Czech University of Life Sciences Prague

**Faculty of
Engineering**

TAE 2019

Proceeding of 7th International Conference on

Trends in Agricultural Engineering 2019

17th - 20th September 2019

Prague, Czech Republic

CZECH UNIVERSITY OF LIFE SCIENCES PRAGUE

CZECH
UNIVERSITY
OF LIFE SCIENCES PRAGUE

Faculty of Engineering

Czech University of Life Sciences Prague
Faculty of
Engineering

7th International Conference on Trends in Agricultural Engineering 2019

Proceeding of 7th International Conference on

Trends in Agricultural Engineering 2019

September 17th 2019 – September 20th 2019

Prague

Czech Republic

Editor in chief: David Herák

7th International Conference on Trends in Agricultural Engineering 2019

September 17th 2019 – September 20th 2019

Conference TAE 2019 publishes research in engineering and physical sciences that represent advances in understanding or modelling of the performance of biological and physical systems for sustainable developments in land use and the environment, agriculture and amenity, bioproduction processes and the food chain, logistics systems in agriculture, manufacturing and material systems in design of agriculture engineering.

Conference venue:

Faculty of Engineering**,** Czech University of Life Sciences Prague**,** Kamýcká 129, Praha 6, Prague, 16521**,** Czech Republic

The 7th TAE conference is organized under the auspices of dean of Faculty of Engineering **doc. Ing. Jiří Mašek, Ph.D.**

Chairman of the conference: David Herák, Czech Republic

Scientific committee:

Nikolay Aldoshin – Russia	Manoj Karkee - USA
Vigen Arakelyan – France	Marián Kučera - Slovakia
Feto Berisso - Ethiopia	František Kumhála - Czech Republic
Jiří Blahovec - Czech Republic	Martin Libra - Czech Republic
Volodymyr Bulgakov - Ukraine	José Machado - Portugal
Roberto D'Amato - Spain	Simon Popescu - Romania
Luis Caicedo - Equador	Alessandro Ruggiero - Italy
Richard Godwin - UK	John Schueller - USA
Gurkan Gurdil - Turkey	Riswanti Sigalingging - Indonesia
Rostislav Chotěborský - Czech Republic	Willi Toisuta - Australia
Jaime Janairo - Philipine	Sotos Voskarides - Cyprus
Vytenis Jankauskas - Lithuania	Stavros Yanniotis - Greece
Algirdas Jasinskas - Lithuania	

All manuscripts in conference proceedings have been reviewed by peer review process.

Reviewers:

Z. Aleš, V. Arakelyen, A. Brunerová, O. Dajbych, G. Gurdil, D. Herák, P. Hrabě, R. Chotěborský, J. Chyba, V. Jurča, A. Kabutey, A. Kešner, P. Kic, M. Kroulík, F. Kumhála, J. Kumhalová, M. Libra, M. Linda, J. Mašek, Č. Mizera, M. Müller, R. Napitupulu, P. Neuberger, P. Novák, S. Pandiangan, M. Petrů, M. Pexa, K. Selvi, R. Sigalingging, E. Simanjuntak, P. Šařec

Warm Welcome to Trends in Agriculture Engineering 2019

The progressive prestige that Trends in Agriculture Engineering international conference has reached during the last 25 years has made it as a world-wide reference about fast development of agriculture from its engineering point of view, and the meeting point for professionals with responsibilities in the improvement of this essential area of whole nations. 108 scientific papers have been selected for TAE 2019 through the Scientific committee of the conference to be presented in a wide thematic spectrum, to promote and to share the newest and the most relevant aspects of agricultural engineering area. Trends in Agriculture Engineering conference become the scientific hub of the global agricultural engineering research and a forum for the future of agri-food production.

The Faculty of Engineering, Czech University of Life Sciences Prague, organizer of this 7th TAE conference, welcomes you in this event. Prague, capital and the largest city of the Czech Republic, welcomes you with its cordiality for making you stay with us the most pleasant possible.

Sincerely

Assoc. prof. Ing. Jiří Mašek, Ph.D.
Dean of Faculty of Engineering
Czech university of Life Sciences Prague

CONTENTS

DRAWBAR PULL OF SMALL TRACTOR WITH SPECIAL LUG WHEELS

Rudolf ABRAHÁM[1], Tomáš ZUBČÁK[1], Radoslav MAJDAN[1]

[1]Department of Transport and Handling, Faculty of Engineering, Slovak University of Agriculture in Nitra, Tr. A. Hlinku 2, 949 76 Nitra, Slovak Republic

Abstract
This contribution is aimed at increase in drawbar pull of small tractor. The special lug wheels were designed for standard tractor driving wheels. If lugs are in base position, a tractor uses standard tires to transport on roads. Protruded position of the lugs allows to improve tractive properties of the tractor in terrain. Drawbar pull at 100% driving wheels slip was measured on cultivated soil at soil moisture 30.98%. Field measurements were repeated seven times to eliminate measurement errors. The results of experiments with special lug wheels were compared with standard tires. The test tractor developed the greater drawbar pull due to the special lug driving wheels. The experimental results show the increase in drawbar pull 23.1% in case of the tractor in second gear.

Key words: tire; wheels slip; tractive performance; agricultural machinery.

INTRODUCTION

Today's agricultural tractors are characterised by high rates of standardisation and feature a range of additional attachments which allow the wider use of each tractor and greatly facilitate its operation *(Kosiba et al., 2012)*. The need for tractors and agricultural machinery to be tested from the point of view of their suitability to agricultural use will grow continuously because these machines directly affect agricultural production *(Hujo et al., 2017)*.

Driving wheels are significant part of a tractor construction because they transmit power to a ground. Therefore, tractor wheels affect a total energy efficiency *(Vitázek et al., 2016; Vitázek et al. 2018)*, a fuel consumption *(Uhrinová et al., 2013)*, and a soil compaction *(Malý et al., 2015; Rataj et al. 2009; Hrubý et al., 2013)*.

Agricultural tractor loses a lot of energy by a driving wheels slip. To reduce the wheels slip, an additional ballast load loads the tractors. This solution improves a drawbar property of the tractors but on the other hand increases the soil compaction and tires wear on a hard surface *(Semetko et al., 2002)*.

The drawbar efficiency affects the fuel consumption and an emission production. The wheels slip reduction improves the fuel consumption, reduces the emission production and so improves an economy and an ecology of a tractor operation.

Many authors *(Kučera et al., 2016; Adamchuk et al., 2016)* researched an impact of driving wheels on the tractor drawbar properties and an environment. This paper is aimed at a research on a new type of the special driving wheels to improve the tractor drawbar pull without a need for the addition ballast load.

MATERIALS AND METHODS

Special lug wheels

The special lug wheels are shown in Fig. 1 and were designed at the Department of Transport and Handling of the Slovak University of Agriculture in Nitra. A support tube (1) is a basic part of the whole mechanism. It enables the remaining parts of the whole mechanism to be attached to each other. On the support tube, there are welded three locking tabs (2), three brackets (3) by which the whole mechanism is connected to the tractor wheel, and a driving disc (6) containing blades (5) mounted by means of ten pins. On the support tube, there are also welded spacer plates (4) through which the mechanism position is centred with respect to the tractor wheel disc. After the driving disc (6), the support tube contains a freely rotating blade control disc (7) for the control of blades. The blade control disc contains, on its circumference, twenty pressed guide pins by means of which blades move into the protruded or base positions. On the other side of the blade control disc, there are four locking holes (9) to fix the position of blades in the protruded position. Three buffer plates (11), attached by six screws to the locking tabs (2), fix the blade control disc on the support tube.
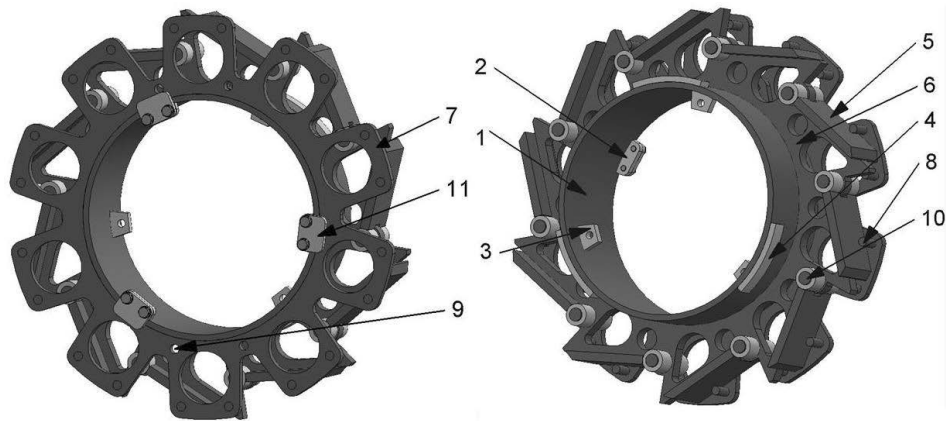
Fig. 1 Special lug wheels: 1 – support tube, 2 – locking tab, 3 – bracket fastening the mechanism to the wheel disc, 4 – spacer plates, 5 – blade, 6 – driving disc, 7 – blade control disc, 8 – guide pin, 9 – locking hole, 10 – blade pin, 11 – buffer plate

Drawbar pull measurement

Drawbar pull at 100% wheels slip was used to compare the special lug wheels with standard tires. The test tractor was equipped with standard tires TS-02 6.5/75-14 4PR TT type (Mitas a. s., Czech Republic). The drawbar pull measurements were realized in accordance with STN ISO 789-9 *(Simikić et al., 2014)*.
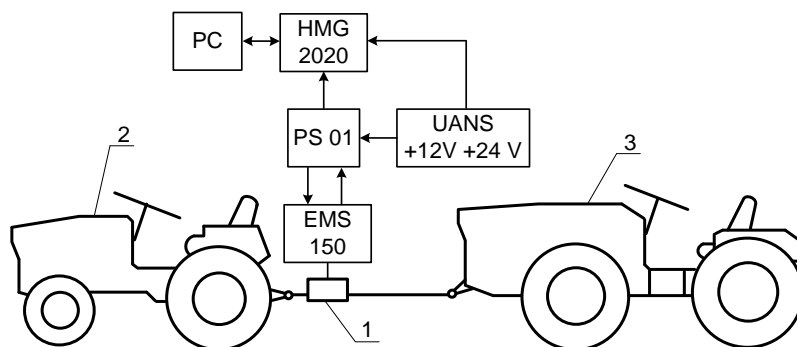
Fig. 2 Schematic diagram of the drawbar pull measurement: 1 – force sensor EMS 150 type, 2 – test tractor Mini 070 type, 3 – load tractor T4K10 type, HMG 2020 – data logger, UANS – universal battery source, PC – personal computer, PS 01 – junction box.

Main parts of a measurement system (Fig. 2) are as follows:
- The test tractor MT8-070 Mini type (Agrozet, Czech Republic) is characterised by gasoline engine with volume capacity 400 ccm, ratted engine power 8 kW and ratted engine speed 3,600 min^{-1}. The test tractor total weight is 310 kg. This tractor drew the load tractor to generate the drawbar pull. The special lug wheels were mounted to the test tractor to compare wheels properties with standard tires on the basis of the drawbar pull. The test tractor with standard tires was equipped with the addition ballast weight in wheel discs to compensate the weight of the special lug wheels. Therefore, there was the same weight of the test tractor under all measurements. The test tractor was operated in second gear.
- The load tractor 4K-14 type (Agrozet, Czech Republic) is characterized by diesel engine with volume capacity 661.6 ccm and maximal output power 13 kW. The load tractor total weight is 870 kg. This tractor loaded the test tractor during the measurement of the drawbar pull.
- The force sensor type EMS 150 (manufacturer: Emsyst s. r. o., Slovak Republic) with strain-gauge bridge in a steel housing (accuracy class: 0.2, rated capacity: 10 kN, rated output: 0 – 10 V). Drawbar pull measurement of tractor Mini 070 is implemented by means of strain tensometric force sensor marked as 150 EMS. Force sensor is connected between the load tractor and test tractor through the steel chain.

- The data logger type HMG 2020 (manufacturer: Hydac GmbH, Germany) is a high-performance portable measuring and data-logging device (Chrastina, et al., 2013) with accuracy $\leq \pm 0.1$. 1 kHz of a sampling frequency was set. Digital recording unit HMG 2020 was used to record electrical signals from force sensor.

- A power supply contains two accumulators (12 V) connected in series or parallel to supply the sensor and the data logger with a direct voltage (12 V or 24 V). The power supply was manufactured in our Department of transport and handling as a portable device (Cviklovič et al., 2012).

The measurements were performed on the field with a cultivated soil of the Slovak Agricultural Museum in Nitra (Slovak Republic) at soil moisture 30.98% (STN 72 1012) in the spring (May 2015). The Chernozem soil type (World Reference Base for Soil Resources) is typical for the area where the field tests were performed.

Drawbar pull calculation

The driving wheels sank to the ground during the measurements. Rocks, stones or another ground inhomogeneity can negatively affect the value of drawbar pull. Therefore, the measurements were repeated seven times to minimize the measurement errors.

To calculate the drawbar pull of one measurement (Fig. 3), a time interval from a start point 1 to a finish point 2 has to be stated. These points are intersection of two lines namely dotted line (minimum level) and solid line (measured course of drawbar pull). Using drawbar pulls of seven measurements, the mean drawbar pull X of the tractor with the different driving wheels types was calculated. The same methodology was published by *Abraham et al., (2019)*.

$$X = \frac{x_1 + x_2 + ... + x_n}{n} \qquad (1)$$

where $x_1, x_2 ..., x_n$ are values of drawbar pulls repeated seven times (N), n is the measurement repetition.

The special lug wheels and standard tires will be compared according to 95% confidence interval *CI*. *Švenková et al. (2010) and Kozelková et al. (2018)* present, that the 95% confidence interval is adequate for experiments in agricultural praxis.
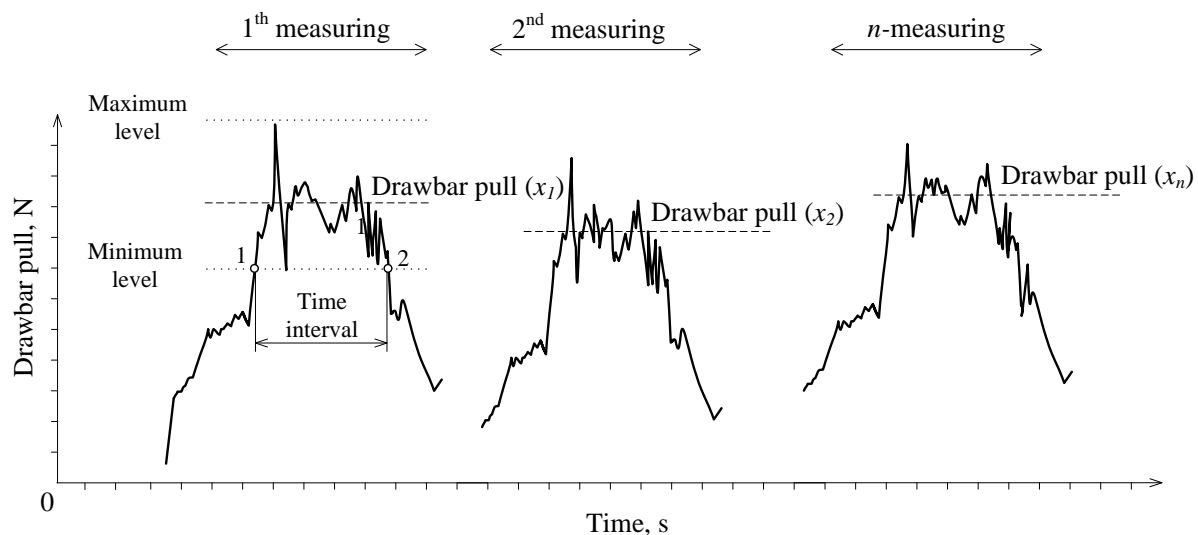
Fig. 3 Methodology of drawbar pull calculation.

RESULTS AND DISCUSSION

Fig. 4 and 5 show the measured courses of drawbar pull during the seven measurements on the cultivated soil. When the tractor was stopped, the driving wheels were slipping at 100% wheels slip. In this moment, the drawbar pulls reached the maximum values. The mean values were calculated and marked by broken lines in graphs.
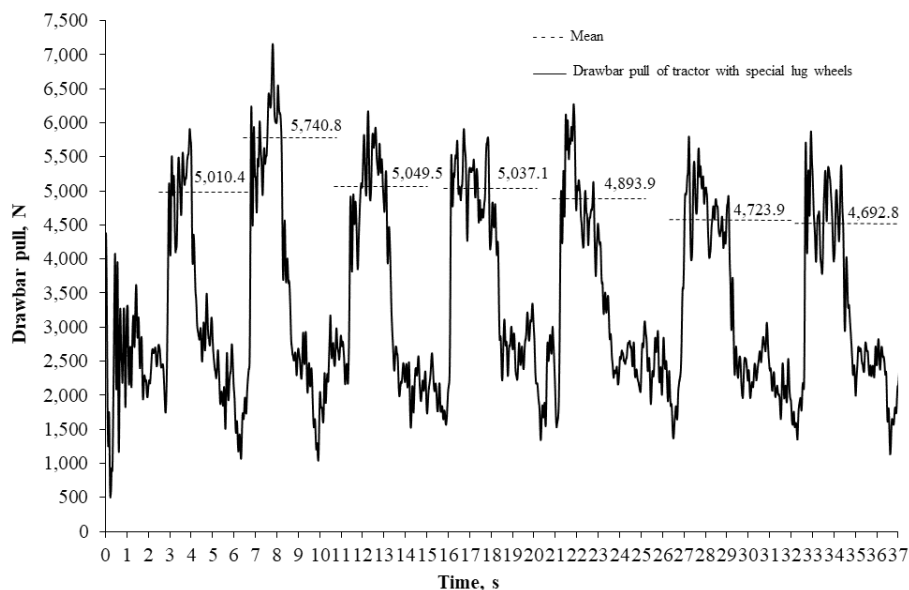
Fig. 4 Drawbar pulls of the tractor with the special lug wheels.
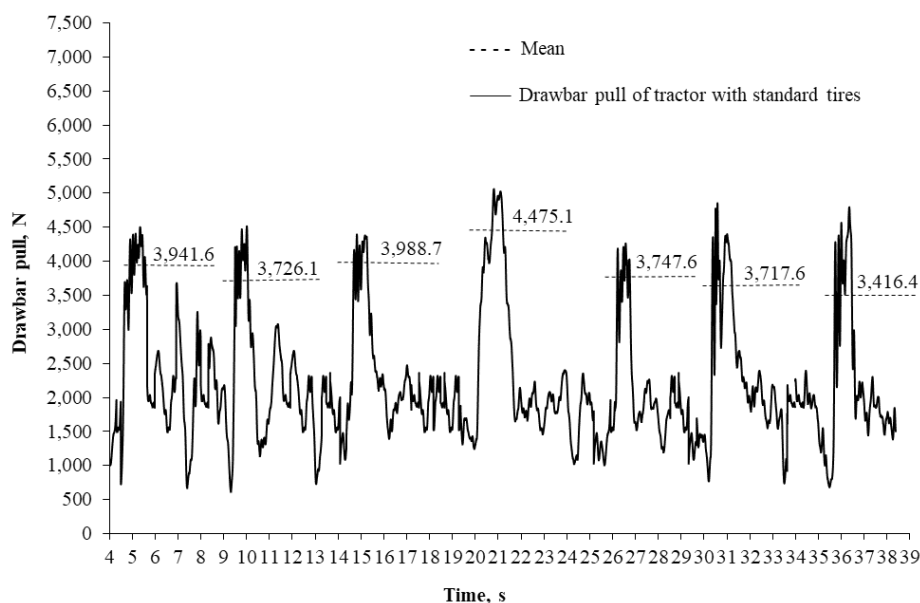
Fig. 5 Drawbar pulls of the tractor with the standard tires.

Tab. 1 shows the calculated values of drawbar pulls, and 95% confidence intervals (*CI*). Considering 95% confidence interval, Fig. 6 shows the statistically significant differences 23.1% between standard tires and special lug wheels.

Tab. 1 Data of drawbar pulls (N) of tractor with different driving wheels.

Wheels type	Drawbar pull N							X N	CI N
Standard tires	3,941.6	3,726.1	3,988.7	4,475.1	3,747.6	3,717.6	3,416.4	3,859.1	608.3
Special lug wheels	5,010.4	5,740.8	5,049.5	5,037.1	4,893.9	4,723.9	4,692.8	5,021.2	645.8
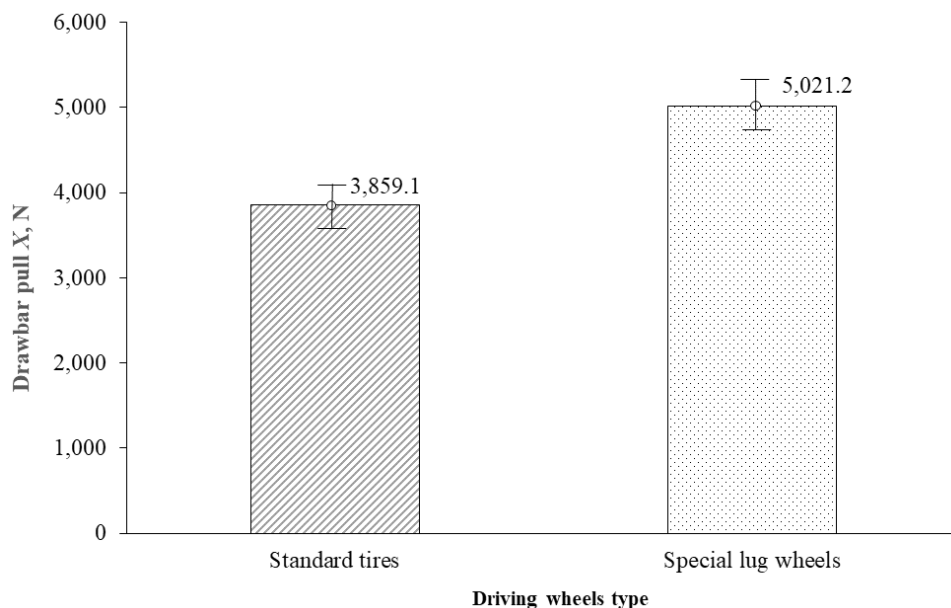
Fig. 6 Comparison of special lug wheels and standard tires.

Battiato and Diserens (2013) present in their work that, although the tractor developed higher drawbar pull both when tire inflation pressure was decreased and wheel load was increased, only the decrease in tire pressure produced improvements in terms of coefficient of traction, tractive efficiency, power delivery efficiency, and specific fuel consumption, while the only significant benefit due to the increase in wheel load was a reduction in the specific fuel consumption at a tire pressure of 160 kPa and a slip of under 15%. *Gee-Clough et al. (1977)* presents the tractive performance of tractor depending on tire inflation, too. When comparing these results with those obtained in our study, we improved the tractor performance using the special lug wheels. In this case the wheel load and tire inflation do not be changed. Traction performance tests were presented by *Turner et al. (1997)* to compare two different rubber belt tractors with two similar radial tire equipped mechanical front wheel drive tractors. Three different test methods were used in both tilled and untilled clay loam soil. The optimized systems showed only small differences in overall performance and efficiency in good traction conditions. This was also where both types of vehicle showed their best power delivery performance. Belted tractors showed their greatest benefit when operated at worse traction conditions in soft or loose soils. Similarly, the special lug wheels improved the traction performance of the test tractor, too.

CONCLUSIONS
The tractive performance affects effective usage of an engine power because a lot of energy is lost between the driving wheels and ground. The transformation of engine power to drawbar pull is a problem relating older and modern tractors, too. The paper presents the design, practical application and tests of special lug wheels to improve the tractive performers of the small tractor. The special lug wheels can be used not only in case of special agricultural conditions (rise grooving) but also in case of all tractors in all difficult tractive conditions. The tests of special driving wheels showed high potential of special lug wheels because the statistically significant increase in drawbar pull reached 23.1%.
The next interest will be aimed at automatization of lugs extension and influence of the special lug wheels on fuel consumption because the lower wheel slip improves this factor.

ACKNOWLEDGMENT

REFERENCES

1. Abrahám, R., Majdan, R. & Drlička, R. (2019). Special tractor driving wheels with two modification of spikes inclination angle. *Agronomy Research, 17, 333-342.*

2. Adamchuk, V., Bulgakov, V., Nadykto, V., Ihnatiev, Y. & Olt, J. (2016). Theoretical research into the power and energy performance of agricultural tractors. *Agronomy Research, 14*, 1511-1518.

3. Battiato, A. & Diseren, E. (2013). Influence of Tyre Inflation Pressure and Wheel Load on the Traction Performance of a 65 kW MFWD Tractor on a Cohesive Soil. *Journal of Agricultural Science, 5,* 197-215.

4. Chrastina, J., Janoško, I. & Polonec, T. (2013). Testing the system to sensing a selected parameter of tractor. *Traktori i pogonske mašine, 8*, 54-60.

5. Cviklovič, V., Olejár, M., Palková, Z. & Pap, M. (2012). Methodology for measuring the efficiency of sine wave inverters. *Acta technologica agriculturae, 15*, 60-63.

6. Gee-Clough, D., McAllister, M. & Evernden, D., W. (1977). Tractive performance of tractor drive tyres. *Journal of Agricultural Engineering Research, 22,* 385-395.

7. Hrubý, D., Bajla, J., Olejár, M., Cviklovič, V. & Tóth, L. (2013). New generation portable vertical penetrometer design. In *Trends in agricultural engineering 2013* (pp. 223-227). Czech University of Life Sciences Prague.

8. Hujo, Ľ., Tkáč, Z., Jablonický, J., Uhrinová, D. & Halenár, M. (2017). The action of force measurement for the three-point hitch of a tractor. *Agronomy Research, 15*, 162-169.

9. Kosiba, J., Varga, F., Mojžiš, M & Bureš, Ľ. (2012). The load characteristics of tractor Fendt 926 Vario for simulation on test device. *Acta Facultatis Technicae, 17,* 63-72.

10. Kozelková, D., Országhová, D., Matejková, E., Fikselová, M., Horská, E., Ďurdíková, D. & Matysik-Pejas, R. (2018). Eggs and their consumption affected by the different factors of purchase. *Slovak Journal of Food Sciences, 12,* 570-577.

11. Kučera, M., Helexa, M. & Molenda, M. (2016). Selected tire characteristics and their relation to its radial stiffness. MM Science Journal, *12*, 1524-1530.

12. Malý, V., Tóth, F., Mareček, J. & Krčálová, E. (2015). Laboratory test of the soil compaction. *Acta Universitatis Agriculturae et Silviculturae Mendelianae Brunensis, 63,* 77-85.

13. Rataj, V., Galambošová, J. & Macák, M. (2009). Experiences with Implementing of CTF System in Slovakia. In *GPS autopiloty v zemědělství.* (pp. 34-38). Czech University of Life Sciences Prague.

14. Simikić, M., Dedović, N., Savin, L., Tomić, M. & Ponjičan, O. (2014) Power delivery efficiency of a wheeled tractor at oblique drawbar force. *Soil and Tillage Research, 141,* 32-43.

15. Semetko, J., Janoško, I. & Pernis, P. (2002). Determination of driving force of tractor and trailer wheels. *Acta Technologica Agriculturae, 5,* 1-4.

16. STN 72 1012 Laboratory determination of moisture content of soils. 1989.

17. Švenková, J. Dědina, M. & Matejková, E. (2010). Verifying ammonia emissions factors currently valid in breeding of livestock. *Acta technologica agriculturae, 13,* 29-32.

18. Turner, R., Shell, L. & Zoz, F. (1997). Field Performance of Rubber Belted and MFWD Tractors in Southern Alberta Soils. *SAE Technical Paper, SP-1291,* 75-85.

19. Uhrinová, D., Jablonický, J., Hujo, Ľ., Kosiba, J., Tkáč, Z., Králik, M. & Chrastina, J. (2013). Research of limited and unlimited emission effect on the environment during the burning of alternative fuels in agricultural tractors. *Journal of Central European Agriculture, 14,* 1402-1414.

20. Vitázek, I., Klúčik, J., Jablonický, J. & Vereš, P. (2016). Ideal cycle of combustion engine with natural gas as a fuel. *Research in agricultural engineering, 62,* 14-20.

21. Vitázek, I., Tkáč, Z. & Mojžiš, M. (2018). Evaluation of drive type properties on the basis of engine-speed maps. In *37th meeting of departments of fluid mechanics and thermodynamics.* (pp 4-12). AIP Publishing.

Corresponding author:
Doc. Ing. Radoslav Majdan, PhD. Department of Transport and Handling, Faculty of Engineering, Slovak University of Agriculture in Nitra, Tr. A. Hlinku 2, Nitra, 94976. Slovak Republic, phone: +421 37 641 4618, e-mail: radoslav.majdan@uniag.sk

HORIZONTAL GROUND HEAT EXCHANGERS – LOW-TEMPERATURE ENERGY SOURCE

Radomír ADAMOVSKÝ[1], Pavel NEUBERGER[1]

[1]*Department of Mechanical Engineering, Faculty of Engineering, Czech University of Life Sciences Prague*

Abstract
The aim of this paper is to analyse and compare the temperatures of heat carrier fluids, thermal resistances, specific outputs and extracted energies for horizontal ground heat exchangers used in the function of low-temperature energy source for heat pumps. Linear and Slinky type horizontal ground heat exchangers, the most commonly used ones in Europe, were verified. The temperatures of the heat carrier fluids did not reach negative temperatures in the two horizontal exchangers throughout the monitored period. The results of the verification indicated that, in terms of the monitored parameters, the linear horizontal exchanger seemed to be more effective than the Slinky type. The temperatures of the heat carrier fluid were on average higher at the linear exchanger by 1.43 ± 2.12 K, with a specific output of 5.76 W per 1 m^2 of the heat exchange surface. The thermal resistance was higher at the Slinky than at the linear exchanger by 50%.

Key words: heat exchanger; temperature; heat carrier fluid; energy accumulation; energy extraction; thermal resistance.

INTRODUCTION

According to *Stefánson (2000)*, low-temperature heat pump energy sources should be renewable and sustainable. The author specified the term "renewable" as a feature of energy source and "sustainable" as a way of using energy. *Wei et al. (2013)* considered the ground mass as a renewable energy source. However, as mentioned by *Kupiec et al. (2018)*, given the time intervals between accumulation and energy extraction, the ground mass can lose its sustainability due to long-term, unbalanced extraction. The temperatures of the ground mass, temperatures of heat carrier fluids in the heat exchangers, extracted outputs and energies are important parameters that affect not only the efficiency and performance of the heat pump, but also the recoverability and sustainability of the low-temperature energy source.

Kayaci, Demir (2018) paid attention to modelling inlet and outlet temperatures of horizontal ground heat exchangers (HGHEs) and its verification. The temperatures of heat carrier fluid in the mode of heat extraction from the ground mass during heating and its supply during cooling a building was monitored by *Gyu et al. (2015)*. The HGHE simulation model was developed and successfully verified in long-term experiments by *Fujii et al. (2012)*. They presented specific outputs of HGHEs depending on the volume flow of the heat carrier fluid. *Verda et al. (2016)* studied the dependence of the depth of HGHEs deposition in the ground mass on its specific output value. *Kupiec et al. (2015)* described the relationships between the energy accumulated in the ground mass during the summer season and the possibilities of its extraction during winter. *Bottarlli et al. (2015)* verified the possibilities of accumulation of energy in the ground mass during summer using PCM materials operating on the principle of phase change. They also analysed the effect of this accumulation on heat carrier fluid temperatures and HGHEs outputs. A series of experiments to determine the specific resistances of HGHEs was carried out by *Zeng et al. (2013)*.

The aim of this contribution was to analyse and compare the temperatures of the heat carrier fluids delivered to the heat pump evaporator, the HGHEs thermal resistances, their specific outputs and energies extracted by HGHEs from the ground mass during a heating season.

MATERIALS AND METHODS

The verification was conducted at the experimental workplace of VESKOM s.r.o. based in Prague, Dolní Měcholupy, during the heating season 2012/2013 from 17 September 2012 to 22 April 2013 (218 days, 5 232 hours). The workplace is located at 50°3'32" north latitude and 14°33'31" east longitude at an altitude of 266 m. Linear and Slinky type HGHE were the subjects of the verification. Linear HGHE

consisted of 330 m (41.47 m^2) piping PE 100RC 40 x 3.7 mm (LUNA PLAST as, Hořin, Czech Republic) deposited at 1.8 m depth in 3 loops with a length of 54.6 m and pipe spacing of 1.0 m. For Slinky HGHE, the total length of piping PE 100RC 32 x 2.9 mm was 220 m (20.11 m^2). This exchanger consisted of 53 loops with a spacing of 0.38 m, deposited at a depth of 1.5 m. *Adamovsky et al. (2015)* presented a detailed scheme of HGHEs installation. Tested HGHEs, along with vertical ground exchangers, were low-temperature energy sources for 3 heat pumps (Industriell Värme Teknik, Tnanas, Sweden) – one PremiumLine EQ E13 (heat output of 13.3 kW at 0/35 °C) and two GreenLine HT Plus E 17 (heat output of 2x 16.2 kW at 0/35°C). The temperatures of the heat carrier fluids were measured by Pt100 sensors at quarter-hour intervals and recorded by the ALMEMO 5990 measuring station (AHLBORN Mess-und Regulungstechnik GmbH, Holzkirchen, Germany). Volume flows of heat carrier fluids were recorded by MTW 3 electronic meters (Itron Inc. Liberty Lake, USA). Ground mass reference temperatures were measured at installation depth at a distance of about 14m from HGHEs. They were measured by GKF 125 and GKF 200 sensors (GREISINGER electronic GmbH, Regenstauf Germany) and recorded at half-hour intervals by the ALMEMO 5990 measuring station. Ambient temperatures were measured by ATF 2 KTY 81.210 sensor (S + S Regeltechnik, Nürnberg, Germany) at a height of 2.5 m above the mass surface. The STATISTICA program (StatSoft, Inc. 2013) and MS Excel 2016 were used to evaluate and analyse the measured values.

RESULTS AND DISCUSSION

1. Heat carrier fluid temperatures

The average daily temperatures of the heat carrier fluids exiting the exchangers, t_L, t_S and the ambient temperatures throughout the heating season are shown in Figure 1. The reaction of the average daily temperatures of the heat carrier fluids to the ambient temperatures is evident. With the exception of the beginning and the end of the heating season, the temperatures of the heat carrier fluid, t_L were higher at linear HGHE than the temperatures, t_S at Slinky HGHE. The quadratic equations of the trend lines of the HGHEs heat carrier fluid temperatures have the form of (1) and (2). Determination coefficients R^2 indicate very good data-curves matching. In equations (1) and (2), τ_d is the duration of the heating season from its beginning, expressed in days.

$$t_S = 0.0007\tau_d^2 - 0.2105\tau_d + 18.74 \quad (R^2 = 0{,}970) \tag{1}$$
$$t_L = 0.0005\tau_d^2 - 0.1784\tau_d + 19.185 \quad (R^2 = 0{,}980) \tag{2}$$
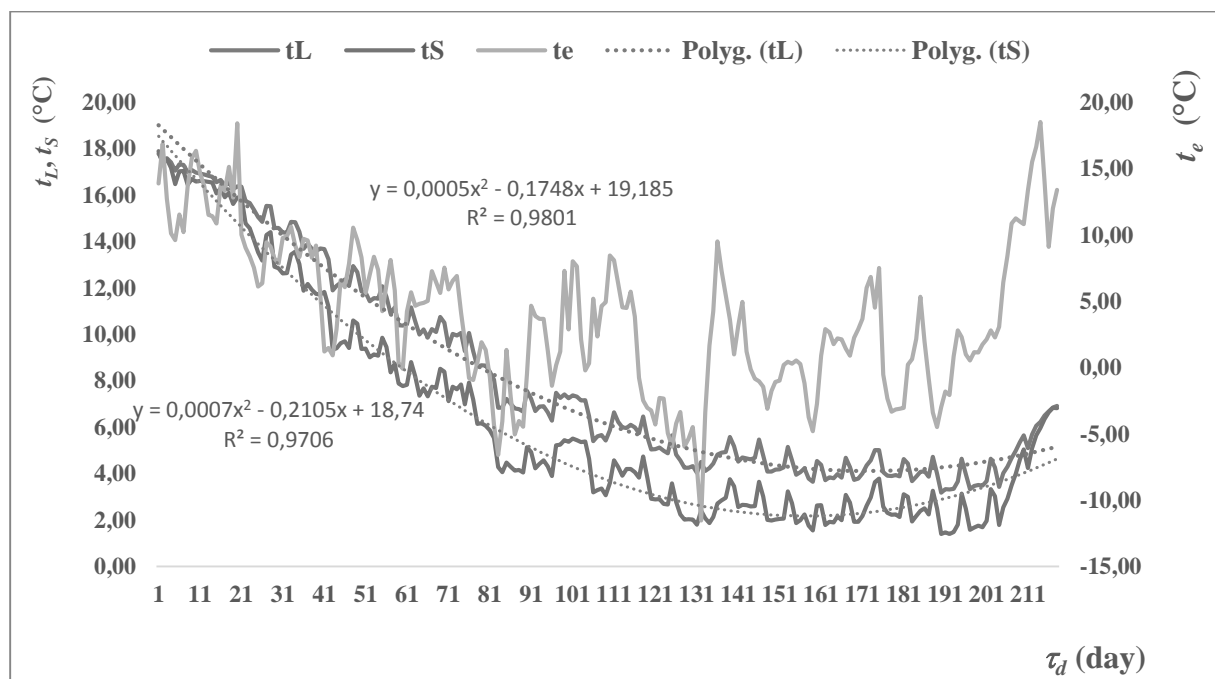
Fig. 1 Average daily temperatures of heat carrier fluids from Slinky HGHE, t_S and from linear HGHE, t_L and ambient temperatures, t_e.

The distribution of the heat carrier fluid temperatures during the heating season is better described by the histogram in Figure 2. It shows the frequency of average hourly temperatures, f_i (5232 values) and temperature modes, $Mod(t)$ (the most frequent temperatures) at 2 K intervals throughout the heating season. The horizontal axis of the histogram shows the temperatures defining the interval, the so-called class representative r in the range of <-1.0; 19.0> ° C.

The histogram indicates that $Mod(t_S)$ of Slinky HGHE occurred in a temperature range of <2.10; 4.00> ° C ($r = 3$ ° C) with relative frequency $f_i = 32.91\%$. The mode of linear HGHE, $Mod(t_L)$ had higher relative frequency $f_i = 34.04\%$ at higher interval <4.10; 6.00> ° C ($r = 5$ ° C). The temperatures t_S occurred with quite high relative frequency $f_i = 12.77\%$ in an interval as low as <0.10; 2.00> ° C ($r = 1$ ° C). Since the higher frequency of the heat carrier fluid temperatures at higher temperature intervals indicate the advantage of a low-temperature energy source, the linear HGHE can be considered more advantageous in terms of temperatures of heat carrier fluids. This conclusion is based on the reversed Carnot cycle. At a constant condensation temperature, an increase in the evaporation temperature, influenced by the temperature of the heat carrier fluid supplied to the evaporator, will increase the heat pump's heating factor. The distribution of heat carrier fluid temperatures in HGHEs is closely related to the distribution of temperatures in the ground mass mentioned in publication by *Adamovsky et al. (2015)*.

Class representative r (°C)	-1	1	3	5	7	9	11	13	15	17	19
tL	0,00	0,84	11,72	34,04	16,34	4,99	9,00	6,57	6,69	9,81	0,00
tS	0,00	12,77	32,91	15,94	8,41	8,54	4,42	5,14	4,17	7,70	0,00
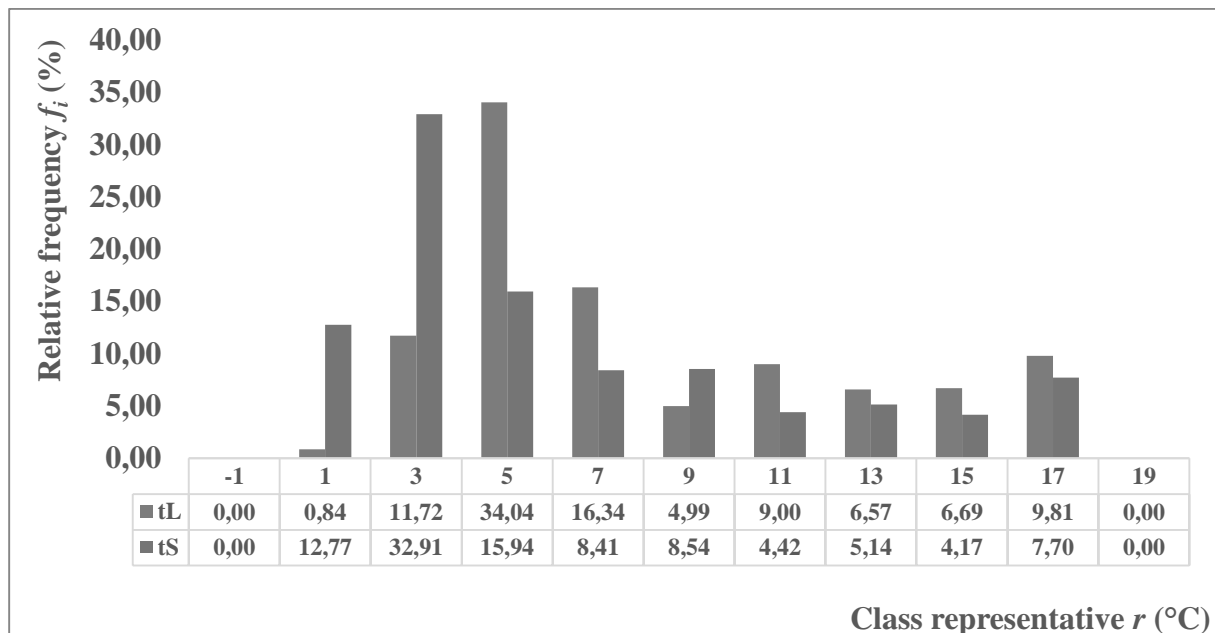
Fig. 2 Relative frequencies of average hourly temperatures of heat carrier fluids from HGHEs, t_L and t_S

2. Heat outputs and extracted energies

The specific heat outputs ($q_{\tau,a}$, $q_{\tau,max}$) and the energy extractions (q_a, q_{max}) were determined on the basis of the difference between the temperatures and the flow rates of the heat carrier fluid (V_τ), the specific heat capacity and the density corresponding to the mean temperature of the heat carrier fluid.

Table 1 presents the average and maximum hourly flow rates of the heat carrier fluids, $V_{\tau,a}$ and $V_{\tau,max}$, respectively, the overall volume of heat carrier fluid, V_Σ flowing through the exchangers during the heating season, the average and maximum specific outputs, $q_{\tau,a}$ and $q_{\tau,max}$, respectively, recalculated to 1 m pipe length and 1 m² of the exchanger's heat transfer surface, average and maximum specific energies, q_a and q_{max}, respectively, transferred from the ground mass by 1 m² of the exchanger in 1 day of the heating season, the overall energy, q_Σ transferred from the mass and overall time of energy extraction by the exchangers, τ_Σ during the heating season.

The overview presented in Table 1 shows that both the specific powers and the extracted energies were higher for linear than for Slinky HGHE. However, the values are determined at different volume flows of the heat carrier fluid and different heat transfer surfaces of the HGHEs. But if the volume

flows of the heat carrier fluids are converted to 1 m^2 of heat exchanger surface, this value is higher for HGHE Slinky. The values of the recorded average specific outputs of HGHEs correspond to those reported by *Rosen et al. (2006)*. At a heating factor of 3.5, they indicated the heat pump's specific output 13 W/m for linear HGHE with a pipe diameter of 40 mm and 7 W/m for Slinky HGHE. The HGHEs outputs and extracted energies were certainly influenced by the special character of the operation of the production halls and administrative building, such as interrupted operation and required low outputs of the heating system, especially at the beginning and end of the heating season.

Tab. 1 Heat carrier fluid flows, heat outputs and extracted energies

Parameter	Linear HGHE	Slinky HGHE
$V_{\tau,a}$ (m^3/h)	0.47±0.22	0.35±0.12
$V_{\tau,max}$ (m^3/h)	0.89	0.72
V_{Σ} (m^3)	1 183.70	592.82
$q_{\tau,a}$ (W/m)	4.92±3.60	3.35±2.42
$q_{\tau,max}$ (W/m)	15.25	12.48
$q_{\tau,a}$ (W/m^2)	39.14±28.67	33.38±24.11
$q_{\tau,max}$ (W/m^2)	121.42	124.20
q_a (kJ/m^2.day)	1 614.15±1 076.40	938.31±677.70
q_{max} (kJ/m^2.day)	4 407.73	4 258.86
q_{Σ} (MJ/m^2)	351.88	204.55
τ_{Σ} (h)	2 497	1 703

Figure 3 presents the course of specific energies extracted by HGHEs during the heating season. As in the case of the heat carrier fluid temperatures, there is a clear dependence of the extracted energy values on the ambient temperatures. The extracted energy values are lower for Slinky HGHE than for linear HGHE due to lower heat carrier fluid temperatures. The reported values of the energy extracted from the ground mass are in accordance with the limit values recommended in the publication by *Kyriakis, Michopoulus (2006)*.
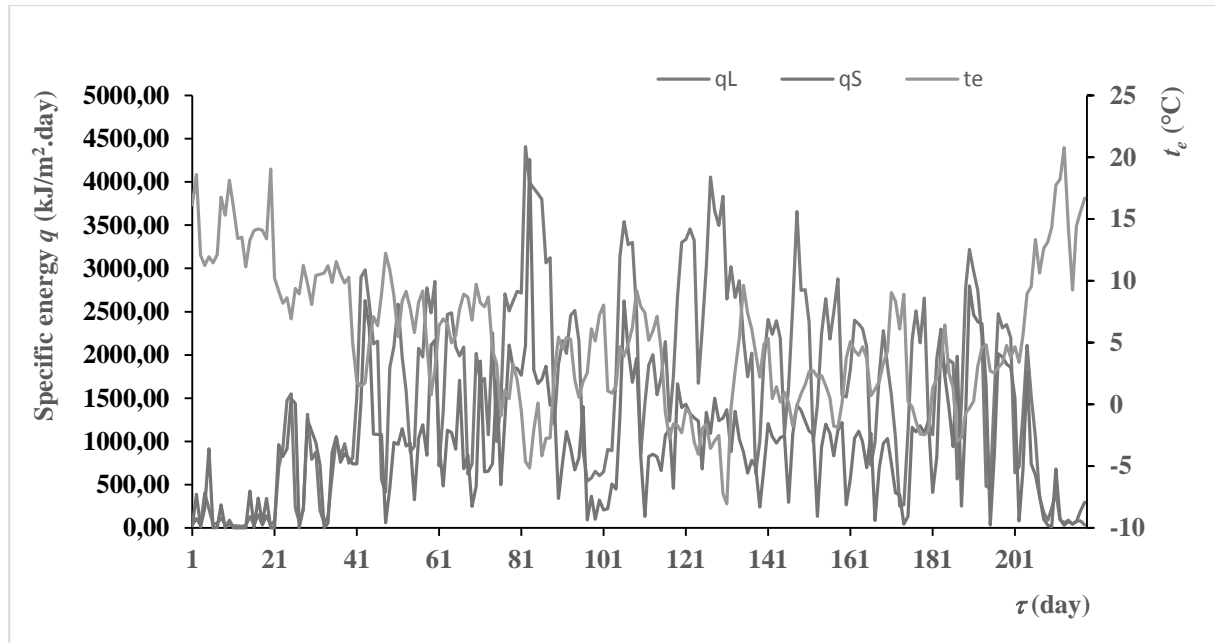
Fig. 3 Energies extracted from the ground mass by HGHEs

3. HGHEs Thermal resistances

The process of heat transfer between ground mass and heat carrier fluid can be evaluated by the relationship published by Z e n g at al. (2003). They relate specific thermal resistance to 1 m length of vertical ground borehole. In terms of HGHEs comparison, it seems to be more advantageous to specify the specific thermal resistance per 1 m² of the heat exchanger surface according to the relation:

$$R = \frac{t_{r.m.} - t_a}{q_\tau} \qquad (3)$$

where:

$t_{r.m.}$ – temperature of reference ground mass (°C);

t_a – temperature of heat carrier fluid (°C);

q_τ – specific heat output of HGHEs (W/m²).

The average thermal resistance value R ranges from 0.07±0.02 m².K/W for linear HGHE and 0.14±0.06 m².K/W for Slinky HGHE. The maximum R value for Slinky HGHE is more than double the value for linear HGHE. A lower thermal resistance value indicates a higher intensity of heat transfer between the ground mass and the heat carrier fluid.

CONCLUSIONS

The above analysis and comparison of the verification results indicate that linear HGHE appears to be more advantageous than Slinky HGHE in terms of the evaluated parameters. This conclusion is confirmed by the courses of the average daily temperatures of the heat carrier fluids, equations (1) and (2) and by the intervals of the modes of the average hourly temperatures and their relative frequencies. Specific heat outputs and energies extracted from the ground mass were also higher at the linear HGHE than at Slinky HGHE. The thermal resistance of linear HGHE was approximately half the resistance monitored at HGHE Slinky.

However, these conclusions are based only on the results of the verification in one heating season. Further measurements will show whether the trends of the monitored parameters do not change under other climatic conditions.

REFERENCES

1. Adamovský, D., Neuberger, P., & Adamovský, R. (2015). Changes in energy and temperature in the ground mass withhorizontal heat exchangers—The energy source for heat pumps. *Energy and Buildings, 92*, 107-115.

2. Bottarelli, M., Bortoloni, M., & Su, Y. (2015). Heat transfer analysis of underground thermal energy storage in shallow trenches filled with encapsulated phase change materials. *Applied Thermal Engineering*, *90*, 1044–1051.

3. Fujii, H., Nishi, K., Komaniwa, Y., & Chou, N. (2012). Numerical modeling of slinky-coil horizontal ground heat exchangers. *Geothermics*, *41*, 55-62.

4. Gyu, H. G., Seung, R. L., Nikhil, N.V., & Seok, Y. (2015). A new performance evaluation algorithm for horizontal GCHPs (ground coupled heat pump systems) that considers rainfall infiltration. *Energy*, *83*, 766 - 777.

5. Kayaci, N. & Demir, H. (2018). Long time performance analysis of ground source heat pump for space heating and cooling applications based on thermo-economic optimization criteria. *Energy and Buildings*, *163*, 121-139.

6. Kupiec, K., Larwa, B., & Gwadera, M. (2015). Heat transfer in horizontal ground heat exchangers. *Applied Thermal Engineering*, *75*, 270-276.

7. Kyriakis, N. & Michopoulos, F. (2006). On the maximum thermal load of ground heat exchangers. *Energy and Buildings*, *38*, 25-29.

8. Rosén, B., Gabrielsson, A., Hellström, G., & Nilsson, G. (2006). Systems for heating and cooling of the land - Demonstration object of geothermal plants (in Swedish). *Varia 556*, Linköping, Sweden: Swedish Geotechnical Institute.

9. Stefánsson, V. (2000). The renewability of geothermal energy. In P*roceedings of the*

World Geothermal Congress 2000 (pp. 883-888).

10. Verda ,V., Cosentino, S., Russo ,S. L., & Sciacovelli, A. (2016). Second law analysis of horizontal geothermal heat pump systems. *Energy and Building*, *124*, 236-240.

11. Wei, W., Baolong, W., Tian, Y., Wenxing, S., & Yiating, L. (2013). A potential solution for thermal imbalance of ground source heat pump systems in cold regions: Ground source absorption heat pump**.** *Renewable Energy*, *59*, 39-48.

12. Zeng, H., Diao, N., & Fang, Z. (2003). Heat transfer analysis of boreholes in vertical ground heat exchangers. *International Journal of Heat and Mass Transfer*, *46*, 4467-4481.

Corresponding author:

doc. Ing. Pavel Neuberger, Ph.D., Department of Mechanical Engineering, Faculty of Engineering, Czech University of Life Sciences Prague, Kamýcká 129, Praha 6, Prague, 16521, Czech Republic, phone: +420 22438 3179, e-mail: neuberger@tf.czu.cz

A DEVICE TO MEASURE WALL FRICTION DURING UNIAXIAL COMPRESSION OF BIOMATERIALS

Olaosebikan Layi AKANGBE[1], Jiří BLAHOVEC[2], Radomír ADAMOVSKÝ[1], Miloslav LINDA[3], Monika HROMASOVÁ[3]

[1]*Department of Mechanical Engineering, Faculty of Engineering, Czech University of Life Sciences Prague, Czech Republic*
[2]*Department of Physics, Faculty of Engineering, Czech University of Life Sciences Prague, Czech Republic*
[3]*Department of Electrical Engineering and Automation, Faculty of Engineering, Czech University of Life Sciences Prague, Czech Republic*

Abstract
A device is reported for the acquisition of the effects of friction between compressed biomaterials along the interface between the material and the wall, parallel to the axis of compression. Results of equipment calibration test as well as uniaxial compression tests on a selected food powder are reported. Wall friction had highly significant effect on transmissibility of pressure in the compressed material and significantly affected effective utilisation of the input energy. The results are of importance with respect to the densification, handling and storage of food materials of the type described.

Key words: wall friction; food powder; effective pressure.

INTRODUCTION

Friction along the internal walls of product compression dies or large storage facilities for related feedstock and products has profound effect *(Cheng, Zhang, Yan, & Shi, 2015; Tien, Wu, Huang, Kuo, & Chu, 2007)*, especially on longitudinal transmissibility of pressure *(Briscoe & Rough, 1998; Michrafy, Haas, Kadiri, Sommer, & Dodds, 2006)* – which determines the degree of achievable deformation *(Li, Liu, & Rockabrand, 1996)* and uniformity of the distribution of density *(Adams, Briscoe, Corfield, Lawrence, & Weert, 1998)* along the lengths of compressed products – and the magnitude of radially transmitted pressure. Dissipation of energy, severe barrel wear and failure of machine elements are some of the effects of friction during food processing *(Adams et al., 1998; Tumuluru, Wright, Kenny, & Hess, 2010)*. Wall friction is therefore an important factor considered during the design and operation of product densification and storage schemes. Available studies document some of these effects in relation to bulk storage of biomaterials *(Horabik & Molenda, 2002; Molenda & Horabik, 2005)*. The effect of wall friction during product densification is however scantily reported, especially in relation to high pressure uniaxial compression. Instrumented bins and dies have been employed in various ways to sense both applied and transmitted loads *(Bek, Gonzalez-Gutierrez, Moreno Lopez, Bregant, & Emri, 2016; Rusinek & Molenda, 2007)* and to estimate internal friction parameters for bulk materials in storage *(Molenda et al., 2006; Rusinek & Molenda, 2007)*. Similar constructs *(Jiří Blahovec & Kubat, 1987)* may be employed to sense frictional drag along the walls of product densification devices. This study reports one such technique.

MATERIALS AND METHODS
Description and working principles of the test apparatus
The device (Fig. 1) consists of a stepped cylindrical ring supported on four slender columns rising from a base ring which is supported in a groove on a flat, circular solid base. A base plug whose smaller end fits in a product compression vessel sits on the base plate and maintains a clearance with the slender arms along its circumference. The product compression vessel sits on the stepped ring. During product compression, friction drag along the internal wall of the die is sensed through deflections in the support arms while reaction to the applied compression force is offered through the plug. Deflections in the support arms are sensed through strain gauges affixed at midpoints on their outer faces. The signals are subsequently relayed and amplified using a data acquisition unit which is
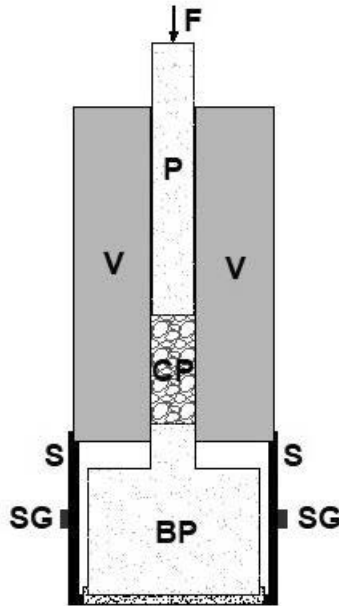
Fig. 1 Schematic layout of the friction drag sensing and data acquisition device indicating the applied force (F), piston (P), compression vessel (V), compressed product (CP), base plug (BP), vessel support (S) and strain gauge (SG)

connected to a personal computer. As shown in the setup (Fig. 1), the small end of the plug is designed to fit in the compression vessel only partially; sufficient clearance is maintained between the bottom of the compression vessel and the stepped face of the base plug. The plug acts as a stationary base while the piston moves vertically downwards during compression. Axially applied pressure induces radial transmission of stress through the material, normal to the face of the wall of the compression vessel. Deformation of the compressed material implies reduction in its volume which progresses mainly axially (downwards), relative to the wall of the die. Drag is thereby imposed on the internal wall of the compression vessel, due, chiefly, to frictional resistance. A threshold magnitude of this resistance is sensed as static friction. Consequently, a dynamic phase is established within which kinetic friction dominates, which is wall friction. The compression vessel is mounted on the support (S) whose slender arms deflect accordingly as a result of frictional drag. Strain transducers are mounted on the four arms in full bridge configuration with compensation for transverse strain in two of the arms to sense the drag. Output analog signals are fed to an amplifier and subsequently through a microprocessor control unit to the input/output devices. The signal gain employed was 20. A user interface (Radlice v.1.1.0.0), developed at the Czech University of Life Sciences was used.

Equipment calibration
The assembled apparatus was mounted on a Labor Tech® LabTest 6.50 electromechanical universal test rig (LABORTECH s.r.o., Opava, Czech republic.) on which calibration tests were done for replicate measures of applied forces acting on the support as would net friction loads. The forces were applied through the top face of the compression vessel. During the test, applied forces were logged against output voltage readings on a multi-meter, connected separately to the data acquisition unit.

Test procedure
Compression tests were carried out on a Tempos ZDM 50 universal test rig (TEMPOS, spol. s.r.o., Czech Republic). Dry powder of *Ceratonia siliqua* L. (carob) at moisture content of 4.51%, in dry basis, was fed into the compression vessel for a product aspect ratio of 1.0. The internal diameter of the vessel was 25 mm. The apparatus (Fig. 1) was mounted on the test rig and axial force applied on the piston through a hemisperical disc at a deformation rate of 10 mm/min. The force was increased steadily from 0 N to a peak force of 10 kN, corresponding to an applied pressure of 20 MPa. Compression data were logged using the TiraTest software (TIRA GmbH, Schalkau, Germany) while friction data were separately logged using the Radlice v.1.1.0.0 software. Both data sets were subsequently

synchronised using their logged time data. The tests were repeated three times. Product moisture content was determined according to ISO 712:2009 *(International Organization for Standardization, 2009)* with the aid of a Gallenkamp type hot air oven (Memmert GmbH, Germany). Product masses were weighed using the Kern 440–35N (Kern & Sohn GmbH, Stuttgart, Germany).

Evaluation of the indices of densification

Procedures and equations employed for evaluating the relevant indices of densification presented here are well reported in literature *(Akangbe, Blahovec, Adamovský, Linda, & Hromasova, 2019; Akangbe & Herak, 2017)*. For a measure of product deformation, gross energy input may be computed using equation (1).

$$E = \sum_{n=0}^{n=i-1} \left[\left(\frac{F_{n+1} + F_n}{2} \right) \times (\delta_{n+1} - \delta_n) \right] \qquad (1)$$

where n refers to subdivisions of the deformation axis or incremental deformation, as logged by the test equipment *(Akangbe & Herak, 2017)* and F_N (N) is force applied for an observed deformation, δ_n (mm). With respect to the mass of the material compressed, specific energy demand, E_m (J.kg^{-1}) was calculated as shown in equation (2).

$$E_m = {E}/{m} \qquad (2)$$

where m (kg) is the mass of the material compressed. The specific power, $\dot{E}$ (J.kg^{-1}.s^{-1}) was subsequently calculated as the time rate of expenditure of this energy, using equation (3).

$$\dot{E} = {E_m}/{t} \qquad (3)$$

where t is deformation time, s. The effective deformation force (F_{net}), net specific energy demand and net specific power requirement were computed using equations (1) – (3), having deducted the measured frictional drag from the applied compression force and replacing F_N (above) with the net force, F_{net} (N), such that

$$F_{net} = F_N - f_N \qquad (4)$$

where f_N (N) is the attendant frictional drag. Deformation moduli were established as ratios of applied and effective compressive stress to the strains obtaining. Bulk density of the compressed material was determined as a function of the established material volume upon compression.

Data analysis

Regression analysis was run on calibration data and treatment means for the test data as well as other ancillary statistics were established using the MS Excel platform.

RESULTS

From the calibration tests conducted, frictional drag along the wall of the compression vessel was found to be related to the output voltage parabolically as presented in equation (5). This relationship was found to be a fitting representation of the interaction of the two parameters (p<0.001) and provided estimates of a significant proportion of the system's behaviour ($R^2 = 0.999$) appropriately.

$$f = 776.09V^2 + 2984.1V \qquad (5)$$

where f is frictional drag (N) and V is output voltage (Volts).

Force and deformation profiles of the compressed food material are presented in Fig. 2. Frictional resistance progressed in a pattern similar to that observed with the steadily applied force. Both trends were curvilineal and appeared to be transcendantal. This means that as the applied force increased, friction along the wall of the vessel also increased, attaining a peak value at the maximum applied force. As a result of this, the effective force acting to compress the powdery material was significantly reduced compared to the applied force (Fig. 2). This net force however exhibits curvilineal trend similar to those of the interacting forces producing it. An intersection of the profiles of wall friction and

the effective compressive force is apparent at about 3027.75 N or a deformation of 8.05 mm. Beyond this point (Fig. 2), effective compressive force was lower than the magnitude of friction along the material-wall interface. This means that a substantial proportion of the force applied beyond the indicated point of interaction, at the given magnitude of applied pressure, is absorbed as frictional resistance. At the applied pressure of 20 MPa and strain of 0.368, induced at a rate of 0.007 s^{-1}, the effective compressive pressure on the powdery material was 8.53 MPa (Fig. 3). This means that, for the gross energy demand of 2.58 kJ.kg^{-1}, the net energy utilised for deforming the material was 1.46 kJ.kg^{-1}. It may be inferred, therefore, that friction energy uptake during the compression of the product
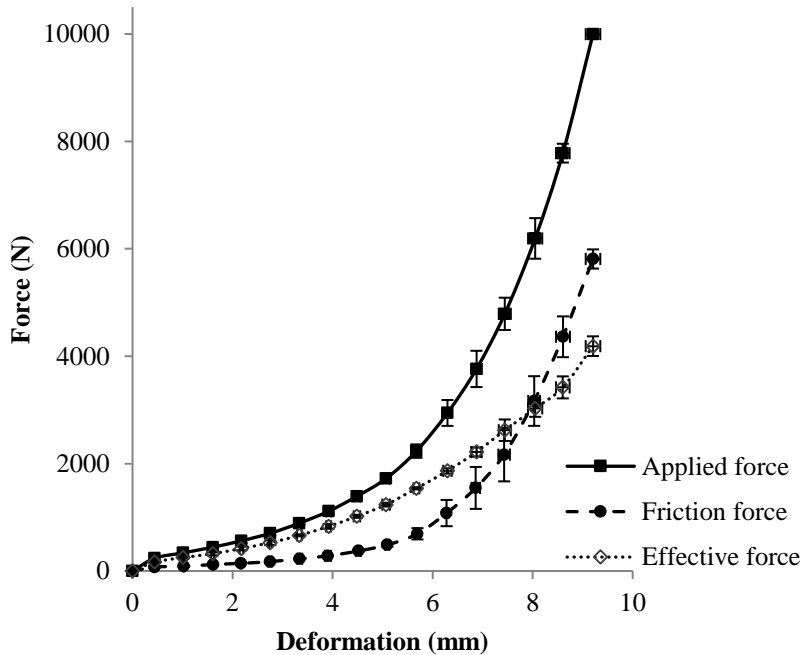
Fig. 2 Force profiles during the compression of dry carob powder
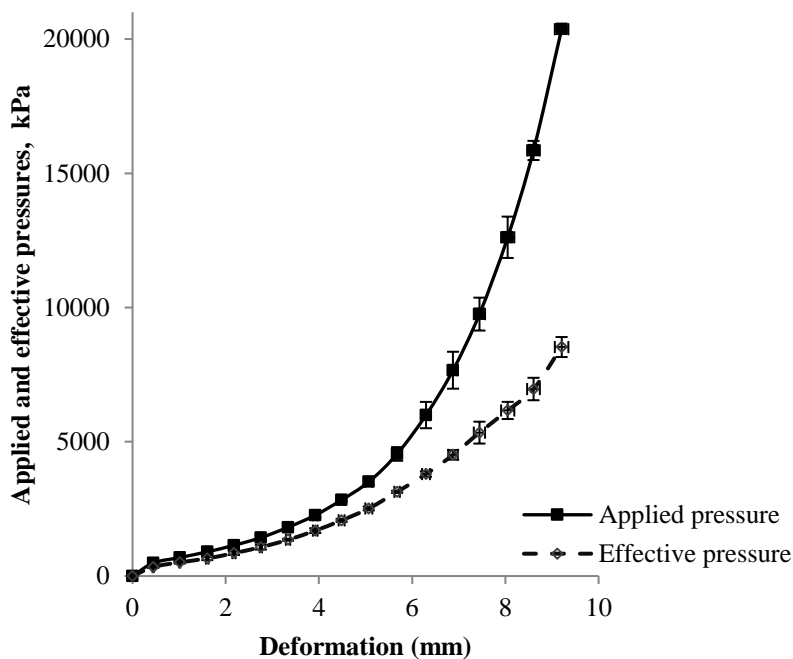
Fig. 3 Applied and effective pressure profiles during the course of product deformation

was responsible for a significant loss (1.12 kJ.kg^{-1}) of the input energy, which represented 43.4% of the total energy supplied. The final bulk density of the compressed carob powder was 1154.55 kg.m^{-3}. At the applied pressure, gain in bulk density of 58.3% occurred in the material, its porosity having been lowered from 50.2% – 24.4%. The time rate of the expenditure of energy by the material for this gain in density was 26.25 kW.kg^{-1}. This was energy use following losses to friction. The attendant modulus of deformation given friction loss (64.9 kPa) was also less compared to what may obtain at the full magnitude of the applied pressure of 20 MPa, which is 187 kPa.

DISCUSSION

Wall friction has a limiting effect on the force acting on the compressed material *(Briscoe & Rough, 1998)*; it significantly reduces the effective compression force and grows with the applied force *(Tien, Wu, Huang, Kuo, & Chu, 2007)*. Contributory effects of the, so called, stick-slip phenomenon *(Stasiak & Molenda, 2004)* translate to significant reductions in transmissibility of applied pressure *(Michrafy, Ringenbacher, & Tchoreloff, 2002)*. Along the material-wall interface, modifications of the layer of the compressed material in contact with the wall occurs. This is associated with friction coefficient, magnitude of radially transmitted force and the comencement and degree of thermal excitations *(Li, Liu, & Rockabrand, 1996; Persson, 1999)*. The onset of such activity is indicated by the occurrence of stick and slip. High fibre content of carob powder *(Yousif & Alghzawi, 2000)* is, in part, responsible for the high frictional resistance, consequent thermal excitation and modification of the material in contact with the wall of the die. *Stasiak, Molenda, Horabik, Mueller, & Opaliński (2014)* report lessening or near elimination of this effect through the use of some lubricating media, although under low compressive pressures. Density attained by the bulk material is therefore attributable, essentially, to the effective compressive pressure. There are important implications of these in respect of achievable product densification and densification energy requirement.

CONCLUSIONS

A method for direct acquisition of data on frictional drag along material-wall interface of product compression dies is presented. Wall friction was satisfactorily related to output voltage and the effect of friction on product densification was found to be pronounced and limiting to effective compression force beyond some critical point for the reported test conditions. Understanding the effects of friction along the interface between compressed products and the wall of compression dies is vital to product densification and food handling and storage schemes.

ACKNOWLEDGMENT

REFERENCES

1. Adams, M. J., Briscoe, B. J., Corfield, G., Lawrence, C. J., & Weert, X. (1998). Optimisation of wall friction in food processing. In *D. Dowson, C. M. Taylor, T. H. C. Childs, G. Dalmaz, Y. Berthier, L. Flamand, ... A. A. Lubrecht (Eds.), Proceedings of the 24th Leeds-Lyon symposium on Tribology: Tribology for energy conservation*, *34*, 347–356. London, UK: Elsevier Science B.V.

2. Akangbe, O. L., Blahovec, J., Adamovský, R., Linda, M., & Hromasova, M. (2019). Effects of selected process parameters on the compaction of carob powder. *Agronomy Research, 17*(1), 13–21.

3. Akangbe, O. L., & Herak, D. (2017). Mechanical behaviour of bulk seeds of some leguminous crops under compression loading. *Scientia Agriculturae Bohemica, 48*(4), 238–244.

4. Bek, M., Gonzalez-Gutierrez, J., Moreno Lopez, J. A., Bregant, D., & Emri, I. (2016). Apparatus for measuring friction inside granular materials - Granular friction analyzer. *Powder Technology, 288*, 255–265.

5. Blahovec, J., & Kubat, O. (1987). Compression of dry porous agricultural materials. *Zemědělská Technika, 33*(5), 289–302.

6. Briscoe, B. J., & Rough, S. L. (1998). The effects of wall friction in powder compaction. *Colloids and Surfaces A: Physicochemical and Engineering Aspects*, 137, 103–116.

7. Cheng, X., Zhang, Q., Yan, X., & Shi, C. (2015). Compressibility and equivalent bulk modulus of shelled corn. *Biosystems Engineering, 140*(2013), 91–97.

8. Horabik, J., & Molenda, M. (2002). Properties of grain for silo strength calculation. In *J. Blahovec & M. Kutílek (Eds.), Physical Methods in Agriculture* (pp. 195–217). Boston, MA: Springer.

9. International Organization for Standardization. (2009). ISO 712: 2009, Cereals and cereal products -- Determination of moisture content -- Reference method.

10. Li, Y., Liu, H., & Rockabrand, A. (1996). Wall friction and lubrication during compaction of coal logs. *Powder Technology, 87*, 259–267.

11. Michrafy, A., Haas, S., Kadiri, M. S., Sommer, K., & Dodds, J. A. (2006). The effects of ambient temperature on the compaction of pharmaceutical powders. *Proceedings of the Institution of Mechanical Engineers, Part E: Journal of Process Mechanical Engineering, 220*(1), 1–6.

12. Michrafy, A., Ringenbacher, D., & Tchoreloff, P. (2002). Modelling the compaction behaviour of powders: Application to pharmaceutical powders. *Powder Technology, 127*(3), 257–266.

13. Molenda, M., & Horabik, J. (2005). Characterization of mechanical properties of particulate solids for storage and handling. In *J. Horabik & J. Laskowski (Eds.), Mecahanical properties of granular agro-materials and food powders for Industrial practice, Part I.* Lublin: Institute of Agrophysics PAS.

14. Molenda, M., Stasiak, M., Moya, M., Ramirez, A., Horabik, J., & Ayuga, F. (2006). Testing mechanical properties of food powders in two laboratories - degree of consistency of results. *International Agrophysics, 20*, 37–45.

15. Persson, B. N. J. (1999). Sliding friction. *Surface Science Reports, 33*, 83–119.

16. Rusinek, R., & Molenda, M. (2007). Static and kinetic friction of rapeseed. *Research in Agricultural Engineering, 53*(1), 14–19.

17. Stasiak, M., & Molenda, M. (2004). Direct shear testing of food powders flowability - Influence of deformation speed and apparatus stiffness. *Acta Agrophysica, 4*(2), 557–564.

18. Stasiak, M., Molenda, M., Horabik, J., Mueller, P., & Opaliński, I. (2014). Mechanical properties of potato starch modified by moisture content and addition of lubricant. *International Agrophysics, 28*, 501–509.

19. Tien, Y. M., Wu, P. L., Huang, W. H., Kuo, M. F., & Chu, C. A. (2007). Wall friction measurement and compaction characteristics of bentonite powders. *Powder Technology, 173*, 140–151.

20. Tumuluru, J. S., Wright, C. T., Kenny, K. L., & Hess, J. R. (2010). A Review on biomass densification technologies for energy application. Idaho Falls: Idaho National Laboratory, U.S. Department of Energy.

21. Yousif, A. K., & Alghzawi, H. M. (2000). Processing and characterization of carob powder. *Food Chemistry, 69*, 283–287.

Corresponding author:

Olaosebikan Layi Akangbe, Department of Mechanical Engineering, Faculty of Engineering, Czech University of Life Sciences Prague, Kamýcká 129, Praha 6 - Suchdol, Prague, 16521, Czech Republic, phone: +420 22438 3186, e-mail: akangbe@tf.czu.cz

HARVESTING OF MIXED CROPS BY AXIAL ROTARY COMBINES

Nikolay ALDOSHIN[1], Otari DIDMANIDZE[1], Bakhadir MIRZAYEV[2], Farmon MAMATOV[3]

[1] *Russian State Agrarian University - Moscow Timiryazev Agricultural Academy, Russia*
[2] *Tashkent Institute of Irrigation and Agricultural Mechanization Engineers, Tashkent, Uzbekistan*
[3] *Karshi Engineering Economic Institute, Karshi, Uzbekistan*

Abstract
The choice verification of operating modes of axial-rotary combine harvesters for harvesting mixed crops of cereal grain and leguminous crops has been carried out. A mathematical model has been compiled to determine the operating modes of axial-rotary threshing and separating systems for harvesting mixed crops. Transfer coefficients have been introduced, one of themcharacterizes a complete threshing of the cereal grain, and the other reflects minimal damage to the grain legume component. The dependences of macro- and microdamages of grains and legumes in mixed crops during harvesting by combines of this type are obtained. The operation modes of the combine harvester RSM-181 "TORUM" for cleaning mixed sowings of white lupine and triticale were substantiated. A clearance between the rotor and the deck of 35 mm and a rotor speed is from 400 to 450 min^{-1} were recommended.

Key words: harvesting; mixed crops; grain losses; grain damage.

INTRODUCTION

Mixed crops (the duplicate term is heterogeneous crops) are crops of two or more crops on the same arable land diseases (*Miu, 2016*). They cannot be attributed to compacted crops, where the cultivation of one crop (usually tilled) in between rows sow another crop. But their use was one of the methods of increasing the productivity of arable land, increasing soil fertility and reducing the pesticide load on the environment.

In such crops, higher photosynthetic productivity is achieved by increasing the total leaf surface area to 60 thousand m^2 / ha, which is 15–20% more than in single-species crops. In this case, the efficiency of photosynthesis was achieved by increasing the multi-tiered agroecosystem, a more uniform distribution of leaves in height, more complete absorption of solar energy due to the suppression of the weed component in crops (*Constable, Somerville, 2003*). The synergistic effect of increasing the productivity of mixed sowing due to more economical consumption of moisture, improved plant nutrition, better use of sunlight and reduced yield losses from a decrease in the numerical composition of the weed component and the prevalence of. The creation of lupine-cereal mixed crops, allows you to get a protein-balanced grain yield without the use of mineral fertilizers, herbicides and other plant protection products (*Aldoshin, 2018*). The most difficult technological method is the cleaning of mixed crops due to the difference in the properties of the crops belonging to them (*Aldoshin, 2016*). The purpose of the study is to evaluate the effectiveness of harvesting lupine-cereal mixed crops with axial-rotary combine harvesters RSM-181(RostSelMash) "TORUM".

MATERIAL AND METHODS

The axial-rotary local control system of the RSM -181 "Torum 740" combine includes four sections: a receiving chamber with a solid, smooth casing, a threshing and separating section, a discharge zone. The angle of the rotor coverage with the lattice surface of the casing in the threshing and separating sections is 360 °. The rotor case rotates at a frequency of 8 min-1. The diameter of the rotor is 762 mm, length 3200 mm. The combine can be equipped with engines of 300 and 370 kW (*Aldoshin, 2018*).

Modes of operation for axial-rotor threshing separating device are more benign. The gap between the rotor and the deck is larger than in the "classical". At the same time, the time spent by the device is much longer, so it allows it to inflict significantly more strikes on the mass, providing threshing of the

grain crop, which is the part of the mixed crops. In addition, the separation area significantly exceeds the parameters of the "classical", which ensures a good selection of both the grain and cereal crops (*Jech, 2011*).

RESULTS AND DISCUSSION

The task of high-quality threshing of grain without exceeding the limit of damage can be solved in a compromise manner (*Aldoshin, 2016*). On the one hand, it is necessary to ensure high-quality threshing of the cereal grain crop, excluding grain losses underground, on the other hand, to ensure a fairly low level of damage to the grain-legged component of mixed crops (*Zhalnin EH.V, 2016*)

We introduce the transfer coefficients characterizing the fragmentation and loss of grain, representing the ratio of the increment of the output parameter to its input value

$$R_i = \frac{d_i}{d_{i-1}}, \tag{1}$$

where d_i, d_{i-1} are respectively, the fragmentation of the *i*-th and *i-1* objects of the combine, and when assessing the loss of grain

$$R_i' = \frac{\Pi_i}{\Pi_{i-1}}, \tag{2}$$

where Π_i, Π_{i-1} losses of the *i*-th and *i-1* objects of the combine.
The total damage to the grain can be represented as a function

$$\partial_\Sigma = f_0(q, w, s, k_n \dots) R_\Sigma \tag{3}$$

where f_0 (*q, w, s, k_p ...*) is the initial input effect, depending on the supply of the grain mass q, its moisture w, contamination s, uneven supply of the threshed mass to the local government k_n, etc.
Gear ratios depend on factors that differ in the nature of origin: structural (K), technological (*T*), and operational (Э). Therefore, they are vector quantities.
$$R = \{K, T, Э\}. \tag{4}$$

Then
$$K = \{K_1, K_2, K_3 \dots \dots K_i \dots\},$$
$$T = \{T_1, T_2, T_3 \dots \dots T_i \dots\}, \tag{5}$$
$$Э = \{Э_1, Э_2, Э_3 \dots \dots Э_i \dots\},$$
where K_i, T_i, $Э_i$ are respectively the *i*-th constructive, technological and operational factors.

In this case, the ratio of their actual values to the required values is determined.

$$K_\mu = W_\mu / w_\mu^{mp}, \tag{6}$$
where W_μ is the actual value of the parameter; $w_\mu{}^{mp}$ is the required parameter value.

As an aggregation function can be taken:
additive function
$$\varphi(W) = \sum_{i=1}^m \gamma_i w_i; \tag{7}$$
where γ^i is the coefficient of relative importance of the particular indicator w_i, *m* is the number of particular indicators of the efficiency of the combine harvester;
multiplicative function
$$\varphi(W) = \prod_{i=1}^m w_i{}^{\gamma_i}; \tag{8}$$

aggregate function

$\phi\ (W) = \min_{\top} \mathrm{i}^{\overline{m}}\ \llbracket\{w\_i /\ \llbracket\gamma\_i\};\rrbracket$

$$\varphi(W) = \min_i \left\{\frac{w_i}{\gamma_i}\right\};$$
$$\gamma_i \neq 0; i = \overline{1, m}; \tag{9}$$

power function

$$\varphi(W) = \left[\frac{1}{m}\sum_{i=1}^{m} w_i^p\right]^{\frac{1}{p}}, p \neq 0, \tag{10}$$

where p is an indicator that reflects the required level of compensation for small values of some equivalent indicators with large values of others.

As p=∞, no compensation is allowed, and the limiting form of the aggregation function (10) coincides with (9). In the case of p=0, it is necessary to ensure the same levels of partial indicators; function (10) coincides with (8), therefore, to select a combine harvester with the best indicators of function (8), (9) and (10), they cannot be used in this form.

The aggregated function in the form of additive (7) is not advisable to use to solve our problem. This is due to the fact that the selected performance indicators are heterogeneous. Threshing separator can be used as a function of one indicator to another:

$$\varphi(W) = \frac{\prod_{i=1}^{m_1} w_i}{\prod_{i=m_1+1}^{m} w_i}; \tag{11}$$

where i = (1, *m₁*) - partial indicators, the values of which it is desirable to increase, i = (*m₁* + 1, m) reduce.

Indicators i = (1, *m₁*)‾, can be identified with the provision of full grain threshing in local government, and indicators, i = (*m1* + 1, m)‾ - with minimization of grain damage during harvesting mixed crops.

However, the indicators of the first and second groups are heterogeneous, have different physical meaning and dimension. Also, the aggregation function from expression (11) is a vector quantity. To bring it to a scalar form and to compensate for the heterogeneity of particular indicators, their different physical meaning and dimension, we use an equivalent transformation. In this case, the function of the aggregated indicator will take the form:

$$\varphi(W) = \frac{\prod_{i=1}^{m_1} \frac{w_i}{w_i^{TP}}}{\prod_{i=m_1+1}^{m} \frac{w_i}{w_i^{TP}}}; \tag{12}$$

Designating

$$\prod_{i=1}^{m_1} \frac{w_i}{w_i^{TP}} = k_1, \qquad \prod_{i=m_1+1}^{m} \frac{w_i}{w_i^{TP}} = k_2, \tag{13}$$

Will get

$$\varphi(W) = \frac{k_1}{k_2} \tag{14}$$

Then the performance indicator will take the form

$$k_э = m\{k_{1i}/k_{2i}\} \tag{15}$$

Using the method of "Least squares", one can evaluate the measure of approximation of the actual result to the desired. Using the efficiency function (12), we note that in order to increase the efficiency of an axial-rotary control, private efficiency indicators w should tend to the values

In this case, the indicator k_{1i} has the meaning of the effect of complete threshing of the grain of ear crops, and k_2 - reflects the minimal damage to the leguminous component.

An increase in the indicators of the first group k_{1i} is aimed at achieving one goal, while the second group k_{2i} leads to the opposite result. In case of heterogeneity, the particular efficiency indicators included in the function φ ($\Pi_э$) may differ according to their influence on the threshing process and separation in axial-rotary local self-government. Then it becomes necessary to introduce in expression) the coefficients γ of the relative importance of the elements k_{1i}. In this case, it is legitimate to assume that the value of γ for the element k_{1i} will correspond to the coefficient of relative importance of the i-th particular efficiency indicator. The values of the coefficients of the relative importance of partial performance indicators can be determined by the method of expert evaluation. Considering the possible options for the inclusion of in dependence (15), we arrive at the following:

Since $\sum (i = 1)^{(i = m)}$ ⟦$\gamma = 1$⟧ ,

with the number of particular indicators m> 1, γ⟧ _i ≠ 1 and γ_i 0.

When γi 1, the influence of ki on the complex index should increase, and when γi → 0, it should weaken.

With the growth of the value of γi, the coefficient k_{1i} should increase, and k2i should decrease.

When γi → 0, the influence of the i-th partial index on the complex index should not be completely rejected.

Since we have chosen two particular indicators to study the quality of the axial-rotary LSG of combine harvesters - direct losses and grain damage, which need to be reduced, then the efficiency indicator takes the form

$$k_э = m\{1/k_{21}k_{22}\}, \tag{16}$$

and taking into account the coefficients of the relative importance γ of particular indicators, a comprehensive performance indicator is determined as follows:

$$k_э = m\left\{\frac{1}{\gamma_1 k_{21}\ \gamma_2 k_{22}}\right\},\ \gamma_2 k_{22} \tag{17}$$

Given the expression of the coefficients k_{21} and k_{22}, we get

$$k_э = m\left\{\frac{1}{\gamma_1 \dfrac{\Pi_э}{\Pi_э^{\partial on}}\gamma_2 \dfrac{\Pi_{\partial p}}{\Pi_{\partial p}^{\partial on}}}\right\}, \tag{18}$$

Suppose that ⟦$\gamma_1 = \gamma$⟧ , then, we obtain an expression to determine the complex criterion of the effectiveness of the quality of work of the local government:

$$k_э = m\left\{\frac{\Pi_э^{\partial}\ \Pi_{\partial p}^{\partial}}{\Pi_э\ \Pi_{\partial p}}\right\}, \tag{19}$$

The dependence of direct losses and grain crushing can be obtained on the basis of experimental data, investigating the influence of various factors 〚X1, X〛, Xn on the operation of an axial-rotor. According to the results of processing the results of experiments, we obtained the following dependences (Fig. 1, 2).
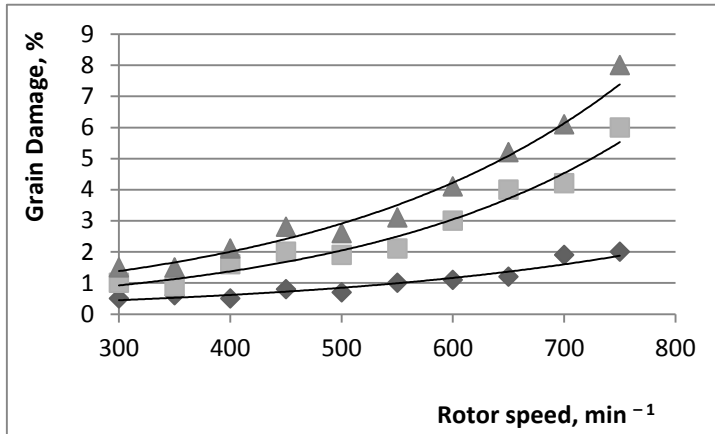
Fig. 1 Dependence of grain damage on rotor speed, min $^{-1}$, (gap between rotor and deck 35 mm):general damage; ◆ macrodamage; ■ microdamage
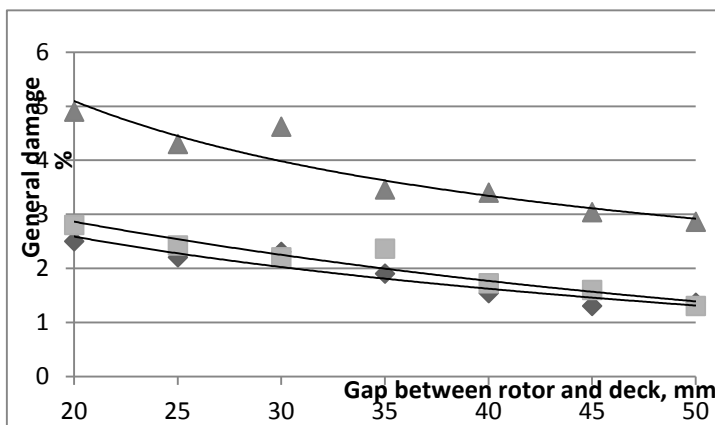
Fig. 2 Dependence of grain damage on the gap between the rotor and deck:
▲ rotor speed, 350 min ^{1} ◆ –; rotor speed, 450 min $^{-1}$; ■ rotor speed, 550 min $^{-1}$

CONCLUSIONS

The results show that, a sharp increases in grain damage occurs with an increasing in the rotor speed of more than 450 min^{-1}As the gap between the rotor and the deck increases, the damage to the grain decreases at all the considered rotor speeds. It should also be noted that with large gaps between the rotor and the deck (from 40 to 50 mm) there is undersized ground triticale.

 Axial-rotary combine harvesters can be used for harvesting mixed crops of cereal crops and leguminous crops. In this case, it is necessary to set the rotor speed from 400 to 450 min^{-1}, and the gap between the rotor and the deck should be 35 mm.

REFERENCES

1. Aldoshin, N. & Didmanidze, O. (2018). Harvesting lupines albus axial rotory combine harvesters. *Research in Agricultural Engineering, 64*(4), 209–214.

2. Aldoshin, N. (2016). Methods of harvesting of mixed crops. In *Proceedings of 6ᵗʰ International Conference on Trends in Agricultural Engineering 2016* (pp. 26-32). Part 1. Czech University of Life Sciences Prague – Faculty of Engineering.

3. Combine Harvesters. (2016). *Theory, Modeling, and Design by Petre Miu*. CRC.

4. Constable, G. & Somerville, B. (2003). A Century of Innovation: Twenty Engineering Achievements That Transformed Our Lives, Chapter 7. *Agricultural Mechanization*. Washington, DC: Joseph Henry Press.

5. Jech, J. et al. (2011). *Stroje pre rastlinnu vyrobu 3*. Nitra: Slovenska Poľnohospodarska Univerzita, 368 p.

6. Lomakin, S. & Berdyshev, V. (2017). Analiz tekhnicheskogo urovnya zernouborochnyh kombajnov "ROSTSEL'MASH". *Vestnik Federal'nogo gosudarstvennogo obrazovatel'nogo uchrezhdeniya vysshego professional'nogo obrazovaniya Moskovskij gosudarstvennyj agroinzhenernyj universitet im. V.P. Goryachkina, 6*(82), 34-42.

7. Zhalnin, EH.V. Cench YU.S., & P'yanov V.S. (2018). Metodika analiza tekhnicheskogo urovnya zernouborochnyh kombajnov po funkcional'nym i konstruktivnym parametram. *Sel'skohozyajstvennye mashiny i tekhnologii, 12*(2), 4-8.

Corresponding author:
Nikolay V. Aldoshin, doctor of the technical sciences, professor, Russian State Agrarian University - Moscow Timiryazev Agricultural Academy, 49 Timiryazevskaya, Moscow, 127550, Russia,
E-mail: naldoshin@yandex.ru

RELIABILITY CHARACTERISTICS OF MECHANICAL OBJECTS OF AGRICULTURAL MACHINES

Zdenek ALES[1], Jindrich PAVLU[1], Marian KUCERA[2], Vaclav LEGAT[1],

[1]*Department for Quality and Dependability of Machines, Faculty of Engineering, Czech University of Life Sciences Prague, Czech Republic*
[2]*Technical University in Zvolen, Faculty of Environmental and Manufacturing Technology, Department of Mechanics, Mechanical Engineering and Design, Slovak Republic*

Abstract
Weibull distribution is commonly used as theoretical distribution of probability in the field of mechanical parts reliability. One of the advantages of using Weibull distribution is that the failure rate can have a rising, falling or constant trend. Weibull distribution is flexible and adaptable for data of all over a wide range. When processing data for all objects, it is necessary to keep track of the operation time to failure, cycles to failure, transport distance, mechanical stress or similar continuous or discrete parameters. It is not always possible to process with a complete data set. The purpose of the paper is to acquaint the readers with the method of processing data of reliability of mechanical parts of agricultural machines based on Weibull analysis of incomplete data of time to failure.

Key words: reliability characteristics; Weibull distribution; machine dependability.

INTRODUCTION

Quite often Weibull distribution is used theoretical distribution of probability during solve of question in field of reliability of mechanical parts. This distribution is applied to data modelling, regardless of whether the failure rate is rising, falling or constant. Weibull distribution is flexible and adaptable for data of all over a wide range. For all objects it is necessary to record the time to failure, cycles to failure, transport distance, mechanical stress or similar continuous or discrete parameters. (*Nassar, et al., 2017; Teringl, et al., 2015*). The method of data processing is focused on incomplete data in the paper. This method is demonstrated on the data of operation time to failure of the taper pins of the disc cultivators. This group includes cases in which there is no failure in all monitored objects during the monitored period (operational time). The processing of incomplete reliability data is typical for data collection in operation, because it is not possible to obtain information of all operating time to failure within a limited time interval in many cases. The Weibull distribution parameters obtained can also be used to apply theory of renewal for decision making between preventive maintenance and corrective maintenance. The aim of the article is to provide information about the reliability data processing when obtained data is not complete, which it means that many of the monitored mechanical parts are in operation state and have not failed.

MATERIALS AND METHODS

When analysing of reliability data, it is necessary to include data of objects that have not broken down during monitored period.

As an example of data processing was used incomplete data of operational time to failure of taper pins of the disc cultivators. A total of 92 machines were analysed and 35 machines failed. The disadvantage of the data obtained is the fact that there are no exact values of the operating time to failure. The operational time to failure t were determined only in intervals, as the area worked in hectares. Excessive damage or fracture of the taper pins of the disc cultivators was considered as a failure. Analysis object is excluded or censored if it has not been broken down by a given manner. If the objects are without a failure, then the data is called censored.

Types of censored data:
- censored by time - the test is terminated at the specified time T before than all objects are broken.
- censored by failure - the test is terminated when the specified number of failure.

When determining of point estimate of Weibull distribution parameters are followed of several steps:

- Ascending order of input data,
- Bernard's approximation,
- Substitution to modified distribution function *F(t)*,
- Linear regression – equation of line
- Calculation of shape α and scale β parameters of Weibull distribution *(ČSN EN 61649, 2009)*.

Firstly, it is necessary to sort the individual values in ascending order $i = 1, 2, 3,\dots n$. For the estimation of the distribution function *F(t)* is used order statistic with the median order (Table 1). Usually, Bernard's approximation is used to calculate the median order:

$$F_i(t) = \frac{i - 0{,}3}{n + 0{,}4} \tag{1}$$

Where: $F_i(t)$ – estimate of median value (-),
   i – rank of serial number of time to failure *t,*
   n – total number of failures.

In contrast, the calculation procedure for complete data is necessary to take into account of influence of censored data - modified procedure:

$$i_{t_i} = i_{t_{i-1}} + m_{t_i} \tag{2}$$

$$m_{t_i} = \frac{(n+1) - i_{t_{i-1}}}{1 + (n - m)} \tag{3}$$

$$F_i(t) = \frac{i_{t_i} - 0{,}3}{n + 0{,}4} \tag{4}$$

Where: m_{ti} – modified number of previous objects (events),
   i_{ti} – adjusted number of time to failure *t.*

Then linear regression is used. This represents the approximation of values by least-square fit of a straight line. The following relations represent the derivation of calculations of the shape parameter α and the scale parameter β of Weibull distribution from the distribution function *F(t):*

$$F(t) = 1 - exp\left[-\left(\frac{t}{\beta}\right)^{\alpha}\right] \tag{5}$$

$$1 - F(t) = exp\left[-\left(\frac{t}{\beta}\right)^{\alpha}\right] \tag{6}$$

$$ln[1 - F(t)] = -\left(\frac{t}{\beta}\right)^{\alpha} \tag{7}$$

$$ln\left[\frac{1}{1 - F(t)}\right] = \left(\frac{t}{\beta}\right)^{\alpha} \tag{8}$$

$$ln\left\{ln\left[\frac{1}{1 - F(t)}\right]\right\} = \alpha \cdot ln(t) - \alpha \cdot ln(\beta) \tag{9}$$

Tab. 1 Bernard's approximation of the function $F_i(t)$ and the calculation of the values for the *x*-axis and *y*-axis of time to failure *t* (partial data)

Number of event	Adjusted number of failure i_{ti}	Operational time to failure t	Event	Bernard's approxima-tion $F_i(t)$	x	y
…	…	…	…	…	…	…
85	71,9714	750	Failure	0,7757	6,6201	0,4019
86	74,6000	750	Failure	0,8041	6,6201	0,4887
87	77,2286	750	Failure	0,8326	6,6201	0,5806
88	79,8571	750	Failure	0,8610	6,6201	0,6797
89	82,4857	1000	Failure	0,8895	6,9078	0,7895
90	85,1143	1000	Failure	0,9179	6,9078	0,9162
91	87,7429	1000	Failure	0,9464	6,9078	1,0734
92	90,3714	1500	Failure	0,9748	7,3132	1,3031

After simple mathematical modifications and two logarithms, the distribution function *F(t)* can be transformed into a line equation:

$$y = k \cdot x + q \tag{10}$$

where:
y – dependent variable,
x – independent variable,
k – slope of a line,
q – point of intersection of line with *x*-axis and *y*-axis, absolute term.

X-axis and *y*-axis are represented by (Table 1):

$$x = \ln(t) \tag{11}$$

$$y = ln\left\{ ln\left[\frac{1}{1-F_i(t)} \right] \right\} \tag{12}$$

The least-square fit of a straight line is used to find the line equation, where it is necessary to solve a set of equation in a normal form:

$$q \cdot \sum_{i=1}^{n} x_i + k \cdot \sum_{i=1}^{n} x_i^2 = \sum_{i=1}^{n} x_i y_i \tag{13}$$

$$n \cdot q + k \cdot \sum_{i=1}^{n} x_i = \sum_{i=1}^{n} y_i \tag{14}$$

Then, coefficient *k* and *q* can be count by:

$$k = \frac{n \cdot \sum_{i=1}^{n} x_i y_i - \sum_{i=1}^{n} x_i \cdot \sum_{i=1}^{n} y_i}{n \cdot \sum_{i=1}^{n} x_i^2 - \left(\sum_{i=1}^{n} x_i \right)^2} \tag{15}$$

$$q = \frac{\sum_{i=1}^{n} x_i^2 \cdot \sum_{i=1}^{n} y_i - \sum_{i=1}^{n} x_i \cdot \sum_{i=1}^{n} x_i y_i}{n \cdot \sum_{i=1}^{n} x_i^2 - \left(\sum_{i=1}^{n} x_i \right)^2} = \bar{y}_i - k \cdot \bar{x}_i \tag{16}$$

By applying a set of equation in a normal form of linear regression, we obtain relation of linear function in the form:

$$y = 0{,}1933x - 6{,}5403 \tag{17}$$

It is also important to verify the statistical significance of the calculated regression equation. For this purpose is used coefficient of determination r^2, which it can be interpreted as the ratio of the sum of squares of the aligned (predicted) values and the sum of the squares of the observed values. (*Berrehal & Benissaad 2016; Garmabaki, et al., 2016*)

Coefficient of determination r^2 is defined by:

$$r^2 = \frac{\left(n \cdot \sum_{i=1}^{n} x_i y_i - \sum_{i=1}^{n} x_i \cdot \sum_{i=1}^{n} y_i\right)^2}{\left[n \cdot \sum_{i=1}^{n} x_i^2 - \left(\sum_{i=1}^{n} x_i\right)^2\right] \cdot \left[n \cdot \sum_{i=1}^{n} y_i^2 - \left(\sum_{i=1}^{n} y_i\right)^2\right]} \tag{18}$$

$$r^2 = \frac{\{35 \cdot (-130,377) - [-22,098 \cdot (-224,639)]\}^2}{[35 \cdot 73,208 - (-22,098)^2] \cdot [35 \cdot 1445,052 - (224,639)^2]} = 0,678 \tag{19}$$

The coefficient of determination takes values between 0 and 1. If the coefficient of determination approaches 1, it is a strong dependence. Otherwise if the coefficient of determination approaches 0, it is a weak dependence. The standard recommends the calculations in which the *x* and *y* axes are swapped in the Figure 1.

The authors used Visual Basic for Applications for all calculations of parameters of Weibull distribution. Programmed algorithms can be used to easily calculate results when changing input data, which helps to refine reliability characteristics.

Values of Weibull distribution parameters (Figure 1) for time to failure *t* can be counted by

$$\alpha = \frac{1}{k} = \frac{1}{0,1933} = 5,173 \tag{20}$$

$$\beta = exp(q) = exp(6,5403) = 692,5 \tag{21}$$
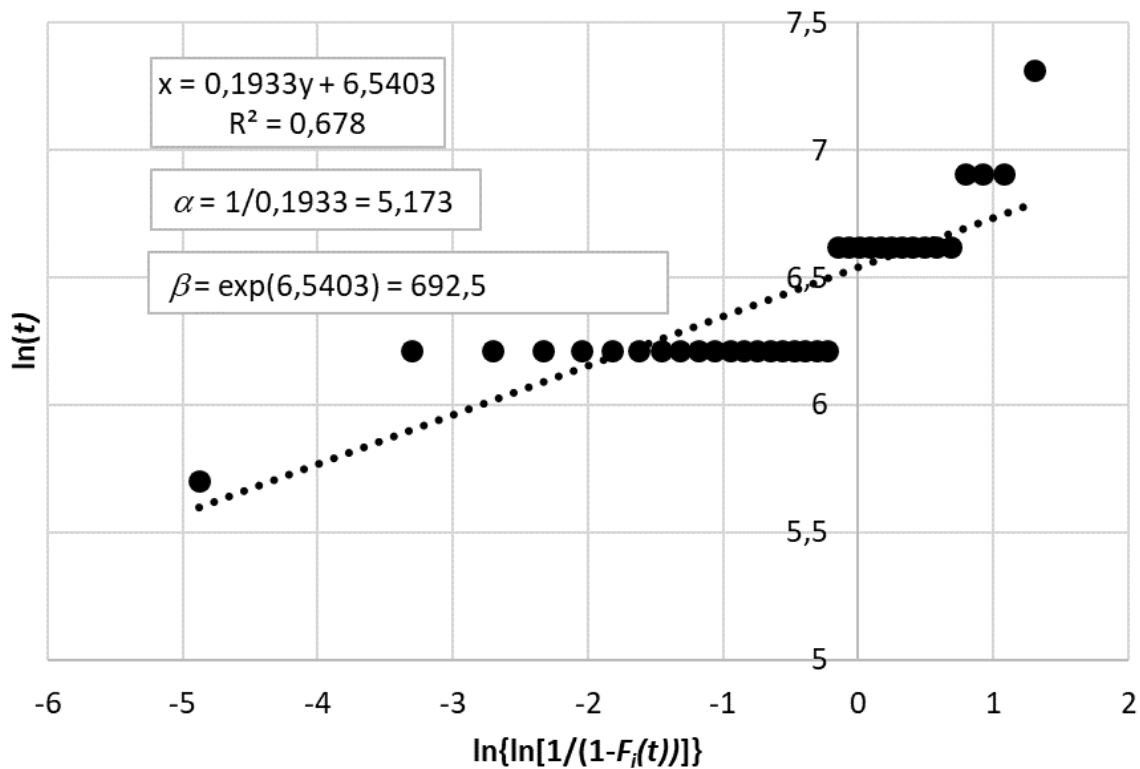
Fig. 1 Graph of calculation of equation of line by linear regression

RESULTS AND DISCUSSION

After calculation of values of Weibull distribution parameters can be used these parameters in calculation of reliability characteristics (service life):

- Probability density function of failure *f(t)*,
- Probability of failure *F(t)*,
- Reliability function *R(t)*,
- Failure rate *λ(t)*. (*Legat, et al., 2016*)
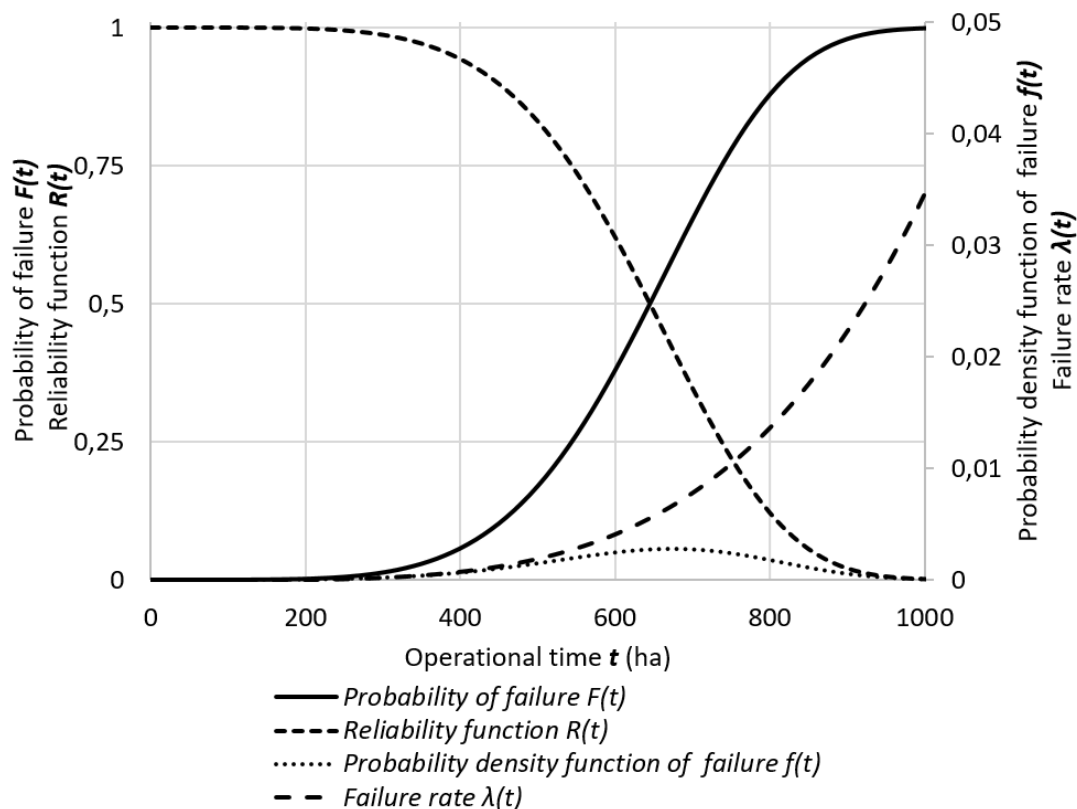
Fig. 2 *Reliability characteristics F(t), f(t), R(t), λ(t) for calculated Weibull distribution for shape parameter α=5,173 and scale parameter β=692,5*

For completeness, it appropriate to mention calculation of *MOTTF* (Mean Operating Time to Failure).

$$MOTTF = \beta \cdot \Gamma\left(1 + \frac{1}{\alpha}\right) = 692,5 \cdot \Gamma\left(1 + \frac{1}{5,1727}\right) = 637 \ ha \qquad (22)$$

When calculation of *MOTTF* is necessary to use formula for function Γ – GAMMA in MS Excel. It is evident from the obtained reliability characteristics that the increase in the probability of failure is relatively steep and the monitored mechanical object has a low reliability, which is also evidenced by the low *MOTTF* value, which is 637 ha. Such low *MOTTF* is several times lower than commonly used objects of the same character. An equally important characteristic of reliability is failure rate, which represents the probability that a mechanical object that has not broken down to operational time *t* will break down immediately after operational time *t* (*Legat, et al., 2017*; Pacaiova & *Izarikova, 2019*). Too steep the course of the failure rate *λ(t)* is shown in Figure 2. It is obvious from the course of reliability characteristics that manufacturer of the disc cultivator must implement corrective actions to improve reliability parameters.

CONCLUSIONS

Weibull's analysis represents a suitable tool for determining the distribution of the probability density function of failure $f(t)$, respectively the distribution function of the probability of failure $F(t)$ when processing of the reliability data of agricultural machinery systems. The paper presents one of the way of calculation of Weibull distribution parameters for an incomplete data, which is obtained from agricultural machinery operation. The results show that the calculated values of *MOTTF* are relatively low, which it is obvious from the reliability characteristics. In this particular case, the disc cultivator manufacturer made structural adjustments that resulted in a significant increase in machine operating life. Big weaknesses in general are input data, which are not always accurate and they are obtained in range of various intervals. With the development of modern technologies, it is assumed that there will be more suitable data collection from diagnostics sensors for already use processed algorithms. The main contribution of the authors is that they programmed automation of algorithms using the Visual Basic for Applications programming language in addition to the calculation methodology described. The computational algorithms created allow simple recalculation when new and more accurate data is obtained. The Weibull distribution parameters obtained can also be used to apply theory of renewal for decision making the between preventive maintenance and corrective maintenance.

ACKNOWLEDGMENT

REFERENCES

1. Berrehal, R., & Benisaad, S. (2016). Determining the optimal periodicity for preventive replacement of mechanical spare parts. *Mechanics, 22*(2). doi: 10.5755/j01.mech.22.2.12269. ISSN 2029 6983.

2. CSN EN 61649 (010653). (2009). Weibull analysis (In Czech).

3. Garmabaki, A., Ahmadi H. S., & Ahmadi A. M. (2016). Maintenance Optimization Using Multi-attribute Utility Theory. *Current Trends in Reliability, Availability, Maintainability and Safety* (pp.13-25). Cham: Springer International Publishing. Lecture Notes in Mechanical Engineering. doi: 10.1007/978-3-319-23597-4_2. ISBN 978-3-319-23596-7.

4. Legat, V., et al. (2016). Management and maintenance engineering (in Czech). Prague: Professional Publishing. ISBN 978-80-7431-119-2.

5. Legat, V., Mosna, F., Ales, Z., & Jurca, V. (2017). Preventive maintenance models – higher operational reliability. *Eksploatacja i Niezawodnosc – Maintenance and Reliability*, *19*(1):134141. doi: http://dx.doi.org/10.17531/ein.2017.1.19.

6. Nassar, M. A., Alzaatreh, M., & Abo-kasem, O., (2017). Alpha power Weibull distribution: Properties and applications. *Communications in Statistics - Theory and Methods,* (pp.1-17).
doi: 10.1080/03610926.2016.1231816. ISSN 0361-0926.

7. Pacaiova, H., & Izarikova, G. (2019). Base Principles and Practices for Implementation of Total Productive Maintenance in Automotive Industry. *Quality Innovation Prosperity*, *23*(1), 45-59. doi: 10.12776/qip.v23i1.1203. ISSN 1338-984X.

8. Teringl, A., Ales, Z., & Legat, V. (2015). Dependability characteristics - indicators for maintenance performance measurement of manufacturing technology. *Manufacturing Technology*, *15*(3), 456-461. ISSN: 1213-2489.

Corresponding author:
doc. Ing. Zdeněk Aleš, Ph.D., Department of Quality and Dependability of Machines, Faculty of Engineering, Czech University of Life Sciences Prague, Kamýcká 129, Prague 6, 16521, Czech Republic, e-mail: ales@tf.czu.cz

THE EFFECT OF POST-HARVEST PROCESSING IN MODEL LINE AT FOOD MAIZE GRAINS EXTERNAL AND INTERNAL QUALITY

Marek ANGELOVIČ[1], Koloman KRIŠTOF[1], Michal ANGELOVIČ[1], Ján JOBBÁGY[1]

[1]*Department of Machines and Production Biosystems, Faculty of Engineering, Slovak University of Agriculture in Nitra*

Abstract
Experimental measurements of post-harvest line were realized in work conditions during maize cleaning and drying. Measurements were realized during maize harvesting with grain moisture 23 - 35 %. Structure of material was monitored before and after cleaning and the external grain quality before and after drying. Grain bulk density, impurities, grain damage and total cleaning effect were evaluated. The purpose of coarse and light trash analysis was the next step to find out the losses of grain quality. The analysis of the internal grain quality from the starch, fats and proteins were then conducted.

Key words: *cleaning; drying; dimension and weight characteristics of grains; cleaning effect; grain quality.*

INTRODUCTION

Cleaning, grading, drying is a basic working operation in post-harvest grain processing. These working operations affect the quality of cleaned and dried grain like a grain dedicated to food and another purpose in a positive and also in a negative way (*Ružbarský et al., 2005*). Requirement for grain purity is made by STN standards. According to the standards, the purity of the grain and the content of the ingredients are decisive for the recognition of cereal grains in their individual quality classes. These requirements place high demands on cleaning, sorting and drying machines in terms of construction and overall machine solutions (*Kroupa et al., 2004*).

The structure and extent of threshing damage depend on not only the threshing conditions (e.g., collision speed), but also the seed properties (*Chowdhury & Buchele 1976; Khazaei et al., 2007*). In maize, seed properties that affect threshing damage degree include seed size, seed shape, and seed moisture content (MC), as these properties affect interaction strengths between seed and threshing cylinder when seeds are threshed from cobs. Of these properties, MC was found to show a significant influence on seed physical damage in French bean; and also affect threshing damage in maize (*Keller et al., 1972; Dauda, 2001; Greven et al., 2001*). Several methods have been developed to evaluate mechanical damage degree. The most commonly used method is visual inspection. Seeds with any visual damage or cracks are picked from the sample to estimate the damage percentage. Mechanical damage level and position in a seed can also be determined by extracting the damaged area stained by use of iodine, fast green, methylene blue, or other stains (*Ng et al., 1998; ISTA, 2015*). Visual inspection and chemical stains can only evaluate external injuries in a seed. Seed vigor test is another way that can evaluate both external and internal damages, where mechanical damage level is estimated by correlating the ability of seed to emerge and develop a healthy seedling. The previous studies conducted on mechanical threshing majorly focused on the damage percentage, with few studies conducted on the influence of damage on seed vigor (*Ajayi et al., 2006; Li et al., 2007*).

Recently, the assessment of the external and internal quality of treated grains on post-harvest lines has been at the forefront. As *Loewer et al. (1994)* and *Jech et al. (2011)* concluded the quality is closely related to Hazard Analysis and Critical Control Points (HACCP). For these reasons, the objective of the study was to evaluate how the post-harvest treatment of maize affects the quality of the treated crop in cleaning, handling, and drying.

MATERIALS AND METHODS

Characteristics of monitored grain material in the process of post-harvest treatment

To assess the cleaning, sorting and drying efficiency of the treated grains in post-harvest treatment, it is necessary to carry out basic experimental measurements of various quantities, which are determined by the relevant standards on the basis of which we have characterized the quality of the work of the machines, the quality of the resulting product and the line as a whole. The monitored parameters in the post-harvest process were separated into two separate sections (a, b):

(a) Monitoring of external quality of food maize grains in the cleaning and drying process

To assess the external quality of the grains, the following factors were monitored before and after drying: grain moisture following standard STN 460610; grain volume weight (kg.m^{-3}, STN 460609); grain size (dimensional) and weight characteristics (STN 460610); grain purity (STN 461100-2); additional mixtures (STN 461050); impurity (STN 461050); grain damage (only macro damage) and characteristics of critical maize grains speed.

(b) Monitoring of internal quality of food maize grains after drying

Internal grain quality is understood the nutritional value, presence of moulds, microorganisms, pests and undesirable substances. For the internal grain quality options the limitations were set to the following analyzes: germinations of whole grains (STN 460311); starch and fat contend, protein content and sediments.

These analyses were performed in an automated laboratory AMYLUM Slovakia, s.r.o. Boleráz.

Brief characteristics of the post-harvest line

Post-harvest line located in AgroDivízia, s.r.o. in Selice has become a model line for carrying out experimental measurements. Due to the fact that this type of machinery is used by several enterprises, a model example is being developed to solve problems that reduce some line quality parameters during post-harvest treatment. The post-harvest grain processing line is mainly oriented on corn processing, but it can also provide post-harvest treatment, expedition, or storage of grains (cereals, maize, legumes, and oilseeds). The technology consists of receiving (underfloor basket), bucket conveyor, pre-cleaning, cleaning, belt conveyor, drying and transport into the grain silo or floor storage (Fig. 1).
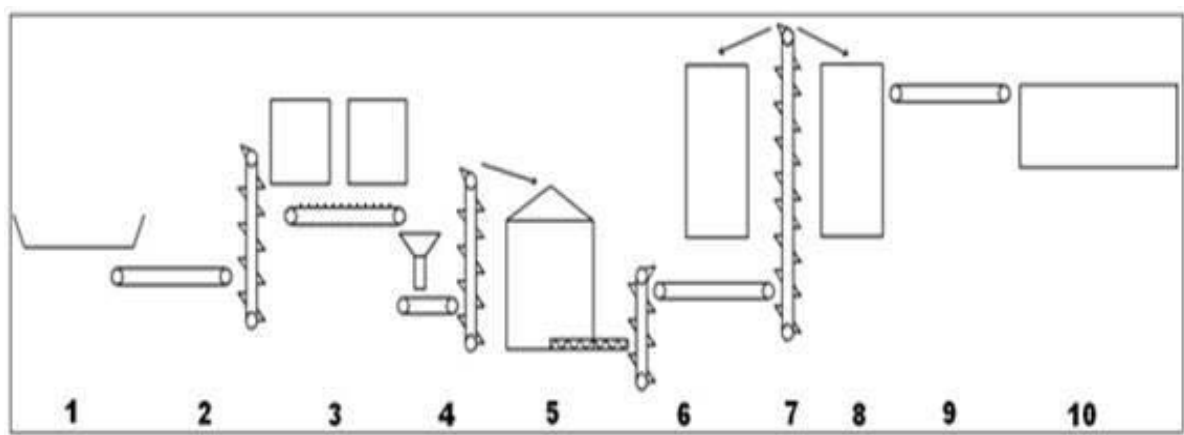
Fig. 1 Composition of the selected (model) post-harvest treatment line (1 – receiving; 2,4,6,7,9 – transport; 3 – pre-cleaning, cleaning; 5 – drying; 8 – grain silo;10 – floor storage).

Used machines, devices and equipment

The machines and equipment of the post-harvest line at AgroDivízia, s.r.o., in Selice were used for experimental measurements. Specialized instruments and equipment that belong to the laboratory equipment at the department DMPB were used to determine the agro-physical properties. They are a sieve cleaner, a humidity meter, digital scales, a grain counter, a volume weight measuring instrument and others.

Evaluation methods used in experiments

Validated statistical calculation procedures were used to evaluate the measured values on the post-harvest line and to evaluate the measured agro-physical characteristics. For determination of basic statistical quantities, evaluation program STATGRAFICS and MS Office 2010 (EXEL 2010) was used.

RESULTS AND DISCUSSION

Evaluation of dimensional and weight characteristics of the grains on monitored crop-plant

In terms of cleaning and grading grains, the most important characteristics of the grains are their dimensions (length, width, thickness), as their size directly influences the choice of size and shape of grain sieve. Further, the variability of the dimensions (the large interval of the respective dimension) affects the lower yield and the grain increase in the II. III. class and waste (Fig. 2-3). The grain size was determined using a digital caliper with an accuracy of 0.01 mm (Traceable).
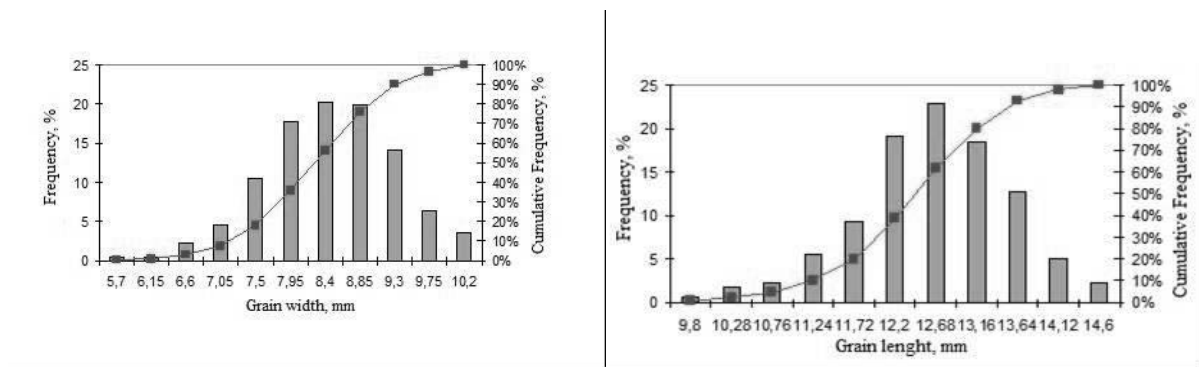
Fig. 2 Histogram of maize grains dimensional characteristics based on the width (left) and length (right)
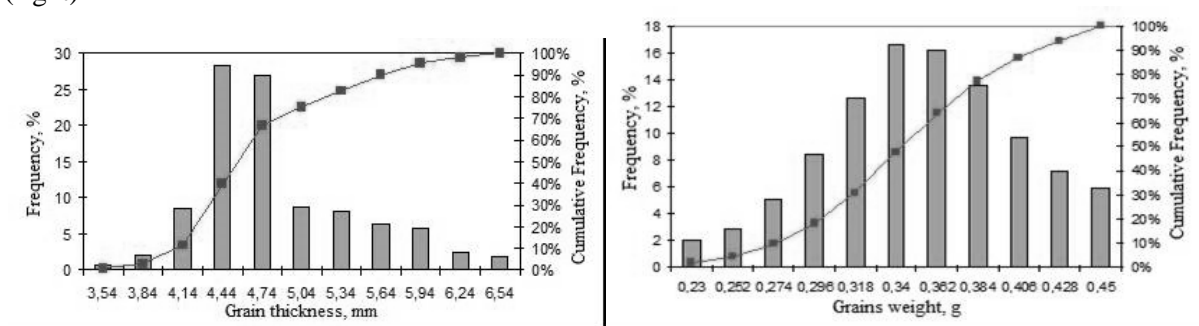
Fig. 3 Histogram of maize grains dimensional characteristics based on the thickness (left) and maize grains weight characteristics (right)

The grain size variation of maize is various. The grain width is in the range of 5.7 to 10.2 mm with an average of 8.24 mm, and length of 9.8 to 14.6 mm with an average of 12.4 mm, and a grain thickness of maize between 3.54 and 6.54 with an average value of 4.72 mm. Corn grain weight ranges from 0.23 to 0.45 grams with an average of 0.34 grams. It should be noted that maize is harvesting at a moisture content of 34% to 20%, resulting in a grain weight fluctuation when cleaning immediately after harvesting.

Determining the critical speed of maize grains in the air stream (flow)

For the purpose of adjusting the airflow speed in the cleaning machines the laboratory measurements of the given quantities were conducted. Based on the measured values, it was determined the critical velocity of the maize grains in the air stream. For maize it represents 8.5 - 13.14 m.s^{-1} with an average value of 10.97 m.s^{-1}.
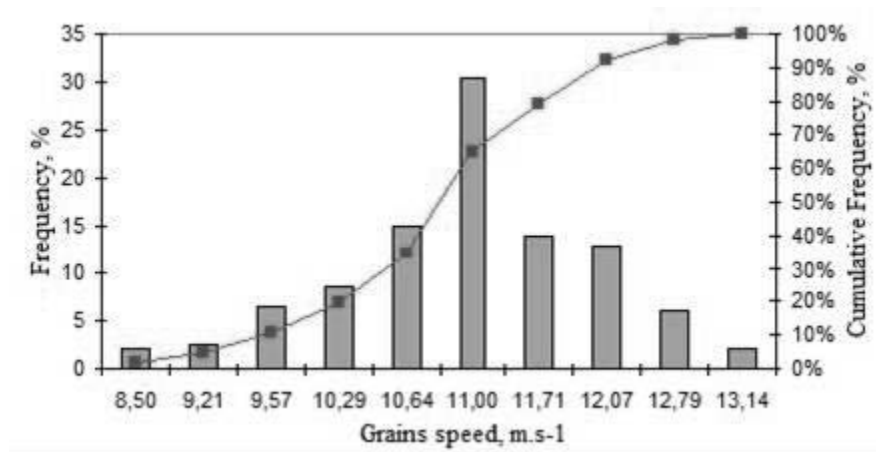
Fig. 4 Characteristics of critical maize grains speed

Evaluation of the external quality of maize grains in the cleaning and drying process
From the point of view of HACCP and food safety, it is necessary to monitor the external and internal quality of the processed product, in the case of this study, it was food maize. The analysis of samples of maize grains collected was performed according to Tab. 1 and Tab. 2 (*n=24*). Tab. 1 and 2 shows the summary results of the monitored external quality parameters of maize grains after the pre-cleaning (treatment) and drying process. The cleaning effect (purification efficiency) of the pre-treatment operation was good to very good 47.5% on average. The bulk density of the grains varied from 882 to 780 kg.m^{-3} depending on humidity. Damage to the grains before and after pre-treatment slightly decreased by separating debris and chopped grains (Tab. 1). A sharp increase in macro damage was observed after drying (Tab. 2). The causes of significant grains damage are more. In authors experience and lessons learned, these are: (a) Failure to comply with threshing system parameters. Corn thresh out was carried out at a high drum speed (17 m.s^{-1}), resulting in higher macro damage, which in some cases was up to 11% compared to the desired 3-5%, (b) Micro damage has been significantly increased, causing grain crumbling in the drying and subsequent handling process. Authors did not monitor what impact on damage has mixing auger in the oven and unloading (push out) auger. As *Gu et al. (2019)* stated, seed postharvest processing is necessary to prepare maize seeds for planting. However, process operations often subject seed to mechanical damage, which reduces seed quality due to external breakage and bruising and internal physiological damage (*Cicero et al. 1998; Ajayi et al. 2006*). Mechanical threshing is one of the processes where damage is caused by abrasions and impacts when seed passes through the machine (*Ajayi et al. 2006; Li et al. 2007*). Thus, mechanical threshing must be controlled to minimize damage during seed production.

Assessment of the effect of the drying process on the internal quality of maize grains
Analysis of the nutritional value of maize grains and their germination was provided in a specialized certified laboratory AMYLUM Slovakia s.r.o. in Boleraz. These analyses were conducted on mixed samples made from two samples previously taken for evaluation of the external quality (*n=12*).Germination is a major indicator of grain quality and viability after drying. An analysis of the internal quality of maize grains from the crop is given in Tab. 3. Germination rates ranged from 86% to 100%. The average germination rate was 92.3%, which is an excellent result for food maize. Other parameters such as starch, fat, and protein are evident from Tab. 3. The content of these variables is conditioned by several factors, especially the hybrid, locality, fertilization, year and post-harvest treatment. Moreover, *Coradi et al. (2019)* concluded that the changes in water contents in the grains during the drying and storage operations intensify the physical losses, even if at the end the grains remain with water content favourable to storage. As mentioned above, the internal quality of the dried maize was excellent and Agriculture Company converted it into cash in the first quality class. It is desirable to note that the temperature of the drying medium ranges from 52 ° C to 65 ° C.

Tab. 1 Assessment of the external maize grain quality before (INPUT) and after (OUTPUT) pre-cleaning (*n=24*)

sample	RAW MATERIAL INPUT							RAW MATERIAL OUTPUT								
	volumetric weight, $g.l^{-1}$	WTG, g	impurity, %	admixture, %	damaged grain, %	clean grain, %	moisture, %	volumetric weight, $g.l^{-1}$	WTG, g	impurity, %	admixture, %	damaged grain, %	clean grain, %	moisture, %	cleaning effect, %	difference, %
1	865.00	264.11	6.00	0.08	5.92	94.00	22.00	815.00	289.00	3.25	0.29	2.96	96.75	21.80	45.77	2.96
2	853.00	321.00	9.38	0.18	9.19	90.62	22.60	861.00	257.84	4.54	0.04	4.50	95.46	22.50	51.63	4.69
3	881.00	276.54	8.49	0.00	8.49	91.51	24.00	904.00	312.38	5.70	1.24	4.47	94.30	23.40	32.83	4.02
4	874.00	260.10	7.73	0.81	6.92	92.27	26.00	780.00	248.04	4.04	0.04	4.00	95.96	25.00	47.80	2.92
5	800.00	342.98	8.58	0.67	7.91	91.42	27.50	915.00	275.12	4.70	0.01	4.70	95.30	28.00	45.19	3.21
6	882.00	348.12	11.69	0.43	11.26	88.31	27.50	880.00	209.56	4.82	0.06	4.77	95.18	28.50	58.74	6.49
7	870.00	296.32	10.70	0.70	10.00	89.30	29.00	847.00	371.12	6.96	0.38	6.58	93.04	31.50	34.89	3.41
8	831.00	272.96	15.51	0.70	14.81	84.49	29.50	860.00	390.74	5.01	0.79	4.22	94.99	31.50	67.69	10.59
9	780.00	387.46	8.20	1.69	6.51	91.80	30.00	859.00	368.12	3.86	0.27	3.59	96.14	31.50	52.99	2.92
10	820.00	348.72	8.88	0.25	8.63	91.12	30.50	845.00	387.10	5.66	0.25	5.42	94.34	32.00	36.19	3.21
11	862.00	350.84	11.56	1.37	10.19	88.44	30.50	800.00	345.34	4.45	0.28	4.17	95.55	32.00	61.52	6.02
12	860.00	358.10	15.66	1.43	14.22	84.34	31.50	800.00	335.00	9.61	1.11	8.51	90.39	32.50	38.61	5.72
13	865.00	264.11	6.00	0.08	5.92	94.00	22.00	815.00	289.00	3.25	0.29	2.96	96.75	21.80	45.77	2.96
14	853.00	321.00	9.38	0.18	9.19	90.62	22.60	861.00	257.84	4.54	0.04	4.50	95.46	22.50	51.63	4.69
15	881.00	276.54	8.49	0.00	8.49	91.51	24.00	904.00	312.38	5.70	1.24	4.47	94.30	23.40	32.83	4.02
16	874.00	260.10	7.73	0.81	6.92	92.27	26.00	780.00	248.04	4.04	0.04	4.00	95.96	25.00	47.80	2.92
17	800.00	342.98	8.58	0.67	7.91	91.42	27.50	915.00	275.12	4.70	0.01	4.70	95.30	28.00	45.19	3.21
18	882.00	348.12	11.69	0.43	11.26	88.31	27.50	880.00	209.56	4.82	0.06	4.77	95.18	28.50	58.74	6.49
19	870.00	296.32	10.70	0.70	10.00	89.30	29.00	847.00	371.12	6.96	0.38	6.58	93.04	31.50	34.89	3.41
20	831.00	272.96	15.51	0.70	14.81	84.49	29.50	860.00	390.74	5.01	0.79	4.22	94.99	31.50	67.69	10.59
21	780.00	387.46	8.20	1.69	6.51	91.80	30.00	859.00	368.12	3.86	0.27	3.59	96.14	31.50	52.99	2.92
22	820.00	348.72	8.88	0.25	8.63	91.12	30.50	845.00	387.10	5.66	0.25	5.42	94.34	32.00	36.19	3.21
23	862.00	350.84	11.56	1.37	10.19	88.44	30.50	800.00	345.34	4.45	0.28	4.17	95.55	32.50	61.52	6.02
24	860.00	358.10	15.66	1.43	14.22	84.34	31.50	800.00	335.00	9.61	1.11	8.51	90.39	32.50	38.61	4.49
x	846.77	324.47	9.99	0.73	9.26	90.01	27.97	851.15	311.19	5.14	0.37	4.77	94.86	28.71	47.50	4.49
s	32.10	45.85	2.96	0.55	2.83	2.96	3.45	42.71	59.62	1.64	0.41	1.42	1.64	4.15	10.73	2.28
Vk. %	3.79	14.13	29.59	75.15	30.61	3.28	12.33	5.02	19.16	31.95	89.66	29.76	1.73	14.45	22.60	50.72

Tab. 2 Assessment of the external maize grain quality before (INPUT) and after (OUTPUT) drying (*n=24*)

sample	RAW MATERIAL INPUT							RAW MATERIAL OUTPUT							
	volumetric weight, g.l⁻¹	WTG, g	impurity, %	admixture, %	damaged grain, %	clean grain, %	moisture, %	volumetric weight, g.l⁻¹	WTG, g	impurity, %	admixture, %	damaged grain, %	clean grain, %	moisture, %	difference, %
1	859.00	368.12	3.86	0.27	3.59	96.14	31.50	850.00	270.82	16.27	0.82	15.45	83.73	10.10	12.42
2	898.00	268.63	4.12	0.04	4.08	95.88	21.50	870.00	264.32	18.60	0.00	18.60	81.40	10.10	14.48
3	830.00	290.92	6.18	1.11	5.08	93.82	20.60	895.00	300.10	12.11	0.06	12.05	87.89	10.20	5.93
4	815.00	289.00	3.25	0.29	2.96	96.75	21.80	905.00	272.71	14.49	0.15	14.34	85.51	10.20	11.24
5	900.00	254.08	9.08	0.03	9.05	90.92	22.00	891.00	271.90	12.28	0.10	12.18	87.72	10.40	3.20
6	860.00	390.74	5.01	0.79	4.22	94.99	31.50	846.00	303.56	15.38	1.50	13.88	84.62	10.50	10.37
7	849.00	335.20	7.32	0.24	7.08	92.68	26.00	850.00	249.50	13.70	0.37	13.33	86.30	10.50	6.38
8	780.00	248.04	4.04	0.04	4.00	95.96	25.00	750.00	250.12	13.05	0.12	12.93	86.95	10.50	9.02
9	899.00	256.08	4.21	0.07	4.14	95.79	33.00	882.00	246.20	15.28	0.16	15.12	84.72	10.70	11.07
10	859.00	368.12	3.86	0.27	3.59	96.14	31.50	879.00	240.40	18.49	0.34	18.15	81.51	10.80	14.63
11	861.00	257.84	4.54	0.04	4.50	95.46	22.50	885.00	278.42	7.57	0.06	7.51	92.43	10.80	3.03
12	878.00	366.88	7.07	0.36	6.70	92.93	24.80	857.00	303.26	15.98	2.20	13.78	84.02	11.10	8.91
13	859.00	368.12	3.86	0.27	3.59	96.14	31.50	850.00	270.82	16.27	0.82	15.45	83.73	10.10	12.42
14	898.00	268.63	6.18	1.11	5.08	93.82	21.50	870.00	264.32	18.60	0.00	18.60	81.40	10.10	14.48
15	830.00	289.00	3.25	0.29	2.96	96.75	20.60	905.00	300.10	12.11	0.06	12.05	87.89	10.20	5.93
16	815.00	254.08	9.08	0.03	9.05	90.92	21.80	891.00	272.71	14.49	0.15	14.34	85.51	10.20	11.24
17	900.00	390.74	5.01	0.79	4.22	94.99	22.00	846.00	303.56	15.38	1.50	13.88	84.62	10.40	3.20
18	860.00	335.20	7.32	0.24	7.08	92.68	31.50	850.00	249.50	13.70	0.37	13.33	86.30	10.50	10.37
19	849.00	248.04	4.04	0.04	4.00	95.96	25.00	750.00	250.12	13.05	0.12	12.93	86.95	10.50	6.38
20	780.00	256.08	4.21	0.07	4.14	95.79	33.00	882.00	246.20	15.28	0.16	15.12	84.72	10.70	9.02
21	899.00	368.12	3.86	0.27	3.59	96.14	31.50	879.00	240.40	18.49	0.34	18.15	81.51	10.80	11.07
22	859.00	257.84	4.54	0.27	4.50	95.46	22.50	885.00	278.42	7.57	0.06	7.51	92.43	10.80	14.63
23	861.00	366.88	7.07	0.36	6.70	92.93	24.80	857.00	303.26	15.98	2.20	13.78	84.02	11.10	3.03
24	878.00	314.43	5.92	0.35	5.57	94.08	27.07	873.56	278.48	14.86	0.99	13.88	85.14	10.79	8.94
x̄	853.78	314.43	5.92	0.35	5.57	94.08	27.07	873.56	278.48	14.86	0.99	13.88	85.14	10.79	8.94
s	39.27	52.03	2.46	0.47	2.34	2.46	4.36	38.31	24.78	4.55	1.76	3.37	4.55	0.51	5.24
Vk, %	4.60	16.55	41.61	75.17	42.03	2.62	16.12	4.39	8.90	30.61	56.06	24.31	5.34	4.69	58.62

Tab. 3 The internal maize grain quality (*n=12*)

Sample	Cultivar	Moisture, %	Starch, %	Germinability, %	Sediment, %	Fats, %	Proteins, %
1		14.6	75.2	98	65	3.0	7.7
2		14.4	74.3	90	70	3.4	9.2
3		12.9	75.3	92	69	3.6	7.9
4		12.9	72.4	90	68	3.2	9.7
5	DK-391	13.2	73.2	100	72	3.2	8.4
6		13.3	73.6	86	62	3.3	10.9
7		13.5	74.2	90	68	3.2	9.7
8		13.7	73.0	88	70	3.3	10.0
9		13.5	72.0	92	64	3.6	8.0
10		14.1	73.0	90	68	3.2	8.4
11		13.9	72.4	90	68	3.0	7.9
12		14.3	73.0	92	66	3.0	8.4
$\bar{x}$		**13.9**	**73.4**	**92.3**	**67.6**	**3.2**	**8.9**

In these circumstances, the maize grain internal quality is affected by numerous variables which drastically change their values. In addition to these observations other issues can be defined as well even more alarming. Agricultural soil and products are severely polluted by heavy metals, owing to the natural weathering of parent materials, mining, industries, melting, and agricultural activities (*Bilos et al., 2001*). However, contaminations of Cd, Cu, Hg, Pb and Zn in soil and crops caused by agricultural activities or natural weathering processes have only seldom been considered (*Árvay et al., 2013; Tomáš et al., 2014; Stanovič et al., 2015; Demková et al., 2017*).

CONCLUSIONS

The quality of the grain cleaners' work is not only judged by the cleanness of the cleaned product, but also by its performance and the loss of quality grains in the waste. It was also analyzed the gross and fine waste. There were whole grains in the gross (rough) waste, but they were under-sized, poor-quality. There were no whole grains in the fine waste. At this stage, the technical condition of the harvest line can be assessed as good. The first critical point that significantly affects the external quality of maize grains is the actual harvesting and threshing as mentioned above. Overall, the most critical element in the model harvest line is the drying process and its impact on the macro damage.

ACKNOWLEDGMENT

REFERENCES

1. Ajayi, S.A., Ruhl, G., & Greef, J.M. (2006). Impact of mechanical damage to hybrid maize seed from harvesting and conditioning. *Seed Technology, 28*, 7–21.
2. Árvay, J., Stanovič, R., Bajčan, D., Slávik, M., & Miššík, J. (2013). Content of heavy metals in soil and crop from middle Spiš area. *Journal of Microbiology, Biotechnology and Food Science, 2*(Special issue on BQRMF), 1988-1996.
3. Bilos, C., Colombo, J.C., Skorupka, C.N., & Rodriguez Presa, M.J. (2001). Sources, distribution and variability of airborne trace metals in La plata city area Argentina. *Environmental Pollution, 111*(1), 149–158.
4. Cicero, S.M., Heijden, G.W.A.M., Van der Burg, W.J., & Bino, R.J. (1998). Evaluation of mechanical damage in seeds of maize (Zea mays L.) by X-ray and digital imaging. *Seed Science and Technology, 26*, 603–612.
5. Coradi, P.C., de Souza, A.H.S., Camilo, L.J., Lemes, A.F.C. & Milane, L.V. (2019). Analysis of the physical quality of genetically modified and conventional maize grains in the drying and wetting processes. *Revista Ciencia Agronomica, 50*(3), 370-377.

6. Dauda A. (2001). Effect of threshing methods on maize grain damage and viability. *Agricultural Mechanization in Asia, Africa and Latin America, 32*, 43–46.

7. Demková, L., Árvay, J., Bobuľská, L., Tomáš, J., Stanovič, R., Lošák, T., Harangozo, L., Vollmannová, A., Bystrická, J., Musilová, J & Jobbágy, J. (2017). Accumulation and environmental risk assessment of heavy metals in soil and plants of four different ecosystems in a former polymetallic ores mining and smelting area (Slovakia). *Journal of Environmental Science and Health, Part A Toxic/Hazardous Substances and Environmental Engineering, 52*(5), 479-490.

8. Greven, M.M., McKenzie, B.A., Hampton, J.G., Hill, M.J. & Hill, G.D. (2001). Some factors affecting seed quality during the mechanical threshing of dwarf French bean (Phaseolus vulgaris L.). *Agronomy New Zealand, 31*, 121–126.

9. Gu, R., Huang, R., JIA, G., Yuan, Z., Ren, L., Li, L., & Wang, J. (2019). Effect of mechanical threshing on damage and vigor of maize seed threshed at different moisture contents. *Journal of Integrative Agriculture, 18*(7), 1571–1578.

10. Chowdhury, M.H. & Buchele, W.F. (1976). Development of a numerical damage index for critical evaluation of mechanical damage of corn. *Transactions of the ASAE, 19*, 428–432.

11. ISTA (International Seed Testing Association). (2015). *International Rules for Seed Test*. Zurich, Switzerland.

12. Jech, J. et al. (2011). *Machinery for crop production 3: Machinery and equipment for post-harvest processing and storyge of plant materials*. Prague: Profi Press. 368 p. ISBN 978-80-86726-41-0.

13. Keller, D.L., Converse, H.H., Hodges, T.O., & Chung, D.S. (1972). Corn kernel damage due to high velocity impact. *Transaction of the ASAE, 15*, 330–332.

14. Khazaei, J., Shahbazi, F., & Massah, J. (2007). Evaluation and modeling of physical and physiological damage to wheat seeds under successive impact loadings: Mathematical and neural networks modeling. *Crop Science*, *48*, 1532–1544.

15. Kroupa, P. et al. (2004). Decreasing of qualitative and quantitative losses in treatment and storage of grain crops at agricultural company. In *Final project report QD 1201* (pp. 103). Prague: VÚZT. Report N° Z-2432.

16. Li, X.P., Gao, L.X., Ma, F.L., Yu, Y.Z., & Zhang, Y.L. (2007). Experimental research of corn seed kernel on the impacting damage. *Journal of Shenyang Agricultural University*, *38*, 89–93.

17. Loewer, O. J., Bridges, T. C., & Bucklin, R. A. (1994). On-Farm Drying and Storage Systems. American Society of Agricultural Engineers. In *ASAE* (pp.214-282). ISBN 0-929355-53-9.

18. Ng, H.F., Wilcke, W.F., Morey, R.V., Meronuck, R.A., & Lang, J.P. (1998). Mechanical damage and corn storability. *Transactions of ASAE*, *41*, 1095–1100.

19. Ružbarský, J., Groda, B., Jech, J. & Sosnowski, S. (2005). *Food technology* (pp.122 - 148). ISBN 80-8073-410-0.

20. Stanovič, R., Kujovský, M., Vollmannová, A., Árvay, J., & Musilová, J. 2015. The content of Cd, Pb and Hg in the grain of maize (Zea Mays L.) harvested in the alluvial soils of the upper reaches of the river Nitra. *Journal of Microbiology, Biotechnology and Food Science, 4*(special issue 3), 142-144.

21. Tomáš, J., Árvay, J., Tóth, T., Vollmannová, A., Kopernická, M., & Slávik, M. (2014). The level of crop plants contamination by heavy metals from the historical mines areas. *Journal of Microbiology, Biotechnology and Food Science, 3*(special issue 3), 294-297.

Corresponding author:
Ing. Koloman KRIŠTOF, PhD., Department of Machines and Production Biosystems, Faculty of Engineering, Slovak University of Agriculture in Nitra, Tr. A. Hlinku 2,Nitra, 94976, Slovakia, phone: +421 37 641 4368, e-mail: koloman.kristof@uniag.sk

SIMULATION OF LINEAR ELECTRIC MOTOR FOR ELECTROMECHANICAL PRUNER

Sergey ANTONOV [1], Gennady NIKITENKO [1]

[1]*Department of Using Electric power in Agriculture, Russian Stavropol State Agrarian University*

Abstract

Gardening is a complex system for the production of berries and fruits, which includes material, financial and labor resources aimed at obtaining the maximum economic effect. Electromechanical pruners based on linear electric motors have several advantages over manual, pneumatic and hydraulic. The use of linear electric motors is one of the promising areas for the development of electric hand tools. The analysis of existing designs of linear electric motors revealed a number of drawbacks. These disadvantages are low efficiency, large mass and size, low armature thrust. The proposed electric motor has the design features of the magnetic system of the stator and the armature. Features are a combination of the design parameters of the magnetic pole of the stator and the armature magnetic circuit. They allow you to increase the power of the armature thrust, increase the efficiency, reduce the weight and size of the electric motor. One of the main tasks in the design of a linear electric motor is to obtain the maximum value of the armature thrust force. To do this, it is necessary to conduct its computer simulation, in order to determine the rational design of the magnetic system. The main factor is the design features of the magnetic system in the air gap, where the energy of the stator magnetic field is converted to the force of the armature. The design parameters affecting the magnitude of the thrust force of the armature determined the bevel angle of the magnetic pole of the stator and the bevel angle of the armature magnetic circuit. The combination of these parameters in different combinations allows you to get a rational design of the magnetic system of a linear electric motor with the maximum value of the armature thrust force.

Key words: Linear motor; thrust force; magnetic system; pruner.

INTRODUCTION

Get high productivity, durability, winter hardiness of trees, regulate growth, as well as product quality allows timely and high-quality pruning of trees.

Detailed pruning of tree branches is done by hand. To increase labor productivity when pruning of branches, we can use mechanization and electrification of works. The analysis of the existing devices of increasing in labor productivity allowed developing the following classification (Fig. 1.).
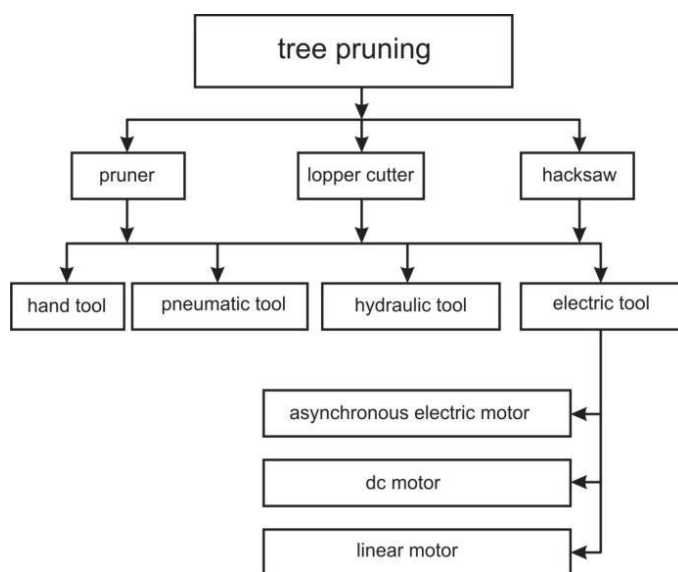
Fig. 1 Classification of mechanization process of trees pruning

Each of the considered tool types has positive and negative sides. The most promising is the use of electrified hand tools for trees pruning (*Hedrick, 1922; Csanády, Magoss, 2013*).
For branches pruning, there are many electromechanical pruners manufactured by industry. These are such as: Makita 4603PW, Makita DVP361Z, Bosch Ciso, Electrocoup F3010, HDP08G, etc. (Fig. 2.)

a)   b)

Fig. 2 Electromechanical pruners: a - HDP08G; b - Electrocoup Infaco

All considered models of electric pruners use direct current motors to drive blades. One of the disadvantages of these engines is high power consumption. This leads to the use of a large mass and overall dimensions battery for powering the electric motor (*Antonov, Nikitenko, Grinchenko, Molchanov, & Avdeeva, 2018*). The main task in the development of a linear electric motor, for hand tools, is to obtain the maximum value of the armature thrust force. To obtain this force of armature thrust it is necessary to optimize the design of the magnetic system of a linear electric motor.

MATERIALS AND METHODS
The linear electric motor (Fig. 3.) consists of a stator (1), which contains a magnetic body (2), a magnetizing coil (3), a non-magnetic frame (4), an upper magnetic pole (5), the cross section of which has the shape of a rectangular trapezium, an end magnetic pole (6), a bolt (7) and a lower magnetic pole (8), having a sample in the form of a cylinder, fixed by bolt (9) to the magnetic body (2), and a non-magnetic insert (10). An armature (11) of a linear electric motor consists of an upper magnetic circuit (12) having the shape of a truncated cone, a lower magnetic circuit (13), non-magnetic bushing (14) put on a non-magnetic rod (15). The armature (11) is mounted in the stator (1) by means of a non-magnetic frame (4) and the non-magnetic insert (10), which are sliding bearings. The return spring (16), the washer (17) and the nut (18) are required to return the armature (11) to its original position.
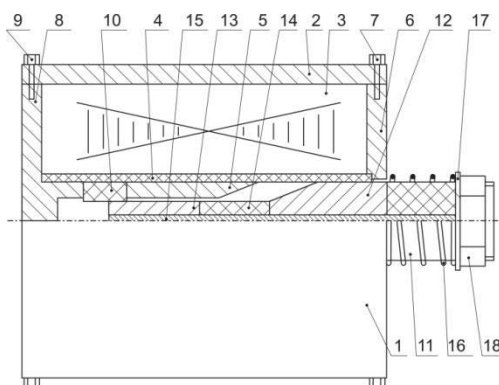
Fig. 3 Linear electric motor: 1 is a stator; 2 is a magnetic body; 3 is a magnetizing coil; 4 is a non-magnetic frame; 5 is an upper magnetic pole; 6 is an end magnetic pole; 7 is a bolt; 8 is a lower magnetic pole; 9 is a bolt; 10 is a non-magnetic insert; 11 is an armature; 12 is an upper magnetic circuit of the armature; 13 is a bottom magnetic circuit of the armature; 14 is a non-magnetic bearing; 15 is a non-magnetic rod; 16 is a return spring; 17 is a washer; 18 is a nut

The proposed linear electric motor works as follows (Fig. 4.): in the absence of power supply to the magnetizing coil (3), the armature (11) takes the upper position under the action of the return spring

(16). When voltage is applied to the magnetizing coil (3), a current creating a magnetic flux Φ starts to flow through it and closes through the magnetic body (2), the end magnetic pole (6), the upper magnetic circuit (12), the upper magnetic pole (5), the lower magnetic circuit (13) and the lower magnetic pole (8).
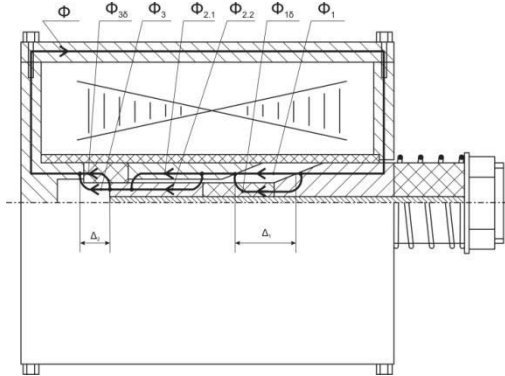
Fig. 4 Magnetic fluxes of linear motor

The magnetic flux Φ in the air gap Δ_1 is divided into magnetic fluxes Φ_1 and $\Phi_{1\delta}$, and in the air gap of length Δ_2 it is divided into magnetic fluxes Φ_3 and $\Phi_{3\delta}$. The magnetic fluxes $\Phi_{2.1}$ and $\Phi_{2.2}$ pass through the upper magnetic pole (5) and the lower magnetic circuit (13). Separation of the magnetic fluxes Φ_1 and $\Phi_{1\delta}$, Φ_3 and $\Phi_{3\delta}$ is possible due to the magnetic resistances commensurability of the air gap and the non-magnetic insert (14). As a result of the passage of magnetic fluxes Φ_1, Φ_3, an electromagnetic force appears, which causes the displacement of the armature (11).

The simulation of a linear electric motor begins with the calculation of magnetic fields. The main characteristic of a magnetic field is magnetic induction, which is a vector quantity. To calculate the magnetic system, we use a two-dimensional magnetostatic problem. The Poisson equation describing the magnetic state of an electric motor in partial derivatives and cylindrical coordinates (r, z). It is recorded as follows:

$$\frac{\partial}{\partial r}\left(v\frac{1}{r}\partial r(rA)\right) + \frac{\partial}{\partial z}\left(v\frac{1}{r}\frac{\partial}{\partial z}(rA)\right) = J \tag{1}$$

where $v = \dfrac{1}{\mu_0 \mu}$ - specific magnetic resistance;

   r, z - cylindrical coordinates;
   J - current density;
   A - vector magnetic potential.

When building a model on the internal and external borders of areas, the following types of boundary conditions are possible.

Dirichlet condition, which sets on the part of the border the known vector magnetic potential A_0, at the top or on the edge of the model. This boundary condition determines the behavior of the normal induction component on the boundary. This condition is most often used to specify a zero value or a complete attenuation of the magnetic field at a border remote from the sources (2).

$$rA_0 = a + bzr + \frac{cr^2}{2} \tag{2}$$

where a, b, c - constant values for each edge.

To analyze the calculation results, it is necessary to operate with the following local and integral quantities.

Magnetic induction vector ($B = rotA$)

$$B_z = \frac{1}{r}\frac{\partial(rA)}{\partial r}, \; B_r = -\frac{\partial A}{\partial z} \tag{3}$$

The total magnetic force acting on the anchor of a linear electric motor is determined by the formula:

$$F = \frac{1}{2}\oint \left(H(n \cdot B) + B(n \cdot H) - n(H \cdot B)\right)dS \qquad (4)$$

Where n - unit vector of the outer normal to the surface.

On the basis of the above formulas, the calculation of the magnetic static field, which is incorporated in the algorithms for calculating the ELCUT program, is constructed. To solve linear problems, the iterative method of conjugate gradients is used.

RESULTS AND DISCUSSION

The purpose of modeling a linear electric motor is to determine the thrust force of the armature. To simulate magnetic fields, we use the professional version of the ELCUT program (*Antonov, Gabriyelyan, Mastepanenko, Zorina & Nozdrovicky, 2016*). As a result of the calculation, we obtain a picture of the magnetic fluxes distribution (Fig. 5.).

a)
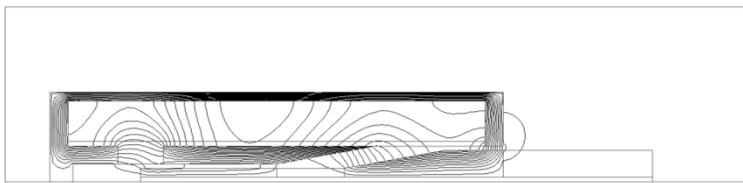
b)
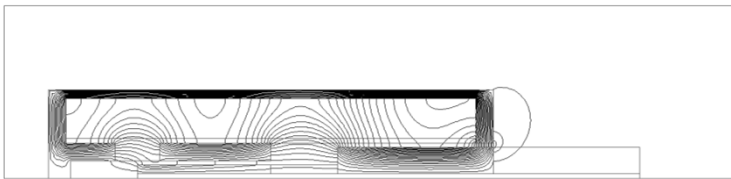
Fig. 5 Calculation result of the magnetic system of the linear motor program ELCUT: a – $\alpha = 10^0$, $\beta = 10^0$; b – $\alpha = 90^0$, $\beta = 90^0$

The main task of modeling a linear electric motor is to rationalize the design of the magnetic system, in order to obtain maximum values of the armature thrust force. The main factor influencing the magnitude of the armature thrust force is the value of the magnetic fluxes Φ_1 and Φ_3 in the air gaps Δ_1 and Δ_2. To rationalize the design of the magnetic system, we change the inclination angle of the magnetic pole of the stator 5 (α) and the inclination angle of the upper magnetic circuit of the armature 12 (β) (Fig. 6a.) from 10^0 to 90^0 at a pitch of 10^0.
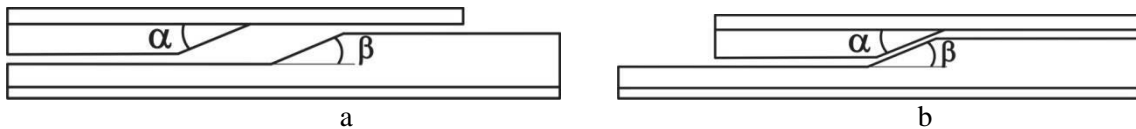
Fig. 6 Magnetic system modeling of a linear electric motor: a - at the beginning of the working stroke; b - at the end of the working stroke

Based on the design features of the magnetic system and the dynamics of the armature (11) relative to the magnetic pole of the stator (5), it is necessary to take into account when modeling their joint at the end of the working stroke (Fig. 6.b). This means that the angle α must be equal to the angle β.

Modeling results of the magnetic system of the linear motor pruner are shown in Table 1.

Tab. 1 Calculation result of the armature thrust force (F_a) of a linear electric motor, N

inclination angle of the magnetic pole of the stator (α) and the upper magnetic circuit of the armature (β)								
α - β								
10^0-10^0	20^0-20^0	30^0-30^0	40^0-40^0	50^0-50^0	60^0-60^0	70^0-70^0	80^0-80^0	90^0-90^0
55,52	52,66	45,61	43,31	43,29	41,59	40,972	39,33	38,33

Considering the obtained data, it should be noted that with an increase in the inclination angle of the upper magnetic circuit of the armature (β) and the inclination angle of the magnetic pole of the stator (α) from 10^0 to 90^0, the armature force F_a decreases from 55.52 to 38.33 N. The maximum value of the armature thrust force is calculated as F_a = 55.52 N.

CONCLUSIONS

The use of a linear electric motor for electrified pruners, as compared to direct current motors, will reduce the mass and dimensional parameters of the device.

Modeling of a linear electric motor in the ELCUT program allowed us to confirm the pattern of magnetic fluxes distribution. Conformity of changes in the armature thrust force, from the inclination angles of the magnetic system elements of a linear electric motor was studied. Based on the obtained results, it can be concluded that the maximum value of the armature thrust force $F_a = 55,52N$ is obtained at $\alpha = 10^0$ and $\beta = 10^0$.

REFERENCES

1. Antonov, S.N., Gabriyelyan, S.Z., Mastepanenko, M.A., Zorina, E.B., & Nozdrovicky, L. (2016).The device of magnetic processing of water for boiler greenhouse. *Research in agricultural engineering*, *62*(Special Issue), 27-33.
2. Antonov, S., Nikitenko, G., Grinchenko, V., Molchanov, A., & Avdeeva, V. (2018). Electromechanical secateurs based on a linear electric motor and determination of the cutting force of branches of fruit trees. In *Ingineering for rural development* (pp. 514-518). Jelgava, Latvia.
3. Csanády, E. & Magoss, E. (2013). Mechanics of Wood Machining. *2-nd ed. Springer-Verlag* Berlin Heidelberg, 199 p.
4. Hedrick, U.P. (1922). *Cyclopedia of Hardy Fruits*. New York: The MacMillan Company. 370 p.

Corresponding author:

Ing. Sergey Antonov, Ph.D., Department of Using Electric power in Agriculture, Russian Stavropol State Agrarian University, Chekhova 37, ap.118, Stavropol, Stavropol Territory, 355013, Russian Federation, phone: +79283054566, e-mail: antonov_serg@mail.ru

GRAVITY COMPENSATION IN ROBOTICS – A REVIEW

Vigen ARAKELIAN [1, 2]

[1] MECAPROCE, Institut National des Sciences Appliquées (INSA)
de Rennes, 20 Avenue des Buttes de Coësmes, CS 70839
F – 35708 Rennes, FRANCE
[2] LS2N-ECN UMR 6004, 1 rue de la Noë, BP 92101,
F-44321 Nantes, France

Abstract
Gravity compensation is a well-known technique in robot design to achieve equilibrium throughout the range of motion and as a result to reduce the loads on the actuators. Therefore, it is desirable and commonly implemented in many situations. Various design concepts for gravity compensation are available in the literature. This paper proposes an overview of gravity compensation methods applied in robotics. In order to classify the considered balancing schemes three principal groups are distinguished due to the nature of the compensation force: counterweight, spring or active force developed by an auxiliary actuator. The author believes that such an arrangement of gravity compensation methods allows one to carry out a systematized analysis and provides a comprehensive view on the problem. Particular attention has been given to the coupled Hand-operated Balanced Manipulator (HOBM) and Lightweight Robot (LWR). The aim of such a cooperation is to displace heavy payloads with less powerful robots.

Key words: *gravity compensation; balancing; actuator power; Hand-operated Balanced Manipulator (HOBM); effort minimization.*

INTRODUCTION

Many robotic systems are operated at low speed to ensure the different tasks. In this situation gravitational torques generated by the masses of links are often much greater than dynamic torques. Thus, gravity compensation is beneficial by which a robotic system can be operated with relatively small actuators generating less torque. The potential energy of such a robotic system is constant (or quasi-constant) for all possible configurations, which leads to the self-balancing of the mechanical system. Nature of the forces that must compensate gravity and its emplacement in the robotic systems may be diverse. In the present paper, the typical gravity compensation solutions are systematized and their effectiveness is considered.

It should be noted that the gravity compensation can also be achieved by optimal control of input torques. In this case the control law combines terms that cancel the gravity effects on the robot link dynamics with a PD-type error feedback on the motor variables *(Gosselin, 2008)*. However, in this survey, the mechanical solutions of the gravity compensation will only be reviewed.

The given systematization can be presented as follows *(Arakelian, 2016)*:

1. Gravity compensation by counterweights.
1.1. Gravity compensation by counterweighs mounted on the links of the initial system.
1.2. Gravity compensation by counterweights mounted on the auxiliary linkage connected with the initial system.
2. Gravity compensation by springs.
2.1. Balancing by springs jointed directly with manipulator links.
2.2. Balancing by using the cable and pulley arrangement.
2.3. Balancing by using auxiliary systems.
2.3.1. Balancing by using an auxiliary linkage.
2.3.2. Balancing by using a cam mechanism.
2.3.3. Balancing by using a gear train.
3. Gravity compensation by using auxiliary actuators.

1. GRAVITY COMPENSATION BY COUNTERWEIGHS

The use of counterweights has been applied to the design of mechanical systems for a long time. The classical approach consists in adding counterweights in order to keep the total centre of mass of moving links stationary. With regard to the several approaches employed for the redistribution of movable masses, the developed design concepts could be divided into two principal sub-groups.

1.1. GRAVITY COMPENSATION BY COUNTERWEIGHS MOUNTED ON THE LINKS OF THE INITIAL SYSTEM

It is obvious that the adding of the supplementary mass as a counterweight is not desirable that it leads to the increase of the total mass, overall size of the robot-manipulator and the efforts in joints. That is why in many constructions of industrial robots, for example KUKA R360 or PUMA 200, the masses of the motors are often used for gravity compensation. The review slowed that the gravity compensation by counterweights mounted on the links is more appropriate for serial and planar parallel manipulators. It is much more difficult for spatial parallel manipulators. Gravity compensation has been successfully applied on hand-operated balanced manipulators (HOBM). The balanced manipulator is a handling system with a simple mechanical system in which the manipulated object in any position of the workspace is balanced. Such a state of constant gravity cancellation allows displacements of heavy objects manually. The term "balanced manipulator" shows that in the operating procedure of these systems is very important to achieve an accurate compensation of gravity. Many studies and design concepts have devoted to the gravity compensation of these manipulators by counterweights. It was shown that for the balancing of these manipulators it is necessary to apply to the pantograph mechanism a sinusoidal balancing moment. The general approach for determination of balancing conditions was proposed by the study of the motion of the center of mass of the pantograph actuator. In many HOBM the balancing by counterweights is combined with actuators, which carried out an active balancing.

1.2. GRAVITY COMPENSATION BY COUNTERWEIGHTS MOUNTED ON THE AUXILIARY LINKAGE CONNECTED WITH THE INITIAL SYSTEM

At first, let us define an auxiliary linkage. We will use this term for any mechanical system that mounted between the balancing element and the initial structure of a robot. The goal of these linkages is to improve the compensation and design conditions via optimum location of balancing elements. There are also some solutions in which it is proposed to cancel the weight of the payload via a moving counterweight. The counterweight balancing of the mine detection vehicle with a pantograph manipulator has been developed. It has been shown that the robot arm with properly dimensioned balancing counterweights can efficiently actuated with very low power and energy consumption.

Many schemes illustrate the parallel manipulators comprising auxiliary systems equipped with counterweights. However, the industrial applications of such approaches are often quite complicated because of limitation of the overall size of manipulators and the possibility of collision of extended moving links carrying counterweights.

2. GRAVITY COMPENSATION BY SPRINGS

Firstly, let us disclose the properties of two types of springs that are used for gravity compensation in robotic systems: zero-free length and non zero-free length springs. The author believes that it is important to provide a comprehensible and short background on these two types of springs. It will be particularly useful for young scientists and engineers. Zero-free length spring is a term for a specially designed coil spring that would exert zero force if it had zero length. Obviously, a coil spring cannot contract to zero length because at some point the coils will touch each other and the spring will not be able to shorten any more. Zero length springs are made by manufacturing a coil spring with built-in tension, so if it could contract further, the equilibrium point of the spring, the point at which its restoring force is zero, occurs at a length of zero. In practice, zero length springs are made by combining a "negative length" spring, made with even more tension so its equilibrium point would be at a "negative" length, with a piece of inelastic material of the proper length so the zero force point would occur at zero length. It is important to emphasize that the use of a zero free length spring for complete gravity compensation is basically used when the spring is connected directly with the robot links and such a necessity

mainly disappears when the spring is connected with the robot links via a cable or an auxiliary mechanism. To preserve the structure of the systematization adopted above, i.e. the first step of classification by the nature of compensation forces and the second step by the structural features, let us gather the spring compensators in following three sub-groups.

2.1. BALANCING BY SPRINGS JOINTED DIRECTLY WITH MANIPULATOR LINKS

In order to create springs with adjustable stiffness the "Jack spring" concept based upon the principle of adding and subtracting coils from a spring has been developed. Thus, with this method, by changing the number of coils in a spring, the actual or intrinsic stiffness of the spring is structurally changed. The gravity balancing of the leg was also solved. The gravity balancing mechanism, proposed in these studies, consists of two springs with the same stiffness coefficients: one compression and another extension connected with the shank of the leg and permitting the complete gravity compensation of the leg's weight. In order to improve the gravity compensation quality the spring mass has been included in the balancing condition. It was shown that the mass of the balancing spring increases the unbalanced moment and it cannot be neglected. The numerical simulations showed that the error caused by neglect of the spring mass can be reached until 8%. Various design concepts have been also developed for adjustment of gravity equilibrators.

2.2. BALANCING BY USING THE CABLE AND PULLEY ARRANGEMENT

The adding of the cable and pulley allows full compensation of gravity by using non-zero free length spring. The gravity compensation with non-circular pulleys and springs has also been examined. After preliminary verification of the design methodology for a single pendulum system, the weight compensation mechanism has been extended to the two degrees of freedom parallel five-bar linkage arm. It has been shown that the introduction of the weight compensation mechanism reduces the maximum static torque up to 50-80%. The spiral pulley with spring are already succefully used.

It should be mentioned that the several error sources in the practical implementations decrease the efficiency of the gravity compensation with springs and pulleys. Errors are mainly caused by the non-linearity of the springs due to the manufacturing tolerance. Often the nominal values of the calculated springs are different to the real values. Therefore, the values of springs´ stiffness must be adjusted. Another error source is the radius of the pulleys.

2.3. BALANCING BY USING AUXILIARY MECHANICAL SYSTEMS

The auxiliary mechanisms have the same effect that the cables and the pulleys. In most cases, they allow the gravity compensation by using non-zero free length springs. The advantage of the adding of an auxiliary mechanism consist also in increase of free parameters of the system which allows one optimize the gravity compensation by applying the linkage synthesis methods. The known solutions can be arranged into three sub-groups: i) Balancing by using an auxiliary linkage that can be un four-bar, slider-crank or coulisse mechanism, the pantograph is also has been applied as an supplementary system. ii) Balancing by using a cam mechanism. In this case, by using the conservation of energy and balance conditions, the optimal profiles of cams can be found in order to compensate the gravity of links or a payload. iii) Balancing by using gear trains.

1. GRAVITY COMPENSATION BY USING AUXILIARY ACTUATORS

In this case, a pneumatic or hydraulic cylinder is connected with manipulator links or directly with the moving platform. There are also some approaches based on counterweights, which are fluid reservoirs connected with an auxiliary actuator. Continuous gravity compensation is achieved by the pumping of the fluid from the first reservoir-counterweight to the second. Electromagnetic effects were also used.

The gravity compensation of spatial parallel architectures is a complicated problem because it can be achieved either by unavoidable increase of the total mass of moving links or by a considerably complicated design of the initial parallel mechanism. It seems that an optimal approach is to combine an auxiliary linkage with pneumatic or hydraulic cylinders. An illustrative example of such a system developed at the INSA of Rennes *(Baradat et al., 2008)*, is shown in Fig. 1. The suggested approach involves connecting an auxiliary mechanism to the initial structure, which generates a vertical force applied to the manipulator platform. The minimization of the input torques was carried out by constant and variable

forces for static and dynamic modes of operation. It was shown that a significant reduction in input torques can be achieved by the suggested balancing mechanism: the reduction of the root-mean-square value of the input torque due to the gravitational forces is 99.5% and the maximum value is 92%.
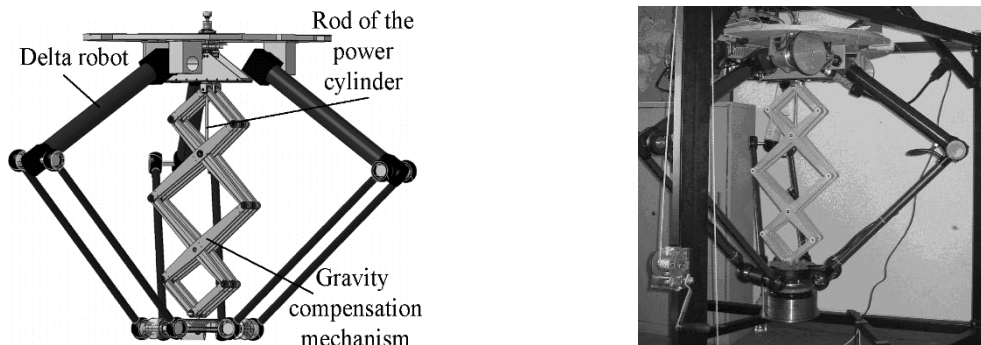
Fig. 1. CAD model and prototype of the balancing mechanism implemented in the structure of the Delta robot.

The positioning errors of the unbalanced and balanced parallel manipulators have been provided. It was shown that the elastic deformations of the manipulator structure due to the payload, change the altitude and the inclination of the platform. A significant reduction in these errors has been achieved by using the balancing mechanism (from 86.8% to 97.5%). The theoretical results obtained by numerical simulations were confirmed by experimental study carried out by means of the developed prototype.

It should be noted that the gravity compensation for the manipulators in which the vertical motion is decoupled from other Cartesian degrees of freedom has also been studied. In the latter situation, only one degree of freedom needs to be gravity compensated in order to eliminate actuator torque due to the weight of the moving parts and the payload. The specificity of this technique it is easy to see on the example of the PAMINSA manipulator developed at the INSA of Rennes. An energetic analysis shows that the gravity work of a body moving in the horizontal plane is equal to zero (the gravitational forces are always perpendicular to the displacements). But the work of the same force moving along the vertical axis is other than zero (the gravitational forces are parallel to the displacements). This phenomenon is used in the design of the hand operated manipulators, in which the horizontal displacements of the payload are carried out manually and the vertical displacements are actuated. This principle is also applied in the design of the parallel manipulators called PAMINSA (Parallel Manipulator of the INSA) *(Briot et al., 2009)*.

Let us consider the mechanical architecture of this manipulators. The aim was to develop a parallel architecture in which displacements of the platform in the horizontal plane are independent of its vertical displacements. For this purpose, the pantograph linkage is used as a leg. The pantograph is a mechanical system with two input points A_i and B_i and one output point C_i (Fig. 2a). These input points linearly control the displacement of the output point C_i. Thus, one linear actuator connected with input point B_i can control the vertical displacement of the output point C_i and one other linear actuator with horizontal axis is able to control its horizontal displacements. Please note that these motions are completely decoupled, i.e. they can be carried out independently.

Now let us connect three Scheiner pantograph linkages with the base and the platform as shown in Fig. 2b. In the obtained structure, one vertical actuator M_v controls the vertical displacement of point B_i of the pantograph linkages, resulting in the vertical displacement of joints C_i of the moving platform. The generation of motion in the horizontal plane is achieved by the actuators M_1, M_2 and M_3 moving the input joints A_i.

Among the obvious advantages of the suggested manipulator architecture, we would like to note the following:

(i) the decoupling of the control powers into two parts, making it possible to raise an important payload to a fixed altitude with powerful actuators and then to displace it on the horizontal plane with less powerful actuators;

(ii) a great accuracy in the horizontal positioning because the payload can be locked in the horizontal plane using mechanical architecture of the manipulator (in other words, if the position of the vertical actuator is fixed, the altitude of the platform cannot change);

(iii) the cancellation of the loads of gravity on the rotating actuators which displace the platform in the horizontal plane;

(iv) the simplification of the vertical control which is based on linear input/output relationships.
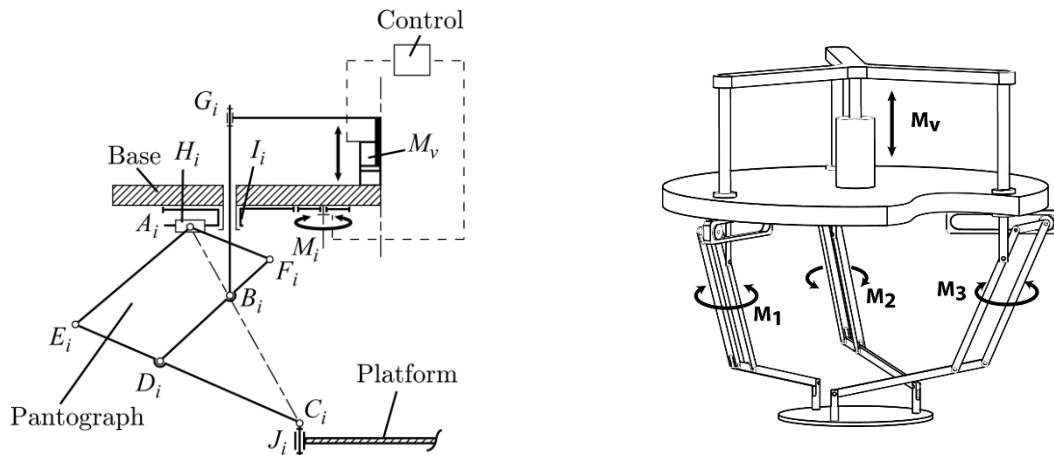
Fig. 2. PAMINSA: a) kinematic chain of each leg; b) 3D view.
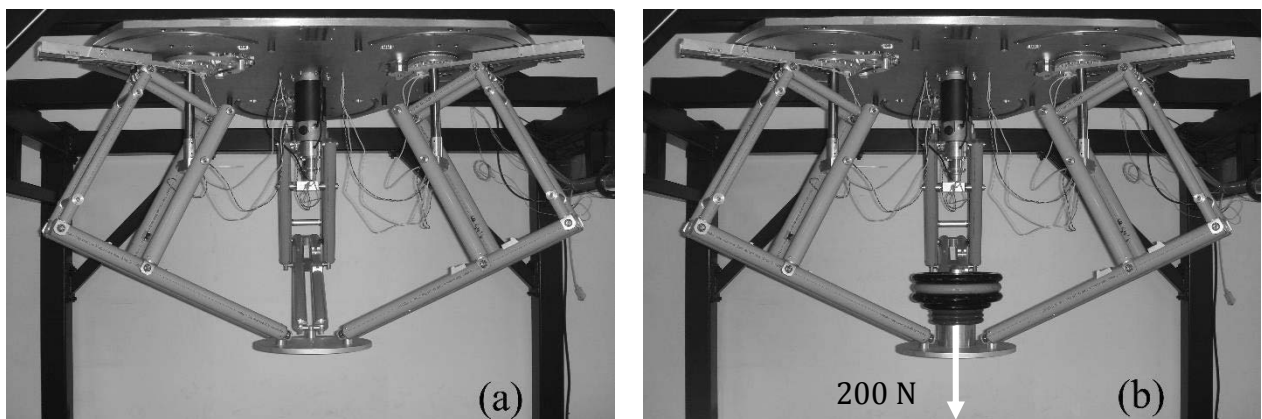
Fig. 3. The prototype of PAMINSA developed at the I.N.S.A. of Rennes.

The design concept has been validated via experimental tests carried out on the prototype (Fig. 3). The curves with and without payload (200N) for the 3 rotating actuators have been superposed. It has been shown that they are similar. Regarding the vertical actuator, it supports the payload and the increase of the input force is significant.

Workers in industries such as manufacturing and assembly, frequently manipulate heavy objects. However, manual processing is often repetitive and becomes tedious, it reduces efficiency and leads to back pains, injuries and musculoskeletal disorders. It is obvious that traditional robot installations can offer several benefits compared to manual operation: improved repeatability, increased precision and speed. However, industrial robots still have many weaknesses compared to humans. For example, currently industrial robots have a limited ability to perceive their surroundings, which requires costly safety arrangements in order to avoid serious injury. These safety arrangements are particularly important and costly when working with installations of large and powerful industrial robots. It is obvious that serial robots have a poor payload-to-weight ratio. For a six-degrees-of-freedom general-type serial robot, it is less than 0.15. For example, a robotic arm handling an object of $50 kg$ must have a weight of at least $350 kg$. The purchase, installation and operation of such a robot are quite expensive. In addition, the

heaviness of the robot and of the payload complicates the dynamics of the system, making it difficult to move accurately and quickly. This becomes especially noticeable during assembly processes, when heavy parts must be installed on a surface with guiding pins. In such a case, the robotic arm has to move smoothly and any sudden movement may damage the mechanical surface of the part.

Such a task is not easy to achieve. Thus, autonomous manipulation does not always provide expected reliability and flexibility. Balancer – robot systems such as power assist robotic systems may be perfectly used for heavy object manipulation. The combination of motion programming of a lightweight robot and simplicity of a hand-operated balanced manipulator (HOBM) may make the system far better than the application of an individual robot arm. Detailed descriptions of gravity compensation methods can be found in the monography *(Arakelian & Briot, 2015)*.

Fig. 4. Coupled «Balancer-lightweight robot» system.

CONCLUSIONS

Despite its ancient history, gravity compensation methods continue to develop and new approaches and solutions are constantly being reported. It seems promising the development of new gravity compensation solutions for the exoskeletons, rehabilitation devices and walking assist devices. The use of active and passive actuations allows a significant reduction of the size and weight of walking assist devices with bodyweight support. However, the several error sources in the practical implementations decrease the efficiency of the gravity compensation in robotics systems. Errors are mainly caused by the non-linearity of the springs due to the manufacturing tolerance. Often the nominal values of the calculated springs are different to the real values. Other error sources are the manufacturing tolerances of equilibrator's links, their stiffness and clearance in joints. In the case of auxiliary linkages, the balancing is carried out for discrete positions due to the non-linearity of transmission characteristics, which leads to an approximate balancing.

REFERENCES

1. Gosselin C. (2008), Smart Devices and Machines for Advanced Manufacturing pp. 27–48. (Chapter: Gravity compensation, static balancing and dynamic balancing of parallel mechanisms). Springer, London (2008).
2. Vukobratovic M., Milojevic M., Tzafestas S., Jovanovic M., & Potkonjak V. (2011). Human and humanoid postures under external disturbances: modeling, simulation, and robustness. Part 2: simulation and robustness. Intelligent & Robotic Systems, 63(2), 211–231.
3. Arakelian V. (2016). Gravity compensation in robotics. Advanced Robotics, 30(2), 79-96.
4. Baradat C., Arakelian V., Briot S., & Guegan S. (2008). Design and prototyping of a new balancing mechanism for spatial parallel manipulators. Transactions of the ASME. Journal of Mechanical Design, 130(7), 072305 (13 pages).
5. Briot S., Arakelian V., & Guegan S. (2009). PAMINSA : A new family of partially decoupled parallel manipulators. Mechanism and Machine Theory, 44(2), 425-444.
6. Arakelian V., & Briot S. (2015). Balancing of linkages and robot manipulators. Advanced methods with illustrative examples. Springer.

Corresponding author:

Full Professor Vigen ARAKELIAN, INSA Rennes / LS2N, 20 avenue des Buttes de Coësmes, CS 70839, F-35708 Rennes Cedex 7, France, phone: +33(0)223238492, e-mails: vigen.arakelyan@insa-rennes.fr & vigen.arakelyan@ls2n.fr

TESTING AUTOMOBILE BRAKING PARAMETERS BY VARYING THE LOAD WEIGHT

Dainis BERJOZA[1], Ilmars DUKULIS[1], Vilnis PIRS[1], Inara JURGENA[2]

[1]*Latvia University of Life Science and Technologies, Faculty of Engineering, Motor Vehicle Institute*
[2]*Latvia University of Life Science and Technologies, Faculty of Economics and Social Development, Institute of Business and Management Science*

Abstract
Modern automobiles are equipped with advanced braking systems and auxiliary safety systems, yet there is an opinion that the braking distance and time considerably increase if increasing the weight of the automobile, e.g. reaching the gross weight. The research performed tests on automobiles of three different size classes: small, medium and large, determining the key parameters – time, distance and deceleration – for braking from a speed of 50 km h^{-1}. The automobiles were road tested by loading them up with the driver or the driver and a load that increased the weights of the automobiles almost to their gross weights. The tests found that for the automobiles with a load, the braking time increased on average by 5.12% and the braking distance increased by 5.9%, while the braking deceleration, compared with no-load driving, decreased by 4.94%.

Key words: braking time; braking distance; braking deceleration; road surface.

INTRODUCTION

Driving safety depends on the braking parameters of the automobile. Braking is the capability of the automobile to decelerate fast and come to a complete stop within a minimum distance. When braking, the kinetic energy of the automobile transforms into thermal energy in the braking mechanisms and in the tyres' contact area with the road surface.

The key braking parameters of the automobile are braking force and deceleration, yet in practice mostly braking time and distance are used. The adhesion parameters of the automobile could be changed, e.g. by driving the automobile on diverse road surfaces and equipping it with new tyres with good tread as well as by varying the weight of the automobile, e.g. driving it loaded or unloaded. If the automobile is loaded, the distribution of load on the axes, the height of the centre of mass and the area of tyre contact with the road surface could change. In accordance with physics laws, the brake factor does not change if varying the load on the tyre.

The adhesion of the tyre to the road surface is characterised by the coefficient of adhesion, which varies, depending on the kind of road surface. Friction is important if driving on a hard surface road, yet ground resistance to shear is important if driving on a deformable surface road. If driving on a wet hard surface road, the movement of tyres cause hydrodynamic pressure on the water. At high speeds, tyres with a small tread depth could lead to aquaplaning – the tyres lose contact with the road surface *(Wong, 2008)*.

As the load on the automobile changes, the area of tyre contact with the road changes as well. At a constant weight of the automobile, the area of tyre contact with the road can change if tyre pressure changes *(Effects of, 2011)*. A change in the area of tyre contact could affect braking distance. According to research investigations done by Slovakian researchers, a 20% lower tyre pressure than that recommended by the tyre manufacturer slightly decreases braking distance. A 20% higher tyre pressure increases braking distance by 15% *(Rievaj, et al., 2013)*. Varying the load of an automobile requires for some automobile models to change the tyre pressure. As the load on the tyre increases, the area of tyre contact with the road also increases, which could change the adhesion parameters of the tyre. Other research investigations that have analysed the effect of change in tyre pressure on braking stated that lower tyre pressure increased braking distance if braking in a linear motion, making no manoeuvre or braking in a curvilinear motion *(Parczewski, 2013)*.

Increasing the load on the automobile, the following other characteristics change:
- ✓ load on springs and automobile ground clearance;
- ✓ height of the centre of mass;

✓ distribution of load on the axles;

✓ wheel radius and the area of tyre contact with the road surface *(Berjoza, 2008; Wong, 2008)*.

Danish researchers conducted a number of braking tests involving 22 drivers. The tests involved 16 nonprofessional drivers and 6 professional ones. The braking was done from speeds of 80, 110 and 130 km h^{-1}. The braking parameters were registered electronically *(Greibe, 2007)*. The braking was done on an asphalt road with the coefficient of adhesion ranging from 0.4 to 0.8 (dry and wet road surfaces).

To register braking operations, the automobiles were equipped with a fifth wheel for taking measurements, a pressure sensor was installed on the brake pedal and a computer was used for collecting and saving the data. The fifth wheel was attached to the automobiles' tow hooks and pressed to the road surface by means of a hydraulic system. The measurements were taken every 0.1 m distance *(Greibe, 2007)*. The speed and the deceleration were computed based on time measurement. The pressure force gauge installed on the brake pedal had an accuracy of 0.15 kg. Two automobiles – a Fiat Grande Punto and an Opel Vectra – were used in the braking tests *(Greibe, 2007)*.

Both automobiles were equipped with an ABS and a manual transmission. The initial tread depth of tyres was 7-8 mm. The professional drivers achieved, on average, a 15-20% shorter braking distance than the nonprofessional drivers did. The dispersion of test replication data was found lower for the professional drivers than the nonprofessional ones. An analysis of the force applied to the brake pedal revealed that at the initial stage, the professional drivers applied even a two-fold larger force than the nonprofessional drivers did, which resulted in a shorter braking distance.

Some scientists have tested automobiles with and without a load *(Roos, Zimmermann, 2004)*. One test driver was involved in all the braking tests. The tests were done by using three diverse automobiles, with a 400 kg load as well as without a load. The braking tests were done on dry and wet roads, with initial speeds before braking at 70, 100 and 130 km h^{-1}. Two automobiles with a load had a longer braking distance. The increase in braking distance was estimated at 4%, while the deceleration was 0.5 m s^{-2} slower. Varying the load, no difference in braking distance was found for the third automobile *(Roos & Zimmermann, 2004)*.

There have been some experimental investigations into braking under various braking regimes. The deceleration of automobiles without an ABS ranged from 6.9 to 7.8 ms^2. With an ABS, the deceleration was in the range of 8.0-8.8 ms^2. A trend was observed – the deceleration of automobiles without an ABS tended to decrease if increasing the initial speed before braking, whereas that of automobiles with an ABS tended to increase if increasing it. The experimental investigations also analysed braking force increase time, which was two times shorter for automobiles with an ABS than without *(Sokolovskij, 2005)*.

Road testing trucks revealed that a correctly position load on the truck deck was important in braking. In N2 category vehicles, a load could be placed in four different positions. Braking an automobile from a speed of 65 kmh^{-1}, the deceleration was in the range of 5.18-5.89 ms^2. The shortest braking distance, 29.91 m, was achieved when the load was positioned on the rear axle. In this case, the braking time was 3.36 s *(Skrucany, et al., 2017)*.

USA researchers tested 10 various automobiles, varying the weights of the automobiles *(National, 2003)*. All the automobiles, including trucks, pickup trucks and a four-wheel drive automobile were manufactured in the USA. The test registered braking distances on dry and wet roads from an initial speed of 100 km h^{-1}. On a dry road, a loaded automobile had a 5-8% longer braking distance than an automobile without a load. On a wet road, the difference in braking distance was larger, in the range of 10-15% *(National, 2003)*.

Automobile users are of the opinion that a heavier load – near the gross weight level – considerably increases braking time and distance. Accordingly, the research aim is to identify the effect of the weight of an automobile on the braking parameters.

MATERIALS AND METHODS

The authors carried out the experiment on three automobiles: a Renault Traffic, a Volvo V70 and a Renault Clio II. The experimental automobiles were equipped with summer tyres with a tread depth in the range of 4-7 mm. The tyre pressure was set as recommended for the weight. All the auto-

mobiles had an ABS and a ventilated disc brake in the front axle. Only the Renault Clio II had a drum brake in the rear axle. The characteristics of the experimental automobiles are presented in Tab. 1.

Tab. 1 Characteristics of the experimental automobiles

No	Characteristics	Automobile make and model		
		Renault Traffic II	Volvo V70	Renault Clio II
1	Manufacture year	2007	2001	2002
2	Kerb weight, kg	1957	1605	1035
3	Gross weight, kg	2835	2100	1515
4	Tyre size	195/65R16	195/65R15	175/65R14

During the experiment, the tyre pressure was adjusted according to the load.

The experiment employed a scientific radar Stalker ATS. The technical characteristics of the radar were as follows: speed accuracy: $\pm$ 1.609 km h^{-1}; measuring speed range: 1-480 km h^{-1}; time accuracy: 0.01 s; and maximum measuring distance: 1.80 km. A digital calliper Insize 1112 was employed to measure the depth of tyre tread. A GPS logger Holux GPS Sport 245 was used to accurately control the speed of the automobiles during the experiment. A brake and shock absorber diagnostic device VT1200 was used to weigh the automobiles; its resolution was 1 kg.

The present research aimed to identify the braking distance and time and compute the deceleration. The automobiles were not equipped with specific auxiliary equipment for measuring the driver's response time and the brake effect increase time.

The experiment was conducted on a road section with low traffic. The asphalt road was dry, with the coefficient of adhesion φ=0.75. The air temperature was in the range of +10-15ºC. During the experiment, the wind speed did not exceed 2-3 m s^{-1}. A scheme of the experiment is shown in Fig. 1.
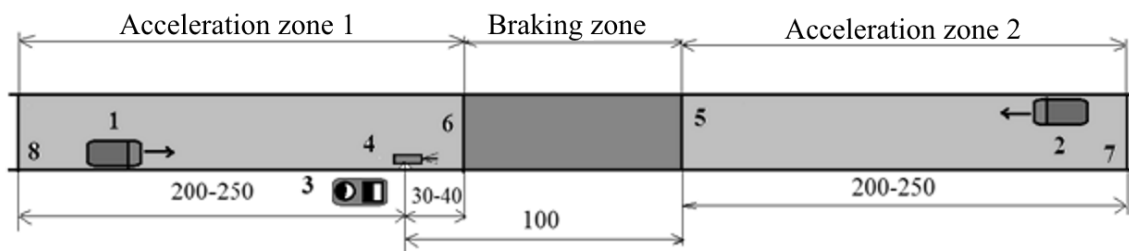
Fig. 1 Scheme of the experiment:
1 – automobile moves away from the radar; 2 – automobile moves towards the radar; 3 – operator's work zone; 4 – scientific radar Stalker; 5 and 6 – start of braking; 7 and 8 – start of acceleration

The measurements were taken in both directions. The acceleration was started either at start point 7 or at start point 8. The experiment was done in both directions to take into account the effects of wind and the road slope. Accelerating from start point 8, the radar operator turned on the radar when the automobile passed by the radar and started braking about 30-40 m behind the radar. The braking was started at a speed of 55±3 km h^{-1}. Afterwards, the automobile was turned around and the acceleration was started at start point 7. When the automobile reached a speed of more than 60 km h^{-1}, the driver signalled by headlights the moment when to activate the radar. The braking was started at a distance of approximately 80-100 m from the radar. The radar was stopped when the automobile came to a complete stop. The measurements were repeated 6-8 times, and five most accurate measurements were selected for data processing. All the measurements were taken with the engine disengaged and the gear-shift lever put in the neutral position.

The experiment was begun with the automobiles being loaded. Tractor counterweights were used as the load for the automobiles. The counterweights were fastened inside the automobiles so that they could not change their positions when braking. The counterweights were placed in the interiors in a way to simulate passengers – 80 kg per seat.

After the experiment, the radar data files were processed and readings were taken. Stalker ATS software was used to take the readings. A screenshot of the monitor for the braking zone is presented in Fig. 2. The screenshot shows two test replications carried out towards the radar (shorter distance) and two replications done away from the radar (longer distance).
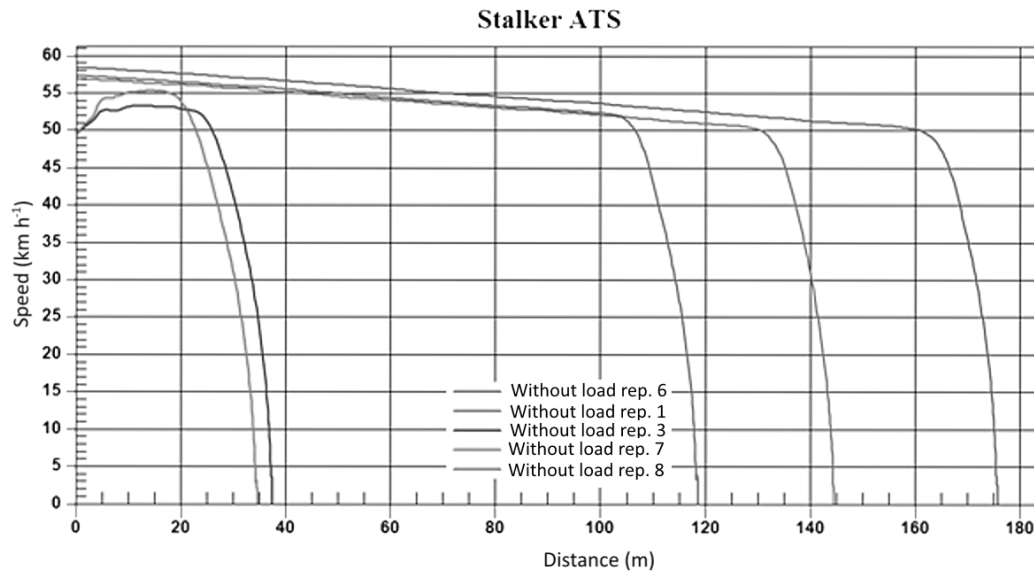
Fig. 2 Screenshot of a radar software chart v=f(s) for a loaded Renault Traffic during braking

The radar software can read the coordinates of points on the chart. Since the braking was not started exactly at a speed of 50 km h^{-1}, it was necessary to find a point being in the closest position to the initial speed. At this speed, the start time of braking was determined (since the moment the radar was activated). Afterwards, the finish time of braking was determined. The period of braking was computed by the equation (1)

$$t_\tau = t_2 - t_1 \tag{1}$$

where t_1- start time of braking (s), t_2- finish time of braking (s).
Using a chart, the data for braking distances were acquired in a similar way. The braking distances were computed by the equation (2)

$$s_\tau = s_2 - s_1 \tag{2}$$

where s_1- start of braking (m), s_2- finish of braking (m).
The average braking acceleration was computed by the equation (3)

$$j_\tau = \frac{v_1 - v_2}{t_\tau} \tag{3}$$

where v_1- start speed of braking (m s^{-1}), v_2- finish speed of braking (m s^{-1}), t_τ- period of braking (s).

RESULTS AND DISCUSSION
The automobiles were weighed before the experiment. The data for the automobiles with no load are shown in Tab. 2.

Tab. 2 Distribution of the weights of the automobiles with no load and driver

No	Automobile	Front axle	Rear axle	Kerb weight, kg	Weight of automobile	
					no load, kg	with load kg
1	Renault Traffic	1130	774	1904	1989	2779
2	Renault Clio II	667	398	1075	1160	1515
3	Volvo V70	826	774	1600	1685	2080

Before the experiment, the force of braking was measured on a roll test bench. The measurements are presented in Tab. 3.

Tab. 3 Force of braking measured on a roll test bench for the automobiles

Automobile	Force of braking, kN			
	Front left wheel	Front right wheel	Rear left wheel	Rear right wheel
Renault Traffic	3.30	3.65	2.07	1.93
Volvo V70	2.47	2.14	2.26	2.82
Renault Clio II	1.58	1.72	1.00	1.13

The experimental results for all tested cars with and without a load are presented in a graph in Fig. 3., Fig. 4. and Fig. 5.

In all the cases, the Renault Traffic, Volvo V70 and Renault Clio performed better without a load than with a load, yet the differences were insignificant. The Renault Traffic braking time with a load was 0.02 s or 1.15% longer than that without a load. The Volvo V70 braking time with a load was 0.11 s or 6.83% longer than that without a load. The braking time for Renault Clio with a load was 0.12 s or 7.36% longer than that without a load.

Without a load, the Volvo V70 had the shortest braking time, 1.61 s, whereas the Renault Traffic had the longest braking time. The Renault Clio II had only a slightly longer braking time. With a load, the braking times for all the automobiles were quite similar, in the range of 1.72-1.76 s. Comparing the braking times measured with and without a load, the largest difference was found for the Renault Clio II that had a drum brake in the rear axle. The smallest differences were found for the Renault Traffic.
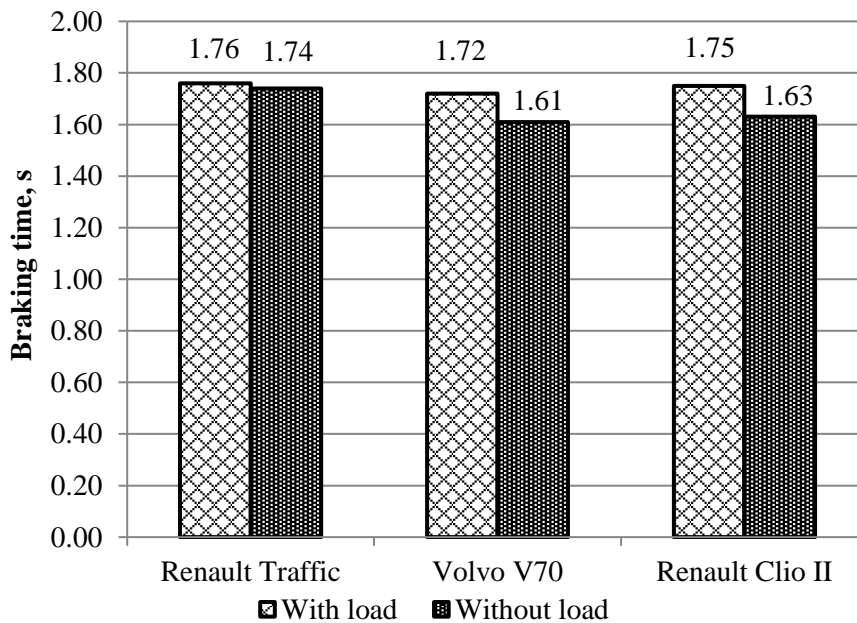
Fig. 3 Comparison of braking times for the experimental automobiles

The braking distances are presented in Fig. 4. Braking distance is one of the most important parameters pertaining to driving safety. The Renault Traffic braking distance with a load was 0.30 m or 2.46% longer than that without a load, but for Volvo V70 the braking distance with a load was 1.06 m or 9% longer than that without a load. The Renault Clio braking distance with a load was 0.73 m or 6.25% longer than that without a load Without a load, the Renault Clio II had the shortest braking distance – 11.68 m. With a load, the Renault Clio II also performed the best – 12.41 m. Performing a comparison of the braking distances with and without a load, the largest difference was found for the Volvo V70, whereas the smallest one – for the Renault Traffic.
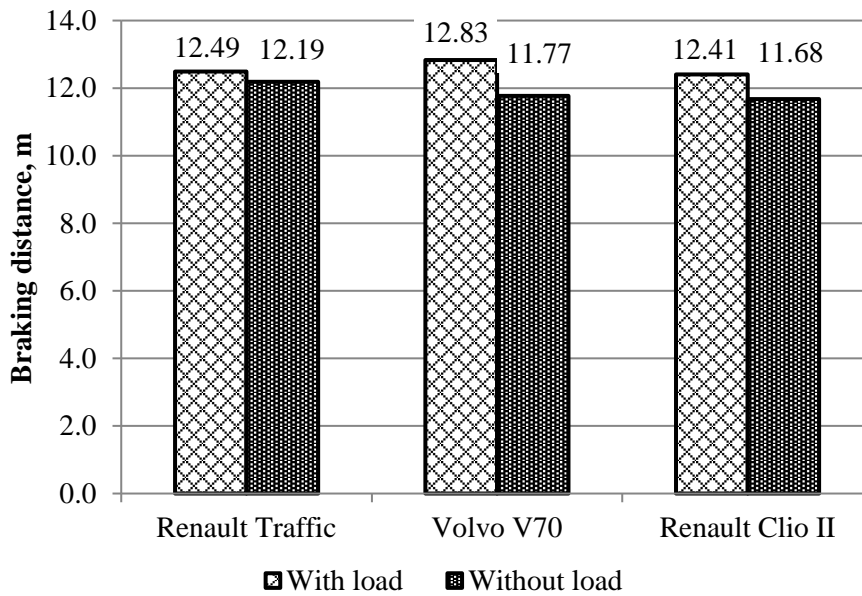
Fig. 4 Comparison of braking distances for the experimental automobiles

Fig. 5 presents data on braking decelerations for all the experimental automobiles. The braking deceleration for Renault Traffic with a load was 0.1 m s^{-1} or 1.25% slower than that without a load, but for Volvo V70 the braking deceleration with a load was 0.51 m s^{-1} or 5.99% slower than that without a load. The braking deceleration for Renault Clio with a load was 0.65 m s^{-1} or 7.59% slower than that without a load. The Volvo V70 had the fastest deceleration, 8.6 m s^{-2}, and the lighter Renault Clio II had almost the same deceleration, 8.57 m s^{-2}, regardless of its simpler rear brake system. With a load, however, the Renault Clio II had a considerably slower deceleration and almost reached that of the Renault Traffic (7.92 and 7.91, respectively).
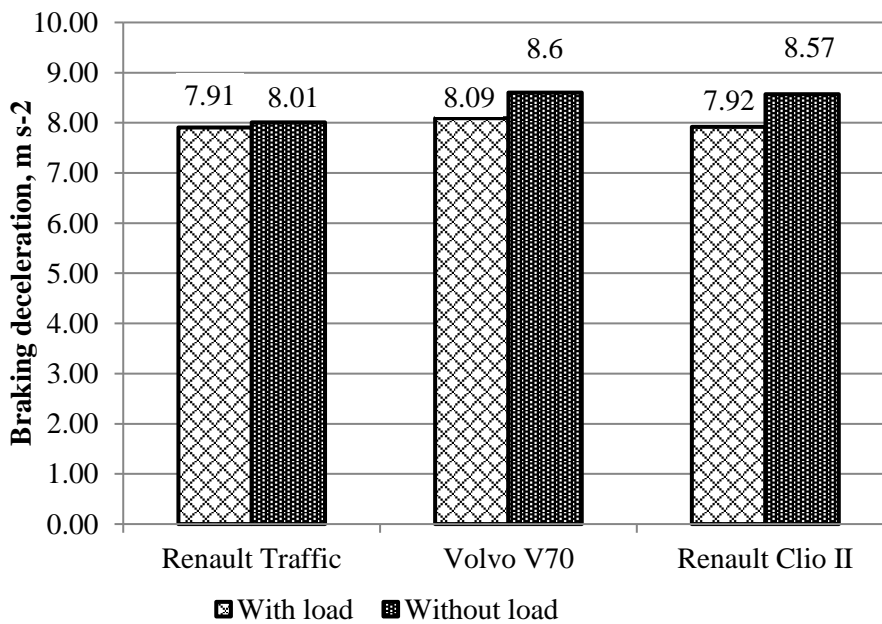
Fig. 5 Comparison of braking distances for the experimental automobiles

The small differences of parameters for Renault Traffic could be explained by the fact that the automobile was in good condition and intended for carrying loads as well. The automobile was initially designed as a freight van, and later it was industrially redesigned into a passenger automobile.

The larger differences of Volvo V70 parameters could be explained by corrosion on rear brake discs. However, the automobile performed the best in terms of force of braking (Table 3).

The decelerations identified in the experiment were similar to those established in investigations by other authors – in the range of 7.91-8.6 m s^2 for automobiles with an ABS *(Sokolovskij, 2017)*. An analysis of average braking parameters for all the automobiles tested revealed that the differences in braking time, distance and deceleration between loaded and non-loaded automobiles were 1-2% less than those reported by other authors *(National, 2003)*.

CONCLUSIONS

1. The research designed and approbated an experimental methodology for identifying braking parameters by use of a scientific radar Stalker ATS.
2. The braking systems of all the experimental automobiles were in good technical condition because the differences in force of braking among the wheels were less than 19.8%.
3. The braking distance of the Renault Traffic was only 2.46% longer with a load than without. The braking time was 1.15% longer, while the deceleration was 1.25% slower. Among all the automobiles, the Renault Traffic performed the best, which could be explained by the appropriateness of it for transporting large loads.
4. The Volvo V70 had a 0.11 s or 6.83% longer braking time, a 9% longer braking distance and a 5.99% slower braking deceleration with a load than without.
5. The Renault Clio II had a 7.36% longer braking time, a 6.25% longer braking distance and a 7.59% slower braking deceleration with a load than without.
6. All the experimental automobiles had, on average, a 5.12% longer braking time, a 5.9% longer braking distance and a 4.94% slower braking deceleration with a load than without. Overall, the changes in braking parameters were relatively small.
7. The experiment demonstrated that without a load, the Renault Clio II had the shortest braking distance – 11.68 m, whereas the Renault Traffic had the longest one – 12.19 m. With a load, the Renault Clio II had the shortest braking distance – 12.41 m, whereas the Volvo V70 had the longest braking distance, 12.83 m.
8. Braking a fully loaded automobile on high-adhesion roads requires applying more force to the brake pedal than necessary for an automobile without a load. This aspect causes a false impression that it takes a longer braking distance and time for the automobile to stop, yet the experiment demonstrated that not a single braking parameter deviated by more 6%.

REFERENCES

1. Berjoza, D. (2008). *Automobile Theory*. Jelgava: LLU.
2. Effects of Tyre Pressure on Braking Distance (in Latvian). (2011). Retrieved from https://www.tvnet.lv/5306624/riepu-spiediena-ietekme-uz-bremzesanas-celu
3. Greibe, P. (2007). *Braking distance, friction and behaviour. Findings, analyses and recommendations based on braking trials.* Lyngby.
4. National Highway Traffic Safety Administration (NHTSA) (2003). Consumer Braking Information.
5. Parczewski, K. (2013). Effect of tyre inflation preassure on the vehicle dynamics during braking manouvre. *Eksploatacja i Niezawodnosc –Maintenance and Reliability*, *15*(2), 134–139.
6. Rievaj, V., Vrabel J., & Hudak A. (2013). Tire inflation pressure on a vehicle stopping distances. *International journal of traffic and transportation engineering*, *2*, 9-13
7. Roos, R., & Zimmermann, M. (2004). *Mogliche Bremsverzogerung in Abhangigkeit von der Griffigkeit*. Univesitat Karlsruhe.
8. Skrucany, T., Vrabel, J., Kendra, M., & Kazimir, P. (2017). Impact of cargo distribution on the vehicle flatback on braking distance in road freight transport. *MATEC Web of Conferences, 134*, 00054.

9. Sokolovskij, E. (2005). Experimental investigation of the braking process of automobiles. *Transport*, *20*(3), 91-95.
10. Wong, J.Y. (2008). *Theory of Ground Vehicles*. 4rd edition Wiley John & Sons, Inc.

Corresponding author:

Dr.sc.ing. Dainis Berjoza, Motor Vehicle Institute, Faculty of Engineering, Latvia University of Life Science and Technologies, 5 Cakstes boulv., Jelgava, LV 3001, Latvia, phone: +371 2935949, e-mail: dainis.berjoza@llu.lv

THE TIME-TEMPERATURE DEPENDENCIES OF POLYCRYSTALLINE PHOTOVOLTAIC MODULE DIFFERENT PARTS

Matúš BILČÍK[1], Monika BOŽIKOVÁ[1], Martin MALÍNEK[1], Patrik KÓSA[2], Marián KIŠEV[2], Juraj BALÁŽI[2], Ana PETROVIĆ[1], Ján CSILLAG[1]

[1]Department of Physics, Faculty of Engineering, Slovak University of Agriculture in Nitra
[2]Department of Electrical Engineering, Automation and Informatics, Slovak University of Agriculture in Nitra

Abstract
The main aim of this research is creation of thermal model for photovoltaic module which is usable in real climatic conditions with localization in Central Europe region. The measuring system for temperature measurement of the photovoltaic module was designed and built at Department of Physics Slovak University of Agriculture in Nitra. Climate characteristics were measured by weather station. The measurements were done during the summer on photovoltaic module. From obtained results is clear that the response of the module temperature is dynamic with irradiance changes, particularly during periods of irradiance fluctuating. Based on the previous facts were made mathematical descriptions of obtained time-temperature and time-irradiance relations. For every graphical relation was obtained polynomial function of the second degree with relatively high coefficients of determination. Temperature model of photovoltaic module was obtained after application of fitting procedure to real dependencies and correlation analysis.

Key words: external factor; relation; solar system; energy.

INTRODUCTION

Solar energy can be directly converted into electrical energy by photovoltaic cells. Photovoltaic have a lot of applications. These applications described author's (*Olejár et al., 2015; Milićević et al., 2012*). The usage of PV system depends on many factors as: solar radiation, ambient temperature, wind speed, material of PV module, composition and mounting structure. Mentioned factors were described by the authors (*Amstrong & Hurley , 2010; Bilčík & Božiková, 2018; Malínek et al., 2018; Libra et al., 2017*). The temperature of PV module especially the temperature of PV cells is important parameter for assessing the long term performance of PV system and its energy production. The authors (*Amstrong & Hurley, 2010; Jones & Underwood, 2001*) reported that PV module efficiency strongly depends on its cells operating temperature. The increasing cell´s temperature has negative influence on the electric power production of PV module (*Duffie & Beckman, 1980; Schott, 1985, Servant, 1985; Cviklovič & Olejár, 2013*). However, in real operating conditions, the temperature measurement of a photovoltaic cell is relatively difficult, so it is more appropriate to measure the surface temperature of PV module active and passive parts. Based on presented facts the main aim of this research was to identify real time-temperature dependencies of the polycrystalline PV module different parts. The next aim of this work is creating the simplified mathematical model for temperature and solar radiation which could be used for prediction operational parameters of PV module. For these measurements was designed and created fully autonomous measuring system with 24 temperature sensors. The measurements were performed on the photovoltaic system, which is located in area of CULS in Czech Republic. The climate parameters were measured by weather station which was located near the PV system.

MATERIALS AND METHODS

For temperature measurement was designed and constructed the measuring system (Fig.1). The measuring system contains these components: 24 temperature sensors with accuracy $\pm$ 0.75 %, control module, communication module, measuring module (B&R, Austria), It works fully automatically. The control software of the measuring system was programmed in Automation Studio. The position of the temperature sensors was chosen according to the temperature changes of the PV module different parts. The temperature changes were detected by the thermovision using the

termocamera Fluke TiR1 (Fluke, USA) (Fig. 2).
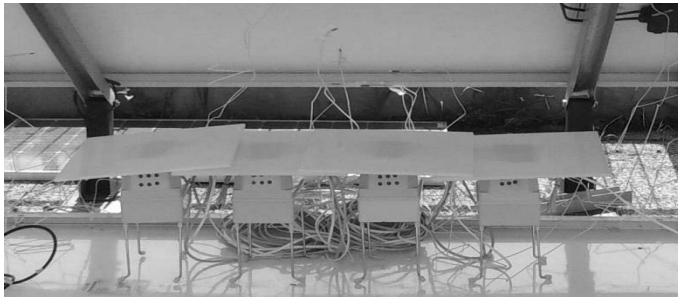
Fig. 1 Measuring system

This weather station measures quantity as: ambient temperature, humidity, air pressure, rainfall, wind velocity, wind direction and global solar radiation. Ambient temperature was measured by sensor HMP45C with accuracy ± 0.5 °C (Vaisala, Inc., Germany). The intensity of solar radiation was detected by pyranometer CM11 with accuracy < 10 W·m^{-2} (Kipp & Zonen, Holland).
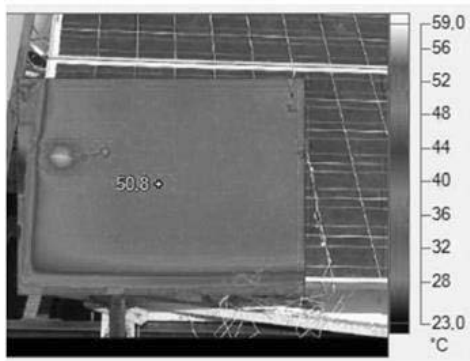
Fig. 2 Identification of temperature changes by termocamera Fluke TiR1

The measurements were performed on the polycrystalline PV module (Yingli Solar, China). The technical parameters of this PV module are presented in Tab. 1. The efficiency of the polycrystalline PV module was 14 %.

Tab. 1 Technical parameters of PV module

Module type	YL230P-29b
Rated maximum power	230 W
Rated voltage	29.5 V
Rated current	7.8 A
Size	1590 mm x 990 mm x 45 mm

RESULTS AND DISCUSSION

At the first were detected the temperature changes by the thermocamera (Fig. 2). These measurements identified differences between upside and downside temperatures of PV module, so the temperatures were measured on the upside parts of PV module and also on downside of PV module. The results of experiments are presented as graphical dependencies. Especially, the time-temperature relations and the relations of global solar radiation intensity in the same time range were identified. The temperature was measured of PV module active part, no active white part of PV module and also in the frame of PV module. The graphical relation on Fig. 3 represents a certain deviation from the expected trend of temperature, which is known from the theoretical models presented in literature (*Amstrong & Hurley, 2010; Jones & Underwood, 2001; Duffie & Beckman, 1980; Schott, 1985; Servant, 1985*).
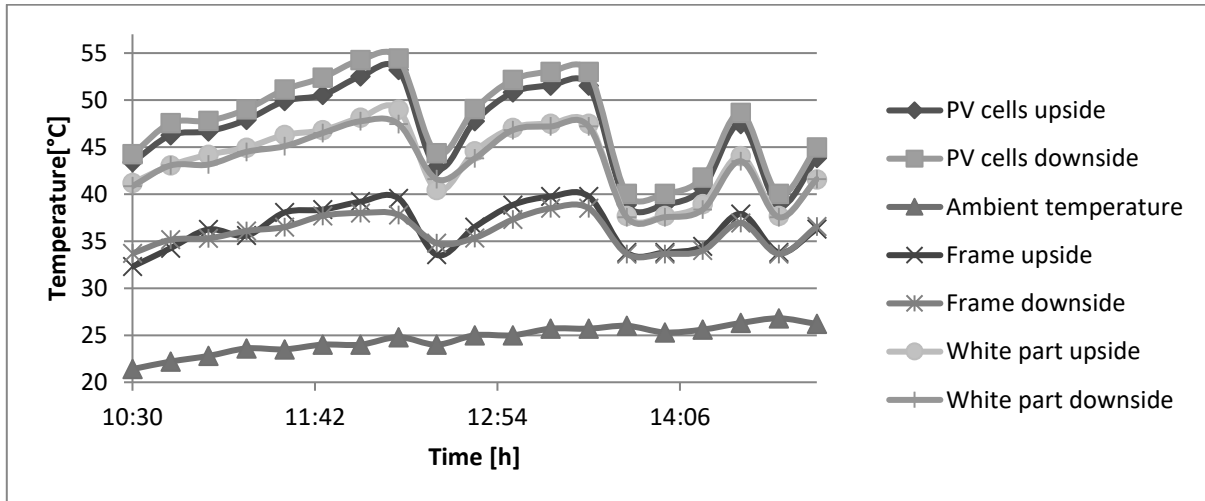
Fig. 3 The time-temperature dependencies of PV module different parts and ambient temperature – real curves

The fitting procedure was applied on the graphical dependences, because from the mathematical point of view it was necessary to smooth out extreme parts of the time-temperature graphical dependences. It eliminates extremes of graphical dependencies which did not correspond to the assumed trend of the graphs.
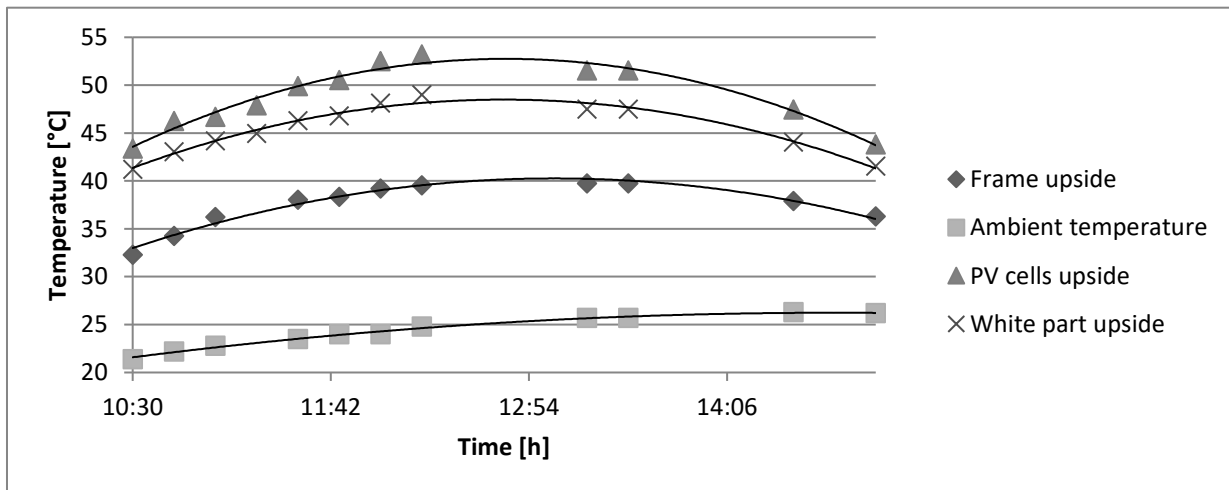
Fig. 4 The time-temperature dependencies of PV module different parts and ambient temperature after fitting procedure and regression analysis

The next step of graphical dependencies processing was regression analysis. The regression analysis allowed the selection of the most appropriate graphical dependence. Based on the descriptive characteristics (coefficients of regression equation, coefficients of determination etc.) of graphical dependencies were selected in all cases the second degree polynomial functions, which are represented by the regression equation (1).

$$T = At^2 + Bt + C \tag{1}$$

Where T – is the temperature of PV module part, t – is time. Coefficients of the regression equation and coefficients of determinations are presented in Tab. 2. In our case was obtained polynomial function for time-temperature relations, but in literature (*Amstrong & Hurley, 2010; Jones & Underwood, 2001; Duffie & Beckman, 1980; Schott, 1985; Servant, 1985*). are presented mainly linear or exponential graphical dependencies.

Tab. 2 Table of statistical coefficients for time-temperature relations

Part of PV module	A	B	C	Coefficients of determinations	Coefficient of correlation	Degree of correlation
PV cells	-1035.7	1101.4	-240.06	0.97	0.34	mild
Frame	-642.8	699.13	-149.84	0.97	0.7	high
White part	-814.68	865.29	-181.27	0.98	0.32	mild

The next part of this research was identifying the influence of the ambient temperature on the temperature of different parts of PV module, so there was performed correlation analysis on all graphical dependencies. The results of correlation analysis are presented in Tab. 2 as coefficients of correlations and degree of correlation. The correlation coefficients were found in the range from 0.32 to 0.7. Especially, the correlation coefficient of 0.34 was found for correlation between the ambient temperature and the temperature of the PV cells, which means middle degree of correlation. The temperature of the PV module frame and ambient temperature correlate on the high degree with a correlation coefficient 0.7 and for the correlation between the temperature of PV module and white area was identified a mild correlation degree with correlation coefficient 0.32. Based on presented results is clear the influence of ambient temperature on the temperature of individual parts of the PV module. This result is new because all known mathematical models presented in literature (*Amstrong & Hurley, 2010; Jones & Underwood, 2001; Duffie & Beckman, 1980; Schott, 1985; Servant, 1985*). assume the constant temperature of all PV module parts which is contrary to the results obtained under real conditions. In the next part of results are presented the time-temperature and solar radiation dependencies. Fig. 6 shows the fluctuations in the intensity of sunshine due to cloudiness change. These fluctuations also affected temperature of PV cells. These extremes were inappropriate for creating of a mathematical model, so fitting procedure was applied.
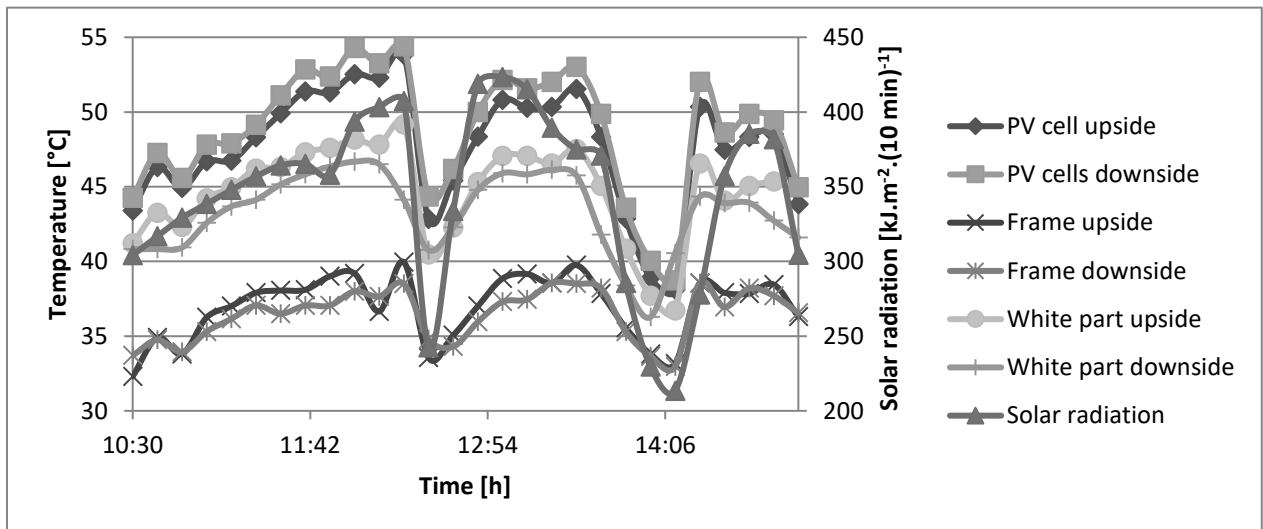
Fig. 5 The time-temperature and solar radiation dependencies – real curves

After fitting procedure were created graphs with smooth curves (Fig. 7.) and by using of regression analysis were chosen model regression equations. The model relations can be described by the polynomial function of second degree (Equation 2).

$$I = Et^2 + Ft + G \qquad\qquad (2)$$

Where I – is the solar radiation, t – is the time. Tab. 3 presents the coefficients of this regression equation and the coefficients of determinations. Determination coefficients are relatively very high, they are from range $R^2 = (0.8 - 0.92)$. The polynomial function of second degree was chosen correctly, not only from the mathematical point of view, but also from the physical theoretical point of view. It

predicts the polynomial progress of temperature relation during the culmination of the sun's intensity.

Tab. 3 Table of statistical coefficients for time relations of solar radiation

Part of PV module	E	F	G	Coefficients of determinations	Coefficient of correlation	Degree of correlation
PV cells	-844.75	909.13	-192.33	0.8	0.8	high
Frame	-590.66	645.21	-135.68	0.92	0.89	high
White part	-542.29	577.58	-105.98	0.82	0.69	high
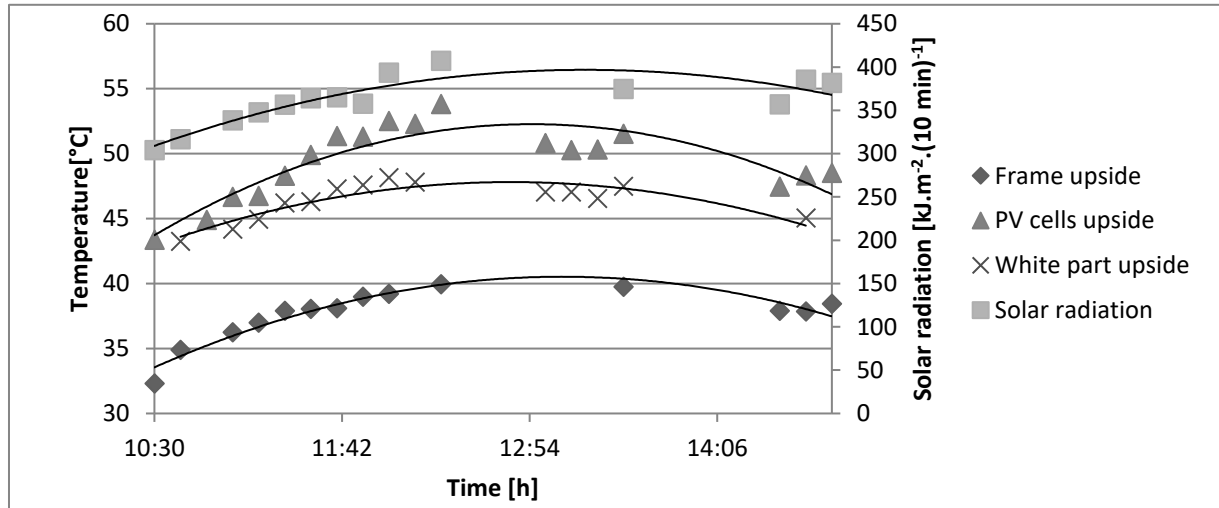
Fig. 6 The time-temperature dependencies of PV module different parts and solar radiation after fitting procedure and regression analysis

A basic correlation analysis was performed for evaluation of graphical dependencies as in previous cases. The correlation between the temperature of PV module different parts and the solar radiation intensity was high with correlation coefficients in range (0.69 - 0.89). The results of the measurement and statistical evaluation of the measured data confirmed from the literature well-known fact, that the intensity of solar radiation most significantly affects the temperature of the PV module.

$$T_m = T_a + \alpha G_T(1 + \beta T_a)(1 - \gamma v_W)(1 - 1.053\eta_c) \qquad (3)$$

The Equation (3) presents temperature model by (*Servant, 1985*) and Equation (6) present temperature model by (*Schott, 1985*). The models for PV module temperature T_m contain physical quantities as ambient temperature T_a , global solar radiation G_T, module electrical efficiency η_c and constant wind velocity v_w with value 1 m·s^{-1}. The parameters in Equations (3) and (6) have values $\alpha = 0.0138$, $\beta = 0.031$, $\gamma = 0.042$ and a, b (Eq. 4, 5) are coefficients of empirical functions of PV and ground emissivities ε_{PV}, ε_g and a cloudiness factor, ε_c.

$$a = 208\varepsilon_{PV} + 297.14\varepsilon_a - 594.3\varepsilon_g \qquad (4)$$

$$b = 6\varepsilon_{PV} + \varepsilon_a - 2\varepsilon_g \qquad (5)$$

$$T_m = T_a + \frac{(\alpha - \eta_c).G_T + (a + bT_a)}{17.8 + 2.1v_w} \qquad (6)$$

Equations (3) and (6) predict temperature of PV module with the linear trend. From presented results is clear that there is high correlation between the intensity of solar radiation and temperature of PV module different parts. From the physical theory is known fact that the culmination of sun intensity has polynomial trend too. It was the main reason for usage the polynomial functions of second degree.

CONCLUSIONS

Results obtained by PV module temperature measurements and measurements of solar radiation intensity confirmed that the reaction of PV module temperature is dynamic in real conditions. This fact is clear for periods where are detected changes of solar radiation intensity which were affected by the cloudiness. The next result is that temperature changes of PV module different parts can be characterized by polynomial function of the second degree. This result was determined by regression analysis of experimental data and by application of the fitting procedure. The significant influence of solar radiation intensity and partial influence of ambient temperature to temperature of polycrystalline PV module was confirmed by correlation analysis. From results is evident, that the temperature of PV module depends on the material of PV module components. The obtained results are in good agreement with the literature (*Amstrong & Hurley, 2010; Jones & Underwood, 2001; Duffie & Beckman, 1980*).

ACKNOWLEDGEMENT

REFERENCES

1   Amstrong, S., & Hurley, W.G. (2010). A thermal model for photovoltaic panels under varying atmospheric conditions. *Applied Thermal Engineering*, *30*, 1488-1495.

2   Bilčík, M., & Božiková, M. (2018). Wind speed and the selected time temperature dependencies for photovoltaic module. *Physics – Applications and Inovations*. SUA in Nitra.

3   Cviklovič, V., & Olejár, M. (2013). Temperature dependence of photovoltaic cells efficiency. In *Trends in agricultural engineering 2013* (pp. 128-131).

4   Duffie, J.A., Beckman, W.A. (1980) *Solar Engineering of Thermal Processes*. New York: John Wiley & Sons.

5   Jones, A.D., & Underwood, C.P. (2001) A thermal model for photovoltaic systems. *Solar Energy*, *70*(4), 349-359.

6   Libra, M., Poulek, & V., Kouřím. P., (2017). Temperature changes of I-V characteristics on photovoltaic cells as consequence of the Fermi energy level shift. *Research in Agricultural Engineering*, *63*(1), 10–15.

7   Malínek, M., Bilčík, M., Božiková, M., Petrović, A., Kotoulek, P., & Hlaváč, P. (2018). The selected time temperature and wind speed dependencies for photovoltaic module. *Journal on Processing and Energy in Agriculture*, *22*(2), 82-84.

9   Milićević, D., Popadić, B., Dumnić, B., Čorba, & Z., Kalić, V. (2012) Possibility of solar potential utilization in Republic of Serbia – practical example. *Journal on Processing and Energy in Agriculture*, *16*(3), 109 – 112.

10   Olejár, M., Cviklovič, V., Hrubý, D., & Lukáč, O. (2015). Autonomous control of biaxial tracking photovoltaic system. *Research in agricultural engineering.* *61*, 48-52.

10   Servant J.M. (1985). Calculation of the cell temperature for photovoltaic modules from climatic data. In *Bilgen E, Hollands KGT, editors. Proceedings of the 9th biennial congress of ISES – Intersol 85* (pp. 370).

11   Schott T. (1985). Operation temperatures of PV modules. In *Proceedings of the sixth E.C. photovoltaic solar energy conference* (pp.392–396).

Corresponding author:
Ing. Matúš Bilčík, Department of Physics, Faculty of Engineering, Slovak University of Agriculture in Nitra, Tr. A. Hlinku 2, SK - 949 76 Nitra, Slovak Republic, phone: +421 917 048 772, e-mail: bilcikmatus@gmail.com

THERMAL ANALYSIS OF POTATO AND CARROT TISSUES AFTER PROCESSING BY PULSED ELECTRIC FIELD

Jiří BLAHOVEC[1], Pavel KOUŘÍM[1]

[1]Department of Physics, Czech University of Life Sciences in Prague, Czech Republic

Abstract
The article is focused on DiElectric thermal analysis of potato and carrot tissues during heating from 30 to 90 °C with possible application of pulsed electric field. Our results show that the temperature scale can be divided into subcritical, critical (70-80 °C) and supercritical parts. Big changes are detected in the critical stage and there are combined with destruction role of the electric field. Destruction role of high temperature and electric field is resulted by the capacity changes in the supercritical change. The observed destruction is higher in potato. This difference can be caused by a destruction role of swelling potato starch.

Key words: dielectric; thermal analysis; model; resistance; capacitance.

INTRODUCTION

The main part of a cooking process used to bring the product texture to such a state that is savoury to a consumer. Recently, the combination of the thermal processing with the application of electric pulses (PEF – pulse electric field: application of short electric pulses of high potential) has been proposed for this purpose (*Blahovec, Lebovka, & Vorobiev 2017*). Previously, it was known that the application of an external pulsing electric field (*Tsong & Su, 1999; De Vito et al., 2008; Vorobiev & Lebovka, 2010*) can damage the integrity of cellular membranes. The disintegration effect of the PEF application to a cellular product is determined by parameters of the pulse procedure, by temperature of the thermal processing and also by the time schedule (*Asavasanti, Stroeve, Barrett, Jernstedt, & Ristenpart, 2012*) of the whole process that is termed pulse protocol.

The important role of temperature as an external parameter for living matter is generally known and there is used as a fundamental technological parameter in cooking of most biological products. There is still lack of information about details of the parallel processes taking place in living cells and tissues during heating (*Vilgis, 2015*). The indirect methods has to be used in this cases, in which only some characteristic states are indicated. For such purposes the methods of thermal analysis (*Haines, 2002*) were developed, provided that specimens' drying due to increasing temperature is prevented (*Blahovec, Lahodová, & Zámečník, 2012; Xu, & Li, 2014*). The combination of electric pulses and simple heating procedures could form a new way of processing in the culinary area and cooking technology. Any reduction of heating in food processing is a source of energy conservation and reduction of food components losses. This is important mainly in fruits and vegetables where heating is followed by losses of vitamins and other unstable important nutrients. Combination of two experimental technics: DMA – Dynamic Mechanical Analysis and DETA – DiElectric Thermal Analysis, see *Haines, 2002*) was used in our previous papers (*Blahovec & Kouřím, 2019a,b*) for studying the changes caused by electric pulses in potato and carrot. It was found that application of PEF causes nontrivial changes of the tested specimens at temperatures 30-90 °C. Even if some changes can be classified as "additive" to the changes caused by temperature, the development some of them can be classified as rather strange (see also *Imaizumi, Tanaka, Hamanaka, Sato & Uchino, 2015; Vorobiev & Lebovka, 2010).*

The aim of this paper is to include some knowledge into differences in behaviour of potato and carrot during their heating in DMA and DETA tests (at temperatures 30-100 °C). For this purpose, the data that were obtained for potato and carrot in two separated research projects in last two years (*Blahovec and Kouřím, 2019a,b*) were used. In these projects, the same PEF protocols were applied to the specimens of the same dimensions so that the obtained electrical parameters can be compared directly.

MATERIALS AND METHODS

The carrots used (variety Jereda) were cultivated in the university garden (for details see *Blahovec & Kouřím, 2019b*) and potatoes were produced by Potato Research Institute in Havlíčkův Brod (Czech Republic) – see *Blahovec & Kouřím, 2019a.*

Rectangular specimens (5.1 - width × 3.8 - thickness × 35 - length) mm with their long axis parallel to the root grow direction were cut from the external part of a root (carrot) or the internal parenchyma (potato) by a knife using special cutting jigs keeping constant the dimensions and the rectangular shape of the specimens. The following procedures were performed with every specimen: measurement of its impedance after its fixation to the DMA tester (see further) at temperature 20 °C (the initial specimen impedance).This measurement gave the initial values of the specimen impedance: real component R_0 and imaginary component X_0. The DMA instrument was arranged so that the electric properties of the tested specimen could be continuously measured as a real conductor described by the complex impedance: an RLC meter (Hameg 8118 with voltage 1 V eff, frequency 20 kHz and 3 sampling per minute) was used for this purpose. The specimen was carefully mechanically fixed in two points so that the longitudinal axis was perpendicular to the fixing jaws. The free length of the specimen between the jaws was 10.8 mm. The height of the fixed specimen was appr. 3.8 mm.

One set of the specimens (5 repetitions) was used for a standard DMA/DETA test (*Blahovec & Kouřím, 2019a*); this set was denoted as the basic, shortly b. One of the jaws was fixed and the other was moving up and down with constant amplitude of 0.5 mm and a frequency of 0.2 Hz in the dynamic cantilever test. The force necessary for the oscillation was recorded, being the basis for the complex modulus determination. Every experiment started at 30 °C. The air humidity in the test chamber (90 %,) was kept constant during the whole experiment. The control of the air humidity in the test chamber was based on direct humidity measurement by a special hygrometer and water vapour ejection into the chamber. The temperature scan proceeded up to 90 °C with a rate of 1 K/min.

The results of the DETA test were analysed on temperature plots of the impedance components: real R_r and imaginary X_r. Also, in this case, we preferred to present the results of our experiments as relative results: $R = R_r/R_0$, and $X = X_r/R_0$, where R_0 is the initial value of the real component of the specimen at 20 °C. This recalculation helps to reduce potential dimensional and surface variations in the prepared specimens. We used simple electrical model of the tested tissues as a parallel connection of a resistor R_e and a capacitor C giving by the following formulas:

$$R_e = \frac{R^2+X^2}{R}; \qquad \omega C = \frac{-X}{R^2+X^2} \qquad (1)$$

where ω is the circular frequency of the electric current.

The specimens included in the sets for further testing (5 repetitions in every case) were removed from the DMA instrument after measurement of the initial impedance (see above) and prepared for PEF loading. It was done in a special equipment between two steel electrodes 2 cm in diameter that were placed in the central parts of the specimen perpendicularly to their 5.1 x 35 mm^2 sides. Pulse loadings were performed using a special equipment: the basic AC sinusoidal signal with a frequency of 20 kHz was modulated into a nearly rectangular form of 10 ms length and height corresponding to the field intensity of 500 V/cm into the tested specimen. In this paper we will limit to the case that was denoted in previous papers (*Blahovec and Kouřím, 2019a,b*) as e: the set of specimens loaded by two pulses with interval 1 s. Using this information, we determined for every specimen its initial parameter R_0 that plays key role of the norm for calculation of R and X after pulsing. Specimens included into set e were tested just after pulsing in the same DMA/DETA combined test as the specimens of the basic test (b).

The results obtained in at least five replications were analysed using the standard laboratory software Origin®, OriginPro Ver. 7 (*OriginLab, Northampton, MA, USA*). The data obtained for a specimen set were unified into a group of data. This group of data was classified according to temperature and analysed sequentially so that the results of all measurements falling into interval of one centigrade increase were evaluated statistically and the corresponding mean values and standard deviations were calculated by a special FORTRAN programme. The applied sampling of data (3 per minute), the rate of heating

(1K/minute) and 5 repetitions of the measurement led to the final statistics of at least 15 measurement for one point/K in the analysed temperature scale. For proving statistical hypotheses 95 % level is used.
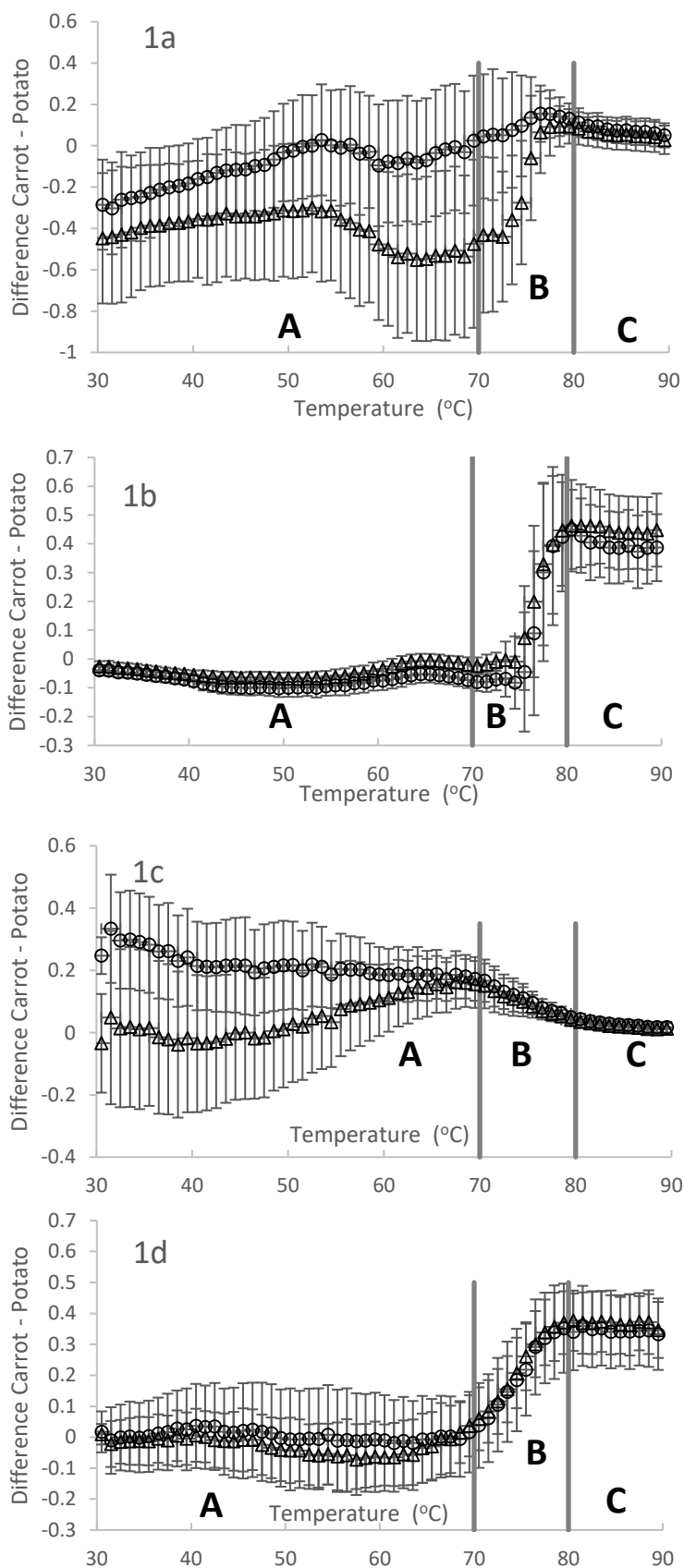
Fig. 1 Difference between values obtained for carrot and the corresponding values for potatoes (triangles mark data for Dali and rings mark data for Agria). The bars represent estimation of standard errors. 1a and 1b: specimens without PEF application, 1c and 1d: specimens after PEF application. 1a and 1c denote R_e; 1b and 1d denote data for capacitance. The marks A, B, and C denote respectively subcritical, critical and supercritical stages in tissue cell wall transformations *(Blahovec & Kouřim, 2019a,b)*.

RESULTS AND DISCUSSION

We will concentrate to differences that we obtained between the values given by Eq. (1) for carrot and potatoes. The resulting data are given in Fig. 1. This figure illustrates either different role of PEF or the potato variety in the DETA plots. Figure 1 shows that the obtained differences in the basic states (without PEF application) are accompanied by a higher level of statistical error at the resistivity of tissue (Fig. 1a) than at its capacitance (Fig. 1b). In stage A and at the lower temperatures in stage B the dispersion of the capacitance data for products without application of PEF is so low that we are able to detect differences in capacitance between different potato varieties: the capacitance of Dali is lower than the capacitance of Agria. The increasing level of statistical dispersion in stage B causes loss of possibility to detect any differences between varieties at higher temperatures. Application of PEF to the tested tissues leads to higher statistical dispersions in the capacitance differences even in the subcritical stage (Fig. 1d) and it also leads to lack of capacitance differences between different potato varieties. At the stage B, there is observed a big change of all differences presented in Fig. 1. Whereas in case of resistance these changes lead to reduction of the differences in the absolute values, in case of capacitance the changes lead to increases of the differences in the positive values. This trend means that in the stage B the differences between carrot and potato in resistance decrease and the opposite change was observed for capacitance differences. Both quantities: the resistance and the capacitance in stage C are approximately constant and of the same value for both potato varieties (see Table 1). But whereas the resistances of all the tested tissues (carrot and two varieties of potato) are approximately the same in stage C (the difference in Table 1 is close to zero in all cases), the capacitance of carrot is much higher than capacitance of potato (Table 1 and Fig. 1b,d). The obtained differences in the capacity of carrot comparing to the potato in stage C indicate that in stage C there still exists some important structural difference between the potato and carrot structures. This difference cannot have important influence on the tissue conductivity whereas it should play the important role in the tissue capacity. Under our opinion, the high difference in capacitance could be caused by the primary cell walls that are destroyed in potatoes in stage B by the swelling starch, but they still exist in carrot. The primary cell walls in carrot can form some structure that is responsible for the observed capacitance differences between potato and carrot (Fig. 1b,c).

The critical stage (B) is typical by destruction of cellular structure, for potato *see Imaizumi et al. (2015)*. Our previous results on potato and carrot (*Blahovec & Kouřím, 2019a,b*) showed that the model capacitance responds in this stage a typical peak that could be reduced by the PEF treatment. The capacitance differences in Figs. 1b, 1c are without any peak, it means that the peak has the same shape either for carrot or potatoes, so that the peaks are cancelled by the applied difference operation.

Tab. 1 Mean carrot-potato differences of model parameters in stage C

Product and parameter	b	e
	Without PEF	With PEF
Dali - R_e	0.054	0.020
Agria - R_e	0.078	0.026
Dali - Capacitance	0.449	0.368
Agria - Capacitance	0.400	0.345

Figure 1 shows that the difference operation gives for R_e variable results that limit our ability to distinguish the variety differences for potatoes. In the basic state (Fig. 1a) and at the initial temperature the plotted difference is less than zero for both potato variety, so that the relative resistance of potato is higher than the relative resistance of carrot. With increasing temperature the plotted difference increases for both potato varieties. In case of Agria we are not able to prove difference in R_e between carrot and potato at temperatures above cca 40 °C. In case of Dali we obtained different results. The difference in R_e between carrot and potato of this variety can be proved at temperatures lower than 75 °C: in this temperature range there is relative resistance of potato variety Dali higher than the relative resistance of carrot. The highest difference in R_e between carrot and potato variety Dali was observed at temperature about 65 °C and in temperature range 50-75 °C it can be proved that R_e in var. Dali is higher than in Agria.

After application PEF the results are little different, because the relative resistance is changed not only in potatoes but also in carrot. At the lowest temperatures, up to about 55 ℃ the relative resistance of Dali behaves similarly as in carrot; after small decrease at higher temperatures (55-80 ℃) it moves to the carrot values in the range C (the resistance difference moves to zero – Fig. 1c, see also Table 1). In case of Agria we observed at low temperatures values of R_e lower than the corresponding values for carrot. The different behavior of Agria and Dali can be proved up to temperature about 55 ℃. After reaching this temperature the relative resistance of Agria behaves similarly as in Dali. It could be concluded that the PEF application leads to reductions of differences between potatoes of different varieties.

CONCLUSIONS

The electric behavior of carrot and potato during its heating up to 90 ℃ can be classified into three stages: subcritical (up to about 70 ℃), critical, and supercritical (above about 80 ℃). The electric properties of the tested products were described by a simple model with parallel connected resistor R_e and capacitor with capacitance ωC. In supercritical stage all parameters are relatively stable, and R_e is approximately the same for all the tested products. This is not true for capacitance: its value for carrot is much higher than for potato (variety difference was not proved). In subcritical stage of the tissues in the basic state, the capacitance is highly stable so that the variety differences can be detected. PEF application leads to the increasing level of statistical dispersion so that no variety differences in the capacitance can be observed. The relative resistance in the subcritical stage is accompanied by a higher level of statistical dispersion even in the basic state. Differences between different varieties can be proved also in the subcritical stage, but only in some special cases.

ACKNOWLEDGMENT

REFERENCES

1. Asavasanti, S., Stroeve, P., Barrett, D.M., Jernstedt, J.A., & Ristenpart, W., (2012). Enhanced electroporation in plant tissues via low frequency pulsed electric fields: Influence of cytoplasmic streaming. *Biotechnological Progress 28*, 445-453.
2. Blahovec, J. & Kouřím, P. (2019a). Pulsed electric stimulated changes in potatoes during their cooking: DMA and DETA analysis. *Journal of Food Engineering 240*, 183-190.
3. Blahovec, J. & Kouřím, P. (2019b). Cooking of carrot previously processed by PEF: DMA and DETA analysis and comparing with Potato. *Innovative Food Science and Emerging Technologies,* in submission.
4. Blahovec, J., Lahodová, M. ,& Zámečník, J., (2012). Potato DMA analysis in area of starch gelatinization. *Food and Bioprocess Technology, 5*, 929–938.
5. Blahovec, J., Lebovka, N. & Vorobiev, E. (2017). Pulsed Electric Fields Pretreatments for the Cooking of Foods. *Food Engineering Reviews 9*, 226-236.
6. De Vito,F.,Ferrari, G., Lebovka, N.I.,Shynkaryk, N.V., & Vorobiev,E., (2008). Pulse duration and efficiency of soft cellular tissue disintegration by pulsed electric fields. *Food Bioprocess Technology 1*, 307-313.
7. Imaizumi, T., Tanaka, F., Hamanaka, D., Sato, Y., & Uchino, T., (2015). Effects of hot water treatment on electrical properties, cell membrane structure and texture of potato tubers. *Journal of Food Engineering 162*, 56-62.
8. Haines, P.J. (2002). *Principles of thermal analysis and calorimetry*. Cambridge: The Royal Society of Chemistry.
9. Ratnayake, W.S., & Jackson, D.S., (2007). A new insight into the gelatinization process of native starches. *Carbohydrate Polymers 67*, 511-529.
10. Ratnayake, W.S., & Jackson, D.S., (2009). Starch Gelatinization. *Advances in Food and Nutrition Research, 55,* 221-268. Elsevier Inc.
11. Schwan, H.P., (1957). Electrical properties of tissue and cell suspensions. *Advances in Biological and Medical Physics 5*, 147-209.
12. Trainito, C., (2015). *Study of cell membrane permeabilization induced by pulsed electric field – electrical modeling and characterization on biochip* [PhD Thesis]. University of Paris-Saclay, 184 pp.

13. Tsong, T.Y., & Su, Z.–D., (1999). Biological effects of electric shock and heat denaturation and oxidation of molecules, membranes, and cellular functions, *Annals New York Academy of Sciences 888*, 211-232.
14. Vilgis T.A. (2015). Soft matter food physics-the physics of food and cooking. *Reports on Progress in Physics 78*, 124602.
15. Vorobiev, E., & Lebovka, N., (2010). Enhanced extraction from solid foods and bio-suspensions by pulsed electric energy. *Food Engineering Reviews 2*, 95-108.
16. Xu, C., & Li, Y., (2014). Development of carrot parenchyma softening during heating detected in vivo by dynamic mechanical analysis. *Food Control 44*, 214-219.

Corresponding author:
Prof. RNDr .Ing. Jiří Blahovec, DrSc., Department of Physics, Faculty of Engineering, Czech University of Life Sciences Prague, Kamýcká 129, Praha 6, Prague, 16521, Czech Republic, phone: +420 22438 4281, e-mail: blahovec@tf.czu.cz

THE EFFECT OF THE CHANGE IN THE COMPOSITION OF THE SUBSTRATE IN THE AGRICULTURAL BIOGAS PLANT ON THE LOGISTICS OF MAIZE CHAFF

Sylwester BOROWSKI[1]

[1]UTP University of Science and Technology, Faculty of Mechanical Engineering, Al. prof. S. Kaliskiego 7, 85-796 Bydgoszcz

Abstract

The paper presents the effect of changing the composition of the substrate on the transport of maize chops to the agricultural biogas plant. The new substrate composition reduced the demand for maize from 25,000 tons to 12,000 tons. Apart from the obvious reduction in the number of transports and the distance traveled, a new delivery model was used. The change in the composition of the sub-plants allowed the reduction of the maize area for the biogas plant. This situation has reduced the maximum transport distance from over 30 km to 25 km in 2017. Maize straw was supplied by an external company with larger transport units. The use of larger transport sets in 2017 resulted in a decrease in the number of kilometers driven even by 59% for a distance of 5.1-10 km. This is directly relevant to the amount of CO_2 produced by biomass transport. However, this solution may cause dissatisfaction among farmers who have previously earned money on biomass transport.

Key words: *transport; biogas power plant; substrates; transport units.*

INTRODUCTION

Biomass of various origins can be used to produce biogas. It must, however, contain more than 30% biodegradable organic matter. The selection of biogas substrates has a significant impact on a number of important factors determining the kinetics of the fermentation process. Maize silage is a particularly useful biogas substrate. The advantage of silage as a substrate for biogas plants is to obtain a relatively large green yield from 1 ha. Not without significance is good susceptibility to ensiling and a large yield of biogas and methane in the anaerobic digestion process. This makes the plant used for energy purposes. The most important positive feature of maize silage is that in the operation of agricultural biogas plants, it ensures biogas production at a stable level and stable operation of the cogeneration unit (*Szlachta & Tupieka 2013*). However, its main disadvantage is the cost of growing corn and producing and transporting chaff (*Borowski et al., 2016, Zastempowski et al., 2013*)

The availability of substrates as close as possible to the installation should determine the size of the biogas plant and the power of the energy equipment. The assessment of raw material resources, their composition and biogas potential is the first step undertaken by the investor. The smallest distance from the installation can be considered for obtaining raw materials with low efficiency, low bulk density or low content of dry matter. In turn, the transport of substrates from larger distances is rational, provided they have a high biogas productivity. According to the Myczko (*2011*) assessment, the profitability of supplying substrates occurs within a radius of 10-30 km from a biogas plant. In turn, Podkówka et al. (*2012*) state that a distance greater than 4 km from a biogas plant means that the cost of transporting maize accounts for over 40% of the total costs of obtaining this substrate.

Each type of biomass requires a different logistic process and raises other problems related to harvesting, processing, storage or delivery. With other devices and barriers, you have to deal with solid biomass processing, and with others with liquid substrates. These difficulties result from the diversity of substrates processed for biogas. For this purpose, the change in the composition of the agricultural biogas plant substrate through the addition of waste is applied. However, such a change may cause a decrease in the quality of biogas (*Kaszkowiak et al., 2017*).

Technologies in the field of biomass use for energy purposes due to its low energy density should be related to distributed generation. The production of electricity and heat should develop in small generating units that use energy crops and agricultural waste (*Jasiulewicz & Janiszewska, 2012*).

This is related to the general trend to limit energy expenditure on biomass production for energy purposes (*Zastempowski et al., 2013, Zastempowski & Bochat, 2016*).

The ideal situation would be to use the raw material at its place of origin. In many cases this is impossible, therefore the transport distance should be as small as possible.

The maize biomass is harvested using a high-efficiency forage harvester, which allows to obtain the grinding of the raw material at a level of approx. 4 mm. Such good fineness allows for high biogas yield and satisfactory organic matter distribution. Maize chop is transported from the field using at least 3 farm tractors and 3 trailers.

The aim of the analysis was to determine the impact of the use of waste biomass from the production of gelatine on the cost of transporting maize biomass due to the reduction in demand for it. The real transport of biomass was taken as the basis for the research.

MATERIALS AND METHODS

Agrarian biogas power plant has been buying raw material (substrate) from farmers from the area around Rypin (Poland). It is maize and slurry. Slurry is collected from pigs farms. Farmers delivering products for biogas generation may in exchange receive postfermentation substance free from harmful substances which can also be used for fields' fertilizations.

Maize for biogas generation, is harvested from about 300 hectares. On average, from 1 ha of corn cultivation about 40 tons of green fodder may be harvested what gives the total sum of about 12000 tons. Demand for maize fell by 50% compared to the previously described situation *(Borowski et al., 2016)*. This situation is caused by the use of waste after the production of gelatin as substrates.

The raw material is colected at the turn of September and October. The harvest and transport of biomass in 2017 were carried out by a commercial external company, independent of the biogas plant. This is a significant difference from the situation in 2013. In that year, transport units were used for transport. In 2017, transport units with a capacity of 23 tons (average) were used for transport.

Then, ensilage is prepared at the territory of the biogas power plant.

Maize ensilage is prepared by green fodder's shredding and pressing. The process of ensilage's forming lasts for about 6 weeks, when by appropriate coverage and cutting off air, earlier prepared corn undergoes the process of ensilaging.

The study analyzed data on changes in the transport of maize biomass in 2017 as compared to 2013. Due to the reduction in the quantity of maize purchased, it is not possible to directly compare changes in the field of transport organization. In 2013, about 25,000 tons of maize chaff were purchased. It was transported by various transport units that belonged to farmers. In 2017, 12,000 tons of maize chaff were purchased. It was transported through large, identical transport units that belonged to one company.

In order to analyze the impact of the organization of transport on the number of transports and the number of kilometers traveled, it was decided to simulate. The simulation consisted in making for 2013 calculation of the number of transports and kilometers driven for the weight of maize chaff purchased in 2017.

RESULTS AND DISCUSSION

The analysis for the purposes of the article was carried out in accordance with the previously described methodology (*Borowski et al., 2016*). For the analysis the field of which was collected biomass was divided because of the distance from the biogas plant. Determined ranges about the size of 5 km.

The amount of the collected biomass (percentage of the total weight) is shown in Fig. 1.

As shown in Figure 1 in 2017, the largest amount of biomass expressed as a percentage was collected within the distance of 5.1-10.0 km from the biogas plant. This result coincides with that obtained in 2013. For 2013, the total amount of purchased biomass was about 25,000 tons. Biomass has been purchased in the entire range of transport decays. In 2017, the total amount of purchased biomass was 12,000 tons. The reduction of the demand for biomass from maize resulted in the rejection of the location above 25 km from the biogas plant.
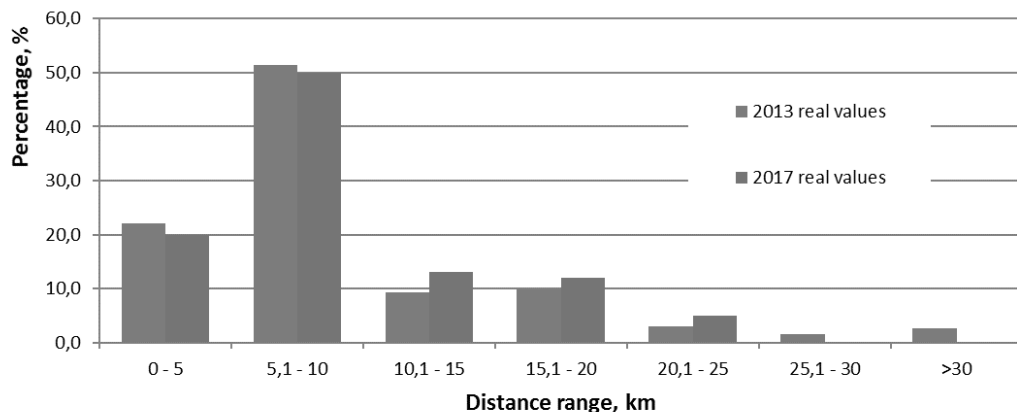
Fig. 1 The amount of biomass collected depending on the transport distance
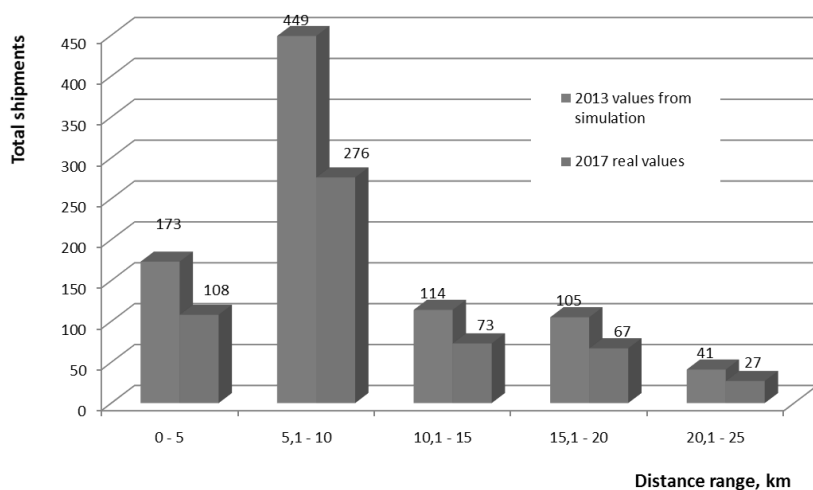
Fig. 2 Comparison of the number of shipments

As can be seen from Figure 2, the use of larger transport units has resulted in a significant reduction in the number of passes. The largest reduction to 59% occurred in the range of 15.1-20 km. This is due to the largest number of fields on which maize was harvested.
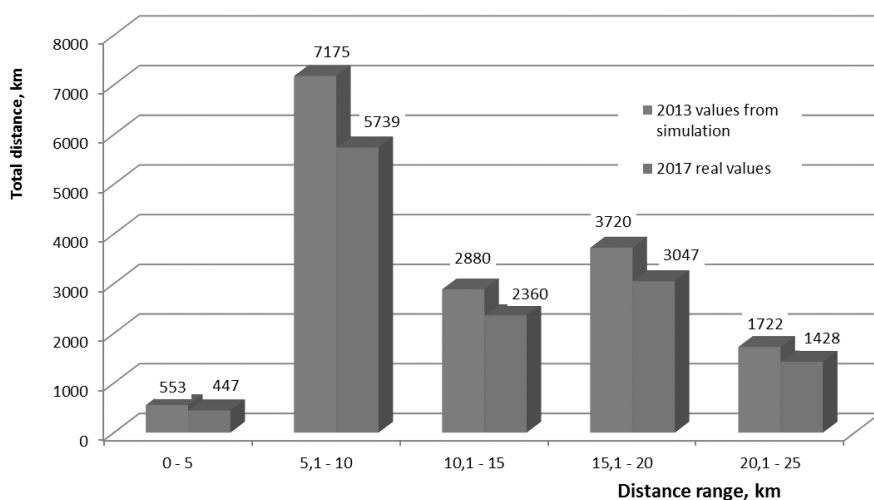
Fig. 3 Comparison of the number of distance

Figure 3 shows the reduction in the number of kilometers driven. In all compartments, the use of a larger transport unit has allowed to reduce the number of kilometers driven to around 80% of the value from 2013.

CONCLUSIONS

The use of waste from gelatin caused a change in the composition of the agricultural biogas plant substrate. In 2017, the amount of purchased biomass from maize was reduced from 25,000 tons to 12,000 tons. This situation has reduced the maximum transport distance to 25 km. A quick delivery model was also used, which involved using an external company to harvest and transport maize chaff. The company has the same, larger transport units. Their use results in a significant reduction in the number of transports and the distance traveled. Any changes introduced had a positive effect on the reduction of CO_2 emissions. However, the calculation of this reduction will constitute a separate scientific work.

REFERENCES

1. Borowski, S., Knopik, L., Markiewicz-Patalon, M., & Brzostek, A. (2016). Assessment of transport substrates for selected agricultural biogas plant. In *Proceedings of 6th international conference on trends in agricultural engineering* (pp. 76-80).
2. Divišová, M., Herák, D., Kabutey, A., Šleger, V., Sigalingging, R., & Svatoňová, T. (2014). Deformation curve characteristics of rapeseeds and sunflower seeds under compression loading. *Scientia agriculturae bohemica, 45*(3), 180-186.
3. Kaszkowiak, J., Borowski, S., Dorszewski, P., & Markiewicz-Patalon, M. (2017). Influence of composition of biogas on selected engine oil values. In *Proceedings of 58th international conference of machine design departments* (pp. 150-153).
4. Myczko A. (red.). (2011). *Budowa i eksploatacja biogazowni rolniczych*. Warszawa-Poznań: ITP.
5. Podkówka, W., Podkówka, Z., Kowalczyk-Juśko, A., & Pasyniuk P. (2012). Biogaz rolniczy – odnawialne źródło energii. Warszawa: PWRiL.
6. Szlachta, J., & Tupieka, M. (2013). Analysis of profitability of maize production designated for silage as a substrate for a biogas plant. *Agricultural Engineering, 3*(145), 375-386.
7. Zastempowski, M. & Bochat, A., (2016). Innovative constructions of cutting and grinding assemblies of agricultural machinery. In *Proceeding of 6th international conference on trends in agricultural engineering 2016* (pp. 726-735).
8. Zastempowski, M., Borowski, S., & Kaszkowiak, J. (2013). New solutions in harvesting plants for power purposes. In *Trends in agricultural engineering 2013* (pp. 673-676).

Corresponding author:
dr inż. Sylwester Borowski, UTP University of Science and Technology, Faculty of Mechanical Engineering, Al. prof. S. Kaliskiego 7, 85-796 Bydgoszcz, e-mail: sylwester.borowski@utp.edu.pl

OBJECTIFICATION OF FMEA METHOD PARAMETERS AND THEIR IMPLEMENTATION ON PRODUCTION ENGINEERING

Marián BUJNA[1], Paweł KIEŁBASA[2]

[1]Department of Quality and Engineering Technologies, Faculty of Engineering, Slovak University of Agriculture
[2]Department of Department of Machinery Management, Ergonomics and Production Processes, Faculty of Production and Power Engineering, University of Agriculture in Krakow

Abstract
We applied the conventional PFMEA (process Failure mode and effect analysis) and identified the RPN risk number on production engineering (the work process on the lathe). Then we added the costs of failures to the method and applied Extended FMEA. After determining the costs and calculations, we identified the ERPN (extended risk priority number). We compared the individual methods and we also compared the proportion of failures in total risk generation (RPN - ERPN). We proposed an action. Finally, we evaluated the applicability of individual methods and models. The ERPN, in contrast to the conventional PFMEA, specifies the risk number. After including the costs necessary for elimination of the failures and costs arising from failures, we have obtained another risk prioritization. The use of the economic effect of the FMEA brings not only an increase in the quality and reduction of defective products, but also the influence of the financial costs on the creation of the risk number.

Key words: PFMEA; extended risk number; increase quality; economic aspect, suggested action.

INTRODUCTION

An FMEA (Failure mode and effect analysis) is an engineering analysis done by a cross-functional team of subject matter experts that thoroughly analyses product designs or manufacturing processes, early in the product development process. Its objective is finding and correcting weaknesses before the product gets into the hands of the customer. (*Jankajová, Kotus, Holota & Zach, 2016; Žitňák, Macák, & Korenko, 2014; Tsai, Zhou, Gao, 2017*).

FMEA being the most widely used risk assessment method in Slovakia and globally in the world, is a part of quality improvement models and methods. Therefore, our findings are used in most manufacturing organizations to improve processes. We can say that the presented methodology, even without modifications, can be used (*Korenko, Földešiová & Beloev, 2015; Girmanová, Šolc, Kliment, Divoková & Mikloš 2017).*

Applying the EFMEA (Extended FMEA) analysis offers a refinement of the results of the conventional PFMEA, which has a significant effect on improving the quality of the resulting products, time savings (less downtime due to malfunctions or failures and subsequent repairs), improving overall safety and, last but not least, reducing operating costs (*Nguyen, Shu, & Shu, 2016; Holota, Hrubec, Kotus, Holienčinová & Čapošová, 2016; Polák, Prístavka & Kollárová, 2015).*

The aim of the paper is to objectivising criteria of FMEA (Failure Mode and Effect Analysis) and consequently their application within our study. The used manufacturing process is the Doosan V-Puma Doom PUMA V550R.

MATERIALS AND METHODS

In this paper, we focused on the risk analysis of the Doosan PUMA V550R lathe (tab. 1).

The component used in brakes in the automotive industry consists of the following processes: preparation of base material, turning (diameters, thickness, grooves), milling, hole drilling, finishing operations, packaging. Our task was to evaluate the production process itself.

The analysis of the work on this lathe was chosen based on the need to reduce the number of defective products. In this post we focused only on turning diameters.

The Doosan Lathe is designed for treating material and performing operations such as:

- external turning - removal of material from the outer surface of the workpiece,
- internal turning - removal of material from the inner surface of the workpiece,
- threading - removal of material from the workpiece surface to form a thread.

Tab. 1 Doosan lathe technical specifications

Manufacturer	Doosan Infracore CO., LTD Korea	Spindle speed	20 - 20 000 RPM
Model type	PUMA V550R	X axis travel	390 mm
Serial No	MT0013-001161	Y axis travel	780 mm
Year	2011	Rapid traverse rates X,Y	12/16 m/min
Power	50.04 kW	Turret	8 positions
Chuck - average	450 mm	Machine weight	ca 9000kg

Basic methodology:
- application of the conventional FMEA process method,
- application of the extended FMEA,
- comparison of the FMEA methods and models and making conclusions.

The minimized steps of applying conventional process FMEA *(IEC 60812:2006)*:
1. Review the process
2. Brainstorm potential failure modes (tab. 3)
3. List potential effects of each failure (tab.3)
4. Determination of failure causes for each single failure (tab. 3)
5. Assign Severity, Occurrence and Detection rankings (tab. 5)
6. Calculate the RPN =Severity x Occurrence x Detection (tab. 5)
7. Take action (tab. 5)

Tab. 2 Minimized rating of severity, occurrence and detection *(IEC 60812:2006)*

No.	Aspect	1	Rating Values -------->	10
1.	Severity	insignificant	-------->	catastrophic
2.	Occurrence	extremely unlikely	-------->	inevitable
3.	Detection	absolutely certain to detect	-------->	no control exists

The steps of ERPN *(Nguyen, Shu, & Shu, 2016).*
1. After we create a PFMEA, we determine - internal failure costs (IFC) - IFC are the costs of scrap, rework, retest, failure analysis, downtime and yield losses, etc.
2. We determine external failure costs (EFC) - as a part of external costs (EFC), we consider cost-free costs; it means a part called WoC – without-casualty costs or CC – casualty costs. This includes the costs of handling complaints from customers that have occurred in almost all cases of failures and are included in this study.
3. We calculate the occurrence probability of the mode – PO (1). PO is based on the classical O (occurrence) parameter and is calculated according to:
$$PO = \frac{O}{10} \tag{1}$$
4. We calculate the detection probability of the mode – PD (2). The PD is based on the conventional D (detection) parameter of the conventional PFMEA.
$$PD = \frac{(10-D)}{9} \tag{2}$$
5. We calculate SI (3)- severity level from an economic perspective in internally dealing with the mode; thus, it closely relates to so-called "internal failure costs IFC".
$$SI = \frac{IFC}{FCmin} \qquad \text{FC}_{min} \text{ - minimum costs by all failures and causes.} \tag{3}$$
6. We calculate SE (4)- severity level from an economic perspective in externally dealing with the

mode.

$$SE = \frac{WoC}{FCmin} \tag{4}$$

7. We calculate SC (5)- severity level of the external failure costs. We place this point in the procedure only if we consider casualty costs – CC.

$$SC = \frac{CC}{FCmin} \tag{5}$$

8. We determine poc - probability of a casualty caused. The _poc_ is either 0 at WoC costs and 1 at CC costs, as there is a breakdown on the machine and a break in the process.

9. Final ERPN (6) calculation for the extended FMEA is calculated according to:

$$ERPN = PO.ST.[PD.SI + (1 - PD).(poc.SC + (1 - poc).SE)] \tag{6}$$

10. All parameters (according to procedure 1-9) will be included into the table 4 and 5.

11. We make conclusions and compare the RPN calculated for the conventional PFMEA with the calculated ERPN (fig. 1).
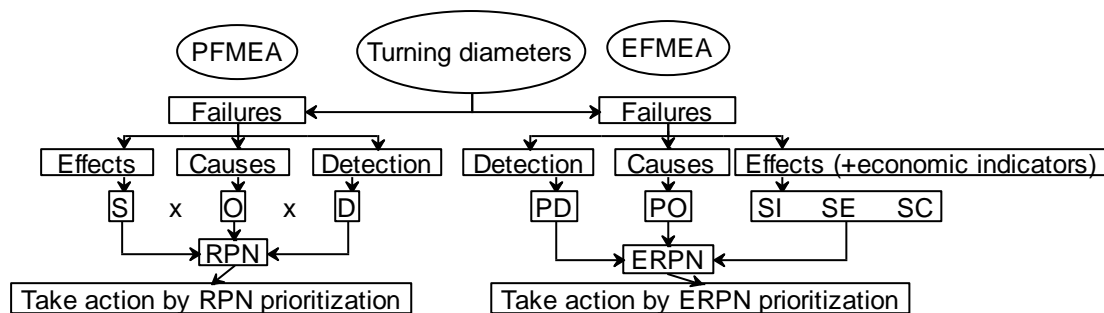
Fig. 1 The steps of PFMEA and EFMEA

RESULTS AND DISCUSSION

When FMEA is applied to a manufacturing process, this procedure is known in industry as the Process FMEA, or PFMEA *(IEC 60812:2006)*.

Based on methodology steps for process FMEA and ERPN we create the table 3, 4 and 5.

Tab. 3 Minimized conventional PFMEA for Operation – Turning diameters *(Bujna, Kotus & Matušeková, 2019)*

Failure	Effects	Causes	Suggested action
Outside diameter is below the tolerance issue	Parts are out of tolerance Customer complaint	Too high feed rate	Set according to the cover sheet
Outside diameter is above the tolerance issue	Customer complaint Scrap Unmountable parts Termination of contract due to frequent complaints	Too low feed rate	Set according to the cover sheet
Inside diameter is below tolerance	Customer complaint Scrap Unmountable parts Termination of contract due to frequent complaints	Cutting blade is worn out	Replace worn out cutting blade. Replace supplier
Inside diameter is above tolerance	Customer complaint Parts are outside specification	Incorrectly chosen measurement method or measurement device	Choose the right measurement method and measuring device
Pitch diameter is below tolerance	Customer complaint Parts are outside specification	Infeed turned off late	Set according to the cover sheet

Thickness of the pitch is above the tolerance	Customer complaint Parts are outside specification	Cutting blade is worn out	Replace worn out cutting blade
Chamfer of the piston ring ID/OD	Rework	The use of manual chamfering	Complete a cover sheet
Concentricity is too high	Customer complaint Parts outside specification	Incorrect measurement methodology	Continuous measurement of units
Pitch radius is too large	Customer complaint Parts are outside specification	Incorrectly selected cutting blade	Set according to the cover sheet
Incorrect chamfer width	Customer complaint Parts are outside specification	Incorrectly set in-feed	Set according to the cover sheet
Roughness height	Customer complaint Parts are outside specification	Feed too high	Set according to the cover sheet
Unturned outer diameter	Rework	Skipped operation	Retrain staff

Tab. 4 Preparatory table for ERPN calculation for operation Turning diameters

Failure	IFC	WOC
Outside diameter is below the tolerance issue	50	110
Outside diameter is above the tolerance issue	105	150
Inside diameter is below tolerance	50	160
Inside diameter is above tolerance	90	110
Pitch diameter is below tolerance	56	110
Thickness of the pitch is above the tolerance	73	110
Chamfer of the piston ring ID/OD	74	140
Concentricity is too high	80	110
Pitch radius is too large	90	110
Incorrect chamfer width	86	110
Roughness height	40	100
Unturned outer diameter	50	140

In the tab. 4 we determined the costs that arise as a result of the Turning diameters operation. Internal costs (IFC) were the costs of scrap, rework, retest, failure analysis, downtime and yield losses, etc. As a part of external costs (EFC), we considered cost-free costs; it means a part called WoC - without-casualty costs. This includes the costs of handling complaints from customers that occurred in almost all cases of failures and are included in this study.

Example for the first line of tab.4:

IFC – by the first failure we assume that the component could be reworked, so no major damage occurs, only the costs for the re-make and a certain time loss – the quantified amount - 50, - €.

FC_{min} – we recorded minimum costs by failure "Roughness height" - 40, - €. FC_{min} is also used to calculate SI (severity level of internal failure costs), SE (severity level of external failure costs), and SC (severity of external fatalities by fatal losses).

WoC represents "no-casualty costs" and are mainly in the form of complaints and handling these complaints. In our study they were of 110, - €.

Tab. 5 Extended FMEA – the determination of ERPN for operation Turning diameters

Failure	Conventional PFMEA - RPN					Extended FMEA - ERPN						
	S(ST)	O	D	RPN	Cl.	PO	PD	SI	SE	poc	ERPN	Cl.
Outside diameter is below the tolerance issue	7	3	4	84	5/6	0.3	0.667	1.25	2.75	0	3.68	8
Outside diameter is above the tolerance issue	9	3	4	108	3	0.3	0.667	2.63	3.75	0	8.10	3
Inside diameter is below tolerance	9	7	2	126	2	0.7	0.889	1.25	4	0	9.80	1
Inside diameter is above tolerance	7	3	2	42	10	0.3	0.889	2.25	2.75	0	4.84	6
Pitch diameter is below tolerance	7	3	5	105	4	0.3	0.556	1.4	2.75	0	4.20	7
Thickness of the pitch is above the tolerance	7	5	2	70	7	0.5	0.889	1.83	2.75	0	6.75	4
Chamfer of the piston ring ID/OD	4	2	6	48	8/9	0.2	0.444	1.85	3.5	0	2.21	12
Concentricity is too high	6	4	2	48	8/9	0.4	0.889	2	2.75	0	5.00	5
Pitch radius is too large	7	2	1	14	12	0.2	1.000	2.25	2.75	0	3.15	9/10
Incorrect chamfer width	7	5	5	175	1	0.5	0.556	2.15	2.75	0	8.46	2
Roughness height	7	3	4	84	5/6	0.3	0.667	1	2.5	0	3.15	9/10
Unturned outer diameter	4	2	2	16	11	0.2	0.889	1.25	3.5	0	1.20	11

If we do not take into account the full external costs, we do not take into account the probability of a casualty caused (poc = 0).

Based on Tab. 5 (it's just part of the whole study) we can say the following conclusions. After the ERPN was determined, we obtained different results than when determining the classical RPN. Importantly, the proportion of individual failures in the overall risk figure was significantly different. As described in the methodology section, the main objective was to reduce the number of defective products in the turning process, where there was the greatest loss in the production. After the introduction of conventional PFMEA, the percentage of defective products decreased from 5.2% to 3.72%. The organization's management was still dissatisfied. We decided to apply an extended FMEA (EFMEA) after a thorough study. EFMEA has only been tested in one particular case in China. Although the application of the EMFEA lasts longer, after a number of staffs training it is a minimum of time losses. It's important to say that by different failures prioritization by ERPN, we focused on suggesting and applying action to failures that were with lower priority solutions by conventional PFMEA.

Benefits of EFMEA:
- Reduction of defective products below 2.5%,
- inclusion of costs in the analysis - an overview of the financial losses for each product failure (defect),
- large use of analysis results,
- significantly reducing of scrap, reworks …,
- increasing operation efficiency.

CONCLUSIONS

Why have we dealt with the ERPN? However, the conventional approach fails to provide satisfactory explanation of the aggregate effects of a failure from different perspectives such as technical severity, economic severity, and production capacity in some practical applications. This can be explained by the fact that the ERPN considers the severity of failures from not only a technical perspective but also an economic one including internal and external costs for any failures undetected before the products are delivered to customers.

Extended FMEA offers an efficient and effective identification of key failure modes. From them, we can easily deduce the root causes and propose corrective measures to reduce the ERPN, there-by minimizing the impact of the failures, or completely eliminating them. Appropriately designed and applied measures increase our production productivity, do not interrupt it and thus do not increase costs. The low failure rate of the processes not only significantly decreases the waste of related resources in terms of materials, labour, and time, thereby reducing the overall cost of the manufacturing operations, but also assures the production capacity and quality of the products, which are actually the key factors for the sustainable survival and development of an industrial manufacturer in the fierce competition market these days. There are several answers why - delivering the product to customers within a specified time, expected product quality, customer confidence, competitiveness.

The benefits of EFMEA are described in the work of Nguyen (*Nguyen, Shu & Shu, 2016*). The performance of their extended index ERPN was tested in an empirical case at a non-woven fabric's manufacturer. Analytical results indicated that the proposed approach (EFMEA - ERPN) outperforms the traditional one (PFMEA - RPN) and remarkably reduces the percentage of defective fabrics from about 2.41% before the trial period to 1.13%, thus significantly reducing wastes and increasing operation efficiency, thereby providing valuable advantages to improve organizational competition power for their sustainable growth.

This study is for the management of engineering technology organizations a sign that the organization prospers.

ACKNOWLEDGMENT

REFERENCES

1. Bujna, M., Kotus, M. & Matušeková, E. (2019). Using the DEMATEL model for the FMEA risk analysis. *Cz OTO 2019*, *1*(1), 550-557. SCIENDO

2. Girmanová, L., Šolc M., Kliment J., Divoková A. & Mikloš V. (2017). Application of Six Sigma Using DMAIC Methodology in the Process of Product Quality Control in Metallurgical Operation. *Acta Technologica Agriculturae. 2*(4). 104-109.

3. Holota, T., Hrubec, J., Kotus, M., Holienčinová, M. & Čapošová, E. (2016). The management of quality costs analysis model. *Serbian journal of management. 11*(1), 119-127. ISSN 1452-4864.

4. ICE 60812:2006 - Analysis Techniques for System Reliability – FMEA.

5. Jankajová, E., Kotus, M., Holota, T. & Zach, M. (2016). Risk assessment of handling loads in production process. *Acta Universitatis Agriculturae et Silviculturae Mendelianae Brunensis. 64*(2) 449-455.

6. Korenko, M., Földešiová, D. & Beloev, Ch. I. (2015). *Risk assessment in quality management*. 1. ed. Ruse: Angel Kanchev University of Ruse, ISBN978-954-712-680-0.

7. Nguyen, T. L., Shu, M. H. & Shu, B. M. (2016). Extended FMEA for sustainable manufacturing: An empirical study in the non-woven fabrics industry. *Sustainability, 8*(9), 939

8. Polák, P., Prístavka, M. & Kollárová, K. (2015). Evaluating the effectiveness of production process using pareto analysis. *Acta technologica agriculturae. 18*(1) 18-21. ISSN 1335-2555.

9. Tsai, S.B, Zhou, J & Gao Y, et al. (2017). Combining FMEA with DEMATEL models to solve production process problems. *ed. Plos One,12*(8):e0183634.

10. Žitňák M., Macák, M. & Korenko, M. (2014). Assessment of risks in implementing automated satellite navigation systems. *Research in agricultural engineering. 60*, 16-24.

Corresponding author:
Ing. Marián Bujna, PhD., Department of Quality and Engineering Technologies, Faculty of Engineering, Slovak University of Agriculture, Tr. A. Hlinku 2, Nitra, 94976, Slovak Republic, phone: +421 641 4762, e-mail: marian.bujna@uniag.sk

INFLUENCE OF MACHINE-TRACTOR SET CONSTRUCTIONAL PARAMETERS ON KINEMATIC DISCREPANCY IN TRACTOR WHEELS

Volodymyr BULGAKOV[1], Valerii ADAMCHUK[2], Volodymyr NADYKTO[3], Volodymyr KYURCHEV[3]

[1]*National University of Life and Environmental Sciences of Ukraine*
[2]*National Scientific Centre "Institute for Agricultural Engineering and Electrification" of Ukraine*
[3]*Tavria State Agrotechnological University, Ukraine*

Abstract
The article discusses methods of influencing a kinematic discrepancy K_v in a tractor with identical wheels as a part of the trailed unit. A net traction of the trailed unit in this case is represented by vertical and horizontal components. While draft resistance must be increased, fulfillment of the condition $K_v = 1$ requires relevant increasing of the air pressure in tractor's wheels. In real using conditions the tractor has to be equipped with a device for automatic changing tires air pressure of the wheels depending of the trailed machine draft resistance. The greater the horizontal component value of the trailed unit net traction, the greater horizontal coordinate application of this component must be shifted to the left relatively to the vertical axle which passes through the rotation center tractor's rear wheels. Ideally, the tractor should have a pendulous mechanism which will keep the value of the kinematic discrepancy K_v close to 1.

Key words: *air pressure; slippage; kinematic discrepancy.*

INTRODUCTION

One of the main trends in the development of modern tractor construction is the four-wheel drive tractors production. The drives of their front and rear axles have a blocked mechanical joint. These axles have the same speed of step forward motion, while the circumferential velocities of the front and rear wheels are usually not equal even if they are of the same size. As a result, due to the difference in the slippage of front (δ_r) and rear (δ_r) tractor wheels a kinematic discrepancy arises, being estimated by the coefficient K_v (*Gurevicius et al.*, 2016).

Analysis of the published articles shows that the researchers mostly emphasized the effect of the coefficient K_v value on the performance of the tractor with different agricultural machines (including trailed). But at the same time, they usually a) considered only horizontal component of the machine draft resistance; b) do not researched the effect of the joining coordinates of the agricultural machine with tractor on realization of the condition $K_v = 1$.

In the paper (*Gurevicius et al.*, 2016) it has been proved that increasing $K_v > 1$ leads to an increase tractor's rolling resistance in all investigated field conditions.

In order to provide, for example, the condition $K_v = 1$ for Case IH Farmall U Pro 115 tractor you should set the air pressure in the front tires of its wheels at 0.7 bar and in the rear tires − 2.3 bar.

The cases, when increasing tractor's rolling resistance under kinematic discrepancy in the drive of its wheels take place, have been given in the papers (*Hegazy and Sandu*, 2013) and (*Damanauskas and Janulevičius*, 2015).

Reducing traction effort and increasing fuel consumption with an increased value of the K_v coefficient have been determined by researchers in the studies (*Senetore and Sandu*, 2011) and (*Molari et al.*, 2012).

The authors Vantsevich and Asme (Vantsevich and Asme, 2014) tried to determine the influence of the kinematic difference in the drive of the tractor wheels not only on its traction characteristics, but also on the stability of movement in the horizontal plane.

As the researchers prove (*Stoilov and Kostadinov*, 2009), the difference in the coefficient $K_v > 1$ is due to the difference in the rolling radii tractor's front and rear wheels. This difference is caused by fluctuations in the vertical load on tractor's axles. Influence changing of the mentioned load on the value of coefficient K_v has been considered in the paper (*Janulevičius et al.*, 2013).

At the same time, the load has been considered by the authors is formed by external forces, having only

vertical direction. Under actually operating conditions of the tractor the external load acting on it has either a horizontal direction or it is inclined to the horizon at some angle (*Bulgakov et al., 2016*).

In this connection, the aim of this work was impact study of the joining coordinates of the agricultural machine with tractor, represented by the horizontal and vertical components of its draft resistance, on the kinematic discrepancy coefficient and to do an experimental review of theoretical research.

MATERIALS AND METHODS

In the paper *(Gurevicius et al., 2016)* it was proposed to determine the kinematic difference coefficient by the following dependence:

$$K_v = (1 - \delta_r) \cdot (1 - \delta_f)^{-1}$$

Very often a different formula is used to calculate this coefficient *(Guskov, 2008)*:

$$K_v = (R_r - \omega_r) \cdot (R_f - \omega_f)^{-1} \qquad (2)$$

where R_r, R_f, and ω_r, ω_f – rolling radius and rotation frequencies of rear and front tractor wheels respectively.

For a tractor with identical front and rear wheels the equation for defining the kinematic discrepancy coefficient ($K_v = 1$) may be calculated from the following equation:

$$K_v = \rho_b \left(2\pi \cdot \rho_a \cdot \sqrt{R_k^3 \cdot r_0} - N_a \right) \cdot \left[\rho_a \left(2\pi \cdot \rho_b \sqrt{R_k^3} \cdot r_0 - N_b \right) \right]^{-1} \qquad (3)$$

where ρ_a, ρ_b – tires air pressure of the front and rear tractor's wheels respectively, MPa; R_k, r_0 – the outer radius and cross-section radius tractor's wheel tire, m; N_a, N_b – the vertical load applied to the front and rear tractor's axles respectively, N.

For the case, when $K_v = 1$ the equation (3) with enough accuracy for practice takes the following form:

$$\rho_b \cdot (\rho_a)^{-1} = N_b \cdot (N_a)^{-1} \qquad (4)$$

As we can see, at the lack of kinematic discrepancy in drive of the tractor running gear with identical wheels, the ratio of the air pressure in their tires is directly proportional to the ratio of the vertical loads on the axles. This leads to significant conclusion. Namely, having got the values of N_a and N_b in advance, it is possible to choose such values of the air pressure in the tractor tires ρ_a and ρ_b that will provide exact fulfillment of the condition (4).

It should be noted that a similar task has been already decided by *(Janulevicius et al., 2014)*. However, the forces they had examined on the tractor were mainly of the vertical direction.

As a practical example of the problem being solved by us, let us consider the procedure for determining N_a and N_b parameters for the trailed version of the machine-tractor set (MTS).

Let us agree, that the trailed MTS in the longitudinal-vertical plane is being affected by horizontal (R_x) and vertical ($R_x \cdot \tan \beta_z$) draft resistance components of the agricultural machine (Fig. 1).
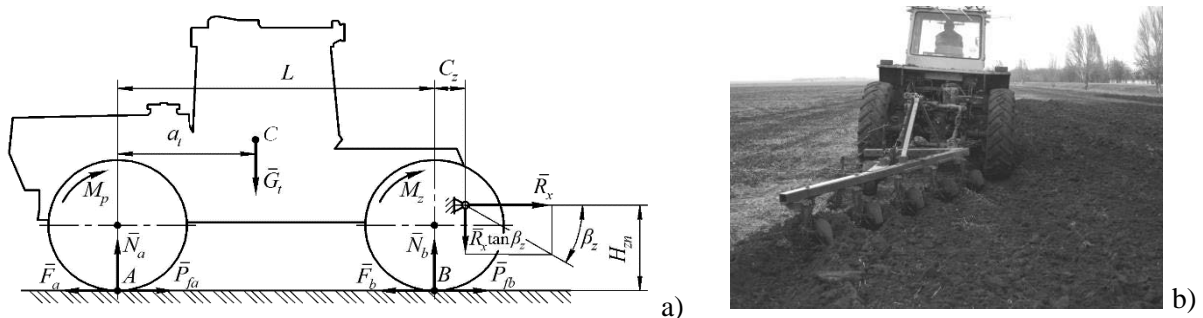
Fig. 1 Trailed version of the machine-tractor set (MTS):
   a)   The scheme of forces acting on the tractor in the longitudinal-vertical plane;
   b)   Tractor HTZ-160 with five-bottom plow PLN-5-35

Brief technical description of the tractor HTZ-160: Total mass (kg) – 8400; Mass on front wheels (kg) – 5000; Mass on rear wheels (kg) – 3400; Wheel base (*L*, mm) – 2860; Tires – 16,9R38; Coordinate a_t (Fig. 1a, m) – 1.16.

Together with the tractor's weight G_t the gross tractions F_a and F_b, the rolling resistances P_{fa} and P_{fb}, as well as the rolling resistance moments M_p and M_z form some distribution of the surface vertical reaction forces N_a and N_b.

To determine the reactions N_a and N_b, as it is well known, it is sufficient use two equations of forces and moments equilibrium acting at MTS under consideration. In this case, such equations can be the sum of the all vertical forces as well as the sum of the moments acting, for example, with respect to point A (see Fig. 1):

$$N_a + N_b - G_t - R_x \cdot \tan \beta_z = 0$$
$$G_t \cdot a_t - N_b \cdot L + R_x \cdot \tan \beta_z \cdot (C_z + L) + R_x \cdot H_{zn} = 0 \tag{5}$$

The essence of the constructional parameters β_z, a_t, L, C_z and H_{zn} have been included in the equation (5), is quite clear from Fig. 1.

The solution of the equations system (5) leads to the following result:

$$N_a = \left[G_t \cdot (L - a_t) - R_x \cdot (\tan \beta \cdot C_z + H_{zn}) \right] \cdot L^{-1}$$
$$N_b = \left[G_t \cdot a_t + R_x \cdot (\tan \beta_z \cdot (C_z + L) + H_{zn}) \right] \cdot L^{-1} \tag{6}$$

Taking into account the formula system (5), the equation (3) takes the form:

$$\rho_b \cdot (\rho_a)^{-1} = \left(G_t \cdot a_t + R_x \left[\tan \beta_z \cdot (C_z + L) + H_{zn} \right] \right) \cdot \left[G_t (L - a_t) - R_x (\tan \beta_z \cdot C_z + H_{zn}) \right]^{-1} \tag{7}$$

The equation (7) as well as formula (2) was used for subsequent calculations.

This formula is absolutely new. It is this one that allows to select such coordinate values of the machine's connection to the tractor, which allow to fulfill the condition $K_v = 1$. At the same time, here both horizontal (R_x) and vertical ($R_x \cdot \tan \beta_z$) components of the agricultural machine draft resistance are taken into account.

The HTZ-160 tractor with the same front and rear wheels (Fig. 2) was taken as the physical object of research. It was used with the five-bottom plow PLN-5-35 (Fig. 1b). Its working width (B_p) is equal 1.75 m.

Fig. 2 Tractor HTZ-160 with the same front and rear wheels

Fig. 3 Tractor's wheel with sensor-hermetic contact

The reliability of equation (7) was determined by the following method. Three options for installing air pressure in the tractor's tires were adopted. In the tires of front axle air pressure was constant and equal $\rho_a = 0.100$ MPa. In the rear axle tires it had three different values: $\rho_b = 0.100$, 0.108 and 0.115 MPa.

From equation (7) for each option of the pressure installation in the tractor's tires the plow's draft resistance horizontal component R_x was determined. The calculations were carried out with the following values of the parameters incoming into the equation (7): $G_t = 82.4$ kN; $a_t = 1.16$ m; $L = 2.86$ m. $C_z = 0.58$ m; $H_{zn} = 0.6$ m; $\beta_z = 8°$.

Parameter β_z – it is inclination angle of the lower links of the tractor's three-point hitch linkage during its work with plow. The value of this parameter was determined by protractor while plowing set was stopped.

Tractor's weight G_t was determined by weighting it with a dynamometer DPU-5. The measurement accuracy was equal 0.5 kN.

Plow draft resistance (R_x) and plowing depth (h) are connected by such well-known equation:

$$R_x = K_o \cdot h \cdot B_p, \tag{8}$$

where K_o – specific plow's draft resistance. According to our research the mean of this parameter in the soil conditions of south Ukraine, for example, is equal 65 kN·m^{-2}.

For each values of force R_x the plowing width from formula (8) was determined. In field conditions the plow was adjusted to three tillage depths (22, 26 and 28 cm). The experiments were performed on soil with a moisture content of 15.4% and a density of 1.28 g·cm^{-3}.

In each adjusting option the plowing set moved on the test section of 200 m each. The replication of each experiment was threefold. After each pass of the plowing set the real plowing depth and value of the cinematic discrepancy K_v were measured.

For the tractor with identical wheels equation (2) taking into account equation (4) looks like this:

$$K_v = \omega_r \cdot \left(\omega_f\right)^{-1} \tag{9}$$

For measuring wheels rotation frequencies (ω_r, ω_f) we used sensor-hermetic contacts (Fig. 3). The electrical signal from them was given by analog-to-digital converter and were transferred to a computer, where the main statistical characteristics were determined.

The real values of the coefficient K_v, calculated using the formula (9), were compared with 1. After this the decision was made on the adequacy of the equation (7).

In the end, using equation (7), we established the laws of such a choice of parameters ρ_a, ρ_b, C_z and H_{zn} that would ensure the fulfillment of the condition $K_v = 1$.

The following statistical characteristics were calculated for the data obtained during the experimental studies: average value; mean square deviation σ and the coefficient of variation v.

RESULTS AND DISCUSSION

Analysis of the experimental data shown that plowing depth real values were in such confidence intervals: a) for the first plow adjustment option – 22.3±1.2 cm; b) for second one – 26.4±2.1 cm; c) for third one – 29.8±1.3 cm. All variation coefficient do not exceed 8%.

Tab. 1 Results of determining the actual depth of ploughing

Indicator	Processing results		
	Plot 1	Plot 2	Plot 3
Specified depth, cm	22	26	28
Average value, cm	22.3	26.4	29.8
Average square deviation σ, cm	1.2	2.1	1.3
Coefficient of variation v, %	5.38	7.95	4.36

As a result, for all options of plowing depth the calculated values of the coefficient K_v is very close to 1 (Fig. 4). The maximum difference of the compared data does not exceed 1.4%.
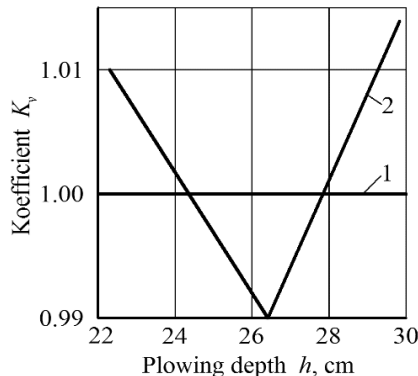
Fig. 4 Deviation of the coefficient K_v values (2) from $K_v = 1$ (1) at different plowing depth

This, as statement in article (Damanauskas, 2018), is almost perfect result. In this study it allows us to consider the equation (7) adequate and therefore suitable for use in further analysis.

Ensuring of the condition $K_v = 1$ while the draft traction is acting ($R_x \neq 0$) may be reached by means of corresponding air pressure increase in the tractor's rear tires (ρ_b) or decrease in front ones (ρ_a) (Fig. 5).

Let us try to analyze the dependence presented in Fig. 5. The average value of the trailed agricultural machine draft resistance, for example, is $R_x = 36$ kN. As practice shows, such value of the tractor HTZ-160 net traction is typical when it using with a majority of a tillage machines. Furthermore, an oscillation variation coefficient of the force R_x is an average of 10%. This means that the draft resistance of the trailed machine will vary within the range from 32 to 40 kN. But in this case, as it follows from Fig. 5, the air pressure in the rear tires of the tractor should vary from 0.128 to 0.148 MPa. In the tractor's front tires the air pressure should decrease from 0.112 to 0.098 MPa.

The horizontal (R_x) and vertical ($R_x \cdot \tan \beta_z$) components of the trailer traction resistance are applied to the tractor at the point with C_z and H_{zn} coordinates (Fig. 1).

As calculations of the formulae system (7) show, the dependence of the H_{zn} parameter from the value of draft resistance (R_x) is insignificant (Fig. 6). Namely, with an increasing R_x force from 30 to 40 kN and providing the condition $K_v = 1$, H_{zn} value decreases at 16 cm only (Fig. 6).
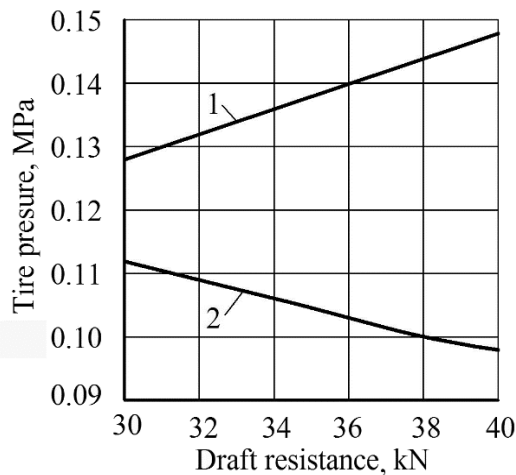
Fig. 5 Influence draft resistance of trailed agricultural machine on air pressure in tractor's rear (1) and front (2) tires
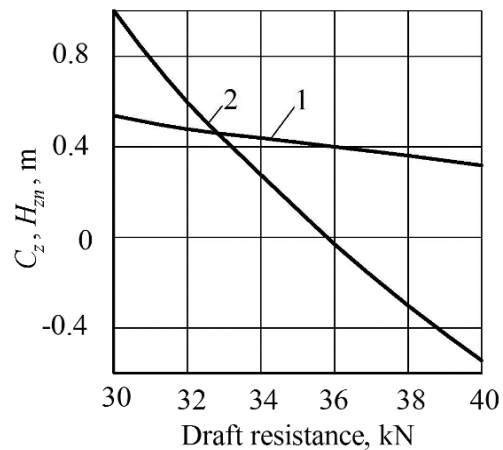
Fig. 6 Influence draft resistance of trailed agricultural machine (R_x) on H_{zn} (1) and C_z (2) parameters

But we have absolutely different situation with the parameter C_z. By means of calculations of the formulae system (6) it has been found that if $R_x = 30$ kN, then the value of C_z is equal 1 m (Fig. 6).

As the value of the force R_x increases, the horizontal coordinate of the application of the trailer traction resistance must be shifted to the left of the vertical axis passing through the rotation center of the tractor rear wheels. For the case of $R_x = 40$ kN this displacement should be 0.55 m ($C_z = -0.55$ m, Fig. 6).

This result may testify that the tractor should have a mechanism for automatic longitudinal displacement of the trailer attachment point to it. The value of this displacement depends from the draft resistance of the agricultural machine.

In practice such the constructional decision can be carried out by means of the well-known pendulous mechanism. As a result, it enables to keep the kinematic discrepancy K_v value in a value close to 1.

CONCLUSIONS

1. The mathematical model, allowing to define the coefficient of kinematic discrepancy of K_v of wheeled all-wheel drive tractor axles by changing some construction parameters is developed.

2. Experimental studies have confirmed the adequacy of the presented mathematical model. At application of the recommended constructional parameters the coefficient of kinematic discrepancy K_v is close to one.

3. To ensure the condition $K_v = 1$ increasing of the trailed machine draft resistance requires a corresponding change of the air pressure in tractor's front and rear tires. Namely, the bigger trailed machine's draft resistance, the bigger air pressure in tractor's rear tires and lower in the front ones.

4. Under the real conditions of the tractor operation it should be equipped with a device that automatically changes the air pressure in the tires of its wheels depending on the value of the trailed machine draft resistance.

REFERENCES

1. Bulgakov, V., Adamchuk, V., Arak, M., Nadykto, V., Kyurchev, V., & Olt, J., (2016). Theory of vertical oscillations and dynamic stability of combined tractor-implement unit. *Agron. Res. 14*, 689–710.

2. Damanauskas, V. & Janulevičius, A., (2015). Differences in tractor performance parameters between single-wheel 4WD and dual-wheel 2WD driving systems. *J. Terramechanics 60*, 63–73. doi: https://doi.org/10.1016/j.jterra.2015.06.001.

3. Damanauskas, V. & Janulevičius, A., (2015). Differences in tractor performance parameters between single-wheel 4WD and dual-wheel 2WD driving systems. *J. Terramechanics 60*, 63–73. doi: https://doi.org/10.1016/j.jterra.2015.06.001.

4. Gurevicius, P., Janulevicius, A., & Pupinis, G., (2016). Kinematic discrepency and moving resistance dependance on tires air pressure in 4X4 tractors, in: Malinovska, L., Osadcuks, V. (Eds.), *15th International Scientific Conference: Engineering for Rural Development, Engineering for Rural Development. Latvia Univ Agriculture, Jelgava* (pp. 574–578).

5. Guskov, A.V., (2008) Opredeleniye ratsionalnogo koeffitsienta kinematicheskogo nesootvetstviya i skhemy privoda vedushchikh mostov kolesnogo traktora. *Vestn. BNTU 8*, 64–67.

6. Hegazy, S., & Sandu, C., 2013. Experimental investigation of vehicle mobility using a novel wheel mobility number. *J. Terramechanics 50*, 303–310. doi: https://doi.org/10.1016/j.jterra.2013.09.005

7. Janulevičius, A., Pupinis, G., & Damanauskas, V., (2013). Effect of Tire'S Pressure on the Kinematic Mismatch of Four Wheel Drive Tractor. *Mechanika 19*, 73–80.

8. Janulevicius, A., Pupinis, G., & Kurkauskas, V., (2014). How driving wheels of front-loaded tractor interact with the terrain depending on tire pressures. *J. Terramechanics 53*, 83–92. doi: https://doi.org/10.1016/j.jterra.2014.03.008.

9. Molari, G., Bellentani, L., Guarnieri, A., Walker, M., & Sedoni, E., (2012). Performance of an agricultural tractor fitted with rubber tracks. *Biosyst. Eng. 111*, 57–63. doi: https://doi.org/10.1016/j.biosystemseng.2011.10.008.

10. Okunev, G.A., Kuznetsov, N.A., & Brazhnikov, A.V., (2014). Substantiation of the air pressure in the tires of HTZ-150K-09 tractor at field works. *Vestn. Chelyabinskoy Gos. agroinzhenernoy Akad*. 70, 99–107.

11. Senetore, C. & Sandu, C., (2011). Torque distribution influence on tractive efficiency and mobility of off road wheeled vehicles. *J. Terramechanics* 372–383.

12. Stoilov, S. & Kostadinov, G.D., (2009). Effect of weight distribution on the slip efficiency of a four-wheel-drive skidder. *Biosyst. Eng.* 104, 486–492. doi: https://doi.org/10.1016/j.biosystemseng.2009.08.011.

13. Vantsevich, V. & Asme, V. (2014). AWD vehicle dynamics and energy efficiency improvement by means of interaxle driveline and sreering active fusion. In *Proceedings of the Asme International Design Engineering Technical Conferences and Computers and Information in Engineering Conference, 2013*, vol. 1. New York: Amer Soc Mechanical Engineers.

Corresponding author:
Volodymyr BULGAKOV, Ph.D., Department of Mechanics, National University of Life and Environmental Sciences of Ukraine, Heroiv Oborony Str.15, Kyiv, 03041, Ukraine phone: +380 44 527-82-63, e-mail: vbulgakov@meta.ua

THE IMPACT OF MULCHING MATERIALS ON THE SOIL MOISTURE DYNAMICS IN CENTRAL EUROPEAN VINEYARDS

Patrik BURG[1], Alice ČÍŽKOVÁ[1], Vladimír MAŠÁN[1], Jana BURGOVÁ[2], Bożena GŁADYSZEWSKA[3]

[1]*Department of Horticultural Machinery, Faculty of Horticulture, Mendel University in Brno, Czech Republic*
[2]*Department of Breeding and Propagation of Horticultural Plants, Faculty of Horticulture, Mendel University in Brno, Czech Republic*
[3]*Department of Biophysics, Faculty of Production Engineering, University of Life Science in Lublin, Poland*

Abstract
This study discusses the evaluation of moisture changes in soil in the area of the vineyard intersection that is covered with different kinds of mulching materials. The experiment was based on four variants in which three kinds of covering materials were chosen to protect the soil surface – grain straw (var. A: the consumption of cover material - 12 t per ha⁻¹) and wood chips (var. B: the consumption of cover material - 40 t per ha⁻¹) and compost (var. D: the consumption of cover material - 20 t per ha⁻¹). The fourth control variant (C) was formed from a cultured spacing without intersection covering material. The soil moisture was measured all year round by using VIRRIB moisture meters located at a depth of 0.1-0.3 m. The measured data was recorded by using a VIRRIBLOGGER recording unit. Analysis of the results obtained confirms the positive effect of grain straw on higher soil moisture values. In this variant, in 2017, soil moisture was higher by 4.37 % and in 2018 by 10.37 % compared to the control variant. In overall, the highest soil moisture values, over a two-year period, were achieved with grain straw and wood chips.

Key words: soil moisture; mulching; grain straw; wood chips; vineyard.

INTRODUCTION

The soil water containing dissolved mineral and organic substances and its efficient use are critical to the sustainable productivity of permanent crops under the context of climate change in typical semiarid regions (*Li et al., 2018*). Water shortage especially during reproductive stage can significantly reduce the yield and quality of fruit (*Li et al., 2016*). Therefore, in order to ensure sustainable production, new methods and procedures are being sought and used in intensive production areas, enabling maximum utilization and retention of natural rainfall in the soil profile. These include, for example, terracing, ridge tillage, changing the gradient, slope length, and roughness of slopes. Moreover, in recent years, increasingly, there have been also used the methods of mulching.

Mulching is referred to as the agronomic practice of leaving mulch on the soil surface for soil and water conservation and to favour plant growth (*Jordán et al., 2011*). The covering layer of mulch represents any material other than soil or living vegetation that performs the function of a permanent or semi-permanent protective cover over the soil surface *(Jordán et al., 2011)*. Therefore, for the mulching purposes, there might be different kinds of materials, such as vegetative residues, biological geotextiles, gravel and crushed stones (*Jiménez et al., 2016*). Mulching has been shown to confer several beneficial effects. Furthermore, mulching allows improved infiltration capacity (*Wang et al., 2016*) and increases water intake and supplies of usable water in the soil *(Mulumba & Lal, 2008)*. Experimental measurements shows that mulching positively influences the topsoil temperature for more optimal growth and development of the plant roots (*Dahiya, Ingwersen & Streck, 2007*) and to decrease evaporation (*Cerdà & Doerr, 2005*). Among these beneficial mulching effects, the reduction of water loss rates is one of the most significant and remarkable (*Díaz-Raviña et al., 2012; Prosdocimi et al., 2016*).
The aim of this work was to evaluate the different influence of mulching materials covering the soil, on the dynamics of changes within the soil moisture in the Central European vineyards.

MATERIALS AND METHODS

Experimental site

For experimental measurements, specific test site, in the south of the Czech Republic, was selected. This was wine-growing sub-region "Velke Pavlovice", the area of "Rakvice", the track / land called "Kozi Horky" (Latitude: 48°51′29″N, Longitude: 16°48′48″E). This site is in the corn production area, where the climate is very warm and dry, with an altitude of 164 meters above the sea level. The land has a flat surface. The average annual temperature in 2017 was 12.3 °C and the total rainfall was 480.0 mm. In 2018, the average annual temperature was 12.5 °C and the total rainfall was 512.8 mm. In terms of the amount of natural rainfall, it is a typical semiarid region, with an annual precipitation of around 450-550 mm.

The soils are classified as a pelic chernozem on very heavy substrates (clays, marshes, carpathian flysch and tertiary sediments), on a scale from heavy to very heavy with a lighter horizon, rarely gravely, with a tendency of moisture on the surface in the profile. Skimmer is classified from none up to 10 %. The slope of the land is up to 10 %.

At the beginning of the vegetation, the initial physical state of the soil was always detected at the site using "Kopecky physical cylinders", the samples were analysed using a valid methodology (*Jandák, 2003*). Samples were taken at five reps from each depth the resulting values are provided in Tab.1 and Tab.2.

Tab. 1 Physical character of soil (at the beginning of vegetation in 2017)

| Soil depth (m) | Density (g·cm⁻³) | Porosity (%) | Volume | | Maximum capillary capacity | Minimal air capacity |
| | | | Water | Air | | |
			(% volume)		(% volume)	
0–0.1	1.05	59.95	59.95	25.40	34.55	45.91
0.1–0.2	1.23	53.23	53.23	26.47	26.76	37.48
0.2–0.3	1.29	50.95	50.95	24.13	26.83	36.99
Average	1.19	54.71	54.71	25.33	29.38	40.13

Tab. 2 Physical character of soil (at the beginning of vegetation in 2018)

| Soil depth (m) | Density (g·cm⁻³) | Porosity (%) | Volume | | Maximum capillary capacity | Minimal air capacity |
| | | | Water | Air | | |
			(% volume)		(% volume)	
0–0.1	1.39	47.11	23.66	23.45	35.83	11.28
0.1–0.2	1.36	48.14	24.01	24.13	36.09	12.06
0.2–0.3	1.42	45.64	26.40	19.24	35.41	10.23
Average	1.39	46.96	24.69	22.27	35.78	11.19

Character of the mulching materials and experiment variants

The experiment was based on four variants, for which three kinds of cover material were chosen to cover of soil cover by the layer of mulching material. The area of tested plots were 13.8 m² (2.3 x 6.0 m), the first mulching material was crushed grain straw (variant A) when consumption of covering material was 1.200 g·m⁻² and volume weight was 100 kg·m⁻³. The second mulching material was wood chips (variant B) when consumption of cover material was 4.000 g·m⁻² and volume weight was 400 kg·m⁻³. And the third mulching material was compost made from grape pomace, grass, wood chips and vegetable waste (variant D). The consumption of covering material at this variant was 2.000 g·m⁻² and volume weight was 560 kg·m⁻³. The fourth control variant (C) consisted of a cultivated interlayer without covering material.

Measuring of the meteorological data and soil moisture

A weather station installed in the experimental vineyard recorded data on air and soil temperature, rainfall and soil moisture at a depth in between 0.1 and 0.3 m. In all experimental variants, the soil moisture values were measured by "VIRRIB" moisture meters, located at a depth in between 0.1 and

0.3 m. The soil moisture expressed as a percentage by weight was recorded during the vegetation every day at a regular fifteen-minute intervals using the "VIRRIBLOGGER" recording unit.

Statistical analysis
A statistical analysis was performed using the software package "Statistics 12.0" (StatSoft Inc., Tulsa, Oklahoma, USA). Analysis of variance was conducted, and the results were compared using Tukey's multiple range assay at a significance level $\alpha = 0.05$.

RESULTS AND DISCUSSION
The Figure 1 and Figure 2 show all year round values of soil moisture, air temperature and natural rainfall distribution at experimental site. The highest soil moisture was recorded, in both years, in variants that use crushed grain straw as a mulching material covering the soil. In 2017, the average value of soil moisture was 26.95 %, in 2018 the average value of soil moisture was 32.28 %.
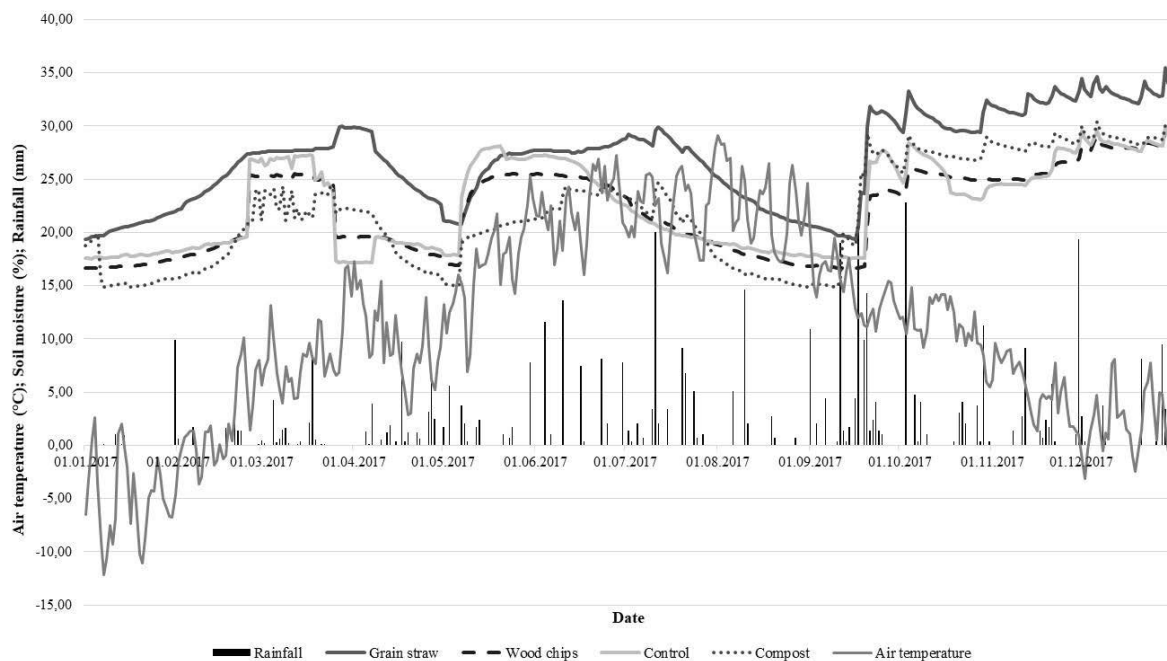
Fig. 1 The value of air temperature, soil moisture and rainfalls in 2017

The Fig. 1, as well as the Fig. 2 show the uneven distribution of rainfall, especially during vegetation. *Vanek (1996)* reports that in terms of water consumption for wine, the starkest period is from June to August. Fig. 3 shows in detail the monthly rainfall sums for both evaluated years. From the values it is clear that there is a higher amount of precipitation especially at the time of harvest or after harvest, but not during the critical period for grapevine.

According to *Vanek (1996)*, depending on the intensity of foliage, the wine shrub consumes 3-7 litres of water per day, which corresponds to approximately 90-210 litres of water per month. However, the monthly rainfall shows that this amount of water needed for wine shrubs is not fully covered, which results in stress conditions. This trend can be further multiplied by vineyards growing on sloping land. The reason for this is the higher risk of surface runaway of water that is not retained by the soil (*Čížková et al., 2018*).
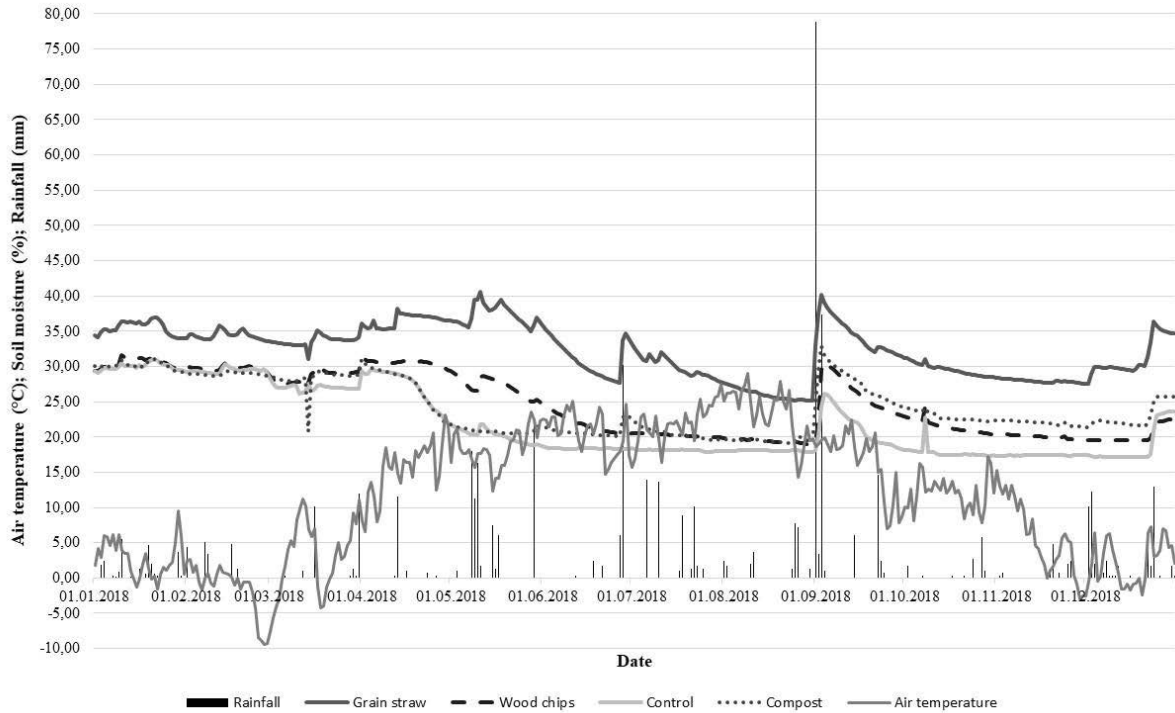
Fig. 2 The value of air temperature, soil moisture and rainfalls in 2018
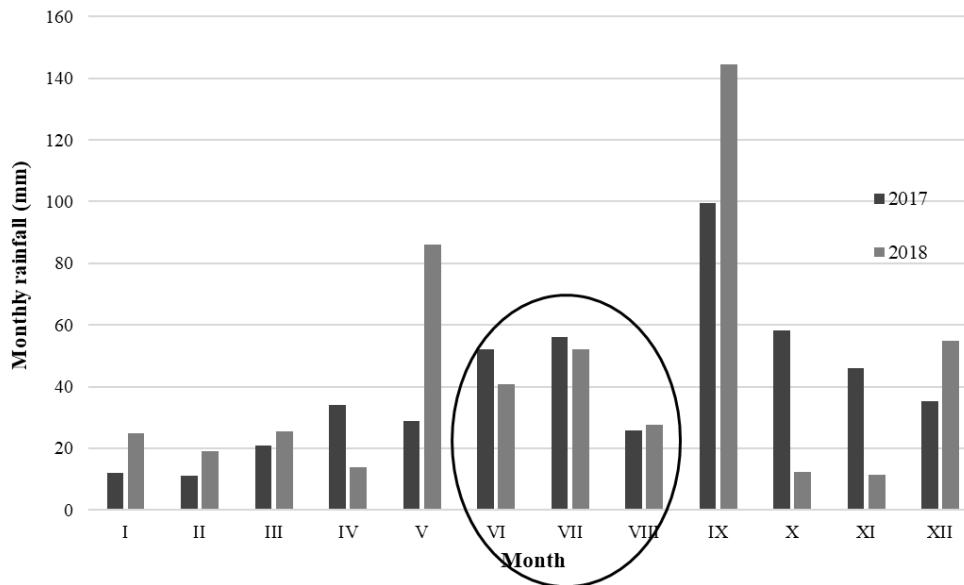
Fig. 3 Monthly rainfall on the experimental site during the years of 2017 and 2018

The statistical evaluation of the results of soil moisture values, which was carried out by the analysis of variance, show that there is a statistically significant difference between the evaluated variants and the years.

Tab. 3 The values of soil moisture

The year of measurement	Experiment variant	The soil moisture (percentage of weight)
2017	crushed grain straw (A)	26.95±0.06[e]
2017	wood chips (B)	22.03±0.08[a]
2017	control (C)	22.58±0.01[b]
2017	compost (D)	21.81±0.06[a]
2018	crushed grain straw (A)	32.28±0.09[f]
2018	wood chips (B)	24.61±0.08[d]
2018	control (C)	21.92±0.10[a]
2018	compost (D)	24.29±0.01[c]

Legend: Data are expressed as means ± standard deviation, different letters in the same columns represent significant difference ($P < 0.05$).

Also, in this case, the results confirm the positive effect of straw mulch on soil moisture. In 2017, the soil moisture was higher by 4.37 % in this variant and in 2018 by 10.37 % compared to the control variant. Overall, in 2018, all variations covered by the mulch layer were higher in soil moisture compared to the uncovered control variant. *Li et al. (2018)* states that the use of mulching materials presents an effective way of reducing soil evaporation in semiarid agroecosystems.

Covering the surface with the materials in terms of straw, film or branches can reduce radiation and wind speed at the surface and, hence, reduce evaporation (*Singh et al., 2011*). Also *Mahdavi et al. (2017)* showed that the crushed straw mulching practice significantly reduced total cumulative evaporation up to 40% as compared to the bare soil plot in a field experimental plot. The mulching decreases soil water content loss by evaporation and the variation in the soil temperature by insulating the surface and treatments increased root zone soil water content, which is expected to lead to higher root water uptake (*Jiménez et al., 2017*).

CONCLUSIONS

This work brings the results of two-year experiment focused on the impact of three kinds of mulch materials - crushed grain straw, wood chips and compost on the dynamics of soil moisture changes. There was also used the control variant which consisted of cultivated interlayer without covering material. The highest values of soil moisture were measured in experimental variants using crushed grain straw. In 2017 the average soil moisture was 26.95 % and in 2018 it was 32.28 %. The results show that wood chips are a suitable alternative for mulching the soil surface. In the broader context, the results obtained suggest that mulching materials and their use in vineyards may have an economic and ecological benefit in semiarid hillslopes. The farmers in the south Moravia region should be encouraged to apply the comprehensive agricultural measures to sustain agroecosystems on sloping field management of vineyards.

REFERENCES

1. Cerdà, A., & Doerr, S. H. (2005). The influence of vegetation recovery on soil hydrology and erodibility following fire: An eleven-year research. *Internatiolnal Journal of Wildland Fire, 14*(4), 423–437.

2. Čížková, A. Burg, P. Mašán, V., Burgová, J. & Visacki, V. (2018). Observing the soil erosion on sloping vineyards when different soil cover applied. In *MendelNet 2018: Proceedings of International PhD Students Conference* (pp. 218-223). Mendel University in Brno.

3. Dahiya, R., Ingwersen, J., & Streck, T. (2007). The effect of mulching and tillage on the water and temperature regimes of a loess soil:

Experimental findings and modeling. *Soil and Tillage Research, 96*(1), 52–63.

4. Díaz-Raviña, M., Martín, A., Barreiro, A., Lombao, A., Iglesias, L., Díaz-Fierros, F., & Carballas, T. (2012). Mulching and seeding treatments for post-fire soil stabilisation in NW Spain: Short-term effects and effectiveness. *Geoderma*, *191*, 31–39.

5. Jandák, J. (2003). *Exercise of Soil Silence* (in Czech). Brno: Mendel University of Agriculture and Forestry in Brno.

6. Jiménez, M. N., Fernández-Ondoño, E., Ripoll, M. A., Castro-Rodríguez, J., Huntsinger, L., & Navarro, F. B. (2016). Stones and organic mulches improve the Quercus ilex L. afforestation success under Mediterranean climatic conditions. *Land Degradation & Development, 27*(2), 357–365.

7. Jiménez, M. N., Pinto, J. R., Ripoll, M. A., Sanchez-Miranda, A., & Navarro, F. B. (2017). Impact of straw and rock-fragment mulches on soil moisture and early growth of holm oaks in a semiarid area. *Catena, 152*, 198–206.

8. Jordán, A., Zavala, L. M. & Muñoz-Rojas, M. (2011). Mulching, effects on soil physical properties. In *Encyclopedia of Agrophysics* (pp. 492-496). Dordrecht: Springer.

9. Li, H. C., Gao, X. D., Zhao, X. N., Wu, P. T., Li, L. S., Ling, Q., & Sun, W. H. (2016). Integrating a mini catchment with mulching for soil water management in a sloping jujube orchard on the semiarid Loess Plateau of China. *Solid Earth, 7*(1), 167–175.

10. Li, H. C., Zhao, X. N., Gao, X. D., Ren, K., & Wu, P. T. (2018). Effects of water collection and mulching combinations on water infiltration and consumption in a semiarid rainfed orchard. *Journal of Hydrology, 558*, 432–441.

11. Mahdavi, S. M., Neyshabouri, M. R., Fujimaki, H., & Heris, A. M. (2017). Coupled heat and moisture transfer and evaporation in mulched soils. *Catena, 151*, 34–48.

12. Mulumba, L. N., & Lal, R. (2008). Mulching effects on selected soil physical properties. *Soil and Tillage Research, 98*(1), 106–111.

13. Prosdocimi, M., Jordán, A., Tarolli, P., Keesstra, S., Novara, A., & Cerdà, A. (2016). The immediate effectiveness of barley straw mulch in reducing soil erodibility and surface runoff generation in Mediterranean vineyards. *Science of The Total Environment, 547*, 323–330.

14. Singh, B., Eberbach, P.L., Humphreys, E., & Kukal, S.S. (2011). The effect of rice straw mulch on evapotranspiration, transpiration and soil evaporation of irrigated wheat in Punjab, India. *Agricultural Water Management, 98*(12), 1847–1855.

15. Vanek, G. (1996). *Vine 3 – Growing: Integrated Grape Production. Ecological and conomic Cultivation, Nutrition and Protection* (in Slovak). Bratislava: PRÍRODA a.s.

16. Wang, J., Huang, J., Zhao, X. N., Wu, P. T., Horwath, W. R., Li, H. C., Jing, Z., & Chen, X. (2016). Simulated Study on Effects of Ground Managements on Soil Water and Available Nutrients in Jujube Orchards. *Land Degradation & DevelopmenT, 27*(1), 35–42.

Corresponding author:
prof. Ing. Patrik Burg, Ph.D., Department of Horticultural Machinery, Faculty of Horticulture, Mendel University in Brno, Zemědělská 1, Brno, 613 00, Czech Republic, phone: +420 519 367 373, e-mail: patrik.burg@seznam.cz

IMPACT OF MANURE AND SELECTED CONDITIONNERS ON PHYSICAL PROPERTIES OF CLAY SOIL

Nikola ČERMÁKOVÁ[1], Petr ŠAŘEC[1], Oldřich LÁTAL[2]

[1]*Dep. of Machinery Utilization, Faculty of Engineering, Czech University of Life Sciences Prague*
[2]*Agrovyzkum Rapotin s.r.o., Czech Republic*

Abstract
The article discusses the results of measurement of soil physical properties that has been done within field trial established at Sloveč in the year 2014 comparing with 2018. There were different variants of fertilizing and soil activator (NeoSol and Z'fix) used. Soil physical properties, i.e. soil bulk density and cone index were measured. The results indicate that at soil upper layer, cone index of all the trial variants dropped relative to control regardless of the manure treatment with Z'fix, or the application of NeoSol. Concerning soil bulk density, a drop in values can be discerned with the application of cattle manure. One variant was increase with no apparent pattern of treatment. Subsequently, draft of chosen tillage implements was measured.

Key words: *activator of organic matter; cattle manure; soil properties; draft; bulk density.*

INTRODUCTION

According to *Bünemann et al. (2018)*, the minimum soil characteristics indicators should include physical, chemical and biological indicators. *Bünemann et al. (2018)* include soil organic matter and structure among the most important indicators of soil quality. One of the basic problems of modern agriculture is soil compaction. Soil compaction results in loss of yield and high soil density. Soil compaction has negative impact on environment. The negative effect of soil compaction is manifested through increased bulk density, soil cone index, and other variables. This all leads to reduction in porosity, hydraulic soil properties, stability and other variables (*Alakukku, 1996*). All these parameters are connected together and influence crop yields. *Celik et al. (2010)* confirmed organic applications to significantly lower the soil bulk density and penetration resistance. According to *Javůrka and Vach (2008)*, it has been shown that excessive soil compaction reduces the growth rate of crop roots, extends them and penetrates into the lower soil layers (rooting depth). In compacted soils, crops that make up the economic yield of underground organs - sugar beets or potatoes - are most affected. For other crops, soil compaction results in lower water and nutrient intake compared to the normally developed root system. Soil compaction occurs in a vast array of soils and climates. Deteriorates with low organic matter content in soil. The low supply of water to the soil, due to compaction, leads to additional fertilizer requirements, leading to increased production costs (*Hamza, 2005*).

The impact of using soil activator of organic matter is among the less explored topics. It can have effect on physical and chemical properties of soil. It can be also assumed that changes in soil properties will be reflected in the long term rather than immediately after application. According to *Podhrázská et al. (2012)*, repeated conventional tillage and application of PRP Sol did not demonstrate any improvement in soil physical properties (density, porosity, soil compaction, reduced water content in soil).

In terms of economy and operation, energy demand of soil tillage is one of the crucial elements. Tillage is the base operation in agricultural systems and its energy consumption represents a consid-erable portion of the energy consumed in crop production (*Larson and Clyma, 1995*). *McLaughlin et al. (2002)*, *Liang et al. (2013)* and *Peltre et al. (2015)* reported manure amendments to have significant effect on reduction in tillage implement draft. Prolonged application and higher rates brought advanced reduction. The primary aim of the project supported by the Technology Agency of the Czech Republic is verify the impact of cattle manure and biological activator of soil on soil production properties.

MATERIALS AND METHODS

Trails field examining effect of substance for soil amendment and fermented manure were established in 2014. The research was carried out until 2017, when other variants were added. The measurement were done in autumn every year. In 2014 were done on 2nd October after the barley harvest. In 2018

measurement were done on 1st November. The trial field is located near Sloveč in Central Bohemia (GPS: N 50°14.256', E 15°20.705', altitude: 273 m). The topography is gently sloping, facing southwest. Soil type on the location Sloveč is very heavy and the soil is thus difficult to cultivate. The content of clay particles under 0.01 mm was 30 % of weight at the depth from 0 to 0.3 m. Volumetric moisture in the top soil layer (0 to 0.30 m) was 35.65 % and total porosity was 40.15 %. Bulk density was 1.46 g.cm^{-3}.

Each trial fields was 45 meters wide and 140 meters long selected to be homogenous and to avoid headland. On this plot was applicated fertilizer out according to the plan. There were used cattle manure, NPK 15-15-15 (Lovofert), NeoSol, Z'fix. Fertilizers were Cattle manure and NPK. NeoSol is soil activator from PRP Technologies company, which is formed by a matrix of calcium and magnesium carbonates that is well bind to the soil solution and regulate the environment, where microorganisms can develop. Z'fix is a granular mix composed of calcium and magnesium carbonates, designed to control fermentation processes in manure and compost. Z'fix was applied directly to the bedding in the presence of animals. Both activators is not a fertilizers, they are supposed to improve conditions for the transformation of organic matter.

Fertilization of individual variants is shown in Table. 1. The difference in variants was in used fertilizers, biological transformers of organic matter. Dosage of cattle manure was 50 t.ha-1, of PRP Sol 200 kg.ha-1, and of NPK 200 kg.ha-1. Than the field was ploughed afterwards. In spring, seedbed preparation was carried out.

Tab. 1 Fertilization of individual variants of trial fields at Sloveč.

Variant	Fertilization
I a	cattle manure with Z'fix + NPK
II a	cattle manure with Z'fix + NeoSol+ NPK
III a	cattle manure+ NPK
IV a	cattle manure + NeoSol + NPK
V a	NeoSol + NPK
VI a	NPK (Control)

There were used Two basic methods for measuring physical properties of soil. Firstly it was undisturbed soil samples using Kopecky's cylinders (volume 100 cm3). Secondly, cone index measuring method was used by registred penetrometer PEN 70 developed at CULS Prague was employed. Moisture was measured by Theta Probe (Delta-T Devices Ltd, UK). The proposed soil tillage implements were measured by means of a drawbar dynamometer with strain gauges S-38/200 kN (LUKAS, Czech Republic) between two tractors (see Fig. 1). Data acquisition system NI CompactRIO (National Instruments Corporation, USA) was employed and its sample rate was set at 0.1 s. The data were then processed by MS Excel (Microsoft Corp., USA) and Statistica 12 (Statsoft Inc., USA) programs.

Fig. 1 Photo of draft measurement of chisel plough Horsch Tiger 5 AS at Sloveč in autumn 2018.

RESULTS AND DISCUSSION

Table 2 shows the overall average values of the basic physical properties of soils. There is a clear difference in volumetric soil moisture between the two years due to exceptionally dry weather over the whole vegetative period of the year 2018. This clearly increased the values of cone index which depends on soil moisture. Illustrative aggregate values at three different depths are presented in the Table 2. Because of drastically different climatic conditions in both year is more interesting relative differences to the control variant than absolute values.

Tab. 2 The overall averages of soil moisture and bulk density, and operating conditions and overall results of measurement of soil tillage implement drafts at Sloveč in autumn of 2014 and 2018.

	Fall 2014	**Fall 2018**
Soil properties		
vol. moisture at 0.00 – 0.05 m [%]	35.16	20.78
cone index at 0.08 m [10^6 Pa]	1.124	0.913
cone index at 0.12 m [10^6 Pa]	1.326	1.477
cone index at 0.16 m [10^6 Pa]	1.571	2.977
bulk density at 0.05- 0.10 m [g.cm^{-3}]	1.763	1.518
red. bulk density at 0.05- 0.10 m [g.cm^{-3}]	1.367	1.248
Draft measurement		
tractor	NH TG285	JD 9560 RT
engine power [HP]	285	560
implement	chisel plough	tine cultivator
implement type	Strom Terraland TN 3000	Horsch Tiger 5 AS
working width [m]	3	5
working depth [m]	0.117	0.122
working speed [km.hour^{-1}]	7.81	7.94

Year-on-year changes in relative cone index values at upper soil layer are presented in Fig. 2 and 3. Cone index of all the trial variants dropped relative to control regardless of the manure origin, manure treatment with PRP Fix, or the application of PRP Sol.
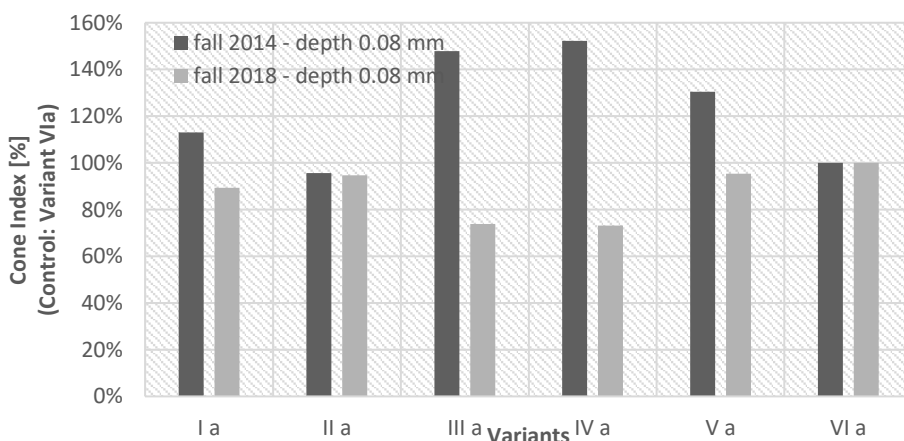
Fig. 2 Graph comparing relative differences of soil cone index values at the depth of 0.08 m at Sloveč in autumn 2014 and 2018 (Variant VIa – 100 %).
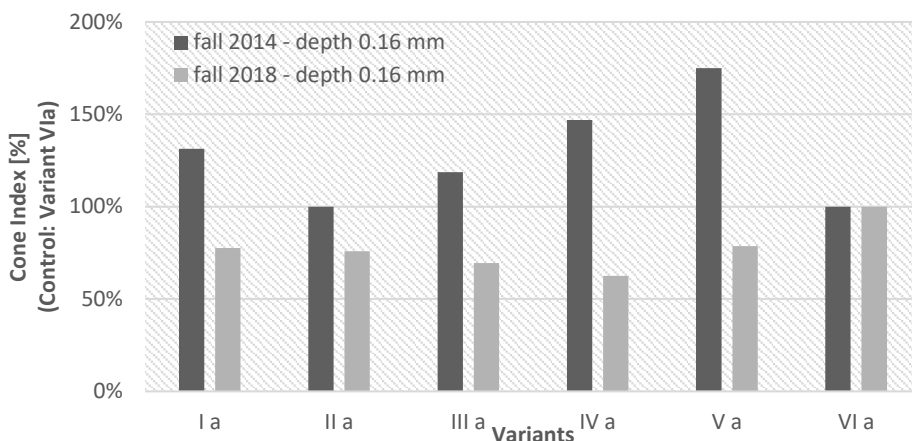
Fig. 3 Graph comparing relative differences of soil cone index values at the depth of 0.16 m at Sloveč in autumn 2014 and 2018 (Variant VIa – 100 %).

On the other hand, overall soil bulk density values decreased, although moderately only. Fig. 4 demonstrates relative comparison to the control variant. A drop can be discerned with the application of cattle manure. Small differences is in variant Va. The increase occurred without obvious cause.
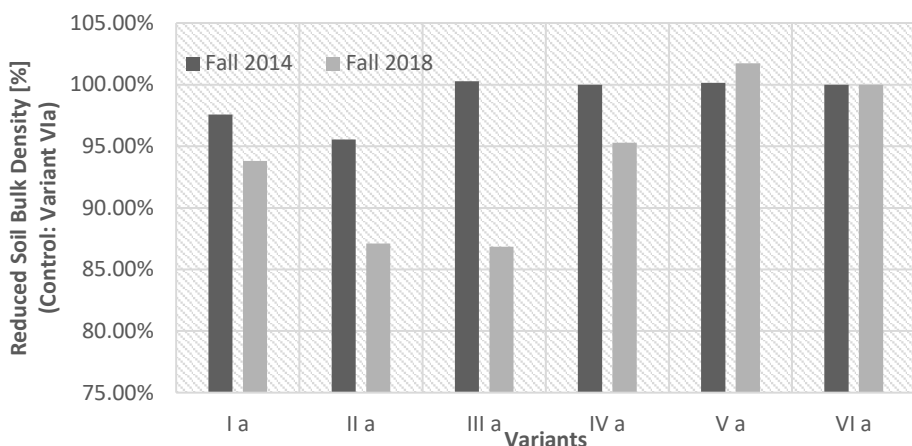
Fig. 4 Graph comparing relative differences of reduced soil bulk density at Sloveč in autumn 2014 and 2018 (Variant VIa – 100 %).
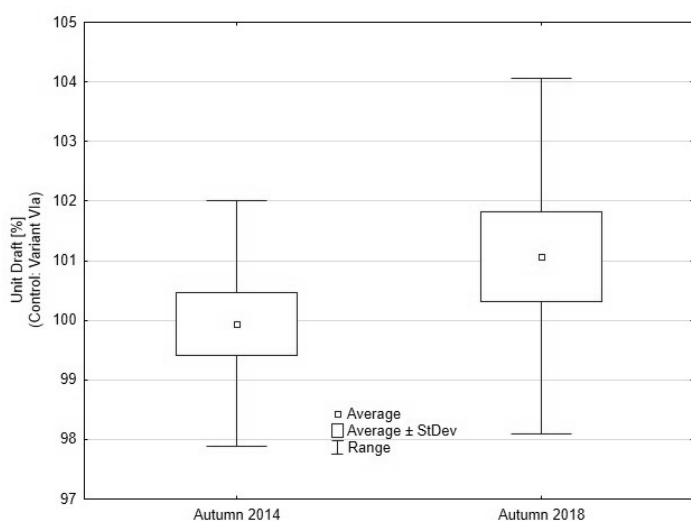
Fig. 5 Graph comparing relative differences of implement unit draft related to control at Sloveč in autumn 2014 and 2018 (control variant VIa excluded).

Fig. 5 presents aggregate unit draft values compared to the control. Due to the different climatic conditions and soil tillage implements used, absolute values cannot be considered. The ratio of individual measured unit draft values to the average value of the control variant is therefore used for evaluation. There a slight increase in unit draft after manure and soil and manure activators.

When taking into account relative differences of individual variants (Fig. 6), the increase was attained in three cases. It was variant IIIa, Iva and Va. The majority differences were in Iva with application Cattle manure, NeoSol and NPK.
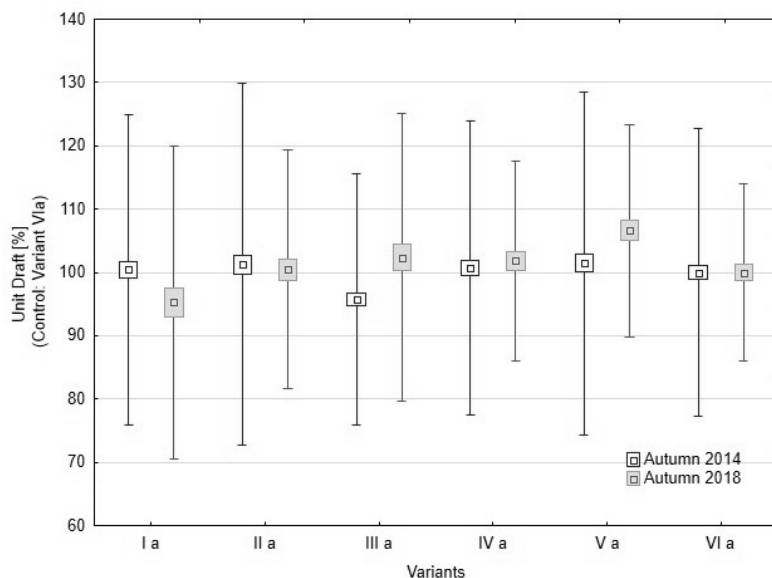
Fig. 6 Graph comparing relative differences of implement unit draft with respect to individual variants at Sloveč in autumn 2014 and 2018

The original assumptions of the research were not mostly confirmed. The experimental measurements confirmed conclusions of *Podhrázská et al. (2012)* that says there is no relationship between the application of the biological soil activator NeoSol and the improvement of the physical properties of the soil. In opposite, *Schjønning et al. (1994)* suggested, that long term fertilizer application can be rewarding to improve soil strength and soil density than manure or inorganic fertilizer treatments. *Celik et al. (2010)* re-ported, that cone index values can be decrease compared to the control variant. With higher application rates of manure, soil bulk density as well. Both these two assumptions was not confirmed

CONCLUSIONS

So far, the work has not proved the beneficial effect of substances for soil (NeoSol) and manure amendment (Z'fix) and of cattle manure on soil cone index and on implement draft force reduction. At soil upper layer, cone index of all the trial variants dropped relative to control regardless of the manure origin, manure treatment with Z'fix, or the application of NeoSol. Concerning soil bulk density, a drop in values can be discerned with the application of cattle manure. One variant was increase with no apparent pattern of treatment.

Subsequently, draft of chosen tillage implements was measured. The unit draft remained practically unchanged relative to the control within one variant, decreased within two variants, and increased within another three variants. The latter two were the variants where the most treatments were accomplished, i.e. application of cattle manure (with and without Z'fix), of NeoSol, and of NPK. It could be therefore assumed that higher number of machinery passes may have resulted in the increased implement draft. The assumed benefits of manure and soil activators may not have had time to take effect. Instead, the impact of higher number of machinery passes due to their application may have been manifested.

The necessity of long-term examination of the effects of activators of organic matter should be emphasized. Research needs to be validated in more locations in order to eliminate the influence of the local

environment. The effects of activators of organic matter are among the less explored topics. In connection with changing composition of organic fertilizer (fewer manure and slurry but more compost and waste from biogas plants), the increased importance of activators of organic matter can be expected.

REFERENCES

1. Alakukku L. (1996). Persistence of soil compaction due to high axle load traffic. I. Short-term effects on the properties of clay and organic soils. *Soil and Tillage Research, 37*, 211-222.

2. Bünemann, E.K., Bongiorno, G., Bai, Z., Creamer, R.E., De Deyn, G., de Goede, R., & Mäder, P. (2018). Soil quality - A critical review. *Soil Biology and Biochemistry,* 105–125.

3. Celik, I, Gunal, H., Budak, M. & Akpinar, C. (2010). Effects of long-term organic and mineral fertilizers on bulk density and penetration resistance in semi-arid Mediterranean soil conditions. *Geoderma, 160*, 236-263.

4. Javůrek, M. & Vach, M. (2008). *Negative effects of soil compaction and a set of measures to eliminate them,* Crop Research Institute, v.v.i.

5. Larson, D.L. & Clyma H.E. (1995). Electro-osmosis effectiveness in reducing tillage draft force and energy forces. *Transactions of ASAE*, *38*, 1281-1288.

6. Liang, A., McLaughlin, N.B., Ma, B.L., Gregorich, E.G., Morrison, M.J., Burtt, S.D., Patterson, B.S., & Evenson, L.I. (2013). Changes in mouldboard plough draught and tractor fuel consumption on continuous corn after 18 years of organic and inorganic N amendments. *Energy*, *52*, 89-95.

7. Hamza, M.A. & Anderson, W.K. (2005). Soil compaction in cropping systems, *Soil Tillage Res., 82*, 121-145.

8. McLaughlin, N.B., Gregorich, E.G., Dwyer, L.M., & Ma, B.L. (2002). Effect of organic and inorganic soil nitrogen amendments on mouldboard plow draft. *Soil & tillage research*, *64*, 211-219.

9. Peltre, C., Nyord, T., Bruun, S., Jensen, L.S. & Magid, J. (2015). Repeated soil application of organic waste amendments reduces draught force and fuel consumption for soil tillage. *Agriculture, Ecosystems and Environment, 211*, 94-101.

10. Podhrázská, J., Konečná, J., Kameníčková, I., & Dumbrovský, M. (2012). Survey of the impact of PRP SOL (NeoSol) subsidiary substance on the hydrophysical properties of soil at cultivation of sugar beet. *Listy cukrovarnické a řepařské*, *128*, 128-133.

11. Schjønning P., Christensen B.T. & Carstensen B. (1994). Physical and chemical-properties of a sandy loam receiving animal manure, mineral fertilizer or No fertilizer for 90 years. *European Journal of Soil Science, 45,* 257-268.

Corresponding author:

Ing. Nikola Čermáková, Department of Machinery Utilization, Faculty of Engineering, Czech University of Life Sciences Prague, Kamýcká 129, Praha 6, Prague, 16521, Czech Republic, e-mail: zemlickovan@tf.czu.cz

SOIL TESTS OF RENOVATED PLOUGHSHARE POINTS

Peter ČIČO[1], Róbert DRLIČKA[1], Radovan ŠOŠKA[1], Zdenko RÓNA[2]

[1]Department of Quality and Mechanical Engineering, Faculty of Engineering, Slovak University of Agriculture in Nitra, Slovak Republic
[2]Transmisie Engineering, a. s. Martin, Slovak Republic

Abstract
The paper deals with operational (soil) tests of selected hardfacing materials allowing extend the life of the ploughshare point. The results showed that the highest wear occurred in the front part of the ploughshare points. EB 520 RB with ledeburitic structure and chromium and vanadium carbides has achieved the highest wear resistance among the materials studied. The ploughshare points welded with the NiCrBSi-based NP 60 WC 20 powder also achieved a relatively high wear resistance. High wear resistance values are mainly due to the presence of tungsten carbide hard structures. NP 62, also based on NiCrBS, but without tungsten carbide particles, has achieved significantly lower wear resistance.

Key words: *ploughshare point; wear; deposit; soil tests.*

INTRODUCTION

In agriculture, various processing tools are used which counter degradation processes during operation. Wear of cutting edges of working tools in operating conditions significantly affects the quality of work and energy demands of soil tillage processes (*Hrabě & Müller, 2013; Kováč, Vanko & Vysočanská, 2014; Mikuš, Balla & Žernovič, 2006; Müller & Hrabě, 2013*).

Farmers and suppliers are looking for different ways to extend the technical life of working tools. One option is to apply materials with increased hardness to the working part of the tool, which is expected to achieve increased wear resistance in the soil. There are several ways of creating hard layers, which are distinguished from each other by technological parameters, filler materials used, as well as by the properties of the created hard layers (*Hrabě, Chotěborský, Ružbarský & Žarnovský, 2010; Kováč, Vanko & Vysočanská, 2014; Viňáš, J., Brezinová, J., Guzanová, A., & Kotus, M., 2013*).

The application possibilities of specific wear resistant materials can be verified in laboratory tests. Despite the excellent results of some materials in laboratory conditions, the results in operational tests will not conform to these evaluations. The evidence can be found in the results of several authors (*Brožek, Nováková & Mikuš, 2010; Mikuš, Kováč & Žarnovský, 2014; Müller & Hrabě, 2013*).

The most accurate results of soil resistance of materials in soil conditions can be obtained through operational tests. It should be noted that the same type of material may have quite different wear values in various operating or soil conditions. These differences are influenced by several factors, e.g. soil (soil type, soil moisture), tillage tool (material and geometry of the tool) and so on (*Hrabě & Müller, 2013; Mikuš, Balla & Žernovič, 2006*).

Therefore, the aim of this paper is to find out the possibilities of extending the life of the ploughshare point by welding-on the selected wear resistant materials and to evaluate the wear on the basis of operational tests.

MATERIALS AND METHODS

The operating tests were focused to examining the wear of the most exposed part of the plough - ploughshare point. A total of fourteen ploughshare points included in the experiment were mounted on the plough Ostroj Europa. The two original ploughshare points were used as a standard, the remaining twelve ploughshare points (divided into three parts by four) were welded-on with two types of powder filler materials based on NiCrBSi (NP 62 and NP 60 WC 20) and hardfacing rod (E 520 RB). The chemical composition of the additive materials used is shown in Tab. 1.

Tab. 1 Chemical composition and hardness of the filler materials used

Filler material	Standard chemical composition (% weight)									Hardness HRC
	C	Si	B	Fe	Cr	WC	V	Mn	Ni	
NP 62	0,9	5,5	4	5	20	-	-	-	remainder	58-65
NP 60 WC 20	0,6	5	3,9	5	20	20	-	-	remainder	75-82
E520 RB	3,5	0,8	-	-	25	-	1,7	0,8		61

The powder filler materials NP 62 and NP 60 WC 20 were applied by an oxygen-acetylene flame (NPK-3 torch, neutral flame, 3-4 mm.s $^{-1}$ welding speed). The material E 520 RB was applied by manual metal arc welding-on (direct current, positive electrode, welding current 80 to 100 A, welding voltage 24 to 25 V, welding speed 3-4 mm.s $^{-1}$). Before welding, grooves with a width of 20 mm and a depth of 2 mm were machined on the front face (Fig. 1). The grooves were then filled with deposit materials, with a weld thickness of 2 mm. The same geometric shape as in case of the original ploughshare points were achieved by this way.
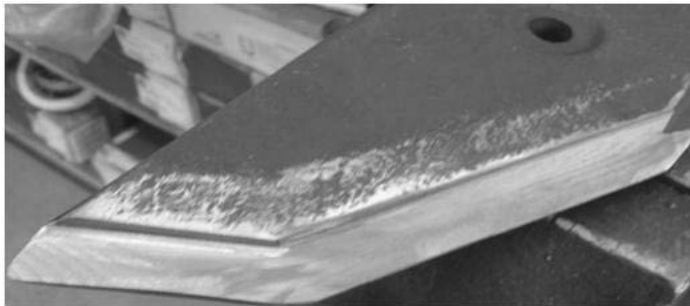
Fig. 1 Groove for hardfacing on the functional face part of the ploughshare point

In operational tests, the size of the linear wear of the ploughshare point was monitored after the 40 and 80 ha area processed. Wear was determined as the difference between the dimensions in the defined planes (Fig. 2) of original and worn ploughshare points after specific area ploughed. The measurements were made with a calliper with an accuracy of 0.02 mm.
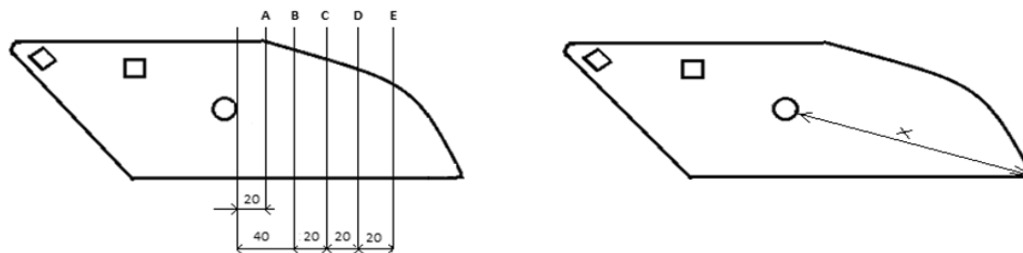
Fig. 2 Measurement planes of linear wear of the ploughshare point

RESULTS AND DISCUSSION
Field tests were realized in loam soil with moisture of 17.5%. The first ploughshare point wear measurement was carried out after 40 h of ploughed area and the results obtained are shown in Fig. 3. The highest wear was found on the standards. The arithmetic mean of their linear loss was 3.32 mm. The lowest wear was achieved by ploughshare point hardfaced with the material E 520 RB, the average loss reached the value of 1.76 mm in the defined planes, which represents 88% better wear resistance compared to standards. Ploughshare points welded-on with NP 62 powder material reached average loss of 1.83 mm width (81% better wear resistance compared to standards) and ploughshare points hardfaced with NP 60 WC 20 reached an average width loss of 2.11 mm (57% better wear resistance compared to standards). The largest lost in linear dimensions were identified in the X plane

(Fig. 2). NP62 deposit was 65.6% better than the standard, NP 60 WC 20 was 148% and the EB 520 RB was 162% more durable than not hardfaced ploughshare point.
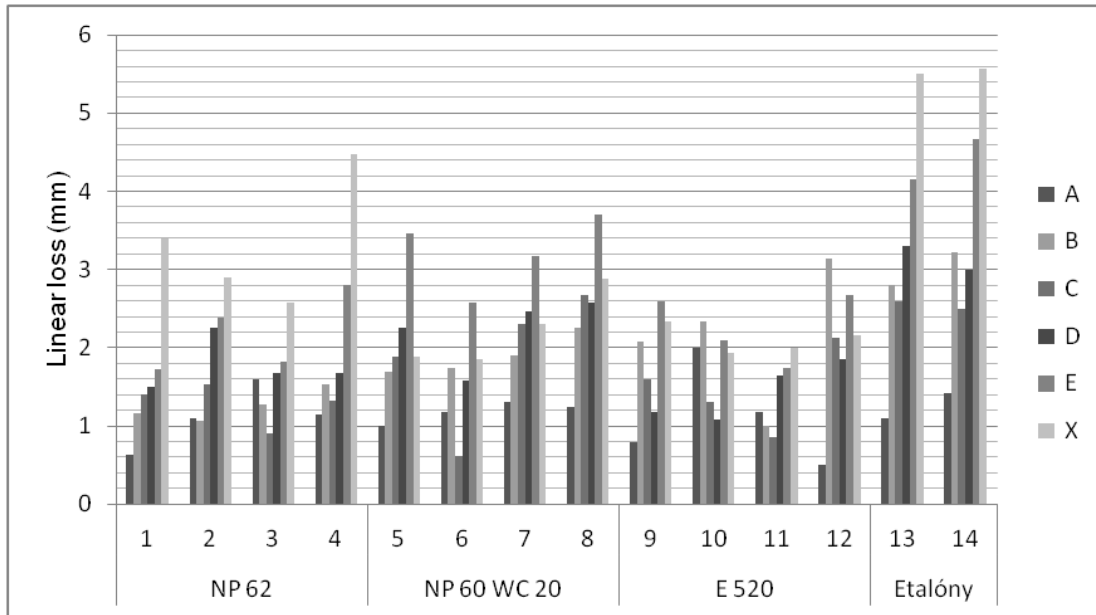
Fig. 3 Linear loss of ploughshare point after 40 ha of ploughed area

The following measurements were made after 80 ha of ploughed area, with average soil moisture of 16.8%. The values of linear loss of the ploughshare point are shown in Fig. 4. The standards showed the highest wear. Their average linear loss in the measured planes was 6.42 mm. E 520 RB with an average linear loss of 3.15 mm, the 103% increase in wear resistance versus standards, achieved the best results from the filler materials. Metal powders had similar losses after ploughing 80 ha. The NP62 deposit achieved an average loss of 3.66 mm (75% better wear resistance compared to standards), the NP 60 WC 20 achieved an average loss of 3.87 mm (65% better wear resistance than standards). Again, the greatest wear was recorded in the X plane (Fig. 2), with the NP62 deposit 70.2% better value than the standard, the NP 60 WC 20 176% and the EB 520 RB 183.5% better durability as not welded ploughshare points.
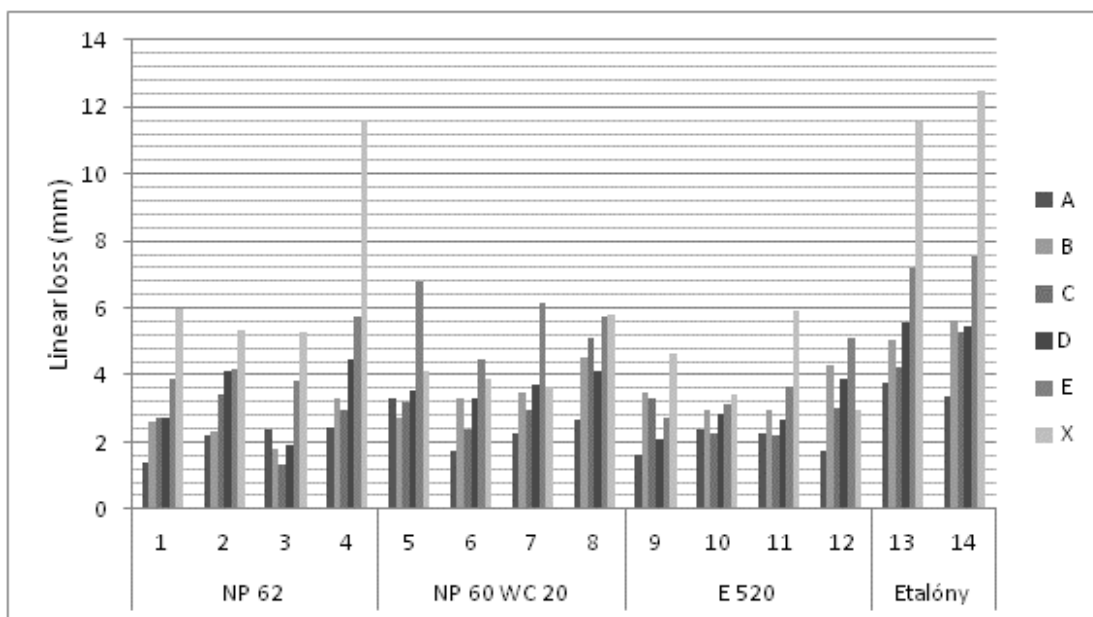
Fig. 4 Linear loss of ploughshare points after 80 ha of ploughed area

The results achieved fully correspond to the results presented by several authors in their works (*Hrabě & Müller, 2013; Kováč, Vanko & Vysočanská, 2014; Mikuš, Balla & Žernovič, 2006; Müller & Hrabě, 2013; Viňáš, J., Brezinová, J., Guzanová, A., & Kotus, M., 2013*). The material NP 60 WC 20 wear of the ploughshare point cutting edge was positively influenced by the presence of WC particles in the structure, being significantly reduced in comparison to the material NP 62, which is in accordance with the results reported by *Mikuš, Balla & Žernovič, 2006; Mikuš, Kováč & Žarnovský, 2014*. EB 520 RB achieved the best results from all materials tested, which can be attributed mainly to the presence of ledeburitic structure (high carbon content) as well as chromium and vanadium carbides in the material structure. The carbide structure seems to be the most suitable in terms of the wear resistance in the soil environment (*Hrabě, Chotěborský, Ružbarský & Žarnovský, 2010*).

CONCLUSIONS

The results achieved showed that the highest wear was in the first third of ploughshare point. When comparing the wear at the particular measuring points, it can be stated that the ploughshare points welded-on with EB 520 RB with ledeburitic structure and chromium and vanadium carbides have the best wear resistance. The ploughshare points hardfaced with NP 60 WC 20 also have 150 to 180% higher resistance comparing to standards. High wear resistance values are mainly due to the presence of hard tungsten carbide structures. The material NP 62, without tungsten carbide particles, was only 70-80% higher than the standards.

Protective deposit can therefore prolong significantly the technical life of the ploughshare point. This issue needs to be further explored and new possibilities for extending the lifetime and reducing the cost of operating tools are sought.

ACKNOWLEDGMENT

REFERENCES

1. Brožek, M., Nováková, A., & Mikuš, R. (2010). Study of wear resistance of hard facings using welding powders on the NiCrBSi basis. In *Trends in agricultural engineering 2010* (pp. 115-118).

2. Hrabě, P., Chotěborský, R., Ružbarský, J., & Žarnovský, J. (2010). Comparison of high chromium and boride hardfacing. In *Trends in agricultural engineering* 2010 (pp. 228-231).

3. Hrabě, P., & Müller, M. (2013). Research of overlays influence on ploughshare lifetime. *Research in agricultular engineering*, 59 (4), 147-152.

4. Kováč, I., Vanko, N., & Vysočanská, M. (2014). Verification of the working life of a ploughshare renovated by surfacing and remelting in the operation. *Research in agricultural engineering*, *60*, 98-103.

5. Mikuš, R., Balla, J., & Žernovič, M. (2006). Forming of hard-layer-hardened blade shape during wear. In *Intertribo 2006* (pp. 119-123).

6. Mikuš, R., Kováč, I., & Žarnovský, J. (2014). Effect of Microstructure on Properties of NiCrBSi Alloys Applied by Flame-Powder Deposition. *Advanced Materials Research*, *1059*, 1-9.

7. Müller, M., & Hrabě, P. (2013). Overlay materials used for increasing lifetime of machine parts working under conditions of intensive abrasion. *Research in agricultular engineering, 59*, 16-22.

8. Viňáš, J., Brezinová, J., Guzanová, A., & Kotus, M. (2013). Application of hard surfacing for repairing of agricultural parts. *Research in agricultural engineering, 59*, (2), 61-67.

Corresponding author:
doc. Ing. Peter Čičo, CSc., Katedra kvality a strojárskych technológií, Technická fakulta SPU v Nitre, Tr. A. Hlinku 2, 949 76 Nitra, Slovensko. Tel.: +421376415686, e-mail: peter.cico@uniag.sk

COMPARISON OF RHEOLOGICAL PROPERTIES OF NEW AND USED BIOLUBRICANTS

Ján CSILLAG[1], Ana PETROVIĆ[1], Vlasta VOZÁROVÁ[1], Matúš BILČÍK[1], Monika BOŽIKOVÁ[1], Tomás HOLOTA[2]

[1]Department of Physics, Faculty of Engineering, Slovak University of Agriculture in Nitra, Slovakia
[2]Department of building equipment and technology safety, Faculty of Engineering, Slovak University of Agriculture in Nitra, Slovakia

Abstract
This paper deals with research focused on possibilities of usage of physical methods while evaluating the chosen technological characteristics of biodegradable lubricants. Biodegradable lubricants UTTO were the subject of examination and they were compared with a sample of mineral oil Ultra. We focused on density, viscosity, fluidity and pour point. Results show that the temperature is an important factor which influences thermophysical properties. Results of the thesis include the acquired dependencies of density and viscosity on temperature described by linear and exponential regression equation of Arrhenius type. Pour point of individual samples was determined by usage of the differential scanning calorimetry.

Key words: *biodegradable lubricants; density; viscosity; fluidity; thermal analysis.*

INTRODUCTION

The term ecological lubricant is not well defined in the literature. Such materials that do not have a negative impact on the environment are generally considered as organic substances. In the case of lubricants, these are biodegradable lubricants, or biomass and require rapid and particularly complete biodegradability by microorganisms. Ecological lubricants can equally replace lubricating oils and greases on mineral base. The economic benefits of organic products are largely because the operating costs are reduced when they are used. The use of ecological lubricants is the best alternative in practice (*Beleš & Zelenka, 2010). Bhusham (2001)* adds that in the future, the environmental properties of a lubricant should take precedence over performance. The aim of our paper is a comparison of ecological lubricant with mineral oil by using the physical methods. It is mainly about measuring the temperature dependencies, such as the dependence of viscosity and density on temperature and their comparison. We will compare new samples and samples which were cyclically stressed in a special test device.

MATERIALS AND METHODS

Dynamic viscosity η (Pa.s), which is the ratio of shear stress τ (Pa) and share rate γ (s^{-1}) as shown in eq. 1.

$$\eta = \frac{\tau}{\gamma} \tag{1}$$

was measured on the digital rotary viscometer Brookfield DV2TLV. Generally, the dynamic viscosity depends on several quantities or variables, such as physical-chemical structure of the sample, temperature, pressure, time, and shear rate (*Severa & Los, 2008*). Measurements of the dynamic viscosity in the temperature interval from temperature 20 °C to 100 °C, are provided. Density of oils is measured by the digital density meter Mettler Toledo DM40 in the temperature interval from 0 °C to 100 °C. The measuring principle of density is based on the electromagnetic induced oscillation of the U-shaped glass tube. The fluidity is an ability of matters to flow. The measure of fluidity is expressed by viscosity. It is defined as a reciprocal of dynamic viscosity. Lubricating oil gradually stops flowing at low temperature until it reaches the point which is referred to as the pour point. The pour point is the highest temperature at which the lubricant no longer flows under the prescribed test conditions. The result is reported in °C (*Stopka, 2014*). The changing of the liquid to the solid can be defined in two stages. The first stage starts to exclude fine hydrocarbon crystals from the oil, the second stage forms a crystal lattice by gradual cooling which prevents the movement of the liquid. This temperature is called a pour point. The value of the pour point largely depends on the chemical composition of the oils and generally increases with the size of the molecules. The pour point of most engine and gear oils ranges from -10 °C to -30 °C

(*Lahučký & Tóth, 2011*). The pour point is also the limit of oil usability. It characterizes the ability of the oil to flow at low temperatures. As *Abdullah et al. (2016)* published in his article, a large proportion of ecological lubricants are used in industrial machines that operate at low temperatures. Exploring the pour point is therefore an important information for the application of lubricants. To measure the pour point we used Mettler Toledo DSC 1. In the case of DSC calorimeters with thermal flow the power difference is measured directly, but this quantity is derived from the temperature difference between the sample and the reference substance (*Šimon, 2000*). From the difference between the temperature of the sample and the temperature of the reference cup (DSC sensor), the DSC 1 module calculates the heat flow signal and offers the possibility of differential calorimetry. The initial peak temperature is counted when the curve begins to deviate from the baseline. The onset and endset temperatures (extrapolated start and end) are the points where the tangents, guided by the inflection points of the curve, intersect with the baseline. The peak temperature is the point which is corresponded by the maximum heat flow, and the final temperature is the point at which the curve stops deviating from the baseline (*Klubal & Ostrý, 2014*). The resulting peak, or the course of the whole measurement, can be influenced by several factors that appear on the graph. The issue of undesirable DSC artefacts was addressed by *Tarasov (2012)*.

We will measure the ecological lubricant Mol Farm Bio UTTO which is also a biodegradable tractor oil. The oil is made from vegetable natural oil and special additives. The oil is designated for use in the gearbox and hydraulic circuit of agricultural and construction machines. It is used for lubrication of gearboxes, hydraulic circuits, for agricultural and construction machinery. Primary biodegradation per CEC L-33-A-93 is 90% within 21 days and test method CEC L-33-A-93 (28 days) is 91 % (*Majdan et al., 2011a*). For comparison, we had MOL Traktol NH Ultra. It is a mineral oil of the same use as UTTO, but the primary biodegradation is almost 45%. Sample was worn in special laboratory equipment, which was at the Department of Transport and Handling at Faculty of Engineering, Slovak University of Agriculture in Nitra. The laboratory equipment was constructed from the elements of the hydraulic systems of the tractors. The equipment uses a tractor gear pump type UD 25 (*Jihostroj Velešín, Czech Republic*), which is used by Zetor Forterra (*Zetor Brno, Czech Republic*). The laboratory equipment of the hydraulic system makes it possible to simulate the pressures of the tractor's hydraulic system in a significantly shorter time than during the operating of the tractor. Hydraulic pump was loaded with cyclically changing pressure from 0.1 MPa to the nominal pressure of the hydraulic pump 20 MPa during the test. It is these pressure surges that burden the tractor's hydraulic system the most (*Tkáč, Majdan & Kosiba 2014*).

RESULTS AND DISCUSSION

In Fig. 1 – Fig. 4 we monitor the temperature dependence of dynamic and kinematic viscosity, density and fluidity of biodegradable oil Mol Farm Bio UTTO.
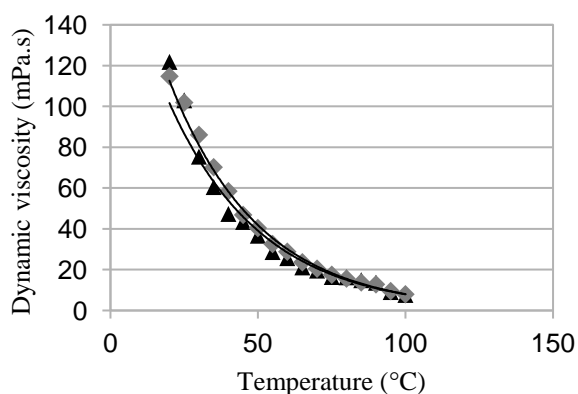
Fig. 1 Temperature dependencies of new oil UTTO ▲ and oil after 750 000 cycles ◆ of dynamic viscosity.
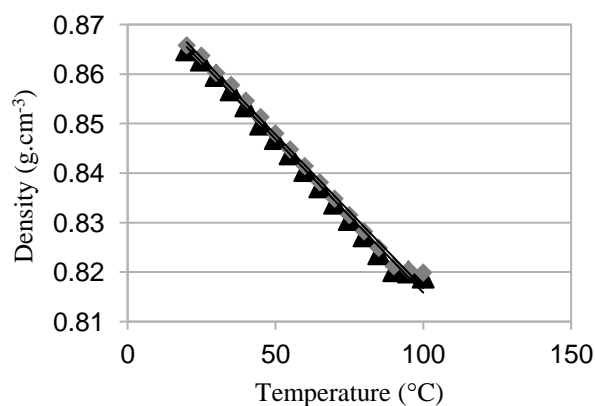
Fig. 2 Temperature dependencies of new oil UTTO ▲ and oil after 750 000 cycles ◆ of density.
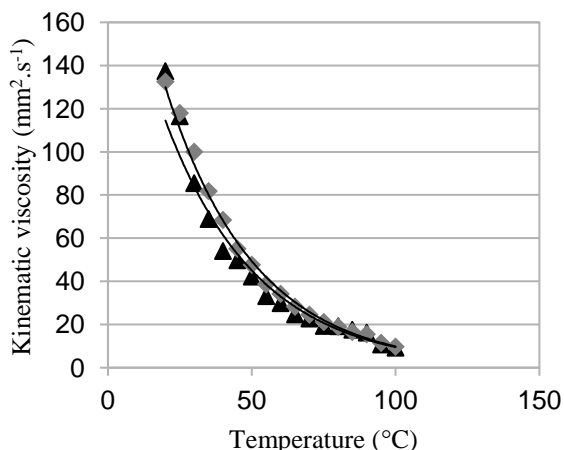
Fig. 3 Temperature dependencies of new oil UTTO ▲ and oil after 750 000 cycles ◆ of kinematic viscosity.
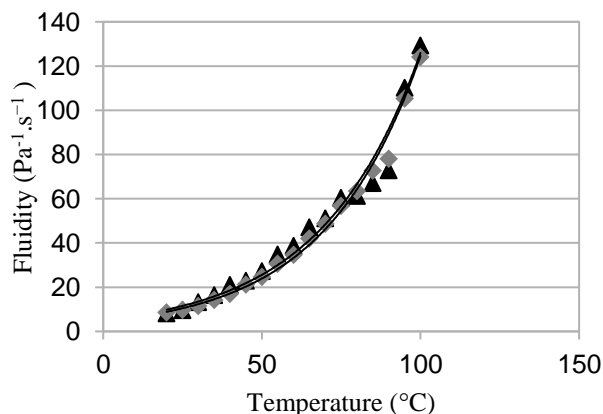
Fig. 4 Temperature dependencies of new oil UTTO ▲ and oil after 750 000 cycles ◆ of fluidity.

Listed dependences for all samples were described by the mathematical regression equation – decreasing exponential dependence of the Ahrrenius type:

$$\eta = A e^{-Bt} \tag{2}$$

where A and B are coefficients of the regression equation.

The new sample reached the highest viscosity values at temperature up to 25 °C. With the rising temperature, the viscosity of the new sample decreased most significantly. At the temperature of 40 °C, the new sample had a dynamic viscosity value of 47.35 mPa.s and for the cyclically burdened sample the value was 58.53 mPa.s. This phenomenon was up to about 75 °C. From this temperature, the viscosity of the new sample increased again, in the comparison with the cyclically burdened sample. The determining coefficients of the exponential regression equation reach a high value, for the new sample it was $R^2 = 0.9786$ and after 750 000 cycles it was $R^2 = 0.9954$. From these values we can say that the given regression equations describe the obtained dependences very accurately. Measurement results of oils density are presented in the graph on the Fig. 2. It is shown that density linearly decreases with temperature of oil. *Kosiba et al. (2016)* dealth with the effect of biodegradable synthetic fluid on operation of tractor hydraulic circuit, using the same biodegradable lubricant UTTO. Density, they measured, at 15 °C was 931 kg.m^{-3} and ours was 867 kg.m^{-3}. Their sample also was subject to a measuring of kinematic viscosity at 40 °C (67.52 mm^2.s^{-1}), while our new sample had 54.15 mm^2.s^{-1}. The manufacturer reports the values of kinematic viscosity at the temperature of 40 °C equal 58.14 mm^2.s^{-1}. Our measurement revealed a value of 68.48 mm^2.s^{-1} after the cyclic stressing of the sample. Similar small differences were also at the temperature of 100 °C, where the manufacturer's kinematic viscosity value for both samples differed from our measured value by 1 mm^2.s^{-1}. From Fig. 4, we can see that the fluidity increases with the increasing temperature. The new sample reaches higher values of fluidity except for the temperature range between 80 – 90 °C. At the temperature 85 °C, the stressed sample had a fluidity of 72.85 Pa^{-1}.s^{-1} and the new sample of 67.08 Pa^{-1}.s^{-1}. The fluidity of the new sample increased again from this temperature.

Tab. 1 Defining the exothermic course of the pour point for the UTTO sample

	New Sample	Sample after 750 000 cycles
Pour point (°C)	-34.11	-33.75
Initial exothermic reaction temperature (°C)	-32.61	-31.89
Final exothermic reaction temperature (°C)	-35.97	-35.6

From the measured values from the DSC module (Tab. 1), we see that the interval of the temperature stability for the new sample ends at the value of -32,61 °C, when the exothermic reaction begins. The new UTTO sample reached the pour point at the temperature of -34.11 °C, while the *Kosiba et al. (2016)* got the -48 °C. A sample after 750 000 cycles had an exothermic peak value and a pour point at the temperature of -33.75 °C. For this sample, the end of the temperature stability interval is at the value of -31.89 °C.

In Fig. 5 – Fig. 8 we monitor the temperature dependence of dynamic and kinematic viscosity, density and fluidity of mineral oil MOL Traktor NH Ultra.
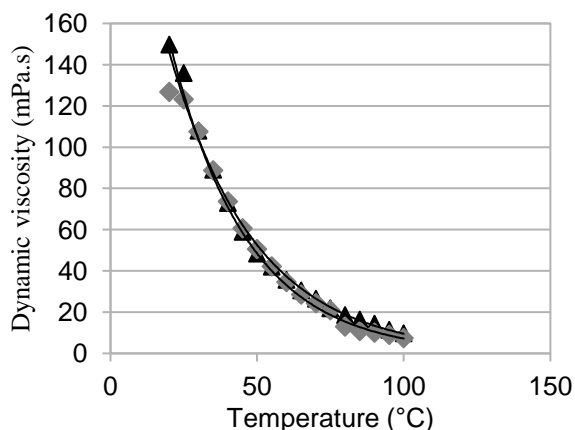
Fig. 5 Temperature dependencies of new oil Ultra ▲ and oil after 750 000 cycles ◆ of dynamic viscosity.
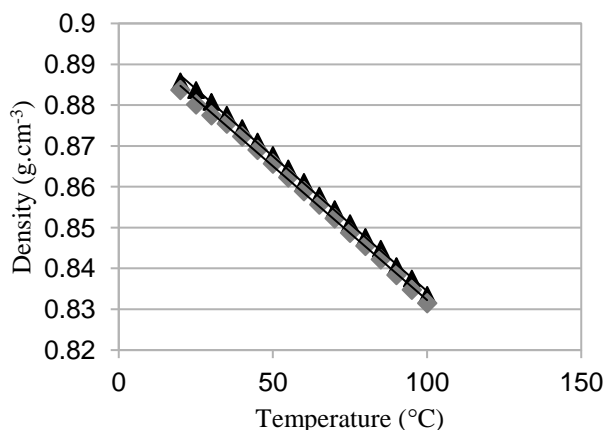
Fig. 6 Temperature dependencies of new oil Ultra ▲ and oil after 750 000 cycles ◆ of density.
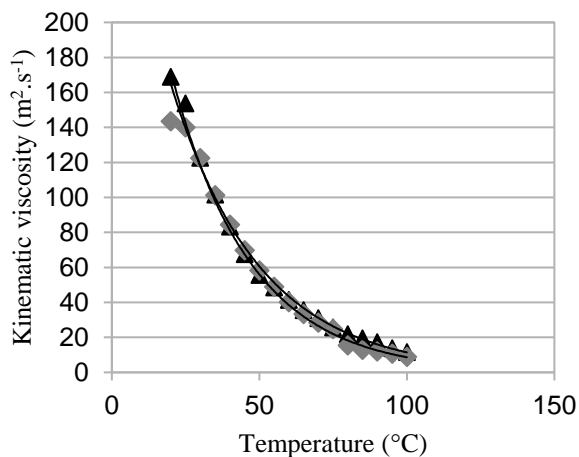
Fig. 7 Temperature dependencies of new oil Ultra ▲ and oil after 750 000 cycles ◆ of kinematic viscosity.
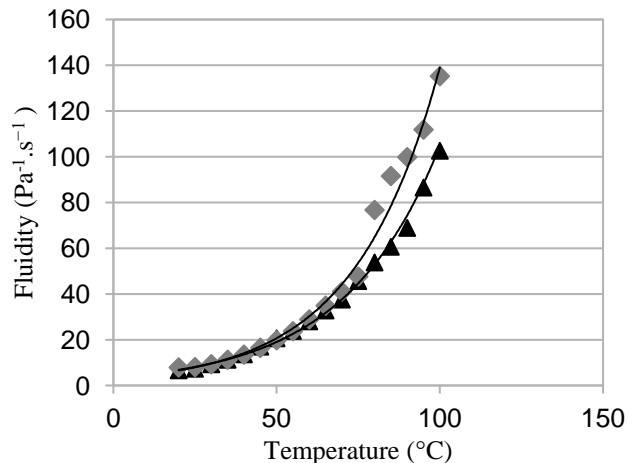
Fig. 8 Temperature dependencies of new oil Ultra ▲ and oil after 750 000 cycles ◆ of Fluidity.

For both samples we can see that with increasing temperature the dynamic viscosity exponentially decreases. In the range between 25 °C – 35 °C the new sample achieved very similar values of dynamic viscosity as the sample after the 750 000 cycles. At the temperature of 40 °C the sample after 750 000 cycles reached the viscosity value of 73.74 mPa.s while the new sample reached the value of 72.86 mPa.s. From the temperature of 55 °C we can see the increase of viscosity value again for the new sample. The sample after 750 000 cycles reached lower values of viscosity from the temperature of 80 °C. The coefficients of determination reach high values, for the new sample a value of 0.995 and for the sample after cyclic stressing the value of 0.988. The sample after 750 000 cycles had lower values

of density – the new sample had a density value of 0.8755 g.cm^{-3} at the temperature of 40 °C and the sample after 750 000 cycles reached the density value of 0.8723 g.cm^{-3}. It is shown that density linearly decreases with temperature of oil. The manufacturer lists a kinematic viscosity value of 80 mm^2.s^{-1} at the temperature of 40 °C. We measured the value of 83.35 mm^2.s^{-1} for the new sample, and a value of 84.53 mm^2.s^{-1} for the cyclically stressed sample. The value of the new sample differs from the data given by the manufacturer by 0.8 mm^2.s^{-1} at the temperature of 100 °C. With the cyclically stressed sample the kinematic viscosity dropped by 1.9 mm^2.s^{-1} from the manufacturer's data. The fluidity exponentially increases with the increasing temperature and from the temperature of 80 °C, the sample after cyclic stressing has higher values than the new sample.

Tab. 2 Defining the course of the exothermic pour point for the ULTRA sample

	New Sample	Sample after 750 000 cycles
Pour point (°C)	-33.12	-36.32
Initial exothermic reaction starting temperature (°C)	-31.17	-35.17
Final exothermic reaction temperature value (°C)	-36.06	-38.19

In the Tab. 2 we can see that the temperature stability for the new sample ends at -31.17 °C and the pour point is at the value of -33.12 °C. The sample after 750 000 cycles reaches the end of the temperature stability at -35.17 °C and the pour point reaches the value of -36.32 °C. For mineral oil, the cyclically stressed samples reached lower initial peak rising values, thus the exothermic reaction in these samples had occurred at a lower temperature. This may be related with a change in the lubricant structure in cyclic stress and thus the transition from liquid to solid occurs at lower temperatures.

CONCLUSIONS

Measured temperature dependencies of density, dynamic and kinematic viscosity, and fluidity show good accordance with published results (*Hlaváč et al., 2014*; *Božiková & Hlaváč, 2014*). Presented linear and exponential dependencies of physical properties on the temperature indicate significant impact of the temperature on oils thermal properties. Both lubricants have the same use and the results presented by our measurements prove only small differences between the mineral and ecological lubricants.

Several authors state that the comparison of biodegradable and mineral oils has yielded comparable results (*Kardjilova et al., 2013, Majdan et al., 2011b, Tkáč et al.,2012*). *Beleš & Zelenka (2008)* also devoted their works to the ecological lubricants and their broad usage in practice. These lubricants help to clean the equipment from deposits and carbon. *Kačmár (2014)* emphasizes the use of ecological lubricants mainly in agriculture, forestry and environment protection.

REFERENCES

1. Abdullah, B., Zubairi, S., Huri, H., Hairunisa, N., Yousif, E., & Basu, R. (2012). Polyesters Based on Linoleic Acid for Biolubricant Basestocks: Low-Temperature, Tribological and Rheological Properties. *Plos one*, *11*, 51 – 60

2. Bart, J., Gucciardi, E., & Cavalloro, S. (2012). Biolubricants: Science and Technology. *Series: Woodhead Publishing Series in Energy*, 944 p.

3. Beleš, B. & Zelenka, L. (2010). Ekologické alternatívy v olejoch a mazivách. *Tribotechnika.*

4. Bhushan, B. (2001). *Modern Handbook of tribology*. Boca Raton: CRC Press.

5. Božiková, M. & Hlaváč, P. (2014). Thermophysical properties of chosen biooils. *Journal of Central European Agriculture*, *18*(1), 8-10.

6. Brown, E. & Gallagher, P. (1998). *Handbook of Thermal Analysis and Calorimetry*. Elsevier, 755 p.

7. Hlaváč, P., Božiková, M., & Presová, R. (2014). Temperature relations of selected engine oils dynamic viscosity. *Acta technologica agriculturae*, *17*, 104 – 107.

8. Kačmár, M. (2014). Biooleje. *Rezbárstvo.*

9. Kardjilova, K., Vozarova, V., & Valah, M. (2013). Influence of Temperature on Energetic and Rheological Characteristics of PLANTOHYD Bio Lubricants – a Study in the Laboratory. *ETASR - Engineering, Technology & Applied Science Research*, *3*(3), 424-428, ISSN 1792-8036.

10. Klubal, T. & Ostrý, M. (2014). Vliv sálavého chlazení a vytápění s PCMs na vnitřní mikroklima a spotřebu energie Vliv sálavého chlazení a vytápění s PCMs na vnitřní mikroklima a spotřebu energie. *TZB-info.*

11. Kosiba, J., Jablonický, J., Bernát, R., & Kuchar, P. Effect of ecological hydraulic fluid on operation of tractor hydraulic circuit. In *6th International Conference on Trends in Agricultural Engineering* (pp. 317–322). Czech University of Life Sciences Prague; Faculty of Engineering.

12. Lahučký, L. & Tóth, T. (2011). *Aplikovaná chémia*, 4. ed., Nitra: SPU Nitra, 147 p.

13. Majdan, R., Cvičela, P., Drabant, Š., Tkáč, Z., Kosiba, J., & Abrahám, R. (2011a). *Hodnotenie ekologických prevodovo-hydraulických kvapalín na základe skúšok prevádzkovým zaťažením*. Nitra: SPU, pp. 127.

14. Majdan, R., Kosiba, J., Tulík, J., Kročková D., & Šinský, V. (2011b). The comparison of biodegradable hydraulic fluid with mineral oil on the basis of selected parameters. *Research in Agricultural Engineering*, 57, 43-49.

15. Perić, S., Nedić, B, & Grkić, A. (2014). Applicative Monitoring of Vehicles Engine Oil. *Tribology in industry*, 36(3), 308−315.

16. Rusnák, J., Kadnár, M., & Kučera, M. (2009). *Biologicky odbúrateľné oleje z pohľadu ich tribologických vlastností*. Monografia, Nitra: SPU, 85 p.

17. Severa, L. & Los, J. (2008). The influence of temperature on dynamic viscosity of dark beer. *Acta Universitatis Agriculturae et Silviculturae*, LVI (2), 303-307. Mendel. Brun.

18. Šimon, P. (2000). Diferenčná kompenzačná kalorimetria a jej využitie pri štúdiu materiálov. *Ropa, uhlie, plyn, 42*(3).

19. Stopka, J. (2014). Syntetické mazivá. *Tribotechnika.*

20. Tarasov, A. Thermal analysis, Lecture series heterogeneous catalysis, *Lectures Series*, FHI MPG.

21. Tkáč, Z., Drabant, Š., Kleinedler, P., Žikla, A., & Bolla, M. (2012). The test of biodegradace transmission and hydraulic fluid designed for agricultural tractors. *Savremena poljoprivredna tehnika, 38*(3), 191-199. Novi Sad: Centre for Evaluation in Education and Science.

22. Tkáč, Z., Majdan, R., & Kosiba, J. (2014). *Výskum vlastností ekologických kvapalín a nových testovacích metód mazacích olejov*. Nitra: SPU (pp. 94).

Corresponding author:
Ing. Ján Csillag, Ph.D., Department of Physics, Faculty of Engineering, Slovak University of Agriculture in Nitra, Slovakia, Tr. A. Hlinku 2, 949 76 Nitra, e-mail: jan.csillag@uniag.sk

BIO-ENERGY POTENTIAL FROM LEMON ORCHARDS

Metin DAĞTEKIN[1], Gürkan A. K. GÜRDİL[2], Bahadır DEMİREL[3]

[1]*Ceyhan Vocational School, Çukurova University, Adana Turkey*
[2]*Department of Agricultural Machines and Technologies Engineering, Faculty of Agriculture, Ondokuz Mayıs University, Samsun Turkey*
[3]*Department of Biosystem Engineering, Faculty of Agriculture, Erciyes University, Kayseri Turkey*

Abstract
Biomass has increasing popularity day by day as the fossil fuel sources consumed away in the world. Biomass can be both plant based and animal based residues. The potential of plant based biomass resources is huge but, most of these sources are idle. Not used for any purposes unfortunately. Pruning residues from fruit orchards are a good solution to compensate this energy source. Lemon is a popular fruit especially in the Mediterranean region of Turkey. Thus, is a good source for biomass. In this study, the pruning residues of lemon trees were converted into solid bio-fuel in the form of pellets. Thermal properties such as; gross calorific value, ash content and flue gas emissions of the produced pellets were analyzed. Also, some physical mechanical properties were determined. Bulk and pellet particle densities were 521.33 and 1236.70kg.m^{-3}, respectively. Firmness of the pellets was 2951 N and mechanical durability (MD) was 88.57%. Results showed us that the pruning residues of lemon orchards could be a good solution to be utilized as solid bio-fuel both in terms of physical-mechanical and thermal properties.

Key words: biomass; energy; lemon; pellet; pruning.

INTRODUCTION

As we are living in an energy age and any sources of energy are vital in today's world. The main source of energy comes from fossil fuels but they are subject to disappear in the coming years. People are in seek of alternative energy sources to survive. Biomass can be a good solution for that since it's plant and animal based residues. There is a huge residue potential in the world due to agricultural production. Unfortunately, most of these potential is not used for any purposes and they are just left on the fields or on the gardens for natural decomposition or just burned randomly near the garden. That is the case for lemon punning residues, as well (Fig.1.).

Fig. 1 Random burning of lemon pruning residues

Shaping the grinded material under pressure to smaller sizes (approx. 30 mm) is called pelleting *(Öztürk, 2012)*. Pellets can be produced from sawdust, wood chips, tree barks, agricultural products, straw, hazelnut shell, almond shell, walnut shell and even from waste papers. The density of material is increased and the transportation and storing costs are decreased by pelleting process. Moreover, homogeneity is provided in size and shape which make them more suitable for automatic feeding sys-

tems and effective usage of material is provided *(Werther et al., 2000; Mani et al., 2003; Holm et al., 2006; Nilsson et al., 2011; Theerarattananoon et al., 2011; Celma et al., 2012)*. Pelleted biomass is low and uniform in moisture content. It can be handled and stored cheaply and safely using well developed handling systems for grains *(Fasina & Sokhansanj, 1996)*. Turkey is an important producer of lemon in her region. Also, she is an important producer of fresh fruit and vegetable with about 51 million tons of production. Turkey's citrus production reached approximately 4.29 million tons in the last decade, with an increase of 44% *(TUIK, 2018)*. Lemon supply and consumption in Turkey is presented in Tab. 1 *(MFAA, 2018)*.

Tab. 1 Lemon supply and consumption in Turkey (1000 tons)

Season	2013/14	2014/15	2015/16	2016/17
Production	726	725	751	851
Import	2	2	3	4
Total supply	728	727	754	855
Export	404	449	394	493
Consumption	324	278	359	362

Lemon orchards need maintaining and care in order to keep and enhance the yield. The most common procedure for this is pruning, of course. The crown of the tree is pruned periodically to strengthen the tree and to boost the productivity. Hence, a big amount of pruning residue is produced in those particular periods and this wood based biomass is not used for any purposes. The aim of this study is to utilize lemon orchard pruning residues as solid biofuel in the form of pellets. Some physical-mechanical and thermal properties of produced fuel pellets such as; gross calorific value, ash content and flue gas emission values were analyzed.

MATERIALS AND METHODS

This study is carried out in labs and workshop of Agricultural Machines and Technologies Engineering Department of Samsun Ondokuz Mayıs University in Turkey. Pruning residues of lemon tree were provided from lemon orchards in Mediterranean Region of Turkey (Fig. 2). Up to date European standards (*EN 14961-2 & EN ISO 17225-6*) were taken as a reference for this research.

Fig. 2 Pre-fragmentation of lemon branches
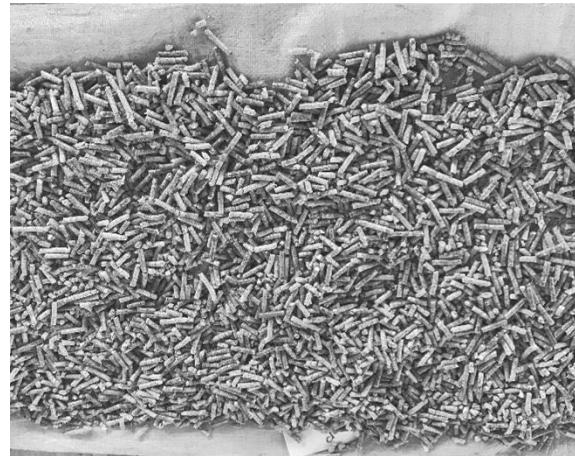
Fig. 3 Pellets from lemon pruning residues

The pre-chopped material was sun-dried under normal conditions until their moisture content was reduced to M10 (8-10 %). Then the dried material was ground in a 3-kW electric hammer mill consisting of 8 hammers rotating at a speed of 2,850 rpm. Once particles of the required sizes PS: 4 mm was obtained, moisture contents were re-measured, and the particles were pelleted using a pelleting machine (Fig. 3).

Lower heating value of pellets were determined by a calorimeter according to the instructions given in standard (*EN 14918*, 2009). Before testing, the pellets were disintegrated in a shredder and kept at 105 °C for 24 hours to remove the moisture. Samples dried at a weight of 0.5-1 g were burned in oxygen atmosphere in a calorimeter bomb under standard conditions and the calorific value was automatically determined in $cal.g^{-1}$ according to the increase in the temperature of the water in the calorimeter chamber and the average actual heat capacity of the system. Then the values are converted into $MJ.kg^{-1}$ as specified in standard (*EN 14961-2, 2010*). The ash contents of the pellets were determined using an ash furnace according to standard (*EN 14775, 2009*) and the flue gas emissions like $O_2(\%)$, $CO(ppm)$, $CO_2(\%)$, $NO(ppm)$, $NO_x(ppm)$ were measured and recorded with a gas analyzer.

RESULTS AND DISCUSSION

Ash content of the pellets made from lemon pruning agricultural residue was found as 5.20%, which is in line with the reference value (A10≤10%) given in standard (*EN ISO 17225-6, 2015*). Heating value of pellets was found as 18.60 $MJ.kg^{-1}$. That is also compatible with the value (Q14.5≥14.5 $MJ.kg^{-1}$) indicated in the above mentioned standard. The results showed us that the heating value of pellets produced from lemon tree pruning residues are higher than the wood (17.57 $MJ.kg^{-1}$). That is a promising result indeed. Especially, when the huge idle potential is concerned. The flue gases of the pellets are presented in Tab.2., below.

Tab. 2 Flue gas emissions of pellets

Water content after burning (%)	NOx (ppm)	CO₂ (%)	O₂ (%)	CO (ppm)	NO (ppm)
8.23	85.66	4.16	16.73	566.67	81.33

All the measured emission values were in the limits given in Regulations for Air Pollution Control (*IKHKKY, 2014*). Ash content was higher than the ash content of pellets produced from hazelnut husks (7.19%) (*Gürdil et al., 2016*). That can be due to content of material since the pruning residues of lemon trees are woody based elements so their ash contents could be higher than a plant based material. But on the other hand, CO and NO concentrations were lower than plant based materials (*Gürdil et al., 2016*). CO_2 emission was higher in fuel pellets produced from lemon pruning residues. But, this is an expected resulted because the higher CO_2 emissions the better burning of material. Physical mechanical properties of pellets are in Tab. 3.

Tab. 3 Some physical mechanical properties of pellets

Bulk density (kg.m⁻³)	Particle density (kg.m⁻³)	MD (%)	Firmness (N)
512.33	1236.70	88.57	2951

As compared to the results of previous researches bulk and particle densities were slightly lower than that of pellets from plant based residues. But, firmness of pellets was higher than them. As a conclusion the pellets produced from lemon orchard pruning residues was found to be very suitable in order to be used as bio-pellets.

CONCLUSIONS

Utilization of idle lemon orchard residues as source of solid biofuel in the form of pellets were investigated in this study. The pellets were produced with 4mm PS and M10 moisture content. Thermal properties of fuel pellets such as; lower heating value, ash content and flue gas emissions were determined. All the tests were done according to the latest EU standards. The results showed that the fuel pellets have very good thermal properties as a fuel. Besides, as from the environmental point of view flue gas emissions were within the defined limits. We believe in that further studies of this kind will help agricultural engineers, scientific researches, farmers and even the policy makers to think more globally and wisely for the future and will definitely have a positive contribution to sustainable development in the world.

REFERENCES

1. Celma, A.R., Cuadros, F., & Rodriguez, F.L. (2012). Characterization of pellets from industrial tomato residues. *Food and Bioproducts Processing, 90*(4), 700-706.

2. EN 14961-2. (2010). Solid biofuels- Fuel specifications and classes- Part 2: Wood pellets for non-industrial use. *European Committee for Standardization*: Management Centre, Avenue Marnix 17, B-1000 Brussels.

3. EN ISO 17225-6. (2015). Solid biofuels -- Fuel specifications and classes -- Part 6: Graded non-woody pellets. *European Committee for Standardization*: Management Centre, Avenue Marnix 17, B-1000 Brussels.

4. EN 14918. (2009). Solid biofuels – Determination of calorific value. *European Committee for Standardization*: Management Centre, Avenue Marnix 17, B-1000 Brussels.

5. EN 14775. (2009). Solid biofuels – Determination of ash content. *European Committee for Standardization*: Management Centre, Avenue Marnix 17, B-1000 Brussels.

6. Fasina, O. O. & Sokhansanj, S. (1996). Storage and handling characteristics of alfalfa pellets. *Powder Handling and Processing, 8*(4): 361-365.

7. Gürdil, G. A. K., Demirel, B., Baz, Y. O., & Demirel, C. (2016). Pelleting hazelnut husk residues for biofuel. In *TAE2016 International Conference on Trends in Agricultural Engineering, Prague, Czech Republic* (pp. 162-165).

8. Holm, J.K., Henriksen, U.B., Hustad, J.E., & Sorensen, L.H. (2006). Toward an understanding of controlling parameters in softwood and hardwood pellet production. *Energy and Fuel, 20*, 2686-2694.

9. IKHKKY. (2014) Regulations for Air Pollution Control Caused by Burning. Retrieved from http://www.mevzuat.gov.tr/.

10. Mani, S., Tabil, L. G., & Sokhansanj, S. (2003). An overview of compaction of biomass grinds, *Power Handling and Process, 15*, 160-168.

11. MFAA, (2018). Citrus report. *Ministry of Food, Agriculture and Animal, Turkish Republic*. ISBN: 978-605-9175-92-0, p: 66.

12. Nilsson, D., Bernesson, S., & Hansson, P.A. (2011). Pellet production from agricultural raw materials- a systems study, *Biomass and Bioenergy, 35*, 679-689.

13. Öztürk, H.H. (2012). *Energy plants and biofuel production*. Hasad yayıncılık Ltd. Şti, İstanbul, p: 272.

14. Theerarattananoon, K., Xu, F., Wilson, J., Ballard R., Mckinney, L., Staggenborg, S., Vadlani, P., Pei, Z.J., & Wang, D. (2011). Physical properties of pellets made from sorghum stalk, corn stoves, Wheat Straw and Big Bluesterm, *Industrial Crops and Products, 33*(2), 325-332.

15. TUIK. (2018). Statistics for plant production. *Turkish Statistical Institute*, Ankara.

16. Werther, J., Saenger, M., Hartge, E.U., Ogada, T., & Siagi, Z. (2000). Combustion of agricultural residues, *Progress in Energy and Combustion Science*, 26, 1-27.

Corresponding author:
Assoc. Prof. Dr. Gürkan A. K. Gürdil, Ph.D., Department of Agricultural Machines and Technologies Engineering Mechanical Engineering, Faculty of Agriculture, Ondokuz Mayıs University, Atakum 55200, Samsun, Turkey, phone: +90 5355949294, e-mail: ggurdil@omu.edu.tr

ULTIMATE TENSILE STRENGTH OF THE STRING DETERMINATION USING SPECTRAL ANALYSIS

Oldřich DAJBYCH[1]

[1]*Department of Mechanical Engineering, Faculty of Engineering, CULS Prague*

Abstract
The paper is focused on ultimate strength of guitar string using spectral analysis of rupture process sound recording from which the frequency of vibration right before failure was determined. The tension thus the stress can be calculated from fundamental frequency of the string. Two materials – High Carbon Steel and Nylon – were tested. Also two diameters of the string for each material were used. The results were verified by classic tension test and also by modal analysis in ANSYS Workbench environment. It was shown that this method gives relevant results.

Key words: *spectral analysis; ultimate strength; guitar string; modal analysis.*

INTRODUCTION

Ultimate tensile strength of material is usually determined using classic tension test *(Davis, 2004; Campbell, 2013)*. There are also other methods such as small punch testing *(Holmström, 2019)* or for dynamic tensile strength using Charpy data *(Lucon, 2016)*.

It is not always possible to provide or use appropriate equipment due to time, operational or economic conditions. But there is possibility to record the sound on almost every mobile device and also applications for spectral analysis or frequency measurement to be done "in the field" are available. There are also numerous possibilities how to apply tension to the object when applied force is not needed to be known. This could be useful in less developed countries or remote location when strength properties of constructional part needs to be verified.

Aim of this article was to introduce contactless method for measurement of ultimate tensile strength of straight vibrating object with constant cross-section what was represented by guitar string. The method shows that it is possible to determine ultimate strength without direct force measurement using shredding machine or similar testing device.

MATERIALS AND METHOD

Selected strings were attached to the guitar and the process of tightening was recorded as audio wav file. For steel strings audio recording electric guitar Fender Stratocaster (made in China) equipped with custom R.M. Pickups was used. Bridge pickup type RS3000 was selected. The guitar was connected over USB soundcard UGM96 into MacBook Pro 13' early 2015 running OSX 10.14.5. Audacity 2.3.0 free software was used for recording and editing. Electromagnetic pickups cannot obviously pick sound from nylon strings therefore acoustic guitar Nashville NW-020N with Thrust Emita USB Studio microphone was used for audio input. Sonic Visualiser version 3.3 what is free software developed at the Centre for Digital Music, Queen Mary, University of London was used for spectral analysis.

Not many string manufacturers offer more detailed information about their products, thus d'Addario strings were chosen because this manufacturer provides enough input parameters for this test to be executed. According to d´Addario tension chart *(d'Addario 2019)* high carbon steel strings PL009 and PL020 and nylon strings J4501 and J4503 were chosen. All strings are plain which means it has no wound therefore its physical and mechanical properties depend only on basic material and cylindrical shape. Required parameters are provided in Tab. 1. Some parameters had to be converted to international system or calculated from others, such as material density which is calculated from unit weight and string dimensions. The density was needed for correct material definition in FEA analysis. Length of all strings was 647.7 mm which is typical scale length of guitar thus 25.5 inches. It was also verified by measurement on the instruments.

Tab. 1 String properties

String	diameter inch	diameter mm	unit weight lb. $\cdot$ inch^{-1}	ρ kg $\cdot$ m^{-3}
PL009	0.090	0.229	$17.94 \cdot 10^{-6}$	7779
PL020	0.200	0.508	$88.61 \cdot 10^{-6}$	7807
J4501	0.280	0.711	$20.92 \cdot 10^{-6}$	941
J4503	0.403	1.024	$46.79 \cdot 10^{-6}$	1015

For each string 5 tests were carried out. The string was attached to the guitar and tuned on its nominal frequency what was verified by guitar tuner. Then the recording was started and the string was tightened using tuning knob of the guitar. The string was lightly hit with guitar pick each 1-2 seconds so that the sound can be recorded but the added force was as low as possible. When the string broke the recording was stopped. The audio wave was then shortened from dozens of seconds even minutes to only last seconds before rupture using editing software. After that the file was saved as wav and opened in spectral analysis software where fundamental frequency of the string in the moment before failure was obtained.

The ultimate strength of the string was calculated as stress for measured frequency using equation (2) which can be simply derived from equation (1) *(Rayleigh; 1945; Raichel, 2006; Inman, 2017)*.

$$f = \frac{1}{2 \cdot L} \cdot \sqrt{\frac{T}{m_1}} \tag{1}$$

where f is frequency of the string (Hz), L is length of the string (m), T is string tension (N) and m_1 is unit weight (kg $\cdot$ m^{-1}).

$$\sigma = \frac{16 \cdot f^2 \cdot L^2 \cdot m_1}{\pi \cdot d^2} \tag{2}$$

where σ is tensile stress in the string (Pa), f is frequency of the string (Hz), L is length of the string (m), d is string diameter (m) and m_1 is unit weight (kg $\cdot$ m^{-1}).

Subsequently all types of strings were tested using testing machine MPTest 5.050 for verification of ultimate tensile strength values. Custom made fixations were used for considerate string attachment. For steel strings testing speed 5mm $\cdot$ min^{-1} was used. Speed 20mm $\cdot$ min^{-1} was used for nylon strings to reduce test time according to much lower Young's modulus.

Also ANSYS Workbench 2019 R1 modal analysis using obtained material properties and ultimate stress values converted to tension used as bolt pretension load was used to verify values of frequency.

RESULTS AND DISCUSSION
The sound wave example with obvious failure moment is presented in Fig.1. Peak frequency spectrogram is shown in Fig.2. Horizontal-like lines show frequencies of clean tone. The lowest one is fundamental frequency of the string which was used for measurement in moment before string failure. Higher frequencies are harmonics which influence the sound of the instrument. The software is showing frequency of selected point in spectrogram on mouse over.

Tab.2. shows results of spectral analysis including standard deviation compared with tensile test ultimate strength results and FEA modal analysis for mean value of ultimate stress obtained from spectral analysis.
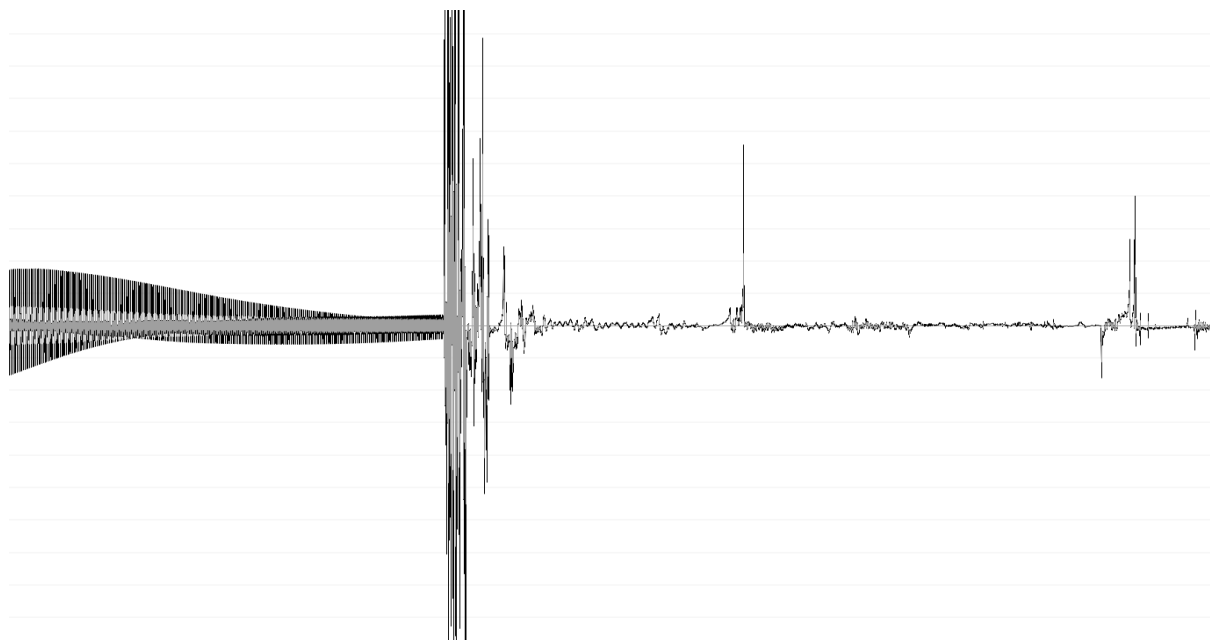
Fig. 1 Sound wave for string P009
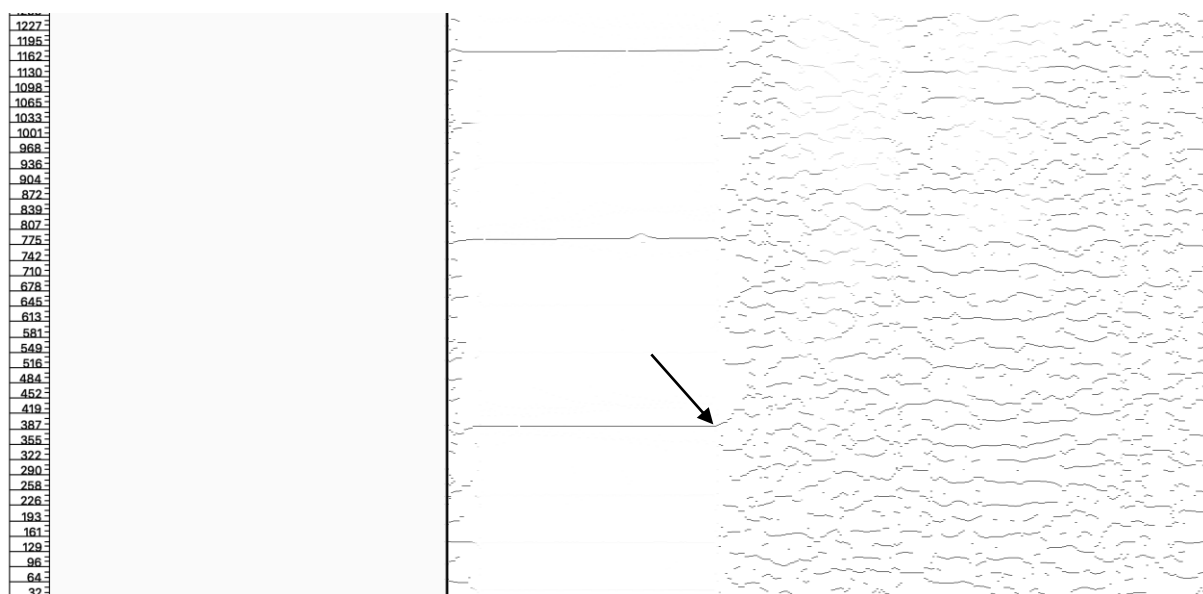
Fig. 2 Peak frequency spectrogram (the arrow is showing place of frequency measuring)

Tab. 2 Results

String	frequency Hz	ultimate strength MPa	tensile test MPa	FEA frequency Hz
PL009	405 ± 10	2143 ± 112	2306	403.2
PL020	350 ± 7	1606 ± 67	1623	350.1
J4501	431 ± 9	293 ± 13	292	408.5
J4503	432 ± 6	318 ± 9	308	424.2

From Tab.2. it is obvious that spectral analysis method gives relevant results. Lower values for steel strings can be explained by added stress of vibrating string in contrast to static tensile test. Result for nylon strings were also influenced by vibration but tensile test was influenced with pressing fixation of softer material what could also reduce the maximal value. The modal analysis for steel strings showed that equation (2) gives correct correlation between frequency and stress. On the other hand, Young's modulus of nylon strings is strongly dependent on stress *(Lynch-Aird & Woodhouse, 2017)* thus its correct definition in ANSYS analysis would require deeper research in mechanical properties of current strings which is out of aim of this study. Therefore, the results of modal analysis for nylon strings are not as relevant as for steel because nylon material provided in ANSYS has constant Young's modulus defined – in this case 3GPa what was estimated from tensile test.

According to *(Olmer, 2007)* music wire with diameter under approx. 0.3mm can have ultimate tensile strength up to 2600MPa what corresponds with obtained results. Decreasing ultimate strength with increasing diameter of the steel strings also corresponds to *(Ono, 2019)*. This effect was not observed at nylon strings what can be caused by different technology in steel and nylon string production. Also different material density thus slightly different basic material or process for each nylon string can explain the results.

CONCLUSIONS

Method for determination of ultimate tensile strength of straight vibrating object with constant cross-section represented by guitar string was introduced. It was shown that it gives relevant results. This method could be used at much enhanced condition with optimized fixations, automated tightening and recording or direct frequency measurement. Or, on the other hand in field conditions with mobile sound recording and analyzing or whenever advanced equipment is not available.

REFERENCES

1. Campbell, F.C. (2013). Inspection of metals. *ASM International: Materials Park*. ISBN 978-1-62708-000-2
2. d`Addario. (2019). String Tension specifications. *d`Addario, Farmingdale (NY)*. Retrieved from http://www.daddario.com/upload/tension_chart_13934.pdf
3. Davis, J.R. (2004). Tensile testing. *ASM International: Materials Park*. ISBN 0-87170-806-X
4. Holmström, S. et al. (2019). Developments in the estimation of tensile strength by small punch testing. *Theoretical and Applied Fracture Mechanics, 101*, 25-34.
5. Inman, D.J. (2017). *Vibration with Control*. Chichester: Wiley & Sons. ISBN 978-1-119-10821-4
6. Lucon, E. (2016). Estimating dynamic ultimate tensile strength from instrumented Charpy data. *Materials and Design 97*, 437–443
7. Lynch-Aird, N. & Woodhouse, J. (2017). Mechanical Properties of Nylon Harp Strings. *Materials (Basel), 10*(5), 497.
8. Olver, A.V et al. (2007). Investigation of service failures of steel music wire. *Engineering Failure Analysis, 14*(7), 1224-1232.
9. Ono, K. (2019). Size Effects of High Strength Steel Wires. *Metals, 9*(2), 240.
10. Raichel, D. R. (2004). *The science and applications of acoustics*. New York: Springer, ISBN 978-0387-26062-4.
11. Rayleigh J.W.S. (1945). *The Theory of Sound*. 2nd ed. Volume 1. New York: Dover Publications.

Corresponding author:
Ing. Oldřich Dajbych, Ph.D., Department of Mechanical Engineering, Faculty of Engineering, Czech University of Life Sciences Prague, Kamýcká 129, Praha 6, Prague, 16521, Czech Republic, phone: +420 22438 3178, e-mail: dajbych@tf.czu.cz

FAST AND RELIABLE POWER MEASUREMENT FOR ENERGY SOURCES TO ENHANCE DISTRIBUTION GRID STABILITY

Milan DANEČEK[1], Ivan UHLÍŘ[1]

[1] *Czech University of Life Sciences Prague, Faculty of Engineering, Department of Physics, Kamýcká 129, CZ165 00 Prague*

Abstract

This paper deals with measurement of fast active power for monitoring the renewable sources connected to a distribution grid. Fast measurement of active power is the key point of a reliable operation of the distribution grid. In past years we have observed increasing ratio of generated power from renewable energy sources. Renewable energy sources have specific behaviour under a specific weather condition. The term "specific behaviour" should be understood here as the oscillations of output power supplied to the distribution grid. This oscillation could be caused e.g. by wind gusts – wind turbine, or passing clouds – photovoltaics. Such kind of active power oscillation could lead to a large blackout. To prevent large blackouts, we have to perform fast active power measurement. This paper will disclose the method of the fast active power measurement and its application for monitoring the dynamic response of the distribution grid.

Key words: renewable sources; distribution grid; power generation; blackout.

INTRODUCTION

Electric power measurement is a general measurement being done in distribution grid monitoring. Any energy source needs a fast power measurement to monitor the operability and the stability of the distribution grid *(Madruga, Bernardon, Vieira, & Pfitscher, 2018; Milligan, 2018)*. Usual methods for measuring electric power are based on digital principle. However, it could be beneficial to use analogue signal processing for some application, especially if we want to investigate dynamic effects in the distribution grid related to the renewable sources. Distribution grid with certain penetration of renewable sources is in the middle of our interest. Renewable sources for instance PV cells (Photovoltaic) can be the source of instabilities for the distribution grid *(Chuang, Chang, Hsiao, Lu, & Yang, 2019; Fiedler, 2019)*.

Digital measurement is widely deployed. It is a part of complex monitoring systems delivered with hardware and equipped with SCADA (Supervisory Control and Data Acquisition) software or the like. Nevertheless, digital measurement has basic limitations. It goes about higher sampling frequencies and the equality of sampled value in a range of one sample. The requirement of higher sampling frequency is often achieved by raw estimation, which might be insufficient, e.g. for making measurements in the systems operating at 50 Hz – distribution grid.

Digital measurement is based on sampling of instantaneous values. The principle of digital active power measurement is that we measure voltage u(t) and current i(t) as a function of time. An instantaneous value of active power is then calculated from the instantaneous values of voltage and current *(Calleja, 2006; Sarkar & Sengupta, 2010)*.

Its median value for the selected time interval gives active power. Similarly, reactive power is determined as the displacement u(t) versus i(t) by 1/4 period. Typical problem of digital power measurement is how to set sampling frequency fs to respect higher harmonic trends expressing deformation of the voltage and current sine wave. We consider that the system frequency is fo is equal 50 Hz. Sampling frequency is as shown in equation (1), which is too low for most of the cases.

$$f_s = 20 \cdot f_0 = 20 \cdot 50 = 1 \, kHz \tag{1}$$

Frequency 1 kHz cannot affect harmonic trends, especially if the semiconductor converters (commonly used for renewable sources – PVE, wind turbine) are used. There also appear errors of measured active power due to interference of the sampling frequency with the measured parameters. Choosing a higher sampling frequency e.g. 10 kHz and higher helps us to avoid all the problems mentioned above, but it

is resulting in higher hardware requirements *(Cataliotti, Cosentino, Di Cara, Lipari, & Nuccio, 2015; Cataliotti, Cosentino, Lipari, Nuccio, & Serazio, 2013).*

Digital power measurement does not fit into the HW (Hardware) and SW (Software) of ordinary small PLC (Programmable Logic Controller). The solution leads to electrical power measurement on DSP (Digital Signal Processor) or programmable gate arrays. The measurement unit and its price range then contrast with a simple control system of the energy device itself.

Additional option for power measurement is the analogue method. It is a simple, cost-effective and reliable method, which is based on multiplication of analogue signal of voltage and current by analogue multiplier. After the multiplication we have to use an analogue filter. For instance, filtered signal can be connected to analogue input of common PLC (Programmable Logic Controller)*(Twigg & Hasler, 2009).* The solution for three phases P, Q, U_{RMS}, and I_{RMS} it means 12 measured variables would cost $120. The frequency range is up to 50 kHz for each channel, if the maximum frequency is not limited by measurement transformers.

Besides digital and analogue methods, which are often used for such kind of measurements, are so called PMUs (Phasor Measurement Units). PMUs allow to measure various phenomenon within the distribution grid. PMUs have several disadvantages and the first one is the investment cost. PMUs are in current scale suited for distribution grid operators such as for WAMS (Wide Area Monitoring Systems). Although to use PMUs for monitoring simple gensets or RES operation is not cost-effective.

Second disadvantage is the measurement of hardware and software. PMUs use sophisticated data processing methods, but cheaper PMUs use nominal value of the frequency (50Hz) instead of actual frequency. To measure dynamic trends, we need fast and responsive measurements, which can be seen below. Collecting and monitoring of operational data for long term periods is not the aim of the proposed solution.

The aim of this paper is to demonstrate the functionality of designed wattmeter for fast active power measurement applicable for local traditional/renewable sources to investigate their dynamic behavior related to rotational inertia.

MATERIALS AND METHODS

Due to the above-mentioned drawbacks of digital active power measurement were designed and assembled wattmeter utilizing analogue measurement method. Designed wattmeter is designed for three phases. The main purpose of designed wattmeter is to investigate the dynamic behaviour of renewable sources and their influence on the distribution grid with special focus on the stability.

Wattmeter construction

The measuring board/wattmeter has 6 inputs and 3 outputs. The inputs are voltage and current signals of corresponding phases. The outputs are then active power signals or resulting total active power from three phases.

The main elements of the board are three analogue multipliers AD633 one per phase. They are serving for multiplication voltage and current signal to gain active power. In the Figure 1. can be seen the schematic of the designed wattmeter.
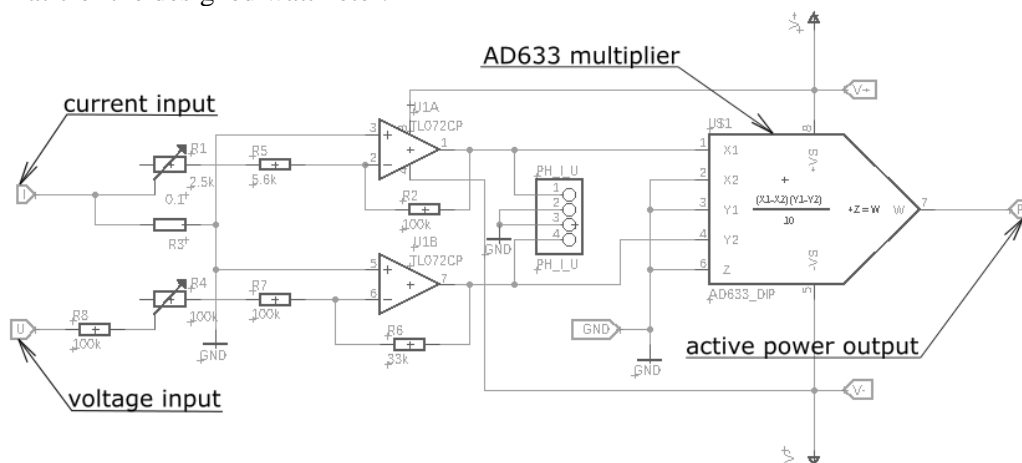
Fig. 1 Exemplary schematic of the designed wattmeter. Shown schematic corresponds to one phase measurement.

Wattmeter testing and calibration

The function of the designed wattmeter was tested and calibrated on the diesel genset with nominal power 1,3 MW. Nominal parameters of the genset are voltage 6.3 kV, 1000 rpm, 50Hz and cosϕ 0.8. Experimental measurement was done in Prague metro emergency power station in Radlicka station (line B). Testing conditions were chosen due to the variability under various testing states (power output, parallel operation etc.). The Figure 2A shows just the test condition. The designed wattmeter could be applied in the same manner for wind turbine or for photovoltaics cells.
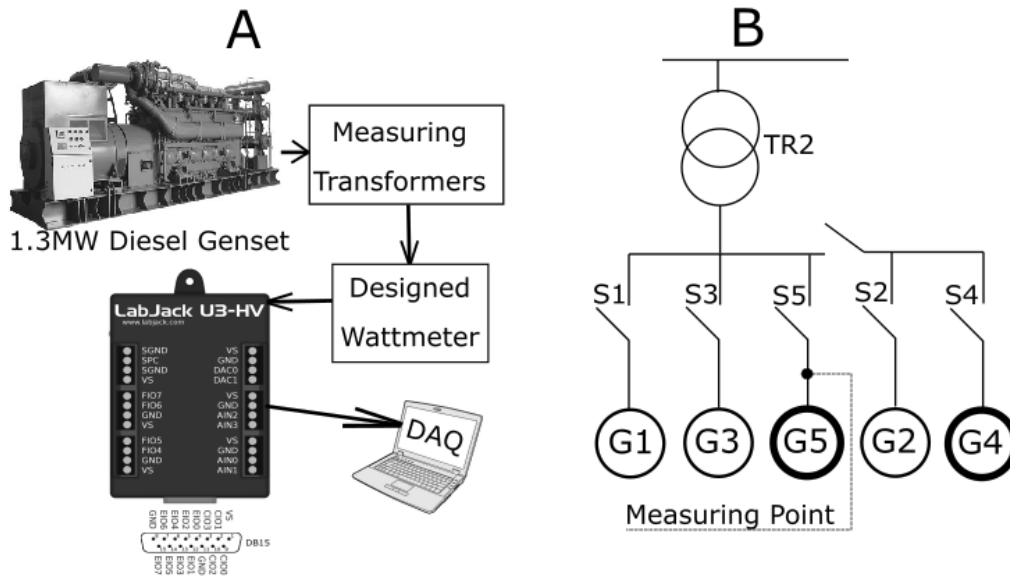
Fig. 2 A – Instrumentation arrangement, **B** – Location of the measuring point (G-generator, S-switch, TR-transformer).

In the Figure 2 we can see the instrumentation arrangement and location of the measuring points. Designed wattmeter was connected to the measuring transformers.

The current transformer has nominal current of primary winding 200 A and secondary winding 5 A. Maximal apparent power for primary and secondary winding is 10 VA. Nominal voltage on the primary winding is 6 kV and on the secondary winding is 0.1 kV. The voltage transformer has maximal load on the secondary winding 50 VA. Voltage transformers are in the set consisting of three transformers for each phase. They are connected in delta/star connection.

The measuring transformers are used also for operational measurement (monitoring). Analogue output from the designed wattmeter was then connected to the USB DAQ module LabJack U3-HV. Data was sampled with 10 kHz frequency.

Measured data was recorded by laptop equipped with LabJack software LJLogUD. Obtained data was then analyzed using MATLAB software. MATLAB analysis consists of filtering the data sets and selecting the sections closed to the phasing action of the gensets.

Statistical analysis to compare independent separate measurements was done using ANOVA method, results are shown in the Tab. 1.

Tab. 1 ANOVA test results

ANOVA						
Source of Variation	*SS*	*df*	*MS*	*F*	*P-value*	*F crit*
Between Groups	0.229474	2	0.114737	2.868421	0.017103	3.354131
Within Groups	1.08	27	0.04			
Total	1.309474	29				

Measurement comparison device was based on the same measuring transformers using measurement card connected to the SCADA system. The difference between reference measurement and designed wattmeter was maximally 10 %. However, the purpose of designed wattmeter is to diagnose and disclose possible failures of the power generation system, so the accuracy of 10 % is still tolerable.

The measurement was done using one wattmeter connected to G5 according to the Figure 2B. We have investigated the influence of two generators running in parallel operation. Testing condition was that G5 was synchronized to the grid (upper trends) and then synchronized with G4 (bottom trends). Measurement then monitored the influence of synchronizing G4 into parallel operation with G5.

RESULTS AND DISCUSSION

Following trends show the result of phasing G4 into parallel operation with G5. Phasing both generators was done under 100 kW load. To verify the functionality of designed wattmeter (monitoring of dynamic behavior of energy sources) we phased the G4 with slight phase displacement, so that it generated power impulse delivered to the distribution grid. Thus, on the top trend in each figure we can see dynamic response of the distribution grid to G5 phasing. Similar trends can be observed in the discontinuous power generation or lost of synchronism, which can be observed in renewable energy sources area (Madruga et al., 2018).

Connecting another genset G4 to electrical grid caused oscillation in the distribution grid, which needs to be regulated by various regulation mechanisms, e.g. frequency regulation (Milligan, 2018). This led to a visible response from already phased G5.

In the Fig.3 we can see first set of measurements on the G4 and G5 in parallel operation with 2s resolution, above we can see significant peak during synchronizing G5 causing the disturbances (disturbance is damped within 13 seconds), below is the response of already synchronized connected genset to the G4 connection. Based on this measurement we can conclude, that G4 is the source of irregularities, which cause fluctuation of delivered G5 power.
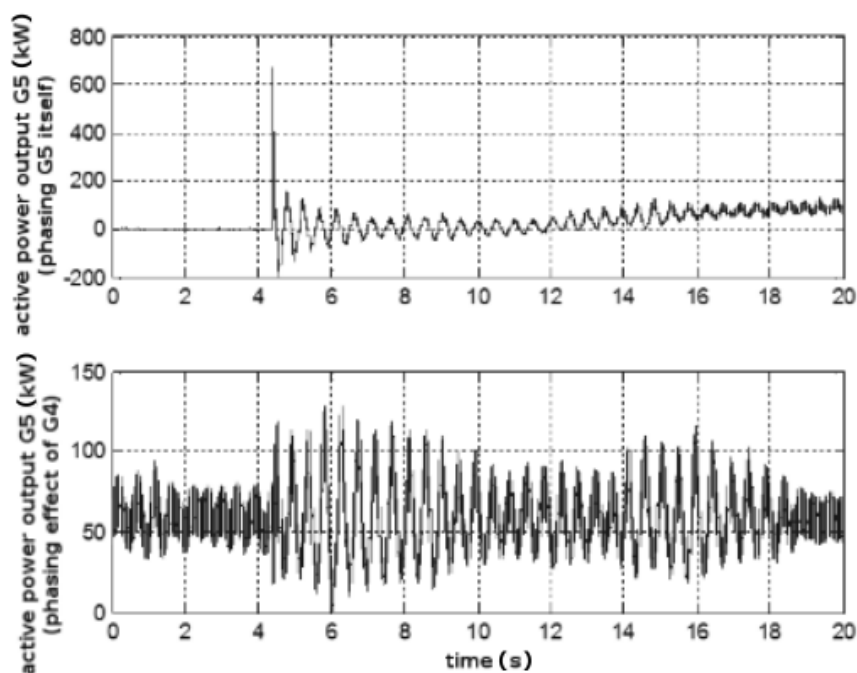
Fig. 3 Set of measurement of active power of G5 – plot with 2s resolution (upper –synchronizing genset to electrical grid, bottom – response of synchronized genset to synchronization event of 2nd genset.

In the Fig. 4 we can see similar trends like in the Fig. 3, but with 1s resolution. We can see significant fluctuations in the G5 power output. Shown state could be potentially dangerous, but we can observe that the damping factor is still high, so the fluctuations are lowered.
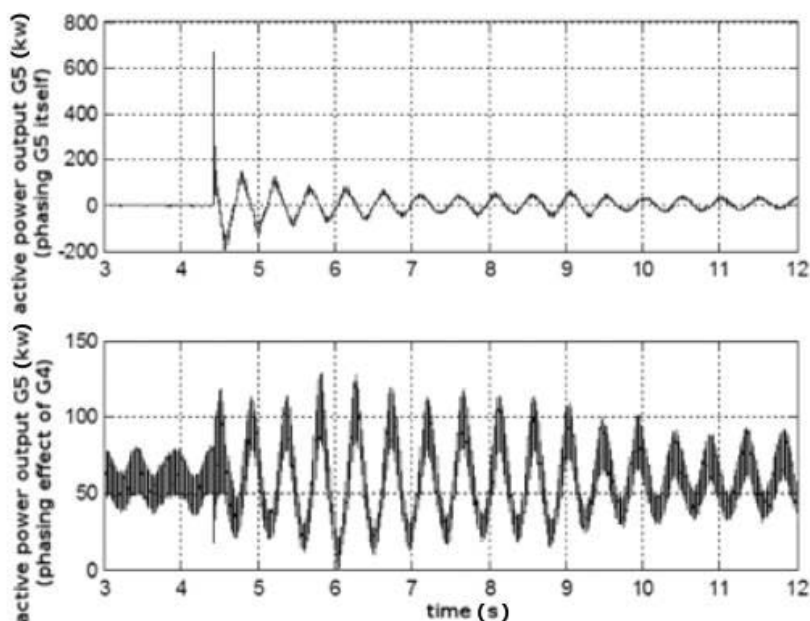
Fig. 4 Set of measurement of active power of G5 genset – plot with 1 s resolution (upper –synchronizing genset to electrical grid, bottom – response of synchronized genset to synchronization event of 2nd genset.
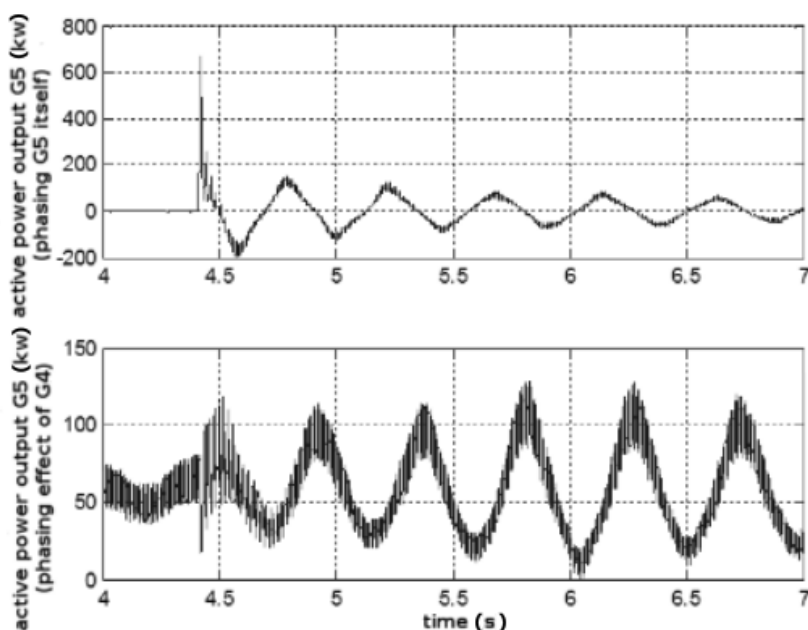
Fig. 5 Set of measurement of active power of G5 genset – plot with 0.5s resolution (upper –synchronizing genset to electrical grid, bottom – response of synchronized genset to synchronization event of 2nd genset

In the Fig. 5. we can see the trends with 0.5 s where damping factor is low, so the amplitude has growing trend. This is state is emergency and could lead to the breakdown of the gensets and to the interruption of delivered power.

CONCLUSIONS
The measurement with developed wattmeter proved that analogue method can provide very fast and reliable outputs. This is very important for monitoring of the energy sources with special regards to their dynamics.

Another point of interest is the accuracy of the measurement. We compared our data with standardized digital measurement done by operators. We achieved maximal error for approximately 10 % of measured value. The error is not satisfying, but main purpose of developed wattmeter is to monitor the dynamics, such as the dynamic response of the distribution grid, damping coefficient, etc. The dynamic response of the distribution grid can be used to find the correlation between the traditional energy power sources output and the renewable power sources output. This type of correlation can be used for distribution grid modelling.

The developed wattmeter will be further used for long term monitoring of the PV panels with focus on dynamic behaviour based on weather conditions (e.g. temperature, clouds…).

The methodology of fast active power measurement provides the values corresponding with the instantaneous torque magnitude according to the Park's equations. It means that foregoing method could be used to investigate mechanical irregularities. Developed wattmeter was used to discover the source of problems e.g. the genset's cylinder (combustion issues), mechanical defects (bearings) or to detect higher order of harmonic functions in the power output. Measured results were used to correct rotational speed regulation. The method is usable for monitoring of electromechanical systems and in comparison, with PMU is much cheaper and more reliable.

REFERENCES

1. Calleja, H. (2006). A simple VFC based wattmeter suitable for application at industrial frequency. *Measurement: Journal of the International Measurement Confederation*, *39*(1), 73–79. doi: https://doi.org/10.1016/j.measurement.2005.07.007

2. Cataliotti, A., Cosentino, V., Di Cara, D., Lipari, A., & Nuccio, S. (2015). A DAQ-based sampling wattmeter for IEEE Std. 1459-2010 powers measurements. Uncertainty evaluation in nonsinusoidal conditions. *Measurement: Journal of the International Measurement Confederation*, *61*, 27–38. doi: https://doi.org/10.1016/j.measurement.2014.10.033

3, Cataliotti, A., Cosentino, V., Lipari, A., Nuccio, S., & Serazio, D. (2013). DAQs-based wattmeters for high accuracy measurements. Comparison with the Italian power primary standard. *Measurement: Journal of the International Measurement Confederation*, *46*(9), 3460–3468. doi: https://doi.org/10.1016/j.measurement.2013.05.031

4. Chuang, M. T., Chang, S. Y., Hsiao, T. C., Lu, Y. R., & Yang, T. Y. (2019). Analyzing major renewable energy sources and power stability in Taiwan by 2030. *Energy Policy*, *125*(October 2018), 293–306. doi: https://doi.org/10.1016/j.enpol.2018.10.036

5. Fiedler, T. (2019). Simulation of a power system with large renewable penetration. *Renewable Energy*, *130*, 319–328. doi: https://doi.org/10.1016/j.renene.2018.06.061

6. Madruga, E. P., Bernardon, D. P., Vieira, R. P., & Pfitscher, L. L. (2018). Analysis of transient stability in distribution systems with distributed generation. *International Journal of Electrical Power & Energy Systems*, *99*(1), 555–565. doi: https://doi.org/10.1016/j.ijepes.2018.01.039

7. Milligan, M. (2018). Sources of grid reliability services. *Electricity Journal*, *31*(9), 1–7. doi: https://doi.org/10.1016/j.tej.2018.10.002

8. Sarkar, A., & Sengupta, S. (2010). Design and implementation of a high accuracy sampling wattmeter under non-sinusoidal and off-nominal frequency conditions. *Measurement: Journal of the International Measurement Confederation*, *43*(3), 312–319. doi: https://doi.org/10.1016/j.measurement.2009.11.003

9. Twigg, C., & Hasler, P. (2009). Configurable analog signal processing. *Digital Signal Processing: A Review Journal*, *19*(6), 904–922. doi: https://doi.org/10.1016/j.dsp.2007.09.013

Corresponding author:
Ing. Milan Daneček, Department of Physics, Faculty of Engineering, Czech University of Life Sciences Prague, Kamýcká 129, Praha 6, Prague, 16521, Czech Republic, e-mail: danecek@tf.czu.cz

ELLIPSE ROTATION UNDER A PRESSURE

Šárka DVOŘÁKOVÁ[1], Josef ZEMAN[2]

[1]*Czech University of Life Sciences in Prague, Faculty of Engineering, Department of Mathematics, Kamýcká 129, 165 21 Prague 6 – Suchdol, Czech Republic*
[2]*Czech University of Life Sciences in Prague, Faculty of Engineering, Department of Physics, Kamýcká 129, 165 21 Prague 6 – Suchdol, Czech Republic*

Abstract
The paper deals with the turning of an ellipse or an ellipsoid in a situation when a normal force affects on it from opposite sides. We assume that the friction with the contact areas is shear and the parameters of the ellipse are known. Potential applications of this task are very varied. For example, it can be the orientation of an elliptical sample by covering and underlying glass of a microscope, the orientation of pebbles or beans in the press, or a simple measurement of the diameter of a wire with a sliding scale.

Keywords: ellipse; ellipsoid; orientation; normal force.

INTRODUCTION

The authors of this article have run into the problem of determining transverse dimensions of the sample of nearly elliptical shape (in space this is an ellipsoid, for which the derived formulas are identical) several times. In practice, it is often the subject of a cylindrical shape with a significant ellipticity, which is exposed to effects of parallel surfaces during the measurement. In this article, we focus on the situation when the device determines distance of these parallel areas adjacent to the measured ellipse.

A similar task would come in case of optical microscope, where the orientation of ellipsoid is affected by the force of planparallel surfaces of covering and underlying glass and the dimension is set by a photograph orthogonal to their flat surface. Taking into consideration our assumption that there is a shear friction between an ellipsoid and planparallel surfaces, the angle of rotation will be given by the curvature of ellipse surface as well as the coefficient of shear friction μ.

The aim of this study is to find an equation for the angle formed by the main halfaxis of the subject of the elliptical shape with planparallel planes, which compress this subject, and that with the coefficient of shear friction between the planes and the subject being known.

MATERIALS AND METHODS

To illustrate and demonstrate the application of discovered connections, a situation when we try to set the exact cross dimension of a human hair using micrometre will be presented. For the measurements we used a digital micrometer JIGO-YT12.7 with a resolution of 0.001 mm.

After this measurement, the sample was repeatedly dehydrated in ethanol baths and deluged by resin and after hardening by mikrotom we took a series of transverse sections of the thickness of 15 μm. Their geometry was subsequently determined under an optical microscope. Cut surface was approximated by ellipse, therefore, the dimension of the main and secondary half-axis was identified. When compressing the flat jaws of the micrometer on the hair 30 year old woman it comes to continual orientation of hair ellipse between the jaws of micrometre (fig. 1) until the moment when sliding friction equals the force rotating the hair. Proportion of the main and adjacent half-axis of hair of white man is approximately 1.62 *(Skřontová, et al., 2017)*. Our goal is to set the final angle, or more precisely the angle interval, in which the oriented ellipse is located towards the flat surface orthogonal to planparallel surfaces. If the angle will be smaller than critical angle α_c, there will be no orientation caused by sliding friction. However, if the initial orientation of ellipse will be bigger, it would cause its rotation and the result angle will be α_c. Micrometre measures transverse dimension, which is slightly bigger than the dimension of the smallest dimension of an ellipse and thus the length of its adjacent half-axis.
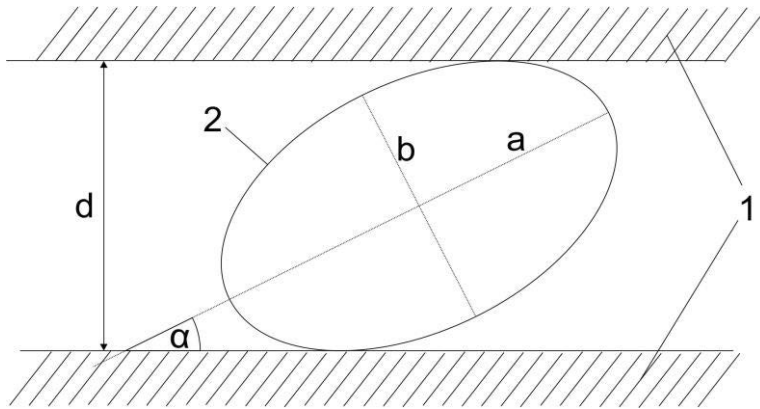
Fig. 1 1-jaws, 2-sample

The aim is to establish the value of this variance on account of the coefficient of shear friction of the pair of materials μ and parameters of ellipse a,b.

Our fundamental assumption is that curvature in a touching point, which means its second derivative in a critical angle must equal shear friction μ. From this attribute we come to the conclusion of this article thanks to the attached method *(Makovický, et al., 2013)*.

RESULTS AND DISCUSSION

Without loss of generality we can transform the task of fig. 1 and solve the easier task (fig. 2).
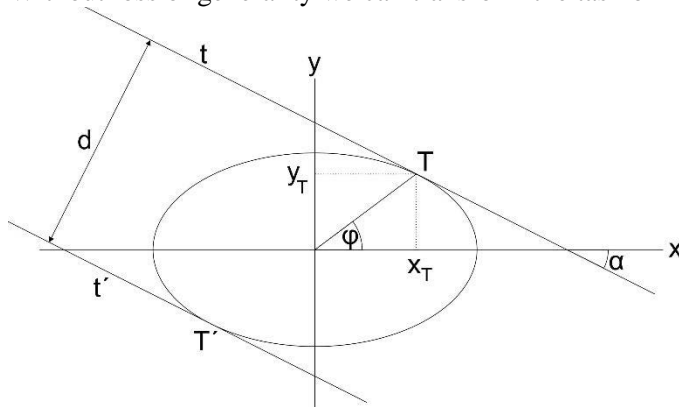
Fig. 2 Ellipse scheme

The sample (ellipse) is placed with its centre at the beginning of the coordinates system and with half-axes parallel with the axes of the system of coordinates *(Mošna, 2014)*. At an angle $\alpha \in (0, -\pi/2)$ we create two parallel tangents with tangent points in the 1st and the 3rd quadrant and we denote them by t and t′. The equation of such an ellipse we can write in the usual form

$$\frac{x^2}{a^2} + \frac{y^2}{b^2} = 1 \tag{1}$$

The slope of the tangent line to this ellipse has evidently the form *(Dvořáková, et al., 2015)*

$$y' = \frac{-bx}{a^2 \sqrt{1 - \frac{x^2}{a^2}}} \tag{2}$$

For the tangent point of the line with the slope $tg\ \alpha$ and our ellipse then holds

$$y_T = b\sqrt{1 - \frac{x_T^2}{a^2}} \tag{3}$$

For the slope of the tangent line then the equality is

$$y'(x_T) = tg\,\alpha = \frac{-bx_T}{a^2\sqrt{1-\frac{x_T^2}{a^2}}} \tag{4}$$

From which we get the coordinate x_T of the tangent point

$$x_T = \sqrt{\frac{a^4\,tg^2\alpha}{b^2+a^2\,tg^2\alpha}} \tag{5}$$

After substituting into the equation (3) we get also y-coordinate of the tangent point T

$$y_T = b\sqrt{\frac{b^2}{b^2+a^2\,tg^2\alpha}} \tag{6}$$

For tg φ of the line connecting the beginning of the coordinates and the tangent point T then holds

$$tg\,\varphi = \frac{b^2}{a^2\,tg\alpha} \tag{7}$$

The equation of the tangent line is then

$$x\,tg\alpha - y + \frac{b^2-tg^2\alpha\,a^2}{\sqrt{b^2+a^2\,tg^2\alpha}} = 0 \tag{8}$$

For the distance of the tangent from the beginning of the coordinates we get the relationship

$$\frac{d}{2} = cos\alpha\,\frac{b^2-a^2\,tg^2\alpha}{\sqrt{b^2+a^2\,tg^2\alpha}} \tag{9}$$

According to the above assumption, the rotation of the elliptical sample occurs if the second derivative of the surface of the sample is greater than the module of the shear friction

$$y'' > \mu.$$

$$y'' = \frac{-ba}{(a^2-x^2)^{3/2}} \tag{10}$$

For the limit angle φ_c, in which compensation of the friction and rotational forces occurs we can write for the coordinates of the critical rotation

$$x_c = \sqrt{a^2 - \sqrt[3]{\left(-\frac{ba}{\mu}\right)^2}} \qquad , y_c = \sqrt{b^2\left(1 - \frac{a^2-\sqrt[3]{\left(-\frac{ba}{\mu}\right)^2}}{a^2}\right)} \tag{11}$$

For $tg\,\varphi$ is therefore

$$tg\varphi = \frac{\frac{b}{a}\sqrt[3]{\frac{ab}{\mu}}}{\sqrt{a^2-\sqrt[3]{\left(-\frac{ba}{\mu}\right)^2}}} \tag{12}$$

Using the equation (7), we get

$$tg^2\alpha = \frac{b^2}{a^2}\cdot\frac{a^2-\sqrt[3]{\left(-\frac{ba}{\mu}\right)^2}}{\sqrt[3]{\left(-\frac{ba}{\mu}\right)^2}} \tag{13}$$

And by using the equation (9) we finally get the critical distance d_c .
Our main question is, what is the relationship between the half-axis b and d/2. Let's take the specific values for human hair:

For half-axis a = 47,5 μm, b = 29,3 μm, μ = 0,11 is $\alpha_c = 47,6^o$ a $d_c = 41,8$ μm *(Jelen, et al., 2014)*. The deviation amounts to 43 %. In case of human hair, the determination of the minimum dimension b of the ellipse with the help of a micrometer is only therefore possible with a tolerance of 43%.

Another comparison we can make based on these measurements, from which we know the cross-sectional dimensions a,b of the female hair identified from the ortogonal cut and at the same time from data measured by a digital micrometer. These measurements then indicate that the maximum measured value actually corresponds with the limit angle specified by equation 13. These measured data served to validate our designated equations, which are the main result of this article.

DISCUSSION

As we have just shown, when using the real values the deviation of the measured value from the length of the minor half-axis of the ellipse may be up to 50 %. Such a value can be significant e.g. in the case that we want to read the diameter of the hair of the horse, where the length of the horse hair we use as a time-recording medium of the condition level of the horse and the diameter of the horse hair in a given location corresponds to the condition of the horse at the time of the growth of this section.

In such cases, in the measurement of soft materials is, however, at the same time necessary to count with the fact that the deformation of the material during a mechanical measurement occurs by the influence of pressure, and it may be even greater than our 43 %.

Another factor influencing the similar measurement is certainly the imperfection of elliptical shape in cross-section of the sample. We consider, however, the elliptical approximation to be an essential second step to the expression of the shape of the sample.

Similar relations corresponding to our relationship 2 are the same result as derived by *Mošna (2014)*.

CONCLUSIONS

Formulas derived above present the base for error estimation while measuring loosely placed samples in a contact way. It is a reflection, which every experimenter facing such problem should take into consideration. It is clear that relatively complicated resulting formulas (12), (13) could be in case of particular samples with a small dispersion of values simplified and some components could be omitted. This could be also done in case of hair, which we have chosen as illustrative. Intentionally we present the formulas in full version, so that their future use would be as general as possible.

REFERENCES

1. Dvořáková, Š. & Mošna, F. (2015). *Diferenciální počet*. Česká zemědělská univerzita v Praze.
2. Jelen, K., Skřontová, M., Šimková, L., Zeman, J., Tlapáková, E., & Fanta, O. (2014). Changes in the mechanical parameters of hair in a group of women in reproductive age. *Neuroendocrinology letters, 35*(6), 481-489.
3. Makovický, P., Horáková, P., Slavík, P., Mošna, F., & Pokorná, O. (2013). The use of trigonometry in bloodstain analysis. *Soudni Lekarstvi, 58*(2), 20-25.
4. Mošna, F. (2014). From Newton to Kepler. One simple derivation of Kepler´s laws form Newton´s ones. *Italian Journal of Pure and Applied Mathematics, 32*, 393-400.
5. Skřontová, M., Šimková, L., Bittner, V., Chalupa, B., Zeman, J., & Jelen, K. (2017). Selected mechanical parameters of women's hair in the Caucasian population. *Neuroendocrinology letters, 38*(3), 199-207.

Corresponding author:
Ing. Šárka Dvořáková, Ph.D., Department of Mathematics, Czech University of Life Sciences in Prague, Faculty of Engineering, Kamýcká 129, 165 21 Prague 6 – Suchdol, 16521, Czech Republic, e-mail: dvorakovas@tf.czu.cz

INNOVATION MEASUREMENT DEVICE OF CAR SEATS

Vítězslav FLIEGEL[1], Petr LEPŠÍK[1], Rudolf MARTONKA[1]

[1]*Department of Mechanical Engineering, TU of Liberec, Studentska 2, Liberec 1*

Abstract

The comfort of sitting on car seats depends on many parameters and the people sitting on it are different. Every person is different, behaves differently, and feels different. We will put such an original-man on a unique car seat and want it to suit everyone without distinction. Then we need to require the car seat to adapt to the person sitting on it, preferably automatically. That is why we are testing a car seat in real-life conditions in the car, i.e. under the conditions of simultaneous multi-axis loading. The content of this article is the innovation of car seat measurement equipment in laboratory conditions. The existing device allows only the vertical movement of the car seat to realize. The aim of the innovation is to complement the device so that the horizontal movement of the car seat can realize simultaneously with the vertical movement.

Key words: car seat; testing; multi-axis loading; human; hard dummy.

INTRODUCTION

Testing of car seats in laboratory condition is done according to the relevant standards (*Standard JASO B407-87: Test code of seating comfort for automobile seats*). There are a number of these standards, and each of them conforms to a certain automobile seat load regime. Also important is the interaction of the car seat with the human, which depends on the comfort of sitting and the level of fatigue after a long car ride. Aim of this article was to provide new method and new testing laboratory equipment for testing of cars seats of loading hard dummy.

MATERIALS AND METHODS

The existing testing device complies with the standards prescribing only one-axis vertical movement of the car seat. So, only with the vertical loading in the "z" axis. Fig. 1.

Fig. 1 Testing device

total
high 1800
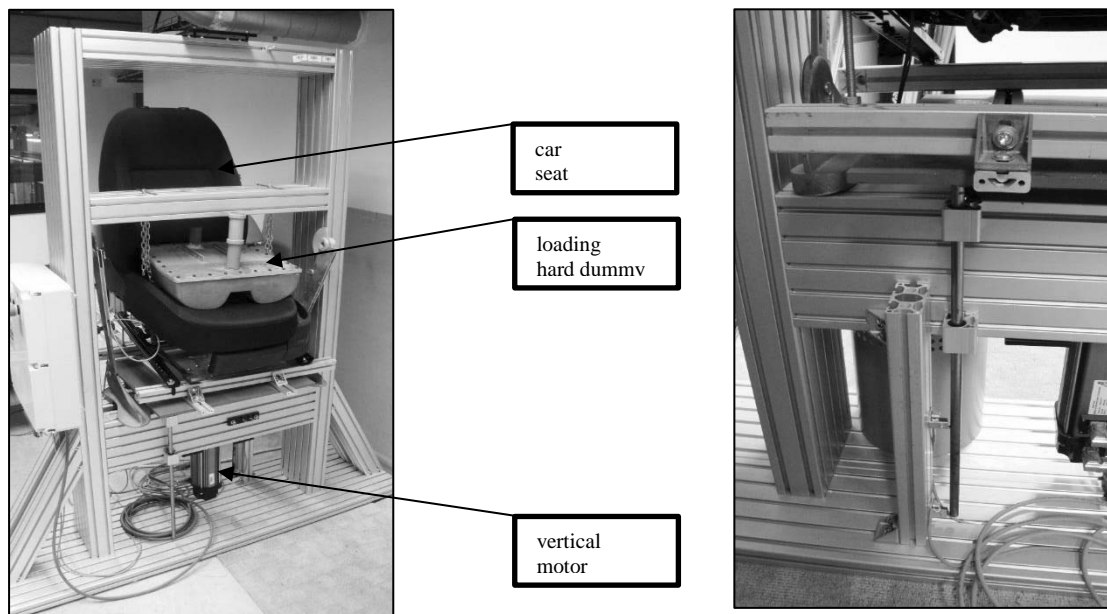
control
panel
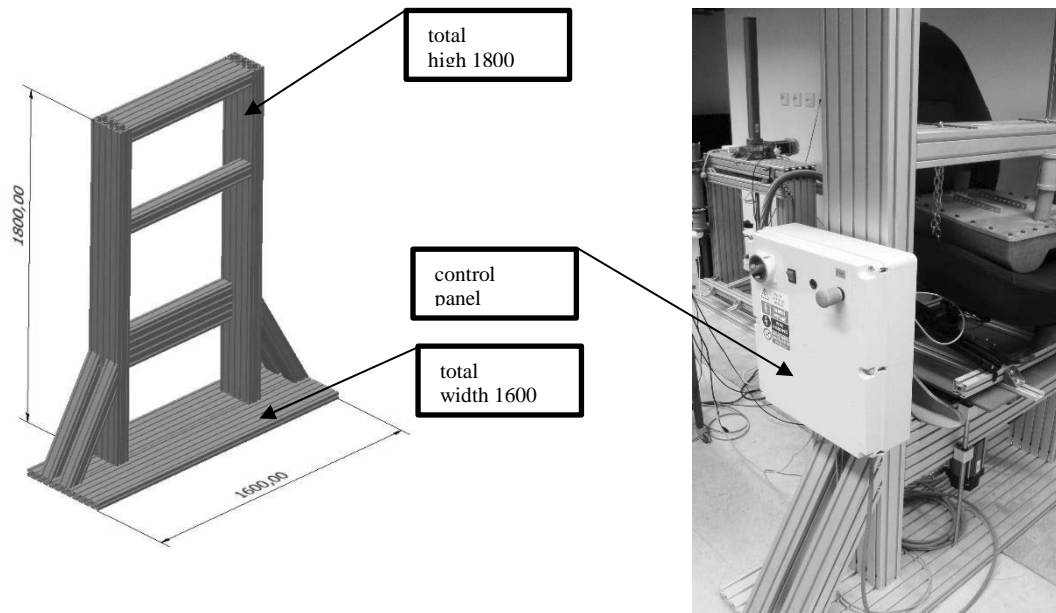
total
width 1600

Fig. 2 Testing device control

Also its total height of the machine is limited to 1800 mm Fig. 2. To test full automobile seats with full load, this height needs to be increased. In addition, according to current standards prescribing car seat testing in laboratory conditions, it is necessary to add the horizontal movement of the seat during testing. When designing the test equipment upgrade, the working height was increased to 2400mm Fig. 3. For the new concept, a new vertical load management Fig. 4, the guide and the guide bearing have been reinforced Fig. 5, between which was placed the linear Servo motor Actuator series GSM40. Have been designed three variants of the horizontal guide Fig. 5-6. The first solution uses standardized elements of the item system. The other two solutions are based on the principle of vertical guidance with a movable profile or with a movable guide rod. The final price calculation of the device innovation leads us to a certain price economy and consequently to simplification of the whole innovated construction. Therefore, the cheapest price option was chosen.

total
height 1800 mm

new
height 2400 mm
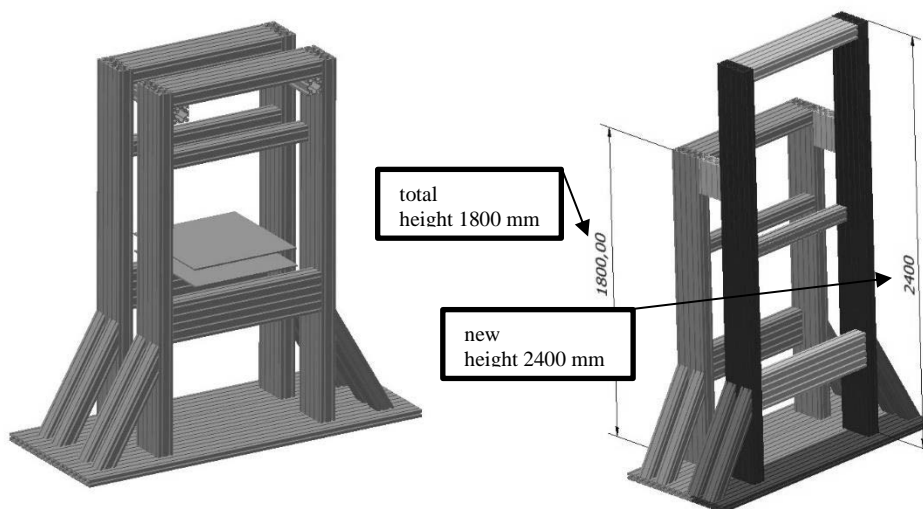
Fig. 3 New testing device
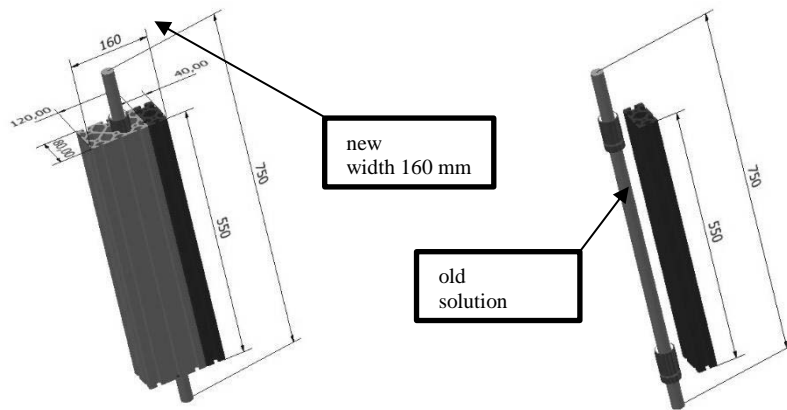
Fig. 4 Vertical movement
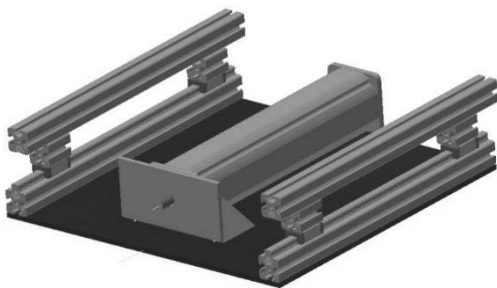
Fig. 5 Horizontal movement
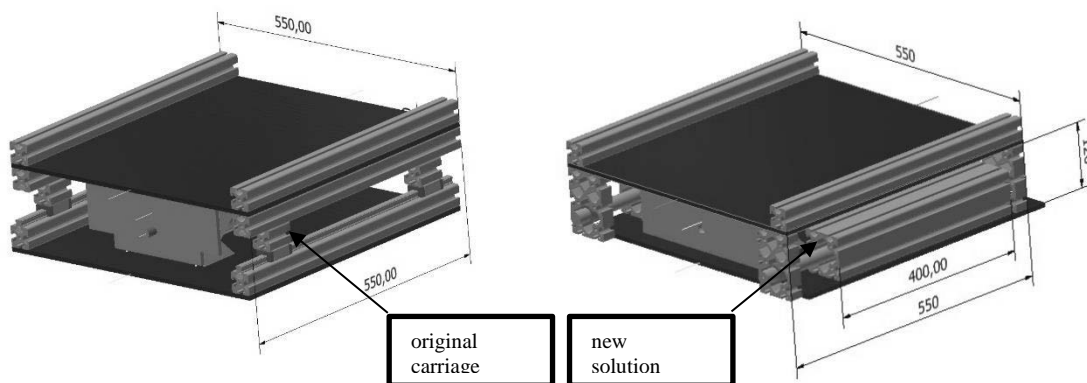
Fig. 6 Horizontal movement variants

For the new device will be designed completely new software Management and regulation in SW LabViev. Conclusions for innovation testing equipment, we can do based on measurements made on the TUL Hexapod device, which show the dependence on the methodise of loading the car seats Fig. 7. Dynamic and static loading in the vertical direction and at the same time by horizontal movement represent new conclusions and measurement results Fig. 8.
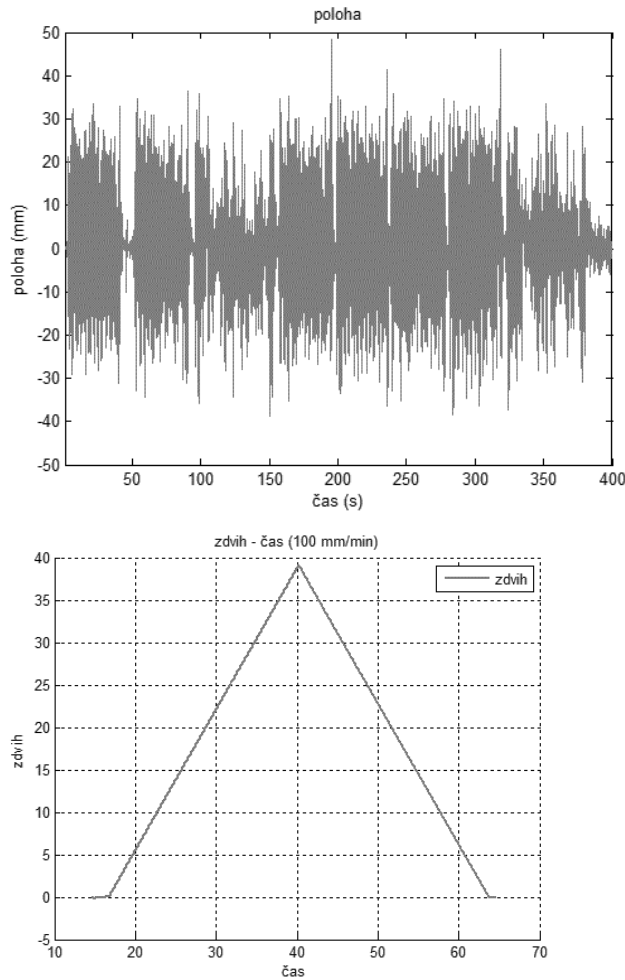
Fig. 7 Vertical and horizontal movement variants

By combining exactly defined dynamic loading cycles in both horizontal and vertical directions with static pauses over time, we obtain characteristics of the properties of automobile seats very close to the real loading in the car. Therefore, we can realize the loading very similar to real traffic in laboratory. The time dependent loading is presented, for example, in Fig. 8, where measured hysteresis character-istics-banana were. The first curve at the beginning of the measurement characterizes the state of the car seat before the fatigue effect. After 180 hours of loading, the comfort layer fatigue is evident, with a moderate load reduction with moderate stiffness decreasing during medium loading. In addition, the damping properties are diminished. Peak loadings are actually the same at finish loading time. When we measure transmission characteristics, there are even greater differences by varying the loading method. Fig. 8 shows the statically evaluated characteristics of 10 repeated measurements by the same conditions.
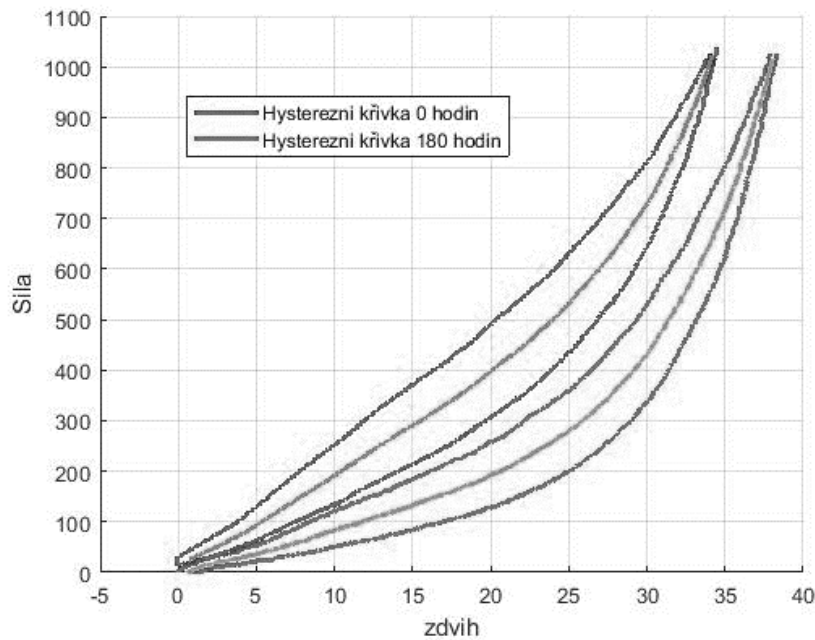
Fig. 8 Vertical and horizontal movement variants

RESULTS AND DISCUSSION

The new device allows to increase the working height from 318 mm to 981 mm Fig. 7. Realizes the possibility of vertical loading of the car seat up to 100 kg of load in the interval up to 100 mm, and at the same time it enables to realize horizontal movement of the car seat in the interval up to 50 mm. This corresponds to the current regulations for laboratory testing of automobile seats with load. The device is original, is not described in any literature, and corresponds only to the requirement of corresponding standards, which prescribe an independent testing signals in two orthogonal directions - the horizontal and vertical. This is original device on TUL.
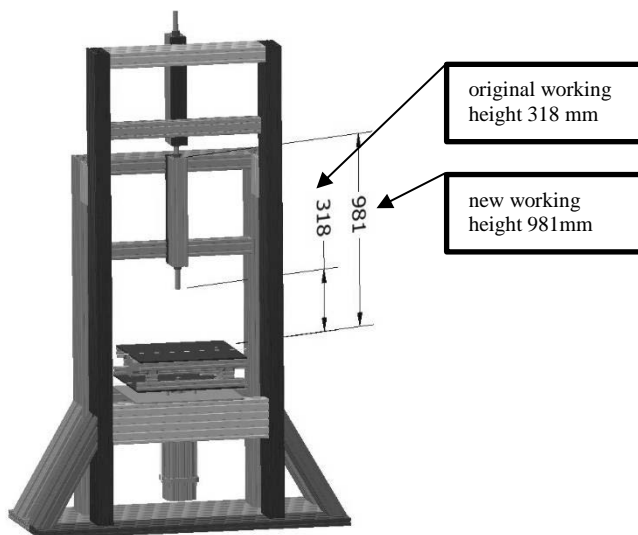
Fig. 7 Final design testing device

CONCLUSIONS

It was constructed universal testing laboratory device for laboratory testing automobile seats in the two directions of movement, both vertical and horizontal. This corresponds to the requirement of the current standard for determining the comfort of car seats. At the present, all structural elements are purchased and the installation of the equipment has been started.

ACKNOWLEDGMENT

REFERENCES

1. Standard: ASTM D3574-11. Standard Test Methods for Flexible Cellular Materials—Slab, Bonded, and Molded Urethane Foams.
2. Standard JASO B407-87: Test code of seating comfort for automobile seats.
3. Standard DIN EN ISO 3385: Flexible cellular polymeric materials - Determination of fatigue by constant-load pounding.

Corresponding author:

Ing. Rudolf Martonka, Ph.D., Department of Mechanical Engineering, Faculty of Engineering, Technical University of Liberec, Studentska 2, Liberec 1, 461 17, Czech Republic, phone: +420 48535 3308, e-mail: rudolf.martonka@tul.cz

THE EFFECT OF ALTERNATIVE TRAFFIC SYSTEMS AND TILLAGE ON SOIL CONDITION, CROP GROWTH AND PRODUCTION ECONOMICS - EXTENDED ABSTRACT

Richard GODWIN[1], Paula MISIEWICZ[1], David WHITE[1], Edward DICKIN[1], Tony GRIFT[3], Emily POPE[2], Anthony MILLINGTON[1], Rayhan M. SHAHEB[1, 3], Magdalena DOLOWY[1]

[1]*Harper Adams University, Newport, Shropshire, United Kingdom.*
[2]*Agriculture and Horticulture Development Board, Stoneleigh Park, Kenilworth, Warwickshire, United Kingdom.*
[3]*University of Illinois at Urbana-Champaign, Illinois, United States of America.*

Extended Abstract
The effect of soil compaction, depending upon its severity, can significantly reduce crop yields by 10 to 15%, increase tillage energy requirements by 200 to 300% and drastically reduce infiltration rates, increasing the problems of run-off, diffuse pollution and flooding. The pressure on the soil at depths of 0.5m has been estimated to have increased by a factor of 10 over the past 80 years, due to the increase in vehicle weight. Work in the Czech Republic has shown that crops grown using traditional mouldboard plough (deep) tillage systems have 85% of the field covered by wheel tracks, this reduces to 65% and 45% when using wider equipment for shallow and no-till practices respectively. This paper reports the detailed effect of improved traffic management on soil conditions and crop yield by focusing on the results of two major studies:

1. *A seven-year programme at Harper Adams University, UK to compare controlled traffic farming (CTF) practices, reduced inflation (very high flexion) pressure tyres and standard inflation pressure tyres for deep, shallow and no-till practices. For a rotation of winter wheat, winter barley (x2), spring oats, spring wheat and field beans on a sandy loam soil.*

2. *A three-year programme at the University of Illinois, USA to compare reduced inflation (very high flexion) pressure tyres and standard inflation pressure tyres for deep, shallow and no-till practices. This consisted of a maize and soya bean rotation in two adjacent silty clay loam fields.*

Both studies have shown, using both classical soil physical measurements and X-ray computed tomography, that soil macro-porosity is enhanced by both CTF and reduced tyre inflation pressure systems.
The results from the six cropping seasons in the UK study have shown 3 years where the CTF practices have significantly improved crop yield, 2 years where the yields have been higher, but not significantly so and one year (2017: spring wheat) where they were significantly lower. This was a year where overall spring wheat yields were approximately 50% of the norm due to abnormally low rainfall in April, May and June. Discounting the 2017 data, the overall economic yield benefit for CTF (with a wheeled area of 30%) was 4.6%. The economic yield benefit for CTF with a reduced wheeled area of 15% was estimated to increase to 8.8%. The yield benefit of the reduced inflation pressure tyres was 2%. The deep and shallow tillage yields where significantly greater than those of the no-till for winter wheat, winter barley and spring oats.
The results from the two cropping seasons in the US study have shown significant increases (4.3% and 2.7%) in maize yield in 2017 and 2018 respectively from the use of reduced inflation pressure tyres. There was no increase in soya bean yield in 2017 but a significant 3.7% increase in 2018. The effect of tillage was significant for the soya bean yield in 2017 and maize yield in 2018, when for both crops the deep tillage yield was greater than the shallow tillage, which was greater than no-till. The economic analysis, which included the additional cost of the very high flexion tyres, showed that the maize/soya bean rotation would produce a benefit of US$38/ha and US$43/ha for the 200ha and 800ha farms respectively.

Key words: *plough, tillage, management, soil, compaction, Czech, USA, UK*

Corresponding author:
Prof. Richard Godwin, Harper Adams University, Newport, Shropshire, TF10 8NB, United Kingdom, Tel: +44 (0) 1952 820280,

A PORTABLE ROVER AS A TOOL FOR SOIL WATER MONITORING

Ioannis GRAVALOS[1], Theodoros GIALAMAS[1], Avgoustinos AVGOUSTIS[1], Dimitrios KALFOUNTZOS[1], Martin LIBRA[2]

[1]*School of Agricultural Sciences, University of Thessaly, Greece*
[2]*Department of Physics, Faculty of Engineering, Czech University of Life Sciences Prague, Czech Republic*

Abstract

Advances in soil water content (SWC) monitoring technology continue to provide new and significant benefits to agriculture. An innovative approach for observing SWC is introduced using a portable rover platform traveling through in-ground horizontal access tubes and monitors the SWC in real time. A series of tests for evaluating the prototype portable rover were designed and conducted. It demonstrated very good mobility and produced records of the SWC in different horizons. The recorded values were then plotted as three dimensional (3D) patterns with high accuracy. The results show potential applications for this sensing approach, yielding horizontal monitoring of soil water in the root zone or deeper subsurface.

Key words: soil water status; monitoring locations; rover platform; access tubes.

INTRODUCTION

Soil water content (SWC) is an indicator of the amount of water in soil and an important factor on many biophysical processes. It affects the plant growth and nutrition, nutrient transformations in the root zone, microbial decomposition of the soil organic matter, etc. (*Bitteli, 2011*). There are two common methods to measure soil water status: direct and indirect. Gravimetric is the only direct method to determine how much water is in the soil. The volumetric and tensiometric (water potential) are indirect methods because they measure other properties of the soil that vary with water content. Most of the available soil water measuring instruments (sensors and probes) are based on indirect methods for measuring the soil water status.

Charlesworth (2000) & Muňoz-Carpena (2004) present several field devices which measure SWC, such as the Time-Domain Reflectometry (TDR), Frequency Domain Reflectometry (FDR), etc. The application of TDR technique to soil water measurements was first reported by *Topp et al. (1980)*. This research linked the measured travel time of an electromagnetic wave with the soil water (θv). FDR soil water sensing systems operate at relatively low frequencies. They are affected by salinity, clay and organic matter, water content, bulk density, temperature, compaction and texture (*Evett & Parkin, 2005; Evett et al., 2006; Paltineanu & Starr, 1997*). FDR sensors are portable, can be used with access tubes, unattended, and can also be automated and multiplexed, while their initial costs may be lower than those of TDR systems or neutron meters. However, a bad soil-sensor contact or small disturbances of the soil around the sensor have a negative impact on the sensor performance (*Fares et al., 2004*).

Gravalos et al. (2012) proposed horizontal monitoring of SWC using a mobile electromagnetic sensor-based platform that moves in access tubes. This integrated system included a soil water sensor and two circular articulated wheeled bases, each of them driven by a small wheeled electric motor. The recorded values of SWC allow the composition of two-dimensional (2D) or three-dimensional (3D) images with high accuracy and on a large scale *(Gravalos et al., 2013). Sun et al. (2014)* also presented an alternative prototype, in which an EM sensor moves through a horizontal access tube while measures SWC distribution at a fixed depth. Two cabled pulleys were affixed to and driven by two individual motors, one being a stepper-motor and the other a dc-motor. During a given scanning event, the stepper motor turned counterclockwise to proceed the sensor in 5 cm increments along the X-axis. Meanwhile, the dc-motor turned clockwise with some resistance against the drawing force to maintain tension on the nylon string. When the mobile sensor reached a Hall-switch at the right end of the tube, the dc-motor reversed direction and retracted the nylon string drawing the sensor back to the starting point.

In this paper, we present the design and prototyping of a portable rover platform that carries a capacitance sensor for easy accessing in an in-ground tube for horizontal monitoring of SWC.

MATERIALS AND METHODS

The schematic illustration of the prototype rover platform that travels through the in-ground access tubes and monitors the SWC is shown in Fig. 1(a). It was constructed with a modified commercial soil water sensor (*Diviner 2000, Sentek Pty Ltd, Stepney South Australia*), placed on two articulated wheeled bases, which are linked via universal joints. The body of the wheeled bases is circular in shape, and it serves to support the driving and sliding wheels. The driving wheels are supported via bumper suspensions. The suspension system allows motion only along the vertical direction and relies its function on flexible members (compression springs), to hold the bumper loosely in place. The deflection of the bumper suspension gives foldable characteristics to the driving wheels, which maintain steady contact with the access tubes. This way, whether it is for straight or curved tubes, the rover platform is always guided to the direction of them. Two motors are engaged in the rover movement. These are high quality DC motors that are installed close to the driving wheel parts. The total length of the rover is 235 mm and its outer diameter may vary from 48 mm to 54 mm. The dynamic behavior of the rover platform was described in detail in reference to *Gravalos et al. (2017)*. In addition, the portable version of the rover platform (Fig. 1(b & c)) includes a stainless steel cable reel (770(L) x 371(W) x 810(H) mm). The electronic control module of the rover platform is installed in the cable reel. It contains all the drivers necessary to drive the motors and allows the speed to be controlled in both the forward and reverse directions.
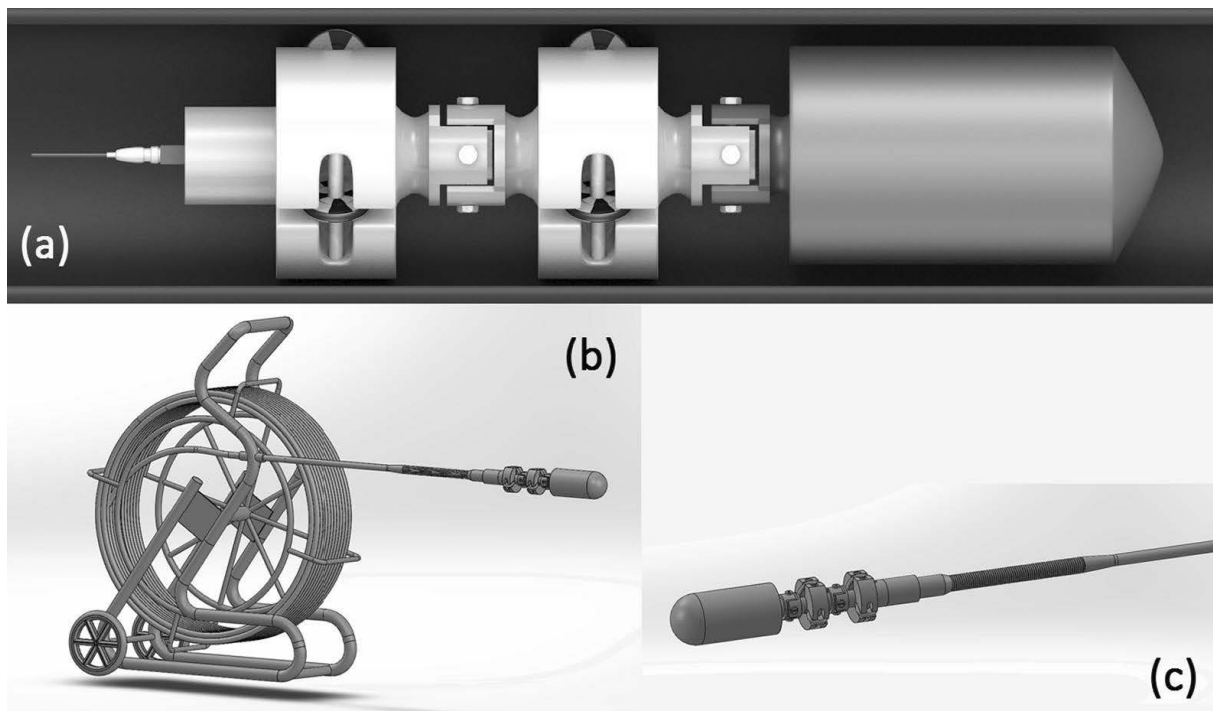
Fig. 1 (a) The schematic illustration of the prototype rover platform, (b) and (c) The portable version of the rover platform for easy accessing in in-ground access tubes.

The experimental tests were conducted in a field plot (1.5 m long and 1 m wide) at the School of Agricultural Sciences, University of Thessaly, Larissa (Greece). Analyses of the soil samples were performed, including: soil particle size distribution (sand 41%, silt 25%, clay 34%), bulk density (1.33 g.cm^{-3}), water retention characteristics (field capacity 27 vol.% and permanent wilting point 13 vol.%) and electrical conductivity (EC) of 0.20 dS.m^{-1}. In addition, three PVC access tubes were placed horizontally, along the field plot, at a depth of 0.15 m under the soil surface, and at uniform distances. In order to build a good knowledge of SWC conditions within the root zone requires measurements to

be taken at several locations. SWC measurements within the root zone can be used to evaluate soil water available to the plant, while deeper measurements below the root zone can show the deep percolation of water. The shallowest SWC measurements should be about 10-15 cm below the surface, while the deepest should be at least 20% deeper than the bottom of the plant's root zone. Special attention was paid to the installation of the tubes in the soil, in order to avoid air pockets between the tubes and the soil. The irrigation occurs only when the daily mean SWC is below the refill point of 0.18 $m^3.m^{-3}$ and this only in locations with a SWC lower than that limit. After 6 weeks of experimental procedure with the above irrigation constraints, 88 mm of water was applied to the total surface of the field plot. Water was distributed across the field plot through manual labor and watering cans.

Calibration of the Diviner 2000 sensor was done under laboratory conditions. The calibration equation was derived from regression analysis of sensor measurements of scaled frequency (*SF*) against the soil water *θv*, according to *Groves & Rose (2004)*, *Giraldi & Iannelli (2009)*.

The observations of SWC were conducted every day for a period of 6 weeks. The portable rover platform measures the SWC at fixed positions of the access tube spaced out every 24 cm of length increment (move-stop-measure case). Thus, for the 3 access tubes a total number of 18 measurements are conducted where every single value is the average value of three readings. A sensor data logger is the data storage, display and conversion device. Then it was connected to the laptop via a standard serial port. A software application is used to download and store data in a backup file or to export backed up data to a comma-separated variables (CVS) file format. This text-based file format can be viewed and analyzed with a third party software.

RESULTS AND DISCUSSION

Box plot of Fig. 2 compares the distributions of SWC between 18 fixed positions of the field plot over the 6 weeks of experimental procedure. At first glance more boxes seem to balance around refill point or to have higher SWC except the boxes of the fixed positions 1, 5, 12 and 17 that shows the lower values of soil water content. In addition, the box of position 4 shows the highest values of SWC much greater than the field capacity. If we ignore the outliers, the variation in the more boxes is very short and similar, except the boxes for fixed positions 4, 9, 10, 15, and 16 whose interquartile range is larger.
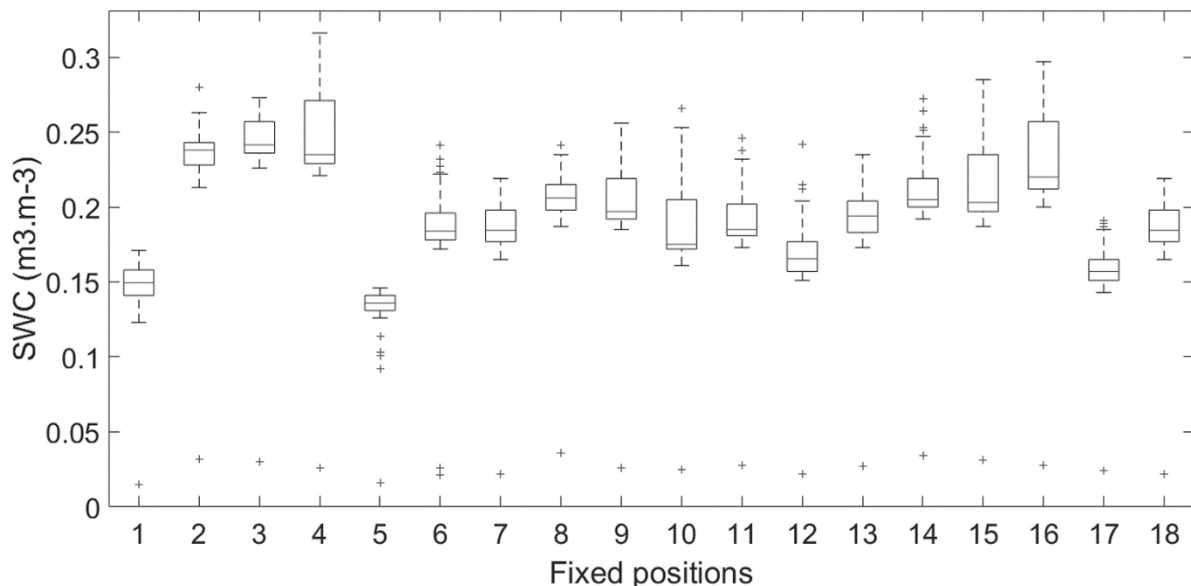
Fig. 2 Box plot of SWC for the eighteen fixed positions of the field plot over the 6 weeks.

Fig. 3 depicts 3D patterns of SWC observed by the rover platform. Each pattern represents a different week (1st until 6th week). The distribution of SWC was characterized by a significant difference between poorly and well-drained regions of the field plot. The soil water did not uniformly infiltrate

downwards but selectively penetrated the deepest layers, according to how good was the spatial drainage system. The SWC fluctuated between 0.01 and 0.316 $m^3.m^{-3}$ in the entire subsurface of the field plot. We may conclude that the variable drainage system in the plot or the soil physical conditions or both control water movement. This information is very useful for precise crop irrigation scheduling.

The combination of portable rover platform moving inside in-ground access tubes is a new approach that allows topological extension of SWC readings and aims at the creation of 2D or 3D soil water images across or along the investigated field plot. Furthermore, it provides an interesting perspective for the assessment of soil water distribution at different horizons of vertical soil profile (we assume that PVC access tubes are installed at different soil depths). It offers quantitative and qualitative spatial soil water data at large scale (>1 m^2), which is not possible with other methods and instruments that only provide local SWC readings. Comparing the results of this method to the much smaller sampling volumes of the sensors or probes installed in predefined points into the soil profile gives an idea of the amount of instrumentation that would be needed if these devices were to be used in order to get precise patterns of the SWC.
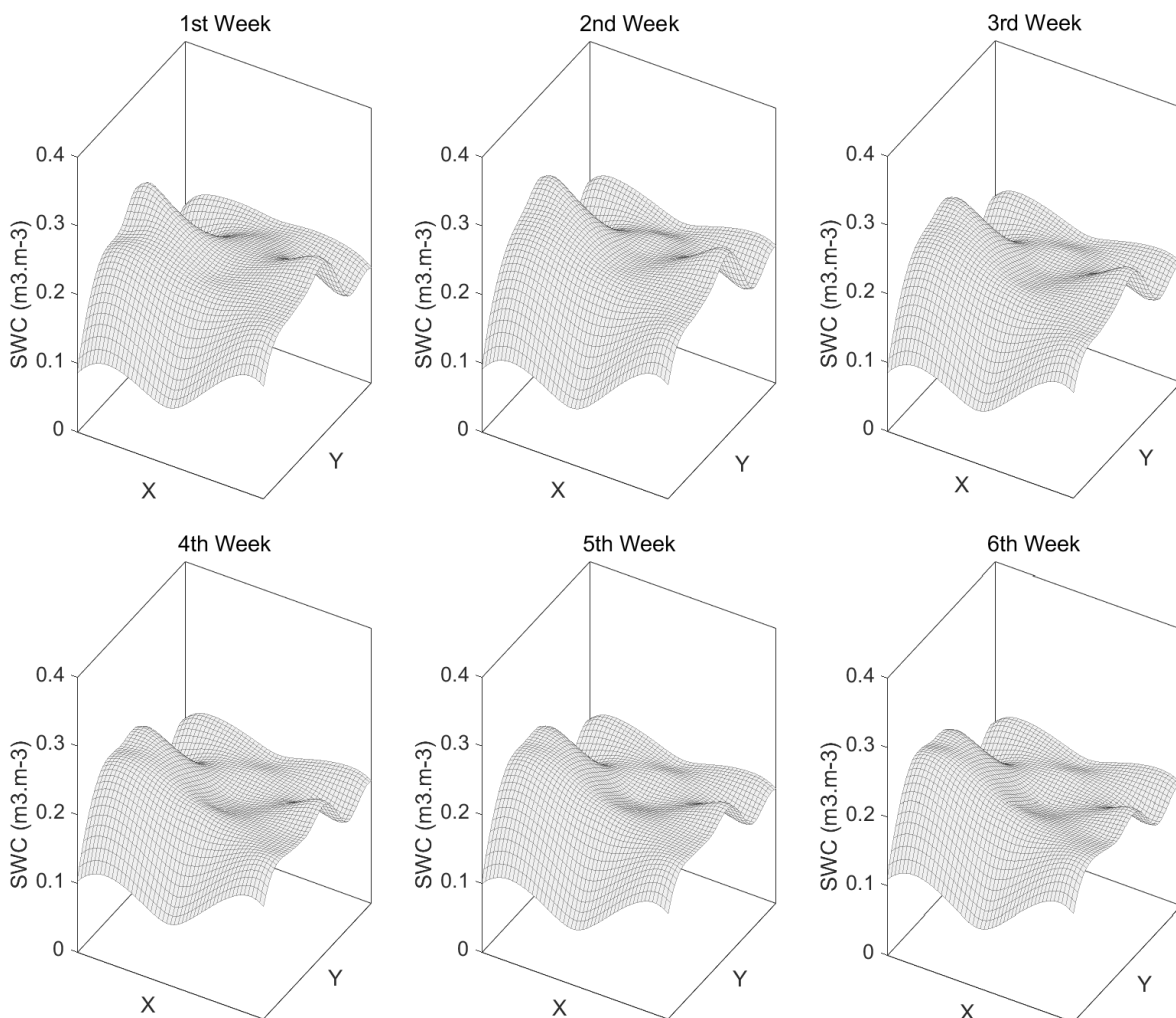
Fig. 3 Three dimensional (3D) soil water patterns at a depth of 0.15 m under the soil surface.

The proposed rover platform for imaging spatial SWC is thus a very attractive alternative. Soil water images will play an increasingly important role in the control of resource gradients, such as, soil water and nutrients and therefore for determining field vegetation patterns. The rover platform method depends on the choice of the capacitance sensor (Diviner 2000). This type of sensor is less accurate than other types due to changes in soil bulk electrical conductivity (including temperature changes) that

often occur in irrigated soils. However, by using sensor specific soil water calibration, the rover platform method could easily become a standard measurement procedure. Alternatively, the capacitance sensor (Diviner 2000) could be replaced by other types of sensors of higher accuracy. Some of them can be easily adapted to the rover platform and have suitable form and dimensions so that they can move in the access tubes with no further modification. Furthermore, being impractical to implement calibration against gravimetrically observed data on a constant basis, meaning that the sensor performance cannot be always guaranteed, geostatistical interpolation methods could be used to interpolate these data, while the actual sensor measurements could be used as a secondary source of information (*Vanderlinden et al., 2008*).

A review of the relevant literature indicates that a satisfactory number of soil water monitoring geophysical methods and technologies are available nowadays (*Galagedara et al., 2003; Grote et al., 2003; Lunt et al., 2005*). In recent years, some researchers used electrical resistivity systems to monitor soil water changes (*Aizebeokhai and Olayinka, 2010*). The spatial distribution of the SWC may also be determined by measuring the bulk soil electrical conductivity (ECa) using non-contacting electromagnetic induction (EMI) instruments. As a future project, field comparative studies need to be carried out so that the proposed rover platform is directly compared to other geophysical methods so that reliable conclusions about their effectiveness and accuracy can be drawn.

CONCLUSIONS

The series of tests have proved that the portable rover platform presented in this study can function effectively inside the in-ground access tubes. It is a new and cost effective way for efficient irrigation water management because it can cover a large irrigated area, and offers rapid and easy measurements. Compared to the majority of the commercial dielectric sensors and probes, which are installed in fixed predefined points into the soil for a long time, the proposed rover platform has a significant advantage, because it is able to record the actual soil water content in horizontal, vertical or other orientation. It can also record the spatial variability of the water content, so that precise information about the soil and plant environment can be gathered.

REFERENCES

1. Aizebeokhai, A. P., & Olayinka, A. I. (2010). Anomaly effects of arrays for 3d geoelectrical resistivity imaging using orthogonal or parallel 2d profiles. *Afr. J. Environ. Sci. Technol.*, *4*, 446-454.

2. Bittelli, M. (2011). Measuring soil water content: A review. *HortTechnology*, *21*(3), 293-300.

3. Charlesworth, P. (2000). *Irrigation insights number one*. Canberra, Australia: Soil Water Monitoring, CSIRO Land and Water.

4. Evett, S. R., & Parkin, G. W. (2005). Advances in soil water content sensing: the continuing maturation of technology and theory. *Vadose Zone Journal, 4,* 986-991.

5. Evett, S. R., Tolk, J. A., & Howell, T. A. (2006). Soil profile water content determination: sensor accuracy, axial response, calibration, temperature dependence, and precision. *Vadose Zone Journal, 5,* 894-907.

6. Fares, A., Buss, P., Dalton, M., El-Kadi, A. I., & Parsons, L. R. (2004). Dual field calibration of capacitance and neutron soil water sensors in a shrinking-swelling clay soil. *Vadose Zone Journal, 3,* 1390-1399.

7. Galagedara, L. W., Parkin, G. W., & Redman, J. D. (2003). An analysis of the ground penetrating radar direct ground wave method for soil water content measurement. *Hydrol. Process.*, *17*, 3615-3628.

8. Giraldi, D., & Iannelli, R. (2009). Measurements of water content distribution in vertical subsurface flow constructed wetlands using a capacitance probe: benefits and limitations. *Desalination*, *243*, 182-194.

9. Gravalos, I., Moshou, D., Loutridis, S., Gialamas, T., Kateris, D., Tsiropoulos, Z., & Xyradakis, P. (2012). Design of a pipeline sensor-based platform for soil water content monitoring. *Biosystems Engineering, 113*, 1-10.

10. Gravalos, I., Moshou, D., Loutridis, S., Gialamas, T., Kateris, D., Bompolas, E., Tsiropoulos, Z., Xyradakis, P., & Fountas, S. (2013). 2D and 3D soil moisture imaging using a sensor-based platform moving inside a

subsurface network of pipes. *Journal of Hydrology, 499,* 146-153.

11. Gravalos, I., Loutridis, S., Gialamas, T., Kateris, D., Xyradakis, P., & Tsiropoulos, Z. (2017). Dynamic behaviour of an in-pipe sensor-based platform for soil water monitoring. *Computers and Electronics in Agriculture*, *134*, 11-18.

12. Grote, K., Hubbard, S., & Rubin, Y. (2003). Field-scale estimation of volumetric water content using ground-penetrating radar ground wave techniques. *Water Resour. Res.*, *39*, 1321-1335.

13. Groves, S. J., & Rose, S. C. (2004). Calibration equations for Diviner 2000 capacitance measurements of volumetric soil water content of six soils. *Soil Use Manag.*, *20*, 96-97.

14. Lunt, I. A., Hubbard, S., & Rubin, Y. (2005). Soil moisture content estimation using ground penetrating radar reflection data. *J. Hydrol.*, *307*, 254-269.

15. Muňoz-Carpena, R. (2004). *Field devices for monitoring soil water*. USA: Agricultural and Biological Engineering Department, Florida Cooperative Extension Service, Institute of Food and Agriculture Sciences, University of Florida.

16. Paltineanu, I. C., & Starr, J. L. (1997). Real-time soil water dynamics using multisensor capacitance probes: laboratory calibration. *Soil Science Society of America Journal, 61,* 1576-1585.

17. Sentek Pty Ltd. (2007). Diviner 2000 user guide version 1.4. South Australia: Stepney.

18. Sun, Y., Zhou, H., Qin, Y., Schulze Lammers, P., Berg, A., Deng, H., Cai, X., Wang, D., Jones, S. B. (2014). Horizontal monitoring of soil water content using a novel automated and mobile electromagnetic access-tube sensor. *Journal of Hydrology, 516,* 50-55.

19. Topp, G. C., Davis, J. L., & Annan, A. P. (1980). Electromagnetic determination of soil water content: measurement in coaxial transmission lines. *Water Resources Research, 16,* 574-582.

20. Vanderlinden, K., Jiménez, J. A., Muriel, J. L., Perea, F., García, I., & Martínez, G. (2008). Interpolation of soil moisture content aided by FDR sensor observations. *Geostatistics for Env. Applications,* 397-407.

Corresponding author:

Prof. Ing. Ioannis Gravalos, CSc., School of Agricultural Sciences, University of Thessaly, Larissa, 41110, Greece, phone: +30 2410 684216, e-mail: gravalos@teilar.gr

DETERMINING PELLETING PARAMETERS FOR ORANGE PRUNING RESIDUES

Gürkan A. K. GÜRDİL[1], Metin DAĞTEKIN[2], Bahadır DEMİREL[3], Çimen DEMİREL[4] Vaclav NOVAK[5], Mahmut DOK[6]

[1]*Department of Mechanical Engineering, Faculty of Engineering, Czech University of Life Sciences, Prague Czech Republic*
[2]*Ceyhan Vocational School, Çukurova University, Adana Turkey*
[3]*Department of Biosystem Engineering, Faculty of Agriculture, Erciyes University, Kayseri Turkey*
[4]*Department of Agricultural Machines and Technologies Engineering, Faculty of Agriculture, Ondokuz Mayıs University, Samsun Turkey*
[5]*Department of Machinery Utilization, Faculty of Engineering, Czech University of Life Sciences, Prague Czech Republic*
[6]*Department of Energy Agriculture, Black Sea Agricultural Research Institute, Samsun Turkey*

Abstract
This study evaluates the pelleting parameters of fuel pellets made from orange tree pruning residues. Physical-mechanical and thermal properties of pellets were studied and their suitability were checked according to latest EU standards. The pruning residues collected from orange orchards were first pre-chopped and then sun dried at outside conditions till the desired moisture content M10 (8-10%) is achieved. Then the material grinded with varying particle sizes (PS: 4, 6 and 8 mm) to produce pellets. Pruning residues from fruit orchards are a good solution to generate alternative energy sources. Orange cultivation is very popular worldwide so the unused pruning residues of the trees must be utilized for energy in today's energy based world. Some physical-mechanical properties such as; pellet particle density, bulk density, mechanical duration, firmness, pellet moisture content and some thermal properties such as; lower heating value, ash content and flue gas emissions of the produced pellets were analyzed. Results showed us that the pruning residues of orange trees were suitable both in technical and environmental aspects for energy utilization.

Key words: energy; orange; pellet; pruning; residue.

INTRODUCTION

The demand for alternative energy sources increases as the depletion of fossil fuels increases. People are in need for renewable energy sources and biomass could be a very choice. Generally, biomass from agricultural production like residues are not utilized sufficiently. Unfortunately, most of these potential is just left on the fields or on the gardens for natural decomposition or just burned randomly near the garden. An example of it is given in Fig. 1., below.

Fig. 1 Pruning and random burning of orange pruning residues

Shaping the grinded material under pressure to smaller sizes (approx. 30 mm) is called pelleting (*Öztürk, 2012*). The density of material is increased and the transportation and storing costs are decreased by pelleting process. Moreover, homogeneity is provided in size and shape which make them more suitable

for automatic feeding systems and effective usage of material is provided (*Werther et al., 2000; Mani et al., 2003; Holm et al., 2006; Nilsson et al., 2011; Theerarattananoon et al., 2011; Celma et al., 2012*). Pelleted biomass is low and uniform in moisture content. It can be handled and stored cheaply and safely using well developed handling systems for grains (*Fasina & Sokhansanj, 1996*). However, pellets can be easily produced from agricultural residues, too. Orange cultivation is very popular in Turkey. It's also important since it contains vitamin C. Turkey is an important producer of fresh fruit and vegetable with about 51 million tons of production. Turkey's citrus production reached approximately 4.29 million tons in the last decade, with an increase of 44% (*TUIK, 2018; MFAA, 2018*). The most common procedure for maintaining the orange gardens is pruning. Pruning improves the strength and productivity of trees. It's also a good way of fighting against diseases. But, it generally ends up with residue problem. So, one must utilize this idle potential in advantage of energy generation. The aim of this study is to utilize orange orchard pruning residues as solid biofuel in the form of pellets. Therefore, some physical-mechanical and thermal properties of produced fuel pellets were analyzed with regards to particular EU standards.

MATERIALS AND METHODS

This study is carried out in labs and workshop of Agricultural Machines and Technologies Engineering Department of Samsun Ondokuz Mayıs University in Turkey with collaboration of Çukurova University in Adana, Czech University of Life Sciences in Prague and Black Sea Agricultural Research Institute in Samsun. Pruning residues of orange tree were provided from the orchards in Adana and Mersin provinces in Mediterranean Region of Turkey. Up to date European standards (*EN 14961-2 & EN ISO 17225-6*) were taken as a reference for this research. The pre-fragmented and chopped material (Fig. 2) was sun-dried under normal conditions until their moisture content was reduced to M10 (8-10 %).

Fig. 2 Pre-fragmentation and chopping of orange branches

Then the dried material was ground in a 3-kW electric hammer mill consisting of 8 hammers rotating at a speed of 2,850 rpm (Fig. 3). Once particles of the required sizes PS: 4, 6 and 8 mm were obtained, moisture contents were re-measured, and the particles were pelleted using a pelleting machine (Fig. 4). Particle density of pellets were calculated according to standard (*EN 15150, 2011*). As defined in that standard the volume of the cylindrical properly shaped pellets was calculated by stereo-metric method and the averaged volume is proportioned to the average mass of the pellet (g.cm^{-3}). Likewise, the bulk

density was calculated as defined in the particular standards (*EN 15103, 2009*). Mechanical durability of the pellets was tested according to standard (*EN 15210-1, 2009*). In this test 500 g of test portion is placed into this rotating chamber. It's rotated 500 times at 50 rpm speed and then the sample is removed and weighed again. The weight difference before and after the test gives us the mechanical durability of the pellets. Pellet firmness parameter is important during transportation and storage of pellets. The firmness values were determined with a special device (Fig. 5).

Fig. 3 Grinding   **Fig. 4** Pelleting   **Fig. 5** Pellet firmness tests

As for the thermal properties; lower heating value of pellets were determined by a calorimeter according to the instructions given in standard (*EN 14918*, 2009). Before testing, the pellets were disintegrated in a shredder and kept at 105 ºC for 24 hours to remove the moisture. Samples dried at a weight of 0.5-1 g were burned in oxygen atmosphere in a calorimeter bomb under standard conditions and the calorific value was automatically determined in cal.g^{-1} according to the increase in the temperature of the water in the calorimeter chamber and the average actual heat capacity of the system. Then the values are converted into MJ.kg^{-1} as specified in standard (*EN 14961-2, 2010*). The ash contents of the pellets were determined using an ash furnace according to standard (*EN 14775, 2009*) and the flue gas emissions like O_2(%), CO(ppm), CO_2(%), NO(ppm), NO_x(ppm) were measured and recorded with a gas analyzer.

RESULTS AND DISCUSSION
The effect of particle size on pellet particle and bulk densities was found statistically significant at M10 (Tab. 1).

Tab. 1 Pellet bulk and particle densities

Particle size (mm)	Pellet bulk density* (kg/m^3)	Pellet density* (kg/m^3)
4	542.40 ± 4.75a	1220.10 ± 6.28b
6	537.82 ± 4.75a	1300.17 ± 2.87a
8	530.21 ± 1.08c	1280.83 ± 1.63c
Sig.	<0.001	0.003

The difference between the values carrying the same letter is insignificant

Although the study is done in single moisture content (M10) but, some studies proved that the moisture content of the pellets have significant effect on pellet particle and bulk densities (*Colley, 2006; Mani et al., 2006; Liu et al., 2014*). The results for pellet bulk densities were more than the values found for the tomato residues (200 kg.m^{-3}) at M10 (*Celma et al., 2012*). This can be because of the structure of the material since the orange pruning residues have woody and harder structure. According to Colley (2006), durability is regarded as high if exceeding 80%, medium if measured as 70–80% and low if values do not reach 70%. The MD of pellets at al PS was high since they changed among 87.20% to 92.58%.

The effect of pellet particle size (PS) on pellet mechanical durability (MD) and firmness parameters has been found statistically significant (Tab. 2).

Tab. 2 Mechanical durability and firmness of pellets

PS (mm)	MD (%)	Firmness (N)
4	92.58 ± 0.11a	3504.90 ± 24.80d
6	91.30 ± 0.09b	2634.50 ± 19.74b
8	87.20± 0.06c	3163.40 ± 12.70c
Sig.	<0.001	<0.001

It's seen that the firmness of the pellets was relatively higher then pellets produced from plant based residues. This because of the woody structure of the pruned branches. The pellets with smaller PS values had the higher MD values always. Which can be explained by the smaller particle sized material has a better compaction characteristics and has smoother surfaces but, this case was not true for the firmness. Some researchers indicated that the pellet quality is high when the MD value is 80% and higher, medium when MD is ranging from 70 to 80% and low quality when MD≤70% (*Tabil & Sokhansnj, 1996; Tabil & Sokhansnj, 1997*). Materials loose some moisture from their structure during pelleting process due to over-heated mold cause of friction. As a result of this some moisture is removed from the material itself when pelleting the material. Moisture contents (MC) of pellets is given in Tab. 3., below.

Tab. 3 Pellet moisture contents

PS (mm)	Pellet moisture content (%)
4	5.00 ± 0.04b
6	4.88 ± 0.06c
8	4.63 ± 0.03a
Sig.	<0.001

The effect of material PS on pellet's moisture content was found statistically significant. Ironically, the pellets produced from smaller particle size had the highest MC, and MC values decreased as the PS increased. The results were in line with the references given in standards (*EN 14961-2, 2010 & EN ISO 17225-6, 2015*).

Ash content of the pellets made from orange pruning agricultural residue was found as 5.57%, which is in line with the reference value (A10≤10%) given in standard (*EN ISO 17225-6, 2015*). Heating value of pellets was found as 18.65 MJ.kg^{-1}. That is also compatible with the value (Q14.5≥14.5 MJ.kg^{-1}) indicated in the above mentioned standard. The results showed us that the heating value of pellets produced from orange tree pruning residues are higher than the wood (17.57 MJ.kg^{-1}). That is a promising result especially, when the huge idle potential is concerned. The flue gases of the pellets are presented in Tab.4., below.

Tab. 4 Flue gas emissions of pellets

Water content after burning (%)	NOx (ppm)	CO$_2$ (%)	O$_2$ (%)	CO (ppm)	NO (%)
8.46	100	4.00	16.90	456.33	95.33

All the measured emission values were in the limits given in Regulations for Air Pollution Control (*IKHKKY, 2014*).

CONCLUSIONS

Energy is the biggest issue on today's world. Renewable energy is a good choice for that since it' sustainable. Biomass energy from agricultural residues is very promising since it's everywhere and environmental friendly, too. Utilization of orange tree pruning residues as source of solid biofuel in the form of pellets were investigated in this study. The pellets were produced with 4, 6 and 8 mm PS at M10 moisture content. Physical-mechanical and thermal properties of fuel pellets were determined and screened out. All the tests were done according to the latest EU standards. The results showed that the fuel pellets have very good physical-mechanical and thermal properties as a fuel. Besides, as from the environmental point of view flue gas emissions were within the defined limits. But, certainly further researches of this kind must be done in order to increase its impact on science. We hope that the obtained results will positively contribute to science and will help agricultural engineers, scientific researches, farmers and even the policy makers to think more globally and wisely for the future and will definitely have a positive contribution to sustainable development in the world.

ACKNOWLEDGMENT

REFERENCES

1. Celma, A.R., Cuadros, F., & Rodriguez, F.L. (2012). Characterization of pellets from industrial tomato residues. *Food and Bioproducts Processing, 90*(4), 700-706.

2. Colley, Z.J. (2006). *Compaction of switchgrass for value added utilization* [MSc Thesis]. Department of Chemical Engineering, The Graduate Faculty of Auburn University. Alabama USA. Retrieved from https://etd.auburn.edu/handle/10415/483.

3. EN 14961-2. (2010). Solid biofuels- Fuel specifications and classes- Part 2: Wood pellets for non-industrial use. *European Committee for Standardization*: Management Centre, Avenue Marnix 17, B-1000 Brussels.

4. EN ISO 17225-6. (2015). Solid biofuels -- Fuel specifications and classes -- Part 6: Graded non-woody pellets. *European Committee for Standardization*: Management Centre, Avenue Marnix 17, B-1000 Brussels.

5. EN 14918. (2009). Solid biofuels – Determination of calorific value. *European Committee for Standardization*: Management Centre, Avenue Marnix 17, B-1000 Brussels.

6. EN 14775. (2009). Solid biofuels – Determination of ash content. *European Committee for Standardization*: Management Centre, Avenue Marnix 17, B-1000 Brussels.

7. EN 15150. (2011). Solid biofuels – Determination of particle density. *European Committee for Standardization*: Management Centre, Avenue Marnix 17, B-1000 Brussels.

8. EN 15103. (2009). Solid biofuels – Determination of bulk density. *European Committee for Standardization:* Management Centre, Avenue Marnix 17, B-1000 Brussels.

9. EN 15210-1. (2009). Solid biofuels – Determination of mechanical durability of pellets and briquettes – Part 1: Pellets. *European Committee for Standardization:* Management Centre, Avenue Marnix 17, B-1000 Brussels.

10. Fasina, O. O. & Sokhansanj, S. (1996). Storage and handling characteristics of alfalfa pellets. *Powder Handling and Processing, 8*(4), 361-365.

11. Holm, J.K., Henriksen, U.B., Hustad, J.E., & Sorensen, L.H. (2006). Toward an understanding of controlling parameters in softwood and hardwood pellet production. *Energy and Fuel, 20*, 2686-2694.

12. IKHKKY. (2014) Regulations for Air Pollution Control Caused by Burning. Retrieved from http://www.mevzuat.gov.tr/.

13. Liu, Z., Quek, A., & Balasubramanian, R. (2014). Preparation and characterization of fuel pellets from woody biomass, agro-residues and their corresponding hydro-chars. *Applied Energy, 113*, 1315-1322.

14. Mani, S., Tabil, L. G., & Sokhansanj, S. (2003). An overview of compaction of biomass grinds. *Power Handling and Process, 15*, 160-168.

15. Mani, S., Tabil, L. G., & Sokhansanj, S. (2006). Effects of compressive force, particle size and moisture content on mechanical of biomass pellets from grasses. *Biomass and Bioenergy, 30*(7), 648-654.

16. MFAA, (2018). Citrus report. *Ministry of Food, Agriculture and Animal, Turkish Republic*. ISBN: 978-605-9175-92-0, p. 66.

17. Nilsson, D., Bernesson, S., & Hansson, P.A. (2011). Pellet production from agricultural raw materials- a systems study. *Biomass and Bioenergy, 35*, 679-689.

18. Öztürk, H.H. (2012). *Energy plants and biofuel production*. Hasad yayıncılık Ltd. Şti, İstanbul, p. 272.

19. Tabil, L.G. & Sokhansnj, S. (1996). Process conditions affecting the physical quality of alfalfa pellets. *Applied Engineering in Agriculture, 12*(3), 345-350.

20. Tabil, L.G. & Sokhansanj, S. (1997). Bulk properties of alfalfa grind in relation to its compaction characteristics. *Applied Engineering in Agriculture, 13*(4), 499-505.

21. Theerarattananoon, K., Xu, F., Wilson, J., Ballard R., Mckinney, L., Staggenborg, S., Vadlani, P., Pei, Z.J., & Wang, D. (2011). Physical properties of pellets made from sorghum stalk, corn stoves, Wheat Straw and Big Bluesterm, *Industrial Crops and Products, 33*(2), 325-332.

22. TUIK, (2018). Statistics for plant production. Ankara: *Turkish Statistical Institute*.

23. Werther, J., Saenger, M., Hartge, E.U., Ogada, T., Siagi, Z. (2000). Combustion of agricultural residues, *Progress in Energy and Combustion Science*, 26, 1-27.

Corresponding author:
Assoc. Prof. Dr. Gürkan A. K. Gürdil, Ph.D., Department of Agricultural Machines and Technologies Engineering Mechanical Engineering, Faculty of Agriculture, Ondokuz Mayıs University, Atakum 55200, Samsun, Turkey, phone: +90 5355949294, e-mail: ggurdil@omu.edu.tr

DESIGN OF A CMM ACTUATION SYSTEM

Ondřej HADAČ[1], Petr LEPŠÍK[2]

[1]Department of Machine Elements and Mechanisms, Faculty of Mechanical Engineering, Technical University of Liberec
[2]Department of Machine Elements and Mechanisms, Faculty of Mechanical Engineering, Technical University of Liberec

Abstract
The article deals with the design of a coordinate measuring machine (CMM) Somet Berox XYZ 464B actuation system. The goal was to transform an existing archaic CMM into a semiautomatic CMM driven by three stepper motors and controlled via the Arduino platform. Within the parametr of maintaining precision, it was not possible to make holes or perform other machining operations on the frame of the CMM. Only existing holes and clamping elements were acceptable to use to modify the machine. The existing holes remained after the disassembly of the old and unnecessary magnetic belt clutches.

Key words: *coordinate measuring machine; CMM, actuation design; Arduino; metrology; low-cost.*

INTRODUCTION

Nowadays, when the demands on precision, quality and accuracy of produced parts are ever higher, continuous improvement, upgrading and acceleration of CMMs is necessary *(Vermeulen, et al., 1998; Kunzmann & Wäldele, 1988)*. State of the art CMMs can almost eliminate fails which arise from human factor. These fails are inherent in large volume in measurement results *(Melichar et al., 2016)*.

CMM Somet Berox was fully movable only by human power. There was a high percentage of fails deriving from human factor. For this reason the idea of modernizing this CMM located on the department of manufacturing systems and automation on the Technical University of Liberec emerged. A Czech CMM Somet Berox XYZ 464B was used for this purpose of rebuild. His typical bridge structure excelled particularly with quill structure and with the system of magnetic clutch used for micro movement. The aim of this article was to rebuild the actuation system of an old CMM Somet Berox, in compliance with today's required standards of accuracy and at low-cost *(Hadač, 2017)*.

MATERIALS AND METHODS

The decision regarding which new type of positioning system should be used was the initial stage of developing this rebuild. Two variants were considered: Variant A - using three stepper motors controlled by the Arduino platform - low-coast modernization, and variant B - using a commercial system and with DC servomotors and commercial control system from Pantec/Deva company. The decision was made using the multi-criteria evaluation of variants employing the points method (Metfessel's alokation). The more appropriate variant A, realization with three stepper motors, was chosen as the result of these evaluation methods.

A mechanical belt drive was used for the power transfer between the stepper motors and the movement devices. The following mathematic formulas (1) (2), were used to determine the toothed timing belt *(Pešík, 2010)*.

$$\frac{\beta}{2} = arcsin \frac{D_{w2} - D_{w1}}{2a} \qquad (1)$$

where β is the belt contact angle (rad), D_w is the pulley diameter (m), a is the toothed pulleys center distance (m).

$$L = \boldsymbol{\pi}\frac{D_{w1} + D_{w2}}{2} + \frac{D_{w1} - D_{w2}}{2}\beta + 2acos\frac{\beta}{2} \qquad (2)$$

where Dw is the pulley diametr (m), β is the belt contact angle (rad), a is the toothed pulleys center distance (m).

Design of the clamping elements for axis XYZ

Stepper motor clamping elements for axes X, Z and Z positioning were among the first parts to be designed shown in Fig. 1 and Fig. 2. These parts were drafted using Autodesk Inventor CAD software and subsequently were cut on a CNC laser cutting machine. All elements were designed considering the current holes and spaces which remained after the disassembly of unnecessary parts from the original CMM. Due to insufficient space on the CMM, methods such as design for manufacturing (DFM) and design for assembling (DFA), were used in the designing of the elements.
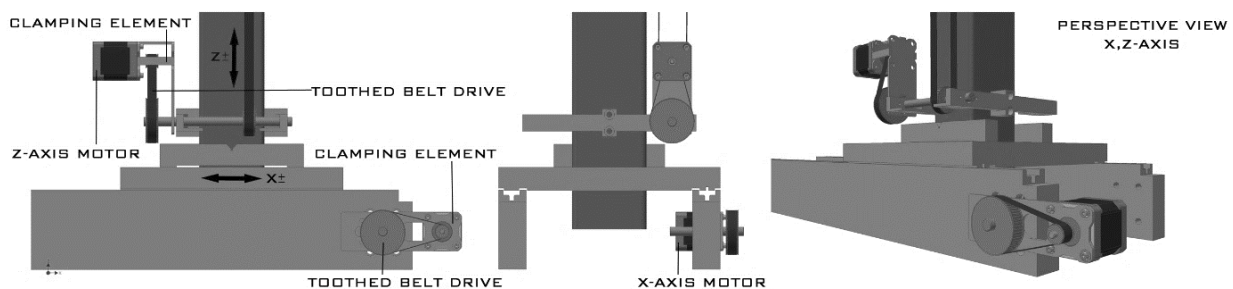
Fig. 1 3D model of X- axis and Z - axis CMM parts
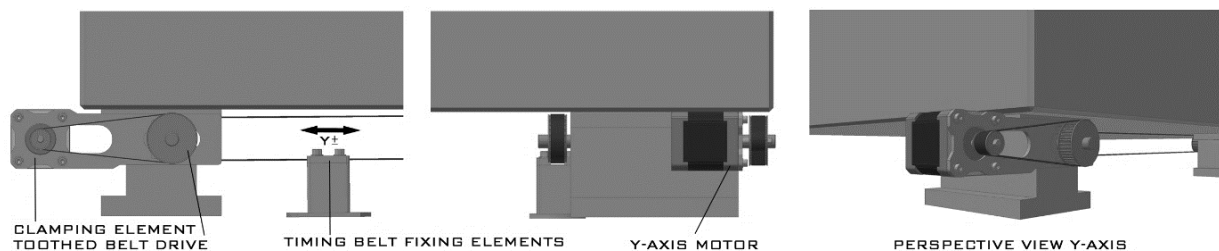
Fig. 2 3D model of Y-axis CMM parts

Arduino hardware connection

Commercially purchased low-coast Arduino platform components were used for this project. The Arduino platform began to emerge in 2005 at Ivrea Institute in Italy as a student project. Arduino motherboards are available for all of the different operation systems, along with a large amount of relevant training information and an intuitive interface IDE (Integrated Development Enviroment), making Arudino a widely-used and very popular platform all over the world *(Candelas et al., 2015)*.

The connected of Arduino components shown in Fig. 3.

The list of components used:

- **The microcontroller board Arduino AtMega 2560** - this board is designed for 54 digital input, which is enough for connection to all components.
- **Expanding 3D CNC Shield V3 Printer Expansion Board** - which is especially usable for 3D printers. There exists a large similarity between 3D printers and CMMs and for this reason this expandable board was used for this project as well.
- **Three Arduino motor drivers DRV8825 with microstepping** - these drivers are intended for bipolallar stepper motors operating from 8,2V to 45V and can deliver maximal 2,2A with additional cooling. These drivers can be expanded by microstep elements with 1/32 step resolution.

- **Two joysticks PS2** - the first is for controlling motors in X and Y axes, and the second for controlling the motor in the Z-axis.
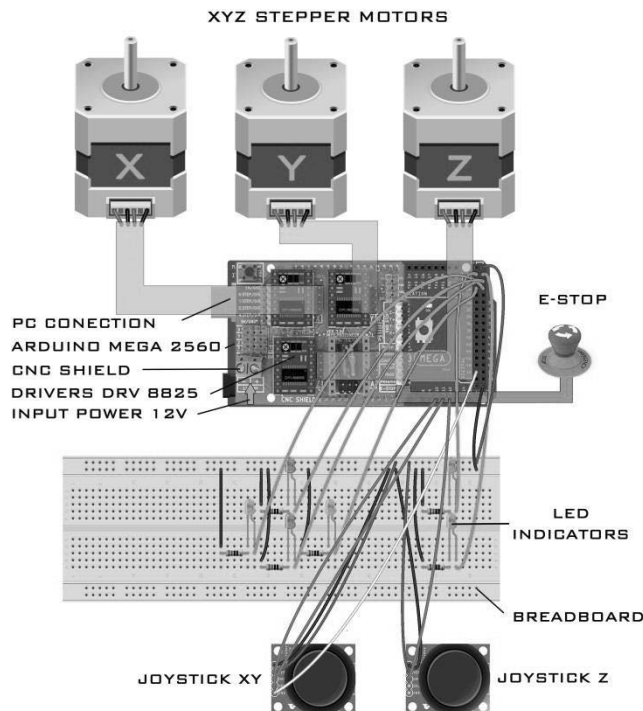
Fig. 3 Conected of Arduino components

Arduino control code to coordinate actual joysticks movements with motors rotations was written in the first step of programing. Three variants for controlling the CMM were considered:
- Var. A – Motor rotation depending on the angle of joystick rotation
- Var. B – Motor rotation depending on pressing of the joystick and adjusting the present speed
- Var. C – A combination of variants A and B.

Variant C was chosen as the most suitable for this rebuild. The reason was simple: the inexperienced personnel will work with the CMM, and the sensitivity of the low-cost joysticks is not sufficient. The potentiometers inside the joysticks are not capable of linear movement during manipulation. It seems clear that potenciometrs with linear movement abilities would be more advantageous for this kind of aplication.

RESULTS AND DISCUSSION

Fig.4 shows the realization of the upgraded CMM with clamped elements mounted, Arduino hardware, toothed pulleys, toothed belts, stepper motor, electric wires and fasteners fully assembled.

The acquisition costs (less than 290€) for the components purchased prove that one of the main aims of this article the low-cost CMM upgrade was achieved. The final price is up to 50 times lower than professional two or three-axes actuators.

Subsequent to this article, there are some future upgrades to recommend on this CMM Somet Berox, which could lead to streamlining of the work processes.

An upgrade of the Arduino control code is especially recommended which will make it possible to work with CMM in a fully automatic mode. This recommended upgrade in cooperation with an optimal algorithm and correct sampling strategy definition could chiefly lead to reduction of a measurement cycle time for CMM that can enhance efficiency of inspection process *(Mian & Al-Ahmari, 2014; Moroni & Petro, 2011)*.
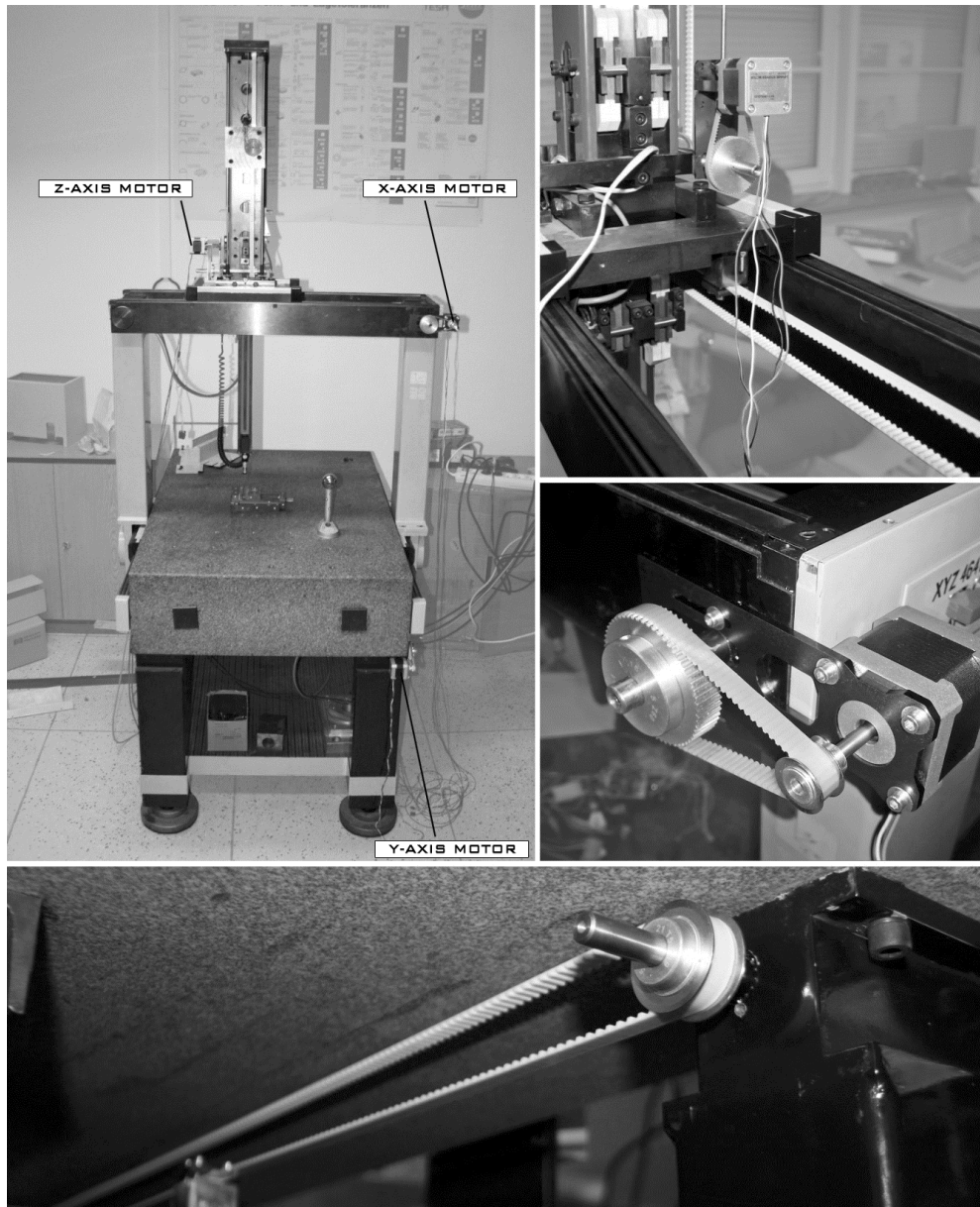
Fig. 4 Final realization of the CMM

A second upgrade regards the connection between touch probe signals and stepper motor signals by which the safety of CMM components will be ensured.

Should these recommended modifications of the CMM Somet Berox be realized, the speed increase, safety, accuracy, general modernization and technical approach to modern CMM of this originally manual CMM will be achieved *(Hocken, 2016)*.

At the end of the rebuild measurations was carried out. For this a reason simplified model to estimate uncertainty in CMM could be very beneficial in some cases as reported by *(Arencibia et al., 2015)* but for our project gauge blocks were used for the verification of accuracy of the measured dimensions. Fig.5 shows the measured values for the 80 and 100 mm gauge blocks. *(Bosch, 1995)*. Software Tango!3D from Topmes company was used for the verification of the measurements. This software was integrated with the CMM Somet Berox in previous modification. As can be seen, there are no deviations from nominal values of the steel gauge blocks. The results of the measurements with acceptable variations of +- 0,01 mm from the nominal values are affected with several sources of CMMs error such as errors from the axes of the CMM, errors from the probing system etc. *(Nafi, 2011)*. Verified by these measurements it can be said, that the rebuild of the CMM Somet Berox was completely succesfull. *(Hadač, 2017)*.

	Actual	Nominal	Hi-Tol	Lo-Tol	Difference	Error	Graph
Distance Plane1,Plane2							mm, dec
⏄	99.99	100.00	0.01	-0.01	-0.01		
Distance Plane5,Plane6							mm, dec
⏄	79.99	80.00	0.01	-0.01	-0.01		
	Actual	**Nominal**	**Hi-Tol**	**Lo-Tol**	**Difference**	**Error**	**Graph**
Distance Plane4,Plane5							mm, dec
⏄	80.01	80.00	0.01	-0.01	0.01		
Distance Planeyz,Plane3							mm, dec
⏄	100.01	100.00	0.01	-0.01	0.01		

Fig. 5 Output from Tango!3D measurement software - Measurement of the gauge blocks

By comparing CMM Somet Berox linear measuring tolerance $MPE_E = \pm (7+L/100)$ (µm) where L is a measured length given in (mm), with modern studies of CMM - $MPE_E = \pm (4.5 + L/100$ and better) *(Sładek, 2016)* suggests that the machine is unable to compete with modern CMMs, but is still sufficient for teaching and occasional measurement purposes.

CONCLUSIONS

The main research effort in this article was the exploring of low-cost modernizing possibilities for a 3-axis machine (CMM) and its transformation via open-platform Arduino controlling.

The complete realization of the selected variant included measuring, concept design of stepper motors and their holding elements in Autodesk Inventor software, cutting the holding elements on a CNC machine, purchasing all necessary components, disassembling all unnecessary elements, writing Arduino control code, connecting all electronic components, assembling all new components, and finally testing functionality of the whole system. The result of the project was a low-cost modernization, fully functional, readily modifiable, semiautomatic CMM, moved by stepper motors and controlled by the Arduino platform using a pair of joysticks.

REFERENCES

1. Arencibia, R., V., Souza,C.C., Costa, H.L. & Piratelli-Filho, A. (2015). Simplified model to estimate uncertainty in CMM. *Journal of the Brazilian Society of Mechanical Sciences and Engineering. 37*(1), 411-421.

2. Bosch, J. A. (1995). *Coordinate measuring machines and systems*. New York: M. Dekker.

3. Candelas, F.A., García, G.J., Puente, S., Pomares, J., Jara, C.A., Pérez, J., Mira D. & Torres F. (2015). Experiences on using Arduino for laboratory experiments of Automatic Control and Robotics. *IFAC-PapersOnLine, 48*(29), 105-110.

4. Hadač, O. (2017). Design of the CMM Somet Berox propulsion systém (in Czech) [Master thesis]. Technical university of Liberec, Faculty of Mechanical engineering, Department of manufacturing systems and automation.

5. Hocken, R.J. & PEREIRA, P.H. (2016). *Coordinate Measuring Machines and Systems.* CRC Press. DOI: 10.1201/b11022. ISBN 9780429114229.

6. Kunzmann, H. & Wäldele, F. (1988). Performance of CMMs. *CIRP Annals. 37*(2), pp. 633-640.

7. Melichar, M., Kubatova, D. & Kutlwaser, J. (2016). CMM Measuring Cycle and Human Factor. *Proceedings of the 27th International DAAAM Symposium 2016. DAAAM International Vienna* (pp. 0371-0376).

8. Mian, H.S. & Al-Ahmari, A. Enhance performance of inspection process on Coordinate Measuring Machine. (2014). *Measurement 47*, 78-91.

9. Moroni, G. & Petro, S. (2011). Coordinate Measuring Machine Measurement Planning. In *Geometric Tolerances* (pp.111-158). London: Springer London.

10. Nafi, A., Mayer, J.R.R. & Wozniak, A. (2011). Novel CMM-based implementation of the multi-step method for the separation of machine and probe errors. *Precision Engineering. 35*(2), 318-328.

11. Pešík, L. (2010). *Machine elements* (in Czech). Liberec: Technical university of Liberec. ISBN 978-80-7372-574-7.

12. Sładek, J.A. (2016). Accuracy of Modern Coordinate Measuring Systems. *Coordinate Metrology*. In *Springer Tracts in Mechanical Engineering* (pp. 337-382). Berlin, Heidelberg: Springer. DOI: 10.1007/978-3-662-48465-4_6. ISBN 978-3-662-48463-0.

13. Vermeulen, M.M.P.A., Rosielle, P.C.J.N. & Schellekens, P.H.J. (1998). Design of a high-precision 3D-coordinate measuring machine. Eindhoven University of Technology, Precision Engineering Section.

Corresponding author:

Ing. Ondřej Hadač, Department of Machine Elements and Mechanisms, Faculty of Mechanical Engineering, Technical University of Liberec, Studentská 2, Liberec 461 17, Czech Republic, phone: +420 721 944 794, e-mail: ondrejhadac@gmail.com

ANALYSIS OF WIRELESS TRANSMISSION LATENCY IN THE 2.4 GHZ AND 5 GHZ ISM UNDER LOAD OF NETWORK WITH DATA STREAM

Jan HART[1], Veronika HARTOVÁ[1], Martin KOTEK[1], Veronika ŠTEKEROVÁ[1]

[1]*Department of Vehicles and Ground Transport, Faculty of Engineering, Czech University of Life Sciences Prague*

Abstract

The Industry 4.0 initiative is currently a very topical and widely used notion, both in the area of information and communication technologies (ICT), academia and commercial sphere. This leads naturally to the development of new technologies that are designed to control and manage wireless terminal devices including data transfer. Some of these devices may be able to transmit large-capacity data, which considerably slows down the wireless network. The aim of this work was to analyze the risks associated with high-capacity data transmission through ISM bands, to find out the real latency of wirelessly transmitted data under different loads and to compare the efficiency of individual technologies from different manufacturers. It has been found that the real latency of wireless transmitted data reaches exponential dependence. At 150 Mbps the average latency of the tested technologies on the 2.4 GHz frequency band ranged from 220 to 255 ms and on the 5 GHz frequency band from 108 to 132 ms.

Key words: *latency; wi-fi; wireless network; ISM bands; frequency.*

INTRODUCTION

The Industry 4.0 initiative is currently a very topical and widely used notion, both in the area of information and communication technologies (ICT), academia and commercial sphere (*Piketty, 2015; Mařík, 2015; Dostál, 2017; Heřman, 2008*). From the side of "Industry 4.0" is the requirement that all attachable devices were connected to the internet to allow these devices to be remotely control, to be easier access to data sharing options or summarize of the data thus obtained, for example, a cloud storage is used (*Piketty, 2015; Mařík, 2015; Chang & Chen, 2017*). This leads naturally to the development of new technologies that are designed to control and manage wireless terminal devices including data transfer (*Han, Liang, Chen & Soong, 2016; Tahir & Shah, 2008; Oppermann, Stoica, Rabbachin, Shelby & Haapola, 2004*). Some of these devices may be able to transmit large-capacity data, which considerably slows down the wireless network (*Chang & Chen, 2017; Powell & Shim, 2012*). As a result, it can lead to latency eg. Driving instructions, where is the need for real-time processing (*Vlček, 2001; Šícha & Tichý, 1998; Dobeš & Žalud, 2006*). Before will be customized sophisticated devices are used, currently will be used at least initially available technologies such as wi-fi access points (*Tahir & Shah, 2008; Powell & Shim, 2012*).

Although the proposition of latency of data packets on wi-fi networks was pursued several authors, one did not address of direct latency of large data flows, but only simple date information (*Chang & Chen 2017; Gao, Ito & Shiratori, 2016; Krivchenkov & Sedykh, 2015*). Mostly, a direct endpoint response was addressed by analyze the data flow through ping commands, and the like (*Gao, Ito & Shiratori, 2016; Vikram & Sahoo, 2017*).

Another important aspect is to answer the question whether specialized systems for mass-data transmission can will defend the usual wi-fi solution from common Wi-Fi access point manufacturers and whether common wi-fi systems can be included in the "Industry 4.0" concept or it will need to use specialized technologies designed specifically for this purpose in the future.

The aim of this work was to analyze the risks associated with high-capacity data transmission through ISM bands, to find out the real latency of wirelessly transmitted data under different loads and to compare the efficiency of individual technologies from different manufacturers.

MATERIALS AND METHODS

The devices were tested in a local network consisting of a router and a switch. Wi-fi access points will be connected through the switch. Then, a data traffic generator is connected to the network, and a system

through which the maximum network throughput and latency of flow of high capacity data. This connection and measurement will be repeated for different access point models. For measurements were used the following devices:

- Generator of network traffic on LAN
  - Tester XtendLan ETHERTEST100G
- Tester of network availability, transmission errors and response times
  - PingerPlus (manufactured by Psiber)
- Router to create a local network
  - ASUS RTAC86U
- Switch to connect the network on the router
  - Cisco SG110D-05
- Wifi access points with client function
  - (tab. 1)

Tab. 1 Wifi access points with client function

Wifi access point	Frequency [GHz]	Speed [Mbps]
CAMIBOX-SET_M1-C2	5	100
MikroTik RBwAPG-5HacT2HnD	2,4 + 5	300 + 1300
Ubiquiti NanoStation M2 Loco	2,4	150
TP-LINK CPE220	2,4	300
Ubiquiti NanoStation M5	5	150
TP-LINK CPE520	5	300

The wiring topology (fig. 1), where the router is connected to the WAN (Internet) and also to the switch. To this is connected tester for testing latency PingerPlus and one of two identical wifi access points. Further, the Wifi access point is wirelessly connected to a second identical access point that is connected to a network traffic generator.
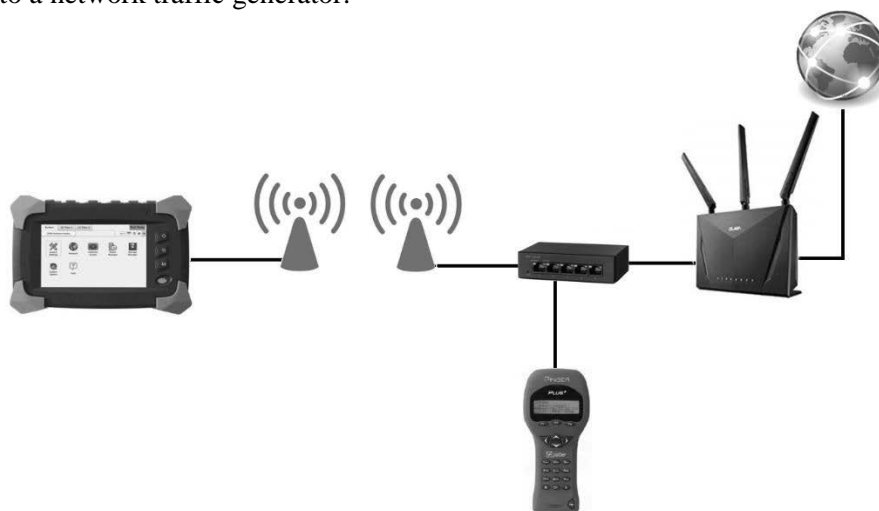
Fig. 1 Topology of wiring of test file

By each measurement was performed 20 repetitions. At the end of the results created average values, which have been further processed. The data flow was chosen to respect the maximum transmission capabilities of each device (1–150 Mbps). A base scale was created that was divided by 10 Mbps. At each measurement was on generator of traffic on LAN network created communication about that volume of data through TCP protocol. This generator was connected to the access point, which sent the data to the same type of device that was 10 m away from it (direct view) and was connected to the switch. This data communication was targeted (routed) to the router, which was also connected to the

switch. Size of latency transfer was monitored by the tester network availability, transmission errors and response times. It verified this latency by function ping and from which individual results were recorded.

RESULTS AND DISCUSSION

From the measured values, several fundamental things can be concluded. The results show that the maximum transmission rate for the individual devices does not affect the resulting of latency. Both of the frequency of 2.4 GHz and at 5 GHz is from the transmission amount of data of 50 Mbps constant of latency. When exceeding 50Mbps latency value increases sharply (fig. 2, fig. 3). We can also conclude from these graphs that apart from the access points from MikroTik manufacturer, individual products from the same manufacturer are on the same level. This means that we cannot say that TP-LINK has products with better quality than Ubiquiti because although it was better in the 5 GHz bands, it was worse in the 2.4 GHz bands.
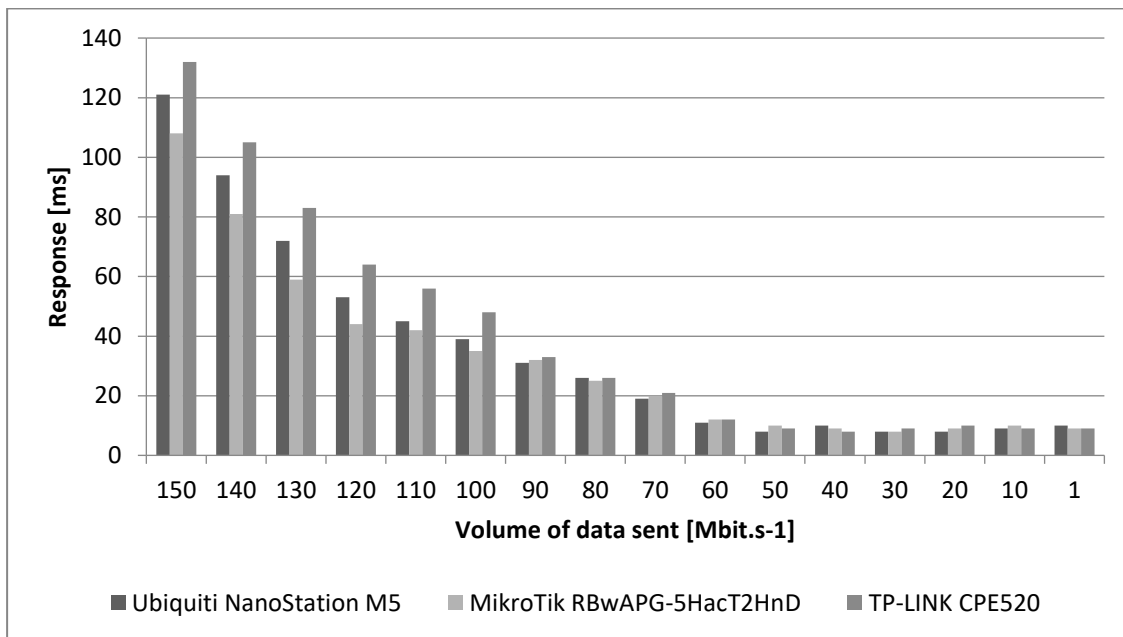
Fig. 2 Testing access points at 5 GHz frequency
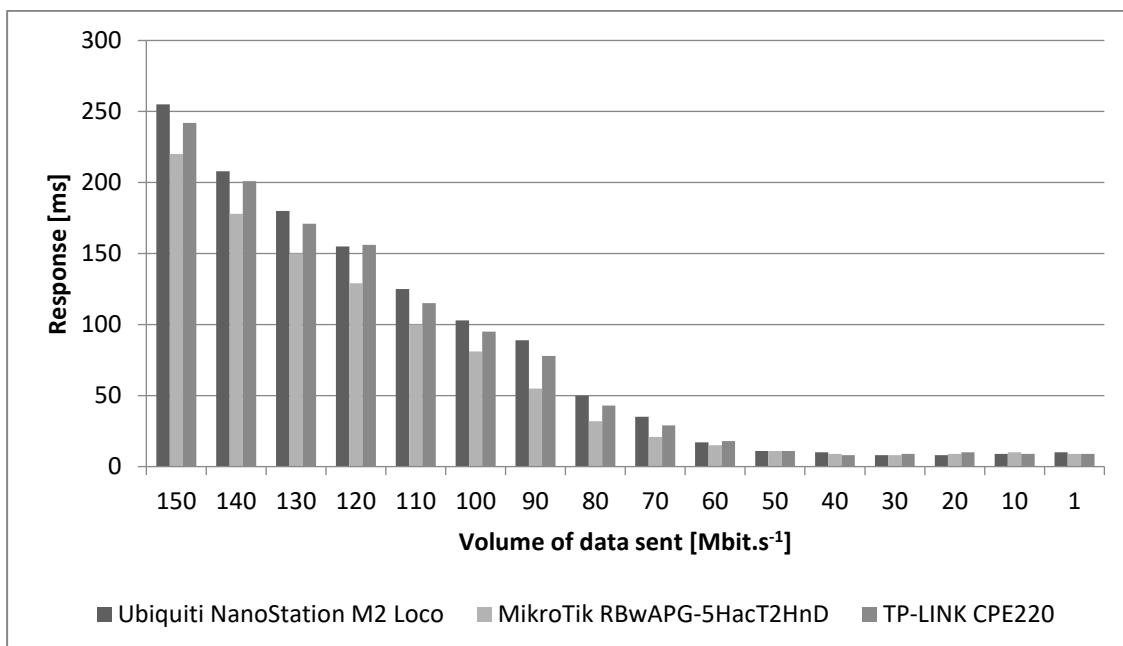
Fig. 3 Testing access points at 2,4 GHz frequency

They were also addressed values for the ISM 2.4GHz, and 5GHz ISM for all the products tested, including professional product variants CamiBOX (fig. 4).
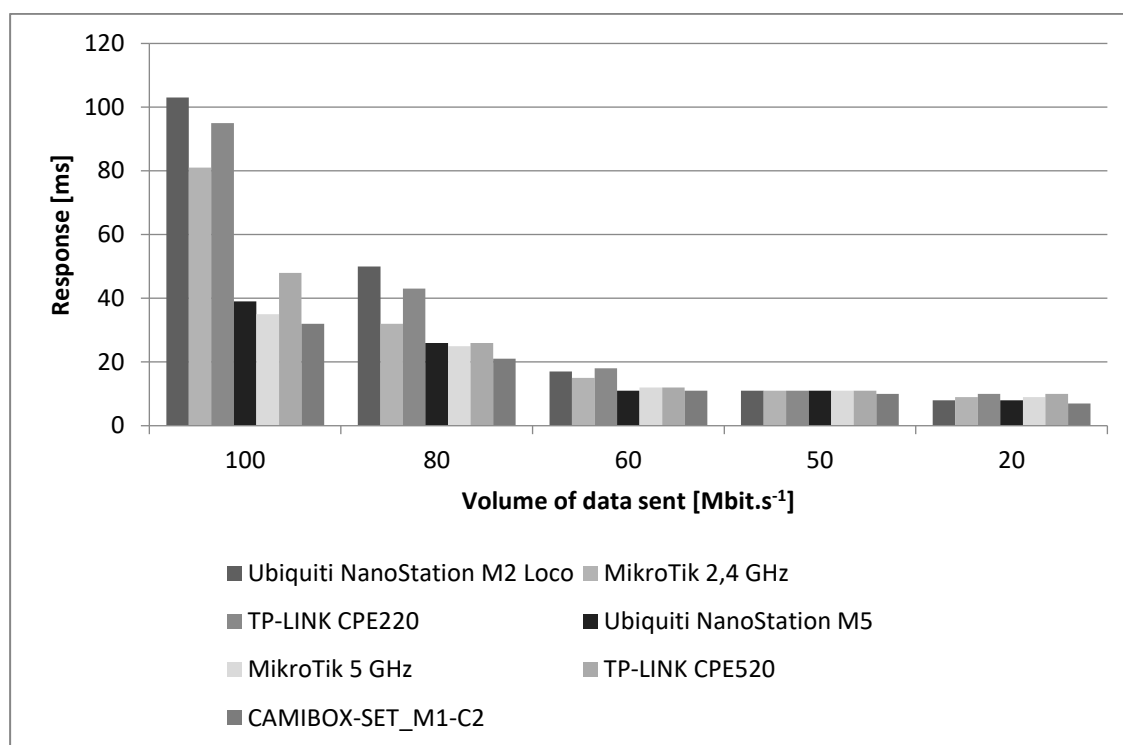
Fig. 4 Comparison of Standard Access Points with Professional Version

Latencies that arise from wireless over wifi are still a problem. Individual scientists are trying to minimize latency in wireless devices through various methods. For example, QAir has a different approach to transfer the distributed queue to the host queue and can reduce the average wifi latency by 50-75% (*Pei, Zhao, Liu, Tan, Zhang, Meng & Pei, 2017*). Another similar process is described by the authors of the article "Uplink ultra-reliable low latency communications assessment in unlicensed spectrum", where they are looking for an alternative to reduce the resulting transmission latency (*Cuevas, Rosa, Frederiksen & Pedersen, 2018*).

In practice, we mostly encounter classic old wifi technologies, through which users also want to control individual automation elements. The problem is that for some operations that require real-time control, latency can cause considerable trouble. Thanks to the exponential increase in latency due to the volume of transmitted data via wifi, it is necessary that at the time of such broadcasting there is no excessive data transmission. Otherwise, the desired operation may be delayed, which can lead to decisive consequences.

Wifi is increasingly used in IoT applications and many others where wireless data communication between two or more devices is needed. The size of IoT data is not fixed. There is an effort to minimize them, but it can also be data in tens or hundreds of MBytes (simple binary commands - bits, video and audio records - tens to hundreds of MBytes, etc.). One such application is the idea of communication between vehicles where individual vehicles exchange information with each other. This communication can lead to more effective information about the accident, traffic and location of the vehicle (*Guan, He, Ai, Matolak, Wang, Zhong & Kurner, 2019*). It is therefore important that the latency of data transfer was minimal, as at increased latency threatens to limit of size the transmission of messages due to the range wifi and movement of vehicles. This also affects the fact that it is time consuming to connect with the wifi access point (*Pei, Wang, Zhao, Wang, Meng, Pei, Peng, Tang & Qu, 2017*).

Similar tests have been addressed in article "Hybrid Communication Architectures for Distributed Smart Grid Applications", although this was strictly related to low-energy communication with photo-voltaic

panels. Even so, this article presents the results latency UDP transmissions depending on the size of packets sent (*Zhang, Hasandka, Wei, Alam, Elgindy, Florita & Hodge, 2018*).

Until a new technology is developed, wifi technology is currently the most widely used wireless local area network technology, so it is important that its testing and improvement does not cease and, on the contrary, continues to grow.

CONCLUSIONS

The results showed that the real latency of wireless transmitted data reaches exponential dependence. At 150 Mbps the average latency of the tested technologies on the 2.4 GHz frequency band ranged from 220 to 255 ms and on the 5 GHz frequency band from 108 to 132 ms.

According to the results it can be stated that the professional CAMIBOX product, which is used for industrial data transmission, has achieved the best results. The second in terms of lowest latency was the manufacturer MikroTik, who achieved similar results to CAMIBOX. Other tested devices TP-LINK and Ubiquiti reached inconsistent results with worse latency than previous devices.

In the future, it is contemplated to continue in testing, taking into account the size of the test packets, and the possibility of using other network topologies as well as extending the number of transmitters to more accurately determine to what extent the latency is dependent on the number of devices on the network.

ACKNOWLEDGMENT

REFERENCES

1. Cuevas, R. M., Rosa, C., Frederiksen, F., & Pedersen, K. I. (2018). Uplink ultra-reliable low latency communications assessment in unlicensed spectrum. In *2018 IEEE GLOBECOM WORKSHOPS (GC WKSHPS)*. Abu Dhabi: U ARAB EMIRATES.

2. Dobeš, J. & Žalud V. (2006). *Moderní radiotechnika*. Praha: BEN - technická literatura.

3. Dostál J. (2017). *Průmysl 4.0 a Společnost 5.0 – výzvy pro změnu (nejen) technického vzdělávání*. Technika a vzdelávanie, pp. 49-54.

4. Gao, J. T., Ito, M. & Shiratori, N. (2016). Optimal Scheduling for Incentive WiFi Offloading under Energy Constraint. In *2016 IEEE 27TH ANNUAL INTERNATIONAL SYMPOSIUM ON PERSONAL, INDOOR, AND MOBILE RADIO COMMUNICATIONS (PIMRC)* (pp.1865-1870).

5. Guan, K., He, D. P., Ai, B., Matolak, D. W., Wang, Q., Zhong, ZD., & Kurner, T. (2019). 5-GHz Obstructed Vehicle-to-Vehicle Channel Characterization for Internet of Intelligent Vehicles. *IEEE INTERNET OF THINGS JOURNAL, 6*(1), 100-110.

6. Han, S. Y., Liang, Y. C., Chen, Q., & Soong, B. H. (2016). Licensed-Assisted Access for LTE in Unlicensed Spectrum: A MAC Protocol Design. *IEEE JOURNAL ON SELECTED AREAS IN COMMUNICATIONS*, *34*(10), 2550-2561.

7. Heřman J. (2008). *Elektronické a telekomunikační instalace*. Praha: Verlag Dashöfer.

8. Chang, B. J. & Chen, S. P. (2017). Cross-layer-based adaptive congestion and contention controls for accessing cloud services in 5G IEEE 802.11 family wireless networks. *COMPUTER COMMUNICATIONS*, *106*, 33-45.

9. Krivchenkov, A. & Sedykh, D. (2015). ANALYSIS OF PACKETS DELAY IN WIRELESS DATA NETWORKS. *TRANSPORT AND TELECOMMUNICATION JOURNAL*, *16*(4), 330-340.

10. Mařík V. (2015). Národní iniciativa Průmysl 4.0. [s.l.]: Ministerstvo průmyslu a obchodu ČR. 42 p.

11. Oppermann, I., Stoica, L., Rabbachin, A., Shelby, Z., & Haapola, J. (2004). UWB wireless sensor networks: UWEN - A practical example. *IEEE COMMUNICATIONS MAGAZINE, 42*, 27-32.

12. Pei, CH., Wang, Z., Zhao, YJ., Wang, ZH., Meng, Y., Pei, D., Peng, YQ., Tang, WL., & Qu, XD. (2017). Why It Takes So Long to Connect to a WiFi Access Point. *IEEE INFOCOM 2017 - IEEE CONFERENCE ON COMPUTER COMMUNICATIONS, IEEE INFOCOM*. Atlanta, GA.

13. Pei, CH., Zhao, YJ., Liu, YX., Tan, K., Zhang, JS., Meng, Y., & Pei, D. (2017). Latency-Based WiFi Congestion Control in the Air for Dense WiFi Networks. In *2017 IEEE/ACM 25TH INTERNATIONAL SYMPOSIUM ON QUALITY OF SERVICE (IWQOS)*. Vilanova i la Geltru, Spain.

14. Piketty T. (2015). *Kapitál v 21. století*. Praha: Euromedia Group, 664 p.

15. Powell, S. & Shim, J. P. (2012). *Wireless Technology: Applications, Management, and Security*. New York: Springer-Verlag, 276p.

16. Šícha, M. & Tichý M. (1998). *Elektronické zpracování signálů základní analogové, digitální techniky*. Praha: Karolinum.

17. Tahir, H. & Shah, S. A. A. (2008), Wireless Sensor Networks - A Security Perspective. In *INMIC: 2008 INTERNATIONAL MULTITOPIC CONFERENCE* (pp. 189-193).

18. Vikram, K. & Sahoo, S. K. (2017). LOAD AWARE CHANNEL ESTIMATION AND CHANNEL SCHEDULING FOR 2.4GHZ FREQUENCY BAND BASED WIRELESS NETWORKS FOR SMART GRID APPLICATIONS. *INTERNATIONAL JOURNAL ON SMART SENSING AND INTELLIGENT SYSTEMS*, *10*(4), 879-902.

19. Vlček J. (2001). *Modulace a přenos signálu*. Praha

20. Zhang, JH., Hasandka, A., Wei, J., Alam, S. M. S., Elgindy, T., Florita, AR., & Hodge, BM. (2018). Hybrid Communication Architectures for Distributed Smart Grid Applications. *ENERGIES*, *11*(4), art. num. 871.

Corresponding author:
Ing. Jan Hart, Ph.D., Department of Vehicles and Ground Transport, Faculty of Engineering, Czech University of Life Sciences Prague, Kamýcká 129, Praha 6, Prague, 16521, Czech Republic, phone: +420 734170850, e-mail: jhart@tf.czu.cz

QUALITY OF HOPS AT DIFFERENT DRYING TEMPERATURES IN CHAMBER DRYER

Petr HEŘMÁNEK[1], Adolf RYBKA[1], Ivo HONZÍK[1]

[1]*Department of Agricultural Machines, Faculty of Engineering, Czech University of Life Sciences Prague, Czech Republic*

Abstract
The drying temperature during the measurement reached 60°C (conventional method) and 40°C (low temperature method). During this measurement, we monitored the output qualitative parameters of the Saaz hop variety in the form of essential oils. During the measurement, an analytical method to determine humulinones, which are one of the components of essential oils in hops and hop products, was newly developed. The measurement confirmed that when drying hops in chamber dryer at a temperature of the drying medium being 40°C, the drying period is extended by approx. 46%. The graphs clearly show the difference in the amount of essential oils contained in the hops dried at 60°C and 40°C. Based on the analytical results it can be concluded that by drying a large majority of the essential oil components is reduced to the approximately same extent, therefore the relative representation in the mixture does not change significantly.

Key words: hop; drying; belt dryer; moisture.

INTRODUCTION

This paper builds on the previous articles covering the comparison of drying process in an experimental chamber dryer at the conventional drying method and low-temperature drying.

Currently, there are 205 fully functional hop dryers available in the Czech Republic. Out of this number, 79 pcs are chamber dryers. Based on the international experience, their drying principle has the potential for further use (*Doe & Menary, 1979*).

Hops are composed of numerous substances. The hop quality both in their fresh and dried state can be assessed in several ways – for instance by means of the moisture content, HIS (Hop Storage Index), alpha and beta bitter acids, prenylflavonoids, humulinones, or hop essential oils. Hop essential oils are the most important group of substances contained in hops responsible for the hop aroma. Depending on the variety, hops contain 0.5 to 3.0% of essential oils which, together with resins and other substances, accumulate in lupulin glands during the process of cone formation and maturation. Hop essential oils are a mixture of several hundreds of natural volatile substances of different chemical composition. Some of these are represented in the order of tens of percent (myrcene, humulene), some other occur in small or even trace amounts. However, all of these together are involved in the formation of the characteristic hop aroma. The constituents of hop essential oils can be divided into three groups. The largest share accounts for the hydrocarbon fraction which forms 70-80% of the total essential oil weight, 20-30% account for the oxygen fraction. The remaining share accounts for the oxygen and sulphur substances (*Krofta, et al., 2017; Münsterer, 2006*).

During the process of drying the moisture content in hop cones reduces from initial approx. 75 up to 85% to approx. 10-12%. Inside the dryer hops are exposed to a drying temperature of 55-60°C for 6-8 hours (conventional method) (*Podsedník, 2001; Kořen, et al., 2008; Rybka, et al., 2018*). With this drying method the temperatures are too high, particularly in the final stage of drying. This is bad for some heat-labile substances and it leads to their losses. In particular, these are hop essential oils contained in quantities between 0.5 and 3.5%, depending on the hop variety (*Hofmann, et al., 2013; Kumhála, et al., 2013*).

Another technology is the method of low-temperature drying (with the drying medium temperature being approximately 40°C) (*Heřmánek, et al., 2017*). This drying method enables to optimize the drying parameters (the drying medium temperature and the hop layer height) mainly for the special hop varieties in which it is desirable to preserve their original composition to the largest degree possible (*Rybáček, et al., 1980; Srivastava, et al., 2006; Kumhála, et al., 2016*). The heat-labile substances will be able to

be used in the manufacture of medicines and food supplements (*Aboltins & Palabinskis, 2016; Aboltins & Palabinskis, 2017; Jokiniemi, et al., 2015*).

Hop drying follows the hop picking line and constitutes an operation which is very important for maintaining the quality of hop product. Low-temperature technology of drying at a temperature of the drying medium of 40°C is suitable for preserving greater amounts of the essential oils contained in a dry hop product (*Vitázek & Jurik, 2015*).

Hop aroma depends on the amount of essential oils contained in hops. Depending of their variety, hops contain 0.5 to 3.0% of essential oils. Hop essential oils are a mixture of several natural volatile substances with various chemical composition. Some occur in the order of tens of percent (e.g. myrcene, humulene), others are present in small or trace quantities. Yet all of these together are the primary contributors of the distinctive hop aroma.

The object of this measurement was to find out whether hops can be dried in an operational chamber dryer at 40°C and at the same time to compare the qualitative characteristics in the form of selected essential oils when hops are dried using the conventional method and low-temperature method.

MATERIALS AND METHODS

By comparing the above-mentioned technologies, it is possible to support or refute the presumed hypothesis. We carried out the in-process measurements of both drying technologies at the researcher Rakochmel Ltd. in Kolešovice in its 4KSCH chamber dryer (Fig. 1). In recent years, during the measurement we put the emphasis on the assessment of the solution benefits in a small experimental chamber dryer (*Heřmánek, et al., 2017; Rybka, et al., 2018*). In 2017 and 2018 we carried out these measurements in an operating dryer in order to assess the impact of preserving the maximum amount of thermally labile substances contained in hop cones – the essential oils.
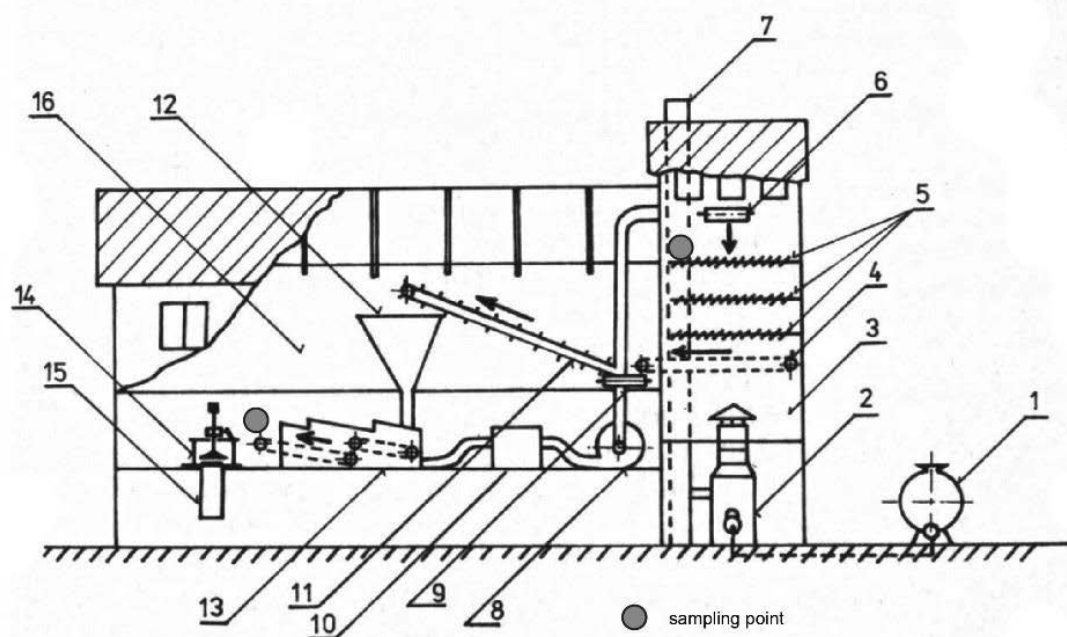
Fig. 1 Scheme of chamber dryer with sampling points for the purposes of laboratory analyses.
1 – fuel tank, 2 – hot-air aggregate, 3 – drying chamber, 4 – discharge conveyor (4th slat box), 5 – slat system, 6 – filling conveyor, 7 – stack, 8 – draught fan, 9 – unloading cross conveyor, 10 – air purifier, 11 – staging conveyor, 12 – hopper, 13 – conditioning, 14 – press, 15 – prism, 16 – storage space.

The hop variety used in this experiment was Saaz. This variety had been chosen because it forms approximately 80% of the hop production in the Czech Republic and that company grows it. The measurement was carried out in two chambers of the dryer, at a temperature of 60°C in its first chamber and at a temperature of 40°C in its third chamber.

During the measurements the drying air temperature and relative humidity were monitored in both chambers by means of data loggers and installed fixed sensors (*Heřmánek, et al., 2017*). Samples were taken from dried hops to determine a decline in the content of essential oils (*Krofta, et al., 2017*). The hop resins include these substances: beta-Pinene, limonene, linalool, geraniol, 2-Undecanone, caryophyllene, caryophyllene-epoxide, humulene epoxide II, myrcene, farnesene and humulene.

Graph courses were drawn up (Fig. 2) based on the drying cycle in both chambers. The essential oils content is illustrated in Fig. 3 and 4.

RESULTS AND DISCUSSION

The above-mentioned measurement proved that drying hops in a operating chamber dryer at a temperature of 40°C will extend the drying period by approx. 45% while maintaining the consumption of LFO per a ton of dry hops (during drying at a temperature of 40°C the layer of inserted hops had been lowered).

The courses of the values of the drying ambient temperature and relative humidity from both measurements are depicted in the graph of Fig. 2 which clearly shows a decline in moisture depending on the measurement time, and differences between drying at a temperature of 60°C and 40°C. The drops in temperature and rises in the drying air relative humidity are due to the technology of pouring the hops, when heaters and fans are stopped because this is the time when the operator fills the upper slat box with green hops.
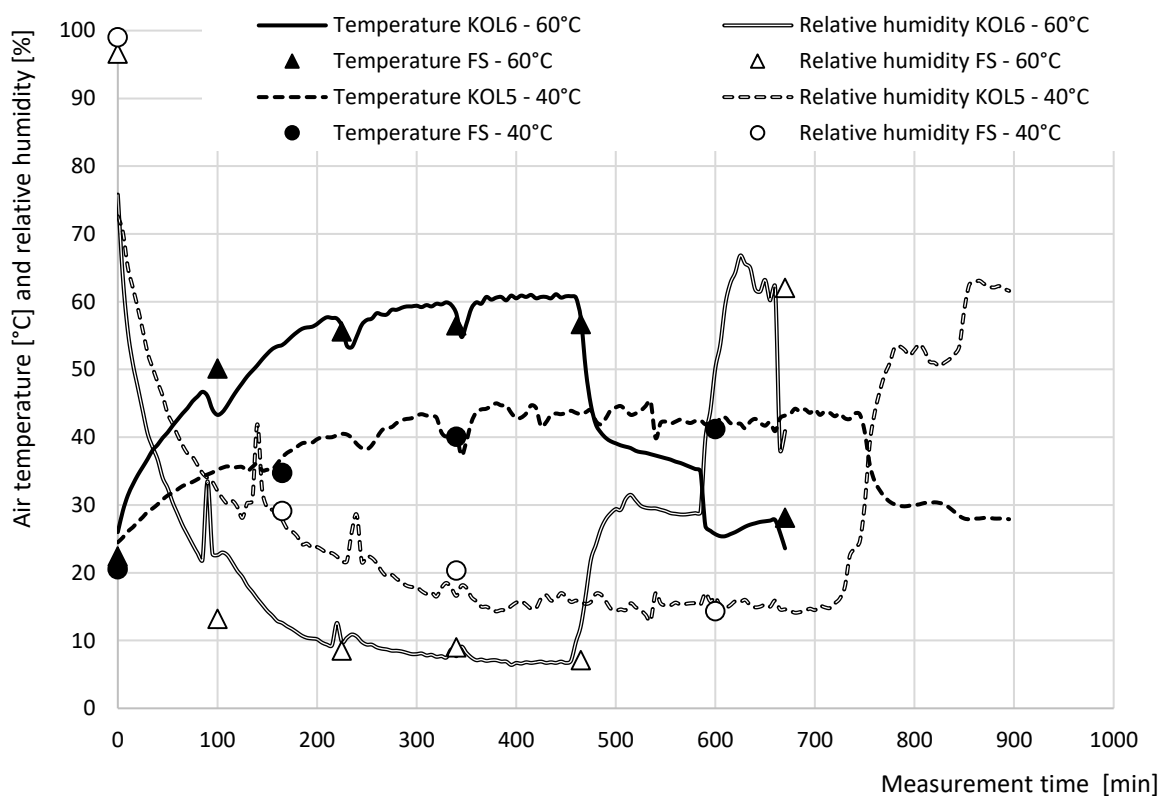
Fig. 2 Dependence of drying air temperature and relative humidity on measurement time (FS – fixed sensors, KOL5, KOL6 – data loggers).

Samples of hop cones were taken during the measurement at the completion of pour and upon leaving the conditioning. Sampling was carried out in both chambers in order to compare the effect of different drying air temperatures. The samples were assessed for the presence of preserved essential oils.

As the etalon was set the content of essential oils in green hops taken at the pour into the dryer. The measurement results are shown in Tab. 1.

Tab. 1 Results of laboratory analyses of hop cones to determine the content of essential oils in green cones, in cones dried at a temperature of 40°C and 60°C in 2018.

Variety	Drying conditions	Essential oils amount	Relative ratio [%]
Saaz	Green hops	0.52	100
	Drying at a temperature of 40°C	0.44	84.6
	Drying at a temperature of 60°C	0.41	78.8

The qualitative assessment of the essential oil composition is expressed as a relative percentage, as a ratio of integrated constituent area to the total integrated area of all essential oil constituents. In quantification the integration parameters are selected so that 50-70 parts of essential oil constituents are quantified. The largest share is formed by terpenic hydrocarbons myrcene, caryophyllene, humulene, farnesene and selinenes that constitute 50-70% of the total essential oils weight.

The graphs in Fig. 3 and 4 show the difference between the drop in the essential oils contained in hops dried at a temperature of 60°C and 40°C.
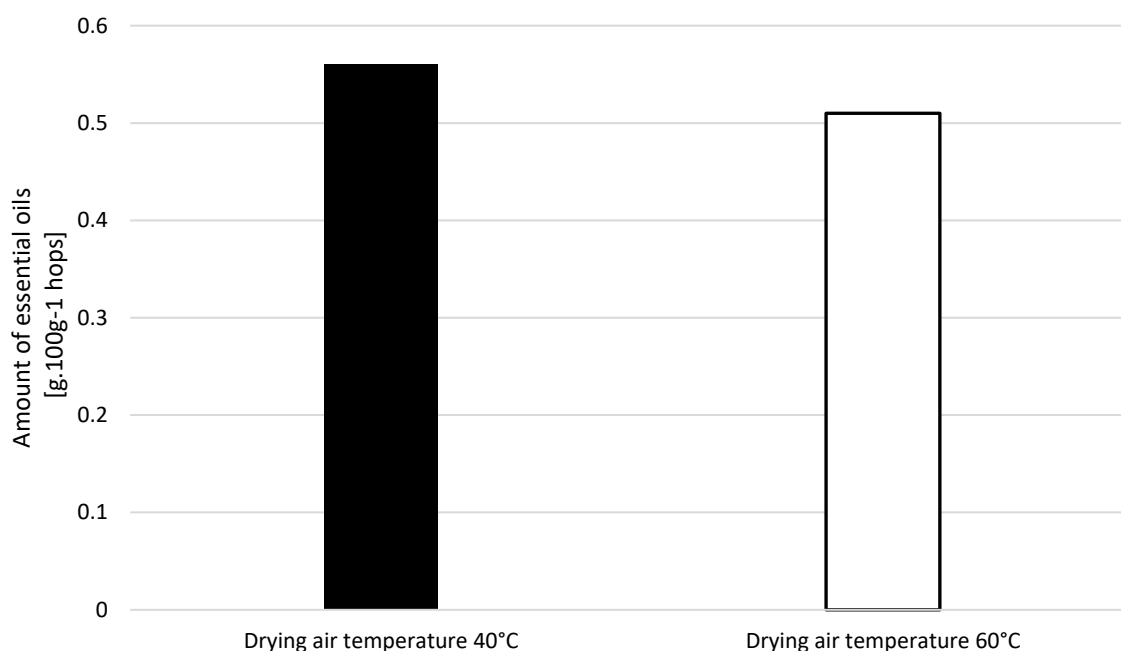
Fig. 3 Content of essential oils in hops dried at different drying air temperatures in a chamber dryer – Saaz 2017.

At a temperature of 60°C, the essential oil content was 0.51 g . 100 g^{-1}, while at a temperature of 40°C the essential oil content was higher, that is 0.56 g . 100 g^{-1}. Although this value is very low in absolute terms, the difference when the drying temperature changes is noticeable. This is shown even more clearly in the following graph (Fig 4).

The graph in Fig. 4 clearly shows the significant difference in the given substances when implementing various drying technologies. Except for geraniol, there is an increase in the amount of all the substances at a lower drying temperature. This is particularly noticeable with terpene hydrocarbon farnesene, but also with humulene and caryophyllene, which together with myrcene form 60 % of the total essential oil weight.
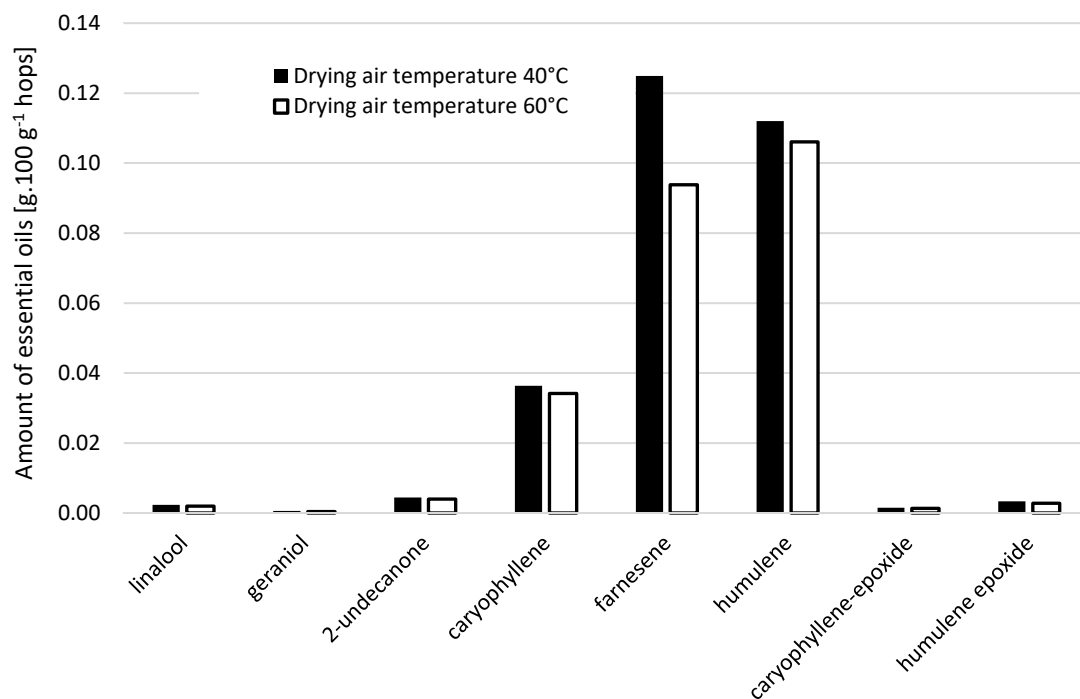
Fig. 4 Content of essential oils in hops dried at different drying air temperatures in a chamber dryer – Saaz 2017.

A study of different temperatures during hop drying has already been published. In the article *(Rybka, et al., 2018)*, the authors dealt with the drying of hops in an experimental chamber dryer. The results of the above measurement in the operating chamber hop dryer show that the lower temperature of drying is preferable from the point of view of maintaining essential oils in hops.

CONCLUSIONS
The object of this measurement was to find out whether hops can be dried in an operational chamber dryer at 40°C and at the same time to compare the qualitative characteristics in the form of selected essential oils when hops are dried using the conventional method and low-temperature method.
With the drying medium temperature being 60°C, hops lose on average 10% of the essential oils content. Based on the analytical results, by drying a major part of essential oils constituents decreases to approximately the same extent, thus the relative representation in the mixture does not change substantially.
Thus, our hypothesis was confirmed both in 2017 and 2018 measuring. When applying the low-temperature technology of drying for aroma hop varieties the result should be at least identical and even better, regarding the higher content of essential oils. In the future we assume further experiments in this area.

REFERENCES

1. Aboltins, A. & Palabinskis, J. (2017). Studies of vegetable drying process in infrared film dryer. *Agronomy Research, 15*(Special issue 2), 1259–1266.

2. Aboltins, A. & Palabinskis, J. (2016). Fruit Drying Process Investigation in Infrared Film Dryer. *Agronomy Research, 14*(1), 5–13.

3. Doe, P.E. & Menary, R.C. (1979). Optimization of the Hop Drying Process with Respect to Alpha Acid Content. *J. Agric. Engng Res., 24*, 233–248.

4. Heřmánek, P., Rybka, A., & Honzík, I. (2017). Experimental chamber dryer for drying hops at low temperatures. In *8th International Conference on Biosystems Engineering 2017, Agronomy Research, 15*(3), 713-719, Estonian University of Life Sciences and Latvia University of Agriculture. ISSN 1406-894X.

5. Hofmann, R., Weber, S., & Rettberg, S. (2013). Optimization of the Hop Kilning Process to Improve Energy Agric. Efficiency and Recover Hop Oils. *Brewing Science, 66*(March/April), 23–30.

6. Jokiniemi, T., Oksanen, T., & Ahokas, J. (2015). Continuous airflow rate control in a recirculating batch grain dryer. *Agronomy Research, 13*(1), 89–94.

7. Kořen, J., Ciniburk, V., Podsedník, J., Rybka, A., & Veselý, F. (2008). *Hop drying in chamber dryers* (in Czech). Hop Research Institute Co. Ltd., Žatec, 31 pp.

8. Krofta, K., Pokorný, J., Ježek, J., Klapal, I., Mravcová, L., Vondráčková, P., Rybka, A., Heřmánek, P., Honzík, I., Podsedník, J., Melč, J., Šrámek, K., Kolman, Z., & Nádvorník, J. (2017). *Evaluation of hops qualitative parameters during drying and storage* (in Czech). CHI s.r.o., Žatec a ČZU v Praze, 17 p., ISBN 978-80-86836-6-4.

9. Krofta, K. (2008). *Evaluation of hop quality* (in Czech). Hop Research Institute Co. Ltd., Žatec, 55 pp.

10. Kumhála, F., Kavka, M., & Prošek, V. (2013). Capacitive throughput unit applied to hop picking machine. *Agric. Computers and Electronics in Agric, 95*(7), 92–97.

11. Kumhála, F., Lev, J., Kavka, M., & Prošek, V. (2016). Hop-picking machine control based on capacitance throughput sensor. *Applied Engng in Agric, 32*(1), 19–26.

12. Münsterer, J. (2006). *Optimale Trocknung und Konditionierung von Hopfen*. Bayerische Landesanstalt für Landwirtschaft, Arbeitsgruppe Hopfenbau, Produktionstechnik, Wolnzach, 26 p., Germany.

13. Podsedník, J. (2001). Hop harvesting technology in the Czech Republic 1996-2000. In *Proceedings of the Technical Commission I.H.G.C. of the XLVIIIth International Hop Growers Congress.* Canterbury-England.

14. Rybka, A., Heřmánek, P., & Honzík, I. (2018). Analysis of Hop Drying in Chamber Dryer. *Agronomy Research, 16*(1), 221-229. ISSN: 1406-894X.

15. Rybka, A., Krofta, K., Heřmánek, P., Honzík, I., & Pokorný, J. (2018). Effect of drying temperature on the content and composition of hop oils. *Plant, Soil and Environment, 64*(10), 512-516. ISSN 1214-1178

16. Rybáček, V., Fric, V., Havel, J., Libich, V., Kříž, J., Makovec, K., Petrlík, Z., Sachl, J., Srp, A., Šnobl, J., & Vančura, M. (1980). *Hop production* (in Czech). SZN Prague, 426 pp.

17. Srivastava, A.K., Goering, C.E., Rohrbach, R.P., & Buckmaster, D.R. 2006. *Engineering Principles of Agricultural Machines.* 2nd Edition. Michigan: ASABE, 569 pp.

18. Vitázek, I. & Jurík, I. (2015). *Grain drying and storage technology*. Nitra: SPU, 136 p. ISBN 978-80-5521419-1.

Corresponding author:
Petr Heřmánek, Department of Agricultural Machines, Faculty of Engineering, Czech University of Life Sciences Prague, Kamýcká 129, Prague, 165 00, Czech Republic, phone: +420 22438 3126, e-mail: hermanek@tf.czu.cz

SELECTED RHEOLOGICAL PROPERTIES OF SOME TOMATO KETCHUPS

Peter HLAVÁČ[1], Monika BOŽIKOVÁ[1], Zuzana HLAVÁČOVÁ[1]

[1]*Department of Physics, Faculty of Engineering, Slovak University of Agriculture in Nitra*

Abstract
This article is focused on monitoring and evaluation of rheological properties of tomato ketchups. Influence of temperature in range (5 – 30) °C and short storage time was investigated. Dependencies of rheological properties on temperature and storage time were evaluated by the regression equations and the coefficients of determination. Ketchup is a non-Newtonian material, so apparent viscosity was measured using digital rotational viscometer Anton Paar DV-3P. Densities of samples were determined according to definition. Apparent viscosity of samples decreased exponentially with increasing temperature, so the Arrhenius equation is valid. Ketchup's apparent fluidity was increasing exponentially with the temperature. We also found out that apparent viscosity had decreased with storage time and on the other hand apparent fluidity was increasing with storage time, which can be caused by structural changes in samples during storing. Temperature dependencies of ketchup densities were sufficiently characterized by decreasing linear function in measured temperature range.

Key words: *ketchup; rheological parameters; density; temperature, dependency.*

INTRODUCTION

Precise knowledge of physical quantities of materials is required at controlled processes in manufacturing, handling and holding. For the quality evaluation of food materials it is important to know their physical properties particularly, mechanical (*Kubík et al., 2017*), rheological and thermophysical (*Glicerina et al., 2013*). Tomatoes are often consumed in fresh state, but several varieties are processed into various products such as tomato sauce, soup, paste, puree, juice, ketchup and salsa. Authors noted that several studies had investigated the benefits of tomatoes in reducing the risk of heart disease, improving bone health, and decreasing the risk of cancer (*Tan & Kerr, 2015*). The industrial processing of tomatoes leads to a great variety of output products. Some of the most relevant are the following: concentrated tomato products, either as puree or paste depending on the percentage of natural soluble solids; pizza sauce, from peels and seeds; tomato powder, as dehydrated concentrated tomato; peeled tomato, either whole or diced; ketchup, tomato sauce seasoned with vinegar, sugar, salt and some spices, etc. (*Ruiz Celma et al., 2009*). New design of experimental double piston filament stretching apparatus that can stretch fluids to very high extensional strain rates was presented by *Mackley et al. (2017)*. Authors had used high speed photography for determination of filament deformation and breakup profiles of a strategically selected range of fluids including low and higher viscosity Newtonian liquids together with a viscoelastic polymer solution, biological and yield stress fluids at extensional strain rates in excess of 1000 s^{-1}. *Mackley et al. (2017)* had also reported that numerical modelling can be used with the fluids correct rheological characterization to gain physical in-sight into how rheologically complex fluids deform and breakup at very high extensional deformation rates. *Chandrapala et al. (2012)* had stated that ultrasonic pulses in combination with rheological measurements could be used at the solids concentration determination in various highly concentrated and industrial food suspensions (tomato, vegetable and pasta sauces, seafood chowder, strawberry yoghurt, cheese sauce with vegetables). Low intensity ultrasound-based techniques could be used during the detection and identification of foreign bodies in food products (e.g. tomato ketchup) (*Chandrapala et al., 2012*). The rheological behaviour of some food dispersions were investigated and modelled with the Herschel–Bulkley model by *Herrmann et al. (2013)*. Several rheologic parameters were studied in dependency on composition of various ingredients (fats, carbohydrates, proteins, water). The effects of manothermosonication or thermal treatment on tomato pectic enzymes and tomato paste rheological properties were compared by *Vercet et al. (2002)*. The quality of tomato concentrate was studied by *Fadavi et al. (2018)* using ohmic vacuum, ohmic, and conventional-vacuum heating methods. Authors had indicated that ohmic heating under vacuum condition had a good effect on quality during the concentration of tomato juice and that vacuum condition decreased the time required for processing and

heating rate. Small amplitude oscillatory shear (SAOS) and large amplitude oscillatory shear (LAOS) behaviour of tomato paste was investigated by *Duvarci et al. (2017)*. Authors had stated that the semi-empirical Bird-Carreau constitutive model can be used in small amplitude oscillatory shear behaviour of tomato paste. Authors also used Ewoldt-McKinley theory for determination of non-linear rheologic properties in large amplitude oscillatory shear behaviour of tomato paste. This method offered parameters which can be used for better understanding of structural changes which occur at different deformations or time scales (*Duvarci et al., 2017*). Rheological properties of tomato products are considered as one of the most important quality attributes, since they influence product processing parameters, especially flow properties during transport, as well as consumers' acceptability (*Torbica et al., 2016*). Investigation of rheological properties and microstructure of tomato puree using continuous high pressure homogenization was done by *Tan & Kerr (2015)*. Influence of rheological and structural characterization of tomato paste on the quality of ketchup was investigated by *Bayod et al. (2008)*. According to *Sharoba et al. (2005)* ketchup is time-independent, semi-solid non-Newtonian fluid having a definite yield stress. The effect of temperature on viscosity of fluids at a specified shear rate could be described by the Arrhenius equation, in which the apparent viscosity decreases as an exponential function with temperature (*Sharoba et al., 2005*). According to *Bayod et al. (2008)* viscosity of tomato ketchup is a major quality component for consumer acceptance. Several parameters affect the flow behaviour of tomato ketchup, including the quality of the raw material (e.g. tomato paste) and the processing conditions. To achieve a constant and desirable quality in the final product (i.e. ketchup), high quality paste and continuous control and adjustment of the variables for its processing are required (*Bayod et al., 2008*). Tomato ketchup could be presented as concentrated dispersion of insoluble matter in aqueous media, and its complex structure causes that it exhibits non-Newtonian, shear-thinning and time-dependent rheological behaviour with yield stress (*Torbica et al., 2016*). Ketchup can be included into one of the most commonly consumed condiment which is made either from fresh tomatoes or from the concentrates such as tomato purees and tomato pastes (*Mert, 2012*). Effect of temperature and concentration on rheological properties of ketchup–processed cheese mixtures was analysed using steady and dynamic oscillatory shear by *Yilmaz et al. (2011)*. Temperature dependency of the apparent viscosity at a specified shear rate (50 s^{-1}) could be described by the Arrhenius model (*Yilmaz et al., 2011*). *Torbica et al. (2016)* have evaluated nutritional, rheological, and sensory properties of tomato ketchup with increased content of natural fibres made from fresh tomato pomace and compared the results with five commercial products. Authors found out that the rheological properties of the ketchup with increased fibre content depend mostly on total solids and insoluble particles content, but properties remained in the limits for standard tomato products.

Apparent viscosity is defined as ratio of shear stress and corresponding shear rate and its physical unit is (Pa·s). Viscosity changes with temperature, for most of the liquids decreases with increasing temperature. According to Eyering theory molecules of liquids continuously move into the vacancies (*Bird et al., 1960*). The temperature effect on viscosity can be described by an Arrhenius type equation

$$\eta = \eta_0 \, e^{-\frac{E_A}{RT}}$$

(1)

where η_0 is reference value of viscosity, E_A is activation energy, R is gas constant and T is absolute temperature (*Figura & Teixeira, 2007*). Density of material ρ is defined as a ratio between mass of material m and its volume V

$$\rho = \frac{m}{V}$$

(2)

The definition is valid for solids, liquids, gases and disperses (*Figura & Teixeira, 2007*). The standard SI unit of density is (kg·m^{-3}). Reciprocal value of apparent viscosity η is called apparent fluidity φ and unit of apparent fluidity is (Pa^{-1}.s^{-1}) (*Figura & Teixeira, 2007*).

$$\varphi = \frac{1}{\eta}$$

(3)

Almost all parameters are influenced by temperature, so mainly these effects were analysed as a main aim in this article.

MATERIALS AND METHODS

Measurements were performed in laboratory settings on four samples of tomato ketchup, purchased in local market (Heinz tomato ketchup, soft ketchup Hellmann´s, sweet ketchup Hamé and soft ketchup Snico). As ketchup is not Newtonian material, apparent viscosity had to be measured. Density (Eq. 2) and apparent fluidity (Eq. 3) were also determined. The measurements of all samples were carried out under the same conditions in approximate temperature range (5 – 30) °C. Measuring of apparent viscosity was performed by digital rotational viscometer Anton Paar (DV-3P). First measurements were performed at the beginning of storing, second measurements were done after three weeks of storing and last measurements were realised after four weeks of storing. There were constructed dependencies of rheological properties on temperature and storage time and evaluated by the regression equations and the coefficients of determination. Temperature dependencies of apparent viscosity can be described by decreasing exponential function (4), in the case of temperature dependencies of apparent fluidity can be used increasing exponential function (5), and temperature dependencies of density were described by decreasing linear function (6).

$$\eta = A e^{-B\left(\frac{t}{t_o}\right)} \; ; \; \varphi = E e^{F\left(\frac{t}{t_o}\right)} \; ; \quad \rho = -G\left(\frac{t}{t_0}\right) + H \tag{4, 5, 6}$$

where t is temperature (°C), t_0 is 1 °C, A, B, E, F, G, H are constants dependent on kind of material, and on ways of processing and storing .

RESULTS AND DISCUSSION

On Fig. 1 are presented temperature dependencies of ketchup apparent viscosity. It is possible to observe from Fig. 1 that apparent viscosity of ketchups is decreasing with increasing of temperature. The progress can be described by decreasing exponential function, which is in accordance with Arrhenius equation (1). Comparable rheological results for ketchup were reported by *Sharoba et al. (2005)*. It is also visible on Fig. 1 that highest apparent viscosities were obtained for sample of Ketchup Snico, and lowest values for Ketchup Hamé, which could be caused by different composition of ketchups.
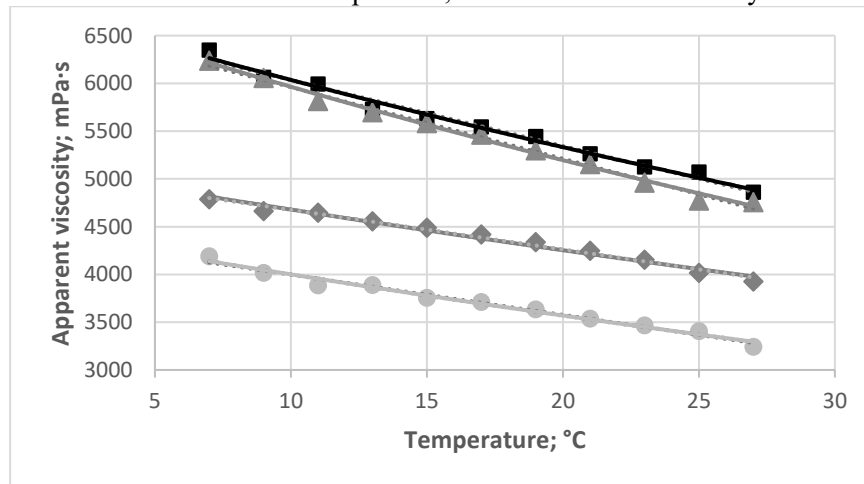
Fig. 1 Relations of ketchup apparent viscosity to the temperature Snico (■), Hellmanns (▲), Heinz (♦), Hamé (●)

Temperature dependencies of ketchup density are shown on Fig. 2. It can be seen that values of density are decreasing with increasing temperature for all samples of ketchup. Similar decreasing progress was found for different samples by *Kumbár & Nedomová (2015)*. In this temperature range was used linear decreasing function. Same type of dependency was used also by *Thomas et al. (2015)* and *Kelkar et al. (2015)*. Highest density values were obtained for Ketchup Snico and on the contrary lowest values for Ketchup Hamé. Apparent fluidity dependencies on temperature are presented on Fig. 3. Increasing exponential character of dependency was used for all samples. Due to the fact that apparent fluidity is defined as reciprocal value of apparent viscosity, highest fluidities were found for Ketchup Hamé and lowest for Ketchup Snico. Regression coefficients and coefficients of determination for all dependencies are shown in Tab. 1.
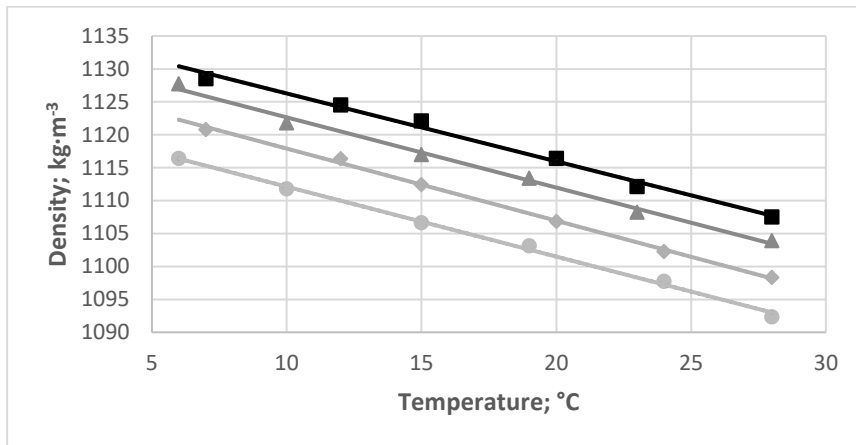
Fig. 2 Relations of ketchup density to the temperature Snico (■), Hellmanns (▲), Heinz (♦), Hamé (●)
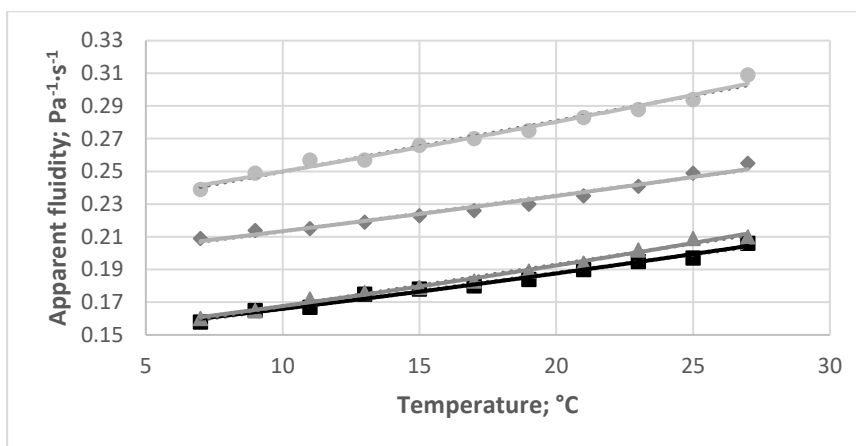
Fig. 3 Relations of ketchup apparent fluidity to the temperature Snico (■), Hellmanns (▲), Heinz (♦), Hamé (●)
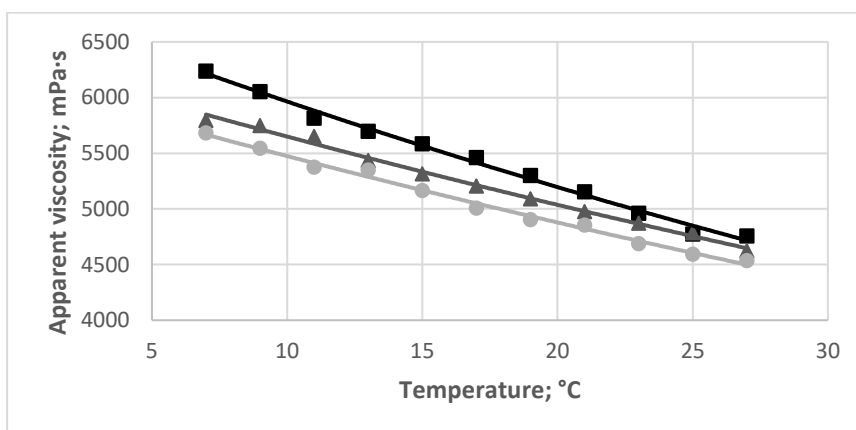
Fig. 4 Relations of ketchup Hellmann´s apparent viscosity to the temperature: first measurement (■), next measurement (▲), last measurement (●)

Influence of storage time for sample of Ketchup Hellmann´s could be seen on Fig. 4. It is clear from Fig. 4 that highest apparent viscosity values were obtained in the beginning of storage, lower values were after three weeks of storing and lowest values after four weeks of storing. This proportion could be caused by structural changes in sample during storing. Similar results were found for other three samples of ketchup. It can be seen from Tab. 1 that coefficients of determination reached very high values in the approximate range (0.980 – 0.998).

Tab. 1 Coefficients A, B, E, F, G and H of regression equations (4 – 6) and coefficients of determinations (R^2)

Sample of ketchup	Coefficients of regression equations (4 – 6)		
	A mPa·s	B -	R^2
Snico	6 832.3	0.012	0.988 4
Hellmann´s	6846.7	0.014	0.992 2
Heinz	5 147.8	0.010	0.980 3
Hamé	4 482.6	0.011	0.981 4
Sample of ketchup	E $Pa^{-1} \cdot s^{-1}$	F -	R^2
Snico	0.146 8	0.012 3	0.987 1
Hellmann´s	0.146 0	0.013 8	0.9919
Heinz	0.193 9	0.009 6	0.978 4
Hamé	0.223 0	0.011 4	0.982 7
Sample of ketchup	G $kg \cdot m^{-3}$	H $kg \cdot m^{-3}$	R^2
Snico	1 136.6	1.031 3	0.991 9
Hellmann´s	1 133.3	1.066 6	0.994 2
Heinz	1 128.9	1.095 6	0.998 2
Hamé	1 122.7	1.061 8	0.997 1
Ketchup Hellmann´s/ measurement	A mPa·s	B -	R^2
First	6 846.7	0.014	0.992 2
Next	6 337.1	0.011	0.994 0
Last	6 143.7	0.012	0.992 6

CONCLUSIONS

Composition of food materials is different so their physical properties are very complex. Physical properties of food materials depend on the manipulation, external conditions and other factors, which determine their behaviour. Rheological properties of tomato ketchups were measured and analysed in this paper. Apparent viscosity is relevant for non-Newtonian materials. Effect of temperature and storing time on measured samples of tomato ketchups was searched and comparison of used samples was made. We found out that apparent viscosity of samples decreased exponentially with increasing temperature, so the Arrhenius equation is valid. Comparable rheological results for ketchup were reported by *Sharoba et al. (2005)*. Proportion of the curves in Fig. 1 could be caused by different composition of analysed samples. Ketchup's apparent fluidity was increasing exponentially with the temperature. Apparent viscosity had decreased with storage time and on the other hand apparent fluidity had increased with storage time, which can be caused by structural changes in samples during storing. Temperature dependencies of ketchup densities were sufficiently characterized by decreasing linear function in measured temperature range, which is in accordance with authors (*Kumbár & Nedomová, 2015*; *Thomas et al., 2015*; *Kelkar et al., 2015*; etc.). The calculated rheological characteristics can be used for designing of technological equipment or containers for distribution of the product to the final users. The knowledge of flow behaviour is also important for the development of new recipes and direct qualitative assessment of the products.

REFERENCES

1. Bayod, E., Willers, E. P. & Tornberg, E. (2008). Rheological and structural characterization of tomato paste and its influence on the quality of ketchup. *LWT - Food Science and Technology*, *41*, 1289 – 1300.

2. Bird, R. B., Stewart, W. E. & Lihgtfoot, E. N. (1960). *Transport Phenomena*. New York, John Wilie & Sons.

3. Chandrapala, J., Oliver, Ch., Kentish, S. & Ashokkumar, M. (2012). Ultrasonics in food processing – Food quality assurance and food

safety. *Trends in Food Science & Technology*, *26*, 88 – 98.

4. Duvarci, O. C., Yazar, G. & Kokini, J. L. (2017). The SAOS, MAOS and LAOS behavior of a concentrated suspension of tomato paste and its prediction using the Bird-Carreau (SAOS) and Giesekus models (MAOS-LAOS). *Journal of Food Engineering*, *208*, 77 – 88.

5. Fadavi, A., Yousefi, S., Darvishi, H. & Mirsaeedghazi, H. (2018). Comparative study of ohmic vacuum, ohmic, and conventional-vacuum heating methods on the quality of tomato concentrate. *Innovative Food Science and Emerging Technologies*, *47*, 225 – 230.

6. Figura, L. O. & Teixeira, A. A. (2007). *Food Physics, Physical properties – measurement and applications* (1ˢᵗ ed.), Verlag, Berlin, Heidelberg, New York: Springer.

7. Glicerina, V., Balestra, F., Dalla Rosa, M. & Romani, S. (2013). The influence of process steps on microstructural, rheological and thermal properties of dark chocolate. *Journal on Processing and Energy in Agriculture*, *17*(2), 59 – 63.

8. Herrmann, J., Alayón, A. B., Trembley, J. & Grupa, U. (2013). Development of a rheological prediction model for food suspensions and emulsions. *Journal of Food Engineering*, *115*, 481 – 485.

9. Kelkar, S., Boushey, C. J. & Okos, M. (2015). A method to determine the density of foods using X-ray imaging. *Journal of Food Engineering*, *159*, 36–41.

10. Kubík, Ľ., Brindza, J., Brovarskyi, V. & Velychko, S. (2017). Perga under compressive loading. *Journal on Processing and Energy in Agriculture*, *21*(1), 23 – 26.

11. Kumbár, V. & Nedomová, Š. (2015). Viscosity and analytical differences between raw milk and UHT milk of Czech cows. *Scientia Agriculturae Bohemica*, *46*, 78–83.

12. Mackley, M. R., Butler, S. A., Huxley, S., Reis, N. M., Barbosa, A. I. & Tembely, M. (2017). The observation and evaluation of extensional filament deformation and breakup profiles for Non Newtonian fluids using a high strain rate double piston apparatus. *Journal of Non-Newtonian Fluid Mechanics*, *239*, 13 – 27.

13. Mert, B. (2012). Using high pressure microfluidization to improve physical properties and lycopene content of ketchup type products. *Journal of Food Engineering*, *109*, 579 – 587.

14. Ruiz Celma, A., Cuadros, F. & López-Rodríguez, F. (2009). Characterisation of industrial tomato by-products from infrared drying process. *Food and Bioproducts Processing*, *87*, 282 – 291.

15. Sharoba, A. M., Senge, B., El-Mansy, H. A., Bahlol, H. E. I. M. & Blochwitz, R. (2005). Chemical, sensory and rheological properties of some commercial German and Egyptian tomato ketchups. *European Food Research and Technology*, *220*, 142 – 151

16. Tan, J. & Kerr, W. L. (2015). Rheological properties and microstructure of tomato puree subject to continuous high pressure homogenization. *Journal of Food Engineering*, *166*, 45 – 54.

17. Thomas, M. J., Bramblett, K. A., Green, B. D. & West, K. N. (2015). Thermophysical and absorption properties of brominated vegetable oil. *Journal of Molecular Liquids*, *211*, 647 – 655.

18. Torbica, A., Belović, M., Mastilović, J., Kevrešan, Ž., Pestorić, M., Škrobot, D. & Dapčević Hadnađev, T. (2016). Nutritional, rheological, and sensory evaluation of tomato ketchup with increased content of natural fibres made from fresh tomato pomace. *Food and Bioproducts Processing*, *98*, 299 – 309.

19. Vercet, A., Sánchez, C., Burgos, J., Montañés, L. & Buesa, P. L. (2002). The effects of manothermosonication on tomato pectic enzymes and tomato paste rheological properties. *Journal of Food Engineering*, *53*, 273 – 278.

20. Yilmaz, M. T., Karaman, S., Cankurt, H., Kayacier, A. & Sagdic, O. (2011). Steady and dynamic oscillatory shear rheological properties of ketchup–processed cheese mixtures: Effect of temperature and concentration. *Journal of Food Engineering*, *103*, 197 – 210.

Corresponding author: Mgr. Peter Hlaváč, Ph.D., Department of Physics, Faculty of Engineering, Slovak University of Agriculture in Nitra, Tr. A. Hlinku 2, Nitra, SK-949 76, Slovakia, phone: +421 376414749, e-mail: Peter.Hlavac@uniag.sk

INFLUENCE OF DIESEL – BUTANOL FUEL BLENDS ON PRODUCTION OF SOLID PARTICLES BY CI ENGINE

Michal HOLÚBEK[1], Jakub ČEDÍK[1], Hien VU[1], Martin PEXA[1]

[1]*Department for Quality and Dependability of Machines, Faculty of Engineering, Czech University of Life Sciences, holubekm@tf.czu.cz*

Abstract
The paper deals with the size distribution and count of solid particles produced by agricultural CI engine, operated on fuel blends of butanol and fossil diesel fuel in comparison with 100% diesel fuel. 5 and 20% concentrations of n-butanol in diesel fuel were used as a test fuels. For measurement the turbocharged engine Zetor 1204, mounted in the tractor Zetor Forterra 8641, was used. The particles were evaluated by means of EEPS (engine exhaust particle sizer) made by TSI, Inc. according to their size and count. The engine was measured in stabilized conditions at rated speed of 2200 min^{-1} under 50%, 75% and 100% engine load. The results showed lower total count of produced solid particles when using both of blended fuels in comparison with diesel fuel. Also, the size of the particles tended to decrease with increasing proportion of n-butanol in the fuel blend.

Key words: solid particles; CI engine; n-butanol; blended fuel; tractor.

INTRODUCTION

Simple alcohols such as butanol, ethanol or methanol as well as vegetable oils are considered as promising potential biofuels. They can be used as additives or blended fuels in CI engines. It is proven that diesel blended with alcohols decrease NO_x and PM emissions *(Killol et al., 2019)*. Compared to ethanol and methanol, n-butanol has some different qualities, such as higher energy content, enabling it to be directly blended and the advantage of not being strongly hygroscopic. Properties of butanol are also considerably closer to diesel fuel *(Rezgui & Guemini, 2016)*. Mentioning the fuel delivery methods, burning butanol in diesel engines can be realized through direct injection of neat butanol or blends with diesel *(Abdullah et al., 2019)*. Butanol has a lower auto-ignition temperature and thus it can be burned easier *(Li et al., 2019)*. Engine oil dilution is one of the problems which occurs in the diesel engine. During the cold start of the engine, the unburnt non-vaporized feedstock is condensed on the cylinder liner wall and is blown through the piston ring and dilutes with the lubricating oil in the crankcase. Fuel dilution also reduces the viscosity of engine oil, which makes lubrication oil film weaker and leads to crankcase bearing wear *(Choi, Lee & Park, 2016)*. Although there are many studies about butanol and vegetable oil blended in biofuel, but there is still limited information of combustion characteristics over a range of blends of n-butanol and diesel including vegetable oils *(Lampe et al., 2018)*. The aim of this paper was to compare the size distribution and count of solid particles produced by agricultural CI engine, operated on butanol-diesel fuel blends and 100% diesel fuel.

MATERIALS AND METHODS

During this experiment three different fuels were compared. Firstly, 100% diesel fuel (D100) with no added bio-component was used as a reference for experiment. Consequently, two fuel blends were used as tested fuels: 95% diesel fuel blended with 5% of n-butanol (BUT5) and 80% diesel fuel blended with 20% of n-butanol (BUT20). Density, kinematic viscosity and calorific value of the tested fuels are shown in Tab. 1. The values of density and kinematic viscosity were measured by means of Stabinger Viscometer SVM 3000 made by Anton Paar GmbH (measuring accuracy < 1%, repeatability 0.1%).

The values of calorific value of the fuels were reached by means of isoperibol calorimeter LECO AC600 (measuring range 23.1–57.5 MJ kg^{-1} for a 0.35 g sample, accuracy 0.1% RSD) according to ČSN DIN 51900-1 and ČSN DIN 51900-2.

Tab. 1 Fuel properties ([1]data obtained from *EN 590*, [2]data obtained from *Imtenan et al. 2015* and *Atmanli et al. 2015*, [3]data obtained from *Rakopoulos et al. 2010*)

	Calorific value MJ.kg^{-1}	Kinematic viscosity mm^2.s^{-1}	Density at 15°C	Cetane number
D100	43.151	1.8013	819.133	50[1]
BUT5	42.438	1.7125	817.971	-
BUT20	41.076	1.7052	817.083	-
BUT100	33.101	2.226	815.270	17[3]-25[2]

The measurements were carried out using compression ignition engine Zetor 1204 with turbocharger, mounted in the tractor Zetor Forterra 8641. The given specifications of the engine are shown in Tab. 2. The engine is in factory setup and it has never been used in outdoor conditions, only for laboratory testing. Its overall operating time does not exceed 160 operating hour.

Tab. 2 Parameters of the tractor engine

Manufacturer and type	Zetor 1204
Cylinders	4, in-line
Air flow	Turbocharged
Rated power	60 kW at 2200 min^{-1} (53.4 kW on PTO)
Maximum torque	351 Nm (312 Nm on PTO)
Engine displacement volume	4.156 l
Cylinder bore X stroke	105 X 120 mm
Compression ratio	17
Fuel system	Mechanical in-line injection pump
Injection type	Direct injection
Combustion chamber	Bowl-in-piston
Injector noozle	Multihole
Start of injection (SOI)	12° before top dead center
Injection pressure	22 MPa
Valve mechanism	OHV
Valves per cylinder	2

A data acquisition unit, provided by manufacturer, was used to store the data from the dynamometer to the computer with the frequency of 10 Hz. The tractor was loaded via PTO (Power Take Off) using mobile dynamometer MAHA ZW 500. Specification of the dynamometer can be seen in Tab. 3.

Tab. 3. Basic dynamometer specification

Manufacturer and type	MAHA ZW 500
Max. power	500 kW
Max. torque	6,600 Nm
Max. speed	2,500 min^{-1}
Torque inaccuracy	< 1% over the full speed range

TSI Engine Exhaust Particle Sizer 3090 (EEPS) was used for measuring of the production of solid particles. The basic operational parameters of the EEPS particle analyser is shown in Tab. 4. This device evaluates particles as the count of particles in volume 1 cm^3.

Tab. 4. EEPS 3090 specification

Particle Size Range	5.6–560 nm
Particle Size Resolution	16 channels per decade (32 total)
Electrometer Channels	22
Charger Mode of Operation	Unipolar diffusion charger
Inlet Cyclone 50% Cutpoint	1 μm
Time Resolution	10 size distributions s^{-1}

The exhaust gas is diluted before entering the particle analyser (dilution ratio 0.01007, dilution factor 99.2667) and then cooled down to temperature approx. 23°C. The pressure of the measured gas is kept at approx. 90 kPa. Data from the particle analyser were stored to the hard drive of PC with the frequency of 1 Hz.

The measurements were carried out at rated engine speed 2200 min^{-1} in stabilized conditions. The loads of the engine were calculated from maximum torque at 2200 rpm for each fuel. The load of the engine was maintained at 50%, 75% and 100%. At each measurement point the monitored parameters were stabilized. After stabilization the monitored parameters were recorded for approx. 80 s. The mechanical losses in gearbox have no real influence on comparative measurement and therefore they were not taken into account. The MS Excel was used for evaluation of the measured data.

RESULTS AND DISCUSSION

In Fig. 1 the particle size distribution for all tested fuels at 50% engine load is shown. It is evident that the concentration of produced solid particles was lower when using both of blended fuels in comparison with D100, which can be explained by higher oxygen content of the blended fuels.

Also, the blended fuels showed lower mean size of the produced solid particles compared with D100. With increasing proportion of n-butanol in the fuel blend the mean size of solid particles decreased (D100 – 55.53 nm, BUT5 – 52.98 nm, BUT20 – 49.47 nm). This can be explained by lower viscosity of the fuel blends in comparison with D100 and therefore better atomization. Also, higher volatility of n-butanol in the fuel blends could contribute to lower size of particles, especially during premixed combustion phase.
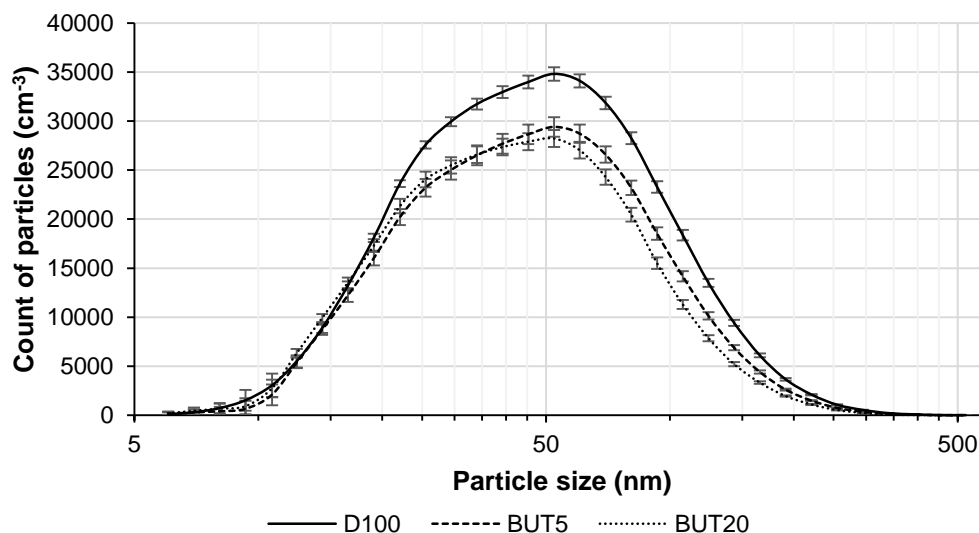
Fig. 1 Particle size distribution for all tested fuels at 50% engine load

In Fig. 2 the particle size distribution for all tested fuels at 75% engine load is shown. From the figure it can be seen that both of the blended fuels reached lower concentration of solid particles in practically all sizes in comparison with D100. However, the difference between BUT5 and BUT20 is more significant than in the case of 50% engine load. The higher particles concentration, reached with BUT20 in comparison with BUT5 may be caused by the properties of n-butanol in the fuel blend, especially by its

lower cetane number. Lower cetane number of BUT20 fuel cause later ignition of the fuel and therefore affects the combustion process, while BUT5 have its properties closer to D100.

Similarly to 50% engine load, the mean size of the particles decreased with increasing proportion of n-butanol in the blend (D100 – 56.28 nm, BUT5 – 54.83 nm, BUT20 – 50.64 nm).

Fig. 3 shows the particle size distribution for all tested fuels at 100% engine load. It is evident that both of blended fuels decreased production of solid particles in comparison with D100, similarly to other measured engine loads. However, similarly to 75% engine load, higher production of solid particles in the size range of approx. 10–70 nm was reached using BUT20 in comparison with BUT5.

Using all tested fuels the mean size of the produced solid particles increased with increasing engine load. Due to lower viscosity of the fuel blends, the mean size of produced solid particles was lower when using both of the blended fuels in comparison with D100 (D100 – 68.7 nm, BUT5 – 65.88 nm, BUT20 – 57.25 nm).

Similar results, concerning lower production of solid particles and size when using n-butanol–diesel fuel blends, were also found by *Jindra et al. (2016)*, especially at higher engine load. Other authors *(Zhang & Balasubramanian, 2014; Geng et al., 2019)* also found lower concentration and lower mean diameter of produced solid particles after addition of n-butanol into biodiesel–diesel fuel blends.
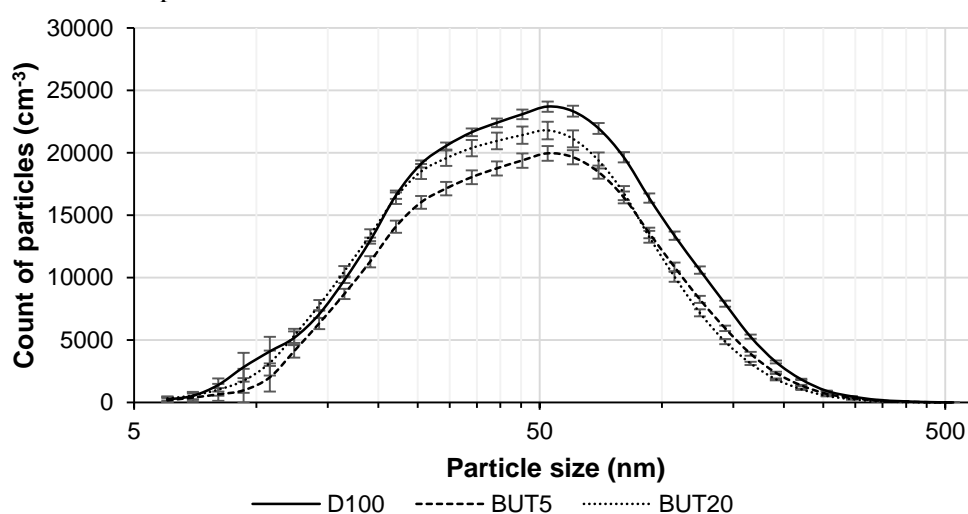
Fig. 2 Particle size distribution for all tested fuels at 75% engine load
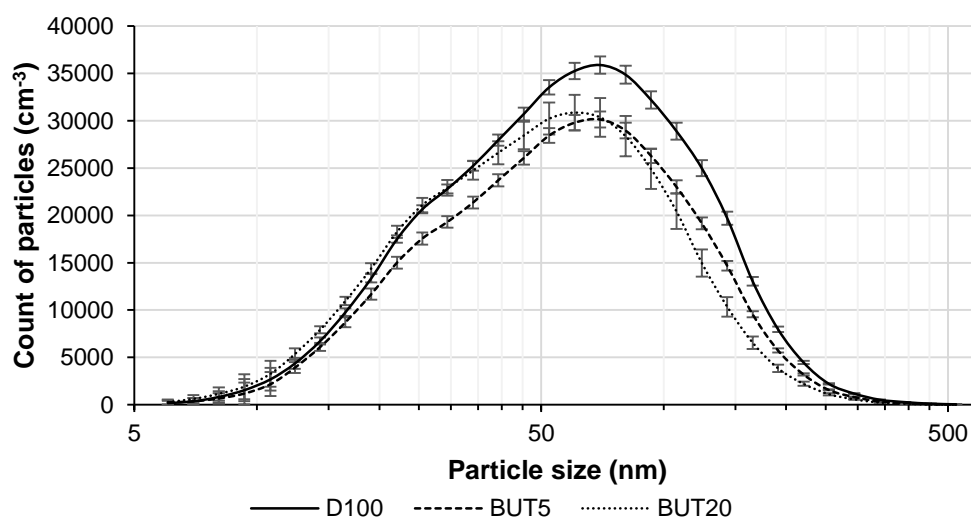
Fig. 3 Particle size distribution for all tested fuels at 100% engine load

In Fig. 4 the total particles count, reached with all tested fuels at all measured engine loads can be seen. It is evident that the lowest concentration of solid particles was reached at 75% engine load. Also at all

measured engine loads the both of blended fuels decreased the total solid particles production. Using BUT5 the decrease was approx. 16.9% at 50% engine load, 17.8% at 75% engine load and 17.3% at 100% engine load. When running on BUT20 fuel blend the decrease of solid particles production was approx. 19.8% at 50% engine load, 10.7% at 75% engine load and 14.5% at 100% engine load. The statistically significant difference was found between all tested fuels in all measured engine loads using the analysis of variance (ANOVA). Tab. 5 shows ANOVA, complemented with Tukey HSD post-hoc test for all tested fuels at all measured engine loads.
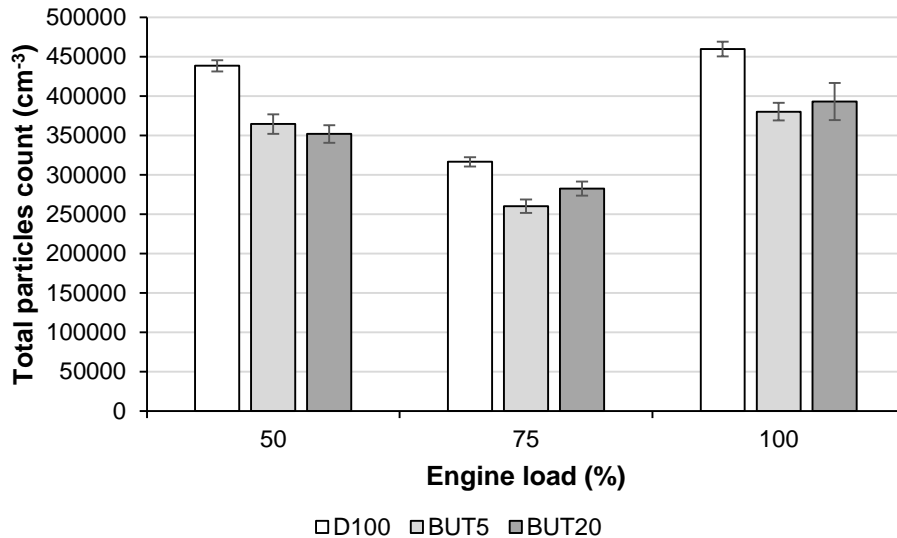
Fig. 4 Total particles count for all tested fuels at all measured engine loads

Tab. 5 ANOVA with Tukey HSD post-hoc test for total particles count at full engine load ($\alpha = 0.05$)

ANOVA

	Sum of squares	Degrees of freedom	Variance	F
Between groups	2.14E+11	2	1.07E+11	448.4478
Within groups	4.09E+10	171	2.39E+08	
Total	2.55E+11	173		

Tukey HSD Post-hoc Test

D100 vs BUT5: Diff=-79544.6571, 95%CI=-86154.4040 to -72934.9102, p=0.0000

D100 vs BUT20: Diff=-66771.9298, 95%CI=-73817.7415 to -59726.1181, p=0.0000

BUT5 vs BUT20: Diff=12772.7273, 95%CI=5957.5440 to 19587.9106, p=0.0000

CONCLUSIONS

From the results of the performed measurement the following conclusions were made:

- The count of produced solid particles decreased at practically all sizes for both of the fuel blends except fuel BUT20 at size range of approx. 10–70 nm.
- Statistically significant difference in total solid particles production was found between all tested variants at all measured engine loads while at higher engine load (75% and 100%) BUT5 fuel showed the lowest solid particles production.
- The mean size of the particles decreased with increasing proportion of n-butanol in the fuel blend.

The paper is focused on comparison of solid particles production of turbocharged CI engine operating on n-butanol–diesel fuel blends and 100% diesel fuel. From reached results it can be stated that addition

of n-butanol into diesel fuel have positive effect on decrease of the number of produced solid particles by CI engine.

ACKNOWLEDGMENT

REFERENCES

1. Abdullah, B., Syed Muhhamad, S., Shokravi, Z., Ismail, S., Kassim, K., Mahmood, A., & Aziz, M. (2019). Fourth generation biofuel: A review on risks and mitigation strategies. *Renewable and Sustainable Energy Reviews*, *107*, 37-50.

2. Atmanli, A., Ileri, E., & Yüksel, B. (2015). Effects of higher ratios of n-butanol addition to diesel-vegetable oil blends on performance and exhaust emissions of a diesel engine. *Journal of Energy Institute*, *88*, 209–220.

3. Choi, J., Lee, S., & Park, S. (2016). Friction losses modelling of piston rings for various combustion pressures in diesel engine. *Journal of Mechanical Science*, *30*, 5739-5747.

4. EN 590. (2013). Automotive fuels. Diesel. Requirements and test methods.

5. Geng L, Chen Y, Chen X., & Lee C. F. (2019). Study on combustion characteristics and particulate emissions of a common-rail diesel engine fueled with n-butanol and waste cooking oil blends. *Journal of Energy Institute, 92*, 438–449.

6. Imtenan, S., Masjuki, H., Varman, M., Rizwanul Fattah, I., Sajjad, H., & Arbab, M. (2015). Effect of n-butanol and diethyl ether as oxygenated additives on combustion–emission-performance characteristics of a multiple cylinder diesel engine fuelled with diesel–jatropha biodiesel blend. *Energy Conversion and Management*, *94*, 84–94.

7. Jindra, P., Kotek, M., Mařík, J., & Vojtíšek, M. (2016). Effect of different biofuels to particulate matters production. *Agronomy Research, 14*, 783–789.

8. Killol, A., Reddy, N., Paruvada, S., & Murugan, S. (2019). Experimental studies of a diesel engine run on biodiesel n-butanol blends. *Renewable Energy*, *135*, 687-700.

9. Lampe, A., Dittmar, A., Heyen, C., & Kiefer, J. (2018). Butanol as a potential biofuel: A spectroscopic study of its blends with n-decane and diesel. *Fuel*, *222*, 312-318.

10. Li, Y., Tang, W., Chen, Y., Liu, J., & Lee, Ch. (2019). Potential of acetone-butanol-ethanol (ABE) as a biofuel. *Fuel*, *242*, 673-686.

11. Rakopoulos, D.C., Rakopoulos, C.D., Giakoumis, E.G., Dimaratos, A.M., & Kyritsis, D.C. (2010). Effects of butanol–diesel fuel blends on the performance and emissions of a high-speed DI diesel engine. *Energy Conversion and Management*, *51*, 1989–1997.

12. Rezgui, Y. & Guemini, M. (2016). Benefits of n-butanol, as a biofuel, in reducing the levels of soot precursors issued from the combustion of benzene flames. *Kinetics*, *57*(6), 731-737.

13. Zhang, Z. H. & Balasubramanian, R. (2014). Influence of butanol addition to diesel–biodiesel blend on engine performance and particulate emissions of a stationary diesel engine. *Applied Energy, 119*, 530–536.

Corresponding author:
Ing. Michal Holúbek, Department for Quality and Dependability of Machines, Faculty of Engineering, Czech University of Life Sciences Prague, Kamýcká 129, Praha 6, Prague, 16521, Czech Republic, phone: +421 902611630, e-mail: holubekm@tf.czu.cz

THE COMBINATION OF RETROREFLECTIVE MATERIALS ON ROAD SIGNS

Lukáš Jan HRABÁNEK[1]

[1]*Department of Vehicles and Ground transport, Faculty of Engineering, Czech university of Life Sciences Prague*

Abstract
Combination of retroreflective materials from the perspective of optical performance is essential for temporary road signs placed in areas of road works while driving at night. The measurements of white traffic sheetings in the measured viewing angle α = 0.33° and the illumination angle β = 5° proved, that there are more significant optical differences in the tapes formally included in the RA2 class, as the two tapes 3M 3930 and OR 5910 have values of around 600 cd·lx^{-1}·m^{-2}. However, the third tape tested, AD 6500, only has values of around 405 cd·lx^{-1}·m^{-2}. Significant differences are seen in traffic sheetings formally classified as RA3, since the AD 7500 and OR 6910 samples have values of around 430 cd·lx^{-1}·m^{-2}. However, the third 3M 4090 traffic sheeting in the same formal class has values up to 764 cd·lx^{-1}·m^{-2}.

Key words: *road works; traffic sheeting; retroreflective material; road signs.*

INTRODUCTION

Road signs provide important traffic information and thus a safer road traffic environment through prohibitions, orders, warnings or otherwise (*Koyuncu & Amado, 2008*). The aim of putting on the key traffic signs, especially the priority or speed limit ones, is to increase road safety *(Baratian-Ghorghi, Zhou, Jalayer, & Pour-Rouholamin, 2015*) day and night and to improve the quality of road transport services (*International commission on illumination CIE, 1988*). The EUROSTAT statistical office's demographic surveys show that Europe is aging, as the relative ratio of persons over the age of 65 has increased for the European population from 10.5 % in 1970 to 15.9 % in 2005. By 2020, according to the medium-sized version of the United Nations projection, the share of European seniors can be expected to grow to 19 %. According to Eurostat data from 20 July 2017, persons over 65 will be 23.9 % in 2030, 27 % in 2040 (*Vácha, 2010*). Older drivers need 40 % more time and 8 times better light conditions to respond adequately to objects or traffic signs than younger drivers do.

If we different eye defects of drivers (according to the Institute of Health Information and Statistics of the Czech Republic based on the EHIS 2014 survey, 19.7 % of respondents reported impaired vision even while using their glasses or other visual aids) (*ÚZIS, 2016*), impaired abilities of quick accommodation of the eye for changes in the level of incident light of older drivers, poor weather conditions, bedazzlement by oncoming vehicles, driver fatigue and possible dirtiness of the road sign and windscreen, then we can better understand why night driving is dangerous and so that we need to ensure that traffic signs are visible in this period.

In the case of night driving, fatal accident rate is 2.5 fatal accidents per 1 million miles travelled (*FHWA, 2008*). While only 25 % of the total driving time is being performed at night, 50 % of fatal accidents happen during this time (*NSC, 2018*). The visibility of traffic signs is ensured by special retroreflective materials that reflect a certain amount of light back to the driver. Especially in the field of road works and traffic restrictions, the use of several types of special retroreflective materials (blind technology) of varying optical performance in one cross section is common, which, especially if combined, can cause the night traffic to miss important traffic information. Traffic signs provide drivers with important information (*M. Khalilikhah, Fu, Heaslip, & Carlson, 2018*). However, road signs are fully effective only if they are clearly visible. With retroreflective material, the traffic signs are visible also at night, even if they are not illuminated by external lights *(Majid Khalilikhah & Heaslip, 2016*).

The usage of retroreflective materials in the field of road works and traffic restrictions is regulated in detail by special technical regulations. They state that on the road signs, only traffic sheetings of RA2 class shall be used on motorways, first road class and local roads (*Ministerstvo dopravy ČR, 2015*). Furthermore it is possible to use RA1 class of retroreflective materials on other roads.

Nevertheless, the continuous higher optical performance in the field of retroreflective materials shows that the three existing classes of formal classification according to EN 12899-1 *("ČSN EN 12899-1," 2003*) are insufficient and significant differences can be observed according to the measurements made.
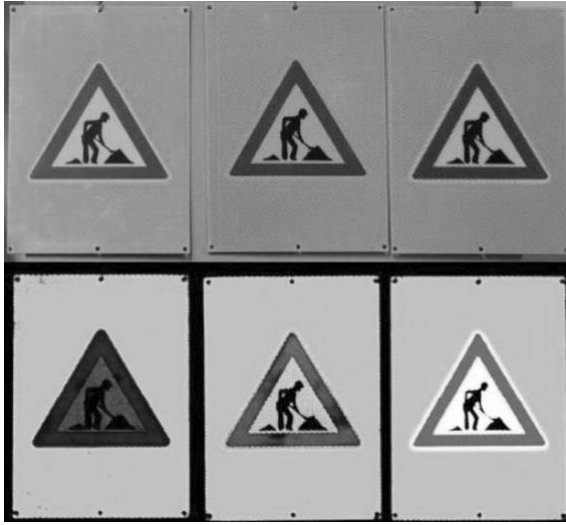
Fig. 1 Combination of traffic sheetings on a traffic sign "Work" on a fluorescent substrate

Fig. 1 in the top row shows pictures of traffic signs taken at daytime. In the lower row, pictures of traffic signs as seen by the driver at night are shown. On the left, there are traffic signs where classes RA1 and RA3 are combined. In the middle a combination of RA2 and RA3 traffic sheeting is used. On the right a complete RA3 class sign is pictured. From the structural point of view the retroreflective materials are differentiated into ballotine (GB) and microprismatic (M). Ballotine materials are made of glass beads. This type of ballotine retroreflective materials has been used since 1930s, and it is no longer possible to increase its performance, since the values of the most powerful ballotine retroreflection materials are around 264 $cd \cdot lx^{-1} \cdot m^{-2}$. Especially for this reason, the more powerful, microprismatic traffic sheetings have been developed. Those have been used since the 1970s. In principle the surface of the microprismatic traffic sheeting is formed by prismatic reflectors. In some microprismatic traffic sheeting a rotational symmetry is being measured, i. e. to what extent the retroreflection is affected by the rotation of the traffic sheeting.

There are many studies dealing with retroreflection of traffic signs. Recently, there have been scientific articles such as the evaluation of background materials leading to increased visibility safety *(Obeidat, Rys, Rys, & Du, 2016)*, basic retroreflective materials maintenance procedures for road signs, automatic retrieval of traffic signs retroreflection by mobile device LIDAR *(Ai & Tsai, 2016)*, Traffic sign damage analysis *(Boggs, Heaslip, & Louisell, 2013)*, Improvement of Traffic Signs Indicating Animal Occurrence *(Majid Khalilikhah & Heaslip, 2017)*, Lifetime of Retro-Reflective Materials (*Unhola, 2016*), (Kai Sørensen, 2011). However, none of these articles have previously dealt with a possible combination of retroreflective materials in one cross section, although in practice it is a common problem and the appropriate combination has a major impact on visibility and thus road safety. Therefore the main aim of the research is to assess the combination of selected retroreflective materials to enhance understanding of their usage. From the perspective of road traffic safety it is desirable to introduce more classes within EN 12899-1, which would take materials of similar optical performance into account.

MATERIALS AND METHODS

The amount of 30 samples, were examined to determine optical properties of white, red, green and blue traffic sheetings with dimensions of 210 × 297 mm. All of them are produced by the three worldwide companies (3M, Avery Dennison and Oralite) and those are the most commonly used traffic sheetings in ordinary road traffic. Retroreflective materials produced by Nikkalite were not investigated, because they are not used by Czech traffic sign manufacturers. Samples that were displayed on the roof of the building of the Faculty of Engineering of the Czech University of Life Sciences in Prague, were repeatedly examined as a part of study (Fig.2). Retroreflection measurement results are limited by this factor, since the sample being examined can be made from a different quality retroreflection materials part during the manufacturing process.
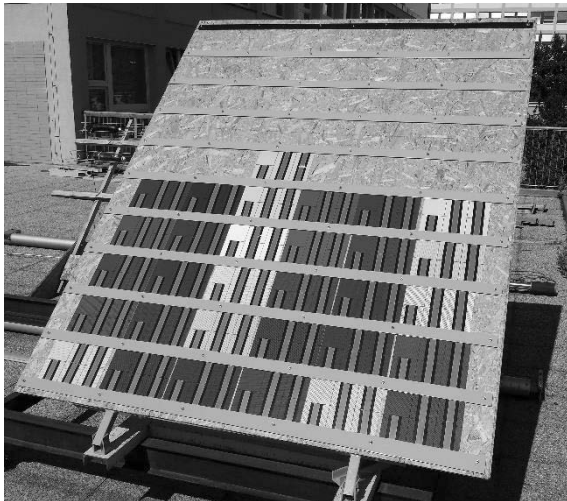
Fig. 2 Traffic sheetings exposed on the roof of building

Retroreflection measurement results are limited by this factor, since the examined samples can be produced of retroreflective materials of different quality during the manufacturing process or during the subsequent treatment of the traffic sheeting by the manufacturer of the traffic signs. The results of traffic sheeting sample measurements also do not promote or uphold the individual products not traffic sheeting manufacturer, but they are merely the basis for an article published in a scientific journal. From a formal point of view, the performance class RA1 according to ČSN EN 12899-1 is represented by the samples of 3M 3200, AD 1500, OR 5710 and 3M EGP type of microprismatic traffic sheetings. From the performance class RA2, the microprismatic traffic sheetings of the type 3M 3930, AD 6500 and OR 5910 were subject to measurements. The functional lifetime of RA1 traffic sheeting is 7 years. The functional lifetime of RA2 and RA3 traffic sheetings is 10 years. Ballotine traffic sheetings are tested according to ČSN EN 12 899-1 and microprismatic retroreflective materials according to European Technical Approval ETA *("ČSN EN 12899-1," 2003)*. RA1 and RA2 class traffic sheetings are measured according to these technical regulations at an viewing angle $\alpha= 0.2°$, $0.33°$ and $2°$ and in the illumination angle $\beta1 + 5°$, $+30°$, $+40°$. RA3 class traffic sheetings are measured at an viewing angle of $0.33°$, $1°$, $1.5°$ and $+ 5°$, $+ 20°$, $+ 30°$, $+40°$ in the illumination angle. For uniform measurement conditions, the illumination angle $\beta1 = 5°$ and the viewing angle α $0.33°$ were chosen to compare the traffic sheeting samples. The individual traffic sheeting samples have been clearly marked and exhibited since the beginning of August 2017. The individual traffic sheetings were consequently optically divided into six individual fields of approximately 0.1 m x 0.1 m. Before the taking of actual measurements, the individual traffic sheetings were always thoroughly cleaned with a cotton cloth so that possible dust and pollen particles would not distort the retroreflexion measurements.

RESULTS AND DISCUSSION

The actual measurements of the traffic sheetings were performed by a certified measuring device Zenther 6060 that is able to measure in three observation angles $\alpha = 0.2°$, $0, 33°$ and $2°$ and in one illumination angle $\beta1 = 5°$, while according to the requirements of ČSN EN 12 899-1 the value of $\beta2 = 0$. The traffic sheetings were measured before being exposed on the roof of the building both horizontally

and vertically to eliminate the effect of rotational symmetry, which can significantly affect the measured values for some types of traffic sheeting. Subsequently, measurements were undertaken after exposure to meteorological effects after 1, 4, 8, 12, 16 and 20 weeks.

The Table 1 shows the retroreflection values (R_A) of $cd \cdot lx^{1} \cdot m^{-2}$ for pre-exposure (A) and 20 weeks after exposure (B), including the minimum retroreflection values (R_A) required by technical regulations (C) and the retroreflection coefficient value (KR) that serves to determine possible combinations of traffic signs in one cross section from the point of their optical performance. The results of the white, red and blue traffic sheeting measurements are presented clearly in the Table 1. The most efficient out of the RA1 class ballotine traffic sheetings is the OR 5710, where the retroreflection value measured after 20 weeks, was exceeding 99.2 $cd \cdot lx^{-1} \cdot m^{-2}$. The lowest value after 20 weeks of measurement was detected for the AD 1500 traffic sheeting, 75 $cd \cdot lx^{-1} \cdot m^{-2}$.

The minimum value according to ČSN 12 899-1 for RA1 class is 50 $cd \cdot lx^{-1} \cdot m^{-2}$. None of the RA1 ballotine traffic sheetings tested has significantly differed in their optical performance according to previous measurements. The 3M EGP class RA1 type microprismatic traffic sheeting has a retroreflection value of about 125.5 $cd \cdot lx^{-1} \cdot m^{-2}$, which is the lowest value achieved among all examined microprismatic traffic sheetings. However, more significant optical differences are already apparent for traffic sheetings formally classified as RA2 class. Two of them, the 3M 3930 and OR 5910 traffic sheetings, have values of about 600 $cd \cdot lx^{-1} \cdot m^{-2}$, while the third tested sample, the AD 6500, achieves values of only about 400 $cd \cdot lx^{-1} \cdot m^{-2}$. Even more significant differences are seen in traffic sheetings formally classified as class RA3, as the AD 7500 and OR 6910 samples have values 418-427 $cd \cdot lx^{-1} \cdot m^{-2}$ and the third one, the 3M 4090 belonging to the same formal class achieved a value of around 764 $cd \cdot lx^{-1} \cdot m^{-2}$.

Tab. 1 Samples of white, red and blue traffic sheetings

| Colour | White | | | | Red | | | | Blue | | | |
| R_A | $cd \cdot lx^{1} \cdot m^{-2}$ | | | | $cd \cdot lx^{1} \cdot m^{-2}$ | | | | $cd \cdot lx^{1} \cdot m^{-2}$ | | | |
Sample	A	B	C	KR	A	B	C	KR	A	B	C	KR
3M 3200 (GB)	85.1	82	50	1	16.9	16.2	10	1	1.1	0,6	2	-
AD 1500 (GB)	79	75	50	0.91	15.5	15.2	10	0.93	5.9	5.4	2	1
OR 5710 (GB)	105.9	99.2	50	1.2	18.7	17.7	10	0.95	7.5	6.2	2	1.14
3M EGP (M)	127	125.5	50	1.53	22.8	22.6	10	1.39	9.1	8.8	2	6.5
3M 3930 (M)	665	654	180	7.97	125.4	120.9	25	7.46	42.5	41	14	7.59
AD 6500 (M)	405	401	180	4.87	75.5	76.5	25	4.72	36.8	31.5	14	8.83
OR 5910 (M)	591.5	589.2	180	7.18	127	125	25	7.71	63.9	63.1	14	11.68
3M 4090 (M)	768.1	764	300	9.3	129	128	60	7.9	51.8	49.5	19	9.16
AD 7500 (M)	419.9	418	300	5.09	66	59.3	60	3.66	29.5	28.9	19	5.62
OR 6910 (M)	431	427	300	5.2	102	101	60	6.23	43	42.5	19	7.87

The obtained results of carried out measurements confirm significant differences in optical performance, especially among the traffic sheetings that are classified as RA2 and RA3 *(Unhola, 2016)*, *(Obeidat et al., 2016)*, *(Kai Sørensen, 2011)*. Thus, the current required values of the European standard EN12899-1 are insufficient and an adjustment should be made to create more formal classes as in the USA, that will have similar optical performance and design *(Carlson, et al., 2017)*. Before the new standard becomes effective, it is therefore always desirable to identify the approximate values of the traffic sheetings with respect to their age before the application of the content of the sign. Most of the samples provided were screened using the ink. Several samples were produced by digital printing, respectively without modification by the manufacturer. Therefore, it would be desirable in further research to compare, on a larger number of samples, the extent to which the optical production process can be influenced by the traffic sheeting production process, since the production process also might have a significant effect on the possible combination of individual traffic sheeting types.

CONCLUSIONS

The combination of different retroreflective materials from the perspective of their optical performance on one temporary traffic sign is only possible when determining the retroreflection coefficient, which serves to simplify the determination of the appropriate combination of materials. The measurements indicate that in the area of temporary traffic signs, in terms of optical performance, no traffic sheeting should be used in one cross-section when the values of the difference of retroreflection constants are higher than 2.

The results of measurements taken of white traffic sheetings show that at the basic measured viewing angle $\alpha = 0.33°$ and the illumination angle $\beta = 5°$ for the RA1 class a combination of all ballotine traffic sheetings is possible, since their maximum optical performance ranges from 79-105 $cd \cdot lx^{1} \cdot m^{-2}$. The RA2 microprismatic traffic sheetings tested had an optical performance of 405 to 665 $cd \cdot lx^{1} \cdot m^{-2}$, thus a combination of 3M 3930 and OR 5910 traffic sheetings is possible. From the perspective of the RA3 traffic sheetings the optically most powerful traffic sheeting is the 3M 4090 type with a value of about 764 $cd \cdot lx^{1} \cdot m^{-2}$, that makes it impossible to combine with any other samples tested in the same class. The experiment will continue for next years and it might be assumed that with a longer period of external influences, the differences in retroreflection of different types of traffic sheetings will become more evident.

REFERENCES

1. Ai, C., & Tsai, Y. J. (2016). An automated sign retroreflectivity condition evaluation methodology using mobile LIDAR and computer vision. *Transportation Research Part C: Emerging Technologies*, *63*. doi: https://doi.org/10.1016/j.trc.2015.12.002

2. Baratian-Ghorghi, F., Zhou, H., Jalayer, M., & Pour-Rouholamin, M. (2015). Prediction of Potential Wrong-Way Entries at Exit Ramps of Signalized Partial Cloverleaf Interchanges. *Traffic Injury Prevention*, *16*(6), 599 604. doi: https://doi.org/10.1080/15389588.2014.98 1651

3. Boggs, W., Heaslip, K., & Louisell, C. (2013). Analysis of sign damage and failure. *Transportation Research Record*, *5*(2337), 83-89. doi: https://doi.org/10.3141/2337-11

4. Carlson, P., Brimley, B., Chrysler, S. ., Gibbons, R., & Terry, T. (2017). Recommended guidelines for nighttime overhead sign visibility (2017). *Transportation Research Record*, *2617*, 27–34. doi: https://doi.org/10.3141/2617-04

5. ČSN EN 12899 1. (2003). *Český Normalizační Institut*.

6. FHWA. (2008). *Traffic sign retroreflectivity* (p. 118). US Department of transportation.

7. International commission on illumination CIE. (1988). *CIE 1988*. Vienna: Central Bureau of the CIE.

8. Kai Sørensen. (2011). *Durability test of retro-reflecting materials for road signs at Nordic test sites - Ageing model for the retro-reflectivity after further exposure*. (April), 1-13.

9. Khalilikhah, M., Fu, G., Heaslip, K., & Carlson, P. (2018). Analysis of in-service traffic sign visual condition: Tree-based model for mobile LiDAR and digital photolog data. *Journal of Transportation Engineering Part A: Systems*, *144*(6). doi: https://doi.org/10.1061/JTEPBS.0000132

10. Khalilikhah, M., & Heaslip, K. (2016). The effects of damage on sign visibility: An assist in traffic sign replacement. *Journal of Traffic and Transportation Engineering (English Edition)*, *3*(6), 571.581. doi: https://doi.org/10.1016/j.jtte.2016.03.009

11. Khalilikhah, M., & Heaslip, K. (2017). Improvement of the performance of animal crossing warning signs. *Journal of Safety Research*, *62*, 1-12. doi: https://doi.org/10.1016/j.jsr.2017.04.003

12. Koyuncu, M., & Amado, S. (2008). Effects of stimulus type, duration and location on priming of road signs: Implications for

driving. *Transportation Research Part F: Traffic Psychology and Behaviour*, *11*(2), 108-125. doi: https://doi.org/10.1016/j.trf.2007.08.005

13. Ministerstvo dopravy ČR. (2015). *TP 66* (p. 160). p. 160.
Retrieved from http://www.pjpk.cz/data/USR_001_2_8_TP/TP_66.pdf

14. NSC. (2018). National Safety Council. Retrieved from https://www.nsc.org/driveithome/teen-driver-risks/night-driving

15. Obeidat, M. S., Rys, M. J., Rys, A., & Du, J. (2016). Evaluation of overhead guide sign sheeting materials to increase visibility and safety for drivers. *Applied Ergonomics*, *56*, 136-143. doi: https://doi.org/10.1016/j.apergo.2016.03.016

16. Unhola, T. (2016). *Durability of retro-reflecting materials for road signs* (p. 27). Helsinki: Finnish Transport Agency.

17. ÚZIS. (2016). EHIS 2014. Retrieved from https://www.uzis.cz/node/7495

18. Vácha, J. (2010). *Ageing of European population Ageing of European population* (in Czech). Masarykova univerzita v Brně. Retrieved from file:///C:/Users/lukas1/Desktop/Starnuti_evropske_populace.pdf

Corresponding author:
Ing. Lukáš Jan Hrabánek, Department of vehicles and ground transport, Faculty of Engineering, Czech University of Life Sciences Prague, Kamýcká 129, Praha 6, Prague, 16521, Czech Republic, e-mail: hrabanek@tf.czu.cz

LABORATORY RESEARCH OF TRANSMISSION – HYDRAULIC FLUID

Ľubomír HUJO[1], Štefan ČORŇÁK[2], Zdenko TKÁČ[1], Michaela JÁNOŠOVÁ[3]

[1]*Department of Transport and Handling, Faculty of Engineering, SUA in Nitra, Slovakia*
[2]*Department of Combat and Special Vehicles, Faculty of Military Technology, University of Defence in Brno, Czech Republic*
[3]*Nemak Slovakia s. r. o., Žiar and Hronom, Slovakia*

Abstract
The article is focused on the laboratory research of the qualitative properties of transmission – hydraulic fluid type MOL Farm NH Ultra and its impact on the technical and operational characteristics of the hydraulic pump type QHD 17. Laboratory testing device allowed to simulate the variable testing conditions of the real conditions under which the hydraulic system of agricultural wheel tractor operates. The flow properties of the hydraulic pump with tested hydraulic fluid at precisely defined intervals were monitored during testing. Based on the measured data, the flow properties of the MOL Farm NH Ultra were evaluated by mathematical – statistical analysis.

Key words: *hydraulic pump; hydraulic system; hydraulic pump flow.*

INTRODUCTION

There are high requirements of hydraulic fluids that serve as energy carriers in hydraulic systems. Their producers must consider their demands for quality improvement and simultaneously reducing the burdening of environment (*Rusnák et al., 2009; Vitázek et al., 2018*). The quality of the transmission – hydraulic fluid is an important indicator of the proper operation of the hydraulic system and it has a major influence on the individual components operation of the hydraulic circuit (*Janoško et al., 2016; Kučera et al., 2016*). Reported by *Hujo (2016, 2017),* accelerated fluid testing is used to optimize the testing time, simulating the operational loading under laboratory conditions. After the testing completion, the physical – chemical properties analysis is done. Impact of the tested fluid on the technical characteristics of the hydraulic pump focusing on the changes of the flow characteristics is also monitored. The basic precondition for proper operation and efficient care about hydraulic fluids is the suitably chosen method of the fluid testing with monitoring of the contamination level of the fluid (*Helebrant, 2001; Janoško et al., 2014*). The aim of study was the research of qualitative properties of transmission-hydraulic fluid and its impact on technical state of hydraulic tractor pump. The fluid properties were monitored by the bulk density, kinematic viscosity and pour point. The technical state of hydraulic pump was evaluated by the flow and decrease of flow efficiency.

MATERIALS AND METHODS

Laboratory testing of transmission – hydraulic fluid was realized based on the method below:
- provision of the physical – chemical analysis of the reference fluid sample,
- verification testing of the hydraulic circuit with operating pressures simulation by electro – hydraulic proportional valve,
- the first measurement was realized after 125 Eh and the values of the flow, pressure and temperature sensors were recorded at hydraulic pump speed 500, 750, 1000, 1250, 1500, 1750, 2000, 2250, 2500 and 2750 min $^{-1}$,
- after recording the data mentioned above, before the next measurement, it is necessary to take the sample of the tested hydraulic fluid, further sampling of the fluid will be carried out after 250, 375 and 500 Eh,
- next, the samples of the fluid had been physically and chemically analysed.

To simulate the operational loading of the gear pump used in the tractor's hydraulic system by applying the tested hydraulic fluid, the laboratory testing device was designed. The device allows to realize laboratory testing based on the signals monitored during testing (*Hujo et al., 2015; Majdan et al., 2013*). Signal progress whereby simulated real operational conditions during testing is presented in Fig. 1.

The signal is provided by electro – hydraulic proportional valve connected to hydraulic circuit (*Tkáč et al., 2014 and 2014; Kosiba et al., 2013*).

The methodical sampling procedure of tested hydraulic fluid was regulated by the standard STN 65 6207 (Hydraulic oils and fluids. Sampling to determine the content of mechanical impurities). In order to access the suitability of hydraulic fluid testing in hydraulic circuit of agricultural, forestry, and handling machinery, it is necessary to know the input parameters of the system in which the hydraulic fluid will be tested. It means to know the technical parameters of the hydraulic pump that is connected to the hydraulic circuit during testing. The technical parameters of the hydraulic pump are shown in Tab. 1.
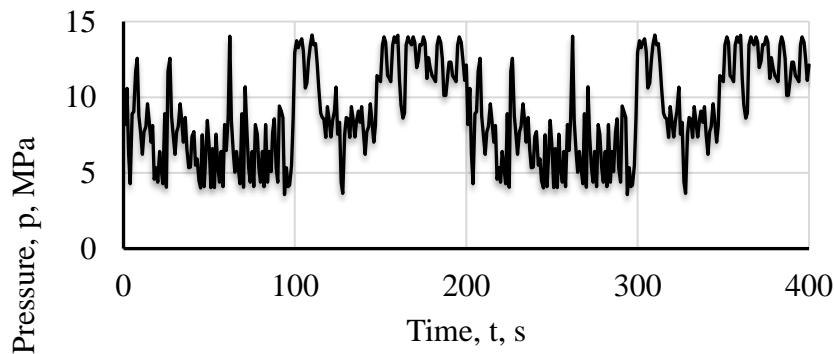
Fig. 1 Pressure signal progress to simulate the operational loading

As tested fluid, it was used the transmission – hydraulic oil type MOL Farm NH Ultra. Its characteristics featured by producers are shown in Tab. 2. This tractor's oil was specially developed for the Case New Holland Group machinery producers. Versatile, long – life oil is aimed on power – shift gearboxes, differentials, wet brakes and high-performance agricultural machinery hydraulic systems.

Tab. 1 Parameters of the hydraulic pump type QHD 17

Parameters		Marking	Unit	Value
Real geometric volume		V_g	dm^3	$17.24.10^{-3}$
Speed	rated	n_n	min^{-1}	1500
	minimal	n_{min}	min^{-1}	350
	maximal	n_{max}	min^{-1}	3200
Input pressure	minimal	p_{1min}	MPa	-0.03
	maximal	p_{1max}	MPa	0.05
Output pressure	max. state	p_{2n}	MPa	29
	maximal	p_{2max}	MPa	31
	peaked	p_3	MPa	32
Rated output flow (min.) at n_n and p_{2n}		Q_n	$dm^3.min^{-1}$	23.2
Maximal flow at n_{max} and p_{2max}		Q_{max}	$dm^3.min^{-1}$	54.3
Input power – rated (max.) at n_n and p_{2n}		P_n	kW	14.8
Maximal rated power at n_{max} and p_{2max}		P_{max}	kW	33.6
Mass		m	kg	10.9

Tab. 2 Characteristics of the transmission – hydraulic fluid type MOL Farm NH Ultra

Characteristics	Unit	Values
Bulk density at 15 ⁰C	$kg.m^{-3}$	875
Kinematic viscosity at 40 ⁰C	$mm^2.s^{-1}$	64.2
Kinematic viscosity at 100 ⁰C	$mm^2.s^{-1}$	10.9
Viscosity index	-	162
Freezing point	⁰C	-36
Flash point in open crucible	⁰C	210

RESULTS AND DISCUSSION

Presented in Fig. 2, the course of **bulk density** changes at 40 ⁰C of tested fluid depending on the hours of operation is shown. The tested oil sample shows the highest bulk density at 0 Eh, as it can be seen from the graphical course. Subsequently, after the others sampling at precisely defined intervals, a negligible decrease of the bulk density was recorded. It might be caused by filtration of the impurities. The measured value of the bulk density of the tested transmission – hydraulic fluid before the testing was 860.70 $kg.m^{-3}$. The measured value is defined by linear function with coefficient of determination R = 0.7449. Based on this value, it could be concluded that linear function is not appropriately chosen, but the use of the fourth-degree polynomial function would be physically inaccurate due to insufficient data. Although, the polynomial would go through the all points with determination coefficient $R^2 = 1$ but in this case, the linear function has higher equity of redemption.
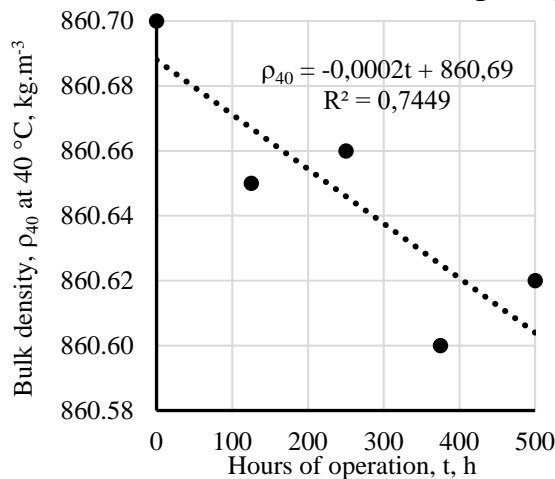
Fig. 2 Course of bulk density at 40 °C depending on the hours of operation
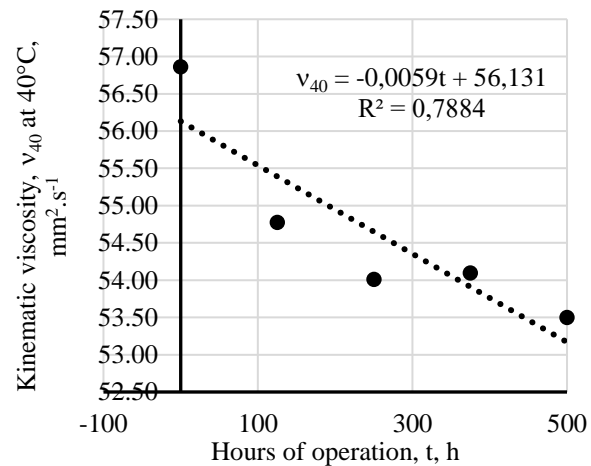
Fig. 3 Course of kinematic viscosity at 40 °C depending on the hours of operation

Kinematic viscosity is one of the basic parameters used to assess the quality of hydraulic oil. Viscosity may increase or decrease during its utilization in hydraulic circuit. Reported by *Helebrant et al. (2001)* the increase of viscosity may be cause by oxidative products or impurities in the oil. The decrease of viscosity is caused by mechanical and thermal degradation of additional additives. Kinematic viscosity values at 40 °C and 100 °C are shown in Fig. 3 and Fig. 4. The values are defined by linear function. The linear function of kinematic viscosity at 40°C can be calculated by equation (1)

$$\nu_{40} = -0{,}0059t + 56{,}131 \qquad mm^2.s^{-1} \tag{1}$$

where *t* is time in engine hours (Eh). Determination coefficient of the kinematic viscosity $R^2 = 0.7884$ at 40 ° C, so it can be state that the type of function is suitably selected. Through the linear function for kinematic viscosity given by equation (1) it is possible to calculate the values for any number of operational hours with hydraulic oil MOL Farm NH Ultra with accuracy of 78.84%. *Asaff et al., (2014)* compared the properties based on DIN 51562-1:1999. At the kinematic viscosity, the authors noted similar changes from 2 to 10%, they recorded similar conclusion that the kinematic viscosity did not achieve a higher change from the initial state by more than 20%.
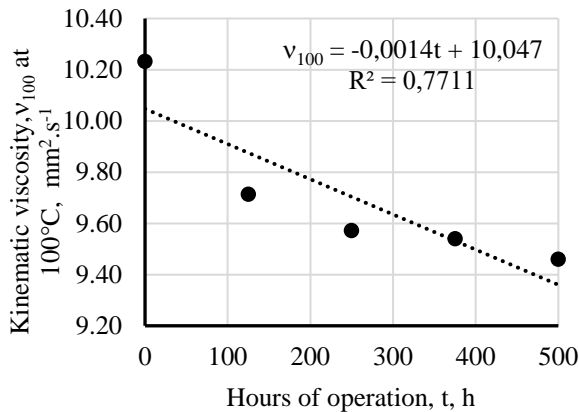
Fig. 4 Course of kinematic viscosity at 100 °C depending on the hours of operation
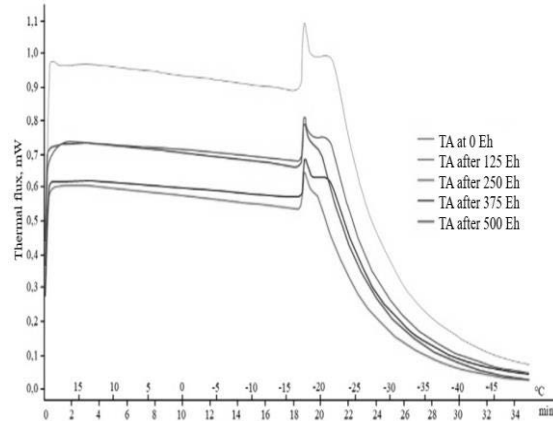
Fig. 5 Thermal analysis (TA) of the hydraulic ´ fluid sample MOL Farm NH Ultra

Testing of the hydraulic fluid sample MOL Farm NH Ultra was also focused on monitoring of the **pour point**. An exothermic peak was recorded at -17.42 °C in the freezing process of the reference sample after 0 Eh. This point is defined as freezing point and the temperature is almost the same as a melting point whereby this temperature depends on the purity of the sample. Since the oil is an amorphous mass, the pour point is performed not only at one point but at the temperature range from -16.99 °C to -18.94 °C. An exothermic peak was recorded at -17.51 °C in the freezing process of the reference sample after 125 Eh. In this case, the recorded temperature range was noted from - 17.02 °C to – 25.29 °C. An exothermic peak was recorded at -17.50 °C in the freezing process of the reference sample after 250 Eh. In this case, the recorded temperature range was noted from - 17.01 °C to – 19.63 °C.
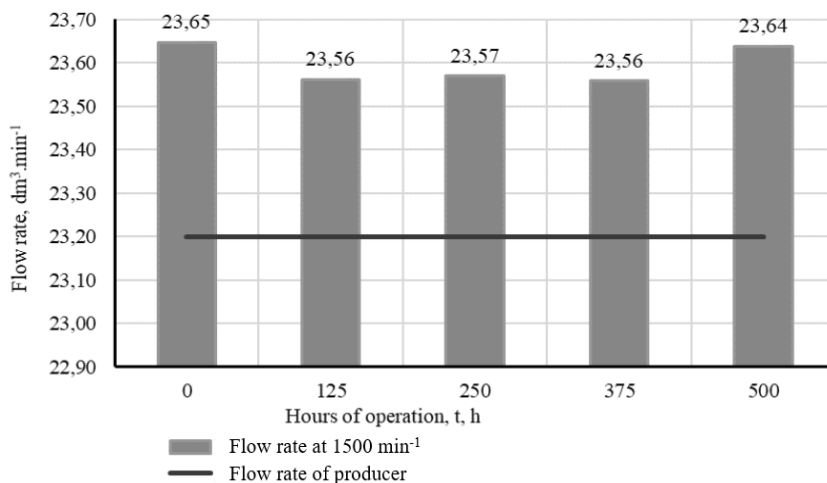
Fig. 6 Flow rate for nominal hydraulic pump speed 1500 min^{-1}

An exothermic peak was recorded at -17.48 °C in the freezing process of the reference sample after 375 Eh. In this case, the recorded temperature range was noted from - 17.05 °C to – 19.45 °C. An exothermic peak was recorded at -17.53 °C in the freezing process of the reference sample after 500 Eh. Autors *Kosiba et al., (2017)*, reached similar course of pour point in their research of degradation process of hydraulic fluids. In this case, the recorded temperature range was noted from - 17.07 °C to – 19.45 °C. Thermal analysis of tested fluid is shown in Fig. 5. The producer of the fluid Mol Farm NH Ultra presents as freezing point the value - 36 °C (*MOL Farm NH Ultra, 2016*). Repeated measurements demonstrated the change of tested fluid properties by an average value of exothermic peak -17.49 °C. The hydraulic pump **flow** was measured according to the methodological procedure and the values were used to determine the average flow rates depending on the operational hours for speed from 500 min^{-1} to 2750 min^{-1}. For nominal hydraulic pump speed 1500 min^{-1}, the processing of measured data is shown in Fig. 6. Stated speed is indicated by producer as rated parameters of the hydraulic pump. From the dependence

mentioned above, it can be state that the physical – chemical characteristics of the tested hydraulic fluid MOL Farm NH Ultra does not affect flow characteristics of QHD 17 hydraulic pump neither elements of transmission – hydraulic system. The value of the average flow rate depending on operational hours is about 1.7% higher. The same conclusions of hydraulic fluids research under laboratory conditions were reached by authors *Halenár et al., (2018), Tkáč et al., (2017), Tulík, et al., (2013) and Kosiba et al., (2013)*. The maximal decrease of the **flow efficiency** was 0.34% after 375 Eh but after 500 Eh, the decrease of the flow efficiency was 0.03% compared to the reference value at 0 Eh. The graphical dependency of the flow efficiency at 1500 min^{-1} is shown in Fig. 7. In accordance with ISO 15380: 2011, it is possible to confirm that the tested fluid does not affect the flow characteristics of QHD 17 hydraulic pump because the flow efficiency decrease did not exceed the value of 20%. Presented in Fig. 8, the course of flow efficiency decrease depending on the hours of operation is shown. Flow efficiency course correspond to the measurement results of *Yoshida and Inaguma (2014)* where the authors concluded that a given flow efficiency is due to the fluid remaining in the gaps while increasing the centrifugal force acting on the liquid as the speed increases.
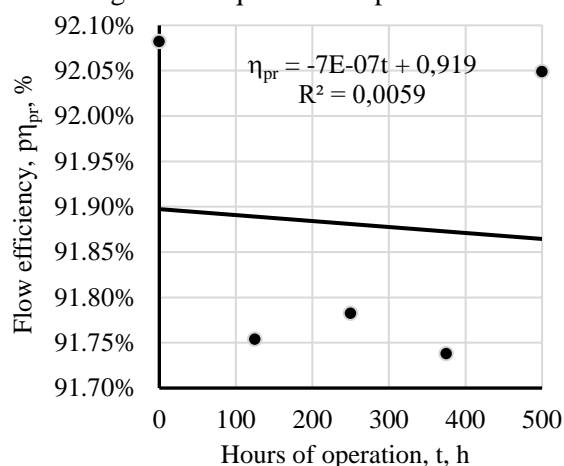
Fig. 7 Flow efficiency for nominal hydraulic pump speed 1500 min^{-1}
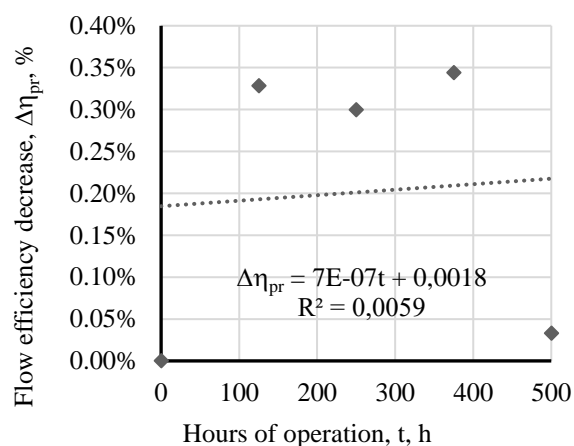
Fig. 8 Flow efficiency decrease for nominal hydraulic pump speed 1500 min^{-1}

CONCLUSIONS

Laboratory testing was focused on qualitative assessment of the transmission - hydraulic fluid MOL Farm NH Ultra, intended for utilization in transmission – hydraulic system of mobile energetic machinery and examine for its impact on QHD 17 hydraulic pump technical and operational characteristics. The laboratory testing device allowed to simulate variable testing condition to simulate the real agricultural wheel tractor operational condition. The flow properties of the hydraulic pump with tested hydraulic fluid at precisely defined intervals were monitored during testing. Based on the measured data, the flow properties were evaluated by mathematical – statistical analysis. Tested transmission – hydraulic fluid MOL Farm NH Ultra was evaluated based on its physical properties from the samples taken at defined intervals. Monitored physical properties of tested hydraulic fluid as bulk density and kinematic viscosity were within the appropriate tolerances after testing. The values of freezing point did not correspond to the data of the hydraulic fluid producer. Based on the results of the MOL Farm NH Ultra transmission – hydraulic fluid testing and its influence on the hydraulic system, it can be stated that hydraulic fluid is able to operate in tractor's hydraulic fluid system without any negative impact on hydraulic pump flow characteristics.

ACKNOWLEDGMENT

REFERENCES

1. Asaff, Y., Negrill, V., Theissen, H., & Murrenhoff, H. (2014), Analysis of the influence of contaminats on the biodegradability characteristics and ageing of biodegradable hydraulic fluids. *Journal of Mechanical Engineering, 60*(6), 417–424. ISSN 0039-2480

2. Halenár, M., Nosian, J., Kuchar, P., Tulík, J., & Furstenzeller, A. (2018). Evaluation of hydraulic fluid during of the operating test. In *Acta Facultatis Technicae, 23*(2), 73-80.. ISSN 1336-4472,

3. Hujo, Ľ., Jablonický, J., & Tkáč, Z., (2017) *Návrh inovatívneho laboratórneho simulačného zariadenia na skúšanie hydrostatických prevodníkov a hydraulických kvapalín*. Nitra: SPU. ISBN 978-80-552-1645-4.

4. Hujo, Ľ., Kangalov, Plamen G., & Kosiba, J. (2015). *Laboratory test devices for evaluating the lifetime of tractor hydraulic components: (proceedings, methods and applications)*. 1st ed. Ruse: University "Angel Kanchev" of Ruse. 69 p. ISBN 978-954-712-665-7.

5. Hujo, Ľ., Tkáč, Z., Tulík, J., Kosiba, J., Uhrinová, D., & Jánošová M. (2016). Monitoring of operation loading of three-point linkage during ploughing. *Research in agricultural engineering, 62*(1), 24-29. ISSN 1212-9151.

6. Helebrant, F., Ziegler, J., & Marasosová, D., (2001) *Technická diagnostika a spolehlivost I. Tribodiagnostika*. Ostrava: VŠB – Technická univerzita, ISBN 80-7078-883-6.

7. Janoško, I., Černecký, J., Brodnianska, Z., & Hujo, Ľ. (2016). *Environmentálne technológie a technika*. 1. ed. Nitra: Slovenská poľnohospodárska univerzita. 306 p. ISBN 978-80-552-1604-1.

8. Janoško, I., Polonec, T., & Lindák, S. (2014). Performance parameters monitoring of the hydraulic system with bio-oil. *Research in agricultural engineering, 60*(special iss.), 37-43. ISSN 1212-9151.

9. Kosiba, J. & Hujo, Ľ. (2017). *Research of hydraulic fluids degradation process under operating condition*. Nitra: SUA in Nitra, 94 p. ISBN 978-80-552-1733-8.

10. Kosiba, J., Tkáč, Z., Hujo, Ľ., Stančík, B., & Štulajter, I. (2013). The operation of agricultural tractor with universal ecological oil. *RAE, 59*(special iss.), 27-33. ISSN 1212-9151.

11. Kučera, M., Aleš, Z., & Pexa, M. (2016). Detection and characterization of wear particles of universal tractor oil using of particles size analyser. *Agronomy Research 14*(4), 1351-1360.

12. Majdan, R. Tkáč, Z., & Kangalov, P. G. (2013). *Research of ecological oil-based fluids properties and new test methods for lubrication oils: scientific monograph*. 1st ed. Rousse: Angel Kanchev University of Rousse, 98 p.

13. Rusnák, J., Kadnár, M., & Kučera, M. (2009) *Biologicky odbúrateľné oleje z pohľadu ich tribologických vlastností*. Nitra: SPU. ISBN 978-80-552-0166-5.

14. Tkáč, Z., Čorňák, Š., Cviklovič,V., Kosiba, J., Glos, J., Jablonický, J., & Bernát, R. (2017). Research of biodegradable fluid impacts on operation of tractor hydraulic system. *Acta technologica agriculturae, 20*(2), 42-45. ISSN 1335-2555.

15. Tkáč, Z., Kangalov, Plamen G., & Kosiba, J. (2014). *Getting ecological of hydraulic circuits of agricultural tractors*. 1st. ed. Ruse: University of Rousse "Angel Kanchev". 120 p. ISBN 978-619-7071-63-4.

16. Tkáč, Z., Majdan, R., & Kosiba, J. (2014). *Výskum vlastností ekologických kvapalín a nových testovacích metód mazacích olejov*. Nitra: Slovenská poľnohospodárska univerzita v Nitre, 94 p. - ISBN 978-80-552-1140-4.

17. Tulík, J., Hujo, Ľ., Stančík, B., & Ševčík, P. (2013). *Journal of Central European Agriculture, 14*(4), 1384-1393. ISSN 1332-9049.

18. Vitázek, I., Tulík, J., & Klúčik, J. (2018). Combustible in selected biofuels. *Agronomy Research, 16*(2), 593-603. ISSN 1406-894X.

19. Yoshida, N. & Inaguma, Y. (2014). Mathematical Analysis of Efficiencies in Hydraulic Pumps for Automatic Transmissions. In *JTEKT Engineering Journal*. no. 1011E.

Corresponding author:
doc. Ing. Ľubomír Hujo, PhD., Department of Transport and Handling, Faculty of Engineering, Slovak University of Agriculture in Nitra, Tr. A. Hlinku 2, Nitra, 949 01, Slovak Republic, phone: +421 37 641 4530, e-mail: lubomir.hujo@uniag.sk

THE TIDAL COMPONENT OF NATURAL RADIATION BACKGROUND

Bohumil CHALUPA[1], Josef ZEMAN[1]

[1]Department of Physics, Faculty of Engineering, Czech University of Life Sciences Prague

Abstract
The paper contains temporal analysis of radiation fluctuations on the Kokonín farm. Our main goal was to ascertain whether tidal forces affect the magnitude of the fluctuations in this location. From a nine-month measurement, carried out by minutes, components were obtained with periods corresponding to the tidal frequencies. The value of sum of the amplitudes was correlated with phases of the Moon, as the main tidal agent. This way one can extrapolate that the amplitude of the tidal component constitutes about 15 % of local natural radiation background.

Key words: Fourier transform; solar and lunar periods; radon.

INTRODUCTION

Gravitational attraction of the sun and the moon are responsible for the tidal motions on the globe, in all three media, the atmosphere, the oceans and the solid Earth. We will not go into great detail regarding this topic and the interested readers are referred to excellent books on the topic (for example Chapter 13 of *Pond & Pickard, 1989;* Chapter 11 of *Dietrich et al., 1980*). However, we will give enough information here so that the reader can appreciate the nature of tidal processes around the globe.

The rhythmic rise and fall of sea level along the world's coastlines are the most apparent manifestation of tides in the global oceans. In some coastal locations, tides are noticeable but not spectacular, but in other places like the West coast of Korea and the Bay of Fundy, the tides are spectacularly large. In some places, the sea level rises and falls with a period of about half a day (these are called semi-diurnal tides), whereas in other places the period is more like a day (called diurnal tides). Yet again, in some locations the tides are mixed. And there are periods during the year, when the sun and moon line up with the Earth when the tides are unusually large.

Natural radiation can be divided into two main components, one coming from above and the other coming from below. While tide of the atmosphere is arguable and can virtually never be identified from experimental data, and while the periodicity of cosmic radiation can be successfully ruled out, indications exist that looking for tidal periods in the ground component of the radiation background could be successful. Such an indication is first of all the presence of tidal components in small water courses and wells. E.g. the flow of Starosuchdolský stream with mean flow rate of abt. 1.75 l/s is modulated by 30 % by the tidal component in the rain-less period. Similarly, the KV4 water-well has the tidal amplitude of 125 mm. These facts may justify sufficiently the idea that different fluids may be squeezed out from the underlying layers with varying gravitational force. When the gravitational force changes periodically, one can also observe, with a certain delay dependent on local structure, radiation oscillations with the same periods, caused e.g. by the outburst of radon.

Tidal periods can be divided mostly to the ones caused by the effect of the Moon and the ones caused by the effect of the Sun. Following Table 1 shows the tidal periods we were using for the analysis in this work.

Table 1 gives the period and relative size of each of these constituents. While in some isolated situations, where other constituents become important, it is seldom essential to include many more to obtain accurate tidal predictions. In shallow water, the so-called compound tides generated by non-linear interaction of primary constituents become important. For example, M4, generated by non-linear self-interaction of the M2 constituent has half the period of M2.

The aim of study was ascertaining of periodic tidal component in natural radiation background in Western Sudetes region.

Tab. 1 Primary Tidal Components

Tidal Component	Period solar hours	Description	Nature
M1	12.42	Principal lunar	semi-diurnal
S2	12.00	Principal solar	semi-diurnal
N2	12.66	Larger lunar elliptic	semi-diurnal
K2	11.97	Luni-solar	semi-diurnal
K1	23.93	Luni-solar diurnal	diurnal
O1	25.82	Principal lunar diurnal	diurnal
P1	24.07	Principal solar diurnal	diurnal
Q1	26.87	Larger lunar elliptic	diurnal
MF	327.90	Lunar fortnightly	Long term
MM	661.30	Lunar monthly	Long term
SSA	4383.00	solar semi annual	Long term
M4	6.21		Compound
MS4	6.10		Compound

MATERIALS AND METHODS

Data from Marek Drápal from his station by the farm in Kokonín (50°42'00.5"N 15°10'24.1"E), three meters above ground surface, were used for the analysis. The data were collected in the period 21. 8. 2018-22. 1. 2019. Pulses from a SBM-20 GM tube were stored each minute, time synchronized through NTP. The data were scanned with three-day rectangular window (of 4320 samples) with Fourier transformation for periods MS4, M4, K2, S2, M2, N2, K1, P1, O1, Q1 from Table 1. The intervals were shortened to the nearest integral multiple of the sought period. The periods found have been visualised with the gnuplot program ver. 5.2 patchlevel 2.

RESULTS AND DISCUSSION

Data for the given period are displayed in Figure 1.

The sum of periodical components is represented in Figure 2.

The data presented show that tides influence is at most up to 10 % of measured signal of radiation fluctuations in the given location, but they can be successfully detected in it. Step signal changes may easily complicate their identification though. To a certain extent, an interpretation problem is constituted by the advancing of the maxima of tidal periods from the full moon. This is to some extent caused by the data processing method. By cropping the three-day interval to the multiple of the sought period, we albeit avoided unpleasant artefacts of non-integer periods on one hand, however on the other hand we moved the sought signal by sometimes the whole period to anterior time, and generally blurred the signal during the summing. Thus we more asked to what extent the period was present in the given three-day period, without demanding to specify the exact moment when it occurred.

Groves-Kirkby et al. (2004) in their domestic radon measurement study in Northampton, England found that the tide vs. radon concentration correlation and lag depends (among others) on the location and on meteorological conditions. And radon, in fact, accounts for a substantial component of the radiation background researched by us. Later the same group *Crockett et al.* (2006) tried to cross-correlate the radon time-series against the modelled variation in tidal force. They found the lag to be about 3-4 days, the correlation coefficient being cyclic with the 14–15-day tidal cycle, reaching about ±0.15.
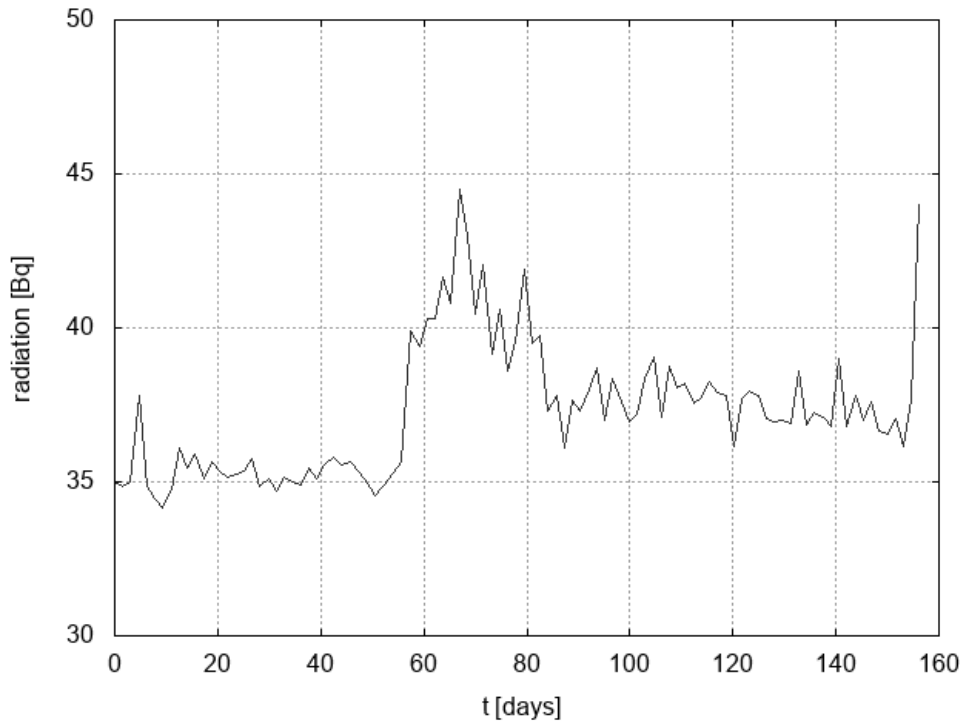
Fig. 1 Recorded period from 2018/08/21 to 2019/01/22. Starting with day 56, i.e. October 16ᵗʰ 2018, one can see increasing radiation level in atmospheric undulation that declines exponentially from November, in total this presumably Belorussian escapade increases the radiation background by 10 % almost permanently.
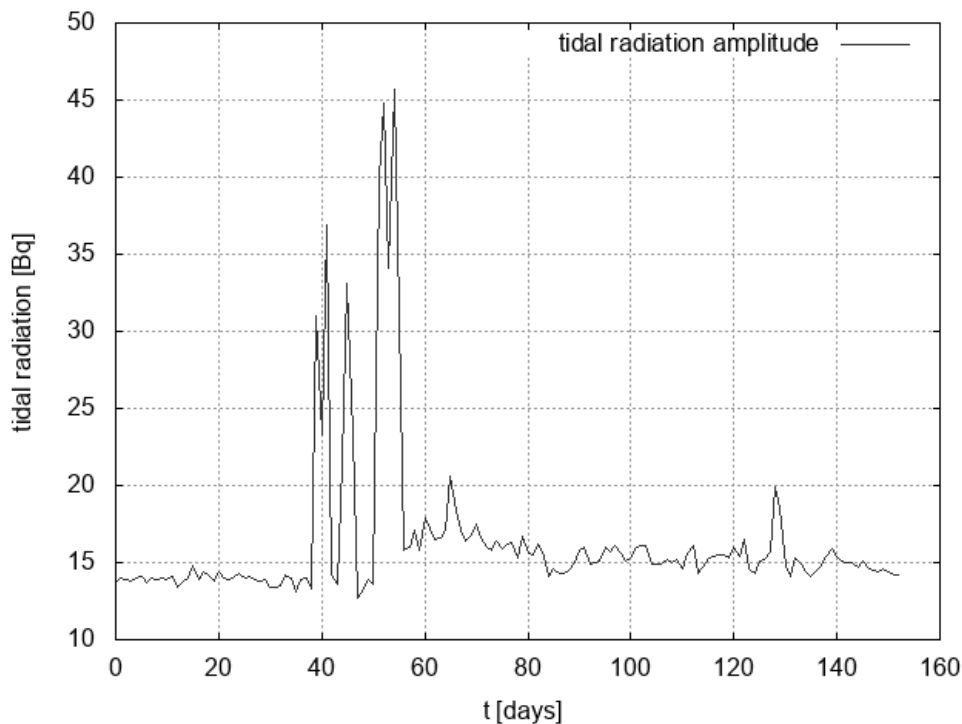
Fig. 2 The data are shifted slightly (by four points against Figure 1); this is caused by the window width. The period displayed is thus 2018/08/24–2019/01/21. Pronounced step increase can be seen in the period of rapid radiation changes in days 39–55 of the record that is more likely an artefact, and further peaks in days 64 (October 25ᵗʰ) and 128 (December 27) in the period of perigee moons of October 24ᵗʰ and December 22ⁿᵈ

CONCLUSIONS

Periodical components have been identified in the radiation background data in Kokonín that one can interpret partially as tidal ones. For verification of this analysis, a longer time series analysis is necessary, and a correlation of computed retarded gravitation with measured radiation background intensity. I seems though that even this analysis carried out by us strengthens the indication (ZD) on the influence of tides on the movement of subsurface fluids.

ACKNOWLEDGMENT

REFERENCES

1. Crockett R. G. M., Gillmore G. K., Phillips P. S., Denman A. R. & Groves-Kirkby C. J. (2006). Tidal synchronicity of built-environment radon levels in the UK. *Geophys. Res. Lett. 33*(5).

2. Dietrich, G., Kalle, K., Krauss, W. & Siedler, G. (1980). *General Oceanography. An Introduction* 2nd Ed., pp. 626.

3. Dvořáková, Š. & Zeman, J. (2016). Tidal effects on small catchments. In *Proceeding of 6th International Conference on Trends in Agricultural Engineering* (pp. 150-154). Czech University of Life Sciences Prague.

4. Fletcher, C.A.J. (1987). *Computational Techniques for Fluid Dynamics, vol. 1 and 2*. Springer-Verlag.

5. Groves-Kirkby C. J., Denman A. R., Crockett R. G. M. & Phillips P. S. (2004). Periodicity in Domestic Radon Time Series – Evidence for Earth Tides. In *Proceedings of 11th International Congress of the International Radiation Protection Association,* Madrid.

6. Kantha, L. & Piacsek, S. *Ocean Models.* Retrieved from https://www.phy.ornl.gov/csep/om/node25.html, (kantha@csep1.phy.ornl.gov).

7. Pond, S. & Pickard, G. L. (1989). *Introductory Dynamical Oceanography,* Second Edition, Pergamon Press, pp. 329.

Corresponding author:
Mgr. Bohumil Chalupa, , Department of Physics, Faculty of Engineering, Czech University of Life Sciences Prague, Kamýcká 129, Praha 6, Prague, 16521, Czech Republic, phone: +420 22438 3291, e-mail: chalupab@tf.czu.cz

THE IMPACT OF USED DIFFERENT COLORED RAW MATERIALS ON COLOUR OF PRODUCED BEER

Ladislav CHLÁDEK[1], Pavel KIC[1], Petr VACULÍK[1], Pavel BRANÝ[1]

[1]*Department of Technological Equipment of Buildings, Faculty of Engineering, Czech University of Life Sciences Prague, Kamýcká 129, 165 21 Prague, Czech Republic*

Abstract
The aim of this article is to analyse the impact of the colour of the main raw materials used for beer production on the colour of brewed beer. The colour of beer is an important user standard whereby the consumer evaluates the beverage first, before the smell and taste are applied. The process of beer brewing using two mash process was provided in the experimental brewery in the Department University of Life Sciences Prague (the beer brand "Suchdolsky Jenik"). Laboratory trials were focused on the study of influence of the colour of malt, hops and brewer's yeast. These raw materials were tested by spectrophotometric measurements according to the colours CIELAB system by the Spectrophotometer CM-600d Konica Minoltaand Spectrophotometer HACH Lange DR 500. The effect of four different types of malts and malt grist (Pilsner Malt, Munich Malt, Caramel Malt and Colouring Malt), Saazer Variety of hops on colour of produced beer was analysed.

Key words: *brewhouse; hops; malt; spectrophotometer; yeast.*

INTRODUCTION

The beer is very old cultural drink, our knowledge of beer production fades into the dim an distant past. This time is probably linked to the settling of the hunter-gatherers and the beginning of grain cultivation, around 12 000 years ago. Colour of beer is an integral and important part of its degustation. When beer is poured into a clear glass, the colour is the first thing the prospective beer drinker will notice. Colour invariably conjures up expectations, usually subliminal, of the flavour experience ahead. A bright golden beer may lead one to expect refreshment and to recall sunny days spent in beer gardens, whereas a reddish–black beer with a thick brown head may evoke expectations of malty roasted flavours and thoughts of sitting in front of a roaring fireplace. Because colour works so powerfully upon the mind, chefs, winemakers, and brewers alike will pay very close attention to achieving the right hues for their creations. It is ironic, therefore, that colour can be an unreliable indicator of flavour. This is because colour exists more in the mind than in reality; technically, colour is the mere reflection or refraction of light as it strikes an object, solid, liquid, or gaseous. Our eyes register the wavelengths of light they receive, and the brain translates these into the colours we see. In beer, colour is determined in various ways. The most significant source of beer colour is pigments in the grain. The malt used in the brewhouse is kilned; the longer the drying process and the higher the drying temperature, the darker will be the grist for the mash and the more opaque will be the beer made from it. In very simple way the measurement of beer colour will be done visually by colour comparison with standardised colour discs (*Kunze, 2010*). Samples and colour discs are adjusted in a comparator until the same colour is obtained. In the case of dark beer measurement is often necessary to dilute it by liquid with known dilution factor (K). This method can be influenced by different factors (*Basařová et al., 2010*): type of lighting, angel of observation, the thickness of the liquid layer, haze of the liquid, design of the apparatus, optic properties of coloured glass. The Lovibond "52" system for the measurement of colour in beer was invented in 1893 by Joseph W. Lovibond in Greenwich, England. It involved the visual comparison of standardized colours, in the form of coloured glass discs, with samples of beer. This was superseded in 1950 when L.R. Bishop proposed the use of a revised set of slides. Bishop's revised system was adopted as the EBC standard in 1951 and the standard slides were manufactured by Tintometer Co, UK, as they are to this day. On the Lovibond scale, a pale golden lager might have a colour of 2˚ or 3˚, a pale ale 10˚– 13˚, a brown ale or dark lager 17˚–20˚, all the way through to the near black of imperial stout at 70˚.

SRM

The Standard Reference Method (SRM) is a unit for measuring beer colour in the US. The European Brewery Convention (EBC) is a similar unit used in Europe. Finding SRM is a laboratory procedure based on measuring the light that passes through a small sample of beer. The beer to be tested is put into a 1 centimetre square cuvette made of glass. Deep blue light (430 nm) is shown through the cuvette. The entering light has a known intensity and the intensity of the exiting light can be measured. SRM is proportional to the physics quantity called Absorption = (Intensity in / Intensity out). Darker coloured beers appear dark because they absorb a larger proportion of the light passing through them. They also have a higher SRM due to higher absorption. The palest beers have an SRM around 1 or 2. Beers that appear totally black have SRM values of 40 or higher, but all beers with SRM greater than about 40 will look very similar.

$SRM = 12.7 \times D \times A\_430$, where D is a dilution coefficient equal to volume sample / volume beer, equal to one for an undiluted sample and equal to two for a sample diluted 1:1 with water. A_430 is the absorption through the cuvette at 430 nm. The multiplier 12.7 was chosen to make SRM values similar to Lovibond values. The two scales are very similar for pale coloured beers, but diverge substantially for darker coloured beers. Our visual experience is based on light at many wavelengths, but SRM data is only produced from one wavelength. Therefore, SRM cannot fully describe apparent colour, but it does a reasonable job of describing most beers with one number. Variations between red-tinted and yellow-tinted browns in the middle of the scale are a particularly noticeable weakness of the SRM method.

European Brewery Convention

European Brewery Convention (EBC) is an organisation representing European breweries. EBC is also the name for a method of measuring beer colour codified by this organization. The EBC colour value is measured in a way that is essentially the same the way SRM is measured. The two values are exact multiples of each other. $EBC = 1.97 \times SRM$. Both are based on absorption of 430 nm light through a sample of beer in cuvette 1 x 1 cm.

The number of EBC units will be calculated by $EBC = 25 \times D \times A(430)$, where D is a dilution coefficient equal to volume sample / volume beer, equal to one for an undiluted sample and equal to two for a sample diluted 1:1 with water. A_430 is the absorption through the cuvette at 430 nm. SRM differs only by using a multiplier of 12.7 instead of 25. An earlier version of the EBC scale was based on light with a wavelength of 530 nm. EBC shares the simplicity and limitations of SRM.

Normal beer colour colours are following (*Olšovská et al., 2017*): Pilsner beer 5.0-12.0 EBC, Pale full gravity beers 7.0-15.0 EBC, Dark full gravity beers 30.0-40.0 EBC, Export pale beers 7.0-15.0 EBC, Export dark beers 45.0-100.0 EBC, Märzen, pale type 9.0-15.0 EBC, Bock beer, pale type 8.0-15.0 EBC. Malt Colour Units (MCU) is an easy way for brewers to calculate the amount of colour expected in a given recipe. This is especially useful for recipes that you are making for the first time. Unfortunately, the relationship between the calculated value MCU and directly measured values of colour (visual inspection, SRM, and EBC) is not straightforward. There are many formulas that attempt to provide a conversion between MCU and SRM. The issue of beer colour in some scientific articles is also addressed. Mostly traditional brewing methods are using official European Brewery Convection (EBC) analysis, e.g. Benard, 2000; Seaton & Cantrell, 1993. The problems of beer colour is also given some attention in some scientific articles. Smedley, 1995 uses CIELAB's colour space to demonstrate how the beer colour differences can be used commercially.

MATERIALS AND METHODS

The laboratory measurements were carried out at the Faculty of Engineering CULS Prague. The process of beer production using two mash process was provided in the experimental small scale brewery in the Department of Technological Equipment of Buildings of Faculty of Engineering at the Czech University of Life Sciences Prague (the beer brand "Suchdolsky Jenik").

Some research were focused on the experimental brewery construction and beer production (*Chládek, 2007; Chládek et al., 2013*). This microbrewery (founded 2006) is equipped with brewhouse, which consists of two stainless steel (SS) vessels. One is a wort kettle with agitator blade, heated by steam (temperature 130°C, pressure 0,3 MPa), second one is lauter tun, with raking and cutting unit, equipped with SS false bottom. The volume of one brew is 10 hl (1,000 litres), two mash process was used. The

wort is clarified in whirlpool, cooled down in two section heat exchanger using tap water and glycol, aerated pitched by the yeast W96, fermented and aged in cylindroconical vessels (20 hl) cooled down by circulation of glycol, than without any filtration or pasteurisation beer is filled in glass bottles 0,5 l and kegs 30 l and 50 l and sold in University Shop. Supplier of floor Pilsner malt is Brewery Ferdinand located in town Benešov, variety of hops is Saaz, supplied by Hops Institute in the town Saaz, partly from University Hops Garden, belonging to the University Brewery. The yeast No W96 was supplied by the Laboratory propagation station of the brewery Krušovice (Member of Heineken Group). Both brewery and hops Garden were under supervision operated by students. For each brew (10 hl water) were used 200 kg of malt, 3 kg of hops and 10 litters of aerated yeast W96. For darker colour of brewed beer was per brew of any kind of beer added 4 kg of Colouring malt grist. The effect of four different types of malts and malt grist (Pilsner Malt, Bavarian malt, Caramel malt and Colouring malt), Saazer Variety of hops on colour of produced beer was analysed. Laboratory trials were focused on the study of influence of the colour of malt, hops and brewer's yeast. These ingredients were tested by spectrophotometric measurements according to the colours CIELAB system by the Spectrophotometer CM-600d Konica Minolta. The colour attributes L* value (lightness), redness (a* values) and yellowness (b* values) were measured five times of each sample, first in its original intact state and subsequently also after milling in the hammer mill. The colours attributes of hops and brewer's yeast were measured as well. The average values of all measured results were calculated. The colours of tested malt and produced beer were compared with the official European Brewery Convection (EBC) scale used for the beer evaluation and found good agreement. For the measurement using method of EBC was used spectrophotometer HACH Lange DR 5000 wavelengths range 190 – 1,100 nm.

The method of evaluation of the test sieving data

This method is described by Chládek et al. (2018). The data obtained from the sieve analysis is relatively difficult to evaluate in a reproducible way. Therefore, a graphical interpretation of the data is often used as it helps in more easily imagining the analytical form of the function (which describes the granulometric composition of the sample). From the analytical form of the function, it is possible to obtain the essential characteristics of the bulk materials. There are important characteristics such as, 'the coefficient of polydispersity' and the mean statistical size of the particle $\bar{x}$ which determines the precision of milling.

RESULTS AND DISCUSSION

Main results from measuring are shown in the Table 1.

Tab. 1 Colour range coordinates (L*, a* and b* mean values with SD) of tested hops, brewer's yeast, malts, malts grist and EBC values of produced beer

Raw material	Parameter			
	L* ± SD	a* ± SD	b* ± SD	EBC units
Hops	47.67 ± 0.57	1.64 ± 0.13	13.34 ± 0.27	-
Brewer's yeast	65.63 ± 0.04	5.40 ± 0.02	21.43 ± 0.14	-
Colouring malt	39.68 ± 0.23	3.23 ± 0.10	3.84 ± 0.17	-
Col. malt grist	41.29 ± 0.51	3.69 ± 0.09	4.68 ± 0.14	-
Pilsner malt	59.99 ± 0.24	4.64 ± 0.09	17.83 ± 0.11	-
Pilsner malt grist	75.50 ± 1.11	2.27 ± 0.25	11.48 ± 0.76	-
Pilsner malt beer	-	-	-	5.9
Munich malt	59.81 ± 0.93	3.47 ± 0.14	12.17 ± 0.04	-
Munich malt grist	69.97 ± 1.02	3.22 ± 0.23	13.30 ± 0.51	-
Munich malt beer	-	-	-	12.5
Caramel malt	54.74 ± 1.09	7.11 ± 0.29	18.96 ± 0.76	-
Caramel malt grist	55.62 ± 0.31	6.98 ± 0.48	16.85 ± 0.38	-
Caramel malt beer	-	-	-	27.5

SD – Standard deviation

In Table No 2 are shown measured results of light beer, for its production was used Pilsner malt only. According EBC System the average value of beer was appr. 8 unit of EBC. To compare with colour of pilsner malt grist is the increase in colour of brewed beer nearly three times, the reason for colour increase are, of course, Maillard reactions (chemical reaction between an amino acids and a reducing sugar, usually requiring the addition of heat, similary as browning).

Tab. 2 Parameters of Light beer

Light beer									
Pilsen malt (200 kg)					Pilsner malt grist (200 kg)				light beer**
EBC		CIELAB System			EBC	CIELAB System			EBC
No	Colour	L*	a*	b*	Colour	L*	a*	b*	Colour
1	2.90	59.99	4.64	17.83	2.90	75.50	4.64	17.83	8.10
2	2.80	59.32	4.84	17.92	2.80	75.60	4.84	17.92	7.50
3	3.00	58.00	4.74	17.88	3.10	75.40	4.74	17.88	8.30
4	2.70	61.20	4.65	17.69	2.70	75.60	4.65	17.69	8.50
5	2.80	59.20	4.64	17.95	2.80	75.40	4.64	17.95	8.40
6	2.90	59.10	4.66	17.66	2.90	75.20	4.66	17.66	7.40
7	2.90	59.10	4.59	17.88	2.90	75.20	4.59	17.88	7.70
8	2.90	49.30	4.40	17.84	2.90	76.10	4.40	17.84	7.90
9	2.50	62.30	4.65	17.82	3.00	75.20	4.65	17.82	7.80
10	2.60	57.20	4.63	17.83	3.10	75.80	4.63	17.83	8.20
Mean	2.80	58.47	4.64	17.83	2.91	75.50	4.64	17.83	7.98
SD	0.16	3.53	0.11	0.09	0.13	0.29	0.11	0.09	0.38
CV	5.58	6.04	2.39	0.52	4.42	0.38	2.39	0.52	4.76

Brewed beer was not possible in System **CIELAB System measured
SD – Standard deviation; CV – coefficient of variation

In the Table 3 are shown measured results of semi-dark beer, for its production were used next to Pilsner malt, Munich malt and Caramunich malt.. According EBC System the average value of beer was appr. 8 unit of EBC. To compare with colour of pilsner -, Munich- nad Caramunich grist is the increase in colour of brewed beer nearly 6 times (for pilsner grist due to its weight).

Tab. 3 Parameters of Semi-dark beer

Semi-dark beer												
Pilsner malt grist (110 kg)				Munich malt grist (60 kg)				Caramunich malt (30 kg)				Beer**
EBC	CIELAB Systém			EBC	CIELAB Systém			EBC	CIELAB Systém			EBC
No	Colour	L*	a*	b*	Colour	L*	a*	b*	Colour	L*	a*	b*	Colour
1	2.90	75.5	2.27	11.48	23.5	69.7	3.42	13.3	130	55.72	7.12	16.85	38.00
2	2.60	75.6	2.13	11.6	23.9	69.9	3.12	13.7	130	55.72	7.12	16.40	36.00
3	2.80	75.4	2.18	12.00	23.1	69.9	3.36	12.8	130	55.72	7.12	16.25	37.00
4	2.67	75.6	2.16	11.49	22.1	70.4	3.28	13.5	130	55.72	7.12	16.50	37.00
5	2.71	75.4	2.14	11.56	22.8	69.4	3.38	12.5	130	55.72	7.12	16.30	37.00
6	2.81	75.2	2.30	12.00	23.2	69.8	3.41	14.1	140	54.74	7.11	17.20	37.00
7	2.76	75.2	2.44	17.88	22.8	69.9	2.98	13.1	130	54.74	7.11	17.50	38.00
8	3.17	75.3	2.11	17.84	22.6	68.9	2.80	13.3	130	54.74	7.11	17.20	39.00
9	3.36	75.9	2.18	17.82	22.8	70.4	3.22	13.1	130	54.74	7.11	16.90	41.00
10	3.07	71.3	2.79	17.83	23.2	70.2	3.22	13.4	130	54.74	7.11	17.20	39.00
Mean	2.89	75.04	2.27	14.15	23.0	69.9	3.22	13.3	131	55.23	7.12	16.83	34.45
SD	0.24	1.33	0.20	3.19	0.49	0.46	0.20	0.45	3.16	0.52	0.01	0.44	11.51
CV	8.30	1.70	9.17	22.50	2.17	0.65	6.29	3.38	2.41	0.94	0.07	2.64	33.40

Brewed beer was not possible in System **CIELAB System measured, SD – Standard deviation; CV – coefficient of variation

Tab. 4 Dark Beer

Dark beer

No	Pilsner malt grist (100 kg) EBC Colour	CIELAB Systém L*	a*	b*	Munich malt grist (50 kg) EBC Colour	CIELAB Systém L*	a*	b*	Caramunich malt (30 kg) EBC Colour	CIELAB Systém L*	a*	b*	CARAFA malt grist (30 kg) EBC Colour	CIELAB Systém L*	a*	b*	Beer EBC Colour
1	2.9	75.5	4.64	17.83	23.5	69.7	3.42	13.3	130	55.7	7.12	16.9	1350	41.29	3.69	4.68	62.0
2	2.8	75.6	4.84	17.92	23.9	69.9	3.12	13.7	130	55.7	7.12	16.4	1350	41.39	3.59	4.28	61.0
3	3.1	75.4	4.74	17.88	23.1	69.9	3.36	12.8	130	55.7	7.12	16.3	1350	41.29	3.54	4.93	63.0
4	2.7	75.6	4.65	17.69	22.1	70.4	3.28	13.5	130	55.7	7.12	16.5	1350	40.35	3.79	4.72	61.0
5	2.8	75.4	4.64	17.95	22.8	69.4	3.38	12.5	130	55.7	7.12	16.3	1350	40.75	3.65	4.70	62.0
6	2.9	75.2	4.66	17.66	23.2	69.8	3.41	14.1	140	54.7	7.11	17.2	1350	41.25	3.68	4.62	62.0
7	2.9	75.2	4.59	17.88	22.8	69.9	2.98	13.1	130	54.7	7.11	17.5	1350	41.3	3.71	4.71	61.0
8	2.9	76.1	4.40	17.84	22.6	68.9	2.80	13.3	130	54.7	7.11	17.2	1350	42.05	3.65	4.69	60.0
9	3.0	75.2	4.65	17.82	22.8	70.4	3.22	13.1	130	54.7	7.11	16.9	1350	42.15	3.71	4.75	62.0
10	3.1	75.8	4.63	17.83	23.2	70.2	3.22	13.4	130	54.7	7.11	17.2	1350	41.05	3.75	4.68	61.0
Mean	2.91	75.5	4.64	17.83	23.0	69.9	3.22	13.3	131	55.2	7.12	16.8	1350	41.29	3.68	4.68	61.5
SD	0.13	0.29	0.11	0.09	0.50	0.46	0.2	0.45	3.16	0.52	0.01	0.44	0	0.53	0.07	0.16	0.85
CV	4.42	0.39	2.4	0.52	2.17	0.65	6.29	3.38	2.41	0.94	0.07	2.64	0	1.29	1.99	3.45	1.38

Brewed beer was not possible in System **CIELAB System measured,

SD – Standard deviation; CV – coefficient of variation

From the previous experimental activity found, that the impact of yeast and hops was negligible, that's why those raw material were not considered.

The results of lightness L* in the Table 1 indicate that the lightest malt is the Pilsner Malt (L* = 59.99 ± 0.24), which even increased the lightness by the milling to the value of Pilsner Malt grist (L* = 75.50 ± 1.11), which causes the difference ΔL* = 15.51. There are recognised also changes in colour shades, a* and b*. The redness of Pilsner Malt (a* = 4.64 ± 0.09) was reduced by milling to the value of Pilsner Malt grist (a* = 2.27 ± 0.25), which causes the difference Δa* = 2.37. Also the yellowness of Pilsner Malt (b* = 17.83 ± 0.11) was reduced by milling to the value of Pilsner Malt grist (b* = 11.48 ± 0.76), which causes the difference Δb* = 6.35. The colour of beer using Pilsner Malt is the lightest (5.9 EBC units) from tested samples. The results of lightness L* of the Munich malt (L* = 59.81 ± 0.93) is very similar to the Pilsner Malt, but the change of lightness of the Munich Malt grist (L* = 69.97 ± 1.02) is not so high, which causes the difference ΔL* = 10.16. The changes in colour shades, a* and b* are small in comparison with Pilsner malt. The redness of Munich Malt (a* = 3.47 ± 0.14) was reduced by milling to the value of Munich Malt grist (a* = 3.22 ± 0.23), which causes small difference Δa* = 0.25. The yellowness of Munich Malt (b* = 12.17 ± 0.04) was slightly increased by milling to the value of Munich Malt grist (b* = 13.30 ± 0.51), which causes the difference Δb* = 1.13. The use of Munich Malt resulted in colour 12.5 EBC units. The most dark malt is the Caramel Malt with lightness L* = 54.74 ± 1.09. The increment of the lightness of Caramel Malt grist (L* = 55.62 ± 0.31) is very small, which causes the difference only ΔL* = 0.88. The changes in colour shades, a* and b* are small in comparison with Pilsner malt. The redness of Caramel Malt which was the highest from three tested malts (a* = 7.11 ± 0.29) was slightly reduced by milling to the value of Caramel Malt grist (a* = 6.98 ± 0.48), which causes small difference Δa* = 0.13. The yellowness of Caramel Malt, which was also the highest from three tested malts (b* = 18.96 ± 0.76) was reduced by milling to the value of Caramel Malt grist (b* = 16.85 ± 0.38), which causes the difference Δb* = 2.11. The use of Caramel malt resulted in colour 27.5 EBC units. Hops was used the same in all three cases, so its influence in the colour of the beer to be compared cannot be proved. Perhaps it is only possible to state that the colour of the hops shows a fairly slight green colour (a * = - 1.64 ± 0.13). The results of this measurement could be used in the future, for comparison with other types of hops. The same applies to brewer's yeasts that showed a certain shade of redness (a * = 5.40 ± 0.02) and a more significant shade of yellowness (b * = 21.43 ± 0.14).

CONCLUSIONS

The results of this research had shown the leakage of information about relationship between colours of raw materials and brewed beer. From the point of view of quickly growing number of new founded craft breweries and new types of beer (IPA, Ale, Stout etc.) is important to recognize all important parameters including the colours of raw materials for this process.

The results of measurements of different malts presented in this paper can be used with advantage for prediction of colour next brewing beer according demand of future customers. The colour of yeast and hops do not have any impact on brewing beer.

The future research and development in this field of science should be focused on the study of the further research of relationship between properties of used raw materials and quality of brewed beer.

ACKNOWLEDGMENT

REFERENCES

1. Basařová, G., Šavel, J., Basař, P., & Lejsek, T. (2010). *Brewery: the theory and practice of beer production* (in Czech). 1st edition. Prague: Vydavatelství VŠCHT, pp. 863.

2. Benard, M. (2000). Determination of repeatability and reproducibility of EBC accepted methods: V – beer. *J. Inst. Brew. 106*, 135-138.

3. Chládek, L. (2007). *Brewing* (in Czech). 1st edition. Prague: Grada, pp. 207.

4. Chládek, L., Vaculík, P., Přikryl, M., Vaculík, M., & Holomková, M. (2013). Impact of malt granulometry on lauter proces. In *5th International Conference on Trends in Agricultural Engineering 2013, TAE 2013 03.09.2013*, (pp. 244-248). Prague: Czech University of Life Sciences.

5. Chladek, L., Vaculik, P., & Vagova, A. (2018). The measurement of energy consumption during milling different cereals using the sieve analyses. *Agronomy research 16*(Special Issue 2), 1341-1350.

6. Kosař, K. & Procházka, S. (2000). *Technology of malt and beer production* (in Czech). 1st edition. Prague: Výzkumný ústav pivovarský a sladařský, pp. 398.

7. Kunze, W. (2010). *Technology Brewing and Malting* (in German). 4th updated English Edition. Berlin: Versuchs- und Lehranstalt für Brauerei in Berlin (VLB), pp. 1047.

8. Olšovská, J., Čejka, P., Štěrba, K., Slabý, M., & Frantík, F. (2017). *Sensory analysis of beer* (in Czech). Prague: Výzkumný ústav pivovarský a sladařský, pp. 398.

9. Seaton, J. C. & Cantrell, I. C. (1993). The determination of beer colour – collaborative trial. *J. Inst. Brew, 99*, 21-23.

10. Smedley, S. M. (1995). Discrimination between beers with small colour differences using the CIELAB colour space. *J. Inst. Brew. 10l*, 195-201.

Corresponding author:
Ass. Prof. Ing. Ladislav Chládek, CSc., Department of Technological Equipment of Buildings, Faculty of Engineering, Czech University of Life Sciences Prague, Kamýcká 129, 165 21 Prague, Czech Republic, phone: +420 22438 2357, e-mail: chladekl@tf.czu.cz

WEAR RESISTANT HIGH BORON STEEL FOR AGRICULTURE TOOLS

Rostislav CHOTĚBORSKÝ[1]

[1]*Department of Material Science and Manufacturing Technology, Faculty of Engineering, Czech University of Life Sciences*

Abstract
The article is focused on high boron steel applicable in agriculture mainly for agriculture tools such as chisels, rings and other. Experimental procedure included two different chemical composition of high boron cast iron with and without chromium content. The samples were in cast state and after heat treatment used in dry rubber wheel test for determination of wear resistant properties. Results show that the best wear resistant properties are received if the heat treatment and forging was used.

Key words: *High boron steel; wear resistance; agriculture tools; heat treatment.*

INTRODUCTION

Wear on tillage tools can be caused by the abrasive action of soil particles. Abrasive wear depends on the abrasive interaction, which is characterized by large surface plastic deformations occurring when two mutually sliding bodies are in contact. The phenomenon occurs when a hard body exerts a smoothing action on a softer body. Wear rate is mostly affected by soil texture, water content, bulk density, and particle angularity and the relative hardness of the tool material with respect to that of soil particles, the operating speed and depth and soil-tool pressure distribution. Especially in very abrasive soils, wear can be dramatic, indeed a tool can be worn out in one working day. An opportunity to reduce wear, largely used in the field of industrial cutting tools, is surface hardening; this can be done as a heat treatment, but above all as a superficial coating. Superficial coating techniques applied to soil engaging components include hard facing *(Jankauskas, Katinas, Skirkus, & Alekneviciene, 2014)*, edge tipping with alumina ceramic *(Müller, M., Chotěborský, R., Valášek, P., Hloch, 2013)*, boriding *(Yazici & Çavdar, 2017)* and thin coating *(Sidorov, Khoroshenkov, Lobachevskii, & Akhmedova, 2017)*.

The toughness and the hardness of the tillage tool materials should be optimized for specific operating conditions *(Abo-Elnor, Hamilton, & Boyle, 2004; Arvidsson, Keller, & Gustafsson, 2004; Cui, Défossez, & Richard, 2007)*. Steels which are often employed in the agriculture industry where soil has to be ground or transported. Although these steels are wear resistant after their heat treatment, they are low or medium carbon steel with hardness up to 55 HRC and their microstructure is tempered martensite *(D. Liu, Xu, Yang, Bai, & Fang, 2004)*. The low cost steel for agriculture tools are steel with small amount of expensive element but there are microalloyed by boron. The way how to obtain material for agriculture industry may be steels on metal matrix composite basis because material in agriculture for a tools like chisel or ploughshare must be toughness.

High-boron alloy steels (0.5 %B to 4.0 %B) are used as wear-resistant materials. At present, the change of structures and properties of high boron cast steel at different homogenization temperatures has seen relatively little study, and wear resistant high boron cast steel has yet to find broad applications *(Cen, Zhang, & Fu, 2014; Fu, Xing, Lei, & Huang, 2011; Liu, Chen, Li, & Hu, 2009)*. It is well known that boron can improve the hardenability of steels and enhance their thermal stability. The solubility of boron, however, is very low in iron, and the addition of excessive boron leads to the formation of continuous network of eutectic boride M2B (M represents Fe, Cr or Mn) along the grain boundaries, which is detrimental to the mechanical properties and results in the embrittlement of high boron Fe–B alloys *(Chen, Li, & Zhang, 2011; Y. Liu et al., 2010)*. Powder metallurgy routes have been used to produce the alloys to prevent the formation of M2B network *(Röttger, Weber, & Theisen, 2012)*. Alloying *(Baron, Springer, & Raabe, 2016; Jian et al., 2016)*, heat treatment and rare earth modification are the most common methods used to improve the toughness of high boron cast steel *(Chotěborský, Rostislav; Bryksí-Stunová, Barbora; Kolaříková, 2013; Savková, Jarmila; Chotěborský, Rostislav; Bláhová, 2013)*. Therefore, plastic deformation is also used to break up boride network. The best cutting of sheets made of high boron steel can be done by WEDM technology. Where the surface roughness can be optimized by setup of parameters *(K. Mouralova, Prokes, & Benes, 2019; K. Mouralova, Benes, et al., 2019;*

Katerina Mouralova, Kovar, Prokes, Bednar, & Hrabec, 2017). Other technological cutting can leads to crack in edges thanks to rapid heating and cooling (laser) or high wear rate of tool for machining. The present research is to study the effect of chemical composition and heat treatment on the microstructural transformation, hardness and wear properties of medium boron steels.

MATERIALS AND METHODS

The medium boron cast steel was melted in a 1 kg medium frequency induction furnace with SiO_2 furnace lining, with charge materials of steels, ferroboron and ferroalloys. The liquid metal was superheated at 1550-1600°C and then deoxidized with a 0.2 wt. % aluminium. Subsequently, the liquid metal was poured into a ceramics mould. The chemical composition of medium boron cast steel is given in Table. 1. It was determined with a spark emission spectrometer.

Before forging, the samples were first annealed at 1000 °C for 4 h to homogenize the chemical composition and improve hot plasticity in high boron cast steel. Process of forging is used repeatedly to break up boride network. Forging temperature of high boron cast steel according to Fe-B phase diagram changes from 900 to 1050 °C. Heat treatment included from quenching (920 °C cooling in water) and tempering (400 °C in air). Wear test was done on a three body abrasion machine based on ASTM G65. The load was 98.1 N, abrasive was sand fraction 0.2 to 0.315 mm. Test cycle of each specimen included ten times 210 m trace. The weight loss was measured after every trace on balance with accuracy 0.1 mg. Weight loss was recalculate to volume loss. To discuss the wear mechanism, worn surface was observed with SEM.

Tab. 1 Chemical composition of tested steel (wt. %), rest is Iron.

	Boron	Carbon	Neodymium	Chromium
Sample 1	0.62	0.5	0.0	0.21
Sample 2	0.61	0.52	0.38	1.12

RESULTS AND DISCUSSION

The cast alloy is generally comprised of white and white-black phases. Previous studies *(Chen et al., 2011; Z. Liu, Li, Chen, & Hu, 2008; Lv, Fu, Xing, Ma, & Hu, 2016a)* shown that white phase are borides and white-black phase is ferrite-pearlite. Fig. 1 shows microstructures of the heat treated samples. As shown in Fig. 1 cast alloy with heat treatment is comprised of white and black phases. Black phase in this case is martensite. The borides vividly present fish-bone, net-like and rod-like morphological characteristics.

Fig. 2 shows microstructures of forged samples. As shown in Fig. 2 forged alloy is generally comprised of white and black phases. White phase are undeformed borides which were cracked by forging of samples. Black phase is martensite and tempered martensite.
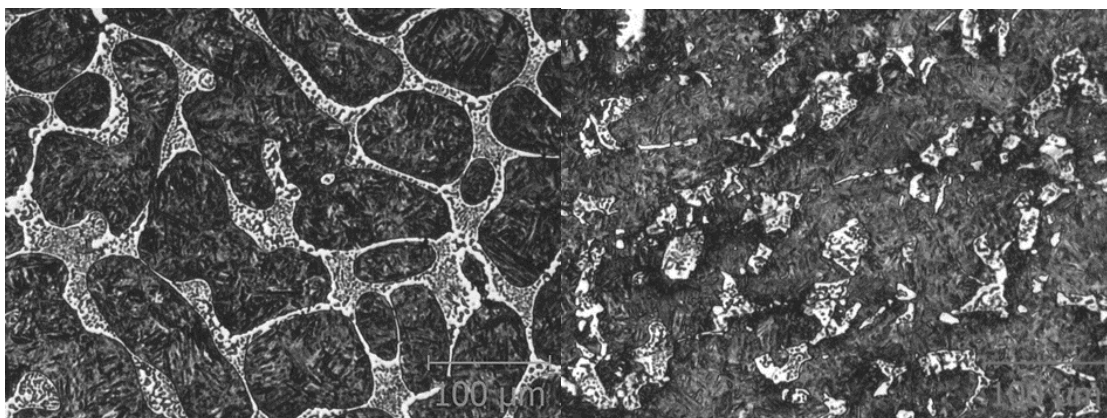
Fig. 1 Boride netlike casted sample   **Fig. 2** Boride particles after forging

As a hard phase, M2B will resist the abrasive particles, protecting F-P from being a shoveled off directly. In return, F-P will support and fix M2B. Also martensite or tempered martensite show a good fix of M2B. The synergic reaction of these two constituents plays an important role in abrasive wear resistance. Richardson's theory said that the material wear resistance would be relatively poor in case of hard abrasive and can be improved effectively by hardness improvement in case of soft abrasive.

Fig. 3a shows the three body abrasive wear weight losses of Fe-B cast alloys (quenched in oil) in case of relative soft abrasive SiO2. Agriculture tool are usually made of Boron 27 steel (typical hardness is 45 HRC), this steel after heat treatment (quenching and low tempering) has a wear loss 0.12 mg per meter (mg/m). The tested high boron steel have wear loss lower then Boron 27. Results are presented in Fig. 3b, where 1 – Boron 27, 2 – sample 1 casted, 3 – sample 2 casted, 4 – sample 1 forged, 5 – sample 2 forged, 6 – sample 1 forged and quenched, 7 – sample 2 forget and quenched.
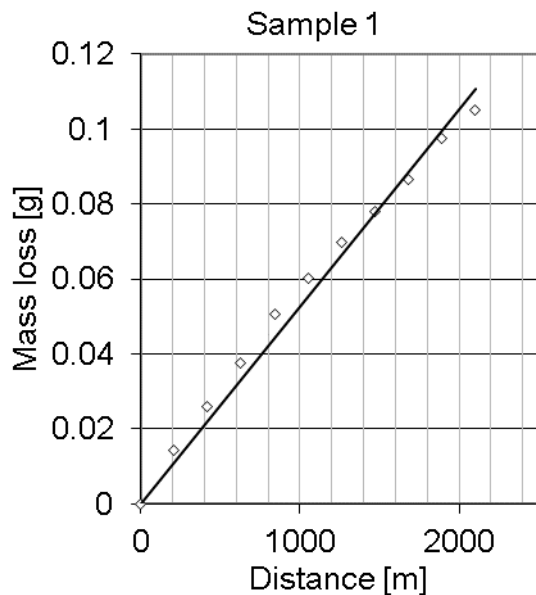
Fig. 3a Result of ASTM G65 DRWT
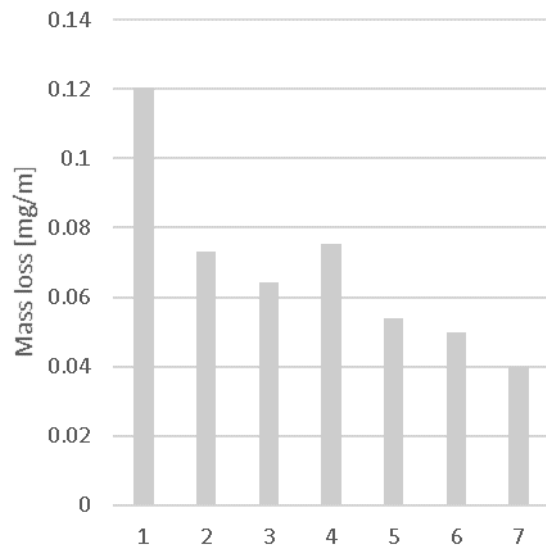
Fig. 3b Comparison of selected samples

Fig. 4. shows the worn surface of Fe-B alloy with and without forging. Worn surface in case sample without forging are covered parallel but chaotic plowing grooves and fractured borides.

Plowing grooves on the worn surfaces are relatively wide and uneven. Peeling and fragments phenomenon appear obviously for borides on the worn surface of 0Cr sample, while worn surface of 1.2Cr sample is relatively smooth. It is likely that the sharp edges and corners of SiO2 particles may be worn down during the interaction with borides. Thus, the grooves in following micro-cutting are supposed to become wider. Owning higher hardness, boride can resist the cutting by SiO2 abrasive effectively. Hence, SiO2 particles may scratch martensite firstly, resulting in their regularity of plowing grooves. For boride with high brittleness, it is easy to fracture during the interaction with SiO2 abrasive on worn surface. The fractured borides will be easily worn down in the following cratches, causing bad wear resistance of the alloy. Inreverse, borides with good toughness will retain relatively good resistance to SiO2 abrasive for along time. Wear resistance of Fe–B cast alloy will certainly make a good performance.
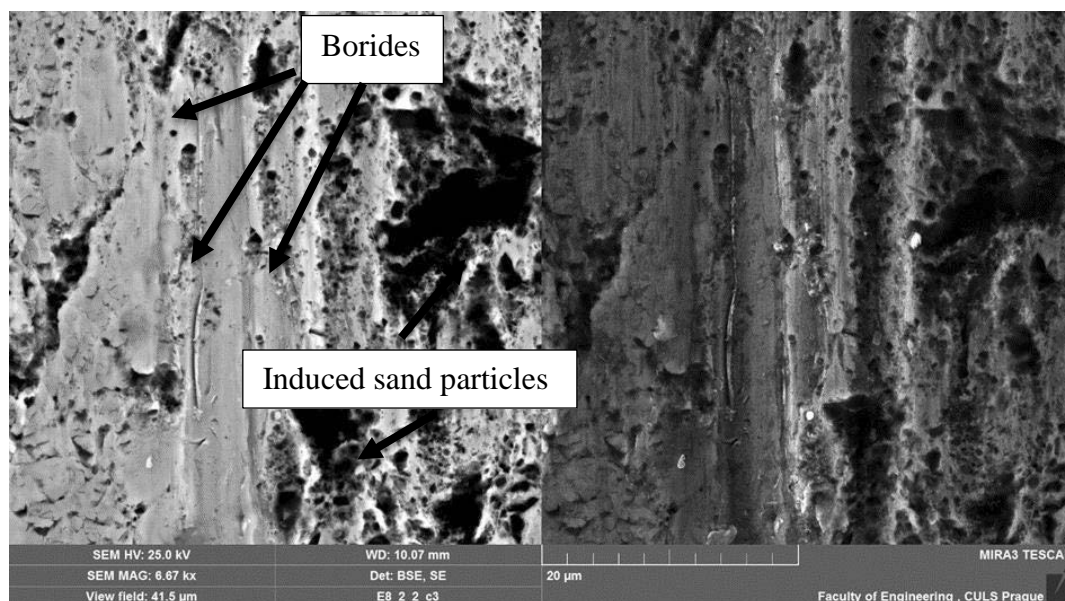
Fig. 4 Worn surface of sample 1 in casted state

Wear resistance of high boron steel so could be increased with alloying so that chromium content will be higher than tested sample. Other way can be complex alloying with aluminum and chromium which leads to higher hardness and toughness like are show in other research *(Christodoulou & Calos, 2001; Lv, Fu, Xing, Ma, & Hu, 2016b; Ren, Fu, Xing, & Tang, 2018)*. In principle it can be same such as alloying the carbide cast iron alloys for wear resistant overlay which are describe in research including wear results *(Berns, Saltykova, Röttger, & Heger, 2011; Chotěborský & Hrabě, 2013; Chotěborský et al., 2009; Kučera & Chotěborský, 2013; Lin, Chang, Chen, Hsieh, & Wu, 2010)*.

CONCLUSIONS

Hard phase of hypoeutectic Fe–C–B alloy containing 0.5 wt.% C and 0.62 wt.% B presents continues network morphology and results in poor wear resistant properties in cast state. Thermomechanical treatment can improve the morphology of hard phase and enhance the impact toughness of the alloy effectively. Hypoeutectic Fe-C-B alloys with low amount of chromium and neodymium can be one of famous and low cost material for agriculture tools like chisel, rings, etc.

REFERENCES

1. Abo-Elnor, M., Hamilton, R., & Boyle, J. (2004). Simulation of soil–blade interaction for sandy soil using advanced 3D finite element analysis. *Soil and Tillage Research*, *75*(1), 61–73.
2. Arvidsson, J., Keller, T., & Gustafsson, K. (2004). Specific draught for mouldboard plough, chisel plough and disc harrow at different water contents. *Soil and Tillage Research*, *79*(2), 221–231.
3. Baron, C., Springer, H., & Raabe, D. (2016). Efficient liquid metallurgy synthesis of Fe–TiB2 high modulus steels via in-situ reduction of titanium oxides. *Materials & Design*, *97*, 357–363. doi:10.1016/j.matdes.2016.02.076
4. Berns, H., Saltykova, A., Röttger, A., & Heger, D. (2011). Wear Protection by Fe-B-C Hard Phases. *Steel Research International*, *82*(7), 786–794. doi:10.1002/srin.201000255
5. Cen, Q., Zhang, H., & Fu, H. (2014). Effect of Heat Treatment on Structure and Wear Resistance of High Chromium Cast Steel Containing Boron. *Journal of Iron and Steel Research, International*, *21*(5), 532–538. doi:10.1016/S1006-706X(14)60083-2
6. Cui, K., Défossez, P., & Richard, G. (2007). A new approach for modelling vertical stress distribution at the soil/tyre interface to predict the compaction of cultivated soils by using the PLAXIS code. *Soil and Tillage Research*, *95*(1-2), 277–287.
7. Fu, H.-G., Xing, J.-D., Lei, Y.-P., & Huang, L.-M. (2011). A study on the wear behavior of Cast Boron Steel. *Journal of Materials Engineering and Performance*, *20*(9). doi:10.1007/s11665-010-9808-9

8. Chen, X., Li, Y., & Zhang, H. (2011). Microstructure and mechanical properties of high boron white cast iron with about 4 wt% chromium. *Journal of Materials Science*, *46*(4), 957–963. doi:10.1007/s10853-010-4840-6

9. Chotěborský, R., & Hrabě, P. (2013). Effect of destabilization treatment on microstructure, hardness and abrasive wear of high chromium hardfacing. *Research in Agricultural Engineering*, *59*(4), 128–135.

10. Chotěborský, R., Hrabě, P., Müller, M., Válek, R., Savková, J., & Jirka, M. (2009). Effect of carbide size in hardfacing on abrasive wear. *Research in Agricultural Engineering*, *55*(4), 149–158.

11. Chotěborský, Rostislav; Bryksí-Stunová, Barbora; Kolaříková, M. (2013). Effect of rare earth element on microstructure of Fe-B cast alloy. In *22nd International Conference on Metallurgy and Materials, METAL 2013* (pp. 203–207). TANGER Ltd.

12. Christodoulou, P., & Calos, N. (2001). A step towards designing Fe–Cr–B–C cast alloys. *Materials Science and Engineering: A*, *301*(2), 103–117. doi:10.1016/S0921-5093(00)01808-6

13. Jankauskas, V., Katinas, E., Skirkus, R., & Alekneviciene, V. (2014). The method of hardening soil rippers by surfacing and technical-economic assessment. *Journal of Friction and Wear*, *35*(4), 270–277. doi:10.3103/S106836661404014X

14. Jian, Y., Huang, Z., Xing, J., Liu, X., Sun, L., Zheng, B., & Wang, Y. (2016). Investigation on two-body abrasive wear behavior and mechanism of Fe–3.0wt% B cast alloy with different chromium content. *Wear*, *362-363*, 68–77. doi:10.1016/j.wear.2016.04.029

15. Kučera, M., & Chotěborský, R. (2013). Analysis of the process of abrasive wear under experimental conditions. *Scientia Agriculturae Bohemica*, *44*(2), 102–106. doi:10.7160/sab.2013.440206

16. Lin, C.-M., Chang, C.-M., Chen, J.-H., Hsieh, C.-C., & Wu, W. (2010). Microstructure and wear characteristics of high-carbon Cr-based alloy claddings formed by gas tungsten arc welding (GTAW). *Surface and Coatings Technology*, *205*(7), 2590–2596. doi:10.1016/j.surfcoat.2010.10.004

17. Liu, D., Xu, H., Yang, K., Bai, B., & Fang, H. (2004). Effect of bainite/martensite mixed microstructure on the strength and toughness of low carbon alloy steels. *Jinshu Xuebao/Acta Metallurgica Sinica*, *40*(8), 882–886.

18. Liu, Y., Li, B., Li, J., He, L., Gao, S., & Nieh, T. G. (2010). *Effect of titanium on the ductilization of Fe–B alloys with high boron content. Materials Letters* (Vol. 64). doi:10.1016/j.matlet.2010.03.013

19. Liu, Z., Chen, X., Li, Y., & Hu, K. (2009). High Boron Iron-Based Alloy and Its Modification. *Journal of Iron and Steel Research, International*, *16*(3), 37–54. doi:10.1016/S1006-706X(09)60041-8

20. Liu, Z., Li, Y., Chen, X., & Hu, K. (2008). Microstructure and mechanical properties of high boron white cast iron. *Materials Science and Engineering: A*, *486*(1), 112–116. doi:10.1016/j.msea.2007.10.017

21. Lv, Z., Fu, H., Xing, J., Ma, S., & Hu, Y. (2016a). Microstructure and crystallography of borides and mechanical properties of Fe–B–C–Cr–Al alloys. *Journal of Alloys and Compounds*, *662*, 54–62. doi:10.1016/j.jallcom.2015.11.171

22. Lv, Z., Fu, H., Xing, J., Ma, S., & Hu, Y. (2016b). Microstructure and crystallography of borides and mechanical properties of Fe–B–C–Cr–Al alloys. *Journal of Alloys and Compounds*, *662*, 54–62. doi:10.1016/J.JALLCOM.2015.11.171

23. Mouralova, K., Benes, L., Bednar, J., Zahradnicek, R., Prokes, T., Matousek, R., … Otoupalik, J. (2019). Using a DoE for a comprehensive analysis of the surface quality and cutting speed in WED-machined hadfield steel. *Journal of Mechanical Science and Technology*, *33*(5), 2371–2386. doi:10.1007/s12206-019-0437-4

24. Mouralova, K., Kovar, J., Prokes, T., Bednar, J., & Hrabec, P. (2017). OPTIMISATION OF WEDM SETTINGS PARAMETERS WHEN MACHINING PURE ALUMINIUM USING THE DOE. *MM Science Journal*, *2017*(05), 2105–2108. doi:10.17973/MMSJ.2017_12_201795

25. Mouralova, K., Prokes, T., & Benes, L. (2019). Surface and Subsurface Layers Defects Analysis After WEDM Affecting the Subsequent Lifetime of Produced Components. *Arabian Journal for Science and Engineering*, 1–13. doi:10.1007/s13369-019-03887-7

26. Müller, M., Chotěborský, R., Valášek, P., Hloch, S. (2013). Unusual possibility of wear

resistance increase research in the sphere of soil cultivation. *Tehnicki Vjesnik*, *20*(4), 641–646.

27. Ren, X., Fu, H., Xing, J., & Tang, S. (2018). Effect of Aluminum on Borocarbides and Temper Softening Resistance of High-Boron High-Speed Steel. *Metallurgical and Materials Transactions A*, *49*(11), 5636–5645. doi:10.1007/s11661-018-4861-3

28. Röttger, A., Weber, S., & Theisen, W. (2012). Supersolidus liquid-phase sintering of ultrahigh-boron high-carbon steels for wear-protection applications. *Materials Science and Engineering: A*, *532*, 511–521. doi:10.1016/j.msea.2011.10.118

29. Savková, Jarmila; Chotěborský, Rostislav; Bláhová, O. (2013). Effect of forging on microstructure of Fe-B cast steel. In *22nd International Conference on Metallurgy and Materials, METAL 2013* (pp. 822–827). TANGER Ltd.

30. Sidorov, S. A., Khoroshenkov, V. K., Lobachevskii, Y. P., & Akhmedova, T. S. (2017). Improving Wear Resistance of Agricultural Machine Components by Applying Hard-Alloy Thick-Layer Coatings Using Plasma Surfacing. *Metallurgist*, *60*(11-12), 1290–1294. doi:10.1007/s11015-017-0443-7

31. Yazici, A., & Çavdar, U. (2017). A Study of Soil Tillage Tools from Boronized Sintered Iron. *Metal Science and Heat Treatment*, *58*(11-12), 753–757. doi:10.1007/s11041-017-0091-3

Corresponding author:
Asc. Prof. Ing. Rostislav Choteborsky, Ph.D., Department of Material Science and Manufacturing Technology, Faculty of Engineering, Czech University of Life Sciences Prague, Kamýcká 129, Praha 6, Prague, 16521, Czech Republic, phone: +420 22438 3274, e-mail: choteborsky@tf.czu.cz

EXPLORING IOT BASED BROILER CHICKEN MANAGEMENT TECHNOLOGY

Shigeru ICHIURA[1], Tomohiro MORI[2], Ken-ichi HORIGUCHI[2], Mitsuhiko KATAHIRA[2]

[1]*Department of Agricultural and Environmental Engineering, Biotic Environmental Science, The United Graduate School of Agriculture Sciences, Iwate University (UGAS)*
[2]*Department of Faculty of Agriculture, Yamagata University, 1-23, Wakabamachi, Tsuruoka, Yamagata, 998-8555, Japan.*

Abstract
The article reports on the development of labor-saving chicken production management techniques with IoT (Internet of Things)) technology. Ip based video cameras, a variety of sensors (atmospheric pressure, illumination, body temperature (4x4 segments)), and RFID (radio frequency identifier, this is for short-range wireless communication based on the electromagnetic fields, radio waves) technology were utilized. RFID was used for getting the chicken's unique embedded ID (identification) which was recorded from RFID tag. As 1st step, we focused on analyzing the individual chicken's weight which is linked with the RFID tag and conducted a trial of video-based chicken weight inference system by Artificial Intelligence (Deep Learning). The study demonstrates the potential of video-based chicken production monitoring system.

Key words: Broiler; Chicken's behaviours; RFID; Artificial Intelligence; Deep Learning; IoT.

INTRODUCTION

As wealth increases, consumers become more particular about what they consume. They are more concerned about food safety and about how their food was produced. This denmand has created a new category of food referred to as premium foods. Research was done on improving the traceability of beef using RFID in China with the aim of meeting consumers rising food safety demands *([1]Feng, J., Fu et al., 2013, [2]Wanjie Liang et al., 2015)*. In broiler chicken production, there is a lack of labour and cost-efficient method/technology to manage individual birds. Domestic consumption of chicken meat in Japan was 2,298 thousand tons in 2015, and 2,369 thousand tons in 2016, an increase of 3.1% over the previous year. Similarly, the domestic production volume is expanding in conjunction with the consumption volume, with 1,517 thousand tons in 2015 and 1,545 thousand tons in 2016. The number of domestic broiler chicken farms (brooders) is on the decline with 2,590 units in 2006 and 2,360 units in 2016, mainly for small-scale feeder groups while the number of shipments have increased from 103,687 thousand in 2006 to 138,776 thousand in 2018, where large-scale chicken farmers had more than 500,000 shipments accounting for 11.3% of the whole 2016. This is mainly due to consolidation of the smaller farms, resulting in more large-scale brooders *([3]Livestock Statistics, MAFF Japan, 2018)*. However, at production sites, 5 to 6% of chickens are expected to die during feeding, and even after post-shipment inspection, they are destroyed due to disease. In addition, in recent years the brooding system has been focused on creating comfortable environments for the reduction of diseases. Regarding the individual recognition, in recent years, with the evolution of IoT technology, increase in storage capacity and the technology of artificial intelligence have been established, as such, all growth records can now be stored as electronic data. In addition, food safety requirements are increasing worldwide, and IoT technology can be incorporated into production process management, to establish a high-quality and safe meat production system with minimum human intervention.

In this research, we manage the broiler chicken growth with IoT technology, and improve the brooding environment of chickens in brooding space from the viewpoint of Welfare (animal welfare) and produce safe and high-quality chicken. The purpose is to develop a system for high quality and safe meat production with minimum human intervention. In this study, we used RFID as a method of individual management of chicken and verified a method of chicken's behaviour detection by Deep Learning based on chicken brooding video.

MATERIALS AND METHODS

(1) Individual management technology of chicken

1) Feeding facility

An experiment on the management of individual chickens was conducted at the experimental feeding facility at the Faculty of Agriculture, Yamagata University in Tsuruoka City, Yamagata Prefecture in Japan. The feeding facility was assembled using a total of four panels for two types of general-purpose gardening panels (890 cm x 1800 cm, 900 cm x 900 cm), and the experimental feeding facility as shown
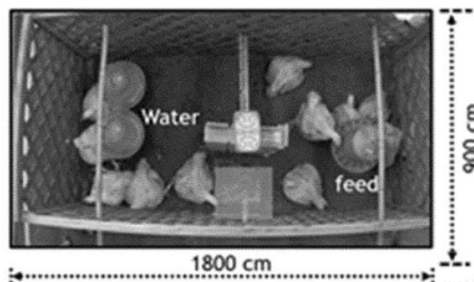
Fig. 1 the experimental feeding facility
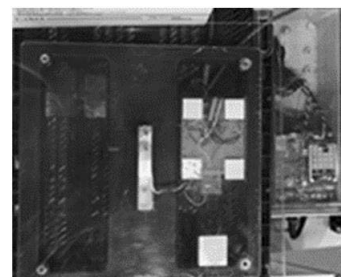
Fig. 2 RFID Tag receiver built-in weight scale as IoT device

Table 1. The Experimental Feedings

Number of experiment Feedings	Feeding Schedule		Feeding Dates	Number of chickens
1st	Oct.11th - Dec. 5th	2017	56	10
2nd	Jun 23rd - Aug. 14th		53	14
3rd	Oct.26th - Nov. 10th	2018	14	11
4th	Nov. 27th - Dec. 19th		23	10

in Fig. 1. It was divided into two in the vertical direction by a partition plate (mesh type) (arrangement of feeding unit) and a section (arrangement of water supply). We installed an RFID Tag receiver built-in weight scale which was located in the single passage of the sections as IoT device (Fig.2). The chicken's

Fig.3 The single passage between area of eating and drinking

video was taken with a wide-angle camera recorded directly from above the weight scale. At the same time, 7 segment LED values which are showed the chicken's ID and each weight were recorded as text data. There was a single passage between area of eating area and drinking, in order for the chickens to pass (Fig.3). For this experiment, we selected a common "*Chunky*" young bird, which were fed four times. Table 1 shows the feeding schedule and number of chickens.

(2) System configuration of experimental feedings.

1) Chicken weight scale

Since it is difficult to identify chickens by visual inspection, we developed RFID Tag receiver built-in weight scale using a commercially available RFID. The weight scale used the load cell (SC133-5kg by Sensor and Control), A/D converter, microcomputer, micro SDXC card and WiFi module. The scale sends the data to storage (Micro SDXC) and into cloud server via WiFi. The obtained data was recorded every 0.5 second, and was saved as text data in csv format which showed Chicken's ID and weight as real-time with 7 segments LEDs. The block diagram of RFID Tag receiver built-in weight scale is shown in Fig. 4 and the working status is shown in Fig. 5.

For RFID tag selection, we used the Low-frequency 125 KHz band. Low-frequency transponder has
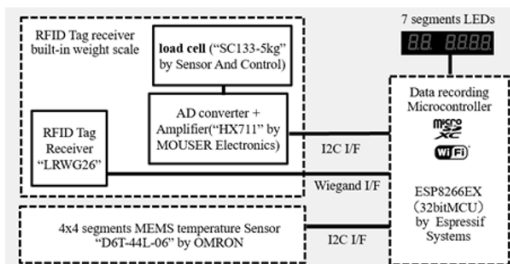
Fig. 4 The block diagram of RFID Tag receiver
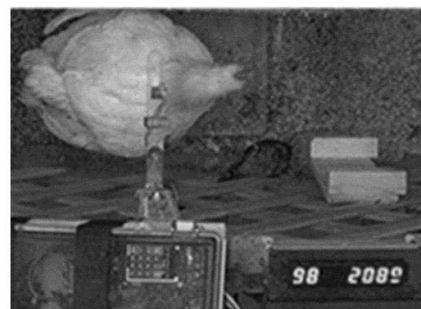
Fig. 5 The RFID Tag receiver built-in weight scale with 7 segments of LED (Chicken's ID and weight (g))

two different reading protocols and 2 frequencies (125KHz and 134.2KHz) and there are others (High-Frequency and Ultra-HIGH Frequency types) ([*4]T.M. Brown-Brandl et al.,2017). These types are different characteristic, Low-frequency and 125KHz has a wide radio directivity and is less susceptible to metal and water. The RFID is a passive ultra-compact Tag (FAREAD Technology, FRD-LF-GT3: φ2.12x12 mm) that does not have a built-in power supply as a coil antenna wound around a core rod shape using an electromagnetic induction system. RFID was used by Feng et. al, (2013) in a traceability system for cattle in China who found that it could greatly improve automation, efficiency

Fig 6. The RFID tag mounting for chicken leg ring with a hot melt adhesive (ethylene vinyl acetate)

and convenience in cattle/beef enterprises management as a controlling tool for product quality and safety. The RFID mounting on a chicken was attached to a commercial chicken leg ring with a hot melt adhesive (ethylene vinyl acetate) as shown in Fig.6.

2) Chicken behavior recording system

Video camera and video server system is shown in Fig.7.

Three IP cameras were set to record the behavior of chickens. Video was shot as sequential JEPG photos than captured the chicken's behavior, ID and weight on 7 segments LED. The video was stored into network attached storage (NAS: Buffalo, Terastation 5400 DN (RAID 4 Drive 8TB)) as JEPG format (Table 2, Fig.8). NAS had enough capacity to record during the experimental feedings.

Table 2. The equipment list of chicken behavior recording system

Items	Vendor	Product Name and Specification	Number of Items
IP camera	Mobitix	M25(horizontal 60 °, vertical 45 °, aperture F1.8)	1
		M25(horizontal 90 °, vertical 67 °, aperture F1.8)	2
NAS(Network attached storage)	Buffalo	Terastation 5400DN (RAID 4 Drive 8TB)	1
PoE(Power over ethernet) ethernet switch	Allied Telesis	AT-SH230-10GP	1
Potable Notebook PC	NEC	Windows10 + Motix Control Center	1
Broadband Router	Corega	CG-WLR300N	1
Dust-proof Cabinet	Nitto Kogyo		1

Fig.7 Video camera and video server system

Fig.8 Chicken behavior recording system

3) Weight inference system

The recorded weight data and the recorded Chicken's shape video were utilized for training data of the weight inference system by AI. In this case, Deep Learning was used.

The chicken shape labeled with displayed weight value. The displayed value was dynamically changed every 0.5 second, we considered the actual weight value of each chicken in order to avoid miss labeling. For training the AI chicken images were selected from the 3rd experimental feedings. We set the 4 weight ranks as 1,700 g, 1,800 g, 1,900 g, 2,000 g. 500 pieces of each rank was labeled for training data for Deep Learning analysis.

We selected the Deep Learning frame work "Darknet (Open Source Neural Networks in C language)" and "Yolo V3" ([*5]Designed by Joseph Redmon et al., 2018) for the inference algorithm. This framework was strong to make the inference as real-time for detecting the chicken weight based on image shape. This was acceptable inference performance for chicken's rapid actions. We executed

10,000 times, 20,000 times and 30,000 times traning with 500 images which were classified into a verification image and a learning image at 8:2. The total number of training data learned was 1,596, and learning accuracy was evaluated with 100 verification images (total: 400 images for 4 ranks) using the trained weight data.

(3) Survey items

The survey was conducted to verify the performance of Chicken weight scale method with regards to ; 1- whether the leg ring attached the RFID tag can keep during the feeding or not. 2-whether it can be measured each chicken's weight data with RFID tag stably or not. 3- whether the measured weight data was accurate or not. 4- whether the weight inference system can be used for getting the progress of growth for chicken's weight, generated by AI(Deep Learning) based on Chicken's photos with Chicken weight scale.

RESULTS AND DISCUSSION

(1) Attachability of RFID Tag to leg ring

The attached RFID tag was dropped twice during the 4 feeding experiments, also there was a problem of the bonded part in the durability. It resulted from a lot of friction between the leg ring and the leg generated from the growth of chicken's activities and deterioration of the adhesion of glue by the manure and high environment temperature (around over 25 ℃). As a countermeasure, we devised a method of fixing RFID to a leg ring with a heat-shrinkable tube. This method was inexpensive and easy to install. In the 4th feeding experiment, the dropout of RFID did not occur. A picture of solution is shown in Fig.9. However, in future, we hope to make available suitable size leg ring with integrated RFID in the market.

Fig 9. Mounted the RFID tag with a heat-shrinkable tube for leg ring

(2) Chicken weight scale

In 4th feeding experiment, Chicken weight scale could record the weight data. We could show the weight gain transition of 10 chickens in Fig 10. Each data was generated based on the histogram of the chicken weight by day. There were some fluctuations of data. The following factors can be considered potential design issues. The representative weight data of each chicken might not be maximum frequency weight value. We observed the scene which the chicken stayed one leg with RFID put on the scale, the other leg put on the ground for long time, in this case, the scale generated lower weight value , (since chicken weight was lower than actual weight) was recorded every second. In other case, if one chicken remains on the scale, other chicken pass over, the scale could not capture the pass though chicken's ID. Also in some cases, when the chicken passed through the scale quickly, the weight value was on transition to target value, but the weight could not reach the target number due to slow response of load
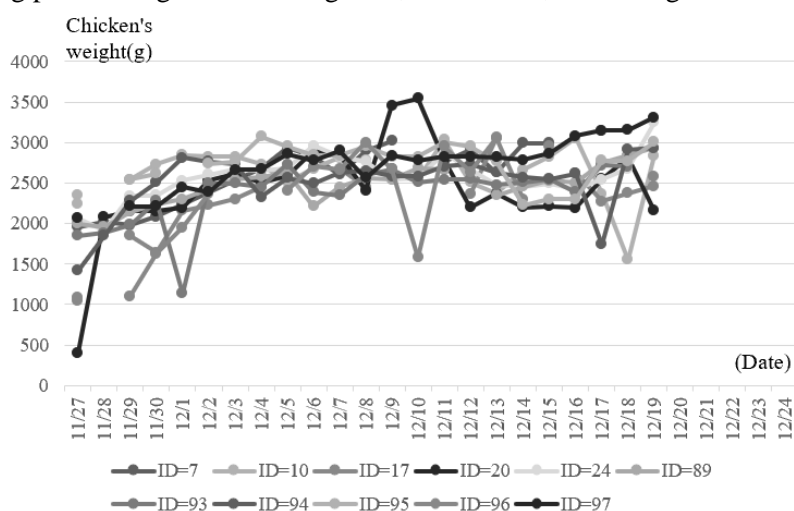
Fig. 10 The weight gaming of 10 chickens on 4th feeding experiments captured with Chicken weight scale

cell. It could not record over 2,500g weight, there were gaps between the actual weight value which are shown in Fig.11 and weight scale value which showed in Fig. 12 as one chart. The solution should be set multiple load cell to make the quick response and capture the more accurate weight.

There is absence of weight data for some birds, this can be attributed to the chicken's quick passing through over the scale. Or it might be the health problem, where the chicken was not active. This is one of key indicator to check the chicken's health, behavior.

From the feeding experiments, it was pos-
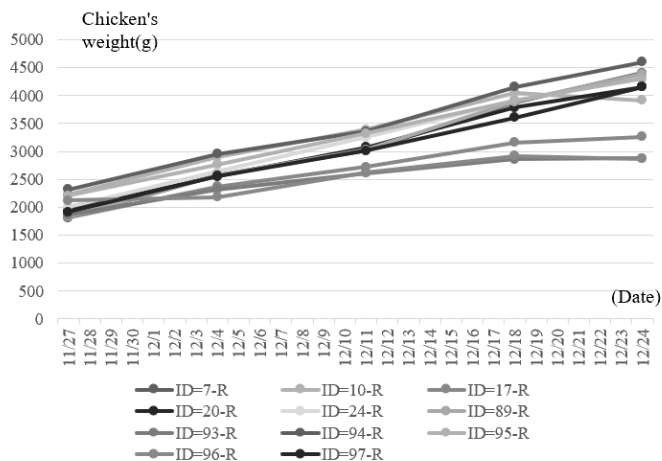
Fig. 11 The weight gaming of 10 chickens on 4th feeding experiments Actual measured weight
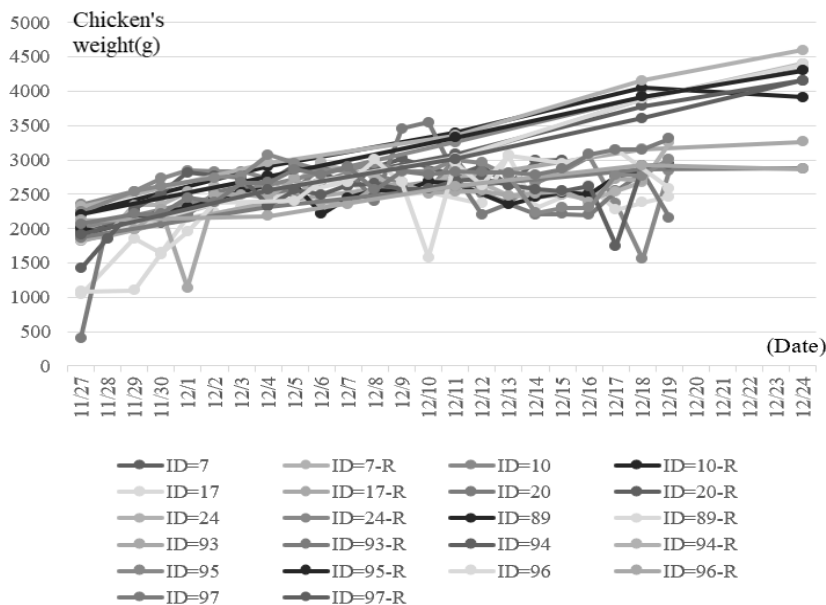
Fig. 12 The weight gaming of 10 chickens on 4th feeding experiments captured with Chicken weight scale and Actual measured weight (-R)

sible to obtain the behavior and weight transition of the chicken in day by day, and it will help to estimate the target date when they will achieve the target weight based on the feeding curve. It will help for preparation of shipping beforehand.

(3) Chicken weight inference by Deep Learning

The weight inference performance result by Deep Learning (AI) is shown in Table 3. and weight inference by AI picture is shown in

ght classification by AI

Fig.13 (Example, ID=97, 2,000g) . We tested 10 pcs of test images for each class (1,700g, 1,800g, 1,900g, 2,000g) and 5 times testing to make sure the AI performance. As a result, the recognition rates of the 2,000g class was 100%, which was acceptable performance, however for the 1,700g, 1,800 g and 1,900 g classes the recognition rate were under 30%, these need to

	Chicken's weight range(g)	1st test(%)	2nd test(%)	3rd test(%)	4th test(%)	5th test(%)	Average(%)
10,000 times tranined weight file	1,700	10	10	40	50	10	24
	1,800	10	10	0	10	30	12
	1,900	20	20	40	0	10	18
	2,000	100	100	100	100	100	100
	Average	35	35	45	40	37.5	**38.5**
20,000 times tranined weight file	1,700	10	10	40	50	10	24
	1,800	10	10	0	10	30	12
	1,900	30	20	40	0	10	20
	2,000	100	100	100	100	100	100
	Average	37.5	35	45	40	37.5	**39**
30,000 times trained weight file	1,700	10	10	40	50	10	24
	1,800	10	10	0	10	30	12
	1,900	30	20	40	0	10	20
	2,000	100	100	100	100	100	100
	Average	37.5	35	45	40	37.5	**39**

improve. This resulted from insufficient training images and missing labelled images which should be include varieties of scenes of chicken's behaviour. Usually automating and tracking behavorial measurement of animals is challenging especially when there is more than one animal in close proximity as they often cross touch resulting in partial occlusion ([*6]Hong et al., 2015). The chicken's captured shape should be considered as against the stable shape, example is the closing of the wings almost the same as captured position. Training with a variety of chicken shapes/pose should be explored. In addition, the classified weight ranks range should be considered and expanded, the classified ranks of example are 1,000 g, 1, 500g, 2,000g, 2,500g.

Fig.13 ID=97, 2,000g weight inference by AI

CONCLUSIONS

In this study, we used RFID as a method for individual management of chicken and verified a method of chicken's behaviour detection by Deep Learning based on chicken brooding video. From the experiments:

1) A robust method of attaching the RFID tag on leg ring during the experimental feedings was determined.

2) We discovered a mechanical architecture issue in chicken weight scale it should prevent other chickens from passing over when a chicken is staying on scale, the aisle will have to be   re-designed.

3) We found the accuracy issue of weight data when it is close to 2,000g, multiple load cells should be used to get quick response to measure the weight.

4) The possibility of utilizing video-based chicken growth management system by AI was demonstrated. The future progress, this system could be useful for the management of the growth situation based on the change of chicken weight and the shipping forecast without human resource.

REFERENCES

1. Brown-Brandl T. M. et al. (2017). A Review of passive Radio Frequency Identification System For Animal Monitoring In Livestock Facilities. In *Applied Engineering in Agriculture (in press)* (pp. 2-4).

2. Feng, J. et al. (2013). Development and evaluation on a RFID-based traceability system for cattle / beef quality safety in China. *Food Control*, *31*(2), pp 314-325. doi: https://doi.org/10.1016/j.foodcont.2012.10.016

3. Hong, W., Kennedy, A., Burgos-artizzu, X. P., Zelikowsky, M., Navonne, S. G., & Perona, P. (2015). Automated measurement of mouse social behaviors using depth sensing, video tracking, and machine learning (pp. 1). doi: https://doi.org/10.1073/pnas.1515982112

4. Ministry of Agriculture, Forestry and Fisheries (2018). *Livestock statistic.* Retrieved from http://www.maff.go.jp/e/data/stat/

5. Redmon, J. et al. (2018). YOLOv3: *An Incremental Improvement*. University of Washington.

6. Wanjie L. et al. (2015). Modeling and Implementation of Cattle/Beef Supply Chain Traceability Using a Distributed RFID-Based Framework in China.

Corresponding author:

Shigeru Ichiura., Agricultural and Environmental Engineering, Biotic Environmental Science, The United Graduate School of Agriculture Sciences, Iwate University (UGAS), (Production Machinery Lab, Faculty of Agriculture, Yamagata University), 1-23 Wakaba-cho, Tsuruoka, Yamagata,, 997-0028, Japan phone: +81 90-3499-3352, e-mail: axk308@tds1.tr.yamagata-u.ac.jp

TORREFACTION UPGRADING OF PALM OIL EMPTY FRUIT BUNCHES BIOMASS PELLETS FOR GASIFICATION FEEDSTOCK BY USING COMB (*COUNTER FLOW MULTI-BAFFLE*) REACTOR

Dewi Agustina IRYANI[1,6], Agus HARYANTO[2,6], Wahyu HIDAYAT[3,6], AMRUL[4,6], Mareli TALAMBANUA[2,6], Udin HASANUDIN[5,6], Sihyun LEE[6]

[1]*Department of Chemical Engineering, Faculty of Engineering, University of Lampung, Indonesia*
[2]*Department of Agricultural Engineering, Faculty of Agriculture, University of Lampung, Indonesia*
[3]*Department of Forestry, Faculty of Agriculture, University of Lampung, Indonesia*
[4]*Department of Mechanical Engineering, Faculty of Engineering, University of Lampung, Indonesia*
[5]*Department of Agro-industrial Technology, Faculty of Agriculture, University of Lampung, Indonesia*
[6] *Research and Development Center for Tropical Biomass,University of Lampung, Indonesia*
[7]*Climate Change Research Division, Korea Institute Energy Research, Republic of Korea*

Abstract
The paper is focused on upgrading of Palm oil empty fruit bunches (EFB) pellets by using rapid torrefaction process. This study aims to evaluate the effects of torrefaction on the main energy properties of EFB pellets. The torrefaction process was conducted on range temperature of 250-350 ˚C by using COMB (Counter Flow Multy-Baffle) Reactor with 3 minutes of residence time. The properties of raw pellets and torrefied pellets such as the caloric value, energy density, ash content and mineral compositions, fixed carbon, volatile materials, lignin, holocellulose, extractives, and water immersion of pellets were analyzed in order to study the effect of torrefaction process on the pellets properties changes. The analytical results showed that the initiating heating value and carbon content of raw EFB pellet are 15.82MJ/kg, and 47 .24 % increased up to 16.20 MJ/kg. 17.90 MJ/kg, 47.70 and 62,06 wt%d.b, subsecquentially for brown and black pellets. In case of moisture content, the initial EFB pellets has 9.21% decreased up to 8.97, and 7.80 %, subsecquentially for brown and black pellets. The obtained results revealed significant differences for all of main physical and energy properties of pellets. The torrefaction is able to upgrade the EFB pellets which having higher caloric value, carbon content, and lower water adsorption.. Therefore, the torrefied EFB pellets are potential to apply as a solid fuel for gasification feedstock or others thermal applications.

Key words: Pellet biomass, Palm oil solid waste, Torrefaction, Biomass pellets, Solid biofuel

INTRODUCTION

The production of palm oil in the world is dominated by Indonesia and Malaysia, with the account for around 85 to 90 percent of total global palm oil production. Indonesia is the largest producer and exporter of palm oil worldwide. Palm oil production in Indonesia has increased dramatically over the past decade. The data Indonesian Palm Oil Association (Gapki) stated that Indonesia would able produce 40 million tons of crude palm oil per year starting from 2020.

Production of crude palm oil consist of several stages from the sterilization of the EFB to the digestion, threshing and clarification of the oil cooking. In palm oil industry, to produce 1 ton of crude palm oil required five tonnes of fresh fruit bunches (FFB) *(Hambali, & Rivai, 2017)*. Alongside palm oil production, the industry also produce several different form of waste as well, such as liquid palm oil mill effluent (POME), empty fruit bunches (EFB), mesocarp fibres, shell, and kernel . Presently, the solid waste such as fibres and shell are used as boiler fuel to produce high pressure steam for turbines in power generation of energy in palm oil mill. While, another solid waste such as EFB and shell are not being utilized.

In the palm oil mill with plantation, EFB mainly utilized as mulch or compost for palm oil plantation. The EFB which placed around the young palms is able to control weeds, prevent erosion and maintain the soil moisture *(Oviasogie, et al., 2010)*. However, in the mill with no plantation, the EFB is untilized properly. Whereas, in the palm oil mill, the utilization of EFB as a source of energy is avoided due to hydrophilic nature, high moisture content and low bulk density, low calorific value. Moreover, the EFB also contains high alkali metal especially potassium and silica *(Stemann, et al., (2013)*.

Therefore, in order to improve the fuel properties of EFB, the combination of pelletization and torrefaction were performed in order to alleviate the issues. Torrefaction was also known as mild form of pyrolysis that is carried out at temperatures range between 200 °C and 30 °C in a non-oxidising environment *(Nyakuma, et al., 2015; Uemura, et al., 2011; Prins, et al., 2006)*. The purpose of torrefaction is for drying and partial devolatization of biomass without affecting the energy content. Torrefaction is able to changes the properties to provide a better fuel quality for combustion and gasification applications *(Prins, et al., 2006)*. In this study, the effects of torrefaction on the main energy and the properties of the EFB pellets such as the caloric value, ash content and mineral compositions, fixed carbon, volatile materials, lignin, holocellulose, extractives, and water immersion of pellets were evaluate. In addition, torrefaction process was conducted on the temperature range of 250-300 ˚C by using COMB (Counter Flow Multy-Baffle) Reactor with 3 minutes of residence time.

MATERIALS AND METHODS
2.1 Material

Palm oil (*Elaeis guineensis*) empty fruit bunch (EFB) pellets from one of pellet producer which is located in Tebing Tinggi, south Sumatra (Toba Hijau Sinergy Corp.) was used for torrefaction feedstock. Prior torrefaction and drying by using COMB Reactor, the samples are characterized by using several analyst methods such as the caloric value, carbon content, energy density, ash content and mineral compositions, fixed carbon, volatile materials, lignin, holocellulose, extractives, and water immersion of pellets. The calorific value of pellets were analyzed using a Parr bomb calorimeter according to ASTM D240. The functional groups of feedstock and products were analyzed by using a Fourier Transform Infrared (FT-IR) spectrophotometer model Perkin Elmer 2000. All of characterization method were conducted in order to understand the effect of torrefaction treatment into the material. Therefore, the raw and the torrefied pellet were dried at 105°C until constant weight.

2.2. Methods
2.2.1. Torrefaction Process

The experiment on the EFB pellets torrefaction was mainly focusing on the determination of process parameters to produce torrefied pellet (black pellet) with optimum yield. Prior the torrefaction experiment, EFB pellets were sieved to separate find dusts and sorted/grouped based on pellet size, particularly its length. The sample of pellets was then torrefied in several experiment attempts, at least 5 runs for each biomass pellets were conducted prior to a successful black pellet production. The target temperature applied during torrefaction of pellets biomass was ± 300°C with a column difference between column-in and colum-top was ± 50°C. While, the other process parameters such as column pressure (flow rate), and feedstock feeding rate was varying depend on the feedstock characteristics such as pellet size, weight, and density. Prior to torrefaction process, feeding test was performed to determine the feedstock feeding rate during the torrefaction.

2.2.2. Characterization of Pellets

The moisture content of samples was determined through the air-dry and oven dry weights measurement using an analytical balance (Sartorius AZ6101,Göttingen, Germany) with a sensitivity of 0.01 g. The density of samples were evaluated by measuring their air-dry weight and volume. The composition of raw and torrefied pellets were determined following the method adapted from *Datta, et al. (1981)* with some modification. Before analyzing the composition of the EFB pellets as the raw material, a sample was extracted using ethyl alcohol to determine the wax content using a soxhlet extractor over 8 h at 80 °C. 150 mg of the de-waxed sample was then dried and treated with 1.5 ml of 72 wt% H_2SO_4 at 30 °C for 1 h. 42 ml of water was added to the treated sample and hydrolyzed for 1 h in an autoclave at 121°C. The hydrolyzed sample was cooled, and then filtered and washed several times with hot water. The residue was noted as a Klason lignin (i.e. acid insoluble solid residue) and was dried at 105°C overnight. The composition of polysaccharide such as hemicellulose and cellulose were determined by using the method which adapted from *Datta (1981)*. The raw and torrefied pellets were further characterized by several methods. Proximate analysis was performed following ASTM standard E-870-06. The ash content was determined by measuring the weight of sample before and after heating a 1.0 g sample at 575°C

for 5 h. The EAS Vario EL cube CHN elemental analyzer was used to measure the elemental composition of the solid products. The caloric value or energy content was determined by using Milne Bomb Calorimeter CAL2K ECO.In addition, for the purpose to identify the chemical structure and functional groups of the raw and torrefied pellets, the Fourier transforms infrared (FTIR) spectrometer (100 Perkin Elmer, MID IR spectrometer) was also performed by using the KBr disk technique (1 mg of sample/100 mg of KBr). The samples were recorded in the range of 400 - 4,000 cm^{-1}.

RESULTS AND DISCUSSION
The Appearance of torrefaction feedstock and products

Figure 1 shows the alteration colors of pellets before and after the torrefaction. The samples are denoted; **a** – Raw (un-torrefied) EFB pellets; **b** – Brown torrefied pellets**; c** – Black torrefied. The alteration color of torrefied EFB pellets from brown to black is mainly attributed to chemical compositions of biomass changes *(Salca, et al., 2016)*.
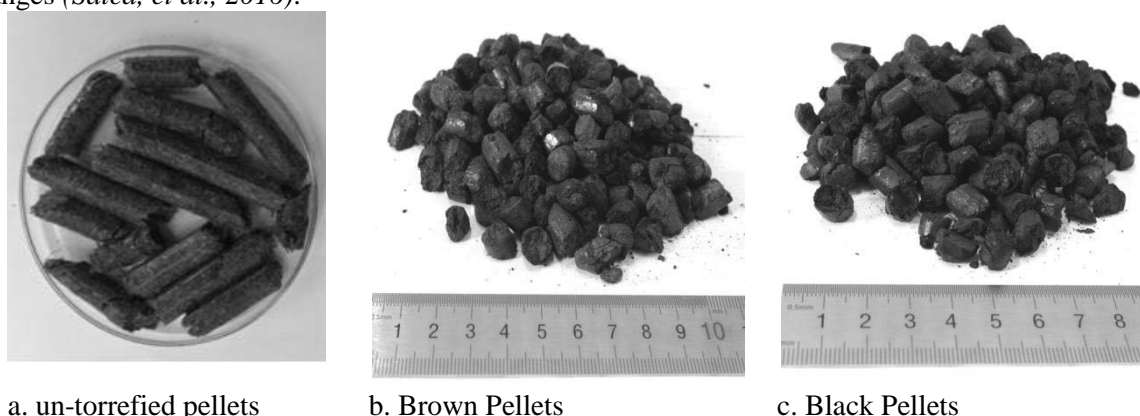
a. un-torrefied pellets   b. Brown Pellets   c. Black Pellets
Fig.1 The apperance of raw and torrefied samples of EFB pellets

Ultimate and Proximate Properties

Table 1 presents the results of the ultimate and proximate values of raw EFB pellets and torrefied. The content of carbon (C) of the torrefied pellets was enhanced by 1.3 times higher than raw EFB pellets, while oxygen (O) and hydrogen (H) content were drastiscally decreases. The reduction of H and O content leads to the dehydration and deoxigenation reactions occurred during the treatment, thus significantly enhancing the heating value (HV) of the torrefied products. The values of atomic H/C and O/C ratios in raw sample were 0.14 and 0.96, respectively. After the torrefaction, the values were changed into 0.12–1.10 and 0.95–0.49, respectively. This result implies that the H/C and O/C values decreased due to the deoxygenation, dehydration and carbonization reactions occurred during the processes. The reaction occurs due to the oxygen-containing functional groups with high activity, moreover low activation energy were easy to crack or recombine to release the CO and CO_2 *(Chen, et al., 2011)*. Moreover, as it was state in the previous paper *(Prins, et al., 2006)* that the solid fuel with low O/C ratios produce the higher gasification efficiencies than fuels with high O/C ratio. Furthermore, the biofuels with highly oxygenated are not perfect fuels for gasifiers from an exergetic point of view. Therefore, the modification of the properties of biomass are more attractive than gasifying these biomass as fuel directly *(Prins, et al., 2006)*.

Tab. 1 Ultimate and proximate properties of raw and torrified EFB pellets (% d.b)

Pellets Sample	C	H	N	O (diff)	MC	VM	FC	AC	HV (MJ/kg)
Raw	47.24	6.63	0.82	45.32	9.21	27.08	63.61	9.0	15.82
Brown	47.70	6.35	0.99	45.54	8.97	22.21	69.84	13.0	16.20
Black	62.06	5.76	0.63	30.96	7.81	18.05	72.84	11.0	17.90

d.b dry basis, *diff*. difference, *VM* volatile matter, *FC* fixed carbon, *AC* ash content, *HV heating value*

Chemical Composition Analysis Results of EFB Pellets

The chemical compositional changes were measured by gravimetric quantification of each component, as indicated in Tab. 2. The fraction of each component in the raw and torrefied samples is presented based on 100 g of the initial biomass. The result shows those hemicelluloses fractions are more easily degraded by thermal treatment compared with cellulose and lignin. The hemicellulose was easier to be decomposed than other polymers due to its branched structure and lower degree of polymerization *(Iryani, et al., 2017)*. Differ with hemicellulose, the cellulose has a greater thermal stability due to their structure which is consist of a long glucose polymer without branches, linked by strong β-(1,4)-glycoside bonds. In case of lignin, the analytical result shows that, the content of lignin tends to increase after the torrefaction. The lignin content increased due to char, re-polymerization products, condensation reactions, and saccharide decomposition products of hemicellulose attached on the surface of the solid material which then leads the dark solid color. This result is in line with the previous research *(Salca, et al., 2016)* which was stated that the alteration of biomass color after torrefaction is related to the degradation of hemicellulose during the process.

Tab. 2 Chemicals composition of pellets (% d.b)

No	Sample	Hemicellulose	Cellulose	Lignin	others
1	Raw EFB Pellets	26	35	17	22
2	Brown Pellets	17	35	21	27
3	Black Pellets	15	35	31	19

Fourier Transforms Infra Red (FTIR) Results Analysis

The FTIR spectroscopy was used to investigate the change of chemical structure before and after the torrefaction. The spectral data provides a simple characteristic comparison between the raw and the torrefied pellets. All of the peaks were confirmed with literature data *(Iryani, et al., 2017; Pastorova, et al., 1993)*. The FTIR spectral data showed a peak around 3300 cm^{-1} that is attributed to an –OH group. Comparing the FTIR spectra of the raw and torrefied pellets, the –OH group peak tend to decreased after the treatment. This result is in line with the data of MC presented in Tab. 1. This result indicates that the hydrogen-bonded –OH groups of hemicellulose of wood was gradually degraded. The peak changes were most apparent in black pellets. The peak in the range of 2928–2940 cm^{-1} is attributed to the aliphatic CH$_n$ groups and also weakens indicating fragmentation and decomposition of the polymer chains. The peak in the range of 1720–1740 cm^{-1} represents C=O stretching vibrations of un-conjugated ketone, carbonyls, ester groups; and C=O of acetyl group in xylan (hemicellulose) become weaker after the torrefaction. The peak of the C–O–C aryl–alkyl ether linkages was detected around 1247 cm^{-1}. The peak of the β-glycosidic linkages between glucose in cellulose was observed in the range of 874–897 cm^{-1}. The peaks around 1608, 1500, and 1408 cm^{-1} correspond to the C=C linkages of aromatic groups in the lignin. The peaks around 1608 and 1408 cm^{-1} suggest that lignin in the feed material was almost stable during the torrefaction and remained in the torrefied product.
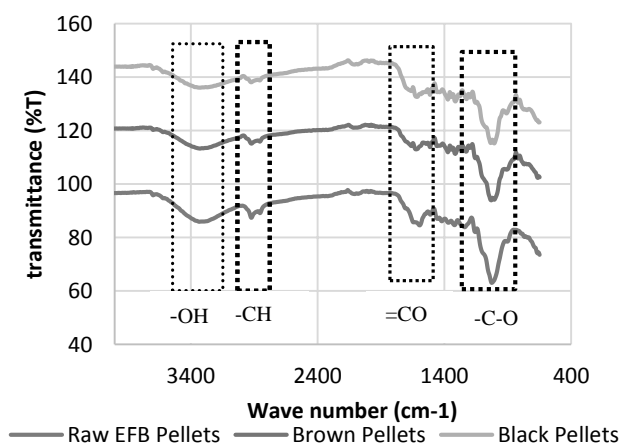
Fig 2. FTIR spectra of raw and torrefied Pellets

Hygroscopic property of EFB pellets
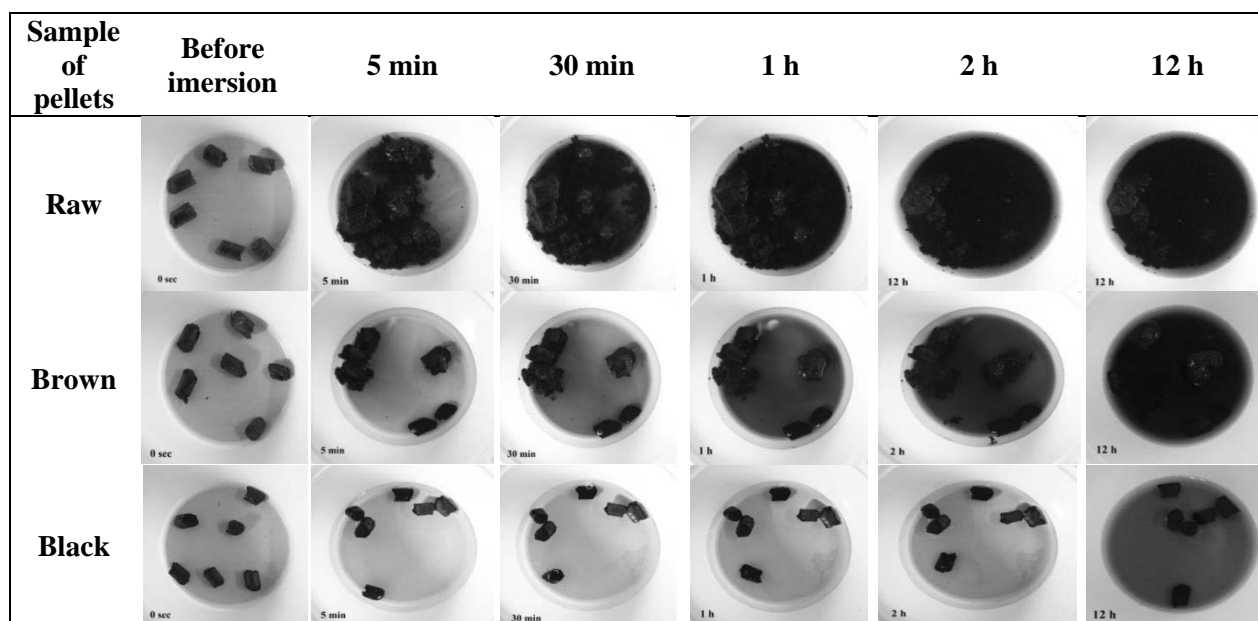
Fig. 3 Water absorption test of the raw and torrefied pellets.

The hygroscopic property of biomass pellets was tested by water absorption test (**Fig. 3**). The water immersion test which was conducted for 5 min, 30 min, 1 h, 2 h, and 12 h showed that the raw pellets fully disintegrated after 30 min. The Black pellets showed no significant disintegration even after 12 h test which is an advantage for long period storage of pellets. The results showed that the hygroscopic property of the raw pellets altered from hydrophilic into hydrophobic after torrefaction. The hydrophobic property of the torrefied pellet is one of their main advantage because moisture uptake by torrefied pellets is almost negligible even under severe storage conditions. It is generally known that the uptake of water by raw biomass is due to the presence of OH groups. Torrefaction produces a hydrophobic product by destroying -OH groups and causing the biomass to lose the capacity to form hydrogen bonds *(Pastorova, et al., 1993)*. Due to these chemical rearrangement reactions, non-polar unsaturated structures are formed, which preserve the biomass for a long time without biological degradation, similar to coal *(Prins, et al., 2006; Chen, et al., 2011)*.

The mineral Compositions Comparison of Raw and Torrefied Pellets

Tab. 3 presented the comparison of the mineral compositions of raw and torrefied pellets. The minerals compositions were analyzed using the X-ray fluorescence (XRF) analysis. The results confirmed the presence of K_2O, CaO, SiO_2, Al_2O_3 and Fe_2O_3 in the sample the result shows that the torrefaction can be slightly reduced the mineral content such as SiO_2, P_2O, CaO and K_2O.

Tab. 3 The mineral composition of raw and torrefied pellets

Element	Unit	Raw	Brown Pellet	Black Pellet
MgO	%	1.21	1.35	1.44
Al_2O_3	%	0	10.06	10,36
SiO_2	**%**	**10.45**	**0**	**0**
P_2O_5	%	2,457	1,292	0
SO_3	%	3.57	2,418	2.34
Cl	%	6.60	6.62	5.97
K_2O	**%**	**51.58**	**44.25**	**46.19**
CaO	%	17.71	14,87	14.83
TiO_2	%	0.19	1.03	1.03

Cr_2O_3	%	0.31	0.48	0.68
MnO	%	0.35	0.83	0,869
Fe_2O_3	%	5.08	15.94	15.76
ZnO	%	0.733	0.19	0.18
Rb_2O	%	0.22	0.45	0.500

CONCLUSIONS

The torrefied pellets or the black pellets of EFB was succesfully produced with good main energy properties. The results showed the reduction of moisture content after the torrefaction of biomass pellets. The improvement in the hygroscopic behaviour was also observed, showing a more hydrophobic product after torrefaction. The heating value of pellets remarkably increased after the torrefaction with COMB. The results proposed that torrefaction by using COMB technology could produce could produce friable, hydrophobic, and energy-rich fuel which ideal for gasification feedstock.

ACKNOWLEDGMENT

REFERENCES

1. Hambali, E. & Rivai M. (2017). The Potential of Palm Oil Waste Biomass in Indonesia in 2020 and 2030. IOP Conf. Series: Earth and Environmental Science 65 012050, 1-10.
2. Oviasogie, P.O., Aisueni, N.O., & Brown, G. E. (2010). Oil Palm Composted Biomass: A Review of the Preparation, Utilization, Handling and Storage. African Journal of Agricultural Research 5(13), 1553-1571.
3. Stemann, J., Erlach, B., & Ziegler, F. (2013). Hydrothermal carbonisation of empty palm oil fruit bunches: Laboratory trials, plant simulation, carbon avoidance, and economic feasibility, Waste and Biomass Valorization 4(3), 441–454.
4. Nyakuma B.B, Ahmad, A. Johari, A, Abdullah, A.T., & Oladokun, O. (2015). Torrefaction of Pelletized Oil Palm Empty Fruit Bunches, Proceeding of The 21st International Symposium on Alcohol Fuels – 21st ISAF, Gwangju, Korea.
5. Uemura, Y., Omar, W.N., Tsutsui, T., & Yusup S.B. (2011) Torrefaction of Oil Palm Wastes, Fuel 90, 2585–2591.
6. Prins. M.J, Ptasinski, K.J., & Jansen F.J.J.G. (2006). More efficient biomass gasification via torrefaction, Energy 31, 3458‑3470.
7. Datta, R. (1981). Acidogenic Fermentation of Lignocellulose-Acid Yield and Conversion Of Components, Biotech. and Bioeng. 23(9): 2167-2170.
8. Salca, E. A., Kobori, H., Inagaki, T., Kojima, Y., & Suzuki, S. (2016). Effect of heat treatment on colour changes of black alder and beech veneers. J. Wood Sci. 62(4): 297-304.
9. Chen Q., Zhou J.S., Liu B., Mei Q.F., & Luo Z.Y. (2011). Influence of Torrefaction Tretreatment on Biomass Gasification Technology, Energy Science & Technology 56(14), 1449–1456.
10. Iryani, D.A., Kumagai, S., Nonaka, & M., Sasaki, K., Hirajima, T. (2017). Characterization and production of solid biofuel from sugarcane bagasse by hydrothermal carbonization. Waste Biomass Valor. 8:1941–1951.
11. Pastorova, I., P.W. Arisz, & J.J. Boon. (1993) Preservation of d-glucose oligosaccharides in cellulose chars. Carbohydrate Research. 248:151–165.

Corresponding author:

Dr. Eng. Dewi Agustina Iryani, Department of Chemical Engineering, Faculty of Engineering, University of Lampung, Indonesia phone: +6281293638980, e-mail: dewi.agustina@eng.unila.ac.id

INFLUENCE OF ECOLOGICAL FLUID ON THE WET DISC BRAKE SYSTEM OF THE TRACTOR

Juraj JABLONICKÝ[1], Peter OPÁLENÝ[2], Daniela UHRINOVÁ[1], Juraj TULÍK[1], Lazar SAVIN[3]

[1]*Department of Transport and Handling, Faculty of Engineering, SUA in Nitra, Slovakia*
[2]*Klueber Lubrication Austria, Salzburg*
[3]*Department of Agricultural Engineering, Faculty of Agriculture, University of Novi Sad, Serbia*

Abstract
The article is focused on the operating measurements of the wet disc brake system of the tractor. Operating measurements were evaluated after tractor's operation of 500 Eh on the 3rd, 4th and 5th gear. The reference fluid and the ecological fluid were tested during operation. In addition, the results of the work include the evaluation of the fluid samples taken from the operational tests to monitor the tractor's braking performance with wet disc brakes. Fluid samples were also tested for changes in their physical properties. Results of the operating measurements evidence that applied reference fluid neither the ecological fluid had negative effect on the minimum braking performance. Also, the physical properties analysis of the tested fluids did not prove their negative impact on the tractor wet disc brake system.

Key words: *agricultural machinery; deceleration; biodegradable oil; physical analysis.*

INTRODUCTION

Agricultural technology has a negative impact on all elements of the environment (*Kučera et al, 2016, Vitázek et al. 2018*). The constant increasing of vehicles number causes air pollution and soil and water contamination by ecologically harmful substances. It was reported that over 60% of all lubricants end up in soil and water (*Majdan et al, 2013*). Environmental protection is an actual topic already for several years, and it becomes a preferred problem in the established trend of economic development (*Tóth et al, 2014; Majdan et al, 2018*). Therefore, the producers of mobile energy machinery together with the oil and lubricants manufacturers develop special products that save the environment (*Vitázek et al., 2018*). Application of suitable biodegradable oils markedly reduces the environmental, sewerage and pathway damage by oil leakage into the environment (*Janoško et al., 2014; Vitázek et al., 2018; Janoško et al. 2010*). Reported by *Tkáč et al. (2014)*, vegetable oils are capable to contribute to the goal of energy independence and security since they are a renewable resource. The amount of biodegradable oils in the market is quite low. There is a catch-up to make a stronger pressure for using biodegradable oils as fillings of hydraulic circuits and gearboxes (*Hujo et al. 2015; Kosiba et al. 2013*). Green technologies and machinery will become an essential part of everyday life *(Janoško et al., 2016)*.

In addition to acceleration, the movement of the mobile energy machinery also results to deceleration, uses the braking system. Study (*Kamiński & Czaban, 2012*) states that effective braking system of the vehicle is essential for safety during the transportation. Regards to the road safety, the braking systems of agricultural vehicles must meet several requirements, including the braking performance. The one type of braking system which uses an oil charge is wet disc brake. Friction elements and applied oil fillings are important parts of the wet disc brakes. Reported by *Mang (2010)*, friction is a passive resistance with opposite direction of action, such as relative motion of the friction surfaces. Especially, the oil filling in the wet disc brakes can affect durability of friction elements, heat dissipation and associated braking performance. Reported by *Tkáč et al. (2014)*, mineral oils, synthetic fluids and ecological fluids are the most widespread in praxis to lubricate transmissions. Authors of the research Study (*Hujo, 2017*) and Study (*Tulík, 2013*) report as the main physical properties of lubricating and energy transfer fluids – viscosity, viscosity index, stability, oxidation, compressibility and shear stability. Viscosity may decrease of increase during the oil utilization. Reported by *Helebrant et al. (2001)*, the increase of viscosity may be caused by oxidation products or impurities in the oil. On the contrary, its decrease may be caused by mechanical and thermal degradation of its additives. *Stopka (2017)* states, that oils with low viscosity index provide the thin thickness of lubricating film resulting

in lubrication boundary conditions. That leads to metal to metal contact and the damage of system components. If two moving metal surfaces contact each other due to insufficient lubrication, excessive wear may occur as a result of so-called cold welding.

Aim of this article was to provide the operational measurements in Zetor Super 5321 tractor's wet disc brake system. The oil reference sample and biodegradable oil sample were tested. The results were evaluated in accordance with established methodology. Subsequently, the braking performance of the tractor's wet disc brake was evaluated, and the physical properties of the used fillings were determined. Testing of these oils should demonstrate whether the reference oil sample can be fully replaced with biodegradable oil and find out the extent to which the wet disc brakes affects the degradation processes in tested oils.

MATERIALS AND METHODS
Characteristics of the reference fluid
As the reference fluid, it was used the oil containing additives to increase the loading capacity of the lubricating film. Basic parameters of the reference fluid are shown in Tab. 1. It is a mineral oil that always guarantees good lubricating properties, high oxidation resistance and high loading capacity. The reference fluid is designed to lubricate the mechanical transmissions of vehicles and drive axles if required oils SAE 80W – 90 with API GL – 4 performance level. The oil can be used for lubrication of mechanical transmissions and axle drives of cars and trucks, construction and agricultural machinery and other transmission applications.

Tab. 1 Basic parameters of the reference fluid

Properties	Units	Values
Density at 40ºC	kg. m^{-3}	878
Kinematic viscosity at 40ºC	mm^2.s^{-1}	146
Kinematic viscosity at 100ºC	mm^2.s^{-1}	15
Viscosity index	–	103
Freezing point	ºC	–27

Characteristics of the ecological fluid
Ecologic universal synthetic tractor oil was used as biodegradable oil. Basic parameters of the ecological fluid are shown in Tab. 2. This oil is assigned for manual gearboxes, axle drives, crankshaft transmissions, steering and gearing transmission, hydraulic systems of tractors and their auxiliary units, for wet brakes, clutches and hydrodynamic transmissions.

Tab. 2 Basic parameters of the ecological fluid

Properties	Units	Values
Density at 40ºC	kg. m^{-3}	899
Kinematic viscosity at 40ºC	mm^2.s^{-1}	80
Kinematic viscosity at 100ºC	mm^2.s^{-1}	15
Viscosity index	–	202
Freezing point	ºC	–48

Service brake measurement methodology
The service brake was measured according to the Methodological Guideline of SR No. 71/2011 that specify control sequence relating to the vehicles braking system. The purpose of the measurement was to determine the maximum braking performance values of the tractor's oil brakes. Under the prescribed conditions, the vehicle shall be capable to achieve prescribed minimal braking performance values of the service brake expressed by deceleration (z_{min}). For comprehensive assessment of the service brake and to assess the effect of biodegradable oil on the service brake, the measurements were executed after 500 Eh of the machine's operation and three gears engaged. Therefore, tractor was monitored for deceleration values with gradual engagement of 3rd, 4th and 5th gear. The tractor uses the reference fluid as an oil fill. The reference fluid had been replaced by ecological fluid at service interval. Based on the

measurements of service brake deceleration with reference fluid, it was possible to compare these data with those obtained with the measurements with ecological fluid. At 3rd and 4th gear, the tractor did not exceed the rate 25 km. h^{-1}, so the deceleration values were compared with minimal value of deceleration $z_{min} = 23\%$. At 5th gear, the tractor achieves maximal rate 30 km. h^{-1}, so the deceleration values were compared with minimal value of deceleration $z_{min} = 28\%$.

The methodical sampling procedure of tested hydraulic fluid was regulated by the standard STN 65 6207 (Hydraulic oils and liquids). After the operational tests, the physical properties analysis of tested oils was executed. The evaluation process was focused on the changes of water content, acidity number, density and dynamic viscosity after 500 Eh of tractor's operation. The viscosity and density measurements were performed by Stabinger viscometer "Anton Paar" method by the standard STN EN 16896 – kinematic viscosity test, petroleum and related products. Total acid number (TAN) is used to test the number of acidic components in the oil sample. Methodical sampling evaluation procedure on the change of TAN was executed by the standard ASTM D 644 A. The measurement of the water content in the oil was performed by the Karl Fischer (KF) titration method.

RESULTS AND DISCUSSION

Deceleration is defined as the ratio between the total braking force F to the axle (axles) of the vehicles and causal static total mass forces Gv (vehicle mass). The deceleration corresponds to the braking deceleration and gravitational acceleration ratio. Reported by *Rybiansky et al. (2009)*, if the prescribed deceleration is reached or exceeded, the deceleration value is enough.

Minimal deceleration values with reference fluid

Based on the achieved results, minimal deceleration values given by legislation were exceeded by 2.70% (3rd gear), by 10.00% (4th gear) and by 6.50% (5th gear). The average values from three consecutive measurements at 3rd, 4th and 5th gear at 500 Eh are shown in Tab. 3.

Tab. 3 Deceleration values with reference fluid

	3rd gear	4th gear	5th gear	
Braking path, s_0	3.59	5.12	11.26	m
Initial speed, v_0	12.11	19.52	29.94	km. h^{-1}
Braking time, T_{br}	1.75	1.81	3.30	s
Braking deceleration, MFDD	2.52	3.24	3.39	m. s^{-2}
Deceleration, z	25.70	33.00	34.50	%

Minimal deceleration values with ecological fluid

Based on the achieved results, minimal deceleration values given by legislation were exceeded by 9.60% (3rd gear), by 9.10% (4th gear) and by 1,35% (5th gear). The average values from three consecutive measurements at 3rd, 4th and 5th gear at 500 Eh are shown in Tab. 4.

Tab. 4 Deceleration values with ecological fluid

	3rd gear	4th gear	5th gear	
Braking path, s_0	2.50	6.67	18.10	m
Initial speed, v_0	12.47	19.96	29.97	km. h^{-1}
Braking time, T_{br}	1.30	2.10	3.26	s
Braking deceleration, MFDD	3.20	3.15	2.88	m. s^{-2}
Deceleration, z	32.60	32.10	29.35	%

Evaluation and physical analysis of the tested oils – change of dynamic viscosity

Dynamic viscosity values are defined by linear function. The linear function of dynamic viscosity at 40°C for reference sample can be calculated by equation (1)

$$\eta_{40} = -0.0226t + 127.53 \qquad \text{mPa. S} \qquad (1)$$

where t is time in engine hours (Eh).

The linear function of dynamic viscosity at 40°C for ecological fluid can be calculated by equation (2)

$$\eta_{40} = -0.0116t + 72.232 \qquad \text{mPa. s} \qquad (2)$$

Presented in Fig. 1, the course of dynamic viscosity at 40°C depending on the hours of operation is shown. It is possible to observe the decrease of dynamic viscosity values depending on the hours of operation. Reported by *Paar (2019)*, brake liquids must fulfil specifications mainly at -40 °C and +100 °C. Most producers state values at + 40 °C and give the viscosity index. There are three main types of brake fluids which are classified by their different chemical base as polyglycolether/borate ester, silicone oil and mineral oil. This is the reason why they do not mix with each other. Reported by *Wójcik (2019),* it was noted that used brake fluid was characterized by lower viscosity and higher density. The viscosity stays constant in the whole range of a shear rate. Additionally, the decrease of viscosity with the increase of temperature was also observed. By *Čorňák & Skolil (2008),* the change of brake fluid viscosity is affected not only by temperature but also by water content.

Evaluation and physical analysis of the tested oils – change of density at 40°C

Density is expressed as a ratio of mass to a given volume. For liquids, temperature is an important factor that can affect a liquids density. In general, as liquid temperature increases, density decreases. Presented in Fig. 2, the course of density at 40°C depending on the hours of operation is shown. It is possible to observe the higher density values of ecological fluid compared to reference fluid. Study *(Koshizuka et al., 2018)* states that fluid density is important for fluid simulations because mass conservation is expressed by the fluid density and the pressure is calculated by fluid density.
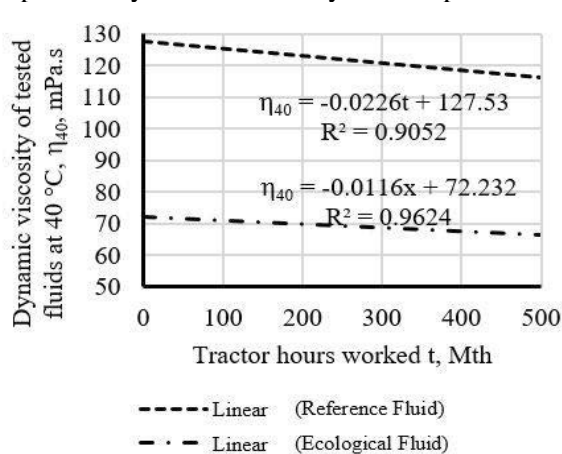
Fig. 1 Course of dynamic viscosity at 40°C depending on the hours of operation
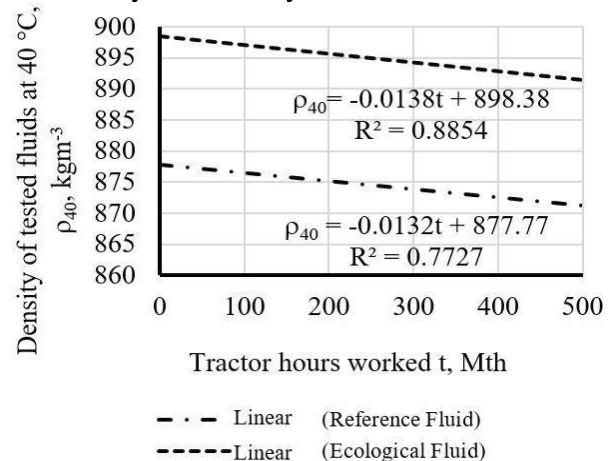
Fig. 2 Course of density at 40°C depending on the hours of operation

Evaluation and physical analysis of the tested oils – change of TAN

Acid Number or Total Acid Number (TAN) is used to test the quantity of acidic components in an oil sample. Presented in Fig. 3, the change of TAN depending on the hours of operation is shown. It is possible to observe the higher TAN values depending on the hours of operation. By *Mantech (2016)*, acid number results are used as a guide in the quality control of lubricating oils. The rate of change of the acid number is more important than its absolute value. A rapid increase can be caused by many factors, including excessive degradation due to hotspots from dirty oil ways, top-up with different oil, or a change in fuel sulphur content. More commonly, a steady increase in acid number may be caused by oxidation over time or temperature effects. High operating temperatures can generate increasing levels of weak organic acids. Oils with a high acid number will form undesirable gums and lacquers on metal surfaces. High acid numbers are also associated with increased viscosity of pumping losses and system corrosion – especially in the presence of water.

Evaluation and physical analysis of the tested oils – change of water content

Water content values are defined by linear function. The linear function of water content for reference sample can be calculated by equation (3)

$$S_{H2O} = -2E - 06t + 0.0038 \qquad \% \qquad (3)$$

where *t* is time in engine hours (Eh).

The linear function of water content for ecological fluid can be calculated by equation (4)

$$S_{H2O} = -2E - 06t + 0.0212 \qquad \% \qquad (4)$$

Reported by *Giani (2018),* brake fluid is an essential part of a vehicle's hydraulic braking system. Above the critical moisture content, the force applied to the brake pedal is not be transferred to the rest of the system, and the brake system fails. Presented in Fig. 4, the course of water content change depending on the hours of operation is shown. It is possible to observe, that the course of line is almost linear.
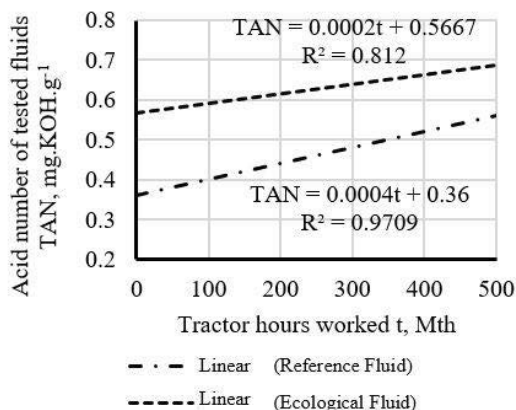
Fig. 3 The change of TAN depending on the hours of operation
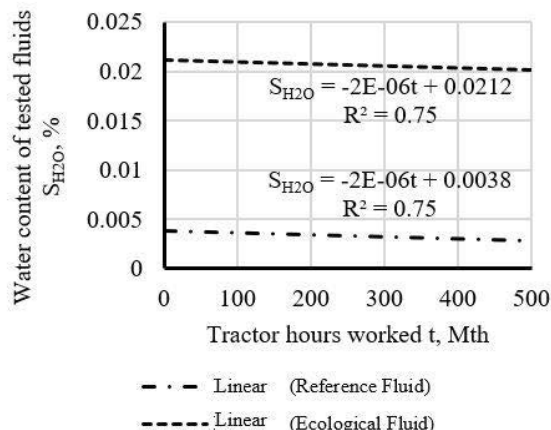
Fig. 4 The water content change depending on the hours of operation

Based on the laboratory analysis of the tested oils, the above – mentioned limits of water content had not been exceeded. The coefficient of water content determination for both tested oils is $R^2 = 0.75$. Maximal permissible value for hydraulic oils is 0.1% and for gear oil 0.3%. The results presented in this paper cannot be compared with already published studies, as it is an innovative research. The comparison of the influence of the oils (mineral and synthetic) on the wet discs brake system and deceleration had not been published yet. Wet braking system measurement methodology used in this contribution was developed during measurement based on the Methodological Guideline of SR No. 71/2011.

CONCLUSIONS
Operating measurements in Zetor Super 5321 wet disc brake system were determined. Two types of the oil fluids were tested – reference oil sample and biodegradable oil. Results of the operating measurements evidence that applied reference fluid neither the ecological fluid had negative effect on the minimum braking performance. Physical properties changes of the tested oils are included in the results as graphical dependencies. The course of individual curves was defined by linear functions to determine the coefficient of determination. The values of determination coefficient and consistent counted mean error of correlation coefficient σ_r certified the reliability of the correlation coefficient which establishes the cleanness degree of the tested oils. The correlation coefficient confirms the results of physical analysis of the tested oils. Both of oils show only minor changes of their physical properties after completion of operating measurements. They do not cause corrosion and any negative impact on the tractor wet disc brake system had not been found.

REFERENCES

1. ASTM D644 (2015). Standard Test Method for Acid Number of Petroleum Products by Potentiometric Titration [Standard]. - [s.l.]: Hach Company/Hach Lange GmbH.

2. ASTM D6595 – 00 (2011). Standard Test Method for Determination of Wear Metals and Contaminants in Used Lubricating Oils or Used Hydraulic Fluids by Rotating Disc Electrode Atomic Emission Spectrometry [Standard]. - [s.l.]: ASTM International.

3. Čorňák, Š. & Skolil, J. (2008). Research of brake fluids viscosity properties. *Advances in Military Technology, 3*(2): 5-10.

4. Giani, S. (2018). Boiling point and water content determination in hydraulic brake fluid testing. In *UserCom Analytical Chemistry No. 22*. Mettler Toledo International.

5. Helebrant, F., Ziegler, J. & Marasová, D. (2001). *Technická diagnostika a spolehlivost I*. Tribodiagnostika – Ostrava: VŠB – Technická univerzita, ISBN 80-7078-883-6.

6. Hujo, Ľ. (2017). *Návrh laboratórneho zariadenia pre skúšanie hydrostatických prevodníkov a hydraulických kvapalín využívaných v mobilných energetických prostriedkoch* [Habilitačná práca]. Nitra: Slovenská poľnohospodárska univerzita v Nitre, p. 158.

7. Hujo, Ľ., Kangalov, Plamen G. & Kosiba, J. (2015) *Laboratory test devices for evaluating the lifetime of tractor hydraulic components:(proceedings, methods and applications)*. 1st ed. Ruse: University "Angel Kanchev" of Ruse. 69 p. ISBN 978-954-712-665-7.

8. Janoško, I., Černecký, J., Brodnianska, Z. & Hujo, Ľ. (2016). *Environmentálne technológie a technika*. 1. ed. Nitra: Slovenská poľnohospodárska univerzita. 306 p. ISBN 978-80-552-1604-1.

9. Janoško, I., Polonec, T. & Lindák, S. (2014). Performance parameters monitoring of the hydraulic system with bio-oil. *Research in agricultural engineering, 60*(special iss.), 37-43. ISSN 1212-9151,

10. Janoško, I., Šimor, R. & Chrastina, J. (2010). The bio-oil testing used in the hydraulic system of the vehicle for waste collection. *Acta technologica agriculturae, 13*(4), 103-108. ISSN 1335-2555.

11. Kamiński, Z. & Czaban, J. (2012). Diagnosing of the agricultural tractor braking

15. Majdan, R., Olejár, M., Abrahám, R., Šarea, V., Uhrinová, D., Jánošová, M. & Nosian, J. (2018). Pressure Source Analysis of a Test Bench for Biodegradable Hydraulic Oils. *Tribology in Industry 40*(2), 183-194.

16. Majdan, R. Tkáč, Z. & Kangalov, P. G. (2013). *Research of ecological oil-based fluids properties and new test methods for lubrication oils: scientific monograph.* 1st ed. Rousse: Angel Kanchev University of Rousse, 98 p.

17. Mang, T., Bobzin, K. & Bartels, T. (2010). *Industrial Tribology: Tribosystems, Friction, Wear and Surface Engineering, Lubrication.* ISBN 9783527320578.

18. Mantech Inc. (2016). Application Note #67 – Total Acid Number (TAN).

19. Metodický pokyn č. 71/2011, ktorým sa stanovujú kontrolné úkony týkajúce sa brzdovej sústavy vozidla vykonávané pri technických kontrolách vozidiel (kontrolné úkony skupiny 200) (2011). MDV SR. TESTEK SK.

20. Paar, A. (2019). Viscosity of Automotive brake fluid – viscosity table and viscosity chart.

21. Rybianský, M., Kuchynka, R., Ondrejka, P. & Hron, P. (2009). *Použitie valcovej skúšobne na vyhodnotenie účinku bŕzd v znaleckej praxi*. Bratislava: TESTEK, s. r. o.

22. Tkáč, Z., Kangalov, Plamen G. & Kosiba, J. (2014). *Getting ecological of hydraulic circuits of agricultural tractors*. 1st. ed. Ruse: University of Rousse "Angel Kanchev", 2014. 120 s. ISBN 978-619-7071-63-4.

23. Tkáč, Z., Majdan, R., & Kosiba, J. (2014). *Výskum vlastností ekologických kvapalín a nových testovacích metód mazacích olejov*. Nitra: Slovenská poľnohospodárska univerzita v Nitre, 94 p. ISBN 978-80-552-1140-4.

24. Tóth, F., Rusnák, J., Kadnár, M. & Váliková, V. (2014). Study of tribological properties of chosen types of environmentally friendly oils in combined friction conditions. *Journal of Central European Agriculture 15*(1), 185-192.

25. Tulík, J. (2013). *Analýza vlastností hydraulických kvapalín používaných v hydraulických systémoch dopravnej a manipulačnej techniky* [Dizertačná práca].

system within approval tests. *Eksploatacja i Niezawodnosc – Maintenance and Reliability, 14*(4), 319–326.

12. Kosiba, J., Tkáč, Z., Hujo, Ľ., Stančík, B. & Štulajter, I. (2013). The operation of agricultural tractor with universal ecological oil. *RAE, 59*(special iss.), 27-33. ISSN 1212-9151.

13. Koshizuka, S., Shibata, K., Kondo, M. & Matsunga, T. (2018). Chapter 2 – Fundamentals of Fluid Simulation by the MPS Method. Moving Particle Semi – Implicit Method (A Meshfree Particle Method for Fluid Dynamics), pp. 25 – 109.

14. Kučera, M., Aleš, Z. & Pexa, M. (2016). Detection and characterization of wear particles of universal tractor oil using of particles size analyser. *Agronomy Research 14*(4), 1351-1360.

Nitra: Slovenská poľnohospodárska univerzita v Nitre.

26. Vitázek, I., Majdan, R. & Mojžiš, I. (2018). The speed maps of selected combustion engines. In *KOKA* (pp. 220-227). 1. ed., 237 p. ISBN 978-80-552-1880-9. Nitra: SPU,

27. Vitázek, I., Tulík, J. & Klúčik, J. (2018). Combustible in selected biofuels. *Agronomy Research, 16*(2), 593-603. ISSN 1406-894X.

28. Vitázek, I., Tkáč, Z. & Mojžiš, I. (2018). Evaluation of drive type properties based on engine-speed maps. In *37th meeting of departments of fluid mechanics and thermodynamics*. 1. ed. ISBN 978-0-7354-1716-8. Melville: AIP Publishing, 4 p.

29. Wójcik, M (2019). Rheological properties of new and used brake fluids. *Acta Mechanica Slovaca 22*(4), 50-54. ISSN 1335-2393.

Corresponding author:
Ing. Daniela Uhrinová, Ph.D., Department of Transport and Handling, Faculty of Engineering, Slovak University of Agriculture in Nitra, Tr. A. Hlinku 2, Nitra, 949 01, Slovak Republic, phone: +421 37 61 4537, e-mail: daniela.uhrinova@uniag.sk

THE EFFECT OF DIESEL ADDITIVE ON EMISSIONS AND ENGINE PERFORMANCE

Ivan JANOŠKO[1], Patrícia FERIANCOVÁ[1]

[1]Department of Transport and Handling, Faculty of Engineering, Slovak University of Agriculture in Nitra

Abstract
The article is focused on the impact assessment of the additives used in diesel fuel to improve the power and emission parameters of the vehicle and its consumption. The usage of additives in engine fuels have an increasing tendency. The manufacturers claim that additives have positive impact on engine operating parameters, cleaning the fuel supply system and decreasing fuel consumption by improving the engine combustion process. In the diesel fuel is often used as 2-ethylhexyl nitrate ($C_8H_{17}NO_3$) based fuel additives summer version. Measurements were performed under laboratory conditions with the help of the MAHA MSR 500 test bench where we performed driving cycles selected by authors with pre-selected external conditions and time intervals (constant engine speed and constant load). Focus have been given on tracking of the vehicle's external speed characteristic and measurement of selected parameters: CO, NO_x, fuel consumption and smoke. The resultant values of the driving cycles measured before and after application of additives to the fuel was compared. The result of the experiment was find, that when was used the fuel additive, performance and torque, fuel consumption and emisssions were improved.

Key words: *fuel additive VIF; smoke; diesel engine; engine speed characteristic.*

INTRODUCTION

The increase of road transport (especially the individual transport) is a worldwide problem in the major part of cities. The fast growth of the world population and industrial development is linked with an increasing consumption of fossil fuels (*Rievaj et al., 2018*; *Jindra et al., 2016).* The increasing traffic intensity brings many negative impacts. The most significant negative impacts of transport include the noise, vibration and production of harmful exhaust emissions as CO, CO_2, NOx, HC and particulate matters. The exhaust gases emitted from the engine often get into the human respiratory tract and may cause headaches, irritation of the mucous membranes in eyes and throat and cause cancer (*Küüt et al. 2015*). The European Union annually orders automakers to reduce the production of harmful pollutants into the air. Therefore automakers are trying to reduce the amount of pollutants generated by combustion. Methods of reducing emissions are provided by various technologies such as particulate filters. Emissions can also be reduced by reducing of the engine volume, reducing fuel consumption or using charged engines. Developments in the field of technology bring with their positive impact and increase of life quality also undesirable side effects. One of the severe adverse effects of the scientific and technical progress is environmental pollution (*Lenďák, et al., 2014; Jablonický, et al., 2012; Králik, et al., 2015; Jablonický, et al., 2019*). Fuel consumption can be affected by driving, but also with the right choice of fuel or additive to fuels. Since diesel fuel has a biofuel content, which also has negative characteristics such as clogging injectors, it also causes rapid oxidation in the fuel system, the formation of deposits in the fuel tank and in the winter months reduces the fuel filtration point. The main goal of the additive is to improve the basic properties such as increasing the cetane number, improving the lubricity properties, avoiding oxidation, which ultimately has a positive effect on the life of the engine as well as on the lifetime of the fuel system (*Jablonický et al., 2012*).

Several additive manufactures such as: Castrol TDA, STP, Liqui Moly, Sheron, Ekolube, Valvoline, VIF and Tectane claim that their products improve technical state of fuel injection system by cleaning and improve cold engine starts, increase octane number. Some manufacturers guarantee decreases of fuel consumption in range of 2-7 % and improvement in emissions. For testing, we chose an additive from company Lang Chemie whose name is VIF because it is one of the most commonly used in Central Europe.

The aim of study was to assess the impact of the additives used in diesel fuel on the vehicle's power, emission parameters and consumption.

MATERIALS AND METHODS

The aim of the contribution was to evaluate the effect of selected Super diesel from VIF manufacturer on the power and emission parameters along with the fuel consumption for the diesel. The tested vehicles is Volkswagen Passat (Fig.1) category M1 with the 2.0 TDI diesel engine with CR injection pump. The vehicle's main parameters are displayed in Table 1.

Fig. 1 Tested vehicles Volkswagen Passat 2.0 TDI (164k km)

Tab. 1 Main parameter of tested vehicle

Vehicle	Volkswagen Passat
Year of manufacture	2011
Engine type	TDI, CR
Cylinders capacity	1,968.0 cm³
Emission regulations	EURO 4
Post-treatment emission systems	NKAT, EGR
Highest engine power/speed	103 kW / 4,150 min⁻¹
Operating weight	1,601 kg
Number of driven axles	1 / front
Number of driven kilometres	164,500

Characteristics of working mediums

During measurements were used fuel from brand Slovnaft. It was a basic range of fuels without the additive with the trade name Tempo plus diesel. In the tank contained approximately 25 liters what was half the capacity of the tank. Pumped diesel fuel met the requirements of standard EN 590 and also satisfies the conditions of the World Association of Automobile Manufacturers. During the testing was used winter diesel fuel, which has a lower temperature of filterability compared to summer diesel fuel. As tested additive was chosen known and in practice often used Super diesel additive made by VIF in a plastic bottle with 125 ml. It is a product constructed on the basis of 2-ethylhexyl nitrate, the manufacturer indicates improvement in the cetane number by 5 units, better combustion, reduced engine noise and lower fuel consumption by 5%. The additive serves to disposable one for 40 to 60 liters of fuel. In the tests, the entire volume of the additive was used, ensuring a dosing ratio of up to 1: 200 or, 0.125 l: 25 l.

Characteristics of the instruments
Fuel flowmeter

Due to inaccurate measuring of fuel consumption by a vehicle on-board computer, it was necessary to use a different, more accurate system. We used an AIC-5004 Fuel Flowmaster external fuel meter from AIC SYSTEMS AG, which joined the car's fuel system in its engine compartment

Performance roller dynamometer:
To measure the performance of the vehicle was used performance dynamometer by the German manufacturer MAHA with the designation MSR 500 with the possibility of measuring 4-wheel drive.

Fig. 2 Performance roller dynamometer MAHA MSR 500

Exhaust gas analyser

To detect quantity of emissions in the exhaust gas was used analyser from brand MAHA and model MGT 5 / MDO2 - LON. It is a dual instrument to record the production of both petrol and diesel emissions.
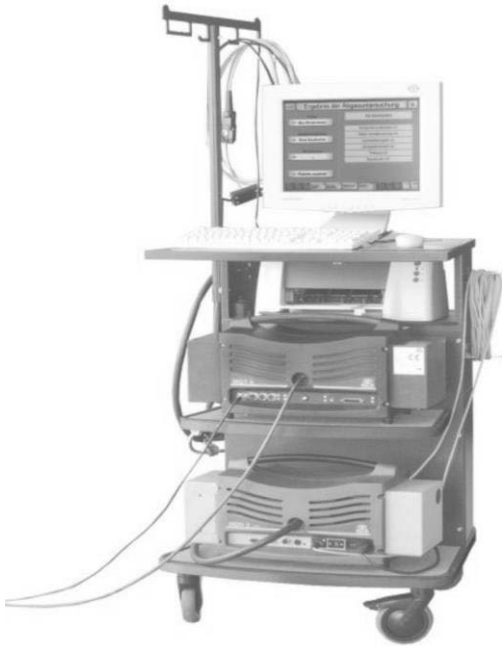
Fig. 3 Exhaust gas analyser - MGT 5 / MDO2 – LON by brand MAHA

The course of measurement

The measurement process itself consisted of several important steps: fixing the car on the roller, connection of the flowmeter, exhaust gas analyser, oil temperature probe and pairing the vehicle via OBD diagnostics with a computer to record all values from the control unit and the devices to the computer. After completion of the initial steps, the engine had to be warmed to the operating temperature to ensure the most accurate and trusted results.

It was necessary to calculate and analyse measured parameters using the basic following relationships:

Calculation of performance P

$$P = M_k . \omega = M_k . 2 . \pi . n \qquad \text{[kW]} \qquad (1)$$

Calculation of torque M_k

$$M_k = \frac{P}{2.\pi.n} \qquad \text{[Nm]} \qquad (2)$$

The quantity of fuel V'' consumed for the selected period of time

$$V' = V_2 - V_1 \qquad \text{[dm}^3. (30s^{-1})] \qquad (3)$$

Hourly fuel consumption V

$$V = \frac{V'.\rho_{fuel}}{t} . 3600 \qquad \text{[kg.hod}^{-1}] \qquad (4)$$

RESULTS AND DISCUSSION

Based on the external engine speed characteristics obtained from the MAHA performance dynamometer, it was possible to assess and compare the performance parameters of the vehicles. As can be seen in Table 2, after comparing the results, it was concluded that the diesel power increased by 0.8 kW and torque by 3.3 Nm, that was in range of dynamometer measurement inaccuracy (2%). Therefore, we do not consider measured values as significant in terms of performance improvement.

Tab. 2 Comparison of average performance parameters before and after adding additive to diesel

Vehicle	Parameter	Before using the additive	After using the additive
Volkswagen Passat	Corrected performance [P_{norm}]	108.6 kW 4405 min^{-1}	109.4 kW 4385 min^{-1}
	Torque [M_{norm}]	316.6 N.m^{-1} 2345 min^{-1}	319.9 N.m^{-1} 2395 min^{-1}

Another examined parameter was the influence of fuel additive on engine emissions. This was performed as a sequence of 5 consecutive measurements before and 5 measurements after addition within the specified time range. Similarly, to the measurement of emissions we measured the fuel consumption by using a flow meter that was connected to the fuel system of the car. The values of these measurements were averaged and statistically analysed. The results are shown in Tables 3.

Tab. 3. The results of measuring emissions and fuel consumption on the VW Passat

Volkswagen Passat	Time of measurement	Value	Different	Standard deviation	Variation coefficient
Carbon monoxide CO (% of vol.)	before addition	0.10	- 0.07	0.015	0.103
	after addition	0.03		0.013	0.205
Oxid nitride NO$_x$ (ppmo)	before addition	102	- 4.0	0.65	0.164
	after addition	98		0.84	0.143
K-value (m^{-1})	before addition	0.131	- 0.04	0.028	0.183
	after addition	0.091		0.019	0.054
Fuel consumption (kg.hod^{-1})	before addition	5.84	+ 0.08	0.08	0.067
	after addition	5.92		0.07	0.058

The results of the experimental measurements show partially the positive effect of the selected additive on the fuel consumption and the emissions of the tested passenger car.

Measurement in Volkswagen Passat showed that CO emission decreased by 70 %, NO$_x$ emission decreased by 4 %. However, fuel consumption increased by 1 % therefore claimed statements by VIF producer to decrease fuel consumption in range of 5 % for diesel engine has not been confirmed by our measurements.

Janoško et al., 2018 presented in other works, that improvement alternatively worsening of emissions and performance parameters also depended on the mileage performance. Measurement in Renault Clio with gasoline engine volume 1,149.0 cm^3, 43 kW, 73k km mileage showed that CO emission decreased by 39.76 %, HC decreased by 60.27 %. However, fuel consumption increased by 7.36 %. Measured parameters in Škoda Octavia 1,9 TDI, diesel engine with the higher mileage (approx. 388k km) showed that smoke (K-value) decreased by 29.20 % and fuel consumption decreased too by 3.39 % while VIF producer claims decrease by 5%.

Other such complex works by other authors have not yet been monitored / published. There are only partial additive evaluations for some parameters listed in the introduction chapter. The assumptions for improvement of CO, NOx and smoke emissions have been confirmed (*Küüt et al. 2015; Lenďák, et al., 2014; Jablonický, et al., 2012, 2019*).

CONCLUSIONS

The aim of the paper was to evaluate the impact of the additives on the vehicle's power and emission parameters along with fuel consumption. This complex approach of additives testing brings more precise answers on energetical and emission changes in petrol and diesel engines.

Experimental measurements were performed in a test laboratory on preselected vehicle. For testing purpose, vehicle Volkswagen Passat with engine volume of 1,968 cm^3, 103 kW, 164k km mileage were chosen. The measurements partiality confirmed the additive manufacturer's claims about emissions improvement and performance parameter. In the case of a diesel engine, the difference was minor in range of dynamometer inaccuracy. We assume that the diesel additive does not have a significant effect on the engine's performance parameter, but it has a positive cleaning impact on the combustion chamber and emissions.

ACKNOWLEDGMENT

REFERENCES

1. Jablonický, J., Tkáč, Z., Majdan, R., Uhrinov,á D., Hujo Ľ, Vozárová, V. (2012). *Properties evaluation of biofuels and bio-lubricants.* Slovak University of Agriculture in Nitra.
2. Jablonický, J., Uhrinová, D., Tulík, J., Polerecký, J. (2019). Measurement of limited and unlimited emissions during burning of alternative fuels in the tractor's engines. In *Biofuels,* (pp. 67-80). 188 p. ISBN 978-1-78985-535-7. London: Intech Open. Retrieved from <https://www.intechopen.com/chapter/pdf-download/63045>.
3. Janosko, I. & Kuchar,P. (2018). Evaluation of the fuel commercial additives effect on exhaust gas emissions, fuel consumption and performance in diesel and petrol engine. ITMS 26220220180. *Agronomy Research*, *16*(3), 737-748
4. Jindra, P., Kotek, M., Mařík, J., & Vojtíšek, M. Effect of different biofuels to particulate matters production. *Agronomy Research*, *14*(3), 783–789.
5. Küüt, A., Ilves, R., Hönig, V., Vlasov, A., & Olt, J. The impact of bioethanol on two-stroke engine work details and exhaust emission. *Agronomy Research*, *13*(5), 1241–1252.
6. Králik, M., Jablonický, .J, & Nikolov, MI. (2015). *Monitoring of NOx emissions at selected diesel engine*. Angel Kanchev University of Ruse.
7. Lenďák P., Jablonický J., Uhrinová, D., Kosiba, J., & Polerecký, J. (2014). Possible solutions for checking particulate matter filters (DPF) in motor vehicles. *Advanced Materials Research, 1059* (spec. iss.), 119-125.
8. Rievaj, V., Vrabel, J., Synak, F., & Bartuska, L. (2018). The effects of vehicle load on driving characteristics. *Advances in science and technology-research journal*, *12*(1), 142-149. ISSN 2299-8624
9. Skrucany, T., Synák, F., Semanová, Š., Ondruš, J., & Rievaj, V. (2018). Detection of road vehicle's centre of gravity. In *11th International Science and Technical Conference Automotive Safety, AUTOMOTIVE SAFETY 2018* (pp.1-7).

Corresponding author:
Doc. Ing. Ivan Janoško, CSc., Department of Transport and Handling, Faculty of Engineering, Slovak University of Agriculture in Nitra, Tr. A. Hlinku 2, 949 76 Nitra, Slovak Republic, email: ivan.janosko@uniag.sk

STRAW PELLETS UTILIZATION FOR REDUCTION OF LIQUID MANURE HARMFUL GAS EMISSIONS

Algirdas JASINSKAS[1], Jonas ČĖSNA[2], Nerijus PAŠVENSKAS[2], Rolandas DOMEIKA[1], Kęstutis ROMANECKAS[3], Jiří MAŠEK[4]

[1]*Vytautas Magnus University, Agriculture Academy, Institute of Agricultural Engineering and Safety, Studentu 15A, Akademija, LT-53361,Kaunas reg., Lithuania*
[2]*Vytautas Magnus University, Agriculture Academy, Institute of Energy and Biotechnology Engineering, Studentu 15A, Akademija, LT-53361, Kaunas reg., Lithuania*
[3]*Vytautas Magnus University, Agriculture Academy, Institute of Agroecosystems and Soil Sciences, Studentu 11, Akademija, LT-53361, Kaunas reg., Lithuania*
[4]*Czech University of Life Sciences Prague, Faculty of Engineering, Kamycka 129, CZ – 165 21, Prague 6 – Suchdol, Czech Republic*

Abstract
Integrated pollution prevention and control systems are necessary to reduce the environmental impact of pollution from livestock farms and to prevent the transfer of pollutants from one environment to another. In intensive livestock farms, various technological and administrative measures should be taken in order to reduce environmental pollution, as the compatibility of these measures avoids the risk of contamination of the environment. The work was performed in Vytautas Magnus University Laboratory of Thermal Energy Processes and Emissions in 2018. The paper analyses the physical properties of wheat and rapeseed straw pellets and their application possibilities for liquid manure reservoir covering and the impact of straw granules on ammonia emission reduction. It has been found that ammonia emissions from liquid manure are reduced by 72-78% when coated by rapeseed pellets.

Keywords: *wheat; rapeseed; straw pellets; pollution; liquid manure; harmful emissions.*

INTRODUCTION

In livestock farms, the accumulation of manure is the main source of ammonia emissions. Evaporating chemicals enter the atmosphere and return to the soil with precipitation. Therefore, in order to solve such problems as climate change, soil erosion, air and environmental pollution, biodiversity loss, we must ensure that the development of livestock farming is based on the principles of sustainable development (*Aleknavičius, 2008*; *Maciukas, 2015*).

There are no reliable measures to protect the environment from harmful pollutants; however, ammonia emissions are decreasing in a loose cow barn, with more cattle shed and manure spreading (*Prakupimaite, 2009*). The impact of livestock farming reduces biodiversity, soil depletion, and water and air pollution. The most important greenhouse gases emitted from manure during anaerobic digestion are methane (CH_4) and nitrous oxide (N_2O) released during storage and use for fertilisation (*Bleizgys & Cesna, 2008*; *Juska, 2010*). Additional gas from manure is ammonia (NH_3) and nitrogen oxides (NO_x), which have an effect on odour generation and are an indirect source of nitrous oxide.

Ammonia is an atmospheric pollutant that promotes acidification of soil and surface water, eutrophication, deforestation (*Pereira et al., 2010*). It is formed by dropping manure, urine, and feed residues. It has been determined that 40% of all nitrogen (N) compounds polluting the atmosphere is ammonia. Another important source of ammonia release is liquid manure and slurry manure (*Mendes & Pieters, 2017*). Liquid manure is usually stored in metal or concrete reservoirs, less often in ponds, and slurry manure is kept in manure storages. To reduce ammonia release, manure storage is covered with various coatings (thick manure, chopped straw, wooden, plastic, clay granules, 2-3 mm thick oil layer, etc.) or roofing. All coatings have their own advantages and disadvantages that need to be assessed when choosing the method of covering the store (*Environmental requirements, 2011*).

The article analyses the use of straw granules for coverage of slurry manure reservoir. Pellets from wheat and rapeseed straw were selected for this purpose; physical properties of the pellets were evaluated, and their influence on ammonia emissions was measured. The aim of this article is to analyse the

physical properties of straw pellets and their application possibilities for liquid manure reservoir coating and to evaluate the influence of straw pellets on ammonia emission reduction.

MATERIALS AND METHODS

The research was carried out at Vytautas Magnus University, Agricultural Academy, Faculty of Agricultural Engineering, Laboratory of Thermal Energy Processes and Emissions. Liquid manure was used for the investigation of harmful gas emissions. The tested manure was taken from a 50-seat cowshed where manure was removed by a wheeled mini-loader, pushing it out of the manure removal path.

Firstly, pellets of wheat and rapeseed straw with the diameter of 9 mm were produced, using a small capacity granulator with a horizontal granulator matrix. Before the plants entered the granulator, they were mixed thoroughly to achieve homogeneity and moistened if were too dry for granulation. Using the dosage unit, the mixture was supplied to the press chamber, where it was moved by rollers through the matrix holes and pressed to form 9 mm pellets. When the pellets cooled, their biometric and physical-mechanical parameters (dimensions, moisture content, volume and density) were evaluated. The parameters of 10 pellets were determined by measuring their height and diameter (accurate to 0.05 mm), and pellet density was calculated.

Pellet moisture was determined by using a special drying oven. The pellets of both straw types were weighed before and after drying. The average humidity of the straw pellets was calculated.

Later, pellet strength (compression strength) was measured by using a physical-mechanical test instrument *Instron 5960*. Pellet strength properties are important for pellet transportation, storage and spreading on the manure surface, etc. Five repetitions with both types of pellets were performed. The test data was stored on the computer, then processed and analysed.

In order to determine which sort of straw pellets were the most suitable for liquid manure surface coating, pellet swelling properties and the optimal pellet layer were investigated. Pellets were immersed into water, and it was observed as they expand. The tests were performed 50 times with each type of granule, marking each pellet in a separate vessel with water and waiting for the pellet to swell. The length and diameter of the bead were measured after swelling. Subsequently, by comparing the granule expansion results and density, one type of bead was selected to cover the surface of the plastic container filled with liquid manure.

When determining the optimal pellet layer, four different pellet layers were tested. Each layer was weighed in order to calculate what amount of granules would be needed for slurry coverage. Tests were performed with 10 mm, 20 mm, 30 mm and 40 mm wheat straw and rapeseed straw granules. The layers were measured every two hours.

To determine the emissions and their variations, liquid cow manure was poured into separate plastic vessels. During the test, the first vessel was not mixed and in no way affected; the second and other containers were covered with straw pellets, increasing the coverage with every container. The emission changes were observed in each container, every minute; the data was collected by a meter-analyser.

RESULTS AND DISCUSSION

Firstly, physical-mechanical properties of produced wheat and rapeseed straw pellets were determined. Moisture content of wheat straw granules was $12.58 \pm 0.53\%$, and moisture content of rapeseed straw was about 20% lower and reached $10.08 \pm 0.17\%$. The average density of investigated wheat straw granules was 1074.6 ± 60.05 kg m^{-3}, and the average density of rapeseed straw granules was very similar and reached 1013.6 ± 47.42 kg m^{-3}. If compared to the results of other researchers, which have investigated biofuel and fodder pellets and briquettes, the density of pellets was-high enough and exceeded 1000 kg m^{-3} (*Siaudinis et. al., 2015; Kakitis et. al., 2011*).

The compression resistance of both types of granules was determined by using the Instron 5960 physical-mechanical test equipment. The results obtained by compressing the wheat straw pellets are presented in Fig. 1, and the results of the rape straw granules are presented in Fig. 2.
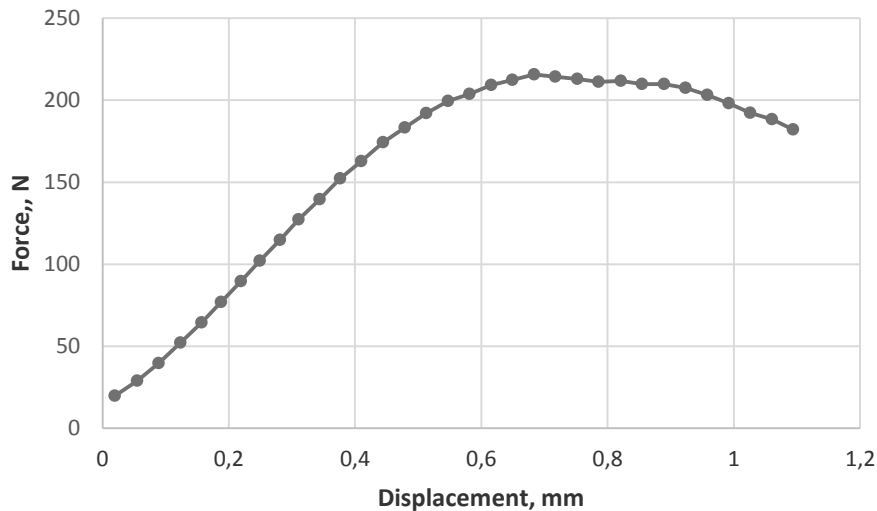
Fig. 1. Research results of wheat straw pellets strength
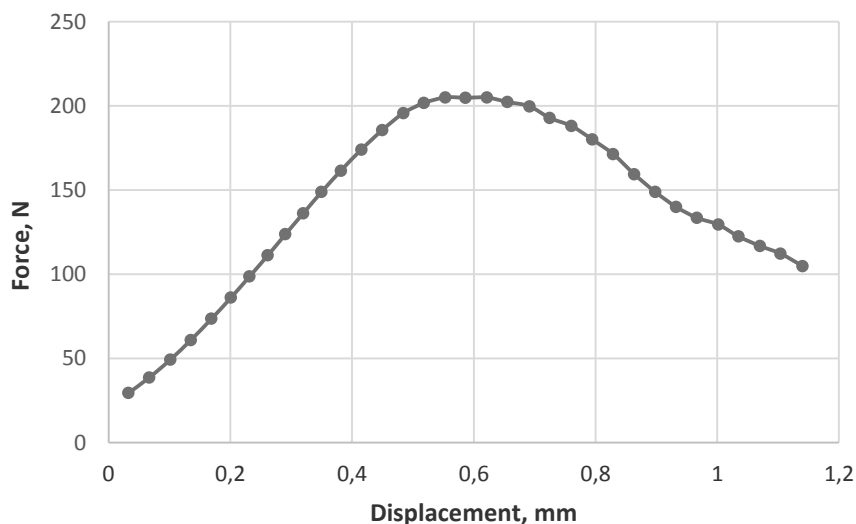
Fig. 2. Research results of rapeseed straw pellets strength

From the results presented in the graphs, it can be seen that–the strength of wheat straw pellets (average force is N, 215 N) is a little higher than that of rapeseed straw – the average force of 205 N is required for crushing rapeseed straw pellets. Therefore, wheat straw granules are more resistant to compression.

It can be noted that the investigated granule properties – moisture content, density, length, diameter and strength – meet the quality requirements for pellets made from plant biomass of the Ministry of Energy of the Republic of Lithuania. Therefore, further research is possible with the selected wheat straw and rapeseed straw pellets (*LAND 43-2013; Siaudinis et. al., 2015*).

After the investigation of the optimal pellet layer for liquid manure surface coating, it was detected that at the beginning, when pellets are filled with water, they float on the surface, but then settle down quickly on the bottom and then rise again. The tests of swelling duration of 10 mm and 20 mm pellet layers showed that the rapeseed pellets swelled up faster and formed a maximum protective layer approximately 12 hours after the start of the test, which changed slightly during the period of the observation hours (Fig. 3, Fig. 4).

To conclude, rapeseed straw pellet swelling duration is higher than that of wheat straw pellets, thus rapeseed straw pellets are more recommended for liquid manure surface coating.
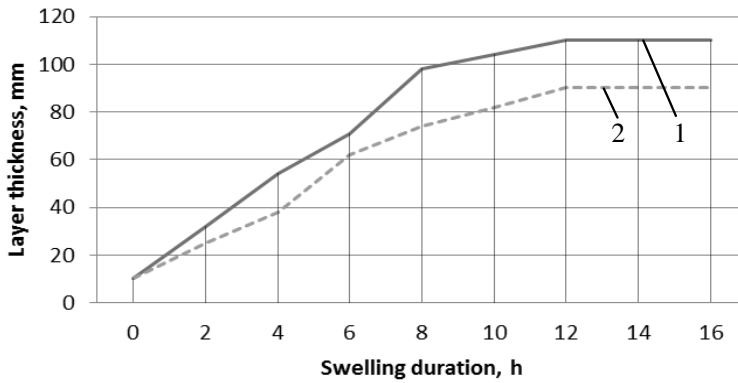
Fig. 3. Swelling duration of 10 mm pellet layer: 1 – rapeseed straw pellets; 2 – wheat straw pellets
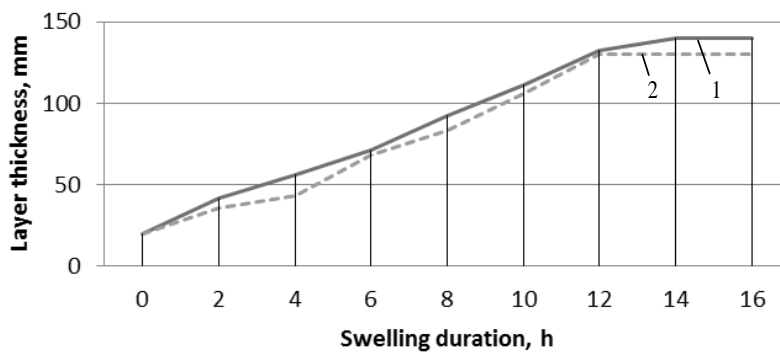
Fig. 4. Swelling duration of 20 mm pellet layer: 1 – rapeseed straw pellets; 2 – wheat straw pellets

The expansion of the rape straw granules layer was determined irrespective of the thickness of the deposited layer, which was always higher than that of the wheat straw pellets. On the average, wheat straw granule lengthens by 3.57 times, and the diameter increases by 1.45 times. Rapeseed straw granule lengthens by 3.1 times, but the diameter increases by 1.8 times. Therefore, rapeseed straw pellets were used for further research.

Further studies were carried out to determine the variation in ammonia emissions by comparing the uncovered liquid manure vessel with the vessel filled with rapeseed straw granules. 44 hours after the start of the test, the rapeseed pellets disintegrated.

From the graph presented in Fig. 5 it can be seen that the ammonia concentration in both vessels was similar at the start of the study and reached the 45 ppm in the first 20 hours of testing.
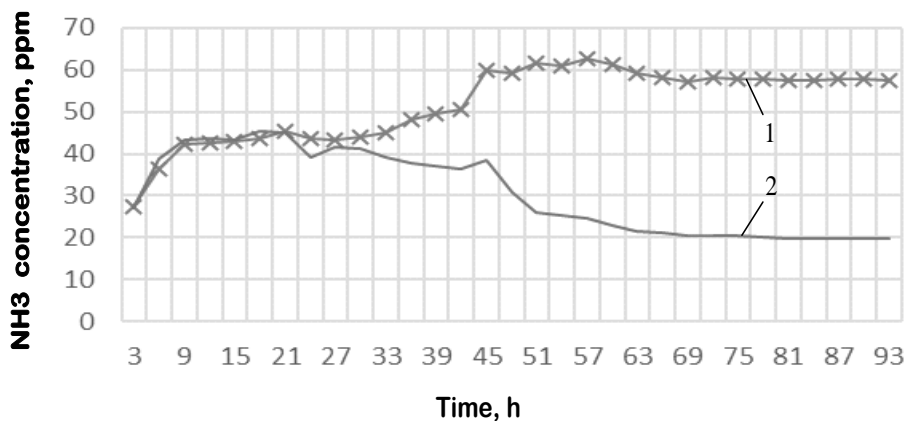
Fig. 5. Variation of ammonia emissions: 1 – liquid manure without coating; 2 – liquid manure with rape-seed straw pellets cover

Later, after 17 more hours, a clearer difference was apparent. In the first vessel, the concentration of ammonia was 50 ppm, and in the second vessel, which had been covered by pellets, the emissions decreased to 36 ppm. At the end of the test, 93 hours after the start of the test, the ammonia concentration in the dish without coating was 59 ppm; and in the container with the rapeseed straw granules it was 19.7 ppm.

Research results showed that a vessel, the surface of which was covered with rapeseed straw pellets, reduced emissions by 75%. Repeated studies showed similar data; emission reduction ranged from 72% to 78%.

These studies shall be continued and will evaluate other plant materials pressed to granules. The content of material and chemical analysis will be evaluated.

Based on the results of our research and other existing studies, it can be said that rape straw pellets are better suited for covering of liquid manure surface, because these plants contain more oil that better retains the emission of noxious gases (*Bleizgys & Cesna, 2008*; *Juska, 2010*).

CONCLUSIONS

Having analysed the main physical-mechanical properties of the produced wheat and rapeseed straw granules, it has been determined that the moisture of the granules varied from 10.08±0.17% to 12.58±0.53%; the average densities of investigated wheat and rapeseed straw granules were very similar and varied from 1013.6 ± 47.4 kg m^{-3} to 1074.6 ± 60.0 kg m^{-3}; the average critical compression resistance force of rapeseed straw reached 204.9 N and was smaller than the critical compression resistance force of wheat straw (215.8 N). Having performed granule swelling tests, it has been determined that the layer of swelled rapeseed straw is always higher than the layer of wheat straw. The impact of rapeseed straw granules on reduction of emissions was observed after 4 hours after the covering; the emission concentration varied from 43.5 ppm in a vessel without coating to 39 ppm in a vessel with rapeseed straw coating. After 93 hours, the emissions stabilised; the emissions of harmful gases were 75% lower in a vessel covered with rapeseed straw granules, comparing to the emissions of the vessel without coating.

REFERENCES

1. Aleknavičius, P. (2008). *Environmental and Environmental Management Law: Educational Book*. Kaunas. 84 p.

2. Bleizgys, R. & Čėsna, J. (2008). *Animal Husbandry Engineering. Educational Book*, 84 p.

3. Environmental requirements for manure and slurry management. (2011). Minister of Agriculture of the Republic of Lithuania, July 14 by Order no. D1-367 / 3D-342 (edit of order No. D1-735 / 3D-700 of the Minister of Environment of the Republic of Lithuania and Minister of Agriculture of the Republic of Lithuania of 26 September 2011) (in Lithuanian).

4. Juška, R., Juškienė, V. & Matulaitis V.R. (2018). Estimation of greenhouse gas (CH4 and N2O) emissions from different manure management systems (in Lithuanian). Retrieved from https://zum.lrv.lt/uploads/zum/documents/files/LT_versija/Veiklos_sritys/Mokslas_mokymas_ir_konsultavimas/Moksliniu_tyrimu_ir_taikomosios_veiklos_darbu_galutines_ataskaitos/darbasLGImeslsistatask.pdf.

5. Kakitis, A., Nulle, I., & Ancans, D. (2011). Mechanical properties of composite biomass briquettes, Environment. Technology. Resources. *Proceedings of the 8th international scientific and practical conference, 1*, 175–183.

6. LAND 43-2013. Emission rates for combustion plants (in Lithuanian).

7. Mačiukas, A. (2015). Manure Management. Retrieved from http://www.agrozinios.lt/portal/categories/217/1/0/1/article/12369/meslo-tvarkymas.

8. Mendes, B. & Pieters, J. (2017). Reduction of ammonia emissions from dairy cattle cubicle houses via improved management or design-based strategies: A modeling approach. *Sience of the Total Environment, 574*, 520-531.

9. Pereira, J., Misselbrook, T.H., Chadwick, D.R., Coutinho, J. & Trindade H. (2010). Ammonia emissions from naturally ventila-

ted dairy cattle buildings and outdoor concrete yards in Portugal. *Atmospheric Environment*, *44*(28), 3413-3421.

10. Prakupimaitė, I. (2009). Investigations of gas emissions from manure processes. Retrieved from http://gs.elaba.lt/object/elaba: 1869864/. 72 p.

11. Šiaudinis, G., Jasinskas, A., Šarauskis, E., Steponavičius, D., Karčiauskienė, D., & Liaudanskienė, I. (2015). The assessment of Virginia mallow (Sida hermaphrodita Rusby) and cup plant (Silphium perfoliatum L.) productivity, physicoemechanical properties and energy expenses. *Energy*, *93*(1), 606–612.

Corresponding author:

Ing. Algirdas Jasinskas, Ph.D., Institute of Agricultural Engineering and Safety, Faculty of Agricultural Engineering, Agriculture Academy, Vytautas Magnus University, Studentu 15A, Akademija, LT-53361 Kaunas reg., Lithuania, phone: +370 612 04002, e-mail: algirdas.jasinskas@vdu.lt

STUDY OF HHO GAS INFLUENCE ON OPERATING PARAMETERS IN CI ENGINE

Petr JINDRA[1]

[1]*Department of Department of Vehicles and Ground Transport, Czech University of Life Sciences Prague*

Abstract

Over the last decade, we have seen sustained growth in oil consumption. This has an adverse environmental impact. From a global point of view, there is a problematic increase in CO_2 production. Locally the increase in oil consumption manifests itself most often by environmental pollution by particulate matters or nitrogen oxides. In the European Union, individual car traffic accounts for about 20% of CO_2 production and continues to grow. The result is social and political pressure to reduce harmful emissions.

This study deals with an alternative way to reduce harmful emissions with HHO gas. That is generated by electrolysis. The resulting gas is mixed in the intake of the vehicle with ambient air. The presence of additional hydrogen and oxygen during combusting should affect the emissions produced without impact of power. A decrease in performance was observed during measurement, while CO_2 and NO_X emissions increased.

Key words: CO_2; NO_X; power; torque; emission.

INTRODUCTION

HHO is a mixture of oxygen and hydrogen produced by electrolysis of water. This mixture is colorless, odorless but extremely flammable. The main problem of HHO gas production is its energy intensity. This is changing due to material developments. Today's HHO generators have much higher efficiency than before *(Laurie Donaldson, 2016)*. This made it possible to reduce the size of the generator and thereby allow installation into the vehicle. HHO is a promising alternative fuel in this this time. Many scientists have conducted many researches and experiments about diesel or biodiesel and hydrogen usage *(Usta, Öztürk, Can, Conkur, Nas, Çon, Can & Topcu, 2005; Al-Baghdadi & Al-Janabi, 2000)*. Hydrogen presents properties that are unique from those of hydrocarbon fuels like a addition, this type of fuel does not contain carbon *(Rimkus, Matijošius, Bogdevičius, Bereczky, Török, 2018; White, Steeper, Lutz, 2006)*. The use of HHO gas in a combustion chamber is expected to increase performance *(Bari, Mohammad Esmaeil, 2010; Kumar & Rao, 2013)*. Furthermore, CO_2 and NO_X emissions are expected to decline *(Baltacioglu, Arat, Özcanli & Aydin, 2016)*.

The aim of this study was to determine the impact of using HHO gas on diesel engine operating parameters. The gas generator was additionally added to the internal combustion engine and used electricity from the onboard network. Electrolysis of the water yielded HHO gas, which was subsequently blended into the intake air. The monitored parameters were engine power and torque. CO_2 and NO_X were monitored for emissions.

MATERIALS AND METHODS

The Škoda Roomster was used for the experiment. It is a three-cylinder turbocharged CI engine. Manufacturer's specifications are in the Tab. 1.

Tab. 1 Škoda Roomster specifications

Parameter	Unit	Value
Engine volume	dm^3	1.422
Max. power (speed)	kW (rpm)	59 (4000)
Max. torque	Nm (rpm)	195 (2200)
European emission standards		EURO 4
Fuel consumption	dm^3 per 100km	5.2
Emission CO_2	$g \cdot km^{-1}$	135

The chassis dynamometer Schenk 3604 was used for vehicle testing under laboratory simulated driving cycle and for power measuring. The driving cycle tested was WLTP in Fig.1. The Worldwide Harmonized Light Vehicles Test Procedure (WLTP) is a worldwide unified procedure for measuring emissions and consumption of passenger cars and light commercial vehicles. To increase the measurement accuracy, each cycle was repeated 3 times.
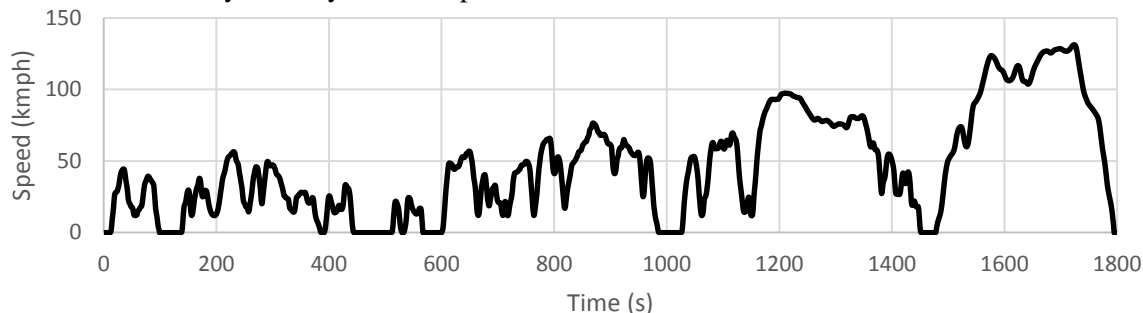
Fig. 1 WLTP driving cycle

The HHO gas generator was a commercially available DCT212 model manufactured by Atthero s.r.o. The main generator parameter is the amount of gas generated. According to the manufacturer, the DCT212 produces 180 $dm^3 \cdot h^{-1}$ at a current of 30A. During the experiment, the current to 20A was reduced due to generator overheating. This caused a reduction in the amount of gas generated to 105 $dm^3 \cdot h^{-1}$.

Exhaust gas components were measured using a Matrix MG-5 analyzer by Bruker. Exhaust gas solids using the EEPS 3090 by TSI analyzer.

RESULTS AND DISCUSSION

An ordinary driver will be concerned if the fuel, air, and HHO mixture will affect engine performance. Engine power measurement was the first step in this study. Fig. 2 shows the results of motor power and torque measurements. The results show that the use of HHO gas has led to a reduction in performance. The maximum power of 64kW was achieved when measuring on diesel. When HHO gas is used, power drops to 60kW. The way in which performance is distributed is more important for drivers. It can be seen from Fig. 2 that there has been a significant distortion of the torque course using HHO gas. This leads to worse engine performance. These results are consistent with the values found by Adrian Birtas *(Birtas & Chiriac, 2011)*.

However, there are many studies whose results are exactly the opposite. In 2013, Le Anh carried out a measurement of both power and torque in percent *(Le Anh, Nguyen Duc, Tran Thi Thu & Cao Van, 2013)*. Increases brake power by 13%, brake torque by 9% and reduces Brake Specific Fuel Conception (BSFC) by 10% on average compared to diesel *(Bahng, Woong, Dongsoon, Youngtae & Misoo, 2016)*.
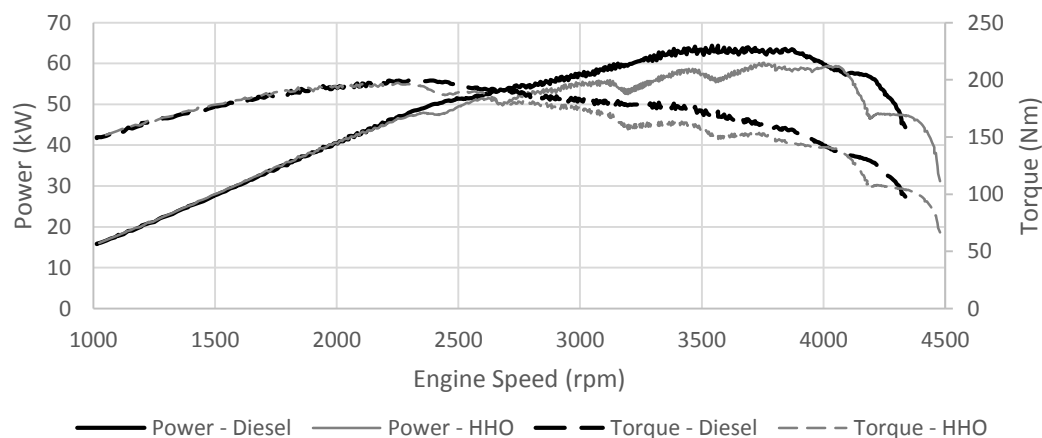
Fig. 2 Brake power output and torque versus engine speed

The production of gaseous emissions was solved as the average mass production per 1 km cycle according to the WLTP measurement methodology. Tab. 2 shows the emission measurement results. The results are converted to total concentration. The results show that with HHO gas production of CO_2 increased by 7%. This will lead to an increase in fuel consumption.

In these studies was reduces CO_2 by 12% or more on average compared to diesel *(Le Anh, Nguyen Duc, Tran Thi Thu & Cao Van, 2013; Bahng, Woong, Dongsoon, Youngtae & Misoo, 2016)*.

Tab. 2 Emission CO_2

	Diesel (g·km⁻¹)	HHO (g·km⁻¹)	Different (%)
WLTP #1	141,3	146,9	
WLTP #2	135,7	149,9	
WLTP #3	138,6	148,5	
Average	138,5	148,4	7% increase

N_2O, NO_2 and NO gases are the most common nitrogen oxide emissions. For the purposes of this study, the results of individual gas measurements are summed and represented as NO_X. The measurement results are shown in Tab 3. During the measurement, the use of HHO in the internal combustion engine has been shown to result in a significant increase in NO_X production by up to 34%.

A subtle result was also achieved in this study where NO_X emissions increased from 345 ppm to 406 ppm *(Birtas & Chiriac, 2011)*. The decrease in NO_X emissions by up to 34% was in study in 2016 *(El-Kassaby, Eldrainy, Khidr & Khidr, 2016)*.

Tab. 3 Emission NOX

	Diesel (mg·km⁻¹)	HHO (mg·km⁻¹)	Different (%)
WLTP #1	164	172	
WLTP #2	108	182	
WLTP #3	121	174	
Average	131	176	34% increase

CONCLUSIONS

The results show that it is not appropriate for the user to use HHO gas in the fuel-air mixture. When HHO gas was used, the power dropped by 6.25%. A change in the composition of the air / fuel mixture leads to engine control instability. The presence of hydrogen gas in the combustion chamber increases the burning rate of the fuel, resulting in harder engine running.

Reducing engine power forces the engine control unit to call this deficit. This leads to increased fuel consumption and thus higher CO_2 production. During the measurement, CO_2 production increased by 7%.

Furthermore, there was another lack of hydrogen combustion in the measurement. It burns at a very high temperature, up to 2 500 °C. At this high temperature, the nitrogen is oxidized in the combustion chamber. This leads to a significant increase in NO_X production. This was well documented during this study because NO_X production increased by 34%.

In conclusion, the retrofitting of the HHO generator to the vehicle is not recommended. From a practical point of view, this is not an easy matter. There is a risk of permanent engine damage during installation. The expected benefits of this technology have not been confirmed during the measurement. On the contrary, during the measurement it turned out that the engine is running in a non-standard mode, its operation is much harder. This makes it difficult to control, which is not user-friendly.

REFERENCES

1. Al-Baghdadi, M. & Al-Janabi, H. (2000). Improvement of performance and reduction of pollutant emission of a four stroke spark ignition engine fueled with hydrogen-gasoline fuel mixture. *Energy Conversion and Management, 41(1),* 77-91.

2. Bahng, G. W., Jang, D., Kim, Y., & Shin, M. (2016). A new technology to overcome the limits of HCCI engine through fuel modification. *Applied Thermal Engineering, 98,* 810-815. ISSN 13594311. doi:10.1016/j.applthermaleng.2015.12.076.

3. Baltacioglu, M. K., Arat, H. T., Özcanli, M. & Aydin, K. (2016). Experimental comparison of pure hydrogen and HHO (hydroxy) enriched biodiesel (B10) fuel in a commercial diesel engine. *International Journal of Hydrogen Energy, 41(19),* 8347-8353. ISSN 03603199.
doi:10.1016/j.ijhydene.2015.11.185.

4. Bari, S., & Esmaeil, M. (2010). Effect of H2/O2 addition in increasing the thermal efficiency of a diesel engine. *Fuel, 89(2),* 378-383. ISSN 00162361. doi:10.1016/j.fuel.2009.08.030.

5. Birtas, A., & Chiriac, R. (2011). A study of injection timing for a diesel engine operating with gasoil and HRG gas. *UPB Scientific Bulletin, Series D: Mechanical Engineering, 73(4),* 65-78. ISSN 14542358.

6. Donaldson, L. (2016). *Materials Today 19 (9).*

7. El-Kassaby, M. M., Eldrainy, Y. A., Khidr, M. E., & Khidr, I. K. (2016). Effect of hydroxy (HHO) gas addition on gasoline engine performance and emissions. *Alexandria Engineering Journal, 55(1),* 243-251. ISSN 11100168. doi:10.1016/j.aej.2015.10.016.

8. Kumar, G. A., & Rao, G. V. (2013). Performance Characteristics of Oxy Hydrogen Gas on Two Stroke Petrol Engine. *International Journal of Engineering Trends and Technology (IJETT), 6(7),* 358-366.

9. Le Anh, T., Nguyen Duc, K., Tran Thi Thu, H., & Cao Van, T. (2013). Improving Performance and Reducing Pollution Emissions of a Carburetor Gasoline Engine by Adding HHO Gas into the Intake Manifold. doi:10.4271/2013-01-0104.

10. Rimkus, A., Matijošius, J., Bogdevičius, M., Bereczky, Á., & Török, Á. (2018). An investigation of the efficiency of using O2 and H2 (hydrooxile gas -HHO) gas additives in a ci engine operating on diesel fuel and biodiesel. *Energy, 152,* 640-651. ISSN 03605442. doi:10.1016/j.energy.2018.03.087.

11. Usta, N., Öztürk, E., Can, Ö., Conkur, E. S., Nas, S., Çon, A. H., Can, A. Ç., Topcu, M. (2005). Combustion of bioDiesel fuel produced from hazelnut soapstock/waste sunflower oil mixture in a Diesel engine. *Energy Conversion and Management, 45(5),* 741-755. ISSN 01968904. doi:10.1016/j.enconman.2004.05.001.

12. White, C. M., Steeper, R. R., & Lutz, A. E. (2006). The hydrogen-fueled internal combustion engine: a technical review. *International Journal of Hydrogen Energy, 31(10),* 1292-1305. ISSN 03603199. doi:10.1016/j.ijhydene.2005.12.001.

Corresponding author:

Ing. Petr Jindra, Ph.D., Department of Department of Vehicles and Ground Transport, Faculty of Engineering, Czech University of Life Sciences Prague, Kamýcká 129, Praha 6, Prague, 16521, Czech Republic, phone: +420 22438 3153, e-mail: jindrap@tf.czu.cz

DETERMINATION OF SOME ENGINEERING PROPERTIES OF KUMQUAT RELATED TO DESIGN PARAMETERS

Onder KABAS[1], K. Cagatay SELVI[2], İlker UNAL[1]

[1]*Akdeniz University, Vocational School of Technical Science, Antalya, Turkiye*
[2]*19 Mayıs University, Department of Agricultural Machinery and Technology Engineering, Samsun, Turkiye*
[1]*Akdeniz University, Vocational School of Technical Science, Antalya, Turkiye*

Abstract

The production of kumquat from the genus Fortunella of Rutaceae family is gradually increasing in South of Turkey. In this study, it is aimed to determine some mechanical properties of the kumquat for the design of the machines to be used harvesting and postharvest. The some mechanical properties of the kumquat grown in the Bati Akdeniz Agricultural Research institute were determined with the help of the texture analyzer device. Mechanical properties such as the elasticity modulus, puncture force, deformation, hardness, Poisson rate, stress and energy in puncture force have been determined. The tests were carried out in three harvest time (optimum harvest time, before and after 10 days from optimum harvest time).Published benchmark data that was generally statistically different will be useful to engineers to new equipment design for different kumquat varieties. These differences that founded can be attributed to environmental and growth conditions.

Key words*: design; mechanical properties; kumquat; puncture.*

INTRODUCTION

Kamquat is native to China but nowadays production is carried out in Japan, Taiwan and Philippines *(Ladaniya, 2008; Quijano & Pino, 2009)*. In recent years, production of kumquat in our country also tends to increase especially in the Mediterranean Region it is grown like other citrus fruits. *(Gölükcü, et al., 2017).*

Mechanical properties of agricultural products are the most important parameters in pre-harvest, harvest and post-harvest operation. To design and improve of relevant machines and facilities used in sowing, harvesting, sorting, conveying, storing, handling and transport, there is a need to know the various engineering parameters of kumquat

Many studies have been reported on the mechanical properties of fruits, such as peach (*Emadi et al., 2011*), oak fruits *(Jalilian, et al., 2011),* pear *(Wang, 2004),* persimmon *(Altuntas, et al., 2011),* oil palm *(Akinoso & Raji, 2011),* kiwifruit *(Larijani, et al., 2014).* There is no much detailed studies concerning the mechanical properties of kumquat have been performed till now. Bohdziewicz & Czachor (2016) conducted studies on changes of mechanical properties of kumquat and cape gooseberry fruit during storage and Jalilian et al. (2013) determined physical and mechanical properties of kumquat variety grown in North of Iran.

The aim of this research was to determine the puncture properties of kumquat fruits in three harvest time for design processing machines.

MATERIALS AND METHODS

The Nagami Kumquat (*Fortunella.margarita*) variety that most grown in Turkey used for all the experiments in this study. Forty five kumquat samples that randomly selected were used in the experimental study for the purpose of measure their some mechanical properties in three harvest time They were grown in the Batı Akdeniz Agricultural Research Institute at Aksu, Antalya in the West Mediterranean region of Turkey and kept at room temperature of 20-21ºC in the laboratory. The tests were conducted within the Biological Test Devices Laboratory of Akdeniz University and BATEM, Antalya, Turkiye.

Mechanical Properties of Kumquat

A texture analyses device was used with a force measurement range of 0–100 N to determine the some mechanical properties of kumquat. Force-deformation data were recorded by its software during punc-

ture test and saved as Excel file for all tests (Fig. 1). Also, force-time curves were recorded by software during tests (Fig. 1). The measurement accuracy was ±0.001 N in force and 0.001 mm in deformation. A curve-ended cylindrical probe 2 mm in diameter was used to compress the fruit at 0.5 mm/s loading velocity during all the tests (*ASAE, 1994*).
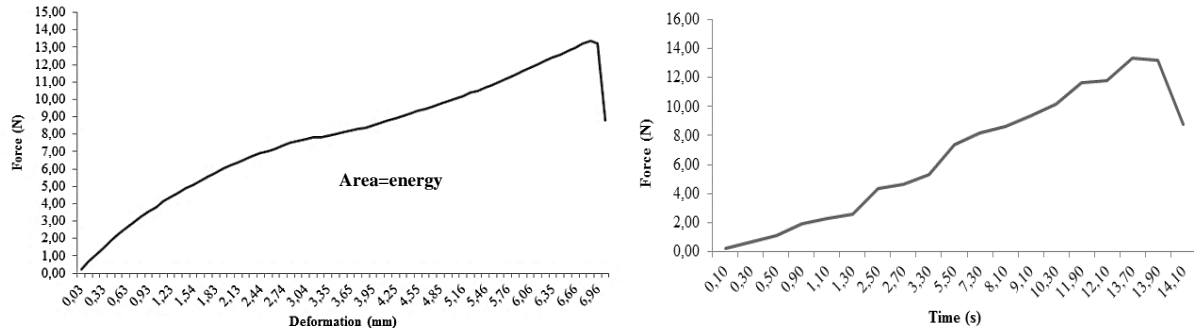
Fig. 1 Force-deformation and time curve from puncture test for Kumquat

Some mechanical properties such as force, energy and deformation at puncture were determined by using these force-deformation curves. The energy absorbed was determined directly from the diagram by measuring the area under the force-deformation curves (Fig. 1)

Poisson ratio, (ν) and Hardness, (H, Nmm^{-1}) were determined by using the following equation (*Finney, 1969; Mohsenin, 1980*).

$$\nu = \frac{(\Delta d | d_0)}{(\Delta l | l_0)} \tag{1}$$

where, d_0 (orginal diameter of sample, mm), d (diameter of sample after compression, mm), Δd (d-d_0), l_0 (orginal length of sample, mm), l_0 (length of sample after compression, mm) and $\Delta l(l_0$-l) are in mm.

$$H = \frac{F_{max}}{D} \tag{2}$$

where, F_{max} (maximum puncture force in curve, N) and D (deformation in maximum puncture force, mm).

The modulus of elasticity *E (*Nmm^{-2}*)* of the test fruits was calculated using Boussinesq techniques as follows (*Mohsenin, 1980*)

$$E = F(1 - \nu^2)/2aD \tag{3}$$

where E is the modulus of elasticity in compression, F(N) is the force in puncture, ν is the Poisson ratio, D(mm) is the deformation, a(mm) is the diameter of the cylindrical probe (2 mm)

Stresses (σ, Nmm^{-2}) were obtained from the following equation (*Sitkei, 1986*)

$$\sigma = F/A \tag{4}$$

where, F (N) is force and A (mm^2) is an initial cross section of the sample.

RESULTS AND DISCUSSION

The means and significant levels of puncture force, deformation stress, puncture energy, hardness, Poisson ratio and modulus elasticity for the initial rupture of the kumquat fruits as a function of harvest time are presented in Tab. 1.

Tab 1.Some engineering properties of Kumquat according to harvest date

	Before 10 days from optimum harvest time	Optimum Harvest time	After 10 days from optimum harvest time	Sig. Level
Puncture Force (N)	9.827b	15.813a	16.714a	**
Deformation (mm)	5.913b	6.724ab	7.12a	*
Stress(N/mm^2)	3.120b	5.036a	5.323a	**
Energy(Nmm)	30.840b	54.446a	59.864a	**
Hardness (N/mm)	1.642b	2.409a	2.385a	**
Poisson ratio	0.280	0.281	0.283	n.s
Modulus of elasticity(N/mm^2)	45.711b	47.383ab	50.065a	*

All data represent the mean of three replications with 15 determinations; a;b letters indicate the statistical difference in rows; *; ** significant levels at 5%, 1% respectively; ns: not significant.

As seen in Tab. 1, some mechanical properties of the kumquat in three harvest time were found to be statistically significant at the different probability levels (5% or 1%), with the exception that the Poisson ratio was found to be insignificant.

The puncture force, stress, energy and hardness of the kumquat were found to be statistically significant at the 1% probability level and Deformation and modulus of elasticity value were determined to be statistically significant at the 5% probability level, also, Poisson ratio was found to be insignificant.

The puncture force of the kumquat (9.827 N) before 10 days from optimum harvest time was significantly greater than other harvest times. There is no difference statistically between optimum harvest time and 10 days after optimum harvest time. The results show that the puncture force increased by increasing harvest time from 9.827 N to 16.714 N. *Jaliliantabar, et al. (2014)* found that the average rupture force of the kumquat was 24.1 N.

In all cases the highest deformation for kumquat fruits (7.120 mm) was obtained at 10 days after optimum harvest time while the lowest for fruits (5.913 mm) was at 10 days before optimum harvest time. The results show that the deformation increased by increasing harvest time from 5.913 mm to 167.120 mm.

According to the test data in Tab. 1, the average values of stress of kumquat 10 days before optimum harvest time, optimum harvest time and 10 days after optimum harvest time were 3.120 Nmm^{-2}, 5.036 Nmm^{-2} and 5.323 Nmm^{-2}, respectively. *Bohdziewicz and Czachor, (2016)* carried out on kumquat fruit and found similar result.

According to harvest time, the highest energy value of the kumquat was 59, 864 (Nmm) 10 days after optimum harvest time while the lowest for fruits (30.840 Nmm) was at 10 days before optimum harvest time. The energy value of the kumquat before 10 days from optimum harvest time was significantly greater than other harvest times.

The results show that the hardness was grading increased by increasing from 1.642 to 2.409 Nmm^{-1} by harvest time then decreased from 2.409 to 2.385 Nmm^{-1}. As shown in Table 1, there is no difference statistically between optimum harvest time and 10 days after optimum harvest time for hardness. Also, the results show that the modulus of elasticity increased by harvest time from 45.711 Nmm^{-2} to 50.065 Nmm^{-2}.

CONCLUSIONS

Effects of harvest time on some engineering properties of kumquat (*Citrus fortunella*) related to design parameters wood were investigated. The results of study indicate that harvest date significantly affect the mechanical properties of kumquat such as the puncture force, stress, energy and hardness of the kumquat were found to be statistically significant at the 1% probability level and Deformation and modulus of elasticity value were determined to be statistically significant at the 5% probability level, also, Poisson ratio was found to be insignificant.

REFERENCES

1. Akinoso, R., & Raji, A.O. (2011). Physical properties of fruit, nut and kernel of oil palm. *Int. Agrophys*, *25*(1), 85-88.

2. Altuntas, E., Cangi, R., & Kaya C. Physical and chemical properties of persimmon fruit. *Int. Agrophys*, *25*(1), 89-92.

3. ASAE. (1994). *Compression test of food materials of convex shape. In Agricultural Engineers Yearbook.* American Society of Agricultural Engineers, St. Joseph, MI.

4. Bohdziewicz, J., & Czachor, G. (2016). Changes of mechanical properties of Kumquat (*citrus japonica* thunb.) and Cape Gooseberry (*physalis peruviana* l.) fruits during storage. *Agricultural Engineering, 20*(3), 15-25.

5. Emadi, B., Abolghasemi, R., Aghkhani, M.H., & Beyraghi, T.S. (2011). Physical and Mechanical Properties of Peach. *World Applied Sciences Journal, 12*(1), 119-122.

6. Finney, E.E. (1969). To Define Texture in Fruits and Vegetables. *Agric. Eng., 50*(1), 462–465.

7. Gölükcü, M., Toker, R., Tokgöz, H., Çınar, O., & Özdemir, M. (2017). Kamkat (*Fortunella margarita* Swing.) kabuk uçucu yağ oran ve bileşiminin anaçlara göre değişimi. U. Ü. Ziraat Fakültesi Dergisi, *31*(1), 69-76

8. Jalilian, T.F., Lorestani, A.N., Gholami, R., Behzadi, A., & Fereidoni, M. (2011). Physical and mechanical properties of Oak (*Quercus Persica*) fruits. *Agric Eng Int: CIGR Journal, 13*(4), 1-4.

9. Jalilian T. F., Lorestani, A.N., & Gholami, R. (2013). Physical properties of Kumquat fruit. *Int. Agrophys, 27*(1), 107-109.

10. Ladaniya, M. 2008. *Citrus fruit: biology, technology and evaluation*. San Diego: Academic Press.

11. Larijani, M.R., Salar, M.R., & Kargarpour, H. (2014). Mechanical analysis Kiwi's texture and skin using texture analyzer set. *International Journal of Farming and Allied Sciences, 3*(1), 99-102,

12. Mohsenin, N.N. (1980). *Physical properties of plant and agricultural materials.* New York: Gordon and Breach Science Publishers.

13. Quijano, C.E., & Pino. J.A. (2009). Volatile compounds of round kumquat (Fortunella japonicaSwingle) peel oil from Colombia. *Journal of Essential Oil Research*, *21*(6), 483-485

14. Sitkei, G. (1986). *Mechanics of Agricultural Materials*. New York: Elsevier.

15. Wang, J. (2004). Mechanical properties of pear as a function of location and orientation. *International Journal of Food Properties*, *7*(2), 155-164.

Corresponding author:
Ing. Kabas Onder, Ph.D., [1]Akdeniz University, Vocational School of Technical Science, Dumlupınar Bulvarı, 07100, Antalya, Turkiye, phone: +90 5055145961, e-mail: okabas@akdeniz.edu.tr

PRELIMINARY EXPERIMENT ON COMPRESSION AND RELAXATION BEHAVIOUR OF BULK SESAME SEEDS AT VARYING FORCES AND SPEEDS

Abraham KABUTEY[1], Cestmir MIZERA[1], David HERAK[1], Petr HRABE[2]

[1]*Department of Mechanical Engineering, Faculty of Engineering, Czech University of Life Sciences Prague, Kamycka 129, 165 21, Prague 6, Prague, Czech Republic,*
[2]*Department of Material Science and Manufacturing Technology, Faculty of Engineering, Czech University of Life Sciences Prague, Kamycka 129, 165 21, Prague 6, Prague, Czech Republic.*

Abstract
The article examined the loading and unloading behaviour of bulk sesame seeds in relation to different forces between 1.5 and 4.5 kN and speeds between 1 and 10 mm·min^{-1}. The testing device (Labortech, MPTest 5.050, Germany) of a maximum load of 5 kN was used for the compression test. The bulk sesame seeds sample was measured at an initial height of 40 mm using the vessel diameter of 60 mm with a plunger. Based on the compression test; the loading time of 737.150±15.127, 500±10.267 and 60.500±9.334 s was observed at speeds of 1, 5 and 10 mm·min^{-1} and maximum force of 4.5 kN. Maximum deformation of 12.320±0.269 mm with a corresponding strain of 0.308±0.007 (-) and deformation energy of 25.495±0.191 J was observed at the lowest speed and maximum force. The applied forces at the various speeds did not initiate rupture of the bulk sesame seeds sample, hence there was no oil recovery. Using the multivariate analysis technique, the calculated parameters were statistically significant (p<0.05).

Keywords: Bulk sesame seeds sample; compression test; loading rate; multivariate analysis.

INTRODUCTION
The loading and relaxation behaviour of agricultural products is vital in food processing and storage as well as transport technologies for characterization of products (*Leblicq, Vanmaercke, Ramon & Saeys, 2015*; *Chakespari, Rajabipour & Mobli, 2010a*; *Chou, Sydow, Martin, Bridgwater & Wilson, 2003*). In the linear compression test, constant force and speed have been mostly applied for analyzing the mechanical and relaxation behaviour of bulk oilseeds (*Herak, Sleger, Mizera & Sedlacek, 2015*; *Divisova, Herak, Kabutey, Sleger, Sigalingging & Svatonova, 2014*; *Herak, Kabutey, Sedlacek & Gurdil, 2012*; *Herak, Kabutey & Sedlacek, 2011*). The relaxation time is also an important rheological property which shows how fast a material can dissipate stress after receiving a sudden deformation (*Maraldi, Molari, Regazzi & Molari, 2017*; *Chakespari, Rajabipour & Mobli, 2010a*; *Bargale, Irudayarj & Marquis, 1995*). The relaxation time of 30.33 s and 90 s has been reported on pear and apples (*Chakespari, Rajabipour & Mobli, 2010a*; *Wang, 2003*). Theoretically, the compression or load-deformation curve can be transformed into stress and strain relationship where the linear elastic region reaching the proportional limit or at the point of the relaxation process is extremely relevant for the design of an optimal processing technology (*Herak & Sedlacek, 2017; Hrabe & Sedlacek, 2016*; *Bargale, Irudayarj & Marquis, 1995*). It is important, however, to understand the varying compression factors such as force and loading rates on the mechanical behaviour of bulk oilseeds to identify the key processing parameters. The objective of the preliminary study was to describe the loading and unloading curves of bulk sesame seeds sample at different forces and speeds. Maximum deformation (mm), deformation energy (J), strain (-), and volume energy (J·m^{-3}) were also calculated.

MATERIALS AND METHODS
Bulk sesame seeds procured from the Czech Republic was used for the experiment. The moisture content of the sample was determined to be 8.42±0.24 % (w.b.) using the standard oven drying method (*Deli, Farah Masturah, Tajul Aris & Wan Nadia, 2011*; *Izli, Unal & Sincik, 2009*; *ISI, 1996*). The compression device (Labortech, MPTest 5.050, Germany) of a maximum load of 5 kN was used to

record the loading and unloading curves of bulk sesame seeds sample measured at an initial pressing height of 40 mm using a vessel diameter of 60 mm with a plunger (Fig.1). Compression forces of 1.5, 3 and 4.5 kN and speeds of 1, 5 and 10 mm·min⁻¹ were applied. The relaxation time of 5 minutes after maximum compression was allowed. The test was repeated twice and the results averaged. The deformation, strain, deformation energy and volume energy were respectively calculated from the relations given by (*Kabutey, Herak, Dajbych, Divisova, Boatri & Sigalingging, 2014; Chakespari, Rajabipour & Mobli, 2010b*). The SPSS software was used to analyse the calculated parameters.
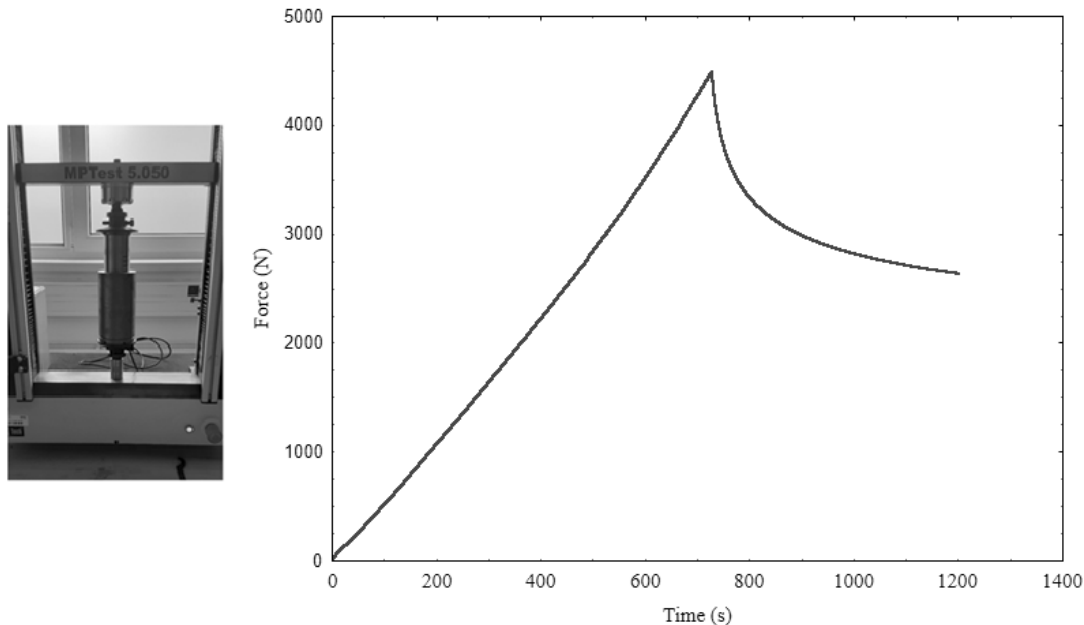
Fig. 1 Compression and relaxation test of bulk sesame seeds at force 4.5 kN and speed 1 mm·min⁻¹

RESULTS AND DISCUSSION

The characteristic load-deformation curves of bulk sesame seeds sample showed a smooth behaviour without any serration effect (*Divisova, Herak, Kabutey, Sleger, Sigalingging & Svatonova, 2014; Gupta & Das, 2000*). Maximum deformation of 12.320±0.269 mm with a corresponding strain of 0.308±0.007 (-) and deformation energy of 25.495±0.191 J was observed at the lowest speed and maximum force. There was no permanent deformation of the bulk sesame seeds sample. The loading time of 737.150±15.127, 500±10.267 and 60.500±9.334 s was observed at speeds of 1, 5 and 10 mm·min⁻¹ and maximum force of 4.5 kN. The mean and standard deviation values of the calculated parameters are presented in Tab. 1.

Tab. 1 Calculated parameters of bulk sesame seeds at different force and speed

Force kN	Speed mm·min⁻¹	Maximum deformation mm	Strain	Deformation energy J	Volume energy $\cdot 10^4$ J·m⁻³
	1	4.805±0.049	0.120±0.001	3.435±0.078	3.037±0.069
1.5	5	4.245±0.064	0.106±0.002	3.235±0.021	2.861±0.019
	10	4.455±0.205	0.111±0.005	3.255±0.134	2.878±0.119
	1	8.925±0.375	0.223±0.009	12.795±0.304	11.312±0.269
3	5	8.080±0.693	0.202±0.017	11.955±0.778	10.569±0.706
	10	8.150±0.424	0.204±0.011	11.900±0.684	10.521±0.688
	1	12.320±0.269	0.308±0.007	25.495±0.191	22.541±0.169
4.5	5	10.630±0.863	0.266±0.022	22.945±0.559	20.285±0.494
	10	10.060±1.556	0.252±0.039	22.255±1.464	19.675±1.294

The limit deformation of the bulk sesame seeds sample without oil leakage showed that the forces applied at different speeds were not great in magnitude to initiate rupture. Therefore, a greater force at a specific speed is required to recover the optimum oil (*Kabutey, Herak, Choteborsky, Dajbych, Sigalingging & Akangbe, 2017*). The normality test of the calculated parameters is given in Tabs. 2 and 3 respectively. From the Shapiro-Wilk test (for small dataset) it can be seen that the data is normally distributed since the p-values were greater than the significance level of 5%. The normality test results of strain and volume energy were similar to the deformation and deformation energy since the strain was determined based on the ratio of the deformation and the initial pressing height of the bulk sesame seeds sample while the volume energy was determined based on the ratio of the deformation energy and volume of the pressing vessel.

Tab. 2 Test of normality of deformation and deformation energy of bulk sesame seeds sample in relation to force

Determined parameters	Force kN	Kolmogorov-Smirnov[a]			Shapiro-Wilk		
		Statistic	df	P-value	Statistic	df	P-value
Deformation, mm	1.5	0.260	6	0.200*	0.887	6	0.302
	3	0.211	6	0.200*	0.955	6	0.780
	4.5	0.214	6	0.200*	0.948	6	0.723
Deformation Energy, J	1.5	0.185	6	0.200*	0.968	6	0.876
	3	0.300	6	0.098	0.846	6	0.146
	4.5	0.220	6	0.200*	0.931	6	0.589

*This is a lower bound of the true significance
[a] Lilliefors significance correction

Tab. 3 Test of normality of deformation and deformation energy of bulk sesame seeds sample in relation to speed

Determined parameters	Speed mm·min⁻¹	Kolmogorov-Smirnov[a]			Shapiro-Wilk		
		Statistic	df	P-value	Statistic	df	P-value
Deformation, mm	1	0.206	6	0.200*	0.879	6	0.264
	5	0.209	6	0.200*	0.910	6	0.435
	10	0.211	6	0.200*	0.919	6	0.498
Deformation energy, J	1	0.210	6	0.200*	0.855	6	0.174
	5	0.200	6	0.200*	0.871	6	0.229
	10	0.191	6	0.200*	0.894	6	0.339

*This is a lower bound of the true significance
[a] Lilliefors significance correction

The multivariate analysis of the calculated parameters (deformation, deformation energy, strain and volume energy) is shown in Tab. 4. The results were statistically significant (p<0.05). The corrected model indicated R squared values of 0.971 and 0.997 respectively. However, the interaction effect of force and speed on the calculated amounts was not statistically significant (p>0.05). The regression coefficients and the statistical significance of each parameter are given in Tabs. 5 to 8. The determined coefficients were statistically significant (p<0.05).

Tab. 4 Multivariate analysis of determined parameters of bulk sesame seeds

Source	Dependent variables	Sum of sqaures	df	Mean square	F-value	P-value
Corrected Model	Deformation	135.141[a]	8	16.893	37.212	0.000
	Deformation energy	1249.657[b]	8	156.207	365.027	0.000
	Strain	0.084[a]	8	0.011	37.212	0.000
	Volume energy	97672760738.748[b]	8	12209095092.344	365.027	0.000
Intercept	Deformation	1141.464	1	1141.464	2514.484	0.000
	Deformation energy	3056.056	1	3056.056	7141.431	0.000
	Strain	0.713	1	0.713	2514.484	0.000
	Volume energy	238860300087.757	1	238860300087.757	7141.431	0.000
Force	Deformation	128.415	2	64.208	141.440	0.000
	Deformation energy	1236.951	2	618.476	1445.262	0.000
	Strain	0.080	2	0.040	141.440	0.000
	Volume energy	96679682391.941	2	48339841195.970	1445.262	0.000
Speed	Deformation	4.694	2	2.347	5.170	0.032
	Deformation energy	7.118	2	3.559	8.317	0.009
	Strain	0.003	2	0.001	5.170	0.032
	Volume energy	556374297.748	2	278187148.874	8.317	0.009
Force *speed	Deformation	2.032	4	0.508	1.119	0.406
	Deformation energy	5.587	4	1.397	3.264	0.065
	Strain	0.001	4	0.000	1.119	0.406
	Volume energy	436704049.058	4	109176012.265	3.264	0.065
Error	Deformation	4.086	9	0.454		
	Deformation energy	3.851	9	0.428		
	Strain	0.003	9	0.000		
	Volume energy	301024097.580	9	33447121.953		
Total	Deformation	1280.691	18			
	Deformation energy	4309.565	18			
	Strain	0.800	18			
	Volume energy	336834084924.085	18			
Corrected Total	Deformation	139.226	17			
	Deformation energy	1253.508	17			
	Strain	0.087	17			
	Volume energy	97973784836.328	17			

df = Degree of freedom; [a] R Squared = 0.971; [b] R Squared = 0.997;

Tab. 5 Regression coefficient of the dependent variable: Deformation (mm)

| Source | Unstandardized coefficients | | Standardized coefficients | t value | P-value |
	B	Standard error	Beta		
Intercept	2.107	0.546		3.861	0.002
Force, kN	0.002	0.000	0.954	14.671	0.000
Speed, mm·min^{-1}	-0.121	0.049	-0.160	-2.463	0.026

Tab. 6 Regression coefficient of the dependent variable: Deformation energy (J)

| Source | Unstandardized coefficients | | Standardized coefficients | t value | P-value |
	B	Standard error	Beta		
Intercept	-6.399	0.749		-8.548	0.000
Force, kN	0.007	0.000	0.991	33.322	0.000
Speed, mm·min^{-1}	-0.155	0.067	-0.068	-2.303	0.036

Tab. 7 Regression coefficient of the dependent variable: Strain (-)

| Source | Unstandardized coefficients | | Standardized coefficients | t value | P-value |
	B	Standard error	Beta		
Intercept	0.053	0.014		3.861	0.002
Force, kN	$5.418 \cdot 10^{-5}$	0.000	0.954	14.671	0.000
Speed, mm·min^{-1}	-0.003	0.001	-0.160	-2.463	0.026

Tab. 8 Regression coefficient of the dependent variable: Volume energy (J·m^{-3})

| Source | Unstandardized coefficients | | Standardized coefficients | t value | P-value |
	B	Standard error	Beta		
Intercept	-56569.493	6618.168		-8.548	0.000
Force, kN	59.695	1.791	0.991	33.322	0.000
Speed, mm·min^{-1}	-1372.497	595.933	-0.068	-2.303	0.036

CONCLUSIONS

The loading test in relation to the applied forces and speeds did not initiate rupture of the bulk sesame seeds sample. The loading time of 737.150±15.127, 500±10.267 and 60.500±9.334 s was observed at speeds of 1, 5 and 10 mm·min^{-1} and maximum force of 4.5 kN. The calculated parameters (deformation, deformation energy, strain and volume energy) were statistically significant (p<0.05) based on the general linear model analysis. The normality test based on Shapiro-Wilk significance indicated that the data is normally distributed (p-value>0.05) confirming the reliability of the results. The follow-up communication would consider applying a higher compressive force at similar speeds for recovering the maximum oil and describing the load-deformation curves and the stress relaxation behaviour of bulk sesame seeds sample using appropriate mathematical models.

REFERENCES

1. Bargale, P. C., Irudayarj, J., & Marquis, B. (1995). Studies on Rheological Behaviour of Canola and Wheat. *Journal of Agricultural Engineering Research*, *61*, 267-274.

2. Chakespari, A. G., Rajabipour, A., & Mobli, H. (2010). Anisotropic Relaxation and Creep Properties of Apple (cv. *Shafi Abadi* and *Golab Kohanz*). *Advance Food Science and Technology*, *2*(4), 200-205.

3. Chakespari, A. G., Rajabipour, A., & Mobli, H. (2010). Strength Behaviour Study of Apples (cv. *Shafi Abadi* and *Golab Kohanz*) under compression loading. *Modern Applied Science*, *4*(7), 173-182.

4. Chou, S., Sydow, K., Martin, P. J., Bridgwater, J., & Wilson, D. I. (2003): Stress relaxation in the extrusion of pastes. *European Ceramic Society*, *23*, 637-646.

5. Deli, S., Farah Masturah, M., Tajul Aris, Y., & Wan Nadia, H. W. A. (2011). The effects of physical parameters of the screw press oil expeller on oil yield from *Nigella sativa* L. seeds. *International Food Research*, *18*(4), 1367-1373.

6. Divisova, M., Herak, D., Kabutey, A., Sleger, V., Sigaliinggging, R., & Svatonova, T. (2014). Deformation curve characteristics of rapeseeds and sunflower seeds under compression loading. *Scientia Agriculturae Bohemica*, *45*(3), 180-186.

7. Gupta, R. K. & Das, S. K. (2000). Fracture resistance of sunflower seed and kernel to compressive loading. *Food Engineering, 46*, 1-8.

8. Herak, D., Kabutey, A., & Sedláček, A. (2011). Mathematical description of rapeseeds (*Brassica napus* L.) mixture mechanical behaviour under compression loading. *Scientia Agriculturae Bohemica*, *42*(1), 31-36.

9. Herak, D., Kabutey, A., Sedláček, A., & Gurdil, G. (2012). Mechanical behaviour of several layers of selected plant seeds under compression loading. *Research in Agricultural Engineering*, *58*, 24-29.

10. Herak, D., Sleger, V., Mizera, C., & Sedlacek, A. (2015). Mechanical behaviour of bulk rapeseeds under quasi dynamic compression loading. *Engineering for Rural Development*, 28 p.

11. Herak, D., & Sedlacek, A. (2017). Utilization of rheological model for description of mechanical behaviour of rapeseeds under compression loading. In *58th ICMD2017* (pp.110-113).

12. Hrabe, P., & Sedlacek, A. (2016). Mechanical behaviour of oil rapeseeds during relaxation and creep. In TAE2016 *Conference on Trends in Agricultural Engineering* (pp.197-200).

13. Izli, N., Unal, H., & Sincik, M. (2009). Physical and mechanical properties of rapeseed at different moisture content. *International Agrophysics*, *23*, 137-145.

14. Kabutey, A., Herák, D., Dajbych, O., Divišová, M., Boatri, W. E., & Sigalingging, R. (2014). Deformation energy of *Jatropha curcas* L seeds under compression loading. *Research in Agricultural Engineering*, *60*, 68-74.

15. Kabutey, A., Herák, D., Choteborsky, R., Dajbych, O., Sigalingging, R., & Akangbe, O. L. (2017). Compression behaviour of bulk rapeseed: Effects of heat treatment, force and speed. *International Journal of Food Properties*, *20*(S1), S654-S662.

16. Leblicq, T., Vanmaercke, S., Ramon, H., & Saeys, W. (2015). Mechanical analysis of the bending behaviour of plant stems. *Biosystems Engineering*, *129*, 87-99.

17. Maraldi, M., Molari, L., Regazzi, N., & Molari, G. (2017). Analysis of the parameters affecting the mechanical behaviour of straw bales under compression. *Biosystems Engineering, 16*, 179-193.

18. Wang, J. (2003). Anisotropic relaxation properties of pear. *Biosystems Engineering*, *85*, 59-65.

Corresponding author:
Ing. Abraham Kabutey, Ph.D., Department of Mechanical Engineering, Faculty of Engineering, Czech University of Life Sciences Prague, Kamýcká 129, Praha 6, Prague, 16521, Czech Republic. Phone: +420 22438 3180, e-mail: kabutey@tf.czu.cz

PRODUCTION OF POLLUTANTS FROM ORGANIC LITTER FOR DAIRY COW

Ingrid KARANDUŠOVSKÁ[1], Jana LENDELOVÁ[1], Štefan BOĎO[1], Štefan MIHINA[1], Štefan POGRAN[1]

[1]Department of Building Equipment and Technology Safety, Faculty of Engineering, Slovak University of Agriculture in Nitra, SLOVAKIA

Abstract

The aim of the experiment was to analyse the production of ammonia and greenhouse gases in dairy farms depending on the type of litter used. Two stables A and B – with the same structure situated next to each other - were used for the analysis. Straw litter was utilized in the deepened cubicles in building A; the bedding based on recycled manure solids (RMS) was used in building B. A significant difference in concentration of all gases were observed in stable A and B (P <0.01). Production of ammonia and methane was significantly lower in stable A ($NH_{3,(straw,AVG)}$ = 0.86 $mg.m^{-3}$ ±0.53 and $CH_{4,(straw,AVG)}$ = 8.36±2.93 $mg.m^{-3}$) than in stable B ($NH_{3,(RMS,AVG)}$ =2.35 $mg.m^{-3}$ ±0.69 and $CH_{4,(RMS,AVG)}$ = 20.61±12.26 $mg.m^{-3}$), while other microclimatic conditions in both were not statistically different. However, the average and maximum values of ammonia and other monitored gases in stable A, as well as in stable B with RMS, did not exceed permitted limit values.

Key words: dairy cattle; organic bedding; harmful gases concentration.

INTRODUCTION

Global atmospheric concentrations of the most important gases: carbon dioxide (CO_2), methane (CH_4), nitrous oxide (N_2O), and ammonia (NH_3), have increased significantly in the last 150 years (*Monteny et al., 2006*). Livestock farming systems are a major source of trace gases contributing to atmospheric pollution locally and globally. Emissions from dairy cow production systems need to be reduced to limit the environmental problems associated with livestock (*Saha et al., 2014*). The membership of the Slovak Republic in the EU imposes obligations to implement EU directives into Slovak laws amending the responsibility of production enterprises for the environment. Increasing demands on the quality of animal products make it necessary to deal with the improving of the animal housing conditions (*Balková and Pogran, 2009*); however, monitoring and reduction of emissions of greenhouse gases must be also ensured (*Pogran et al., 2011*). Currently, great attention is paid to usage of livestock manure so that it can be re-evaluated in the further agricultural activity. Dairy farms are under gradual pressure to improve their management of manure. Bedding is a very costly component of dairy farming that has significant implications for animal health, as well as environment. The cost and availability of bedding fluctuates, and good bedding materials can be expensive and difficult to obtain. Farmers using RMS report greater cow comfort than with other bedding materials they have used (*Harrison, et al., 2008*). Recent technological advancements in the dairy sector have enabled the dairy farms with liquid manure to use mechanical solid-liquid separation systems equipped with active composting of the separated solids. Farmers consider this desirable, because liquid manure storage requirements are reduced, and composted solids are used as bedding material, avoiding thus an increase in cost of purchased bedding (*Husfeldt et al., 2012*). Appropriate manure separators allow separation of the solid part from the liquid component up to 40% of dry matter and its subsequent usage as a plastic litter that improves animal welfare (*Jelinek et al., 2006*). Selection of bedding materials by farms is related to the manure system used, availability and cost of materials. Increased promotion of high-performance slurry separation machinery that can produce separated manure solids with dry matter (DM) exceeding 30% has provoked interest in this practice in European farms, in which there are very different climatic conditions. Scientists also try to address the issue of bacteriology and hygiene risks of organic litter. With increasing temperature, the production of specific harmful gases also increases (*Zhang et al., 2005, Rong et al., 2014*). The aim of this work was to compare the concentrations of harmful gases in two dairy housing units, using the straw bedding and bedding from the recycled manure solids during summer.

MATERIALS AND METHODS

INNOVA Air Tech Instruments Photoacoustic Multi-Gas Monitor with a 1309 multichannel sampling system was used to measure NH_3, CO_2, CH_4, N_2O concentrations. This equipment was installed in two buildings A and B with the same ground plan dimensions and roof height. Dairy cows are housed in comfortable lying cubicles with a length of 2.5 m and a width of 1.2 m, which are located at the external walls in two rows. Manure corridor is between them. The feeding passes are in the middle of the stall. During the experiment, 170 dairy cows were housed in each stable, the Holstein-Friesian breed with an average weight of 580 kg. The experiment was conducted in the summer months of June, July and August on selected days when the indoor air temperature ranged from 14 to 34 °C. Temperature and relative air humidity were recorded using a Comet datalogger. Straw is used as bedding in cow cubicles in the stable A; and the identical cubicles with the same location are filled with litter of separated slurry (RMS) in the stable B. The produced liquid manure and urine are continuously removed by a hydraulic blade scraper into the cross-channel and from there to the two-chamber pumping sump and then to a slurry separator where the liquid is separated from the solid part. The liquid part – slurry is pumped into above-ground storage tanks and the solid part is sprinkled from the separator into the transport mechanism and is used as litter for the cubicle lying in the cowshed. Both stables have longitudinally opened walls protected by a net with hexagonal openings that can be covered with a controllable flow system from a height of 600 mm above ground. Natural ventilation is ensured by roof ridge that is 56 m long. The measuring points of livestock gases production were at eight locations in both buildings (Fig. 1).
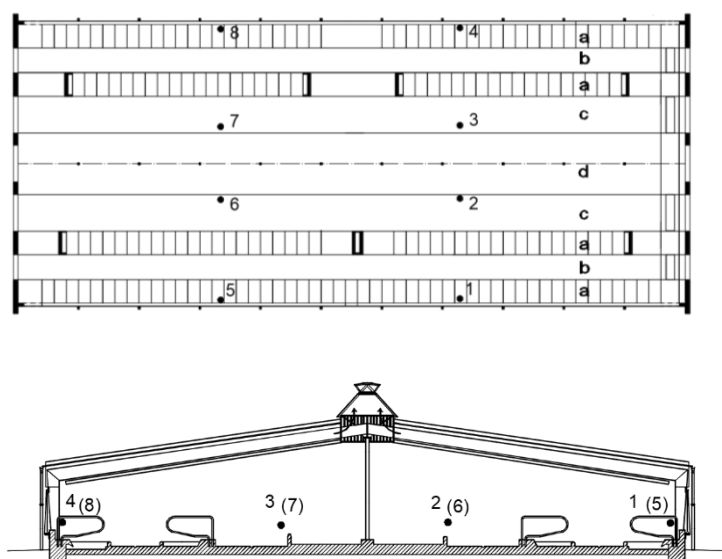
Fig. 1 Ground plan and cross-section of the stable (A and B) with air sampling locations
Legend: a - cubicles; b - manure corridor; c – feeding area; d - feeding passage; 1, 4, 5, 8 - measuring points in the cubicles; 2, 3, 6, 7 - measuring point in the feeding area (with liquid manure)

RESULTS AND DISCUSSION

Indoor and outdoor temperatures, relative humidity of air and gas concentrations recorded during the measurement periods are presented in Tab. 1. The Statistica 10 software, one-factor ANOVA, the Tukey HSD test at the significance level $\alpha = 0.05$ was used to evaluate and compare the gas production in the monitored stables in terms of used litter material in the lying cubicles. Test results show that the average values of the gas concentrations observed in measurements at stables A and B were significantly different (Tab. 2). Ammonia production was statistically significantly lower in building A (0.86 mg.m^{-3}±0.53), in which the straw was used for litter than in building B (2.35 mg.m^{-3}±0.69), in which the separated slurry was used. However, microclimatic conditions in both housings were not statistically different. The average and maximum values of ammonia and other monitored gases in stable A, as well as in stable B with litter of separated slurry did not exceeded permitted limit values.

Tab. 1 Evaluated gas concentrations, indoor and outdoor temperature and relative humidity during measurement in housing stable A (straw litter) and stable B (litter from RMS), P<0.01

	unit of measur.	stable	N valid	average	min.	max.	stand. dev.	var. coefic.
NH_3	mg.m^{-3}	A	3328	0.9	0.1	6.6	0.5	61.4
		B	3328	2.4	0.2	3.3	0.7	29.2
CO_2	mg.m^{-3}	A	3328	1032.2	787.0	1692.3	120.9	11.7
		B	3328	1370.7	821.5	2573.5	384.8	28.1
CH_4	mg.m^{-3}	A	3328	8.4	0.3	29.0	2.9	35.0
		B	3328	20.6	4.6	61.5	12.3	59.5
N_2O	mg.m^{-3}	A	3328	1.0	0.7	1.3	0.1	8.2
		B	3328	1.2	0.8	1.6	0.2	16.2
indoor air temperature	°C	A	3328	24.6	14.5	33.4	4.2	17.2
		B	3328	24.3	14.9	32.7	4.1	16.9
relative humidity of indoor air	%	A	3328	60.2	30.6	83.4	13.7	22.7
		B	3328	61.1	30.9	87.5	14.0	22.8
outdoor air temperature,	°C		3328	23.8	12.7	34.3	5.0	21.1
relative humidity of outdoor air	%		3328	58.6	23.0	97.2	18.7	31.8

Tab. 2 Statistical analysis of gas concentrations, indoor temperature and relative humidity during measurement in stable A (litter from straw) and stable B (litter from RMS), Tukey´s HSD, P<0.05

		unit of meas.	stable	average value	p-value
1	NH_3	mg.m^{-3}	A	0.9	0.000009
2			B	2.4	
1	CO_2	mg.m^{-3}	A	1032.2	0.000008
2			B	1370.7	
1	CH_4	mg.m^{-3}	A	8.4	0.000009
2			B	20.6	
1	N_2O	mg.m^{-3}	A	1.0	0.000007
2			B	1.2	

Similar results in terms of ammonia concentrations in free dairy housing utilizing deep straw litter were reported by *Herbut and Angrecka (2014)*, who recorded average values of ammonia as follows: 0.98 mg.m^{-3} in June; 0.79 mg.m^{-3} in July; and 0.86 mg.m^{-3} in August. Straw is frequently used bedding material, and it is characteristic with an ability to absorb the water and gases, as well as with high content of dry mass (approx. 85%). For many years, these two factors determined the popularity of its application (*Adamski et al., 2011*). One kilogram of straw absorbs approx. 2-5 g of ammonia. In absorption is increased in modified straw, (treated by i. e. cutting or gridding). This experiment also included investigation of the physical properties of materials used in the cubicles, namely the dry matter content under operating conditions. Results are reported in *Lendelova et al. (2016)*, who found an average dry matter content value of 27.18 ± 0.96% by measuring the dry matter content of the RMS prior to its supplying to the cubicle without significant differences at each sampling site (P <0.01). After four days, the average RMS dry matter content in the selected samples taken from the cubicle was 51.61% and 65% after another 4 days. The average dry matter content of straw was 90.88 ± 0.79% prior to its spreading to the cubicles, dropping to 88.12% after supplying with litter, and continued to drop to 68.38% before being removed from the storage. Results showed that after spreading the separated sludge slurry into cubicles in the stable with free stalls filled with separated raw manure solids, there was a significant increase in

dry matter during 2–8 days from starting dry matter content of 27% to 65%, which is positive in terms of hygiene and comfort. Situation is quite the opposite in wet and cold environments, where RMS farmers are sceptical (*Leach et al., 2015*) and the research was subsequently devoted to the chemical and bacteriological characteristics of RMS and their impact on milk quality and welfare (*Gooch et al., 2005, Bradley et al., 2018*). Efficiency of DM removal is greatly variable depending on the type of used separators: 16-78% for screw pressers, 14-40% for roller presses, and 25-77% for decanter centrifuges (*Godbout et al., 2002, Gooch et al., 2005*). According to *Rumburg et al. (2004*) and *Rogge et al. (2006)*, the quality of beddings and their moisture influence the emissions of organic compounds, and odour and dust into the air and are assessed on the basis of animal behaviour standards that are an important determinant of welfare in addition to other things (*Adamski et al., 2011*). *Fillingham et al. (2017)* reported that solid-separation and composting are potential greenhouse gas mitigation practices for dairy farms. Separation reduces carbon in the liquid fraction entering the manure storage, hence reducing the potential methane emissions, with a high global warming potential. Carbon dioxide is emitted only as a part of the short (biogenic) carbon cycle and does not contribute to the net atmospheric concentration (*Vergé et al., 2013*). Nitrous oxide is a potent greenhouse gas with climate-carbon feedback emitted from solid manure and compost. Manure emits ammonia, which is an indirect greenhouse gas and has adverse health effects (*Harrison and Yin, 2000*). According to *Misselbrook and Powell (2005),* there is a number of ways, influencing the emissions from different bedding materials. These include physical structure, chemical composition of bedding and different capacity to absorb deposited urine. Absorption may reduce emissions by increasing the resistance to gaseous transport. For example, mixture of peat and chopped straw reduced emissions from young cattle in bedded pens by approximately 50% compared to long straw, chopped straw, or wood shavings; this reduction was attributed to high ammonia absorbing capacity of this bedding (*Jeppsson, 1999*). Considering the recycled manure solids with the much greater absorbance capacity presented by *Misselbrook and Powell (2005)*, it was suggested that the majority of the urine was retained in the upper layers of bedding with a lower resistance to transport, resulting in higher emissions in comparison to sand bedding. Generally, the presence of bedding material can reduce NH_3 emissions from cattle housing. *Chambers et al. (2003)* reported emissions lower from a deep straw litter in cattle housing system to be lower by 30% in contrast to a slurry-based system. Our possibilities at experimental farm did not allow us to compare the absorption capacity of RMS with sand or non-bedded system. However, a partial analysis of concentration of ammonia and other gasses over the cow beds in stable A and stable B did not show any significant difference in stable utilizing the RMS in contrast stable using the straw litter. Nevertheless, this claim will be subject to detailed analysis of litter exposed to different litter cycles and with a different rate of excrement removal from the manure corridors, both of which may have a significant impact on the overall result for cubicles filled with straw and cubicles filled with bedding from recycle manure solids.

CONCLUSIONS

The classic organic litter is well formable, flexible and usually thermally insulated, but problem lies in its availability, labour demands and cost. The issue of their influence on the internal and subsequently external environment, which is dependent on changes in physical properties in relation to changes in air chemistry, is also essential. The recycled sludge bedding gives the impression of non-hygiene, unpleasant odour and undesirable production of emissions. The work is based on the assumption that ammonia and methane productions increase with increasing ambient temperature. Therefore, the first experiments were focused on monitoring of production of pollutants in the building with litter made of separated sludge slurry in the summer and opportunity of simultaneous measurements in the same neighbouring building utilizing straw as litter had allowed us to compare the obtained data. The experiment was conducted in two phases, the first phase included observation of litter physical properties, the second phase included measurement of differences in the concentrations of produced gases. On the basis of the results of our measurements, we have determined the following conclusions. Considering the two neighbouring buildings (each with 170 cow cubicles), the average concentrations of NH_3, CO_2, CH_4, resp. N_2O were significantly higher in the building with recycled sludge slurry bedding (2.35 $mg.m^{-3}$, 1370 $mg.m^{-3}$, 20.61 $mg.m^{-3}$, 1.19 $mg.m^{-3}$, respectively) than in building with the straw bedding (0.86 $mg.m^{-3}$, 1032.24 $mg.m^{-3}$, 36 $mg.m^{-3}$, 0.98 $mg.m^{-3}$ respectively). Increased concentrations of NH_3, CO_2, CH_4 and N_2O did

not show that RMS litter absorbs produced pollutants, however, observed concentrations did not exceed permitted limits for dairy farming.

ACKNOWLEDGEMENTS

REFERENCES

1. Adamski, M., Glowacka, K., Kupczynski, R., & Benski, A. (2011). Analysis of the possibility of various litter beddings application with special consideration of cattle manure separate. *Acta Scientiarum Polonorum: Zootechnica, 10*, 5-12.

2. Balková, M. & Pogran, Š. (2009). Assessment of microclimatic parameters in a building for heifers. *Acta technologica agriculturae*, *12*, 15-18.

3. Bradley, A.J., Leach, K.A., Green, M.J., Gibbons, J., Ohnstad, I.C., Black, D.H., Payne, B., Prout, V.E., & Breen, J.E. (2018). The impact of dairy cows' bedding material and its microbial content on the quality and safety of milk-A cross sectional study of UK farms. *International Journal of Food Microbiology*, *269*, 36-45.

4. Fillingham, M.A., VanderZaag, A.C., Burtt, S., Baldé, H., Ngwabie, N.M., Smith, W., Hakami, A., Wagner-Riddle, C., Bittman, S., & MacDonald, D. (2017). Greenhouse gas and ammonia emissions from production of compost bedding on a dairy farm. *Waste Management, 70*, 45–52.

5. Godbout, S., Pelletier, F., Larouche, J.P., Belzile, M., Feddes, J.J.R., Fournel, S., Lemay, S.P., & Palacios, J.H. (2012). Greenhouse Gas Emissions Non-Cattle Confinement Buildings: Monitoring, Emission Factors and Mitigation. In *Greenhouse Gases-Emission, Measurement and Management* (pp. 101-126). Guoxiang Liu, IntechOpen.

6. Gooch, C.A., Inglis, S.F., & Czymmek, K.J. (2005). Mechanical solid-liquid manure separation: performance evaluation on four New York State dairy farms. In *ASAE Annual Meeting*. Paper number 054104.

7. Harrison, E.Z., Bonhotal, J., & Schwarz, M. (2008). Using manure solids for dairy barn bedding. Ithaca, NY: *Cornell Waste Management Institute*.

8. Harrison, R.M., & Yin, J., (2000). Particulate matter in the atmosphere: which particle properties are important for its effects on health? *Science of the Total Environment*, *249*, 85-101.

9. Herbut, P. & Angrecka, S. (2014). Ammonia concentrations in a free-stall dairy barn. *Annals of Animal Science*, *14*(1), 153-166.

10. Husfeldt, A.W., Endres, M.I., Salfer, J.A., & Janni, K.A. (2012). Management and characteristics of recycled manure solids used for bedding in Midwest freestall dairy herds. *Journal of Dairy Science, 95*(4), 2195-2203.

11. Chambers, B.J., Williams, J.R., Cooke, S.D., Kay, R.M., Chadwick, D.R., & Balsdon S.L. (2003). Ammonia losses from contrasting cattle and pig manure management systems. In *Waste and the Environment* (pp. 19-25). Edinburgh.

12. Jelínek, A., Kraus, R., & Dědina, M. (2006). New technology of slurry processing from cattle breeding as a plastic litter for improvement of the environment and welfare of farmed animals. In *Separated slurry as plastic litter in cattle farms* (pp. 8-13). Praha VUZT.

13. Jeppsson, K.H. (1999). Volatilization of ammonia in deep-litter systems with di!erent bedding materials for young cattle. *Journal of Agricultural Engineering Research*, *73*, 49-57.

14. Leach, K. A., Archer, S. C., Breen, J. E., Green, M. J., Ohnstad, I. C., Tuer, S., & Bradley, A. J. (2015). Recycling manure as cow bedding: Potential benefits and risks for UK dairy farms. *The Veterinary Journal, 206*, 123-130.

15. Lendelová, J., Žitňák, M., Bošanský, M., Šimko, M., & Piterka, P. (2016). Testing of property changes in recycled bedding for dairy cows. *Research in agricultural engineering*, *62*, S44-S52.

16. Misselbrook, T.H. & Powell, J.M. (2005). Influence of Bedding Material on Ammonia Emissions from Cattle Excreta. *Journal of Dairy Science*, *88*, 4304-4312.

17. Monteny, G.J., Bannink, A., & Chadwick, D. (2006). Greenhouse gas abatement strategies

for animal husbandry. *Agriculture, Ecosystems and Environment*, *112*, 63-170.

18. Pogran, Š., Bieda, W. Gálik, R., Lendelová, J., & Švenková, J. (2011). *Quality of the indoor environment in the housing buildings.* Nitra: SUA.

19. Rogge, W.F., Medeirosb, P.M., & Simoneit, B.R.T. (2006). Organic marker compounds for surface soil and fugitive dust from open lot dairies and cattle feedlots. *Atmospheric Environment, 40*, 27-49.

20. Rong, L., Liu, D., Pedersen, E.F., & Zhang, G. (2014). Effect of climate parameters on air exchange rate and ammonia and methane emissions from a hybrid ventilated dairy cow building. *Energy Building, 82*, 632-643.

21. Rumburg B., Neger M., Mount G.H., & Yonge D., Filipy J., Swain J., Kincaid R., Johnson K. (2004). Liquid and atmospheric ammonia concentrations from a dairy lagoon during an aeration experiment. *Atmospheric Environment, 38*, 1523-1533.

22. Saha, C.K., Ammon, C., Berg, W., Fiedler, M., Loebsin, C., Sanftleben, P., Brunsch, R., & Amon, T. (2014). Seasonal and diel variations of ammonia and methane emissions from a naturally ventilated dairy building and the associated factors influencing emissions. *Science of The Total Environment*, *468*, 53-62.

23. Vergé, X. P., Maxime, D., Dyer, J. A., R. L. Desjardins, R.L., Arcand, Y., & Vanderzaag, A. (2013). Carbon footprint of Canadian dairy products. *Journal of dairy science, 96,* 6091-6104.

24. Zhang, G., Strom, J. S., Li, B., Rom, H.B., Morsing, S., Dahl, P., & Wang, E. (2005). Emission of ammonia and other contaminant gases from naturally ventilated dairy cattle buildings. *Biosystem Engineering*, *92*, 355-364.

Corresponding author:
doc. Ing. Jana Lendelová, PhD., Department of Building Equipment and Technology Safety, Faculty of Engineering, Slovak University of Agriculture in Nitra, Tr. A. Hlinku 2, Nitra, 949 76, Slovakia, phone: +421 37 641 5777, e-mail: jlendelovauniag@gmail.com

IMPACT OF THE APPLICATION OF BIOESTERS' ADDITION TO DIESEL OIL ON THE COURSE OF TURNING MOMENT AND POWER WITHIN THE SCOPE OF LOW ROTATIONAL SPEED AT VARIABLE SETTINGS OF FUEL INJECTION

Jerzy KASZKOWIAK[1], Marietta MARKIEWICZ[1], Paweł KRZACZEK[2]

[1]UTP University of Science and Technology, Faculty of Mechanical Engineering, Al. prof. S. Kaliskiego 7, 85-796 Bydgoszcz
[2]University of Life Sciences in Lublin, Faculty of Production Engineering, 28 Głęboka Street 20-612 Lublin,

Abstract
Combustion engines with self-ignition, are the basic source of drive in vehicles and machines. The fuel used by them is the diesel oil.
At present, the basic fuel for powering engines with self-ignition is the diesel oil of fossil origin. The increase in the use of bioesters obtained from products of organic origin, creates problems as far as correct operation of the above mentioned engines are concerned. The features of diesel oil of connate origin and of biocomponent as similar, however there occur many adverse effects. In the study there are presented the studies on the drive unit powered with the mixtures of diesel oil and fatty acid methyl esters. There was studied the course of changes of power and the turning moment within the scope of the rotational speed up to 2250 rev./min at variable injection parameters' settings. It has been established, that the addition of bioesters has an impact on lowering of power and the turning moment. Obtaining of satisfactory results is possible following adjustment of the fuel's dose and the supercharging pressure. It has been found, that the addition of bioester results in lowering of power and the turning moment, however increase of the fuel's dose and supercharging allows to obtain a similar or even a higher power and of the turning moment.

Key words: biofuels; environment protection; turning moment; power of a diesel engine; means of transport; working machines.

INTRODUCTION

Exhausting resources of fossil fuels and striving after limitation of CO_2 emission, result in an increasing interest in fuels of renewable origin. For diesel engines with self-ignition, the use of bioesters as a fuel, is conductive for limiting emission of CO_2 and NOx *(Hosain S. et al. 2008)*. Bioesters may be obtained from the fat of plant or animal origin, and even from fat obtained from wastes. However, production of fuels should not be a competition for food production that is why sources of bioesters from other raw materials, for ex. from algae are sought *(Lin L. 2011)*. Bioesters obtained from products of renewable origin, may have very differentiated properties. They depend on both the raw material, as well as on the technology of their processing. On the performance parameters of fuel there have the impact the following features: temperature of ignition, temperature of filter's blocking, cetane index, heat of combustion *(Hoekman K. et al. 2011)*. Moreover, the conducted studies point at lower emission of particulate solids at the time of fuel's combustion with bioesters' additive. However, a drop in power has been noticed together with the content of biocomponent (lower fuel's calorific value). It has been found in the studies, that the change of the fuel injection's beginning may be a way to maintain the power *(Monyem A. & Van Gerpen J. 2001)*. There are also analysed other manners of powering engines with self-ignition just as the use of the additive of alcohol or water emulsion to diesel oil *(Kowalski M. & Jankowski A. 2018)*. Most often, the drop of power caused by the use of the additive of bioesters to diesel oil, is proportionate or higher than the one resulting from the drop of the fuel's calorific value *(Lapuerta M. et al. 2008)*.

More and more restrictive requirements demanded from combustion engines, aim at lowering of the global emission of greenhouse gases. However, it is encountered by resistance on the side of both the producers as well as users. The willingness to maintain good performance parameters as well as high reliability result in the increase of the costs of production and servicing of combustion engines.

The rape-seed oil following treatment is one of the most popular raw material used for production of biofuels *(Uzdowski M., 2006; Uzdowski M., 2008)*.

Maintaining of a constant, high quality of fuels of renewable origin is very important, as it is one of the main factors influencing the parameters of machines and vehicles' operation *(Markiewicz-Patalon M., Muślewski M., Kaszkowiak K., 2018; Markiewicz-Patalon M., et al.,2018)*.

Low contents of bioesters in fuel do not result in occurring of bigger differences in properties of fuels as well as the effects of their use. Noticeable changes, both in physio-chemical as well as in performance properties, occur most often only with the content above 25-30% *(Markiewicz-Patalon M., Kaszkowiak K., 2017; Markiewicz-Patalon M., et al., 2017)*. For the vehicles in which engines with self-ignition are used, particularly important for the correct usage are both the maximum values as well as the course of the value of power and of turning moment, especially within the range of low and medium turning values. They influence both the fuel consumption as well as the comfort of the vehicle's handling. The purpose of the study was to determine whether it is possible to achieve satisfactory engine operation parameters in the range of low rotational speeds fed with a blend of diesel and bioester when changing the settings of the fuel injection controller.

MATERIALS AND METHODS

The tests were conducted on the chassis dynamometer type DynoTech – weight bearing, with Eddy current brake consisting of a frame, rollers with housing, measuring controller and with software. The vehicle was powered with an engine with self-ignition, supercharged, with the ignition system Common Rail. The operating parameters (maximum power and maximum moment) measured for standard settings, for an engine powered with standard fuel, differed from the ones declared by the producer. Precise, real data of the engine are presented in the table 1. That unit is commonly used both in delivery trucks as well as in passenger vehicles. Design of the engine, its fittings and the type of fuel's injection, are typical for the solutions applied at present also in units of higher power that is why it will be possible to make an attempt of the obtained results' transposition. The results obtained for the analysis purposes, consider the losses in the vehicle's mechanical elements (an engine, power transmission system).

Tab. 1 Real technical data of a power unit

swept capacity [cm^3]	1560
engine power [KM]/[kW]	102/78
maximum turning moment [Nm]	238
number of cylinders	4
diameter of a cylinder [mm]	73
piston stroke [mm]	88.3
number of valves	16
type of injection	direct, Common Rail
Supercharging	turbocompressor
filter of particulate solids	does not have

The tested engine was broken-in and fully technically efficient, air filter was replaced into a new one prior to the cycle of tests' commencement. Prior to commencement of the measurements, the engine was heated up to the temperature corresponding to average usage conditions (temperature of liquid in cooling system 85-90^{0}C). The power transmission system was efficient, had no clearances and other defects. The exhaust system was not equipped with particulate solids' filter. View of the power unit is presented in drawing 1. The power unit cooperates with the dual-mass flywheel and a turbocompressor of variable geometry, what has an impact of the engine's performance increase.

During the studies, the engine was powered with a mixture of a diesel oil (of mineral origin) and the additive of fatty acid methyl esters. The tests were conducted for pure diesel oil (fuel I) and mixture of diesel oil and the content of bioester 50% (by weight) (fuel II). The results obtained for powering engine with fuel without the additive of bioesters at factory's setting, have been assumed as the reference level.

Fuels used for powering the engine during the tests, have been assessed as far as parameters are concerned. The selected real properties of the fuels used for tests, are presented in table 2.

Tab. 2 Properties of fuel used in the studies (average values)

Feature	Diesel oil 100% (Fuel I)	50% of diesel oil and 50% of bioester (Fuel II)
Viscosity [mPa • s]	6.46	8.56
Mass density [$kg • dm^{-3}$]	0.83	0,86
Cetane number	53.3	58.4
Heat of combustion [J/g]	44277	41770
Calorific value [J/g]	43097	40590

The tests were conducted in turn for pure diesel oil (fuel I) ND for fuel comprising 50% of diesel oil and 50% of bioesters (fuel II), changing in the software of the computer controlling the injection parameters (dope of fuel and supercharging). Each time, for the change of the injection's parameters settings, the disassembly of the computer was performed, and modified software was installed. There were tested the maximum values and the course of the power and the turning moment one by one for: standard settings, dose of fuel increased by 2%, dose of fuel increased by 4%, does of fuel increased by 6%. Moreover, for the dose of fuel increased by 6%, the measurement was conducted at the supercharging increased from 50 to 150 hPa. The studies were conducted one by one for fuels of the content of bioesters: 0% and 50%. Each test was repeated 10 times.
An exemplary injection map for a 2% increased fuel dose is shown in Figure 1.
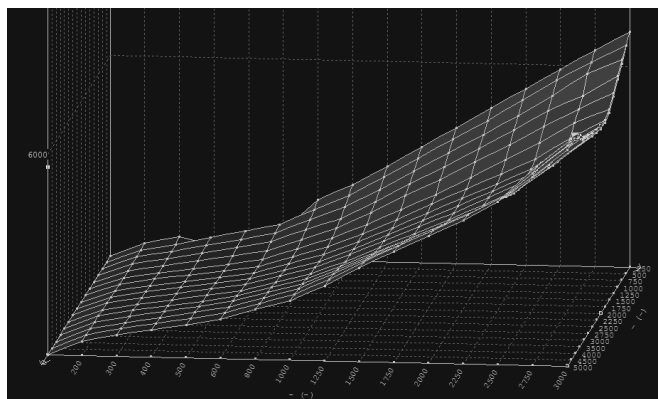
Fig. 1 Injection map for the fuel dose increased by 2%.

The view of the stand for introducing changes in the unit controlling the engine is presented in drawing 2.
The following results have been used for further analysis: powering of the engine with fuel I and at standard settings (A), for fuel II at standard settings (B), dose of fuel increased by 2%(C), dose of fuel increased by 6%(D) and supercharging increased by 50 hPa, and the dose of fuel increased by 6% and supercharging up to 150 hPa(E). The obtained results were exposed to the statistical analysis with the use of the STATISTICA programme.

Fig. 2 The stand for the engine controller's software modification

RESULTS AND DISCUSSION

Based on the conducted tests it has been found, that in case of powering with fuel with 50% of bioesters' additive for standard settings (B), the drop of power and turning moment was observed almost within the whole scope of turning speeds with reference to the engine powered with diesel oil of mineral origin (A). The differences were statistically important and changed within the range from 0 to 18 kW. The biggest differences occurred within the scope of low revolutions (up to 1350 rev/min). Within the range of low rotating speeds 0– 2250 rev/min, the differences occurred within the whole range. Within the range from 1250 rev/min up to 2150, the differences were statistically essential (p=0,05). Similar results were observed by many researchers, including *Orliński (2013) and Kurczyński et al. (2012)*. However, no test results were found on the modification of the injection controller settings. A slight decrease in power and torque was observed by *Xue et al. (2011)*, however, their research was conducted at a lower bioester content in the fuel.

Increasing of the fuel's dose by 2% (with the use of fuel II) (C) made it possible to obtain the power not differing statistically from the power reached by the engine for the fuel I, at standard settings. Increasing of the fuel's dose by 6% and supercharging increased by 50 hPa resulted in subsequent increase of power as compared to the values obtained for fuel I and II at manufactory's settings and for the fuel II at the dose increased by 2%. The obtained mean values are presented in Fig 3. Within the analysed range it has been found, that the most favourable as far as the reached power for fuel II is concerned, is application of the increased dose of fuel and increase of supercharging by 50 hPa. It makes it possible to reach the values higher than for the remaining variants.

Fig. 3 Dependency of power and rotating speed for the tested types of fuels and settings of the engine work's controller.
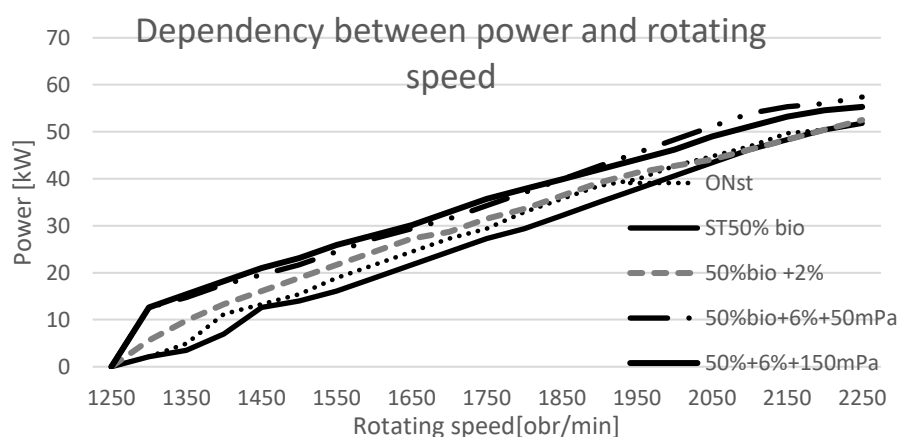
The course of power's increase for the engine powered with fuel II at the dope of fuel increased by 6% and supercharging in turn with 50 hPa and 150 hPa, had the highest value within the range up to 2250 rev/min. Similar results were obtained by *Buyukkaya (2010)*, where the maintenance of high torque and

power required an increase in the amount of fuel supplied by about 8-9%, however in relation to the maximum values.

For these two conditions, within the range of the rotating speed up to 1850 rev/min, the power values did not differ statistically significantly between themselves. At the speed above 1800 rev/min, higher power was reached by the engine at supercharging increased by 50 hPa. The differences were statistically significant.

The engine's turning moment for the tested types of fuels and settings, had the course of a character close to the course of the power changes. The course of the changes of the turning moment is presented in fig. 4. The lowest values of the moment within the whole tested range, has been established for the fuel II at standard settings. For the scope 1350 rev/min-2250 rev/min, the difference between the value of the turning moment for an engine powered by fuel I and II at standard settings, substantially differed statistically and oscillated within the limits 10 – 66 Nm.
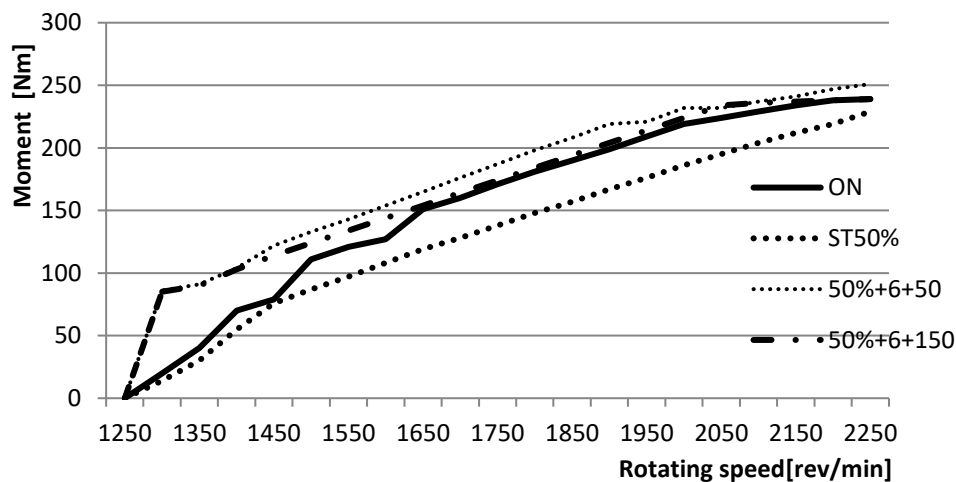
Fig. 4 Course of the turning moment's changes depending on the rotating speed for the tested types of fuel and settings of the engine's controller

A smaller power drop for the 1200-2600 rev / min rotating speed when using the addition of bioesters was observed by Adaileh and AlQdah (2012). However, the bioesters used by them in the studies were preoxidated, which increased their energy value.

CONCLUSIONS

Usage of the addition of biofuel results in reduction of power and of the turning moment. It has been established in many tests conducted in different centers. As a result of the conducted tests it has been found, that powering of the engine with fuel II (50% of bioester) caused the drop in power within the tested range of rotating speeds even by 18 kW. The decrease of power was observed within the whole tested range.

A similar drop was observed for the course of turning moment. The biggest drop in the turning moment amounted to 33 Nm. Such a big drop in power and moment, in particular within the range of lower and medium rotating speeds, shall result in worsening of the traction vehicles' properties, the engines of which are powered with such fuels.

As a result of the conducted experiment covering changes of the engine's operating parameters it has been pointed out, that it is possible to reach the engine's performance parameters not worse than while powering with fuel of connate origin. However, making changes in the manufactory's settings of the engine's operation shall be necessary. Increase of the fuel's dose by 2% as compared to the manufactory's settings (provided for fuel comprising 10% of bioester), has resulted in reaching of engine's performance not differing from the results obtained for I at manufactory's settings.

Further adjustment of the settings of the unit controlling the engine's operation has showed, that it is possible to reach values of power and turning moment higher than for standard settings in case of powering with fuel I (diesel oil of connate origin). The increase of the fuel's dose by 6% and supercharging by 50 hPa, has resulted in the increase of turning moment and power. The difference of the turning

moment for the engine powered with fuel with addition of 50% of biocomponent at standard settings (B) and the setting in which the dope has been increased by 6% and supercharging by 50 hPa (D), amounted maximally to 72 Nm (at 1300 rev/min). A similar increase was observed for the course of power. Increase of power within the range of low rotating speeds amounted from 5- 12 kW. Further increase of supercharging resulted in lowering of power and moment.

REFERENCES

1. Adaileh, M. W & AlQdah, K. S. (2012). Performance of Diesel Engine Fuelled by a Biodiesel Extracted From A Waste Cocking Oil. *Energy Procedia, 18.*

2. Buyukkaya, E. (2010). Effects of biodiesel on a DI diesel engine performance, emission and combustion characteristics. *Fuels, 89*(10).

3. Hossain, ABM S., Salleh, A., & Nasrulhaq, A. (2008). Biodiesel Fuel Production from Algae as Renewable Energy. *American Journal of Biochemistry and Biotechnology 4*(3), 250-254.

4. Hoekmana, S., Brocha, A., Robbinsa, C., Cenicerosa, E., & Natarajanba, M. (2012). Review of biodiesel composition, properties, and specifications. *Renewable and Sustainable Energy Reviews, 16*(1), 143-169.

5. Kowalski, M. & Jankowski, A. (2018) Reasearches of a Combustion Engine Fueled with a Fuel-Water Microemulsion. *Journal of KONES, 25*(4), 186-196.

6. Lapuerta, M., Armas, O., & Rodríguez-Fernández, J., (2008). Effect of biodiesel fuels on diesel engine emissions. *Progress in Energy and Combustion Science, 34*(2), 198-223.

7. Lin, L., Cunshan, Z., Vittayapadung, Shen Xiangqian, S., & Mingdong, D., (2011). Opportunities and challenges for biodiesel fuel. *Applied Energy, 88*(4), 1020-1031.

8. Markiewicz-Patalon, M., Kaszkowiak E., Zbytek, Z., & Szymczak, M. (2017). Comparison of Calorific Values of Petroleum-Driver Fuels with Alternative Fules of Vegetable Origin. *Proceedings of 58th International Conference of Machine Design Departments* (pp. 222-225). p-ISBN 978-80-213-2769-6.

9. Markiewicz-Patalon, M., Muślewski Ł., Kaszkowiak J., & Knopik L. (2018). Analysis of selected operating parameters of engine powered by a mixture of biocomponents and diesel oil. *Jurnal of Kones Powertrain and Transport, 25*(4). ISNN 1231-4005.

10. Markiewicz-Patalon, M., Muślewski, Ł., Kaszkowiak, J., & Sójka M. (2018). Analysis of efficiency of the vehicle transport facilities powered with diesel oil with additive of biocomponent. Kraków: KONMOT.

11. Markiewicz-Patalon, M., Muślewski, M., Kaszkowiak, J., & Landowski B. (2017). Assessment of the suitability of the fuels with component power engines. *Jurnal of Kones Powertrain and Transport, 24*(4). p-ISSN 1231-4005

12. Monyem A., & Van Gerpen J. (2001). The effect of biodiesel oxidation on engine performance and emissions. *Biomass and Bioenergy 20*(4), 317-325

13. Orliński, P. (2013). Ocena wybranych wskaźników pracy silnika rolniczego o zapłonie samoczynnym zasilanego olejami roślinnymi. *Zeszyty Naukowe Instytutu Pojazdów, 1*(93).

14. Uzdowski, M. (2006). Możliwości wykorzystania mieszanin paliw tradycyjnych i alternatywnych do zasilania silników ZS. *Motrol, 8A.*

15. Uzdowski, M. (2008). Problematyka wykorzystania paliw alternatywnych do zasilania silników trakcyjnych. *Motrol, 10.*

16. Xue, J., Grift, E., & Hansen, T. (2011). Effect of biodiesel on engine performances and emissions. *Renewable and Sustainable Energy Reviews, 15*(2).

Corresponding author:

dr inż. Jerzy Kaszkowiak UTP, UTP University of Science and Technology, Faculty of Mechanical Engineering, Al. prof. S. Kaliskiego 7, 85-796 Bydgoszcz, e-mail: jerzy.kaszkowiak@utp.edu.pl

THE DEGRADATION RATE OF RETROREFLECTIVE MATERIALS

Mariia KHRAPOVA[1], Lukáš Jan HRABÁNEK[1], David MARČEV[1]

[1]*Department of Vehicles and Ground transport, Faculty of Engineering, Czech university of Life Sciences Prague*

Abstract
The paper is focused on the comparison of retroreflective levels of traffic sign materials. These samples were exposed to the accelerated natural weathering. Ten types of tree colours have been installed on the test desk on the building flat roof for 16 months. The coefficient of retroreflection was measured by handled retroreflectometer and subsequently was found out the degree of degradation. It was found out that the degradation rate for different types of retroreflective materials is unequal. The lowest difference between measurement was observed for white 3M 4090 film – about 1%, the highest was found for blue samples OR 5710 and 3M EGP films - about 17%. The degree of degradation in terms of colour is the lowest for white and the highest for blue.

Keywords: retroreflectivity; traffic signing; safety; maintenance.

INTRODUCTION

Traffic signs should be visible and readable for all age groups of drivers because signs provide important traffic information and increase safety on roads *(Baratian-Ghorghi, Zhou, Jalayer & Pour-Rouholamin, 2015)*. It is especially important for elderly drivers because they need 8 times more light to respond adequately to a traffic sign than younger drivers. The brightness of signs is also crucial for drivers who have various eye defects. According to the European health interview survey, 19.7% of the respondents have reported eye problems (even if they use glasses or contact lenses) *("Ústav zdravotnických informací a statistiky ČR," 2016)*. The impaired ability of aged drivers to accommodate the eye to different luminance level, a relatively high percentage of drivers with eye defects, poor weather conditions and darkness might significantly affect the visibility of a traffic sign.
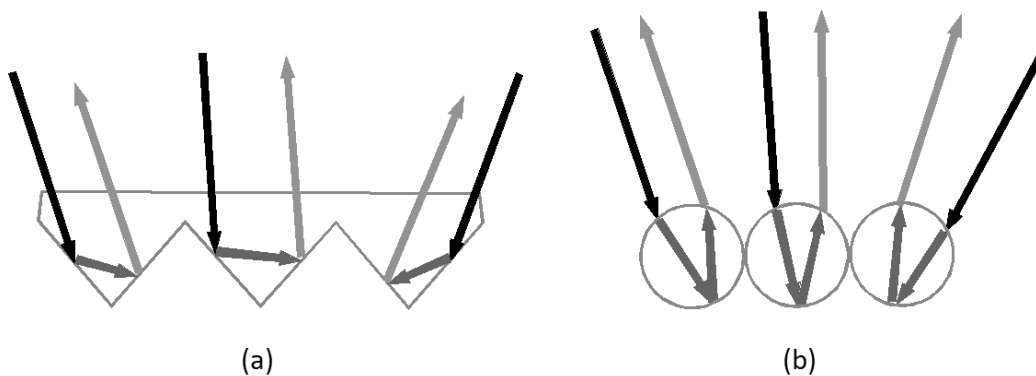
Fig. 1 Compositions of retroreflective sheeting. (a) Microprismatic type is consisted of prisms. (b) Glass bead type is consisted of small glass spheres. *(Source: Authors' work)*

Visibility of traffic signs at night, when about 50% of road accidents occur *(FHWA, 2008; National Safety Council, 2018)*, is ensured with special retroreflective sheeting upon the signs. This type of sheeting increases the brightness of the signs by reflecting light from the car headlights directly toward the driver *(Austin & Schultz, 2009)*. Nowadays, there are two main types of retroreflective sheeting, glass bead and microprismatic (Fig.1). They do not only have different structural units – glass spheres or prisms – they also have different tendencies to deterioration in the course of time *(Brimley & Carlson, 2013; Oloufa, 2017; Ré, Miles & Carlson, 2011; Rizenbergs, 1974; Sørensen, 2011)*.

Taking into account the degradation rate of retroreflective sheeting makes it possible to create a predictive model thus optimize the maintenance activities and replacement of road signs *(Babić, Babić, &*

Macura, 2017; Wolshon, Swargam, & Degeyter, 2002). Maintenance programs allow traffic signs not only to be visible enough but also to cut down the expenses of road agencies *(Bischoff & Bullock, 2002; Jackson, Carlson, Ye & Jackson, 2013)*.

The goal of this article is to determine the degradation rate of different types of retroreflective materials after accelerated natural weathering.

MATERIALS AND METHODS

The study encompassed 30 samples of white, red and blue retroreflective sheeting commonly used in signing production in the Czech Republic. The Tab. 1 represents all the test samples with dimensions 210 (mm) by 297 (mm) produced by different manufacturers - 3M, Avery Dennison (AD) and Oralite (OR). The samples were placed on the test desk that was installed on the flat roof of the Faculty of Engineering of CULS Prague. It was inclined at an angle of 45° and was oriented face to the south for the accelerated natural weathering *(ČSN EN 12899-1 Stálé svislé dopravní značení - Část 1: Stálé dopravní značky, 2003)*. Samples were exposed to natural weathering for sixteen months. Due to natural weathering the results similar to the degradation rate of the in-service traffic signs can be provided (Ketola, 1999).

Tab. 1 Test samples according to the manufacturer, type and colour. W – white, R – red, B – blue; GB – glass bead, M – microprismatic.

Class*	Number of sheeting	Manufacturer and serial number	Colour			Type
			W	R	B	
	1	3M 3200	X	x	x	
RA1	2	AD 1500	X	x	x	**GB**
	3	OR 5710	X	x	x	
	4	3M EGP	X	x	x	
	5	3M 3930	X	x	x	
RA2	6	AD 6500	X	x	x	
	7	OR 5910	X	x	x	**M**
	8	3M 4090	X	x	x	
RA3	9	AD 7500	X	x	x	
	10	OR 6910	X	x	x	

* - according to *(EN 12899-1 Fixed, vertical road traffic signs, 2007)*

Before putting out the sheeting samples, the measurements of their coefficient of retroreflection were made according to the standards *(ČSN EN 12899-1 Stálé svislé dopravní značení - Část 1: Stálé dopravní značky, 2003; EAD 120001-00-0106 Microprismatic retro-reflective sheetings, 2016)*. The measurement of the retroreflective films was carried out by a certified measuring device - retroreflectometer Zehnther 6060, which allowed to set the coefficient of retroreflection in compliance with the requirements of *(ČSN EN 12899-1 Stálé svislé dopravní značení - Část 1: Stálé dopravní značky, 2003)*. The device also provided with information about the average value of three measurements of each sample. The mean value was used for further analysis.

In the Czech Republic, there is not common unified standard for measuring of different retroreflective sheeting materials. For example, glass bead sheeting should be tested according to *(ČSN EN 12899-1 Stálé svislé dopravní značení - Část 1: Stálé dopravní značky, 2003)* and microprismatic retroreflective materials – in accordance with the European Technical Assessment *(EAD 120001-00-0106 Microprismatic retro-reflective sheetings, 2016)*. RA1 and RA2 glass bead materials are measured according to these technical regulations with observation angle $\alpha = 0.2°$, 0.33° and 2° and illumination angle $\beta_1 = +5°$, +30°, +40°. RA3 film is measured with observation angle of 0.33°, 1°, 1.5° and illumination angle + 5°, + 20°, + 30°, +40°. The identical measurement was carried out with the chosen illumination angle $\beta_1 = 5°$ and the observation angle $\alpha = 0.33°$ to compare the test samples. A summary of the minimal performance

requirements for chosen illumination and observation angles of retroreflective sheeting is presented in Tab. 2.

Tab. 2 Requirements for minimal values of coefficient of retroreflection (cd·lx⁻¹·m⁻²) for different colours and retroreflective classes according to *(ČSN EN 12899-1 Stálé svislé dopravní značení - Část 1: Stálé dopravní značky, 2003)*

Class	Colour		
	White	Red	Blue
RA1	50	10	2
RA2	180	25	14
RA3	300	60	19

In order to determine the rate of degradation of individual samples, repeated measurement of the samples was carried out 16 months after exposing them to natural weathering. According to the standards *(ČSN EN 12899-1 Stálé svislé dopravní značení - Část 1: Stálé dopravní značky, 2003; EAD 120001-00-0106 Microprismatic retro-reflective sheetings, 2016)*, the samples were always cleaned before the measurement in order to avoid the influence of dirtiness. To specify the results, the meteorological conditions during this period were taken from the meteorological station that is located approximately 300(m) from the measuring spot.

Tab. 3 Determination of the scale of retroreflective degradation

D (k)	% loss of retroreflection
1	<5
2	5–10
3	11–15
4	> 15

The average values of the first and second measurements of each individual sample were compared by calculating the difference between these two values. The result was presented in a percentage. In order to determine the degree of degradation D(k) of each reflective material, all the results were divided into 4 groups (Tab. 3). Group number 1 corresponded to a decrease in retroreflection up to 5%. Group number 2 corresponded to a decrease in retroreflection from 5 to 10%. Group number 3 corresponded to values of results from 10 to 15%. The difference between the two measurements above 15% is represented by group number 4.

RESULTS AND DISCUSSION

According to the meteorological station, during the period of time the daily temperature fluctuated from -9°C to 30°C, the daily humidity - between 45% and 95%. Global radiation ranged from 1,500 to 22,500 (kJ·m⁻² per day). The barometric pressure was between 953 and 988 (hPa). Daily rainfall ranged from 0.0 to 17 (mm per day). The scale of meteorological data is wide here but average values are not presented in the paper because they would not describe measuring conditions with higher preciseness. They represent usual nowadays continental conditions of the central Europe. Nevertheless, these meteorological conditions have led to the deterioration of the retroreflection level that is presented in Tab. 4 as D (k). This table also shows the average values of retroreflection coefficient of two data sets of measurements ("before" – the first measurement and "after "– the second measurement) that could be used for future researches.

The analysis of Tab. 4 shows that a total of 70% of white test samples can be included in group number 1. 20 % of all white retroreflective sheeting corresponds to group number 2 and only OR 5710 has lost 11.63% of retroreflection and corresponds to group number 3. According to the class division of all white samples, RA2 and RA3 have shown the loss of retroreflection up to 5%.

Regarding the red colour, 50% of all the samples correspond to group number 1, 20% to group number 2, the rest of the samples shows the deterioration of retroreflection above 10%. The highest retroreflection loss is observed in 3M 3200 film with retroreflection loss of 16.5%.

Tab. 4 The average values of measurements of retroreflection coefficient (cd·lx⁻¹·m⁻²) and the degree of degradation of different types of sheeting. W – white, R – red, B – blue, b – before, a – after.

		Number of sheeting									
		1	2	3	4	5	6	7	8	9	10
W	b	85±3	73±3	109±4	132±5	678±28	414±17	530±22	769±32	422±17	434±18
	a	79±3	74±3	97±4	118±5	649±27	400±16	585±24	763±31	417±17	426±17
	D(k)	2	1	3	2	1	1	1	1	1	1
R	b	16±1	16±1	19±1	23±1	125±5	66±3	127±5	129±5	100±4	102±4
	a	14±1	15±1	16±1	22±1	118±5	59±2	125±5	127±5	88±4	99±4
	D(k)	4	1	3	2	2	1	1	1	3	1
B	b	1*	7*	8*	9*	43±2	33±1	64±3	52±2	30±1	43±2
	a	1*	7*	6*	8*	41±2	30±1	63±3	48±2	28±1	42±2
	D(k)	1	1	4	4	1	2	1	2	1	1

* - deviation is negligible, because is less than 0.4

Regarding the red colour, 50% of all the samples correspond to group number 1, 20% to group number 2, the rest of the samples shows the deterioration of retroreflection above 10%. The highest retroreflection loss is observed in 3M 3200 film with retroreflection loss of 16.5%.

Concerning the blue colour, group number 1 includes 40% of samples, 30% belong to group number 2, the rest relates to group number 4. Specifically, the retroreflection coefficient of a blue sample of the 3M 3200 film is between 1.1 - 1.2 (cd·lx⁻¹·m⁻²), which is below the requirements of *(ČSN EN 12899-1 Stálé svislé dopravní značení - Část 1: Stálé dopravní značky, 2003)*. According to the class division, the loss of retroreflection above 15% is found in 75% of the RA1 film samples. However, this comparatively high percentage of deterioration does not mean that the coefficient of retroreflection of all samples will decrease in the same range during their whole service life.

Tab. 5 Comparison of authors' results with the results from study *(CHEN & JIANG, 2016)*

		Authors' results 16 months %		(CHEN & JIANG, 2016) 156 months %	
Colour	**Class**	minimal value	maximal value	minimal value	maximal value
White	RA1	7	12	12	21
	RA2	1	4	15	29
	RA3	1	2	2	9
Red	RA1	3	17	10	26
	RA2	2	10	12	40
	RA3	3	12	1	43
Blue	RA1	5	18	1	9
	RA2	2	10	11	15
	RA3	2	4	0.1	15

Looking at the average D(k) values in terms of colour, white samples show the lowest value since the degradation rate of the retroreflective materials is 1.4. The red samples show the average value of

D(k) 1.9 and for the blue samples, the average D(k) is 2.2. Looking at the average value of D(k) for different classes, the lowest value was presented by the microprismatic films RA3 and RA2 - the average value of D(k) is 1.33. The highest material degradation rates are shown for the RA1 film samples with D(k) equal to 2.58.

Almost all test samples after natural weathering have met the minimal requirements that are presented in Tab.2. Only the 3M 3200 blue sheeting did not meet the requirements of the standard, but even the new one.

In the Tab. 4 some coefficients of retroreflection were higher for the second measurement than for new sheeting samples. It can be explained that points for measurements were selected randomly and the microstructure of retroreflective films is not uniform as well.

The results of current study have been compared with the results of study *(CHEN & JIANG, 2016)* because of the same division of retroreflective materials. However, unlike to this research, *(CHEN & JIANG, 2016)* investigated 230 traffic signs for 13 years in Beijing, China. The minimal and maximal values of degradation rate for different types of retroreflective materials were used for comparison and are presented in Tab. 5. The analysis of Tab. 5 shows that there is no linear dependence on signs deterioration. Over a tenfold period of time, the average degradation rate has tripled. These results cannot be final as there are many factors that can affect the measurement. These factors include the environmental conditions around the traffic signs (*Khalilikhah* & Heaslip, 2015) and ambient temperature and humidity during the measurement *(Khrapova, 2019)*.

CONCLUSIONS

The goal of this paper was to determine the degradation rate of ten types of retroreflective sheeting commonly used on the traffic signs in the Czech Republic. In order to fulfil the main aim of the research two sets of data measurements were made - before and after accelerated natural weathering. The results of the measurements were compared, and the degree of degradation was found. After analysis, it was found that samples of red and blue R A1 were assessed as unstable because the deterioration of the retroreflection level was more than 15% after 16 months of natural weathering. It was also found that the 3M 3200 blue sheeting did not meet the requirements of the standard. The high level of degradation of retroreflective material was observed for the red 3M 3200 sheeting with 16.5% of deterioration, blue samples OR 5710 and 3M EGP films had the highest loss - about 17%.

According to the results of the carried out research, it can be assumed that some types of retroreflective sheeting will not meet the minimal retroreflection requirements before the end of their service life. The comparative analysis showed that degradation rate is not a linear function, it decreases in time. The experiment will continue, as the approved part of doctoral thesis, for several more years to prove that there is no constant degradation rate for different types of retroreflective films. The future results can support the design of the more accurate model of retroreflection degradation.

ACKNOWLEDGMENT

REFERENCES

1. Austin, R. L., & Schultz, R. J. (2009). *Guide To Retroreflection Safety Principles And Retrorereflective Measurements*. San Diego: RoadVista.
2. Babić, D., Babić, D., & Macura, D. (2017). Model for Predicting Traffic Signs Functional Service Life – The Republic of Croatia Case Study. *PROMET - Traffic&Transportation*, *29*(3), 343.
3. Baratian-Ghorghi, F., Zhou, H., Jalayer, M., & Pour-Rouholamin, M. (2015).

Prediction of Potential Wrong-Way Entries at Exit Ramps of Signalized Partial Cloverleaf Interchanges. *Traffic Injury Prevention*, *16*(6), 599–604.

4. Bischoff, A., & Bullock, D. (2002). Sign retroreflectivity study. *Joint Transportation Research Program*, 190.

5. Brimley, B. K., & Carlson, P. J. (2013). The Current State of Research on the Long-Term Deterioration of Traffic Signs. In *Transportation Research Board 92nd Annual Meeting* (p. 14).

6. Chen, Y., & Jiang, M. (2016). Attenuation law of retroreflection coefficient for highway traffic sign retroreflective sheeting. *Journal of Traffic and Transportation Engineering*, *16*(6), 107–113.

7. ČSN EN 12899-1 Stálé svislé dopravní značení - Část 1: Stálé dopravní značky, Český normalizační institut. (2003).

8. EAD 120001-00-0106 Microprismatic retro-reflective sheetings. (2016).

9. EN 12899-1 Fixed, vertical road traffic signs (2007).

10. FHWA. (2008). *Traffic sign retroreflectivity*. US Department of transportation.

11. Jackson, N. M., Carlson, P. J., Ye, F., & Jackson, G. R. (2013). *Use of high intensity reflective sheeting in lieu of external lighting of overhead roadway signs. Transport*. Florida: Dept. of Transportation,

12. Ketola, W. (1999). Laboratory-Accelerated Versus Outdoor Weathering for Retroreflective Sheeting Specifications. *Transportation Research Record: Journal of the Transportation Research Board*, *1657*, 63–70.

13. Khalilikhah, M., & Heaslip, K. (2015). Important Environmental Factors Contributing to the Temporary Obstruction of the Sign Messages.

14. Khrapova, M. (2019). Determining the influence of factors on retroreflective properties of traffic signs. *Agronomy Research*, *17*(S1), 1041–1052.

15. NSC. (2018). National Safety Council.

16. Oloufa, A. A. (2017). Development of a Sign Sheeting Sampling Protocol for the Determination of Service Life of Traffic Signs UCF-CATSS.

17. Ré, J. M., Miles, J. D., & Carlson, P. J. (2011). Analysis of In-Service Traffic Sign Retroreflectivity and Deterioration Rates in Texas. *Transportation Research Record: Journal of the Transportation Research Board*, *2258*(1), 88–94.

18. Rizenbergs, R. L. (1974). *High-Intensity Reflective Materials for Signs*.

19. Sørensen, K. (2011). Durability test of retro-reflecting materials for road signs at Nordic test sites - Ageing model for the retro-reflectivity after further exposure.

20. Ústav zdravotnických informací a statistiky ČR. (2016). Retrieved from http://www.uzis.cz/

21. Wolshon, B., Swargam, J., & Degeyter, R. (2002). Analysis and Predictive Modeling of Road Sign Retroreflectivity Performance. In *16th Biennial Symposium on Visibility and Simulation* (p. 9).

Corresponding author:
Ing. Mariia Khrapova, Department of Vehicles and Ground transport, Faculty of Engineering, Czech University of Life Sciences Prague, Kamýcká 129, Praha 6, Prague, 16521, Czech Republic, e-mail: khrapova@tf.czu.cz

FLOW CHARACTERISTICS OF THE TRACTOR HYDRAULIC CIRCUIT BY APPLICATION OF THE BIODEGRADABLE SYNTHETIC FLUID

Ján KOSIBA[1], Juraj JABLONICKÝ[1], Rastislav BERNÁT[2], Zoltán ZÁLEŽÁK[2]

[1]*Department of Transport and Handling, Faculty of Engineering, Slovak University of Agriculture in Nitra, Slovakia*
[2]*Department of Quality and Engineering Technologies, Faculty of Engineering, Slovak University of Agriculture in Nitra, Slovakia*

Abstract
This paper deals with lifetime test of biodegradable synthetic fluid. This fluid was used in the hydraulic and transmission circuit of a tractor type Zetor Proxima 6321. The test of the biodegradable synthetic fluid was set 500 engine hours (EH). During operating test was monitored the influence of the biodegradable synthetic fluid on flow characteristics and decrease of flow efficiency of the tractor hydraulic pump. The decrease of the flow efficiency of the hydraulic pump by nominal speed after completing 500 EH was Δηpr = 1.701%. The measurements were founded the minimal influence of the fluid on the hydraulic pump wear.

Key words: engine speed; flow efficiency; hydraulic pump.

INTRODUCTION

Hydraulic equipment is widely used in powerful mechanisms of agricultural and forest machines as well as in many other areas. The development of modern hydraulic components is aimed at increasing the transmitted power, reducing the energy intensity, minimizing the environmental pollution and increasing the technical life and machine reliability (*Haas et al, 2016*). Environmental protection is an actual topic already for several years, and it becomes a preferred problem in the established trend of economic development (*Tóth et al, 2014*, *Majdan et al, 2018*). Agricultural technology has a negative impact on all elements of the environment (*Kučera et al, 2016*). It was reported that over 60% of all lubricants end up in soil and water (*Majdan et al, 2013*). Hydraulic line breaks are extremely common. If not attended to, these releases can cause contamination of the soil, ground and surface water. The ecological fluids market is expanding, and ecological oils which can be used in hydraulic and transmission systems are one of the provided products *(Hnilicová et al, 2016)*. Biodegradability has become one of the most important design parameters both in the selection of base fluids and in the overall formulation of the finished lubricant (*Mendoza et al, 2011*).

This paper presents the results of a long-term operational test of the biodegradable synthetic fluid (type HEES – Hydraulic Environmental Ester oil Synthetic). The biodegradable synthetic fluid was applied in the transmission and hydraulic circuit of the tractor type Zetor Proxima 6321. During operating test was monitored the influence of the biodegradable synthetic fluid on flow characteristics of the tractor hydraulic pump. Flow characteristics of the tractor hydraulic pump is a basic indicator its lifetime. The test of the biodegradable synthetic fluid was set 500 engine hours (EH). The majority of tractors are subjected to conditions (especially during the winter) which can cause an undesirable phase transition of fluid in hydraulic systems. It is necessary to further develop and improve fluid flow by means of the correct operation of hydraulic equipment. The flow characteristics are important to the life of the hydraulic system.

MATERIALS AND METHODS

To choose the agricultural tractor for testing, it was taken into account analysis of the sale of agricultural tractors and the utilization of tractors on farms in Slovakia. By these criteria, it was selected Zetor Proxima 6321 tractor. Before application of biodegradable synthetic fluid, there was removed fluid from the transmission and hydraulic circuit and it was purified. At the same time, the new oil filter was fitted to the tractor. To the transmission and hydraulic circuit of the tractor there was applied selected biodegradable synthetic fluid.

Operational test of the biodegradable synthetic fluid was set at 500 engine hours (EH) (the tractor had over 2,450 EH). Measurements of flow characteristics are made after completing 0, 250 and 500 engine hours. The most important condition by measuring of the flow characteristics of hydraulic pumps is the oil temperature. The temperature must be maintained at constant value, because the viscosity of the fluid depends on it. At the same time, by measuring of the flow characteristics, the fluid temperature must be on operating value. Another extremely important parameter is revolution of hydraulic pump. The hydraulic pump revolution will be monitored based on the combustion engine revolution among which is transference. The temperature of oil during measuring of flow characteristics was t = 40°C. Table 1 shows the basic technical parameters of biodegradable synthetic fluid.

Tab. 1 Technical parameters of biodegradable synthetic fluid

Properties	Unit	Amount
Kinematic viscosity at 40°C	$mm^2 s^{-1}$	67.52
Density at 15°C	$kg\ m^{-3}$	931
Flash point	°C	212
Pour point	°C	- 48

The speed of the hydraulic pump will be monitored based on speed of the combustion engine, whereas the internal combustion engine and the hydraulic pump axle ratio $i = 1.467$ reducing. Table 2 shows the speed of the hydraulic pump during measuring of flow characteristics.

Tab. 2 Speed of combustion engine and hydraulic pump

Combustion engine speed (rpm)	Hydraulic pump speed (rpm)
1,600	1,090
2,200	1,500
2,300	1,570

To establish a methodology for the flow of hydraulic characteristics of hydraulic pumps measuring, it is needed to set up the components that would be used to achieve the intended results. The most important components include a flow sensor, pressure sensor, temperature sensor, recording unit, load member and joint flange. By the draft of the measurement chain, it is required to follow the certain measurement conditions. The most important condition by measuring of the flow characteristics of hydraulic pumps is the oil temperature. The temperature must be maintained at constant value, because the viscosity of the oil depends on it. At the same time, by measuring of the flow characteristics, the oil temperature must be on operating value. Another extremely important parameter is speed of hydraulic pump. The speed of hydraulic pump will be monitored based on the combustion engine speed among which is transference (*Tkáč et al, 2014*).

RESULTS AND DISCUSSION

The flow characteristics were measurement at 0 EH, after completing 250 EH and after completing 500 EH. Fig. 1 – 3 shows the flow characteristics of the hydraulic pump type UD 20 at the different speeds and Fig. 4 flow efficiency of the hydraulic pump after statistical processing. The polynomial regression function of 2 orders at analysis of measurement was used.

Standard deviation σ is defined as a positive square root of variance. Standard deviation is calculated if we have a complete set of possible states of the process (system). In probability theory and in statistics, standard deviation or mean square deviation is a measure of statistical dispersion. Simply said, it refers to how widely are the values distributed in a set (*Hill & Lewicky, 2006*).

$$\sigma = \sqrt{\frac{1}{n}\sum_{i=1}^{n}(x_i - \bar{x})^2} \qquad (1)$$

where: n – population size, x_i – individual values of population, $\bar{x}$ – arithmetic average of population.

When selecting a value from the range -2σ, $+2\sigma$, the probability of standard normal distribution is 95.46%. The flow efficiency of the hydraulic pump was calculated from this sample of values.
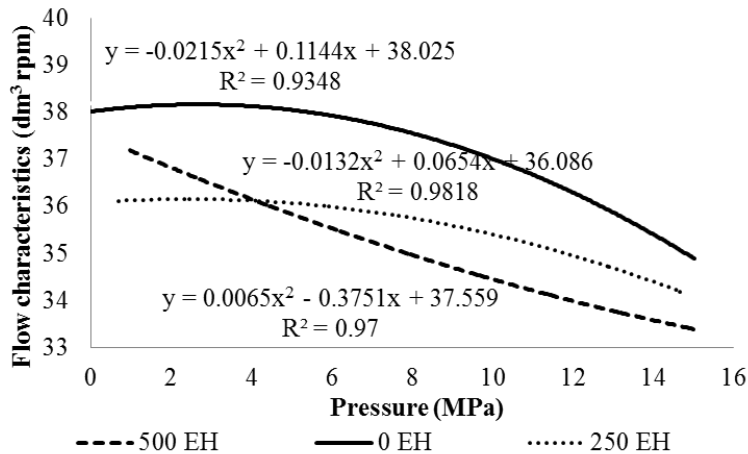

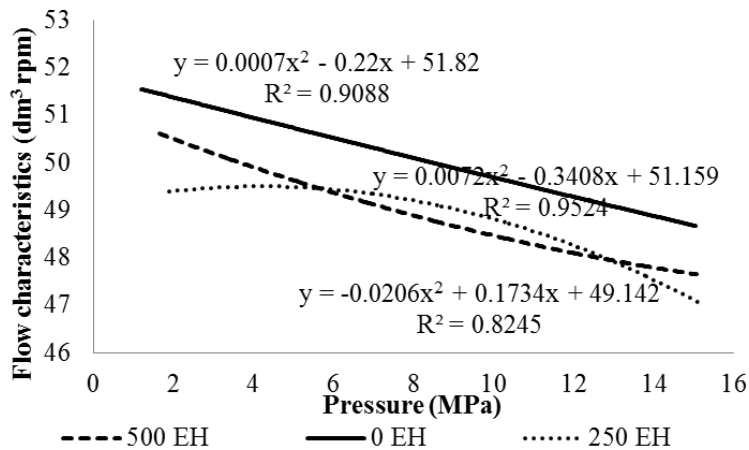**Fig. 1** Flow characteristics of hydraulic pump at n = 1,090 rpm

Fig. 2 Flow characteristics of hydraulic pump at n = 1,500 rpm (nominal speed)
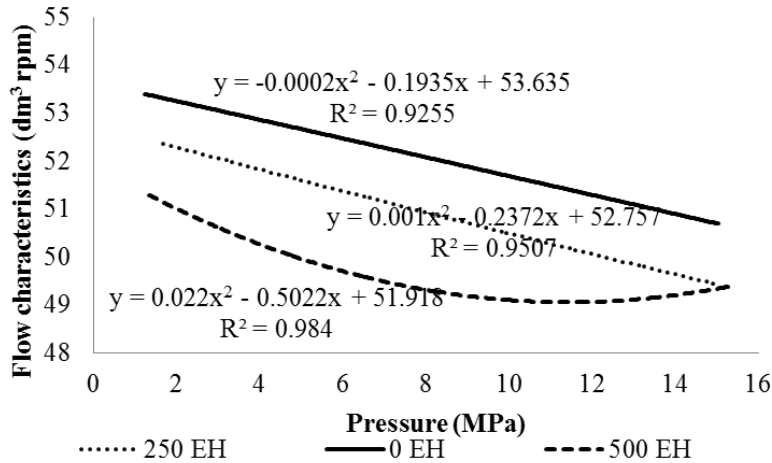
Fig. 3 Flow characteristics of hydraulic pump at n = 1,570 rpm
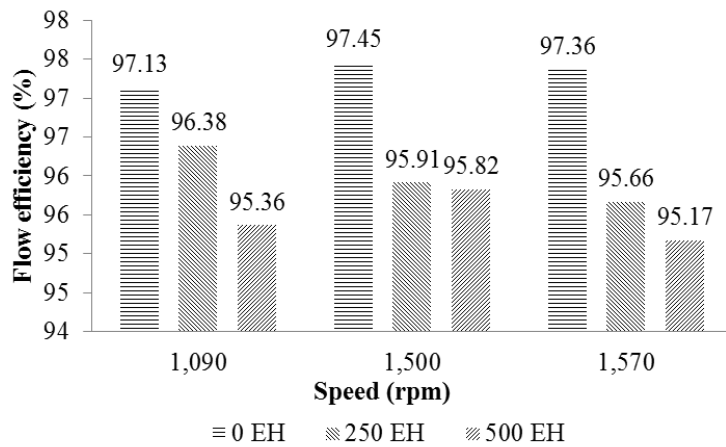
Fig. 4 Flow efficiency of the hydraulic pump

Hydraulic pump-operating conditions affect significantly the pump efficiencies, it is very important to understand how the pump efficiencies depend on the hydraulic pump-operating conditions (*Inaguma & Yoshida, 2013*). At the beginning of the performance test of biodegradable synthetic fluid, the level of flow efficiency by nominal speed of hydraulic pump was at η_{pr0} = 97.45%; at the end of the performance test, it was at η_{pr500} = 95.82%. This means that the decrease of the hydraulic pump flow efficiency after completing 500 EH was $\Delta\eta_{pr}$ = 1.701%. This decrease indicates a minimal impact of biodegradable synthetic fluid on the lifetime of the hydraulic pump of tractor type Zetor Proxima 6321. *Dobrota et al*, (2010) evaluated the flow efficiency of the hydraulic pump at the nominal speed η = 95.73% depending on the pressure p = 20 MPa and *Michael et al*, (2012) evaluated the flow efficiency at the nominal speed η = 95.00%. These values corresponded with our results.

Kinematic viscosity at 40 °C (Fig. 5) is evaluated based on the positive or negative tolerance of the measured values in comparison with the value of new oil (0 engine hours). The decrease of kinematic viscosity at 40 °C does not exceed the limit of 20% which is prescribed for the ISO 15380:2011 standard. The deviation of kinematic viscosity at 40°C is calculated by using the formula:

$$\Delta V = \frac{V_0 - V_{500}}{V_0} \cdot 100 \tag{2}$$

where: ΔV – deviation of kinematic viscosity at 40 °C, V_0 – kinematic viscosity at 40 °C at 0 engine hours, V_{500} – kinematic viscosity at 40 °C at 500 engine hours

Fig. 5 Kinematic viscosity at 40 °C and decrease of kinematic viscosity at 40 °C

The decrease of kinematic viscosity at 40 °C (after completing 500 engine hours) was calculated $\Delta V = 2.41\%$ according to Eq. (3), based on the value of new oil $v_0 = 67.52$ mm^2 s^{-1} and value of used oil $v_{500} = 65.89$ mm^2.s^{-1}. *Alias et al,* (2009) evaluated the kinematic viscosity at 40 °C of palm oil-based TMP este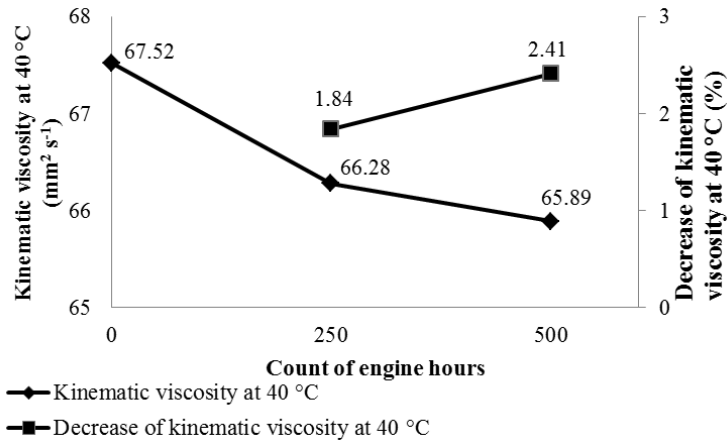r (TMPE) and found the increase of kinematic viscosity after completing 400 hours $\Delta V = 1.72\%$. Decrease of kinematic viscosity of the fluid means too thin oil film and therefore low load capacity. The lower viscosity, the higher wear occurs (*Sejkorová et al, 2017, Majdan et al, 2014*).

CONCLUSIONS
Tribotechnical diagnostics use oils as media that help obtain information about processes and changes in the systems that they lubricate. If tribodiagnostics are applied properly and thoroughly, they result in significant savings in many areas; for example, they contribute to an increase of the lifetime of machines and devices, to a decrease of consumption of energy, to limiting the idle time (*Kučera et al, 2013, Kučera et al, 2017*). The decrease of the hydraulic pump flow efficiency by nominal speed after completing 500 EH was $\Delta\eta_{pr} = 1.701\%$. This decrease indicates a minimal impact of biodegradable synthetic fluid on the lifetime of the hydraulic pump of the tractor type Zetor Proxima 6321. We can say that the biodegradable synthetic fluid does not affect the construction or operation of the tractor type Zetor Proxima 6321.
Biodegradable synthetic fluid has no negative influence on the rubber components in the hydraulic circuit of the tractor type Zetor Proxima 6321. One of the reasons for the high price of environmentally friendly hydraulic fluids is the necessity for the manufacturers of hydraulic pumps to approve the usage of the fluid in the hydraulic system and to verify its compatibility with hydraulic circuit components (*Xuejun et al, 2015, Stojilković & Kolb, 2016).*

REFERENCES

1. Alias, N.H., Yunus, R., Idris, A., & Omar. R. (2009). Effect of additives on oxidation characteristics of palm oil-based trimethylolpropane ester in hydraulic applications. *European Journal of Lipid Science and Technology 111*(4), 368–375.
2. Haas, P., Kadnár, M., Tóth, F., Rusnák, J., & Nógli, D. (2016). Influence of bellows setting on its spring rate and on temperature ad-

justment of electromechanical thermostats. *Acta technologica agriculturae*, *19*(2), 43–48.
3. Hill, T. & Lewicky, P. (2006). *Statistics: Methods and applications*. Statsoft Inc., Tulsa USA.
4. Hnilicová, M., Kučera, M., & Pavlu, J. (2016). Analysis of hydraulic oil in handling lines baljer & zembrod using the methods of

trobotechnical diagnostics. *Key Engineering Materials, 669*, 451–458.

5. Dobrota, D., Lalić, B., & Oršulić, M. (2010). Experimental modelling of volumetric efficiency of high-pressure external gear pump, *Nase More, 57*(5-6), 535–240.

6. Inaguma, Y. & Yoshida, N. (2013) Mathematical analysis of influence of oil temperature in hydraulic pumps for automatic transmissions. *SAE Interantional Jouranl of Passenger Cars – Mechanical Systems, 6*(2) 786–798.

7. Kučera, M., Majdan, R., Abrahám, R., & Haas, P. (2016). Analysis of the effect of loading on tribological system properties. *Acta Universitatis Agriculturae et Silviculture Mendelianae Brunensis, 64*(3), 825–833.

8. Kučera, M., Aleš, Z., Ivandić, Z., & Hujo, Ľ. (2013). Possibility of hydraulic fluids with a low environmental impact application in agriculture and transport machinery. *Journal of Central European Agriculture, 14*(4), 1592–1601.

9. Kučera, M., Aleš, Z., & Pexa, M. (2016). Detection and characterzation of wear particles of universal tractor oil using a particles size analyzer. *Agronomy Research, 14*(4), 1351–1360.

10. Kučera, M. & Aleš, Z. (2017). Morphology analysis of friction particles generated in tractor transmission oils. *Acta Technologica Agriculturae, 20*(3), 57–62.

11. Majdan, R., Tkáč, Z., & Kangalov, P.G. (2013). *Research of ecological oil-based fluids properties and new test methods for lubricating oils : scientific monograph.* 1st ed. Rousse : Angel Kanchev University of Rousse, 98 s.

12. Majdan, R., Tkáč, Z., Abrahám, R., Szabó, M., Halenár, M., Rášo, M., & Ševčík, P. (2016). Proposal for filtration systme for biodegradable lubricants in agricultural tractors. *Agronomy Research, 14*(4), 1395–1405.

13. Majdan, R., Olejár, M., Abrahám, R., Šarea, V., Uhrinová, D., Jánošová, M. & Nosian, J. (2018). Pressure Surce Analysis of a Test Bench for Biodegradable Hydraulic Oils. *Tribology in Industry, 40*(2), 183–194.

14. Majdan, R., Tkáč, Z., Stančík, B., Abrahám, R., Štulajter, I., Ševčík, P., & Rášo, M. (2014). Elimination of ecological fluids contamination in agricultural tractors. *Research in agricultural engineering, 60*(special iss. 1), 9–15.

15. Mendoza, G., Igartua, A., Fermamdez-Diaz, B., Urquiola, F., Vivanco, S., & Arguzoniz, R. (2011). Vegetable oils as hydraulic fluids for agricultural applications. *Grasas y aceites 62*(1), 29–38.

16. Michael, P.W., Khalid H., & Wanke, T. (2012). An Investigation of external gear pump effiecency and stribeck values. *SAE Technical Papers* 8.

17. Sejkorová, M., Hurtová, I., Glos., J., & Pokorný, J. (2017). Definition of a motor oil change interval for high-volume diesel engines based on its current characteristics assessment. *Acta Universitatis Agricultrrae et Silviculturae Mendelianae Brunensis, 65*(2), pp. 481–490.

18. Stojilković, M. & Kolb, M. (2016). Tribological Properties of Biodegradable Universal Tractor Transamission Oil. *Tribology in Industry, 38*(2), 229–234.

19. Tóth, F., Rusnák, J., Kadnár, M., & Váliková, V. (2014). Study of tribological properties of chosen types of environmentally friendly oils in combined friction conditions. *Journal of Central European Agriculture, 15*(1), 185–192.

20. Tkáč, Z., Drabant, Š., Majdan, R., & Cvíčela, P. (2008). Testing stands for laboratory tests of hydrostatic pump of agricultural machinery. *Research in Agricultural Engineering, 54*(1), 183–191.

21. Tkáč, Z., Hujo, Ľ., Tulík, J., Kosiba, J., Uhrinová, & Šinský, V. (2014). Greening of agricultural and forestry tractors. *Acta Universitatis Agriculturae et Silviculturae Mendelianae Brunensis, 62*(5), 1135–1139.

22. Xuejun, H., He, J., & Tenfei, S. (2015) Analysis on design of coiled tubing sliding drilling electronic control tractor with hydraulic-driven in microhole. *Electronic Journal of Geotechical Engineering, 20*(10), 4333–4347.

Corresponding author:

doc. Ing. Ján Kosiba, PhD. Department Transport and Handling, Faculty of Engineering, Slovak University of Agriculture in Nitra, Tr. A. Hlinku 2, 949 76, Nitra, Slovakia, phone: +421 37 641 5776, e-mail: jan.kosiba@gmail.com

ANALYSIS OF PARTICULATE MATTER PRODUCTION DURING DPF SERVICE REGENERATION

Martin KOTEK[1]

[1]Department of Vehicles and Ground Transport

Abstract
The reduction of particulate matter (PM) production generated by diesel engines is important topic of nowadays. One of possible ways to reduce of PM is the usage of diesel particulate filters (DPF). The basic function of DPF is a collecting of PM inside the filter. That is why that the functional DPF must be regularly regenerated and there are several methods of regeneration processes. This article deals with analysis of PM production during the service regeneration process of DPF.
The vehicle Skoda Rapid with turbocharged diesel common-rail engine equipped by DPF was used for the experiment. The results show high PM production during the process of DPF regeneration. The production was approximately 1.5 times higher than production of diesel engine without DPF at the maximum engine load. The summary of total PM concentration during the regeneration is equal to production of diesel car without the DPF during 1-hour normal drive.

Key words: DPF; common rail; particulate matter; TDI; OBD.

INTRODUCTION

Private car use is one of the biggest polluters of modern cities. The main impurities include carbon monoxide (CO), nitrogen dioxide (NO_2), ozone (O_3) and particulate matter (PM) (*Hea J., 2017*). It is becoming increasingly topical issue particulate matter in recent years.

PM in pure form (elementary and organic carbon) are not dangerous but they create conditions suitable for dangerous pollutant. The mutagenicity and carcinogenicity of PM initially was attributed primarily to polycyclic aromatic hydrocarbons (PAH) (*Lewtas, 2007; Vojtíšek-Lom, 2015*). PM may affect reproduction, cardiovascular system or may be involved in cancer (*Lewtas, 2007*). The main impact on health has a PM size. Particles less than tens of nanometres can penetrate through cell membranes into the blood and have a wide and detrimental effect on human health. (*Künzli, 2000*).

Currently there are several ways to reduce the production of PM. One possible way is a higher rate of biofuels use which has a positive impact on PM production. This trend was confirmed in several experiments of biofuel use in agriculture tractor engines (*Jindra, 2016; Pexa, 2014*) as well as in passenger cars (*Mařík, 2014; Kotek, 2015*).

Diesel Particulate Filter (DPF) have been widely used to remove harmful PM. The basic function of DPF is a collecting of PM inside the filter. Therefore DPF must be regularly regenerated to remove accumulated particulates such as soot and organic materials. Regeneration is initiated either actively by additional fuel injection or passively during higher engine load generating high exhaust temperatures. That is why that the large quantities of PM are emitted during regeneration (*Khalek, 2011; Barone, 2010*). This article deals with analysis of PM production during the service regeneration process of DPF like a one of possible way for maintain DPF efficiency.

MATERIALS AND METHODS

The vehicle Skoda Rapid Spaceback 1.6 TDI with 4 cylinder turbocharged compression ignition (CI) engine with diesel particulate filter (DPF) was used in this experiment. Before experiment DPF contained 12 grams of soot. The older vehicle Skoda Roomster 1.4 TDI was used for comparison of PM production of car with and without DPF. Technical specifications of cars are summarized in Table 1.

Tab. 1 Technical information of tested cars

Vehicle	Rapid 1.6 TDI Spaceback	Roomster 1.4 TDI
COMBUSTION ENGINE		
Design	compression ignition, turbo charged	compression ignition, turbo charged
Fuel system	common rail	unit injector system
Number of cylinders and valves	4, in row, 16 valves	3 in row, 6 valves
Fuel	diesel	diesel
Volume of cylinders	1,598 ccm	1,422 ccm
Power	85 kW at 4,400 rpm	59 kW at 4,000 rpm
Torque	250 Nm at 1,500 rpm	195 Nm at 2,200 rpm
EU limit	EU6	EU4
Manufacture year	2016	2006
CAR BODY		
Service weight	1,260 kg	1,240 kg
Total weight	1,740 kg	1,755 kg
DRIVE PERFORMANCE		
Max. speed	190 km·h⁻¹	165 km·h⁻¹
Acceleration 0-100 km·h⁻¹	10.3 s	14.7 s
Fuel consumption	5.0/3.4/4.1 (liter·100 km⁻¹)	5.1/3.76/4.26 (liter·100 km⁻¹)

The diagnostic system BOSCH KTS 520 was used for communication with engine control unit (ECU). This device is able to activate special service function which allows to do so-called service regeneration of DPF. This process is primary intended for diesel particle filter regeneration if the standard processes of regeneration (passive or active regimes of regeneration) not passed. This can happen typically at the very short trips in town traffic. If the content of soot in DPF exceeds 20 g it is necessary to make the service regeneration.

Classification of particulate matter was made with the TSI analyser model EEPS 3090 whose detailed specification is shown in Table 2. The analyser enables detection of particle size and also monitors their number. The obtained data is then presented as a size range of particles produced. The measured sample is taken from the exhaust, and then is diluted by the device. Within the experiments were evaluated only relative changes in the production of particulate matter in the diluted exhaust gas.

Tab. 2 Specification of PM analyser TSI EEPS 3090

Particle size range	5.6 – 560 nm
Particle size resolution	16 channels per decade (32 total)
Electrometer channels	20
Time resolution	10 size distribution per second
Sample flow	10 $l \cdot min^{-1}$
Dilution accessories	Rotation Disk thermodilution

Production of CO_2 was measured using emission analyser Atal-AT-505. The analyser uses nondispersive infrared (NDIR) method to detect CO, CO_2 and HC emissions and electrochemical cell for O_2 and NO_X emissions. The technical data of the analyser are summarized in Table 3.

Tab. 3 Specification of ATAL AT-505

Measured Values	Measurement Range	Resolution	Accuracy
CO	0 ... 10 % Vol.	0.001 % Vol.	0 … 0.67%: 0.02% absolute, 0.67% … 10%: 3% of measured value
CO_2	0 ... 16 % Vol.	0.01 % Vol.	0 … 10%: 0.3% absolute, 10 … 16%: 3% m.v.
HC	0 ... 20, 000 ppm	1 ppm	10 ppm or 5% m.v.
NO_X	0 ...5 000 ppm	1 ppm	0 … 1000 ppm: 25 ppm, 1000 … 4000 ppm: 4% m.v.
O_2	0 ... 22 % Vol.	0.1 % Vol.	0 … 3%: 0,1% 3 … 21%: 3%

RESULTS AND DISCUSSION

The result of instantaneous values of PM total concentration during DPF regeneration is shown in Fig.1. Before start of regeneration process it was necessary to engine warm up to operating temperature. The regeneration process started at raised idling speed when ECU based on the command from KTS device started the increase in exhaust gas temperature inside DPF from 160°C up to 650°C. The additional burning was followed by increase in CO_2 production. The regeneration process took about 20 minutes (1205 s). The volume of soot decreased from 12 to 0 gram which demonstrates good DPF condition (according to car mileage it is expectable result). As is shown in Fig. 2 regeneration process has been splitted into 3 phases. First phase lasted from 100 to 180 seconds and has been characterized by fast high increase in PM production with size about some tens nm. The second phase lasted from 180 to 950 seconds and has been characterized by gradual increase in PM production caused by gradual burning of collected particles with size up to hundreds nanometers. The last third phase lasted from 950 to 1200 seconds and has been characterized by gradual decrease in PM production. As is shown in Fig. 2 the PM size distribution has been concentrated in two size groups (middle and big particles). The similar PM production during DPF regeneration process confirms (*Quirosa, 2014*).
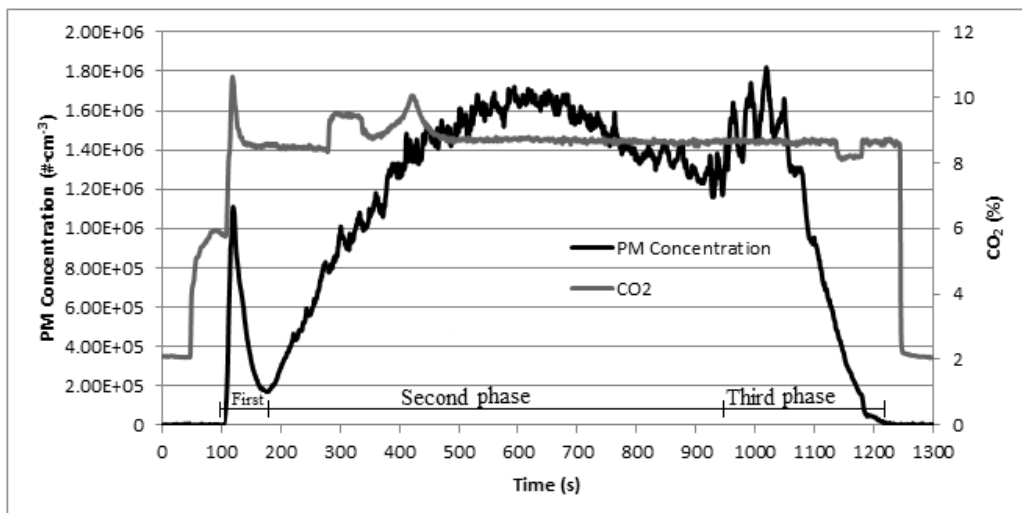
Fig. 1 PM and CO_2 production during service regeneration
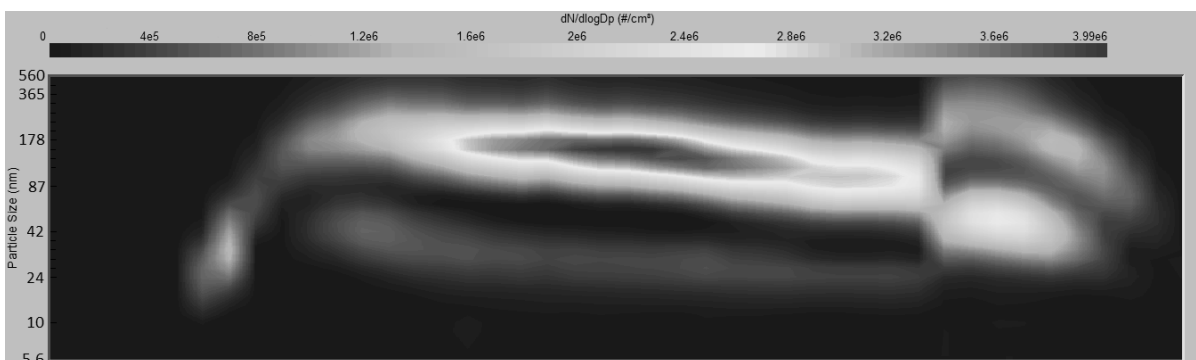

Fig. 2 Size distribution and the number of PM during regeneration

As is shown in Fig. 3, during the regeneration process were produced increased amounts of PM in compare of normal operating state of engine.
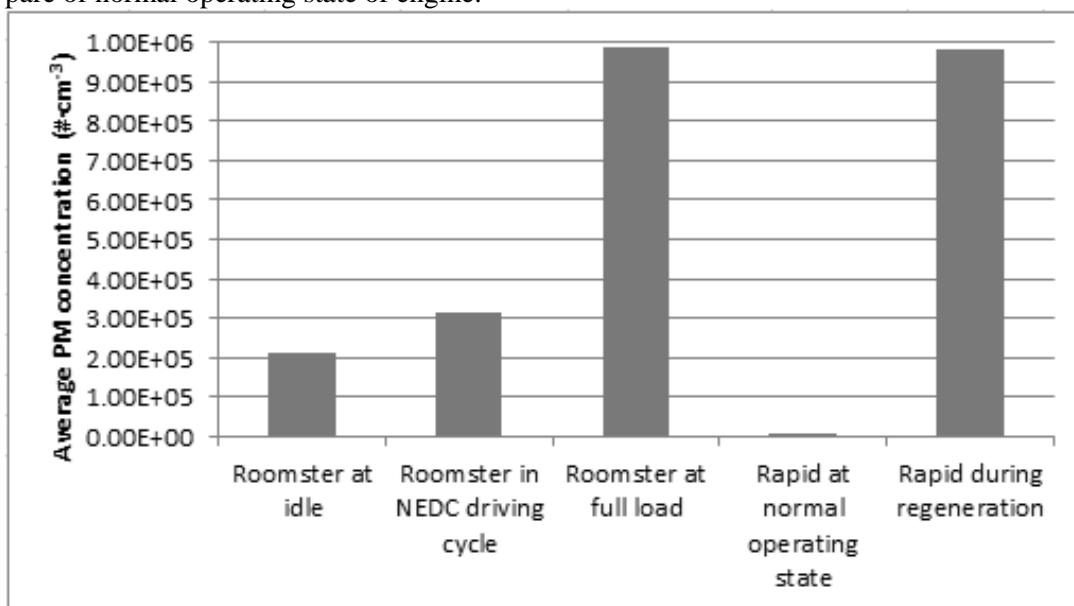

Fig. 3 Compare of average PM concentration of tested cars in various operating states

There is shown different PM production in depend on various operating states. PM production of Skoda Roomster was very dependent to engine operating state when already at idling speed produced substantially higher amount of PM and with increasing engine load the PM production grew. Skoda Rapid produced still very low PM amount independently to engine operating state while at active regeneration process of DPF was accompanied by increased PM production approximately equal to Roomster PM production at full load.

CONCLUSIONS

DPF is well known technology for PM reduction. The vehicles equipped by DPF produce provably minimally amount of PM compared to vehicles without DPF. Disadvantage of DPF is unfortunately necessary regeneration which is followed by big increase in PM production. This article showed immediate PM production during regeneration process which is almost equal to PM production of vehicle without DPF at full load. Although the temperature inside DPF is lower than inside combustion chamber the combustion conditions inside DPF are more stable and combustion process takes significantly longer time. Therefore use of DPF has very positive impact to the PM total concentration regardless to the immediate operation state of engine.

ACKNOWLEDGMENT

REFERENCES

1. Barone, T.L., Storey, J.M.E. & Domingo, N. (2010). An analysis of field-aged diesel particulate filter performance: particle emissions before, during, and after regeneration. *Journal of the Air and Waste Management Association, 60*, 968–976.

2. Hea J., Gonga S., Yuc Y., Yud Y., Wub L., Maob H., Songb C., Zhaoc S., Liua H., Lib X., & Lib R. (2017). Air pollution characteristics and their relation to meteorological conditions during 2014–2015 in major Chinese cities. *Environmental Pollution, 223*, 484-496.

3. Jindra P., Kotek M., Mařík J., & Vojtíšek M. (2016). Effect of different biofuels to particulate matters production. *Agronomy Research*, *14*(3), 783–789.

4. Khalek, I.A., Bougher, T.L., Merritt, P.M., & Zielinska, B. (2011). Regulated and unregulated emissions from highway heavy-duty diesel engines complying with U.S. Environmental Protection Agency 2007 Emissions Standards. *Journal of the Air and Waste Management Association, 61*, 427–442.

5. Kotek T., Kotek M., Jindra P., & Pexa M. (2015). Determination of the optimal injection time for adaptation SI engine on E85 fuel using self-designed auxiliary control unit. *Agronomy Research, 13*(2), 577–584.

6. Künzli, N., Kaiser, R., Medina, S., Studnicka, M., Chanel, O., Filliger, P., Herry, M., Horak, F. Jr., Puybonnieux-Texier, V., Quénel, P., Schneider, J., Seethaler, R., Vergnaud, J.-C., & Sommer, H. (2000). Public-health impact of outdoor and traffic-related air pollution: a European assessment. *The Lancet, 356*(9232), 795–801.

7. Lewtas, J. 2007. Air pollution combustion emissions: Characterization of causative agents and mechanisms associated with cancer, reproductive, and cardiovascular effects. *Mutation Research, 636*, 95–133.

8. Mařík J., Pexa M., Kotek M. & Hönig V. (2014). Comparison of the effect of gasoline - ethanol E85 - butanol on the performance and emission characteristics of the engine Saab 9-5 2.3 l turbo. *Agronomy Research*, *12*(2), 359–366.

9. Pexa M. & Mařík J. (2014). The impact of biofuels and technical engine condition to its smoke - Zetor 8641 Forterra. *Agronomy Research*, *12*(2), 367–372.

10. Quirosa, D. C., Yoonc, S., Dwyerd, H.A., Collinsc, J. F., Zhue & Y., Huaia, T. (2014). Measuring particulate matter emissions during parked active diesel particulate filter regeneration of heavy-duty diesel trucks. *Journal of Aerosol Science*, *73*, 48–62.

11. Vojtíšek-Lom, M., Pechout, M., Dittrich, L., Beránek, V., Kotek, M., Schwarz, J., Vodička, P., Milcová, A., Rossnerová, A., Ambrož A.

& Topinka, J. (2015). Polycyclic aromatic hydrocarbons (PAH) and their genotoxicity in exhaust emissions from a diesel engine during extended low-load operation on diesel and biodiesel fuels. *Atmospheric Environment, 109*, 9–18.

Corresponding author:

Ing. Martin Kotek, Ph.D., Department of Vehicles and Ground Transport, Faculty of Engineering, Czech University of Life Sciences Prague, Kamýcká 129, Praha 6, Prague, 16521, Czech Republic, phone: +420 22438 3681, e-mail: kotekm@oikt.czu.cz

VARIATION OF THE STERILISATION BOTTLE FOR SOLAR WATER DISINFECTION

Pavel KOUŘÍM[1], Bohumil CHALUPA[1], Josef ZEMAN[1]

[1]*Department of Physics, Faculty of Engineering, Czech University of Life Sciences Prague*

Abstract
The project was inspired by the successful Swiss project Sodis (Solar Disinfection), in the frames of which spreading of the ability to disinfect water by the Sun is under way in the tropical areas of the whole world, namely with the help of used PET bottles, thus almost with no expenses. We tried, with a slight modification of the PET bottles used, to attain the desired effect, i.e. making surface water drinkable also in conditions where there isn't sufficient solar intensity, or the temperatures of ambient air cause too intensive cooling of the water sterilized. All our modifications of the disinfection containers increase the water treatment costs only very slightly. Six variations of sterilisation containers were compared in our test: original simple, a simple one placed into a sheath made of a bigger transparent bottle, a bottle fitted with a half-cylinder aluminium foil reflective element, a bottle with the half-cylinder reflective element placed in a sheath made of a bigger transparent bottle, a blacked bottle, and a lacked bottle placed into a bigger transparent bottle. All bottles for the water were 1.5 litre bottles from the Pepsi drink. 2.25-litre Pepsi bottles then form the outer sheaths. The bottles were filled with water from a pond and exposed to the sun for 10 hours; then the water from each bottle and the water from the pond have undergone microbiological analysis. The number of Escherichia Coli, coliform bacteria, the number of cultivated micro-organisms at 20 and 36 °C for 24 hours were determined in all seven samples. The result is a finding that as long as the water temperature does not reach at least 55 °C, the essential sterilisation factor is the UV component of the incident radiation; from that follows that the best results in immediate E. coli and coliform bacteria concentration has the bottle equipped with a half-cylinder aluminium reflector. Black-painted bottles, on the other hand, had reached by 15 degrees higher temperatures though, however this only caused more successful bacteria reproduction, but their die-off did not arrive due to the impenetrability of the bottles for the UV radiation, and the number of bacteria, especially in the cultivated samples, surpassed the original values by orders of magnitude.

Key words: *water disinfection; Sodis; solar disinfection; PET bottles.*

INTRODUCTION

Unsafe drinking water, along with poor sanitation and hygiene, are the main contributors to an estimated 4 billion cases of diarrhoeal disease annually, causing more than 1.5 million deaths, mostly among children under 5 years of age (*WHO 2005*). As part of its Millennium Development Goals, the United Nations expressed its commitment by 2015 to reduce by one half the people without sustainable access to safe drinking water. Current estimates are that there are still 1.1 billion people without this access (*WHO/UNICEF 2006*). However, results from a recent assessment in six pilot countries, found that 31 % of drinking water samples from boreholes exceeded WHO guideline values (GV) and national drinking water standards in the pilot countries for faecal contamination, the leading source of infection and disease (-*RADWQ 2006*). In one of the pilot countries, only 43.6% of samples from stored water were in compliance with the WHO guideline value and national standards, and more than half of household samples showed post-source contamination.

Boiling or heat treatment of water with fuel is effective against the full range of microbial pathogen s and can be employed regardless of the turbidity or dissolved constituents of water. While the WHO and others recommend bringing water to a rolling boil for 1 minute, this is mainly intended as a visual indication that a high temperature has been achieved; even heating to pasteurization temperatures (60 °C) for a few minutes will kill or deactivate most pathogens (*UNICEF, 2008*). However, the cost and time used in procuring fuel, the potential aggravation of indoor air quality and associated respiratory infections, the increased risk of burn, and questions about the environmental sustainability of boiling have led to other alternatives.

One of the possibilities, besides ceramic filters and water chlorination, is also solar sterilisation according to the SoDis system (*Meierhofer & Wegelin*, *2002*). This inexpensive method utilizes cumulative effect of solar heating-up by thermal radiation and the effect of UV radiation in PET bottles with water, exposed to solar radiation for 24 hours.

Solar disinfection has been repeatedly shown to be effective for eliminating microbial pathogens and reduce diarrhoeal morbidity (*Hobbins 2004*) including epidemic cholera (*Conroy 2001*). Among the most practical and economical is the "Sodis" system, developed and promoted by the Swiss Federal Institute for Environmental Science and Technology (http://www.sodis.ch). It consists of placing low turbidity (<30NTU) water in clear plastic bottles (normally 2L PET beverage bottles) after aerating it to increase oxygenation and exposing the bottles to the sun, usually by placing them on roofs. Exposure times vary from 6 to 48 hours depending on the intensity of sunlight. Like filters, thermal and solar disinfection do not provide residual protection against recontamination. Accordingly, householders must have a sufficient number of bottles to allow them to cool and maintain treated water in the bottles until it is actually consumed (*UNICEF, 2008*).

Experiments were also done with various modifications of this method, e.g. glass bottles were used instead of the PET ones (*SODIS, 1998*), with little success though; its reason can be seen in the bad UV transmittance of the glass of the thickness used for common bottles.

The aim of this study was verifying the usability of the SODIS method in higher latitudes (central Europe) using disinfection containers – bottles with several modifications.

MATERIALS AND METHODS

On August 15th 2017 at 8:00 AM seven water samples were taken from an open fire pond at coordinates 50.129788N, 14.374491E in the premises of the Czech University of Life Sciences in Prague, Czech Republic. The samples were placed into six PET bottles according to the SODIS procedure described above; the seventh sample was cooled to 4 °C and left at this temperature in dark place for the whole day. Six variants of sterilisation containers were compared in this test (fig. 1): Original plain one, a plain one placed into a casing of a larger transparent bottle, a bottle equipped with a half-cylinder aluminium foil reflector, a bottle equipped with a half-cylinder aluminium foil reflector placed into a sheath of a larger transparent bottle, a black-painted bottle and a black-painted bottle placed into a sheath of a larger transparent bottle. All bottles for the water were 1.5 litre bottles from the Pepsi drink, the outer sheaths from 2.25 Pepsi then.

Fig. 1 Six variations of sterilisation bottles exposed to the sun.

Besides the temperatures in the bottles, air temperature and solar radiation were measured. Radiation was measured with a CM11 pyranometer from Dutch company Kipp & Zonen B. V. Used thermometers were electronic ones with DS18B20 chip sheathed in stainless steel sheaths, and equipped with a reflexive radiation shield inside the bottles. The air thermometer was equipped with the radiation shield too. After 10 hours elapse, samples were taken from all six bottles into glass containers with ground mouths, see fig. 2, and those stored in dark at 4.5 deg. C till the next morning.

Fig. 2 Samples taken after 10 hours exposition in variously modified containers

Next morning, all seven samples were delivered to an accredited laboratory No. 473-ASLAB T. G. Masaryk Water Research Institute, public research institution, for microbiological analysis, where analysis according to the ČSN EN ISO/IEC 17 025:2005 standard was made.
In the results clarification attempt, GIMP 2.8 program and OceanOptics USB2000+ spectrometer were used for determining relative colours.

RESULTS AND DISCUSSION
On the day of measurement, i.e. August 15th, 2017, it was a nice sunny day; the run of the solar radiation indicates the chart in the following Fig. 3.
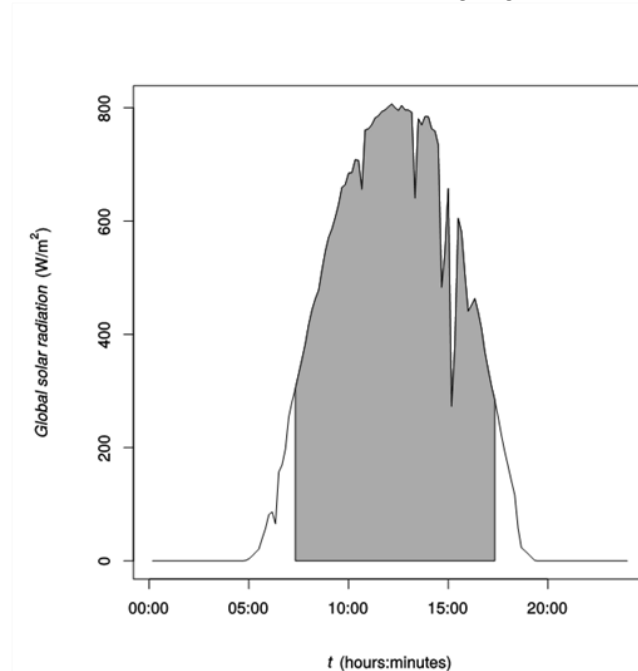
Fig. 3 Solar radiation on the day of measurement. Exposure time of the bottles is highlighted.

Total incident energy per square meter on that day added up to 23.7 MJ, where during the exposure time the energy totalled 22 MJ, i.e. 93 %. Minimum solar radiation during the exposition part of the day was 272.8 W/m^2, maximum 806.8 W/m^2, median 640.7 W/m^2 and mean was 603 ± 172 W/m^2. Incident solar radiation on the PET bottle used totalled about 0.6 MJ.

Following Fig. 4 illustrates that even on a sunny August day, required temperature of above 55 °C necessary for heat pasteurisation of the water *(Luzi et al. 2016)*, cannot be reached with tested bottle combinations. At the same time one can recognize that the influence of the double wall caused usually an 8–9 °C increase, while the black painting a 7 °C one. The bottle with reflector occurred always between the transparent bottle and the black one, in both insulated and non-insulated bottles.

About twice as great mutual thermal differences occurred between bottles with insulation than between bottles w/o insulation. Water temperature maximum over ambient air reached a noon maxima about 10 °C in non-insulated bottles and another 10 °C higher in insulated ones.
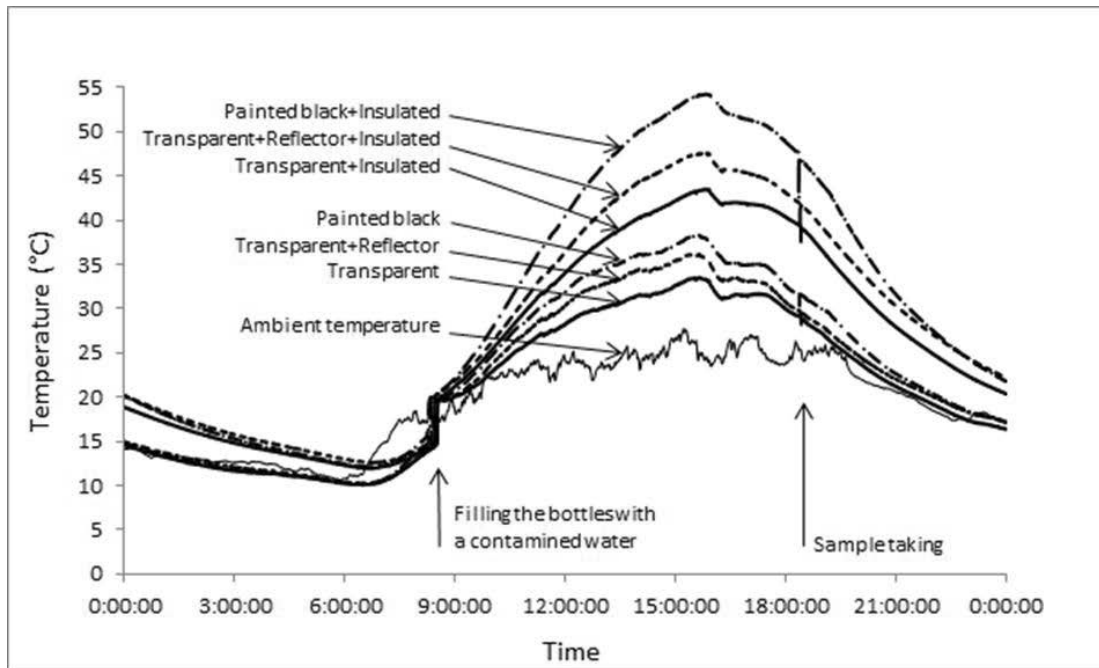
Fig. 4 Temperatures in particular bottles during the measurement day, together with ambient temperature.

Following Table 1 indicates number of organisms in the original water sample REF and in samples treated in six bottle types.

Tab. 1 Results of microbiological analyses of samples. REF – original untreated sample, BL+INS – black painted insulated bottle; BL – black painted bottle; TR+REF+INS – bottle with reflective layer and insulated; TR+REF – transparent bottle with reflective layer; TR+INS – transparent bottle, insulated; TR – transparent bottle; CFU – colony forming units; MO – micro-organisms.

Indicator	Unit	REF	BL+INS	BL	TR+REF+INS	TR+REF	TR+INS	TR
Esch. coli	CFU/100 ml	270±40	<10	180±40	<2	<10	<10	10±40
Colif. bact.	CFU/100 ml	270±40	<10	180±40	<2	<10	<10	10±40
Cultiv. MO at 22 °C	CFU/1 ml	1600±40	56800±40	7000±40	4200±40	5600±40	6400±40	1400±40
Cultiv. MO at 36 °C	CFU/1 ml	1800±40	35000±40	4400±40	6400±40	1800±40	8000±40	2600±40

As a first observation we can state that *Escherichia coli* and coliform bacteria content decreased in all bottle types. After cultivation at 22 °C it appeared though that the number of colonies decreased only in the plain non-insulated transparent bottle. On the other hand, after cultivation at 36 °C, lower number of colonies than in the reference sample was not recorded in any treated sample. Only in the transparent bottle with reflector, the number at least did not increase. Gigantic number of cultivated micro-organism colonies at both 22 °C and 36 °C was reached in the black-painted bottle with insulation. Their number increased 20 and 30 times in comparison to the original sample. Generally it can be stated that more colonies were usually found in the insulated bottles than in the single-walled ones

after cultivation. This applies absolutely after the cultivation at 36 °C, where double-wallness caused 3 to 8 fold increase. Cultivation at 22 °C recognized an increase in colonies caused by two walls in the transparent bottle and in the black one, while in the bottle with a reflector two walls caused a slight decrease. As can be seen from Tab. 1 from the listed deviations, that at the same time constitute the interval of 86% reliability of the result, all results differ significantly from each other, with the exception of very low concentrations of 10 CFU per reference volume and less. The most dangerous bacteria, E. Coli, were practically killed by the sterilisation process in all bottle types with the exception of simple black-painted bottle. This confirms that temperature cannot disinfect the water by itself when it is not high enough and UV radiation is blocked *(Luzi et al. 2016)*.
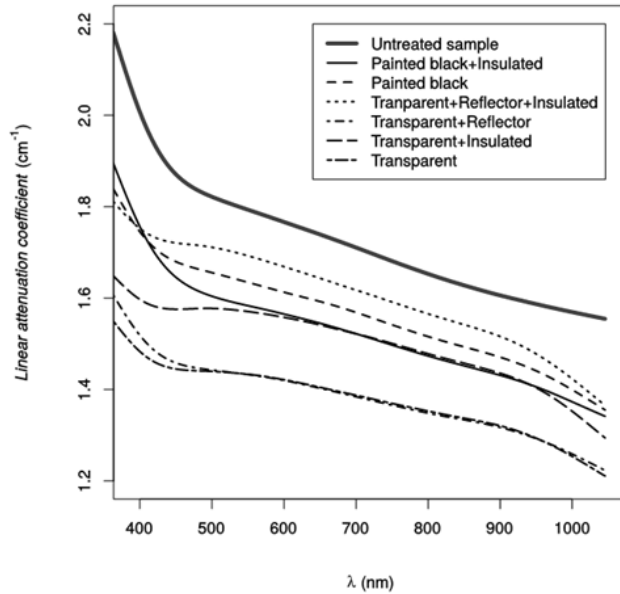
Fig. 5 Coefficient of absorption for non-treated sample and for the six variants of treated samples, for visible and near IR spectra

The absorption coefficient chart indicates that for all samples it applies that they show lowest absorption at the highest wavelengths. The sample that differs most in shape from the other ones by the most increased absorption in the violet spectrum part is the one that was treated in black painted insulated bottle. In this area, the most different from this one is the sample treated in the transparent insulated bottle. Treatment in the plain transparent bottle caused the largest absorption change in the examined wavelength range. The most similar shape to the original absorption curve has the sample treated in black insulated bottle. Mutually most similar shapes have the samples from the transparent bottle and the transparent bottle with reflector.

Following Table 2 shows that relative colour results determined in the GIMP 2.8 program, as mean sample from fig. 1, the spectral curves from Fig. 4 are in accordance with the data in this table.

Tab. 2 Colour composition of bottles with samples from Fig. 1:. REF – original untreated sample, BL+INS – black painted insulated bottle; BL – black painted bottle; TR+REF+INS – bottle with reflective layer and insulated; TR+REF – transparent bottle with reflective layer; TR+INS – transparent bottle, insulated; TR – transparent bottle. Values in the table are 8-bit colour components of the (RGB) colours of respective samples.

colour	REF	BL+INS	BL	TR+REF+INS	TR+REF	TR+INS	TR
Red	157	167	165	160	166	159	165
Green	152	166	163	161	165	159	163
Blue	116	144	121	155	135	136	133

Cardinal result of this work is thus orientation of following studies dealing with water sterilisation by this way in colder conditions, namely in the direction to UV concentration maximisation in the treated sample. At the same time we show that the attempts to cheaply increase the temperature are rather counter-productive. That direction can be successfully omitted from the further optimisation development.

CONCLUSIONS

In the Czech Republic conditions, UV radiation is essential for water sterilisation using bottles. Temperature increase at the cost of UV decrease is highly counter-productive. Intensity of green colouring of the treated water correlates only slightly with the concentration of the dangerous bacteria E. coli and coliform bacteria.

REFERENCES

1. Conroy, R. M., Meegan, M. E., Joyce, T., McGuigan, K., & Barnes, J. (2001). Solar disinfection of drinking water protects against cholera in children under 6 years of age. *Archives of Disease in Childhood.* 85(4), 293–5.

2. Hobbins, M. (2004). *Home-based drinking water purification through sunlight: from effectiveness to health effectiveness*. [PhD thesis]. University of Basel. Retrieved from http://pages.unibas.ch/diss/2006/DabsB_7569.pdf

3. Luzi, S., Tobler, M., Suter, F., & Meierhofer, R. (2016) *SODIS manual* (updated). Eawag, Sandec. Retrieved from http://www.sodis.ch/methode/anwendung/ausbildungsmaterial/dokumente_material/sodis-manual_2016.pdf

4. Meierhofer, R. & Wegelin, M. (2002). *Solar water disinfection — A guide for the application of SODIS* (PDF). Swiss Federal Institute of Environmental Science and Technology (EAWAG).

5. RADWQ (2006). Rapid Assessment of Drinking Water Quality, Summary Report. World Health Organization/UNICEF.

6. SODIS (1998). "SODIS Technical Note # 2 Materials: Plastic versus Glass Bottles". sodis.ch. 20 October 1998.

7. UNICEF (2008). Promotion of Household Water Treatment and Safe Storage in UNICEF Wash Programmes.

8. WHO (2005). Progress towards the Millennium Development Goals. Retrieved from https://unstats.un.org/unsd/mi/goals_2005/goal_2.pdf

9. WHO (2006). Mortality Country Fact Sheet 2006: Ethiopia, Geneva: World Health Organization. Retrieved from http://www.who.int/whosis/mort/profiles/mort_afro_eth_ethiopia.pdf

Corresponding author:
Ing. Pavel Kouřím, Department of Physics, Faculty of Engineering, Czech University of Life Sciences Prague, Kamýcká 129, Praha 6, Prague, 16521, Czech Republic, phone: +420 22438 3291, e-mail: kourim@tf.czu.cz

SURFACE WATER RUNOFF DURING RAINFALL AFTER COMPOST INCORPORATION INTO SOIL

Pavel KOVAŘÍČEK[1], Josef HŮLA[1], David HÁJEK[1], Marcela VLÁŠKOVÁ[1]

[1]Research Institute of Agricultural Engineering, Prague, Czech Republic

Abstract
The effect of compost application on soil hydraulic properties was evaluated in a field trial on a farm with ecological agriculture. A control treatment was without compost application during the trial while in a treatment with compost incorporation a dose of 12-18 t of dry matter/ha was applied every year after the forecrop harvest. Microplots for surface runoff collection were used to measure surface runoff during rainfalls, another method was the use of rainfall simulation by a rainfall simulator. Both measurement methods showed lower values of surface water runoff and higher values of water infiltration into soil in the treatment with every-year compost incorporation into soil compared to the control treatment. The results of the field trial confirmed a contribution of high-quality compost application to an increase in the infiltration capacity of soil during intense rainfalls.

Keywords: *surface runoff; water infiltration into soil; rainfall simulation.*

INTRODUCTION

A change in farming systems on land and technical anthropic activities in landscape underlie changes in the soil environment. Aboveground parts of plants are returned to the soil to a limited extent while humus content in the soil is often reduced and the soil structure is disturbed. Soil disaggregation is the most often caused by mechanical disturbance of the soil by farm machines and by a concurrent reduction in soil organic matter content. These soil processes decrease the infiltration rate of water into soil while surface water runoff and water erosion occur on slopes during intense rainfalls. Drought periods become more severe when the plants are lacking water lost through rapid surface runoff during rainfall. High-quality compost may be a suitable instrument supplying missing organic matter to the soil.

A decrease in the bulk density of soil at the depth of compost incorporation was reported *by Golabi et al. (2007)* and also by other authors *(Courtney & Mullen, 2008; Lynch et al., 2005)*. An improvement in the stability of soil aggregates after organic waste application to the soil was documented by *Rajeswari et al. (2007)*. High-quality soil organic matter has positive effects in conditions where the soil is exposed to the impacts of tractor passes *(Horn et al., 2006)*.

Compost application can be a way of accelerating water infiltration into the soil during torrential rains. An increase in the water-holding capacity is also assumed. Both factors become more and more important under the current climate pattern when alternating dry and wet periods are being extended. The compost application to make up for organic compounds in the soil taken up for crop production and the effect on surface water runoff during rainfall are investigated in specific farming conditions in pilot trials.

The application of high compost doses (200-500 t.ha^{-1}) aimed to influence soil properties was reported by *Pagliali et al. (1981). Thompson et al. (2008)* stated that the infiltration capacity of sandy-loam or loamy-sand soil increased linearly with the supply of a compost and sand mixture or of compost only compared to the soil not treated with compost.

The hypothesis of beneficial effects of compost incorporation on physical and hydrophysical properties of soil has been supported by results of many authors – *Boyle et al.(1989); Pagliali et al.(1981); Stoffela & Kahn (2001)*.

The aim of this study is to evaluate the effect of compost application on soil's hydraulic properties over three-years on a farm that employs ecological farming methods.

MATERIALS AND METHODS

In a pilot trial conducted on a farm with ecological agriculture and where conventional ploughing technology is used for soil tillage, the effect of compost application on soil hydraulic properties was

evaluated. All agricultural practices in the trial were carried out in a direction of contour lines. The compost made from farmyard manure, slurry and grass hay from meadow maintenance and landscape maintenance produced in a farm composting plant was used for fertilization (Tab. 1).

Tab. 1 Quality characteristics of produced compost for fertilization on experimental plot (according to ČSN 46 5735)

Year	Moisture (% weight)	Burned component (% weight)	N - total (%)	Ratio C:N	pH
2012	64.18	41.52	2.37	8.76	8.67
2013	60.86	35.50	1.62	11.00	8.40
2014	42.90	39.90	1.88	10.80	8.41
2015	51.50	39.60	2.02	9.47	8.65

Two parcels of 150x60 m in size were delineated on a slightly sloping plot – a control treatment without compost application during the trial and a treatment with incorporated compost at a dose of 12-18 t dry matter/ha every year after the forecrop harvest.

In each experimental treatment 4 microplots for surface runoff collection were installed after the crop sowing (Fig. 1). The area of the microplot (0.5x0.4 m) for surface runoff collection was delimited by the steel sheet sides. The steel sheet sides were driven into the soil to a depth of 0.10 m and the side height above the ground surface was 0.05 m. Using a collector in the bottom part of the microplot, water was caught into a collection bottle during a runoff event. The collector was covered with a sheet metal so that the surface runoff from the measuring area would not be influenced by a rainfall caught in the collector. The collection of surface runoff by this method was described by *Bagarello & Ferro (2007) or Hudson et al. (1993)*. The rainfall total during a runoff event was read off on a rain gauge placed in each experimental treatment. It was checked under intense rainfall whether any surface water runoff had occurred. If it had, collection bottles were replaced by empty ones and the collected volume of water was weighed to the nearest ±5 g. In the course of the microplot installation the inclination of the microplot measuring area was measured with a digital clinometer (Tab. 2). Investigations were done in four farming years 2012-2016 when the crop rotation of oats, winter triticale, emmer wheat and spring barley was used.

Tab. 2 Average slope of the mini-collectors on the measuring surface during installation

Year	Variant	Slope - average (°)
2012	control	3.7
	compost	4.2
2013	control	3.2
	compost	3.0
2014	control	4.1
	compost	4.0
2015	control	3.8
	compost	3.2

In addition to the study of surface water runoff from the microplots measurements were done during rainfall simulation on a measuring area of 0.5 m² at rainfall intensity of 87.8 mm.h⁻¹ (1.46 l.m⁻².min⁻¹) and at constant water pressure of 100 kPa *(Kovaříček et al. 2008)*. Water flowing from the sprinkled measuring area was conducted to a vessel placed on a digital balance. The weight of cumulative runoff of surface water was logged in a PC at an interval of 5 s. Collected water from surface runoff is filtered, filtered soil is dried and from the dry weight of washed soil a unit soil loss (g.m⁻².h⁻¹) caused by water erosion is determined. Based on the known simulated rainfall intensity and surface runoff volume other derived indicators converted per unit area of 1 m² are calculated: cumulative rainfall, cumulative surface runoff and cumulative infiltration.

Fig. 1 A microplot for surface runoff collection installed after the crop sowing, a collector directing water runoff to a collection bottle is covered with a sheet metal

RESULTS AND DISCUSSION

Figs. 2–4 document the results of evaluation of surface runoff from microplots for surface runoff collection in runoff events during a pilot field trial conducted in three farming years. In the first year of investigation winter triticale was planted on an experimental parcel. The effect of compost application on soil hydraulic properties is expressed by cumulative surface runoff. Fig. 2 shows differences in surface water runoff between experimental treatments for different rainfall totals during the growing season of winter triticale. Very low values of surface water runoff were recorded in the 2013 autumn season, when most water was infiltrated into the soil during rainfalls. The reason was an increased occurrence of macropores in topsoil within a short period after ploughing. The beneficial effect of compost on water infiltration into soil was manifested at the end of April and after mid-May 2014 – on these dates after compost incorporation into soil the surface runoff of precipitation water was 5.5 times and 2.8 times lower, respectively, compared to the control treatment without compost application.
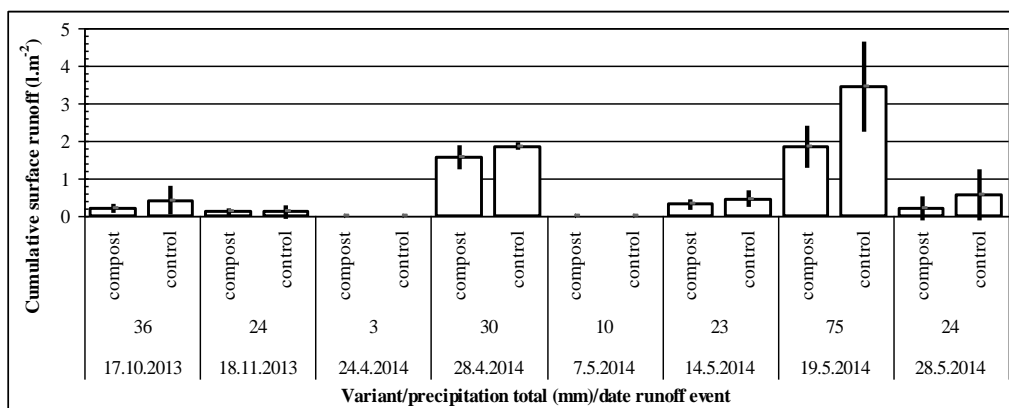
Fig. 2 Surface runoff – 2013-2014 – winter triticale

In the subsequent farming year winter emmer wheat was grown on an experimental parcel. The higher surface runoff of precipitation water occurred at intense rainfall in June 2015 (Fig. 3). On two dates of June 2015 the lower surface water runoff was observed in a treatment with compost incorporation in comparison with the control treatment without compost application.

In 2016 spring barley was sown on an experimental parcel. Surface water runoff occurred after more intense rainfalls in the second half of May and before mid-June 2016 (Fig. 4). Also on these dates surface water runoff was lower in the treatment with compost incorporation into soil. The infiltration capacity of soil during rainfalls is mainly influenced by the instantaneous porosity of soil and by soil moisture.
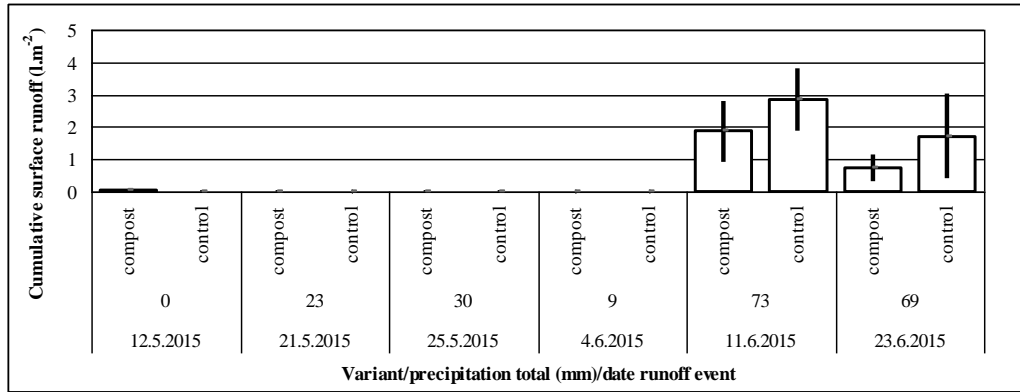
Fig. 3 Surface runoff in 2015 – emmer wheat
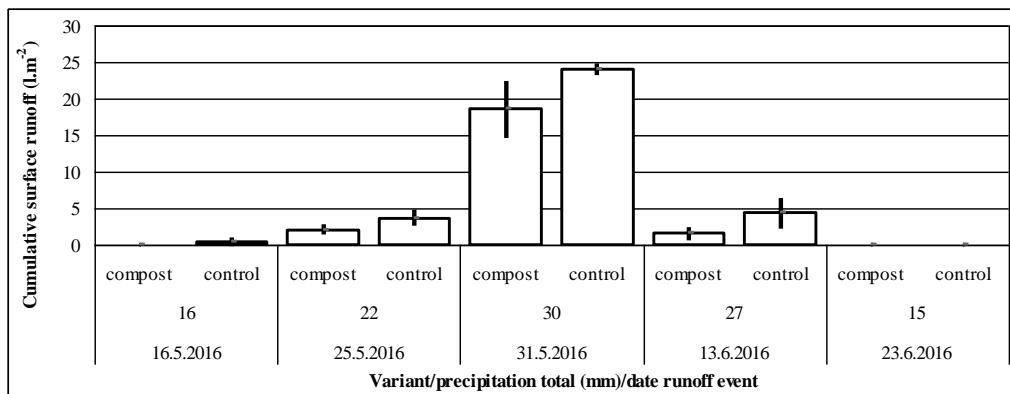
Fig. 4 Surface runoff in 2016 – spring barley

From the measurements when a rainfall simulator was used, results of measuring the surface runoff from a collection area of 0.5 m^2 are given in litres per hour (Fig. 5). Also these measurements indicated a beneficial effect of compost incorporated into soil – higher water infiltration into soil and lower surface water runoff were observed on the parcel with every-year compost incorporation.

The results of measurements of surface runoff during rainfalls and of measurements when rainfall simulation was used confirm a hypothesis that the application of high-quality compost is a contribution to an improvement in the infiltration capacity of soil during rainfall. A reduction in surface water runoff during intense rainfalls is also beneficial from the aspect of lowering a risk of water erosion of soil, which is very urgent in conditions of the CR. The seasonal data were evaluated using Statistica 12CZ software and evaluated at confidence level 0.95. The effect of compost on decreasing surface runoff could be confirmed (p=0.046) using Mann-Whitney U test using data from the whole tested period.
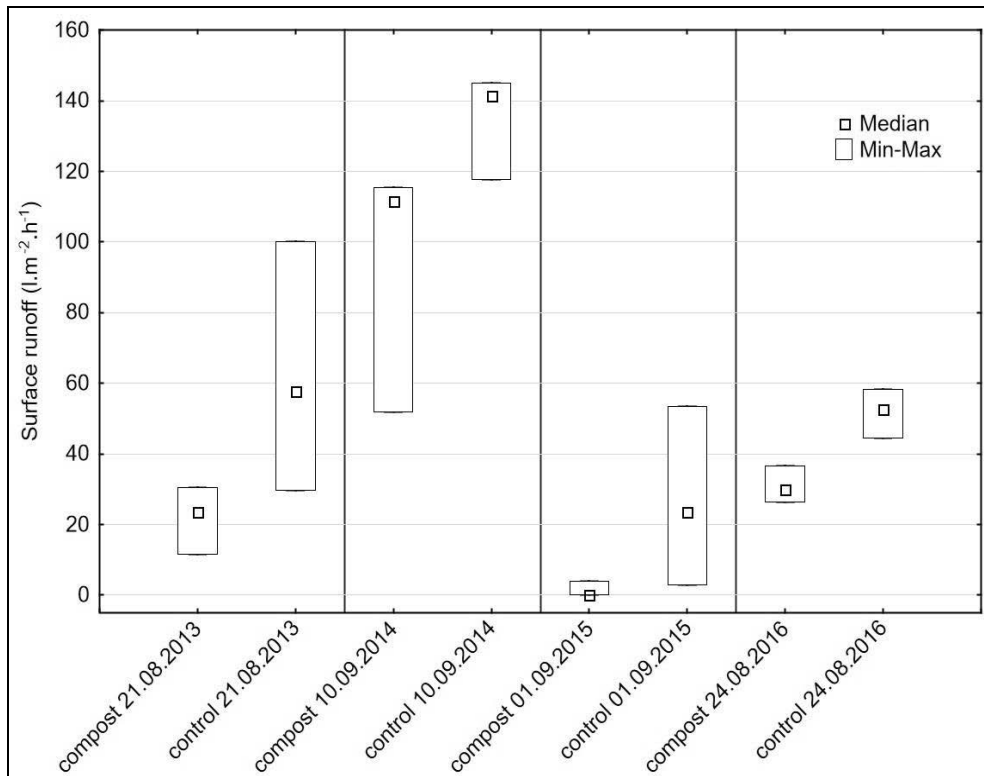
Fig. 5 Surface runoff in 2013-2016

Soil loss results from rainfall simulation are in Tab. 3.

Tab. 3 Soil loss at rainfall simulation (intensity 87.8 $mm.h^{-1}$)

Year	Soil loss ($g.m^{-2}.h^{-1}$)	
	Compost	Control
2013	2.64	43.39
2014	58.40	83.61
2015	0.10	13.10
2016	2.58	14.49

The results of evaluation of surface water runoff during rainfalls and rainfall simulation are consistent with the results of the authors who reported a positive effect of compost incorporation into soil on physical properties of soil and on water infiltration into soil *(Courtney & Mullen, 2008; Lynch et al., 2005)*. The results showing an improvement in the infiltration capacity of lighter soils after compost incorporation were also confirmed *(Thompson et al. 2008)*.

In an overall evaluation of results of this field trial it should be taken into account that the compost was applied every year at a dose of 12-18 t of dry matter/ha after the forecrop harvest. However, in agricultural practice the compost is not applied every year.

CONCLUSIONS

An evaluation of the effect of compost incorporation into soil in three consecutive farming years confirmed a beneficial effect of high-quality compost on the infiltration capacity of soil during rainfall and during rainfall simulation using a rainfall simulator. Besides the direct effect of incorporated compost on mechanical properties of soil a contribution of high-quality compost to an increase in the intensity of biological processes in soil can be assumed. The application of high-quality compost can become a component of soil productivity conservation by means of returning a part of produced plant biomass to the soil.

REFERENCES

1. Bagarello, V., & Ferro, V. (2007). Monitoring plot soil erosion and basin sediment yield at Sparacia experimental area. In *Changing soils in a changing world: the soils of tomorrow (Guide book of the scientific excursion)* (pp. 67-74). ESSC, Palermo 2007.

2. Boyle, M. W. T., Frankerberger, Jr., & Stolzy, L. H. (1989). The influence of organic matter on soil aggregation and water infiltration. *Journal of production Agriculture*, *2,* 290-299.

3. Courtney, R. G., & Mullen, G. J. (2008). Soil quality and barley growth as influenced by the land application of two compost types. *Bioresource Technology, 99*, 2913-2918.

4. Golabi, M. H., Denney, M. J., & Iyekar, C. (2007). Value of composted organic wastes as an alternative to synthetic fertilizers for soil quality improvement and increased yield. *Compost Science & Utilization, 15*(4), 267-271.

5. Horn, R., Fleige, H., & Peth, S. (2006). Soil management for sustainability. Reiskirchen, Catena Verlag GMBH, 497 p.

6. Hudson, N. W. (1993). Field Measurment of soil erosion and runoff. *Unated Kingdom: Silsoe Associates,* 139 p.

7. Kovaříček, P., Šindelář, R., Hůla, J., & Honzík, I. (2008). Measurement of water infiltration in soil using the rain simulation method. *Research in Agricultural Engineering. 54*(3), 123-129.

8. Lynch, D. H., Voroney, R. P., Warman, P. R. (2005). Soil physical properties and organic matter fractions under forages receiving composts, manure or fertilizer. *Compost Science & Utilization, 13*(4), 252-261.

9. Pagliali, M., Guidi, G., La Marca, M., Giachetti, M., & Lucamante, G. (1981). Effects of sewage sludge and composts on soil porosity and aggregation. *J. Environ. Qual., 4*, 556-561.

10. Rajeswari, M., Maruthi Sankar, G. R., Ranghaswami, M. V., & Mistra, P. K. (2007). Screening of soil amendments for efficient water-holding capacity based on a rainfall-infiltration model in a vertisol. In *Journal of Irrigation and Drainage Engineering* (pp. 468-474). ASCE.

11. Stoffela, P. J., & Kahn, B. A. (2001). *Compost Utilization in Horticulture cropping system*. USA: Lewis Publisher.

12. Thompson, A. M., Paul, A. C., & Balster, N. J. (2008). Physical and hydraulic properties of engineered soil media for bioretention basins. *Transactions of the asable, 51*(2), 499-514.

Corresponding authors:
Ing. Pavel Kovaříček, CSc., Research Institute of Agricultural Engineering, p.r.i., Drnovská 507, 161 01 Prague 6-Ruzyně, Czech Republic, phone: +420233022236, +420601587191, e-mail: pavel.kovaricek@vuzt.cz

MEASUREMENT THE VOID OF WOODEN CHIPS BY GAS DISPLACEMENT METHOD

Václav KŘEPČÍK[1], František KUMHÁLA[1], Jakub LEV[2]

[1]*Department of Agricultural Machines, Czech University of Life Sciences in Prague, Faculty of Engineering, Kamýcká 129, 165 00 Praha 6 – Suchdol, Czech Republic*
[2]*Department of Physics, Czech University of Life Sciences in Prague, Faculty of Engineering, Kamýcká 129, 165 00 Praha 6 – Suchdol, Czech Republic*

Abstract
The void of wooden chips is very important factor which significantly affects properties of wooden chips, i.e. dielectric properties, speed of combustion. This paper is focusing for void measurement of pure wooden chips by apparatus for measurement the volume of particular material. The principle of measuring apparatus is based on the gas displacement method. The volume between the parts of wooden chips is calculated on the basis of decreasing pressure by Boyle-Mariott's law. The pressure operating range was from 1000 to 1500 Pa. The moisture content of the wooden chips was reduced by hot-air oven with temperature 105 °C. The difference of measurement volume of wooden chips by displacement method and real volume was determined. The difference between real volume and volume which was measurement by displacement method was change during the drying the samples of the wooden chip. The effect of the internal porosity of the material was detected.

Key words: *Boyle-Mariott's law; void; wooden chips; moisture content.*

INTRODUCTION

Wooden chips are used for the production of heat energy in various devices. Wooden chips are burned in facilities that serve for heating individual houses or in very sophisticated facilities for the heating of a large number of buildings. According to *Díaz-Yáñez, et al. (2013)* in a number of countries, the use of wooden chips for energy purposes can be doubled. The most important characteristic of wooden chips is the moisture content, which clearly influences the heating capacity of the material during combustion *(Nyström & Dahlquist, 2004; Swisher, 1976).* The moisture content of wooden chips ranges from 20% to 55%. With legislative changes, heating companies for the production of heat energy by combustion of wood chips are forced to reduce the content of pollutants in the combustion gases. The regulation of combustion process based on the moisture content before the entry of wooden chips into the combustion chamber can bring about a reduction in the content of pollutants in the combustion gases. *Nelson (2005)* demonstrates in his studies that the dielectric properties of the material are significantly influenced by the moisture content. *James (1975)* published the results of his measurements of dielectric properties of wood and hardboard at various temperatures, frequencies, moisture content ratio and fibre orientation. From the results of experiment (*Nelson, 1991*), it's evident that volume density is another important parameter affecting dielectric properties.

The void can significantly influence the measurement of the moisture content of wooden chips. There are several methods for determining the volume of particular particles, it means their void. One of these methods is the gas displacement method *(Sahin & Summu, 2006). Thompson & Issacs (1967); Fang & Campbell (2000)* used the gas displacement method to measure the volume of the seed in their research. From the results they achieved, it is evident that the porosity of the material influences the results of the measurement of volume by the of gas displacement method. *Křepčík et al. (2017)* carried out the calibration of the measuring apparatus for the measurement of the volume of particulate material respectively the void in their research. From the measured data it was found that the moisture content of the material influenced the results of the measurement of the void because the measuring medium penetrated into the internal pores of the material.

This paper is focused to measurement of volume respectively the void of pure wooden chips by apparatus based on the principle of Boyle-Marriot's law.

MATERIALS AND METHODS

The measuring apparatus for measurement of void of wooden chips (Fig. 1) is composed from two chambers with the same volume and the connection conduit for the displacement of measuring medium (the air in this case). The connection conduit includes the three manual valves for displacement of measuring medium between the comparative and measuring chamber and the pressure values were displayed on the digital pressure gauge. The principle of gas displacement method is used for the measuring the samples with irregular shape and this method using Boyle-Mariott's law (*Sahin & Summu, 2006*).
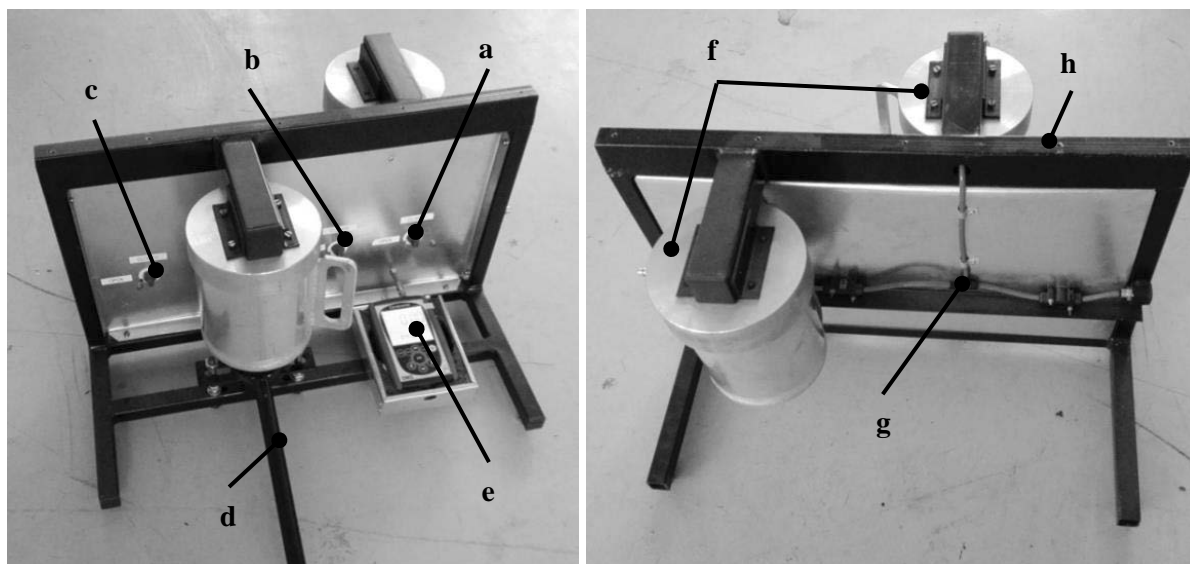
Fig. 1 Measuring apparatus: a) closing valves no. 1; b) closing valves no. 2; c) closing valves no. 3; d) pressure mechanism of measuring chambers; e) digital pressure meter; f) measuring and comparing chambers; g) connecting line; h) bearing frame of the measuring apparatus

The samples were sorted to three fraction of beech wooden chips (Fig. 2). The samples were inserted into the cold water and they were in the water for 24 hours for achievement of the maximal moisture content in the samples. After taking samples out of water they were inserted into the plastic bags for homogenization of the moisture content in all particles of wooden chips. The samples were inside the plastic bags for 24 hours and the excess water was removed in the step, too. The samples were filled to the measuring chamber by gravitational method without mechanical pressuring. The samples were aligned with the top edge of the measuring chamber by ruler. The measuring chamber with the samples were inserted to the pusher mechanism.
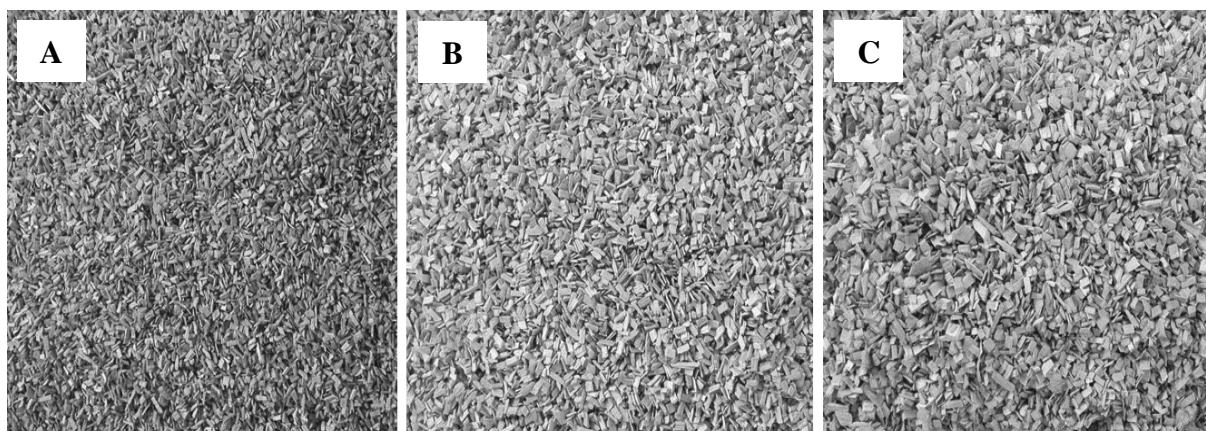
Fig. 2 A) Fraction x < 3.15 mm; B) – Fraction 3.15 mm < x < 5 mm; C) Fraction x > 5 mm

The measuring medium (the air in this case) was pushed into the first part of the connection conduit and the pressure was between 1000 Pa to 1500 Pa. The manual valves no. 1 and 2 were closed. After the

pressure settled in the first part of connection conduit, the value of the pressure in the first part of connection conduit was deducted from the pressure gauge and recorded like pressure P_1. After the pressure recording (P_1) the manual valve no. 2 was opened and the manual valve no. 3 was in the closed position. After the pressure settled in the all connection conduit, the value of the pressure in the all connection conduit was deducted from pressure gauge and recorded like pressure P_2. The manual valve no. 3 was opened for remove the pressure from connection conduit. This measurement was repeated ten times. The volume of the sample can be counted with the help of the following equation. The equation is based on Boyle-Mariot's law *(Sahin and Sumnu, 2006)*:

$$V_S = V_2 - V_1 \left(\frac{P_1 - P_2}{P_2} \right) \qquad\qquad (1)$$

where: V_s – calculated volume of the sample (m^3), V_1, V_2 – volume of the chambers (m^3), P_1, P_2 – measured pressures (Pa).

The samples were subsequently inserted into the hot-air oven and they were dried at the temperature 105 °C (ČSN 72 1012). The drying of the samples continued until the weight of the refuel sample was decreased to determine the moisture content by 10 to 15 g. The samples were mixed every 15 minutes to ensure uniform drying of the sample throughout the profile. After the drying samples, they were inserted into the plastic bags for homogenization of the moisture content in all particles of wooden chips and were left for 24 hours to homogenize the samples and to cool down. The samples were measured by the same system which is described above, after this step.

RESULTS AND DISCUSSION

Results of the measurement are displayed in the Fig. 3. Each of the three diagrams contains four curves. The first curve always presents volumes which were measurement by gas displacement method. The second curve presents the real volume of samples the wooden chips. The third and fourth curves represent the percentage of real sample volume and the volume measured by the gas displacement method.

In the diagrams in the Fig. 3 it is possible to mark two different areas. For all three factions, it can be seen that the accuracy of the measurement of the volume of wooden chips by the gas displacement method increases with the increasing of moisture content the samples. In the first area, the internal pores of the wooded chips were filled with water and the proportion of measuring media penetrated into the internal pores was reduced. This area is different for each fraction by its length. For fractions where the particle size is less than 3.15 mm, this first area extends to a fraction of the moisture content of about 35%. The percentage increase in the volume measurement error for this fraction is almost linear. Very similar to the course is evident in the fraction, where the particle size is greater than 5 mm. The error of measurement of volume by gas displacement method is increased below the 35 % of moisture content. The water was removed from the internal pores of samples under this edge of moisture content and the measuring medium can be penetrate into the internal pores. For a fraction with a particle size of 3.15 mm < x < 5 mm, it is evident that the increase in the measurement error occurred only when the moisture content was below 15%.

The presented results, shows that there can be influence between the volume of wooden chips and the amount of pores in the particles of wooden chips by gas displacement method. This result is positive because the volume of internal pores influences fundamentally dielectric properties of material *(Nelson, 1991)*. Presented results corresponding the conclusions of calibration the apparatus for measurement of volume the particular material which achieved *Křepčík et al. (2017)*. The results of the measurements indicate that the results of the measurements may differ in the individual fractions of the same type of wooden chips.

Fraction x < 3.15 mm

Fraction 3.15 mm < x < 5 mm

Fraction x > 5 mm
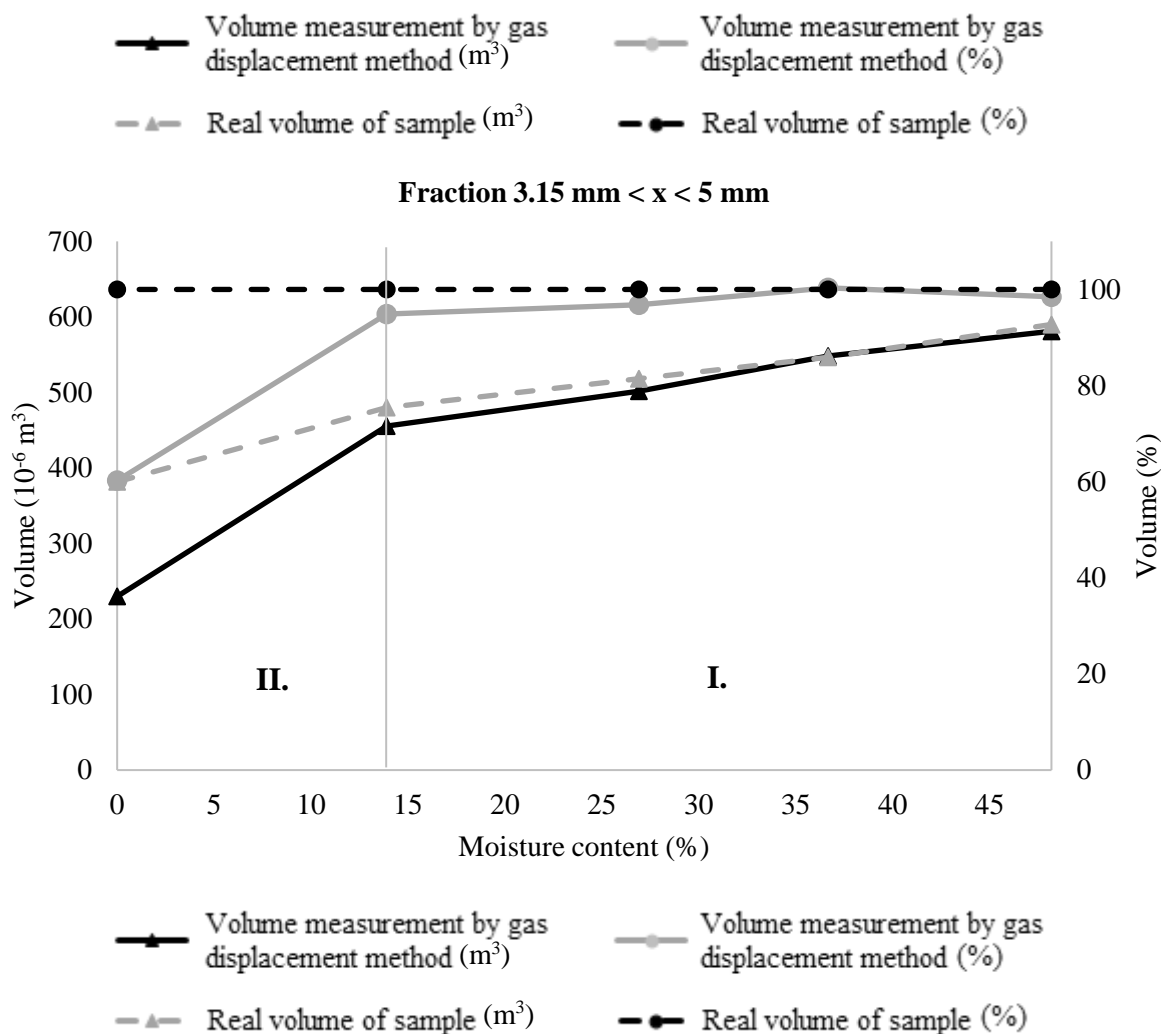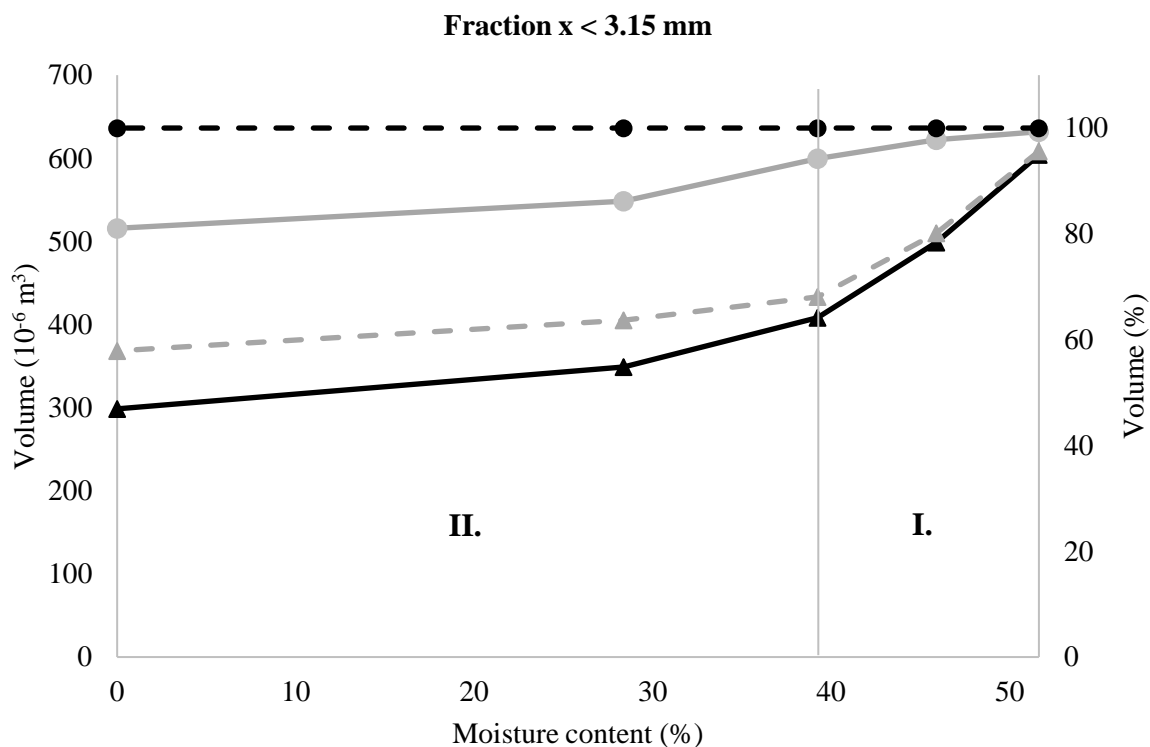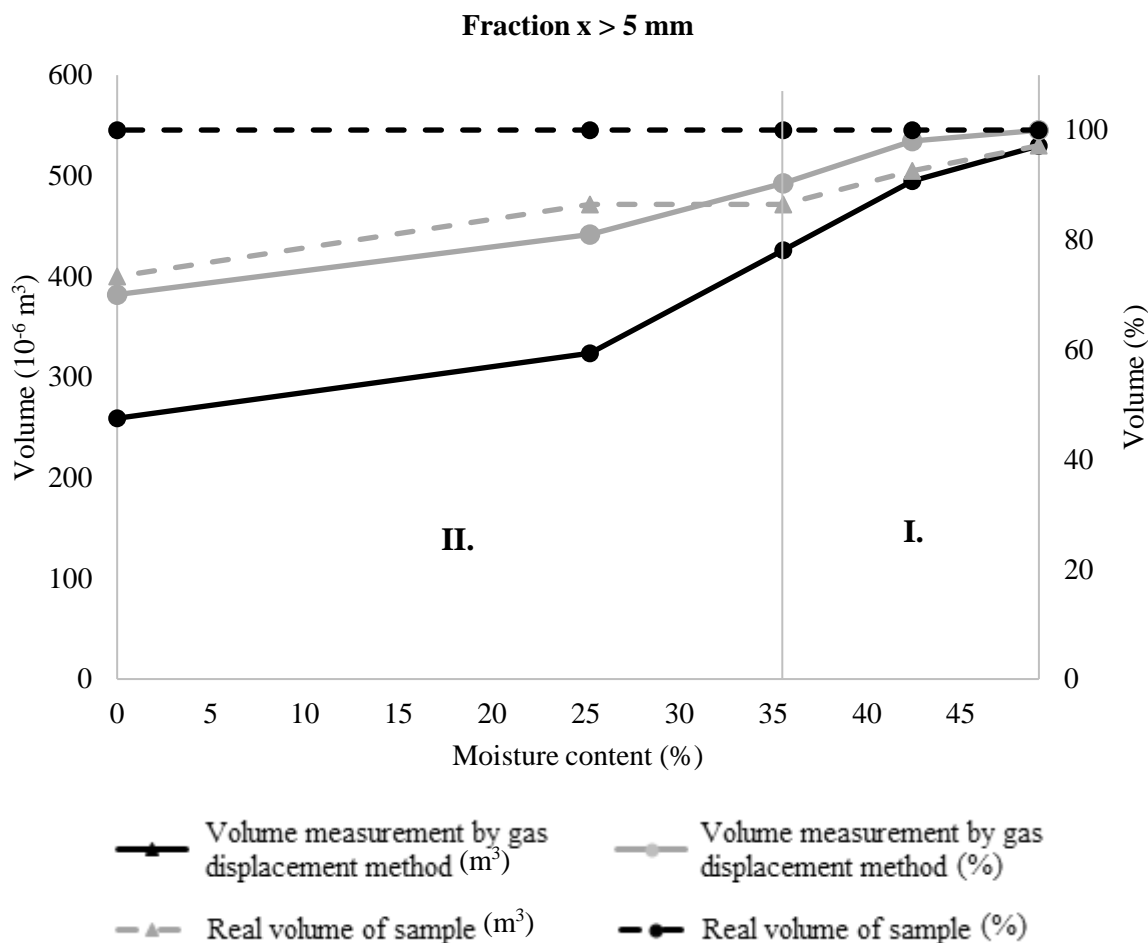
Fig. 3 Results of measurement the volume by gas displacement method for each fraction the pure wooden chips

CONCLUSIONS

The results of the measurements show that wooden chips are heterogeneous material, which can exhibit non-trivial behaviour even in individual fractions of the same type of wooden chips. This fact must be taken into account in the design of the method for continuous measurement of the moisture content of wooden chips. It is possible to use the measuring apparatus for the measuring the volume respectively void of wooden chips because the moisture content of the wooden chips is in the range from 20 % to 55 %.

ACKNOWLEDGMENT

REFERENCES

1. Díaz-YáXez, G., Mola-Yudego, B., Anttila, P., Röser, D., & Asikainen, A. (2013). Forest chips for energy in Europe: Current procurement methods and potentials. *Renewable and Sustainable Energy Reviews*, *21*, 562-571.
2. Fang, C. & Campbell, G.M. (2000). Effect of Measurement Method and moisture Content on Wheat Kernel Density Measurement. *Food and Bioproducts Processing*, *78*, 179-186.
3. James, W. L. (1974). Dielectric properties of wood and hardboard: variation with temperature, frequency moisture content and grain orientation. Madison, WI: US Department of Agriculture, Res. Pap FPL 245.

4. Křepčík, V., Lev, J., & Kumhála, F. (2017). Development and testing of apparatus for wooden chips void measurement. *Agronomy Research, 15*(S1), 1050-1056.

5. Nelson, S. O. (2005). Dielectric Properties Measurement for Agricultural Applications. *ASAE Paper No: 053134.*

6. Nelson, S. O. (1991). Dielectric properties of agricultural product-measurements and applications. *IEEE Transactions on Electrical Insulation, 26*, 845-869.

7. Nystöm, J. & Dahlquist, E. (2004). Methods for determination of moisture content in woodchips for power plants – a review. *Fuel*, *83*, 773-779.

8. Sahin, S. & Summu, S. G. (2006). *Physical Properties of Foods.* Springer New York, 257.

9. Swisher, B. E. (1976). Alternate uses of wood chips. Ohio, USA: Columbus and Southern Electric Company Columbus. *Journal of Arboriculture*, January.

10. Thompson, R. A. & Isaacs, G. W. (1967). Porosity Determinations of grains and Seeds with an Air-Comparison Pycnometer. *Transactions of the ASAE, 10*(5), 0693-0696.

Corresponding author:

Ing. Václav Křepčík, Department of Agricultural Machines, Faculty of Engineering, Czech University of Life Sciences Prague, Kamýcká 129, Praha 6 - Suchdol, Prague, 165 00, Czech Republic, phone: +420 732202607, e-mail: krepcik@tf.czu.cz

EFFECT OF LOAD CONDITIONS ON THE SIZE AND PRODUCTS OF WEAR

Marian KUČERA[1], Milan KADNÁR[1], František TÓTH[1], Jozef RÉDL[1], Jozef NOSIAN[1]

[1]*Department of Machine Design, Faculty of Engineering, Slovak University of Agriculture in Nitra, Tr. A. Hlinku 2, 949 76 Nitra, Slovak Republic*

Abstract

The submitted paper analyzes the effect of loading on the properties of selected sliding pair. Loading regimes were simulated based on two random signals after their statistical processing with a mean value equal to 1000 N. The aim of the study was to confirm the hypothesis of the effect of random loading method on the size and type of wear. It should also confirm the hypothesis of the effect of used lubricant in conditions of limiting friction in terms of its emergency properties. Steel E335 and bronze CC483K were used as material pair. Two oils were selected for lubrication of friction node – the mineral gear oil Madit PP80 and ecological oil Plantohyd 46 S. The result of this study is a ferrographic analysis of oil samples and the analysis of worn surfaces in relation to weight loss, which confirms the hypotheses.

Key words: tribotestor; random process; sliding node; lubrication.

INTRODUCTION

The design of construction nodes is required to fully respect the characteristics of operating loads (*Kučera & Rusnák 2008; Kučera 2014*). An effort to simulate the tribological behaviour of the practical system exists in simulated tribological tests. This area of tribometry is extremely difficult and the use of the system approach is extremely important here (*Blaškovič et al. 1990; Liček 2017; Kučera 2014*). The effect of factors (load cycle, lubricant) on the friction pair was statistically verified by the 2-factor Analysis of Variance (ANOVA). The respective differences between the mean values of each sample were defined by Duncan´s Multiple Range Test with a significance level (p-value) of 0.05 (*Kučera et al. 2016; Kopčanová et al. 2018*). The hypothesis of significant effect of random load was solved in several studies. Under the conditions of experiment, Hydros UNI had more favorable results (*Kostoláni, 2013*). Mogul, Plantohyd, Hydros and Naturelle oils with the same viscosity class of 46 loaded statically and dynamically showed better results compared to mineral oils in terms of friction coefficient (*Tóth et al. 2014; Kučera 2014*). In terms of environmental protection, the decisive factor is also the replacement of mineral and synthetic lubricants with ecological lubricants that are biodegradable (*Kosiba et al. 2013; Majdan et al. 2016; Tkáč et al. 2014; Bošanský et al. 2005*). The aim of this study was to confirm the effect of random loading process and ecological oil on the size and type of wear in terms of emergency properties of friction pair.

MATERIALS AND METHODS

We selected steel E335 as the material sample for the shaft. The sample was pressed on the auxiliary shaft even before grinding to final dimension. The shafts were then grinded to the final dimension of Ø 29.960 mm to achieve the H8/f7 fit, i.e. close clearance fit. We selected a bearing shell as the second friction element. The commercial marking of the bearing shell is B60 and its dimensions are Ø 35r7 × Ø 30F7 × 20 (Fig. 1).
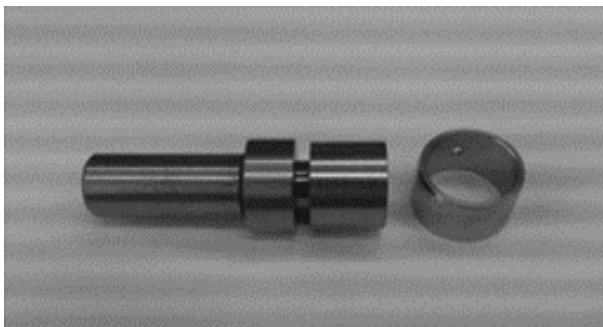
Fig. 1 View of real shaft and bearing shell

Tribological experiments were performed using the laboratory experimental test device Tribotestor M10 (SUA in Nitra, Slovakia).
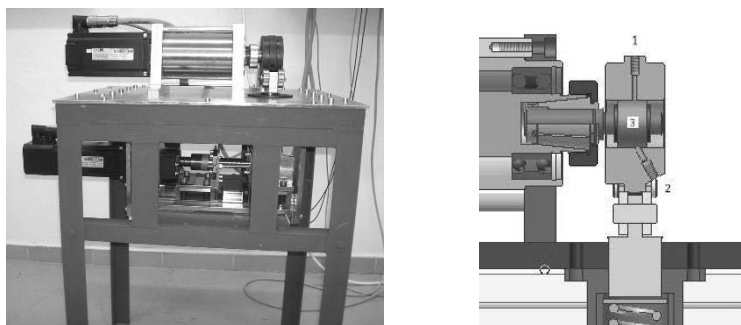
Fig. 2 View of the test device Tribotestor M10 (left) and the tribological node (right)

Test parameters:
- *Loading force 1:* 500–1500 N (dynamic regime D1), according to generated and statistically processed random signal 1, mean value 1000 N (Fig.3);
- *Loading force 2:* 500–1500 N (dynamic regime D2), according to generated and statistically processed random signal 2, mean value 1000 N (Fig.4);
- *Loading force 3:* 1000 N (static regime) – marked as ST (Fig.5);
- *Loading regimes:* according to the processed course of performance of two random processes and comparative (reference) static regime of the test;
- *Operating speed of shaft:* 180 min^{-1};
- *Time of test:* 60 min;
- *Running-up period:* 5 min, loading 500 N;
- *Lubrication method:* gravity feed of lubrication (cup in a height of 500 mm);
- *Oils used:* Madit PP80, producer Slovnaft Bratislava, Plantohyd 46 S – producer Fuchs;
- *Material of shaft:* steel E335; according to standard EN 10025-2 : 2004;
- *Material of counterpart:* a full-bronze bearing shell of material CC483K; according to standard STN 423123.
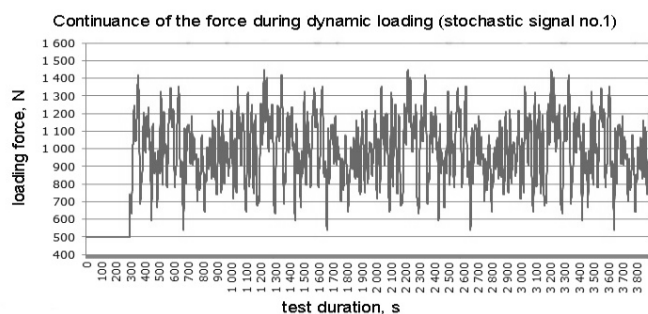
Fig. 3 Course of the loading force during dynamic loading, signal no. 1
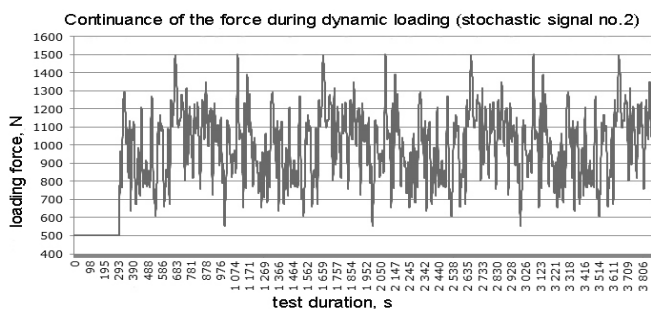
Fig. 4 Course of the loading force during dynamic loading, signal no. 2
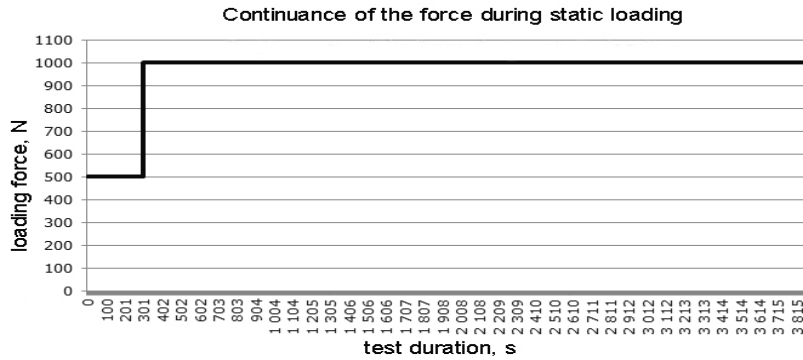
Fig. 5 Course of the loading force during static loading

Oil samples were standardly prepared before implementing the ferrography. Ferrogram was assessed by visual diagnostics and documented with a digital camera and with microscope of Kapa 6000 type (Novel, Xiamen,China), in cooperation with digital camera Moticam 1000 1.3 MP (Motic, Xiamen, China) (magnification was set to 200x). Ferrogram was examined in the area about 5 mm from the start of the flow of oil sample up to the length of 20 mm, i.e. the length of about 15 mm.

RESULTS AND DISCUSSION
We performed 60 tribological tests, i.e. 10 for each type of loading and lubrication. Each of the tests started with a 5 minutes run-up period.

Results of weight loss analysis
Determination of the weight loss of the material pair was performed using laboratory scales Voyager® (Ohaus Corporation, Pine Brook, USA) with an accuracy of 0.001g. Both pre-test and post-test weighing was performed under steady-state conditions to minimize measurement errors. The results (average values) are presented in Tables 1 and 2. Their interpretation in terms of the effect of loading method on the size of wear in experimental conditions is quite clear.

Tab 1. Average values of the bearing shell weight loss

Type of oil	PP 80			Plantohyd 46S		
Loading	ST	D1	D2	ST	D1	D2
Weight loss, g	0.024 4	0.028 2	0.035 2	0.017 5	0.019 5	0.020 5

Tab 2. Average values of the shaft weight loss

Type of oil	PP 80			Plantohyd 46S		
Loading	ST	D1	D2	ST	D1	D2
Weight loss, g	0.011	0.011 2	0.014	0.002 5	0.005 1	0.005 3

Based on the recorded and processed results of the experiment following can be stated:

The smallest wear in the whole set of the bearing shell samples was observed at static loading regime lubricated with oil Plantohyd 46 S and it was 0.017 5 g. On the other hand, the highest wear was observed in the bearing shell samples loaded with dynamic regime D2 lubricated with oil PP 80 and it was 0.035 2 g.

The smallest wear in whole set of the shaft samples was again observed at static loading regime lubricated with oil Plantohyd 46 S and it was 0.002 5 g. The highest wear was observed in the shaft samples loaded with dynamic regime D2 lubricated with oil PP 80 and it was 0.014 g.

Results of the ferrographic analysis

We prepared 3 samples of oil Madit PP 80 for the ferrographic analysis. The samples were randomly taken during the experiment for each loading regime:
-Sample no. 1 – loaded with constant force – marked as static – ST (reference),
-Sample no. 2 – loaded according to generated signal 1 – marked as dynamic – D1,
-Sample no. 3 – loaded according to generated signal 2 – marked as dynamic – D2.

At the same time we also prepared 3 samples of oil Fuchs Plantohyd 46 S. The samples were randomly taken during the experiment for each type of loading regime:
-Sample no. 4 – loaded with constant force – marked as static – ST (reference),
-Sample no. 5 – loaded according to generated signal 1 – marked as dynamic – D1,
-Sample no. 6 – loaded according to generated signal 2 – marked as dynamic – D2.

The effect of loading methods on wear type and wear size of the friction pair materials was demonstrated by observing the ferrograms at 50x magnification (*Kučera et al 2016; Kopčanová et al 2018)*. The aim of observing the ferrograms at 200x magnification (as well as worn surfaces) was to confirm the hypothesis of wear type and transfer of abrasion particles from surface to surface. Based on the observations of the ferrograms (Madit oil) it can be stated that the thickest layer of the ferrographic film is at the sample no. 3 (Fig. 6c). Large particles above 100 µm have been recorded (measured in photo). By observing the surfaces of the shafts lubricated with Madit oil we found small amounts of transferred material with degradation signs regardless of the loading method. The pictures are therefore not mentioned. By observing the samples no. 4 and no. 6 lubricated with oil Plantohyd, their intense coverage has been recorded (Fig. 7). The highest coverage was at the sample no. 6 with signs of tiny shiny particles. The least intensive coverage of this sample set is at sample no. 4 where large numbers of medium-sized particles up to 30 µm have been observed. Several particles of about 100 µm were recorded at sample no. 6. By observing the surfaces of shafts lubricated with oil Plantohyd, substantially larger quantities of transferred material are visible, especially in dynamic loading methods (Fig. 8b, c). Fig. 8b (shaft sample no. 21) shows the areas of continuous surface of transferred material in the form of thin scales after multiple plastic deformation, indicating the presence of adhesive wear. Fig. 8c (shaft sample no. 22) shows, that in addition to the continuous surfaces of the transferred material, there are signs of abrasive wear in the loading cycle D2.

The performed experiments can be characterized as wear tests under the conditions of limiting friction. The effect of dynamic loading is visible in Fig. 8b, c. There are visible continuous layers of transferred material without degradation signs, which resulted in "lower" shaft wear. Finally, the transferred material behaved as a triboactive element, what in the end affected the better friction coefficient *(Kopčanová et al 2018)*.

a   b   c
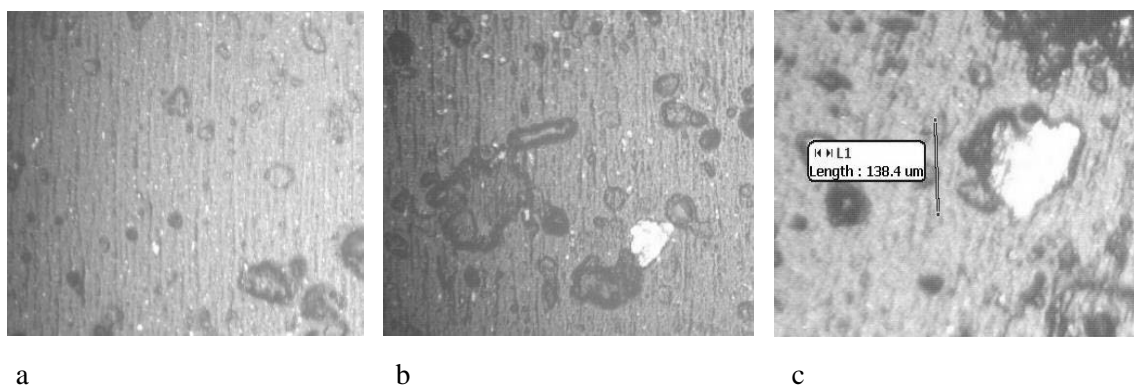
Fig. 6 View of wear particles (200x)

a   b   c
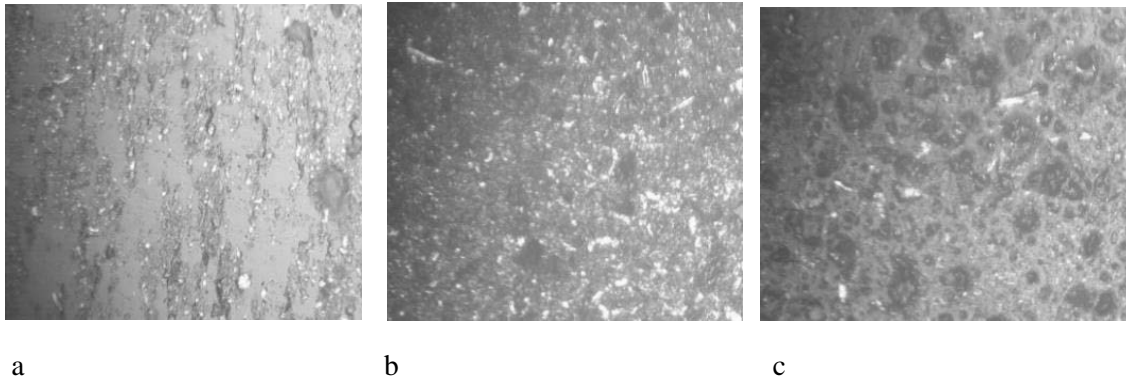
Fig. 7 View of wear particles (200x)

This also confirms the hypothesis of the effect of dynamic loading method on the wear size as a result of the transfer of material from the softer element of the pair.

a   b   c
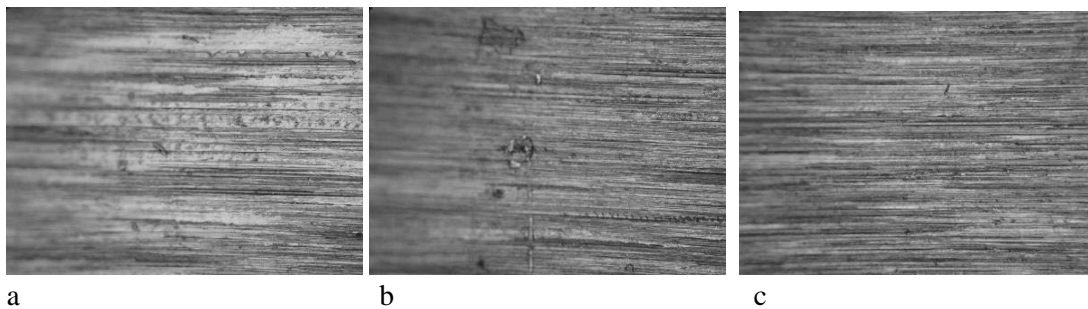
Fig. 8 Surface of the shaft after a - ST, b – D1, c – D2 loading, lubricated by oil Plantohyd 46S (sample no. 20, 21, 22) (20x)

CONCLUSIONS

The selected material pair (steel E335 and tin bronze CC483K) were tested in two-oil-lubricated environment. On a representative sample, dynamic loading has been shown to cause higher wear of the material pair compared to static. Under the conditions of given experiment (limiting friction state), the difference is 0.01 g for shells and 0.003 g for shafts. Friction node degradation occurred in the environment lubricated with Madit PP80. In ecological lubrication with Plantohyd 46S, the transferred material along with the oil acted as a trioactive element. This has also been confirmed for dynamic loading methods. Plantohyd 46S has better properties in terms of emergency properties. This is also evidenced by lower shaft wear (0.005 3 g) compared to Madit PP80 (0.014 g).

REFERENCES

1. Bhushan, B. (2001). *Modern Handbook of Tribology*. Boca Raton: CRC Press.
2. Blaškovič, P., Balla, J., & Dzimko, M. (1990). *Tribology.* (Tribológia). Bratislava: ALFA.
3. Bošanský, M., Vereš, M., & Gaduš, J. (2005). *Possibilities of the use of C-C gearings in agricultural and building machines working in environments with increased environmental.*
4. Kopčanová, S., Kučera, M., Kučera, M., Kučera, M., & V. Kučerová, V, (2018). The Effect of Friction Behaviour and Wear Protection Ability of Selected Base Lubricants on Tribo-pairs Parameters of Machine Components. *Tribology in Industry*, *40*(4), 681-691.
5. Kostoláni, P. (2013). *Study of the influence of the stochastic loading process on the properties of the tribological system* [PhD thesis], (in Slovak). SUA in Nitra.
6. Kučera, M., & Rusnák, J. (2008). *Study of tribological properties of materials deposited on the surface by selected surfacing technologies* (in Slovak). SUA in Nitra.
7. Kučera M., Majdan R., Abraham R., Kučera M., & Haas P. (2016). Analysis of the

Effect of Loading Process on Tribological System Properties. *Acta Universitatis Agriculturae et Silviculturae Mendelianae Brunensis, 64*(3), 825–833.

8. Kučera, M. (2014). *Verifikácia postupov simulácie náhodných procesov zaťažovania v podmienkach experimentu* [PhD thesis]. SUA in Nitra.

9. Licek, R, (2017). Evaluation of Tribological Properties by Using Different Process Fluid by Test Ball on Disc. *Manufacturing Technology*, *17*(2), 217-223. ISSN: 1213-2489.

10. Majdan, R., Tkáč, Z., Abrahám, R., Szabó, M., Halenár, M., Rášo, M., & Ševčík, P. (2016). Proposal for filtration system for biodegradable lubricants in agricultural tractors. *Agronomy Research*, *14*(4), 1395-1405. ISSN 1406-894X.

11. Tkáč, Z., Majdan, R., & Kosiba, J. (2014). *Research of properties of ecological liquids and new test methods of lubricating oils* (in Slovak). SUA in Nitra.

12. Tóth, F., Rusnák, J., & Kadnár, M. (2014). Study of tribological properties of chosen types of environmentally friendly oils in combined friction conditions. *Journal of Central European Agriculture, 15*(1), 185–192.

Corresponding author:
doc. Ing. Marian Kučera,PhD., Department Of Machine Design, Faculty Of Engineering, Slovak University Of Agriculture In Nitra, Tr. A. Hlinku 2, 949 76 Nitra, Slovak Republic,
phone: +421 641 4106, e-mail: marian.kucera@uniag.sk

DEVELOPMENT OF CAPACITIVE THROUGHPUT SENSOR FOR PLANT MATERIALS

František KUMHÁLA[1]

[1]Department of Agricultural Machines, Faculty of Engineering, Czech University of Life Sciences in Prague, 16521 Prague– Suchdol, Czech Republic, E-mail: kumhala@tf.czu.cz, Phone: +420-2-24383135

Abstract
The aim of this article is to introduce the steps of development of capacitance throughput sensor for plant materials. Main results of sensor function with forages, sugar beets, potatoes, chopped maize and hop are discussed. The theory of capacitive throughput sensor function and its influence on sensor behavior in practical conditions is also presented as well as the influence of measured material moisture content changes. Capacitive throughput sensor is a relatively inexpensive and sufficiently robust and accurate alternative to other methods of plant materials throughput measurement.

Key words: *theory of function; forages; potatoes; sugar beet; maize; hop.*

INTRODUCTION

A plant materials throughput sensor can be useful not only in several applications of precision farming. Information about the variable throughput of plant materials can be used e.g. for calculating site-specific crop yield for a yield map, but also in order to control of technological process in more complex agricultural or food processing machines. For this reason, considerable attention has been paid to the development of these sensors in the past.

Plant material throughput sensors first appeared in combine harvesters, i.e. grain harvesting machines. At present, it can be stated that since 1993 farmers have commercially available yield monitors, working on a number of different principles. However, all these yield monitors are located between combine cleaning shoe grain outlet and the grain tank. Monitors can be divided into two large groups. One measures the volume of purified grain on its way to the combine and the other measures its weight (*Stafford et al., 1996; Arslan et al., 2000; Reyns et al., 2002;* and others). Nevertheless, some problems associated with the measurement of grain throughput on the combine harvester were later pointed out e.g. by *Lark, Stafford & Bolam (1997), Arslan & Colvin (2002)* or *Whelan & McBratney (2002).*

In addition to cereals, there have also been an attempt to measured throughput of other plant materials in the past. *DeHaan et al. (1999)* used a bulk yield monitor for potato yield mapping. They reported that after calibration the bulk recorded weighs had been within 5 % of actual weights. *Ehlert & Algerbo (2000)* gave a short overview of possible potato throughput measurement principles. They reported that radiometric measurements, weighing cells in the continuous conveyor belt, optical measurements with photo evaluation, and deflection plate measurements were all known techniques. *Gonigeni et al. (2002)* developed an image-based system for sweet potato yield and grade monitoring. However, when sweet potatoes moved on the harvester conveyor belt, the weight estimations correlated with the actual weights rather poorly. *Hofstee & Molena (2002)* tested a machine vision based yield mapping system of potatoes and recently, *Hofstee & Molena (2003)* used a similar system for estimation of volume with potatoes partly covered with a soil residue. They concluded that there were good prospects for their system using 2 -dimensional information; however, they reported that further research into this method was necessary. *Persson, Eklundh & Algerbo (2004)* developed an optical sensor for tuber yield monitoring.

Sugar beet yield sensors have also been studied. Weight-sensing systems have been studied in several applications (*Isensee & Lieder, 2001; Schwenke et al., 2002; Walter & Backer, 2003; Hall, Backer & Hofman, 2003*). The main disadvantage of all systems is that they are sensitive to contaminants such as mud, plant rests, small stones etc. For that reason, *Schmittmann & Kromer (2002)* tried to measure the mass flow of clean beet. They based their method on online counting of beets and calculating specific yield by multiplying the number of beets the average mass of single beets. They reported that in field tests the system worked successfully, but only under optimized conditions.

Hennens et al. (2003) developed a mass flow sensor for sugar beet harvesters based on the use of a curved impact plate to measure momentum. The sensor was designed in accordance with a mathematical model of beet flow and was installed in the beet harvester cleaning unit. Using only momentum to predict mass flow, errors up to 20 % were discovered. However, this error rate was reduced to 3 % when material velocity corrected momentum was used. *Konstantinovic et al. (2007)* evaluated an ultra wideband radar system for sugar beet yield mapping. They tried to distinguish sugar beet and its dimensions from the surrounding agricultural soil. Sugar beet detection and mass determination potentials under field conditions were evaluated. The simple threshold detection approach to the reflected energy showed insufficiently accurate results and further research into this method is necessary.

Several other systems and methodologies have also been developed for other non-combinable crops which may be suitable for potato and sugar beet as well, e.g. measurement of mass accumulation rate (*Godwin & Wheeler, 1997; Saldana et al., 2006*).

Forages throughput sensors have also been studied in the past. *Vansichen & De Baerdemaeker (1993)* calculated yield from the torque of a forage harvester's blower. Another possibility is to measure the distance between feeder rolls of the harvester *(Ehlert & Schmidt 1995; Auernhammer, Demmel & Pirro., 1996; Barnett & Shinners, 1998; Martel & Savoie, 1999; Schmittmann, Kromer & Weltzien, 2001; Diekhans, 2002)*. A mass flow sensor for a pull type (trailed) forage harvester based on a reaction plate in the spout was constructed and tested by *Missotten et al. (1997)*. Similar sensors were tested by other authors (*Barnett & Shinners, 1998; Martel & Savoie, 1999, Schmittmann, Kromer & Weltzien, 2001*) for self propelled forage harvesters. *Martel & Savoie (1999)* measured electrical capacitance in the spout of a forage harvester and *Schmittmann, Kromer & Weltzien (2001)* measured crop layer thickness. Some of these methods (e. g. distance between feeder rolls, reaction plate, and crop layer thickness) are very interesting and showed a good coefficient of determination ($R^2 = 0.94$ to 0.98). Some methods (e. g. distance between feeder rolls, electrical capacitance in the spout of a forage harvester) have to be supplied with several calibration parameters.

Site-specific measurement of biomass in growing cereal crops has been proposed by *Ehlert, Volker & Kalk (2002)* using a pivoted cylindrical body moving horizontally through a plant population (moving pendulum). The angle of deviation of this pendulum varies with the plant properties.

The feed rate measurement technique for mowing machines was also tested. *Demmel et al. (2002)* used a principle based on belt weighing technology in the windrowing device of a mower. Recently, *Ruhland, Haedicke & Wild (2004)* determined yield by means of determining the torque requirements in the windrowing device of a mower. Both methods are suitable only for mowing machines equipped with a windrowing device. A pulse radar system for grass yield measurements was also introduced (*Wild, Ruhland & Haedicke, 2003*). The results obtained from the measurement showed that the sensors need further improvement.

Shinners, Barnett & Schlesser (2000) developed and evaluated systems to measure material feed rate on a self-propelled forage windrower. They tested conditioning roll force, conditioning roll rise and swath shield impact force as a predictors of material feed rate. The only system to show promise of adequately predicting material feed rate through the machine was impact force on the swath shield. Recently, *Shinners, Huenink & Behringer (2003)* equipped a windrower to measure material feed rate by the following sensors: pressure sensor to measure the load at the platform drive motor; speed pick-up to measure conditioning roll speed, load cell to measure crop impact on the swath forming shield and rotary potentiometers to measure crop volumetric flow past swath forming shield. The crop volumetric flow was well correlated with material feed rate when the sensor output was combined with platform inclination and roll speed. The results from these measurements were meaningful ($R^2 = 0.94$).

In the past, we have also been developing and testing sensors for measuring the throughput of mowing machine. Principles based on torque sensor in machine's conditioner shaft and curved impact plate mounted at the exit of the machine *(Kumhála & Prošek, 2003; Kumhála et al., 2003; Kumhála, Kroulík & Prošek 2007)*. However, while developing and testing these two contact methods, we have faced with some of their disadvantages. Problems can be caused by foreign particles in the harvested forages, such as stones, which can damage the measuring device.

Non-contact measurement methods are preferable from this perspective. For example, the use of capacitive measurement methods could be interesting. The advantages of capacitive sensor are its relative

simplicity, its possible suitability for the often difficult operating conditions found on agricultural machines, and its low cost.

Capacitance sensor techniques can be used for the determining different properties of a range of plant materials. The function of capacitance sensors depends on the fact that the dielectric constant of an air/material mixture between two parallel plates increases with material volume concentration increasing. According to many authors *(e.g. Kim et al., 2003; Nelson, 2005; Wild & Haedicke, 2005; Jones et al., 2006)* the dielectric properties of many materials depend on frequency, moisture content, volume density, temperature, chemical composition, and permanent dipole moment association with water and other constituent molecules.

Capacitance sensors have been widely used for plant material moisture content determination *(Lawrence, Funk & Windham, 2001)*. *Eubanks & Birrell (2001)* determined the moisture content of hay and forages by using multiple frequency parallel plate capacitors. *Osman et al. (2002)* built a parallel plate capacitor with variable spacing for hay and forage moisture measurement. *Snell et al. (2002)* used a radio-frequency application device for sensing dry matter content of various agricultural products.

However, there were also efforts to use a capacitive sensor to measure throughput. *Stafford et al. (1996)* used a capacitive sensor to determine grain mass flow. *Martel & Savoie (1999)* observed a capacitance controlled oscillator placed at the discharge end the forage harvester spout to measure changes induced by forage particles. Recently, *Savoie, Lemire, & Thériault (2002)* used a similar capacitance controlled oscillator for their measurement. *Williams et al. (2000)* used electrical capacitance tomography for particular solids flow rate measurement on a conveyor belt.

Based on the information from this literature review and also our own experience, it was clear that the principles of measuring plant materials throughput are known, but still not often used. Measuring systems are sometimes too complicated and still not enough robust and to use contactless capacitive measurement principle could be a promising way to improve this situation. That is why in 2006 we started to develop capacitive sensor suitable for plant materials throughput measurement. The main aim of this paper is therefore to present the steps of capacitive throughput sensor for plant materials development and the results achieved.

MATERIALS AND METHODS

Since we had experience in measuring the throughput of the forage through the mower and mower was still available, we first tried to develop a capacitive sensor suitable for this machine in 2006.

The parallel plate capacitance sensor consisted of two metal sheets 2 mm thick and with the dimensions 830 mm in length and 260 mm in width. The distance between the plates was 300 mm. The inside parts of metal sheets were insulated by two plastic sheets 1 mm thick with the same dimensions which were stuck on metal sheets. Sides of the capacitance sensor were made from 10 mm thick acrylic glass. A shielding 2 mm thick metal plate with the dimensions 830 mm in length and 280 mm in width were fixed to mentioned acrylic glass sides in the distance 430 mm from the capacitor's shielded plate (see Fig. 1). This metal plate shielded the capacitance sensor from surrounding influences which could affect the measurement. The design of a sensor and its dimensions we tried to develop just ready for practical using on small rotary mower equipped with conditioner (ŽTR 186, Agrostroj Pelhřimov Company).
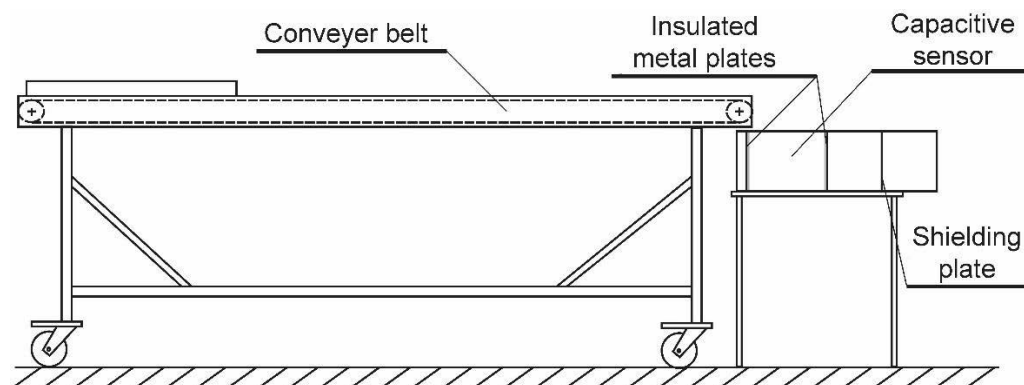

Fig. 1 Arrangement of measurement device for laboratory tests in 2006.

The laboratory set-up consisted of a conveyer belt carrying a measured quantity of material into sensor equipped with the electronic measurement apparatus (Fig. 1). Material from the conveyer belt passed through the sensor between its plates. Material was transported through parallel plate capacitance sensor for approximately five seconds for each test run.

A very important part of our capacitive throughput sensor is its electronic circuit. The sensor - capacitor and the whole oscillating circuit was driven at 27 MHz frequency. The exact connection of the measuring circuit is in the Fig. 2. The capacitor was fed with AC-voltage from the oscillator via resistor or another capacitor with the same reactance. The resistor together with two measuring capacitor plates made up a voltage divider and thus the output voltage of that divider depended on the capacity on the measuring capacitor and that capacity is dependent on the dielectric matter between the plates again. The dielectric constant of the measuring capacitor varied according to the amount and type of material paced between the plates, it means according to proportion material/air. The AC output voltage of the divider was then rectified in an AC/DC rectifying module and amplified with an amplifier. Rectified output voltage just can be measured and saved. In this case we used 0.5 s interval for saving.
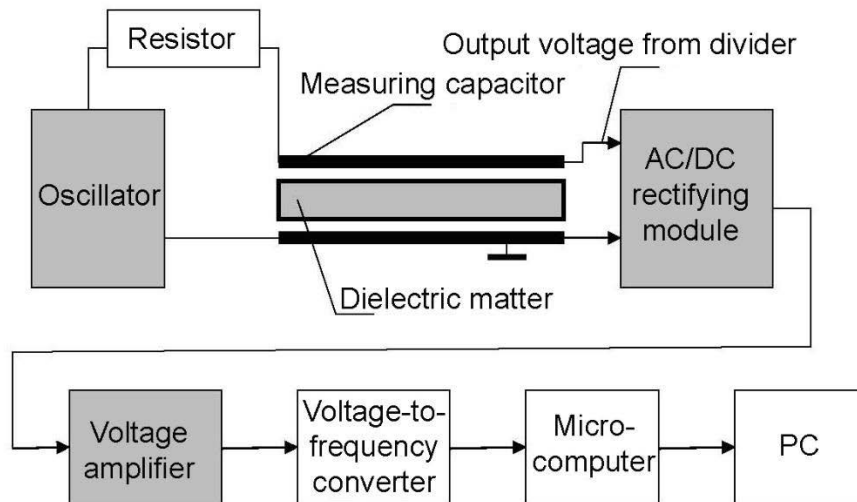
Fig. 2 Block diagram of electronic apparatus arrangement for plant material throughput measurement. Oscillator worked at 27 MHz frequency.

This relatively simple proposed connection of electronic circuit is very sensitive (capable of measuring very small capacitance changes), but within a narrow measuring range. However, this narrow measurement range was perfectly suited to our needs.

In 2006, measured material was grass from natural meadow. Closer description of methodology used in this year can be found in *Kumhála et al. (2007).*

During the measurement in 2006, it appeared that it is necessary to partially change the arrangement of the measuring device. The arrangement was improved with the aim to achieve more uniform material distribution within the sensing volume. The capacitive sensor was mounted directly on the conveyer as follows: bottom metal sheet of the capacitor was inserted under the elastic belt and the center of the belt was just in the middle of the metal sheet length. The capacitor was placed near to the end of the conveyor. This arrangement of measuring device is in Fig. 3. In 2007, this arrangement was used for the measurements repeated with grass during spring period and for the measurements with sugar beets and potatoes in autumn period of this year. Closer description of measuring device can be found in ASABE paper No. 084700 (*Kumhála et al., 2008*).

Measurements with sugar beets and potatoes in 2007 showed the need to determine the theoretical assumptions of the sensor function. The most important conclusions from the theoretical considerations of the capacitive sensor function were as follows.
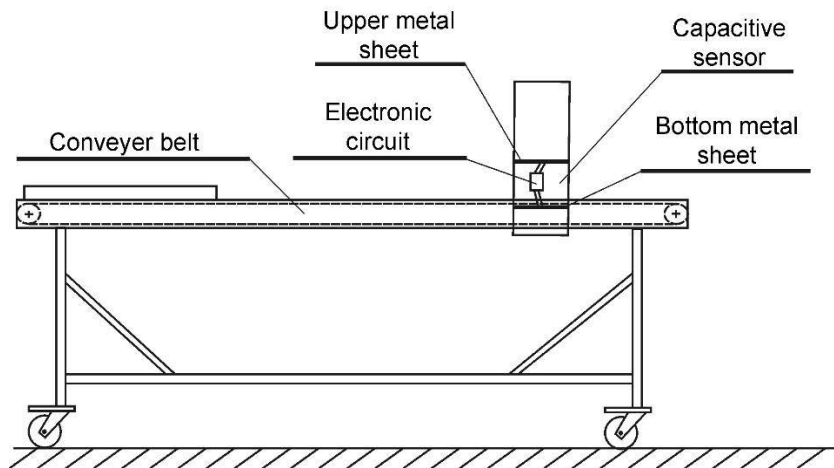
Fig. 3 Arrangement of measurement device for laboratory tests after improvement.

Bearing in mind the filling of the a real capacitive sensor with some dielectric material, two important separate cases have to be considered.

I. Layer filling (LF). This case is characteristic by using the whole plate area for transporting the material through the sensor (Fig. 4 left) and the differences in throughput is realized by increasing thickness c_1 of the analyzed material. This regime of sensor operation is typical for materials formed by small particles when the sensor is used for higher throughput values. Resulted relationship between the sensor capacity C and the throughput value Q is described as an equation of the shifted hyperbola.

II. Filling by simple particles (FSP) In this case the plate area for transport is covered partially (Fig. 4 right) and the throughput differences are solved only by the degree of the plate covering that is expressed by a length a_1 in Fig. 4 right. This case describes lower throughput regimes and/or regimes working with particles with dimensions nearly comparable with the plates distance c. Linear dependence of the sensor capacity and the sensor throughput is achieved in this case.
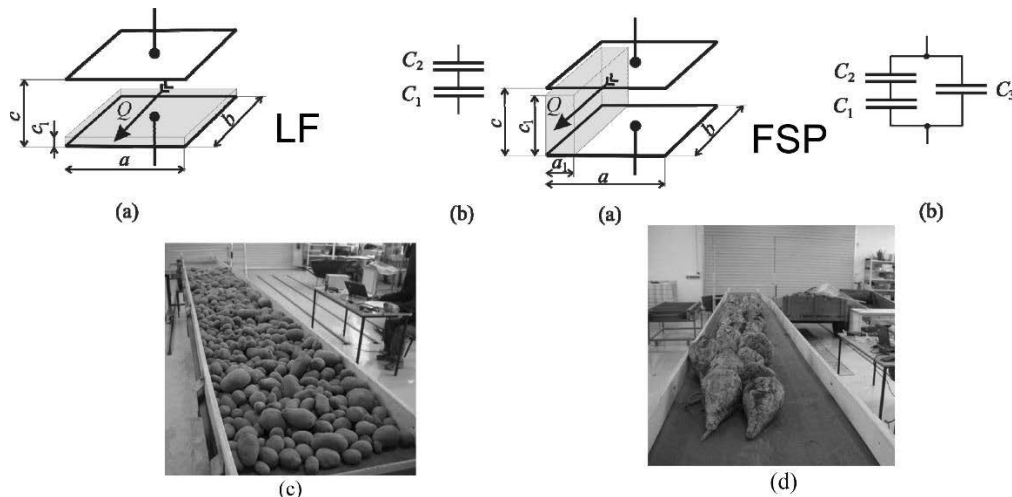
Fig. 4 Material distribution in capacitive throughput sensor in the case of layer filling (LF) and filling by single particles (FSP); (a) initial material throughput layer; (b) substituted model; (c) LF realized using potatoes (Q=12.6 kg s^{-1}); (d) FSP realized using sugar beet (Q=12.7 kg s^{-1}); a capacitive throughput sensor plate length; b capacitive throughput sensor plate width; c distance between capacitive throughput sensor plates; c_1 thickness of material layer in capacitive throughput sensor; C_1, C_2, C_3 capacity of substituted capacitors; Q direction of measured material throughput.

In working conditions both cases (LF and FSP) can be combined. Nevertheless if the average diameter of measured material particle is relatively small compared to the capacitor plates distance the resulting capacity tends to be described as LF depending on material throughput and conversely, when the average

particle dimension approaches the distance c the resulting capacity tends to depend on throughput as FSP. This means that every plot of C versus Q starts at low throughputs as FSP and changes to LF at high throughputs when this is allowed by the sensor construction parameters and the particle dimensions of the product. Closer description of these theoretical considerations including equations can be found in *Kumhála, Prošek & Blahovec (2009)*.

The suitability of capacitive sensor for chopped maize throughput measurement was also tested in 2008. Since the moisture content of chopped maize during harvesting is lower compared to previous materials tested, the experiments were focused on the effect of moisture content on plant material throughput measurement. Stationary laboratory experiments with balsa blocks were arranged. Another, smaller laboratory capacitor was made for that purpose. The capacitor was integrated into an electronic circuit similar to the ones used for other experiments. The dimensions of capacitor plates were 67 mm in length and 40 mm in width. The distance between the plates was 20 mm. Four balsa blocks with the dimensions 57 mm in length, 40 mm in width and 16 mm in height were used for those experiments.

At start of the experiments, balsa blocks were moistened to about 80% of moisture content and then slowly dried in our laboratory. After about 45 minutes of drying, balsa blocks were placed into plastic bags and sealed in order to homogenize moisture content distribution inside each of balsa blocks. After that, each balsa block was separately weighted and placed between smaller capacitor plates. The values of balsa blocks weight and measuring circuit output voltage were logged and used for further calculations of balsa blocks moisture content and charting. This procedure was repeated until balsa blocks equilibrium moisture content was achieved. During the measurements the dimensions of balsa blocks were checked to make sure that they hadn't changed. Detailed description of materials and methods used for these experiments is in *Kumhála, Prošek & Kroulík (2010)*.

Based on the results achieved, in 2011 and 2012 there was an effort to use a capacitive sensor to monitor hop throughput on the hop picking machine. All harvesting experiments were done using a stationary hop picking machine PT-30 produced by Chmelařství družstvo Žatec, CR, and located in Stekník. This machine uses picking conveyer system. At the beginning of the picking process, hop vines are loaded into the picker manually using feed track intake. Then, hop cones are separated from the vine stalk by two picking walls (equipped with picking conveyers) along their entire length with subsequent secondary picking of long ends. Picked hop cones are then separated by air separators and inclined separating conveyers. At the end of the hop picking machine clean hop cones falling down from inclined separating conveyers are transported away from the machine by a horizontal elastic belt conveyer. Main parts of PT-30 can be seen in Fig. 5.
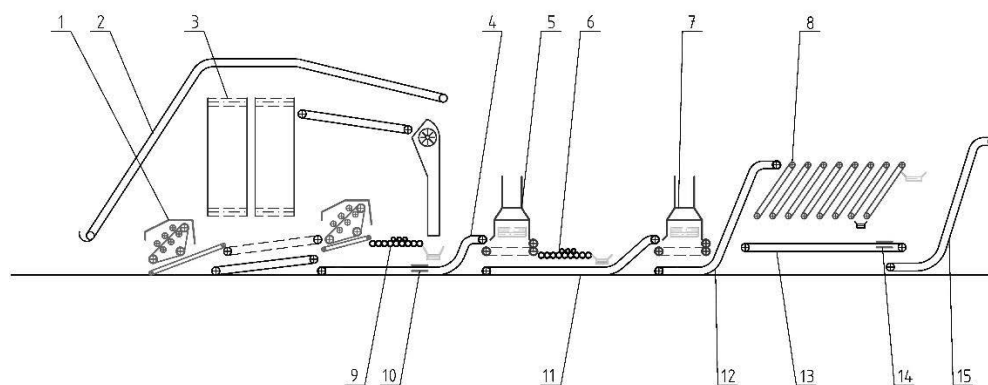
Fig. 5 Main parts of stationary hop picking machine PT-30. 1-lateral pickers for secondary picking of long ends, 2-feed track intake, 3-picking walls, 4-belt conveyer to separation part, 5-primary air separator, 6-pinch rollers, 7-secondary air separator, 8-inclined separating conveyers, 9-waste conveyers, 10-pinch rollers, 11- location of capacitive throughput unit for throughput control, 12-belt conveyer to secondary air separator, 13-belt conveyer to inclined separating conveyers, 14-horizontal elastic belt conveyer, 15-location of tested capacitive throughput unit, 16-belt conveyer to drying machine.

A modified capacitive throughput unit was made to be mounted on our PT-30 hop picking machine. The main difference was in capacitor dimensions. Dimensions of the bottom, grounding plate were 1222 mm in length and 300 mm in width. Dimensions of the upper, active plate were 1170 mm in length and 300

mm in width. Both plates were made of 1.5 mm thick metal sheet. In order to increase the strength of the plates their edges were bent by 90 degrees. The upper plate was insulated from the rest of the machine by two pertinax blocks with dimensions of 300 x 70 x 20 mm. For practical reasons the distance between the plates had to be set to 80 mm. The electronic measurement apparatus of this unit was mounted on the insulation block at the left side of the upper plate and run at 6 MHz frequency in this case. A more detailed description of the materials and methods used in 2011 and 2012 is in *Kumhála, Kavka & Prošek (2013)*.

Based on previous encouraging results, the sensor was used to control the hop picking process in 2013. The parallel plate capacitance sensor was mounted on a PT-30 hop picking machine (label 11 in Fig. 5). The dimensions of the bottom, grounding plate were 1000 mm in length and 300 mm in width. The dimensions of the upper, active plate were 890 mm in length and 300 mm in width. Both plates were made from 1.5-mm thick metal sheet. In order to increase the strength of the plates their edges were bent by 90 degrees. The upper plate was insulated from the rest of the machine by two insulating blocks with the dimensions of 290 x 60 x 8 mm. The distance between the plates was 165 mm. The upper plate was covered from the top by a plastic sheet in order to prevent its clogging by impurities. The capacitance sensor was equipped with an electronic measurement apparatus, which was mounted on the insulation block at the right side of the upper plate and worked at 6 MHz frequency.

For the purpose of wet hop material instantaneous throughput measurement and consequent control, the capacitance sensor was mounted on the pocket belt conveyer transporting picked hop material to the separation part of the machine (Fig. 6). The sensor was placed in the last third of the conveyor, just before the beginning of its sloping part. The total transport length of the conveyor belt was 6.26 m; the transport width was 0.9 m. The conveyor pockets were made from 1-mm thick metal sheet and their height was 70 mm. The conveyor velocity could be set in the range of 0.23–0.46 m s^{-1} using an electric motor drive controlled by a frequency converter. Detailed description can be found in *Kumhála et al. (2016)*.
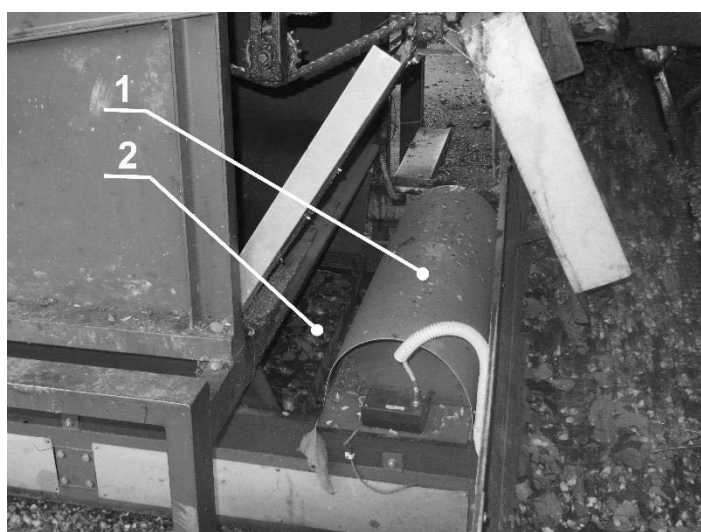
Fig. 6 Location of the capacitance throughput sensor on the pocket belt conveyer of the PT-30 stationary hop picking machine (Fig. 5, label number 11). 1 – capacitance throughput sensor, 2 – pocket belt conveyer with picked hop material.

RESULTS AND DISCUSSION

An example of the measurement results in 2006 is shown in Fig. 7. The forage mass flow determination by means of parallel plate capacitance sensor driven at 27 MHz frequency appeared to be a promising way. The results revealed a strong linear relationship between the feed rates of the wet forage crop material passing through the sensor between its plates and the tested measuring capacitance sensor circuit output. However, the results obtained showed that an improvement of the electronic circuit connection and measuring device arrangement can be recommended.
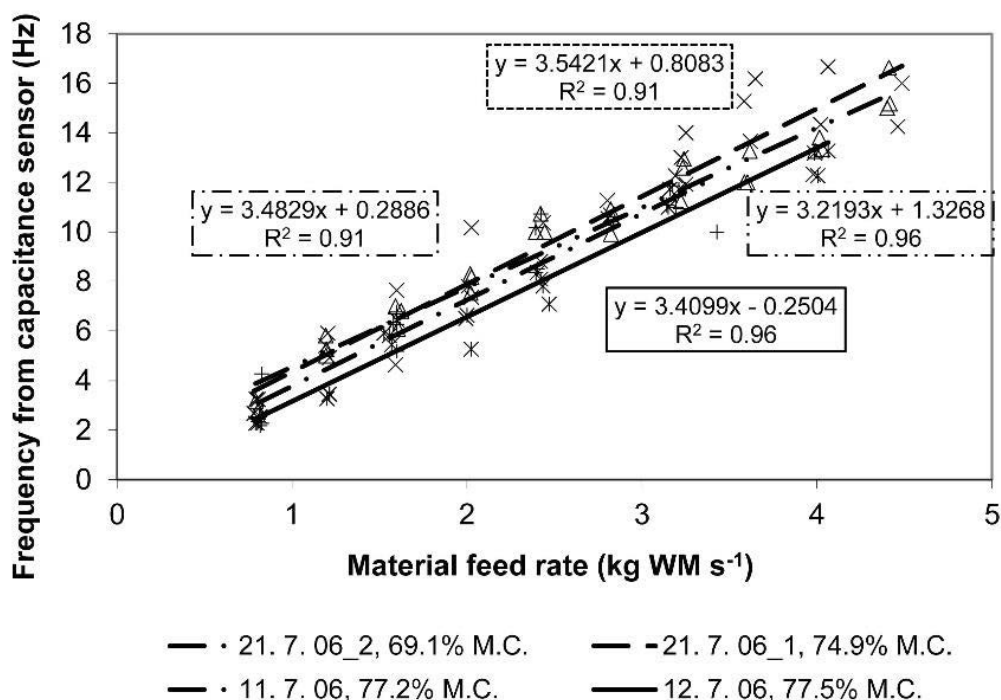
Fig. 7 The dependence of measured circuit output frequency on plant material mass flow (11th, 12th and 21st July 2006). M.C. – moisture content.

An example of the results obtained with partially changed arrangement of measuring device (see Fig. 3) is provided in Fig. 8.
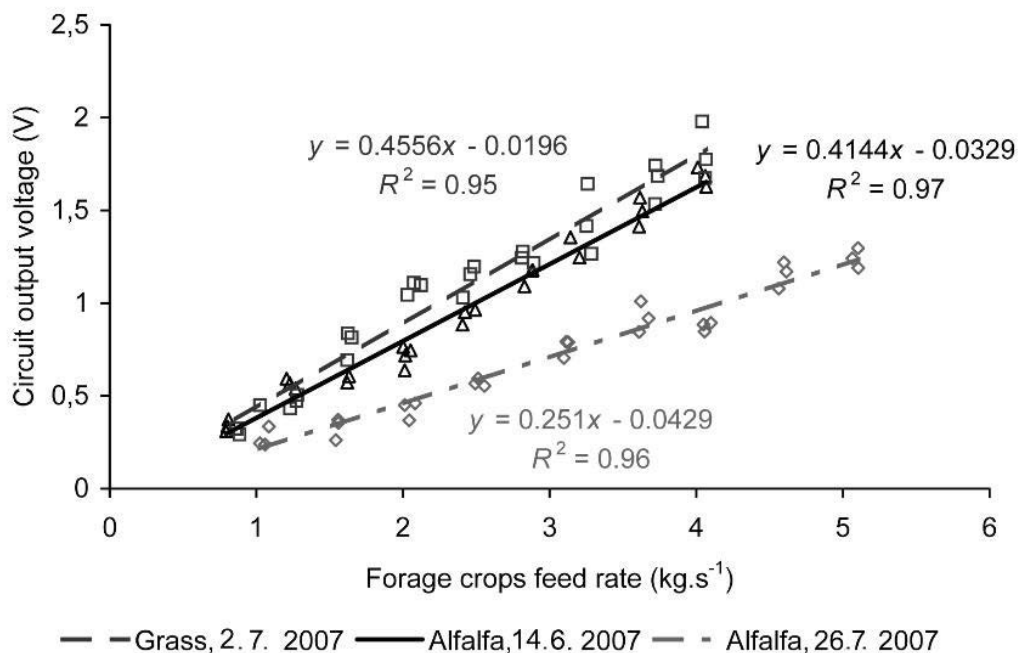
Fig. 8 Dependence of the measuring circuit output on forage crops feed rate (14.6. 2007 alfalfa 66.3 % M.C., 2.7. 2007 grass from natural meadow 74.4 % M.C., 26.7. 2007 alfalfa 75.9 % M.C.).

The linear dependence of the capacitive sensor data on forages throughput was confirmed in 2007. The resulting coefficients of determination were the same or better than in 2006. However, the whole behavior of the measuring apparatus was not entirely logical. It was not clear which of changing factors of

investigated material influenced the measurement more and which less. For example, it was not clear how the measurement was affected by changes in forages moisture content etc.

After measurements with forage crops in the spring and summer of 2007, a functional measuring apparatus remained in our laboratory. During the autumn of 2007, samples of potatoes and sugar beets from other measurements appeared in the same laboratory. Therefore, it was not difficult to decide about testing of our capacitive throughput sensor also with these plant materials. The advantage of potatoes or sugar beets over forage crops lies primarily in the more regular shape of the individual particles.

The results from the measurements with sugar beets and potatoes are in Fig. 9.
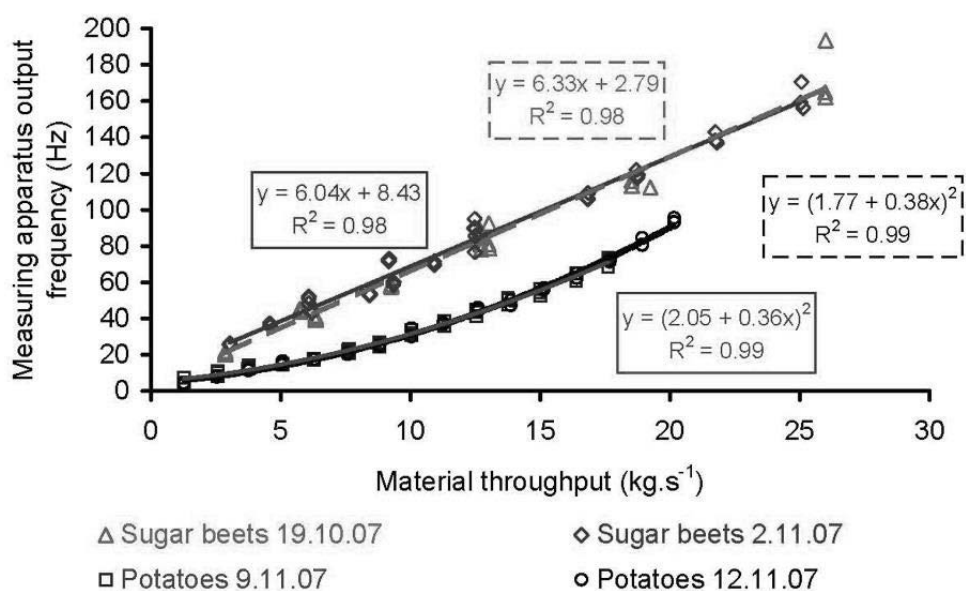
Fig. 9 Dependence of measuring apparatus output frequency (directly proportional to voltage and sensor capacity) on sugar beets and potatoes throughput.

However, the results of this measurement raised more questions than answers. Why we achieved so different output values for comparable material throughput? Why the trend was for sugar beets linear and for potatoes not? It was clear at this point that we do not understand well the behavior of the capacitive throughput sensor. It was necessary to turn back to the theory of capacitive throughput sensor function. The result of theoretical considerations can be seen in Fig. 4. Detailed description of theoretical considerations, its calculation and the results obtained with sugar beets and potatoes can be found in *Kumhála et al. (2008)* or *Kumhála, Prošek & Blahovec (2009)*.

Another often harvested plant material is maize for silage making. As the chopped particles are relatively small, hyperbolic dependence of measured output values on throughput resulting from layer filling was expected and confirmed by our measurements in 2008. As already mentioned, copped maize has less moisture content than previously tested materials. The results from our measurements studying the effect of moisture content on plant material throughput measurement can be seen in Fig. 10.

Although the effect of measured material moisture content changes to its throughput measurement is surprisingly not as great as expected (*Stafford et al., 1996*), still some exists. It can be concluded from our results that if materials with relatively high moisture content are measured (i.e. potatoes, sugar beets, carrots, tomatoes etc.), changes of about 5% of material moisture content have very little influence on capacitive throughput sensor measurement and which can therefore be neglected.
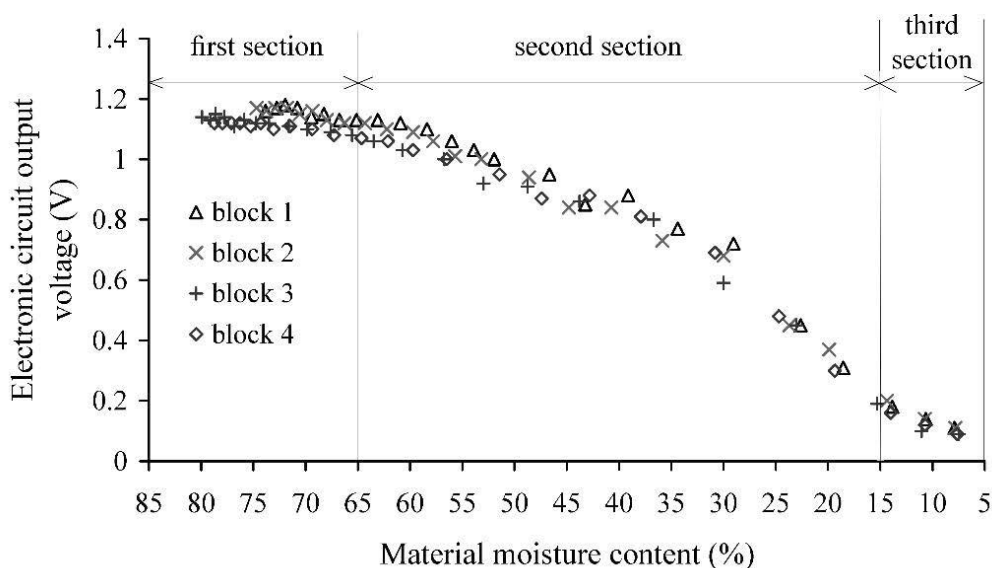
Fig. 10 Dependence of measured capacitive sensor output voltage on balsa blocks moisture content (wet basis) changes. Dry matter content of 1st balsa block was 4.79 g, of 2nd balsa block 4.83 g, of 3rd 3.71 g and of 4th balsa block 3.75 g.

However, in the case when materials with lower material moisture content are measured, the changes in material moisture content itself can influence the results of capacitive throughput measurement. In our case, material moisture content of freshly chopped maize can vary from 40% to about 60%. This is just below 65% and those values fall into the second section of the chart in Fig. 10. This must be respected during the operation of capacitive throughput sensor. Independent measurement of material moisture content can be recommended for plant materials with material moisture content in the range from 65 to 15%.

Results of previous experiments and knowledge of capacitive throughput sensor behavior motivated us to its practical application with the aim to control hop picking process of stationary hop picking machine. The main task of this control was to reduce hop harvest losses resulting from the uneven throughput of the harvested material through different parts of hop harvesting machine (see Fig. 5). An example of the hop picking machine control using signals from capacitive throughput sensor to control it is in Fig. 11.
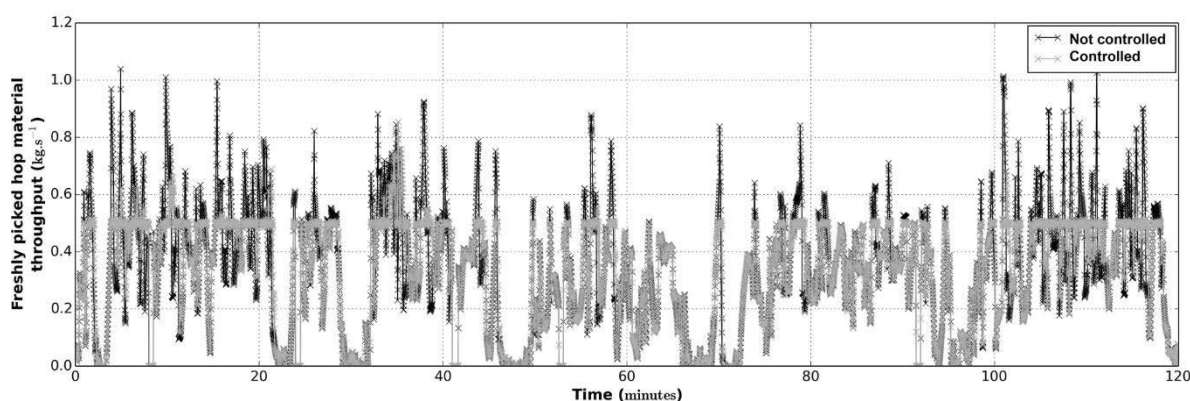
Fig 11 The course of freshly picked material throughput when automatic throughput control is used (gray curve) and when it is not (black curve).

From Fig. 11 it is clear that using the automatic control procedure avoids reaching a material throughput higher than 0.5 kg.s^{-1} (which are the cause of losses) in numerous occasions in comparison with the situation when automatic control is not used. It is realistic to assume that control system functionality can save over 2% of harvesting losses. When harvesting 30 ha per year with the average yield of 1 ton

per ha, this fact represents a saving of 0.6 tons of dry hop cones per one year. When calculating with the estimated control system price of 145 000 Kč (5 650 EUR or 6,250 USD) and the commodity price 150 000 Kč (5 850 EUR or 6,600 USD) per ton of dry hop, the return on investment should be less than two years. Closer description of the results from this practical application of capacitive throughput sensor can be found in *Kumhála et al., 2016*.

Further experiments with capacitive sensor were focused on its division into segments (*Lev, Wohlmuth-ová & Kumhála, 2012*) or on deeper study of the influence of frequency and material moisture content changes on its function (*Lev et al., 2017*). However, these experiments are just beyond the scope of this article.

CONCLUSIONS

It can be concluded on the base of our results that capacitive throughput sensor is a suitable device for measuring the throughput of plant materials. It is a relatively inexpensive and sufficiently robust and accurate alternative to other methods of plant materials throughput measurement. However, it is to be expected that the filling of the capacitive throughput sensor plays a very important role that has to be respected during its use. Independent measurement of material moisture content is recommended for plant materials with material moisture content in the range from 65 to 15%. The potential of the capacitive throughput sensor has also been tested under normal operating conditions during hop harvesting with satisfactory results.

ACKNOWLEDGMENT

REFERENCES

1. Arslan, S. & Colvin, T. S. (2002): An Evaluation of the Response of Yield Monitors and Combines to Varying Yields. *Precision Agriculture 3*(2), 107-122.

2. Arslan, S., Inanc, F., Gray, J., & Colvin, T. (2000). Grain Flow Measurements with X-ray Techniques. *Computers and Electronics in Agriculture 26*(1), 65-80.

3. Auernhammer, H., Demmel, M., & Pirro, P. J. M. (1996). Lokale Ertragsermittlung mit dem Feldhäckslern. (Local Yield Monitoring in a Forage Harvester). *Landtechnik 51*(3), 152-153.

4. Barnett, N. G. & Shinners, K. J. (1998). Analysis of Systems to Measure Mass-flow-rate and Moisture on a Forage Harvester. *ASAE Paper No. 981118*.

5. DeHaan, K. R., Vessey, G. T., Holmstrom, D.A., MacLeod, J. A., Sanderson, J. B., & Carter, M. R. (1999). Relating potato yield to the level of soil degradation using a bulk yield monitor and differential global positioning systems. *Computers and electronics in Agriculture 23*(2), 133-143.

6. Demmel, M., Schwenke, T., Heuwinkel, H., Locher, F., & Rottmeier, J. (2002). Lokale Ertragsermittlung in einem Scheibenmähwerk mit Aufbereiten. (Local Yield Monitoring in a Mower Conditioner with Windrowing Device). In: *Proceedings of Conference Agricultural Engineering 2002* (pp. 139–143). VDI Verlag GmbH.

7. Diekhans, N. 2002. Ein praxisnahes Verfahren für eine Ertragsmessung an Feldhäckslern. (A Practical Solution for Yield Measurement on a Forage Harvester). In: *Proceedings of Conference Agricultural Engineering 2002.* (pp. 133-137). VDI Verlag GmbH.

8. Ehlert, D. & Algerbo, P-A. (2000). Yielding mapping with potatoes. *Landtechnik 55*(6), 436-437.

9. Ehlert, D. & Schmidt, H. (1995). Ertragskartierung mit Feldhäckslern. (Yield Mapping in Forage Harvesters). *Landtechnik 50*(4), 204–205.

10. Ehlert, D., Volker, U., & Kalk, W.-D. (2002). Sensorgestützte Stickstoffdüngung in Winterweizen. (Sensor Based Nitrogen Fertilization in Winter Wheat). In: Proceedings of Conference Agricultural Engineering 2002 (pp. 127-132). VDI Verlag GmbH.

11. Eubanks, J. C. & Birrell, S. J. (2001). Determining moisture content of hay and forages

using multiple frequency parallel plate capacitors. *ASAE paper No. 011072.*

12. Godwin, R. J. & Wheeler, P. N. (1997). Yield mapping by mass accumulation rate. *ASAE paper No. 971061.*

13. Gonigeni, S., Thomasson, J. A., Wooten, J. R., White, J., Thompson, P. G., & Shankle, M. (2002). Image-based sweetpotato yield and grade monitor. *ASAE Paper No. 021169.*

14. Hall, T. L., Backer, L. F., & Hofman, V. L. (2003). Sugarbeet Yield Monitoring for Site-Specific Farming Part II-Field Testing. *Precision Agriculture 4*(4), 433 – 444.

15. Hennens, D. Baert, J., Broos, B., Ramon, H., & De Baerdemaeker, J. (2003). Development of a Flow Model for the Design of a Momentum Type Beet Flow Sensor. *Biosystems Engineering 85*(4), 425 – 436.

16. Hofstee, J. W. & Molena, G. J. (2002). Machine vision based yield mapping of potatoes. *ASAE paper No. 021200.*

17. Hofstee, J. W. & Molena, G. J. (2003). Volume estimation of potatoes partly covered with dirt tare. *ASAE paper No. 031001*, 12 p.

18. Isensee, E. & Lieder, W. (2001). Ertragmessung in der Rübenernte [Yield measurement during sugar beet harvesting]. *Landtechnik 56*(4), 272-281.

19. Jones, C. L., Stone, M. L., Maness, N. O., Solie, J. B. & Brusewitz, G. H. (2006). Plant biomass estimation using dielectric properties. *ASABE paper No. 063092.*

20. Kim, K. B., Lee, J. W., Lee, S. S., Noh, S. H., & Kim, M. S. (2003). On-line measurement of grain moisture content using RF impedance. *Transaction of ASAE, 46*(3), 861-867.

21. Konstantinovic, M., Woeckel, S., Schulze Lammers, P., & Sachs, J. (2007). Evaluation of a UWB Radar System for Yield Mapping of Sugar Beet. *ASABE paper No. 071051.*

22. Kumhála, F., Kavka, M., & Prošek, V. (2013). Capacitive throughput unit applied to stationary hop picking machine. *Computers and Electronics in Agriculture 95*(6), 92–97.

23. Kumhála, F., Kroulík, M., Mašek, J., & Prošek, V. (2003). Development and testing of two methods for the measurement of the mowing machine feed rate. *Plant, Soil Environment 49*(11), 519-524.

24. Kumhála, F., Kroulík, M., Kvíz, Z., Mašek, J., & Prošek, V. (2008). Sugar beets and potatoes throughput measurement by capacitive sensor. In *Agricultural Engineering - Landtechnik 2008* (pp. 199-204). VDI Verlag GmbH, Germany.

25. Kumhála, F., Kroulík, M., & Prošek, V. (2003). Development and evaluation of forage yield measure sensors in a mowing-conditioning machine. *Computers and Electronics in Agriculture 58*(2), 154-163.

26. Kumhála, F.; Kvíz, Z.; Kmoch, J. & Prošek, V. (2007). Dynamic Laboratory Measurement with Dielectric Sensor for Forage Mass Flow Determination. *Research in Agricultural Engineering 53*(4), 149-154.

27. Kumhála, F., Lev, J., Kavka, M., & Prošek, V. (2016). Hop-Picking Machine Control Based on Capacitance Throughput Sensor. *Applied Engineering in Agriculture 32*(1), 19-26.

28. Kumhála, F. & Prošek, V. (2003). Laboratory Measurement of Moving Machine Material Feed Rate. *Precision Agriculture 4*(4), 413-419.

29. Kumhála, F., Prošek, V. & Blahovec, J. (2009). Capacitive throughput sensor for sugar beets and potatoes. *Biosystems Engineering 102*(1), 36-43.

30. Kumhála, F., Prošek, V. & Kroulík, M. (2010) Capacitive sensor for chopped maize throughput measurement. *Computers and Electronics in Agriculture 70*(1), 234–238.

31. Kumhála, F., Prošek, V., Kroulík, M. & Kvíz, Z. (2008). Parallel Plate Mass Flow Sensor for Forage Crops and Sugar Beet. *ASABE paper No. 084700.*

32. Lark, R. M., Stafford, J. V. & Bolam, H. C. (1997). Limitations on the Spatial Resolution of yield Mapping for Combinable Crops. *Journal of agricultural engineering research 66*(3), 183-193.

33. Lawrence, K. C., Funk, D. B., & Windham, W. R. (2001). Dielectric moisture sensor for cereal grains and soybeans. *Transaction of ASAE, 44*(6), 1691-1696.

34. Lev, J., Křepčík, V., Prošek, V., & Kumhála, F. (2017). Capacitive throughput sensor for plant materials - Effects of frequency and moisture content. *Computers and Electronics in Agriculture 133*(2), 22-29.

35. Lev, J., Wohlmuthová, M., & Kumhála, F. (2012). Qualito of Material Distribution Imaging with Segmental Capacitive Sensor using Landweber's Iterative Algorithm. In: *Proceedings of 11th International Scientific Conference on Engineering for Rural Development* (pp. 239-244). Latvia University of Agriculture.

36. Martel, H. & Savoie, P. 1999. Sensors to Measure Forage Mass Flow and Moisture Continuously. *ASAE Paper No. 991050*.

37. Missotten, B., Broos, B., Strubbe, G., & De Baerdemaeker, J. (1997). A Yield Sensor for Forage Harvesters. In: *Precision Agriculture 1997. Proceedings of the 1ˢᵗ European Conference on Precision Agriculture* (pp. 529-536). BIOS Scientific Publishers.

38. Nelson, S. O. (2005). Dielectric properties measurement for agricultural applications. *ASABE paper No. 053134*.

39. Osman, A. M., Savoie, P., Grenier, D., & Thériault, R. (2002). Parallel-plate capacitance moisture sensor for hay and forage. *ASAE paper No. 021055*.

40. Persson, D. A., Eklundh, L., & Algerbo, P-A. (2004). Evaluation of an optical sensor for tuber yield monitoring. *Transaction of the ASAE 47*(5), 1851-1856.

41. Reyns, P., Missotten, B., Ramon, H., & De Baerdemaeker, J. (2002). A Review of Combine Sensors for Precision Farming. *Precision Agriculture 3*(2), 169-182.

42. Ruhland, S., Haedicke, S., & Wild, K. (2004). A Measurement Technique for Determination of Grass. In: *Proceedings of Conference Agricultural Engineering 2004* (pp. 317 – 324). VDI Verlag GmbH.

43. Saldana, N., Cabrera, J. M., Serwatowski, R. J., & Gracia, C. (2006). Yield mapping system for vegetables picked up with a tractor-pulled platform. *Spanish Journal of Agricultural Research 4*(2), 130-139.

44. Savoie, P., Lemire, P., & Thériault, R. (2002). Evaluation of five sensors to estimate mass-flow rate and moisture of grass in a forage harvester. *Applied Engineering in Agriculture, 18*(3), 389-397.

45. Shinners, K. J., Barnett, N. G., & Schlesser, W. M. (2000). Measuring Mass-Flow-Rate on Forage Cutting Equipment. *ASAE Paper No. 001036*.

46. Shinners, K. J., Huenink, B. M., & Behringer, C. B. (2003). Precision Agriculture as Applied to North American Hay and Forage Production. In: *Proceedings of the International Conference on Crop Harvesting and Processing. ASAE Publication Number 701P1103e*.

47. Schmittmann, O. & Kromer, K-H. (2002). Teilflächenspezifische Ertragsmessung von Zuckerrüben [Site-specific yield measurement of sugar beet]. In: *Proceedings of the Conference Agricultural Engineering* (pp. 259 – 264). VDI Verlag GmbH.

48. Schmittmann, O., Kromer, K-H., & Weltzien, C. (2001). Yield Monitoring on Forage Harvester. In: *Proceedings of PMA 2001* (pp. 286 – 291). CUA Prague, Czech Republic.

49. Schwenke, T., Demmel, M., Rothmund, M., & Rottmeier, J. (2002). Ertragsermittlung im selbstfahrenden Zuckerrüben Köpf-Rode-Bunker [Local yield detection in a self-propelled sugar beet harvester]. In: *Proceedings of the Conference Agricultural Engineering* (pp. 253 – 258). VDI Verlag GmbH.

50. Snell, H. G. J., Oberndorfer, C., Lücke, W., & Van den Weghe, H. F. A. (2002). Use of electromagnetic fields for the determination of the dry matter content of chopped maize. *Biosystems Engineering 82*(3), 269-277.

51. Stafford, J., Ambler, B., Lark, R., & Catt, J. (1996). Mapping and interpreting the yield variation in cereal crops. *Computers and Electronics in Agriculture, 14*(2-3) 101-119.

52. Vansichen, R. & De Baerdemaeker, J. (1993). A measurement technique for yield mapping of corn silage. *Journal of Agriculture Engineering Research 55*(1), 1-10.

53. Walter, J. D. & Backer, L. F. (2003). Sugarbeet Yield Monitoring for Site-Specific Farming Part I-Laboratory Tests and Preliminary Field Tests. *Precision Agriculture 4*(4), 421-431.

54. Whelan, B. & McBratney, A. (2002). A Parametric Transfer Function for Grain-Flow Within a Conventional Combine Harvester. *Precision Agriculture 3*(2), 123-134.

55. Wild, K., Ruhland, S., & Haedicke, S. (2003). Pulse radar systems for yield measurements in forage harvesters. In: *Precision Agriculture, Proceedings of the 4th European Conference on Precision Agriculture* (pp. 739-744). Wageningen Academic Publishers.

56. Wild, K. & Haedicke, S. (2005). Improving the accuracy of moisture sensors for forage crops. In: *Book of Abstracts 5 ECPA-2 ECPLF* (pp. 326-328). JTI Sweden.

57. Williams, R. A., Luke, S. P., Ostrowski, K. L., & Bennett, M. A. (2000). Measurement of bulk particulates on belt conveyor using dielectric tomography. *Chemical Engineering Journal 77*(1-2), 57-63.

Corresponding author:
prof. Dr. Ing. František Kumhála, Department of Agricultural Machines, Faculty of Engineering, Czech University of Life Sciences Prague, Kamýcká 129, Praha 6, Prague, 16521 Czech Republic, phone: +420 22438 3135, e-mail: kumhala@tf.czu.cz

LOGISTICS SPRAWL IN PRAGUE'S SUBURB FROM SATELLITE IMAGES

Jitka KUMHÁLOVÁ[1], Miroslav RŮŽIČKA[2], Elena CASTILLO LOPÉZ [3] Martin CHYBA[4]

[1]*Department of machinery utilization, Faculty of Engineering, Czech University of Life Sciences Prague, Czech Republic*
[2]*Department of vehicles and ground transport, Faculty of Engineering, Czech University of Life Sciences Prague, Czech Republic*
[3]*Department of Geographic Engineering and Techniques of Graphical Expression, University of Cantabria, 39005, Spain*
[4]*Department of machinery utilization, student of the Faculty of Engineering, Czech University of Life Sciences Prague, Czech Republic*

Abstract
The construction of logistics centres and the selection of their localities affects not only the activities of urban goods movement, but also the urban environment. The phenomenon called as logistics sprawl, i.e. the relocation of logistics facilities away from inner urban areas to suburban areas has received an increasing level of attention from scientific community and public as well. The paper results are focused on the square increase of logistics centres in Prague's suburb with the use of satellite images. These images were compared with the cadastre of the Czech Republic. Build up squares of logistics centres enlarged about 400.10^4 (m^2) in suburb from the year 2013 to 2018 at the expense of agricultural land. This fact can exacerbate the quality of life in the Prague´s suburban areas.

Key words: logistics centres; remote sensing; land use; environmental impact.

INTRODUCTION

There are many efforts to define and classify logistics centres academically. Using freight village term synonymously, logistics centre is defined as: traffic logistical interconnection points within a logistics network that primarily function is an interface between local and long-distance goods transport (*Winkler & Seebacher, 2011*). In an ideal case, the logistics centres should be located near urban agglomerations and have a quick access to regional and long-distance. The second condition to fulfil requirement for logistics centre is its access to at least two transport modes (*Europlatforms, 2019*), in particular to road and rail (intermodal terminal). Logistics centres or logistics facilities can be distinguished into different types that require land depending on the category and objective of the facility, which can be a warehouse, distribution centres (DC), truck terminal or intermodal facility (*McKinnon, 2009*). As logistics facilities represent a pivotal component of the overall logistics network, urban planners need to carefully assess the merits and limitations of land use allocation related to these facilities. They affect the overall landscape, resource use as well as the future economic and social geography of suburban areas (*Cidell, 2011*). *Lindsey et al.,* (*2014*) indicated that for public stakeholders, the location of logistics facilities affect regional truck traffic patterns and influence the well-being of individuals in local communities by contributing to several issues such as noise, air quality, safety and congestion. *Visser & Francke* (2018) found that the total number of square meters occupied by logistics centres has multiplied by two and half over the past twenty years in the Netherlands. It is evident that particular attention should be given to this progress of land use (land take) especially when the land is primarily devoted to the agricultural purposes or even it is wild nature. *Aljohani &Thomson* (*2016*) presented a summary of the empirical findings illustrating the additional distance trucks travel due to logistics sprawl in several European and North American cities. Furthermore, the paper (*Aljohani &Thomson*, *2016*) provides an overview of the measures and policies implemented in various metropolitan areas to reintegrate small-scale logistics facilities within inner urban areas to act as consolidation centres. They focused on the taxonomy of impacts of logistics sprawl and listed these main impact groups i.e. impacts on urban freight geography, contribution of logistics sprawl to increased distance travelled by trucks, contribution of logistics sprawl to negative environmental impacts and impacts on commuting of logistics employment (*Aljohani & Thomson, 2016*). As the main environmental negative impacts are taken into account the increase of

greenhouse gas emissions and pollutions as well as increasing fuel consumption and unsustainable nature of urban logistics as a result of the additional congestion (*Dablanc and Ross* (*2012*) and *Wygonik et al.* (*2014*) *in Aljohani & Thomson, 2016*). *Aljohani & Thomson* (2016) concluded that impact of logistics sprawl is significantly understudied as much of the prior research has been descriptive in nature while failing to quantity the actual negative environmental impacts.

Remote sensed data, generally from satellites or unmanned aerial systems, can provide accurate and timely geospatial information of urban and peri-urban areas. These data can have various spectral, spatial or temporal resolution (*Taubenböck et al., 2012*). Currently, the most used satellite systems became Landsat with medium spatial resolution (30 m) and Sentinel 2 from European Space Agency Copernicus Programme with 10 m spatial resolution for visible and near-infrared part of electromagnetic spectra. In contrary to relatively new Copernicus programme Landsat images have a regularly sampled historical archive of 40 years (*Ghosh et al., 2014*). Land cover classification seems to be as one of the most studied topics in remote sensing, especially for agricultural, forest or land changes purposes (*Zhu & Woodcock, 2014*). Currently, many advanced tools as classification workflows allow this process make relatively easy. Nevertheless, it is not easy to make it accurate. Higher classification accuracy is usually achieved using different land cover product (*Friedl et al., 2010*).

The main aim of this paper is to describe the increase of quantity of Prague's logistics sprawl during the last 5 years, with the support of supervised classification of satellite images (downloaded for selected areas in the year 2013 and 2018). This result of the main aim will be compared with the supporting information from the cadastre of the Czech Republic to determine and prove the accuracy of input satellite images (from Landsat 8 and Sentinel 2).

MATERIALS AND METHODS

The eight logistics areas were selected to be the aim of conducted survey. Five of them are located in the district Prague-East and three in the district Prague-West. All these surveyed areas are located alongside of highways and one of them near the road of the first class (see Table 1); where large amounts of logistics centres have been constructed up to now and continue to be constructed.

Landsat 8 Operational Land Imager (OLI) images from 15.5.2013 and 13.5.2018 were down-loaded from Geological Survey of U.S. (USGS) (https://earthexplorer.usgs.gov/) in Level 1 – Top of Atmosphere reflectance format. The images were converted to Level 2 Bottom of Atmosphere reflectance format with the help of atmospheric correction module ENVI 5.5 SW. Sentinel 2B Multispectral Instrument (MSI) from 14.5.2018 was downloaded from Copernicus Open Access Hub (https://scihub.copernicus.eu/) in L2A format which equals the Bottom of Atmosphere reflectance. Pre-processing of Sentinel 2 image consisted of individual band resampling to the same spatial resolution. In the case of this image it was 10 m. The surveyed areas were cut and classified into five categories supported of supervised classification tool (ENVI 5.5 software made by Excelis, Inc., McLean, USA). Basic four categories as "arable land", "forest land", "built-up area", and "water area" were selected for better landscape type differentiation. The fifths category was "logistics centres". Result of supervised classification workflow were raster data formats of surveyed areas. Rasters were edited with the help of "Edit Classification Image" post-classification tool and then converted to vector data formats and processed by the geo-processing tool in ArcGIS 10.4.1 software (ESRI, Redlands, CA, USA). The areas were obtained in square metres. Next processing was based on statistical comparison of L8 images from 2013 and 2018 and then L8 from 2013 and S2 from 2018 (S2 images have been available since 2016). The results derived from satellite images were then verified by actual information from the cadastre of the Czech Republic (https://nahlizenidokn.cuzk.cz/, 28.3.2019). It was calculated only for the areas III. and VII., where the highest increase of logistics centres square was monitored.

RESULTS AND DISCUSSION

Overview of surveyed areas, its location and areas derived from satellite images and the cadastre of the Czech Republic is presented in Table 1. The increase of logistics centres square in surveyed areas from 2013 to 2018 are then available in Table 2. Surveyed areas based on Landsat 8 images supervised classification in 2013 was visualized in Fig. 1. Visualization of surveyed areas based on Sentinel 2 images supervised classification in 2018 in Fig. 2.

Tab. 1 Overview of surveyed areas, its location and areas derived from satellite images Landsat 8 (L8) and Sentinel 2 (S2) in 2013 and 2018 and the cadastre of the Czech Republic (CR) in 2019.

Designation of areas	Designation of highways	2013 L8 [$m^2.10^4$]	2018 L8 [$m^2.10^4$]	2018 S2 [$m^2.10^4$]	Cadastre of the CR [$m^2.10^4$] 2019
I. Zdiby, Klecany	D8	44.7	56.1	80.9	-
II. Zápy, Brandýs nad Labem	D10	62.7	102.5	116.2	-
III. Šestajovice, Mochov	D11	114.8	217.7	233.2	221.8
IV. Průhonice, Čestlice	D1	202.0	323.9	307.1	-
V. Mirošovice, Pyšely	I/3	4.1	18.1	21.3	-
VI. Středokluky	D7	42.7	113.3	82.6	-
VII. Hostivice, Jeneč	D6	57.0	109	108.1	100.1
VIII. Rudná	D5	74	85.9	82.9	-
Total square – Praha-East		428.3	718.4	758.7	-
Total square – Praha-West		173.6	308.2	273.5	-
Total		602.0	1026.6	1032.2	-

Tab. 2 Increase of logistics centres in surveyed areas derived from Landsat 8 images (L8 /L8 – 2013 vs. 2018) and L8 and Sentinel 2 images (L8 / S2 – 2013 vs. 2018) and its relative expression.

| Designation of areas	Increase of LC [$m^2.10^4$] Landsat 8	Increase of LC [$m^2.10^4$] Sentinel 2	Increase in % Landsat 8	Increase in % Sentinel 2
I. Zdiby, Klecany	11.3	36.1	4	11
II. Zápy, Brandýs nad Labem	39.9	53.5	14	16
III. Šestajovice, Mochov	102.9	118.3	35	36
IV. Průhonice, Čestlice	121.9	105.1	42	32
V. Mirošovice, Pyšely	14.0	17.2	5	5
VI. Středokluky	70.7	39.9	52	40
VII. Hostivice, Jeneč	52.0	51.1	39	51
VIII. Rudná	12.0	8.9	9	9
Total square – Praha-East	290.0	330.4	100	100
Total square – Praha-West	134.6	99.9	100	100
Total	424.6	430.3	-	-
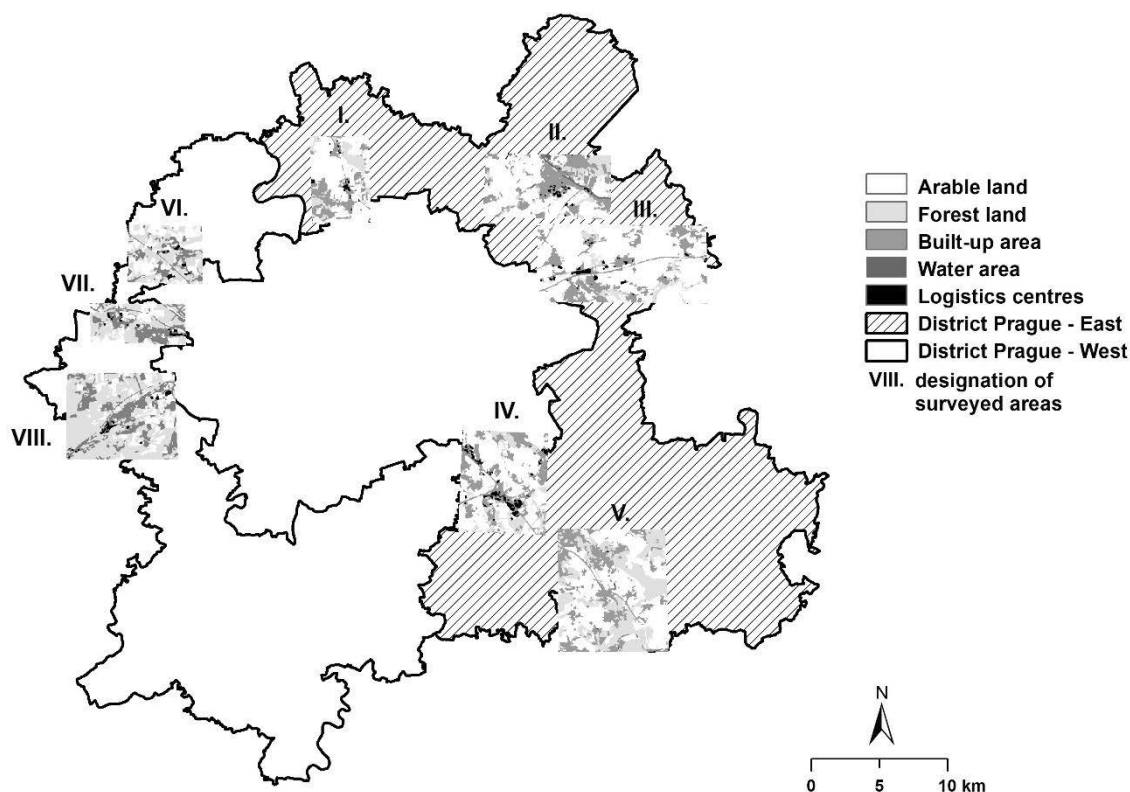
Fig. 1 Surveyed areas based on Landsat 8 images supervised classification in the year 2013.

The highest increase of logistics centres square was detected in the areas: VI. (Středokluky) and VII. (Hostivice, Jeneč) in Prague – West district, and then in areas III. (Šestajovice, Mochov) and IV. (Průhonice, Čestlice) in Prague – East district. On the contrary the lowest increase was found in areas: V. (Mirošovice, Pyšely in Prague – West district) and VIII. (Rudná in Prague – West district) (see Table 1, 2 and Fig. 1, 2).

The results showed that the built-up square of logistics centres differs on the base of satellite images used for this comparison. The satellite images (S2 and L8) used in this study had medium spatial resolution of 10 and 30 m per pixel. This spatial resolution seems to be sufficient and in many case standard for land cover classification and change detection and can provide consistent and repeatable measurements at an appropriate spatial scale (*Verbesselt et al., 2010; Wulder et al., 2008*). Nevertheless, the obtained results found out that the spatial resolution of L8 images were too coarse for the detection of smaller buildings. The calculation carried out in the cadastre of the Czech Republic for areas III. and VII. showed that the better spatial resolution of Sentinel 2 image can exacerbate the image classification for the right object detection. The advantage of using these satellite systems seems to be revisit period (8 days with multiple Landsat sensors in orbit, and 3 days for Sentinel 2) and wide spatial coverage (185 km for Landsat and 290 km for Sentinel 2 field of view). The availability of many images increase the chance of cloud-free data (*Gómez et al. 2016*). That is why it was possible to find two images from different source for almost the same date (13.5. 2013 and 15.5.2018) for this study. Supervised classification with subjectively setting of the classes enables to enhance possibilities how to identify land cover types one by one (*Chen et al. 2014*). This should minimize effects of spectral confusion among land cover classes as in our study. However, the areas surveyed in this study were selected with the aim to identify the logistics centres only on the base of spectral characteristics of detected land cover. Sometimes it can be very difficult to differ the land cover as iron roof and bare soil or concrete surface. In this case should help collection of training samples due the supervised classification workflow. Accuracy of those classification increase by using of many accurate inputs for example from cadastre information, land use / land cover application. This statement is in accordance with *Gómez et al., (2016)* who recommend supervised classification, machine learning or ensemble algorithms for more accurate and efficient classification.
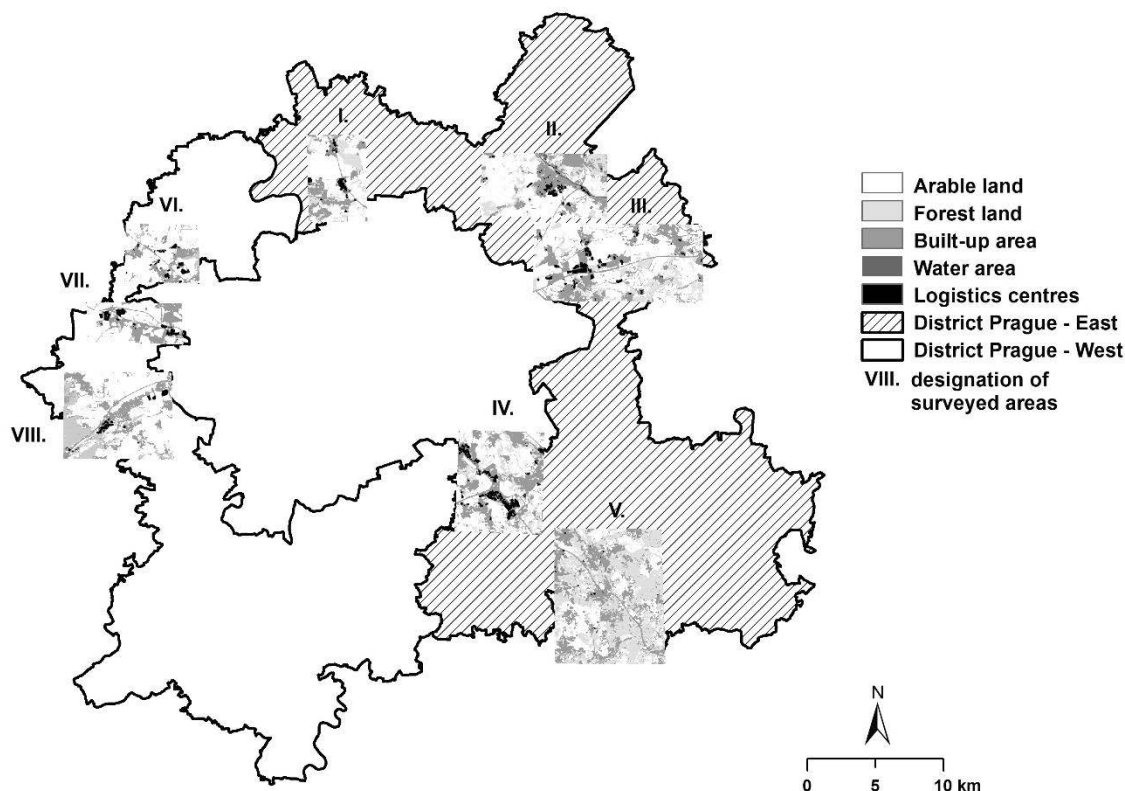
Fig. 2 Surveyed areas based on Sentinel 2 image supervised classification in 2018.

The Fig. 2 showed that the logistics sprawl in the Prague´s suburban areas is at the expense of agricultural land. This fact can exacerbate the quality of life how it is described in the study of *Patino & Duque* (*2013*). Remote sensing can be one of very powerful and efficient tool for the evaluating of life quality together with information from situ. The challenge for the further work, focused on this topic, can derive other various indices describing social and economic dimensions and the environmental aspects of the suburban areas.

CONCLUSIONS
This paper found out and proved that the satellite remote sensing is powerful and efficient tool to detect and evaluate changes within suburban and urban areas. The carried out research illustrates that freely accessible satellite images from Landsat 8 and Sentinel 2 (with medium spatial resolution), can provide sufficiently precise information about logistics sprawl and they can be used for its quantitative evaluation. The eight logistics areas alongside of highways were surveyed in the districts Prague-East and Prague-West. The satellite images from the year 2013 and 2018 were analysed with the aim to get an evidence of the logistics centres sprawl. These procedures were carried out with the support of supervised classification of satellite images and they were compared with information from the cadastre of the Czech Republic. The highest increase of build-up square of logistics centres was determined in the areas "Středokluky" and "Hostivice, Jeneč" in district Prague-West and then in areas "Šestajovice, Mochov" and "Průhonice, Čestlice" in district Prague-East. The build-up square of logistics centres enlarged about 300.10^4 (m^2) in district Prague – East and $100 .10^4$ (m^2) in district Prague-West from the year 2013 to 2018. This total "land take" place at the expense of high quality agricultural land. This fact points out to a low agricultural land preservation that should be paid more attention.

REFERENCES

1. Aljohani, K. & Thompson, R.G. (2016). Impacts of logistics sprawl on the urban environment and logistics: Taxonomy and review of literature. *Journal of Transport Geography, 57*, 255–263.

2. Chen, J., Chen, J., Liao, A., Cao, X., Chen, L., Chen, X., He, Ch., Han, G., Peng, Sh., Lu, M., Zhang, W., Tong, X., & Mills, J. (2015). Global land cover mapping at 30 m resolution: a POK-based operational approach. *ISPRS J. Photogramm. Remote Sens., 103*, 7-27.

3. Cidell, J. (2011). Distribution centres among the rooftops: the global logistics network meets the suburban spatial imaginary. *Int. J. Urban Reg. Res. 35 (4),* 832–851.

4. ČUZK Nahlížení do katastru nemovitostí (cadaster of the Czech Republic). Retrieved from https://nahlizenidokn.cuzk.cz/

5. Friedl, M.A., Menashe, D. S., Tan, B., Schneider, A., Ramankutty, N., Sibley, A., et al. (2010). MODIS collection 5 global land cover: Algorithm refinements and characterization of new datasets. *Remote Sensing of Environment, 114*, 168–182.

6. EUROPLATFORMS. The European Logistics Platforms Association. Retrieved from http://www.europlatforms.eu/?page_id=150

7. Ghosh, A., Sharma, R., & Joshi, P.K. (2014). Random forest classification of urban landscape using Landsat archive and ancillary data: Combining seasonal maps with decision level fusion. *Applied Geography, 48*, 31-41.

8. Gómez, C., White, J.C., & Wulder, M.A., (2016). Optical remotely sensed series data for land cover classification: A review. *ISPRS J. Photogramm. Remote Sens., 116*, 55-72.

9. Lindsey, C., Mahmassani, H.S., Mullarkey, M., Nash, T., & Rothberg, S. (2014). Industrial space demand and freight transportation activity: exploring the connection. *J. Transp. Geogr. 37,* 93–10.

10. McKinnon, A. (2009). The present and future land requirements of logistical activities. *Land Use Policy, 26,* 293–301.

11. Patino, J.E. & Duque, J.C. (2013). A review of regional science applications of satellite remote sensing in urban settings. *Computers, Environment and Urban Systems, 37*, 1-17.

12. Taubenböck, H., Esch, T., Felbier, A., Wiesner, M., Roth, A., & Dech, S. (2012). Monitoring urbanization in mega cities from space. *Remote sensing of Environment, 117*, 162-176.

13. Verbesselt, J., Hyndman, R., Zeileis, A., & Culvenor, D. (2010). Phenological change detection while accounting for abrupt and gradual trends in satellite image time series. *Remote Sens. Environ., 114*, 2970–2980.

14. Visser J., & Francke J. (2018). Logistics sprawl: the spatial structure of logistics centres and hinterland container terminals. Retrieved from *https://www.researchgate.net/publication/324543132*

15. Winkler H., & Seebacher G. (2011). Management of freight villages: findings from an exploratory study in Germany. *Int J Logist Rest Appl,14*(4), 271-283.

16. Wulder, M.A., White, J.C., Goward, S.M., Masek, J.G., Irons, J.R., Herold, M., Cohen, W.B., Loveland, T.R., & Woodcock, C.E. (2008). Landsat continuity: issues and opportunities for land cover monitoring. *Remote Sensing of Environment, 112*, 955–969.

17. Zhu, Z., & Woodcock, C.E. (2014). Continuous change detection and classification of land cover using all available Landsat data. *Remote Sensing of Environment, 144*, 152-171.

Corresponding author:
Doc. Mgr. Jitka Kumhálová, Ph.D., Department of Machinery Utilization, Faculty of Engineering, Czech University of Life Sciences Prague, Kamýcká 129, Praha 6, Prague, 16521, Czech Republic, phone: +420 22438 3148, e-mail: kumhalova@tf.czu.cz

DATA COLLECTION FOR NON LINEAR SOIL MODEL OF DEM

Jiří KUŘE[1], Rostislav CHOTĚBORSKÝ[1], Monika HROMASOVÁ[2], Miloslav LINDA[2]

[1]*Department of Material Science and Manufacturing Technology, Faculty of Engineering, Czech University of Life Sciences, Kamýcká 129, 165 21 Prague – Suchdol, Czech Republic*
[2]*Department of Electrical Engineering and Automation, Faculty of Engineering, Czech University of Life Sciences, Kamýcká 129, 165 21 Prague – Suchdol, Czech Republic*

Abstract
In order to create a model, input parameters need to be provided. The basic step for obtaining these parameters is the execution of the appropriate experimental tests. Establishing stiffness for the specific soil in relation to its consolidation is one of the important parameters. Soil porosity was observed under various consolidation. Tests were carried out in order to determine the amount of force required to compact the soil to a specific degree of porosity, as well as to determine stiffness and derive the relationship between stiffness and porosity. The individual coefficients can be used to set the model in RockyDEM environment.

Key words: Stiffness; ball indentation; porosity; soil.

INTRODUCTION

When creating a mathematical model of a particular substance, a selection of an appropriate contact model between the particles is necessary. Rocky DEM environment *("Rocky DEM Particle Simulator," 2018)* has three particle contact models available. Hysteretic Linear Spring model, Linear Spring Dashpot model and Hertzian Spring Dashpot model *(Obermayr, Vrettos, & Eberhard, 2013; Pasha, Dogbe, Hare, Hassanpour, & Ghadiri, 2013)*. The use of Hysteretic Linear Spring model is advised for creating non-linear soil models. This model was first introduced in the year 1986 *(Walton & Braun, 1986)*. Static and dynamic friction are the fundamental parameters for setting a mathematical model *(Kuře, Hájková, Hromasová, Chotěborský, & Linda, 2019)*. An important parameter for the correct use of the model is Stiffness *(Ucgul, Fielke, & Saunders, 2015)*. Ball indentation method can be used to correctly determine stiffness of a particular substance *(Pasha et al., 2014)*. Principally, it determines hardness of the material. Hardness is defined as the resilience of a material to a plastic deformation. In the case of a loose material, it is possible to determine the stiffness under a specific state of compaction. The aim of this work is to describe the process of determining stiffness, using the ball indentation method, and gaining results for a specific type of soil. These parameters are important in order to create models using the discrete element method.

MATERIALS AND METHODS

This type of soil is located in northwestern part of Prague (Czech Republic). The first step was to determine the soil's moisture. During these tests it is necessary for the moisture to remain at the same value. Moisture of the soil significantly affects its mechanical properties. In order to determine the moisture, a sample was taken, weighted and then left to dry out for 24 hours in a drying room under 105 degrees Celsius (221°F). The moisture was then calculated and determined to be 17%. Another set of tests were performed to determine the dependence of the force affecting the soil in relation to its compaction. A 40mm diameter cylinder was filled with separated soil up to a height of 60mm, followed by a pressure test during which the soil was compressed under constant feed rate. During this test, the force applied to the indentation ball as well as its displacement were observed and recorded (Fig. 1 and 2). In the force/depth of the compaction relation was the force converted to pressure. Deformations were determined from the deformation curve and subsequently a maximal pressures for the soil sample's compaction and consolidation, it is required for the ball indentation test. A size 90x90x60 mm containers were filled with separated soil samples in order to determine its stiffness. Individual load forces were recalculated to the cross section area of 90x90mm. Individual samples were subjected to load forces of 65, 225, 470, 546, 902 and 1841 N. After reaching a specific force load, the samples were hold for 10 minutes in case of soil relaxation and subsequently subjected to the ball indentation test.

The test involves embedding the ball indenter into the sample at a constant deformation rate *(Pasha, 2013; Pasha, Pasha, Hare, Hassanpour, & Ghadiri, 2013)* and then relieving it once again at a constant deformation rate back to the ball's initial position. The test was carried out on a universal tensile machine. The deformation rate was set to 10 mm/min. The force acting on the ball during its retraction is also measured. The cycle is complete after the ball reaches the initial position (Fig. 1). A 25.4 mm diameter Teflon ball was used for the indentation. The result of the test is the dependence of force on the indentation position of the ball into the soil (Fig. 2).
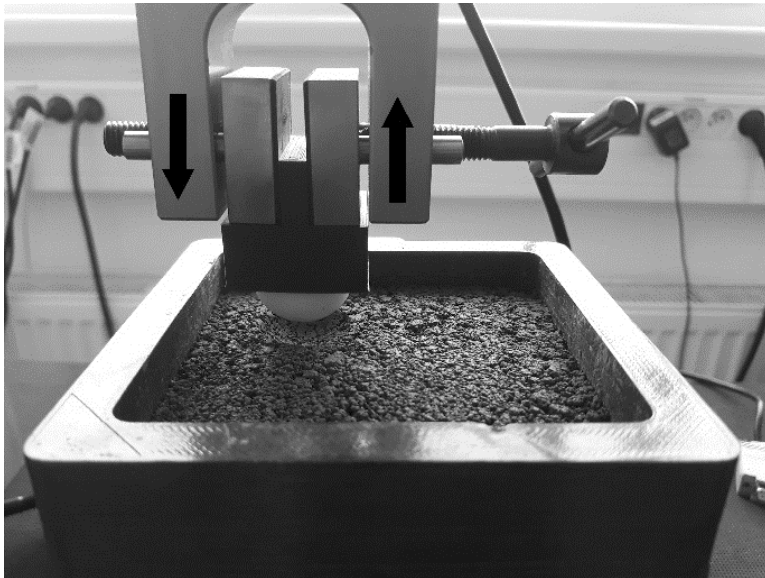
Fig. 1 Cycles of ball indentation into compacted soil

Figure 2 shows the schematic penetration diagram of the test of the test. The graph shows Elastic energy (EE), which indicates the area below the unload curve. Plastic Energy (PE) is the area below the load curve that, at the same time, does not excluded the unload curve. Calculation of areas from the measured data is expressed by equations (1) and (2).
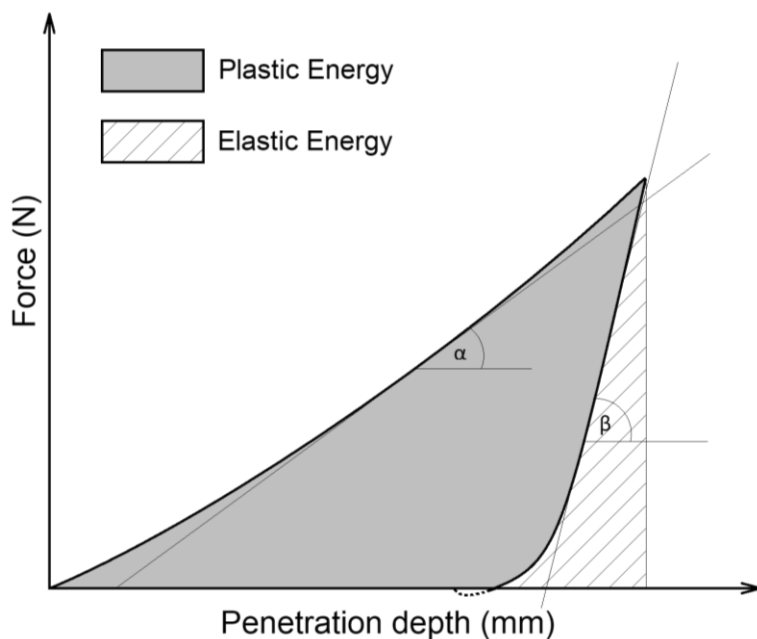
Fig. 2 Loading-unloading curve of ball indentation test

$$EE = \sum_1^i \left(\frac{(d_i - d_{i-1}) * (Fl_i - Fu_{i-1})}{2} + (d_i - d_{i-1}) \cdot Fu_{i-1} \right) \qquad (1)$$

where *EE* is Elastic Energy (N.mm, *d* is displacement (mm) and *Fu* is Force of unloading (N)

$$PE = \sum_1^i \left(\frac{(d_i - d_{i-1}) * (Fl_i - Fl_{i-1})}{2} + (d_i - d_{i-1}) \cdot Fl_{i-1} \right) - EE \qquad (2)$$

where *PE* is Plastic Energy (N.mm), *d* is displacement (mm) and *Fl* is Force of loading (N)

From the obtained energies, the ratio between them can be calculated. This ratio is marked as Er – energy ratio (3).

$$E_r = \frac{EE}{EP} \qquad (3)$$

where E_r is Energy ratio (-)

In order to calculate stiffness it is necessary to know the load curve direction and the unload curve direction (4) and (5). The proportion of these two directions (6) expresses the stiffness coefficient.

$$k1 = \tan \alpha \qquad (4)$$

where *k1* is slope of load curve (N.mm^{-1}) and α is angle of tangent of load curve (°)

$$k2 = \tan \beta \qquad (5)$$

where *k2* is slope of unload curve (N.mm^{-1}) and β is angle of tangent of unload curve (°)

$$\text{stiffness} = \frac{k1}{k2} \qquad (6)$$

Soil porosity was determined from density of bulk matter. Volume and weight were determined at maximum compression of the soil sample (at ε = 41.7% deformation). The soil density is therefore 1839 kg.m-3 ± 53 kg.m-3. In order to determine the bulk density, the soil was separated into measuring cylinder to a defined height of h = 60mm. This sample determined weight and volume. The resulting density for the separated soil is 975 kg.m-3 ± 43 kg.m-3. The porosity can be expressed by the relation for each variable deformation ε ranging from 0 – 41.7% using the equation (7).

$$\varepsilon = 0.53 - 1.272 \cdot x \qquad (7)$$

where ε is deformation (-) and *x* is porosity (%)
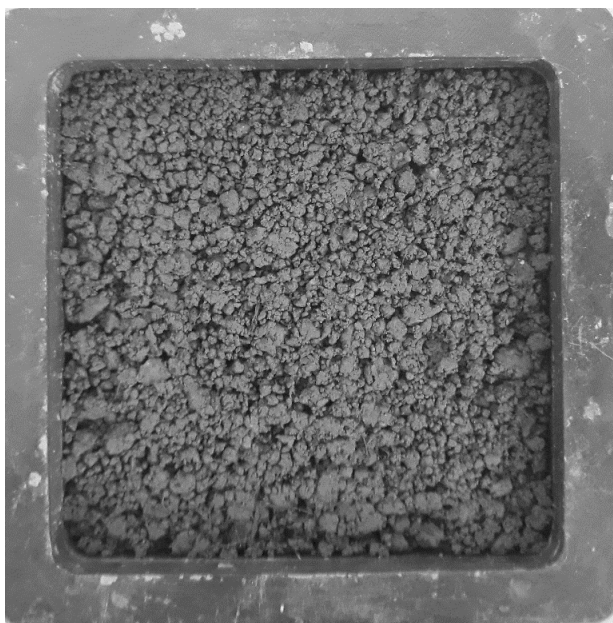
Fig. 3 Compacted specimen soil of 65 N

Once the measuring is done, individual indents can be analysed. The soil must be well spread out before the first load. In case of insufficient separation, larger lumps may occur in the soil. These areas may then distort the result of the test. Fig. 3 shows spread out soil sample after a load of 65 N. Visible pores can be observed between the individual parts of the soil. Fig. 4 shows the same soil sample after the test was carried out. Visible indentations are present in the sample. Measurements were made for a specific maximal load. See Tab. 1 in *Results and discussion* for the measuring parameters. In order to determine the stiffness value, it is important to know the load and unload curve directions. These directions can be obtained from curves for different maximum loads or loading and unloading speeds *(Pasha et al., 2014)*. The measured values were processed and the soil porosity was determined for each load.
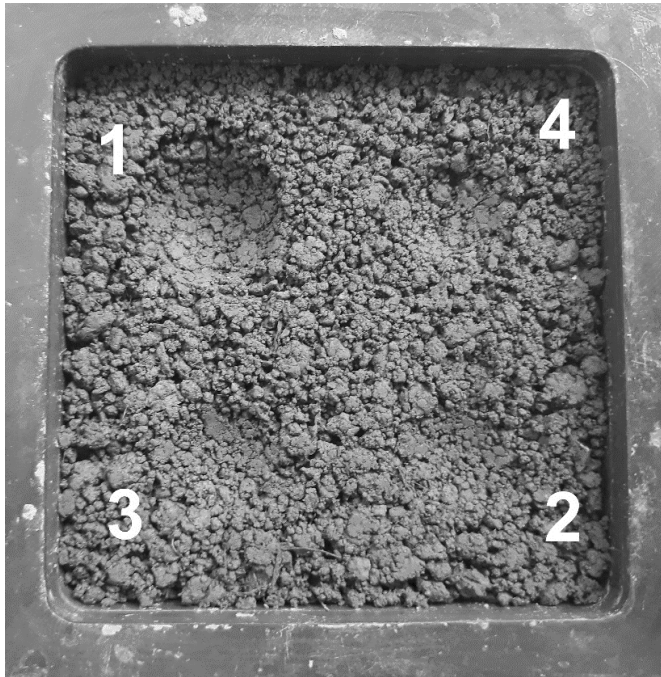
Fig. 4 Soil specimen with dimples

RESULTS AND DISCUSSION
Plastic and elastic energy was determined from the measured curves. EE / PE is defined as the proportion of Elastic energy and Plastic energy, indicated as E ratio. See Tab. 1 for the measured data.

Tab. 1 Energies of ball indentation tests

Pre-load	Plastic Energy	Standard Deviation	Elastic Energy	Standard Deviation	Ball maximum force	E ratio
N	N.mm	N.mm	N.mm	N.mm	N	-
65	27.7	1.26	1.52	0.035	10	0.054
225	169	27.6	10.2	0.127	40	0.060
470	88.8	4.17	9.66	0.317	40	0.108
546	83.0	8.94	9.36	0.127	40	0.112
902	56.3	5.54	8.95	0.233	40	0.158
1841	39.0	1.80	8.84	0.116	40	0.226

See Tab. 2 for the measured load-unload directions. The load curve direction is indicated by the coefficient k1, and the unload curve direction by the coefficient k2. The proportion of these directions indicates stiffness.

Tab. 2 Energies of ball indentation tests

Pre-load	k1 slope	Standard Deviation	k2 slope	Standard Deviation	Coefficient of Stiffness	Standard Deviation
N	N.mm⁻¹	N.mm⁻¹	N.mm⁻¹	N.mm⁻¹	-	-
65	1.70	0.04	44.3	0.71	0.04	0.0012
225	4.07	1.21	97.9	0.46	0.04	0.0125
470	8.24	0.43	101	2.12	0.08	0.0125
546	9.39	0.96	105	1.75	0.09	0.0076
902	12.8	1.31	106	1.39	0.12	0.0119
1841	17.9	0.83	108	3.31	0.16	0.0068

Fig. 3 indicates the relation between stiffness and Energy ratio expressed from the measured values. Based on this ratio it is possible to calculate the stiffness value from the proportion of the individual energies.
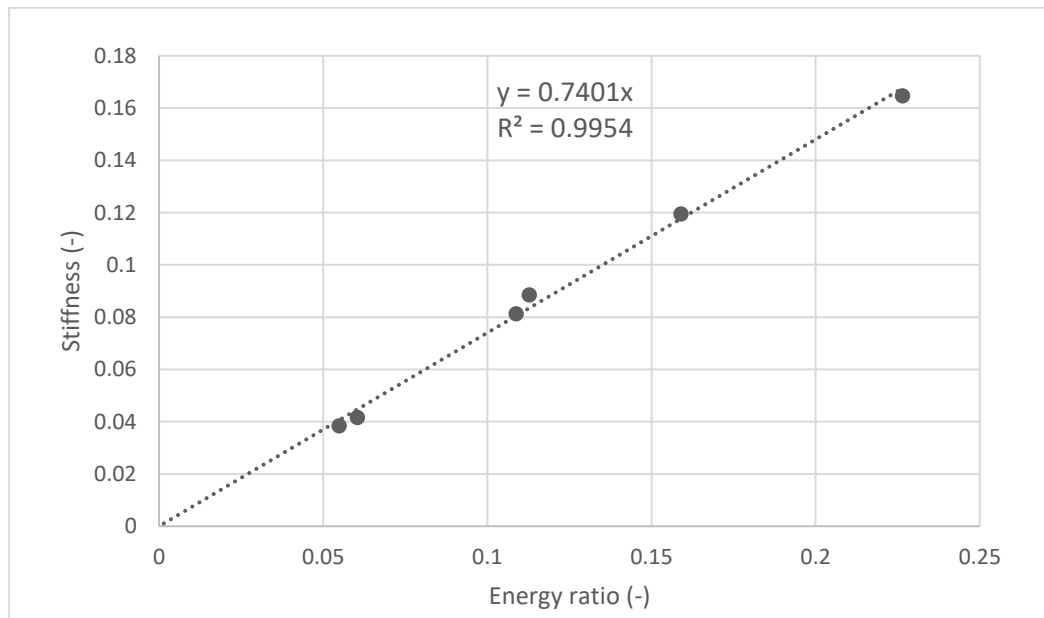
Fig. 5 Curve of stiffness and energy ratio

Tab. 3 shows the relations between energies, stiffness and porosity, which were obtained from the measured data. Equations 1) and 2) express relation between energy and porosity. Equation 3) shows the relation between stiffness and porosity. Knowing these relations, it is possible to calculate individual values for different degrees of porosity.

Tab. 3 Ratio between porosity elastic energy, plastic energy and stiffness where x is porosity

	Equation	
1)	$EE = 15.043 \cdot x^2 + 1.5719 \cdot x + 8.8433$	$R^2 = 0.964$
2)	$EP = 1784.4 \cdot x^2 + 4.6881 \cdot x + 43.815$	$R^2 = 0.916$
3)	$Stiffness = 0.7756 \cdot x^2 - 0.6388 \cdot x + 0.1619$	$R^2 = 0.975$

Stiffness values range, in the case of this soil type, from 0.04 to 0.16. This is a considerable interval within the model setup. Porosity of the material depends on its separation. There is, however, a dependence between porosity and other properties such as Elastic energy, Plastic energy or Stiffness. The porosity was calculated from 0 when reaching the maximum soil pressure. Deformation of the soil is therefore dependent on its porosity. Stiffness value also fundamentally changes based on the type of soil.

In comparison, stiffness values of a sandy soil are lower than those of other types of clay soil *(Chen, Munkholm, & Nyord, 2013)*. The maximal value of stiffness that can be used in the model equals 1. The individual parameters depend on the moisture content *(Ucgul, Fielke, & Saunders, 2015)*. Moisture content was obtained and maintained at 17% throughout the test.

CONCLUSIONS

The measured values indicate that the value of stiffness is directly proportional to the Energy ratio. Stiffness is a very important parameter when creating models using the discrete element method. The measurement method used is a fundamental solution for obtaining important values needed for preparation and usage of a mathematical soil model. Soil porosity affects the stiffness value. With increasing porosity of soil, the stiffness value decreases. In the case of Plastic energy and Elastic energy with increasing porosity of soil, the energy values also increase. However, the Energy ratio decreases with the increasing soil porosity.

ACKNOWLEDGMENT

REFERENCES

1. Chen, Y., Munkholm, L. J., & Nyord, T. (2013). A discrete element model for soil–sweep interaction in three different soils. *Soil and Tillage Research*, *126*, 34–41.
2. Kuře, J., Hájková, L., Hromasová, M., Chotěborský, R., & Linda, M. (2019). Discrete element simulation of rapeseed shear test. *Agronomy Research*, *17*(2), 551–558.
3. Obermayr, M., Vrettos, C., & Eberhard, P. (2013). *A discrete element model for cohesive soil*.
4. Pasha, M. (2013). *Modelling of Flowability Measurement of Cohesive Powders Using Small Quantities*. The University of Leeds.
5. Pasha, M., Dogbe, S., Hare, C., Hassanpour, A., & Ghadiri, M. (2013). *A new contact model for modelling of elastic-plastic-adhesive spheres in distinct element method*. 831–834.
6. Pasha, M., Dogbe, S., Hare, C., Hassanpour, A., Ghadiri, M., Pasha, M., … Ghadiri, · M. (2014). *A linear model of elasto-plastic and adhesive contact deformation*, *16*, 151–162.
7. Pasha, M., Pasha, M., Hare, C., Hassanpour, A., & Ghadiri, M. (2013). Analysis of ball indentation on cohesive powder beds using distinct element modelling. In *Powder Technology*, vol. 233.
8. *Rocky DEM Particle Simulator*. (2018). Retrieved from rocky.esss.co
9. Ucgul, M., Fielke, J. M., & Saunders, C. (2015). Defining the effect of sweep tillage tool cutting edge geometry on tillage forces using 3D discrete element modelling. *Information Processing in Agriculture*, *2*(2), 130–141.
10. Ucgul, M., Fielke, J. M., & Saunders, C. (2015). Three-dimensional discrete element modelling (DEM) of tillage: Accounting for soil cohesion and adhesion. *Biosystems Engineering*, *129*, 298–306.
11. Walton, O. R., & Braun, R. L. (1986). Viscosity, granular-temperature, and stress calculations for shearing assemblies of inelastic, frictional disks. *Journal of Rheology*, *30*(5), 949–980.

Corresponding author:
Ing. Jiří Kuře, Department of Material Science and Manufacturing Technology, Faculty of Engineering, Czech University of Life Sciences Prague, Kamýcká 129, Praha 6, Prague, 16521, Czech Republic, phone: +420 721470890, e-mail: kure@tf.czu.cz

ASSESSMENT OF THE WAY HOLDING STEERING WHEEL IN DIFFERENT TRAFFIC SITUATIONS

Martin KŮRKA[1], Michal HRUŠKA[1]

[1]*Czech University of Life Sciences, Faculty of Engineering, Department of Technological Equipment of Building, Kamýcká 129, 165 21 Prague 6, Czech Republic*

Abstract

This paper deals with assessing the differences in steering wheel holding positions for left-sided and right-sided steering vehicle in three specific driving situations. The collected data is compared to the generally accepted optimal steering wheel position in terms of both active and passive safety. The research described in this work was based on a sample of randomly selected drivers from the Czech Republic, Great Britain and Australia. Data collection was done by means of electronic questionnaires with precisely-described and visualized situations for better understanding and presentation of the examined state. The data was then subjected to statistical evaluation, where the difference between the drivers driving in the right-sided steering countries and the drivers driving in the left-side steering countries. Basis of the statistical evaluation of the data obtained, it was found that there is a difference in the way the steering wheel is held in the assessed traffic situations between drivers driving in left-sided traffic and between the drivers in right-sided traffic. The results of this work can be used in the process of designing passenger car cabins. Especially in the field of adaptation of control or multimedia elements to the needs of drivers in individual countries.

Key words: *driver; safety; hands; traffic; steering wheel.*

INTRODUCTION

Observation techniques are most commonly used today as a tool for assessing the safety of passenger car crews, where the observer usually deals with driver behaviour while driving. The most frequently observed parameters include seat belt use, mobile phone use, seat positioning, etc. Holding the steering wheel correctly is an important aspect of traffic safety *(Thomas, J. A. & Walton, D., 2007; Viano, D. C., Patel, M. & Ciccone, M. A, 2018)*. Multifunctional steering wheels represents a direct link between driver and machine, and the optimal design of these elements, coupled with the design of the various armrests, directly affects the overall driver comfort and thus the safety of the vehicle operation (*Chang, Y. & Chen, Ch.W., 2016*).

Multifunctional steering wheels used in passenger cars today are equipped with a number of controls that make it easier for the driver to operate things such as a mobile phone or the car's multimedia system. These controls are located on the steering wheel so that the driver can control them tactfully, with the thumbs of both hands, only with the use of positional memory. This aims to keep the driver's attention, focusing the field of driver's view on the traffic situation in front of and around the vehicle and provides the ability to respond more quickly to possible changes in traffic conditions while driving.

Although car manufactures try to model the use of the multifunction steering wheel by assuming the steering wheel to hold in a generally recognized optimal position (*Walton, D. & Thomas, J. A., 2005*) but in practice, we know that a statistically significant percentage of drivers hold the steering wheel quite differently.

In traffic safety history, a number of researches *(Hruška, 2018;* Schmidt, S., Seiberl, W. & Schwirtz, A.*, 2015; Walton, D. & Thomas, J. A., 2005*) have drawn attention to how the steering wheel is held, on the findings of which designers base their work. They are usually focused on the effect of grip on passive safety and the subsequent type and extent of injury in the accident. The most frequently quoted optimal value is according to the analogue clock face, i.e. the left hand position on the nine and the right hand on the three, with the driver holding the steering wheel with both hands (*Schiro, J., Gabrielli, F., Pudlo, P. & Barbier, F., 2013; Hault-Debrulle, A., Robache, F., Paxaux, M., P. & Morvan, H., 2010*). This value is specified as the optimum value regardless of the side that the steering wheel is on.

The aim of this work is to assess the hypothesis that there is a statistically significant difference in the way hold of steering wheel by drivers who are driving in right-sided traffic and drivers who are driving in left-sided traffic.

MATERIALS AND METHODS

For the needs of the measurements, a total of 160 participants (82 women and 78 men) from the Czech Republic, Great Britain and Australia were selected, and they were divided into two groups of 80 respondents. Each of the respondent groups comes from countries with different road traffic.

Respondents from the Czech Republic were included in the group of drivers driving on the right-sided traffic (Tab. 1) and respondents from Great Britain and Australia were assigned to a group of drivers driving on the left-sided traffic (Tab. 2).

Tab. 1 Data on tested persons from the group of drivers driving in the left-sided traffic (CZ)

| | Number | Age | | |
		Average	Minimum	Maximum
Men	40	29.7	20	52
Women	40	32.2	19	64
Total	**80**	**30.9**	**19**	**64**

Tab. 2 Data on tested persons from the group of drivers driving in the right-sided traffic (UK, AUS)

| | Number | Age | | |
		Average	Minimum	Maximum
Men	38	38.4	21	65
Women	42	34.7	20	56
Total	**80**	**36.5**	**20**	**65**

Three basic traffic situations were defined for the purpose of the research. These were traffic situations in which the interviewed driver could find him or herself and answer how he or she held the steering wheel in the given situation. These consist of three common situations in which drivers repeatedly find themselves when driving. Each of these situations has been thoroughly verbally described and supplemented with an illustrative photo for better understanding. **Situation A** was described as driving on highways or high-speed roads at low intensity traffic with no psychological pressure on the driver. **Situation B** was described as driving outside of a city on a secondary road with a lot of bends, in medium traffic, with moderate intensity psychological pressure on the driver. **Situation C** was described as driving outside of a city under reduced visibility and very dense traffic, where very high demands are placed on the driver and the driver is subjected to considerable psychological pressure.

Basic data collection was carried out with the help of electronic questionnaires in two language versions. Their translations and semantically-identical content were verified by a professional translation agency. As part of the basic information provided in the questionnaire, respondents were advised to devote sufficient time to filling out individual questions and had schemes available to help them better imagine the situation (Fig. 1). Although the questionnaire method may not be as accurate as real-environment testing, given the set objectives and the number of subjects surveyed, testing in a real environment would be virtually impossible in organizational terms.

The questionnaire consisted of nine questions divided into two groups. The first group were questions about age (in years), gender (female, male), and side preference (right-handed, left-handed) of the subject. In addition, the test subject was interviewed about how long he or she had a driver's licence (in years), how often he or she drove a passenger car (every day, at least once a week, occasionally, exceptionally), with the final data being about the position in which the subject most often sits behind

the steering wheel (a choice of three basic positions divided according to the subject's chest distance from the centre of the steering wheel).

In the second group of questions, the test subject was asked to gradually imagine each of the three traffic situations described above and responsibly state for each of them whether he or she held the steering wheel with one or both hands, and in which position. This was always based on the pre-selected scheme attached to each question (Fig. 1), where, according to the watch face, the range of R12-R6 was defined for the right hand, and for the left hand the analogous range of L6-L12. The overlap at 12 and 6 o'clock is selected because the test groups from left-sided and right-sided traffic were evaluated. The subject was also told to indicate the most prevalent value of the grip on the steering wheel. We dismissed in the first phase extreme values where the test subject crosses the hand and held the steering wheel with, for example, the left-hand on the right, as highly unlikely in view of the objectively high degree of discomfort the driver would experience in such a position. For this reason, we completely discarded these alternatives.
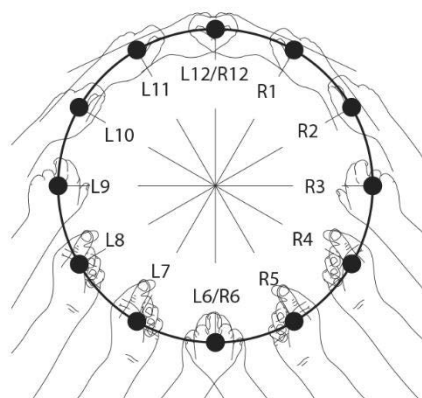
Fig. 1 Scheme of positions of individual grips according to an analogue watch face

RESULTS AND DISCUSSION

The results obtained during the measurements were statistically processed and evaluated using contingency tables, Pearson's chi-squared test and adjusted residuals methods. The percentage of individual hand positions on the steering wheel, regardless of whether the steering wheel is held by one hand or both, obtained from the measured data, is shown in Tab. 3 for right-sided traffic respondents (CZ) and in Tab. 4 for left-sided traffic respondents (UK, AUS).

Tab. 3 Percentage of grips for drivers in right-sided traffic (CZ).

	Position							
Left hand	L6	L7	L8	L9	L10	L11	L12	ΣL
Situation A	0,00 %	8,30 %	9,70 %	31,90 %	40,30 %	5,60 %	4,20 %	100,00 %
Situation B	0,00 %	2,70 %	5,30 %	22,70 %	58,70 %	5,30 %	5,30 %	100,00 %
Situation C	0,00 %	0,00 %	1,30 %	25,00 %	68,60 %	3,80 %	1,30 %	100,00 %
	Position							
Right hand	R12	R1	R2	R3	R4	R5	R6	ΣR
Situation A	0,00 %	0,00 %	36,20 %	25,50 %	21,30 %	10,60 %	6,40 %	100,00 %
Situation B	0,00 %	0,00 %	55,80 %	30,90 %	11,80 %	1,50 %	0,00 %	100,00 %
Situation C	0,00 %	1,30 %	64,00 %	30,70 %	2,70 %	1,30 %	0,00 %	100,00 %

It is clear from Tab. 3 and 4 that there are differences in steering wheel hand positions for drivers who are driving in right-sided traffic and drivers who are in left-sided traffic. The highest percentage of positions, regardless of the combination of both hands for all interviewed drivers, are L10 and R2. From this, it can be concluded that a significant percentage of drivers still use an older hand's position in L10 R2 (*Brown, 2002*). This is confirmed by the average age of interviewed drivers, which can be deduced

from having attended a driving school while this position was part of the curriculum (*Brown, 2002*). It is also evident that drivers do not use L6 and R12 positions in the right-sided traffic at all. This is also true for drivers in left-sided traffic, but these positions are marked L12 and R6 (Fig 1). The second highest percentages, regardless of the combination of both hands, are positions L9 and R3.

Tab. 4 Percentage of grips for drivers in left-sided traffic (UK, AUS).

	Position							
Left hand	L6	L7	L8	L9	L10	L11	L12	ΣL
Situation A	1,60 %	4,80 %	35,60 %	17,70 %	38,70 %	1,60 %	0,00 %	100,00 %
Situation B	0,00 %	0,00 %	26,00 %	26,00 %	45,30 %	2,70 %	0,00 %	100,00 %
Situation C	0,00 %	0,00 %	12,80 %	29,50 %	56,40 %	1,30 %	0,00 %	100,00 %
	Position							
Right hand	R12	R1	R2	R3	R4	R5	R6	ΣR
Situation A	1,60 %	1,60 %	35,50 %	30,60 %	19,40 %	11,30 %	0,00 %	100,00 %
Situation B	0,00 %	6,50 %	49,30 %	22,10 %	18,20 %	3,90 %	0,00 %	100,00 %
Situation C	0,00 %	2,50 %	52,40 %	26,30 %	13,80 %	5,00 %	0,00 %	100,00 %

Tab. 5 and 6 show how the driver holds the steering wheel in each situation. Whether the driver holds the steering wheel with one hand, both or at the optimal position L9 and R3 (*Schiro, J., Gabrielli, F., Pudlo, P. & Barbier, F., 2013; Hault-Debrulle, A., Robache, F., Paxaux, M., P. & Morvan, H., 2010*). It is clear in the PivotTables (Tab. 5 and 6) that if the traffic situation becomes more complex and the driver is perceived as potentially more dangerous, most of the interviewed drivers use both hands to drive. A total of 41 drivers from the Czech Republic hold the steering wheel by one hand, 31 drivers with both and 8 drivers holding the steering wheel in this position in the optimal position. The data from drivers in left-sided traffic is not fundamentally different in any situation. Pivot tables were subsequently supplemented by the method of adjusted residuals. In general, when comparing Tab. 5 and 6, it can be argued that drivers in the UK and Australia driving more carefully than drivers in the Czech Republic.

Tab. 5 Combination of tracked grips for drivers in right-sided traffic (CZ).

CZ	One hand	Both hands	Optimal	Σ
Situation A	41 (+++)	31 (---)	8	80
Situation B	17	50	13	80
Situation C	4 (---)	58 (++)	18	80
Σ	62	139	39	240

Tab. 6 Combination of tracked grips for drivers in left-sided traffic (UK, AUS).

UK, AUS	One hand	Both hands	Optimal	Σ
Situation A	36 (+++)	35 (---)	9	80
Situation B	10 (-)	58 (+)	12	80
Situation C	2 (---)	60 (+)	18	80
Σ	48	153	39	240

To determine whether there is a significant difference in the way in which the steering wheel is being held between drivers in left-sided and right-sided traffic was used Pearson's chi-squared test where the measured data were compared for each situation separately. The data for Pearson's chi-squared test were used data from Tab. 5 and 6, each table being 2x3 for each situation. The number of degrees of freedom for each situation was 2 and the critical value at the selected significance level (0,05) was 5,991465. The result test value was compared to the critical value (5,991465). Cramer's V value was also calculated

from the resulting data. The claim that there is a statistically significant difference in the way in which the steering wheel is held by the drivers in right-sided traffic and the drivers in the left-sided traffic cannot be statistically confirmed in any situation, as shown in Tab. 7.

CONCLUSIONS

The results published in this work are thematically linked to previous researches (*Hruška, 2018; Kůrka, 2019*) and complement the complex view of steering wheel holding issues in various types of traffic and in different traffic situations. In this work, a large amount of data was obtained from a large group of respondents from three different countries with two different traffic types, which may be statistically interesting in terms of possible comparisons with other statistics that could be obtained from respondents with other parameters such as for example, different education, age, etc.

Based on the above results, it can be stated that the primary hypothesis stated in the introduction to the work was not confirmed. There are no statistically significant differences in how drivers are holding the steering wheel in left-sided traffic and right-sided traffic. What can be said with certainty is that drivers, with a deteriorating situation, tend to hold the steering wheel with both hands, regardless of the type of road traffic. From a safety point of view, it was found that a statistically significant number of interviewed drivers held the steering wheel in the wrong way, either with one hand or in the wrong combination of both hands.

The results of this work can be used in the process of designing passenger car cabs, especially in the process of ergonomically shaping the steering wheel and controls elements in such a way that the driver has both hands on the steering wheel voluntarily and comfortably.

The benefit of this work is to provide valid data for further research in this field, where it would be possible to refine the above results or supplement data obtained from field research in other countries.

ACKNOWLEDGMENT

REFERENCES

1. Brown, I. D. (2002). A laboratory comparison of two steering techniques. *In Behavioural research in roadsafety twelfth seminar.*
2. Chang, Y. & Chen, Ch.W. (2016). Kansei assessment of the constituent elements and the overall interrelations in car steering wheel design. *International Journal of Industrial Ergonomics*, *56*, 97-105.
3. Hault-Debrulle, A., Robache, F., Paxaux, M., P. & Morvan, H. (2010). Determination of pre-impact occupant postures and analysis of consequences on injury outcome. Part I: A driving simulator study, *Accident Analysis & Prevention* (pp. 66-74).
4. Schiro, J., Gabrielli, F., Pudlo, P. & Barbier, F. (2013). Steering wheel hand position in low–speed maneuvers, *Transportation Research Part F: Traffic Psychology and Behaviour* (pp. 133-145).
5. Schmidt, S., Seiberl, W. & Schwirtz, A. (2015). Influence of different shoulder-elbow configurations on steering precision and steering velocity in automotive context. In *Applied Ergonomics* (pp. 176-183).
6. Hruška, M. (2018). Assessment of the actual hand position on the steering wheel for drivers of passenger cars while driving. *Agronomy Research*, *16*(4), 1668-1676.
7. Kůrka, M. (2019). Assessment of differences in the way the steering wheel is held by passenger car drivers depending on the complexity of the traffic situation. *XXI. International Conference of Young Scientists* (pp. 105-110).
8. Thomas, J. A. & Walton, D. (2007). Measuring perceived risk: Self-reported and actual hand positions of SUV and car drivers. *Transportation Research Part F: Traffic Psychology and Behaviour*, *10*(3), 201–207.
9. Viano, D. C., Patel, M. & Ciccone, M. A. (1989). Patterns of Arm Position during Normal Driving. *Human Factors: The*

Journal of the Human Factors and Ergonomics Society, *31*(6), 715–720.

10. Walton, D. & Thomas, J. A. (2005). Naturalistic observations of driver hand positions. *Transportation Research Part F:* *Traffic Psychology and Behaviour*, *8*(3), 229–238.

Corresponding author:

Ing. Martin Kůrka, Department of Technological Equipment of Building, Faculty of Engineering, Czech University of Life Sciences Prague, Kamýcká 129, Praha 6, Prague, 16521, Czech Republic, phone: +420 728 428 209, e-mail: kurkam@tf.czu.cz

HARDFACING ELECTRODES RESISTANCE IN LABORATORY CONDITIONS

Ján LILKO[1], Martin KOTUS[2], Peter DOBIAŠ[3], Ondrej PONJIČAN[4]

[1,2]*Department of Quality and Engineering Technologies, Faculty of Engineering, Slovak University of Agriculture, Tr. A. Hlinku 2, 94976 Nitra, Slovak Republic.*
[2]*Department of Quality and Engineering Technologies, Faculty of Engineering, Slovak University of Agriculture, Tr. A. Hlinku 2, 94976 Nitra, Slovak Republic.*
[3]*Secondary agrotechnical school, Tovarnícka 1632, 95501 Topoľčany, Slovak Republic.*
[4]*Department of Agricultural Engineering, Faculty of Agriculture, University of Novi Sad, Trg. Dositeja Obradovića 8, 21101 Novi Sad, Vojvodina, Republic of Serbia.*

Abstract
The article describes abrasive wear resistance determination of selected electrodes. Produced welds has been tested in laboratory conditions for hardness and relative resistance according to the standard (ČSN 01 5084). Achieved results confirmed the increase of welds abrasive wear resistance. Selected electrodes are suitable for a creation of abrasion resistant layers, which can lead to extension of working life cycle of agricultural machinery.

Key words: *tribology; abrasive wear; relative resistance; filler materials.*

INTRODUCTION

The area of the functional parts of agricultural machinery life extension is always up to date. Latest researches results allow solve this problem by application of expensive materials and technologies. Working parts of the machines in agricultural production are subjected to the intensive wear, particularly due to presence of abrasive particles in soil. During the motion of the active parts in the soil, the metal is heavily worn and thereby rapidly changing tool dimension and reducing its life. Improving of the working life cycle of machinery is related to the abrasive wear principles research in laboratory and/or operating conditions.

There are various possibilities of solving this problem in maintenance practice now. A modern solution is to produce active parts using new wear resistant materials (*Votava, & Kumbár, 2014; Bednár et al., 2013*). The main advantage is simple replacement of worn part by new one. Abrasive resistance can be also achieved by mechanical and heat treatment or chemical heat treatment (*Kováč et al., 2014; Mikuš et al., 2012)*. The solution with a future is the creation of abrasive resistant layer on the surface of active parts by harfacing (*Šoška et al., 2014; Müller et al., 2018)*.

A success of the creation the wear resistant layer depends not only on the quality and properties of used materials, but on the type of the application technology as well. Higher hardness and wear resistance, improved fatigue strength and corrosion resistance increase can be achieved by selection of proper material and technology.

The aim of this article is to assess the resistance of selected hardfacing materials to abrasive wear. For comparison we will use two electrodes applicable in agricultural industry with a focus on extending the working life of machinery parts. The difference between electrodes will be in the directional chemical composition. We assume that by increasing the carbon & chromium content it possible to reach a very hard surface already with the first layer. We determine the resistance of used weld deposits by testing in laboratory conditions with measuring hardness & determining the relative wear resistance.

MATERIALS AND METHODS

The abrasive resistance of filler materials is determined using electrodes of WELCO Ltd., Uherský Brod. They are used in renovation to get hardfaced surfaces for small & middle-sized businesses. The hardfacing process was carried out using a common welding supply according the manufacturer recommended technological process.

Short characteristics of selected materials declared by the manufacturer:
- Welco 1701s designed on chromium-carbide basis is used for abrasive wear at moderate impact stress. In comparison to similar types of electrodes, it is characterized mainly by im-

proved control of the weld pool. The deposit is flat with easily removable slag. It is suitable for worn machinery parts used in the coal, earth, gravel, sand mining, for hardfacing welds of dredges, conveyor screws and machine parts with operation temperature up to 200° C.

- Welco 1707s is universal hardfacing electrode. It is applicable for the tools from steel, cast steels and hard Mn-steels worn due to simultaneous shock, pressure and abrasion wear. An application is easy with well removable slag, with very small spraying, no undercuts and with yield of 120%. It is suitable for worn parts of excavators, cylinders, chains, constructions and road machinery and cold cutting tools.

Table 1 describes the chemical composition of additive materials and hardness defined by manufacturer HV30. The hardness of HV30 has been achieved with the welding of first layer.

Tab. 1 Indicative chemical composition of electrodes and hardness HV30

Material	C	Mn	Si	Cr	Mo	V	Nb	W	Fe	Hardness HV30
Welco 1701s	4.3	1.3	-	38	0.8	0.5	0.03	1.3	rest	650-700
Welco 1707s	0.4	0.3	0.8	8	1	0.6	-	-	rest	515-690

Wear resistance and HV30 hardness has been determined in the laboratory of the Department of Quality and Engineering Technologies FE SUA in Nitra. The test instrument has been calibrated and meets relevant standards requirements as well. The hardness test has been carried out according to the standard STN EN ISO 6507 – Vickers hardness test. The penetrating pin is a diamond pyramid with a load of 294 N. To determine the wear resistance standard ČSN 01 5084 – Determination of abrasion resistance of metal materials on abrasive cloth has been used. The standard describes the procedure which has been followed. During the test, weight loss of both welded and standard samples have been measured. Standard test material for comparison has been steel 12014.20 with hardness range HV=95÷105.

As an assessment criterion abrasive wear relative resistance ($\Psi_{abr.}$) has been defined:

$$\Psi_{abr.} = \frac{W_{hE}}{W_h} \tag{1}$$

W_{hE} stands for average weight loss of standard (g), W_h stands for average weight loss of test materials (g).

RESULTS AND DISCUSSION

Evaluation criteria (relative resistance and hardness) are evaluated for one-, two- and three-layer deposits. All results obtained are average values of the measured samples. Table 2 shows measured values for weight loss and HV30 hardness measurements. Figure 1 shows the wear resistance.

Tab. 2 Values of measuring weight loss and hardness HV30

Material	Weight loss			Hardness HV30		
	1st layer	2nd layer	3rd layer	1st layer	2nd layer	3rd layer
Welco 1701s	0.1682	0.1404	0.1069	640	711	785
Welco 1707s	0.2133	0.1940	0.1801	500	577	679
Standard	0.3614			104		

Based on the results obtained, we do conclude that increase of the hardness means higher relative wear resistance. Increase of relative resistance leads to the cut of material loss and it results in improved life cycle of the parts of the machines. This relation has been achieved with both filler materials and with multiple deposit layers as well. Higher resistance to abrasive wear was observed for Welco 1701s electrode.

Increasing wear resistance can also be achieved by using tool steels. The authors *Votava, & Kumbár, 2014; Bednár et al., 2013* achieved the relative resistance in the range of $\psi_{abr.} = 1.91 \div 2.75$.

They have proven their value in practice in laboratory and operational tests. The relation of increased hardness and improved increases wear resistance has also been confirmed by other authors (*Ťavodová et al., 2018; Votava, 2014; Pauliček et al., 2014*) in their research.
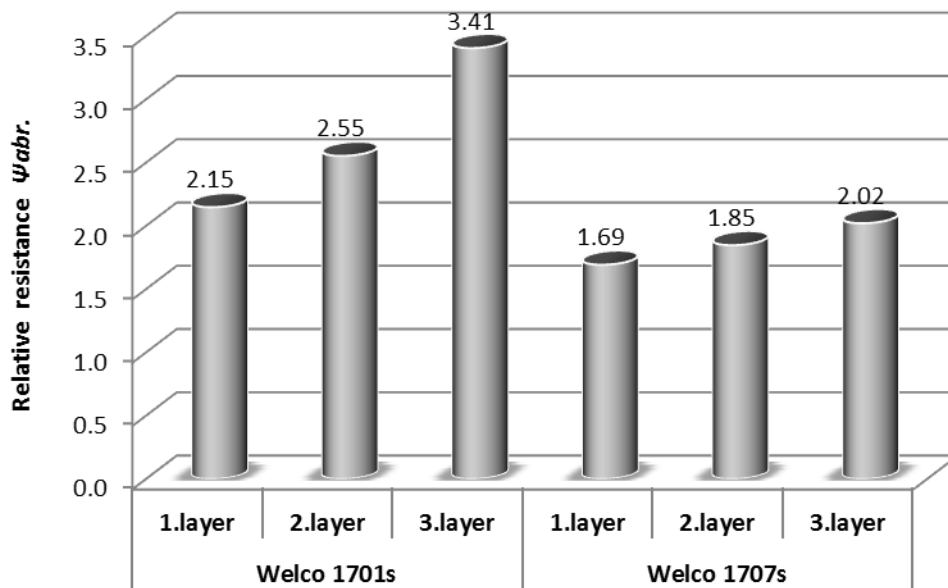

Fig. 1 Graphical representation of wear resistance $\Psi_{abr.}$.

Favourable results of deposit wear resistance can be achieved in testing of filler and powder materials in operation conditions (*Kováč et al., 2014; Mikuš et al., 2012; Müller et al., 2018*). These authors confirm the suitability for the application of such weld deposits on ploughs. Hardfacing deposits created on chisels (*Čičo & Bujna*, 2009; *Čičo & Bujna*, 2011) achieved reduced wear compared to the non-welded ones as well.

The wear resistant layer can also be created by chemical-heat treatment, e.g. with boron saturation. The authors (*Kováč et al., 2013*) state that increase in hardness and relative wear resistance in the range of $\psi_{abr.} = 1.2 \div 1.7$ can be obtained by controlling the diffusion processes. For wear resistance and hardness, it is necessary to ensure that the base metal matrix contains chromium carbides (*Vináš et al., 2013*). Laser application of powder filler material (*Kovaříková et al., 2011*) allow to achieve relative resistance $\psi_{abr.} = 3.2 \div 5.1$.

The Welco 1701s electrode contains significantly increased chromium content. Compared to the Welco 1707s electrode the content of carbon is increased and the electrode has a small fraction of niobium with tungsten. Chromium with carbon produces carbides increasing wear resistance. The hardness values obtained confirmed the influence of alloying elements on wear resistance increase. The hardness also increased with the number of layers, resulting from less mixing of the electrode material with the base materials.

The results of the tests showed that with increasing volume (number of layers) of the weld deposits, the relative resistance to abrasive wear increases. Wear of functional parts should be avoided in order to achieve proper operation of the functional parts. Wear reduction can be achieved by forming abrasion-resistant layers. The electrodes used meet the criteria for choosing lower weight-loss in abrasive wear.

CONCLUSIONS

The low life of the functional parts of the soil tillage machines requires new deposit alloy materials. Assessing the results of relative abrasion resistance and hardness of the tested materials, it is possible to conclude on the suitability of using the materials in soil conditions. However, we must not forget the impact of chemical effects of the soil on the machine functional parts.

For real application of electrodes it is also necessary to carry out operational tests, which also take into account the influence of real soil factors. We assume their decisive importance in the proper selection

of wear resistant materials for specific soil conditions. It is necessary to comprehensively assess the service life of parts of agricultural machinery in the view of mechanical and chemical model of the wear.

The paper deals with the determination of abrasive wear resistance of selected electrodes. We have created deposits using filler materials that are commonly available at the market. Their advantage is the use of simple manual metal arc welding. Based on our results and in comparison with other authors we clearly state the suitability of the use of surfacing in abrasive wear conditions. The tested electrodes are suitable for use in practice in order to form abrasion-resistant layers. With the given electrodes we can increase the service life of some agricultural machines.

ACKNOWLEDGMENT

REFERENCES

1. Bednár, R., Votava, J., Cervinka, & J., Fajman, M. (2013). Suitability of technical materials for machinery subsoilers for soil tillage. *Acta Universitatis Agriculturae et Silviculturae Mendelianae Brunensis, 61*(2), 9-16.

2. Čičo, P. & Bujna, M. (2011). *Odolnosť tvrdonávarových materiálov v prevádzkových podmienkach* (monography), 119 p. SUA Nitra.

3. Čičo, P. & Bujna, M. (2009). Technical life of undermine chisels renovated of the hard surfacing. *Manufacturing engineering*, *8*(4), 41-42.

4. Kotus, M., Pauliček, T., & Holota, T. (2013). Resistance of coated electrodes suitable for renovation of tillage tools. *Journal of Central European Agriculture*, *14*(4), 1295-1302.

5. Kovaříková, I., Šimeková, B., Hodúlová, E., & Ulrich, K. (2011). Properties of composite wear resistant layers created by laser beam. *Annals of DAAAM and Proceedings of DAAAM Symposium, 22*(1). 1193-1194.

6. Kováč, I., Mikuš, R., Drlička, R., & Žitňanský, J. (2013). Boron effect on mechanical properties and structure of steel STN 41 5230 surface layer. *Materials, technologies and quality assurance*, *801*, 123-129.

7. Kováč, I., Vanko, N., & Vysočanská, M. (2014). Verification of the working life of a ploughshare renovated by surfacing and remelting in the operation. *Research in Agricultural Engineering*, *60*, 98-103.

8. Mikuš, R., Kováč, I., Drlička, R., & Hudec, D. (2012). Tribological properties of duble layered hardfacing materials. In *Quality and Reliability of Technical System* (pp. 155-160). SUA Nitra.

9. Müller, M., Novák, P., Chotěborský, R., & Hrabě, P. (2018). Reduction of ploughshare wear by means of carbide overlay. *Manufacturing Technology*, *18*(1), 72-78.

10. Pauliček, T., Votava, J., & Kotus, M. (2014). Abrasive resistance of filler metals in laboratory condi-tions. *Journal of Central European Agriculture*, *15*(1), 208-213.

11. Ťavodová, M., Kalincová, D., & Slováková, I. (2018). Evaluation of some parameters of hard surfacing treatment of the functional surfaces of forestry tools. *Management Systems in Production Engineering*, *26*(4), 222-226.

12. Viňáš, J., Brezinová, J., Guzanová, A., & Svetlík, J. (2013). Degradation of renovation layers deposited on continuous steel casting rollers by submerged arc welding. In *Proceedings of the Institution of Mechanical Engineers, 227*(12), 1841-1848.

13. Votava, J. (2014). Usage of abrasion-resistant materials in agriculture. *Journal of Central European Agriculture, 15*(2), 119-128.

14. Votava, J. & Kumbár, V. (2014). Use of tool st eels in soil processing to increase sugar beet production. *Listy Cukrovarnické a Řepařské, 130*(9-10), 292-296.

Corresponding author:
doc. Ing. Martin Kotus, PhD., Department of Quality and Engineering Technologies, Faculty of Engineering, Slovak University of Agriculture, Tr. A. Hlinku 2, 949 76 Nitra, Slovak Republic, phone: +421 37 641 5689, e-mail: martin.kotus@uniag.sk.

DETERMINING SOIL COMPACTION AT TRAFFIC LINES WITH PROXIMAL SOIL SENSING

Miroslav MACÁK[1], Vladimír RATAJ[1], Marek BARÁT[1], Ján KOSIBA[2], Jana GALAMBOŠOVÁ[1]

[1]*Department of Machines and Production Systems, Faculty of Engineering, Slovak university of Agriculture in Nitra, Tr. A. Hlinku 2, 949 76, Nitra, Slovakia*
[2]*Department of Transport and Handling, Faculty of Engineering, Slovak university of Agriculture in Nitra, Tr. A. Hlinku 2, 949 76, Nitra, Slovakia*

Abstract
Soil compaction introduced by large machineries is one of the major problems in crop production. There is need to assess the soil compaction in quick and reliable way. Soil proximal sensing technologies are robust tools for soil parameters determination. The aim was to assess two selected proximal sensing systems to determine soil compaction. As experimental site a CTF field was used, namely: crop bed (no traffic at all) and a traffic line (lines used for all traffic since 2009) areas. To characterize the differences in soil compaction, a vertical penetrometer was used which showed highly significant differences down to the depth of 70 cm. A horizontal penetrometer developed at Slovak university of Agriculture (measuring at 0.10, 0.15 and 0.20 cm depth) and soil conductivity sensor (EM38 – Geonics Limited) (measuring at depth range of 0.35 and 0.75m) sensors were used, both able to detect the differences at statistically significant difference of 0.01.

Key words: CTF; electric conductivity; horizontal penetrometer.

INTRODUCTION

Soil compaction is a major problem facing modern agriculture (*Hamza & Anderson, 2005*). It significantly affects the behaviour and the rate of physical - chemical and biological processes due to low porosity, low water and air permeability and increased requirements for traction power in seedbed preparation (*Badalíková, 2010; Chamen, 2011*). There are many factors which influence soil compaction. Besides the properties of soil itself (soil type, water and soil organic matter contents, etc.), the major factor is artificial. Other than incorrect management practices, the majority of soil compaction is caused by field machinery and its axle loads, wheel and tyre parameters, number of passes and drive slip. For example, the predicted pressure at 0.5 m depth in soils has increased by a factor of around six due to increasing loads over the past 80 years (*Chamen, 2011*). *Kroulík et al. (2009)*, *Galambošová & Rataj (2011)* showed that 85% and more of the field area is trafficked during the season. Damaged soil structure after field traffic may be partly repaired by deep soil cultivation however the high cost of these operations may be reduced by site- specific tillage (*Chamen et al, 2015*). Other group of action is based on reducing/ avoiding soil compaction. To minimize the trafficked area, controlled traffic farming can be deployed, where the traffic is confined to the least possible area. The basic principle is establishing permanent traffic lines, which are used for all field operations and crop growth is mostly confined to the non-trafficked areas – crop beds (*Chamen, 2011; Chamen, 2003*). This system can be used for all field crops (*Peets et al., 2017*). Also, in these systems, the extent of soil compaction needs to be determined and a proper soil management needs to be design as the permanent traffic lines are drilled in most of the European CTF systems *(Galambošová et. al, 2017; Macák et al. 2018, Smith at al., 2014; Godwin et al, 2015*). Determining soil compaction is possible with tradition methods as sampling of undisturbed soil samples or vertical penetrometer measurements which are, however, time and cost consuming (*Rataj et al., 2014*). Therefore, rapid methods which enable to measure soil properties and produce soil maps with high resolution. Proximal sensing methods are well described in *Gebbers (2019),* he summarizes that as direct methods the penetrometers and draft force sensors can be used. As indirect methods, the electromagnetic induction, galvanic couple electric resistivity or ground penetrating radar methods can be used. There are published results on determining soil compaction by these methods (*Krajčo, 2007; Alaoui & Diserens, 2018; Romero-Ruiz et al. 2019*). However, there is still lack of evidence in terms of direct

assessing the extend of soil compaction by these methods. This paper presents results of a pilot experiment comparing the two soil proximal methods used to determine the soil compaction at traffic lines namely soil conductivity and a horizontal penetrometer at a CTF experimental site.

MATERIALS AND METHODS

This paper presents a pilot assessment of two different soil proximal sensing methods used for soil compaction detection at traffic lines.

Experimental site

Soil sensors were used to determine soil compaction at an experimental site, where a long-term field scale experiment on Controlled traffic farming was established in growing season 2009/2010. The 16ha experimental field is located at University farm in Kolinany with silty loam in the top soil (0-350 mm) (51% silt, 30% sand, 19% clay). The different intensity of soil compaction is introduced through the controlled traffic of machinery at the field. The layout of the experiment and all the details are described in *Macák, et al. (2018)* and *Galambošová et al. (2017)*.

Data from soil proximal sensors were collected at two areas with different soil compaction conditions (Figure 2):

 - Crop bed – non compacted soil (no field traffic since 2009/2010),
 - Traffic line – permanent traffic line of the CTF system, all field traffic at this line since 2009/2010

To characterize the level of compaction at the areas, vertical penetrometer resistance was measured with a vertical penetrometer (Eijlkelkamp Soil & Water, Netherlands) and soil samples for soil moisture determining were taken at the same time. These data were used as etalon for the soil proximal sensing measurements.

Used methods of proximal sensing

Draft force sensor

A draft force sensor developed at Department of Transport and Handling was used (Figure 1). Details of the device are provided in *Varga, et al. (2014)*. The device measures continuously with two blades (one in non-compacted soil and one in compacted soil) and was originally designed to calculate the difference between the two blades which then is used to determine the relative extent of soil compaction. However, this sensor can be used also in conditions such as CTF field, where the traffic during measurement is confined to the traffic lines and different soil compaction conditions can be measured at the same time. The measuring device was aggregated with John Deere 8100 and the forward speed of 1 km.h^{-1} was used. Measurements were taken along a selected permanent tramline as shown in Figure 2 in three depth horizons (10cm, 15cm and 20 cm).

Fig, 1 Horizontal penetrometer using h the two-argument comparative method - photograph from the measurement

Electromagnetic conductivity

The ECa (electromagnetic induction) was measured by EM38 MK2 (Geonics Limited, Canada) which provides measurements in the range to 0.35m and 0.75 m when in the horizontal dipole orientation. Measurements were conducted at the same positions as the soil force sensor described above. To ensure this, the RTK accuracy GNSS receiver (Topcon) was used for guidance during the measurement.

The DC-resistivity method is a method that measures spatially distributed voltages resulting from current injections throughout an array of electrodes typically arranged on the soil surface or in boreholes

Data analyses

Data were analysed with standard methods; one factor ANOVA with the LSD test were used to evaluate the differences of crop bed and permanent traffic line data. Software Statistica was used.

RESULTS AND DISCUSSION

Soil force sensor was used in 2018 and electrical conductivity sensor was used in 2019 season. Figure 2 shows the penetrometric resistance at the areas in those two seasons. *Siqueira et al. (2014)* reported overview of published results that that root growth can be restricted or even impeded when PR values vary between 1.0 and 3.5MPa or 2.0 and 4.0MPa. In 2018 were these limit values recorded for both areas, the crop bed reached the value of 2 MPa at the depth of 12cm and the permanent traffic line at 5cm. In 2019 were the values up to the limit value to the depth of 30 cm for traffic line and 60 cm for the crop bed, respectively. However, differences between the two areas of soil compaction (crop bed and permanent traffic line) were statistically significant in the whole soil profile as it was expected.
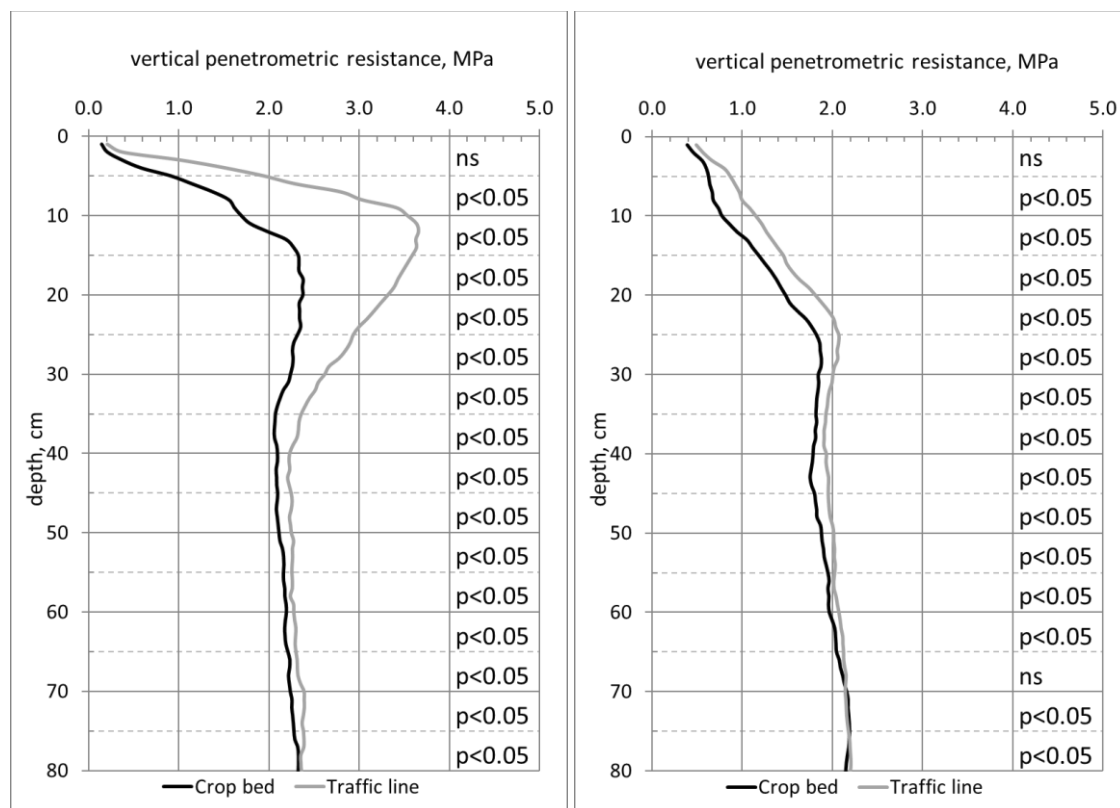

Fig. 2. Intensity of soil compaction in experimental zones represented by vertical penetration resistance (crop bed and trafficked lane) Left in 2018, right in 2019. Note: average of gravimetric soil moisture content in depth horizons 0-20 cm, 20-40cm and 40-80cm were 20.6%, 22.7%, 23.7% in 2018 and 23.4%, 22.5%, 22.6% in 2019, respectively.

Horizontal penetrometer

A horizontal penetrometer measuring the draft force was used in conditions of a soil moisture content of 19%. Results are given in Table 1 and Figure 3. Statistical analyses showed a significant difference

in the median values for all depths and both soil moisture conditions at a level of p<0.010. The difference between the crop bed and traffic line decreases with increasing depth. This corresponds with the vertical penetrometer values, where also the difference decreases with increasing depth in the range between 10 to 20 cm. This shows the ability of the measuring device to detect the soil compaction differences across a small distance, which has potential use in assessing the conditions of permanent traffic lines in a CTF system, or e.g. measuring the effect of irrigation machinery on soil compaction (*Jobbagy et al., 2016*). Also, if used for field scale variability mapping, soil moisture and a GNSS location should be recorded as proposed by authors (*Naderi-Boldaji et al., 2016*) the areas for local tillage could be targeted (*Adamchuck et al., 2004*).

Tab. 1 Mean values, standard deviation and median values for data obtained by draft force sensor, (n>2500),
** p<0.01

Depth of measurement, cm	Compaction	Draft for, N average ± sd		Difference, N / significance
10 cm	Crop bed	1018.0	± 296.3	1260.7 **
	Traffic line	2278.7	± 427.9	
15 cm	Crop bed	1652.3	± 324.8	1186 **
	Traffic line	2838.3	± 374.4	
20 cm	Crop bed	3166.0	± 473.3	837.3 **
	Traffic line	4003.3	± 599.5	

The soil conductivity sensor

Results of soil conductivity measurements are provided in Figure 5. Here, measured values for the different soil compaction conditions (crop bed and traffic line) are presented for both depth ranges (C1 – up to 0.35m and up to 0.75 m).
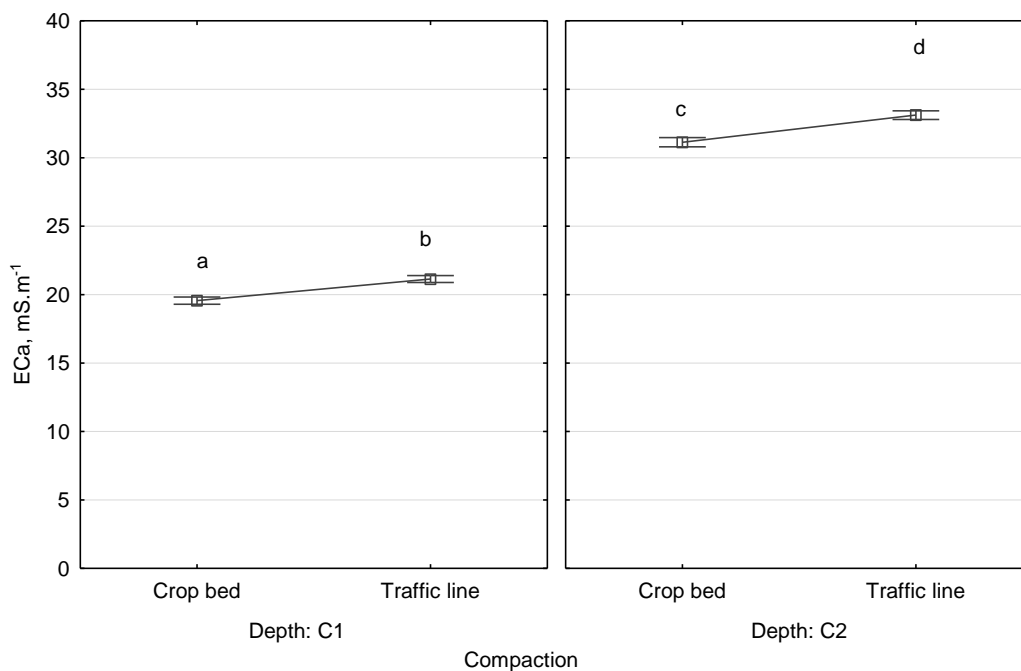

Fig. 5 Mean values of soil conductivity measured in crop bed and traffic line in 0.35m (C1) and 0.75 m (C2) depth, a,b,c,d - different letters denotes to different groups at p<0.01

Values of measured ECa are typical for this type of soil texture (*Domsch & Giebel, 2004*). For both depths, soil compaction increased the ECa values significantly.

The difference between measurement in crop bed and at traffic line were significantly different for both depths (p <0.01). Up to date, there is lack of published knowledge on determining the soil compaction by electric sensors. In 2007, Krajčo compared different sensors and reported that the electromagnetic sensor distinguished the areas with no compaction above 0.3 m and areas with no compaction in whole profile with less precision.

CONCLUSIONS

Paper deals with selected soil proximal methods to determine soil compaction of permanent traffic lines at a CTF field, where permanent separation of crop bed and field traffic line has been used for 10 years. Data from a pilot study showed, that electric conductivity measured by the electromagnetic induction methods is a useful tool to distinguish between the compacted lines and crop bed for the depth ranges up to 0.3 and 0.75 m at a statistically significant level. This was alongside the tramlines. Future research should be done to exam the spatial resolution in the traffic lines should be determined. The horizontal penetrometer showed high sensibility in terms of determining the soil compaction in the upper layer. Here the local maximum of compaction was targeted by the sensor. Future work will be aimed on combining the sensor with soil moisture measurements and GNSS data and possible extension of the sensor in order to be able to measure different depths simultaneously.

ACKNOWLEDGMENT

REFERENCES

1. Alaoui, A. & Diserens, E. (2018) Mapping soil compaction – A review. *Current Opinion in Environmental Science & Health*, *5*, 60–66.

2. Antille, D.L., Chamen, W.C.T., Tullberg, J.N. & Lal, R. (2015a). The potential of controlled traffic farming to mitigate greenhouse gas emissions and enhance carbon sequestration in arable land: A critical review. *Transactions of the ASABE, 58*(3), 707–731.

3. Badalíková, B. (2010). Influence on Soil Tillage on Soil Compaction. In *Dedousis, A.P., Bartzanas (eds.), Soil Engineering*. Springer - Verlag Berlin Heidelberg.

4. Barát, M., Rataj, V., Týr, Š., Macák, M. & Galambošová, J. (2017). Effect of controlled traffic farming on weed occurrence. *Agronomy Research, 15*(4), 1484–1490.

5. Chamen, W.C.T, Alakukku, L., Pires, S., Sommer, C., Spoor, G., Tijink, F.G.J. & Weisskopf, P. (2003). Prevention strategies for field traffic-induced subsoil compaction: a review Part 2. Equipment and field practices. *Soil & Tillage Research*, *73*, 161-174.

6. Chamen, W.C.T. (2011). *The effects of low and controlled traffic systems on soil physical properties, yields and the profitability of cereal crops on a range of soil types* [PhD Thesis]. Cranfield University

7. Chamen, W.C.T. (2015). Controlled traffic farming – From worldwide research to adoption in Europe and its future prospects. *Acta Technologica Agriculturae*, *18*(3), 64–73.

8. Galambošová, J., Macák, M., Rataj, V., Godwin, R. J., Žitňák, M., Vitázková, B., Ďuďák, J., & Chamen, W. C. T. (2014) Yield performance of controlled traffic farming permanent tramlines. Paper Number 142005820, In *ASABE Annual International Meeting 2014*, ASABE. Michigan: St. Joseph.

9. Godwin, R.J., Misiewicz, P.A., Smith, E.K., Millington, W.A.J., White, D.R., Dickin, E.T. & Chaney, K. (2017). Summary of the effects of three tillage and three traffic systems on cereal yields over a four-year rotation. *Aspects of Applied Biology*, *134*, 233–241.

10. Hamza, M.A. & Anderson, W.K. (2005). Soil compaction in cropping systems A review of the nature, causes and possible solutions. *Soil & Tillage Research*, *82*(2), 121-145.

11. Jobbagy, J., Krištof, J. & Findura, P. (2016). Soil compaction caused by irrigation machinery. *Agronomy Research, 14*(3), 790–800.

12. Krajčo, J. (2007). *Detection of soil compaction using soil electrical conductivity* [MSc by Research thesis]. Cranfield University at Silsoe.

13. Kroulík, M., Kumhála, F., Hula, J. & Honzík, I. (2009). The evaluation of agricultural machines field trafficking intensity for diffrent soil tillage technologies. *Soil & Tillage Research*, *105*, 171–175.

14. Mojtaba Naderi-Boldaji, Peter Weisskopf, Matthias Stettler, & Thomas Keller. (2016). Predicting the relative density from on-the-go horizontal penetrometer measurements at some arable top soils in Northern Switzerland. *Soil & Tillage Research*, *159*, 23-32.

15. Peets, S., Chamen, W.C.T., Godwin, R.J., White, D.R., Misiewicz, P.A. & Hargreaves, P.R. (2017). System design and the economics for controlled traffic farming (CTF) in grass silage production. ASABE Paper No.: 1700145. St. Joseph, MI.: *2018 ASABE Annual International Meeting, American Society of Agricultural and Biological Engineers.*

16. Romero-Ruiz, A., Linde, N., Keller, T., & Or, D. (2019). A review of geophysical methods for soil structure characterization. *Reviews of Geophysics*, *56*, 672–697.

17. Smith, E. K., Misiewicz, P. A., Girardello, V., Arslan, S., Chaney, K., White, D. R. & Godwin, R. J. (2014). Effects of traffic and tillage on crop yield (Winter Wheat Triticum aestivum) and the physical properties of a sandy loam soil. *ASABE Paper No 1912652*. Michigan, USA: St. Joseph.

18. Varga, F. Tkáč, Z., Šima, T., Hujo, Ľ., Kosiba, J. & Uhrinová, D. (2014). Measurement of soil resistance by using a horizontal penetrometer working with the two-argument comparative method. *Agronomy Research, 12*(1), 187–196.

Corresponding author:

Ing. Miroslav Macák, Ph.D., Department of Machines and Production Systems, Faculty of Engineering, Slovak university of Agriculture in Nitra, Tr. A. Hlinku 2, 949 76, Nitra, Slovakia, Slovak Republic, phone: +421 64144798, e-mail: miroslav.macak@uniag.sk

INFLUENCE OF OPERATING PARAMETERS OF THE VEHICLE ON THE ROLLING RESISTANCE SIZE WITH THE VARIABLE DIAMETER OF THE TEST ROLLER

Daniel MADER[1], Martin PEXA[1], Jakub ČEDÍK[1], Bohuslav PETERKA[1], Zbyněk VONDRÁŠEK[2]

[1]*Department of Quality and Dependability of Machines*
[2]*Department of Electrical Engineering and Automation*

Abstract:
The paper on the theme "how the tire pressure, vertical load upon wheel, and driving velocity influence the rolling resistance during the measuring cycle on the roller test stand with various roller diameters" is focused on the selected parameters (tire pressure, vertical load upon wheel, and driving speed), which exert, under certain circumstances, more or less significant influence on the rolling resistance at measuring of the performances, consumption rates and/or pollutant emission rates on the road vehicle roller tester. These roller testers, however, may be equipped with rollers differing in diameter, which is the significant parameter that influences the tire rolling resistance and must be taken into account whenever a roller tester is under design.

Key words: roller tester; rolling resistance; vertical load.

INTRODUCTION

Road vehicles and their operation have a significant impact on human health. Therefore, vehicles are approved for road safety and environmental friendliness. Both new and in-service vehicles are approved. New vehicles are approved during homologation tests and vehicles in use during inspection tests that replace demanding homologation tests in service.

Roller dynamometers are used for homologation tests of road vehicles and generally for detailed tests. The use of roller dynamometers simulates road traffic in laboratory conditions. Using the dynamometer, the vehicle's operating parameters are then evaluated, such as emissions, both in the form of particulate matter and in the form of gaseous components, and the fuel consumption is evaluated *(Damanik 2018, Kaya 2018, Aydin 2015)*. Tests such as the NEDC test-New European Driving Cycle *(Wu 2019, Mera 2019, Dimitrakopoulos 2019)*, WLTP World-Harmonized Light-Vehicle Test Procedure *(Massaguer 2019, Park 2019, Solouk 2019)*, JC08 Japan Cycle *(Umihara 2018, Kim 2018, Hagino 2016)* etc.

In order to assess the impact on human health, the technical condition of vehicles in operation is also monitored. As it turned out, it is difficult to describe the technical condition of the vehicle correctly and to identify its shortcomings. Therefore, roller testers designed for inspection measurements are being developed, but also for routine service workplaces.

The design of the roller testers remains essentially the same, and the rollers used, in particular their size, change. The usual diameter of the test roller is between 170 and 250 mm (Maha Consulting, Bosch etc.), there are also test benches with a diameter of 400 mm, and recently test rollers with a small diameter of around 100 mm (Actia) have appeared. The realization of a small roller test room has much less space and thus less demand for input investment. The use of such a wide range of test roller testers means that the tire rolling problem on the test bench rollers is well and correctly solved. In practice, the issue of rolling agricultural tires *(Derafshpour 2019, Farhadi 2018)*, or on rolling flat tires *(Greiner 2018, Lee 2011)* or on large diameter rollers, which are considered straight road simulations for laboratory tests, are often addressed *(Ejmont 2018)*. The issue of rolling on small-diameter rollers in vehicle test rooms is not addressed in detail in the literature.

The aim of the paper is to analyze the influence of the size of the rollers of the vehicle roller testers on the rolling resistance, which is significantly reflected in the measurement accuracy. The analysis is

performed on a 165/70 R13 tire at 1.9 bar and the variables are the vertical tire load, the tire peripheral speed, and the test roller diameter.

MATERIALS AND METHODS

The rolling resistance measurements have been taken on test equipment shown in fig. 1. Its main part is the test roller (the diameters used 90, 110, 170, 220, 320 and 400 mm), against which the tire (165/70 R 13) is pressed by action of a hydraulic system. Powered by the frequency converter the electric drive is responsible for the roller rotation speed. The output power values necessary to overcome the rolling resistance have been established as watt-meter readings.
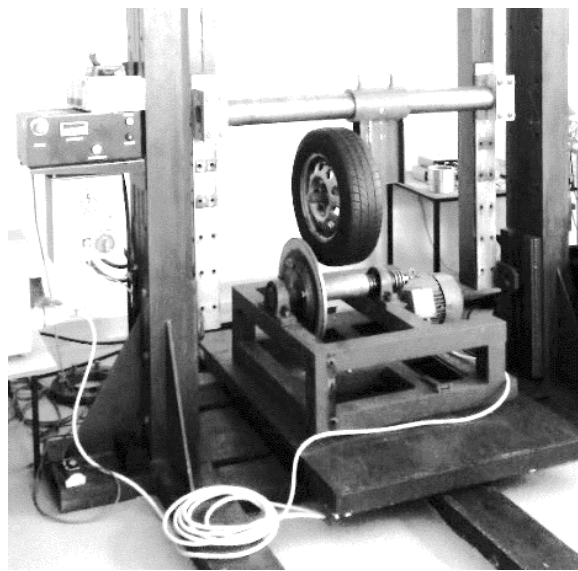

Fig. 1 Testing equipment

Because of the fact that it is the motor input what is actually measured, it is necessary to gradually eliminate other resistances that can influence the measurements, with power losses due to tire air resistance, those attributable to the tire hub bearing, to the roller supporting bearings, to the rotating roller air resistance, to the driving belt slippage, to the motor bearings rolling resistance, to the motor air resistance (ventilation losses), and due to motor electromagnetic efficiency. The output power necessary to overcome the tire-on-roller rolling resistance is the result.

Elimination of these associated losses is realized by measuring the roller without any tire pressed against it and by running out of the separate (not pressed against) tire at such a speed at which the measurements themselves would be taken. Fixed measurement conditions:

- summer tire (165/70 R13) used – temperature range 40–60 °C
- roller diameter (90, 110, 170, 220, 320 and 400 mm),
- vertical load settings (200, 260, 330, 400 kg),
- roller circumferential speed (10, 15, 20, 25, 30, 35, 40, 50, 60, 70 km.h^{-1})
- air pressure is constant inside the tire, not being varied during the measuring session (1.9 bar).

An example of how the resistances can be eliminated is shown in fig. 2. During the measuring session (roller loaded with tire) the output power measurements were taken, shown in utmost grey. The lowest positioned values reflect the situation when the roller alone is in motion, but with no tire pressed against it. They pose most included losses. The lower loss values are attributable to the bearing on which the tire is seated and to the related ventilation losses. They are the values lying just below the zero axis. The black points and the black line represent the rolling resistance resulting values.
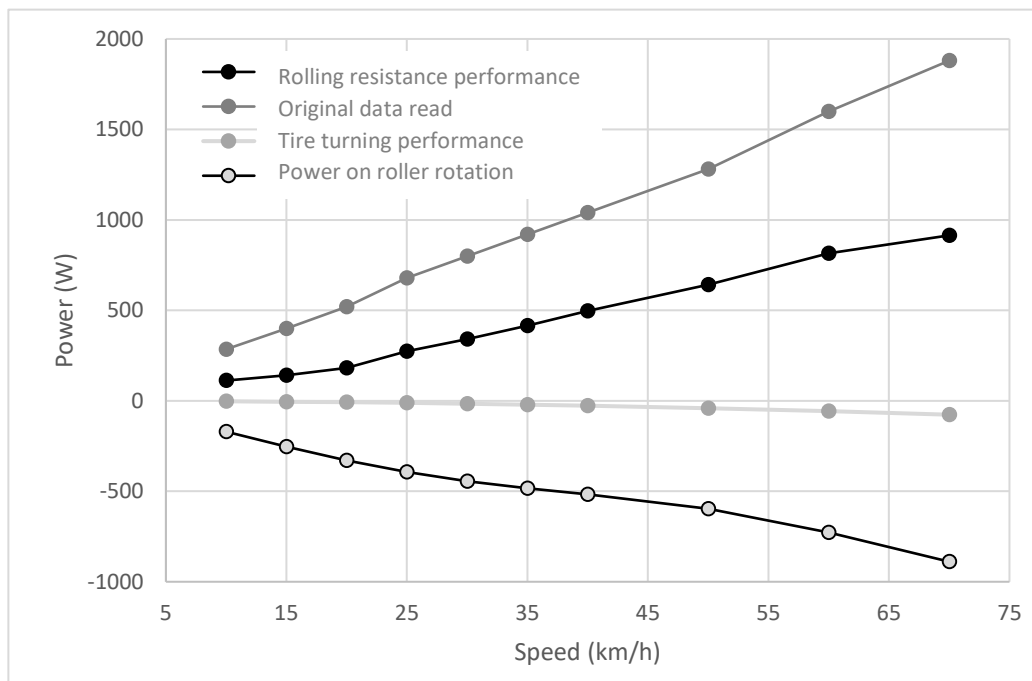

Fig. 2 Example of loss elimination (roller 170 mm, vertical load 205 kg)

RESULTS AND DISCUSION

Examples of the necessary rolling power resistance measurements for the mean vertical load of 205 kg acting upon the 165/70 R13 tire are shown in tab. 1. The watched vertical load upon tire in kg is shown in the first column, the test roller diameter in the second one, and the values of the output power in W, necessary to overcome the rolling resistance, in the following columns as function of speed in km.h^{-1}. The X symbols for the rollers having 90 and 110 mm in diameter at the speeds from 50 to 70 km.h^{-1} imply that no measurements have been taken here. Depending on the test equipment gears used this circumferential speed could not be achieved.

Tab. 1 Example of measured values of required rolling power for medium vertical load 205 kg, tire 165/70 R13

Power W		The circumferential speed of roller									
Load kg	Roller mm	10 km.h^{-1}	15 km.h^{-1}	20 km.h^{-1}	25 km.h^{-1}	30 km.h^{-1}	35 km.h^{-1}	40 km.h^{-1}	50 km.h^{-1}	60 km.h^{-1}	70 km.h^{-1}
203	90	227	296	478	550	622	839	1020	x	x	x
205	110	168	265	359	482	531	581	747	951	x	x
206	170	124	172	227	325	386	451	518	656	867	1010
207	220	119	156	214	252	322	372	445	596	670	862
204	320	101	135	188	230	292	334	386	482	609	738
205	400	103	123	183	231	269	316	364	478	572	646

As plotted against the stand roller diameter, circumferential speed and vertical load upon the 165/70 R13 tire, the curve of the necessary power to overcome the rolling resistance is shown in fig. 3. As widely known, the contribution of the circumferential speed has shown a quite unambiguous manifestation. The higher the tire circumferential speed, the higher is the power necessary to overcome the rolling resistance. As against their larger counterparts, smaller rollers show steeper growth in the power necessary to overcome the rolling resistance, given the growing circumferential speed.

In respect of the dispersal of the power values to overcome the rolling resistance at the individual speeds and vertical loads and with various rollers used the dispersal of the values can be said as lesser at lower circumferential speeds up to 40 km.h^{-1}. Hence the conclusion can be drawn that the roller size exhibits greater influence where higher levels of the test stand roller circumferential speeds are used.
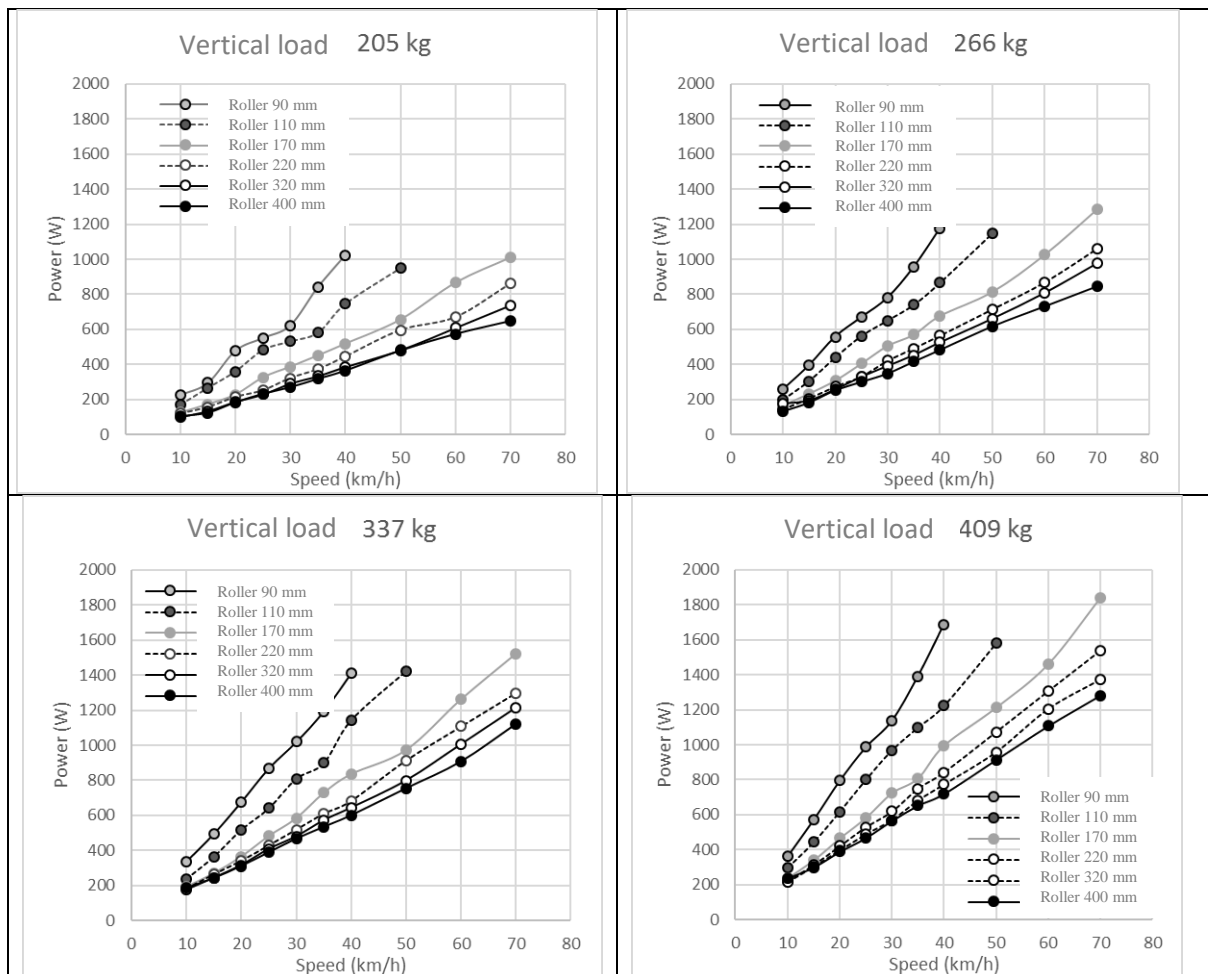

Fig. 3 Rolling resistance performance versus roller diameter, circumferential speed, and 165/70 R13 tire vertical load

For the load influence analysis see fig. 4, showing comparison of the power required to overcome the rolling resistance in per cents, while the 100 % level is to be understood as the measurements with the vertical load of 205 kg. The increase in vertical load to 266 kg can be said to raise the power necessary to overcome the rolling resistance to 128 %, the vertical load increase to 337 kg will raise this necessary power to 159 %, and the vertical load increase to 409 kg will result in this necessary power increase to 191 %.

A look at the dispersal of the power values required to overcome the tire rolling resistance (expressed in % in fig. 4) will reveal greater dispersal of the values at lower circumferential speeds than at higher speeds. Hence, the conclusion can be drawn that the roller diameter is the more significant factor at lower circumferential speed values than at higher ones.
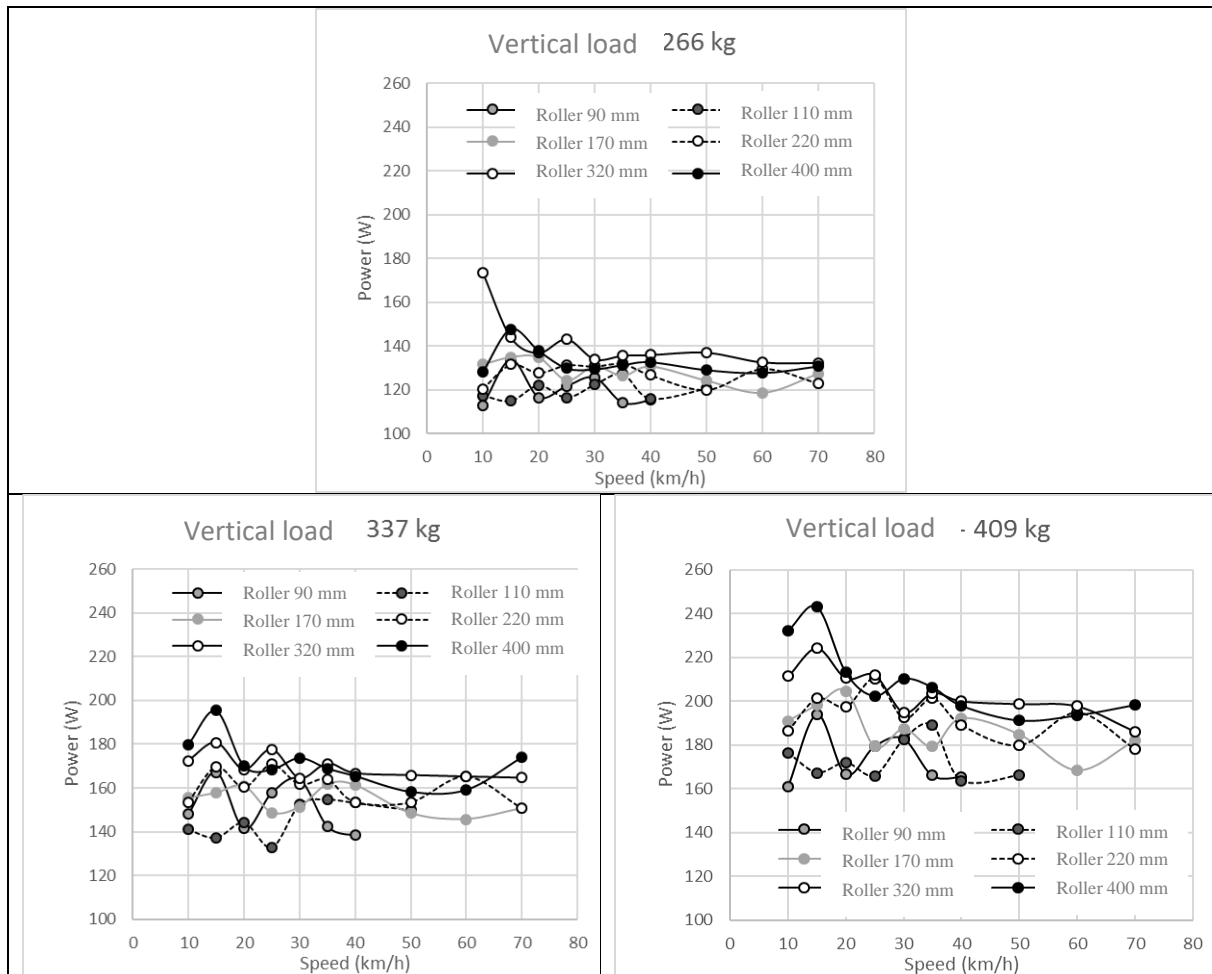

Fig. 4 Percentage comparison of the power needed to overcome the rolling resistance (100 % is the value measured for a vertical load of 205 kg)

For the summarized analysis results see Fig. 5, showing the power values necessary to overcome the rolling resistance with various rollers differing in diameter used, taken relatively to the values obtained on the 400 mm roller. It is obvious from Fig. 5 that the smaller is the roller, the more steeply the required power values grow. This growth is more significant with lesser values of vertical load.

Fig. 5 shows the influence of speed as the value of standard deviation. The greater is the deviation, the more significant is the speed. In this light, the rollers smaller in diameter seem to be less suitable for use on the roller tests stands and this makes correct setting of loading forces more demanding. The power necessary to overcome the rolling resistance with a 200 mm roller will rise by about 20–25 % with a 400mm roller and by about 90–100 % with a 100 mm roller.
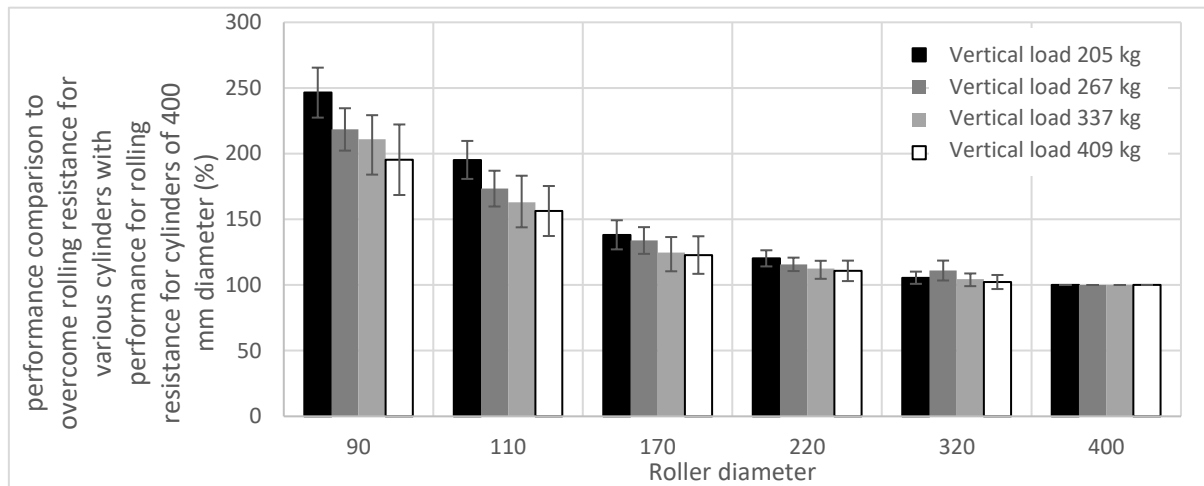
Fig. 5 Overall evaluation of the change in power needed to overcome the rolling resistance at variable speed, vertical load and various roller sizes (%) – 100 % are values for a 400 mm roller diameter.

CONCLUSIONS

Construction of roller test stands is considerably more demanding for investment mainly then in the event of the underground ones. In respect of the maintenance and inspection stations, it would be more interesting to conceive them as of the overground type. This, however, mostly results in use of the rollers having less than obvious diameter cca 200 mm. This change in the roller diameter manifests itself as follows:

- As for the vertical load it can be said that the greater vertical load is used, the greater is the power required to overcome the rolling resistance, growing more rapidly with lesser roller diameters than with the greater ones. Increase in vertical load from 205 to 266 kg will cause 1.3-times growth in power to overcome the rolling resistance. Due to the 205 to 337 kg growth in vertical load the power necessary to overcome the rolling resistance will increase ca 1.6-times, and due to the vertical load increase from 205 to 409 kg the power to overcome the rolling resistance will rise ca 1.9-times.
- Concerning the circumferential speed, it can be stated that the power necessary to overcome the rolling resistance will record an increase. The increase is more significant with the lesser-diameter rollers where broader dispersal of values is moreover achieved.
- As to the roller diameters, it can be stated that the power required to overcome the rolling resistance with a 200 mm roller will rise by about 20–25 % with the 400 mm diameter while with a 100 mm roller the necessary power will increase by 90–100 %, i.e. to a double of its original value.

From the viewpoint of the roller testers the test results yet remain to be transformed as most roller testers work with pair of rollers, not with a single one. This transformation cannot however be generalized otherwise than mathematically when the transformation results strongly depend on diameter of the rollers and their axis-to-axis spacing.

The measurement results show that the use of rollers of small diameter (below 150 mm) for roller testers is possible. A number of publications deal with the problem of rolling tires on the road. However, the publications are focused on large road simulating rollers *(Ejsmont 2019)*, tire wear *(Taryma 2018)* or vehicle emissions issues *(Lee 2018)*. Many authors are engaged in modeling rolling resistance *(Cho 2013, Andersen 2015, Volskaya 2018)*. There is currently no author in the literature available to experimentally determine the tire rolling resistance on rollers.

REFFERENCES

1. Andersen, L.G., Larsen, J.K., Fraser, E.S., Schmidt, B., & Dyre, J.C. (2015). Rolling resistance measurement and model development. *Journal of Transportation Engineering, 141*(2), art. no. 04014075.

2. Aydin, H. & Ilkiliç, C. (2015). Analysis of combustion, performance and emission characteristics of a diesel engine using low sulfur tire fuel. *Fuel, 143*, 373-382.

3. Damanik, N., Ong, H.C., Tong, C.W., Mahlia, T.M.I., & Silitonga, A.S. (2018). A review on the engine performance and exhaust emission characteristics of diesel engines fueled with biodiesel blends. *Environmental Science and Pollution Research, 25*(16), 15307-15325. doi: 10.1007/s11356-018-2098-8

4. Dimitrakopoulos, N., Belgiorno, G., Tunér, M., Tunestål, P., & Di Blasio, G. (2019). Effect of EGR routing on efficiency and emissions of a PPC engines. *Applied Thermal Engineering*, 742-750. doi: 10.1016/j.applthermaleng.2019.02.108

5. Ejsmont, J., & Owczarzak, W. (2019). Engineering method of tire rolling resistance evaluation. *Measurement: Journal of the International Measurement Confederation, 145*, 144-149.

6. Hagino, H., Oyama, M., & Sasaki, S. (2016). Laboratory testing of airborne brake wear particle emissions using a dynamometer system under urban city driving cycles. *Atmospheric Environment, 131*, 269-278. doi: 10.1016/j.atmosenv.2016.02.014

7. Cho, J.R., Lee, H.W., Jeong, W.B., Jeong, K.M., & Kim, K.W. (2013). Numerical estimation of rolling resistance and temperature distribution of 3-D periodic patterned tire. *International Journal of Solids and Structures, 50*(1), 86-96.

8. Kaya, T., Kutlar, O.A., & Taskiran, O.O. (2018). Evaluation of the Effects of Biodiesel on Emissions and Performance by Comparing the Results of the New European Drive Cycle and Worldwide Harmonized Light Vehicles Test Cycle. *Energies, 11*(10), art. no. 2814. doi: 10.3390/en11102814

9. Kim, H., Son, H., Kim, H., & Hwang, S. (2018). Development of an advanced rule-based control strategy for a PHEV using machine learning. *Energies, 11*(1), art. no. 89. doi: 10.3390/en11010089

10. Lee, B., Kim, D., Lee, J., Cha, W., & Seo, Y. (2018). Influence of tire rolling resistance coefficient on road load and fuel economy for passenger car. *Transactions of the Korean Society of Automotive Engineers, 26*(6), 745-754.

11. Massaguer, E., Massaguer, A., Pujol, T., Comamala, M., Montoro, L., & Gonzalez, J.R. (2019). Fuel economy analysis under a WLTP cycle on a mid-size vehicle equipped with a thermoelectric energy recovery system. *Energy, 179*, 306-314. doi: 10.1016/j.energy.2019.05.004

12. Mera, Z., Fonseca, N., López, J.-M., & Casanova, J. (2019). Analysis of the high instantaneous NO emissions from Euro 6 diesel passenger cars under real driving conditions. In *Applied Energy* (pp. 1074-1089). doi: 10.1016/j.apenergy.2019.03.120

13. Park, S., Cho, J., & Park, J. (2019). Numerical methodology on virtual model extension and system-level optimization of light-duty diesel vehicle with dual-loop exhaust gas recirculation. In *Applied Energy* (pp. 1422-1435). doi: 10.1016/j.apenergy.2019.03.181

14. Solouk, A., Kapadia, J., Masterson, B., & Shakiba-Herfeh, M. (2019). Impacts of WLTP test procedure on fuel consumption estimation of common electrified powertrains. *SAE Technical Papers*, 2019-April (April). doi: 10.4271/2019-01-0306

15. Taryma, S., Woźniak, R., Ejsmont, J., Mioduszewski, P., & Ronowski, G. (2018). Tire/road noise and tire rolling resistance on the prototype PERS surface. *IOP Conference Series: Materials Science and Engineering, 421*(2), art. no. 022035.

16. Umihara, T., Tamura, A., Ishibashi, T., & Kawamura, A. (2018). Proposal of soft SOC balancing method to two battery HEECS chopper used for EV power train. In *Proceedings: IECON 2018 - 44th Annual Conference of the IEEE Industrial Electronics Society, art. no. 8592730* (pp. 2128-2132). doi: 10.1109/IECON.2018.8592730

17. Vol'skaya, N.S., Zhileykin, M.M., & Zakharov, A.Y. (2018). Mathematical model of rolling an elastic wheel over

deformable support base. *IOP Conference Series: Materials Science and Engineering, 315*(1).

18. Wu, T., Yao, A., Feng, J., Wang, H., Li, Z., Liu, M., & Yao, C. (2019). A reduced PM index for evaluating the effect of fuel properties on the particulate matter emissions from gasoline vehicles. *Fuel, 253*, 691-702. doi: 10.1016/j.fuel.2019.05.059

Corresponding author:
Ing. Daniel Mader, Department for Quality and Dependability of Machines, Faculty of Engineering, Czech University of Life Sciences Prague, Kamýcká 129, Praha 6, Prague, 16521, Czech Republic, phone: 728943190, e-mail: maderd@tf.czu.cz

INFLUENCE OF BIOFUELS ON SKODA RAPID 1.6 TDI ENGINE'S EMISSIONS AND FUEL CONSUMPTION

Jakub MAŘÍK[1], Veronika HARTOVÁ[1], Martin KOTEK[1]

[1]*Department of Vehicles and Ground Transport, Czech University of Life Sciences Prague*

Abstract
The road transportation increases all around the globe and bio-fuels become the forefront of public interest. The bio-fuels enable to replace completely or partially the existing energetic resources with their limited capacities. The usage of bio-fuels is particularly beneficial in terms of reducing dependence on fossil fuels (petroleum) and consequently negative environmental impacts. According to the Article 3, Directive 2009/28/EC, each member state has to ensure that an energy share from renewable sources in all forms of transportation reaches at least 10% of the final consumption of energy in transportation till 2020. This article analyses and compares selected bio-fuels and their influence on engine's emissions parameters. On diesel engine of Skoda Rapid 1.6 TDI were measured harmful emissions in the testing using the NEDC on chassis dynamometer. As fuels, were chosen pure diesel fuel, pure HVO and pure FAME. Furthemore, fuel consumption were monitored.

Key words: driving cycle; HVO; RME.

INTRODUCTION
The steep population growth over recent decades has led to a significant increase in demand for fossil energies. Most estimates present the world's oil reserves for the next 50 years, and although projections for relatively early depletion of fossil fuels are constantly delaying due to improvements in drilling technology and discovery of large shale gas stocks, efforts are being made to exploit and develop renewable sources such as fuels. The interest in their application and research is not only due to declining oil reserves but also   many others, such as efforts to minimize harmful emissions and impact on the environment and human health, efforts to reduce dependence on oil suppliers *(Bae & Kim, 2017)*.

The consumption of fossil fuels keeps growing together with significant increase of sales of diesel vehicles in Europe. Emissions coming from these vehicles have an impact on both human health and the environment *(Dockery, Schwartz & Spengler, 1992; Pourazar, Frew, Blomberg, Helleday, Kelly, & Wilson, 2004; Goyal, Jaiswal, Kumar, Dadoo & Dwarakanath, 2010; Jacobson, 2001; Koch, 2011)*.

The European Union is increasingly focusing on the use of biofuels. At present, as a biofuel component in the Czech Republic, it is blended (according to legislation at least half of the sales network of the filling station operator up to 5% by volume, especially bioethanol or ethyl-tert-butyl ether (ETBE) produced from bioethanol. Bioethanol is therefore used as a component in conventional automotive gasoline fuels *(Mužíková, Pospíšil & Šebor, 2010)*. Fatty acid methyl esters (FAME) are used as the bio-component in diesel fuels. In the Czech Republic, rapeseed oil methyl esters (RME) are used in particular. At present, up to 7% FAME is added to the diesel fuel. The market also includes so called blended diesel fuels containing more than 30% by volume of FAME *(Šimáček, Vrtiška, Mužíková & Pospíšil, 2017)*.

The aim of the regulations of the European Union is to increase the proportion of renewable energy up to 10% by the year 2020 in order to reduce the production of greenhouse gases, especially CO_2 (Directive 28/2009/CE).

MATERIALS AND METHODS
In the experiment, the emissions and fuel consumption of the Škoda Rapid 1,6 TDI passenger car were measured on chassis dynamometer.

The car was placed on chassis dynamometer by a driven axle and secured by a parking brake and fixed with locking straps. A gas analyzer tube (FTIR) was introduced into the exhaust pipe. Engine speed, particle filter clogging, and other values were recorded and stored at a sampling rate of $\pm 1 Hz$ using the VAG-COM system. The measured quantities from the FTIR gas analyzer and the VAG-COM system

were then synchronized. To the engine will be fuel transported by a fuel pump from an external fuel tank located on a laboratory scale. Using this scale fuel consumption was measured. 67/5000 Measurements were made with the engine warmed to its operating temperature. Car cooling was provided by a suction fan. Emission measurements and other operating parameters were measured during the New European Driving Cycle (NEDC) cycles.

The selected operating parameters selected the emissions and fuel consumption of a passenger car diesel engine using two biofuels - RME (rape oil methyl ester) and HVO (hydrogenated vegetable oil). The reference fuel served pure diesel. Measurements were made on the Škoda Rapid 1.6 TDI passenger car (see Table 1).

Tab. 1 Basic parameters of the Škoda Rapid 1.6 tdi

Engine type	compression ignition, turbo charged
Cylinders volume	1598 cm^3
Cylinders	4
Compression ratio	16,5:1
Injection	Common rail
Power	77 kW at 3000 rpm
Torque	250 Nm at 1500 rpm
Weight	1265 kg
EU norm	Euro 5

During measurement has been used, these devices:
- Chassis dynamometer
- Fan FILCAR AL - 1500 / C
- Gas analyzator MATRIX MG-5
- VIBRA AJ-6200CE Laboratory weight

The chassis dynamometer consists of two cylinders connected by a chain. To improve the adhesive properties, one cylinder is provided with an anti-slip surface. The cylinders are fitted on one side with adjustable flywheels designed to simulate the inertia of the vehicle. On the other side, a direct-current electric motor of 56 kW is connected to one cylinder. A 125 kW turbine brake is connected to the second cylinder for static power measurement purposes. Vehicle cooling during operation was provided by the FILCAR AL - 1500 / C suction fan. Then was used analyzer FTIR. FTIR is infrared spectrometer for automated, high-precision gas concentration monitoring in real time. It allows the detection and quantification of gas occurring in a concentration of only a few ppb (parts per billion) to one hundred percent. It measures up to 5 spectra per second at a spectral resolution of 0.5 cm -1 and up to 30 spectra per second at a spectral resolution of 4 cm $^{-1}$. For accurate measurement of fuel consumption was used laboratory weight, operating on the principle of a vibration cell that is highly resistant to electromagnetic and electrostatic interference and temperature changes (see Fig. 1).

Fig. 1 Connecting the scales to the vehicle

Pure RME and pure HVO (NExBTL from Neste Oil) were tested. The reference fuel was pure diesel. The properties of the individual fuels are described in Table 2.

Tab. 2 Basic properties of tested fuels

Parameter	Diesel	HVO	RME
Calorific value [MJ·kg⁻¹]	43,1	44,1	37,2
Density at 15°C [kg·m⁻³]	833,5	778,6	882,5
Kin. viscosity at 40 °C [mm²·s⁻¹]	2,66	2,89	4,63
Flesh Point [°C]	60	983	>120
Filterability - CFPP [°C]	-24	-38	-26
Cetan number [-]	555	>70.0	60
Cetan index [-]	552,2	793,1	58,5

RESULTS AND DISCUSSION

The results of emissions and fuel consumption measured during the NEDC driving cycle are described in the following text and their calculated averages from the individual measurements are shown in the graphs. These graphs include an error line based on standard deviations. For the same reason, the experiment was started and ended when running on the selected reference fuel - Diesel 1 (start) and Diesel 2 (terminating), see the following graphs for emissions. Emissions were measured according to the above mentioned methodology for the NEDC driving cycle. Three driving cycles (measurements) were performed for Diesel and HVO and 4 driving cycles were performed for RME. For illustration, Fig. 2 show the measured values of the instant CO_2 concentration when running a diesel car for 3 NEDC cycles.
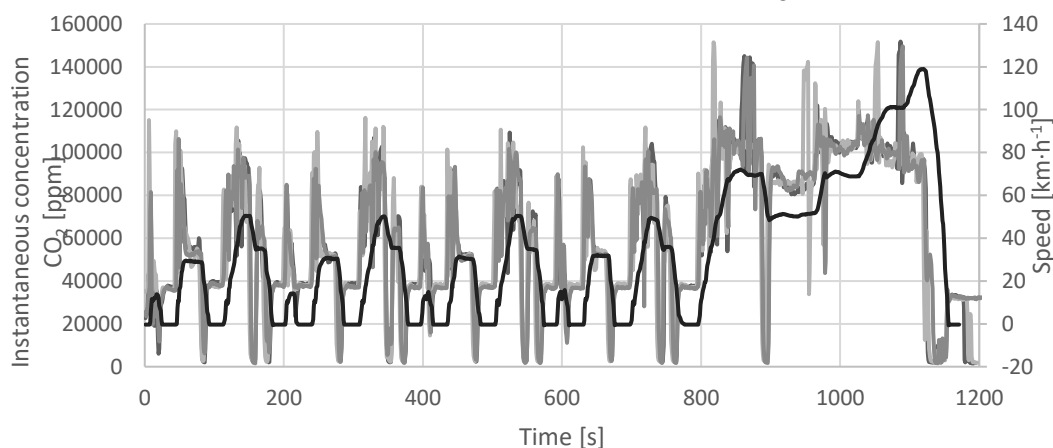

Fig. 2 Instant CO_2 concentration for 3 driving cycles NEDC

The lowest CO_2 emissions were measured during HVO operation. Compared to RME, an average of 10.2 g · km⁻¹ is lower. CO_2 values for diesel were measured higher by 5.6 g · km⁻¹ compared to HVO see on Fig. 3.
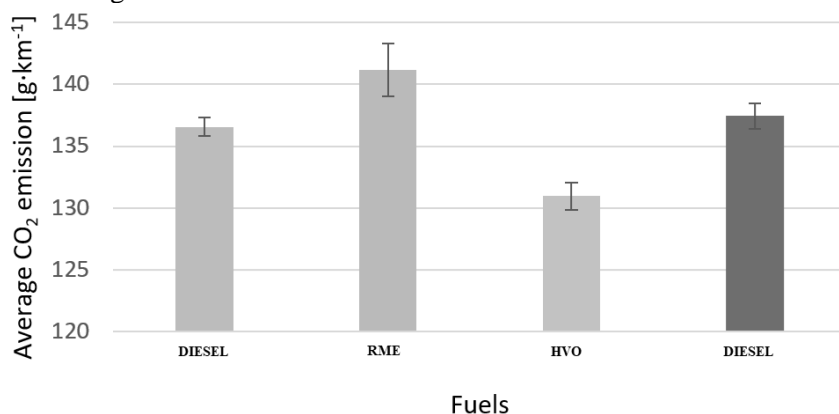

Fig. 3 Emission CO_2

These CO_2 values, as a product of high-quality combustion, correspond to the measured fuel consumption for each fuel. Higher levels of carbon dioxide can also be caused by oxygen, which contains much more fuel than oil and HVO.

The lowest and almost negligible CO emission values were measured at RME, with an average value of $7.710 \cdot 10^{-4}$ g · km^{-1}. This is probably due to the high content of oxygen in RME and therefore its high oxidation (CO_2 generation). Higher values were measured for diesel and HVO, which are probably due to the absence of oxygen in both fuels. The CO emission differences were very low when using diesel as compared to HVO see on Fig. 4. To the same conclusion was reached by the authors (*Millo, Debnath, Vlachos, Ciaravino, Postrioti & Buitoni, 2015*), in their publication they write: CO and HC specific emissions were significantly reduced with both RME and HVO blends. This behavior was more evident for the HVO, likely due to the better ignition quality of this fuel.
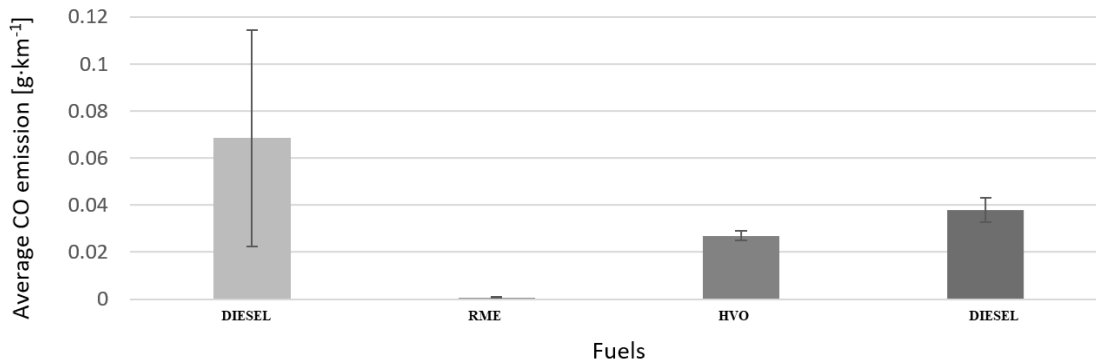

Fig. 4 Emission CO

However, the average CO emission value for diesel distorted one measurement during which the catalyst catalyst was regenerated. This phenomenon has dramatically increased the instantaneous concentrations of most measured emission gases, with the highest increase being measured for CO emissions, which is approximately 7 times the average of the measurable values.

Differences in NO_x production were recorded between HVO and diesel very small, averaging 0.009 g per cycle. Higher values were found for RME for which the average value of this emission was 0.224 g, ie about 0.06 g · km^{-1} more. This may be due to a higher rate of pressure wave propagation in RME than diesel, which typically causes earlier injections of conventional engines, and thus earlier ignition, which may be associated with higher oxygen content in fuel due to higher NO_X emissions, see on Fig. 5.

Authors (*Millo, Debnath, Vlachos, Ciaravino, Postrioti & Buitoni, 2015*) in their study report write that (Millo, Debnath, Vlachos, Ciaravino, Postrioti & Buitoni, 2015) NOx emissions of HVO fuel were generally comparable with of diesel fuel. Most studies for example *(Hajbabaei, Johnson, Okamoto, Mitchell, Pullman & Durbin, 2012)* have shown that HVO generally reduces NOx emissions compared to conventional diesel fuel and biodiesel.
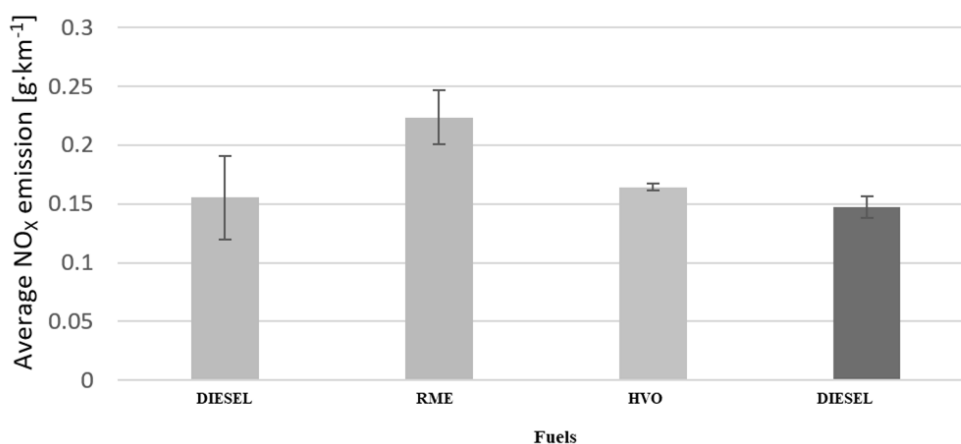

Fig. 5 Emission NO_x

The fuel consumption ratios correspond to their calorific values. Most fuel (540 g) per NEDC cycle was therefore consumed on average when the car is running on RME (calorific value 37.2 MJ · kg⁻¹) About 72 grams less consumed the vehicle while running on diesel (calorific value 43.1 MJ · kg⁻¹) and the lowest consumption was achieved with HVO (calorific value 44.1 MJ · kg⁻¹) by 86 g less than RME, see on Fig 6.
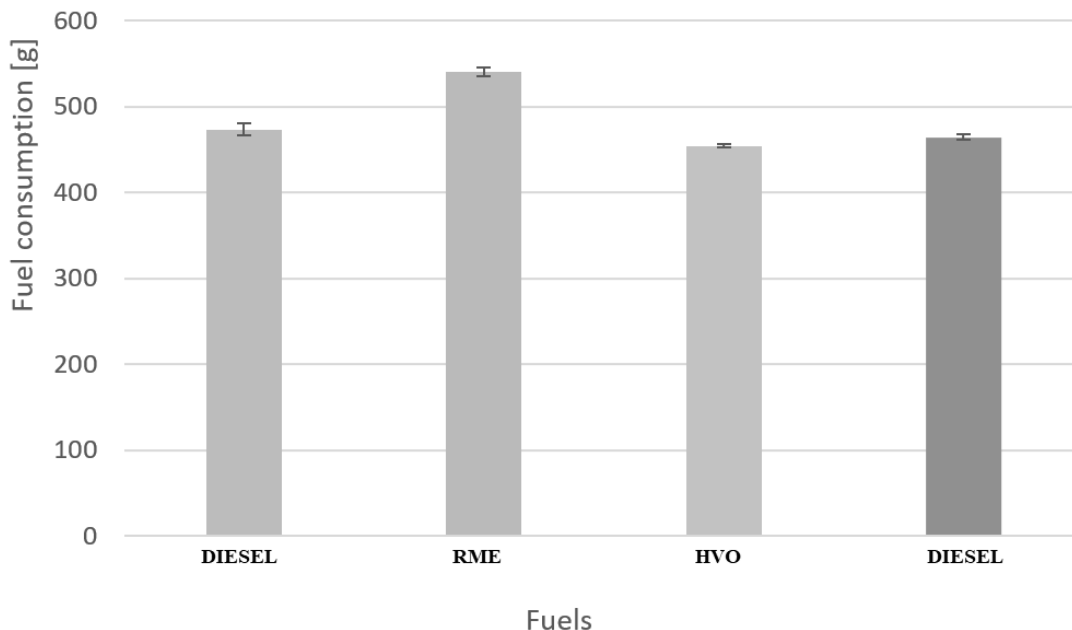

Fig. 6 Fuel consumption per NEDC cyklus

The review of the authors *(Chauhan, Singh, Cho & Lim, 2016)* shows that similar biofuels generally cause an increase in NOx emission and a decrease in CO emissions compared to diesel. HVO has potential advantages with respect to both petrodiesel and biodiesel in terms of production costs, exhaust emissions and adaptability to current engine designs. In the case of renewable diesel, all regulated emissions as well as fuel consumption can be reduced write *(Soo-Young No, 2014)*.

CONCLUSIONS

In the practical part, the effect of the rapeseed oil methyl ester (RED) and hydrogenated vegetable oil on the gaseous emissions and fuel consumption of the Škoda Rapid 1,6 TDI passenger car was evaluated, using diesel fuel as the reference fuel. In total, the smallest amount of the most significant greenhouse gases, CO_2, N_2O and CH_4, produced a test vehicle during the NEDC driving cycle when operating on HVO. Compared to RME, CO_2 emissions averaged about 10 g · km⁻¹ were lower. Similar to slightly higher values than HVO were recorded when running on diesel fuel. In spite of the lowest measured N_2O values for RME, this biofuel appears to be least environmentally friendly in terms of greenhouse gas production. As far as fuel consumption is concerned, the lowest values (about 464 g · km⁻¹) were measured during HVO operation, again very similar to diesel operation (454 g · km⁻¹). With RME, fuel consumption was around 540 g · km⁻¹, which is probably due to its lower calorific value compared to the other two fuels tested.

From the point of view of emissions and fuel consumption, HVO appears to be a good substitute for petroleum naphtha, showing similar and somewhat better properties than this fossil fuel. Another advantage of HVO compared to RME is the possibility of its production from non-food raw materials, which does not affect food prices and does not require the cultivation of extensive monocultural areas degrading the quality of the soil. Some biofuels appear to be a good alternative, sometimes a substitute for fossil fuels. After the depletion of oil stocks, they are likely to play a major role in the transport sector, with transport being further shuffled between alternative drives than before, eg electric drives and hydrogen fuel cells.

The results of the study *(Pexa, Čedík & Pražan, 2016)* also show that biofuels are significantly affected by the combustion engine pollutants. Especially biofuels containing the HVO or butanol exhibit lower smokiness and up to 40% less NO_x production.

ACKNOWLEDGMENT

REFERENCES

1. Bae, C. & Kim, J. (2017). Alternative fuels for internal combustion engines. *Proc. Combust. Inst., 36*(3), 3389–3413.

2. Directive 28/2009/CE of the European Parliament and of the Council. (2009).

3. Dockery, D. W., Schwartz J., & Spengler, J. D. (1992). Air pollution and daily mortality: associations with particulates and acid aerosols. *Environ Res, 59*, 362-70.

4. Goyal, P., Jaiswal, N., Kumar, A., Dadoo, J. K., & Dwarakanath, M. (2010). Air quality impact assessment of NOx and PM due to diesel vehicles in Delhi. *Transp Res Part D: Trans and Environ*, *15*, 298-303.

5. Hajbabaei, M., Johnson, K. C., Okamoto, R. A., Mitchell, A., Pullman, M., & Durbin,T. D. (2012). Evaluation of the impacts of biodiesel and second generation biofuels on NOx emissions for CARB diesel fuels. *Environ Sci Technol*, *46*, 9163-9173.

6. Chauhan, B. S., Singh, R. K., Cho, H. M., & Lim, H. C. (2016). Practice of diesel fuel blends using alternative fuels: A review. *Renewable and Sustainable Energy Reviews, 59,* 1358-1368.

7. Jacobson, M. Z. (2001). Global direct radioactive forcing due to multicomponent anthropogenic and naturals aerosols. *J of Geophys Res*, *106*, 1551-68.

8. Koch, D. (2011). Transport and direct radiative forcing of carbonaceous and sulphate aerosols in the GSISS GCM. *J of Geophys Res*, 106:203, 11-32

9. Millo, F., Debnath, B. K., Vlachos, T., Ciaravino, C., Postrioti, L., & Buitoni, G. (2015). Effects of different biofuels blends on performance and emissions of an automotive diesel engine. *Fuel*, *159*, 614-627.

10. Mužíková, Z., Pospíšil, M., & Šebor, G. (2010). Využití bioethanolu jako pohonné hmoty ve formě paliva E85 (in Czech). In *Chem. List*. (pp. 677–683).

11. No, S-Y, (2014). Application of hydrotreated vegetable oil from triglyceride based biomass to CI engines – A review. *Fuel, 115*, 88-96.

12. Pexa, M., Čedík, J., & Pražan, R. (2016). Smoke and NOx emission of combustion engine using biofuels. *Agronomy Research*, *14*(2), 547-555.

13. Pourazar, J, Frew, A. J., Blomberg, A., Helleday, R., Kelly, F. J., & Wilson, S. (2004). Diesel exhaust exposure enhances the expression of IL-13 in the bronchial epithelium of healthy subjects. *Respir Med*, *98*, 821-25.

14. Šimáček, P., Vrtiška, D., Mužíková, Z. & Pospíšil, M. (2017). Motorová paliva vyráběná hydrogenací rostlinných olejů a živočišných tuků (in Czech). In *Chem. List.*, (pp. 206–212).

Corresponding author:
Ing. Jakub Mařík, Ph.D., Department of Vehicles and Ground Transport, Faculty of Engineering, Czech University of Life Sciences Prague, Kamýcká 129, Praha 6, Prague, 16521, Czech Republic, phone: +420 22438 3112, e-mail: marikj@tf.czu.cz

RESEARCH ON ENGINE POWERED WITH A MIXTURE OF DIESEL OIL AND BIOCOMPONENT AT CHANGE OF FUEL INJECTION SETTINGS

Marietta MARKIEWICZ[1], Jerzy KASZKOWIAK[1]

[1]UTP University of Science and Technology, Faculty of Mechanical Engineering, Al. prof. S. Kaliskiego 7, 85-796 Bydgoszcz

Abstract
The basic fuel for powering engines with self-ignition is the diesel oil, the basic components of which are the products of crude oil's processing. The energy situation prevailing in the world (increase of prices and the decreasing natural resources) resulted in the return to the renewable fuels' concept. The design solutions of the drive units allow for their powering with diesel oil and biocomponent's mixture, due to the similar physio-chemical properties. In the work there are presented studies of the drive unit powered with the mixture of 70% of diesel oil and 30% of fatty acid methyl esters. In the subject matter of the studies, modifications were made in the settings of the fuel injection controller in order to fin dan optimum setting which would make it possible to obtain high effectiveness of the drive unit in case of the mixture's change.

Key words: transport; environment protection; engine with self-ignition; biofuels; effectiveness of an engine; means of transport; working machines.

INTRODUCTION

Protection of the natural environment and of fossil planet's resources, is one of the most important problem taken up by authorities and society. Additives of fatty acids methyl esters to the diesel oil accepted by the European Union, make it possible to reduce consumption of the fossil energy resources. The European Union planned normalization of energy consumption by 2020 within the frames of the ecological commitments *(Ministry of Economy, 2009)*.

The forecasts of the European Union point at the increased share of diesel oil in the transport section and keeping up of the constant consumption as the engine fuel. Release of the market from the supplies of the petroleum-derived fuels is the argument for resuming the idea of plant fuels. Plant oils are the ones which have the broadest application as far as production of biofuels is concerned. Among the renewable fuels of plant origin, there may be singled out the following ones: rape oil, soybean oil, sunflower oil, arachis oil and animal fats *(Bajor K. & Biernat K., 2011)*. The listed fuels of plant origin, commonly called biofuels, have to be exposed to chemical processes in order to obtain physio-chemical properties similar to the ones of the diesel oil. Because of technical, economical, design and technological reasons, the most often used oil is the rape oil, which is exposed to the process of chemical treatment in order to adopt it for self-ignition engines' powering *(Uzdowski M., 2006; Uzdowski M., 2008)*. Reliability of the means of transport and agricultural machines, to a big extend depends on the properties of fuels they are powered with *(Markiewicz-Patalon M., Muślewski M. & Kaszkowiak K., 2018; Markiewicz-Patalon M., et al., 2018)*. Application of transesterified plant oil as an additive to the diesel oil, makes it possible to improve the lubricating properties of fuel and extends the engine's life *(Dzieniszewski G., 2015)*. Additive of biocomponent in the volume provided for in the Directive of the European Union, has the physio-chemical properties similar to the diesel oil. Only the increase of the share of biocomponent in the diesel oil by 30%, shall result in visible differences in the fuel's structure *(Markiewicz-Patalon M. & Kaszkowiak K., 2017; Markiewicz-Patalon M., et al., 2017)*.

On the efficient and ecological engine's operation, apart from the fuel there also has an impact its design that is the systems co-operating with each other. The process of combustion in engines with self-ignition, depends on the correctly prepared air-fuel mixture, characterised by even concentration of fuel in the whole space of the combustion chamber and fuel's fragmentation into drops of the diameter as small as possible *(Luft S., 2011)*. On the fuel combustion's process, there also have the design and performance factors of the drive unit, such as *(Włodarski J., 1982)*: material of a piston, compression degree, the engine's supercharging, design of a combustion chamber, fuel injection's parameters, the angle of the injection advance, composition of a combustible mixture, the engine's loading and the engine's

rotational speed. The systems of the self-ignition engine's powering may be divided into the systems controlled electronically and mechanically. Electronic controlling in these engines is used mainly because of the possibilities of interference in the course of the fuel's injection and its precise control *(Lotko W., 1995)*. Change of the injection's course allows to increase the engine's efficiency.

The aim of the study was to analyze the operational parameters of the self-ignition engine powered by a blend of diesel and fatty acid methyl esters.

MATERIALS AND METHODS

The subject matter of the studies was the engine with self-ignition, which has been widely used in the motor transport and working machines. The technical data of a drive unit used in the studies, are presented in the table 1.

Tab. 1 Technical data of a drive unit

swept capacity [cm^3]	1560
motor capacity [KM]	110
maximum turning moment [Nm]	240
number of cylinders	4
type of injection	direct, Common Rail
injectors	electromagnetic
supercharging	Turbo-compressor

The tested engine is presented in the drawing 1. The driving unit mates with dual-mass flywheel and a turbo-compressor of variable blades' geometry, what has an impact on the increase of the generated engine's performance.

Fig. 1 The driving unit used in the tests

The material under investigation was the mixture of 70% of diesel oil and 30% of fatty acid methyl esters. The fatty acid methyl esters are the plant oils put through to the transesterification process that is the exchange of the chemically bounded glycerin in triacylglycerol's particle into added methyl alcohol in the presence of basic or acid catalysts, which commonly are called biocomponents.

Modification of the engine's electronic system were conducted during the tests, by modification of the computer's driving unit factory software. The purpose of the introduction of the changes in the injection controller's settings was to find out if and how the values of the vehicle's performance parameters change. Because of the specificity of a vehicle's electronic system, disassembly of a dive computer and introduction of changes in the software on a special stand, was required each time. Prior to introduction of the changes in computer software, a diagnostic measurement was conducted in order to establish the possibility and rationality of the engine parameters' increase. Modifications in the vehicle's software consisted in the increase of the fuel dope by 2% and air supercharging by 50 hPa. Also the factory's settings were tested in order to relate the results obtained at the time of conducted modifications. The

injection maps which came into being after the conducted modifications of the fuel injection controller's settings, are presented in the drawings 3 and 4.
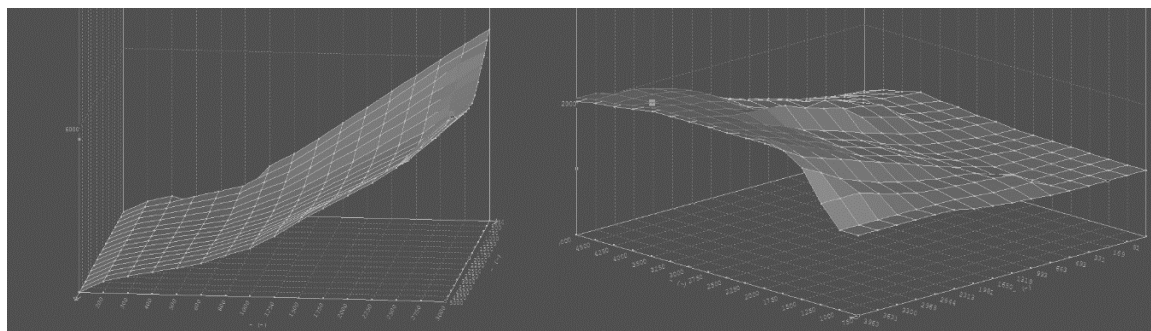

Fig. 3 Injection map for a fuel dope of 2%   **Fig. 4** Injection map for air supercharging 50 hPa

The conducted studies concerned the values of the performance parameters of a driving unit powered with a mixture of diesel oil and the fatty acid methyl esters, at variable settings of the fuel injection's controller. The measurement also covered such parameters as: power, turning moment, emission of noise generated by the engine and the volume of solid particles in exhaust gas.

The studies were conducted with the use of load chassis dynamometer with an eddy current brake. The chassis dynamometer made it possible to obtain the data necessary to determine the characteristics of the driving unit's performances just as power and turning moment *(Kolator B., & Janulin M., 2014; Kołodziej E., & Skrzyniowski A., 2012)*. The device measured the turning moment turned over to the crankshaft and calculated the engine's power based on the value of the turning moment and the rotational speed of the crankshaft *(Michalski R., Gonera J., & Janulin M., 2012)*. The air humidity, changes in the atmospheric pressure and the air temperature had an impact on that measurements. The purpose of conducting the tests on the load chassis dynamometer there were the following: checking of the parameters reached by the driving unit assembled in a vehicle, measurement of the engine's parameters following the changes in the settings of the fuel injection controller, checking of the values of the noise emission's values and solid particles with the use of additional analysers. The chassis dynamometer used in the tests, is presented in the draving 5. The measurement of the solid particles occurred with an optical method, with the use of a solid particles' analysed MPM-4, presented in figure 6. That method consisted in checking of the intensity of the light beam going through the stream of exhaust gas *(Peterson C., et al., 2000)*. The solid particles coming into being at the time of fuel's combustion in self-ignition engines, are the coal particles and smaller particles absorbed by it that is carbon black *(Pelkmans L., & Debal P., 2006)*. The analyser, took the samples of exhaust gas with the use of an instrument stalk, which was exposed to the laser action. Then, with the use of a dispersed light's detector, the measurement of the volume and concentration of solid particles was conducted.

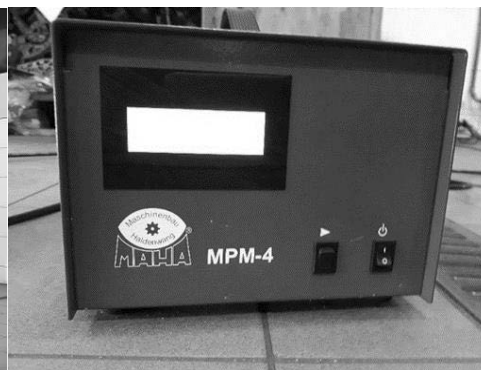**Fig. 5** Chassis dynamometer   **Fig. 6** Solid particles' analyser

The experiment was conducted in order to determine the engine's performance parameters for three settings of the fuel injection's controller. The examinations were conducted in the laboratory's environment, with the use of a load chassis dynamometer, which simulated the road conditions. Preparation of the object of the studies for the experiment, consisted in fastening of the vehicle on the dynamometers with belts, heating up of the driving unit and connection of all the necessary instrument stalks. Before staring of the measurements, the engine was heated up to the temperature of 85°C for cooling liquid. Each measurement of the performance parameters of the examined driving unit was conducted 30 times in the conditions of the maximum engine's loading.

RESULTS AND DISCUSSION

Based on the conducted literature's analysis, the performance parameters of a driving unit powered with the mixture of a diesel oil and fatty acid methyl esters, the values of which were analysed. The analysis concerned also such parameters as: power, turning moment, noise and solid particles. The analysis concerned 30 measurements of the selected values of the driving unit powered with the mixture of 70% of diesel oil and 30% of fatty acid methyl esters, at variable settings of the fuel injection's controller. The values of the basic statistics for the analysed performance parameters of a driving unit and the standard engine's settings, are presented in the table 2.

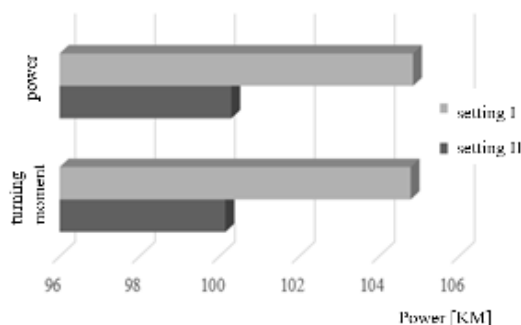**Tab. 2** Statistical analysis of the performance parameters for the setting I

Performance parameters	power [KM]	turning moment [Nm]	noise [dB]	Solid particles [ppm]
Medium value	100.15	233.59	120.8	75.033
Median	100.30	234.35	121.1	75.50
Standard deviation	0.833	2.905	0.764	4.468
Coefficient of variation	0.008	0.012	0.006	0.060
Minimum	96.3	228.3	119.5	68.0
Maximum	100.8	237.6	122.6	85.0

In the table 3 there is presented a statistical analysis of the performance parameters of a driving unit powered with the mixture of 70% diesel oil and 30% of fatty acid methyl esters and the II setting of the fuel injection controller (fuel's dose increased by 2% and air supercharging increased by 50 hPa).

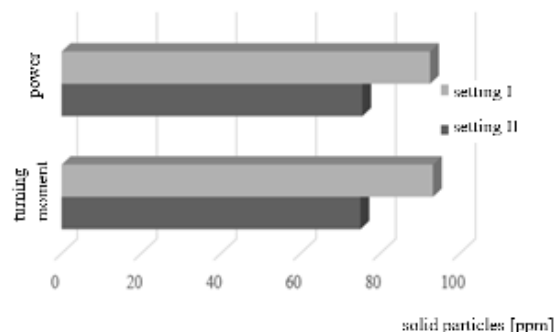**Tab. 3** Statistical analysis of the performance parameters for the setting II

Performance parameters	power [KM]	turning moment [Nm]	noise [dB]	Solid particles [ppm]
Medium value	104.79	241.49	120.52	93.233
Median	104.85	253.90	120.5	92.50
Standard deviation	0.367	0.264	0.344	3.029
Coefficient of variation	0.003	0.001	0.003	0.032
minimum	104.2	241.0	119.9	88.0
maximum	105.5	242.0	121.0	99.0

Measurement of the selected performance parameters was conducted in order to check, how a change of the fuel injection controller's setting influences the driving unit, which is powered with a mixture of 70% of diesel oil and 30% of fatty acid methyl esters. The data from the above table (medium value and median) are presented graphically in figures 7-10.

Fig. 7 Values of power for the setting I and II
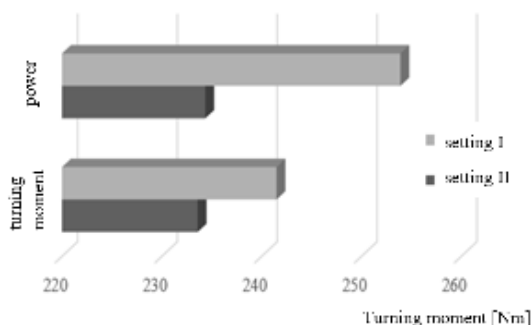
Fig. 8 Values of the turning moment for the setting I and II
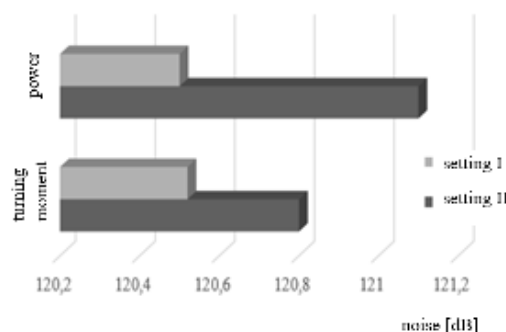
Fig. 9 Values of noise for the setting I and II

Fig. 10 Values of solid particles for the setting I and II

From the statistical analysis of the obtained results of measurements it results, that the change of the fuel injection controller's settings improves the engine's performance and lowering of the volume of solid particles in the exhaust gases. During the studies there was also observed the constant level of noise's emission generated by the driving unit powered with the mixture of 70% of diesel oil and 30% of fatty acid methyl esters.

CONCLUSIONS

Based on the anaysis of the literature and own studies, there have been determined the performance parameters such as: power, turning moment, noise generated by the engine and solid particles included in the exhaust gases *(Agarwal A., et al. 2006, Agarwal A., 2007, Ambrozik A., et al., 2012, Arapski N., et al. 2007, Banapurmath N., 2008, Szlachta Z., 2001)*. Then, the measurement of their value depending on the fuel injection controlling's settings was conducted. The obtained results of the driving unit performance parameters' testing justify the purposefulness of modification of the engine computer's software system. Analysis of the results of the studies, made it possible to determine the number of solid particles formed at the time of combustion of the mixture of 70% of diesel oil and 30% of fatty acid methyl esters at different settings of the fuel injection controller. In the study there are compared two settings: the factory one and the increase dope of fuel by 2% and the increased air supercharging by 50 hPa. It results from the conducted studies, that the change of the fuel injection controller's setting results in the decrease of the solid particles in exhaust gases by 20%. In case of power measurement, there has been noticed the increase by approx. 5%. Emission of noise generated by a driving unit remained on a comparable level. At the time of the conducted studies, there was also observed a higher turning moment for the setting of the increased dope of fuel and the air supercharging, which amounted to about 3%. These were the parameters of power and the turning moment, which proved to be the most sensitive to the change of the fuel injection controller's settings. Studies on the properties of the basic parameters of self-ignition engines fed with mixtures of transesterified vegetable oil and diesel oil were conducted in many centers *(Podolak A., et al. 1998)*. While studying at literary studies, they are not conducted due to

changes in software powered by mixed diesel and ester oil. Engine parameters are available in the literature *(Agarwal A., et al. 2013, Arapaki N., et al. 2007, Armas O., et al. 2010)*.

REFERENCES

1. Agarwal, A. D., Sinhab, S., & Agarwal, A. K., (2006). Experimental investigation of control of NOx emission in biodiesel-fueled compression ignition engine. *Renewable Energy, 31*.

2. Agarwal A. K. (2007). Biofuels (alcohols and biodiesel) applications as fuels for internal combustion engines. *Progress in Energy and Combustion, 33*.

3. Agarwal, A. K., Srivastava, D. K., Dhar, A., Maurya, R. K., Shukla, P. CH., & Singh, A. P. (2013). Effect of fuel injection timing and pressure on combustion, emissions and performance characteristics of a single cylinder diesel engine. *Fuel, 111*.

4. Ambrozik, A., Ambrozik, T., Kurczyński, D., & Łagowski, P. (2012). Ocena sprawności silnika ZS zasilanego biopaliwami, Autobusy-technika, eksploatacja, systemy transportowe.

5. Arapaki, N,, Bekeas, E., Karavalakis, G., Tzirakis, E., Stournas, S., & Zannikos, F., (2007). Regulated and unregulated emission characteristics of diesel vehicle operating with diesel biodiesel blend. *SAE Technical Paper, No 1*.

6. Armas, O., Yehliu, K., & Boehman, A. (2010). Effect of alternative fuels on exhaust emission during diesel engine operation with matched combustion phasing. *Fuel, 89*.

7. Bajor, K., & Biernat, K. (2011). Biopaliwa jako alternatywne nośniki energii w silnikach spalinowych, klasyfikacja i perspektywy rozwoju. *Archiwum Motoryzacji, nr 1*.

8. Banapurmath, N., Tawari, P., & Hosmath, R. (2008). Pperformance and emission characteristics of a DI compression ignition engine operated on Honge, Jatropha And sesame oil methyl esters. *Renewable Energy, 33*.

9. Kolator, B., & Janulin, M. (2014). Wyznaczanie stanów trakcyjnych pojazdu za pomocą hamowni podwoziowej LPS3000. *Studies and Proceedings of Polish Association for Knowledge Management, nr 68*.

10. Kołodziej E., & Skrzyniowski A. (2012). Badania diagnostyczne samochodów na hamowni podwoziowej Autodyn 30. *Mechanika, Politechnika Krakowska 10*(109).

11. Lotko, W. (2008). *Rozwój układów zasilania silników wysokoprężnych*. Radom: Politechnika Radomska.

12. Luft, S. (2011). *Podstawy budowy silników*. Warszawa: Wydawnictwo Komunikacji i Łączności.

13. Markiewicz-Patalon, M., Kaszkowiak, E., Zbytek, Z., & Szymczak, M. (2017). Comparison of Calorific Values of Petroleum-Driver Fuels with Alternative Fules of Vegetable Origin. In *Proceedings of 58th International Conference of Machine Design Departments* (pp. 222-225). p-ISBN 978-80-213-2769-6.

14. Markiewicz-Patalon, M., Muślewski, Ł., Kaszkowiak, J., & Knopik, L. (2018). Analysis of selected operating parameters of engine powered by a mixture of biocomponents and diesel oil. *Jurnal of Kones Powertrain and Transport, 25*(4). ISSN 1231-4005.

15. Markiewicz-Patalon, M., Muślewski, Ł., Kaszkowiak, J., & Sójka, M. (2018). Analysis of efficiency of the vehicle transport facilities powered with diesel oil with additive of biocomponent. Kraków: KONMOT.

16. Markiewicz-Patalon, M., Muślewski, M., Kaszkowiak, J., & Landowski, B. (2017). Assessment of the suitability of the fuels with component power engines. *Jurnal of Kones Powertrain and Transport, 24*(4). p-ISSN: 1231-4005.

17. Michalski, R., Gonera, J., & Janulin, M., (2012). Wyznaczanie charakterystyki zewnętrznej ciągnika kołowego z wykorzystaniem przenośnej hamowni intercyjnej. *Postępy Nauki i Techniki, nr 14*.

18. Ministerstwo Gospodarki. (2009). Polityka energetyczna Polski do 2030 roku. Projekt z dnia 15-07-2009. Warszawa.

19. Pelkmans, L. & Debal, P. (2006). Comparison of on-road emission with emissions measured on chassis dynamometer test cycles. *Transportation Research, 11*.

20. Peterson, C., Toberski, J., Thompson, J., & Chase, C. (2000). The effect of biodiesel feedstock on regulated emission in chassis dyna-

mometer tests of a pickup truck. *American Society of Agricultural of Biological Engineering, 43*(6).

21. Podolak, A., Petransky, I., Zikla, A., & Finorowa, J. (1998). Prewadzkove a ekologicke vlastnosti biopaliw z repky ozimnej. *Acta Technologica Agriculturae*. Slovaca Universitas Agriculturae Nitriae.

22. Szlachta, Z., & Cisek, J. (2001). The Autoignition Delay of Vegetable Fuels at Veried Air Temperatures Inside Combustion Chamber of Diesel Engine. Nitra: Agrotech.

23. Uzdowski, M. (2006). Możliwości wykorzystania mieszanin paliw tradycyjnych i alternatywnych do zasilania silników ZS. *Motrol, nr 8A*.

24. Uzdowski, M. (2008). Problematyka wykorzystania paliw alternatywnych do zasilania silników trakcyjnych. *Motrol, nr 10*.

25. Włodarski, J. (1982). Tłokowe silniki spalinowe- procesy trybologiczne. Warszawa: Wydawnictwo Komunikacji i Łączności.

Corresponding author:
mgr inż. Marietta Markiewicz, UTP University of Science and Technology, Faculty of Mechanical Engineering, Al. prof. S. Kaliskiego 7, 85-796 Bydgoszcz, e-mail: marmar000@utp.edu.pl
dr inż. Jerzy Kaszkowiak UTP, UTP University of Science and Technology, Faculty of Mechanical Engineering, Al. prof. S. Kali-skiego 7, 85-796 Bydgoszcz, e-mail: jerzy.kaszkowiak@utp.edu.pl

ANALYSIS OF TOXIC COMBUSTION COMPONENTS OF THE DIESEL ENGINE POWERED WITH A BLEND OF DIESEL FUEL AND BIODIESEL

Marietta MARKIEWICZ[1], Łukasz MUŚLEWSKI[1]

[1] UTP University of Science and Technology, Faculty of Mechanical Engineering, Al. prof. S. Kaliskiego 7, 85-796 Bydgoszcz

Abstract

One of the most important problems for road transport is environmental protection. A way to reduce the emission of toxic components of exhaust gases emitted by engines and to reduce the consumption of fossil energy sources is to use fuel from renewable sources. The most popular alternative fuel are fatty acid methyl esters, which are used as an additive to diesel fuel. The paper presents a study of toxic products of fuel combustion in diesel engines fuelled with a blend of 70% diesel fuel and 30% fatty acid methyl esters. The conducted tests allowed to determine the quantitative content of toxic products of combustion of the tested blend in comparison to diesel fuel.

Keywords: *transport; environmental protection; diesel engine; compression-ignition engine; biofuels; means of transport; toxic components of exhaust gases.*

INTRODUCTION

The use of alternative fuels to supply internal combustion piston engines is associated with high demand and dwindling natural resources. The first compression-ignition engine developed by Rudolf Diesel was fuelled with peanut oil. Only after the development of oil refining technology did it become clear that diesel is a much more versatile fuel for diesel engines. The advantages of diesel fuel are its good lubricating properties, its viscosity of 2.0-4.5 mm²*s-1 and its high cetane number, which testifies to the engine's ability to self-ignite *(Zając P., 2009).* Despite the superiority of petroleum fuels over vegetable fuels, the concept of supplying combustion engines with alternative fuels was reinstated for environmental reasons. The fuel with intermediate parameters between vegetable oil and diesel fuel turned out to be methyl esters of fatty acids *(Piętak A., Radkowski S., 2006).* FAME (pure fatty acid methyl esters), commonly referred to as biodiesels or biocomponents, are the most popular alternative fuel used to fuel diesel engines. They are most often used as an additive to diesel fuel.

Since 2003, in accordance with the decision of the European Union, biodiesels have been used as a mandatory additive to marketed diesel fuel. The basic legal act which determined the development of the biofuel market was Directive 2003/30/EC (Official Journal of the European Union L 123), which obliged, out of concern for environmental protection, EU member states to participate in the share of fatty acid methyl esters in transport fuels in the minimum amount of 5.75%. In 2009, the regulations were amended by introducing by the European Parliament the Directive 2009/28/EC, which imposes an obligation to share 10% of biofuels in the transport sector by the end of 2020 (Official Journal of the European Union L 140). The Directive also sets out sustainability criteria for the classification of biofuels as renewable energy sources. In the record of development in the liquid biofuels market, the criterion concerning the reduction of greenhouse gas emission in relation to conventional fuels is also taken into account. The level of 35% was expected to be reached by the end of 2017 and then gradually increase to 50%. The transposition of the Directive on the promotion of renewable energy sources in the Member States of the European Union was to take place on 5 December 2010 and ensure an increase in the share of renewable energy sources.

Fuel properties have a major impact on the combustion process and reliability of the facility in operation *(Markiewicz-Patalon M., et al., 2018; Markiewicz-Patalon M., et al., 2018).* The addition of biodiesel to the diesel fuel improves lubricating properties, extends engine life and emits negligible amounts of sulfur. There are also complications associated with the use of the biofuels, such as obtaining a high cetane number, the solubility of plastics, changes in physical properties and viscosity due to temperature increase *(Dzieniszewski G., 2015).* The blend of diesel fuel with 10% biodiesel has physical and chemical properties similar to diesel fuel *(Markiewicz-Patalon M., et al., 2017; Markiewicz-Patalon M., et al., 2017).* The basic properties of both fuel blends are presented in Table 1.

Tab. 1 Properties of diesel fuel and biodiesel blend

Characteristics of blends	BIODIESEL BLEND	DIESEL FUEL
Viscosity [mm² $\cdot s^{-1}$]	3.5-5.0	2.0-4.5
Sulfur content [mg $\cdot kg^{-1}$]	≤ 10	≤ 350
Density [$g \cdot cm^{-3}$]	0.86-0.90	0.82-0.845
Cetane number	≥ 47	≥ 51
Particulate content [$mg \cdot kg^{-1}$]	≤ 24	≤ 24
Water content [$mg \cdot kg^{-1}$]	≤ 500	≤ 200
Carbon residue [%]	≤ 0.3	≤ 0.3
Ignition point [°C]	≥ 101	≥ 55

Additional supply of combustion engines with biodiesel blends reduces the emission of toxic components of exhaust gases such as carbon oxides, hydrocarbons and particulate matter *(Agarwal A. K., et al., 2013; Arapaki N., et al., 2007; Armas O., et al., 2010; Bala B.K., 2005; Choi S., Oh Y., 2006; Dzieniszewski G., 2009; Fontaras G., et al., 2009; Knothe G., et al., 2006; Lapuerta M., et al., 2008; Leung D., et al., 2006).* The exception is nitrogen oxides, which show an increase of several percents in relation to pure diesel fuel *(Merkisz J., Kozak M., 2003).*
The aim of the study was to determine the toxic components contained in the splanons of the propulsion unit of the transport vehicle powered by blends of diesel oil and fatty acid methyl esters.

MATERIALS AND METHODS
The material used in the tests was a blend of 70% of diesel fuel and 30% of fatty acid methyl esters (Blend I) and diesel fuel without biodiesel (Blend II) presented in Figures 1 and 2.

Fig. 1 Blend I   **Fig. 2** Blend II

The conducted tests covered the measurement of performance parameters of the engine fuelled with these blends. The measurement included the composition of exhaust gases and the content of particulate matter in exhaust gases. The measurement of the toxicity of exhaust gases included such compounds as oxygen (O2), carbon monoxide (CO), carbon dioxide (CO_2), hydrocarbons (HC) and nitrogen oxide (NO2).
The tests were conducted on an 81 kW diesel engine with Common Rail direct fuel injection and electromagnetic injectors, which is shown in Figure 3. The engine used in the tests was not equipped with a diesel particulate filter.

Fig. 3 The engine used in the tests

In order to efficiently replace the fuel supplying the engine, modifications to the fuel supply system have been made. The adaptation of the engine fuel supply system has not introduced any changes to the design of the engine, but only covered its accessories. The modifications included the installation of an external fuel tank and disconnecting the fuel supply from the factory tank installed in the vehicle. No additional fuel filters or fuel pump were installed in the engine. The fuel supply system was connected directly to the external tank and the engine. During the study, standard filters for the engine model were used. Excess fuel from the engine supply system returned to the external tank by means of a return line. After changing the fuel from diesel fuel to a blend of 70% diesel fuel and 30% fatty acid methyl esters, the engine ran for about 10 minutes at idle to remove the residues of the previous fuel from the fuel filter and fuel supply system.

The experiment was conducted to determine the engine performance parameters for two tested blends. The tests of these parameters were performed in the laboratory environment with the use of a chassis dynamometer simulating road conditions. The preparation of the object for the experiment was in accordance with the recommendations of the dynamometer manufacturer. In addition, only probes to measure the components of exhaust gases and particulates have been installed. Prior to each measurement, the engine was warmed up to 85 °C of coolant.

The measurement of the concentration of toxic components in exhaust gases was performed with the use of a diagnostic method, which made it possible to determine the quantitative content of components emitted into the environment in the form of exhaust gases. The measurement with the MGT-5 exhaust gas analyzer included the quantitative determination of the volumetric compositions of particular components in the exhaust gas. The view of the toxic exhaust gas analyzer is shown in Figure 4. The exhaust gas analyzer used for the tests met the requirements of the European Parliament and Council Directive 22/2004/EC. During the test, the analyzer was controlled from a PC. The measurement of carbon dioxide, carbon monoxide and hydrocarbons contained in exhaust gases are performed in the form of infrared radiation of exhaust gases, while the measurement of oxygen is performed by electrochemical method.

Fig. 4 MGT-5 exhaust gas analyzer

Particulate emissions were measured using the optical method with the MPM-4 analyzer, shown in Figure 5. The measurement method consisted in measuring the intensity of the light beam passing through the exhaust gas stream *(Pelkmans L., Debal P., 2006)*. The particulate matter produced during fuel combustion in diesel engines is carbon particles and smaller particles absorbed by carbon, i.e. soot *(Peterson C., et al., 2000)*. The analyzer took a sample of the exhaust gas through a measuring probe, which was exposed to a laser. Then, using the scattered light detector, the size and concentration of particulate matter were measured.

Fig. 5 MPM-4 particulate matter analyzer

Each measurement of the performance parameters of the tested engine was carried out 30 times under maximum load.

RESULTS AND DISCUSSION

On the basis of the literature analysis, evaluation criteria for a diesel engine fuelled with a blend of diesel fuel and fatty acid methyl esters have been established. In this study, performance parameters important for environment protection were featured. The following parameters were analyzed: carbon monoxide (CO), carbon dioxide (CO_2), oxygen (O_2), hydrocarbons (HC), nitrogen oxide (NO_2) and particulate matter (PM). The analysis included 30 measurements of selected values of performance parameters of a diesel engine for diesel fuel (Blend I) and blend of 70% diesel fuel and 30% fatty acid methyl esters (Blend II). The main statistical values of the analyzed performance parameters of the diesel engine fuelled with diesel fuel are presented in Table 2.

Tab. 2 Mean values of test results for blend I

Material	CO [% vol.]	CO_2 [% vol.]	O_2 [% vol.]	HC [ppm]	NO_2 [ppm]	PM [ppm]
Mean value	0.13	11.96	17.29	51.46	227.23	95.93
Median	0.11	12.0	17.09	43.5	227.5	96.0
Standard deviation	0.071	0.384	0.694	19.937	12.983	2.249
Coefficient of variation	0.546	0.032	0.04	0.387	0.057	0.023
Minimum	0.04	11.2	16.21	30.0	196	92.0
Maximum	0.43	12.9	18.47	88.0	251.0	99.0

Table 3 presents a statistical analysis of performance parameters of a diesel engine fuelled with a blend of 70% diesel fuel and 30% fatty acid methyl esters.

Tab. 3 Mean values of test results for blend II

Material	CO [% vol.]	CO_2 [% vol.]	O_2 [% vol.]	HC [ppm]	NO_2 [ppm]	PM [ppm]
Mean value	0.068	11.88	10.24	9.033	237.76	75.03
Median	0.04	9.0	9.98	9.0	236.5	75.5
Standard deviation	0.065	0.325	2.069	0.546	16.132	4.468
Coefficient of variation	0.957	0.027	0.202	0.061	0.068	0.06
Minimum	0.04	11.3	6.96	8.0	207.0	68.0
Maximum	0.28	12.7	18.98	10.0	283.0	85.0

The measurement of exhaust gases and particulate matter was performed in order to determine the quantitative content of toxic components for a diesel engine fuelled with a biodiesel blend. Data from the table (mean and median values) are presented graphically in Figures 6-7.
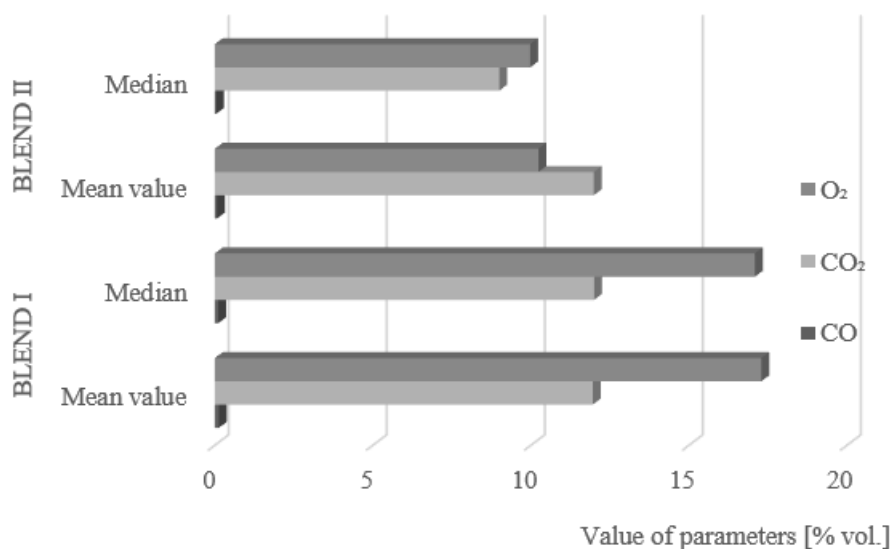

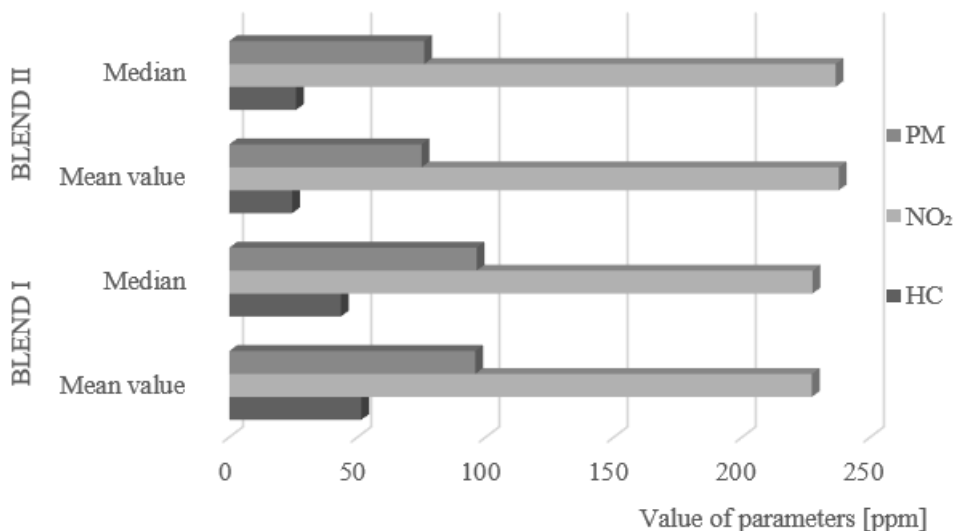**Fig. 6** Performance parameter values for engine

Fig. 7 Performance parameter values for engine

Statistical analysis of the obtained results of measurement of harmful substances in exhaust gases shows that the addition of methyl esters of fatty acids affects the concentration of individual components of exhaust gases. There is a decrease in carbon dioxide, oxygen, and hydrocarbons. During the tests, we also observed an increase in nitrogen oxides and a constant level of carbon oxides, which did not change depending on the changes in the blend supplying the engine. As other authors have pointed out, feeding diesel engines with methyl esters of fatty acids reduces the emission of toxic impurities of exhaust components, such as carbon oxides, hydrocarbons and solid particles *(Agarwal A. K., et al., 2013; Arapaki N., et al., 2007; Armas O., et al., 2010; Choi S., Oh Y., 2006; Fontaras G., et al., 2009; Knothe G., et al., 2006; Lapuerta M., et al., 2008)*. The exception is nitrogen oxides, showing an increase of a dozen or so percent over pure diesel.

CONCLUSIONS

On the basis of literature analysis and own study, performance parameters such as particulate matter in exhaust gases and toxic components of exhaust gases such as carbon monoxide, carbon dioxide, oxygen, hydrocarbons, and nitrogen monoxide were determined. Next, the values of these parameters were measured for tested blends. Obtained results of tests of performance parameters of engine justify the advisability of adding methyl esters of fatty acids to diesel fuel. The analysis of the test results allowed to determine the quantitative content of toxic components and particulate matter emitted during the combustion of individual blends. The study compares two blends: diesel fuel and a blend of 70% diesel fuel and 30% fatty acid methyl esters. The tests show that the use of 30% biodiesel additive reduces particulate matter in exhaust gases by about 20%. In the case of toxic components of exhaust gas, a significant increase in nitrogen oxides was noted during the tests, which increased by about 4.5%. Carbon dioxide remained at a similar level. During the tests, a decrease in oxygen and carbon monoxides was also observed. Hydrocarbons were the most sensitive to changes in the blend. Hydrocarbons decreased from 54 ppm to 9 ppm after the addition of biodiesel to diesel fuel.

REFERENCES

1. Agarwal, A. K., Srivastava, D. K., Dhar, A., Maurya, R. K., Shukla, P. CH., & Singh, A. P. (2013). Effect of fuel injection timing and pressure on combustion, emissions and performance characteristics of a single cylinder diesel engine. *Fuel, 111*.

2. Arapaki, N., Bekeas, E., Karavalakis, G., Tzirakis, E., Stournas, S., & Zannikos, F. (2007). Regulated and unregulated emission characteristics of diesel vehicle operating with diesel biodiesel blend. *SAE Technical Paper, No 1*.

3. Armas, O., Yehliu, K., & Boehman, A. (2010). Effect of alternative fuels on exhaust emission during diesel engine operation with matched combustion phasing. *Fuel, 89*.

4. Bala, B.K. (2005). Studies on biodiesels from transformation of vegetable oils for diesel engines. Energy Edu Sci Technol.

5. Choi, S. & Oh, Y. (2006). The emission effects by the use of biodiesel fuel. *International Journal of Modern Physics B., 20*.

6. Directive 2003/30/EC of the European Parliament and of the Council of 8 May 2003 on the promotion of the use of biofuels or other renewable fuels for transport. Official Journal of the European Union L 123.

7. Directive 2009/28/EC of the European Parliament and of the Council of 23 April 2009 on the promotion of the use of energy from renewable sources and amending and subsequently repealing Directives 2001/77/EC and 2003/30/EC. Official Journal of the European Union L 140.

8. Dzieniszewski, G. (2009). Selected ecological and economic aspects of supplying diesel engines with vegetable fuels (in Polish). *Inżynieria Rolnicza, 6(115)*.

9. Dzieniszewski, G. (2015). Ekologiczne problemy biopaliw (Ecological problems of biofuels). *Journal of Civil Engineering, Environment and Architecture*.

10. Fontaras, G., Karavalakis, G., Kousoulidou, M., Tzamkiozis, T., Ntziachristos, L., Bakeas, E., Stournas, S., & Samaras, Z. (2009). Effects of biodiesel on passenger car fuel consumption, regulated and non-regulated pollutant emissions over legislated and real-world driving cycles. *Fuel, 88*(9), 1608-1617.

11. Knothe, G., Sharp, C., & Ryan, T. (2006). Exhaust emission of biodiesel, petrodiesel, neat methyl esters and alkanes in a new technology engine. *Energy and Fuels, 20.*

12. Lapuerta, M., Armas, O., & Rodriguez-Fernandez, L. (2008). Effect of biodiesel fuels on diesel engine emission. *Progress in Energy and Combstion Science, 34.*

13. Leung, D., Luo, Y., & Chan, T. (2006). Optimization of exhaust emission of a diesel engine fuelled with biodiesel. *Energy and Fuels, 20.*

14. Markiewicz-Patalon, M., Kaszkowiak, E., Zbytek, Z., & Szymczak, M. (2017). Comparison of Calorific Values of Petroleum-Driver Fuels with Alternative Fuels of Vegetable Origin. In *Proceedings of 58th International Conference of Machine Design Departments* (pp. 222-225). p-ISBN: 978-80-213-2769-6.

15. Markiewicz-Patalon, M., Muślewski, Ł., Kaszkowiak, J., & Knopik, L. (2018). Analysis of selected operating parameters of engine powered by a mixture of biocomponents and diesel oil. *Journal of Kones Powertrain and Transport, 25*(4). ISNN 1231-4005.

16. Markiewicz-Patalon, M., Muślewski, Ł., Kaszkowiak, J., & Sójka, M. (2018). Analysis of efficiency of the vehicle transport facilities powered with diesel oil with additive of biocomponent. KONMOT, Kraków.

17. Markiewicz-Patalon, M., Muślewski, M., Kaszkowiak, J., & Landowski, B. (2017). Assessment of the suitability of the fuels with component power engines. *Journal of Kones Powertrain and Transport, 24*(4). p-ISSN: 1231-4005.

18. Merkisz, J. & Kozak, M. (2003). Influence of the blend composition of the biofuel and the conventional fuel on exhaust emissions (in Polish). *Eksploatacja i Niezawodność, 3.*

19. Piętak, A. & Radkowski, S. (2006). Wieloaspektowa analiza stosowania paliw alternatywnych w Polsce ze szczególnym uwzględnieniem biopaliw.

20. Pelkmans L. & Debal P. (2006). Comparison of on-road emission with emissions measured on chassis dynamometer test cycles. *Transportation Research, 11.*

21. Peterson C., Toberski J., Thompson J., & Chase C. (2000). The effect of biodiesel feedstock on regulated emission in chassis dynamometer tests of a pickup truck. *American Society of Agricultural of Biological Engineering, 43*(6).

22. Zając, P. (2009). Silniki pojazdów samochodowych. Wydawnictwo Komunikacji i Łączności. Warszawa.

Corresponding author:

Marietta Markiewicz, M.Sc.Eng., UTP University of Science and Technology, Faculty of Mechanical Engineering, Al. prof. S. Kaliskiego 7, 85-796 Bydgoszcz, e-mail: marmar000@utp.edu.pl

Prof. Łukasz Muślewski, Ph.D. (Eng.), UTP University of Science and Technology, Faculty of Mechanical Engineering, Al. prof. S. Kaliskiego 7, 85-796 Bydgoszcz, e-mail: lukasz.muslewski@utp.edu.pl

EVOLUTIONARY ANALYSIS OF AUTONOMOUS AGRICULTURAL VEHICLES

Ivan MAŠÍN[1]

[1]*Department of the Design of Machine Elements and Mechanisms, Technical University in Liberec, Studentska 2, 46117 Liberec, Czech Republic*

Abstract
The article is focused on application of evolution trends theory in the autonomous agricultural vehicles field. Trends of engineering systems evolution describe natural transitions of the engineering system from one state to another, and are generally valid for all engineering disciplines. Knowledge of these trends can more accurately predict the problems associated with the design of new technologies in the agriculture and thus increases the probability of success of the chosen solution.

Key words: *autonomous agricultural vehicles; design; evolution; trends.*

INTRODUCTION

Technology forecasting is a process that is based on the use of appropriate techniques and methods. Traditional techniques are techniques based on experience, assessment and intuition; market research techniques; time series techniques; techniques using regression analysis; other quantitative techniques (*Phaal, Farrukh, & Probert, 2010; Miles, Saritas, & Sokolov, 2016*; *Daim, Pizzaro, & Talla, 2014*). Information input for the majority of these methods is usually a subjective feeling and intuition, which of these methods makes a real mix of science and art. It is clear that the methods of technology forecasting should more include objective rules of the development of technical systems. As these methods of technology forecasting are not based on objective rules of the development of technical systems, numerous scientific activities were focused on identification of typical trends of engineering systems evolution (*Altshuller, 1984*; *Lyubomirskiy, & Litvin, 2003; Shpakovsky, 2016*). Typical trends of engineering systems evolution have been identified on the basis of a broad analysis of patent databases and historical trends in technology development. Trends occupy a special place in the innovation science and engineering field, as they offer a view of the technical system from a variety of time perspectives - from the past, through the present to the far future. They have a great potential for innovation and conceptual design phase because they describe what happened in the past to successful technology and because they are leading innovators to what is likely to happen in the future. Studies oriented on the fulfillment of evolutionary trends as a source of innovation opportunities identification also focus on agricultural technology *(Mašín, & Petrů, 2018)*. As the field of autonomous agricultural vehicles is developing dynamically, it would be desirable already in the concept generating phase to check whether conceptual proposals are in line with objective trends in technology development. The aim of this article is therefore to compare whether the real development of autonomous agricultural vehicles corresponds to selected identified and described trends of engineering systems evolution.

METHODS AND INFORMATION SOURCES

For evolutionary analysis so-called trends of engineering system evolution (TESE) were used. Trends of engineering systems evolution are eleven and together they form a hierarchical system (*Lyubomirskiy, & Litvin, 2003)*. From the two main trends (the S-curve development and the trend of increasing ideality) are derived the other trends, respectively one trend may be the implementation of another trend (Fig. 1). These open patent databases served as information sources:

- Espacenet (https://worldwide.espacenet.com)
- Patenscope (https://patentscope.wipo.int/search/en/search.jsf)
- USPTO Patent Full-Text and Image Database (http://patft.uspto.gov/netahtml/PTO/search-adv.htm)

The following databases of scientific papers and professional publications also served as sources of information:

- ScienceDirect (https://www.sciencedirect.com)
- *IEEE* Xplore Digital Library (https://ieeexplore.ieee.org)

- IOPScience (https://iopscience.iop.org).

The websites of agricultural technology manufacturers and available publications *(e.g. Berns, & von Puttkamer, 2009)* also served as sources of information.
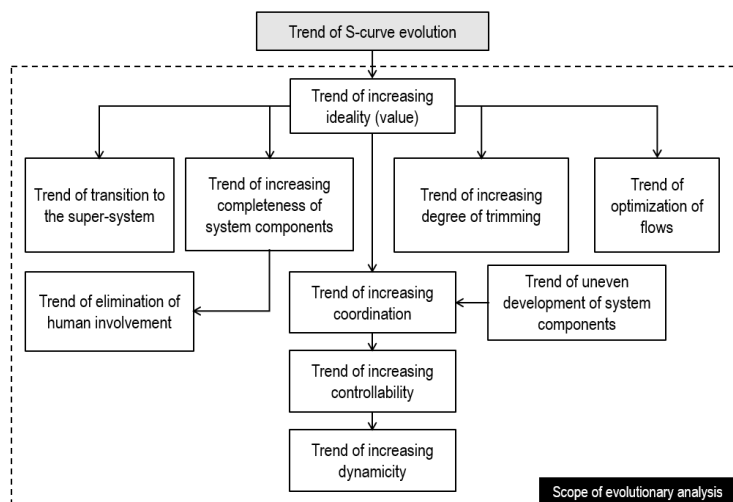

Fig. 1 Hierarchical system of trends of engineering systems evolution (adapted from *Lyubomirskiy, & Litvin, 2003*)

RESULTS AND DISCUSSION

The evolutionary analysis based on the mentioned information sources showed that the development of autonomous agricultural vehicles corresponds best with the following two trends in the evolution of engineering systems:

- trend of increasing coordination
- trend of elimination of human involvement

The trend of increasing coordination is reflected in the evolution of technical systems by gradually coordinating the "behavior" of the system components and consequently coordinating the "behavior" of the super system (*Lyubomirskiy, & Litvin, 2003*). Coordination is also understood as the choice of one parameter with respect to the value of another parameter. This "driving" parameter value can be pre-selected (for example, when manufacturing the agricultural machine) or in the process of its operation (for example during harvesting or weed destroying processes). For example, when developing the outer shape of a system, the shape of the developed system must be coordinated with the shape, properties, and movement of the objects that interact with the system (an example of this trend being the standardization of the dimensions of the interconnected parts or the ergonomic agricultural tool handle solution). From this trend viewpoint we can observe different trend mechanisms – coordination in shape, coordination in rhythm, coordination of materials, coordination of action, coordination of parameter, self-coordination etc.
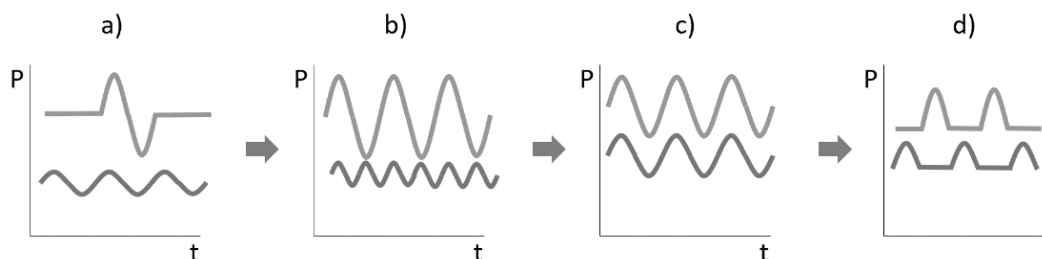

Fig. 2 Trend of increasing coordination of engineering systems (a – incoordinated actions, b – partly coordinated actions, c – coordinated actions, d – interval actions)

The trend of increasing coordination in the form of coordinated actions can be illustrated by example of a system for speed-based coordinated control of agricultural vehicles when on-the-go unloading is utilized (*Ray, 2017*) – Fig. 3a. Another example of this trend may be wireless networking of agricultural machines in a collaborative agricultural process (*Schmidt, 2017*) - Fig. 3b.
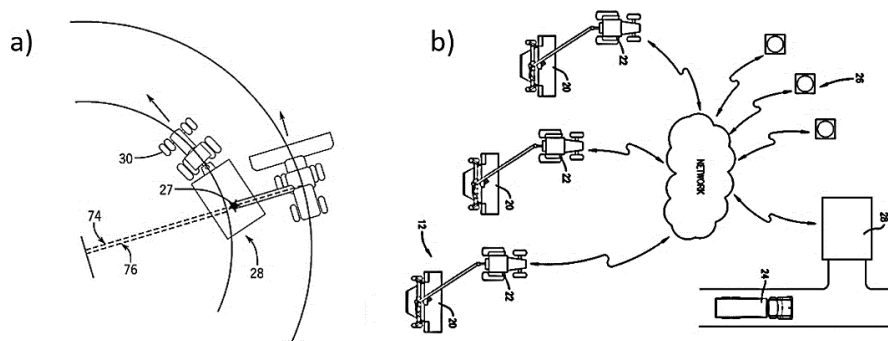

Fig. 3 (a) Automatic coordination of the agricultural vehicles speed (*Ray, 2017*) and (b) synchronization of agricultural vehicles with the help of wireless networking (*Schmidt, 2017*)

The trend of elimination of human involvement in engineering systems trend lies in the fact that during evolution, the number of functions performed in the system by human is reduced (*Lyubomirskiy, & Litvin, 2003*). This trend is particularly relevant for systems where standard subsystems such as the workpiece, transmission, power source, and control system are omitted and initially do not exist (Fig. 4). This is a special case of the trend of increasing completeness of engineering systems, because a man is often an element on which it is usually easiest to transfer the functions, which yet cannot be performed by the system.
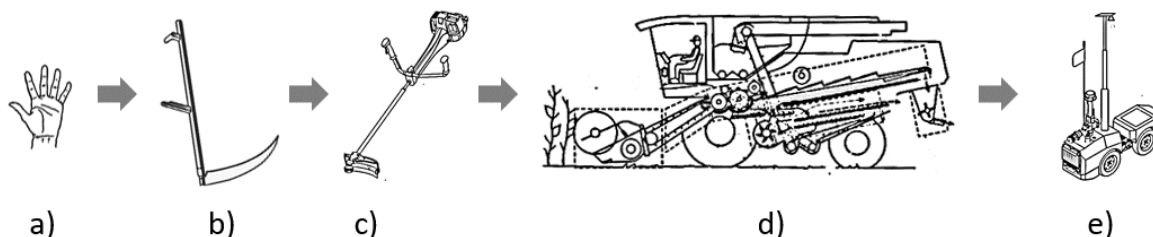

Fig. 4 Trend of elimination of human involvement in engineering systems (human roles: a – man alone, b – tool, c – energy and drive, d – control and supervision, e – only decision making)

Fulfilling this trend in autonomous agricultural vehicles field can be documented on the concept of an autonomous system (*Kavender-Bares, 2017*) or on the unmanaged robotic platform for performing multiple functions in agricultural systems (*Blackwell, Schildroth, Myers, & Becker, 2018*) - Fig. 5.
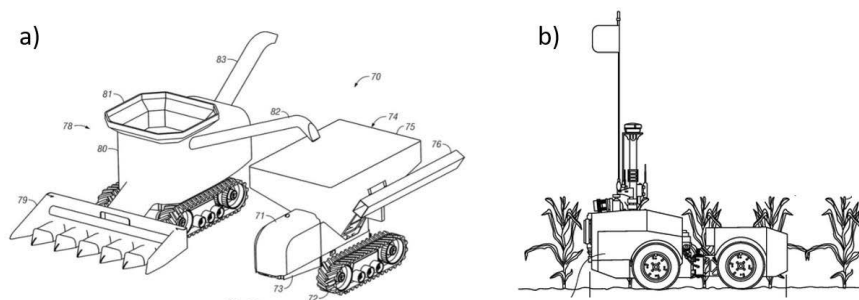

Fig. 5. Trend of elimination of human involvement in agriculture – concept of autonomous system (a) and robotic platform (b) (*Kavender-Bares, 2017; Blackwell, Schildroth, Myers, & Becker, 2018*)

CONCLUSIONS

Prognoses created using evolutionary analysis can provide management and engineers with important and more reliable input into the strategic planning process because they are based on objective patterns in the development of technical systems. Applying evolutionary analysis to the engineering systems guarantees a supply of novel ideas, and conceptual directions. The article contains one of the first applications of trends of engineering system evolution (TESE) to the field of agricultural autonomous vehicles. The study shows that TESE can be a powerful tool for autonomous agricultural vehicles innovation and forecasting. The study indicates that autonomous agricultural vehicles will develop significantly in lines of trend of increasing coordination and trend of elimination of human involvement.

ACKNOWLEDGMENT

REFERENCES

1. Altshuller, G. S. (1984*). Creativity as an Exact Science*. New York: Gordon and Breach Publishing.
2. Berns, K. & von Puttkamer, E. (2009). *Autonomous land Vehicles*. *Steps Towards Service Robots*. Wiesbaden: Vieweg + Teubner.
3. Blackwell, R., Schildroth, R., Myers, M., & Becker D. (2018). Patent Application US2018325009 (A1). Autonomous systems, methods, and apparatus for ag based operations.
4. Daim, T. U., Pizzaro, M., & Talla R., editors (2014). *Planning and Roadmapping Technological Innovations*. Springer International Publishing.
5. Kavender-Bares, K. (2017) Patent Application US20123424A1. Robotic platform and method for performing multiple functions in agricultural systems.
6. Lyubomirskiy A. & Litvin S. (2003). *Trends of Engineering Systems Evolution - Guide*. Boston: Gen 3 Partners.
7. Mašín, I., & Petrů, M. (2018). Trends of Engineering Systems Evolution and Agricultural Technology. In *Automation in Agriculture - Securing Food Supplies for Future Generations* (ed. Stephan Hussmann). London: IntechOpen.
8. Miles, I., Saritas, O., & Sokolov, A. (2016). *Foresight for Science, Technology and Innovation*. Springer International Publishing.
9. Phaal, R., Farrukh, C., & Probert, D. (2010*). Roadmapping for Strategy and Innovation: Aligning technology and markets in a dynamic world*. Cambridge: Institute of Manufacturing - University of Cambridge.
10. Ray, B. R. (2017) Patent Application US2017192419A1. System and method for speed-based coordinated control of agricultural vehicles.
11. Shpakovsky N. (2016). *Tree of Technology Evolution. Ways to New Business Opportunities*. Moscow: CreateSpace.
12. Schmidt, K. K. (2017) Patent Application US2017083026A1. Isobus wireless networking of agricultural machines in a collaborative agricultural process.

Corresponding author:
doc. Dr. Ing. Ivan Mašín, Department of the Design of Machine Elements and Mechanisms, Technical University in Liberec, Studentska 2, 46117 Liberec, Czech Republic, phone: +420 602439258, e-mail: ivan.masin@tul.cz

INFLUENCE OF SOIL TILLAGE ON WATER INFILTRATION IN LIGHT SOIL CONDITIONS OF CENTRAL BOHEMIA

Adéla MELICHAROVÁ[1], Jiří MAŠEK[1], Stanislav KOVÁŘ[1]

[1]*Department of Agricultural Machines, Faculty of Engineering, Czech University of Life Sciences Prague, Kamýcká 129, Praha 6, Prague, 16521, Czech Republic*

Abstract
This paper focuses on the evaluation of infiltration abilities of light sandy loamy cambisoil. Measurements of water infiltration were performed on field experiment in Nesperská Lhota near Benešov (Central Bohemia Region) on sandy-loam soil at an altitude of 390 m. Seven variants of experimental plots with different tillage intensity and crops were evaluated. Simplified falling-head method was used. The measurements showed different infiltration abilities of individual variants. The measurement did not show a clear effect of depth of tillage on soil infiltration capabilities. Also, no clear effect of the crop on infiltration was demonstrated during the 2017 season.

Key words: *soil tillage; hydraulic conductivity; depth of loosening.*

INTRODUCTION

Soil is a non-renewable natural resource that is the main means of producing food in agriculture *(Morgan & Nearing, 2011).* Knowledge of the physical and hydraulics properties of soil is one of the basic cognition that should decide when and how the soil is to be treated *(Titi, 2002).* It is therefore a correct estimation of soil workability with regard to the specific conditions prevailing in the habitat, when the soil handling does not damage its quality, but on the contrary, the optimum condition of the soil environment suitable for plant cultivation is achieved *(Javůrek et al., 2008).*

The beneficial effect of soil protection technologies is often associated with the reduction of soil water erosion. The basic pillar of these technologies is the use of organic matter on the soil surface (biomass of crops, post-harvest residues). This material partially covers the soil surface, thereby reducing surface runoff and soil wash. This is demonstrated by *Portela et al. (2010),* when the highest soil losses were on the surface with minimal plant residues. On this surface was also the highest measured surface runoff.

The reduced soil tillage significantly affects the hydraulic conductivity of the soil and thus the soil infiltration properties. *Kroulík et al. (2007)* found the highest average infiltration properties for ploughed land, while minimum values were recorded for shallow tillage. He also found that soil that is loosened has a higher water capacity than reduced soil tillage.

Reicosky et al. (2005) states that the course of infiltration depends on the amount of water and the way the water is transported to the soil surface (precipitation, irrigation, flooding). Equally important are the soil properties, of which the most important are the structure, granularity, porosity, soil profile construction and soil density.

Franzluebbers (2002) writes that infiltration of water into the intact sample for long-term no-till soil was higher than that of conventional cultivated land. Higher infiltration of untreated soil was measured only if the soil was so treated at the same site for an extended period of time. However, using these technologies for less than a few years, the infiltration of untreated soil may be the same or even lower than that of conventionally treated soil. This is due to the initial technogenic compaction and the lack of biological activity required to create a stable soil structure. This confirms the length of the transition period, which is necessary to create a certain soil structure, which is confirmed by previous authors. Soil-causing soil treatment has a direct effect on soil properties and environmental problems *(Paustian et al., 1997).*

The aim of this work was to assess and evaluate the individual technologies of soil cultivation in the cultivation of various crops in terms of water infiltration into the soil.

MATERIALS AND METHODS

Field trial with 7 variants was established at locality Nesperská Lhota in Central Bohemia Region. Measurements are carried out in the sandy loam Cambisoil during season 2017. The experimental plot is on a slope with a south-east slope, average slope is 4.9°. The variants vary in different tillage and different crops. Plot of land for each variant was 6 m x 50 m in length side is facing the fall line.
Variants of trial:

Variation 1 – oat with conventional tillage. Land was ploughed into the middle depth (0.2 m). It was used moldboard plough the soil was left in rough furrow through the winter. Seedbed preparation was performed using harrows and levelling bars. Last operation was sowing of oats.

Variation 2 – oat with reduced tillage. After the harvest the straw was crushed and left in the field. This was followed by reduced tillage with disc cultivator (into depth 0.08m). The oats were sowed in spring the following year.

Variation 3 – maize with conventional tillage and inter-row crop. Land was ploughed into the middle depth (0.2 m). It was used moldboard plough. The soil was left in rough furrow through the winter. Seedbed preparation was performed using harrows and levelling bars. Oats were seeded into inter-row space (2 rows- 0.125 m). After the germination of oats was sown maize.

Variation 4 – land was ploughed into the middle depth (0.2 m). It was used moldboard plough The soil was left in rough furrow through the winter. Seedbed preparation was performed using harrows and levelling bars. Last operation was sowing of maize. The soil surface was covered at the time of sowing almost by zero organic matter.

Variation 5 – maize with direct sowing. The straw was crushed and left on the land in the autumn of 2015. The soil remained without tillage over the winter. In spring maize was sown directly without any tillage.

Variation 6 – maize with freezable intercrop. After previously harvest tines cultivator was done into a depth of 0.18 meters followed by sowing intercrops (mustard). There was a freezing of intercrops during the winter. Maize was sown without tillage in the spring.

Variation 7 – without vegetation (black fallow). Land was maintained over time without vegetation through total herbicide Roundup (conventional tillage technology).

The method used was simplified falling-head (*Bagarello et al., 2004*). This device consists of a plate with a diameter of 0.15 m and a metal sheet wall thickness – 2 mm. Its height is 0.2 m. This single ring was thoroughly embedded in the soil, taking care to minimize the changes in the measured pore system. The ring was inserted into a depth of 0.1 m. Water volume of 0.5 dm^3 was then poured into a single ring and the time was set off. When the water was soaked into the soil, the time was stopped and the value was subtracted. Consequently soil moisture was measured again using the moisture meter Theta probe (Delta Devices, UK). It was performed in 10 repetitions for each variant. Kopecky cylinders with the volume of 100 cm^3 were taken to determine the basic physical properties of soil (each variation: 12 pieces). Soil sampling was performed prior to measurement (15.6.2017).

The data obtained from the measurements was evaluated in the STATISTICA 12 program. Chart graphs were used to illustrate field trial data. Data were further evaluated by ANOVA analysis using the Tukey HSD test.

RESULTS AND DISCUSSION

Table 1 describes the basic physical properties of soil for each variant. The table shows a small difference between the variants. This is due to a long period between loosening and soil sampling. Meanwhile, the soil has declined and the differences are small. This is true for values of density and porosity. The values can be considered typical of the soil type. However, the whole 2017 season was marked by a significant drought, which was influenced mainly by the measurement of soil hydraulic properties.

Tab. 1 Selected properties of the soil

Variant	Depth [m]	Porosity [%]	Bulk density [g.cm^{-3}]
	0,05-0,1	41,21	1,56
1	0,1-0,15	38,96	1,62
	0,15-0,2	31,44	1,82
	0,05-0,1	42,85	1,51
2	0,1-0,15	42,68	1,52
	0,15-0,2	38,68	1,63
	0,05-0,1	45,52	1,44
3	0,1-0,15	46,06	1,43
	0,15-0,2	51,94	1,27
	0,05-0,1	41,96	1,54
4	0,1-0,15	42,62	1,52
	0,15-0,2	42,66	1,52
	0,05-0,1	39,88	1,59
5	0,1-0,15	41,43	1,55
	0,15-0,2	38,29	1,64
	0,05-0,1	41,47	1,55
6	0,1-0,15	44,92	1,46
	0,15-0,2	42,78	1,52
	0,05-0,1	45,52	1,44
7	0,1-0,15	42,73	1,52
	0,15-0,2	44,89	1,46

The first measurement took place on 15. 06. 2017. In this area since the beginning of May it was max. 15 mm. This long-term absence of precipitation has also been unfavourably reflected in the results of the field trial. The soil in this period was extremely dry and very difficult to absorb water.
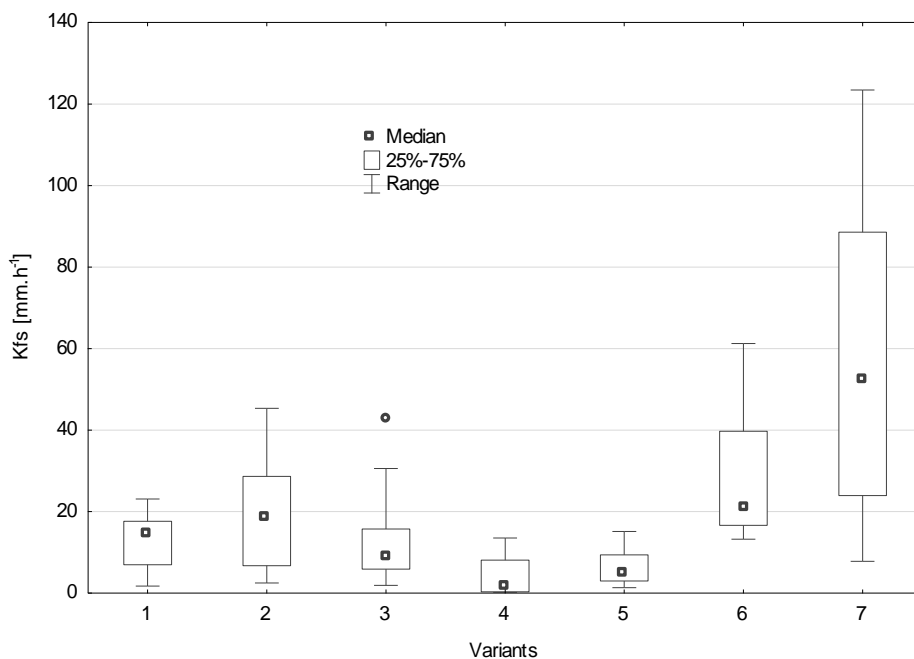

Fig. 1 Saturated hydraulic conductivity 15. 06. 2017

It can be seen from Figure 1 that the variant without vegetation had the highest hydraulic conductivity at the first measurement. By more than half, the maize variant with the freezing crop was second. It was followed by a variant of oats with direct sowing. A similar result was achieved with ploughing oats and maize prepared with ploughed crops. The lowest conductivity was measured in maize tilled by ploughing.

Another measurement took place in about three weeks on 07. 07. 2017. During this period more than 40 mm has already rained, which had a great influence on soil infiltration ability. In this measurement, Figure 44 showed the best cumulative infiltration for the ploughing variant of oats. With a large step, varieties of ploughed maize and intercrops and ploughed maize variants followed. The lowest result was achieved by the oat variant with direct sowing with an infiltration of 1.45 mm.h^{-1}. The second-smallest infiltration was shown by the vegetation-free variant of 3.5 mm.h^{-1}.
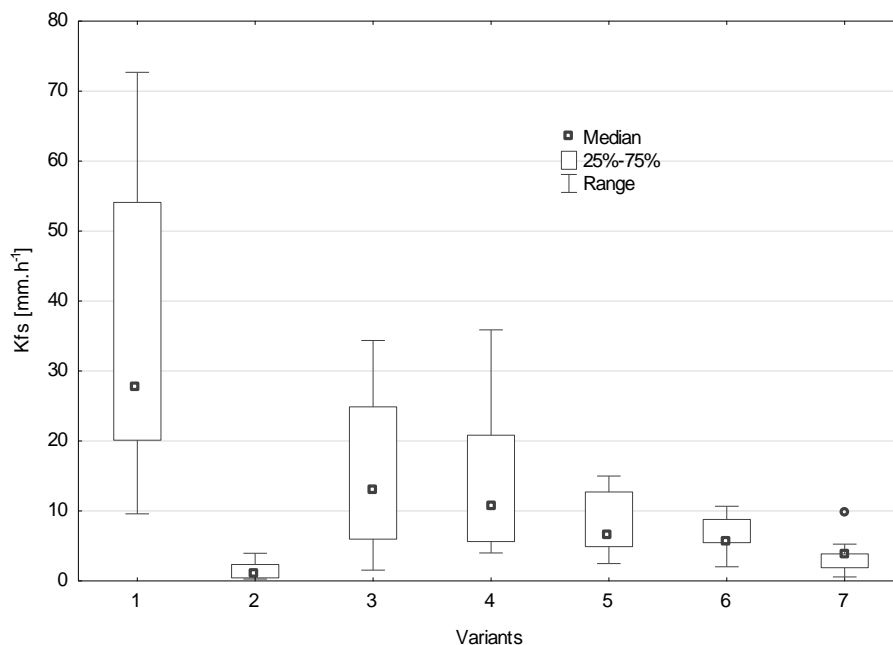

Fig. 2 Saturated hydraulic conductivity 07. 07. 2017

The last measurement in this year took place 08. 08. 2017. By this time the variants with oat were already harvested and there was only stubble.

The results of the last measurement are shown in Figure 36. Here, too, its value was twice as high as the second place. The smallest infiltration ability was shown by the variant of maize prepared by ploughing. Behind it was placed ploughing maize with sown crops.

Most studies confirm the beneficial effect of reduced or no-till technologies on soil hydraulic properties. However, the behavior of different soils cannot be excluded from this issue. In contrast to most studies, *Soracco et al. (2019)* concluded that no-till technology reduces the hydraulic conductivity of the soil, which affects the connectivity of pores, especially for finely structured soils. Conventional technology has shown higher overall pore connectivity in all monitored sites. The authors also used Mini Disks for this measurement. This is in line with our study.
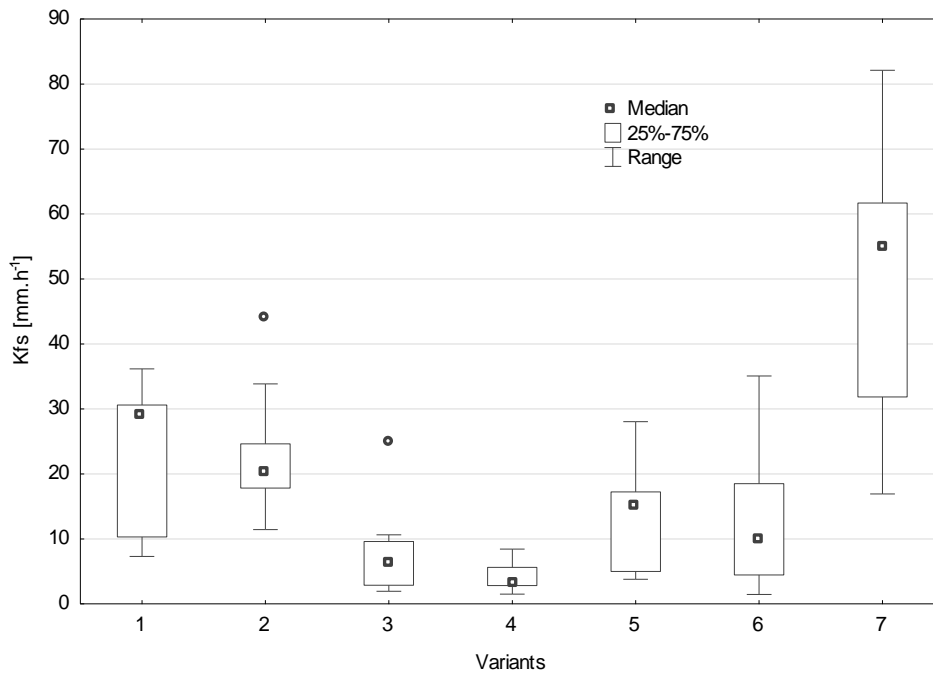
Fig. 3 Saturated hydraulic conductivity 08. 08. 2017

The Single ring method is rather less used. *Castellini et al. (2015)* emphasize the importance of organic matter for improving soil infiltration capabilities. *Alagna et al. (2016)* recommend the use just for the measurement of sandy-clay soils. The authors emphasize frequent fluctuations in values where the effect of soil and crop processing is not clear. The different behavior of the variants during a longer evaluation is confirmed by *Capello et al. (2017)*. This is also in line with the results of this work, when it is not possible to draw clear conclusions from the Single Ring measurement.

CONCLUSIONS

The input hypotheses of the thesis were only partially confirmed. The positive effect of non-tillage technologies on the increase of soil infiltration properties has not been clearly demonstrated. In the case of surface runoff, their meaning is not entirely clear. However, it should be noted that soil loss is far more severe than simple surface runoff. The measurement was certainly influenced by extreme drought during the 2017 season.
It was not possible to find optimal conditions during this season to measure the soil hydraulic properties.

REFERENCES

1. Alagna, V., Bagarello, V., Di Prima, S., & Iovino, M. (2016). Determining hydraulic properties of a loam soil by alternative infiltrometer techniques. *Hydrological Processes*, *30*(2), 263-275.
2. Bagarello, V., Iovino, M., & Elrick, D. (2004). A simplified falling-head technique for rapid determination of field-saturated hydraulic conductivity. *Soil Science Society of America Journal*, *68*(1), 66-73
3. Capello, G., Biddoccu, M., Ferraris, S., Pitacco, A., & Cavallo, E. (2017). Year-round variability of field-saturated hydraulic conductivity and runoff in tilled and grassed vineyards. *Chemical Engineering Transactions*, *58*, 739-744.

4. Castellini, M., Giglio, L., Niedda, M., Palumbo, A. D., & Ventrella, D. (2015). Impact of biochar addition on the physical and hydraulic properties of a clay soil. *Soil and Tillage Research*, *154*, 1-13.

5. Franzluebbers, A. J. (2002). Water infiltration and soil structure related to organic matter and its stratification with depth. *Soil and Tillage Research*, *66*(2), 197-205.

6. Javůrek, M., Hůla, J., Vach, M., & Kroulík, M. (2008). Impact of different soil tillage technologies on soil erosion effect mitigation. *Scientia Agriculturae Bohemica,* 39(2), 218-223.

7. Kroulik, M., Hůla, J., Šindelař, R. & Illek, F., (2007). Water Infiltration into Soil Related to the Soil, Tillage Intensity, *Soil Water Research*, 2(2), pp. 15-24.

8. Morgan, R. P. C., & Nearing, M. A. (Eds.). (2011). *Handbook of erosion modelling*. West Sussex: Wiley-Blackwell, 77 p.

9. Paustian, K., Collins, H. P. &Paul, E. A. (1997). *"Management controls on soil carbon." Soil Organic Matter in Temperate Agroecosystems*. Cole, eds. Boca Raton: CRC Press, pp. 5-49.

10. Portela, J. C., Cogo, N. P., Bagatini, T., Chagas, J. P. & Portz, G. (2010). Restauração da estrutura do solo por sequências culturais implantadas em semeadura direta, e sua relação com a erosão hídrica em distintas condições físicas de superfície. *Revista Brasileira de Ciência do Solo*, *34*, 1353-1364.

11. Reicosky, D. C., Lindstrom, M. J., Schumacher, T. E., Lobb, D. E., & Malo, D. D. (2005). Tillage-induced CO2 loss across an eroded landscape. *Soil and Tillage Research*, *81*(2), 183-194.

12. Soracco, C. G., Villarreal, R., Melani, E. M., Oderiz, J. A., Salazar, M. P., Otero, M. F. & Lozano, L. A. (2019). Hydraulic conductivity and pore connectivity. Effects of conventional and no-till systems determined using a simple laboratory device. *Geoderma*, *337*, 1236-1244.

13. Titi, A. (2002). *Soil tillage in agroecosystems*. USA: CRC press, 384 p.

Corresponding author:
Ing. Adéla Melicharová, Department of Agricultural Machines, Faculty of Engineering, Czech University of Life Sciences Prague, Kamýcká 129, Praha 6, Prague, 16521, Czech Republic, e-mail: melicharovaa@tf.czu.cz

EVALUATION OF ECONOMIC RISKS IN PRODUCING WINTER OILSEED RAPE

Miroslav MIMRA[1], Miroslav KAVKA[1], Petr MARKYTÁN[2]

[1]*Department of Machinery Utilization, Faculty of Engineering, Czech University of Life Sciences Prague, Kamýcká 129, 165 21 Praha 6 – Suchdol, Czech Republic*
[2]*Union of Oilseeds Growers and Processors, Na Fabiánce 146, 182 00 Praha 8 – Březiněves, Czech Republic*

Abstract
This paper analyses two data series covering the period of 5 to 10 years regarding specific selected key parameters for companies using the counselling services of the Union of Oilseeds Growers and Processors in Prague (UOGP) and some other companies that make no use of these services (OTHERS). For the selected key parameters, the risk analysis of reaching the gross profit, the gross margin and the break-even point was conducted with the aid of the Monte Carlo stochastic simulation method. The results of the calculations show that the companies using UOGP consulting achieve on average, at the same level of risk, a gross profit higher by 53%; a gross margin higher by 30% and their break-even point is lower by 11%. Taking advantage of the knowledge and services provided by a consulting company has positive economic benefits, and it increases the competitiveness of companies.

Key words: *gross profit; gross margin; break-even point; Monte Carlo method.*

INTRODUCTION

Oilseed rape is one of the most important agricultural crops in the Czech Republic. Winter oilseed rape on arable land in the production year 2015/2016 amounted to 359,243 hectares, which meant on average 14.4% of the arable land, while the dispersion in individual farms amounted to a number between 0.19% up to 35%, or even more *(Volf and Zeman, 2016)*.

The high amount of winter oilseed rape and its ongoing increase are mainly due to its market attractiveness. This, on the one hand, means a higher market production, mainly due to higher yields and farmer prices. Farmer prices (Tab. 2) and yields (Tab. 1) drive the market production. Both components of market production are under the influence of the market environment, the influence of weather and the level of compliance with the technological discipline in the respective company. Technological discipline means strict adherence to all operational processes and to their technological (cultivating) parameters. Strict adherence to technological discipline also has an impact on input prices and thus on costs *(Janotová, 2016;* also see Tab. 3), concerning items that the farmer generally cannot influence (such as purchase prices, taxes, rent, fees) as well as the items which depend on his decisions (such as number of operations, machine sets, dosages, etc.).

The monitoring of the development of input and output prices for winter oilseed rape production shows considerable price differences; the prices are also influenced by consulting (or in our specific case in the membership in UOGP). The prosperity and competitiveness of the production depends on the mutual relation between costs, prices and revenues in the market environment. For managerial decision-making, it is therefore essential to analyse constantly the available information and to evaluate the degree of feasibility of the managerial targets *(Wolke, 2008; Smejkal and Rais, 2009)*, which includes evaluating risks.

Producing winter oilseed rape is influenced by a number of factors which are intertwined. Unfortunately, greater attention has not been given to the benefits of the expert experience from companies providing counselling on the economic results of winter oilseed rape yet. Against this background, this paper evaluates the economic risks of growing winter oilseed rape based on UOGP's statistical data recorded over the last 5 to 10 years in order to quantify these risks using simulation models. The results are divided into two groups: for members of the UOGP and for non-members of the UOGP (hereinafter referred to as "OTHERS").The reasons for such segmentation are the above-mentioned potential differences between the two groups. The aim of this study was to analyse the economic risks of oilseed rape cultivation based on statistical data obtained over the last 10 years with the support of the Monte Carlo stochastic simulation method.

MATERIALS AND METHODS

Modelling is based on the principle of generating random values *(Gleissner and Berge, 2004)* within boundary conditions for their triangular statistical distribution (Evans et al., 2000). The input parameters are always based on optimistic and pessimistic estimations of the parameter and its most frequent occurrence, which is a so-called distribution peak (Tab. 4).

The risk analysis was conducted with the aid of the stochastic Monte Carlo simulation method's algorithm; its principle was described by *Kroese et al. 2011*, concerning generating a pseudo-random variable for input parameters. The calculation principle is based on simulating a critical variable using 100 000 simulations (of risk situations) and constructing a two-sided frequency distribution interval at a materiality level of 0.05. The mathematical model created in Microsoft Excel using the Crystal Ball Add-In is utilised to determine the mean value of a magnitude that results from a random sample. Consequently, data obtained through simulations can be statistically evaluated.

Parameters which are likely to change were selected. With regard to market production, the parameters concern changes in the oilseed yield and farm prices related to one hectare of winter oilseed rape. On the cost side, they concern changes in variable costs (such as labour, materials, maintenance of machines) or in total costs (= variable costs increased by fixed costs, e.g. overhead costs, annual depreciation, insurance) related to one hectare of winter oilseed rape. As a reference parameter, the value of gross profit (GP – see relation 2) and contribution to the gross margin (GM – relation 3), which were reached per hectare, have been selected. In order to compare the results reached by the group of farmers who were members of the UOGP and a group of non-members, the parameter of an achieved break-even point (BEP – relation 4) was selected.

Yield values were generated based on the input analysis in Tab. 1 and on the boundary conditions in Tab. 4; values of the farm price, according to Tab. 2 and 4, and cost values, according to Tab. 3 and 4.

Market production (MP) is set as:

$$MP = Y \cdot P \qquad \text{(CZK/ha)} \tag{1}$$
$$Y – \text{yield (t/ha)}$$
$$P – \text{price (CZK/t)}$$

Gross profit (GP) is set as:

$$GP = MP − TC \quad \text{(CZK/ha)} \tag{2}$$
$$MP – \text{market production (CZK/ha)}$$
$$TC – \text{total costs (CZK/ha)}$$

Gross margin (GM) is set as:

$$GM = MP − VC \quad \text{(CZK/ha)} \tag{3}$$
$$VC – \text{variable costs (CZK/ha)}$$

Break-even point (BEP) is the variant of relation 2 when:

$$GP = 0 \tag{4}$$

Subsequently, this question was determined for the model: "Which risk can be expected when a certain value of gross profit or gross margin is reached by changing the parameters?" (Tab. 4). The variation of this question was assessing the risk of reaching a break-even point where the GP = 0, or at what farmer price of rape seed this beak-point is reached.

For the risk analysis, the gross profit (excluding overheads, taxes, etc.), gross margin and break-even point values were used; all of them are important indicators for managerial decision-making. Planting technologies are also affected by natural influences and market conditions which the agricultural company cannot control itself. Therefore, special attention should be paid to the point at which planting becomes profitable, as well as to the gross margin analysis.

RESULTS AND DISCUSSION

Analysis of the parameters for calculation

According to the results monitored by **UOGP** (=Union of Oilseeds Growers and Processors) in Prague, in the following four tables, input parameters are analysed in the time series of 10 years, i.e. yield, farm price, cost, market output, gross profit and contribution to reimbursement.

Tab. 1 Development of the average winter oilseed rape yields according to companies which are UOGP members or non-members (OTHERS) in t / ha

Year / Type of the company	2007	2008	2009	2010	2011	2012	2013	2014	2015	2016
UOGP	3.32	3.21	3.47	3.08	3.18	3.06	3.73	4.28	3.71	3.74
OTHERS	2.86	2.73	2.96	2.65	2.54	2.54	3.23	3.69	3.21	3.25

Source: UOGP Prague

Tab. 2 Development of farmer prices for winter oilseed rape according to companies which are UOGP members or non-members (OTHERS) in CZK / t

Year / Type of company	2007	2008	2009	2010	2011	2012	2013	2014	2015	2016
UOGP	7 407	9 542	6 582	7 772	10 911	11 906	10 389	9 433	9 979	9 878
OTHERS	7 207	9 342	6 382	7 572	10 711	11 706	10 189	9 233	9 779	9 678

Source: UOGP Prague

Tab. 3 Development of the average winter oilseed rape production costs according to companies which are UOGP members or non-members (OTHERS) in CZK / ha; (VC = variable costs; FS = fixed costs; TC = total costs)

Year / Type of company		2007	2008	2009	2010	2011	2012	2013	2014	2015	2016
UOGP	VC	15 678	17 761	19 403	16 669	19 004	21 467	22 784	23 478	24 867	25 776
	FC	4 500	5 000	5 000	5 000	5 000	5 500	6 000	6 000	6 000	6 000
	TC	20 178	22 761	24 403	21 669	24 004	26 967	28 784	29 478	30 867	31,776
OTHERS	VC	14 894	16 873	18 433	15 836	18 054	20 394	21 645	22 304	23 624	24 487
	FC	4 500	5 000	5 000	5 000	5 000	5 500	6 000	6 000	6 000	6 000
	TC	19 394	21 873	23 433	20 836	23 054	25 894	27 645	28 304	29 624	30 487

Source: UOGP Prague and www.agroconsult.cz;

Tab. 4 Marginal conditions used for modelling

Indicators	UOGP			OTHERS		
	P	ML	O	P	ML	O
Yield (t/ha)	3.5	3.7	3.9	3.0	3.2	3.4
Farmer price (CZK/ha)	9 760	10 000	10 750	9 560	9 880	10 750
Total costs (CZK/ha)	30 700	29 700	28 400	29 500	28 500	27 300
Variable costs (CZK/ha)	24 700	23 700	22 600	23 470	22 500	21 450

Legend: P – pessimistic estimate; ML – most likely estimate; O – optimistic estimate

1. Yield (Y): According to the results monitored by UOGP (=Union of Oilseeds Growers and Processors) in Prague, the average yield of winter oilseed rape for the last 10 years amounted to 3.48 t / ha for UOGP members and to 2.97 t / ha for non-UOGP members (hereinafter referred to as "OTHERS"). According to an analysis of the last 5 years, the average yield for UOGP members was 3.70 t / ha and for non-members 3.18 t / ha. Based on the comparison of the average yields over the last 10 and 5 years, an increasing tendency was noticeable.

2. Farmer price (P): The farmer price (which in this paper means their selling price) for winter oilseed rape is directly dependent on the growing year, on the EUR to CZK exchange rate, the situation on the commodity exchange MATIF and the initial sales strategy of each agricultural company. Under such market conditions, larger companies which are generally involved with the UOGP have a competitive advantage. For the analysis, the average prices tracked by UOGP were also taken into consideration.

3. Costs: The value of the costs was broken down into variable (VC), fixed (FC) and total costs (TC). It was first analysed on the basis of the data monitored by UOGP Prague and then on the basis of an expert calculation done by the AgroConsult advisory system. During the last 10 years, the average cost was 9 380 CZK / t for members of UOGP and 9 280 CZK / t for OTHERS. In view of the slightly rising trend, the marginal conditions (Tab. 2) were set based on the data from the last 5 years, where the average price for UOGP members was 10 317 CZK / t and for OTHERS 10 117 CZK / t.

Market production (MP), gross profit (GP) and gross margin (GM)

The results of calculations concerning market production, gross profit and gross margin for UOGP members and OTHERS are shown in Tab. 5. The resulting values were calculated by multiplying the relevant input parameters according to the relation 1 to 3. The SAPS subsidies were not included in calculating the market output; this fact is important for the subsequent assessment of the risk connected to producing given that the SAPS subsidies were gradually reduced by the EU. The tables depict a comprehensive view of the situation in the winter oilseed rape production economy.

Tab. 5 Average MP, GP, GM and BEP values

Indicators	UOGP	OTHERS
Market production (CZK/ha)	37 000	31 616
Gross profit (CZK/ha)	7 300	3 116
Gross margin (CZK/ha)	13 300	9 116
Break-even point (t/ha)	2.97	2.88

Discussion

Based on the modelling of the input parameters using the built-in model, the following results were obtained. The results of the risk analysis are shown using the probability distribution graphs of the gross profit, the gross margin and the break-even point. The results obtained from the risk situations were statistically evaluated using descriptive statistics. For interpretation of the simulation results, a frequency curve was used. The frequency curve displays the frequency of the occurrence of the generated values in the scope of the selected range (between the minimum and the maximum value). Based on this range, the variance distribution can be analysed. Each analysed value (parameter) represents the result of one possible situation. The form of the value distribution in the frequency curve indicates the nature of the risk of the analysed parameter. The smaller the height of the curve and the range of the minimum and maximum values, the smaller is also the probable risk connected to the parameter being analysed.

The distribution curve displays the cumulative frequency of occurrence of the analysed parameter. By means of the distribution curve, it is possible to determine the probability with which the occurrence of individual generated values can be expected. In this interval, therefore, the probability of occurrence of any (whichever) value of this parameter can be analysed. The inverted value of probability determines the risk that the values can exceed.
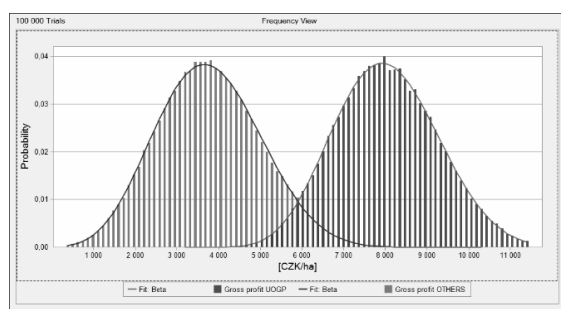

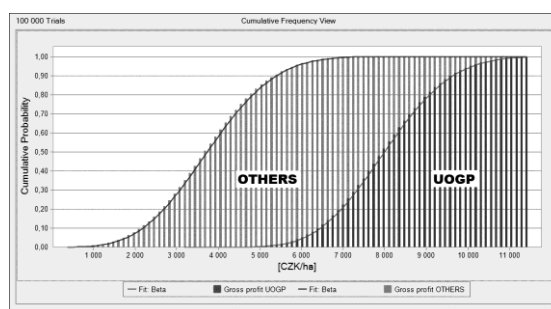**Fig. 1** Distribution curves and the probability of reaching gross profit

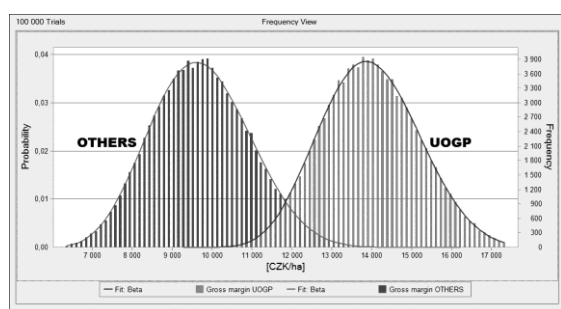**Fig. 2** Cumulative frequency graph of the probability of reaching gross profit

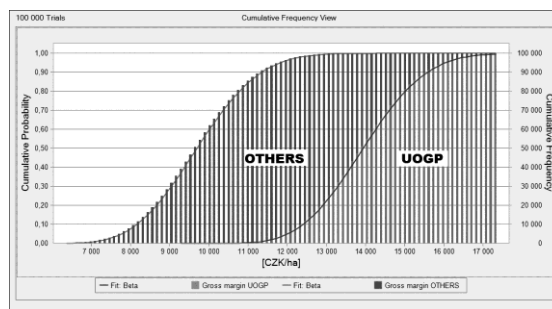**Fig. 3** Distribution curves and distribution of the probability of reaching a gross margin

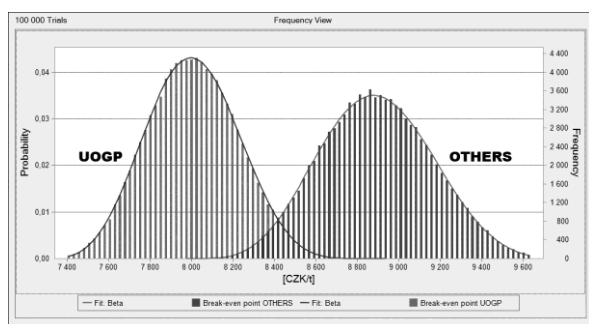**Fig. 4** Cumulative frequency graph of the probability of reaching gross margin

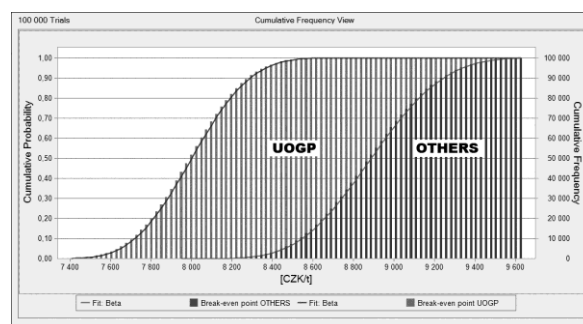**Fig. 5** Distribution curves and distribution of the probability of reaching a break-even point

Fig. 6 Graph of the cumulative frequency of probability of reaching a break-even point

Tab. 7 Prediction of probability distribution of GP, GM and BEP

Indicators	Gross profit (GP) (CZK/ha)		Gross margin (GM) (CZK/ha)		Break-even point (BEP) (CZK/t)	
Percentile	UOGP	OTHERS	UOGP	OTHERS	UOGP	OTHERS
100%	4 025.14	-374.81	9 926.10	5 778.02	7 327.50	8 090.02
90%	6 453.48	2 184.25	12 402.29	8 172.03	7 721.63	8 545.18
80%	6 965.52	2 695.15	12 905.59	8 670.27	7 813.26	8 655.90
70%	7 347.80	3 080.04	13 286.12	9 045.66	7 883.00	8 740.39
60%	7 678.67	3 410.57	13 615.14	9 375.31	7 944.50	8 813.98
50%	7 994.35	3 724.95	13 933.97	9 689.86	8 002.62	8 884.52
40%	8 316.36	4 046.88	14 255.34	10 004.37	8 060.00	8 956.90
30%	8 663.32	4 397.94	14 598.93	10 352.95	8 122.83	9 033.50
20%	9 075.39	4 817.68	15 007.48	10 762.66	8 193.30	9 123.81
10%	9 639.40	5 396.98	15 577.92	11 342.61	8 291.26	9 245.64
0%	12 873.41	8 624.43	18 715.48	14 158.95	8 712.05	9 778.99

CONCLUSIONS

Companies which are taking advantage of the knowledge and services provided by a consultancy company and which comply with a good technological discipline achieve better economic results in winter oilseed rape production, despite the higher costs for the planting technologies. When planning the expected gross profit from the winter oilseed rape production, it is necessary to evaluate the feasibility of the managerial targets and to take into account the connected risks. Marin et al. (2017) applied the stochastic methods in order to model the crop yields. In general, it can be said that the higher the gross profit the company plans to achieve, the higher is the risk of reaching this target. Homolka and Mydlar (2011) found out in their research that profit is significantly influenced by the changes in the farmer prices of winter oilseed rape. When interpreting the issue of crop production risk, it is possible to use a classification where the risk up to 20% is rated as low, 21 to 40% as acceptable, and 41 to 60% as high and above 60% as very high (unacceptable).

Companies that are members of UOGP achieve the same likelihood of both higher gross profits (difference of average values is CZK 4 264 / ha) and gross margin (the average rank difference is 4 241 CZK / ha). An increasing range of winter oilseed rape production reduces unit fixed costs, and this results in growing profits. In addition, these companies achieve lower values of the break-even point (the average value difference is 886 CZK / t). This allows them at a lower purchase price of winter rape seed not to be in the red, in comparison with non-UOGP members.

For UOGP members, the gross profit of CZK 7 300 per hectare, based on the professional estimate, is reached with a probability of 71%. In comparison for UOGP non-members, the gross profit based on the professional estimate of CZK 3 116 / ha is reached with a probability of 69%. Thus, the level of risk is at an acceptable level.

The members of UOGP reach the value of the contribution to the fixed costs of CZK 13 300 per hectare with a probability of 69%, and the OTHERS reach a fixed cost allowance of CZK 9 116 / ha with a probability of 68%. The amount of the gross margin is sufficient to cover the fixed costs of both above-mentioned groups. Accordingly, it enables them to further develop their companies. According to Rayburn (2009), the possible benefits of using the stochastic methods are an improved performance and better economic results of the agricultural company.

The presented method of modelling the economic risks of growing winter oilseed rape can be applied to other crops as well. The accuracy of the modelling results depends on the accuracy of the input parameters of the assessed agricultural company and the growing region. In other words: In order to obtain the most accurate and appropriate results, it is highly recommended not to evaluate the average values collected within a large area (such as an entire EU-country), but rather to apply this method precisely to the input parameters specific for each agricultural company (considering its production technology, used material and machinery, selling price, costs, etc.) or to smaller regions with similar cultivation conditions.

ACKNOWLEDGMENT

REFERENCES

1. Evans. M., Hastings, N., & Peacock, B. (2000). *Statistical distributions*. Third edition (p. 187). New York: John Wiley & Sons Inc., 220 p.

2. Gleissner. W., & Berger, T. (2004). The Monte Carlo: Simulation method for risk aggregation. (Auf nach Monte Carlo: Simulationsverfahren zur Risiko-Aggregation.) *Risknews*, *1*(1): 30–37.

3. Homolka, J., & Mydlar, R. (2011). Efficiency evaluation in intensive growing of winter rape. *Agricultural Economics, 57*(5), 247–257, ISSN 0139570X.

4. Janotová, B. (2016). Rape Growing Economy and its Development for 2015 in the Czech Republic. (in Czech). *In Rapeseed production system, sunflower production system, 33rd evaluation seminar* (pp.95-99). Hluk: UOSP Praha.

5. Kroese, D. P., Taimre, T., & Botev, Z. I. (2011). *Handbook of Monte Carlo Methods*. New York: John Wiley & Sons. 772 p. ISBN 0-470-177 93-4.

6. Marin, F. J., Jones, W., & Boote, K. J. (2017). A Stochastic Method for Crop Models: Including Uncertainty in a Sugarcane Model. *Agron. J. 109*, 483–495. doi:10.2134/agronj2016.02.0103

7. Rayburn, E. B. (2009). Estimating Economic Risk Using Monte Carlo Enterprise Budgets. *Forage and Grasslands, 7*. doi:10.1094/FG-2009-0415-01-MG.

8. Smejkal V. & Rais K. (2009). *Risk management in firms and companies* (in Czech). Prague: Grada, 360 p.

9. Volf, M. & Zeman, J. (2016). Results of rape growing in the Czech Republic (in Czech). In *Rapeseed production system, sunflower production system, 33rd evaluation seminar* (pp. 1-34). Hluk: UOSP Praha.

10. Wolke, T. (2008). *Risikomanagement*. München: Oldenburg Wissenschaftverlag GmBH, 134 p.

Corresponding author:
Ing. Miroslav Mimra, Ph.D., Department of Machinery Utilization, Faculty of Engineering, Czech University of Life Sciences Prague, Kamýcká 129, Praha 6, Prague, 16521, Czech Republic, phone: +420 22438 3145, e-mail: mimra@tf.czu.cz

ANTI-EROSION TWO-STAGE TILLAGE BY RIPPER

Bakhadir MIRZAYEV[1], Farmon MAMATOV[2], Nikolay ALDOSHIN[3], Mansur AMONOV[1]

[1]*Tashkent Institute of Irrigation and Agricultural Mechanization Engineers, Tashkent, Uzbekistan*
[2]*Karshi Engineering Economic Institute, Karshi, Uzbekistan*
[3]*Russian State Agrarian University - Moscow Timiryazev Agricultural Academy, Russia*

Abstract
The aim of the research is to develop a technology and a two-stage ripper for protection of soil from wind and water erosion, as well as improves the accumulation and preservation of soil moisture. The authors proposed a technology of two-stage moldboardless loosening slopes' soil and a cultivator for its implementation. The design of the developed two-stage ripper with the working bodies of the "paraplau" type is given. The type of working bodies and their mutual arrangement were substantiated via theoretical studies. It has been established that the plow scheme with the upper and lower working bodies alternation with the lower bend of the rack is the most rational design scheme of a two-stage ripper with working bodies of "paraplau" type. High-quality loosening with the lowest energy costs is provided with longitudinal and transverse distances between the working bodies of 0.50-0.60 m and 0.35-0.40 m, and field board's width and length are 0.7 m and 0.16 m respectively. The rational values of the loosening plate's parameters were substantiated by theoretical and experimental studies: the maximum plate's installation angle to the surface of the rack is 25º, the plate's length and width are 0.12-0.15 m and 0.9-0.12 m respectively.

Key words: wind erosion; slope; paraplau; chissel; soil protection.

INTRODUCTION

Soil erosion is a major environmental threat to the sustainability and productive capacity of agriculture. During 40 years in 1955-1995, nearly one-third of the world's arable land has been lost by erosion. Potential for water and wind erosion of soil is highest in arid and semiarid regions in which located Uzbekistan. In recent years, erosion has caused considerable damage to Uzbekistan's agriculture. Excessive soil tillage in cultivating different crops leads to the spread of wind and water erosion of soil. Because of soil erosion in individual farms, crop yields are sharply reduced. The lightening of the mechanical composition and repeated blowing, in the strong wind zones is result in a sharp decrease in humus, nitrogen and phosphorus in soil. Wind erosion in arid and semiarid zones also increase ambient air pollution by particulate matters *(Lal, 2017; Amonov, Pulatov, & Colvin, 2006; Stetler, & Saxton, 1996; Pimentel, Harvey, Resosudarmo, Sinclair, Kurz, McNair, & Blair, 1995; Khamraev, Nasriddinov, & Nasriddinov, 1989; Mirzajonov, 1981).*

In this regard, research is aimed to improving the tillage process by developing new technologies for moldboard less tillage of eroded soils and creating technical means to protect the soil from wind and water erosion. In addition, new tillage technology reducing energy costs of tillage, improving the accumulation and preservation of soil moisture.

MATERIALS AND METHODS

The work was carried out using the basic principles and methods of classical mechanics, statistics, and experiment based on mathematical planning, as well as general methods to determine the machines' agro technical, energy and economic performance.

In order to prevent wind and water erosion on sloping lands, a new technology was developed that allows obtaining a stepped bottom of the furrow, which contributes to the retention and accumulation of soil water, especially during heavy rainfall. A two-stage ripper with upper and lower loosening working bodies of the "paraplau" type was developed for implementation of this technology *(Mamatov & Mirzayev, 2013; Mirzaev, Mamatov, Avazov, & Mardonov, 2019; Mirzaev, Mamatov, & Tursunov, 2019).* It includes a frame 1, on which working bodies 2 and 3 are successively and alternately installed (Fig. 1). Each working body of the "paraplau" type consists of a rack 4 inclined in the transverse vertical plane and a knife 5, chisels 6, a field board 7 and a loosening plate 8 fixed on it.

Each working body of the "paraplau" type consists of a rack 4 inclined in the transverse vertical platan where knife 5, chisels 6, field board 7 and loosening plate 8 are fixed on it. The rack's inclined part of the working body 2 is made with a smaller height, and the inclined part of the working body 3 is made with a greater height. On the working body 3 with a greater height, the loosening plate is fixed at the level of the loosening plate of the working body with a lower height.
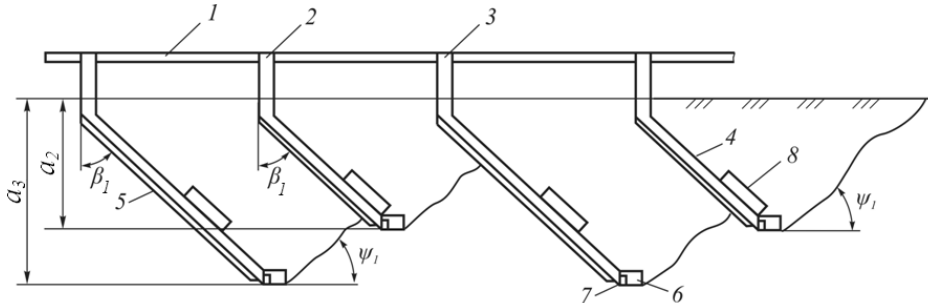

Fig. 1 Technological working process of a two-stage ripper

A stepped bottom of the furrow with periodic indentations (intra soil ridges) intersecting a densified sole is obtained after passing a two-stage ripper. Intrasoil ridges contribute to the complete retention and accumulation of soil water (particularly after heavy rainfall) and water erosion is prevented accordingly.

RESULTS AND DISCUSSION

The loosening plate's angle ε of installation to the rack's surface, its length l_R and width b_R, length l_{pd} and width b_{pd} of the field board, the value of the inter-legged working bodies M and the longitudinal distance L between them are the main parameters of the ripper with working bodies such as "paraplau" (Fig.2.). Loosening technological parameters that determine its effectiveness are the depth and quality of the loosening, the distance between the loosened strips, the width and depth of subsoil stage loosened at the bottom of furrow.

The area of soil's loosened zone of the arable and subsurface layers affects, on the one hand, the energy intensity of tillage, and on the other hand, the ability to retain and accumulate of soil water. Therefore, to select the layout of the working bodies and other parameters of a two-stage cultivator, we investigated their effect on the loosening fullness, the depth of the step and the distance between the loosened strips.

The quality of soil loosening was assessed by fullness of loosening, i.e. the loosening coefficient η, representing the ratio of the loosened soil zone area F_1 to the total area F, located in platan perpendicular to the direction of ripper's movement, limited by working width of grip B_p and maximum loosening depth, i.e. depth processing a_h of the lower working body, i.e. $\eta = F_1/F$ (*Mamatov & Mirzayev, 2014a*).

The energy intensity of tillage was evaluated by the two-stage ripper's resistivity, i.e. $K=P/F$, where P – two-stage ripper's traction resistance; F – total area of the arable and subsurface layers loosened part (*Mamatov & Mirzayev, 2014c*).

The angle that meets these conditions is determined from the following relation: $\varepsilon \leq (\pi/2 - \varphi_{max})/2$, where φ_{max} – maximum angle of soil friction with the plate's working surface, at $\varphi_{max} \approx 40°$ angle $\varepsilon \leq 25°$.

The loosening plate's greatest length l_R was found (condition: excluding soil loading in front of the plate and moving the soil by the plate to the surface of arable land) by the following expressions (*Mamatov & Mirzayev, 2014b*):

$$l_R \leq \frac{2\sigma\cos\varphi}{q\sin(\varepsilon+\varphi)}, \tag{1}$$

q – coefficient of volumetric crumpling of soil, N/m³; σ – temporary soil resistance to compression, Pa; φ – soil friction angle on metal, gr.

Taking into account the conditions for ensuring agrotechnical requirements for the ridges' height formed between the aisles of upper working bodies, the below formula was obtained to determine a lateral distance between the working bodies:

$$M = 2na_2ctg\psi_1 + b_d, \qquad (2)$$

where n – ridge's permissible height ratio to the depth processing of the upper working body.

While determining the longitudinal distance between the working bodies, the tool's condition from being clogged by plant residues and soil was taken into account. (Fig. 3). Below equation was obtained to determine the minimum distance between the working bodies of a two-stage ripper:

$$L_2 \geq (a_3 - a_1)ctg\psi + \frac{\sigma}{\gamma g(1 + \frac{W}{100})}ctg(\alpha_d + \varphi)\cos\alpha_d + (a_3 - a_1 - h)tg\beta_1, \qquad (3)$$

where a_1 – depth of the rack's straight part immersion into the soil, m; ψ – soil spalling longitudinal ; W – soil moisture, %; h – lift height chisels, m; α_d – crumbling chisels angle, gr.
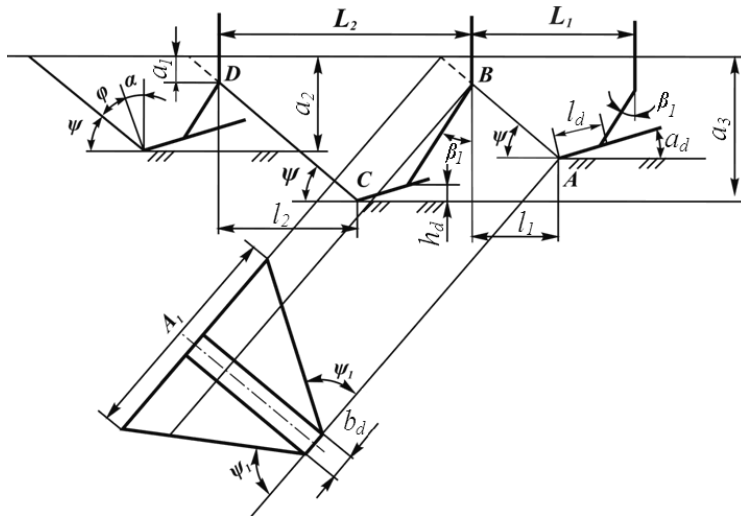

Fig. 2 Scheme for defining the soil deformation zone by the working bodies of a two-stage ripper

Field boards play a central role to support a two-stage ripper and ensure the stability of its travel across the grip's width and the straightness of the unit's movement in a horizontal platan. The field board's width should be less than or equal to the chisel's height h, otherwise the soil coming from the chisel will fall on it, which will lead to an increase in the ripper's resistance. Thus, we have:
$$b_{pd} \leq h = 0,072m, \ b_{pd} = 0,07 \text{ m}.$$

The field board length was determined based on the condition that its pressure on the furrow's wall does not exceed a permissible value:

$$l_{pd} \geq \frac{\eta K a_m b_k \sin(\alpha + \theta)\cos\varphi}{[p]\cos\theta\cos(\alpha + \varphi)}, \qquad (4)$$

where K – soil resistivity while loosening, Pa; η – ripper's coefficient; φ –friction angle on field board, gr; a_m – average depth of processing ripper, m; b_k – grip width of the working body, m; $[p]$ – permissible value of the field board's specific pressure on the furrow wall, Pa; α – the ripper thrust line angle , gr; θ – angle between the resultant force direction on the working body and the translational motion of the ripper, gr.
35 m, $[p]=5 \cdot 10^4$ Pa; $K=5 \cdot 10^4$ Pa; $\theta =20°$ length $l_{pd} \geq 0,16$ m.

To select a type of working body with an inclined rack, the experimental studies of two types of working bodies were carried out: with upper inflection of the rack (above the surface of tillage); with lower inflection of the rack (under the surface of tillage). The studies demonstrated that both types of working bodies on agrotechnical and energy indicators differ slightly from each other. Therefore, we have chosen a working body with a lower inflection, since it is possible to install a disk knife vertically in front of it.

The results from experimental studies showed that soil crumbling, stubble conservation, soil surface

crests and specific traction resistance, as well as the reliability of the ripper, depend on the transverse and longitudinal distances between the working bodies. With a transverse distance between the working bodies of 0.35 and 0.40 m and a longitudinal distance of 0.50-0.60 m, all agrotechnical indicators of a two-stage ripper were observed, the clogging of its working bodies did not occur.

Comparative experimental studies of various schemes for a two-tiered ripper revealed that a two-stage ripper with alternating upper and lower working bodies is the most appropriate. As well as, two-tier ripper with alternating upper and lower working bodies has a lower specific traction resistance by 21.75% compared to a ripper with two lower working bodies.

The results also showed that initially, the working body's traction resistance slightly increased with increasing angle ε of the loosening plate to the rack surface from 5 to 15º, a further increase in the angle ε led to its intensive increase. The drag resistance increased more intensively at high speeds by increasing angle ε. As the angle increased from 5 to 25º, the degree of soil loosening improved. However, a soil displacement towards the furrow was observed with a further increase in the angle of more than 25º, the height of the ridges was beyond the limits of acceptable agrotechnical requirements. Analysis of the results indicated that the traction resistance of the working body increased rapidly with an increase in the plate width from 0.05 to 0.15 m, and the quality of loosening improved. A further increase in the plate width slightly affected the amount of traction resistance. Increasing the plate width from 0.05 to 0.12 m did not significantly affect the height of the ridges. A further increase in width led to an intense increase in the height of the ridges. In this case, its values were beyond the limits of permissible.

It has been established that the rational width and length of the plate should be selected in the range of 0.09-0.12 m and 0.12-0.15 m.

CONCLUSIONS

It has been established that the most rational design scheme of a two-stage ripper with inclined racks was a plow scheme with alternating upper and lower working bodies with the lower inflection of the rack; high-quality loosening with the lowest energy costs was ensured at the longitudinal and transverse distances between the working bodies of 0.50-0.60 m and 0.35-0.40 m and the field board's width and length of 0.07 m and 16 m respectively. The rational values of the loosening plate parameters were within the following limits: the maximum angle of the loosening plate to the rack surface was 25º, the plate length and width were 0.12-0.15 m 0.9-0.12 m respectively.

REFERENCES

1. Amonov, M. O., Pulatov, A. S., & Colvin, T. S. (2006). Machine innovation for inter row cotton cultivation in Uzbekistan. *Applied engineering in agriculture*, *22*(5), 665-674.

2. Khamraev, M. B., Nasriddinov, M. N., & Nasriddinov, M. R. (1989). *Intensification the use of desert soils*. Mehnat.

3. Lal, R. (2017). Soil erosion by wind and water: problems and prospects. In *Soil erosion research methods* (pp. 1-10). Routledge.

4. Mamatov, F. M., & Mirzayev, B. S. (2013). Soil protection and moisture saving technologies and tools for tillage. *European Applied Sciences*, *9*, 115–117.

5. Mamatov, F. M., & Mirzayev, B. S. (2014a). Erosion preventive technology of crested ladder-shaped tillage and plow design. *European Applied Sciences*, *4*, 71–73.

6. Mamatov, F. M., & Mirzayev, B. S. (2014b). The quality of soil loosening theoretical determination by a two-stage ripper with working bordies of an inclined type. *TashSTU*, *3*, 108–112.

7. Mamatov, F. M., & Mirzayev, B. S. (2014c). Theoretical definition of chisel's working body traction resistance of the „paraplau" type. *Problems in Mechanics*, *3*, 172–176.

8. Mirzaev, B., Mamatov, F., Avazov, I., & Mardonov, S. (2019). Technologies and technical means for anti-erosion differentiated soil treatment system. *E3S Web of Conferences, 97*(05036).

9. Mirzaev, B., Mamatov, F., & Tursunov, O. (2019). A justification of broach-plow's parameters of the ridge-stepped ploughing. *E3S Web of Conferences, 97*(05035).

10. Mirzajonov, K. M. (1981). *Wind erosion of irrigated soils in Uzbekistan and the fight against it*. Science.

11. Pimentel, D., Harvey, C., Resosudarmo, P.,

Sinclair, K., Kurz, D., McNair, M., & Blair, R. (1995). Environmental and economic costs of soil erosion and conservation benefits. *Science*, 267(5201), 1117-1123.

12. Stetler, L. D., & Saxton, K. E. (1996). Wind erosion and PM10 emissions from agricultural fields on the Columbia Plateau. *Earth surface processes and landforms*, *21*(7), 673-685.

Corresponding author:

Bakhadir S.Mirzayev, doctor of the technical sciences, professor, Tashkent Institute of Irrigation and Agricultural Mechanization Engineers, 39 Kari Niyazi, Tashkent 100000, Uzbekistan, E-mail: bahadir.mirzaev@tiiame.uz, mirzayev.bakhadir@bk.ru

DESIGN OF COMPOSITE FRAMES USED IN AGRICULTURAL MACHINERY

Jaroslav MLÝNEK[1], Michal PETRŮ[2], Tomáš MARTINEC[2]

[1]Department of Mathematics, FP, Technical University of Liberec, Liberec 1, Studentská 2, Czech Republic
[2]Institute for Nanomaterials, Advanced Technologies and Innovation, Technical University of Liberec, Liberec 1, Studentská 2,Czech Republic

Abstract
At present, composite materials are increasingly used in agricultural machinery. The light weight, long lifespan and minimal maintenance of composites are among the main reasons for their use in agricultural machinery. Frame composites are often produced for the needs of agriculture. The production technology of these composites is based on the winding of fibres (from carbon or glass) on a frame (usually from polyurethane). A fibre-processing head and industrial robot are used in the production of composite frame. This paper describes the calculation of an appropriate off-line trajectory of the industrial robot during the passage of frame through the fibre-processing head. The described mathematical model of the winding process and matrix calculus are used to calculate suitable robot trajectory.

Key words: composite; fibre-processing head; industrial robot; mathematical model; software implementation.

INTRODUCTION

At present, composites are increasingly replacing classic materials (such as iron, steel, aluminium, wood) in industrial production. The main advantages of using composite materials are their low weight (75% lighter than steel and 30% lighter than aluminium), strength, flexibility, weather and corrosion resistance, minimal maintenance, long life span (see (*Gay & Hoa, 2007*), (*Petrů et al., 2015*)). Composites offer an attractive ratio of material properties-to-production costs. The use of composite materials is currently most widespread in the aerospace and automotive industries. However, composites are also currently well-established in other areas. A significant sector in the use of composites is production of agricultural machinery. In addition to the general advantages of composites the use of composites in the production of agricultural machinery makes it possible to achieve special cargo space shapes. The agricultural machine also causes less pressure on arable land due to its lower weight when using composites. Specifically, the use of composite frames is significant in the production of tractors, grain harvesters, various agricultural cultivators etc. In particular, composite frames are often used to reinforce the chassis and driver's cab of agricultural machinery. Composite frames can also be used to reinforce cargo space, cab doors and various covers of machines.

The article is focused on the technology of composite frame production using a fibre-processing head and an industrial robot. All experimental tests were performed at a robotic workplace (see Fig. 1). The fibre-processing head (see Fig. 2 on the left) is fixed in the robot workspace and the frame is fastened to the end-point of the robot (robot-end-effector, REE, see Fig. 2 in the middle and Fig. 3 on the left). The closed composite frame shown in Fig. 3 on the left is used to attach the side window in the tractor cab. The paper presents a mathematical model of the winding of fibres on a frame. The use of matrix calculus (especially matrices of rotations and translations) allows us to find a suitable trajectory of REE when passing the frame through the fibre-processing head. Calculation of robot trajectory is programmed in the Delphi development environment.

MATERIALS AND METHODS

We describe a mathematical fibre winding model to calculate a suitable REE trajectory during the passage of the frame through the fibre-processing head. The winding technology is implemented on the basis of the use of the fibre-processing head and an industrial robot. The fibre-processing head consists of three guide lines, each of which has ten coils with carbon or glass fibres (see Fig. 3 on the right). The composite frame passes through the fibre-processing head and three layers of fibres are

gradually wound on the surface of the frame. The first rotating guide line winds fibres under angle $\pi / 4$, the middle guide is static and winds the second layer of fibres under angle 0 (placement of the fibres in a longitudinal direction). The second rotating outer guide line winds the fibres under angle $-\pi / 4$. The winding process is shown in Fig. 2 on the left (fibre-processing head contains three guide lines). The passage of the frame through the fibre-processing head should be orthogonal to the guide lines and the frame should be go through the head as near the centre of the guide lines as possible. In this way, the correct winding angles and the homogeneity of the fibre windings are ensured. We need to determinate the appropriate trajectory of the REE to meet the above conditions.
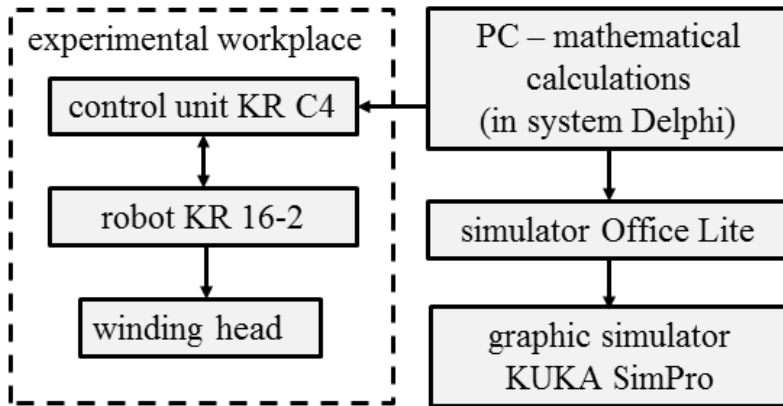
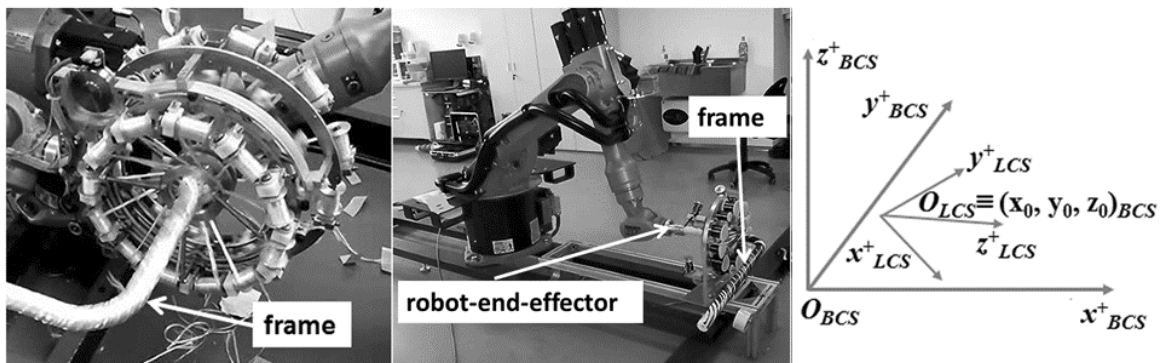**Fig. 1** Schematic representation of the experimental robotic workplace.

Fig. 2 Example of fibre-processing head with three guide lines (on the left); industrial robot with frame fastened in the end-effector, fibre-processing head contains only one guide line (in the middle) and basic coordinate system (BCS) of the robot and local coordinate system (LCS) of REE (on the right).

Industrial robot workspace in our model is defined by the base right-handed Euclidean coordinate system E$_3$ (BCS , see Fig. 2 on the right). Description of location and orientation of individual subjects in the robot workspace is made in BCS . Subsequently, we determine the local right-handed Euclidean coordinate system E$_3$ (LCS , see Fig. 2 on the right). This system describes location and orientation of REE towards BCS . In the following text, we will label the vectors and points with coordinates in BCS with the subscript $_{BCS}$ and vectors and points with coordinates in LCS with the subscript $_{LCS}$.

1/ <u>Robot activity control</u>
The robot central unit controls all working activities of the industrial robot (see Fig. 2 in the middle) using instructions through the REE. The location and orientation of the REE relative to BCS is defined

by the position of LCS relative to BCS. The LCS origin is positioned in the REE. The actual position of the LCS with regard to the BCS is determined by six parameters listed in the tool-centre-point (TCP), where $TCP = (x, y, z, a, b, c)$. The first three parameters specify the coordinates of the origin of the LCS in regard to the BCS. The last three values a, b and c specify the angle of the rotation of the LCS around the axis z, y, and x with regard to the BCS.
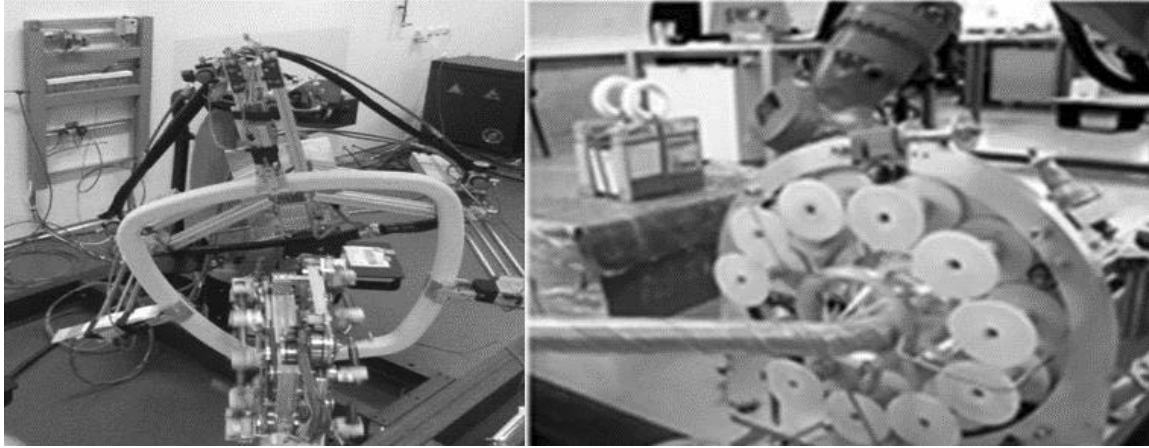

Fig. 3 Industrial robot with connected polyurethane frame and fibre-processing head (on the left) and guide line of fibre-processing head with ten coils with fibres (on the right).

2/ Fibre-processing head representation
The fibre-processing head is fixed in the working space of the robot. Each of the three guide lines of the head has ten coils with carbon fibres (see Fig. 3 on the right). These fibres are gradually wound onto the frame. Individual components of the head are described in BCS. The first outer rotating guide line is presented by circle $k1$ with the centre $S1_{BCS}$ and the second outer rotating guide line by circle $k2$ with the centre $S2_{BCS}$ (see Fig. 4 on the right). The second outer rotating guide line is presented by circle $k2$ with the centre $S2_{BCS}$. The static middle guide line (enables the placement of the fibres in a longitudinal direction) need not be considered in the model. The circles $k1$ and $k2$ have an identical radius r_{CIRCLE}. Centres $S1_{BCS}$ and $S2_{BCS}$ lie on the axis s of the fibre-processing head.

The centre of the fibre-processing head is represented by point H_{BCS}. Unit vector $\mathbf{h1}_{BCS}$ indicates the direction of the passage of the frame through the head. Vectors $\mathbf{h1}_{BCS}$ and $\mathbf{h2}_{BCS}$ are orthogonal. Point H_{BCS} together with vectors $\mathbf{h1}_{BCS}$ and $\mathbf{h2}_{BCS}$ allow us to calculate a REE trajectory when the frame passes through the head.

3/ Composite frame representation
The composite frame has a circular cross-section. The frame can be described by its central axis o and radius $\mathbf{r}_{TUBE}$ ($r_{CIRCLE} > r_{TUBE}$). An example of a vertical section of a polyurethane frame composed of two perpendicular arms is shown in the Fig. 4 on the left. The central axis o is defined in the LCS (of the REE) by a discrete set of points $B(i)_{LCS}$ and the unit tangent vectors $\mathbf{b1}(i)_{LCS}$ at those points, $1 \leq i \leq N$. In addition, the unit vector $\mathbf{b2}(i)_{LCS}$ ($1 \leq i \leq N$) lies in the plane orthogonal to the vector $\mathbf{b1}(i)$. The points $B(i)_{LCS}$ and vectors $\mathbf{b1}(i)_{LCS}$, $\mathbf{b2}(i)_{LCS}$ are prescribed by a composite designer to ensure passage of the frame through the fibre processing head. The variable l represents the distance between point $B(1)_{LCS}$ and a point on the axis o (see Fig. 4 on the left).

4/ Calculation of REE trajectory
We describe the main idea of REE trajectory calculation. A detailed calculation procedure is given in (*Martinec et al.*, 2015). Recall that frame is fastened to the REE. We calculate REE trajectory that ensures the gradual passage of the axis o of the frame through the centre H_{BCS} of the fibre-processing head (see Fig. 5) in the desired direction $\mathbf{h1}_{BCS}$ (and by this way passage frame through head).

The frame's initial point of passage is $B(1)_{LCS}$ and the end point is $B(N)_{LCS}$ (for example see Fig. 4 on the left, end point is $B(106)_{LCS}$).
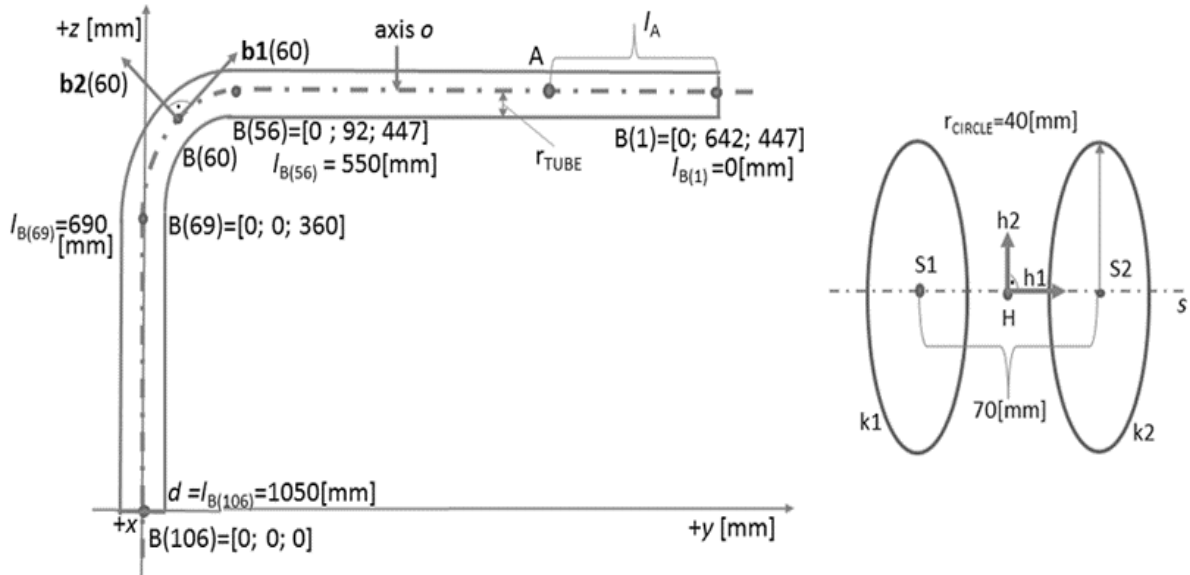

Fig. 4 Example of a vertical section through a composite frame composed of two perpendicular arms (on the left) and two outer rotating guide lines $k1$ and $k2$ of fibre-processing head specified in *BCS* (on the right).
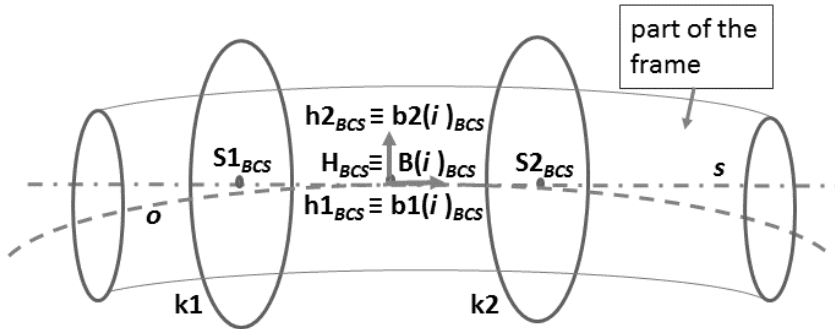

Fig. 5 Schematic representation of the composite frame passing through the fibre-processing head.

We need to find such TCP_i for each i ($1 \le i \le N$) that the following relations are valid (see Fig. 5)

$$B(i)_{BCS} \equiv H_{BCS}, \ \mathbf{b1}(i)_{BCS} \equiv \mathbf{h1}_{BCS}, \ \mathbf{b2}(i)_{BCS} \equiv \mathbf{h2}_{BCS}. \tag{1}$$

It means that the two orthogonal vectors and their common initial point originally defined in the *LCS* are in the same position in the *BCS* as the two fixed orthogonal vectors and their common initial point specified in the *BCS*. The location and orientation of the REE in *BCS* in the i-th step of the passage of the frame through the fibre processing head are uniquely determined by the relation (1). The identification of vectors $\mathbf{b2}(i)_{BCS}$ and $\mathbf{h2}_{BCS}$ allows the performance of the necessary rotation of the frame around the tangent of the axis o at point $B(i)_{BCS}$ when the point $B(i)_{BCS}$ is identified with centre of the head H_{BCS}. We calculate the transformation matrix $\mathbf{T}_i$ from *LCS* to *BCS* for the i-th step of passage of the frame through the fibre processing head. The transformation matrix $\mathbf{T}_i$ is generally the product of the translation matrix $\mathbf{L}_i$ and the rotation matrix $\mathbf{Q}_i$, i.e.

$$\mathbf{T}_i = \mathbf{L}_i \cdot \mathbf{Q}_i. \tag{2}$$

Validity of relation (1) is reached by applying matrix $\mathbf{T}_i$ in relation (2) to *LCS*, i.e. then

$$H_{BCS} \equiv B(i)_{BCS} = \mathbf{T}_i B(i)_{LCS}, \ \mathbf{h1}_{BCS} \equiv \mathbf{b1}(i)_{BCS} = \mathbf{T}_i \mathbf{b1}(i)_{LCS} \text{ and } \mathbf{h2}_{BCS} \equiv \mathbf{b2}(i)_{BCS} = \mathbf{T}_i \mathbf{b2}(i)_{LCS} \text{ is true.}$$

Calculation of translation matrix $\mathbf{L}_i$ and rotation matrix $\mathbf{Q}_i$ in relation (1) is made using matrix calculus (in more detail see (*Sciavicco & Siciliano*, *2004*), (*Martinec et al.*, *2015*)). Rotation matrix $\mathbf{Q}_i$ can be written in the form (see (*Martinec et al.*, *2015*))

$$\mathbf{Q}_i = \mathbf{Rot}(z, a_i) \cdot \mathbf{Rot}(y, b_i) \cdot \mathbf{Rot}(x, c_i), \tag{3}$$

where $\mathbf{Rot}(z, a)$ is the orthogonal matrix of rotation of *LCS* around axis z by angle a, $\mathbf{Rot}(y, b)$ orthogonal matrix of rotation of *LCS* around axis y by angle b and $\mathbf{Rot}(x, c)$ orthogonal matrix of rotation of *LCS* around axis x by angle c (the so-called Euler angles of matrix $\mathbf{Q}_i$).

Now, we can determine $TCP_i = (x_i, y_i, z_i, a_i, b_i, c_i)$, where parameters x_i, y_i and z_i define translation of the REE and are determined by matrix $\mathbf{L}_i$ in relation (2) and the last three parameters a_i, b_i and c_i are given by relation (3) (in more detail see (*Martinec* et *al.*, *2015*)).

RESULTS AND DISCUSSION

The procedure described in paragraph 4/ of previous chapter is used to calculate the sequence TCP_i (for $1 \le i \le N$) on an external PC. Then we enter the calculated set of TCP_i into the robot's control unit. Subsequently, the robot creates by its commands a continuous trajectory of the REE allowing the passage of the frame through the fibre-processing head. The robot's control unit creates the REE trajectory on the principle of linear interpolation or using of cubic splines of the parameters included in TCP_i ($1 \le i \le N$).

The quality of the produced composite frame depends primarily on the quality of the frame itself (often created from polyurethane) and on the quality of wound fibres (usually from carbon or glass). However, keeping the correct angles and homogeneity of the filaments on the frame are also very important for the quality of composite frame. Traditional procedures of composite frames manufacturing based on the manual skills of technicians are labour-intensive and time-consuming. In addition, it is difficult to maintain the correct winding angles of fibres on the frame during manual processing. One of the possible approaches used to produce composite frames is to stretch the fabric from the fibres on a frame. However, if the frame has a complicated 3D shape or if the frame is closed, then this approach is difficult to use. In such cases, the method of winding of endless fibre strands on a frame geometry using rotary fibre-processing head is suitable for use.

Note that using two industrial robots in the production of composite frame can also be used in the case of a closed frame (see Fig. 6). A composite frame is connected to the first robot and during the winding process the composite frame is fastened to the second robot.

Described approach to REE trajectory definition is significantly more effective than the teach-in method. The principle of this method is that the technician finds a suitable trajectory based on repeated use of the robot control panel called the "teach pendant".

CONCLUSIONS

This article describes the procedure of calculating the 3D trajectory of REE of an industrial robot during the manufacturing of a frame composite. This described computational procedure in the article allows us to determine the appropriate off-line REE trajectory based on the use of a mathematical model of winding process and matrix calculus.

Suppliers of industrial robots currently offer specific software tools facilitating control of the REE for specific tasks of the industrial robot (e.g., laser cutting, welding, pressing, packing). But these tools are not applicable for our problem.

Procedure of off-line calculation of REE trajectory described in the article is completely independent of the industrial robot type and software tool of robot unit. Therefore, the described algorithm can be applied to any industrial robot and any manufacturing process.

The procedure for determining the optimized REE trajectory in the winding process can be obtained by modifying the described algorithm in this article (see (*Mlýnek et al.*, *2018*). In contrast, the teach-in method is practically unusable finding the optimal trajectory.
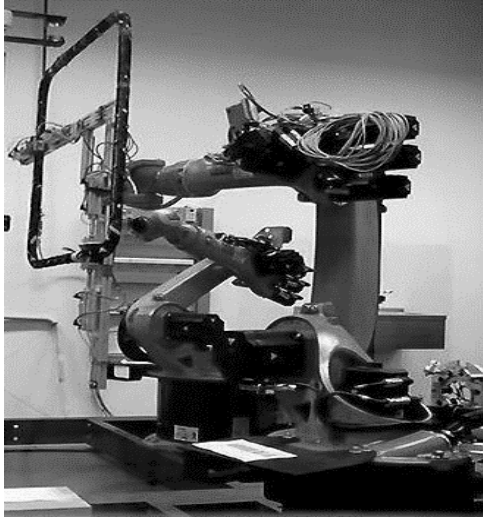
Fig. 6 Cooperation of two industrial robots in the production of closed composite frame.

REFERENCES

1. Gay, D. & Hoa, S. V. (2007). *Composite materials – design and applications.* CRC press. Taylor & Francis Group London. ISBN: 978-1-4200-4519-2.

2. Martinec, T., Mlýnek, J., & Petrů, M. (2015). Calculation of the robot trajectory for the optimum directional orientation of fibre placement in the manufacture of composite profile frames. *Robotics and Computer-Integrated Manufacturing*, *25*, 42-54. ISSN: 0736-5845, doi: 10.1016/j.rcim.2015.02.004.

3. Mlýnek, J., Petrů, M., & Martinec, T. (2018). Optimization of Industrial Robot Trajectory in Composite Production. In *Proceedings of the 18th International Conference on Mechatronics - Mechatronika, ME 2018, Brno* (pp. 270 – 275). Brno University of Technology. ISBN: 9788021455443.

4. Petrů, M., Novák, O., Lepšík, P., & Myšáková, D. (2015). Experimental Analysis and Numerical Modelling of Interphase Interfaces of New Environmental Low-Energy Composites. *Applied Mechanics and Materials*, 732, 95-98. doi: 10.4028/www.scientific.net/AMM.732.95.

5. Sciavicco, L. & Siciliano, B. (2004*). Modelling and Control of Robot Manipulators*. London: Springer. ISBN 978-1-84628-641-4.

Corresponding author:
Doc. RNDr. Jaroslav Mlýnek, CSc., Department of Mathematics, FP, Technical University of Liberec, Studentská 2, Liberec, Czech Republic, phone: +420 485352847, e-mail: jaroslav.mlynek@tul.cz.

EVALUATING THE PERFORMANCE OF AI FOR SORTING GREEN SOYBEAN

Tomohiro MORI[1], Mitsuhiko KATAHIRA[1]

[1]*Department of Faculty of Agriculture, Yamagata University*

Abstract
Almost all farmers who cultivate green soybeans do sorting manually, with a work efficiency of 12kg/h. They desire a sorting machine for green soybeans. In recent years, the performance of AI (artificial intelligence) has been improving because of deep learning. If we can use the AI for sorting by deep learning and mount on sorting machine, it will be possible to develop a high performance sorting machine. In this study, we made an AI to detect the green soybeans' position and judge its quality, and discuss how to make a high-performance AI. Results indicated that it is necessary to prepare both non-defective product and defective product image data when we make AI for sorting. It was found that when many quality characteristics were set and images of two or more varieties were mixed in the dataset, the performance of AI was low.

Key words: *AI; deep learning; YOLOv3; sorting; labor saving.*

INTRODUCTION

In Japan, green soybean is cultivated in many areas. For the past 10 years, the cultivated acreage of green soybean changed little, but the production of green soybean decreased. One of the reason is the sorting which people do manually. The work efficiency is 12kg/h, so many farmers desire a sorting machine for green soybeans. *Katahira, et al. (2011)* made a sorting machine of green soybean on a trial basis, but due to the structure of the detection unit, there were problems in sorting accuracy. In recent years, the performance of AI is improving because of the deep learning, and various research has been conducted to apply AI to the field of agriculture. In addition, the performance of the object detection algorithm is also evolving. Famous object detection algorithms include "Faster R-CNN", "SSD" and "YOLO". If we use AI which is made by using deep learning and the object detection algorithm, we may be able to develop the green soybean sorting machine with high performance and simple structure and save labor in selection work. As a first step to realize this, we must establish a method to make a high-performance AI to sort green soybean quality. The aim of this study was to determine the important elements necessary for making a high-performance AI for sorting green soybean using deep learning.

MATERIALS AND METHODS

(1) Green soybean image collection

The green soybeans used for image data collection were cultivated in the farm of Yamagata University in 2018. We collected the green soybeans' images to use a green soybean's prototype selector (PITA-EDS-mini01, PITA-EDS001, Gaochao Engineering Co. Ltd.). After collecting the images, they were cut into a square of about 250pixels, with one green soybean in each image. Finally the images were rotated in eight directions and to increase the number of pictures.

(2) Dataset preparation

We classified green soybeans by eight quality characteristics (Fig.1). Non-defective product is only "Good" and other seven are defective products. Before doing deep learning, we needed to create teacher data. It is the information about the quality of green soybeans in the image. Therefore, I used the software "LabelImg" and annotated. To investigate how difference in dataset size and composition affect the performance of AI, four datasets were prepared and four types of AI were built (Tab.1).

(3) Development AI by deep learning

The environment of the computer which we used for the deep learning is shown in Tab. 2. We used Darknet (Open Source Neural Networks in C language) as a framework for deep learning and YOLOv3 as an object detection algorithm. Darknet and YOLOv3 were developed in 2018, and they are one of the highest performance framework and object detection algorithm as of 2018 *(Joseph & Ali, 2018)*. The number of times of deep learning is three pattern of 10000 times, 30000 times, and 50000 times. In Total, twelve AIs were made.

(4) Evaluation of AI's performance

First we prepared 20 image datasets of the eight quality items and show to them each AI. Then we counted the number of image data that AI correctly judged the quality of green soybeans. The detection rate was calculated by the equation (1).

$$A = \frac{W}{20} \cdot 100 \tag{1}$$

Where A is the detection rate (%), and *W* is the number of image data that AI correctly judged the quality of green soybeans. Since the datasets A and B (Tab.1) did not include the image data of the quality characteristics of "Good", the AIs of the datasets A and B cannot detect "Good" green soybeans. So we recorded only the detection rates of the seven quality characteristics other than "Good" when we used the AIs made with datasets A and B to get the detection rate data. After that, we summed up the detection rates and divided by the number of quality items to calculate the average detection rate. We collected 5 iterations of the average detection rate data.

Next we selected the AIs with the highest average detection rate in each datasets and showed the AIs the "Non-defective product" and "Defective product" image data which was newly prepared. The "Non-defective product" image dataset included the images of only one quality characteristics of "Good", and the "Defective product" image dataset included the images of seven quality items of defective products. The "Non-defective product" and "Defective product" image dataset contain 25 images respectively. The sorting rate was calculated by the equation (2).

$$\eta = \frac{Wg}{25} + \frac{Wf}{25} - 1 \tag{2}$$

Where η is the sorting rate, and *Wg* is the number of image data that the AIs correctly detected a non-defective item when we showed the AIs the "Non-defective product" image data, *Wf* is the number of image data that the AIs correctly detected defective item when we showed the AIs the "Defective product" image data. If the AIs in datasets A and B did not detect anything when they saw the "Non-defective product" image data, we presumed that they could detect "Non-defective product". We collected 10 iterations of the sorting rate data.

(5) Data analysis

Statistical analysis was performed using SAS (ver.9.4; SAS Institute Japan, Tokyo). The Average detection rate and the sorting rate was analyzed by Tukey's test at 0.05 probability level.
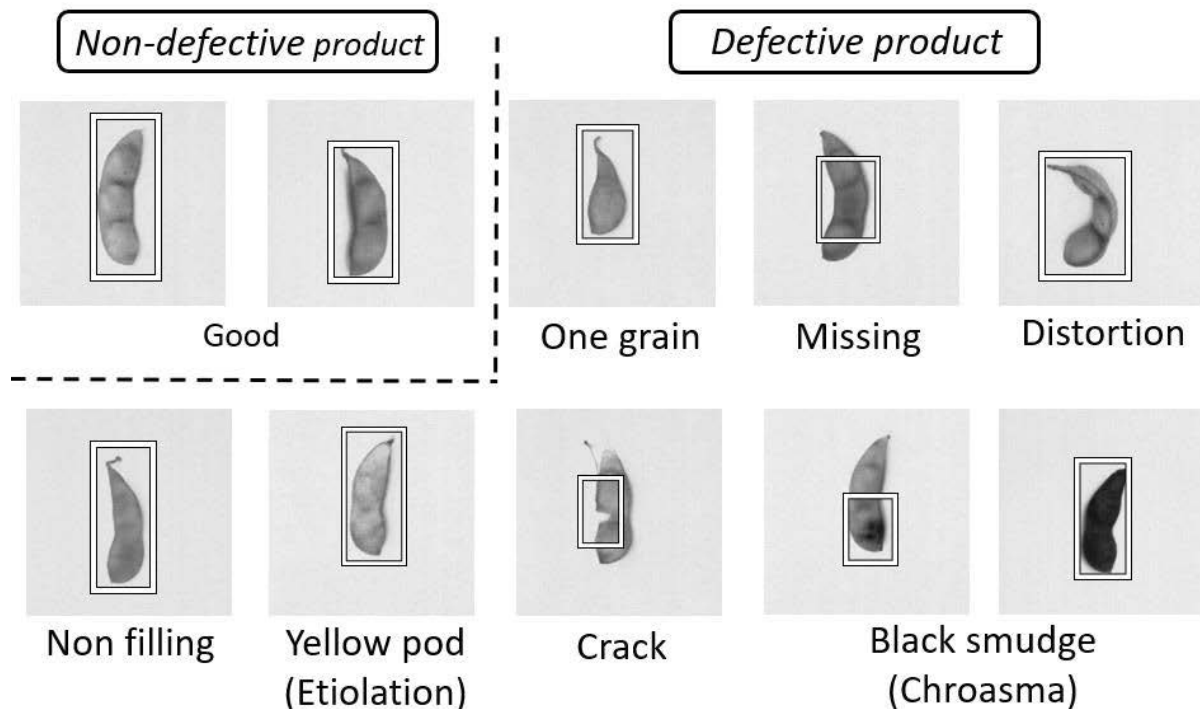

Fig.1 Eight quality items and area of annotation

Tab.1 Content of each dataset

Dataset	Content of data set	The number of image data	Variety of green soybean
A	7 defective characteristics excluding "Good"	1000 image data for each characteristic (total:7000)	Shonai–sango
B	7 defective characteristics excluding "Good"	2000 image data for each characteristic (total:14000)	Shonai–sango, Hiden
C	8 quality characteristics including "Good"	1000 image data for each characteristic (total:8000)	Shonai–sango
D	8 quality characteristics including "Good"	2000 image data for each characteristic (total:16000)	Shonai–sango, Hiden

Tab.2 AI development environment

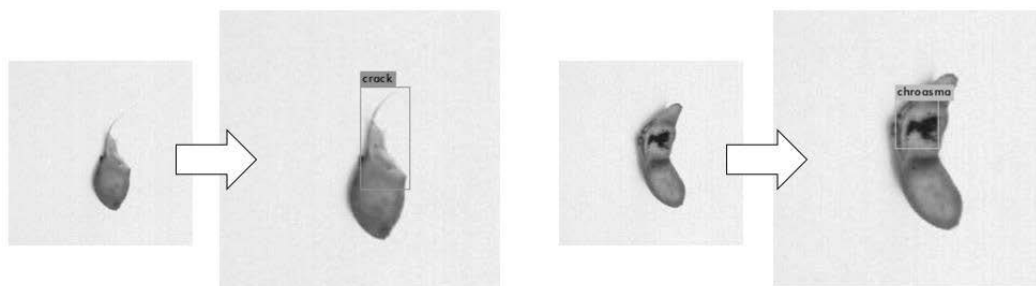| OS	CPU	GPU	NVIDIA Driver	CUDA	cuDNN	OpenCV
Ubuntu 16.04LTS	Intel Core i7–4790S	NVIDIA GeForce GTX1080Ti (11GB)	410.72	10.0	7.4.1	3.4.0

Fig.2 Example of quality judgement and position detection by AI

RESULTS AND DISCUSSION

(1) The average detection rate

The result of the average detection rate by each AI is shown in Fig.3. The average detection rate was highest for the AI of dataset B with 50000 times of deep learning, and the value was 88.6%. On the other hand, the average detection rate was lowest for the AI of dataset D with 50000 times of deep learning, and the value was 43.9%. There was no case that the AI could not detect green soybean at all. The datasets C and D included the "Good" images, so the AIs of datasets C and D have one more quality characteristic to detect compared to the AIs of datasets A and B. Further, the dataset D included the images of two green soybeans' varieties. The shape and color of "Shonai-sango" and "Hiden" are not very similar. In particular, the shape and color of these two varieties of "Good" differ greatly (Fig.4). If there are many quality characteristics that we want AI to detect, with mixed varieties that are not similar in shape and color in the dataset, the performance of AI will be degraded.

(2) The sorting rate

The result of the sorting rate by each AI is shown in Fig.5. The average sorting rate was highest for the AI of dataset C, and the value was 0.59. On the other hand, the sorting detection rate was lowest for the AI of dataset B, and the value was 0.02. Compared to the AIs of the datasets C and D, the AIs of the datasets A and B erroneously detected a non-defective product as a defective product in many cases. This caused the low sorting rate of the AIs from the datasets A and B. This suggested that it is necessary to add the "Good" image data in the dataset when we developing the AI for sorting.
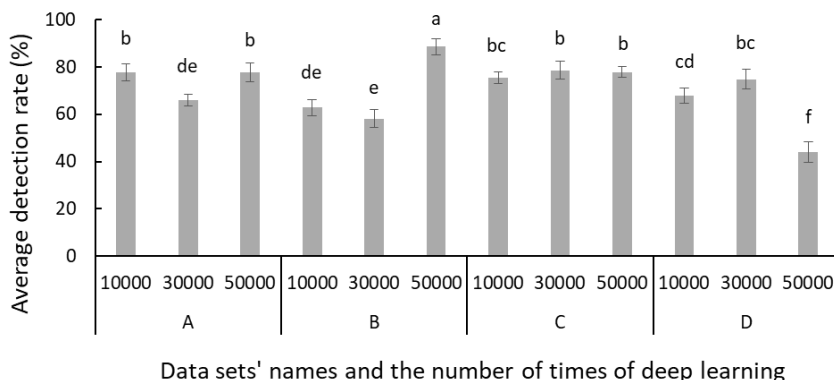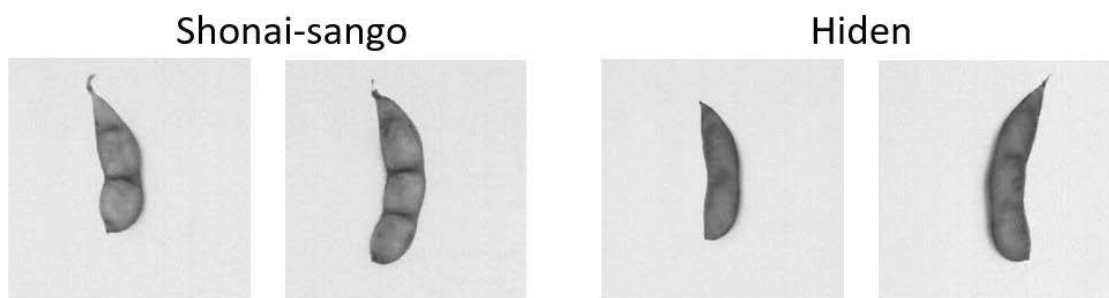

Fig. 3 Average detection rate

Fig.4 Example of "Shonai-sango" and "Hiden" Non-defective product image data
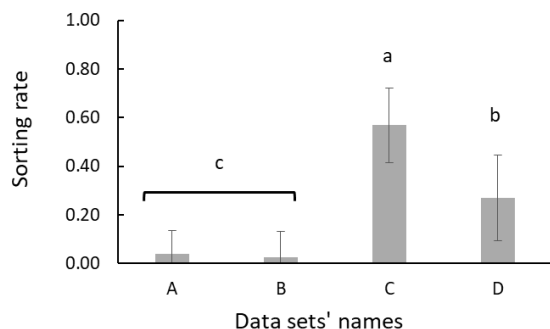

Fig.5 Sorting rate

In the past survey on green soybean sorting, in the case of manual sorting, the result of sorting rate was 0.59. From this, it was found that the sorting ability of AI with the highest performance is equivalent to that of humans.

CONCLUSIONS

This study sought to develop a sorting AI for green soybean that can be mounted on a sorting machine and it was shown that the AI can detect the green soybeans' quality characteristics by looking at the appearance of them. Through this experiment, we determined the elements necessary for developing a high-performance AI. As computer vision technology is evolving every day, we will explore the use of other frameworks and object detection algorithms, and compare the performance of those AIs. In the near future we will be able to develop higher-performance AI and mount on a sorting machine. Finally, the findings from this study will be also useful in developing the AI for other crop sorting and other uses.

REFERENCES

1. Joseph, R. & Ali, F. (2018). YOLOv3: An Incremental Improvement. *arXiv*, 1804.02767v1
2. Joseph, R. & Ali, F. (2016). You Only Look Once: Unified, Real-Time Object Detection. *arXiv*, 1506.02640v5.
3. Katahira, M., Zhang, S., Ohizumi, T., Gotou, T., Unuma, H., Tamura, A., & Gotou, K. (2011). Development of green soybean sorting method using image processing (part2) - Evaluation of green soybean sorting machine prototype performance. *Journal of the JAPANESE SOCIETY of AGRICULTURAL MACHINERY*, *73*(2), 127-134.
4. Li, Z., Jingdun, J., Guan, G., Xia, H., Wanlin, G., & Minjuan, W. (2018). Deep Learning Based Improved Classification System for Designing Tomato Harvesting robot. *IEEE Access, 6*, 67940-67950.
5. Shaoqing, R., Kaiming, H., Ross, G., & Jian, S. (2016). Faster R-CNN: Towards Real-time Object Detection with Region Proposal Networks. *arXiv*, 1506.01497.
6. Wei, L., Dragomir, A., Dumitru, E., Christian, S., Scott, R., Cheng-Yang, F., & Alexander, C. (2016). SSD: Single Shot MultiBox Detector. *arXiv*, 1512.02325

Corresponding author:

Tomohiro MORI, Department of Faculty of Agriculture, Yamagata University, 1-40-202 Midori Town, Turuoka City, Yamagata,Japan, 997-0046, email: a180012m@st.yamagata-u.ac.jp

VERTICAL GROUND HEAT EXCHANGERS – LOW-TEMPERATURE ENERGY SOURCES

Pavel NEUBERGER[1], Radomír ADAMOVSKÝ[1]

[1]*Department of Mechanical Engineering, Faculty of Engineering, Czech University of Life Sciences Prague*

Abstract

The most widely used types of ground exchangers in Europe, single (A) and double (B) U-tube exchangers, installed in 113 meters deep boreholes were verified during our research. The monitored parameters included the temperatures of heat carrier fluids, thermal resistances, specific outputs and extracted energies of vertical rock exchangers used as low-temperature energy sources for heat pumps. It is apparent from the results of the verification that the single U-tube exchanger was more effective than the double U-tube exchanger in terms of the monitored parameters. Temperatures of the fluids were higher for exchanger B and their distribution was more favourable. However, differences in average temperatures were only 0.35 K. The specific heat outputs per 1 m^2 of heat exchange surface area and specific energies extracted from the mass were higher at exchanger A than at B by 11.17 W and 370 kJ/m^2·day, respectively.

Key words: *temperature; heat carrier fluid; heat exchanger; heat output; heat resistance; energy extraction.*

INTRODUCTION

Heat pump energy systems use mainly low-temperature renewable energy sources contained in ground or rock mass, water or ambient air. At the same time, unlike other energy systems, they also make it possible to use anergy, the part of energy that is unusable in the sense of the 2nd Law of Thermodynamics. These facts evoke an urgent need for research into heat pump energy systems, especially in terms of renewability and sustainability of their low-temperature energy sources. This paper is focused on a rock mass as a low-temperature source for heat pumps. The energy contained in the rock mass is utilized by vertical tubular heat exchangers (VGHE), mostly U-shaped, stored in boreholes with depths up to 150 meters. The VGHEs heat carrier fluid temperatures, the extracted heat outputs and the energy values extracted from the rock mass are important parameters influencing the renewability and sustainability of the low-temperature energy source, as well as the overall effect of the energy system.

Michopoulos, Kyriakis (2009) developed and experimentally verified prediction model of the heat carrier fluid temperatures at the VGHEs output. The model demonstrated satisfactory accuracy during the whole verification procedure. *Mesaha et al. (2017)* focused on the temperature changes of the heat carrier fluids, heat outputs and energy values extracted from ground mass in dependence on the VGHEs pipe lengths. Numerical analysis of the VGHEs single and double U-tube dimensional model was performed by *Zeng et al. (2003)*. The results of their verification showed that double U-tube exchangers had higher specific heat output and lower thermal resistance per 1 m of borehole than single U-tube exchangers. *Ren et al. (2018)* monitored the temperatures of the heat carrier fluids, outputs and extracted heat of the VGHEs with steel and polyethylene pipes. Both the outlet temperatures and outputs were higher at the VGHE with steel pipes that those with polyethylene pipes. Long-term operation of VGHE in both heating and cooling modes was simulated by *Choi et al. (2018)* as well as by *Remiorz et al. (2015)*. Verification demonstrated that temperature of the heat carrier fluid and the VGHEs output in the winter period increased significantly when the heat was accumulated in the cooling mode during the summer. The causes of VGHEs degradation indicated by the thermal imbalance of the ground mass were discussed by *You et al. (2016)* and also by *Liet al. (2018)*. They elaborated a very detailed overview of the main problems caused by the thermal imbalance of the mass and what causes it to arise. In case of disruption of the balance, *Dai et al. (2015)* recommended to supplement VGHEs with a solar system used for ground mass regeneration.

The aim of this article was to analyze and compare the temperatures of the heat carrier fluids supplied to the heat pump evaporator, the VGHEs thermal resistances, their specific outputs and energies extracted by VGHEs from the ground mass during the heating season.

MATERIALS AND METHODS

Two types of VGHEs installed in a boreholes with a depth of 113 m were tested. VGHE A in a form of single U-tube was the first one, made of polyethylene piping PE 100RC 40 x 3.7 mm with a total length of 226 m (28.40 m^2). The second was VGHE B in a form of double U-tube made of polyethylene piping PE 100RC 32 x 2.9 mm with a total length of 452 m (45.44 m^2). The piping is resistant to point loads and cracks. Both VGHEs, together with horizontal ground heat exchangers, are sources of low-temperature energy for two heat pumps GreenLine HT Plus E 17 (heat output 2x 16.2 kW at 0/35 °C) and one pump IVT PremiumLine EQ E13 (heat output 13.3 kW at 0/35 °C), (Industriell Värme Teknik, Tnanas, Sweden). The heat pumps are used for heating of administrative building and service halls of VESKOM s.r.o. based in Prague Dolní Měcholupy. The following computation values were used for this location: outdoor temperature t_e = -12 °C, average temperature in the heating season 4.0 - 5.1 °C and the heating system operation time 216-254 days. The temperatures of the heat carrier fluids were measured at quarter-hour intervals on the VGHEs outlet and inlet pipes with Pt100 sensors and recorded by ALMEMO 5990 measuring device (AHLBORN Mess- und Regulungstechnik GmbH, Holzkirchen, Germany). The reference temperature of the ground mass was measured at a depth of 50 m in an empty non-operating borehole. The ambient temperatures t_e were recorded at a height of 2.5 m above the ground surface with ATF 2 KTY 81.210 sensor (S + S Regeltechnik, Nürnberg, Germany). Specific heat outputs ($q_{\tau a}$, $q_{\tau max}$) and energy extractions (q_a, q_{max}) were determined on the basis of the difference of heat carrier fluid temperatures, heat carrier fluid flow rates (V_τ) measured by MTW 3 electronic meters (Itron Inc. Liberty Lake, USA), specific heat capacities and densities corresponding to the medium temperature of the heat carrier fluid. The measurement took place during the heating season 2012/2013 from 17 September 2012 to 22 April 2013 (218 days). STATISTICA program (StatSoft, Inc. 2013) and MS Excel 2016 were used to evaluate the measured quantities.

RESULTS AND DISCUSSION

1. Temperatures of heat carrier fluids

The average daily temperatures of heat carrier fluids of VGHE A (t_A) and B (t_B) are shown in Figure 1. It presents an important observation that the temperatures of fluids did not reach negative values during the monitored period. The reaction of temperatures of the heat carrier fluids to the ambient temperature is evident here. The temperature course indicated an insignificant difference between temperatures t_A and t_B. Heat carrier fluid temperatures of VGHE A were higher on average only by 0.35±0.32 K. The output temperatures of VGHE type A were the same as those monitored by *Remiorz et al. (2015)* when testing similar type of VGHE.

The quadratic equations for the temperature trend lines of the VGHEs are in the form of (1) and (2). Determination coefficients R^2 correspond to the data very well. τ_d in equations (1) and (2) indicates the length of the heating period from its beginning, expressed in days.

$$t_A = 0.0004.\tau_d^2 - 0.1206.\tau_d + 14.731 \qquad (R^2 = 0.908) \qquad (1)$$
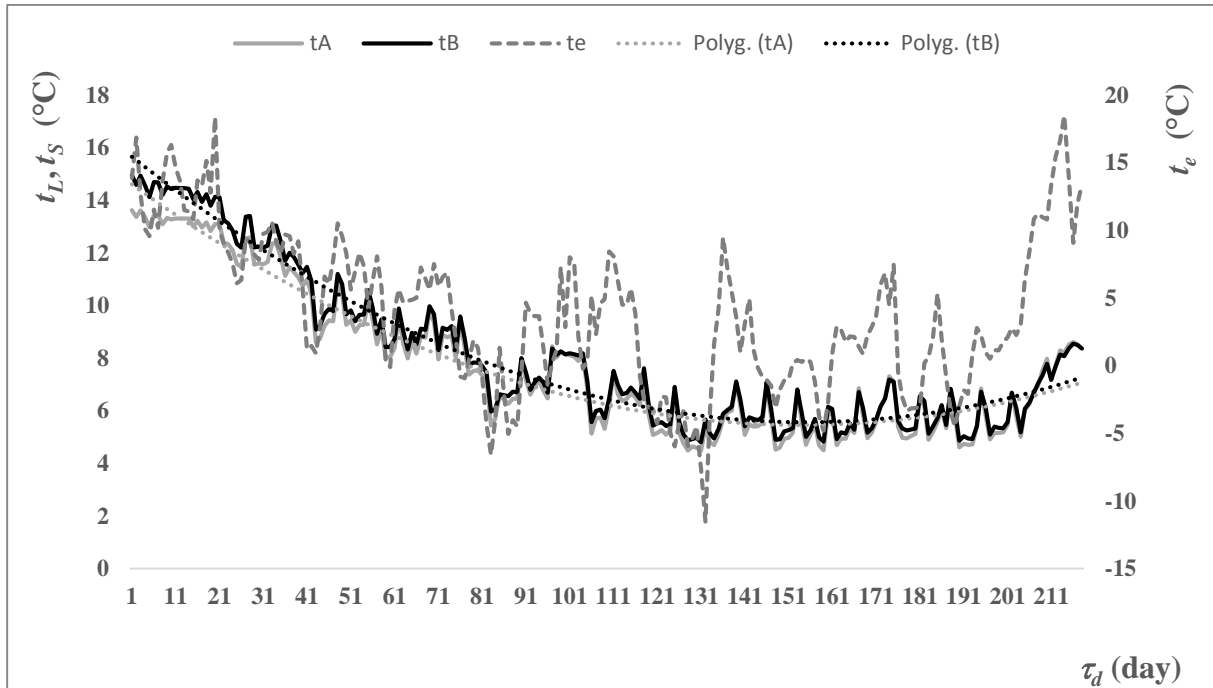$$t_B = 0.0004.\tau_d^2 - 0.1321.\tau_d + 15.798 \qquad (R^2 = 0.936) \qquad (2)$$

Fig. 1 Average daily temperatures of VGHEs heat carrier fluids t_A, t_B and ambient air temperatures t_e.

A different view and more information can be gained from the histogram of temperature distribution of heat carrier fluids during the heating season in Figure 2. This histogram is significant mainly because of the information it gives us on the relative frequency of average hourly temperatures f_i (5.232 values) at 2 K intervals characterized by the so-called class representative r, which ranges from 1.0 to 17.0 °C. The temperature mode $Mod(t)$, determining the interval of the most frequently occurring heat carrier fluid temperatures, is especially important variable of the histogram.
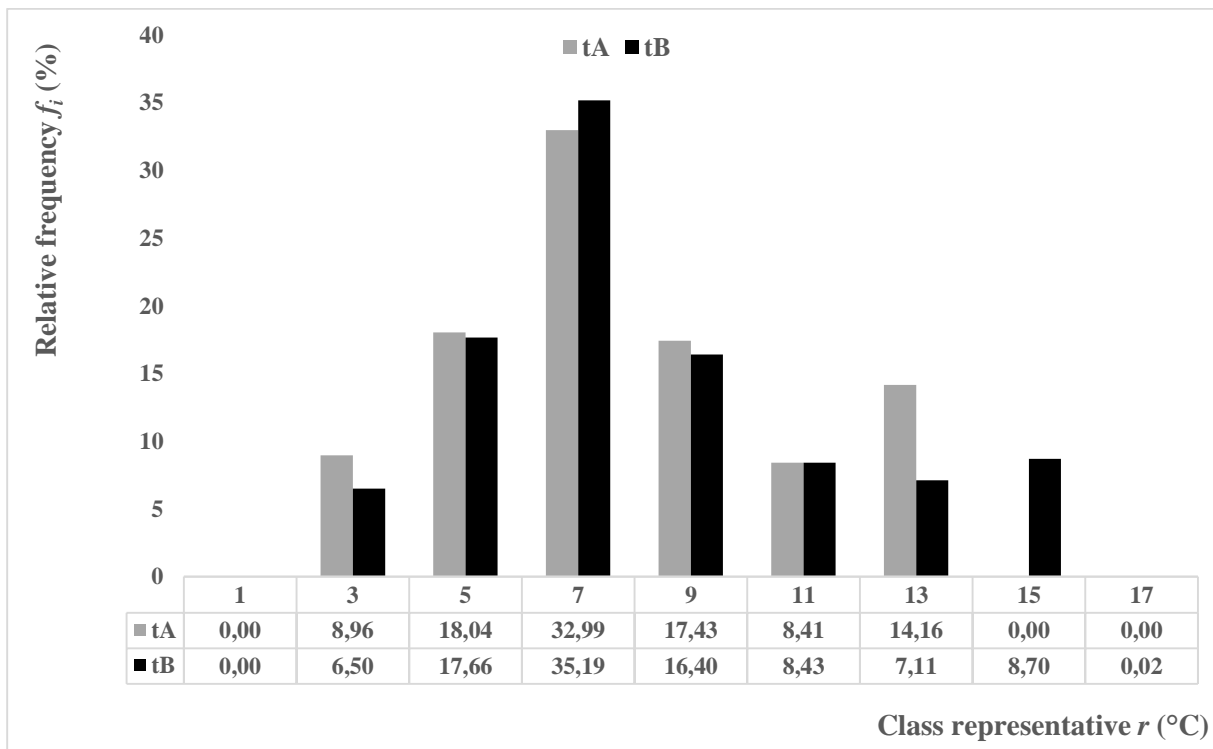

	1	3	5	7	9	11	13	15	17
■ tA	0,00	8,96	18,04	32,99	17,43	8,41	14,16	0,00	0,00
■ tB	0,00	6,50	17,66	35,19	16,40	8,43	7,11	8,70	0,02

Fig. 2 Relative frequencies of average hourly VGHEs heat carrier fluids temperatures t_A a t_B

As indicated by the results, the temperature mode of the heat carrier fluid *Mod(t)* of both VGHEs occurred in the interval 6.10–8.00 °C (r = 7 °C). However, the relative frequency of occurrence was higher at VGHE B (f_i = 35.19%) than at VGHE A (f_i = 32.99%). At the same time, temperatures of VGHE B occurred in higher ranges (r = 15 °C and r = 17 °C) than that of VGHE A (r = 13 °C). The higher frequency of the heat carrier fluid temperatures at higher temperature intervals indicated the advantage of this low temperature energy source.

2. Heat outputs and extracted energies

The following parameters are presented in Table 1: the average and the maximum flow rates of the heat carrier fluid, $V_{\tau a}$, and $V_{\tau max}$ respectively, total volume of the heat carrier fluid that had passed through the exchangers during the heating period, V_Σ, specific and maximum heat outputs converted to 1 m of pipe length and 1 m² of heat transfer surface of the exchangers, $q_{\tau a}$ and $q_{\tau max}$ respectively, average and maximum specific energies transferred from the mass by 1 m² of the exchanger during 1 day of the heating season, q_a and q_{max} respectively, the total amount of energy transferred from the mass by the exchanger during the heating season, q_Σ and also the total time of energy extraction by exchangers during the heating season, τ_Σ .

The specific heat outputs $q_{\tau a}$, $q_{\tau max}$ (W/m, W/m²) as well as the specific energies extracted from the mass q_a, q_{max} (kJ/m²·K) were higher at VGHE A than at B. The observed specific heat outputs of VGHEs corresponded to the values published by *Banks (2012)*. He defined the specific heat output of a heat pump converted to 1 m length of a borehole with a heating factor of 3.4 within the range of 37–104 W, on average 67 W/m. In the monitored heating period, the average specific outputs of VGHEs related to 1m of a borehole length were 15.07±10.50 W/m for VGHE type A and 19.63±13.70 W/m for type B. Similar values of specific outputs were presented by *Zeng et al. (2003)*.

Tab. 1 Heat carrier fluid flows, heat outputs and extracted energies

Parameter	VGHE A	VGHE B
$V_{\tau a}$ (m³/h)	0.52±0.26	0.61±0.31
$V_{\tau,max}$ (m³/h)	1.03	1.27
V_Σ (m³)	1 435.96	1 787.94
$q_{\tau a}$ (W/m)	7.53±5.25	4.90±3.42
$q_{\tau,max}$ (W/m)	29.28	14.18
$q_{\tau a}$ (W/m²)	59.97±41.80	48.80±34.08
$q_{\tau,max}$ (W/m²)	233.08	141.05
q_a (kJ/m².day)	2 723.40±1 785.58	2 353.59±1 540.89
q_{max} (kJ/m².day)	7 495.07	6 564.86
q_Σ (MJ/m²)	593.70	513.08
τ_Σ (h)	2 750	2 920

The graph in Figure 3 shows the course of specific energies extracted from the ground mass by VGHEs during the heating season. The specific energies extracted from the ground mass correspond to the trend of specific heat outputs of VGHEs. There is also evident a relationship of the values of extracted specific energies and ambient temperatures, as confirmed by the verification results of *Todoran, Balan (2016)*.
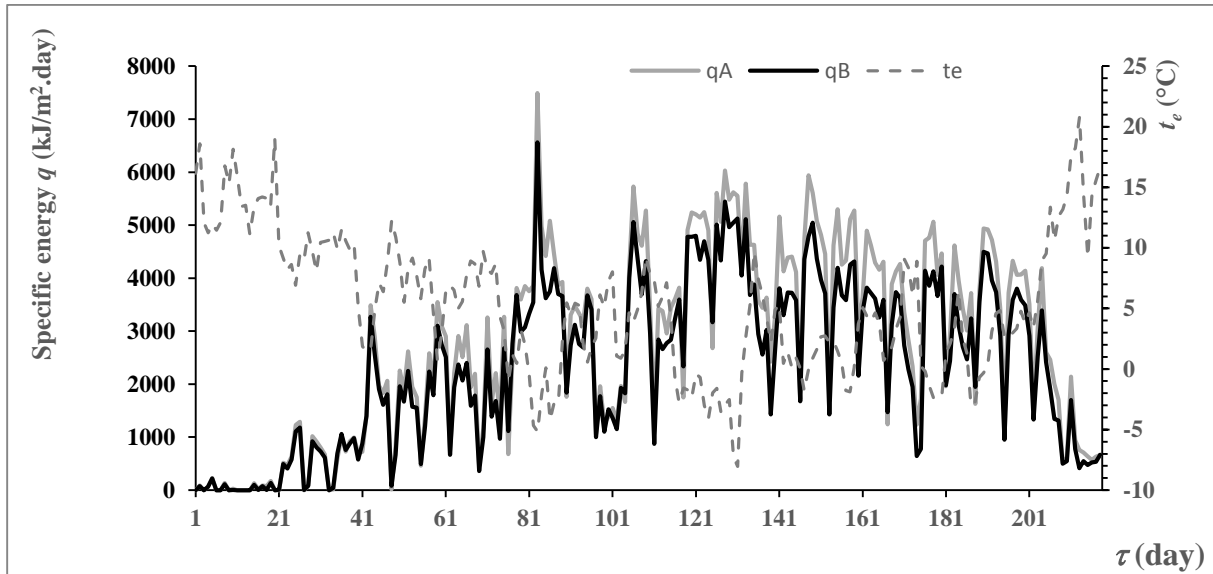
Fig. 3 Specific extracted energies q_A, q_B and ambient temperatures t_e

3. Heat resistances of VGHEs

Zeng et al. (2003) pointed at the dependence of the specific thermal resistances of VGHEs on the pipe diameter and the borehole depth related to 1 m depth of a borehole. They expressed the thermal resistance by relation (3):

$$R = \frac{t_{r.m.} - t_a}{q_\tau} \tag{3}$$

where:
R – specific heat resistance of a borehole (m·K/W);
$t_{r.m.}$ – temperature of reference ground mass (°C);
t_a – temperature of heat carrier fluid;
q_τ – specific heat output converted to 1 m length of a borehole.

They reported that VGHEs thermal resistance decreased as the VGHEs pipe diameter enlarged and increased with a greater depth of a borehole. They also found that the specific thermal resistance was smaller at the double U-tube exchanger than that at the single U-tube VGHE. The results of our verifications confirmed this conclusion. The average specific resistance was 0.36±0,12 m·K/W at VGHE A and 27±0.10 m.K/W at VGHE B.

From the point of view of evaluation and comparison of the heat transfer process between the ground mass and the heat carrier fluid, it seems advantageous to express the specific heat resistance converted to 1 m² of the heat transfer surface of VGHE. In this way, the average specific thermal resistance was 0.09±0.03 m².K/W at VGHE A and 0.11±0.04 m².K/W at VGHE B.

CONCLUSIONS

Higher temperatures of heat carrier fluid, higher relative frequencies in mode of temperature distribution of heat carrier fluid and occurrence of temperatures at higher intervals were more often monitored at VGHE B than at VGHE A. However, graphs in Figures 1 and 2 show that the temperature differences of the heat carrier fluids were not significant.

The average specific heat output calculated per 1 m² of heat transfer surface of the exchanger pipes was higher by 22.89% at VGHE A, at a lower average flow rate of the heat carrier fluid by 14.75%. Also, the specific thermal resistance per 1 m² of heat exchange surface was lower by 18.18% at VGHE A than at B.

The above analysis indicated that VGHE A can be considered to be more effective than VGHE B in terms of monitored parameters.

The objective of further verifications will be presumably monitoring and analysing the temperatures of the heat carrier fluids in terms of confirming the results in different climatic conditions of the heating seasons.

REFERENCES

1. Banks, D. (2012). *An Introduction to Thermogeology: Ground Source Heating and Cooling*. 2nd ed. Chichester: JohnWiley & Sons.

2. Dai, L., Li S., DuanMu, L., Li, X., Shang, Y., & Dong M. (2015). Experimental performance analysis of a solar assisted ground source heat pump system under diferent heating operation modes. *Applied Thermal Engineering*, *75*, 325-333.

3. Choi, W., Ooka, R., & Nam, Y. (2018). Impact of long-term operation of ground-source heat pump on subsurface thermal state in urban areas. *Sustainable Cities and Society*, *38*, 429-439.

4. Li, W., Li, X., Wang, Y., & Tu, J. (2018). An integrated predictive model of the long-term performance of ground source heat pump (GSHP) systems. *Energy and Buildings*, *159*, 309-318.

5. Mensah, K., Jang, Y. S., & Choi, J.M. (2017). Assessment of design strategies in a ground source heat pump system. *Energy and Building*, *138*, 301-308.

6. Michopoulos, A. & Kyriakis, N. (2009). Predicting the fluid temperature at the exit of the vertical ground heat exchangers. *Applied Energy*, *86*, 2065-2070.

7. Remiorz, L. & Hanuszkiewicz-Drapala, M. (2015). Cumulated energy consumption in a heat pump system using a U-tube ground heat exchanger in a moderate climate. *Energy and Buildings*, *96*, 118-127.

8. Ren, CH., Deng, Y., & Cao, S.J. (2018). Evaluation of polyethylene and steel heat exchangers of ground source heat pump systems based on seasonal performance comparison and life cycle assessment. *Energy*, *162*, 54-64.

9. Todoran, T. P. & Balan, M. C. (2016). Long term behavior of a geothermal heat pump with oversized horizontal collector. *Energy and Buildings*, *133*, 799-809.

10. You, T., Wu, W., Shi, W., Wang, B., & Li X. (2016). An overview of the problems and solution of soil thermal imbalance of ground-coupled heat pumps in cold regions. *Applied Energy*, *177*, 515-536.

11. Zeng, H., Diao, N., & Fang, Z. (2003). Heat transfer analysis of boreholes in vertical ground heat exchangers. *International Journal of Heat and Mass Transfer*, *46*, 4467-4481.

Corresponding author:
doc. Ing. Pavel Neuberger, Ph.D., Department of Mechanical Engineering, Faculty of Engineering, Czech University of Life Sciences Prague, Kamýcká 129, Praha 6, Prague, 16521, Czech Republic, phone: +420 22438 3179, e-mail: neuberger@tf.czu.cz

OPTIMIZATION OF THE GROOVE CAM MECHANISM

Ha NGUYEN VAN[1], Ladislav SEVCIK[2]

[1]*Department of Manufacturing Technology of Hung Yen University of Technology and Education, Viet Nam*
[2]*Department of Design of Elements and Mechanism of Technical University of Liberec, Czech Republic*

Abstract
The article deals with the optimization of the groove shapes of the output shaft and the optimization of the shape of the groove side surfaces and the overall design of the middle cam mechanism member to reduce contact pressure. The optimization process results in a reduction of the maximum contact pressure to 863 MPa when the recommended value is up to 800 MPa. It can thus be stated that this embodiment is already practically applicable.

Key words: Ball cam; cam groove optimization; contact analysis; novel cam; groove ball transmission.

INTRODUCTION

Cam mechanisms are widely used in many types of modern machines because of their excellent properties for operation speed, motion accuracy, structural rigidity, and low production cost. Generally, plate cam mechanisms are only one of the larger number of the cam and follower combinations and can be classified in several ways.

Norton (2002) and Rothbart (2004) present a method for classifying a cam mechanism called the force-closed and form-closed cam mechanisms. For kind of force-closed cam mechanisms they describe that in order to ensure constant contact between the cam and follower, an external force is required to be applied. This force is usually provided by a spring of sufficient stiffness or sometimes by an air cylinder. Therefore, as a result, of the force effect, the driving torque and contact stress between the cam and follower in the rise are increased, which cause to make the wear on the cam and follower. Whereas, in the form-closed cam mechanism, contact is obtained by letting the roller follower run in a cam groove or by using a conjugate condition. Thus no force is required to maintain the contact between its cam and the follower. On the other word, the contact stress between the cam and the follower will consequently be smaller and the driving torque in the rise can be reduced.

In recent years, with the rapid development and popularization of mechanical products in modern society, which has been such an important question on designing and producing mechanisms precisely. Besides, with the assistance of the numerical controlled manufacture system being widely applied in this time, which are useful tools for the designer to develop a new type of cam profile.

Therefore, a novel cam mechanism (Fig. 1) is proposed to design for converting a cam rotation to a desired output motion of the output shaft. The mechanism is composed mainly of a rotary input camshaft, a rotary output shaft, a middle part, and two balls and a frame to mount all the parts. In previous work *(Nguyen & Sevcik, 2017b; Nguyen, 2019)*, the author of this paper presented the first design model of the groove cam mechanism. The mechanism includes the input camshaft and the output shaft, which were described in Fig. 2 and Fig . 3.

Fig. 2 describes the shape of the input camshaft, where on one of the tops of the input camshaft has an eccentric circular groove is created with a groove radius is 3 mm, the eccentric is 6mm (the distance length between the center of the shaft axis and the center of the circular groove), the radius of the circular groove from center of rotation is 20 mm.

Fig. 3 depicts the shape of the output shaft. Like as the input camshaft, on one of the tops of the output shaft, which is designed two straight grooves. These straight grooves must have the same groove radius with the circular groove of the input camshaft. And the number of the straight grooves on the output shaft can be designed depends on the requirements of the design.

The main function of the balls is the transfer the moments and velocities from the input camshaft into the output shaft. So when cam works each ball can be easy to roll up and down with respect to their

straight groove on the middle part and the output shaft correspondingly. Moreover, at the same time, these balls must roll along in the circular groove of the input camshaft.

Due to each steel ball only rolls up and down in each straight groove of the middle part. Which plays the role of a roller follower of a cam mechanism. Therefore, the groove cam mechanism model is designed with a pair of followers for one cam but it is not a type of conjugate cam system. Due to the cam mechanism is designed which takes a form-closed, so the groove cam mechanism gets some advantages to other cam mechanisms because of following considerations: compared with a force-closed cam mechanism, the mechanism withstands lower contact stress and no force is required to maintain the contact between its cam and the follower; compared with conjugate cam mechanism in which a set of two cams must be used, the cam mechanism is simpler in construction because only one cam is needed. So, it occupies a small space and has a lower cost.
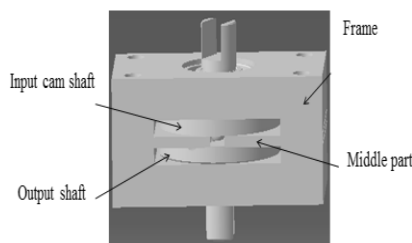

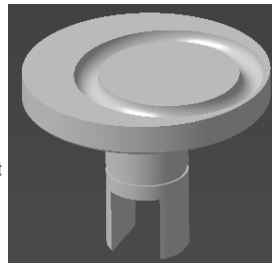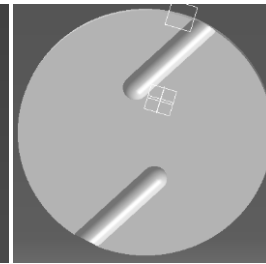**Fig. 1** Groove am mechanism model the first design model   **Fig. 2** The input cam shaft   **Fig. 3** The output shaft of

Another point in its favor of this groove cam model which used the ball followers, where the ball is commonly applied in the bearing and ball screw fields. Therefore, which is easy for replacement and availability from bearing manufacturers stock in any quantities are advantages. Moreover, in recent years, the idea uses the ball for gearing design has been developing by Sincroll Company *(Johnson, 1985)*.

By the technology, the roller or balls connect the wheels or bodies, while the performing pure rolling motion without sliding. Thus, the power efficiency is higher, the sliding friction is approximately eliminated and so on. Therefore, the idea of altering the roller follower by the balls is applied for a groove cam mechanism in this research.

By this design, the surface contacts between the ball with their grooves are always changing when cam working. This contact phenomenon could cause to make the balls can damage easily and the result is the failure of these balls *(Gopalakrishnan &Ruban, 2015)*.Therefore, the task to analyze the contact pressure between the ball and their grooves must pay attention to this research. Based on the results of contact calculation obtained by using the analytical calculation method and FEM for the first design model *(Nguyen, 2019)*. We knew that the resulting deviation in contact stress is 4.52 %. But if we compared these result with the lists the maximum contact pressures and their recommended values for different types of materials according to *(Chablat et al., 2007)*.

Allowable pressure for refined steel is up to 2000 MPa and the maximum pressure obtained from the analyses is 2093 MPa. As recommended pressure is 800 MPa, it was necessary to modify the design of the grooves so as to lower the pressure at the contact surfaces. Therefore, the aim of this study is to design an optimized design a new cam mechanism with respect to the minimum contact pressure to reach the recommended pressure value for steel material based on changing the groove shapes of the output shaft and the middle part of the groove cam mechanism.

MATERIALS AND METHODS

In the design of the cam mechanism, the two main factors must be considered. The first one is the selection of a proper motion curve and the second one is the requirement for the radius of curvature of the cam profile to be greater than a minimum limit to avoid the undercut phenomenon. Therefore, to optimize the groove cam mechanism, the design must meet the above requirements.

In this article, we focus on how to reduce the contact stress between the ball and the groove in design to reach the maximum recommended value contact pressure for steel material, which is a significant key for optimum design of the groove cam.

In our case, when the cam mechanism works each steel ball body in contact with three grooves, which are the groove of the input camshaft, middle part, and the output shaft. The ball is a spherical shape, the groove of the input camshaft is circular and the grooves of the middle part and the output shaft are straight. Therefore, in the previous design *(Nguyen & Sevcik, 2017b; Nguyen, 2019)*.

the calculated we assumed that the contact between the ball and the straight groove is like contact between sphere-on-flat plate. It may cause high contact pressure.

For a given groove cam profile, the maximum value of the Hertz pressure is obtained for the minimum radius of curvature of the groove cam. Obviously, it is easy to know that the Hertz pressure is a maximum when the contact area is a minimum value and the magnitude of the force is a maximum. Consequently, the higher contact area and the smaller force makes the Hertz pressure is lower. This problem was reviewed by Johnson (1985) *(Nguyen & Sevcik, 2017a)*. He first reviews the development of the theory of contact stresses since the problem was originally addressed by Hertz in 1882.

The radius of the contact-patch of the contact depends on several parameters, amongst them, the equivalent radius of the contact (geometry constant B) following equation

$$B = \frac{1}{2}\left(\frac{1}{R_f} + \frac{1}{R_r}\right), \tag{1}$$

R_r is the radius of the ball, which is constant and R_f is the radius of the groove in contact with the ball (in this case which is either of a radius of circular groove cam or the groove of the output shaft or the groove of the middle part). Therefore, B depends only on R_f. Finally, for a given cam profile, a_h is a minimum when R_f is a minimum. Hence, to compute the maximum value of the Hertz pressure, we have to consider the lowest value of R_f.

Obviously, the maximum value of the contact pressure depends on several parameters, namely, the shapes of the parts in contact, the number of the groove of the output shaft, the material of the parts in contact, the load applied. Therefore, we have some different ways to minimize Hertz pressure:

 i)   Increase the number of the groove of the output shaft;
 ii) Decrease the minimum value of the radius of the R_f by changing the shape of the groove cam as well as the groove shape of the output shaft and middle part;
 iii) Decrease the load applied;
 iv) Choose a material with a lower Young modulus;
 v)   Together with change the shape of the frame to make the mechanism is more stable.

Based on the result of the previous studied presented by own author *(Nguyen, 2019)* combines with stated suggestions above, in this section, we can choose the way to optimize the groove cam mechanism following:

Firstly, we changed the straight groove by a curved groove, also changing the shape of the frame.

Secondly, Remained the curved groove of the output shaft in the previous case and changed the flat surface of the straight groove of the middle part by spherical surface. By this replacement, the shape of the ball and the groove of the middle part is the same size. Therefore, it may increase more elements in contact between the ball and the groove of the middle part. Hence, the maximum contact pressure may also reduce.

RESULTS AND DISCUSSION

1. Optimization of the groove cam by changing the groove shape of the output shaft. (the second design model)

To carry out this design we must follow some procedures below.

Find the trajectory of the groove of the output shaft we use inverse model and coordinate systems to analysis follow

The reverse model is used to translate the relative motion of follower with respect to cam into absolute motions, that is, let the cam stationary and the follower and the frame rotate at the same velocity as the cam but in the direction opposite to the cam at the same time, the follower reciprocates in the predefined motion with respect to the frame.

Fig. 4 is a generalized model of the groove cam mechanism, the cam rotates counterclockwise at a constant angular velocity and drives the output shaft. To express the motion of each part in a groove cam, three coordinate systems are set. The first is called a Cam coordinate system (CCS) $X_1O_1Y_1$ with an origin fixed at the axis of the cam to describe the cam shape. The second is a frame coordinate sys-

tem (FCS) XOY with an origin located on the cam axis and its Y-axis normal to the path of translating follower (the trajectory of the ball center in the straight groove of the middle part). This coordinate system coincides with the coordinate system of the middle part. This coordinate describes the position and motion of the ball with respect to the cam. In an initial position where the rotational angular θ is 0 degree; the coordinate axis OX coincides with the axis O_1X_1. The third is an output coordinate system (OCS) $X_2O_2Y_2$ with an origin fixed at the axis of the output shaft used to describe the shape of the groove of the output shaft. In reality, the CCS and OCS are movable, and the FCS is stationary.
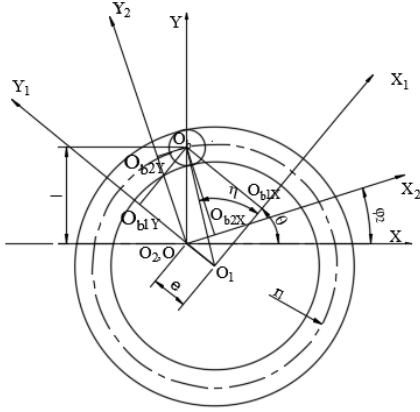

Fig. 4 Generalized model of a groove cam

Vectors are used to represent kinematical quantities and expression such as position. From Fig .4, the position of the ball's center O_b can be expressed in vector form as

$$\overrightarrow{OO_b} = \overrightarrow{OO_1} + \overrightarrow{O_1O_b}. \tag{2}$$

The vector OO_b in the frame coordinate system (FCS) as

$$OO_b{}^o = \begin{bmatrix} 0 \\ l \end{bmatrix}, \tag{3}$$

also, we have the vector $OO_1 \ and \ O_1O_b$ in the frame coordinate system (CCS) as

$$OO_1{}^1 = \begin{bmatrix} 0 \\ -e \end{bmatrix}, \tag{4}$$

$$O_1O_b{}^1 = \begin{bmatrix} r_1 \cdot \cos\eta \\ r_1 \cdot \sin\eta \end{bmatrix}, \tag{5}$$

With l is the distance between the center O and the ball's center at the initial position and e is the eccentric distance between the rotating center of the cam and the center of the circular groove.

Substituting equations 4 and 5 into equation 2 obtained

$$OO_b{}^1 = \begin{bmatrix} r_1 \cdot \cos\eta \\ r_1 \cdot \sin\eta - e \end{bmatrix}. \tag{6}$$

Hence, the vector OO_b in the frame coordinate system (FCS) obtained

$$OO_b{}^o = R_{z,\theta} \cdot OO_b{}^1 = R_{z,\varphi_2} \cdot OO_b{}^2, \tag{7}$$

with $R_{z,\theta}, R_{z,\varphi_2}$ are rotating matrices of the z-axis with respect to θ and φ_2 respectively, and can be expressed following

$$R_{z,\theta} = \begin{bmatrix} \cos\theta & -\sin\theta \\ \sin\theta & \cos\theta \end{bmatrix}, \tag{8}$$

and $R_{z,\varphi_2} = \begin{bmatrix} \cos\varphi_2 & -\sin\varphi_2 \\ \sin\varphi_2 & \cos\varphi_2 \end{bmatrix}. \tag{9}$

Substituting equations 3 and 7 into 6 we got

$$\begin{bmatrix} 0 \\ l \end{bmatrix} = \begin{bmatrix} \cos\theta & -\sin\theta \\ \sin\theta & \cos\theta \end{bmatrix} \begin{bmatrix} r_1 \cdot \cos\eta \\ r_1 \cdot \sin\eta - e \end{bmatrix} = \begin{bmatrix} r_1 \cdot \cos(\theta + \eta) + e \cdot \sin\theta \\ r_1 \cdot \sin(\theta + \eta) - e \cdot \cos\theta \end{bmatrix}. \tag{10}$$

Equation 9 can rewrite by as

$$r_1{}^2 = e^2 \cdot \sin^2\theta + (l + e \cdot \cos\theta)^2 = l^2 + 2 \cdot l \cdot e \cdot \cos\theta + e^2 - r_1{}^2 = 0.$$

In this case the trajectory of the groove of output shaft undefined, therefore, at the initial position we assumed that the output coordinate system (OCS) situated like as Fig. 4.

If we want to design the trajectory of the groove is curved, for a simplification case we assumed that the curve may a circle and can be expressed by an equation in (OCS) as

$(x - a)^2 + (y - b)^2 = R_2{}^2,$ (11)

With *a, b* are coordinates of the circle center and R_2 is the radius of the circular groove of the output shaft.

We can express the position of *A* in the (OCS) following

$OA^2 = \begin{bmatrix} l \cdot sin\varphi_2 \\ l \cdot cos\varphi_2 \end{bmatrix},$ (12)

with φ_2 is the rotational angle of the output coordinate system.

Substituting the values of x and y from equation 11 into 10 we obtained

$(l \cdot sin\varphi_2 - a)^2 + (l \cdot cos\varphi_2 - b)^2 = R_2{}^2.$ (13)

Rewrite equation 12 got

$2 \cdot l \cdot (asin\varphi_2 + bcos\varphi_2) = R_2{}^2 - l^2 - a^2 - b^2,$ (14)

Denoted $sin\mu = \frac{a}{\sqrt{a^2+b^2}}$ and $cos\mu = \frac{b}{\sqrt{a^2+b^2}}.$ (15)

Substituting equation 15 into 14 obtained

$2 \cdot l \cdot (sin\mu \cdot sin\varphi_2 + cos\mu \cdot cos\varphi_2) = \frac{R_2{}^2 - l^2 - a^2 - b^2}{\sqrt{a^2+b^2}},$ (16)

Finally, the obtained equation following as

$2 \cdot l \cdot (cos\varphi_2 - \mu) = \frac{R_2{}^2 - l^2}{\sqrt{a^2+b^2}} - \sqrt{a^2+b^2}.$ (17)

For as simplification case of design, given a value of parameters then solve the equation 16 to find R_2 or *a*.

An example is given *l*=14mm, φ_2=0 degree assumed the center of the circular groove of the output leans on the x-axis, hence, *b*=0. From equation 16 we can choose one of two values and the last parameter can be taken.
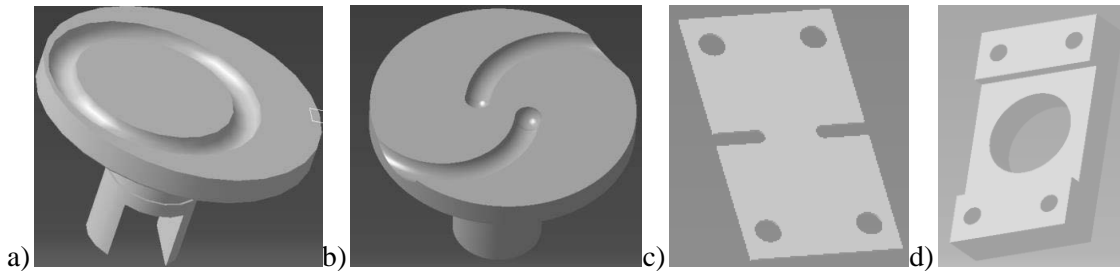

Fig. 5 a) The shape of the input camshaft, b) the shape of the output shaft, c) the middle part, d) one of two frames of the groove cam mechanism for the second design model

1.1 Calculation of contact pressure of the steel ball and the curved groove by Hertz theory
The contact between the ball and the curved groove of the output shaft can be modeled as a contact of sphere-on-cup. With the sphere is the ball and the cup is the curved groove. By applying the Hertz theory and substitution the magnitude of the design parameters we obtained the results of maximum contact pressure between the ball and their grooves.

The average and maximum contact pressure can be found respectively

$P_{aveg} = \frac{F_{A1}}{A} = \frac{30.929}{3.678 \cdot 10^{-8}} = 841(MPa),$

$P_{max} = \frac{3}{2} \cdot \frac{F_{A1}}{A} = \frac{3}{2} \cdot 841 = 1262(MPa).$

1.2 Finite element analysis
The calculation was performed under the same boundary conditions as the previous cases *(Nguyen, 2019)*. The material of all parts made by steel, the elasticity model is 2 E5 MPa, the Poisson's ratio is 0.3. The meshing type is free, element size is set 0.5 mm for each contact pairs. Restrained all degrees of freedom (DOF) of the middle part (fixed support), added frictionless support constraint to the input camshaft and the output shaft, and applied moment load to the input camshaft is given 1000 N.mm.
The result of calculation reveals that the maximum contact pressure reached the value of 1152 MPa, as shown in Fig. 6

From Fig. 6 we can know that the contact pressure change. The biggest pressure was at the contact point between the ball and the curved groove of the output shaft, and the lowest contact pressure existed at the contact between the ball and the groove of input camshaft, which was consistent with the fact *(Norton, 2002)*. From the simulation result of the maximal contact pressure was 1152 MPa while the Hertz theory value was 1262 MPa. The comparison clearly showed that there was good consistency between the Hertz theory solution and the finite element solution. For more information can be seen in Tab. 1.But if compared the maximum contact pressure with the recommended value of the maximum pressure P_{max} for steel material *(Chablat et al., 2007)*, which is still larger. Therefore, we should improve the design to meet the goal of the design.

Also, Fig. 6 b the contact area between the ball and the straight groove of the middle part is the unconventional case. Contact area looks like a circular shape, which is a question for the designer because according to the Hertz theory, the contact area common is ellipse or rectangle shape. Therefore, this problem can be solved in the next section.
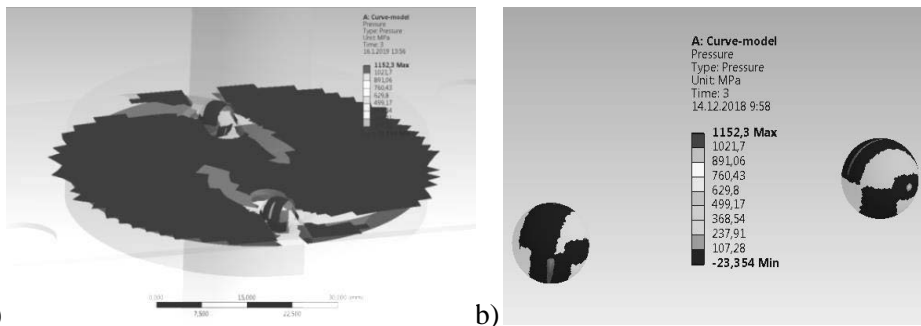

a)   b)

Fig. 6 a) Distribution of contact pressure on the groove cam mechanism, 6 b) cloud chart about contact pressure on the ball in contact with their grooves of the groove cam

Tab. 1 Comparison pressure [MPa] between two methods

Parameter	Hertz theory solution	Finite element solution	Differences
Maximum contact pressure	1262	1152	8.7%

2. Optimization of the groove cam by changing the groove surface of the middle part (the third design model)

2.1 Redesign the surface of the straight groove

The goal of the optimal design of the groove cam mechanism is to reduce the maximum contact pressure between the ball and their grooves to approach the recommended value P_{max} (for steel material is 800 MPa). Therefore, in this section, we may think about changing the contact surface of the straight groove of the middle part, because the middle part is a thin part, and the previous cases, the contact surface of the straight groove participated in contact with the ball is a flat plate. Hence, the contact areas between the ball and the straight groove of the middle part may not enough, which may cause increasing the maximum contact pressure.

If replacing the flat plate of the straight groove of the middle part by a spherical surface, hereby the contact surface between the ball and the groove surface is the same size. Therefore, it can increase elements in contact between the ball and the groove of the middle part. Hence, the maximum contact pressure may also reduce.
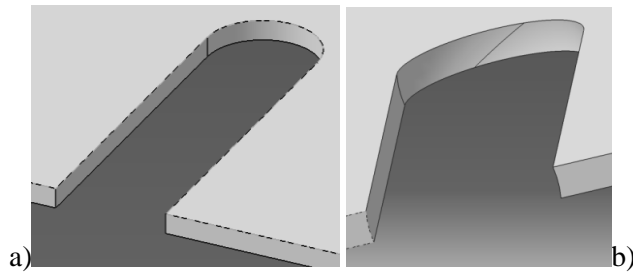
Fig. 7 a) view of the straight groove with the flat-plate surface, b) view of the straight groove with a spherical surface for the third design model

2.2 Finite element solution

For the redesigned model, all parts of the groove cam in the previous design model maintained. We had a changing the surface of the straight groove of the middle part as designed above.

The calculation was performed under the same boundary conditions as the previous cases.

By means of simulation, the contact change status can be got as Fig. 8
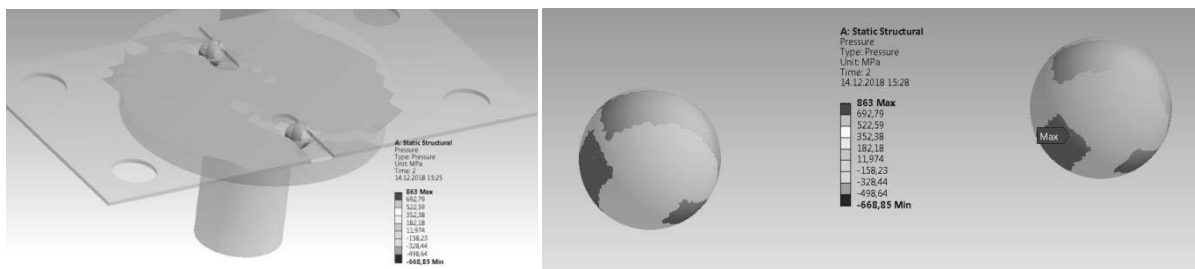

Fig. 8 Distribution of contact pressure on the groove cam mechanism for the third design model

Fig. 8 clearly shows that the maximum contact pressure, which takes the value 863 MPa, occurs at the contact point where the steel ball is in contact with the curved groove of the output shaft. For more details were presented in *(Norton, 2002)*. Moreover, the maximum contact pressure is approaching the recommended value P_{max} (800 MPa). It is a very impressive number. Hence, in this case, it can be proved that the way to optimize the groove cam mechanism was successful in design.

Tab. 2 Comparison contact pressure [MPa] for redesign model and recommended value P_{max}

The redesign model	Recommended value (P_{max})	Differences
863	640 to 800	7.9%

In addition, from Fig. 9, we can clearly know that all the contact areas had an approximate ellipse shape in the contact area of the ball and their grooves, which was consistency with the Hertz contact theory. It means that the question in the previous design model was answered.
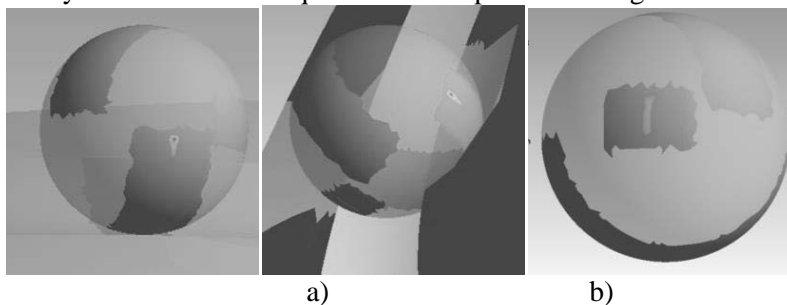

a)   b)   c)

Fig. 9 Cloud charts about contact pressure on the ball in contact with their grooves of the third design model a) the contact area with groove curve of the output shaft, b) the contact area with the groove of input camshaft, c) the contact area with the straight groove of the middle part

DISCUSSION

Tab. 3 Contact pressure [MPa] of all design models

Solution	Fist design model	Second design model	Third design model
Finite element	2093	1152	863

Based on the results obtained, which is obviously revealed that the maximum contact pressure of the second design model is less than the first one is 45% (refer to table 3) and the third design model is less than the second one is 25%. Therefore, the purpose of the optimal design with respect to reducing the Hertz pressure is obtained with the groove shapes of the output shaft and the middle part.

Both Hertz theory and finite element methods were applied to determine the contact pressure between the balls and their grooves of the groove cam. The results have shown that the computational values were consistent with theoretical values.

The study brought out the newest idea design for designing cam mechanism by using the ball, where the ball plays the role of a follower in the cam mechanism. Until now there are very few references can be found in the literature that addresses the issue of the application of the ball for designing the cam field. So the research may help to open the new trend for designing cam mechanism in the years coming up.

At present, the material used for calculation of this research is structural steel, which is a common material used in cam design. Nowadays with developing of the advanced material, it is necessary to expand to other material with a lower Young modulus, i.e., a more compliant material, thus increasing the surface of contact, hence, decreasing the maximum contact pressure. Moreover, when the material is more compliant, its plastic domain occurs for smaller stresses. Therefore, other material must be carried out in the future to obtain the goal of optimal design for the groove cam mechanism.

CONCLUSIONS

From the result of the numerical simulation for the first design model, which was presented in *(Nguyen, 2019)* and the last two design models which were investigated in this article. We can conclude that the maximum contact pressure between the ball and their grooves by applying the ball for cam design is approaching the recommended value P_{max} (800 MPa). Although the calculating value is slightly bigger than the allowable contact pressure of steel material, the differences are not too much (7.9%). It is a very impressive number. Thus the way to optimize the groove cam mechanism was successful in design.

ACKNOWLEDGMENT

REFERENCES

1. Chablat, D et al., (2007). The Optimization of a Novel Prismatic Drive. *Problems of Mechanics, 1*(26), 32-42.
2. Gopalakrishnan, T., Ruban, M. (2015). Contact analysis of roller bearing using finite element method. *Vels Journal of Mechnical Engineering, 2*, 30-33.
3. Retrieved from http://www.sincroll.com/ws.php?page=index.
4. Johnson, K. L. (1985). *Contact Mechanics.* Cambridge University Press.
5. Nguyen Van, H., Sevcik, L. (2017). Apply steel balls for designing the cam mechanism. In *Proceeding of 22ⁿᵈ International Conference Mechanika* (pp. 118-121).
6. Nguyen Van, H., Sevcik, L. (2017) The contact analysis of designing the cam mechanism by using ANSYS. In *ICMD 2017 58ᵗʰ International Conference of Machine Design Departments* (pp.271-274).
7. Nguyen Van, H. (2019). *Modern transmission mechanism of production machine* [Doctoral thesis]. Technical University of Liberec, Czech Republic.

8. Norton, R. (2002). *Cam design and manufacturing handbook*. New York: Industrial Press Inc.
9. Rothbart, H. (2004). *Cam Design Handbook*. USA: McGraw-Hill.
10. Tang Z., Sun J. (2011). The contact analysis for deep groove ball bearing based on analysis. In *International Conference on Power Electronics and Engineering Application* (pp. 423-428).

Corresponding author: Ph.D. Ha Nguyen Van., Faculty of Mechanical Engineering, Hung Yen University of Technology and Education, 39A Road, Khoai Chau District, Hung Yen province, Viet Nam, phone: +840849790998, e-mail: nguyenha.hut@gmail.com

EFFECTIVE DOSE OF BIOCHAR WITHIN THE FIRST YEAR AFTER APPLICATION

Václav NOVÁK[1*], Kateřina KŘÍŽOVÁ[1,2], Petr ŠAŘEC[1], Ondřej LÁTAL[3]

[1]*Czech University of Life Sciences Prague, Faculty of Engineering, Department of Machinery Utilization, Kamýcká 129, 16500 Prague, Czech Republic*
[2]*Crop Research Institute, Division of Crop Protection and Plant Health, Drnovská 507/73, 16106 Prague, Czech Republic*
[3]*Agrovýzkum Rapotín Ltd., Výzkumníků 267, 78813 Vikýřovice, Czech Republic*
Correspondence: novakvaclav@tf.czu.cz

Abstract

Uneven spatial and temporal distribution of precipitation is becoming a major issue of modern agriculture. Biochar, as a natural soil conditioner, is supposed to modify soil properties and enhance water infiltration. Field experiment was conducted in order to evaluate the effective dose and its impact on soil and vegetation properties within the first season. Four small-scale plots were established within a maize field in 2017. Each plot was treated with a different dose of biochar. Penetration resistance measurements were carried out to indicate physical soil properties. Concurrently, the chlorophyll content and Normalized Difference Vegetation Index were estimated. Acquired data variability was calculated and evaluated in relation to results of measurement conducted on the plot that was established in 2014. A conclusion was drawn that biochar stimulates crop growth and the improvement reached by a lower amount after longer period may be substituted by a higher dose in the first season.

Key words: maize; soil properties; chlorophyll content; spectral index; drought.

INTRODUCTION

Nowadays, modern agriculture faces numerous challenges. Most of them are caused by rapid population growth, while the area of agricultural land is simultaneously decreasing. According to Czech Statistical Office (*2018*), more than one third of agricultural land in the Czech Republic was lost in the past 100 years. Concurrently, intensive farming systems have depleted the soil by using mineral fertilizers and various pesticides, very often in overdoses. In connection with the application of these substances, soil compaction has become increasingly serious issue. This phenomenon has had a negative effect, mainly on water infiltration (*Chyba, Kroulík, Krištof, Misiewicz, & Chaney, 2014*). It consequently reduces soil biodiversity and changes roots growth that affects a wide range of key functions staple for crop production (*Stolte et al., 2016*). The root system has a significant effect on plant health, not only the density and length of the roots, but as well the root volume and surface area, which are very important for plant growth (*Saleem, Law, Sahib, Pervaiz, & Zhang, 2018*). It is generally known that crop yields depend not only on soil fertility, but also on the alterations of physical and hydraulic soil properties (*Gülser, Ekberli, & Candemir, 2016*). Crops access to water sources during drought periods has become one of the key factors defining crop yields in the Central European region (*Žalud et al., 2017*). In the Czech Republic, drought is the second most extensive natural disaster (*Potop, Možný, & Soukup, 2012*) and therefore plans on how to prevent crop water stress status must be developed. One promising solution could be the utilization of biochar (*Fischer et al., 2019*).

Biochar is a very stable carbon-based material, which is usually produced from waste biomass during the pyrolysis process. The waste material is usually subjected to the decomposition process and thus it becomes a source of CO_2 emissions. On the contrary, biochar production is considered to be environmentally clean technology, since most of the carbon is incorporated into the pyrolysis product (*Bordoloi et al., 2019*). This material is supposed to be applied directly into the soil where it acts as a soil conditioner (*Zhao & Zhou, 2019; Fang, Zhan, Ok, & Gao, 2018*). Many studies were undertaken to monitor the influence of biochar on soil properties. It was confirmed that the soil physical properties had improved, such as the decrease of penetration resistance or bulk density (*Jien, 2019*). Additionally, due to high organic content and high total pore volume, biochar increased water and nutrient retention (*Abel et al., 2013*) and also reduced the mobility of some organic and inorganic pollutants in a soil

profile (*Bolan et al., 2014*). Regarding this, biochar application on an agricultural plot is beneficial and results in higher crop yields (*Agegnehu, Srivastava, & Bird, 2017*) since naturally all these soil properties benefit plant status as well. Although there are many studies about biochar and its impact on soil properties, the dosing is an issue which has not gained very much attention so far. Hence the main aim of the study was to evaluate biochar dose influence on soil and crop properties within a maize field after one year after biochar application.

MATERIALS AND METHODS
Site and crop management

The study was conducted within an agricultural plot located near the Šumperk town in the Olomouc region, Czech Republic (49° 59' 8.8296" N, 16° 59' 47.0904" E). In total 13.24 ha field was divided into plots with a variable area and also varying agricultural management. Besides biochar, the area dedicated to examining its impact on the soil and crop properties was treated by standard complex fertilizers (N, P, K). According to the FAO Soil Units, the soil type was classified as Gleyic Luvisols, which are usually developed on flat surfaces. Practically no sloping of the plot enables a wide-row crops cultivation without any erosion exposure. In the 2018 growing season, LAVENA variety of a maize crop was cultivated; sown on the 26th April 2018 and harvested on the date 27th August 2018. Biochar used for this study was produced from plant biomass and wooden waste in the Czech Republic. Tab. 1 gives technical specifications more in detail. Five small-scale plots 15 x 30 m with a different dose of microgranular biochar were examined within this study (Tab. 2), where specific doses were applied into the soil profile ± 25 cm during standard tillage in the autumn of 2017.

Tab. 1 Technical specifications of biochar used for the study

Total C in dry matter	min 45	[%]
Total N in dry matter	min 1	[%]
Total P (P_2O_5) in dry matter	16	[%]
Total K (K_2O) in dry matter	17	[%]
pH	9-11	-
Particle size < 2 mm	min 40	[%]
Particle size > 10 mm	max 10	[%]

Tab. 2 Specific doses of biochar applied to small-scale plots under investigation and related maize yield from the 2018 growing season.

Plot code	Biochar dose [t ha^{-1}]	Year of application	Yield [t ha^{-1}]
B15c	15	2014	51.9
B15	15	2017	50.8
B30	30	2017	53.0
B45	45	2017	54.6
B60	60	2017	55.8

Weather conditions

The growing season of 2018 is generally considered extremely dry compared to past years. This drought period was caused not only by high temperatures, but also by sporadic and insufficient rainfall. These conditions had a negative impact on crop yield, specifically 30–40% loss on maize yields in the area of interest (*Intersucho, 2019*). Fig. 1 provides information about the temperature trend and Fig. 2 about precipitation during year-long time period compared to the long-term normal (1981–2010) in the Olomouc region according to the data of Czech Hydrometeorological Institute.

Terrestrial measurements and Data Analysis

On two occasions, on-site terrestrial measurements were conducted in order to acquire empirical soil and vegetation data. The first visit, the 5th June 2018, focused on the leaf development stage (BBCH 18) while the second, 3rd July 2018, concentrated on the stem elongation stage (BBCH 32).

There were 9 sampling points regularly distributed within each of the examined plots, where all measurements were focused.

Regarding the soil properties, penetration resistance (PR) data was obtained during the first field visit. Soil moisture was measured using Theta Probe (Delta-T Devices Ltd, UK). PR was measured using the registered penetrometer PEN 70 (CULS, Prague).

To determine crop condition, Leaf Chlorophyll Content (LCC) was measured using CCM 300 sensor (OptiSciences, USA) that works with proven chlorophyll fluorescence ratio (F735 nm/F730 nm), in three repetitions for each sampling point. Concurrently, a spectral index was derived based on images captured by GreenSeeker handheld sensor (Trimble, USA). This device is designed to calculate NDVI as a basic indicator of vegetation greenness.

Statistical testing on the influence of specified doses on above-mentioned variables was entirely conducted in an open-source software environment R (*R Core Team, 2018*; *Wickham, 2009*). Since the data did not meet the assumption for using one-way ANOVA, Kruskal-Wallis distribution-free test was used to evaluate the data variability.
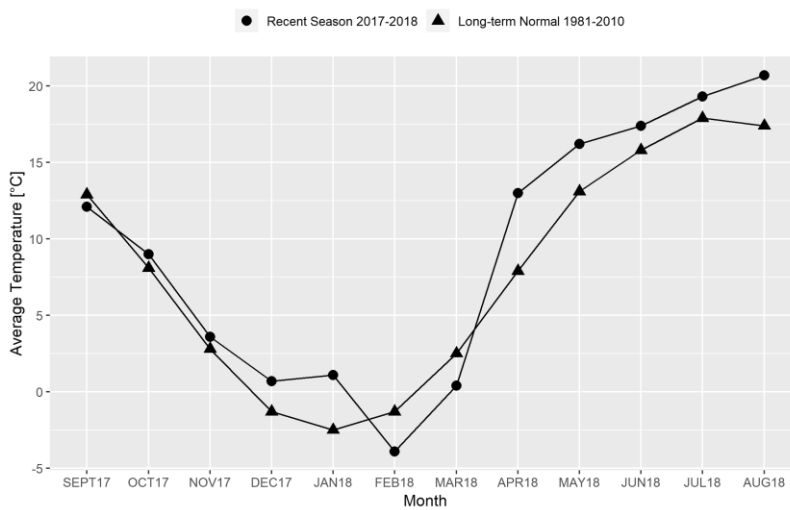

Fig. 1 Temperature conditions in the Olomouc region in the recent season compared to a long-term normal (1981–2010).
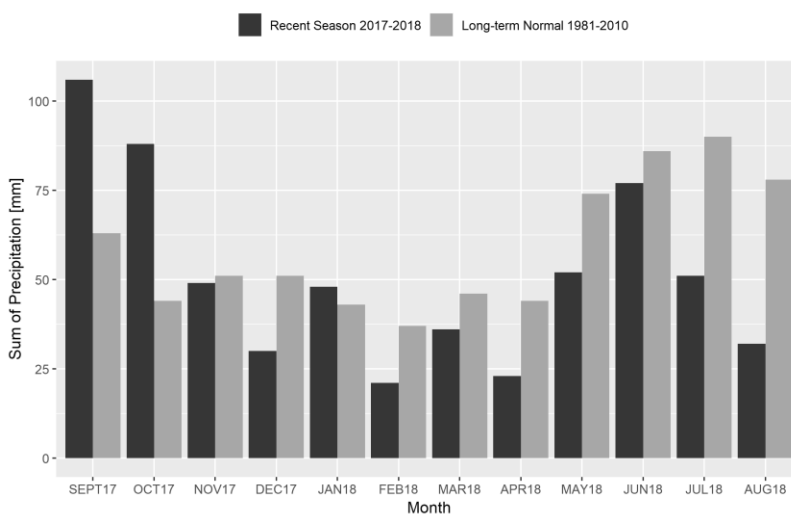

Fig. 2 Precipitation conditions in the Olomouc region in the recent season compared to a long-term normal (1981–2010).

RESULTS AND DISCUSSION

First, the influence of specified biochar doses on soil PR was examined. However, statistical analysis showed that there was no significant difference found between the examined plots. PR as a soil factor may reduce crop growth and yields in its higher values (*Colombi, Torres, Walter, & Keller, 2018*; *Haider, Steffens, Moser, Müller, & Kammann, 2017*). For maize, the top 10 cm of a soil profile is considered the most crucial due to the importance of shoot-borne nodal roots within its root system (*Colombi et al., 2018*). Since PR is a function of soil water content (*Dec, Dörner, & Balocchi, 2011*) and many studies described an increase of soil moisture when treated by biochar (*Haider et al., 2017*), the performance of this soil conditioner may not be considerable in a drought period. Nevertheless, (*Bengough, McKenzie, Hallett, & Valentine, 2011*) determined the value of 3 MPa as a threshold, since when PR becomes a limiting factor for root elongation. The data indicated that the topsoil profile values were below that critical 3 MPa threshold despite the drought period. Therefore, it is likely the short period of biochar effect produced no relevant results in terms of PR.

Regarding the impact of biochar addition on crop yield, current studies do not provide consistent results. Non-economic benefits, such as a decrease in nitrate leaching or an increase in organic carbon in a soil profile rather than direct impact on yield, are highlighted (*Aller et al., 2018*; *Haider et al., 2017*). Spectral index NDVI did not give significant statistical results. For maize, NDVI value is typically increasing during the growing season till the beginning of canopy senescence (*Verhulst et al., 2011*). Study of *Liu et al.* (*2018*) compares the performance of NDVI and chlorophyll fluorescence in periods of drought detected in winter wheat. Their conclusion supports the fact that NDVI is able to indicate a rather a long-term drought conditions, while solar-induced chlorophyll fluorescence appears to be a good indicator of the early drought period.
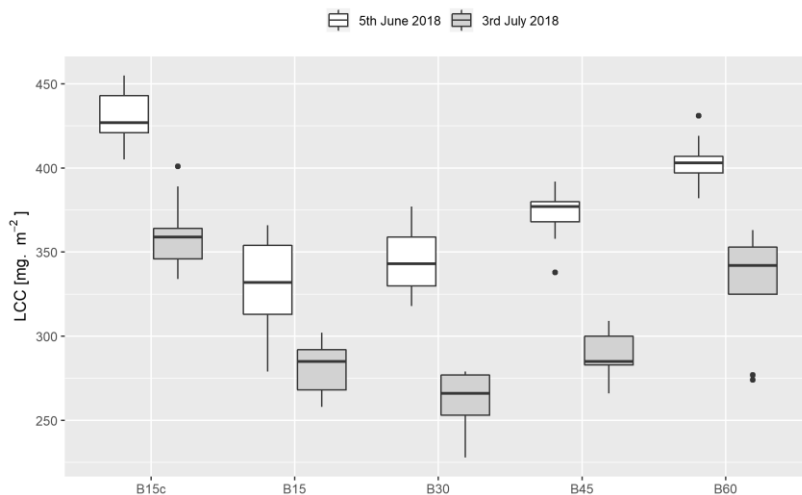

Fig. 3 Leaf Chlorophyll Content (LCC) data variability measured using CCM 300 chlorophyll meter during both field visits.

NDVI is correlated closely with LCC, regarding the study of *Cui, Li, & Zhang* (*2009*). However, in contrast with NDVI values measured in this study, LCC provided significant results for both sampling terms (Fig. 3). Nevertheless, there was no significant difference between plots B15c and B60, even though the latter plot had been treated with four times a higher dose. This, in some way, opens a discussion about the effective biochar management. *Pandit et al.,* (*2018*) conducted a three-year (six cropping seasons) field experiment in Nepal with the aim to evaluate the biochar dosage mostly from an economic perspective. According to their results, 15 t ha-1 is the optimum. Eventually, *Gavili, Moosavi, & Kamgar Haghighi (2019)* point out the fact that based on specific biochar used, higher doses may have had a negative impact on the soil salinity levels. Apparently, the time, respectively the duration of biochar effect, is also a crucial factor, since the impact of the highest dose with short effect duration (B60) on LCC levels may be considered equal to the lowest dose after four years appearance in a soil profile (B15c). Moreover, multi-year studies often describe that there is no observable effect on a crop growth until at least the second or third year (*Pandit et al., 2018*). This study, nevertheless,

gained significant results (LCC) already in the first year after biochar application even though there were no alterations recorded by soil properties, very likely because of the drought period.

CONCLUSIONS

Biochar has gained a lot of attention in recent years. Besides its substantial environmental influence, since it is produced from organic waste material, it is considered to have various positive effects in the field of crop production. This study aimed to evaluate the impact of specific biochar dosage on soil properties together with the growth of maize in the first year after biochar application. Based on the results, it was concluded that biochar stimulates the crop growth. Additionally, the improvement reached by a lower dose over longer period may be substituted by a higher dose already in the first season. However, there are some concerns about the negative influence of high doses of biochar in terms of increasing soil salinity levels as well as being economically demanding. Since there are mainly non-economic benefits highlighted in the studies, such as increasing organic carbon levels or decreasing nitrate leaching, the biochar application should not be considered as a tool for increasing economic income in the first place. To better observe biochar dose effects on soil properties and crop growth alterations, a multi-year study is required. However, the influence of increasing dose on LCC may be observed already within the first year.

REFERENCES

1. Abel, S., Peters, A., Trinks, S., Schonsky, H., Facklam, M., & Wessolek, G. (2013). Impact of biochar and hydrochar addition on water retention and water repellency of sandy soil. *Geoderma*, *202–203*, 183–191. doi: https://doi.org/10.1016/J.GEODERMA.2013.03.003

2. Agegnehu, G., Srivastava, A. K., & Bird, M. I. (2017). The role of biochar and biochar-compost in improving soil quality and crop performance: A review. *Applied Soil Ecology*, *119*, 156–170. doi: https://doi.org/10.1016/j.apsoil.2017.06.008

3. Aller, D. M., Archontoulis, S. V., Zhang, W., Sawadgo, W., Laird, D. A., & Moore, K. (2018). Long term biochar effects on corn yield, soil quality and profitability in the US Midwest. *Field Crops Research*, *227*, 30–40. doi: https://doi.org/10.1016/j.fcr.2018.07.012

4. Bengough, A. G., McKenzie, B. M., Hallett, P. D., & Valentine, T. A. (2011). Root elongation, water stress, and mechanical impedance: a review of limiting stresses and beneficial root tip traits. *Journal of Experimental Botany*, *62*(1), 59–68. doi: https://doi.org/10.1093/jxb/erq350

5. Bolan, N., Kunhikrishnan, A., Thangarajan, R., Kumpiene, J., Park, J., Makino, T., … Scheckel, K. (2014). Remediation of heavy metal(loid)s contaminated soils – To mobilize or to immobilize? *Journal of Hazardous Materials*, *266*, 141–166. doi: https://doi.org/10.1016/J.JHAZMAT.2013.12.01

6. Bordoloi, S., Gopal, P., Boddu, R., Wang, Q., Cheng, Y.-F., Garg, A., & S, S. (2019). Soil-biochar-water interactions: Role of biochar from Eichhornia crassipes in influencing crack propagation and suction in unsaturated soils. *Journal of Cleaner Production*, *210*, 847–859. doi: https://doi.org/10.1016/j.jclepro.2018.11.051

7. Chyba, J., Kroulík, M., Krištof, K., Misiewicz, P. A., & Chaney, K. (2014). Influence of soil compaction by farm machinery and livestock on water infiltration rate on grassland. *Agronomy Research*, *12*(1), 59–64.

8. Colombi, T., Torres, L. C., Walter, A., & Keller, T. (2018). Feedbacks between soil penetration resistance, root architecture and water uptake limit water accessibility and crop growth – A vicious circle. *Science of the Total Environment*. doi:

https://doi.org/10.1016/j.scitotenv.2018.01.1
29

9. Cui, D., Li, M., & Zhang, Q. (2009). Development of an optical sensor for crop leaf chlorophyll content detection. *Computers and Electronics in Agriculture*, *69*(2), 171–176. doi: https://doi.org/10.1016/j.compag.2009.08.00
1

10. Czech Statistical Office. (2018). No Title. Retrieved from https://www.czso.cz/csu/czso/za-sto-let-ubyla-tretina-zemedelske-pudy

11. Dec, D., Dörner, J., & Balocchi, O. (2011). Temporal and spatial variability of structure dependent properties of a volcanic ash soil under pasture in southern Chile. *Chilean Journal of Agricultural Research*, *71*(2), 293–303. doi: https://doi.org/10.4067/S0718-58392011000200015

12. Fang, J., Zhan, L., Ok, Y. S., & Gao, B. (2018). Minireview of potential applications of hydrochar derived from hydrothermal carbonization of biomass. *Journal of Industrial and Engineering Chemistry*, *57*, 15–21. doi: https://doi.org/10.1016/J.JIEC.2017.08.026

13. Fischer, B. M. C., Manzoni, S., Morillas, L., Garcia, M., Johnson, M. S., & Lyon, S. W. (2019). Improving agricultural water use efficiency with biochar – A synthesis of biochar effects on water storage and fluxes across scales. *Science of The Total Environment*, *657*, 853–862. doi: https://doi.org/10.1016/j.scitotenv.2018.11.3
12

14. Gavili, E., Moosavi, A. A., & Kamgar Haghighi, A. A. (2019). Does biochar mitigate the adverse effects of drought on the agronomic traits and yield components of soybean? *Industrial Crops and Products*, *128*, 445–454. doi: https://doi.org/10.1016/j.indcrop.2018.11.04
7

15. Gülser, C., Ekberli, I., & Candemir, F. (2016). Spatial variability of soil physical properties in a cultivated field. *EURASIAN JOURNAL OF SOIL SCIENCE (EJSS)*, *5*(3), 192. doi: https://doi.org/10.18393/ejss.2016.3.192-200

16. Haider, G., Steffens, D., Moser, G., Müller, C., & Kammann, C. I. (2017). Biochar reduced nitrate leaching and improved soil moisture content without yield improvements in a four-year field study. *Agriculture, Ecosystems and Environment*. doi: https://doi.org/10.1016/j.agee.2016.12.019

17. Intersucho. (2019). Relative soil saturation. Retrieved from http://www.intersucho.cz/en/?map=1&from=2018-01-28&to=2019-01-28&current=2018-08-26

18. Jien, S.-H. (2019). Physical Characteristics of Biochars and Their Effects on Soil Physical Properties. In *Biochar from Biomass and Waste* (pp. 21–35). Elsevier. doi: https://doi.org/10.1016/B978-0-12-811729-3.00002-9

19. Liu, L., Yang, X., Zhou, H., Liu, S., Zhou, L., Li, X., … Wu, J. (2018). Evaluating the utility of solar-induced chlorophyll fluorescence for drought monitoring by comparison with NDVI derived from wheat canopy. *Science of The Total Environment*, *625*, 1208–1217. doi: https://doi.org/10.1016/j.scitotenv.2017.12.2
68

20. Pandit, N. R., Mulder, J., Hale, S. E., Zimmerman, A. R., Pandit, B. H., & Cornelissen, G. (2018). Multi-year double cropping biochar field trials in Nepal: Finding the optimal biochar dose through agronomic trials and cost-benefit analysis. *Science of The Total Environment*, *637–638*, 1333–1341. doi: https://doi.org/10.1016/j.scitotenv.2018.05.1
07

21. Potop, V., Možný, M., & Soukup, J. (2012). Drought evolution at various time scales in the lowland regions and their impact on vegetable crops in the Czech Republic. *Agricultural and Forest Meteorology*, *156*, 121–133. doi: https://doi.org/10.1016/J.AGRFORMET.201
2.01.002

22. R Core Team. (2018). R: A language and environment for statistical computing. Vienna: R Foundation for Statistical Computing.

23. Saleem, M., Law, A. D., Sahib, M. R., Pervaiz, Z. H., & Zhang, Q. (2018). Impact of root system architecture on rhizosphere and root microbiome. *Rhizosphere*, *6*, 47–51. doi: https://doi.org/10.1016/j.rhisph.2018.02.003

24. Stolte, J., Tesfai, M., Øygarden, L., Kværnø,

S., Keizer, J., Verheijen, F., … European Commission. Joint Research Centre. Institute for Environment and Sustainability. (2016). *Soil threats in Europe.* Publications Office.

25. Verhulst, N., Govaerts, B., Nelissen, V., Sayre, K. D., Crossa, J., Raes, D., & Deckers, J. (2011). The effect of tillage, crop rotation and residue management on maize and wheat growth and development evaluated with an optical sensor. *Field Crops Research*, *120*(1), 58–67. doi: https://doi.org/10.1016/j.fcr.2010.08.012

26. Wickham, H. (2009). *ggplot2 : elegant graphics for data analysis*. Springer.

27. Žalud, Z., Hlavinka, P., Prokeš, K., Semerádová, D., Balek Jan, & Trnka, M. (2017). Impacts of water availability and drought on maize yield – A comparison of 16 indicators. *Agricultural Water Management*, *188*, 126–135. doi: https://doi.org/10.1016/J.AGWAT.2017.04.007

28. Zhao, Z., & Zhou, W. (2019). Insight into interaction between biochar and soil minerals in changing biochar properties and adsorption capacities for sulfamethoxazole. *Environmental Pollution*, *245*, 208–217. doi: https://doi.org/10.1016/j.envpol.2018.11.013

Corresponding author:
Ing. Václav Novák, Czech University of Life Sciences Prague, Faculty of Engineering, Department of Machinery Utilization, Kamýcká 129, 16500 Prague, Czech Republic, novakvaclav@tf.czu.cz

CAE-JUSTIFICATION OF THE LEADING SHAFT OF THE TEST STAND

Alexander PASTUKHOV[1], Evgeny TIMASHOV[2], Olga SHARAYA[1], Dmitry BAKHAREV[1]

[1]*Belgorod State Agricultural University named after V. Gorin, Russian Federation*
[2]*Belgorod University of Cooperation, Economics and Law, Russian Federation*

Abstract
For assessment of reliability of power knots of transmissions of transport and technological machines, for example, of drive lines, on the basis of resource tests develop special stands which provide realization of service conditions. Purpose - ensuring durability and rigidity of the leading shaft of the stand of the power circuit bearing the leading elements: technological conical tooth gear and the tested cardan joint. The analysis of durability and rigidity has shown that statically definable scheme of shaft does not provide the required working capacity level. Statically indefinable scheme of the leading shaft of power circuit is offered. Justification of design of shaft and test calculations are executed on the basis of CAE-technologies in APM WinMachine with use of the WinShaft module. As a result on the normal tension, reserve factor and deformation of shaft the provision of intermediate bearing part is proved, the operability - is provided.

Key words: power circuit; tests; resource; durability; rigidity.

INTRODUCTION

Due to the expansion of scope of products of agricultural mechanical engineering and complication of the equipment the importance of problem of reliability of modern machines continuously increases. At all stages of life cycle of products, including "scientific research – design – production – operation", definition of indicators of reliability includes complex of works on establishment of quantitative values, and control – assessment of compliance of the reached reliability level to regulatory requirements (*Lamberson L.R., Kapur K.S., 2009*). To definition and confirmation of indicators of reliability at development stage of skilled copies and assessment of quality of the repaired products apply experimental methods, in particular, research resource stand tests. The technical instrument of stand tests is the stand equipment which is the technical device for reproduction of conditions of loading and functioning in operation (*Velichkin I.N., 1999; Kljatis L.M., Khabatov B.Sh., 1990*). At assessment of reliability of power knots of the farm vehicles losing the working capacity because of wear and fatigue for the purpose of obtaining reliable information apply stand resource tests of products in the form of the accelerated tests by toughening of loading or sealing on time at the same time obtain information on reliability of object in shorter terms, than in operation (*Srivastava A.K., et al. 2006; Flick E.P., 1984; Timashov E.P., Pastukhov A.G., 2009*). For load-bearing parts of the stand of loading, created at tests are limit therefore the question of design of the stand and justification of durability and rigidity of its elements is very difficult and relevant. At experimental working off of design of the stand for tests of drive lines (*RU 2134412*) the weak point - the leading shaft is revealed (*Erokhin M.N., Pastukhov A.G., 2008; Pastukhov A.G., 2008*). The initial sizes of the leading shaft have been established on the basis of static calculation on bend with torsion on equivalent tension, however the specified calculation for reserve factor on fatigue strength, shows about violation of condition of strength (*Pastukhov A.G., et al., 2018 a*). The aim of the study – ensuring durability and rigidity of design of the leading shaft by justification of the settlement scheme on the basis of CAE-technology.

MATERIALS AND METHODS

In practice of development of the stand equipment for experimental assessment of durability of drive lines there are three kinds of configuration of power circuit: 1) the direct-flow power scheme - short circuit of power circuit is carried out by frame; 2) the consecutive arrangement of the technological and experienced drives in power circuit – short circuit of power circuit is carried out by the mentioned drives; 3) parallel arrangement of the technological and experienced drives in power circuit – power short circuit by coverage technological drive of the experienced drive. Main shortcomings of schemes of configuration, respectively: 1) level of loading of the experienced drive depends on the power of the

established power source (electric motor); 2) equal loading both the technological, and experienced drives; 3) increased requirements of durability and rigidity to the bearing system of drive gear. Advantages of the provided schemes are obvious, respectively: 1) simplicity of design; 2) universality of design; 3) low loading of technological drive due to seating on the bigger radius of rotation. Thus, stands of the third scheme of configuration are perspective in terms of carrying out resource tests of power elements of transmissions, for example, of drive lines (*Erokhin M.N., Pastukhov A.G., 2008*).

The stand (*RU 2134412*) is developed for resource tests of drive lines taking into account influence of dynamic loads from toothed gearings, which contains electric motor 1, by means of elastic clutch 2 connected to technological gear reducer 3, the tested drive line 4 and the loading device 5, included in power circuit, reduction ratio of reducer 3 is equal to unit, and tooth gears of 6 and 7 conical reducers 3 are established on conducted 8 and the leading 9 shaft located in bearing parts 10 (Fig. 1).
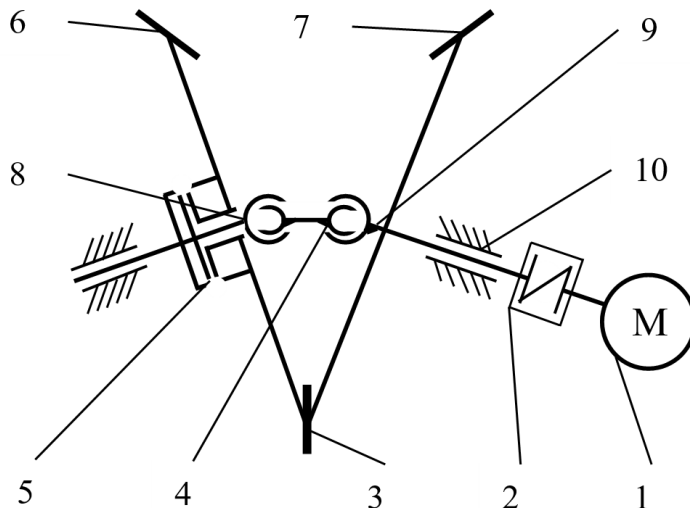

Fig. 1 The kinematic scheme of the stand for test of drive lines

In the course of practical working off of test procedure at the stand it is revealed that considerable conveyance of the end of the leading shaft 9 where the leading tooth gear 7 is established, leads to sidesway in gear reducer 3 that has an adverse effect on providing spot of contact piece in gear gearing. Thus, selection of geometrical characteristics of shaft 8 and 9 under the terms of durability and rigidity does not provide conditions of operability of technological drive. In this regard the hypothesis of introduction of static indefinability in the scheme of installation of the leading shaft is made for what it is necessary to define the provision of additional bearing part.

Due to the invariancy and high labor input of analytical calculations as the settlement tool the program complex of engineering calculations APM WinMashine (STC «Automated Design of Mashines», Russia, Korolyev), in particular, the WinShaft module - is applied to calculation of shaft on durability and rigidity (*Shelofast V.V., et al., 2013; Pastukhov A.G., et al., 2018 b*).

The course of preparation and carrying out calculations contains the following stages: 1) drawing up three settlement schemes of configuration of the leading shaft: statically definable scheme of shaft (Fig. 2), statically indefinable scheme with additional bearing part on the end of shaft (Fig. 3), statically indefinable scheme with additional bearing part of swing on the established ring gear of technological wheels of conical reducer (Fig. 4); 2) establishment of constructive technology factors of design of shaft and the application of loadings from the technological toothed gearing; 3) calculation of values of reserve factor on fatigue strength of n_{fat}, equivalent normal tension σ_{eq} and conveyances of f in 100 sections of shaft on length with the analysis of the 1st own form of deformation of shaft.

On Fig. 2-4 sketch of shaft, constructive and technological elements and coordinates of arrangement of bearing parts are shown full-scale on large-scale sex of the graphic editor of the module. In protocols of calculation numerical values of the calculated sizes and their graphic interpretation are recorded.

As basic data are accepted: nominal torque in power circuit is T_{nom}=600 (Nm), average dividing diameter of tooth gears is d_m=255 (mm), cog cross-section corner is α=20(°), corner of dividing cone of wheel is δ=81(°), district force in gearing is F_t=4706 (N), radial force is F_r=267 (N), axial force is F_a=1692 (N); subject to test is cardan joints IV of standard size on RD 37.001.665-96 with bearings GPZ-804704K5.
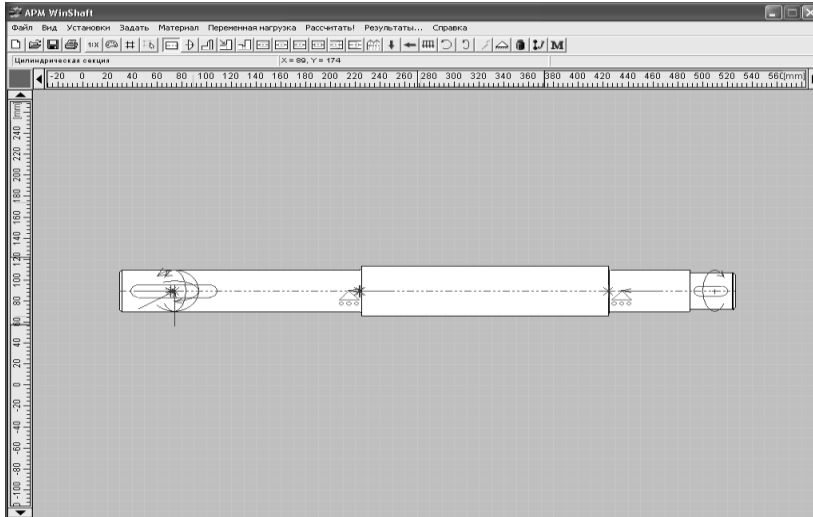
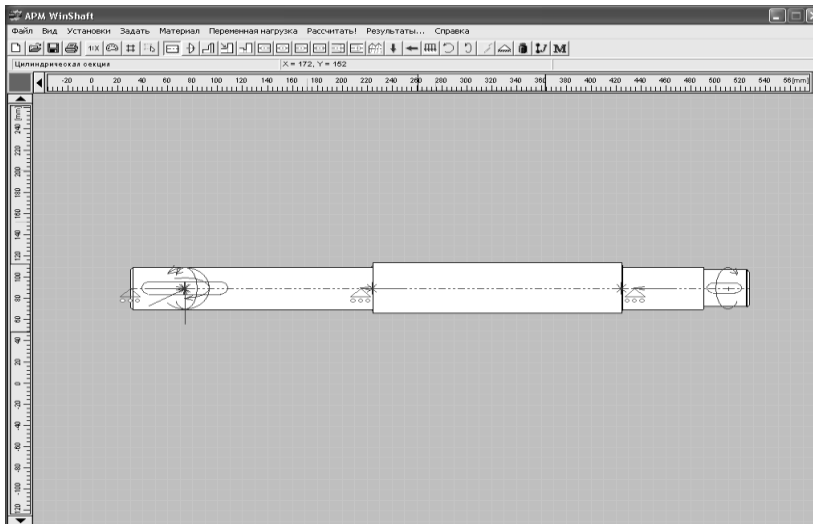**Fig. 2** Settlement scheme of statically definable leading shaft (option 1)

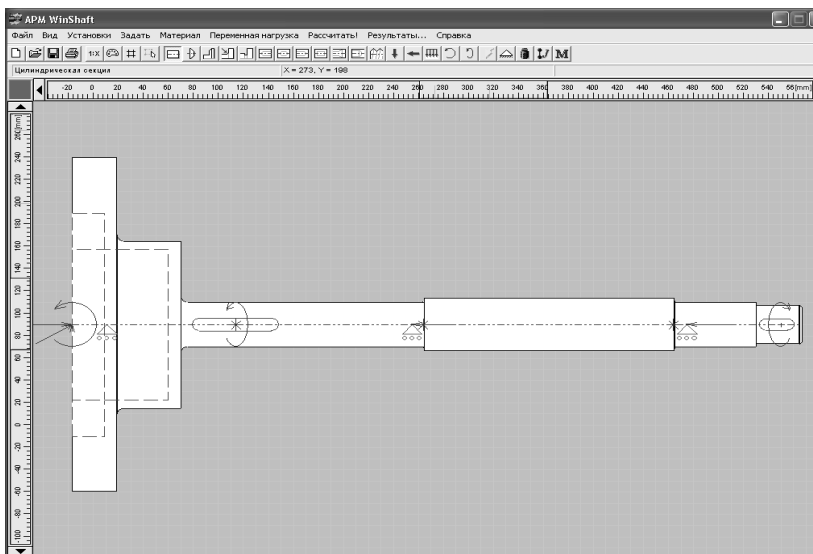**Fig. 3** Settlement scheme of statically indefinable leading shaft (option 2)

Fig. 4 Settlement scheme of statically indefinable leading shaft with wheel (option 3)

RESULTS AND DISCUSSION

As a result of performance of engine calculations for the considered versions of settlement schemes of the leading shaft values of reserve factor on fatigue strength of n_{fat}, equivalent normal tension σ_{eq} and conveyances of shaft of f as the provision of rated section of shaft are received. The maximum values of tension and reserve factor and also conveyance of the console end of shaft of f_{cons} are given in Tab. 1.

Tab. 1 Summary results of calculation of versions of settlement schemes of the leading shaft

Parameters	σ_{eq}, MPa	f_{cons}, mm	n_{fat}
Statically definable scheme of shaft (Fig. 2)	641	0.406	0.385
Statically indefinable scheme of shaft (Fig. 3)	149	0.000	0.804
Statically indefinable scheme of shaft with wheel (Fig. 4)	24.8	0.100	4.210

Analysis of data of Tab. 1 has allowed to draw the following partial conclusions (*Birger I.A. et al., 1993*): 1) equivalent normal tension for of statically definable shaft exceeds (option 1), and statically indefinable shaft (options 2 and 3) the allowed tension at bend for steel 40 (C40 EN) is σ_{adm}=200 (MPa) does not exceed; 2) practical check of conveyance of the console end of the leading shaft assembled with tooth gear at the stand by options 1 and 2 has shown offset of teeths of conical wheel in contact point on 5-10 (mm), in option 3 offset was absent; 3) for ensuring fatigue strength of shaft it is necessary to accept sufficient obtaining reserve factor of strength more than 3 that for options 1 and 2 is impracticable. Therefore, according to Tab. 1 of the compared versions 1, 2 and 3 of settlement schemes of the leading shaft (Fig. 2-4) at the stand it is necessary to apply introduction of the additional bearing parts of swing established to rim of gear conical wheels of reducer to realization i.e. by option 3. Graphic illustrations of calculated parameters are presented on Fig. 5-7.
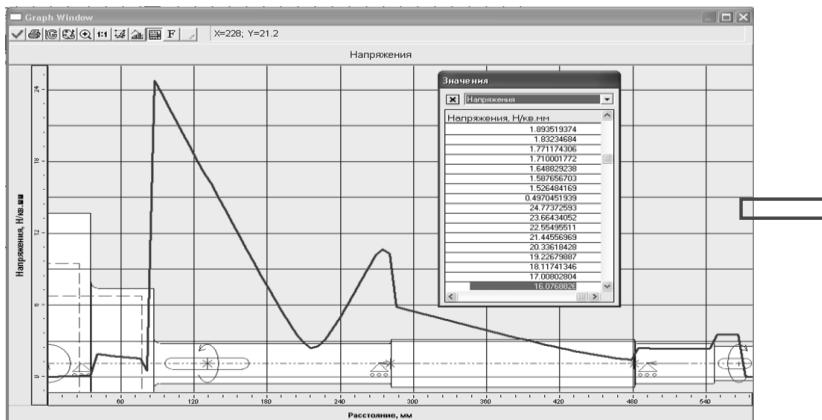

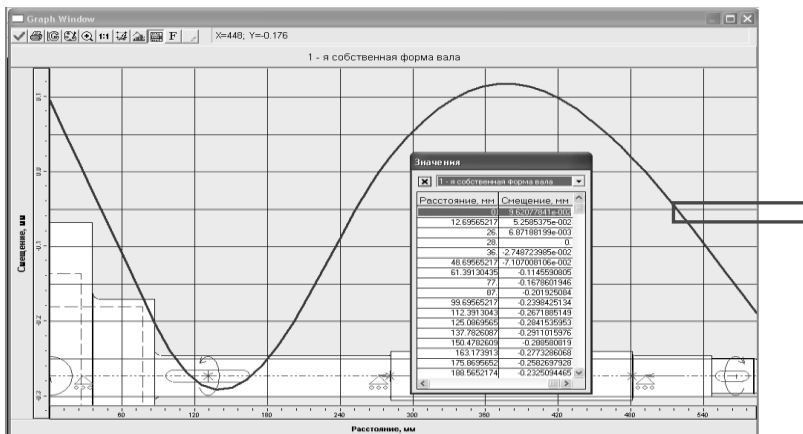**Fig. 5** Results of calculation of normal equivalent tension for shaft (option 3)

Fig. 6 Results of calculation of conveyances of the console end of shaft (option 3)
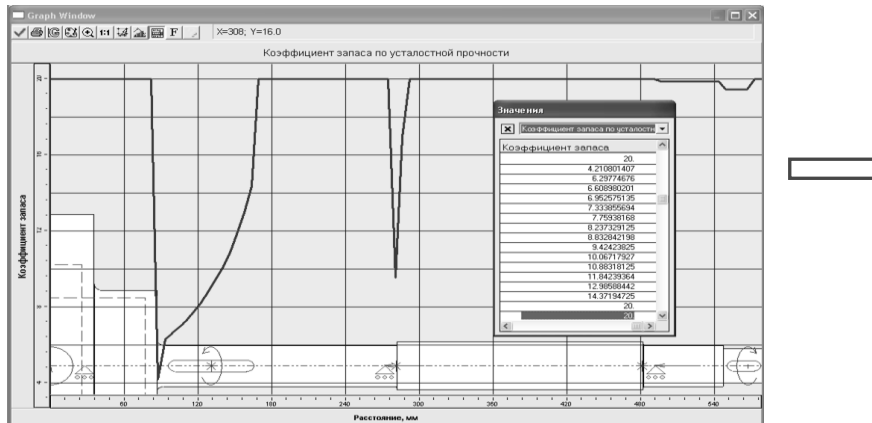
Fig. 7 Results of calculation of reserve factor of strength on fatigue for shaft (option 3)

As a result of production of intermediate bearing parts of swing and their installation in design of the test stand the technical tool for carrying out resource tests of cardan joints of unequal angular speeds is received. The general view of the stand with intermediate bearing part is presented on Fig. 8.
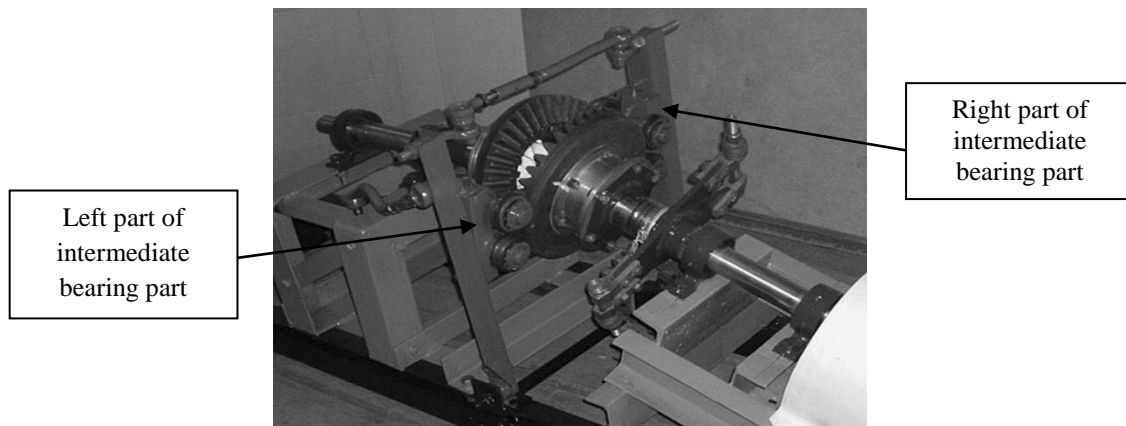

Fig. 8 General view of the stand for test of drive lines with intermediate bearing part

The subsequent technical evaluation of rationality of design has shown fidelity of the made decision on introduction of static indefinability at installation of shaft of the stand on the basis of CAE technologies as the loading of shaft has decreased, and the mass of the stand in comparison with analogs remained minimum (*Ašonja A., et al., 2013; Eresko S.P., 2016*). The metal construction of the stand allows to realize resource tests in the toughened mode. By comparison of results of development of this stand we note that similar technical solutions were applied also by other researchers for the purpose of ensuring durability and rigidity of the bearing shaft (*Ašonja A.N., 2014; Menovshchikov V.A., Eresko S.P., 2006*).

CONCLUSIONS
1. Ensuring durability and rigidity of power elements of the test stand allows to realize variability of the modes of loading of the experienced joints, gears and units of transmissions, both at the level of operation, and at the forced tests.
2. Introduction of static indefinability of design of shaft of the stand has led to ensuring high-quality contact piece of teeths of reducer that allows to realize as much as possible the potential of durability of technological drive of the stand at resource tests.
3. Use of CAE technologies when developing technical means for resource fail-safe tests is priority of development of production of the transport and technological equipment, owing to considerable drop of labor input and improvement of quality of process.

REFERENCES

1. Ašonja, A.N. (2014). The Influence of Diagnostic State of Reliability of Agriculture Double Cardan Shaft (in Serbian). *Scientific Journal Agricultural Engineering, 1,* 405-409.

2. Ašonja, A., Adamović, Ž., & Jevtić, N. (2013). Analysis of Reliability of Cardan Shafts Based on Condition Diagnostics of Bearing Assembly in Cardan Joints. *Journal Metalurgia International*, *18*(4), 216-221.

3. Birger, I.A., Shorr, B.F., & Iosilevich, G.B. (1993). *Calculation on durability of parts of machines* (in Russian). Reference book. Mechanical Engineering, 640 p.

4. Erokhin, M.N. & Pastukhov, A.G. (2008). *Reliability of drive lines of transmissions of agricultural machinery in operation* (in Russian). Monograph. Belgorod: BelSAA, 160 p.

5. Eresko, S.P., Eresko, T.T., Kukushkin, E.V., Menovshchikov, V.A., & Orlov, A.A. (2016). The design of the stand for testing cardan joints on needle bearings in a wide range of sizes with a change in the angle of fracture of the cardan drive (in Russian). *Transport. Transport facilities. Ecology,* 2, 58-73. doi: 10.15593/24111678/2016.02.05.

6. Flick, E.P. (1984). *Mechanical drives agricultural machines* (in Russian). Monograph. Moscow: Mechanical Engineering. 272 p.

7. Klyatis, L.M. & Khabatov, B.Sh. (1990). Features of the development and applications of test stands (in Russian). *Tractors and agricultural machines,* 5, 4-5.

8. Lamberson, L.R. & Kapur, K.S. (2009). *Reliability in engineering design*. Weliy India Pvt. Limited.

9. Menovshchikov, V.A. & Eresko, S.P. (2006). *Research and improvement of needle bearings of drive lines of transport and technological machines* (in Russian). Monograph. Krasnoyarsk State Agrarian University, 250 p.

10. Pastukhov, A.G. (2008). Advanced stands for resource tests of drive lines (in Russian). *Automotive industry, 5*, 35-37.

11. Pastukhov, A.G., Timashov, E.P., & Sharaya, O.A. (2018 *a*). Principles of designing and justification of parameters of the coaxial scheme of the power contour of the stand for resource tests of drive lines. In *Proceedings ISB-INMA TEH "Agricultural and mechanical engineering"* (pp. 101-106).

12. Pastukhov, A., Kolesnikov, A., Bakharev, D., & Berezhnaya, I. (2018 *b*). Assessment of operability of the crankshaft of the compressor. In *Engineering for Rural Development* (pp. 850-855). Jelgava, Latvia. doi: 10.22616/ERDev2018.17.N164.

13. Srivastava, A.K., Goering, C.E., Rohrbach, R.P., & Buckmaster, D.R. (2006). Engineering Principles of Agricultural Machines. *ASABE*.

14. Shelofast, V.V., Zamriy, A.A., Rozinsky, S.M., Shanin, D.V., & Alekhin, A.V. (2013). Practical training course. CAD/CAE APM WinMachine system (in Russian). *Teaching manual*, 144 p. Moscow: Publishing house APM.

15. Timashov, E.P. & Pastukhov, A.G. (2009). *Increase in durability of cardan joints of transport and technological machines in operation* (in Russian). Monograph. Stary Oskol: STI MISIS. 73 p.

16. Velichkin, I.N. (1999). Accelerated testing - the key to the competitiveness of technology (in Russian). *Tractors and agricultural machines,* No 3, 41-43.

Corresponding author:
Alexander Pastukhov, Dr. Sc. Ing., Professor, Hade of Department of Technical Mechanic and Machine Design, Faculty of Engineering, Belgorod State Agricultural University named after V.Gorin, Vavilov's street, 1, Maysky, Belgorod district, Belgorod region, 308503, Russian Federation, phone: +7-960 6276818, e-mail: pastukhov_ag@mail.ru

ESTIMATION TRENDS IN THE MAINTENANCE OF A MANUFACTURING EQUIPMENT RELATION TO THE INDUSTRY 4.0 CHALLENGE

Jindrich PAVLU[1], Vaclav LEGAT[1], Zdenek ALES[1]

[1]*Department for Quality and Dependability of Machines, Faculty of Engineering, Czech University of Life Sciences Prague, Czech Republic*

Abstract
The paper presents a survey of trends and perspectives in asset and maintenance management in the field of maintenance execution, maintenance top management responsibility, maintenance processes, resources for maintenance and maintenance monitoring, analysis and improvement. Every idea is presented in the light of the Industry 4.0 revolution.

Key words: *asset management; maintenance management; maintenance engineering; trends in maintenance.*

INTRODUCTION

Nowadays, many maintenance managers wonder, where maintenance is lead up and what it will look like in the near and far future. The Fourth Industrial Revolution is coming down to us and aspects are already described in many publications, e.g. (*Marik, et al., 2015; Marik, 2016*), usually under the heading Industry 4.0. It is positive that the government of the Czech Republic also supports this challenge and perhaps will provide the necessary financial support in the form of grants to application research and other activities. Admittedly, these publications (*Marik, et al., 2015; Marik, 2016*) do not address maintenance management and engineering independently and move in the industry as a whole.
Nevertheless, the Czech Maintenance Society (CMS) is raising awareness of the application ideas of Industry 4.0 to maintenance in all educational activities since 2016, both in its courses, seminars and conferences. These courses refer and prepare participants for solutions of the Industry 4.0 challenges.

The aim of this paper is to prepare a study of the expected development of maintenance management and engineering in the near future.

MATERIALS AND METHODS

The general idea of maintenance of a manufacturing equipment is based on the principles of maintenace management system, whose main objective is to plan, manage and control material and information flow in order to achieve the performance and economic goals. A substantial part of the maintenance management system is an information system (IS), which goal is to capture, store, process and transmit data (actual and planned). It is beneficial not only for well organized documentation of the maintenance and other activities (it is a starting point, it is not desired goal), but also to save time in preparing and implementing maintenance activities, saving human resources, material and spare parts, quick reduction of weak points, reduction of nonconforming products, increasing of the reliability of production equipment, etc. *(Jurca & Ales, 2012).*

Maintenance 4.0 is based on policies and is supported by Industry 4.0 tools. Key tools include:

- Robotisation,
- Automation,
- Digitalisation,
- IoT (Internet of things),
- comunication (data collection, smart glasses, augmented reality),
- big data (monitoring and diagnostics),
- information and computing technology,

- • methods and techniques of cybernetics and artificial intelligence used for predictive maintenance,
- • spare parts logistics, 3D printer,
- • new materials
- • staff, social aspects, etc.

Will these things going to be all for free, with extra cost? Certainly not, but the assumption is given by the hypothesis that the embedded money will bring more money in the future.

Performance monitoring can be scheduled, on demand or continuous. The development is aimed at continuous monitoring (diagnosis) with various sensors. The development is leading up to continuous monitoring (diagnostics) via various sensors.

Predictive maintenance of status is based on prediction, which is derived from analysis and evaluation of significant degradation parameters of object - see Figure 1.

Predicting is based on analysis and extrapolation of degradation parameters of object (see Figure 2 and 3) or other more sophisticated methods (e.g. neural networks, artificial intelligence, multipara-metric analysis, etc.).

Non-linear extrapolation using nth degree polynomials (1) is not recommended, because it is uncertain how the trend prediction will develop according to this function.

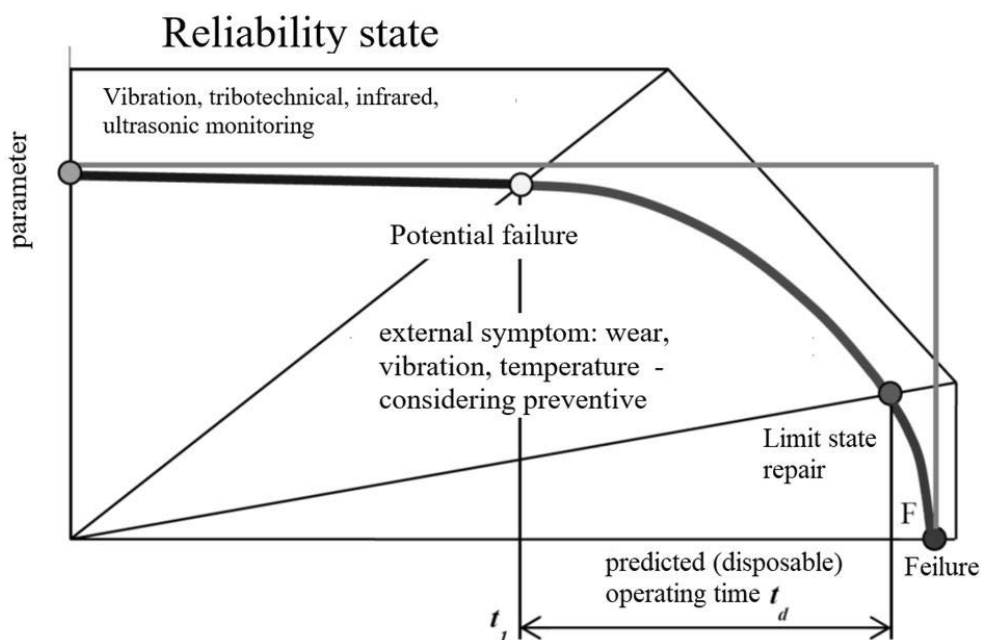$$S(t) = a_0 + a_1 t + a_1 t^2 + \cdots + a_n t^n \qquad a_n \neq 0 \qquad (1)$$

Fig. 1 The Principle of Predicting Time to Repair (Failure)

Principle: Apply predictive maintenance wherever it is technically possible and economically advantageous. This is important perspective requirement to maintenance. Nowadays predictive maintenance is still much mentioned, but there are still a just few fully functional applications in use. [*CSN EN 13306:2017*]

Proactive maintenance will be increasingly applied to all types of maintenance. Proactive maintenance is based on analysis of causes, whether potential or real failures, and the elimination of all undesirable identified causes.
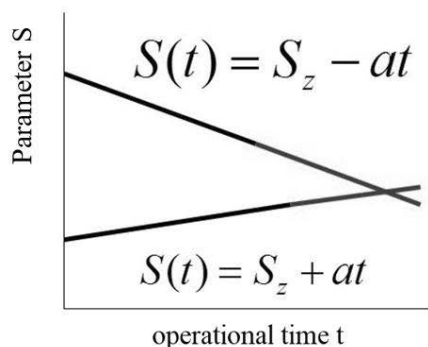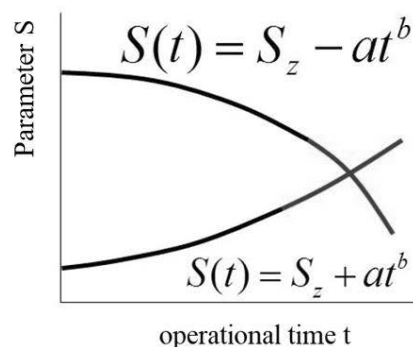
Fig. 2 Linear one-parametric extrapolation

Fig. 3 Nonlinear one-parametric extrapolation

RESULTS AND DISCUSSION

Based on the described analysis of maintenance tools and methods is can presented an overview of what data should the maintenance information system collect and process in the area of maintenance management.

The authors see the biggest problem in the absence of data analysis in general and automated analyses in particular. Sophisticated data analysis, artificial intelligence in diagnostics of technical condition and fault conditions, algorithms for calculating limit state for repair, routine planning of preventive maintenance, shutdowns, spare parts is missing. Unfortunately, the authors have to say that the maintenance management system and maintenance staff (at all levels) is not ready for this challenge at present. The automotive industry has an exceptional position in the Industry 4.0 challenge, but there is not all at the level of excellence. The industry is moving forward at a fast pace to reap the benefits of the Industry 4.0 revolution, but unfortunately standards bodies have not been able to keep up with this pace *(Kaur et al. 2018)*.

Indeed, an analysis approach aimed at preventing the occurrence of progressive defects allows for a drastic reduction of shut-down times inevitably occurring during maintenance phases *(Dinardo, Fabbiano, & Vacca, 2018)*.

However, maintenance information systems will require major improvements in area of processing and evaluation data. Current hardware is already at high level in the field of collection, transfer and storage data (sensors, wireless data transfer, concentrated and shared clouds, internet of things etc.) (*CSN EN 60300-3-14:2005)*.

Quality requirements for maintenance processes are growing and it can generally be expressed in several points:

1. Asset acquisition with high reliability and low life cycle costs in accordance with asset management. (*PAS 55-1:2008*; *PAS 55-2:2008*; *CSN ISO 55000:2015*; *CSN ISO 55001:2014*; *CSN ISO 55002:2014*; *CSN EN 16646:2015*; *Wilson, 2013*).
2. Maintenance of tangible fixed assets in operational and proper condition.
3. Prevention of creates failure and following failure conditions.
4. Operative elimination of failures.
5. Reducing the environmental impact of production equipment
6. Safety of operational and maintenance man
7. Risk mitigation
8. Elimination of critical failure
9. Applying optimal maintenance costs.
10. Leading asset management to applying methods best practice with according to Industry 4.0 challenge

Conception of Industry 4.0 highly requires integration of all development, manufacturing, logistics and maintenance processes. In this area there is much to improve and implement. There are also some weaknesses in administration and maintenance planning, an appropriate information planning system is very small. The corrective maintenance system still prevails. The pressure on predictive and proactive maintenance will grow *(CSN ISO 55000:2015)*.

It is conclusive, consequently, to assert that the main drive behind the fourth industrial revolution is to guarantee the effective availability of reliable, complete, and real-time information by linking together all parties or elements of the value chain (*Alqahtani, Gupta, & Nakashima, 2019*).

Massive implementation of Conception of Industry 4.0, using of sensors detecting the technical situation, analysing RCM and using dates from analysing FMECA are helpful for much more better and efficient identification of preventive maintenance tasks to:

- detect and correct emerging failures either before they occur or before they become critical failures
- reduce the probability of failure
- uncover hidden errors that have occurred
- increase the cost-effectiveness of the maintenance program.

Smart system sand internet-based solutions that characterize Industry 4.0 greatly impact and change manufacturing processes and practices, maintenance strategies and maintenance management *(Koenig, Found & Kumar, 2019)*.

Proper maintenance strategies are drawing increasing attention and facing new challenges as important methods in improving the reliability and availability of manufacturing systems in order to ensure the timely delivery of high-quality products to customers *(He, Han, Gu & Chen, 2018)*.

Maintenance management processes should be significantly change due to the Industry 4.0 challenge. The pressure will increase to transition from maintenance to failure and periodic maintenance to predictive and proactive maintenance wherever it will be technically possible and cost-effective. The technical possibilities of implementing of predictive maintenance are already enabled by offering of wide range of affordable sensors.

a) **Timing data**
- Time to failure and time between failures t and operational time of machines and their elements,
- inspection repair intervals, preventive repair intervals, diagnostic intervals, preventive maintenance – repairs intervals,
- maintenance lead time and laboriousness of maintenance, planned technical - useful life of machine and equipment,
- downtimes of machines and equipment, which are created by:
- organizational downtime, logistic downtime,
- rest time for personal needs,
- preventive maintenance,
- failures,
- setup and adjustment downtime,
- technological failures,

b) **Technical data** – various diagnostic signals,
- vibrotechnical data,
- temperatures,
- the magnitude of voltage and current
- tribotechnical data,
- wear size
- clearance, flow rate, pressure
- change the efficiency of machine
- real performance,

c) **Economic data**
- cost of preventive maintenance,
- revision cost, preventive inspection cost, diagnostic cost,
- maintenance cost after failure,
- downtime cost (function of production losses),
- costs caused by increasing wear on functional surfaces,
- losses from the risk of occurrence of failure and non-compliance if normative for repair to comply with the normative for recovery,

- •   Production price of one product,
- •   labour, material, overheads costs on internal maintenance and external maintenance,

These data require the introduction of a thorough cooperation with financial controlling and fundamental adjustment of information system maintenance (ISM)

- d)   **Reliability data** (reliability, maintainability and maintenance support)
- \-   quantitative data
  - •   time to failure and time between failure,
  - •   time to repair,
  - •   density distribution of probability of failure
  - •   probability of failure, probability of reliability, failure rate and failure intensity,
  - •   time of undetected of failure condition,
  - •   time of administrative delay,
  - •   time of corrective maintenance, time of preventive maintenance,
  - •   number of non-conforming units due to a faulty manufacturing process and the start of production
  - •   spare parts consumption number of maintenance man,
- \-   quality data
  - •   description of mode failure, causes of failure, detectability of failure, consequence of failure,
  - •   type of communication (reporting and repair of failure, maintenance support),

One of the most important property features of the production equipment is operational reliability. With the characteristic (features) of reliability we are measuring availability, sustainability and ensure the maintenance of machinery and equipment, what influences the level of using their nominal efficiency and their overall productivity, quality and production efficiency. Data collection and knowledge of probability of failures features allow to optimize preventive maintenance in general and with monitoring and diagnosis to optimize and apply predictive maintenance.

It follows that the business of these reliability departments should be the collection of reliability data, analysis and processing into relevant characteristics, optimization of preventive maintenance programs and application of reliability tools to improve the reliability of production equipment as well as final products.

CONCLUSIONS

Maintenance requirements for industrial production machine and equipment never fade away. Requires on education and training of maintenance staff will grow progressively, a profession desired will be in mechatronics. Producers will deliver smart machines, i.e. machines more reliable, more powerful, more effective, safer, greener and more ergonomic producing machines with ability to self-management with the support of asset management. Better application of robotics and digitalization of the maintenance processes (smart machines) will not replace fully „the hands" of maintenance staff, just speed up their processes, make them easier and reduce unwanted downtime. Electronic systems will be managed and controlled mainly remotely. Diagnostics and analysis of acquired data using artificial intelligence and predictive maintenance will reduce operational failure rate, resp. improves the reliability and availability of production equipment. The data obtained by monitoring and diagnosing the technical condition of the production facility and the financial control of its operation will be more effectively operated and intensively used in the maintenance management processes. Spare parts logistics will be supported by the 3D printing technology and the assortment of spare parts for storage will be managed scientifically. The Government will support the development of education also in the field of maintenance staff, starting with dual apprenticeships, through secondary education in industrial schools, to higher education with fields of mechatronics, management and maintenance engineering in line with the

Conception Industry 4.0 challenge. General and Production Directors will fully appreciate the importance and will more support the maintenance of production equipment according to the Maintenance conception 4.0 as a necessary prerequisite and resource for improving the organization´s performance.

ACKNOWLEDGMENT

REFERENCES

1. Alqahtani, A. Y., Gupta, S. M., & Nakashima, K. (2019). Warranty and maintenance analysis of sensor embedded products using internet of things in industry 4.0. *International Journal of Production Economics*, *208*, 483-499.
2. CSN EN 13306:2017 Maintenance – Maintenance terminology.
3. CSN ISO 55000:2015 Asset management – Overview, principles and terminology.
4. CSN ISO 55001:2014 Asset management – Management systems – Requirements.
5. CSN ISO 55002:2014 Asset management – Management systems – Guidelines for the application of ISO 55001.
6. CSN EN 16646:2015 Maintenance – Maintenance within physical asset management.
7. CSN EN 60300-3-14:2005 Dependability management - Part 3-14: Application guide - Maintenance and maintenance support.
8. Dinardo, G., Fabbiano, L., & Vacca, G. (2018). A smart and intuitive machine condition monitor-ing in the Industry 4.0 scenario. *Measurement*, *126*, 1-12.
9. He, Y., Han, X., Gu, Ch., & Chen, Z. (2018). Cost-oriented predictive maintenance based on mission reliability state for cyber manufacturing systems. *Advances in Mechanical Engineering, 10*(1), 1-15.
10. Jurca, V., & Ales, Z. (2012) Maintenance management systems in agricultural companies in the Czech Republic. Eksploatacja i Niezawodnosc – *Maintenance and Reliability*, *14*(3): 233-238.
11. Kaur, K., Selway, M., Grossmann, G., Stumptner, M., & Johnston, A. (2018). Towards an open-standards based framework for achieving condition-based predictive maintenance. *In: Proceedings of the 8th International Conference on the Internet of Things - IOT '18*. New York, USA: ACM Press, 1-8.
12. Koenig, F., Found, A. P., & Kumar, M. (2019) Innovative airport 4.0 condition-based maintenance system for baggage handling DCV systems. *International Journal of Productivity and Performance Management*, *68*(3), 561-577.
13. Marik, V., et al. (2015). National Industry Challenge 4.0. Ministry of Industry and Trade.
14. Marik, V. (2016). Industry Challenge 4.0. for Czech Republic, Management Press, ISBN 978-80-7261-440-0.
15. PAS 55-1:2008 Asset Management, Part 1: Specification for the optimized management of physical assets, Institute of Asset Management, London, ISBN 978-0-580-50975-9.
16. PAS 55-2:2008 Asset Management, Part 2 Guidelines for the application of PAS 55-1, Institute of Asset Management, London, ISBN 978-0-580-50976-6
17. Wilson, A. (2013). Asset Management focusing on developing maintenance strategies and improving performance. Published by Conference Communication, Monks Hill, Tilford, Farnham, Surrey HU10 2AJ, 2013. ISBN 978-0-9506465-6-5

Corresponding author:
Ing. Jindrich Pavlu, Ph.D., Department for Quality and Dependability of Machines, Faculty of Engineering, Czech University of Life Sciences Prague, Kamýcká 129, Praha 6, Prague, 16521, Czech Republic, e-mail: pavluj@tf.czu.cz

SOME PHYSICAL PROPERTIES OF BIODIESEL BLENDS WITH GASOLINE

Ana PETROVIĆ[1], Vlasta VOZÁROVÁ[1], Ján CSILLAG[1], Matúš BILČÍK[1]

[1]*Department of Physics, Faculty of Engineering, Slovak University of Agriculture in Nitra*

Abstract
The physical properties of any fuel are significant factors which help to decide whether the oils are suitable for engine or not. The prediction of various properties of biodiesel or blends of biodiesel with gasoline is vital for the design of different systems of diesel engine. Therefore, this paper is dealing with characterization of viscosity and specific calorific value of biodiesels according to present standard testing methods. The basis of this work is experimental material research. The main aim is to evaluate effect of gasoline addition to biofuel. Dynamic viscosity showed high temperature dependence. Results presented that gasoline could effectively lower the viscosity. We concluded that calorific value depends on input raw material. It was concluded that almost all samples are following the standard specified by EN 14214 and ASTM D 6751.

Key words: biodegradable fuels; gasoline; viscosity; specific calorific value.

INTRODUCTION

As the primary liquid fuel – diesel is being used in many sectors e.g. transportation, power, agriculture etc. (*Pantazi et al., 2013*). A significant role in the economic development of a country has the transport sector. This sector represents more than 70 % of the total diesel consumption. Industrial sector also consumes diesel for generator set and agricultural sector for water pumps. Diesel engine is being preferred for its high reliability, energy efficiency, durability and low operational cost by both manufacturers and users (*Acharya et al., 2017*). But the vehicular pollution is a major source of air pollution which is a prime cause of different respiratory diseases and global warming. Beside this, the worrying problems are petroleum reserves and price increase of fossil energy. The current way of using fuels in transport cannot be characterized either as pure or as sustainable (*Angelovič et al., 2016*).

The generation of "greenhouse gases" in the operation of motor vehicles may be impaired by the use of alternative drives or alternative fuels, respectively (*Kosiba et al., 2016*). To compete with this critical situation, a good number of research have been conducted to find alternative to fossil fuels for eco-friendly condition. Biodiesel is considered to be a notable option for at least complementing conventional fuels (*Aransiola et al., 2014*). The quality of biodiesel is regulated by standards, the two most utilized being ASTM D6751 in the United States and EN 14214 in the European Union. Many countries encourage the development and use of biodiesel. ASTM approves biodiesel blends, such as B5, for safe operation in any compression-ignition engine designed to be operated on diesel vehicles including electrical generators, trucks, tractors and boats.

Different researchers have studied the physical and chemical properties of biodiesel and blend it either experimentally or theoretically. Researchers proved that the diverse fatty acid composition of biodiesel has huge impact on properties, which provides an obvious effect on engine performance. Accordingly, it is necessary to research biodiesels according to present standard testing methods (*Atabani et al., 2013*).

Most of the researchers reported biodiesel (BD) – gasoline (G) blends impact on gasoline compressed ignition (GCI) engine performance and emission (*Putrasari & Lim, 2018; Adams et al., 2013*) or common rail diesel engine (*Chen et al., 2017*). And these studies shown that BD – G blends have better low temperature fluidity and vaporization then biodiesel itself. Gasoline addition reduces smoke and ultrafine particle emissions (UFP), while the NOx emissions increases a little. However, detailed study on physicochemical properties not yet been published. *Hlaváčová et al. (2018)* made the same conclusion. The specification for the biodiesel – gasoline blend fuel has lack of information. This paper is dealing with some physical properties – viscosity and specific calorific value.

MATERIALS AND METHODS

Selected biodiesel and biodiesel blends

Commercial gasoline (G) and Rapeseed methyl ester biodiesel (BD) and four gasoline-biodiesel blends (95 % BD + 5 % G (95:5), 90 % BD + 10 % G (90:10), 85 % BD + 15 % G (85:15) and 80 % BD + 20 % G (80:20)) were used in this study. The gasoline-biodiesel blends were prepared by a mixing/shaking process for about (3–5) min to produce homogeneous blends. This homogenization process was repeated before every measurement.

Methods and measuring equipment

Viscosity is the most important property of any fuel as it indicates the resistance of a material to shear or flow and it is strongly influenced by temperature. It therefore affects the operation of the fuel injection equipment and spray atomization, particularly at low temperatures when the increase in viscosity affects the fluidity of the fuel (*Božiková et al., 2016; Atabani et al., 2013*). Dynamic viscosity derived from Newton's law is characterized by a relationship:

$$\tau = \eta \; grad \; v \tag{1}$$

where: $grad \; v = \frac{dv}{dh}$ - the size of velocity gradient (s^{-1}), τ - shear stress (Pa), η - dynamic viscosity (Pa.s).

The fuel as a liquid is said to exhibit ideal viscous flow or Newtonian behaviour. We can divide the viscosity into dynamic and kinematic. For liquids, dynamic viscosity is functionally dependent on temperature and pressure, decreases with ascending temperature and rising when pressure rises. The relationship of kinematic and dynamic viscosity states that the viscosity can be defined as the ratio of dynamic viscosity and density of liquid when measured at the same temperature:

$$\nu = \frac{\eta}{\rho} \tag{2}$$

where: η - dynamic viscosity (Pa.s), ρ - density (kg.m^{-3}).

Viscosity of most of the liquids decreases with increasing temperature according to Arrhenius equation (*Hlaváč et al., 2016*).

$$\eta = \eta_0 e^{\frac{E_A}{RT}} \tag{3}$$

where: η - dynamic viscosity (Pa.s), η_0 - reference value of dynamic viscosity (Pa.s), E_A - activation energy (J.mol^{-1}), R - gas constant (J.K.mol^{-1}), T - absolute temperature (K).

Božiková & Hlaváč (2013) conducted research of rheological properties of rapeseed oil, where relation had exponential decreasing progress and it was described by modified Arrhenius equation. Viscosity of vegetable oil is typically ten times higher than petroleum based diesel. High viscosity leads to a poorer atomization and vaporization, formation of shoots, etc. (*Atabani et al., 2013*). Lower viscosity implies better low-temperature performance (*Alicke et al., 2015; Joshi & Pegg, 2007*). Other literature often presents kinematic viscosity data for biodiesel and its components, and these data are included in our work. Kinematic viscosity is prescribed in biodiesel standards. Often, the authors obtain whole curves to investigate temperature and blend concentration effects on viscosity.

Dynamic viscosity was measured with the Brookfield DV2T Viscosimeter. Measurements of the dynamic viscosity in the temperature interval from temperature 25 °C to 90 °C, are provided. In our case of measuring fuels, we used the ULA (0) spindle. All the samples had volume 16 ml. Accuracy of the viscosity measurement is ± 1.0 % of the full scale.

The specific calorific value of virtually all fatty acid methyl esters occurring in biodiesel exceed 35 000 kJ.kg^{-1} (35 MJ.kg^{-1}), the minimum specific calorific value prescribed in the European standard EN 14213 when using biodiesel for heating purposes. Specific calorific value q_s is the combustion heat calculated per unit of mass. It is reported in J.kg^{-1}.

$$q_s = \frac{Q}{m} \tag{4}$$

where: q_s - specific calorific value (J.kg^{-1}), Q – calorific value (J), m - mass (kg).

Energy value (expressed by calorific value) is an important parameter in the selection of a fuel. This is one of the important criteria as it affects the fuel consumption and output power. The energy value of biodiesel is generally lower than of diesel because of its higher oxygen content (*Atabani et al., 2013*). The measurement method, used for measuring of the specific calorific value, is the calorimetry method with the IKA C 5000 calorimetric system. All samples had volume 0.400 mg and were measured ten times. Measurement accuracy is ± 0.1 %.

RESULTS AND DISCUSSION

From the measured data, we created graphical dependencies of the dynamic viscosity on temperature for all samples and the typical curves were listed in Fig. 1. The dynamic viscosity of 100:0, 95:5, 90:10, 85:15 and 80:20 at 40 °C is 5.35, 4.32, 3.83, 3.67 and 3.07 Pa.s, respectively. So the viscosity of biodiesel with larger ester head group is higher, which is also confirmed by other authors (*Chen et al., 2017; Moser, 2009*). We deliberately measured the wider range of temperatures, because we wanted to obtain a full overview of the behavior of samples.
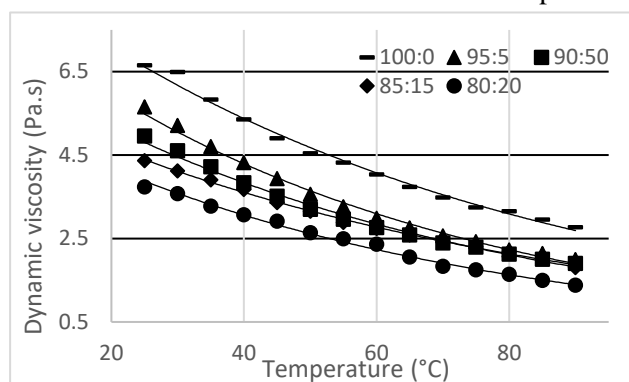

Fig. 1 Dependence of dynamic viscosity on temperature

Tab. 1 Overview of Viscosity Exponential Regression Equations and Determination Coefficients

Sample BD:G	Exponential regression equation	Coefficient of determination R^2
100:0	$y = 9.3465e^{-0.014x}$	0.9933
95:5	$y = 8.2474e^{-0.016x}$	0.9929
90:10	$y = 6.9824e^{-0.015x}$	0.9926
85:15	$y = 6.0912e^{-0.013x}$	0.9949
80:20	$y = 5.7446e^{-0.016x}$	0.9940

From Fig. 1, it can be seen that the measured viscosity values were different for individual samples. The greatest differences were at lower temperatures, where the viscosity is changed within a relatively wide range. Interestingly, the 100:0 sample, reaches the highest viscosity values. So as the temperature increased, the differences between the viscosities are getting smaller, and then the viscosity of 100:0 is greater than those of BD – G blends. In fact, a Newtonian behavior is always observed in this range. As expected, we see in Fig. 1, that the maximum viscosity of 100:0, 6.65 Pa.s is attained at the lowest temperature of 25 °C, and as the sample is heated the viscosity decreases, so we got final temperature of 90 °C and viscosity of 2.77 Pa.s. At temperatures at or above room temperature (25 °C), the ideal behavior of a biofuel is of a Newtonian fluid. The overall decrease in curve behavior is described by the exponential regression equations, which are listed in Table 1. Determination coefficients achieve high values for all samples. We can say, that the given regression equations precisely describe the graphical decreasing dependencies. These results confirmed the validity of Arrhenius exponential relationship. The statistical significance of the regression equation coefficients was tested on the level of significance $\alpha = 0.05$, in the Microsoft Excel software 2016 version 16.0.4266.1001, therefore, with the 95 % probability.

The viscosity tests showed an average precision of ± 0.08 mPa.s for the evaluated samples. The viscosity results are in accordance with the literature, where biodiesel have a higher viscosity than BD – G blends. According to *Joshi & Pegg (2007)* this is due to the composition of alkyl esters of long chain fatty acids. As the literature mostly report kinematic viscosity at 40 °C, in Table 2, we calculated it, according to the equation (2).

Fig. 2 shows a comparison of the kinematic viscosity values of the blends, biodiesel, and the standards applied to fuel mixtures. The ASTM D6751 standard establishes an acceptable range of viscosity for biodiesel from 1.9 to 6.0 $mm^2.s^{-1}$; while the EN 14214 standards defined the range between 3.5 and 5.0 $mm^2.s^{-1}$. Based on these data, $\nu = 6.176\ mm^2.s^{-1}$ for 100:0 is not fully acceptable in referenced standards, and therefore without blending cannot be used in the United States and Europe. Blend 95:5 is

in limits of ASTM, but still too high for EU. Other samples (90:10, 85:15, 80:20) fall under the cited standards.

Tab. 2 Density and calculated kinematic viscosity

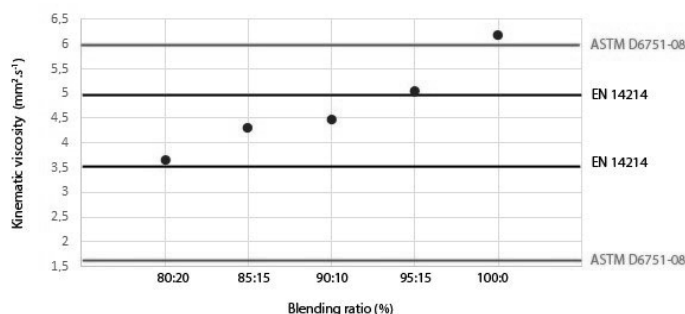| Sample BD:G	Density 15 °C g.cm^{-3}	Density 40 °C g.cm^{-3}	Kinematic viscosity 40 °C mm^2.s^{-1}
100:0	0.8838	0.8662	6.176
95:5	0.8774	0.8611	5.017
90:10	0.8714	0.8550	4.480
85:15	0.8655	0.8491	4.322
80:20	0.8612	0.8432	3.641

Fig. 2 Kinematic viscosity at 40 °C compared to standards EN 14214 and ASTM D6751

A comparison of some results in the present study and those in literature was also conducted. It was found that 100:0 possesses higher kinematic viscosity at 40 °C (6.176 mm^2.s^{-1}) then of *Atabani et al. (2013)* (4.5281 mm^2.s^{-1}), than that of *Karmakar et al. (2010)* with 4.439 mm^2.s^{-1}. *Chen et al. (2017)* has slightly higher viscosity of 6.01 mm^2.s^{-1}, but still below our result. In the same article he reports viscosities for blends 90:10 and 83:17, 4.76 mm^2.s^{-1}, 4.20 mm^2.s^{-1}, respectively. *Putrasari & Lim (2018)* got the result 4.229 mm^2.s^{-1}, while *Baczewski & Szczawinski (2011)* claim this value of viscosity 4.37 mm^2.s^{-1}.

With the increase in the percentage of gasoline present in the blends, the viscosity values slightly decreased. Reduction of the viscosity of 80:20 sample was the most remarkable among all reductions.

The final stage of the life cycle of a fuel is its combustion in an engine. Calorific value is a crucial parameter in the selection of a fuel. It is important to mention that all samples were burned totally, so it was perfect combustion without ash.
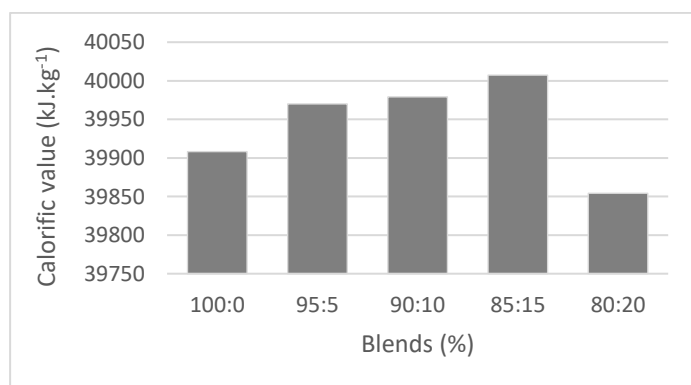

Fig. 3 Average values of measured Calorific value of fuel samples

The graphical representation of average values is shown on Fig. 3. It can be observed that sample 85:15 possesses the highest calorific value of 40007 kJ.kg^{-1} followed 90:10 (39976 kJ.kg^{-1}), 95:5 (39970 kJ.kg^{-1}), 100:0 (39908 kJ.kg^{-1}) and finally 80:20 (39854 kJ.kg^{-1}).

Among the data presented in Fig. 3, it is found that 80:20 biodiesel blend contain lower calorific value (39854 kJ.kg^{-1} on an average 39913 kJ.kg^{-1}) where the calorific value of other biodiesels is nearly 40000 kJ.kg^{-1}. We expected that the calorific value will increase with the increasing percentages of gasoline in blend, but even the measurement was repeated ten times for each sample, that was not confirmed for all blends. It should be noted, that the difference, between 80:20 and other samples, does not exceed 1 % of the average.

Tab. 3 Overview of descriptive statistics

Statistical parameter	100:0	95:5	90:10	85:15	80:20
$\bar{q_s}$	39908	39970	39979	40007	39854
$\bar{S}$	18.83	33.59	35.56	18.40	27.84
V_k (%)	0.047	0.084	0.089	0.046	0.069

It would also be interesting to research blends with even more gasoline, and see how the trend of calorific values would continue. The ASTM D6751 does not provide any limits for calorific values, but EN 14214 standard requires minimum of 35000 kJ.kg^{-1}. All samples are above the standards minimum value, thus they are acceptable.

It was found that our results of 100:0 (39908 kJ.kg^{-1}) possesses higher calorific value than 39790 kJ.kg^{-1} in *Putrasari & Lim (2018)* or 37120 kJ.kg^{-1} in *Adams et al. (2013)*. The one who find higher value is *Atabani et al. (2013)* 40195 kJ.kg^{-1}. *Chen et al. (2017)* declares 39390 kJ.kg^{-1} for 100:0, 39980 kJ.kg^{-1} for 90:10 blend and 40420 kJ.kg^{-1} for 83:17 blend, where it was confirmed that with the increasing of gasoline percentage in blends the calorific value also increases.

CONCLUSIONS

This mainly experimental study highlighted some properties of various biodiesel–gasoline blends. To describe in detail those properties, it assumes the knowledge of the parameters that include the influence of the material on the storage and combustion processes. These properties include viscosity and calorific value. In the present work, attention was paid to the analysis of those parameters, in order to create the widest possible picture of biodiesel behaviour.

We emphasize that the temperature has an important impact on the microstructure, and hence they also have a strong influence on the rheology of the biodiesel. As temperature increases, dynamic viscosity has decreased. During measurement, dynamic viscosity, showed high temperature dependence. Results presented that gasoline could effectively lower the viscosity.

Further, during calorific value measurement, all samples were burned totally, so it was perfect combustion without ash. Based on above mentioned studied literature and our results, we can conclude that calorific value depends on an input raw material.

These properties can also help to predict the quality and performance of biodiesel in diesel or other engines. It was found that those properties of biodiesels are following the standard specified by EN14214 and ASTM D 6751. This research can also be motivation for further technical research and development of special filters for engine.

REFERENCES

1. Acharya, N., Nanda, P, Panda, S. & Acharya, S. (2017). Analysis of properties and estimation of optimum blending ratio of blended mahua biodiesel. *Engineering Science and Technology, an International Journal, 20*(2), 511–517.
2. Adams, C.A, Loeper, P., Krieger, R., Andrie, M.J. & Foster, D.E. (2013). Effects of biodiesel–gasoline blends on gasoline direct-injection compression ignition (GCI) combustion. *Fuel, 111*, 784–790.
3. Alicke, A.A., Leopércio, B.C., Marchesini, F.H. & De Souza Mender, P.R. (2015). Guidelines for the rheological characterization of biodiesel. *Fuel, 140*, 446–452.
4. Angelovič M., Jablonický, J., Tkáč, Z., & Angelovič, M. (2016). *Properties of alternative fuels and their influence on parameters of combustion engines* (in Slovak). SUA in Nitra. ISBN 978-80-552-1569-3.
5. Aransiola, E.F., Ojumu, T.V., Oyekola, O.O., Madzimbamuto, T.F. & Ikhu–Omoregbe, D.I.O.A. (2014). *Review of current technology for biodiesel production: state of the art. Biomass Bioenergy, 61*, 276–297.
6. ASTM (American Society for Testing and Materials) International. D6751. (2017). Standard testmethod for biodiesel fuel blend stock (B100) for middle distillate fuels.
7. Atabani, A.E., Mahlia, T.M.I., Masjuki, H.H., Badruddin, I. A., Yussof Hafizuddin, W. & Chong,W.T. (2013). A comparative evaluation of physical and chemical properties of biodiesel synthesized from edible and non–edible oils and study on the effect of biodiesel blending. *Energy, 58*, 296–304.
8. Baczewski, K. & Szczawinski, P. (2011). Investigation properties of rapeseed oil methyl esters/aviation turbine fuel jet a-1 blends. *Journal of KONES Powertrain and Transport, 18*(1), 15–22.
9. Božiková, M. & Hlaváč, P. (2013). Thermophysical and rheologic properties of biooil Samples. *Journal of Central European Agriculture, 14*(3), 279–290.
10. Božíková, M., Hlaváč, P., Valach, M., Híreš, Ľ., Krišťák, Ľ., Malínek, M. & Regrut, T. (2016). Selected thermal and rheologic parameters of liquid fuels. In *6th International Conference on Trends in Agricultural Engineering* (pp. 81–87). Czech University of Life Sciences Prague; Faculty of Engineering.
11. CEN (European Committee for Standardization). EN 14214. (2009). Automotive fuels – fatty acid methyl esters (FAME) for diesel engines – requirements and test methods.
12. Chen, H., He, J., Yisong, Ch. & Haining H. (2017). Performance of a common rail diesel engine using biodiesel of waste cooking oil and gasoline blend. *Journal of the Energy Institute, 91*(6), 856–866.
13. Hlaváčová, Z., Božiková, M., Hlaváč, P., Regrut, T., & Ardonová, V. (2018). *Selected physical properties of various diesel blends. International Agrophysics, 32*(1), 93–100.
14. Hlaváč, P., Božiková, M., Hlaváčová, Z. & Kubík, Ľ. (2016). Influence of temperature and storing time on selected red wine physical properties. *Acta Universitatis et Silviculturae Mendeliane Brunensis, 64*(2), 433 – 439.
15. Joshi, R.M. & Pegg, M.J. (2007). Flow properties of biodiesel fuel blends at low temperatures. *Fuel, 86*, 143–151.
16. Karmakar, A., Karmakar, S. & Mukherjee S. (2010). Properties of various plants and animals feedstocks for biodiesel production. *Bioresource Technology, 101*(19), 7201–7210.
17. Kosiba, J., Uhrínová, D., Jablonický, J. & Majdan, R. (2016). *Alternative fuels and motor vehicle drives* (in Slovak). SUA in Nitra.
18. Moser, B.R. (2009). Biodiesel production, properties, and feedstocks. *Vitro Cell Dev-Plant, 45*, 229–266.
19. Pantazi, X. E., Moshou, D., Kateris, D., Gravalos, I. & Xyradakis, P.A. (2013). Automatic prediction of gasoline – biofuel blend type in combustion four-stroke engine based on one class support vector machines. In *5th International Conference on Trends in Agricultural Engineering* (pp. 498–502). Czech University of Life Sciences Prague; Faculty of Engineering.
20. Putrasari, Y. & Lim, O. (2018). A study of a GCI engine fueled with gasoline-biodiesel blends under pilot and main injection strategies. *Fuel, 221*, 269–282.

Corresponding author:
Ing. Ana Petrović, PhD., Department of Physics, Faculty of Engineering, Slovak University of Agriculture in Nitra, Tr. A. Hlinku 2, Nitra, 949 76, Slovak Republic, phone: +421 37641 5785, e-mail: ana.petrovic@uniag.sk

BEHAVIOUR OF 3D PRINTED IMPELLERS IN PERFORMANCE TESTS OF HYDRODYNAMIC PUMP

Martin POLÁK[1]

[1]Department of Mechanical Engineering, Faculty of Engineering, Czech University of Life Sciences in Prague, Kamýcká 129, 165 21 Prague, Czech Republic, e-mail: karel@tf.czu.cz

Abstract

The paper summarizes the results of testing the performance characteristics of various types of radial centrifugal pump impellers manufactured by Rapid Prototyping method. Experimental performance characteristics were compared to those of conventional impellers manufactured by sand moulds casting. The operational testing had shown that all tested variants of impellers were able to withstand the maximum load at the highest power output without any damage. In terms of performance, the impellers manufactured by 3D printing had higher efficiency at higher flow rates than conventional casted impellers by a few percentage points. The main advantage of this method is the rapid manufacturing of the prototype – in this case, the production time of one impeller did not exceed 33 hours.

Key words: *Rapid Prototyping; pump; turbine; power characteristics.*

INTRODUCTION

Contemporary Czech, but also Central European landscape is facing increasingly a lack of rainfalls. The rainfall deficiency is particularly noticeable in the soil management sectors - agriculture and forestry.

Lack of irrigation water is also a serious problem in dry-climate areas and underdeveloped countries (*Kazim, 2003*). Micro-irrigation systems (MIS) are ever more frequently being introduced in areas with limited water supplies. The size of such irrigated areas is gradually growing – from 1.1 million hectares in 1986 to approximately 3 million in 2000. Nowadays more than 70 countries use micro-irrigation on a total area exceeding 6 million hectares as mentioned in (*Zamaniyan, Fatahi, Boroomand-Nasab, 2014*). On the other hand, (*Ebrahimian, & Liaghat, 2011*) pointed out that there are many cases of inefficient water utilisation – such as the case of Iran which has a dry climate (average annual rainfall of 240 mm) but uses efficiently only 35% of the total amount of water designated for agriculture.

Due to the lack of rainfall water, our farmers are nowadays also considering increasingly the possibility of using controlled artificial irrigation systems. These systems, consisting usually of a set of storage tanks, water distribution pipes and pumps, are often considerable energy consumers. Some sources, for example (*Melichar, 2009*), indicated that up to 30% of all electricity generated is consumed for pumping liquids. Efforts to save energy lead to the development of technical innovations in the most energy-demanding parts of these systems – pumps, as described in (*Fontana, Giugni, & Portolano, 2011*) and (*Venturini, Alvisi, Simani, & Manservigi, 2017*).

One major driving force for innovations is the effort to improve the efficiency of machines in operation, a trend which in recent time has been supported by EU legislation (*Directive 2009/125/EC*). Nevěřil indicated in his publication (*Nevěřil, 2012)* that Regulations focused specifically on hydraulic machines (*Commission regulation (EU) No 547/2012*) specified a so called minimum energy efficiency index (MEI) of at least 0.1 which meant in practice that 10% of pumps with the lowest efficiency had to be withdrawn from the EU market. From 1st January, 2015, this index has to be at least 0.4, which means it is necessary to replace 40% of the pumps on the European market.

Today, the experimental, research and production activities in engineering cannot do without using 3D-CAD powerful graphics systems. The basis is a parametric graphical three-dimensional model in CAD software. The most widely used software in practice are INVENTOR, SOLIDWORKS, CATIA, CREO, SOLID EDGE, AUTOCAD and others. 3D models can be used not only for various analysis, but also as a basis for production of components by Rapid Prototyping.

As mentioned in (*Mohan, Senthil, Vinodh, & Jayanth, 2017*) and (*Jayanth, Senthil, & Prakash, 2018*), fused deposition modelling (FDM) is the most significant technique in additive manufacturing that refers to the process where successive layers of material are deposited in a computer-controlled environment

to create a three-dimensional object. This technology was also chosen for our experimental verification of properties of the impellers for radial centrifugal pump.

The aim of the testing was to verify the hydraulic parameters of those impellers and to compare them with the parameters of cast iron or cast steel impellers manufactured by conventional casting.

MATERIALS AND METHODS

Impellers manufactured by 3D printing were tested on a hydraulic test circuit where pump and reverse turbine operation was examined in a similar way as in (*Pugliese, De Paola, Fontana, Giugni, & Marini, 2016*).

The META Plus 5 pump, manufactured by ISH Pumps Olomouc, was selected for experimental verification. From a design point of view, this is a one-stage centrifugal pump with a spiral box and impeller with outer diameter $D_1 = 132$ mm (Fig. 1).
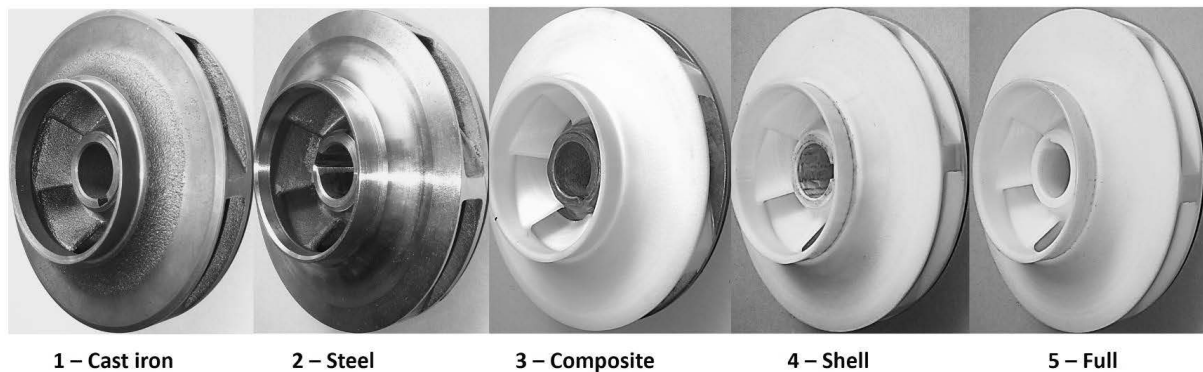

1 – Cast iron **2 – Steel** **3 – Composite** **4 – Shell** **5 – Full**

Fig. 1 Variants of impellers

Five different impeller variants were created for testing in total, all having the same flow section geometry. The impellers were made using Stratasys Dimension Elite 3D Printer 180-00105 from material ABS-P430 (Acrylonitrile Butadiene Styrene, density: $\rho_{ABS} = 1{,}050$ kg.m^{-3}). The impellers parameters and printer settings are summarized in Tab. 1. Temperature settings of printer were the same in all cases – model head: 280°C, support head: 150 °C, chamber environment 75 °C.

Tab. 1 Overview of variants of tested impellers

Variant	Description	Slice height [mm]	Print time [h:min:s]	Used ABS [cm^3]	Weight [g]
1 - Cast iron	Grey cast iron, sand mould				1,400
2 - Steel	Stainless cast steel, sand mould				1,810
3 - Composite	Rear shroud, cast iron + ABS blades	0.18	30:57:01	159.4	710
4 - Shell	Shell ABS - 3D print	0.18	23:21:52	87.9	80
5 - Full	Compound impeller, ABS - 3D print	0.18	32:29:10	187.5	185

Fig. 2 shows the internal structure of the impeller construction used in 3D printing. The lines indicate the paths of the printing head nozzle in one of the printed layer. The structure on the left was used for printing the full and the composite impeller (variant 5 and 3, respectively). The structure in the middle was used to print the shell impeller (variant 4). The structure on the right is another possibility of inner construction; it was not used in our research.
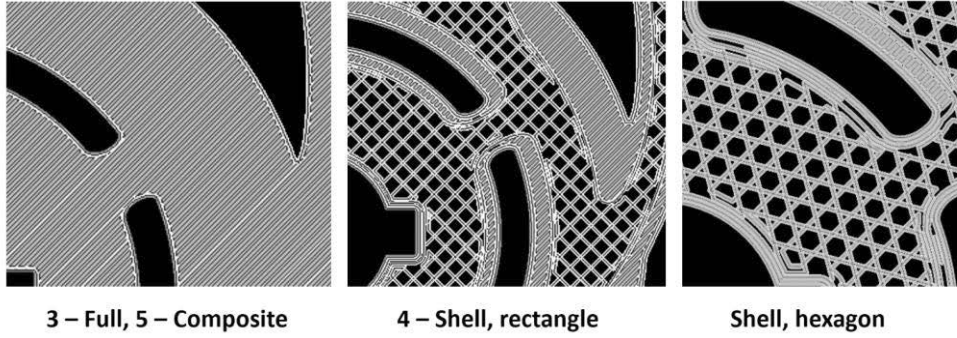
3 – Full, 5 – Composite   4 – Shell, rectangle   Shell, hexagon

Fig. 2 Detail of inner structure of the impeller, ABS – 3D printing

Verification tests were conducted on a hydraulic circuit in the Fluid Mechanics Laboratory at the Faculty of Engineering, Czech University of Life Sciences Prague. The circuit diagram is shown in Fig. 3.
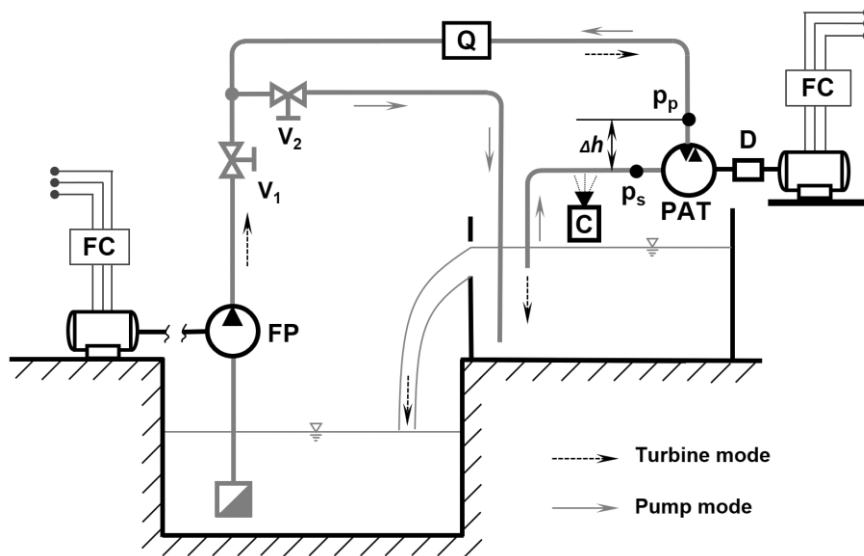

Fig. 3 Hydraulic circuit scheme for testing turbines/pumps. Q – flowmeter, FP – feed pump, PAT – tested pump, V1, V2 – control valves, D – dynamometer, FC – frequency inverter, C – camcoder. (*Polák, 2019*)

The testing circuit consisted of a set of two reservoirs with pipes and control and measuring elements. With this setting, the tested machine was measured in pump and turbine mode – by closing valve V_2 while regulating valve V_1, the water flows in the direction of dashed arrows, while the feeding pump (FP) creates the hydropower potential for the turbine. The dynamometer (D) with momentum sensor Magtrol TMB 307/41 (accuracy 0.1%) allows continuous regulation of shaft speed by frequency inverter LSLV0055s100-4EOFNS. This device enables operation in motor and braking mode. The water flow was measured using an electromagnetic flowmeter (Q) SITRANS F M MAG 5100 W (accuracy 0.5%). Pressures at (p_p) and (p_s) were measured by pressure sensor HEIM 3340 (accuracy 0.5%) installed according to 1st class accuracy requirement (*ČSN EN ISO 9906*).

The mechanical input of the pump, or the output of the turbine is given by:

$$P_m = M_T \frac{\pi \cdot n}{30} \tag{1}$$

where, M_T is the torque on the pump/turbine shaft (Nm) and n, the pump/turbine speed (min⁻¹). The hydraulic potential is determined by:

$$P_W = Q \cdot \rho \cdot \left[\frac{p_p - p_s}{\rho} + \frac{8 \cdot Q^2}{\pi^2} \left(\frac{1}{d_p^4} - \frac{1}{d_s^4} \right) + g \cdot \Delta h \right] \tag{2}$$

where Q is flow rate (m³·s⁻¹), p_p and p_s are pressures (Pa) in pressure and suction pipe respectively, d_p and d_s are inner diameters (m) of pressure and suction pipe, respectively, Δh is the vertical distance (m)

between p_p and p_s, and ρ is the specific weight of water (kg·m⁻³). The element in brackets of equation (2) expresses the specific energy Y (J·kg⁻¹). Detailed investigation of related functions and relations can be found in (*Gülich, 2014*) and (*Kramer, Terheiden, & Wieprecht, 2018*).

The overall efficiency of the pump η_p or turbine η_T is:

$$\eta_p = \frac{P_w}{P_m}, \quad \eta_T = \frac{P_m}{P_w} \tag{3}$$

RESULTS AND DISCUSSION

Based on the measured values, the performance characteristics of all five impeller variants were stated according to (*Pugliese, De Paola, Fontana, Giugni, & Marini, 2016*) and (*Polák, 2019*). Fig. 4 shows the pump operational characteristics, in particular the efficiency courses and the total heads related to flow rates. The characteristics were measured at 1,450 rpm, which corresponds to a pump driven by a four-pole asynchronous motor as indicated in (*Gülich, 2014*). The measurement was carried out at a constant pump rotational speed, where the flow was controlled by the throttle valve V_2 at the pump discharge.
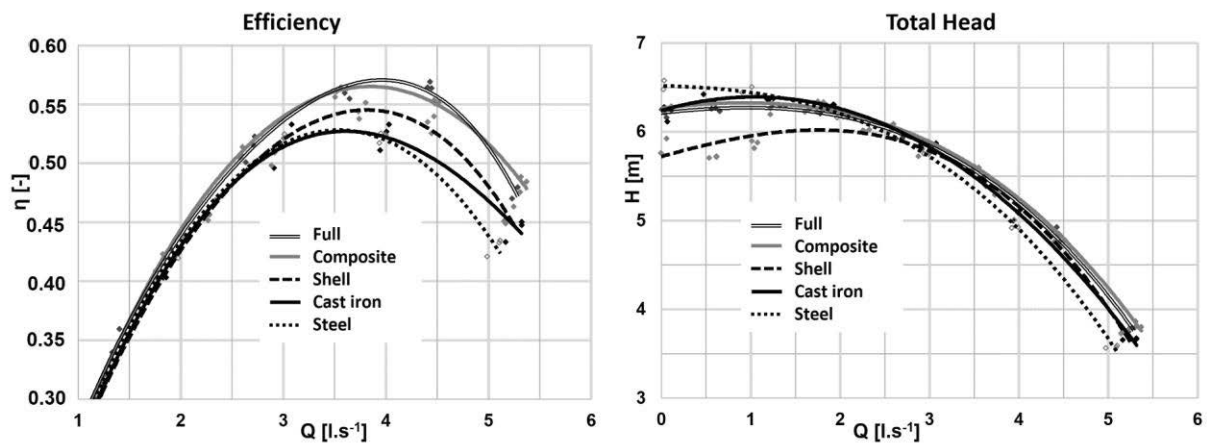

Fig. 4 Performance parameters in pump mode at 1,450 rpm

Fig. 5 presents pump characteristics measured at 2,950 rpm, corresponding to a two-pole asynchronous motor drive. The measurement procedure was the same as in the previous case.
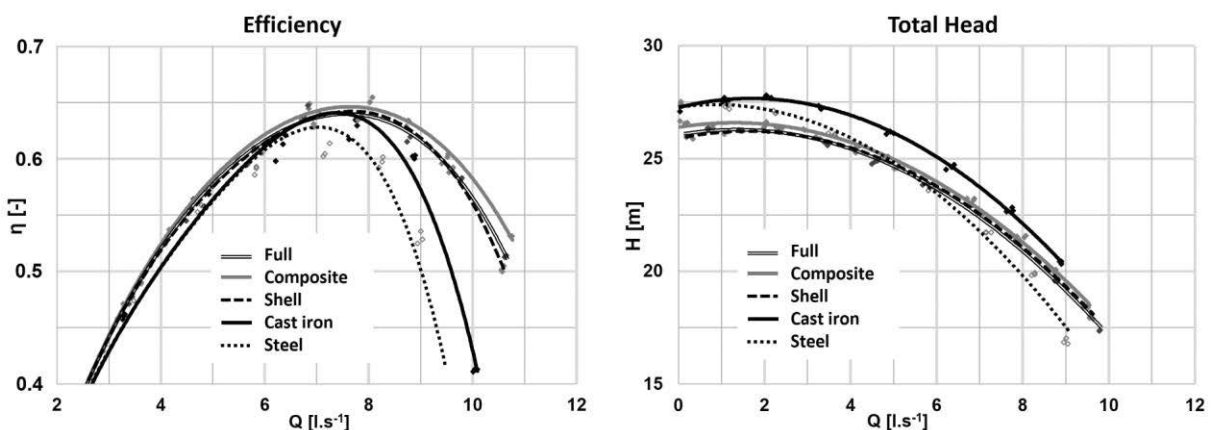

Fig. 5 Performance parameters in pump mode at 2,950 rpm

Fig. 6 below describes the characteristics of reverse turbine operation. The measurement was carried out at constant hydraulic potential (constant speed of feeding pump FP). At this setting, the turbine was gradually loaded from idle speed to 500 rpm.
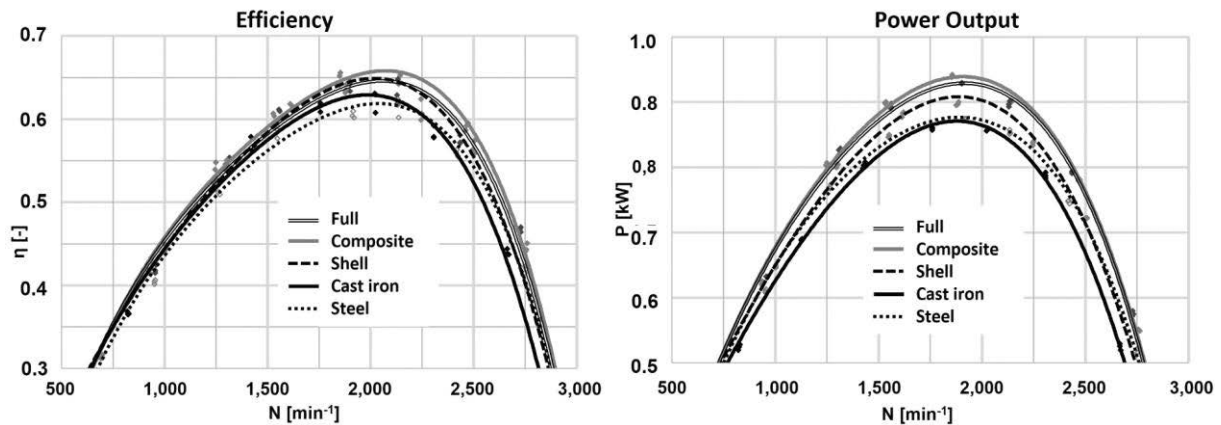
Fig. 6 Performance parameters in turbine mode

The operational tests have proved that all tested impeller variants are able to withstand the maximum load even at the highest output without damage (here pump mode at $n_T = 2{,}950$ rpm, $P_m = 3$kW, $M_T = 9.8$ Nm).

CONCLUSIONS

As far as the pump operation is concerned, the graphs showed that at 1,450 rpm, the total heads of the individual variants were almost the same, with the exception of the Shell variant, which showed a reduction of about 4.8% at the lowest flow rates. Conversely, at 2,950 rpm, all 3D variants showed on average 15% reduction in the total heads compared to the cast iron variant.

Pump operation efficiency courses at the low flower rates were the same for all variants. At higher flow rates, the efficiency of the 3D impellers increased gradually. This is particularly noticeable at 1,450 rpm, where the Composite and Full variants achieved higher overall efficiency (by 5% in absolute value) at optimum operation (= maximum efficiency) compared to a conventional cast iron impeller. Besides, at 2.950 rpm, ABS impellers presented flatter, thus more favourable efficiency courses and higher flow rates. This is due to the lower surface roughness of the flow parts. The roughness (Ra) of the internal coarse flow surfaces at the metal sand mould casted impellers ranged from 50 to 100 μm. The roughness of the impellers produced by 3D printing depended on the surface position. Vertical surfaces had a roughness of 3.2 μm, inclined and horizontal surfaces 6.3 and 12.5 μm, respectively. The metal rear shroud of the composite impeller had a roughness of 0.8 μm. Lower surface roughness results in lower hydraulic losses and higher impeller flow rate, which is also reflected in their performance characteristics.

In terms of turbine operation, the steel and cast iron impellers again presented lower overall efficiency compared to the impellers produced by 3D printing. The difference is particularly noticeable at the Composite variant, which had higher efficiency and especially output compared to cast iron impeller (on average by 4 to 6%). Again, the cause can be found in lower roughness and therefore lower hydraulic losses. This fact is confirmed by the increased machine flow rate when using impellers made with 3D printing.

Based on the results described above, the FDM Rapid Prototyping method can be recommended for testing hydrodynamic pumps. Indisputable advantage of this way of manufacturing is the speed of prototype production - in this case the production time of one impeller did not exceed 33 hours.

ACKNOWLEDGMENT

REFERENCES

1. Commission regulation (EU) No 547/2012. Retrieved from http://extwprlegs1.fao.org/docs/pdf/eur113548.pdf.

2. ČSN EN ISO 9906. (2013). Rotodynamic pumps - Hydraulic performance acceptance tests - Grades 1, 2 and 3 (in Czech). ČSNI.

3. Directive 2009/125/EC. Retrieved from https://eur-lex.europa.eu/legal-content/EN/TXT/?qid=1556369519391&uri=CELEX:32009L0125.

4. Ebrahimian, H., & Liaghat, A. (2011). Field evaluation of various mathematical models for furrow and border irrigation systems. *Soil and water research, 6*(2), 91-101.

5. Fontana, N., Giugni, M., & Portolano, D. (2011). Losses reduction and energy production in water-distribution networks. *Journal of Water Resources Planning and Management*, *138*(3), 237-244

6. Gülich, J. F. (2014). *Centrifugal pumps* (3rd edition). Berlin: Springer.

7. Jayanth, N., Senthil, P., & Prakash, C. (2018). Effect of chemical treatment on tensile strength and surface roughness of 3D-printed ABS using the FDM process. *Virtual and Physical Prototyping*, *13(3*), 155-163.

8. Kazim, A. M. (2003). Thermal and water management in irrigating lands in the arid and semi-arid regions. *Applied thermal engineering*, *23*(7), 807-820

9. Kramer, M., Terheiden, K., & Wieprecht, S. (2018). Pumps as turbines for efficient energy recovery in water supply networks. *Renewable energy*, *122*, 17-25.

10. Melichar, J. (2009). *Hydraulic and pneumatic machines – Part pumps* (in Czech). ČVUT in Prague ISBN 978-80-01-04383-7.

11. Mohan, N., Senthil, P., Vinodh, S., & Jayanth, N. (2017). A review on composite materials and process parameters optimisation for the fused deposition modelling process. *Virtual and Physical Prototyping, 12*(1), 47-59.

12. Nevěřil, J. (2012). Limits of energy demands (in Czech). *Sigmaprofil, 20(4), 10.*

13. Polák, M. (2019). The influence of changing hydrotechnical potential on performance parameters of pump in turbine mode. *Energies 2019, 12(11), 2103.*

14. Pugliese, F., De Paola, F., Fontana, N., Giugni, M., & Marini, G. (2016). Experimental characterization of two Pumps As Turbines for hydropower generation. *Renewable energy*, *99*, 180-187.

15. Venturini, M., Alvisi, S., Simani, S., & Manservigi, L. (2017). Energy production by means of pumps as turbines in water distribution networks. *Energies*, *10*(10), 1666.

16. Zamaniyan, M., Fatahi, R., & Boroomand-Nasab, S. (2014). Field performance evaluation of micro irrigation systems in Iran. *Soil and Water Research*, 9(3), 135-142.

Corresponding author:
Doc. Ing. Martin Polák, Ph.D., Department of Mechanical Engineering, Faculty of Engineering, Czech University of Life Sciences Prague, Kamýcká 129, Praha 6, Prague, 16521, Czech Republic, phone: +420 22438 3183, e-mail: karel@tf.czu.cz

RAIN-FLOW ANALYSIS OF PLOUGH FRAME BEAM

Jozef RÉDL[1], Marian KUČERA[1]

[1]*Department of Machine Design, Faculty of Engineering, Slovak University of Agriculture in Nitra, Slovak Republic*

Abstract

The article is focused on experimental measurement of the acceleration of plough in certain point of construction and the certain direction. The simplified model of plough allows converting the acceleration into the force. The bending moment function of the plough frame was calculated. Differentiating the bending moment we got the shear force acting inside the frame profile. The reduced stress function was calculated by Von Misses hypothesis method. The reduced stress function was processed by rain-flow counting method. Histogram of cyclic stress is created from rain-flow analysis.

Key words: steel fatigue; rain-flow; damage criterion; counting methods.

INTRODUCTION

The assessment of life fatigue of steel constructions in agricultural machines is still very interesting area of research. The derivation of the statistical expression for the fatigue life at a welded connection is outlined which requires only constant amplitude stress/life data and the standard deviation and ruling frequency of the stress history (*Harral, 1987*). The aim of this study is to determine the stress ranges in the beam of plough which operating on the ground. The study is based on the research provided in the Faculty of Engineering in the past. The wide research of the life fatigue prediction of multipurpose agricultural carrier steel frames in Slovakia was done in Slovak Agricultural Testing and Research Centre. Applying the stress gauges for recording the deformation of the steel structure allowed designing the more efficient frames (*Sestak, 2002*). The agricultural machines parts that are influenced to the cyclic loading are still under the intensive research. Not only agricultural machines parts but also the heavy trucks parts are the object of the research. The prediction of life fatigue of front axle of heavy truck was done in system Ansys® (*Zhang et al. 2016*). The all agricultural steel components that are transmitting the loading or power are in most cases welded. From this reason is necessary to determine the life fatigue of welded joints and its residual stress (*Maddox, 1991; Niemi, 1995; Cui et.al. 2019*). The time-domain approach was defined in the form in which the response time history is calculated by static stress analysis by superimposing all stress influences from the applied loads at each time step, lacks the dynamics of the structure especially for vibration-based problems when a loading excites the natural frequencies of the structure (*Anzai, 1995; Aykan, 2005*). The determination of vibrations of structure and measurements with strain gauges needs more sensors. In many cases the location on frame of strain gauges are complicated due the irregular shape of structure. The best way is the using the acceleration gauge to determine the frame acceleration in certain direction. Determination the additional stress of structures from vibrations applying the basic dynamics relationship is very useful method. The main objective of this research was to study the relationship between additional stresses on building induced by vibrations, vibration nature and building dynamic characteristics. The designed models maximum stresses were measured due to each vibration load (*Hashad, 2015*). Assessment of life fatigue in agricultural universal transporters from operation vibration was investigated by many authors. The three motion parameters (displacement, velocity, and acceleration) describing a shock spectrum, velocity is the parameter of greatest interest from the viewpoint of damage potential. This is because the maximum stresses in a structure subjected to a dynamic load typically are due to the responses of the normal modes of the structure, that is, the responses at natural frequencies (see Chap. 21). At any given natural frequency, stress is proportional to the modal (relative) response velocity. Specifically,

$$\sigma_{\max} = C.v_{\max}.\sqrt{\rho.E} \,, \tag{1}$$

where : σ_{max} is maximum modal stress, v_{max} is – maximum modal velocity, ρ is mass density of the structural material, E is modulus of elasticity, C - Constant of proportionality dependent upon the geometry of the structure (often assumed for complex equipment to be $4 < C < 8$ (*Piersol & Bateman et.all, 2010*). The Rain Flow Cycle (RFC) was analysed and reviewed by many authors. Definition of this method from mathematical point of view was done. The method presented by (*Rychlik, 1987*) attaches to each maximum of the strain function the amplitude of a corresponding cycle or two half cycles, which are evaluated independently from each other. Algorithm of RFC was also analysed by (*Schluter, 1991; Baek, 2008*). Practical application of RFC in fatigue life prediction was published by many authors. The application of Palmgren-Miner rule in fracture mechanics was realized by (*Chen et al., 2011*) The Palmgren–Miner rule can be used for fatigue life predictions, if and only if, the damage development rate can be presented as a product of the functions of stress (strain) amplitude and current amount of damage (*Todinov, 2001*).

MATERIALS AND METHODS

Measurement object

Object for measurement was a plough Kuhn Vari-Master 183 depicted on Figure 1. The basic parameters of plough are listed in the Table 1. (*www.khun.com*). Measurement on plough was realized on deep plow. The plowed ground was planar without rough parts. The plough was mounted on tractor John Dere 8220.

Tab. 1 Properties of plough

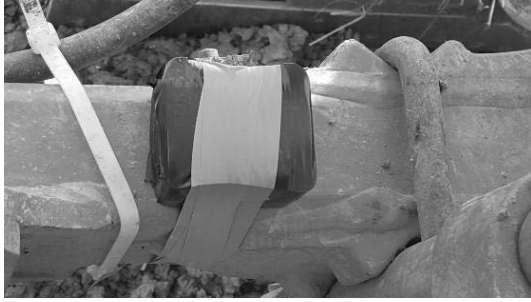| Parameter	m	kg	pieces
Manufacturer	Kuhn		
Type	Vari Master 183		
Mass (m_P)		2840	
Distance between bodies	0.96		
Bodies			6
l_{ef}	5.76		
Beam ($a \times a \times t$)	0,180x0,180x0,008		

Fig.1 Plough Pottinger

Fig. 2 Detail of sensor location

Fig.3 Sensor Eval - ADXL 345Z-DB

For measurement of plough vibration was used the Eval - ADXL 345Z-DB data acquisition board. The board measured accelerations in the XYZ axes. Measured data was recorded to the MiniSD card. The relevant direction for us was the accelerations in Z axis direction.

Mathematical model

The measured vibration data were transformed to the stress data set. We cannot use the mentioned method by Piersol et. because we have a time depend acceleration. We assume that the behaviour of the plough mounted on the three point linkage is similar like behaviour of the cantilever beam. For this reason we used the theory of cantilever beam design theory. We substituted the real plough with model as depicted on Figure 4. For utilizing the designed model we set up the basic assumption as follows:

- three-point linkage stiffness is similar as a fixed connection of the cantilever beam,
- for bending moment is used the effective length of plough,
- plough support wheel damping is contained in the acceleration data,
- used loading is the weight of the plough,
- neutral axis of the beam lay to the beam axis of symmetry,
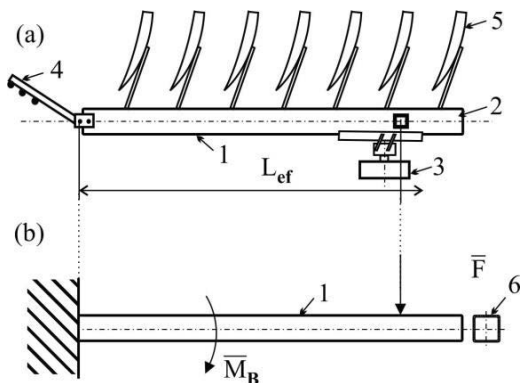- neglecting the shear deformation.

Fig. 4 Plough and its model
a: 1-plough beam, 2-acceleration gauge, 3-wheel, 4-three point linkage mechanism, 5-body
b: 1-plough beam,6-beam profile, $\overline{F}$-force, $\overline{M}_B$- bending moment

The equation for calculating stress we use d the equation 2.

$$\sigma_{(i)} = \frac{m_p.l_{ef}}{W}.a_{(i)} \tag{2}$$

RESULTS AND DISCUSSION

From the experimental measurement we got the technical function of the acceleration in z-axis direction. Based on equations (2) we got the raw data of the stress, depicted in the figure 5 and 6. The raw accelerations data was filtered with Butterworth maximally flat magnitude filter, see Equations (3)

$$B_n(s) = \prod_{k=1}^{\frac{n}{2}} \left[s^2 - 2.s.\cos\left(\frac{2k+n-1}{2n}.\pi\right) + 1 \right], n = even \tag{3}$$

$$B_n(s) = (s+1)\prod_{k=1}^{\frac{n-1}{2}} \left[s^2 - 2.s.\cos\left(\frac{2k+n-1}{2n}.\pi\right) + 1 \right], n = odd , \text{ where :}$$
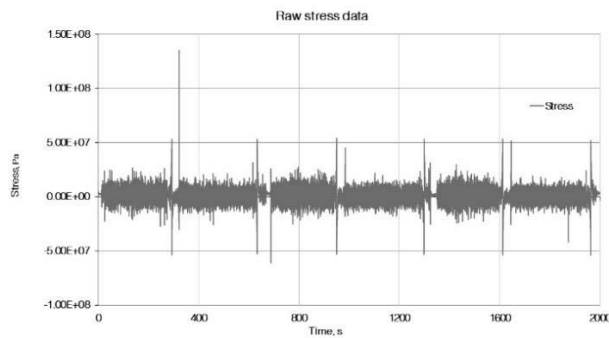
$n -$ order of filter

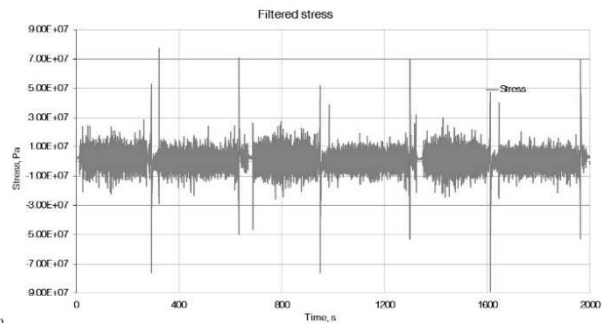

Fig.5 Stress raw data

Fig.6 Filtered stress data

Applying the rain flow method on the filtered stress data we got the rain-flow matrix histogram. The matrix is depicted in the figure 7. The rain-flow matrix was solved with the Matlab® system which is available for academics through the Slovak Centre of Scientific and Technical Information (*http://www.cvtisr.sk/*). The stress and cycles chart is depicted in the figure 8.
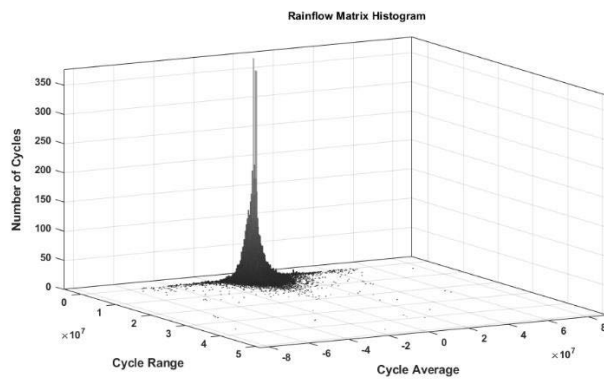

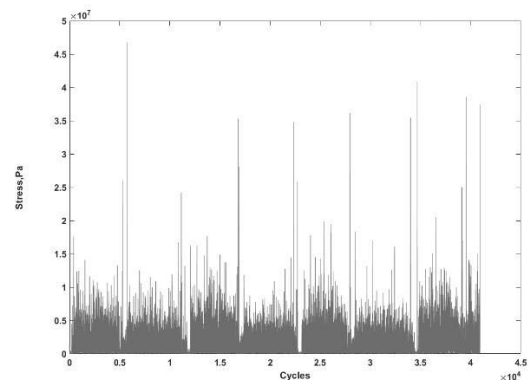
Fig.7 Rain-flow matrix

Fig.8 Stress-cycles chart

From rain-flow analysis we got the values which are necessary for the life fatigue calculation. The range counts and statistical values are in the table 2.

Tab. 2 Rain-flow counting results

Stress	Pa
Min	-8.841604021544859e+07
Max	.694699408809440e+07
Mean	1.055257081702104e+06
Median	1.141895561065718e+06
Deviation	6.420929987293424e+06
Range	1.653630343035430e+08

CONCLUSIONS

The unusual method of beam stress determination was presented. The operating environment was an agricultural ground, where plough supported on the tractor performed the agro-technical operation. The vibrations of the plough were measured and the acceleration was transformed to the acting force. The similar method to determine the steel frame stress was published by *Hashad (2015)*. The designed mathematical model is very simply and utilizing it's we should on the easiest way determine the potential damage of the beam. But the Palmgren-Miner rule must by applied. For application of Palmgren-Miner rule must by the set of the stress data counted by rain-flow counting algorithm as published by *Harral (1987), Anzai (1992)* and *Sestak (2002)*. The results published by *Harral (1987)* was the stress deviation in range 5 to 26 MPa and solved standard stress deviation calculated by us was up to 6,421 MPa. Also the maximum stress counted by Harral was 177 MPa and maximum stress solved by us was 88 MPa in absolute value .These results are very significant and proving our methodology. The similar algorithm of rain-flow counting method and application of Palmgren-Miner rule are published by *Todinov (2001)* and *Piersol and Paez (2010)*. The typical shape of stress histogram of rain-flow counting algorithm was created. From the analysis we get the peaks of stress and the cycles ranges which are the significant properties of the analysis. As denoted by *Cui et al. (2019)* the fatigue life prediction model is based on the elastic fracture mechanics. The our model is also based on the mechanics of the elastic isotropic bodies. For the shorter publication space, we didn't publish the results from application of Palmgren-Miner rule. To validate the presented method must be carried out the experimental measurement with stress gauge.

REFERENCES

1. Anzai, H. (1992). Algorithm of the Rainflow Method. In *The Rainflow Method in Fatigue* (pp. 11-20). Butterworth-Heinemann.
2. Aykan, M. & Çelik, M. (2009). Vibration fatigue analysis and multi-axial effect in testing of aerospace structures. *Mechanical Systems and Signal Processing, 23*(3), 897-907.
3. Baek, S. H., Cho, S.S., & Joo, W.S. (2008). Fatigue Life Prediction Based on the Rainflow Cycle Counting Method for the End Beam of a Freight Car Bogie. *International Journal of Automotive Technology, 9*(1), 95-101.
4. Chen, N., Wang,G., & Guedes-Soares, C. (2011). Palmgren–Miner's rule and fracture mechanics-based inspection planning, *Engineering Fracture Mechanics, 789*(18), 3166-3182.
5. Cui,Ch., Zhang,Q., Baob,Yi., Bu, Yi., & Luoa,Yi. (2019). Fatigue life evaluation of welded joints in steel bridge considering residual stress. *Journal of Constructional Steel Research*, *153*, 509-518.
6. Harral, B.B. (1987). The application of a statistical fatigue life prediction method to agricultural equipment. *International Journal of Fatigue, 9*(2), 1987, 115-118.
7. Hashad,A. (2015). Additional stresses on buildings induced by vibration effects. *Water Science*, *29*(2), 134-145.
8. Hobbacher,A.F. (2016). Recommendations for Fatigue Design of Welded Joints and Components (IIW Collection) 2nd ed. 2016 Edition. *Series: IIW Collection*. 143 p. Springer.

9. Niemi. E. (1995). Stress Determination for Fatigue Analysis of Welded Components (Woodhead Publishing Series in Welding and Other Joining Technologies). *Woodhead Publishing Series in Welding and Other Joining Technologies, 80.*

10. Maddox, S.J. (1991). Fatigue Strength of Welded Structures (Woodhead Publishing Series in Welding and Other Joining Technologies) 2nd Edition. *Woodhead Publishing Series in Welding and Other Joining Technologies*, *208.*

11. Piersol,A. -Paez,T. (2010). *Harris' Shock and Vibration Handbook*, 6th Edition, NY: McGraw-Hill.

12. Rychlik, I. (1987). A new definition of the rainflow cycle counting method. *International Journal of Fatigue*, *9*(2), 119-121.

13. Schluter, L. L. (1991). *Programmer's Guide for LIFE2's Rainflow Counting Algorithm*.

14. Šesták, J. (2002). *Life prediction of framed structures : Monograph* (in Slovak). Nitra: SPU, 62.

15. Todinov, M.T. (2001). Necessary and sufficient condition for additivity in the sense of the Palmgren–Miner rule. *Computational Materials Science*, *21*(1), 101-110.

16. Zhang,M., Ji,X. , & Li, L. (2016) A research on fatigue life of front axle beam for heavy-duty truck. *Advances in Engineering Software, 91*, 63–68.

Corresponding author:
doc. Ing. Jozef Rédl, Ph.D., Department of Machine Design, Faculty of Engineering, Slovak University of Agriculture in Nitra, Tr.A.Hlinku 2, Nitra 94976, Slovak Republic, phone: +421 37 641 5670, e-mail: redl@is.uniag.sk

THE IMPACT OF WEED CONTROL METHODS ON SUGAR BEET CROP

Kęstutis ROMANECKAS[1], Aida ADAMAVIČIENĖ[1], Edita EIMUTYTĖ[1], Jovita BALANDAITĖ[1], Algirdas JASINSKAS[2]

[1]Vytautas Magnus University, Agriculture Academy, Institute of Agroecosystems and Soil Sciences, 53361 Kaunas reg., Akademija, Lithuania
[2]Vytautas Magnus University, Agriculture Academy, Institute of Agricultural Engineering and Safety, 53361 Kaunas reg., Akademija, Lithuania

Abstract

The effect of non-chemical weed control on organically grown sugar beet crop productivity and quality was tested at the Experimental Station of the Aleksandras Stulginskis University in 2015-2016. The aim of the experiment was to ascertain the influence of living mulch, mechanical (mellowing, cutting, mulching) and physical (steaming) weed control methods on sugar beet productivity and quality parameters. There were tested 6 weed control methods: inter-row mellowing (control treatment), cutting and mulching with weeds, Persian clover, white mustard and spring barley, inter-row steaming.

Different alternative weed control methods usually had negative significant impact on the sugar beet crop yield except inter-row steaming treatment. In these plots, decrease of root yield was insignificantly less compared with control treatment. The effect of weed control methods on sugar beet root quality parameters was weak.

Key words: *sugar beet; non-chemical weed control; organic farming; productivity; quality.*

INTRODUCTION

Today's traditional agriculture uses growing technologies based on a chemical pest control system. Sugar beet is one of the most sensitive crop for weeds suppression, as they grow slowly in their early stages of development and cannot compete with the weeds that germinate at that time. Weeds can reduce sugar beet yield by 26–100% *(Vasinauskienė & Brazienė, 2017)*. Usually, in sugar beet crop, herbicides containing the active ingredients as phenmedipham, desmedipham, etofumezate, metamitron, trisulfuronmethyl, clopyralid and chloridazone *(Bennett, et al., 2004; Deveikytė, 2005; Domaradzki, 2007)*. High yields of root crop are obtained, but the extensive use of chemicals causes ecological pollution. Avoiding damage the balance of nature and the risk of contamination of agricultural production with residues of chemicals that are harmful to humans, encourages the transition to organic farming. Weeds are one of the most important agronomic problems in all farming systems, but the most important in organic as the non-chemical methods of weed control are less effective than the use of herbicides in intensive farming systems *(Liebman, et al., 2003; Pilipavičius, et al., 2011)*.

Mechanical inter-row weed control is practiced in organic farms and can significantly reduce crop weediness. The effectiveness of a mechanical weed control depends on the time and intensity of its application. Methods of thermal engineering are also used to kill weeds. The heat source used around the plant creates a high-temperature environment which, when heated, destroys them *(Sirvydas & Kerpauskas, 2012)*.

Cover crops (like as mulch) might suppress weeds and improve the fertility of soil at the same time *(Kader, et al., 2017; Pannacci, et al., 2017)*. Some of inter-cropped catch crops continue vegetation and known as a "living mulch" *(Robačer, et al., 2016)*. The use of the living mulch is a sufficient alternative to the mechanical weed control. As living mulch can be grown clover, black medic, white mustard or cereal grasses *(Den Hollander, et al., 2007a; Kunz, et al., 2016; Masilionyte, et al., 2017)*. However, living mulch crops can compete with the main crop *(Liedgens, et al., 2004)*.

To summarize, sugar beet growing with living mulch crops is not widely investigated. In most cases, the inter-cropping of legumes in cereals *(Duchene, et al., 2017)* or maize *(Adamavičienė, et al., 2012; Verret, et al., 2017)* are investigated. So, the aim of the experiment was to establish the impact of non-chemical weed control methods on the productivity and quality of organically grown sugar beet crop.

MATERIALS AND METHODS

A stationary field experiment was performed in 2015–2016 at the Experimental Station (54º52′ N, 23º49′ E) of the Aleksandras Stulginskis University (ASU), Lithuania. The main objective of experiment was to ascertain the influence of different non-chemical weed control methods on sugar beet crop productivity and quality in the conditions of organic farming. Six weed control methods were established: inter-row mellowing (CT, control treatment), cutting and mulching with weeds (MW), Persian clover (MC), white mustard (MM) and spring barley (MB) living mulches, and inter-row steaming (ST). According to the *Yagioka (2015)*, MW treatment imitates "natural farming" system. By the way, *Lumbanraja et al. (2004)* established, that weeds as a cover plants were a sufficient control method in coffee fields. The soil of experimental site was a silty loam (on average 46% sand, 42% silt, 12% clay) Planosol (*Endohypogleyic-Eutric – Ple-gln-w*) (WRB, 2014), climate – boreal (subarctic) with an average annual temperature by the 6.7°C and precipitation rate – 625 mm. Length of vegetation season with active temperatures (≥ 10 °C) is about 6 months. Meteorological conditions during the investigations are presented in Table 1. Length of vegetation means the period from sugar beet sprouting to harvesting. 2015 and 2016 vegetative seasons were quite different in precipitation rates and temperatures.

Tab. 1 Meteorological conditions during investigations, Kaunas Meteorological Station, 2015–2016

Year	Length of vegetation days	Average temperature of 24 hours ° C	Sum of active temperatures ° C	Precipitation rate mm
2015	159	15.2	2273.9	171.5
2016	137	16.4	2161.7	384.6

The agrotechnical operations and timing are presented in Table 2. Pesticides and mineral fertilizes were not used in the experiment.

Tab. 2 Agrotechnical operations and timing

Agrotechnical operation	Timing
Straw loosening, manure distribution (30 t ha^{-1}), ploughing	2014 October only
Pre-sowing tillage	End of April
Sowing	After pre-sowing tillage
Inter-row mellowing before living mulch plants sowing	End of May, after the emergence of sugar beet sprouts
Sowing of living mulch	After inter-row loosening
Inter-row steaming	The beginning of June, after weed sprouts emergence
Inter-row loosening, cutting and mulching	3 times up to the beginning of July
Harvesting	The beginning of October

Four replication of an experiment were performed, distribution of plots – randomized. In 2014, the pre-crop of sugar beet was spring barley. Since 2015, continuous sugar beet crop was cultivated.

The distance between sugar beet rows was 45 cm, between seeds – about 16 cm. Sugar beet variety – „Firenze". The sowing rate of white mustard and Persian clover as living mulch was 10 kg ha^{-1}, spring barley – 200 kg ha^{-1}. The living mulch plants were cut and distributed on the soil surface 3 times by a hand-operated brush cutter 'Stihl' FS–550. Inter-row steaming was performed with mobile steaming machine, which had been projected and manufactured in ASU (patents LT5620B and LT55332B) (Fig. 1).

Fig. 1 Inter-row steaming machine

The experimental data were statistically evaluated using the ANOVA software.

RESULTS AND DISCUSSION

Results of investigations show, that alternative weed control methods mainly decreased yield of sugar beet root compared with mechanical inter-row mellowing (CT) (Table 3). Inter-row steaming treatment (ST) was effective against weeds. The yield of root crops was about 15 t ha^{-1} less than in control, but difference was insignificant. Due to the concurrence with main crop, mulching methods significantly decreased yields of roots. The most negative effect was observed in MC and MM plots. In our earlier investigations, white mustard living much effectively controlled weeds in sugar beet crop *(Romaneckas, et al., 2009)*, but competed with main crop and decreased yields of root crop *(Adamavičienė, et. al., 2009)*. Similarly, *Kunz et al. (2016)* found, that the most effective was herbicide application (control) compared with living mulch application. Despite that, *Trifolium subterraneum* initiated the highest yield of white sugar.

Tab. 3 Sugar beet root yield and quality, average of 2015–2016

Weed control treatment	Yield t ha^{-1}	Sucrose content g kg^{-1}	Potassium content mmol kg^{-1}	Sodium content mmol kg^{-1}
CT	55.82a	173.9a	31.0a	2.5a
MW	31.86b	167.0a	31.6a	3.0a
MC	28.06b	166.9a	32.0a	3.2a
MM	27.20b	166.4a	32.0a	3.1a
MB	31.48b	168.4a	30.8a	2.6a
ST	40.74ab	174.2a	30.6a	2.4a

Note: CT – inter-row mellowing (control treatment); MW – inter-row cutting and mulching with weeds; MC – inter-row cutting and mulching with the Persian clover; MM – inter-row cutting and mulching with white mustard; MB – inter-row cutting and mulching with spring barley; ST – inter-row steaming. Values with different letters mean significant differences between treatments at 95 % probability level.

In our experiment, different weed control methods included living mulch application, did not have significant effect on sugar beet root crop quality (Table 3). In the case of quality, ST treatment was the most effective. In steamed plots, roots of sugar beet had the higher amount of sucrose and the lowest concentration of impurities (potassium and sodium). In *Afshar et al. (2018)* experiment, living mulch increased sucrose concentration and decreased sodium, potassium and amino-N concentration in the beet roots.

CONCLUSIONS

Different alternative weed control methods usually had negative significant impact on the sugar beet crop yield, except inter-row steaming treatment. In these plots, decrease of root yield was insignificantly less compared with control treatment. The effect of weed control methods on sugar beet root quality parameters was weak. To summarize, inter-row steaming is an effective weed control method, which might be widely used in conditions of organic farming.

REFERENCES

1. Adamavičienė, A., Romaneckas, K., Šarauskis, E., & Pilipavičius, V. (2009). Non-chemical weed control in sugar beet crop under an intensive and conservation soil tillage pattern: II. Crop productivity. *Agronomy Research*, *7* (special issue 1), 143-148.
2. Adamavičienė, A., Romaneckas, K., Pilipavičius, V., Avižienytė, D., Šarauskis, E., & Sakalauskas, A. (2012). Interaction of maize and living mulch: Soil chemical properties and bioactivity. *Journal of Food, Agriculture & Environment*, *10*(3-4), 1219-1223.
3. Afshar, R. K., Chen, C., Eckhoff, J., & Flynn C. (2018). Impact of a living mulch cover crop on sugarbeet establishment, root yield and sucrose purity. *Field Crops Research*, *223*, 150-154.
4. Bennett, R., Phipps, R., Strange, A., & Grei P. (2004). Environmental and human health impacts of growing genetically modified herbicide-tolerant sugar beet: a life-cycle assessment. *Plant Biotechnology Journal*, *2*, 273-278.
5. Deveikytė, I. (2005). Comparison of weed control systems in sugar beet. *Žemdirbystė/ Agriculture*. *92*(4), 93-105 (in Lithuanian with English summary).
6. IUSS working group WRB. (2014). *World reference base for soil resources*. 3th edition. World Soil Resources Reports No. 106. Rome: FAO. Retrieved from http://www.fao.org/3/a-i3794e.pdf.
7. Domaradzki, K. (2007). Optimization of herbicide application in the sugar beet protection system. *Prog. Plant Prot.\Post. Ochr. Roślin*, *47*(3), 64-73.
8. Duchene, O., Vian, J. F., & Celette, F. (2017). Intercropping with legume for agroecological cropping systems: Complementarity and facilitation processes and the importance of soil microorganisms. A review. *Agriculture, Ecosystems & Environment*, *240*, 148-161.
9. Den Hollander, N. G., Bastiaans, L., & Kropff, M. J. (2007). Clover as a cover crop for weed suppression in an intercropping design. II. Competitive ability of several clover species. *European Journal of Agronomy*, *26*, 104-112.
10. Kader, M. A., Senge, M., Mojid, M. A., & Ito, K. (2017). Recent advances in mulching materials and methods for modifying soil environment. *Soil & Tillage Research*, *168*, 155-166.
11. Kunz, C. H., Sturm, D. J., Peteinatos, G. G., & Gerhards, R. (2016). Weed Suppression of Living Mulch in Sugar Beets. *Gesunde Pflanzen*, *68*(2), 1-10.
12. Liebman, M., Bastiaans, L., & Baumann, D. T. (2003). Weed management in low-external-input and organic farming systems. In *Weed Biology and Management* (pp. 285-315). Kluwer Academic Publishers.
13. Liedgens, M., Frossard, E., & Richner, W. (2004). Interactions of maize and Italian ryegrass in a living mulch system: (2) Nitrogen and water dynamics. *Plant and Soil*, *259* (1-2), 243-258.
14. Lumbanraja, J., Adachi, T., Oki, Y., Senge, M., & Watanabe, A. (2004). Effect of weed management in coffee plantation on soil chemical properties. *Nutrient Cycling in Agroecosystems*, *69*, 1-4.
15. Masilionyte, L., Maiksteniene, S., Kriauciuniene, Z., Jablonskyte-Rasce, D., Zou, L., & Sarauskis, E. (2017). Effect of cover crops in smothering weeds and volunteer plants in alternative farming systems. *Crop Protection*, *91*, 74-81.
16. Pannacci, E., Lattanzi, B., & Tei, F. (2017). Non-chemical weed management strategies in minor crops: A review. *Crop Protection*, *96*, 44-58.
17. Robačer, M., Canali, S., Lakkenborg Kristensen, H., Bavec, F., Grobelnik Mlakar, S., Jakopa, M., & Bavec, M. (2016). Cover crops in organic field vegetable production. *Scientia Horticulturae*, *208*, 104-110.

18. Romaneckas, K., Romaneckienė, R. & Pilipavičius, V. (2009). Non-chemical weed control in sugar beet crop under intensive and conservation soil tillage: I. Crop weediness. Agronomy Research, *7* (Special issue 1), 457-464.
19. Sirvydas, P. A. & Kerpauskas, P. (2012). *Thermal weed control: monography*. Akademija-Kaunas: Aleksandras Stulginskis University Press (in Lithuanian with English summary).
20. Vasinauskienė, R. & Brazienė, Z. (2017). Control of pests in the sugar beet crop using the damp water steam. *Optimization of ornamental and garden plant assortment, technologies and environment*. *8*(13), 89-96 (in Lithuanian with English summary).
21. Verret, V., Gardarin, A., Pelzer, E., Médiène, S., Makowski, D., & Valantin-Morison, M. (2017). Can legume companion plants control weeds without decreasing crop yield? A meta-analysis. *Field Crops Research*, *204*, 158-168.
22. Yagioka, A., Komatsuzaki, M., Kaneko, N., & Ueno, H. (2015). Effect of no-tillage with weed cover mulching versus conventional tillage on global warming potential and nitrate leaching. *Agriculture, Ecosystems & Environment*, *200*, 42-53.

Corresponding author:
Agr. Kęstutis Romaneckas, Ph.D., Institute of Agroecosystems and Soil Sciences, Faculty of Agronomy, Agriculture Academy, Vytautas Magnus University, Studentu 11, Akademija, LT53361, Kaunas reg., Lithuania, phone: +370 656 300 44, e-mail: kestutis.romaneckas@vdu.lt

HOP DRYING IN BELT DRYER USING COOLING CHAMBERS

Adolf RYBKA[1], Petr HEŘMÁNEK[1], Ivo HONZÍK[1]

[1]Department of Agricultural Machines, Faculty of Engineering, Czech University of Life Sciences Prague, Czech Republic

Abstract

When drying hop cones, sufficient drying of strigs is the bottleneck. Bracts are then dried up to such a level which makes pressing the hops impossible. That is the reason why hops are conditioned after over-drying to reach an optimum moisture content of 10 to 12 %. This process does not benefit hops, therefore we suggested to substitute the conditioning chamber for two cooling chambers, in which the moisture of bracts and strigs can be equilibrated. This equilibrium is essential for baling. The advantage of this drying method is energy saving and improvement in the quality of the hop product. On the basis of the patented design and a utility model, the apparatus was assembled at the belt dryer PCHB 750 of Agrospol Velká Bystřice Ltd. Comparing the operation with conditioning and the option of the cooling chambers, the gas savings amounted to 2,356 CZK.t^{-1} of dry hops and the electricity savings amounted to 831 CZK.t^{-1} of dry hops. Assuming the reduction of the harvest period by approximately 39 %, the other cost items will be reflected in the overall saving.

Key words: hop cone; drying; conditioning; moisture.

INTRODUCTION

In conventional belt dryers hops are dried down to a moisture content of 8 up to 6 %. They are over-dried by reason of the need for adequate drying of the hop cone strig (*Heřmánek et al., 2018*; *Hofmann et al., 2013*). On the other hand, bracts are then dried to such an extent that baling these hops is impossible. Therefore, after drying, hops are 'conditioned'. After conditioning, the hops have an optimum moisture content of approximately 10 to 12 %. It is obvious that neither over-drying nor subsequent moistening does not benefit the hops (*Henderson & Miller, 1972*; *Rybáček et al., 1980*). With the current setting of belt dryers the optimum moisture content is achieved already by the end of the second belt, yet the strig moisture content being considerably higher (*Mitter & Cocuzza, 2013*; *Srivastava et al., 2006*). Drying on the third belt, where the hops are over-dried, takes up to 1/3 of energy requirements for drying, therefore a design has been created in which the over-drying and subsequent moistening in a conditioning chamber is substituted by a system of two cooling chambers where the hop cones will be left for approximately 4 to 8 hr. or longer if necessary. During this time the moisture levels of bracts and strigs will reach an equilibrium value. This equilibrium is essential for the final baling as the increased moisture in the cone strigs might cause the hops to deteriorate. The designed technological process responds to the requirement for an increase in the efficiency of gentle hop drying in belt dryers, for a reduction of drying costs, and for an increase in the quality of the final product (*Chyský, 1977).*
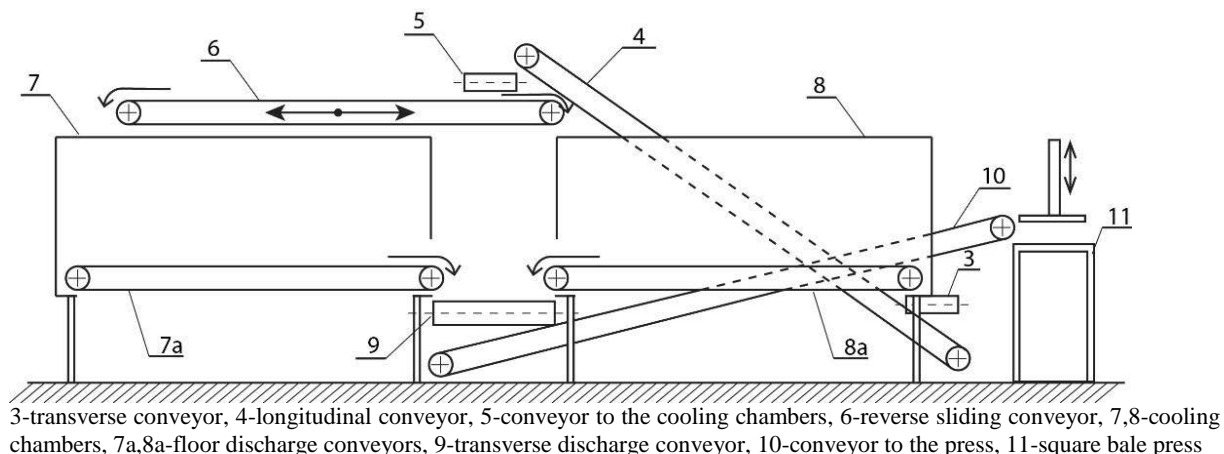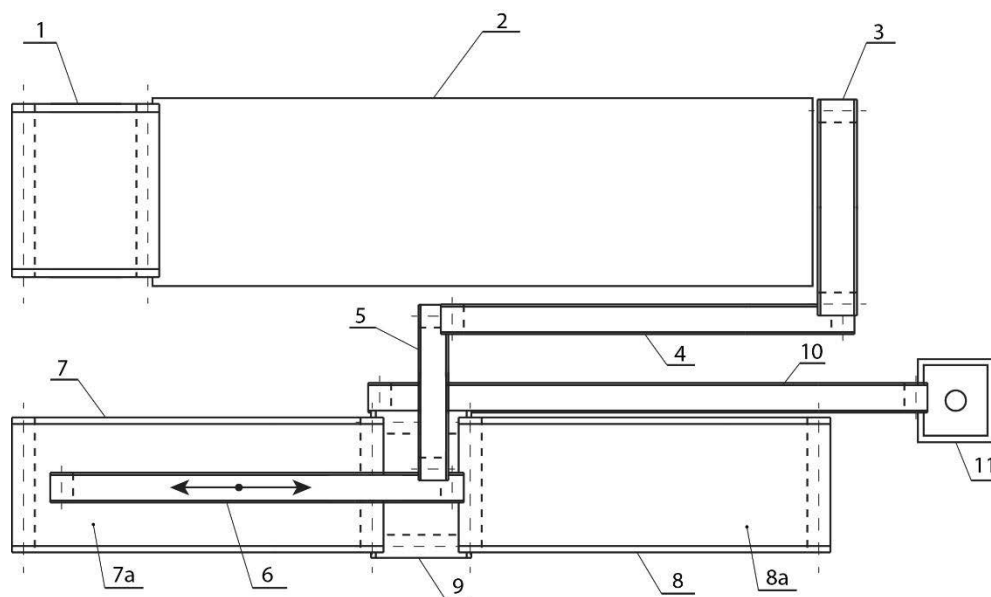

3-transverse conveyor, 4-longitudinal conveyor, 5-conveyor to the cooling chambers, 6-reverse sliding conveyor, 7,8-cooling chambers, 7a,8a-floor discharge conveyors, 9-transverse discharge conveyor, 10-conveyor to the press, 11-square bale press

Fig. 1 Side view of the cooling chambers and system of conveyors

1-filling conveyor, 2-belt dryer, 3- transverse conveyor, 4- longitudinal conveyor, 5- conveyor to the cooling chambers, 6-reverse sliding conveyor, 7,8-cooling chambers, 7a,8a- floor discharge conveyors, 9- transverse discharge conveyor, 10-conveyor to the press, 11- square bale press

Fig. 2 Top view of the deployment of the belt dryer, cooling chambers and system of conveyors

In the proposed technology (Fig. 1 and 2) the dried hop cones are conveyed from the belt dryer (2) with the conditioning switched off into the cooling chambers where the moisture content of the bracts and strigs evens out spontaneously, and the resulting moisture of the dried hop cones rises by 2 up to 4 % to 10 up to 12 % . Chamber filling and emptying system is separated in a way that the first cooling chamber (7) is filled by dried hops which gradually cool down here, and from the other chamber (8) the hops are conveyed (10), during the filling of the first chamber after being cooled down, i.e. after the moisture levels have reached an equilibrium value of 10 to 12 %, to the square bale press (11) where they are baled. Each cooling chamber capacity is 125 m^3 (12.5 x 4.0 x 2.5 m), which corresponds to the belt dryer performance.

The aim of the research, which is presented by the article, is to compare the drying curves with the existing technology of hop drying and using cooling chambers.

Based on the conceptual patented designs and a utility model, in 2018 the apparatus was assembled at the PCHB 750 belt dryer of Agrospol Velká Bystřice Ltd. The proposed technology of the cooling chambers is assembled as follow-up equipment, i.e. a floor plan extension is necessary as well as roofing of the whole space, with regard to the dimensions of the cooling chambers. The assembly was put into operation in the harvest season of 2018.

MATERIALS AND METHODS

The implementation of the new technological process using cooling chambers was preceded by repeated in-process measurements of the dependence of hop cone moisture content, and of bracts and strigs moisture contents separately on the drying time (drying curve) when drying the Saaz variety (*Heřmánek et al., 2016*; *Rybka et al., 2017*). The samples had been taken from each inspection window (Fig. 3) of the dryer (1-9), conditioning (10-11) and conditioning outlet (12). The moisture contents of the whole hops, bracts and strigs were determined by means of the Mettler-Toledo HE43 moisture analyser (*Jech et al., 2011*).

The drying curve shape led us to recommend setting the drying process in a way so that the drying kept going on still on the third belt, not over-drying the hops, with the conditioning switched off, thus the cones reached a moisture content of approximately 9-10 % at the outlet. With the current belt dryers their technological process can be influenced, in that context, by an increased belt speed, or possibly by a change in the dried hop layer height, or even by a highly complicated adjustment of the drying air distribution. Almost all of the adjustments lead to an increase in the hop passage through the dryer and

to a reduction of the drying time. The option covering an increased belt speed was then implemented in such a way so that the hop cone moisture content at the 9th inspection window was approximately 10 %. Following the hops at the dryer outlet, they were continuously loaded into one or the other cooling chamber in which the moisture content of the bracts and strigs evened out spontaneously to a required resulting hop cone moisture, and their temperature stabilized to ambient temperature. The hops were then conveyed to be baled and dispatched.
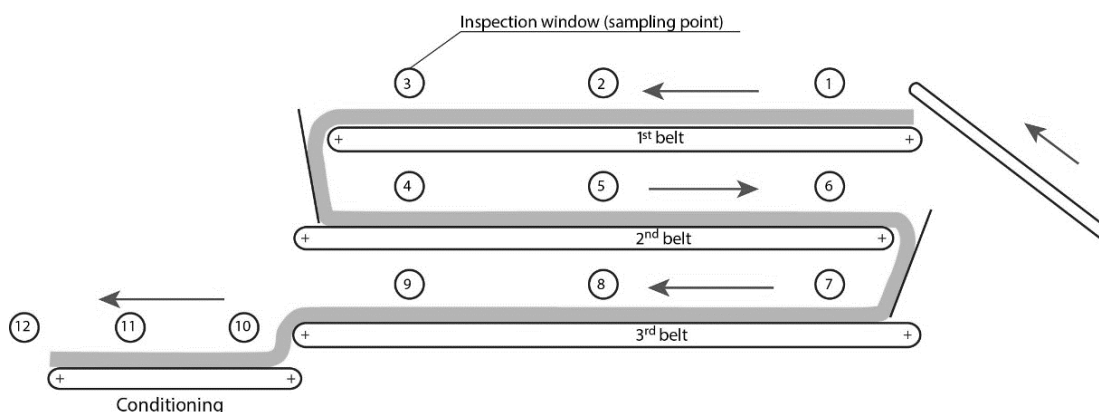
Fig. 3 Scheme of the belt dryer measured area with marked sampling points

RESULTS AND DISCUSSION

1. Dependence of the moisture content of hop cones, bracts and strigs on the drying time (drying curve).

At the beginning of the 2018 harvest season, the drying curve was determined for the Saaz semi-early red-bine hops variety. Several measurements were carried out the results of which did not vary significantly. Fig. 4 shows an example of a drying curve from one of the measurements. The graph makes it possible to assess the relationship between the moisture contents of the whole cones, bracts and strigs. Tab. 1 presents the belt speed and cumulative time of measurement. The drying curve character is defined by the moisture levels at individual inspection windows detected by the moisture analyser for the cones, bracts and strigs (*Kumhála et al.,* 2016; Rybka *et al., 2016*). In order to ensure full drying of the strigs, hops are then over-dried. The product is subsequently moistened by conditioning up to the acceptable moisture level. It is apparent that the strig moisture content declined gradually compared to the bract moisture. Since the ratio by mass of the bracts and strigs was approximately 9:1, in determining the moisture content of cones a value approaching the moisture content of bracts was obtained. The strigs by passing the conditioning were logically gaining a higher moisture more slowly compared to the whole cones the moisture content of which is practically identical to that of the bracts.

The drying curve in Fig. 4 clearly shows that during normal drying the hop cones are considerably over-dried. Already at the beginning of the third belt (inspection window n. 7) the hops are sufficiently dried and even the hop cone strig has a moisture content of 8 to 10 %. Thus, any further drying leads to energy losses, cost increases and to degradation of the hop cone quality. The drying curve illustrates that at least 200 min out of the total drying time is needless drying. The presented dependence resulted in recommendation to set the drying process in a way so that the drying kept going on still on the third belt, not over-drying the hops, with the conditioning switched off, thus the cones reached a moisture content of approximately 9-10 % at the outlet and were subsequently stored in the cooling chambers.

2. Inclusion of the cooling chambers in the technology of hop drying.

In 2018, the issued design was implemented inside the enlarged facility of the picking line and belt dryer of Agrospol Velká Bystřice Ltd. where two cooling chambers were built, interconnected by a system of conveyors following up the PCHB 750 belt dryer outlet (*Rybka et al., 2018*). The entire new technology was subsequently validated. The drying belt speed increased (Tab. 1) in such a way so that the hop cone moisture content at the 9th inspection window was approx. 10 %. Owing to the ratio of the times of passage between the first and ninth inspection window at the initial and the new belt speed, the drying time was reduced by approx. 39 %. Fig. 5 depicts the drying curve of the progress of drying without

conditioning and with the subsequent use of cooling chambers. The graph in Fig. 5 clearly shows that upon leaving the belt dryer the moisture content of the strig is relatively high, however, it gradually evens out with the moisture content of the bracts inside the cooling chambers (Fig. 6).
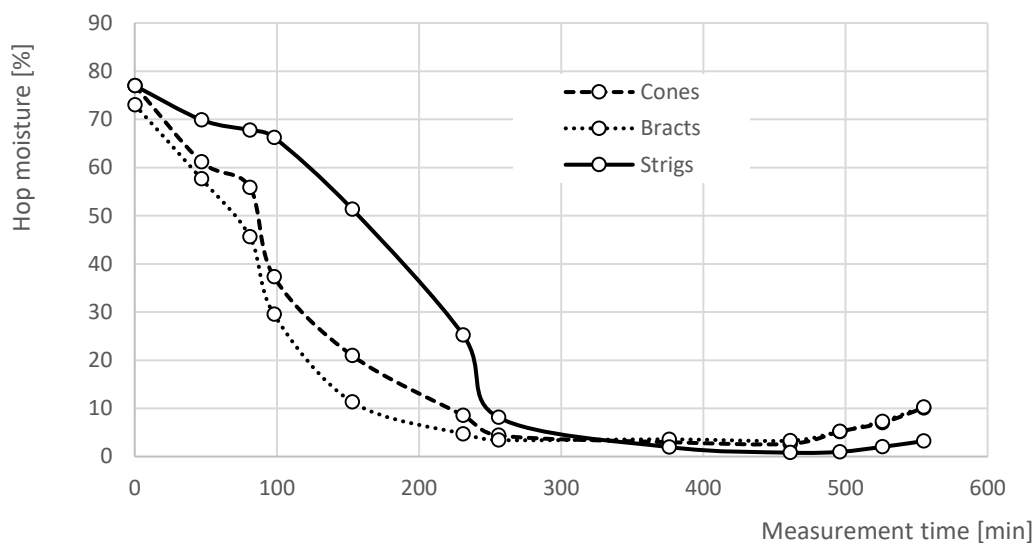

Fig. 4 Dependence of the moisture contents of cones, bracts and strigs on the drying time (points = inspection windows)

Tab. 1 Parameters of hop drying in belt dryer with and without conditioning

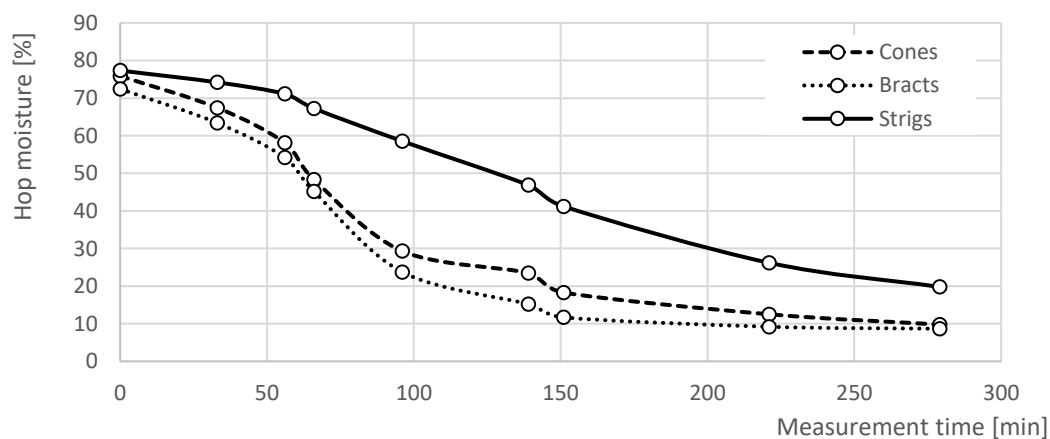| Drying with conditioning												
Sampling point		1st belt			2nd belt			3rd belt			Conditioning	
Inspection window		1	2	3	4	5	6	7	8	9	10	11	Outlet 12
Belt speed	m.s⁻¹	0.0031			0.0019			0.0012					
Measurement time	min	0	47	81	98	153	231	256	376	461	496	526	555
Drying without conditioning												
Belt speed	m.s⁻¹	0.0055			0.0034			0.0019					
Measurement time	min	0	33	56	66	96	139	151	221	279			

Fig. 5 Dependence of the moisture contents of cones, bracts and strigs on the drying time with the use of cooling chambers

Following the accelerated drying process, we monitored the progress of changes in the moisture contents of cones, bracts and strigs inside the cooling chambers. The graph in Fig. 6 illustrates the gradual mutual transmission of moisture for the cones, bracts and strigs, and their approximation. Our assumption that during the cooling process the moisture content of cones increases by approx. 1 % under the influence of the external atmospheric environment has been fulfilled. The hop cone moisture content at the outlet prior to baling complies with the requirements specified by hop purchasers.
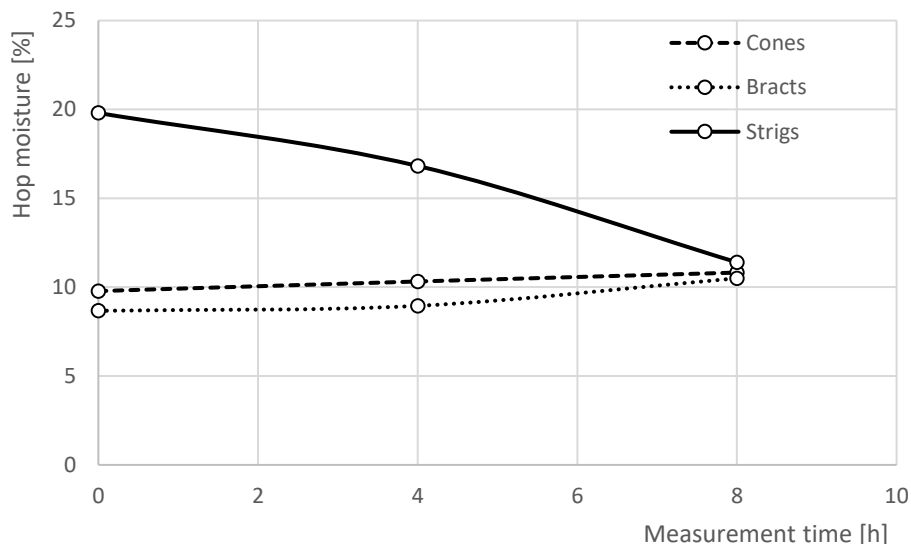
Fig. 6 Dependence of the moisture contents of cones, bracts and strigs on the storage time inside the cooling chambers

CONCLUSIONS

The economic output concerning the inclusion of cooling chambers in the hop drying technology is directly related to the reduced drying time in the belt dryer. This reduction of drying time and elimination of over-drying has significant effects on the increase in the quality of hop cones, reduction of losses in the heat-labile substances, as well as on the final assessment of the hop product (*Krofta, 2008*). Due to our long-standing monitoring of the day-to-day operation it was found out that the inclusion of cooling chambers in the process of hop drying will bring about savings in gas of 2,356 CZK.t^{-1} of dry hops, and savings in electricity of 831 CZK.t^{-1} of dry hops. As a consequence of the anticipated reduction of the harvest period by approx. 39 %, other cost items will be reflected in these savings, such as e.g. salary of the workers participating in the harvest, their use for other activities, savings in the fuel for tractors and in the electrical power for other operations related to the harvest, etc. There are no negative effects that would influence the environmental quality.

ACKNOWLEDGEMENT

REFERENCES

1. Henderson, S. M., & Miller, G. E. (1972). Hop Drying-Unique Problems and Some Solutions. *Journal Agricultural Engineering Research, 17*, 281-287.
2. Heřmánek, P., Rybka, A., & Honzík, I. (2018). Determination of moisture ratio in parts of the hop cone during the drying proces in belt dryer. *Agronomy Research, 16*(3), 723-727.
3. Heřmánek, P., Rybka, A., Honzík, I., Hoffmann, D., Jošt, B., & Podsedník, J. (2016). Construction and verification of an experimental chamber dryer for drying hops. In *6th International Conference on*

Trends in Agricultural Engineering I (pp. 179-185). Czech Republic: CULS Prague.

4. Hofmann, R., Weber, S., & Rettberg, S. (2013). Optimization of the hop kilning process to improve energy efficiency and recover hop oils. *Brewing Science, 66*(March/April), 23-30.

5. Chyský, J. (1977). *Moist air* (in Czech). Prague, Czech Republic: SNTL.

6. Jech, J., Artim, J., Angelovičová, M., Angelovič, M., Bernášek, K., Honzík, I., Kvíz, Z., Mareček, J., Krčálová, E., Polák, P., Poničan, J., Rybka, A., Ružbarský, J., Sloboda, A., Sosnowski, S., Sypula, M., & Žitňák, M. (2011). *Machines for Crop Production 3: Machinery and equipment for post-harvesting and treatment of plant material* (in Czech and Slovak). Prague, Czech Republic: Profi Press Co. Ltd.

7. Krofta, K. (2008). *Evaluation of hop quality.* Žatec, Czech Republic: Hop Research Institute Co. Ltd. (in Czech).

8. Kumhála, F., Lev J., Kavka, M., & Prošek, V. (2016). Hop-picking machine control based on capacitance throughput sensor. *Applied Engineering in Agriculture, 32*(1), 19-26.

9. Mitter, W. & Cocuzza, S. (2013). Dry hopping - a study of various parameters. *Brewing and Beverage Industry International, 4*, 70-74.

10. Podsedník, J., Rybka, A., Heřmánek, P., & Honzík, I. (2019). A method for treating the moisture of hops after drying using cooling chambers and apparatus for carrying out the method (in Czech). Industrial Property Office. Patent No. 307835. Bulletin No. 24/2019.

11. Rybáček, V., Fric, V., Havel, J., Libich, V., Kříž, J., Makovec, K., Petrlík, Z., Sachl, J., Srp, A., Šnobl, J., & Vančura M. (1980). *Hop production* (in Czech). Prague, Czech Republic: SZN.

12. Rybka, A., Heřmánek, P., & Honzík, I. (2017). Theoretical analysis of the technological process of hop drying. *Agronomy Research, 15*(3), 859-865.

13. Rybka, A., Heřmánek, P., Honzík, I., Hoffmann, D., & Krofta, K. (2016). Analysis of the technological process of hop drying in belt dryers. In *6th International Conference on Trends in Agricultural Engineering II* (pp. 557-563). Czech Republic: CULS Prague.

14. Rybka, A., Krofta, K., Heřmánek, P., Honzík, I., & Pokorný, J. (2018). Effect of drying temperature on the content and composition of hop oils. *Plant, Soil and Environment, 64*(10), 512-516.

15. Srivastava, A. K., Goering, C. E., Rohrbach, R. P. & Buckmaster, D. R. (2006). *Engineering Principles of Agricultural Machines*. Michigan, USA: ASABE, 2nd Edition.

Corresponding author:
Doc. Ing. Adolf Rybka, CSc., Department of Agricultural Machines, Faculty of Engineering, Czech University of Life Sciences Prague, Czech Republic,rybka@tf.czu.cz

THE EFFECT OF MOISTURE ON THE MECHANICAL PROPERTIES OF FLAX PREPREG

Martina RYVOLOVÁ[1]

[1]*Institute for Nanomaterials, Advanced Technology and Innovation, Bendlova 1407/7, Liberec, Czech Republic*

Abstract

Natural fiber reinforced laminates have gradually gained their place in the technical application of fiber-reinforced plastics. The strength of the flax fiber is high; compared to other natural fibers. The deterioration percentage during use is very small. Flax fibers have very good resistance to alkalis, acids and their solutions. The fiber is smooth-surfaced; the degree of its soiling is small. Flax fiber absorbs moisture very well and dries very well. The linen fabrics are hypoallergenic, resist mites, mold, and bacterial contamination. They are particularly suitable for people with various types of allergies, asthma, atopic eczema or psoriasis. Woven fabrics (more usually weave are plain and twill), unidirectional oriented fabric (roving, tapes, and non-crimp fabric) and chopped fibers from flax fibers serve as the reinforcement from natural fibers reinforced plastics (NFRP). Applications of linen fibers reinforced composites include for example sandwich panels (automotive), components for boats (nautisme), floor-wall panel, indoor furniture (building), component for special cars and bikes (sport and leisure), smartphone cover, tablet support (electronics), glasses, musical instrument and other (free time). The article described comparison the mechanical properties of flax fibres reinforced plastics, which was exposed to long-term action of moisture.

Key words: Flax fibres; epoxy matrix; moisture; mechanical properties; water absorption.

INTRODUCTION

A composite is defined as a multiphase material; dispersive phase (continuous or particulate) has a reinforcing function, continuous phase is plastic matrix. Synergic effect of phases leads to an improvement in the properties of the composite. Fibres and product of fibres are classified as continuous types of dispersion phases. The type of reinforcement is related to the production technology. The properties of the reinforcement are directly dependent on the types of fibres and production technology. Linum usitatissimum is an annual herb, grown for linen fibre and for seeds containing oil. He was one of the first domesticated plants and used to make textiles. It grows to a height of about 1.2 meters, blooms light blue, the fruit is a capsule. The bast fibre obtained from flax is one of the natural fibres of plant origin. The fibre has a textile use (yarns, threads, fabrics, ropes, medical and food industry) and technical use (flax tow, fow yarns). Flax processing procedure from the plant to the yarn is a technically demanding technological process with many steps. The processing of the stem of the plant yields a technical fibre up to 1 m long, 600 μm in diameter. Technical fibre consists of elementary fibres. The elementary fibre length is 40-60 mm, diameter 20 μm. Nodes are a typical feature of linen fibre, spaced irregularly along the length of the fibre. The microscopic sections show the elementary fibre shape as an irregular polygon with rounded corners (*Fidelis, 2013*). (*Sfiligoj Smole, Hribernik, Stana Kleinschek & Kreže, 2013*) describe detailing the composition of the stem of fibre-forming plants. All plant cells have a primary wall. The secondary cell wall is formed by successive deposition of cellulose layers, which are divided in three sub-layers, of which the middle layer is the most important for fibres mechanical properties. Each of three fibres sub-layers has a different micro fibrillary orientation, which is specific for the fibre type. Study (*Alix, Lebrun, Marais, Philippe, Bourmaud, Baley & Morvana, 2012*) was focused on chemical upgrading functional and mechanical properties of flax fibres with using commercial enzymes. Enzymes influence was monitored by optical microscopy, water sorption measurement and mechanical properties measurement. The moisture absorption and desorption in flax and hemp fibres and yarns investigate (*Mustata & Mustata, 2013*). The results of their experiment supported the conclusion, that the ratio of amorphous and semi crystalline cellulose and the microfibrillar angle defined the difference mechanical properties between other types of fibres. Flax yarns showed an increase in tensile strength in the wet state and during of water absorption in fibres in comparison with the dry state.

When choosing the appropriate type of fibre reinforcement from flax fibres, it is necessary to take into account the method of its preparation - technological process of production. Interesting results brought (*Goutianos, Peijs, Nystrom & Skrifvar, 2006*) in the study the mechanical properties of flax fibres reinforced composites according to technological process of production linen rovings, yarns, woven fabrics and non-crimp fabrics. The results of their study have clearly confirmed that natural firer composites based on continuously produced reinforcement exhibit improved mechanical properties compared to current non-woven reinforcements. They describe a significant influence of twist of longitudinal textiles on the properties of woven and non-crimp composite reinforcements and the effect of twist on the quality of fibre impregnation by the polymer resin. In paper *(Mei-po Ho & all, 2012)* describes the processes for producing composite materials and discusses their suitability for NFRP production. Modelling of mechanical properties of composites requires good knowledge of fibre bundle behaviour during deformation. Paper (*Charlet, Eve, Jernot, Gomina, Breard, 2009*) describes the main characteristics of flax fibre behaviour in connection with their morphology. PhD. thesis (*Aslan, 2012*) deals with the problem of reliable measurement of the real strength of unidirectional composites made from flax fibres. The number of experiments were part of the research; concurrently mathematical models were created using the finite element method. The team (*Zhu, Zhu, Abhyankar & Njuguna, 2013*) investigated the effect of fibre treatment in the bio composite material from linen/tannin and the effect of adjustments on fibre surface appearance and mechanical properties of the composite, because water absorption into bio-composites limits their possibility of outdoor applications. Flax fibres absorb moisture very well and thus changes in mechanical properties. The aim of the study was to test the resistance of flax prepreg to long-term exposure to moisture and determine the size of changes of mechanical properties.

MATERIALS AND METHODS

Flax fibres reinforced composites panel was prepared for experiment. Panel is composed from two perpendicular oriented layers of flax prepreg. Using a two-layer sample for tensile strength test eliminate the need to test the composite in the 0 ° and 90 ° directions. The flax prepreg was composed from unidirectional oriented flax fibres and epoxy resin, weight ratio 50% fibres, 50% epoxy resin. Composite panel was made under conditions recommended by the manufacturer (temperature, humidity pressure). The experiment was based on long-term exposure of water to the flax reinforced polymer plate. The assumption was that when the water was absorbed to flax reinforcement, the strength of the FFRP would change significantly. Parameters of composite plates shows Table 1.

Tab. 1 Flax prepreg panels parameters

No.	Orientation	Weight before water immersion [gm^{-2}]	Weight after water immersion [gm^{-2}]
1	0°/90°	656	658
2	0°/90°	613	612
3	0°/90°	613	615

Three groups of samples were prepared for the tensile strength test. Figure 1 shows specimens preparing for tensile strength test, Figure 2 strength testing machine Tiratest T2400.
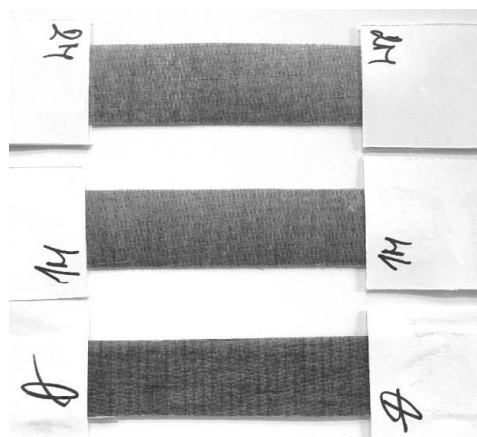

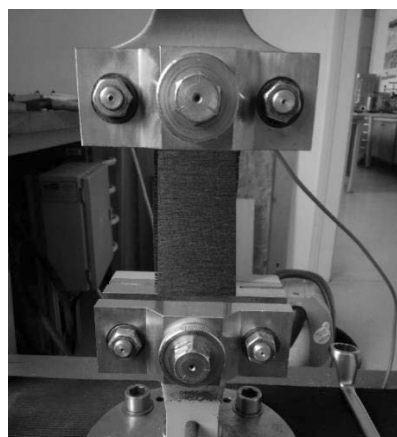**Fig. 1** Specimens for tensile strength test

Fig. 2 Strength testing machine

The first group of samples was exposed to water at room temperature and normal humidity to 500 hours, the second group of samples was exposed to water at room temperature and normal humidity of 1450 hours. The last group of samples was used for comparison; the samples were stored at room temperature and normal ambient humidity. Conditioning the samples (after water action) was performed at room temperature and normal humidity for 24 hours.

The specimens for uniaxial stress test was prepared according Standard ČSN EN ISO 527-4. Thickness of specimens was measured using thickness gauge SDL M 034/1. Tensile strength test was realized on strength testing machine Tiratest T2400, speed of test was 2mm/min. Specimens size (length, width and thickness) was entered individually for each specimen. Tensile curves, values of maximum breaking force (F_{max}), maximal strength (R_{max}) and tensile strength modulus (E) were results of test.

RESULTS AND DISCUSSION

Tensile strength test was realized for prepared flax pepreg specimens after long-term water exposure. Water absorption is typical property of flax fibres and flax products. The study (*Mustata, 2013*) describe differences between the breaking force and the strength of dry and wet flax yarns with different fineness and different finishing of rovings. Article (*Alix, 2012*) describe using of different methods for detection of changes of flax fibres properties using enzymatically upgrading. It was used tensile strength test for comparison mechanical properties befor and after enzymes action. Internal structure of flax stem was inspected using optical microscopy.

The study (*Zhu, 2013*) describe influence of fibre treatment to tensile properties and water absorption of flax/tannin composite material. The effect of different chemical reagents on surface of flax fibres was analysed using the SEM micrograph, pure flax fibres and modified fibres was compared. The treatment of fibres was performed to increase adhesion between the flax fibre and the tannin matrix. The tensile strength test was exploited to confirm the assumption of an increase in the mechanical properties of the composite using the adhesion improvement of resin to surface of flax fibres.

Table 2 presents the specimens parameters and statistically processed results of measurement. Tensile curves, values of maximum breaking force (F_{max}), maximal strength (R_{max}) and tensile strength modulus (E) were results of test. Graph of F_{max} values shows Figure 3 and Figure 4 shows specimens after test.

Tab. 2 Results of measurements

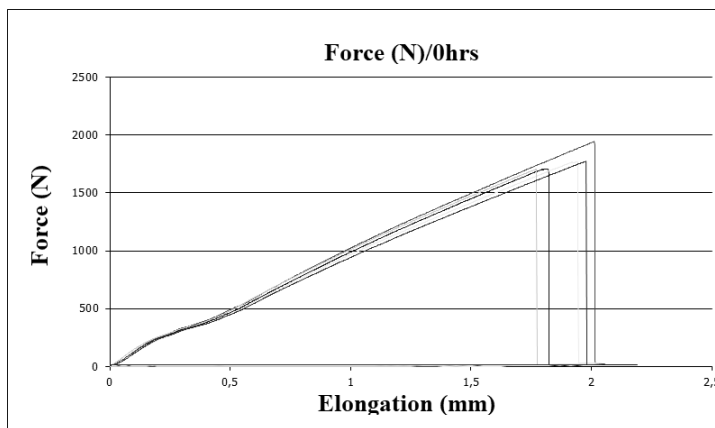| FRP	Thickness [mm]	F_{max} [N]	R_{max} [N/mm^2]
0 (1)	0,75	1780,8	79,146
500h (2)	0,60	1785,0	99,170
1450h (3)	0,61	1775,6	92,056

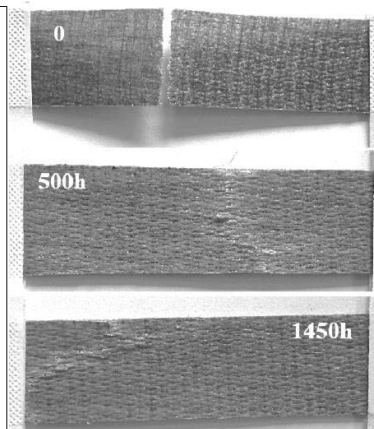**Fig. 3** Graph of maximal force   **Fig. 4** Specimens after test

Studies that deals with the relationship between mechanical properties of flax and moisture clearly shows that water absorption increases the strength of flax fiber. The experiment did not produce clear results in this direction. The experiment showed only that the specimens of flax fibers reinforced plastic (flax prepreg) absorbed only very little or no moisture.

Changes in appearance of the surface of the specimens were monitored by SEM analysis. The images show that the surface of the specimens remained unchanged overall. Images on specimens affected by water was taken at the point where small white spots/clusters appeared on the surface (Fig 5). The clusters did not affect the mechanical properties of the specimens.
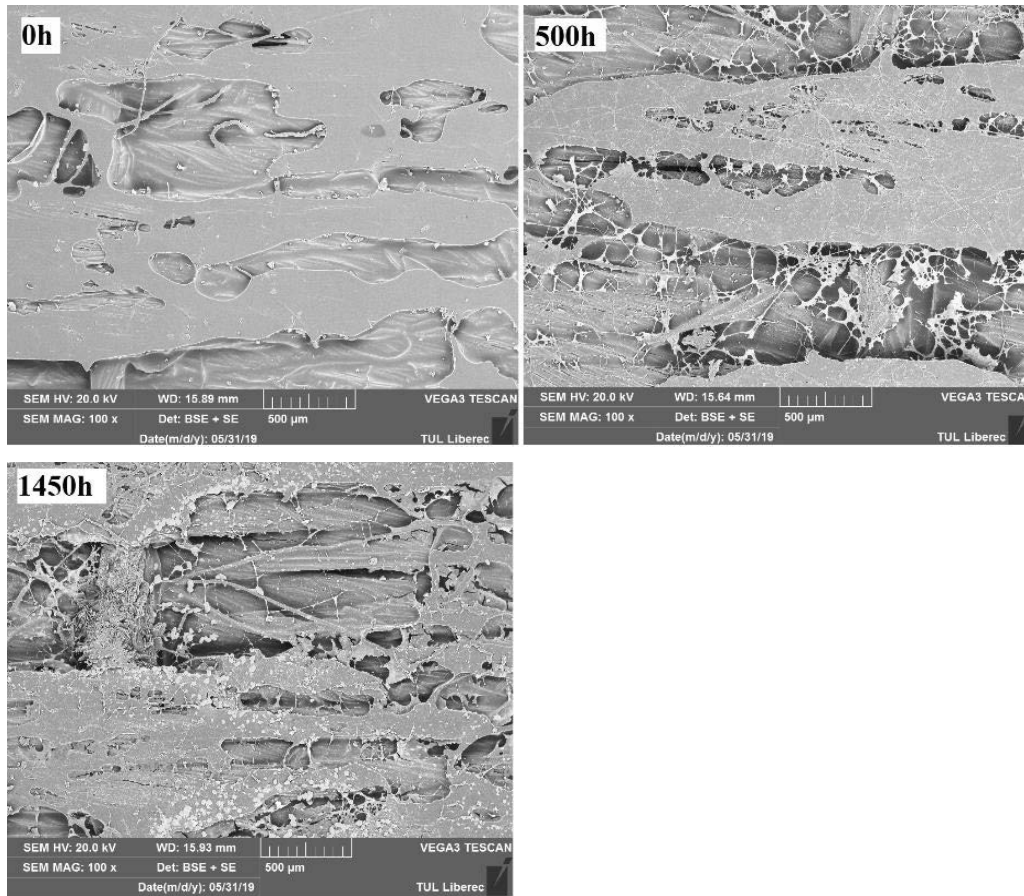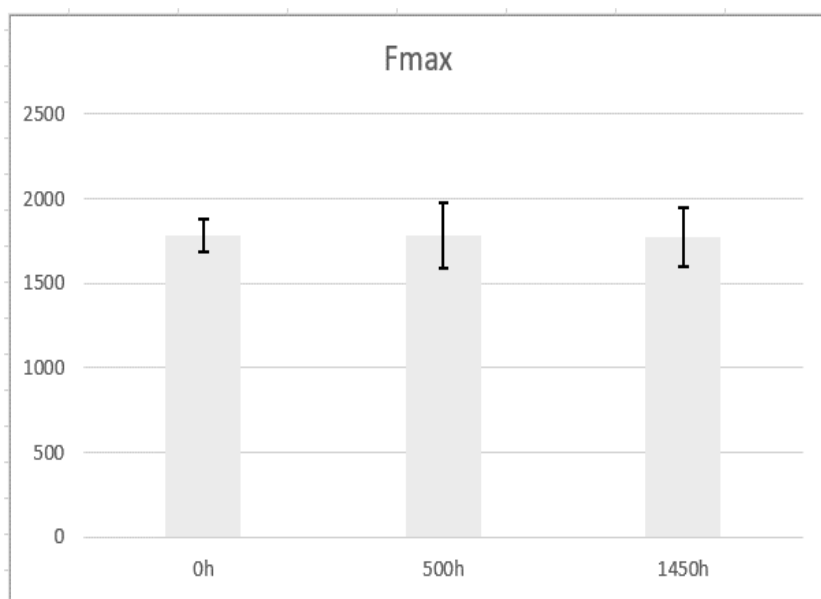

Fig. 5 Surface of composite specimens

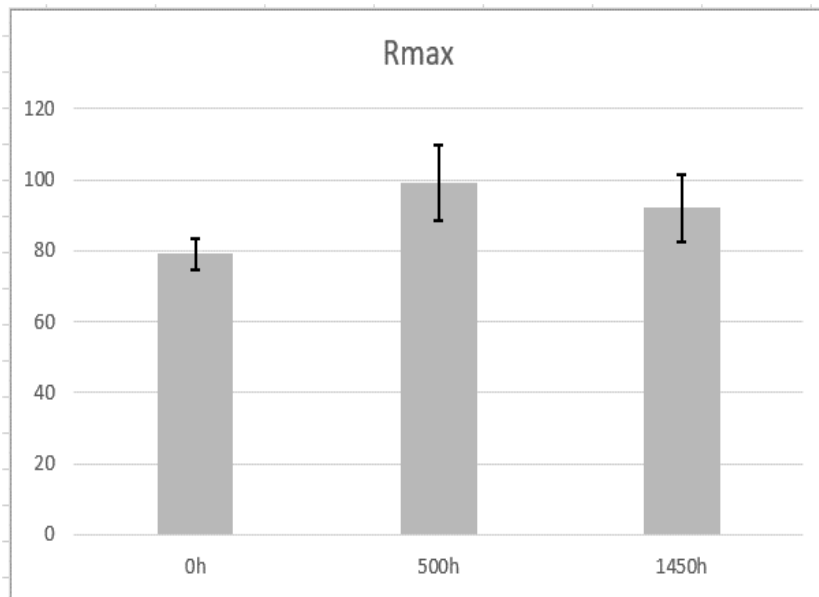**Fig. 6** Comparison of maximal force results

Fig. 7 Comparison of maximal strength results

Comparing the breaking force F_{max} of individual specimens groups is not showing no significant differences. The average values are moving in rang 12N, is not possible to exclude that it is measurement error. The differences for maximal strength R_{max} is more pronounced, but is not possible to exclude that it is measurement error also.

CONCLUSIONS

The influence of moisture on mechanical properties of flax fiber reinforced polymer in this work was studied. Samples made from linseed prepreg were exposed to the long-term effect of water. Results of measurement were obtained during the uniaxial stress test. Statistically processed values were compared. The results cannot be considered conclusive. Differences in values of individual variables are not significantly different.

ACKNOWLEDGMENT

REFERENCES

1. Alix S., Lebrun L., Marais S., Philippe E., Bourmaud A., Baley C., & Morvana C. (2012). *Pectinase treatments on technical fibres of flax: Effects on water sorption and mechanical properties*. doi:10.1016/j.carbpol.2011.07.035

2. Aslan M. (2012). *Characterisation of Flax Fibres and Flax Fibre Composites*. ISBN: 978-87-92896-07-0.

3. Charlet K., Eve S., Jernot J.P., Gomina M., & Breard J. (2009). *Tensile deformation of a flax fiber*. doi:10.1016/j.proeng.2009.06.055

4. Fidelis, M. (2013). The effect of fibre morphology on the tensile strength of natural fibres. *Journal of Materials Research and Technology, 2*(2), 149–157.

5. Goutianos S, Peijs T, Nystrom B, & Skrifvar M. (2006). Development of flax fibre based textile reinforcement for composite applications. *Applied Composite Materials, 13*, 199-215.

6. Mei-po Ho, Hao Wanga, Joong-Hee Lee, Chun-kit Ho, Kin-tak Lau, Jinsong Leng, &

David Hui. (2012). Critical factors on manufacturing processes of natural fibre composites. doi:10.1016/j.compositesb.2011.10.001

7. Mustata A., Mustata F. St. C., Moisture (2013). Absorption and Desorption in Flax and Hemp Fibres and Yarns. *Fibres & Textiles in Eastern Europe, 21, 3*(99), 26-30.

8. Sfiligoj Smole, M., Hribernik, S., Stana Kleinschek K., & Kreže T. (2013). Plant Fibres for Textile and Technical Applications, doi: 10.5772/52372.

9. Zhu J., Zhu H., Abhyankar H., & Njuguna J. (2013). Effect of fibre treatments on water absorption and tensile properties of flax/tannin composites. In *The 19th International Conference on Composite Materials*.

Corresponding author:
Ing. Martina Ryvolová., Department of Machinery Construction, Institute for Nanomaterials, Advanced Technology and Innovation, Bendlova 1409/7, Liberec 1, 460 01, e-mail: martina.ryvolova@tul.cz

CONSTRUCTION AND MONITORING OF THE UNIQUE ROOF PHOTOVOLTAIC SYSTEM IN PRAGUE

Jana ŠAFRÁNKOVÁ[1], Václav BERÁNEK[2], Martin LIBRA[1], Vladislav POULEK[1], Jan SEDLÁČEK[1]

[1]*Department of Physics, Faculty of Engineering, Czech University of Life Sciences Prague*
[2]*Solarmonitoring, Ltd.., Prague*

Abstract
A photovoltaic system with a nominal output power of 449 kW$_p$ has been working reliably for almost 9 years on the roof of a sports stadium in Prague. We have used the monitoring system Solarmon-2.0 developed by us to monitor the data. A roof-mounted structure (RIPV) with flexible photovoltaic modules based on thin layers of amorphous silicon was chosen. These modules are located horizontally and lie flat over the roof so that they can not be seen from the street and do not interfere with the architectural concept of the city district. In this article we describe the unique design of the photovoltaic system and we present interesting results captured from the evaluated data. In the end, we discuss the comparison of the amount of electricity produced with the expected values in the given location and comparison of the data with similar photovoltaic systems.

Key words: *solar energy; energy conversion; flexible PV module; photovoltaic system.*

INTRODUCTION

We have been designing and testing photovoltaic systems for many years and the results have been published in many previous works, see for example *(Poulek et al., 2018)*. The photovoltaic (PV) system on the roof of the sports stadium (see Fig. 1) started working in 2010, so it has already been running for almost 9 years. Flexible PV modules based on thin layers of amorphous silicon, placed horizontally, were used for its construction. Such PV system is not visible from the street and does not disturb the architectural concept of the city district. In this article we present its design and our results of long-term data monitoring. First experiences with this PV system have been published earlier in the work *(Libra et al., 2016)* including unique data during solar eclipse. At work *(Monteiro et al., 2017)*, there is an annual monitoring of a similar PV system on the roof of the Mineirão football stadium in Brazil, and other PV systems on the roofs of the sports stadiums are described. Large flat roofs are considered as very suitable for installation of PV systems.

The aim of study was following. Design of the large photovoltaic system, long-time data monitoring and data evaluation. Data comparison with the similar photovoltaic system and with the expected values according PV GIS (http://re.jrc.ec.europa.eu/pvgis/apps4/pvest.php#). To monitor the data, we use the Solarmon-2.0 monitoring system developed by us, which we have described in detail in the article *(Beránek et al., 2018)*.

We have also tested the flexible PV modules used in our laboratory (see Fig. 2). Tests have confirmed that the modules are suitable for the application. The construction of PV cells based on thin layers of amorphous silicon describes in more detail, for example, work *(Foti et al., 2014)*. For example, work on thin film layers of another semiconductor (CdTe) refers to work *(Khrypunov et al., 2006)*. For example, the works *(Peng et al., 2011, Fung & Yang, 2008)* refer to other possibilities of integrating photovoltaics into building architecture (BIPV). Hybrid PV/PT systems incorporated in buildings are mentioned in the report *(Matuška & Šourek, 2017)*, and about energy self-sufficiency of buildings with integrated PV system, e.g. in report *(Luthander et al., 2015)*.

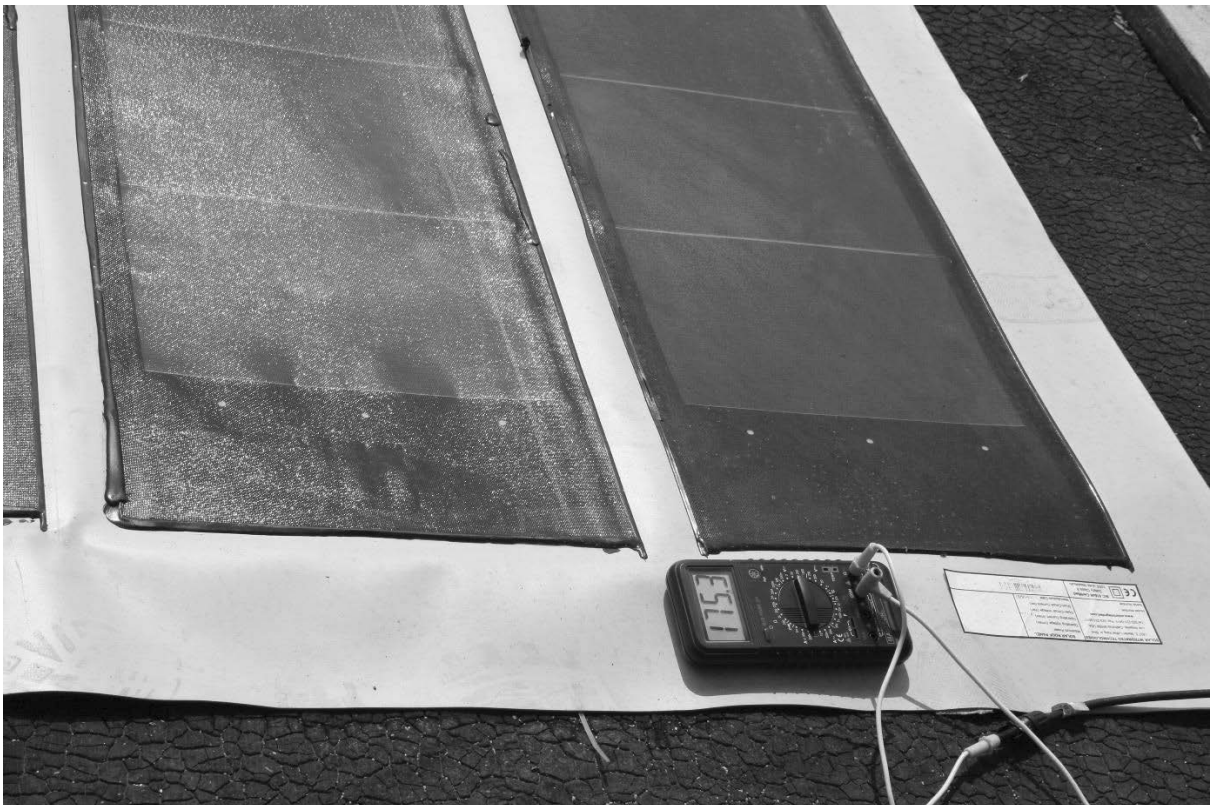**Fig. 1** PV system on the roof of the sports stadium in Prague

Fig. 2 Flexible PV module during testing in our laboratory

MATERIALS AND METHODS

The PV system was integrated into a flat roof with slight rounding. The flexible VAEPLAN V Solar 432 solar modules used in the experiment are shown in Fig. 1. They are oriented horizontally. They cannot be seen from the street and cannot disturb the architectural concept of the city district. Each module has a nominal output power of 432 W_p. The PV system has 8 identical independent sections. There is a merging switchboard in each section and 26 strings are connected to it. In each string there are 5 PV modules connected in series. Switchboards are equipped with fuse disconnecters, overvoltage arresters and ABB OT160E4 DC disconnecters, from which output power goes to the inputs of the electronic inverters. The total number of PV modules is 1040 and the total nominal power of the PV system is approximately 449 kW_p on the DC voltage side.

For connection of the PV system to a three-phase AC network, two inverters from Aurora Power-One (type PVI-CENTRAL-220.0-CZ) with three-phase alternating voltage are used. Each inverter consists of four blocks of 55 kW_p of maximum power. Each block has an output on the central bus which leads the power to the transformer. The eight sections are therefore connected to two inverters and the maximum power on the AC side is 440 kW_p.

RESULTS AND DISCUSSION

Fig. 3 summarizes the results of the monitoring of the PV system within 8 years of operation. For better comparison, the values are converted to 1 kW_p of installed power. The low values of the electricity produced in October and November 2014 are related to the failure of the PV system caused by the storm. If we calculated the electricity produced in these months as in previous years, we would have a value of around 715 $kWh.kW_p^{-1}.year^{-1}$ in 2014.
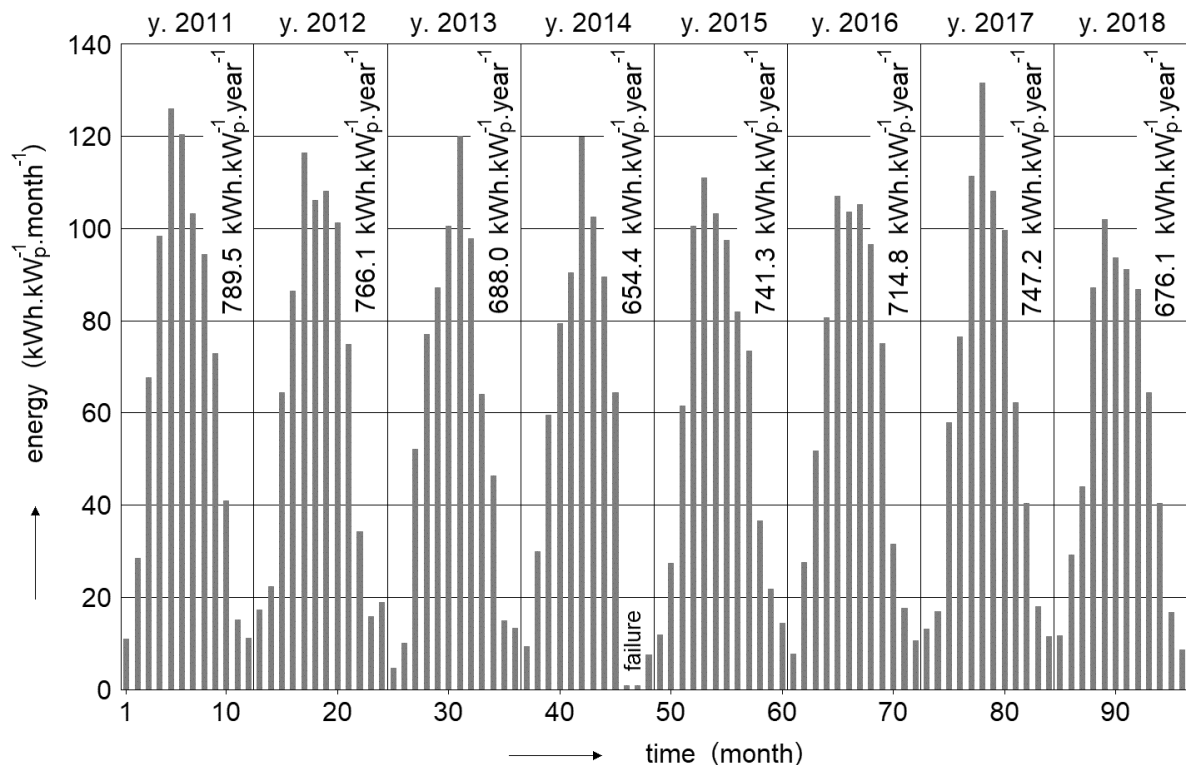

Fig. 3 Summarized results of monitoring of the PV system within 8 years of operation

According to the internationally used photovoltaic geographic information system forecast (http://re.jrc.ec.europa.eu/pvgis/apps4/pvest.php#), the expected amount of electricity produced per 1 kW_p of installed power output should be around 788 $kWh.kW_p^{-1}.year^{-1}$. Because the PV system is located on a flat roof, the "free-standing" module was used for the calculation and not "building integrated". It is clear from Fig. 3 that this value reached the PV system only in the first year of

operation. But we have to take into account the above-mentioned slight rounding of the roof and the slope of some PV modules slightly northwards. In addition, the PV system is in a dusty environment. The railway line is in close proximity. From horizontal PV modules, the dust is not washed away by rain. Although the PV system operator is occasionally cleaning it, the settled dust reduces electricity production. Nevertheless, the fall in electricity production over the past eight years is not dramatic, yet by 2015 and 2017 it has dropped by about 5% compared to the start of operation. In 2018, however, this drop was 14%, but the fall in one year may be in line with the natural fluctuation of meteorological conditions, and it does not mean degradation of the PV system parameters. Real output power will show next years of data monitoring.
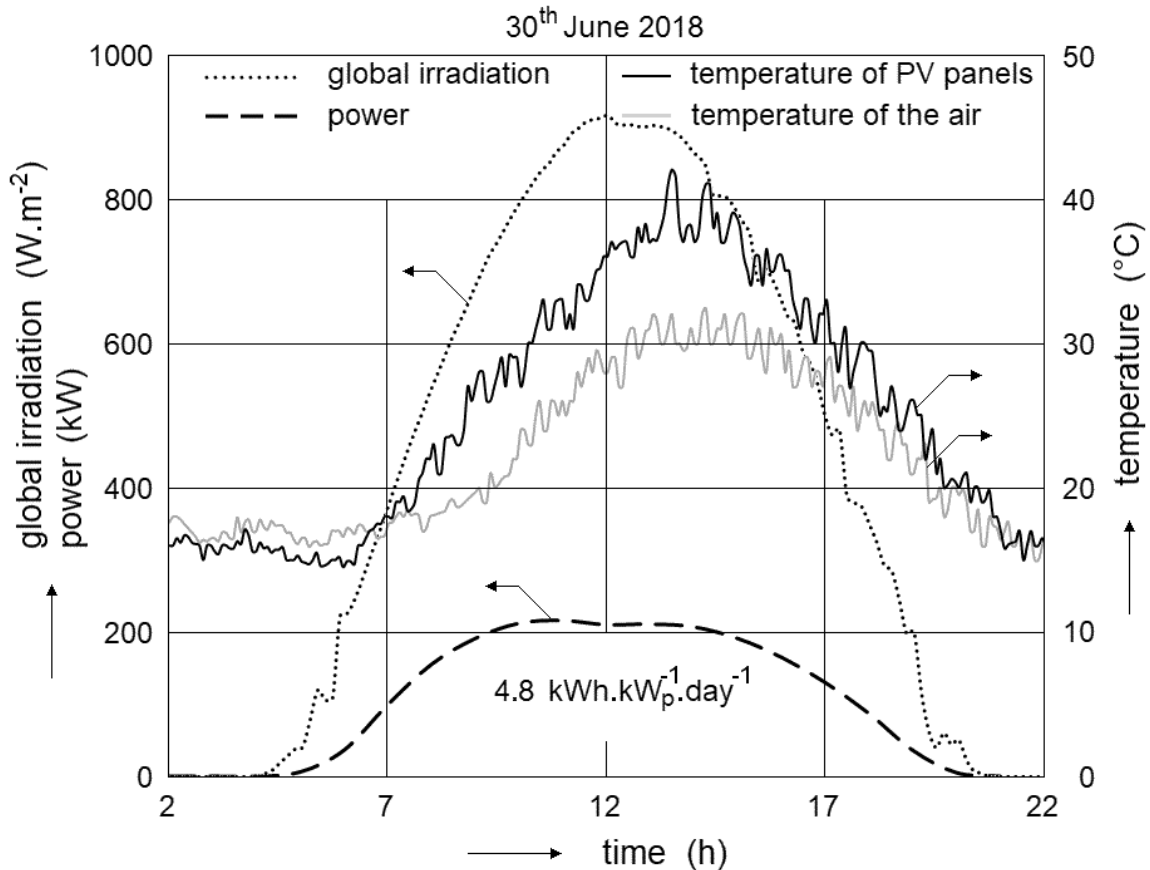

Fig. 4 Time dependence of instantaneous power, global radiation intensity, PV module temperatures and air temperatures for a sunny summer day

Fig. 4 is the time dependence of instantaneous power, global radiation intensity, PV module temperatures and air temperatures for a sunny summer day. Fig. 5 is the same dependence on a sunny winter day. The daily value of the produced electrical energy converted to 1 kW$_p$ of nominal power is also given. However, the air temperature is measured near PV modules and is therefore slightly distorted and is not an exact meteorological value. Moreover, the instantaneous wind influences temperature fluctuations. It is easy to see the alternation of the morning temperature minima and afternoon temperature peaks, during sunny days the temperature differences are much greater on sunny days than during the cloudy days. The temperature of PV modules is usually lower than the air temperature at night due to thermal radiation, while during the day it is on the contrary higher due to the absorption of solar radiation.

With increasing temperature, the efficiency of photovoltaic energy conversion decreases *(Poulek et al., 2018)*. For PV modules used, the manufacturer gives a decrease of 0.21% /°C. PV modules are glued directly to the roof waterproofing membrane, which prevents them from bottom cooling. During summer sunny days, therefore, their temperature reached more than 40°C, as shown in Fig. 4.
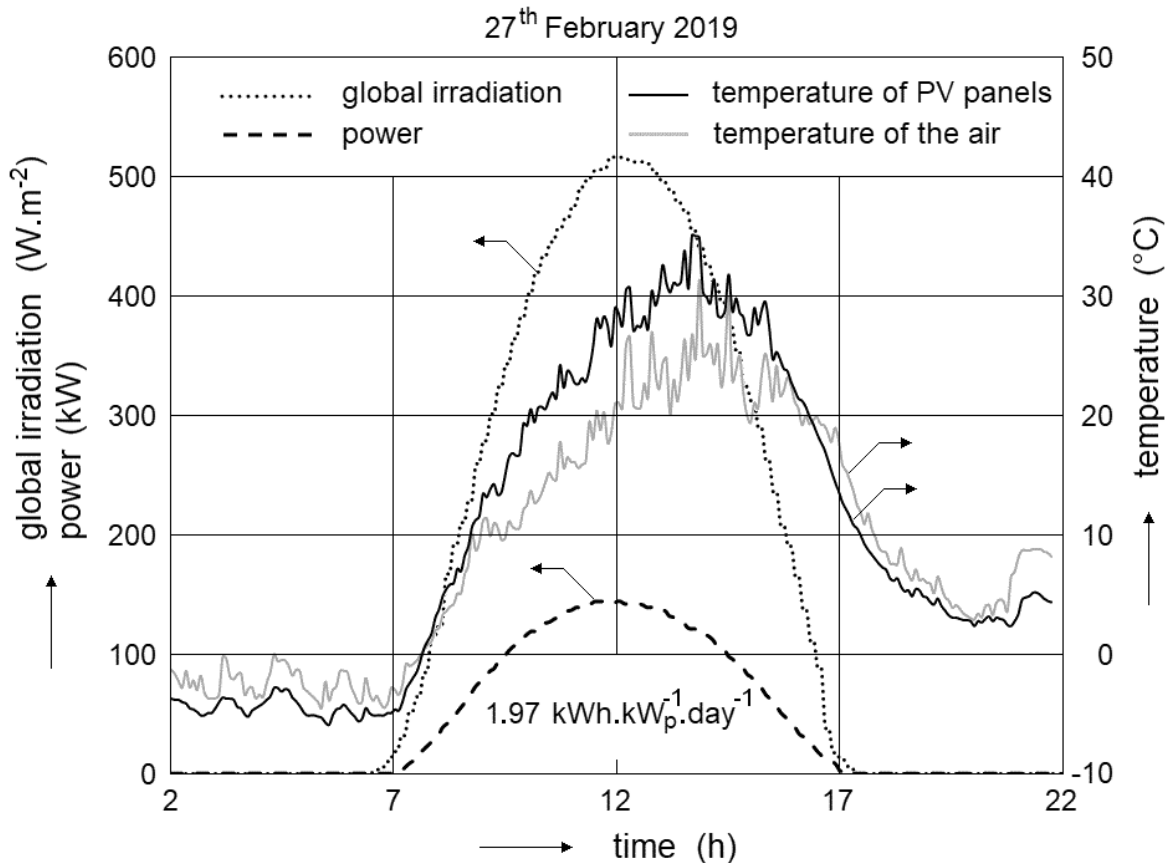
Fig. 5 Time dependence of instantaneous power, global radiation intensity, PV module temperatures and air temperatures for a sunny winter day

Previously, a similar smaller PV system was tested and the results were published in the work *(Libra et al., 2013)*. The distance between these two PV systems is approximately 5 km. In this case, similar flexible PV foils were used. The PV system was not exactly horizontal. A part of the PV system was oriented to the south with the slope approximately 3° and a part was oriented to the north with the same slope. The annual values of the produced electric energy were round 780 kWh.kW$_p^{-1}$.year^{-1} on the north side and round 900 kWh.kW$_p^{-1}$.year^{-1} on the south side. These values are a bit higher. There is the better self-cleaning because of the water flow and the laying dust do not reduce the transparency.

CONCLUSIONS
The PV system installed on the roof of the football stadium is considered a useful use of space. The design of a PV system based on flexible PV modules glued directly to the roof waterproofing membrane was the only option in terms of the design and static assessment of the roof and from the point of view of architectural integration into the city's urban planning concept. In the case of horizontally oriented PV modules, there is a higher summer-to-winter energy production ratio compared to south-sloping modules because the projection of the PV module surface into a plane perpendicular to the direction of the solar radiation is given by the cosine of the angle of incidence.

The PV system had worked without major problems during the past eight years, only in October and November 2014 had a storm failure. The values of the amount of electricity produced initially corresponded to expectations. During the aging of the PV system, there is a certain decrease, which is not dramatic yet. A larger drop in electricity production in 2018 may be in line with the natural fluctuation of meteorological conditions and does not necessarily mean degradation of the PV system parameters. This will show up next data monitoring. We intend to continue to collect the data and in particular to monitor further changes in the value of the electricity produced during the aging of the

entire installation. The expected life of PV modules based on thin layers of amorphous silicon (a-Si) is about 12 years.

Our data can also be used for the construction of other PV systems and for the prediction of the amount of electricity produced in PV systems of similar design. We assume that roof PV systems will become increasingly important as additional energy sources, but the classic large power plants are not yet being replaced.

ACKNOWLEDGMENT

REFERENCES

1. Beránek, V., Olšan, T., Libra, M., Poulek, V., Sedláček, J., Dang, M-Q., & Tyukhov, I.I. (2018). New Monitoring System for Photovoltaic Power Plants' Management. *Energies, 11*(10), Article No. 2495, 1-13.

2. Foti, M., Tringali, C., Battaglia, A., Sparta, N., Lombardo, S., & Gerardi, C. (2014). Efficient flexible thin film silicon module on plastics for indoor energy harvesting. *Solar Energy Materials & Solar Cells, 130*, 490–494.

3. Fung, T.Y.Y. & Yang, H., (2008). Study on thermal performance of semi-transparent building-integrated photovoltaic glazings. *Energy & Buildings, 40(3)*, 341–350.

4. Khrypunov, G., Romeo, A., Kurdesau, F., Bätzner, D.L., Zogg, H., & Tiwari, A.N. (2006). Recent developments in evaporated CdTe solar cells. *Solar Energy Materials and Solar Cells, 90*, 664-677.

5. Libra, M., Avramov, V., & Poulek, V. (2013). Experience gathered with the Prague national theatre PV system. In *Proc. 5th Intenational Conference Trends in Agricultural Engineering, Prague, 3rd-6th September 2013* (pp.386-390).

6. Libra, M., Beránek, V., Sedláček, J., Poulek, V., & Tyukhov, I.I. (2016). Roof photovoltaic power plant operation during the solar eclipse. *Solar Energy, 140*, 109-112.

7. Luthander, R., Viden, J., Nilsson, D., & Palm, J., (2015). Photovoltaic self-consumption in buildings: A review. *Applied Energy, 142*, 80–94.

8. Matuška, T. & Šourek, B. (2017). Performance Analysis of Photovoltaic Water Heating System. *International Journal of Photoenergy, Article ID 7540250*, 1-10.

9. Monteiro, L.G., Macedo, W.N., Torres, P.F., Silva, M.M., Amaral, G., Piterman, A.S., Lopes, B.M., Fraga, J.M., & Boaventura, W.C. (2017). One-Year Monitoring PV Power Plant Installed on Rooftop of Mineirão Fifa World Cup/Olympics Football Stadium. *Energies, 10*(2), Article No. 225, 1-23.

10. Peng, Ch., Huang, Y., & Wu, Z., (2011). Building-integrated photovoltaics (BIPV) in architectural design in China. *Energy & Buildings, 43*(12), 3592–3598.

11. Poulek, V., Matuška, T., Libra, M., Kachalouski, E., & Sedláček, J. (2018). Influence of increased temperature on energy production of roof integrated PV panels. *Energy & Buildings, 166*, 418–425.

12. Photovoltaic Geographical Information System. (2019). Retrieved from http://re.jrc.ec.europa.eu/pvgis/apps4/pvest.php#.

Corresponding author:
Prof. Ing. Martin Libra, CSc., Department of Physics, Faculty of Engineering, Czech University of Life Sciences Prague, Kamýcká 129, Praha 6, Prague, 16500, Czech Republic, phone: +420 22438 3284, e-mail: libra@tf.czu.cz

CONSISTENT MAINTENANCE MANAGEMENT MODEL

Jan SAILER[1], Tomáš HLADÍK[1]

[1]*Department for Quality and Dependability of Machines, Faculty of Engineering, Czech University of Life Sciences Prague, Czech Republic*

Abstract
A number of asset management models, methodologies and tools are available and well known today. However, various organisational approaches to asset management processes are adopted by companies in industry. In the paper, a number of examples of maintenance process models are summarized and comparison of examples (benchmark) of real maintenance organisational structures is presented. The used examples origin from chemical, petrochemical and automotive industries. On this background, a case study of major maintenance organisation change in Unipetrol, a central-european refinery and petrochemical group (part of PKN Orlen) is presented and analysed.
The goal of the authors is to provide readers an overview of the proposed changes in the organisational structure and asset management processes. Furthermore, to show the significance of their impact on number of management positions (reduction by 25%), roles, competences and asset management process flows with respect to KPIs evaluation.

Keywords: maintenance; organisational structure; asset management.

INTRODUCTION

There currently exist a number of asset management methodologies and tools. Even though this term is defined through a set of norms, both national and global ones (*ISO 55000, 2014*; *ISO 55001, 2014*), in the vast majority of cases we see isolated processes and methodologies, even though these are efficient as far as their application and outputs are concerned, they mostly focus only on a s ingle area or sub-process and are not interlinked, they do not form a consistent whole, or do not respect the needs or organisational structure of the production plant (*Leong, 2012*; *Flynn, 1995*). This state is usually caused by the isolated development of individual methodologies, which are often commercial products. An important role is also played by time, since individual methodologies and tools were developed in a certain time frame and thus they logically cannot follow up on each other. As an example, the set of methodologies generally referred to as Risk Reliability Management includes the Reliability Centered Maintenance, Risk Base Inspection and SIFpro© (*Shell Global Solution International, 2003*) methodologies, whose goals are to generate optimized plans for preventive maintenance based on risk assessment. Individual methodologies generate plans for preventive maintenance, but in distinct formats, completely unsuitable for automated or batch transfer to central planning systems for maintenance, where data are still processes within the planning and work implementation sub-process. A frequent representative of such CMMS is SAP – the preventive maintenance management module (*Valesko, 2010*; *Tan, 2009*; *Mourtzis, 2016*). Another factor which reduces the efficient implementation of modern methodologies for asset management is their low adaptability to the organisational structure of the production plant. The imperfect connection of the asset management to the production area, which in this case represents the customer, and with processes supporting the asset management process such as the purchase of spare parts and consumable material, investments, safety and security, or HR, then leads to imperfect communication flows that reduce the organisation's efficiency and in the end lead to suboptimal asset management costs, reduced availability of production equipment and lower process safety. For instance, this could lead to imperfect adherence to requirements of valid legislature, incorrect usage of residual service life of production equipment, or low coverage by predictive maintenance.

The facts specified above force us to view the asset management process as a consistent unit, integrated within the organisational structure of the production plant in a manner allowing efficient communication and goal sharing, whereas the real needs of the production facility, the medium- and long-term plans as well as the mission and vision of the company all need to be respected.

The proposed solution spans all parts of the asset management process, from the method of entering requests, their approval and prioritization, system of technical preparation of a job, optimal planning, transfer for implementation, feedback on implementation and final acceptance and closure of a job,

whereas emphasis is placed on efficient communication, work quality and utilization of work capacities (*Wireman, 2004*; *Kuda, 2012*).

Organisationally, it is necessary to setup the process in a way ensuring that individual decision steps are carried out on the side of the operator of the device and not on the side of the maintenance. On one hand, this results in an independent approval process with respect to costs management, and on the other this leads to clearly defined priorities by the operator, who is then forced to make decisions not only based on the current operating situation but also based on the costs and indicators for long-term operational availability (*ČSN EN 15341, 2010*). As was mentioned earlier, one of the primary tools to achieve optimal decision-making was the sharing of goals within key indicator assessment for processes, whereas the operator shares maintenance goals such as maintenance costs, mechanical availability of devices, Mean time between failures (MTBF) and/or efficiency of the work of the implementer of maintenance. On the other hand, the maintenance side shares operational goals, such as operational availability, use of production facilities, the energy index, or for instance variable costs (*Abreu, 2013*). From an organisational standpoint, the solution is based on the structure of a so-called multi-professional team, where a single organisational element has representatives of all key areas required for efficient administration and management of the entrusted production section. In practice, this means that the team includes representatives of production, technologies and maintenance, as well as other areas such as reliability and quality management who are responsible for the efficiency of central specialized bodies in given areas.

One of the key areas that need to be emphasized is the definition of process efficiency indicators for individual management levels, including the definition of key indicators (*ČSN EN 15341, 2010*). This set of indicators contains not only basic items such as the aforementioned fixed costs for maintenance, MTBF, or mechanical availability of equipment, but also indicators monitoring process safety of equipment such as Loss of Primary Containment (LOPC), number of process alarms per time unit, success rate of diagnostics of rotary machines etc.

The structure of monitored indicators is based on a classical pyramid logic, where the number of monitored items becomes smaller in the direction of top management (*Younus, 2003*).

The primary contribution is the creation of an asset management model which will ensure an improvement of mutual communication and coordination between individual company bodies, improvement of availability indicators for production equipment, optimization of costs for the implementation of maintenance activities, improvement of process safety indicators such as LOPC or number of process alarms. The author intends to demonstrate these properties based on a real-life implementation of the proposed process solution.

For creation of such asset management model, it is vital to reflect current problems and trends in maintenance organisational structures. There are two basic forms of maintenance organisational structures: area and central. In an area organisation, work control is delegated to area shops. In a central organisation, all work orders are controlled from a central shop (*Maynard, c2001*). For smaller maintenance organisations it is typical to use central form, for larger organisations central shop concept is widely used. Combination of both concepts (area-central) might be used for multilevel maintenance, where specialists are assigned to specific areas, maintaining the key equipment. Skills which are not needed on a daily basis are dispatched from the central shop when needed.

Organisational structure can be partly described by the Maintenance Organisation Ratio. This is manager to staff ration and ordinarily it is about 15:1. However this ration must be set carefully with respect to the skills and daily agendas of supervisors, machine shop dispositions and to the form of production (*Maynard, c2001*). Thus The goal of this study is to provide an overview of the proposed changes in the organisational structure and asset management processes.

MATERIAL AND METHODS

One of the main factors for the maintenance organisation is the characteristics of the maintenance needs that are generated by the assets.

A possible scenario of a production plant for chemical products can serve as an example.

Originally all the repair work arising out of the maintenance needs (or demand) of the plant was undertaken by local maintenance department personnel. After a major decrease of 40% in production output due to lack of demand was decided by management to reduce the numbers of production and maintenance personnel.

A further investigation resulted in two main options to choose between: either completely outsource the maintenance function, or outsource as much as possible. For practical reasons it was decided that a maximum of 50% of the work had to be done by maintenance department and 10% by operators undertaking first line maintenance work. So 40% of all work was outsourced, in particular all work on building services installations and all the utility equipment (*Zaal, 2016*).
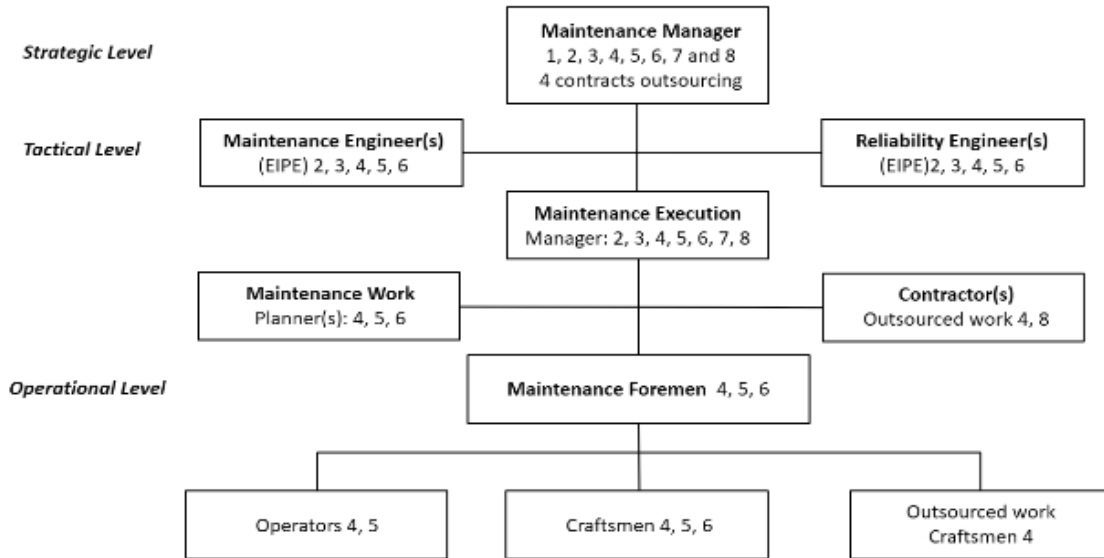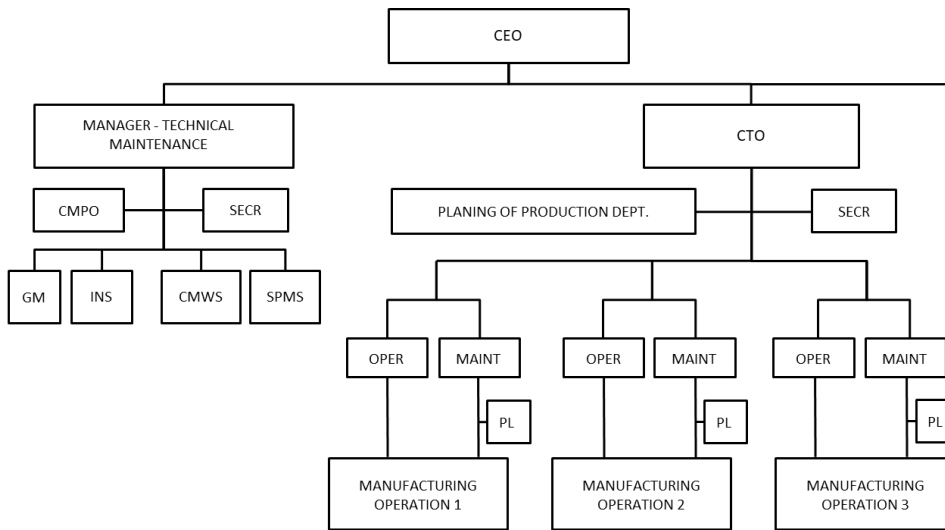

Fig. 1 Possible organisation of the maintenance department for a production plant (*Zaal, 2016*)

CMPO: Central production planning dept. **SECR**: Secretary **INS**: Instruments and tooling management

GM: General repairs workshops **OPER**: Operations manager **MAINT**: Maintenance manager

CMWS: Central maintenance workshops **SPMS**: Spare parts procurement and warehouses management **PL:** Planning

Fig. 2 Example of organisation structure of combined maintenance *(Legát, 2017)*

Regardless of formal structure of the organisation and the position of maintenance within the structure, there are certain generally accepted principles. The employees must know what they are responsible for, and whom they report to. Managers are required to know who is responsible for setting goals and all other activities needed for their success. The organisation structure should represent these responsibilities in the simplest and uncomplicated way. The organisation structure is often clear on the

level where business policy is formulated in the organisation, however, it is essential that the organisation structure is clearly understood on the level of work execution (*Legát, 2017*).

RESULTS AND DISCUSSION

The area maintenance model was in the past been used over the long term for individual production plants in Unipetrol. This was during times when the company had its own in-house executive maintenance including workshops and machinery. Change occurred in the nineties, when the company underwent privatisation and almost all servicing activities were split off and from then on used in the form of outsourcing. Changes in the organisational structures of maintenance were also accelerated at that time, when it was necessary to adapt to a different model of operation. Over the next fifteen years, many changes then occurred, when organisation of maintenance settled on the area model with a specific small role played by centralised services which constituted basic service for individual maintenance operations. The central part included technical diagnostics, cost reporting and basic administration of the maintenance process. There was no central technical engineering, no system of uniform strategic management, for example in the field of reliability, inspection, risk management, planning and strategy for preventative maintenance. Connection with the field of production differed for various production units. This model of maintenance management required a large number of management employees and ensured only minimal options for uniform management of maintenance strategy.
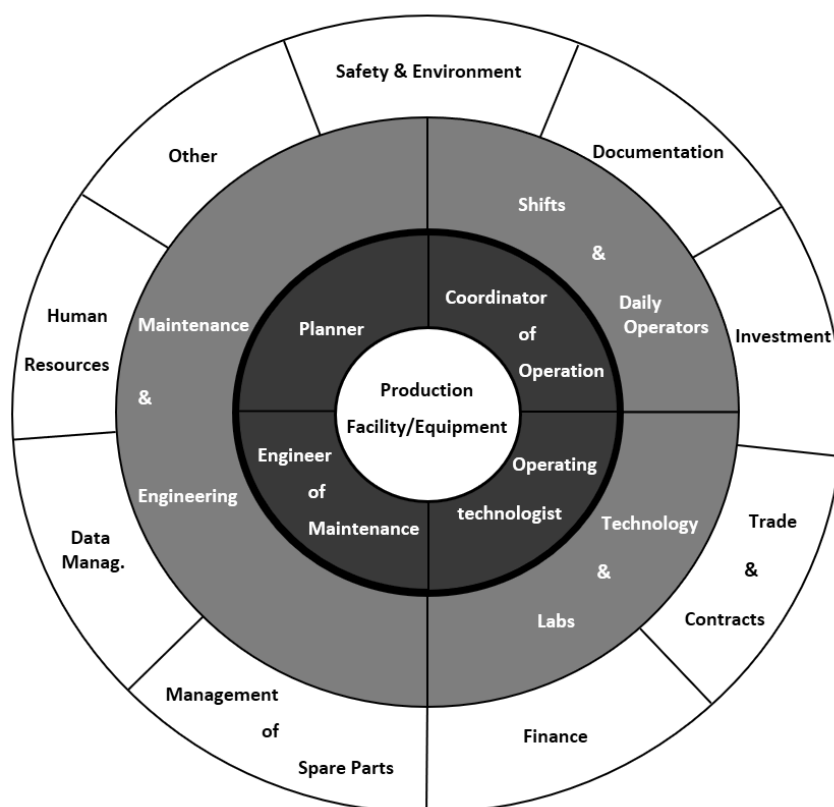

Fig. 3 Roles in production Team

In 2014, the company decided to implement the organisational model of Facility Teams across the board for management in the field of production. This concerns a multiprofessional team which is responsible for comprehensive management of a defined production unit and which also allows for close connection with organisation of maintenance.

Apart from the position of production technologist and energy technologist, the Facility Team is made up of a Reliability Engineer, Main Maintenance Engineer, Operations and Maintenance Coordinator and Scheduler (Fig. 3). It is precisely thanks to these positions that close interconnection with organisation of maintenance and its suppliers is ensured.
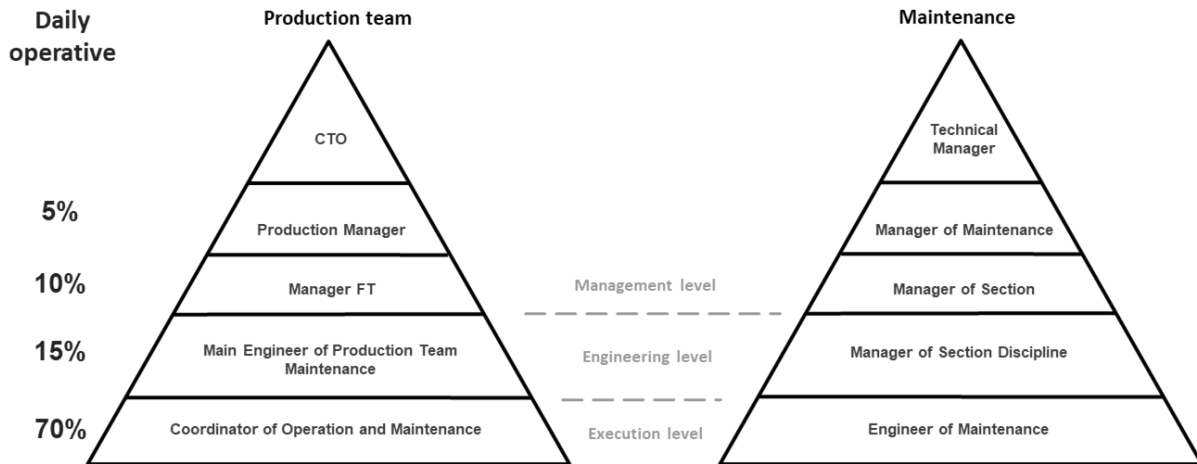
Fig. 4 Organisational Pyramid

So as to ensure that responsibilities and communication between in-house production and maintenance are clearly defined, transition to Facility Teams required change in the organisational structure of maintenance (Fig. 4). These changes were at the same time used to ensure more complex changes in organisation of in-house maintenance, whereas centralization occurred of the executive part of maintenance and the level of technical engineering was created, allocated to departments according to technical expertise (Fig. 5).
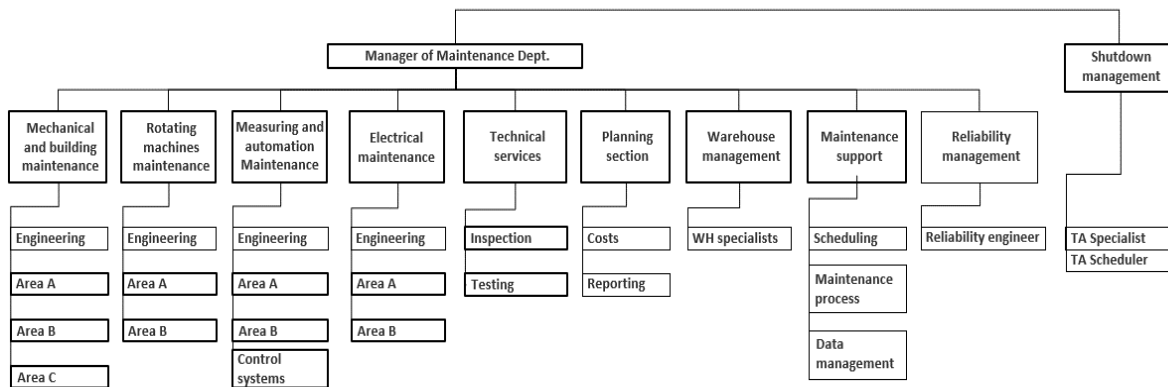

Fig. 5 Organisational chart

CONCLUSIONS

The changes in the organisational structure described above had an impact on the number of employees in management positions, bringing a reduction in their number from 12 to 9, i.e. by 25%.

Tab. 1 Analyzed KPIs

Indicators	Unit	Before the change					After the change		
		2010	2011	2012	2013	2014	2015	2016	2017
Ratio of managerial positions	%	6,9	7,7	7,6	8,4	8,5	6,4	6,3	5,5
Regulatory requirements fulfilment	%	16,5	19,6	15,8	17,2	18,3	7,8	4,7	1,7
High priority works	%	18,3	19,1	19,3	19,7	20,3	15,0	11,5	14,2
Planned vs. unplanned maintenance	%	26,0	25,0	23,5	20,5	21,2	14,0	16,0	14,0
Failure maintenance ratio	%	44,0	56,0	50,5	54,0	51,0	52,0	53,5	52,5

The reason behind these organisational changes was not however reduction of the number of jobs, but increase in the specialist abilities as regards organisation in the field of technical engineering and setup of organisation in such a way that competences and flow of information are clearly defined within the framework of interconnection between organisation of production and organisation of maintenance. For the evaluation, the period of 2010-2017 has been used (Tab. 1), with the year 2014 as the point of change. This period represents a sufficient sample of timeseries of selected KPIs and also avoids impacts of certain historical changes.

REFERENCES

1. Abreu, J., Martins, P. V., Fernandes, S. & Zacarias, M. (2013). Business Processes Improvement on Maintenance Management: A Case Study. In *Procedia Technology, 9*, 320-330. ISSN 22120173.

2. Ales Z, Jurca V, & Legat V. Effectiveness indicators of food processing lines. (2013). In: *Conference Proceeding - 5th International Conference Trends in Agricultural Engineering 2013* (pp. 56-61). Czech Republic: Czech University of Life Sciences in Prague.

3. ČSN EN 15341: Údržba – Klíčové indikátory výkonnosti údržby. (2010). ÚNMZ.

4. Flynn, B. B., Schroeder, R. G., & Sakakibara, S. (1995). The Impact of Quality Management Practices on Performance and Competitive Advantage. In *Decision Sciences, 26*(5), 659-691. ISSN 0011-7315.

5. *Introduction to Risk & Reliability Management*. (2003). Shell Global Solution International. ISBN: 978-80-213-2388-9.

6. ISO 55000: Overview, principles and terminology. (2014). International Organization for Standardization.

7. ISO 55001: Management systems – Requirements. (2014). International Organization for Standardization.

8. Kuda F., Beránková, E., & Soukup, P. (2012). Facility management v kostce: pro profesionály i laiky. Olomouc: Form Solution. ISBN 978-80-905257-0-2.

9. Legat, V., Mosna, F., Ales, Z., & Jurca, V. (2017). Preventive maintenance models – higher operational reliability. In *Eksploatacja i Niezawodnosc – Maintenance and Reliability*, *19* (1):134141.

10. Leong, T. K., Zakuan, N., & Saman, M. Z. M. (2012). Quality Management Maintenance and Practices-Technical and Non-Technical Approaches. In *Procedia - Social and Behavioral Sciences, 65*, 688-696. ISSN 1877-0428.

11. Maynard, H. B. & Zandin, K. B. (2001). *Maynard's industrial engineering handbook*. 5th edition (pp. 2248-2250). New York: McGraw-Hill. ISBN 9780070411029.

12. Mourtzis, D., Vlachou, E., Milas, N. & Xanthopoulos, N. (2016). A Cloud-based Approach for Maintenance of Machine Tools and Equipment Based on Shop-floor Monitoring. In *Procedia CIRP, 41*, 655-660. ISSN 22128271.

13. Tan, W. G., Cater-Steel, A., & Toleman, M. (2009). Implementing it service management: A case study focussing on critical success factors. In *Journal of Computer Information Systems*, *50*(2), 1-12.

14. Valesko, S. (2010). CMMS increases efficiency, cuts downtime. In *The National Provisioner, 224*(3), 20-23.

15. Wireman, T. (2004). *Benchmarking best practices in maintenance management*. New York: Industrial Press. ISBN 9780831131685.

16. Younus, J., Fahad, M., & Khan, M. A. (2016). Evaluation and Benchmarking of Maintenance Organization and Planning/Scheduling at Automotive Industries of Pakistan. In *Procedia CIRP, 40*, 711-715. ISSN 22128271.

17. Zaal, T. M. E. (2016). *Profit-driven Maintenance for Physical Assets.* Maj Engineering Publishing. ISBN 9079182419.

Corresponding author:
Ing. Jan Sailer, Department for Quality and Dependability of Machines, Faculty of Engineering, Czech University of Life Sciences Prague, Czech Republic, e-mail: Jan.Sailer@unipetrol.cz

TILLAGE SYSTEMS OF WINTER OILSEED RAPE (*BRASSICA NAPUS L.*) PRODUCTION WITH RESPECT TO COSTS, ENERGY AND LABOUR CONSUMPTION

Ondřej ŠAŘEC[1], Petr ŠAŘEC[1]

[1]*Dep. of Machinery Utilization, Faculty of Engineering, Czech University of Life Sciences Prague*

Abstract

The objective of this work is to assess different systems of winter oilseed rape production, i.e. reduced (RT) and conventional (CT) tillage, mainly in terms of yields, fuel and labour consumption, machinery and material costs in the conditions of the Czech Republic. Since 2001/02, trials were accomplished in 548 fields. Over the first five years, CT yields generally surpassed RT yields. But gradually, this trend turned over. The potatoes production area proved to be the most favourable in terms of yields. Recently namely, beet production area demonstrated also good results. When excluding cases with organic fertilizer application, the average fuel consumption of RT was by 15.7 % lower than that of the CT, the overall labour consumption again lower by 18.4 %, and finally the machinery costs lower by 10.8 %. All the above mentioned differences proved statistically significant. Concerning earnings per hectare, RT results proved superior to CT in all of the production areas.

Key words: *reduced tillage; conventional tillage; ploughing; fuel, variety; fertilization.*

INTRODUCTION

Over the past decades, numerous tillage techniques have appeared substituting conventional tillage (CT) comprising ploughing. These methods, i.e. conservation or reduced tillage (RT), generally do not over-turn soil and leave substantial share of crop residues on the soil surface (at least 30% of surface covered to be eligible to label 'conservation tillage'). Reduced tillage mainly helps to preserve soil moisture, to lower costs of production and to shield soils from compaction and erosion (*Holland, 2004*).

There has been extensive investigation on the effects of conservation tillage on crop yield in many zones in Europe over the last decades. Often, detailed works were carried out on the environmental and economic consequences of conservation agriculture (e.g. *Bailey et al., 2003; Hocking et al., 2003; Husnjak, Filipović & Košutić, 2002; Kisić et al., 2010; Lopez & Arrue, 1997; Răus et al, 2016; Tebrügge & During, 1999*). However, the conclusions from different works frequently appear conflicting and are therefore problematic to interpret (e.g. *Cantero-Martinez et al., 2003; Huang et al., 2011; Lopez & Arrue, 1997*). This is to be anticipated: both the agro-environmental settings as well as the method of reduced tillage applied differ substantially between individual works. The recent study of *Madarász et al.* (2016) nevertheless suggested that over the ten trial years, tillage type was a more important factor with respect to yields than the highly changeable climate of the studied years. During the first three years of changeover to RT, a reduction of 8.7% was measured, compared to CT. However, the next seven years produced a 12.7% increase of RT yields of all the crops grown.

An assessment of the particular parts of the overall costs disclosed that reduced-tillage involved herbicide costs and larger machinery, but these costs were counterweighed by lower operating costs (*Sanchez-Giron et al., 2004, 2007; Sørensen & Nielsen, 2005*). Other studies established that marginally reduced crop yields can be counter balanced by the lower fuel and labour consumption (*Gemtos et al., 1998; Bonciarelli & Archetti, 2000; Tebrügge, 2000; Šařec P. & Šařec O., 2017*). The systems with lower level of tillage intensity should be prioritized, not only for the sake of costs, but also for the sake of simpler organization due to less machinery and labour requirements (*Grubor et al., 2015*). However, the extend of benefit depends on specific situation such as farm size, cropping system etc. (*Sanchez-Giron et al., 2007*).

The objective of this work is to assess different systems of winter oilseed rape production, i.e. reduced (RT) and conventional (CT) tillage, mainly in terms of yields, fuel and labour consumption, machinery and material costs in the conditions of the Czech Republic. The assessment is based on the long-term operational monitoring of approximately 40 farms that begun in 2001. This work followed experiments carried out by the authors in Opařany in 1998 (*Šařec et al., 2002*).

MATERIALS AND METHODS

Starting in 2001/02, operational experiment has been carried out in the Czech Republic where around 40 farms growing winter oilseed rape took part in. The farms were chosen in order to represent various production zones, i.e. pedoclimatic conditions, and different soil tillage technologies. According to the tillage system used, observations were sorted into one of the two key groups, i.e. conventional tillage (CT) and reduced tillage (RT) group. Other sorting criteria, besides production year, were:

- production area: forage, potato, cereal, beet, maize;
- winter oilseed rape variety: conventional, hybrid, mixed (both types of varieties used in a field);
- application of organic fertilizers (manure, slurry, compost, sugar cane boiling residues etc.);
- application of fertilizers at sowing.

Within the experiment, the following values were monitored or measured:

- characteristics of soil: bulk density (Kopecky's cylinders of a volume of 100 cm3), gravimetric moisture, cone index (registered penetrometer PEN 70 developed at the CULS Prague);
- characteristics of individual fields: size, system of soil tillage and stand establishment, previous crop, manner of crop residue management, year of previous application of farmyard manure;
- data on conducted filed operations: machinery used, fuel and labour consumption, material applied and its rate, costs and other supplementary information;
- characteristics of crop stand: the number of plants per m2, the weight of roots, hybrid / conventional variety, yield.

Machinery costs were determined in a customary way and consisted of ownership (financing costs, depreciation, insurance and taxes, housing) and operation costs (fuel and oil costs, repair and maintenance costs, labour costs). At every farm, the amount of expenses spent, i.e. machinery and material costs, was evaluated compared to the attained seed yield, respectively revenues. Earnings from one hectare were calculated as total costs deducted from revenues, i.e. average annual farm price one ton of oilseeds multiplied by seed yield. Costs related to agricultural land and overhead costs were not comprised.

RESULTS AND DISCUSSION

During seventeen production years since 2001/02, trials were accomplished in 548 fields. Reduced tillage (RT) system of oilseed rape production was employed in 304 cases, conventional tillage (CT) in 244 cases only. This inequity developed over the monitored period, when some of the farms changed their system from CT to RT.

RT prevailed on heavy-textured soils in arid regions, i.e. in maize production area and in most of the beet production area. The most frequent tillage operations consisted of two soil cultivations, followed in some cases by a seedbed preparation. Under RT, deeper (20 cm and more) soil cultivation became regular in the course of time, and has been employed by nearly every farm recently.

CT was used predominantly by farms with lighter soils and higher annual precipitation rates that could be found in potato and marginally beet production area. The common tillage procedures consisted of a stubble cultivation followed by ploughing, and a seedbed preparation done once or twice.

Choice of the tillage system was influenced also by the equipment that a particular agricultural business owned. Disc cultivators prevailed within CT, whereas within RT, where two stubble cultivations were usual, tine cultivators were common, particularly for the second cultivation.

Application of organic fertilizers is another factor influencing costs and operational characteristics. Manure was applied mainly in forage and potato production areas, where the production of manure was sufficient and potatoes production decreasing. Therefore, manure could have been applied prior to oilseed rape. On the other hand in cereal, beet and maize production areas, where manure was applied primarily prior to sugar beet or corn maize, the application prior to oilseed rape displayed lower frequencies.

Over the monitored period of seventeen years, the average oilseed rape yield from all 548 fields was 3.74 t·ha^{-1}. Tab. 1 shows average seed yields according to several sorting criteria. Average yield attained by RT slightly surpassed the one attained by CT.

Over the first five years of the monitoring, CT yields generally surpassed RT yields (Fig. 1). But gradually, this trend turned over and RT reached higher yields. One of the reasons might be that farmers got used to the specific requirements and opportunities of RT system and may have improved it over time,

e.g. by employing the deeper soil loosening. Favorable effect of RT may have been gradual and required time to arise. Yet another reason may relate to recent weather development with higher temperatures and lower precipitations, where RT may have helped with better soil moisture management.

Concerning regionalization, potato production area demonstrated the highest average yield, followed by beet production area, while maize production area, where only RT was used, proved inferior results. Seed yields attained by RT exceeded those produced using CT in all of the production areas except the forage one.

Relatively small frequencies and uneven distribution of cases into individual categories may have influenced the results. For example RT was the only tillage system employed in maize production area. Results of CT were therefore not harmed due to unsuitability of maize production area in terms of winter oilseed rape growing.
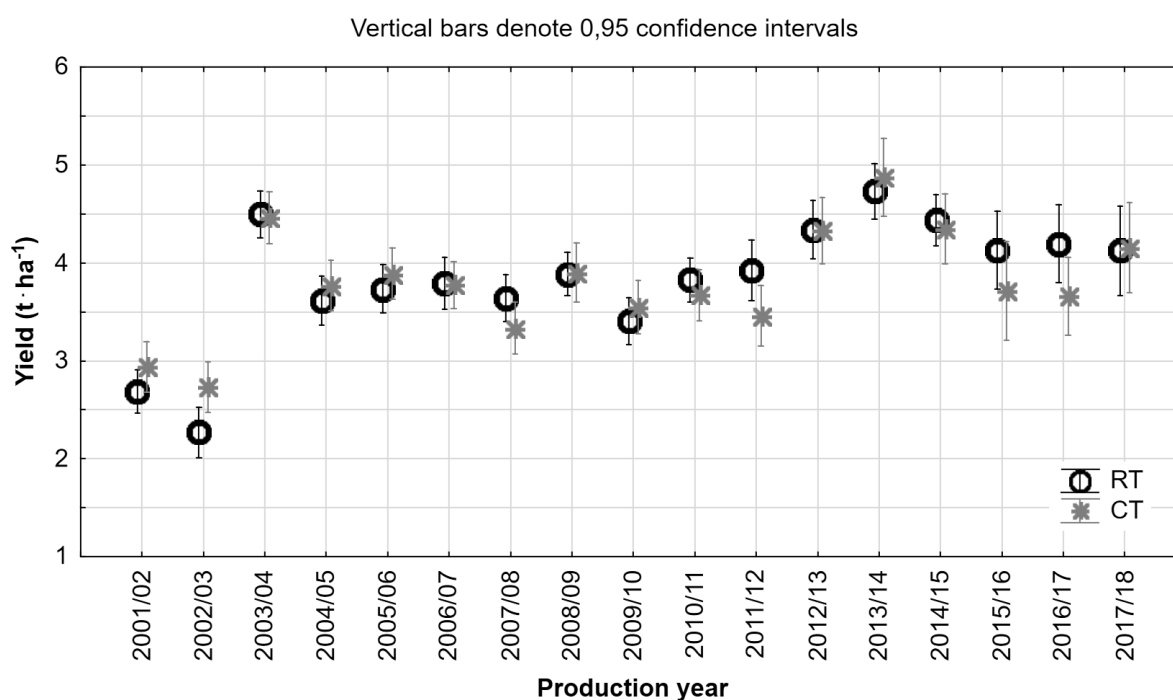

Fig. 1 Graph of time development of oilseed rape yields produced by reduced (RT) and conventional (CT) tillage systems

Statistical analysis of seed yields showed no significant differences with regard to the tillage system used, to fertilizer application at sowing, and to organic fertilizer application. Oilseed rape variety type (*t*-Test, $n = 538$ – mixed varieties excluded, $p = 0,037449$), and production area (*Turkey HSD* test) were the two sorting criteria where significant differences were demonstrated between the average rape yields. The trials thus correspond only partly with what *Madarász et al.* (2016) proved, i.e. by 12.6 % significantly higher rape yield of conservation compared to ploughing technology over ten-year period. One reason might be the monitoring and operational character of the trials, another one the differences in local climatic and other conditions.

Technological and economic variables, i.e. fuel consumption, labour consumption, machinery, material and total costs, unit costs per ton of production and earnings per hectare, were statistically significantly influenced by the application of organic fertilizers. This operation is demanding in terms of fuel, labour as well as costs. In order to avoid its influence, observations with organic fertilizer involved were excluded from further analysis. Tab. 2 thus presents the effect of soil tillage systems on the above mentioned technological and economic variables in the cases, where no organic fertilizers were used. Statistically significant differences between RT and CT were proved in terms of fuel and labour consumption, and machinery costs.

Tab. 1 Oilseed rape yields and frequencies of cases with respect to tillage system, production area and other factors

| | Tillage system | | | | Aggregate | |
| | Reduced tillage (RT) | | Conventional tillage (CT) | | | |
	Yield (t·ha⁻¹)	Frequency	Yield (t·ha⁻¹)	Frequency	Yield (t·ha⁻¹)	Frequency
Production area						
Forage	3.45	32	3.62	12	3.49 [ab]	44
Potato	4.21	22	3.82	71	3.91 [c]	93
Cereal	3.56	92	3.54	51	3.55 [a]	143
Beet	3.93	142	3.73	110	3.84 [bc]	252
Maize	3.33	16	—	—	3.33 [ab]	16
Variety						
Conventional	3.68	123	3.62	88	3.65 [b]	211
Hybrid	3.82	179	3.77	148	3.80 [a]	327
Mixed	2.33	2	3.58	8	3.33	10
Organic fertilizers						
No	3.72	221	3.70	137	3.71 [a]	358
Yes	3.85	83	3.73	107	3.78 [a]	190
Fertilizers at sowing						
No	3.75	188	3.70	239	3.72 [a]	427
Yes	3.76	116	4.07	5	3.77 [a]	121
Aggregate	3.75 [a]	304	3.71 [a]	244	3.74	548

The findings of *Sanchez-Giron et al.* (2004, 2007) on higher herbicide, i.e. material, costs of RT was thus not verified, contrary to the conclusion on lower machinery costs. Decrease in fuel and labour consumption (*Bailey et al., 2003; Bonciarelli and Archetti, 2000; Gemtos et al., 1998; Tebrügge, 2000; Grubor et al., 2015*) was validated entirely.

Tab. 2 Effect of reduced (RT) and conventional (CT) tillage systems on yield, technological and economic variables of oilseed rape production excluding cases with organic fertilizer application (*t*-Test)

Variable	RT	CT	p-value
Frequency	221 [a]	137 [a]	—
Yield (t·ha⁻¹)	3.72 [a]	3.70 [a]	0.814660
Fuel consumption (l·ha⁻¹)	66.02 [a]	78.29 [b]	<0.000001
Labour consumption of stand establishment (hrs·ha⁻¹)	1.16 [a]	1.86 [b]	<0.000001
Labour consumption (hrs·ha⁻¹)	3.32 [a]	4.06 [b]	<0.000001
Machinery costs (CZK·ha⁻¹)	5,983.22 [a]	6,706.03 [b]	0.000002
Material costs (CZK·ha⁻¹)	12,177.81 [a]	11,613.22 [a]	0.062611
Total costs (CZK·ha⁻¹)	18,321.67 [a]	18,542.60 [a]	0.533736
Unit costs (CZK·t⁻¹)	5,249.68 [a]	5,244.37 [a]	0.978239
Revenues per ha (CZK·ha⁻¹)	31,538.84 [a]	31,294.48 [a]	0.833348
Earnings per ha (CZK·ha⁻¹)	13,217.17 [a]	12,751.88 [a]	0.660559

With respect to the earnings per hectare (Fig. 2), the best results were reached in potato and beet production areas with RT in both, followed by CT in potato zone, and by cereal production area with both RT and CT.
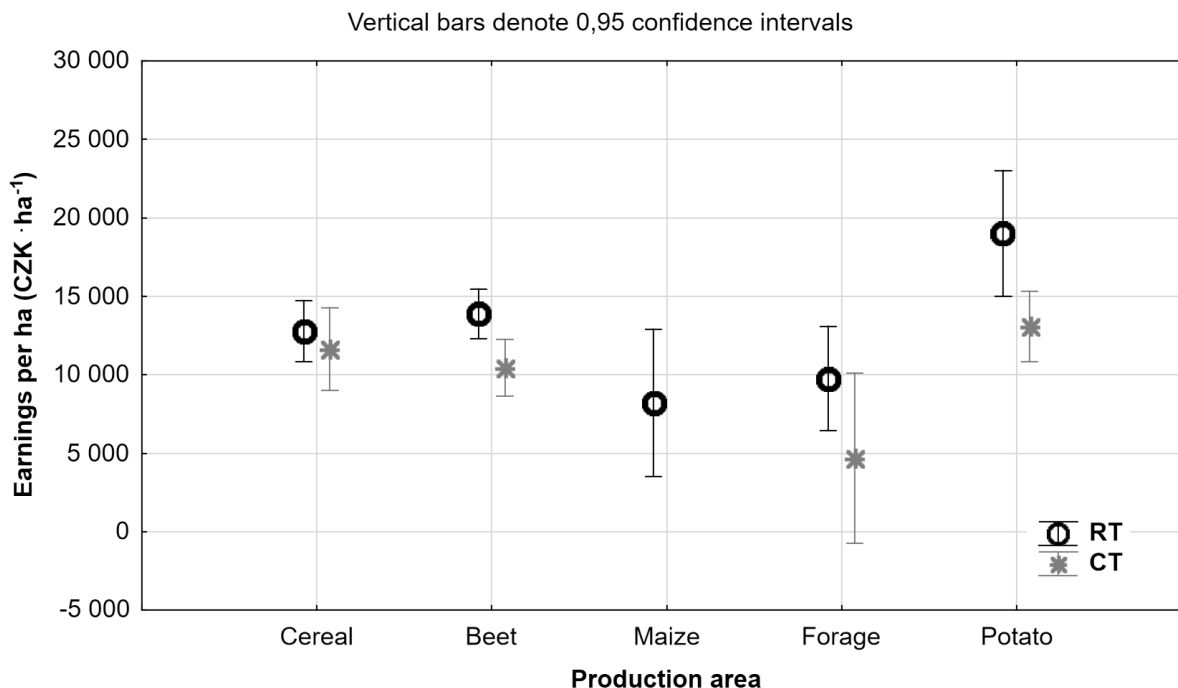
Fig. 2 Graph of earnings per hectare of oilseed rape regarding production areas and reduced (RT) and conventional (CT) tillage systems

CONCLUSIONS

When excluding cases with organic fertilizer application, the average fuel consumption of RT was by 15.7 % lower than that of the CT, the labour consumption of stand establishment was lower by 37.7 %, the overall labour consumption again lower by 18.4 %, and finally the machinery costs lower by 10.8 %. All the above mentioned differences proved statistically significant. The total costs were lower by mere 1.2 %. On the other hand, yields reached by RT were slightly higher, i.e. by 0.6%. The resulting unit costs of seed production were nearly identical. The potatoes production area proved to be the most favourable in terms of oilseed rape yields. Beet production area demonstrated also good results, namely over the recent years. In all of the production areas except the forage one, average seed yields reached by RT surpassed those produced using CT. Concerning earnings per hectare, RT results proved outstanding with regard to CT in all of the production areas.

RT confirmed to be an adequate alternative to CT from the viewpoint of oilseed yields, of economics as well as of fuel and labour consumption, particularly when employed on purpose and systematically. Lately, RT with deeper soil loosening has spread increasingly, namely in order to ensure the disruption of compacted layers.

REFERENCES

1. Bailey, A., Basford, W., Penlington, N., Park, J., Keatinge, J., Rehman, T., Tranter, R. & Yates, C. (2003). A comparison of energy use in conventional and integrated arable farming systems in the UK. *Agriculture Ecosystems & Environment, 97*(1-3), 241-253.
2. Bonciarelli, F. & Archetti, R. (2000). Energy saving through reduction of soil tillage. In: *15th ISTRO Conference*. TX, USA: Fort Worth. [CD-ROM]
3. Cantero-Martinez, C., Angas, P. & Lampurlanes, J. (2003). Growth, yield and water productivity of barley (hordeum vulgare

l.) affected by tillage and N fertilization in Mediterranean semiarid, rainfed conditions of Spain. *Field Crops Research, 84*, 341–357.
4. Gemtos, T.A., Galanopoulou, S. & Kavalaris, C. (1998). Wheat establishment after cotton with minimal tillage. *European Journal of Agronomy, 8*, 137–147.
5. Grubor, M., Maletic, I., Lakic, J., Kovacev, I. & Kosutic, S. (2015). Economic efficiency of winter wheat and oil seed rape production in different soil tillage systems. In *43rd International Symposium on Agricultural Engineering* (pp. 265–274). Agronomski Fakultet

Sveucilista u Zagrebu, Opatija, Croatia.

6. Hocking, P.J., Mead, J.A., Good, A.J. & Diffey, S.M. (2003). The response of canola (Brassica napus L.) to tillage and fertiliser placement in contrasting environments in southern New South Wales. *Australian Journal of Experimental Agriculture*, *43*(11), 1323–1335.

7. Holland, J. (2004). The environmental consequences of adopting conservation tillage in Europe: reviewing the evidence. *Agriculture Ecosystems and Environment*, *103*, 1–25.

8. Huang, M., Zou, Y, Feng, Y., Cheng, Z., Yali Mo, Y., Ibrahim, M., Xia, B. & Jiang, P. (2011). No-tillage and direct seeding for super hybrid rice production in rice–oilseed rape cropping system. *Europ. J. of Agronomy, 34*, 278-286.

9. Husnjak, S., Filipović, D. & Košutić, S. (2002). Influence of different tillage systems on soil physical properties and crop yield. *Rostlinna Vyroba, 48*(6), 249-254.

10. Kisić, I., Bašić, F., Birkas, M., Jurišić, A. & Bićanić, V. (2010). Crop yield and plant density under different tillage systems. *Agriculturae Conspectus Scientificus, 75*(1), 1–7.

11. Madarász, B., Juhos, K., Ruszkiczay-Rüdiger, Z., Benke, S., Jakab, G. & Szalai, Z. (2016). Conservation tillage vs. conventional tillage: long-term effects on yields in continental, sub-humid Central Europe, Hungary. *International Journal of Agricultural Sustainability*, *14*(4), 408-427.

12. Lopez, M. & Arrue, J. (1997). Growth, yield and water use efficiency of winter barley in response to conservation tillage in a semi-arid region of Spain. *Soil and Tillage Research, 44*, 35–54.

13. Răus, L., Jităreanu, G., Ailincăi, C., Pârvan, L. & Țopa, D. (2016). Impact of different soil tillage systems and organo-mineral fertilization on physical properties of the soil and on crops yield in pedoclimatical conditions of Moldavian plateau. *Romanian Agricultural Research*, *33*, 111–123.

14. Sanchez-Giron, V., Serrano, A., Hernanz, J. & Navarrete, L. (2004). Economic assessment of three long-term tillage systems for rainfed cereal and legume production in semiarid central Spain. *Soil and Tillage Research, 78*, 35–44.

15. Sanchez-Giron, V., Serrano, A., Suarez, M., Hernanz, J. & Navarrete, L. (2007). Economics of reduced tillage for cereal and legume production on rainfed farm enterprises of different sizes in semiarid conditions. *Soil and Tillage Research, 95*, 149–160.

16. Šařec, O., Šařec, P. & Kavka, M. (2002). Different methods of cropstand establishment within the system of winter oilseed rape cultivation. *Research in Agricultural Engineering, 48*(2), 66–72.

17. Šařec, O. & Šařec, P. (2017). Results of fifteen-year monitoring of winter oilseed rape (Brassica napus L.) production in selected farm businesses of the Czech Republic from the viewpoint of technological and economic parameters. *Agronomy Research, 15*(5), 2100-2112.

18. Sørensen, C.G., Nielsen, V. (2005). Operational analyses and model comparison of machinery systems for reduced tillage. *Biosystems Engineering, 92*(2), 143-155.

19. Tebrügge, F. (2000). Long-term no-tillage as a tool to protect the environment, results of 20 year field trials on different kinds of soil in different crop rotations. In: *15th ISTRO Conference*. TX, USA: Fort Worth. [CD-ROM].

20. Tebrügge, F. & During, R.A. (1999). Reducing tillage intensity - a review of results from a long-term study in Germany. *Soil & Tillage Research, 53*(1), 15–28.

Corresponding author:
doc. Ing. Petr Šařec, Ph.D., Department of Machinery Utilization, Faculty of Engineering, Czech University of Life Sciences Prague, Kamýcká 129, Praha 6, Prague, 16521, Czech Republic, phone: +420 22438 3147, e-mail: psarec@tf.czu.cz

EFFECT OF ORGANIC FERTILIZERS, BIOCHAR AND OTHER CONDITIONERS ON MODAL LUVISOL

Petr ŠAŘEC[1], Václav NOVÁK[1], Kateřina KŘÍŽOVÁ[1]

[1]Dep. of Machinery Utilization, Faculty of Engineering, Czech University of Life Sciences Prague

Abstract

The paper assesses changes in soil physical properties, i.e. bulk density, cone index, and implement draft, after the application of organic fertilisers, i.e. manure and compost, and manure and soil conditioners, Z'fix, NeoSol, and biochar. Biochar and traditional manure demonstrated favourable influence on soil bulk density, cone index and tillage implement draft. The manure treated by Z'fix demonstrated higher bulk density and draft, though it reached highest silage maize yields. Compost and NeoSol exhibited increased bulk density, but reduced draft on the opposite.

Key words: *cattle manure; NeoSol; Z'fix; compost; cone index; bulk density.*

INTRODUCTION

Over the past few decades, the demands on agricultural production have been growing rapidly. The pressure increases mostly due to the climate change, changes in crop rotation, decreasing area of the arable land, reduction of livestock farming. According to the Czech Statistical Office (*Sálusová, 2018*), cattle production has declined by more than half in the past 30 years. Intensification of agriculture has caused the lack of quality soil organic matter (SOM) that is on the European scale one of the staple causes of decreasing soil productivity (*Stolte et al., 2016*). This phenomenon causes a reduction in the diversity and fertility of arable land and it is associated with other soil degradation issues *(Gardi, Jeffery & Saltelli, 2013*). Besides soil fertility, SOM is associated with soil structure and other properties (*Walsh & McDonnell, 2012*). It is also known that organic matter naturally reduces soil compaction (*Chakraborty & Mistri, 2017*), which is a very serious issue. Only in Europe, even about 33 million hectares are threatened by soil compaction (*Alaoui & Diserens, 2018*). Compaction strongly affects root growth, since the conditions of water and gas transport in the soil are not optimal (*Stolte et al., 2016*). Of course, this situation often results in reduced crop yield. Soil compaction can be easily measured by cone penetrometer. Bulk density is another frequently used option for measurement (*Odey, 2018*).

Organic materials added to soil profile have a beneficial effect on reclaiming and improving the physical quality of degraded soil (*Are et al., 2017*). The application of manure or compost contributes to the increasing content of SOM (*Panagos et al., 2015*). The use of manure improves the physical, biological and chemical properties of soil (*Ludwig et al., 2007*). The manure or directly soil can be treated with so called activators or conditioners that still are not thoroughly explored. However, current studies suggest that activators improve soil properties and plant growth conditions (*Borowiak et al., 2016*). Thus when using activators, there are not only economic benefits, e.g. a reduction of the energy intensity of soil tillage (*Šařec & Žemličková, 2016*), but also a contribution to the environmental sustainability of agriculture (*Šařec & Novák, 2017*).

In recent years, biochar has gained the considerable attention. This carbon-based product of pyrolysis is made mostly of waste plant (*Mukherjee & Lal, 2013*). It is a highly porous material that affects water retention capacity (*Rasa et al., 2018*), and therefore improves soil properties. However, effect of biochar applied into the soil strongly depends on input material for the pyrolysis process and also on the pyrolysis temperature (*Lei & Zhang, 2013*).

The authors of these studies generally agree that activators and biochar should be tested on different soil types and conditions. Therefore, this study aims to determine the effect of activators, compost, and biochar for soil physical properties after one year of application.

MATERIALS AND METHODS

In 2017, experimental variants were established near the town of Větřkovice in the Moravian-Silesian Region of the Czech Republic (N 49°47.232', E 17°50.028', 501 m a. s. l.). In 2018, silage maize (LG 30.248, FAO 250) was grown on the plot, while it was sown on the 26th April 2018 and harvested on

the 30th August 2018. Soil type of the filed was *Modal Luvisol*, and soil texture defined as loam soil. Soil properties are presented more in detail in Tab. 1. The experimental area was divided into eight smaller plots of 170 x 30 m for each variant. Fertilization management of individual variants is shown in Tab. 2. NeoSol (PRP Technologies, France) was used as the activator of biological transformation of soil organic matter. Biochar was used in the same way. Z'fix (PRP Technologies, France) was used as the activator of manure. It was applied to the bedding of cattle deep litter housing at a recommended weekly dose. These conditioners cannot be considered as fertilizers due to their low content of active components. Dosage of cattle manure was 50 t·ha⁻¹ (2017), of NeoSol 150 kg·ha⁻¹ (2017, 2018), of biochar 15 t·ha⁻¹ (2017), of compost 50 t·ha⁻¹ (2017), and of additional NPK according to crop common practice (2017, 2018). All the other field operations and material applied did not differ among variants.

Tab. 1 Soil properties of the field prior to the experiment in 2017

	Soil depth (m)	
	0.00–0.30	0.30–0.60
Soil Aggregate Stability - SAS (%)	62.9	54.7
pH/KCl	4.4	4.5
Humus content (%)	2.8	2.3
Humic Acid / Fulvic Acid ratio	1	2.1
Microbial biomass carbon - Cmic ($\mu g \cdot g^{-1}$)	3.28	2.23
C / N ratio	9.55	5.50

The registered penetrometer PEN 70 (CULS Prague) was used to determine the cone index, while ten measurements were done for each variant. Soil moisture was measured by Theta Probe (Delta-T Devices Ltd, UK). To obtain undisturbed soil samples from the depth of 0.05 to 0.10 m and subsequently soil bulk density, Kopecky cylinders with a volume of 100 cm³ were utilized. The implement draft was measured by dynamometer with strain gauge S-38/200kN (Lukas, the Czech Republic). This device was placed between two tractors. The working tractor was John Deere 6150R (rated engine power 111.9 kW) in 2017, and Fendt 826 Vario (rated engine power 190.9 kW) in 2018. In both years, six furrow plough PHX 6-30 was used as an implement. On each variant, there were several crossings of the measuring set. First, overall draft of the pulled tractor and working implement were measured. The plough worked at a constant speed, and the tillage depth was checked after each pass. After that, the same measurements were carried out with implement not working in order to obtain only machinery rolling resistances and forces induced by potential field gradient. The system NI CompactRIO (National Instruments Corporation, USA) was used for data collection with sampling frequency of 0.1 s. Acquired data were assigned to individual variants using Trimble Business Center 2.70 (Trimble, USA). Measuring dates were 10th September 2017 and 10th October 2018. Data was processed by MS Excel (Microsoft Corp., USA) and Statistica 12 (Statsoft Inc., USA).

Tab. 2 Fertilization of individual variants and maize silage yields in 2018

Variant	Fertilization	Yield ($t \cdot ha^{-1}$)
N-1	Cattle manure with Z'Fix + NPK	44.2
N-2	Cattle manure with Z'Fix + NeoSol + NPK	43.2
N-3	Cattle manure + NPK	41.6
N-4	Cattle manure + NeoSol + NPK	42.4
N-5	NeoSol + NPK	40.2
N-6	NPK - Control	38.2
N-7	Compost + NPK	41.8
N-8	Biochar + NPK	42.8

RESULTS AND DISCUSSION

The variants attained higher silage maize yield than the control (Tab. 2). The variants with manure treated by Z'fix (N-1 and N-2) attained the highest yields, most probably due to its high nitrogen content (*Šařec, Látal & Novák, 2017*). High yield was reached also by the biochar variant (N-8), which is in accordance with the findings of *Are et al.* (2017). NeoSol (N-5) demonstrated favourable effect as well, which confirms the work of *Borowiak et al.* (2016).

All the measured values were analyzed relative to the control Variant N-6 rather than analyzing the absolute values. In this way, differing weather conditions of individual years were allowed for. Bulk density values related to the average value of respective control Variant N-6 that are displayed in Fig. 1 did not differ significantly according to the *Analysis of Variance* with regard to both factors separately, i.e. to the variant and to the measurement date, nor with regard to their combination. Nevertheless, there is a visible bulk density increase after the application of compost (N-7) and of manure treated with Z'fix (N-1 and N-2). The manure treated in such a way contains less straw that is in addition more decomposed and is therefore denser. The condition of the compost was the same case. On the other hand, bulk density slightly decreased after the biochar application (N-8). *Are et al.* (2017), *Mukherjee & Lal* (2013) and *Lei & Zhang* (2013) described also bulk density reduction after biochar application. On the contrary, *Are et al.* (2017) found bulk density reduction also after veticompost application.
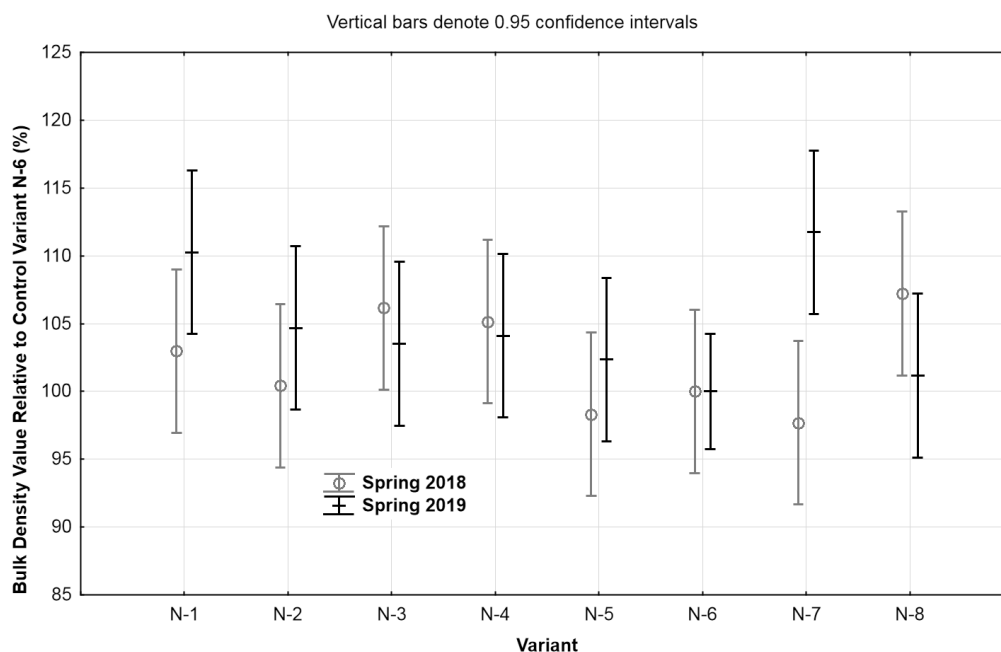

Fig. 1 Graph comparing relative differences of bulk density values from the depth of 0.05 to 0.10 m in spring 2018 and 2019 for individual variants (Variant N-6 as 100%)

Since cone index values depend strongly on soil moisture, they were measured also in spring, i.e. on 22nd April 2018 and on 23rd April 2019, when soil moisture was more likely to be homogenous. Cone index values were again analyzed relative to the control Variant N-6, as is presented in Fig. 2. The *Analysis of Variance* did not prove statistically significant differences for the combination of all the factors in question, i.e. measurement date, variant and depth. Considered separately though, factors' average cone index differences were statistically significant. For the variants with manure application, i.e. N-1 to N-4, cone index values decreased at shallow depths to up to 20 cm. This corresponds with the findings of *Celik et al.* (2010) and *Šařec & Žemličková* (2016). Deeper on the other hand, the values generally slightly increased for the mentioned variants. Since the manure application had taken place before the first measurement was carried out, the increased cone index values below tilled profile cannot be assigned to the additional pass of a manure spreader. The variants with NeoSol and compost used, i.e. N-5 and N-7, demonstrated no evident pattern except for the increased cone index average at the depth of 24 cm. The application of biochar (N-8) decreased cone index values at shallower depths without having increased them deeper.
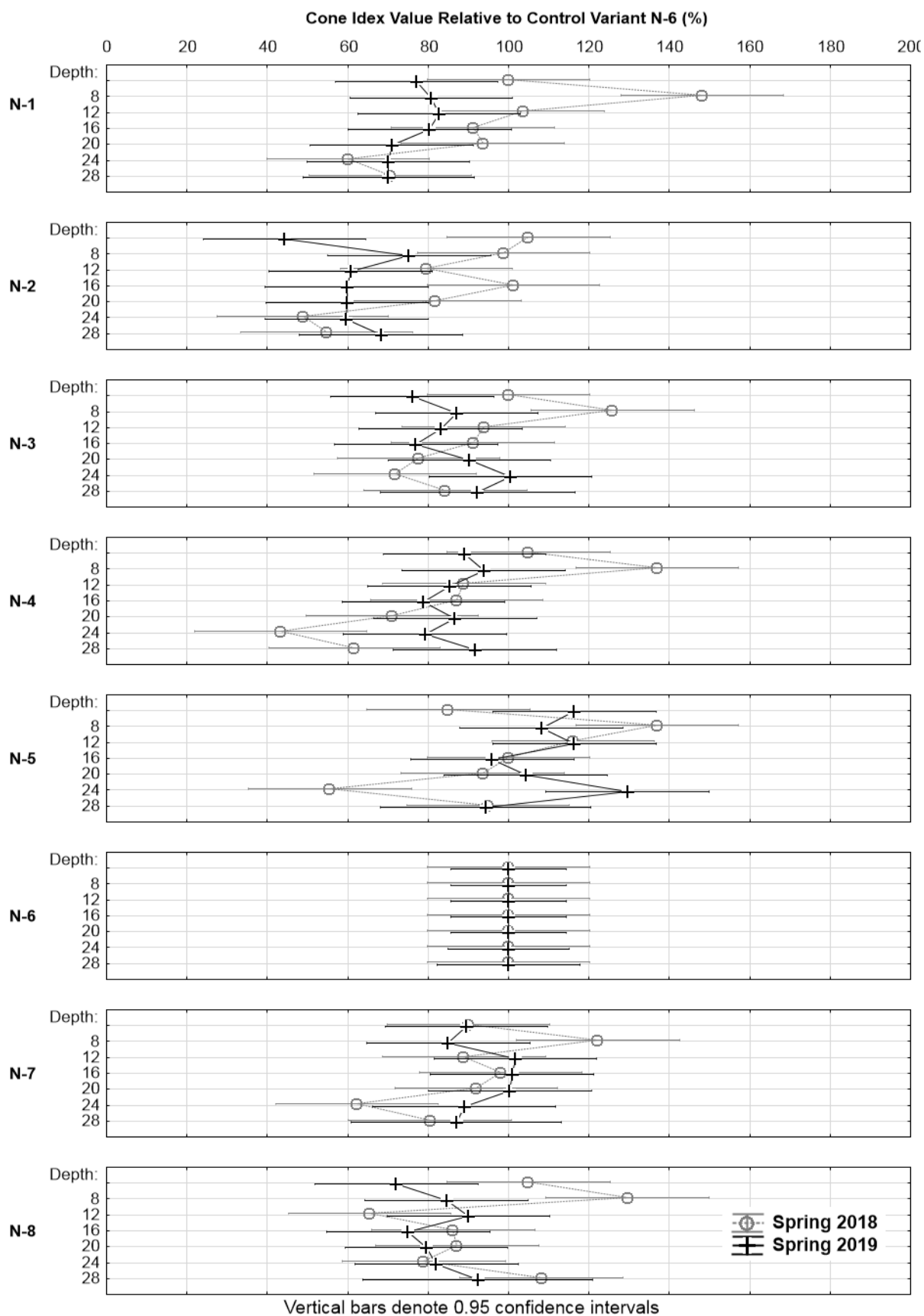
Fig. 2 Graphs comparing relative differences of soil cone index values in spring 2018 and 2019 for individual variants (Variant N-6 as 100%)

Implement draft was measured in autumn, i.e. on 10th October 2017 prior to the application of manure and other substances, and on 10th September 2018. Tillage depth attained in average 0.210 m in 2017 and 0.206 m in 2018. Soil moisture differed statistically significantly (p = 4.89504643598622 · 10^{-23}) having been 27.6% vol. in 2017 and 13.1% vol. in 2018. The decreased moisture caused an increase in overall unit implement draft across all variants, i.e. from 63960.88 N · m^{-2} in 2017 to 65929.05 N · m^{-2} in 2018. The difference was highly significant (p = 0.000845), although the implement used was the same for both years. Draft values were therefore assessed relative to the control Variant N-6, as is shown in Fig. 3. The *Analysis of Variance* confirmed statistically significant differences with respect to the variants, but measurement date and the combination of both factors proved insignificant. Generally, average implement draft values decreased relative to the control, with the exception of the manure treated by Z'fix (N-1 and N-2), which was denser than the untreated one as mentioned above.
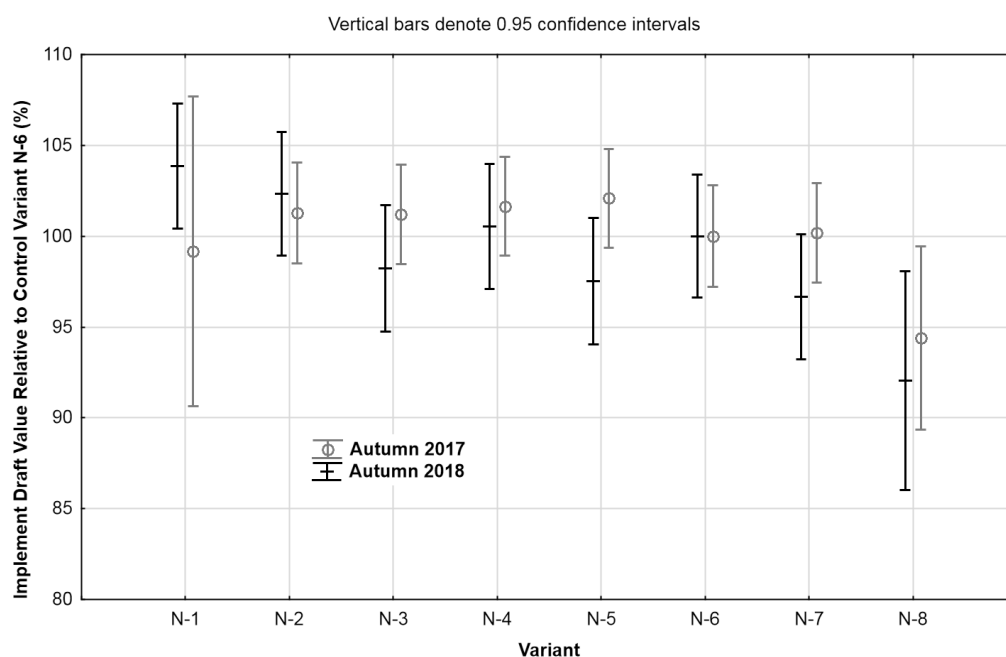

Fig. 3 Graph comparing relative differences of implement unit draft values in autumn 2017 and 2018 for individual variants (Variant N-6 as 100%)

CONCLUSIONS
The experiment focused on the effect of organic fertilizers and conditioners on soil physical properties was conducted. Biochar demonstrated favourable influence on soil bulk density, cone index and tillage implement draft. The same can be to some extent stated on the effect of traditional manure. The manure treated by Z'fix demonstrated higher bulk density and draft, though it reached highest silage maize yields. Compost and NeoSol exhibited increased bulk density, but reduced draft on the opposite. It is necessary to carry on with the research for a prolonged period, so that changes can manifest themselves.

ACKNOWLEDGMENT

REFERENCES

1. Alaoui, A. & Diserens, E. (2018). Mapping soil compaction – A review. *Current Opinion in Environmental Science & Health*, 5, 60–66.
2. Are, K.S., Adelana, A.O., Fademi, I.O. & Aina, A.O. (2017). Improving physical properties of degraded soil: Potential of poultry manure and biochar. *Agriculture and Natural Resources, 51*(6), 454–462.
3. Borowiak, K., Niewiadomska, A., Sulewska, H. Szymanska, G., Gluchowska, K. & Wolna-

Maruwka, A. (2016). Effect of PRP SOL and PRP EBV nutrition on yield, photosynthesis activity and soil microbial activity of three cereal species. *Fresenius Environmental Bulletin, 25*(6), 2026–2035.

4. Celik, I, Gunal, H., Budak, M. & Akpinar, C. (2010). Effects of long-term organic and mineral fertilizers on bulk density and penetration resistance in semi-arid Mediterranean soil conditions. *Geoderma, 160*, 236-263.

5. Chakraborty, K. & Mistri, B. (2017). Estimation of soil compaction from bulk density and its effect on crop production. *Indian Journal of Spatial Science, 8*(2), 101–107.

6. Gardi, C., Jeffery, S. & Saltelli, A. (2013). An estimate of potential threats levels to soilbiodiversity in EU. *Global Change Biology, 19*(5), 1538–1548.

7. Lei, O. & Zhang, R. (2013). Effects of biochars derived from different feedstocks and pyrolysis temperatures on soil physical and hydraulic properties. *Journal of Soils and Sediments*, *13*(9), 1561–1572.

8. Ludwig, B., Schulz, E., Rethemeyer, J., Merbach, I. & Flessa, H. (2007). Predictive modelling of C dynamics in the long-term fertilization experiment at Bad Lauchstadt with the Rothamsted Carbon Model. *European Journal of Soil Science, 58*(5), 1155–1163.

9. Mukherjee, A. & Lal, R. (2013). Biochar impacts on soil physical properties and greenhouse gas emissions. *Agronomy*, *3*(2), 313–339.

10. Odey, S.O. (2018). Overview of engineering problems of soil compaction and their effects on growth and yields of crops. *European Journal of Advances in Enineering and Technology, 5*(9), 701–709.

11. Panagos, P., Borelli, P., Meusburger, K., Alewell, C., Lugato, E. & Montanarella, L. (2015). Estimating the soil erosion cover-management factor at the European scale. *Land Use Policy, 48*, 38–50.

12. Rasa, K., Heikkinen, J., Hannula, M., Arstila, A., Kulju, S. & Hyväluoma, J. (2018). How and why does willow biochar increase a clay soil water retention capacity? *Biomass and Bioenergy*, *119*, 346–353.

13. Sálusová, D. (2018). *Czech agriculture from the viewpoint of statistics* (in Czech). Prague: Czech Statictical Office.

14. Šařec, P., Látal, O. & Novák, P. (2017). Technological and economic evaluation of manure production using an activator of biological transformation. *Res. Agr. Eng.*, *63*(Special Issue), 59-65.

15. Šařec, P. & Novák, P. (2017). Influence of manure and activators of organic matter biological transformation on selected soil physical properties of Modal Luvisol. *Agronomy Research, 15*(2), 565–575.

16. Šařec, P. & Žemličková, N. (2016). Soil physical characteristics and soil-tillage implement draft assessment for different variants of soil amendments. *Agronomy Research*, 2016, *14*(3), 948–958.

17. Stolte, Jannes et al. (2016). *JRC Scientific and Technical Reports - Soil Threats in Europe*. Luxembourg: JRC Science Hub.

18. Walsh, E. & McDonnell, K.P. (2012). The influence of added organic matter on soil physical, chemical, and biological properties: a small-scale and short-time experiment using straw. *Archives of Agronomy and Soil Science, 58*(SI 1), S201–S205.

Corresponding author:

doc. Ing. Petr Šařec, Ph.D., Department of Machinery Utilization, Faculty of Engineering, Czech University of Life Sciences Prague, Kamýcká 129, Praha 6, Prague, 16521, Czech Republic, phone: +420 22438 3147, e-mail: psarec@tf.czu.cz

FORCE REQUIREMENTS OF DIFFERENT MANUAL PRUNING SHEARS WHEN CUTTING ABELIA *(ABELIA GRANDIFLORA)* BRANCHES

Kemal Çağatay SELVİ[1], Önder KABAŞ[3], Mehmet KARATAŞ[2]

[1]*Department of Mechanical Engineering, Faculty of Engineering, Czech University of Life Sciences Prague, Czech Republic*
[2] *Department of Agricultural Machines and Technologies Engineering, Faculty of Agriculture, Ondokuz Mayıs University, Samsun/TURKEY*
[3]*Vocational School of Technical Sciences, Akdeniz University, Antalya, TURKEY*

Abstract
The article is focused on comparative investigation of some pruning shears(bypass) in terms of cutting forces and design when cutting Abelia branches. Three different by-pastype pruning shears were selected to evaluate. Abelia branches were used as a material in the tests. The experiments were carried out at a constant speed of 300 mm/min and 6 replicates in two different diameter groups (4.89 mm and 6.93 mm). The shear force data was obtained using a Lloyd tester and a computer with NEXYGEN software. The diameters of braches were included in the model as covariates and their effect was eliminated from the model and only the effect of the design characteristics of the shears on the force values was investigated. The LSD test was used for comparisons between means and covariance analysis was used for data analysis. The results were statistically significant at 1% significance level. According to the results; the smallest force values were obtained by first shear for both diameter groups (32.54 N-85.11 N). All the data were taken into consideration; it was seen that the first shears performed the same process with less force than the other shears in terms of cutting forces.

Key words: pruning shear; shear force; abelia branch; ergonomic design.

INTRODUCTION
The genus Abelia contains 30 species that vary in many traits including cold hardiness, flower color, and growth habit. Abelia ×grandiflora (André) Rehd. is widely used in the landscape because of its prolific floral displays of pinkish-white flowers and glossy semi-evergreen to evergreen foliage *(Scheiber, Robacker & Lindstrom, 2002)*. (Fig. 1).

Fig. 1 Abelia (Abelia grandiflora)

Pruning process is an important part of cutting flower cultivation. Production costs and power requirement are very high and labor efficiency is lower than the other operations *(Pekitkan, Eliçin & Sessiz, 2019)*. Pruning is regular and productive technique practiced in ornamental plants for controlling the growth, enhancing the yield and shaping the plant *(Akhtar, Akram, Sajjad & Farooq, 2016)*. Furthermore, from an ergonomic point of view, it is possible to say that pruning is also in the category of repetitive work. In general, most manual pruning shears fall into two basic types: anvil and bypass. (Fig.

2). Finally, some pruning shears require a bigger hand force to cut a given thickness of branch than do other models.

Fig. 2 Bypass and Anvil type pruning shears

Fig. 3 Lloyd instrument universal testing machine

Regarding manual repetitive works, some limit values for human health have been reported, such as pruning in agricultural production and maintenance. According to the EN-1005-3 standard, it is desirable that the force to be applied by the hand is not above 300 N and desirable values should be in the rage of 150-200 N, if possible. There are many references to pruning and pruning shears in the literature, but they do not address hand force for repetitive actions or design effect on efficiency. They are generally dealing with information on plant properties and the power or energy requirements of an equipment (*Persson, 1987; Emadi, Kosse & Yarlagadda, 2004; Voicu, Moiceanu, Sandu & Poenaru, 2011; Esehaghbeygi, Hoseinzadeh, Khazaei & Masoumi, 2009; Hoseinzadeh &Shirneshan, 2012; Selvi & Kabaş, 2016*). No references to tests of pruning shear hand force requirements were found enough about ornamentals. The objective of this study was to compare low cost bypass hand pruning shears and which ones required the low hand force especially in terms of their design and also for hand health according repetitive works.

MATERIALS AND METHODS
Plant material
In the shear tests, abelia branches were obtained from a commercial garden in Samsun province located in North of the Turkey. The test samples were randomly cut by hand from garden. The collected branches were transported to the laboratory at the Department of Agricultural Machinery and Technologies Engineering, University of Ondokuz Mayıs which were then placed in a refrigerator at 5 °C until the time of the cutting tests. The test procedure consisted of measuring the force on the handle required to cut abelia branches in two different diameters: 4.89 mm and 6.93 mm.

Pruning shears
Three low cost hand pruning shears were selected for evaluation in this study. The models are listed in Table 1, together with some properties.

Tab.1 Some properties of low cost hand pruning shears

			Dimensions mm	A	150
				B	156
				C	67

Model name	Type	Blade thickness mm	Blade angle °	Weight g	Cost Euro
Bulmax BMX-286	By-pass	2.2	8.25	471	5.21

			A	123
	Dimensions mm		B	136
			C	52

Model name	Type	Blade thickness mm	Blade angle °	Weight g	Cost Euro
Akman	By-pass	3.7	21.05	187	4.78

			A	150
	Dimensions mm		B	150
			C	60

Model name	Type	Blade thickness mm	Blade angle °	Weight g	Cost Euro
Yeniay	By-pass	4.4	13.71	365	3.79

All of the pruning shears were purchased new for this evaluate. The plant materials were pre-experimented to simulate manual cutting, with a repetition of 300 mm/min at constant speed and 2 different diameter groups (4.89 mm and 6.93) with 10 replications.

Testing device and apparatus

The force required to cut hazelnut suckers with different pruning shears was measured by a Lloyd Instrument Universal Testing Machines (Lloyd Instrument LRX Plus, Lloyd Instruments Ltd, An AMATEK Company). The device has three main parts: moving head, driving unit and data acquisition system (load cell, note book and connections and NEXYGEN Plus software). The device was equipment with a load cell of 1000 N and measurement accuracy of load cell was 0.5%.
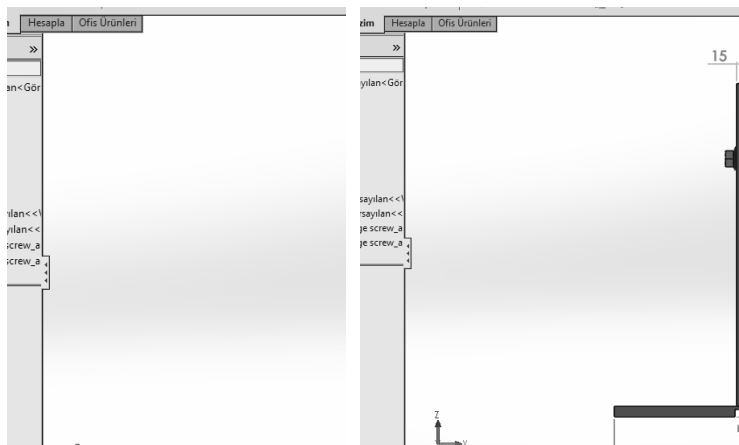

Fig. 4 Clamping apparatus to the Lloyd LRX Plus tester

Load cell was fixed to moving head (Fig.3). In the experiments, a clamping apparatus has been manufactured in order to enable the cutting shears to perform the correct cutting operation and to be mounted on the test device. The detail picture and dimensions of the clamping apparatus is shown in Fig. 4.

RESULTS AND DISCUSSION

The mean forces of the pruning shear to cut abelia branches are shown in Fig.5 and Fig.6. All three hand shears were able to cut all branches belonging to two different diameter groups in the experiment. Significant differences in cutting force requirements were noted. In the first diameter group; the highest shear force value was found to be 163.86 N for second diameter and at second shear, whereas the smallest shear force value was 32.54 N for first diameter group and at first pruning shear.
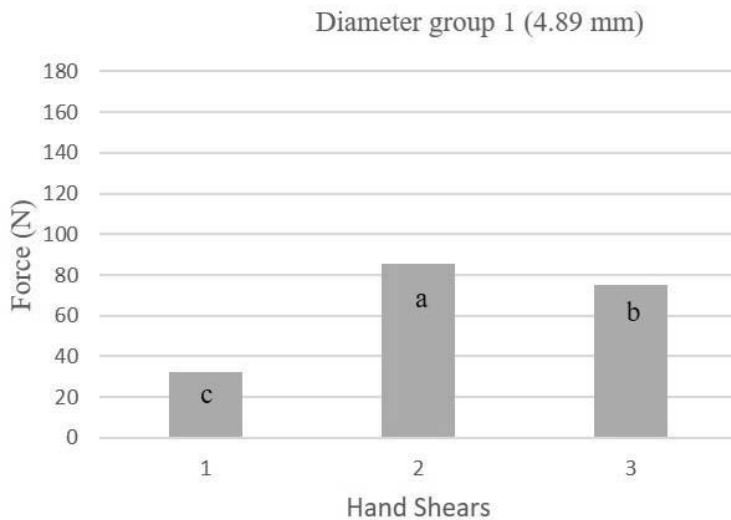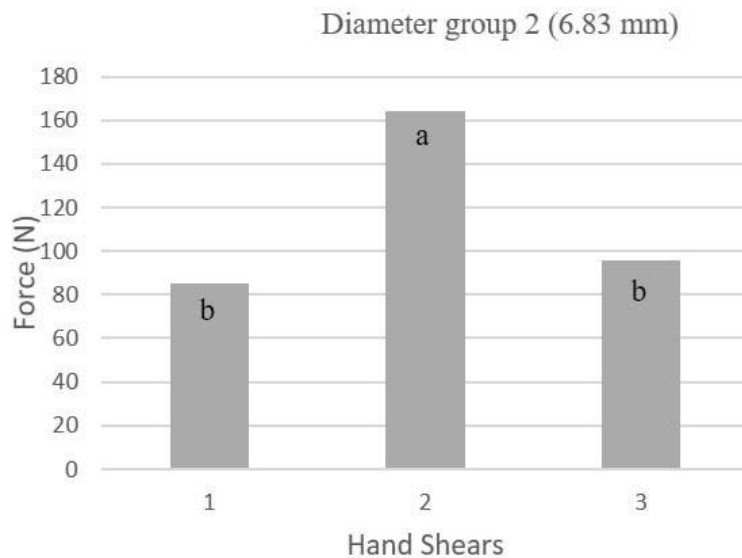

Fig. 5 Measured forces for diameter group 1.

Fig. 6 Measured forces for diameter group 2.

Average shearing force values obtained with different pruning shears were 32.54, 85.68, 75.20 N for first diameter group respectively. The same values were 85.11, 163.86, 95.57 N for second diameter group. It can be seen that from the Fig.5, for the first diameter group, first pruning shear was able to perform approximately 2.5 times less force compared to the other shears. One reason maybe that the

thickness of the first pruning shears is less than the other shears. Thus the blades enter the material with less force and less impact on the lateral frictional resistance.

In addition, blade angle values support this result. In the study of *Mathanker, Grift & Hansen*, 2015, It supports the fact that the regulation of blade angles effects the cutting energy values and is therefore directly related to the force values. On the toher hand the maximum grip strength of a healthy young male using pliers like hand tool is approximately 600 N. For repeated and continuous work 33-50% of the above values is recommended *(Paivinen, 2002)*. From this point of view, three shears tested in this study were able to perform cutting operations below these values. The study results showed that, all pruning shears values tested with abelia branches in this study ergonomically below the limit values.

CONCLUSIONS

All pruning shears in this study required low operating force under ergonomic limits and were inexpensive. The average shear force varied between 35.54 N – 163.86 N. Also, results showed that the average cutting force of first pruning shear (Bulmax BMX-286) was significantly lower than rest of the other both pruning shears.

ACKNOWLEDGMENT

REFERENCES

1. Akhtar, G., Akram, Ahsan., Sajjad, Y., & Farooq, A. (2016). Improving flower yield of two essential oil bearing rosa species through pruning severity. *Pakistan journal of nutrition 15*(4), 328-332.

2. Emadi B., Kosse V., & Yarlagadda P. (2004). Relationship between mechanical properties of pumpkin and skin thickness. *International Journal of Food Properties*, *8*(2), 277-287.

3. Esehaghbeygi A., Hoseinzadeh B., Khazaei M., & Masoumi M. 2009. Bending and shearing properties of wheat stem of alvand variety. *World Applied Sciences Journal, 6*(8), 1028-1032.

4. Hoseinzadeh B. & Shirneshan A. (2012). Bending and shearing characteristics of canola stem. *American-Eurasian J. Agric. & Environ. Sci., 12*(3), 275-281.

5. Mathanker S.K., Grift, T.E. & Hansen A.C. (2015). *Biosystems engineering*, 133, 64-70.

6. Paivinen, M. (2002). The assesment of ergonomics and usability of consumer pruducts-For case studies on hand tools [PhD thesis]. Tampere 2002.

7. Pekitkan, F.G., Eliçin, A.K., & Sessiz, A. (2019). Effects of knives type, cutting angle and loading speed on force and energy requirement of grape cane. *Journal of multidisciplinary engineering science and technology*, *6*(2), 9552-9556.

8. Persson, S. (1987). Mechanics of cutting plant material. *ASAE Publications*, St Joseph, USA.

9. prEN 1005-3. (1995). Safety of Machinery – Human Physical Performance – Part 3. Recommended Force Limits for Machinery Operation. European Committee for Standardisation.

10. Scheiber, S.M., Robacker C.D., & Lindstrom O. M. (2002). Stem and leaf hardiness of 12 Abelia Taxa. *J. Environ. Hort. 20*(4),195–200.

11. Selvi K. Ç. & Kabaş Ö. (2016). Bending and shearing properties of some standard carnation (dianthus caryophyllus l.) varieties stem. *Acta Technica Corviniensis, 4*, 133-136.

12. Voicu G., Moiceanu E., Sandu M., Poenaru I.C., & Voicu P. (2011). Experiments regarding mechanical behaviour of energetic plant miscanthus to crushing and shear stress. In *Engineering for Rural Development Jelgava* (pp. 490-495).

Corresponding author:
Ing. Kemal Çağatay Selvi, Ph.D., Department of Agricultural Machines and Technologies Engineering, Faculty of Agriculture, Ondokuz Mayıs University Samsun, Kurupelit 55200, Samsun, Turkey, phone: +90 507 9262829, e-mail: kcselvi74@gmail.com

UTILIZATION OF ENVIRONMENTAL ENGINEERING TECHNOLOGY IN PALM OIL INDUSTRY: CURRENT STATE

Anna Oktavina SEMBIRING[1]

[1]*Czech University of Life Sciences Prague, Faculty of Engineering, Department of Mechanical Engineering, Kamycka 129, Praha 6, 165 21, Suchdol, Czech Republic*

Abstract
In many attempts, remote sensing has been utilized to assist agriculture in the best management practice to improve production and minimize its impact on the environment. In palm oil agriculture in Indonesia, conversion of high conservation value forest into palm oil plantation area is a continuous major environmental concern. Many efforts have been done using remote sensing technology such as Landsat 8 and Landsat 4-5 TM imagery to obtain information. However, the degree in which the information has been used effectively to assist policy and other decision, limited research has been done. To add to the knowledge, this paper aims to present a review of recent studies on remote sensing and exemplify some of the main challenges to optimally support the attempt to minimize deforestation, at the same time improve palm oil production in Indonesia.

Key words: *Remote Sensing, Palm Oil, Deforestation, Indonesia*

INTRODUCTION

Currently Palm oil became one of the most controversial market-driven crops in the world. Palm oil serves as the main type of vegetable oil consumed by the global market, yet its productions in the producer countries have led to deforestation, distinctions of endangered animals, and displacement of indigenous people *(Lee, Ghazoul, Obidzinski, & Koh, 2014; Obidzinski, Andriani, Komarudin, & Andrianto, 2012)*. Indonesia is currently the main producer of Palm Oil. It dominates the global market with European union and China as the main absorbers of Indonesian Palm Oil *(Teoh, 2010)*.

As part of the government effort to improve the sustainability of Indonesia Palm Oil, In 2016 Indonesian President Jokowi instructed moratorium of palm oil land expansion and intensification of the existing area *(Wicaksono, 2018)*. This instruction was driven mainly by the continuous major environmental concern in Indonesia Palm Oil Industry and that is the conversion of high conservation value forest into palm oil plantation area. There are many debates on the impact of palm oil plantation expansion on deforestation in Indonesia. Data suggested that together with the world's second biggest producer of palm oil, Malaysia, the total areas of palm oil plantation of both countries covered 17.0 Mha as for 2015 and upward trend was shown as from the year 2000 *(Chong, Kanniah, Pohl, & Tan, 2017)*.

To assist the instruction, research has been generated using remote sensing. Satellite data imagery from remote sensing technology such as Landsat 8 and Landsat 4-5 TM imagery was obtained to gain information *(Andrianto, Komarudin, & Pacheco, 2019; Austin et al., 2017; Gaveau et al., 2018)*. However, the degree in which the information has been used effectively to assist policy and other decision, limited research has been done. To contribute to the knowledge, this paper aims to present a review of three recent studies on remote sensing and exemplify some of the main challenges to optimally support the attempt to minimize deforestation, at the same time improve palm oil production in Indonesia.

MATERIALS AND METHODS

The current study used qualitative approach with secondary source of data collection. Secondary data includes journal articles obtained from web of knowledge and google scholar database. To select related journal articles that serve the aim of this study, search was limited to studies derived between year 2016 and 2019 using keywords palm oil, remote sensing, deforestation, and Indonesia.

RESULTS AND DISCUSSION

Recent study on the current application of remote sensing in palm oil agriculture has stated three main aims of advancement of remote sensing for land cover change classification *(Chong et al., 2017)*. These

three aims are firstly, to detect conversion of forest cover and other high conservation value land such as peatland into palm oil plantation, secondly, to identify degraded or other suitable non-forest area for palm oil plantation, and thirdly, to analyze related social and environmental impact of land conversion.

Research on forest loss and industrial plantations in Borneo has been conducted using cloud-free LANDSAT image mosaics to understand land use change between the period 2000 – 2017 *(Gaveau et al., 2018)*. The study has found that in the 17 years period, forest in Borneo has declined by 14% (6.04 Mha) and 3.06 Mha were forest converted into industrial plantation with distribution of forest loss between Indonesian Borneo and Malaysian Borneo as below (Figure 1.). Although both oil palm and pulpwood industry share the total 170 % of plantation expansion, oil palm industry responsible for the 88% of the total. However, after 2016 there was a decline in forest loss in 2017. Possible derived of the decline are low palm oil prices, wet conditions, and improved fire prevention.
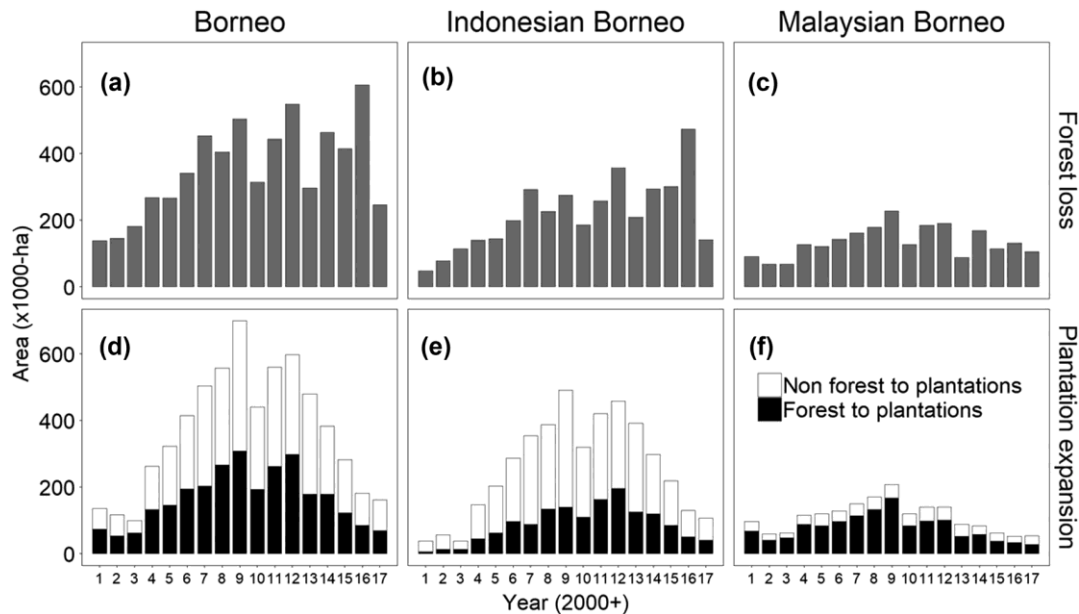

Fig. 1 Time-series (2001-2017) of Borneo's land use change, derived by observing LANDSAT imagery (source: *Gaveau et al. 2018*)

Another study on land cover change conducted by *Austin et al (2017)*. Mapped of large-scale oil palm plantations was done using Global Land Survey Landsat composites and Landsat 4-5 TM imagery by identifying grid patter, and associated infrastructure including roads, mill facilities, and management buildings and recently cleared areas adjacent to existing area that may have been prepared for cultivation of palm oil based on the grid formation *(Austin et al, 2017)*. The study analyzed proportion and area of plantations converted from forest up to 2015 across Sumatra, Kalimantan, and Papua. During 1995 – 2015 expansion of palm oil plantation in Indonesia occur at an average rate of 450.000 ha/year and 117.000 ha/year were forested area.

Information also obtained regarding 30.2 million hectares of non-forest land nationwide that are suitable for palm oil cultivation based on biophysical characteristics of the area. This areal consist of 15.2 Mha located in Sumatra, 13.0 Mha in Kalimantan, and 2.0 Mha in Papua *(Austin et al, 2017)*. However, due to the lack of mechanization of the current regulation for expansion towards suitable non-forest area, utilization of the suitable land was not optimized yet.

Meanwhile, another study was done from 2013 – 2014 to understand investments conducted by five large-scale oil palm plantations and the implications for local landowners and environment in the Boven Digoel and Merauke Districts *(Andrianto et al., 2019)*. Using data gathered by Landsat 8, the study identify some of the area designated for large-scale agricultural development which are located closer to big rivers such as the digoel and Bian Rivers. The benefit of the location is that it will ease the transport of fresh fruit bunch to the mills as well as crude palm oil to the refinery mill. The implication of the plan is the reduced of welfare of the indigenous people due to loss of livelihoods and impacts on food security. However, the

local spatial plan was designed with the aim for job creation, infrastructure provision and wellbeing of the local community.

CONCLUSIONS

Land cover classification of Landsat images is one of the most important and common application used in any research of land cover change *(Phiri & Morgenroth, 2017)*. The information gathered can inform policy makers, company, and community regarding land conditions including social and environmental impacts related to the land use. However, there are challenges on how the data gathered can assist the efforts to minimize deforestation and optimize the suitable non-forest area for palm oil plantation. The research present in this study exemplified some of the challenges. As many studies have confirmed, palm oil development has benefit to higher opportunity for employment, improvement of livelihoods in rural and remote areas *(Dib, Krishna, Alamsyah, & Qaim, 2018; Euler, Krishna, Schwarze, Siregar, & Qaim, 2017; Gatto, Wollni, & Qaim, 2015)* and stimulate growth and infrastructure development in the local areas *(Teoh, 2010)*. For this reason, land expansion towards forest cover area is still an option and gaps on the mechanisation of the current regulation to regulate the practice have hindered the attempts to minimize deforestation. This also includes the mechanisation to optimize suitable non-forest area for palm oil plantation to achieve the national fresh fruit bunch production goal.

ACKNOWLEDGEMENT

REFERENCES

1. Andrianto, A., Komarudin, H., & Pacheco, P. (2019). Expansion of Pal Oil Palm Plantations in Indonesia's Frontier: Problems of Externalities and the Future of Local and Indigenous Communities. Land, 8(4), 56. doi: https://doi.org/10.3390/land8040056

2. Austin, K. G., Mosnier, A., Pirker, J., McCallum, I., Fritz., S., & Kasibhatla, P. S. (2017). Shifting patterns of oil palm driven deforestation in Indonesia and implications for zero-deforestation commitments. Land use policy, 69, 41 - 48.

3. Chong, K. L., Kanniah, K. D., Pohl, C., & Tan, K. P. (2017). A review of remote sensing applications for oil palm studies. Geo-spatial Information Science, 20(2), 184 - 200. doi: 10.1080/10095020.2017.1337317

4. Dib, J. B., Krishna, W., Alamsyah, Z., & Qaim, M. (2018). Land-use change and livelihoods of non-farm households: The role of income from employment in oil palm and rubber in rural Indonesia. Land Use Policy, 76, 828-838. doi: 10.1016/j.landusepol.2018.03.020

5. Euler, M., Krishna, V., Schwarze, S., Siregar, H., & Qaim, M. (2017). Oil Palm Adoption, Household Welfare, and Nutrition Among Smallholder Farmers in Indonesia. World Development, 93, 219-235. doi: 10.1016/j.worlddev.2016.12.019

6. Gatto, M., Wollni, M., & Qaim, M. (2015). Oil palm boom and land-use dynamics in Indonesia: The role of policies and socioeconomic factors. Land Use Policy, 46, 292-303. doi: 10.1016/j.landusepol.2015.03.001

7. Gaveau, D. L. A., Locatelli, B., Salim, M. A., Yaen, H., Pacheco, P., & Sheil, D. (2018). Rise and Fall of Forest Loss and Industrial Plantations in Borneo (2000 - 2017). Conservation Letters. doi: 10.1111/conl.12622

8. Lee, J. S. H., Ghazoul, J., Obidzinski, K., & Koh, L. P. (2014). Oil palm smallholder yields and incomes constrained by harvesting practices and type of smallholder management in Indonesia. Agronomy for Sustainable Development, 34(2), 501-513. doi: 10.1007/s13593-013-0159-4

9. Obidzinski, K., Andriani, R., Komarudin, H., & Andrianto, A. (2012).

Environmental and Social Impacts of Oil Palm Plantations and their Implications for Biofuel Production in Indonesia. Ecology and Society, 17(1). doi: 10.5751/ES-04775-170125

10. Phiri, D., & Morgenroth, J. (2017). Developments in Landsat Land Cover Classification Methods: A Review. Remote Sensing, 9(9), 967.

11. Teoh, C. H. (2010). Key Sustainability Issues in the Palm Oil Sector.

12. Wicaksono, P. E. (2018). Presiden Jokowi Teken Inpres Moratorium Perkebunan Sawit. liputan6. Retrieved from https://http://www.liputan6.com/bisnis/read/3648519/presiden-jokowi-teken-inpres-moratorium-perkebunan-sawit

Corresponding author:
Anna Oktavina Sembiring, Department of Mechanical Engineering, Faculty of Engineering, Czech University of Life Sciences Prague, Kamýcká 129, Prague, 160 00, Czech Republic, email: sembiring@tf.czu.cz

PROTECTIVE ELEMENTS OF AGRICULTURAL ELECTRIC VEHICLES

Ladislav ŠEVČÍK[1]

[1]*Department of Machine Design, Mechanical Faculty, Technical University of Liberec*

Abstract

In the paper, there is a procedure for calculation of strength solutions of protective electric vehicle structures according to EU Regulation No 1322/2014 for agricultural and forestry machinery frames for ROPS "Tractor". The design of the protective elements is made of welded high strength steels.

Key words: *electric vehicle; protective elements; stress transcendent calculation.*

INTRODUCTION

The aim of the research was to design a welded ROPS construction of high-strength sheets to comply with the European Directive, with minimum weight.

The design optimization and the strength calculation of the ROPS frame of the agricultural electric car is carried out according to the EU Regulation No 1322/2014 for agricultural and forestry machinery frames for ROPS "Tractor". Values of the maximum static forces to be applied to the ROPS, acting in the vertical and kinetic energy directions in the longitudinal and lateral directions (see Tables 1 and 2), calculated according to EU Regulation 1322 / 2014 for ROPS "Tractor" for electric vehicle, 2x2 chassis.

Tab. 1 Mass of electric vehicle

Chassis type	2x2
Vehicle storage weight	1200 kg
Vehicle maximum storage weight	1400 kg
Vehicle reference weight- max. technical weight	2600 kg

Note: The vehicle reference mass M is the weight chosen by the manufacturer to calculate the input energy and pressure forces to be used in the tests. It shall not be less than the weight without weight and shall be sufficient to ensure that the weight ratio does not exceed 1,75.

Tab. 2 Load variants

Load type	Value
Min. the amount of energy absorbed by the longitudinal loading E (IL1) = 1.4M	3640 J
Min. the amount of energy absorbed at lateral loading E (IS) = 1.75M	4550 J
Vertical loading force at back F = 20M	52000 N
Vertical loading force at front F = 20M	52000 N
Min. energy at longitudinal loading in opposite direction E (IL2) = 0.35M	910 J

Dimensions of force spreaders, the length of the distribution element for the longitudinal and transverse loading of the frame can be min. 250 mm and max. 700 mm by multiples of 50 mm, the height is always 150 mm. Load locations according to EU regulations are shown in Fig. 1.

For longitudinal loading from the rear (in the direction of travel), the point of application of the force is 1/6 of the width of the frame from the edge, closer to the operator's seat (driver), in the 400 mm task. With regard to the optimized top frame design, the length of the longitudinal load carrier is E (IL1) 600 mm.

For longitudinal loading from the front (opposite the direction of travel) the force is at a distance of 1/6 of the width of the frame W from the edge on the opposite side of the top of the frame, further away from the operator's seat (driver 400 mm). The length of the longitudinal load carrier E (IL2) is 700mm. For lateral loading E (IS), the power point is determined by the position of the clearance zone, precisely by the position of the seat reference point (SIP) by the operator (driver). In the solved task, the point of loading of the side load is only 119 mm from the front edge of the frame and therefore the distributor has the shortest possible length, ie 250mm - see Fig. 1.
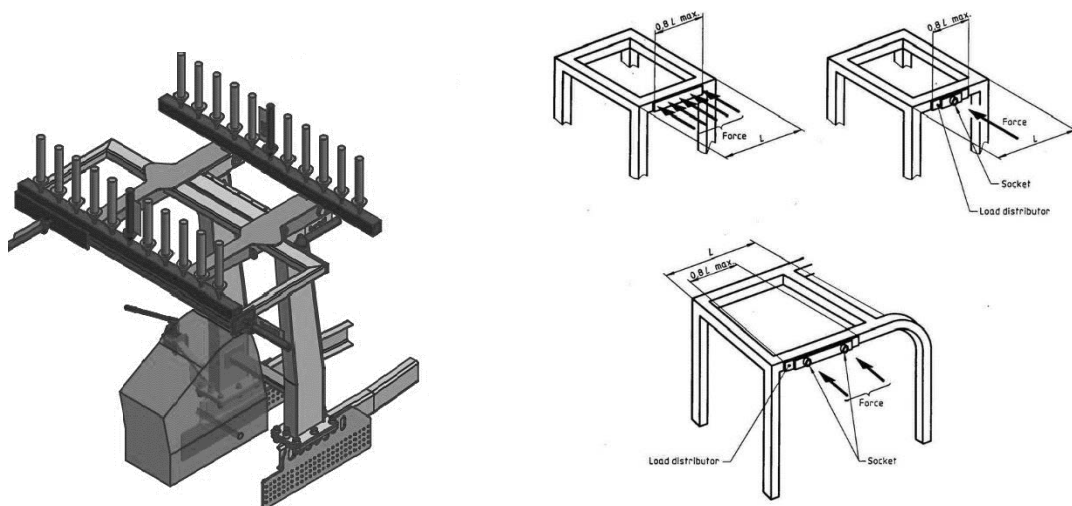

Fig. 1 Design of ROPS "Electro mobile into the field" - loads and their position in tests

Fig.2 Position of lateral force application according to EU Regulation No. 1322/2014

The vertical loading (pressure test) is performed on the rear and front sides of the protective frame with a force of F = 20M by means of a pressure beam (not part of the ROPS frame), which is pressed against its protective frame by two hydraulic cylinders connected by universal joints. The position of lateral force application according to EU Regulation No. 1322/2014 is in fig. 2.
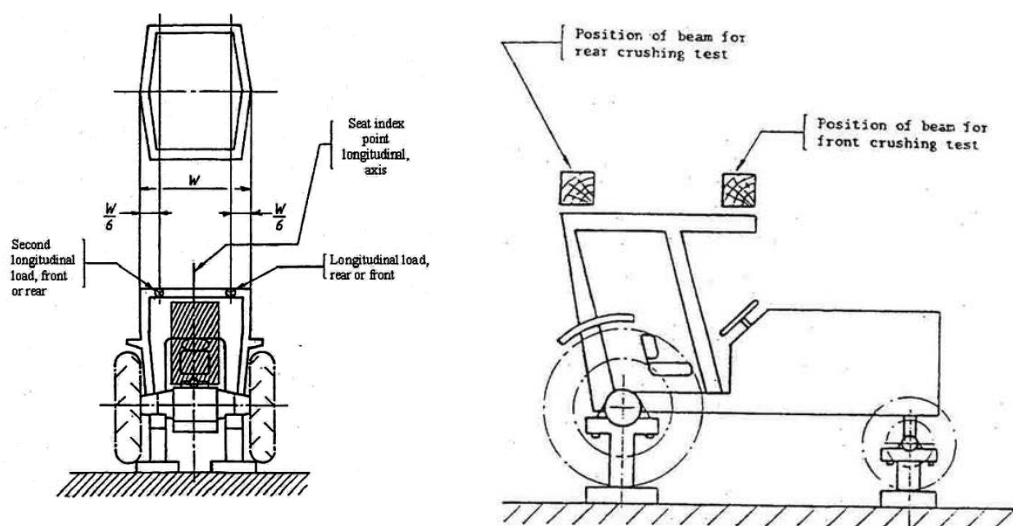

Fig. 3 Positions of longitudinal forces from the rear (in the direction of travel) and from the front (in the opposite direction)

Back and side view, Fig. 3, show loads of electric tractor according to EU Regulation No. 1322/2014. The structure of the protective frame must be such that after the deformations from the gradually loading forces the hatch operator area is not affected.

MATERIALS AND METHODS

High-strength steel S690QL, strength limit 770 - 940MPa, yield strength 690 - 790MPa was used for the main welded vertical beams of the lower frame (webs) and hinged top part of the frame.

Mechanical properties of steel are according to SIJ Acroni certificate.The FEM calculation was based on the tensile test data of the material (*Xiaolin & Yijun, 2019*). Nonlinear calculation respected measured data see. Fig. 4. The device is tested by loading forces in three directions gradually over time. Load first in the direction of travel, then from top and on the end from side. The device deforms plastically. It is then unloaded but partially deformed. As a result of the positive evaluation, the permanent deformation of the device does not reach a certain space.

Furthermore, the loading procedure (tests) according to the standard for the calculation of operator protection during overturning and the size of welds, in particular at welding points, was entered. The plastic and elastic deformations and stresses were calculated in gradual loading by individual tests in Ansys Workbench 17.2, module transient structure. The project scheme is shown in Fig. 5. In linear static structure were counted deformation and stress separately for each load. In transient structural the loading was linked to the previous one from tab. 2. Force from energy calculate by nonlinear gradual system in software.
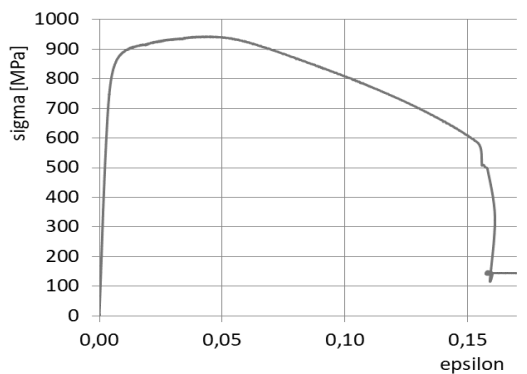

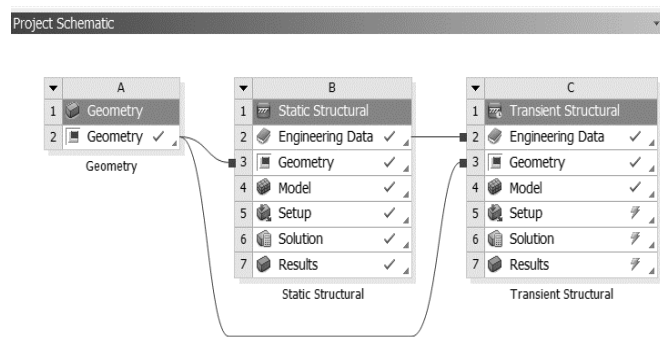**Fig. 4** Material S690 QL welded

Fig. 5 Project scheme

In transient structural the loading given by energy was linked from the static calculation. Steps followed gradually by tab. 2. It only tests one frame per standard load, which probably won't happen in car crush.

RESULTS AND DISCUSSION

The design of the ROPS was changed until it was simulated that it would be distorted outside the area of Fig. 1 and Fig.3 after all tests in Tab. 2 of the device. Furthermore, the condition was that the plastic deformation in welds would not be greater than 3%. The device will be most stressed at the attachment welds, so the stress and strain results after all tests are shown in the following figures.
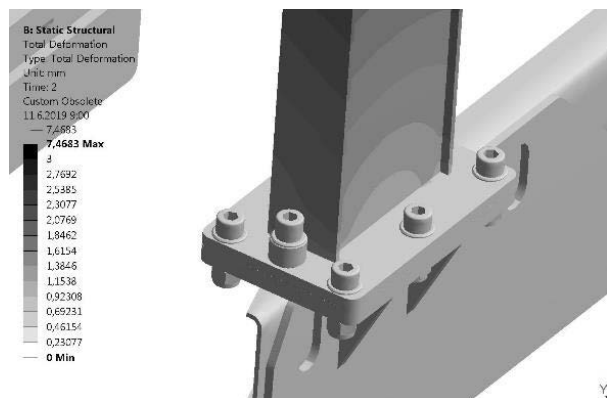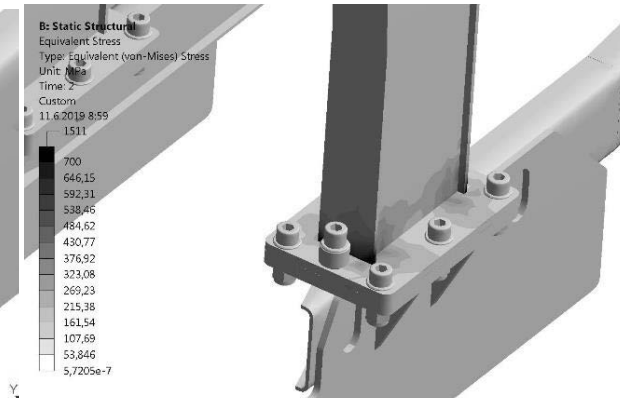

Fig. 6 Deformation after transient loading
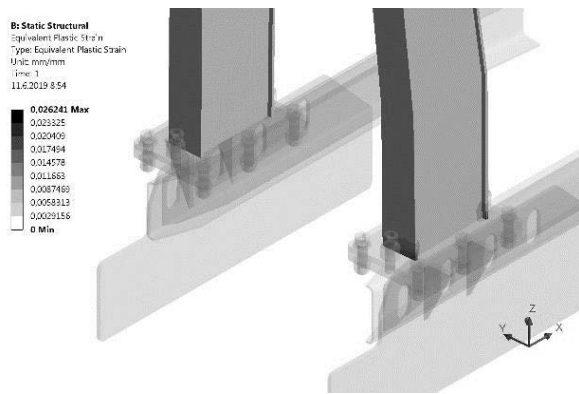
Fig. 7 Stress after transient loading

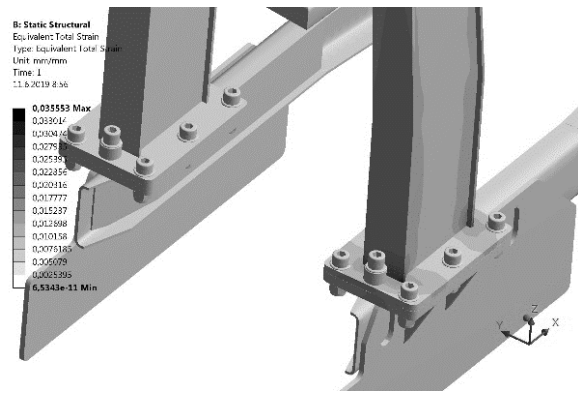**Fig. 8** Equivalent plastic deformation is 2%

Fig. 9 Elastic and plastic deformation is 3.6%

Taking into account the post-test deformation and stress of transient loading, see Fig. 6, 7. Result of equivalent plastic deformation and elastoplastic deformation are in Fig. 8, 9. The required maximum 3% plastic deformation ensures sufficient space for the operator under the protective cover after its plastic deformation. It is important that the elastic and plastic deformation does not exceed 5% in total for the attachment to the electric car. Since the maximal deformation value in Fig. 9 is 3.6%, the design will be on the safety side and can corrected quality of welds (*Xiaolin & Yijun, 2019; Parrish, 2014*).

CONCLUSIONS

As predicted, the resulting load capacity of the electric car frame made of welded high strength plates will depend on the technology of the welds. The welds must be formed sequentially from several layers so that recrystallization does not occur due to the thermal load. The weld tensile test in Fig. 4 shows a 15% total deformation. However, the strength value of the material decreases after 5%. The required 3% plastic deformation and 2% elastic deformation are in the area of maximum possible stress. The design was designed for this value based on simulations. Practical testing after production will be verified.

ACKNOWLEDGMENT

REFERENCES

1. Commission Delegated Regulation (EU) No 1322/2014 of 19 September 2014 supplementing and amending Regulation (EU) No 167/2013 of the European Parliament and of the Council as regards design requirements; General requirements for the approval of agricultural and forestry vehicles.

2. Parrish, A. (2014). *Mechanical Engineer's Reference Book*. 11th Edition. Elsevier.
3. Xiaolin, Ch. & Yijun L. (2019). *Finite Element Modeling and Simulation with ANSYS Workbench*. CRC Press. ISBN-13: 978-1138486294

Corresponding author:
Prof. Ing. Ladislav Ševčík., Department of Mechanical Design, Mechanical Faculty, Technical University of Liberec, Studentská 2, Liberec 1, Liberec, 46117, Czech Republic, phone: +420 485353316, e-mail: ladislav.sevcik@tul.cz

COMPARISON OF GSM AND GPS TECHNOLOGIES FOR TRACKING PEOPLE

Antonín SIROTEK[1], Jan HART[1]

[1]Department of Technological Equipment of Buildings, Faculty of Engineering, Czech University of Life Sciences Prague

Abstract
This article deals with the comparison of a technologies for tracking people. People can be tracked using GSM and GPS. These methods have different properties and are suitable for different applications. For this reason, GPS and GSM receivers have been tested. People were tracked for a period of 90 days. People did not change their behaviour in any way. The accuracy and reliability of these methods was monitored. This makes it possible to determine which method is more suitable for tracking people.

Key words: GPS; GNS; tracking.

INTRODUCTION

Thanks to modern technologies it is possible to not only determine your location but also to track other people or other things. Tracking people use emergency services, firefighters, police in search of missing persons and employers to control their employees. The first way is to track via a mobile network. Mobile network is a telecommunication network designed for telephone calls, data transfer and other services. The network consists of mobile devices, Base Transceiver Station (BTS), Serving Mobile Location Center (SMLC), Gateway Mobile Location Center (GMLC). These networks work most often at frequencies from 300MHz to 3GHz (*Eberspächer, et al., 2009*). Mobile phone users are well-traceable, which they may not be aware of. Tracing of a mobile device in the mobile network is necessary function based on the principle of operation. The mobile device still checks its position and connection to the transmitter BTS. Tracking is not possible in the area outside the BTS range (*Qayyum, et al., 2013*). Another option is using GNSS (Global Navigation Satellite System) localization. GNSS enables global satellite positioning. The current positioning systems in use are the American GPS (Global Positioning System), Russian GLONASS, European Galileo and the Chinese BeiDou. GNSS consists of a universe segment, user segment and control segment. A-GPS (Assisted GPS) has been used in our research. It is known that GPS positioning with code measurements for the civil sector has an accuracy of 5 to 15 m under ideal conditions (*Bona, 2000*). Smartphones typically have an accuracy of 5 meters in ideal conditions (*Diggelen, Enge, 2015*). Positioning using the mobile network has an accuracy of hundreds of meters. The most important thing here is the density of BTS transmitters (*Kos, et al., 2006*). However, it is necessary to test the accuracy and reliability of positioning in real conditions. The aim of this study is to determine which method is the most suitable for tracking people and what characteristics is has.

MATERIALS AND METHODS

It was tested tracking via mobile network, GPS and equipment using both methods. Equipment used methods E-OTD (The Enhanced Observed Time Difference method) in GSM and GPRS mobile networks and OTDOA (Observed Time Difference Of Arrival) method in UMTS networks for tracking in mobile networks. E-OTD method is a terminal based method. The mobile device includes clocks, which are synchronized by the network. The mobile device calculates the delay of the signal emitted from BTS. The result is the Real Time Difference (RTD). Value between two BTS is Geometry Time Difference (GTD). Intersections of GTD values indicate the most likely occurrence of mobile devices (*Dzulkifli, et al., 2017*). OTDOA method works on the same principle as the E-OTD method. The accuracy of localization by mobile networks depends on the density of BTS (*Orlich, 2006*). For the GSM method, we assume less accuracy and greater reliability.

Another method that was tested for determining the position was GPS. The receivers use code measurement methods. The code measurement principle uses the distance between the receiver and the transmitter to determine the position. The distance codes are the marks that determine the time when the satellite signal was broadcast. The receiver detects the broadcast time and code reception time. From the detected difference, the distance between the satellite and the receiver is determined. It is possible to

calculate the position from the signal of four satellites. This method is used in most ordinary GPS receivers (*Bensky, 2006*). In addition, A-GPS has been used for faster positioning. GBAS (Ground Based Augmentation Systems) and SBAS (Satellite Based Augmentation Systems) were not used. For GPS, we assume greater accuracy and low reliability.

Equipments displayed median position error. It is an estimate of accuracy in meters. The magnitude of the medium positional error is affected by the constellation of transmitters, number of transmitters used and the strength of the received signal. That is why, the accuracy of localization depends on the environment in which the receiver is located (*Ge, et al. 2017*). The navigation equipment used was PRA type LX series 1. Equipment includes GMS module and A-GPS receiver. It has a CPU Kirin 655 Octa-Core, 3 GB RAM, a triple virtual antenna, a battery with a capacity of 3000 mAh, for long life and works on the Android 7.0 platform.

Five people were tracked for 90 days. People were tracked using three devices. The first device uses the GSM method, the second GPS and the third device use GPS and GSM simultaneously. All three methods were measured at the same time. The tracking method was set on the device. The results were stored in the equipment memory. Measurements took place in Central Bohemia Region in Czech Republic in the territory with coordinates 50 ° 3′0 ″ N, 14 ° 42′36 ″ E. The measurement took place on weekdays in 2018.

RESULTS AND DISCUSSION

Five people have been monitored for 90 days in three ways of tracking. The tracking results using various methods are shown in Tab. 1., 2. and 3.

Tab. 1 Tracking via GSM and GPS

	m
Best accuracy	4.00
Worst accuracy	100.00
Modus	21.00
Median	21.00
Average accuracy	30.41

Tab. 2 Tracking via GSM

	m
Best accuracy	50.00
Worst accuracy	863.00
Modus	150.00
Median	170.00
Average accuracy	200.00

Tab. 3 Tracking via A-GPS

	m
Best accuracy	4.00
Worst accuracy	98.00
Modus	10.00
Median	38.00
Average accuracy	40.00

The devices worked 24 hours a day and recorded their position every hour. It was not always possible to determine the location. The Tab. 4 shows the number of measured values. If we compare how many times, we could not determine the location for each method, we can judge the reliability of the methods.

Tab. 4 Number of measured values

Method	n
GPS + GSM	10 152
GSM	10 044
GPS	7 020

The reliability of the individual methods is shown in Tab. 5.

Tab. 5 Reliability of the methods

Method	Reliability (%)
GPS + GSM	94
GSM	93
GPS	65

GPS accuracy is 5 to 15 m with conventional devices using the code measurements. The devices reach this accuracy with an excellent view of the sky (*Bhatta, 2011*). But tracked people spend most of their time in buildings or vehicles, where there is poor, or no sky view and GPS signal is weak. As a result, localization accuracy has deteriorated to 40 m. GPS tracking reliability was 65%. *Fischer et al., (2018)* reported a small error rate of 8.2%, because his measurement took place outside buildings. Therefore GPS-only tracking is not appropriate for search for people. This method is useful for cases, where we assume that people will be in an environment with a good view of the sky, for example, measuring sports performance, was described by *Scott et al., (2016)*. It is enough to monitor people's behaviour and health, reported by *Brusilovskiy et al., (2016)*. The average accuracy deteriorated to 200 m when localized via GSM. Reliability increased to 93%. It does not matter if the receiver moves inside or outside the building. Localization is possible everywhere there is a mobile network signal. GSM tracking is a reliable and less accurate method, which responds to our expectations. When using GPS and GMS localization simultaneously, we got surprisingly good results. It achieves the best accuracy and reliability. This method seems ideal for tracking people.

CONCLUSIONS

Tracking via GPS is suitable for applications where is not important reliability, but accuracy. Reliability of 65% does not seem to be enough for searching for people. Reliability is major when searching for persons. Of course, we can assume that tracked people will not be in an environment with a good view of the sky. Tracking via GSM is a reliable method, but worse accuracy in hundreds of meters makes it harder to find people. The device uses localization via GSM and GPS together achieved 93% of high reliability and good accuracy of 30.41 meters. This method seems to be best for tracking people.

ACKNOWLEDGMENT

REFERENCES

1. Bensky, A. (2016). *Wireless positioning technologies and applications*. London: Artech House. 401pp.
2. Bhatta, B. (2011). *Global navigation satellite systems: insights into GPS, GLONASS, Galileo, Compass, and others*. Hyderabad, India: BS Publications, 438pp.
3. Bona, P. (2000). Accuracy of GPS phase and code observations in practice. *Acta Geodaetica et Geophysica Hungarica 35*, 433-451.
4. Brusilovskiy, E., Klein, L.A., & Salzer, M.S., (2016) Using global positioning systems to study health-related mobility and participation. *Soc. Sci. Med. 161*, 134-142
5. Diggelen, F. & Enge, P. (2015). The World's first GPS MOOC and Worldwide Laboratory using Smartphones. In *28th*

International Technical Meeting of the Satellite Division of The Institute of Navigation (pp. 361-369).

6. Dzulkifli, M.A., Sulaiman S., & Saparon A. (2017). *2017 INTERNATIONAL CONFERENCE ON ELECTRICAL, ELECTRONICS AND SYSTEM ENGINEERING (ICEESE).* Tracking System for Missing Person. IEEE 345 E 47TH ST NEW YORK. Kanazawa, pp. 57-60

7. Eberspächer, J. (2009) *GSM: architecture, protocols and services.* Chichester, U.K.: Wiley.

8. Fischer, M., Parkins, K., Maizels, K., Sutherland, D.R., Allan, B.M., Coulson, G., & Di Stefano, J., (2018). Biotelemetry marches on: A cost-effective GPS device for monitoring terrestrial wildlife *PloS one.* 13

9. Ge, X., Gu R.., Lang Y., & Ding Y. (2017). 3rd IEEE Information Technology and Mechatronics Engineering Conference (ITOEC). *Design of Handheld Positioning Tracker Based on GPS/GSM.* IEEE 345 E 47TH ST NEW YORK, Chongqing, pp. 868-871.

10. Kos, T., Grgic, M., & Sisul, G. (2006). Mobile User Positioning in GSM/UMTS Cellular Networks. *Proceedings ELMAR 2006* (pp. 185-188) IEEE.

11. Orlich, M. 2006 *Basic localization methods in GSM. Access Server.* Czech Technical University in Prague, 120pp.

12. Qayyum, E., Moshin Z., & Malik J. (2013). *Real-time Vehicle Tracking System Using GPS and GSM.* Riga: LAP LAMBERT Academic Publishing.

13. Scott, M.T.U., Scott, T.J., & Kelly, Vincent G. (2016) The Validity and Reliability of Global Positioning Systems in Team Sport: A Brief Review. *J. Strength Cond. Res. 30,* 1470-1490

Corresponding author:

Ing. Antonín Sirotek, Department of Technological Equipment of Buildings, Faculty of Engineering, Czech University of Life Sciences Prague, Kamýcká 129, Praha 6, Prague, 16521, Czech Republic, phone: +420 721 354 426, e-mail: siroteka@tf.czu.cz

MINIMIZING OF SETUP ATTEMPTS ON KILNFORMING PROCESS WITH DOE

Vladimír SOJKA[1], Petr LEPŠÍK[1], Petra HENDRYCHOVÁ[2]

[1]Department of Design of Machine Elements and Mechanisms, Faculty of Mechanical Engineering, Technical University of Liberec, Liberec, Czech Republic
[2]Department of Research and Development, Preciosa – Lighting, Kamenický Šenov, Czech Republic

Abstract
Number of setup attempts on kilnforming process can be very high. Because each next attempt to setting up the process correctly is expensive, there is need to face off to this problem. Solution for it could be the Design of Experiment (DOE) method for describing the process in kiln and thereafter predicting the process results. This paper is focusing on use of DOE for glass slumping technology. After DOE is used number of setup attempts is reduced to minimum. That spare time and money on kilnforming technology. Application of DOE on glass kilnforming process was proven by case study on glass slumping technology in Preciosa – Lighting company also included in this paper.

Key words: Design of Experiment; kilnforming; glass slumping; process setup optimization.

INTRODUCTION

Kilnforming processes like glass fusing or glass slumping are good for making variety of different shapes from glass plates. These technologies are often used for art production, where is no need for high productivity. Setting up of kilnforming process is often only guessing from previous experiences with processes. That can lead to many wrong attempts before right dimension of product are done. In cases where kilnforming technologies are used in manufacturing there is need to have a process with a less waste and higher productivity. A cost of setup for production of new parts can be very high. This requires to do setups of processes better. Practically there are only two main parameters for setting up: forming temperature and forming time.

The biggest problem comes when kilnforming is used in a custom production. In a custom production of unique parts, there is need to often re-setup the kiln. If exact setup of a process is not known, it can take numerous of attempts to get a good result. One attempt can sometimes take up to a whole day, and when result is bad, the material and time used for this attempt are wasted and the final price is higher and higher with every try. A ratio between the number of setups and the number of products in custom production is close to 1:1. That all can lead to situations when more time is spent on wrong tries and kiln setups, than manufacturing itself. Either in a serial or custom production, there is need to reduce the number of setup tries to a minimum.

This calls for method determining how to setup the glass kilnforming process as few attempts as possible – in best case on the first attempt. That leads to a statistical method, the Design of Experiment (DOE), which is a great tool for describing of very complex systems. Positive results with DOE method were proved by many authors before. For example, design optimization of composite parts (*Lepšík & Kulhavý, 2017),* heat transfer optimization *(Das & Dwivedi, 2013),* and others (*Weissman & Anderson, 2015*).

The aim of this paper is to use the DOE method for predictable setup of glass kilnforming process, including a case study from workshop producing unique kilnformed parts to chandeliers in the Preciosa – Lighting company.

MATERIALS AND METHODS
Glass kilnforming

Glass forming is an umbrella term for many techniques of glass manufacturing in a kiln. Most significant techniques of kilnforming are glass fusing and glass slumping. Glass fusing is a method when several parts (plates, fragments or shards) of glass are fused together by high temperatures in a kiln. Results depend on forming time and temperature, it can look only like joining of parts together or complete fusion of parts into one object (*Sadakova, 2015*; *Seward, 2003*). The glass slumping is instead, a method when a plate of glass is changing its shape by heat and gravitation. The plate of glass

is heated in kiln and it is becoming plastic. This plastic glass is falling down and copying the shape of the mold or form (*Stokes, 1997*). It can be step after glass fusing or it is possible to do both methods in one step. The plate of glass with smaller parts of glass are fused together and formed via mold in one step. Different time and temperature in kiln causes different results. On dropout forms there can be different depth of dropout of glass during forming temperature.

Design of Experiment (DOE)

The Design of Experiment is a statistical tool for describing of very complex systems, where a mathematical model cannot be applied. An experiment generally is a set of tries (runs) where a goal is to find the best work procedure or to gain a better knowledge about properties of a product or process.

The result of the Design of Experiment is significancy level of factor's effect on system outcome which are calculated by a statistical hypothesis testing. The next result is a regression function, which is calculated from correlation between factors, their significancy and the demanded response (*Anderson & Whitcomb, 2015; Condra, 2001; Weissman & Anderson, 2015*).

Use of DOE for setup of Kilnforming process

A glass manufacturing itself is a complex process with many variables (*Seward, 2003*), that is why the Design of Experiment is good for use in kilnforming processes. This paper is focusing on glass slumping. To setup a process properly it is important to find how to set the parameters of the process to get the result which is needed. In case of glass slumping, it could be a depth of dropout of glass or an angle of bending. At first it is needed to find the intended result, then factors, which have an effect on the process results, are chosen. Here it is simple because factors are parameters of process. The kiln and the material must be the same for each experiment. The factors are: the forming temperature, the forming time, the thickness of the glass plate and the dimension of the mold (for example the diameter of a hole in the mold). After factors are chosen, it is needed to define their upper and lower values. The next step is to make the experiment plan. In basic, a simple plan is enough. For four factors, a solution can be a half plan with one repeating and with middle points.

After a real experiment, which means measurement of each run results, is done, a software calculates which of factors are significant and which are not. The software also calculates a regression model of the process. The main outcome of the Design of Experiment is a regression equation (1) and regression coefficients describing kilnforming process.

$$Y = b_0 + b_1 \cdot x_1 + b_2 \cdot x_2 + b_3 \cdot x_3 + b_4 \cdot x_4 + b_5 \cdot x_1 \cdot x_2 + b_6 \cdot x_1 \cdot x_3 + b_7 \cdot x_1 \cdot x_4 \qquad (1)$$

In the regression equation Y is measured outcome (response), $b_0 - b_7$ are coefficients of regression (-), and $x_1 - x_4$ are factors.

From this equation it is possible to calculate parameters for a setup of process to get required results with necessary conditions of final product.

For example, to make a particular part, a needed material, its thickness and shape of mold is usually in description of part's parameters. Kiln is defined by workshop. Only parameters which is possible to change are forming temperature and forming time. These two are easy to calculate from the equation (1).

Case study

For the case study experiment, a glass slumping technology in the Preciosa – Lighting company was chosen. The Preciosa – Lighting is company in Czech Republic, which makes luxury chandeliers in custom type of production. The goal of experiment was to find values of parameters for setup of a glass slumping process to get a requested depth of dropout of the glass plate. An equation for calculation of values used for slumping of unique parts in future on first attempt. Parameters of glass slumping process are: the forming temperature, forming time, thickness of the glass plate, diameter of a hole in the form. Factors which have an effect on the outcome (a depth of dropout of a glass plate) are: the glass type and its manufacturer, shape of dropout form, position of form in kiln, orientation of tin layer on glass, temperature curve, thickness of glass plate, dimension of dropout hole in form, forming temperature and forming time. Conditions of the experiment were set in a way that the glass manufacturer

was the Pilkington company, type of glass was optifloat, shape of dropout form was circle, orientation of tin layer was upside, position was in the center of kiln, temperature curve is shown in Tab. 1.

Tab. 1 Temperature curve for experiment

Step	Temperature	Time
1.	555 °C	70 min
2.	Forming temperature	30 min
3.	Forming temperature	Forming time
4.	555 °C	50 min
5.	500 °C	120 min
6.	400 °C	120 min

The next step in experiment was to find upper and lower values for experiment factors. These values are shown in a Tab. 2.

Tab. 2 Temperature curve for experiment

Factor	Lower point	Upper point	Middle point
Forming temperature	620 °C	720 °C	670 °C
Forming time	300 s	2700 s	1500 s
Glass thickness	4 mm	12 mm	8 mm
Diameter of hole in form	150 mm	500 mm	325 mm

Values of factors were written into a statistic software and a plan of experiment was automatically generated. The design of experiment used was a half plan with repeating. The next was the experiment itself. Dropout form was a metal plate with round hole. Before measurement, a separator was applied on surface of the form. The separator was Bullseye Shelf Primer which is a mixture with kaolin as a main ingredient. Separator was applied in form of water solution. When separator was dry, Glass plate was putted on a form, and main kilnforming process could began.

Each run taken whole workday and at the end, results was measured. Depth of dropout of glass from each run was collected. After all experiment runs were done, results were written into the software (Minitab®). The software calculated significancy of factors and a regression function. Deformation of the glass after one of experiment runs is shown in Fig. 1.
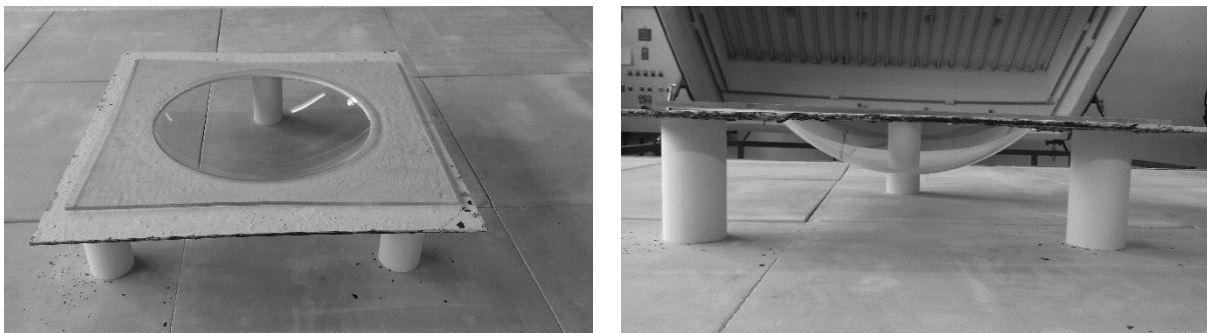

Fig. 1 Deformation of glass plate after experiment

RESULTS AND DISCUSSION

After all measurements, the software calculated a regression function of the kilnforming process. The factor's effects are shown in Fig. 2. As it is seen, every chosen factor had a significant effect on the process outcome which is the depth of the glass dropout. That means that every effect which was included in the DOE has a significant influence on kilnforming process. Factor with biggest effect on response is factor *D*, which is the diameter of dropout form, followed by forming time (factor *A*). Main

effects of factors are shown in Fig. 3. Plots shows that all factors are rising types, that means that when higher value of depth of glass dropout is needed, all factor must be set to its maximum value. From the report also occurs that chosen factors are describing the slumping process with 99.95% of accuracy.
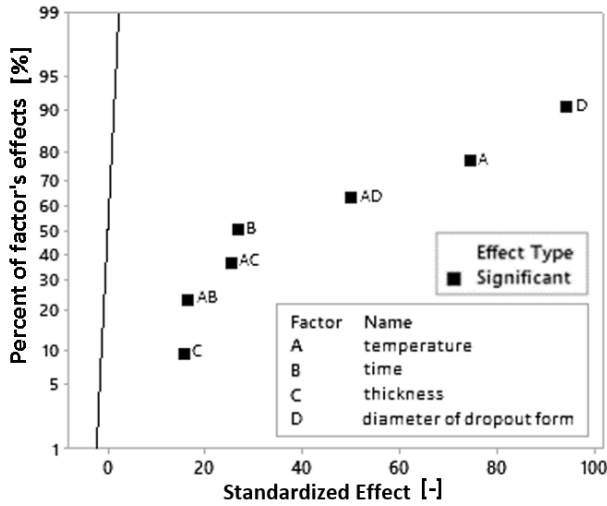

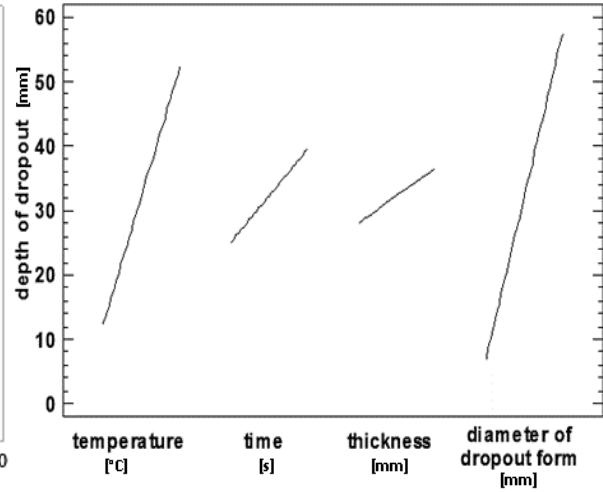**Fig. 2** Normal plot of the standardized effects   **Fig. 3** Main effects plot for depth of dropout

The regression function is visualized by response surface plot shown in Fig. 4.
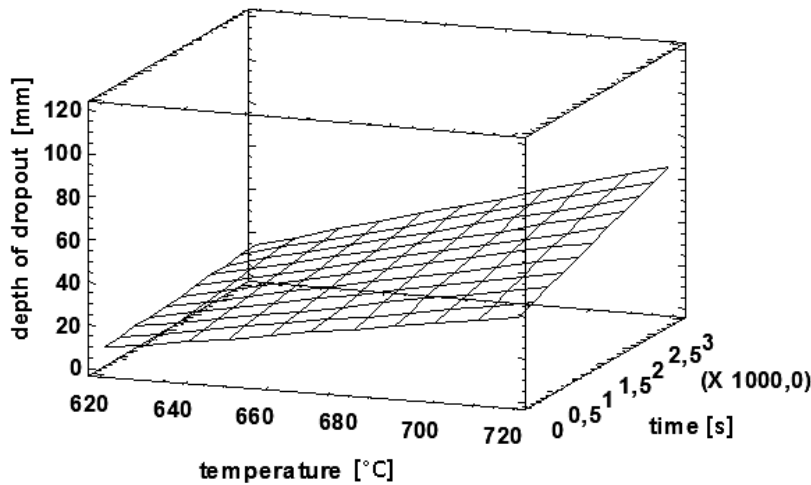

Fig. 4 Estimated response surface (thickness = 8, diameter of dropout form = 325)

The main result was a regression equation which is describing a regression function (2),

$$Y = b_0 + b_1 \cdot A + b_2 \cdot B + b_3 \cdot C + b_4 \cdot D + b_5 \cdot A \cdot B + b_6 \cdot A \cdot C + b_7 \cdot A \cdot D \qquad (2)$$

where Y is depth of glass dropout (mm), $b_0 - b_7$ are regression coefficients (-), A is the forming temperature (°C), B is the forming time (s), C is the thickness of glass plate (mm) and D is the diameter of the hole in the form (mm).

Regression coefficients are: $b_0 = 291$, $b_1 = -0.4811$, $b_2 = -0.04351$, $b_3 = -21.752$, $b_4 = -0.8819$, $b_5 = 0.000074$, $b_6 = 0.03403$, and $b_7 = 0.001532$. When regression coefficients are put into equation (2), final regression equation (3) appears.

$$Y = 291 - 0.4811 \cdot A - 0.04351 \cdot B - 21.752 \cdot C - 0.8819 \cdot D + 0.000074 \cdot A \cdot B +$$
$$+ 0.03403 \cdot A \cdot C + 0.001532 \cdot A \cdot D$$

(3)

From equation (3), it is possible to calculate the setup for the process. Because the shape and materials are given by specification of the product, only parameters which are allowed to change are forming temperature and forming time. When one of these is set, the other one can be easily calculated. That can be used for setting up the process of manufacturing of a new product by kilnforming techniques. Residuals – a difference between real measured depths of a glass dropout and depths calculated form the regression function, was good. It is because of distribution of residuals is symmetric around the regression function. The biggest difference between the regression function and the real depth is approximately 2 millimeters, which is a very good result in a glass industry focused on art manufacturing.

That all means, that it is possible to get really precise results from kilnforming processes on first setup of a process, when the DOE was used before.
For verification of results another measurements were done. In those verifying measurements were values of forming temperature and forming time changed in a way to not be same as upper, lower, or middle value from experiment. In last try the form was not set into the center of kiln to know if position in kiln is also significant or not.

Results from verifying measurements have shown that difference between calculated and real depth is on maximal value 1.2 millimeters. That proves that the experiment was done the right way and the results are usable for next production. These measurements were done only for practical verification, there is no need for this verification every time when DOE is used.

Equation (3) is used for setting up of glass slumping process with maximal dimension differences of 2 millimeters. This results are better than before the DOE was used. Results are better even in comparison with results for setting up the kiln from other authors, for example (*Sadakova & Safin, 2015*), or in comparison with recommendations from manifold guidebooks.

Beside of original state, the number of setup attempt could be reduced to minimum. Use of DOE for kinforming processes optimization is very practical. For more complex shapes there is possibility that final results will have bigger dimension differences than simple shape parts. With very high probability the DOE is good for optimization of all glass manufacturing processes.

CONCLUSIONS
It was proved that the Design of Experiment (DOE) is a great tool for describing of a kilnforming process. When the DOE is done, results can be used for predicting of a process setting, to get a correctly manufactured part on the first try. For every kiln or specific technique particular DOE must be done, because every machine and technique can have different conditions and the final regression equation have different regression coefficients. The number of setup attempts was minimized to few tries in many cases to setting up on first try. With more complex shapes there can be bigger differences between calculated dimension and final outcome.
To describe a whole kilnforming process there is needed to do the DOE for all categories of forms and for many glass types.

ACKNOWLEDGMENT

REFERENCES

1. Anderson, M., Whitcomb, P. (2015). *DOE simplified: practical tools for effective experimentation*. CRC Press, Taylor & Francis Group, (252p). ISBN: 978-1-4822-1894-7.
2. Condra, L. (2001). *Reliability improvement with design of experiments*. Marcel Dekker, (398p). ISBN: 978-0824705275.
3. Das, D., Dwivedi, A. (2013). Parametric Optimization of Heat Transfer from Triangular Fin Array Within a Rectangular Enclosure Using Design of Experiment (DOE): A Comparative Analysis. *Journal of The Institution of Engineers (India): Series C*, *93*(4), 335-343.
4. Lepšík, P., Kulhavý, P. (2017). Design optimalization of composite parts using DOE method. *58th International Conference of Machine Design Departments (ICMD)*, 200-205.
5. Sadakova, V., Safin, R. (2015). Technology of a Glass Mosaic with Use of Tack Fusing. *International Multidisciplinary Scientific Conferences on Social Sciences and Arts*, 639-646.
6. Seward, T. (2003). Modeling of Glass Making Processes for Improved Efficiency. US Project DE-FG07--96EE41262.
7. Stokes, Y. (1997). Creeping-flow computational modelling of optical quality free-surfaces formed by slumping of molten glass. In *CTAC97 Computational Techniques and Applications Conference*, 1-8.
8. Weissman, S., Anderson, N. (2015). Design of Experiments (DoE) and Process Optimization. A Review of Recent Publications. *Organic Process Research & Development*, *19*(11), 1605-1633.

Corresponding author:
Ing. Vladimír Sojka., Department of Design of Machine Elements and Mechanisms, Faculty of Mechanical Engineering, Technical University of Liberec, Studentská 1402/2, Liberec, 461 17, Czech Republic, phone: +420 485353326, e-mail: vladimir.sojka@tul.cz

EFFECT OF NITROGEN FERTILIZATION ON THE COLOUR OF WHEAT LEAVES AS AN INDICATOR OF APPLICATION DEFICIENCY

Jiří SOUČEK[1], Radek PRAŽAN[1], Jan VELEBIL[1]

[1]*Research Institute of Agricultural Engineering, p. r. i., Drnovská 507, Praha 6, Prague, 161 01, Czech Republic*

Abstract

The article is focused on comparing vegetation indices tested on plants grown in controlled environment. The indices were derived from scanned RGB images of leaves of spring wheat, variety Dafne. They were the Kawashima index (R-B)/(R+B), the excess green index (2G-(R+B))/(R+G+B) and hue. The images were processed in the ImageJ program and compared based on histograms of index values over the leaf areas. There were four variants with varying degree of fertilizer, herbicide and fungicide application to the plants, including a control variant with no application. Leaf samples were analysed for 11 weeks after the emergence of plants. The indices did not reliably distinguish between the variants, however greater differences were found between early and later stages of the plant development.

Key words: Triticum aestivum; rgb channels; vegetation index.

INTRODUCTION

The response of plants to environmental factors can express in the change of spectral reflectance of the foliage *(Ayala-Silva & Beyl, 2005)*. However, since getting a full reflectance spectrum requires costly instruments, a cheaper option is to use a hyper-spectral or multi-spectral camera to receive an image with a multitude of channels in various frequency bands ranging from ultraviolet to near-infrared light. *(Akhtman, Golubeva, Tutubalina, & Zimin, 2018)*. Most widely used approach is the employment of vegetation indices, numbers obtained by arithmetic operations usually over intensity values of red, green, blue and near-infrared bands *(Wang, Zhou, Zhu, & Guo, 2017)*. The most well-known such index is the normalized difference vegetation index (NDVI) used to evaluate the proportion of vegetation cover.

A still cheaper option is to use a regular RGB colour camera, which creates an image from three overlapping frequency bands that approximate human colour vision. RGB images can be used to distinguish the maturity status of plants *(Alharbi, Zhou, & Wang, 2018)*, to detect the presence of diseases *(Dhingra, Kumar, & Joshi, 2018)* and even to estimate the nitrogen status of plants *(Gupta, Ibaraki, & Trivedi, 2014)*.

For multiple crop plants, correlations have been found between indices calculated from RGB channels captured by a digital camera and leaf nitrogen content or chlorophyll content *(Baresel et al., 2017; do Amaral et al., 2018; Kawashima & Nakatani, 1998; Niu et al., 2019)*. Such relations have been studied using various methods ranging from simple regression to machine learning algorithms *(Barbedo, 2019)*, but predominantly they have been done on field data. There has been a lack of comparisons on plants grown in controlled environment.

Therefore, this research was focused primarily on determining the effect of different levels of pesticide application and nitrogen nutrition on the colour differences of the spring wheat leaves grown in controlled conditions.

MATERIALS AND METHODS

The research was carried out under laboratory conditions as a pot experiment. The experiment was carried out in a closed phytotron with adjustable air temperature and humidity under artificial light. The main reason was the need for precise application of fertilizers and plant care products, the possibility of adjusting the temperature and the ease of immediate measurements. In this way, unaccountable effects were eliminated. The cultivation area of each pot was 0.24 m^2.

The tested crop was spring wheat, Dafne variety. The experiment was performed at four different dosage levels, each in four replicates. The water input of each individual vessel was monitored. In later

growth stages, it was facilitated through bottom watering in combination with an automatic misting system.

Wheat was sown on March 21, the seed area density was 5.2 10^6 seeds per hectare, the sowing depth was 30 mm. Applied preparations were Roundup Klasik (pre-emergence application), nitrogen (basic fertilization and two-time urea application) and the fungicide ARTEA plus. The dosages were adjusted in multiples (0, 0.5, 1, and 2) of a base application rate. Thus, four variants of different application intensity were tested (see Tab. 1). Plants emerged March 28th.

Tab. 1 Types of application, dates and amounts

Variant	Preemergent herbicide Roundup klasik	Basic fertilization	Preemergent herbicide Roundup klasik	Fertilization – 7% urea	Fertilization – 7% urea	Fungicide ARTEA plus
	10.3. ($l.ha^{-1}$)	15.3. ($kgN.ha^{-1}$)	24.3. ($l.ha^{-1}$)	20.4. ($kgN.ha^{-1}$)	4.5. ($kgN.ha^{-1}$)	5.5. ($l.ha^{-1}$)
0	0		0	0	0	0
0.5	5	36.8	5	18.4	14.7	0.25
1	10		10	36.8	29.4	0.5
2	15		15	73.6	58.8	1

For each analysis 1 leaf was taken from each container. At the tillering stage, they were selected randomly. During the stem extension, heading and ripening stages, the leaves from the penultimate joint were sampled.

The colour of leaves was scanned immediately after removal with the CANON CanoScan 8800F scanner against a white background and saved in 24-bit bmp format. Images were analysed in the program ImageJ 1.52n. First the white background was removed using threshold function and replaced with black. The RGB channels were then split into greyscale images and subsequently arithmetic operations were performed on the split channels using the expression parsing utility of the program. The expressions were selected from literature based on good performance in sources. The expressions based on RGB values were the Kawashima index *(Kawashima & Nakatani, 1998)* (equation 1) and excess green index *(Woebbecke, Meyer, Von Bargen, & Mortensen, 1995)* (equation 2).

$$KI = (R - B)/(R + B) \tag{1}$$

$$ExGI = (2G - (R + B))/(R + G + B) \tag{2}$$

These operations resulted in 32-bit depth images from which histograms were acquired. The histograms were made from values in the range from -1 to 1 and sorted into 256 bins. The histogram counts were converted to relative frequencies and the distribution of expression values was summarized by average value and standard deviation.

As a third index, hue was selected. For this the images were converted into HSB (hue, saturation and brightness) colour model and only hue histogram was used. Hue values are reported in degrees in 360° scale.

All used indices are expected to be reasonably independent on the brightness of the image, significantly more so than the original RGB channels and they have been used to distinguish between plant canopies and soil, therefore being in practice useful also for the estimation of vegetation cover ratio. However, they still could change according to white balance of the image etc. Therefore, each image was taken with the same setting of the device. Figure 1 shows an example of histograms of RGB channels and indices made from the same image. It is evident, that the indices have narrower distributions, thus making them more suitable to distinguish between images.
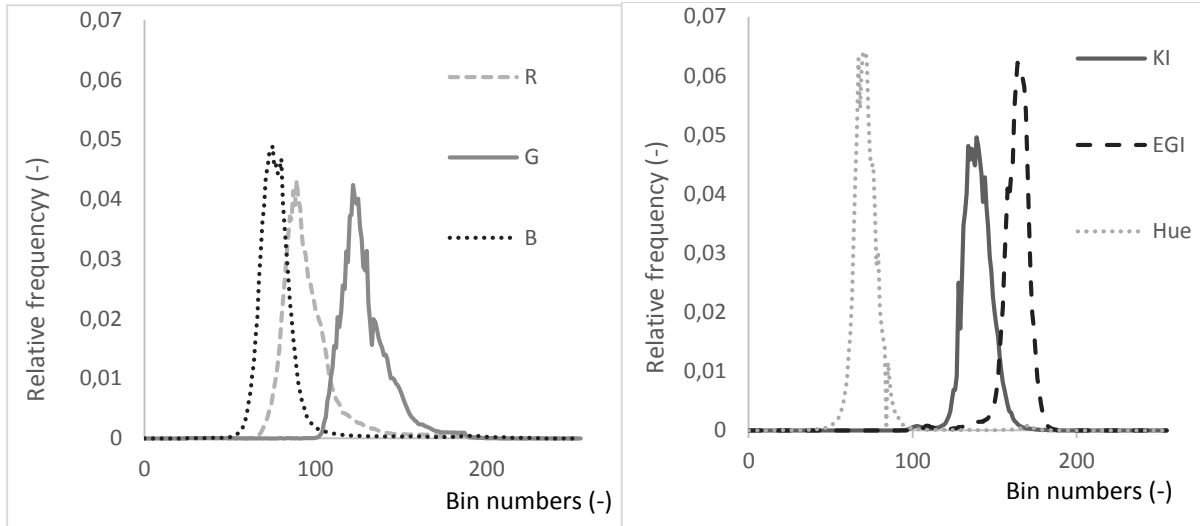
Fig. 1 Histograms of RGB channels and indices of an image, horizontal axes show histogram bin numbers.

RESULTS AND DISCUSSION

Table 1 presents the Kawashima index values. The KI values received were in the range from -0,032 to 0,091 and there was a decreasing tendency with succeeding sampling dates. In *(Kawashima & Nakatani, 1998)* chlorophyll content was correlated with the expression 0.952 – 1.76 KI, however the range of KI values was higher (ca. 0.1-0.5). However, there is a weak tendency towards lower values of KI in variants with more nitrogen input. This is more evident in the last three samplings. However, the differences between variants at the same date are always well within one standard deviation.

Tab. 2 Kawashima index (KI) average values and standard deviations

Variant	weeks after emergence							
	2	5	6	7	8	9	10	11
0	**0,091**	**0,084**	**0,044**	**0,061**	**0,016**	**0,013**	**0,000**	**0,015**
	±0,069	±0,055	±0,054	±0,055	±0,048	±0,050	±0,045	±0,044
0.5	**0,085**	**0,075**	**0,053**	**0,029**	**0,029**	**0,001**	**-0,017**	**-0,008**
	±0,071	±0,049	±0,057	±0,064	±0,059	±0,053	±0,047	±0,049
1	**0,067**	**0,072**	**0,051**	**0,051**	**0,011**	**-0,027**	**-0,027**	**-0,021**
	±0,065	±0,056	±0,052	±0,055	±0,044	±0,046	±0,049	±0,046
2	**0,087**	**0,069**	**0,056**	**0,036**	**0,029**	**-0,017**	**-0,032**	**-0,027**
	±0,069	±0,059	±0,048	±0,054	±0,056	±0,045	±0,049	±0,048

Table 3 shows the values of excess green index. EGI is generally useful to distinguish green plant parts from e.g. soil, however it has been also shown to correlate weakly with chlorophyll content in rice *(Saberioon et al., 2014)* but with varying correlation coefficients in different development stages. In present case it shows similar behaviour to KI since it also tends to decrease with the development of the plants, although with multiple exceptions. The values for variants are very close again except for the last three sampling dates when the variants with lower applications show higher EGI.

Tab. 3 Excess green index (EGI) average values and standard deviations

Variant	weeks after emergence							
	2	5	6	7	8	9	10	11
0	**0,275**	**0,271**	**0,247**	**0,243**	**0,235**	**0,219**	**0,197**	**0,219**
	±0,069	±0,061	±0,056	±0,050	±0,049	±0,053	±0,053	±0,048
0.5	**0,257**	**0,276**	**0,241**	**0,235**	**0,244**	**0,203**	**0,175**	**0,199**
	±0,078	±0,053	±0,058	±0,054	±0,055	±0,055	±0,054	±0,050
1	**0,267**	**0,275**	**0,256**	**0,250**	**0,224**	**0,182**	**0,156**	**0,178**
	±0,079	±0,063	±0,049	±0,055	±0,045	±0,054	±0,058	±0,047
2	**0,268**	**0,267**	**0,255**	**0,253**	**0,233**	**0,188**	**0,154**	**0,172**
	±0,083	±0,060	±0,046	±0,052	±0,058	±0,046	±0,059	±0,045

Table 4 shows hue values expressed in degrees and which can be easily expressed in a circular diagram for easy visual comparison. In studied data the hue values tend from warm green (hue 105) towards mid green and cool green (hue 120-135) with the development of the plants. The variants are very close until week 7. Again, the last three weeks show the largest differences between variants.

Tab. 4 Hue average values and standard deviations in degrees

Variant	weeks after emergence							
	2	5	6	7	8	9	10	11
0	**103**	**102**	**109**	**105**	**115**	**116**	**119**	**115**
	±18	±15	±14	±11	±12	±16	±16	±14
0.5	**104**	**103**	**107**	**113**	**113**	**120**	**125**	**122**
	±23	±10	±17	±14	±14	±17	±18	±16
1	**107**	**105**	**107**	**108**	**116**	**128**	**130**	**126**
	±22	±14	±12	±13	±14	±17	±21	±16
2	**104**	**104**	**106**	**111**	**111**	**125**	**132**	**128**
	±25	±15	±11	±12	±17	±12	±21	±16

In the presented data, varying degrees of fertilizer, herbicide and fungicide application do not show significant differences. Since the values could not be correlated with leaf nitrogen or chlorophyll contents, it cannot be determined whether they are useful for nitrogen measure on spring wheat. On the other hand, differences are more obvious between early and later growth stages. Therefore, they could still be used for comparing development and ripeness level in a field.

In practice, colour sensing methods can be sensitive to light conditions. For example, in sunny conditions the increased surface reflections will yield wider distribution of colour intensities. This makes reliable differentiation between index values more difficult. Also, it means that there is a potential for errors if conditions change during image acquisition over tested area. It is, therefore, reasonable to conduct both experiments in controlled environment and in field to ascertain the effectiveness of an image treatment algorithm.

CONCLUSIONS
Three indices derived from RGB images of spring wheat leaves from a colour scanner have been tested for their differences for 11 weeks after plant emergence in four degrees of fertilizer, herbicide and fungicide application doses. The tested indices were the Kawashima index, excess green index and hue. The indices performed generally similarly in that they were capable of distinguishing between stages, however differences between application variants were not significant, although they were not correlated with chlorophyll or nitrogen content.

REFERENCES

1. Akhtman, Y., Golubeva, E., Tutubalina, O., & Zimin, M. (2018). Application of Hyperspectral Images and Ground Data for Precision Farming. *Geography, Environment, Sustainability*, *10*(4), 117–128. doi: https://doi.org/10.24057/2071-9388-2017-10-4-117-128

2. Alharbi, N., Zhou, J., & Wang, W. (2018). *Automatic Counting of Wheat Spikes from Wheat Growth Images*, (May 2019), 346–355. doi: https://doi.org/10.5220/0006580403460355

3. Ayala-Silva, T., & Beyl, C. A. (2005). Changes in spectral reflectance of wheat leaves in response to specific macronutrient deficiency. *Advances in Space Research*, *35*(2), 305–317. doi: https://doi.org/10.1016/j.asr.2004.09.008

4. Barbedo, J. G. A. (2019). Detection of nutrition deficiencies in plants using proximal images and machine learning: A review. *Computers and Electronics in Agriculture*, *162*(April), 482–492. doi: https://doi.org/10.1016/j.compag.2019.04.035

5. Baresel, J. P., Rischbeck, P., Hu, Y., Kipp, S., Hu, Y., Barmeier, G., & Schmidhalter, U. (2017). Use of a digital camera as alternative method for non-destructive detection of the leaf chlorophyll content and the nitrogen nutrition status in wheat. *Computers and Electronics in Agriculture*, *140*, 25–33. doi: https://doi.org/10.1016/J.COMPAG.2017.05.032

6. Dhingra, G., Kumar, V., & Joshi, H. D. (2018). Study of digital image processing techniques for leaf disease detection and classification. *Multimedia Tools and Applications*, *77*(15), 19951–20000. https://doi.org/10.1007/s11042-017-5445-8

7. do Amaral, E. S., Vieira Silva, D., Dos Anjos, L., Schilling, A. C., Dalmolin, Â. C., & Mielke, M. S. (2018). Relationships between reflectance and absorbance chlorophyll indices with RGB (Red, Green, Blue) image components in seedlings of tropical tree species at nursery stage. *New Forests*, 1–12. doi: https://doi.org/10.1007/s11056-018-9662-4

8. Gupta, S., Ibaraki, Y., & Trivedi, P. (2014). Applications of RGB color imaging in plants. *Plant Image Analysis*, (February 2015), 41–62. doi: https://doi.org/10.1201/b17441-4

9. Kawashima, S., & Nakatani, M. (1998). An Algorithm for Estimating Chlorophyll Content in Leaves Using a Video Camera. *Annals of Botany*, *81*(1), 49–54. doi: https://doi.org/10.1006/anbo.1997.0544

10. Niu, Q., Feng, H., Li, C., Yang, G., Fu, Y., Li, Z., & Pei, H. (2019). *Estimation of Leaf Nitrogen Concentration of Winter Wheat Using UAV-Based RGB Imagery*. doi: https://doi.org/10.1007/978-3-030-06179-1_15

11. Saberioon, M. M., Amin, M. S. M., Anuar, A. R., Gholizadeh, A., Wayayok, A., & Khairunniza-Bejo, S. (2014). Assessment of rice leaf chlorophyll content using visible bands at different growth stages at both the leaf and canopy scale. *International Journal of Applied Earth Observation and Geoinformation*, *32*, 35–45. doi: https://doi.org/10.1016/J.JAG.2014.03.018

12. Wang, L., Zhou, X., Zhu, X., & Guo, W. (2017). Estimation of leaf nitrogen concentration in wheat using the MK-SVR algorithm and satellite remote sensing data. *Computers and Electronics in Agriculture*, *140*, 327–337. doi: https://doi.org/10.1016/j.compag.2017.05.023

13. Woebbecke, D. M., Meyer, G. E., Von Bargen, K., & Mortensen, D. A. (1995). Color indices for weed identification under various soil, residue, and lighting conditions. *Transactions of the American Society of Agricultural Engineers*, *38*(1), 259–269.

Corresponding author:
Ing. Jiří Souček, Ph.D., Research Institute of Agricultural Engineering, p. r. i., Drnovská 507, Praha 6, Prague, 161 01, Czech Republic, phone: +420 233 022 214, e-mail: jiri.soucek@vuzt.cz

STRESS FACTORS IDENTIFICATION USING THERMAL CAMERA

Karel STARY[1], Zdeněk JELÍNEK[1], Jan CHYBA[2]

[1]*Czech University of Life Sciences, Faculty of Engineering, Department of Machinery Utilization, Kamýcká 129, CZ165 00 Prague, Czech Republic*
[2]*Czech University of Life Sciences, Faculty of Engineering, Department of Agricultural Machines, Kamýcká 129, CZ165 00 Prague, Czech Republic*

Abstract
The yields of plant production are limited by a number of stress factors affecting the plants during its vegetation. Heat, water stress, herbivorous organisms and other stress factors have a negative effect on the crop yields. This study is focused on describing the impact of stress factors of plants by monitoring the rape drying process by a thermal camera. The results of the measurement showed that the plant of rape resists heat and water stress for quite a long time without obvious damage, but after three hours of the drying process the damage started to occur very quickly. The plant transpiration stopped and gradually dries from the bottom leaves. Data collection of drying processes can help to decrease the loss of the yield during the heatwaves by setting the right time and amount of water for irrigation of the crops.

Key words: Stress factors; plant production; thermal camera.

INTRODUCTION

The growth of the world population and there to related increasing food consumption requires higher yields from food producers. Therefore the food producers have to seek new options how to increase the yields of their production. Stress factors are one of the main risks for the plant production and plant producers are looking for new methods how to eliminate the negative impacts of the stress factors. Plants are exposed to a variety of abiotic stresses such as drought, flood, salinity, freezing, cold and hot temperature, various light intensity and many others during their growth and development *(Mohanta et al., 2017)*. The living organisms are also interacting with other organisms and the environment. They have positive, negative or neutral impact on the environment. In case of negative influence, the organisms are designated as the biotic stressors. Those could be bacteria, viruses or even humans. Stress factors usually interact in the various combinations together. For instance the high temperature stress is usually accompanied with water stress and high light intensity *(Procházka, 1998)*. When the stress influence crosses the limit of plant stress tolerance, plant organs dysfunction and other disabilities occur *(Bláha, 2003)*. Different crops respond differently to the stress exposure, but high temperatures during days could lead to damage on reproductive processes. Interestingly, certain wild crop species have developed mechanisms to escape the stress damage. This could be examples for breeding field crops that are resilient to heat stress *(Prasad et al., 2017)*.

It is highly relevant to detect the stress early, but it is very hard to achieve it. Near infrared imaging could be used to uncover stress related processes in the early stages *(Behmann et al., 2014)*. Detection of plant stress in the early stages is of utmost importance for breeding crops with a higher stress tolerance as well as for improvement of methods of crop management and therefore, it is vital for irreversible damages and yield loss prevention. *(Tester & Langridge, 2010)*. One of the method how to prevent yield losses and ensure the water supply of the plants is the utilization of the thermal infrared imaging system. This system maintains high measurement accuracy and could be considered for measuring crop water stress at high spatial and temporal resolution. These are required for managing water irrigation. Thermal sensing is sensitive to crop water requirements and leads to efficient allocation of available water resources for irrigation *(Mangus et al., 2016)*. Thermal image analysis have also potential to estimate leaf area index (LAI). The LAI derived from thermal imaging could be a very accurate indicator of the crop biophysical parameters and moisture stress condition *(Banerjee et al., 2018)*. The main aim of this study was utilization of thermal camera to monitor the process of water stress affecting rape plant since it allowed to recognize the stress in its early stages. Such ability is vital in order to take adequate agronomical measures and thus prevent the plant damages and overall yield losses.

MATERIALS AND METHODS

The simulation of the water stress impact on the rape plant was done in growth stage 2, decimal 19. The simulation took place in laboratory. To provide stable temperature, the laboratory was air-conditioned and the windows were darkened for the elimination of reflected heat. Thermal camera FLIR A655sc was used for the measurement. The camera was hold on a frame construction. The construction was built over a measured plant and the camera was hanged under the right angle down above the plant. FLIR A655sc is a R&D thermal camera for science and research purposes. The camera belongs to the LWIR (Long-Wavelength Infrared) category with a spectral range of 7-14 µm. This camera is equipped with a very good temperature stability, homogenous picture, high measuring accuracy and temperature sensitivity (<30mK). The experiment was set up according to the camera producer instructions to reach the highest measuring accuracy.

The results of the measuring were processed with the Workswell CorePlayer software which was optimized for this particular research. The measuring was running for eight hours, therefore the software had to be modified for long sequences recording.

Before the experiment commenced the emissivity of the measured surface had to be specified. The accurate setting of the emissivity is required for the correct measuring results. If the thermal camera was set up for a higher emissivity than what the actual level in the environment in which the object is, the camera would measure lower temperature than what the actual temperature is. And vice versa, if the camera was set for a lower emissivity than what the actual level in the environment in which the object is, the camera would measure higher temperature. The emissivity is governed by following relation:

$$\varepsilon_T = \frac{H_E}{H_{OE}} \tag{1}$$

where: H_E is the radiation intensity of the measured surface and H_{OE} is the radiation intensity of the black object. In this case the emissivity was set on $\varepsilon_T = 0,7$.

The measuring took 8 hours, while a picture was taken every 5 minutes. Shots with a period of 20 minutes were used for evaluation of the experiment. This article includes selected thermal images showing the impact of water and heat stress on a rape plant.

RESULTS AND DISCUSSION

Upon commencement of the experiment (4:19 p.m.) the rape plant did not suffer by heat nor water stress. The processed thermal image showed that the surface of the leaves was cool, the pores in leaves were open and the photosynthesis proceeded. It was confirmed in Fig. 2 where the majority of the plant surface temperatures ranged between 20-22 °C.
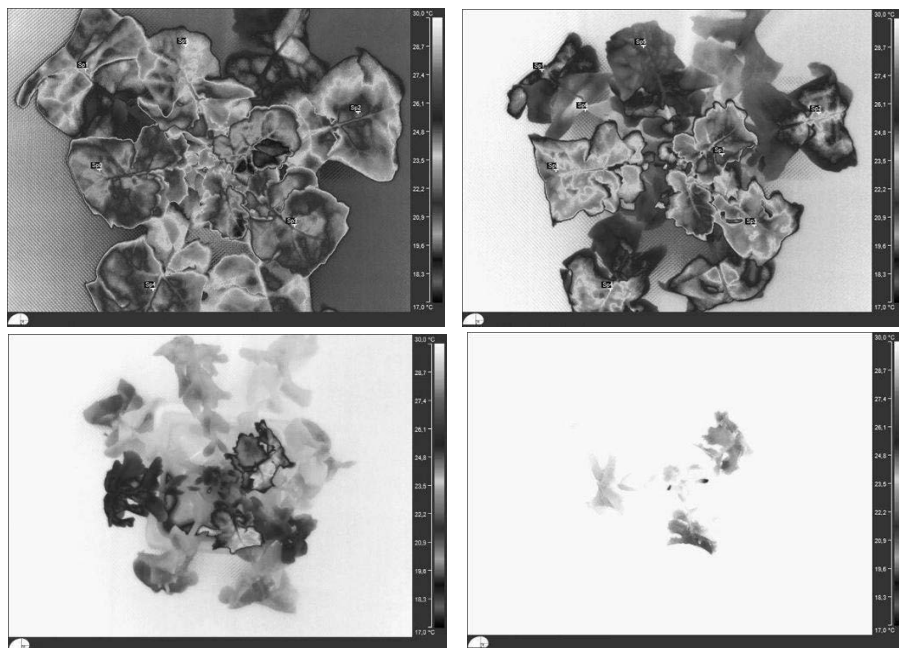

Fig. 1 Plant surface temperature at 4:19 p.m. (top left), 7:39 p.m. (top right), 8:59 p.m. (bottom left) and 10:59 p.m. (bottom right)
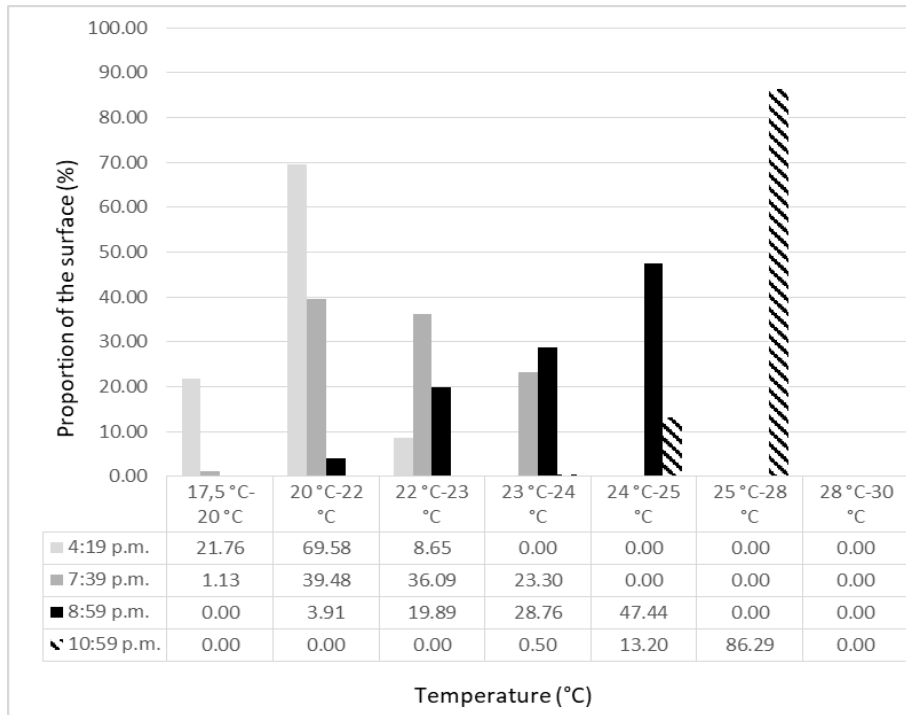
Fig. 2 Representation of temperatures during the experiment.

The water and heat stress began to significantly affect the plant within 3 hours from the start of the experiment. In comparison with the thermal image at the beginning of the experiment, the temperature of leaves on the ground whorl of the plant was increased. The water potential was reduced and the transpiration was decreased. The plant concentrates its water potential to the upper whorl leaves in order to cool them down. The lack of water became critical for the rape plant after next one and half hour of stress influence (at 8:59 p.m.). Water potential was reduced to the critical limits, which resulted in decrease of the turgor pressure down to 0 and fading of leaves. The pores in leaves were closing, the photosynthesis and transpiration was slowed down until it ceased completely. The only leaves ensuring the transpiration were on the top of the plant. The drying process continued very quickly. At 10:59 p.m. the plant was almost completely dried up. In Fig. 1 is clearly proved that the surface of the plant ability to transpire is significantly reduced in comparison with the beginning of the experiment. The only transpiring and cooled down leaves were on the upper part of the plant. The Fig. 3 depicts the whole measuring process in a timescale. Water stress is considered to be one of the main threats for winter oilseed rape plants within the next few decades *(Pullens et al., 2019)*.
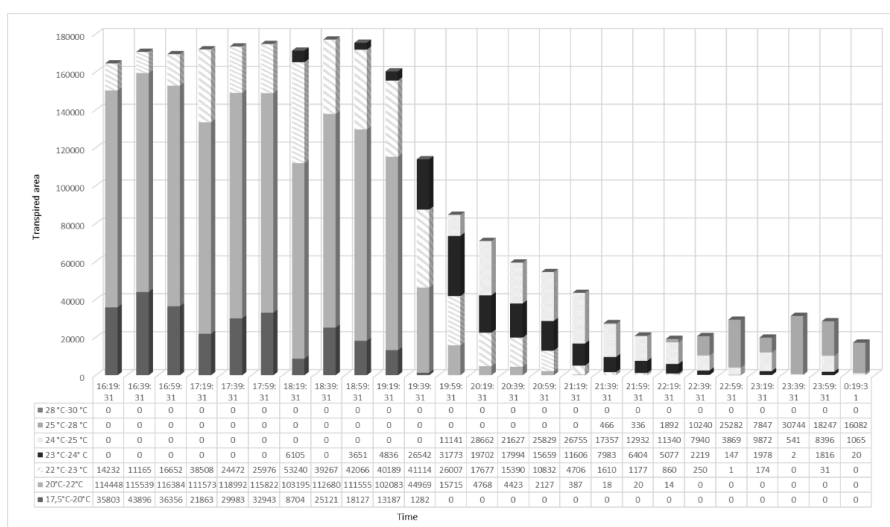

Fig. 3: Transpired area surface during the experiment

Together with other kinds of stresess which have an adverse effect on plants, it is crucial to establish effective strategies in order to maximize the yield. *(Sabagh et al., 2019)* Our measuring not only confirmed results from previous experiments made on different crops *(Mangus et al., 2016)*, *(Banerjee et al., 2018)*, but also proved that the utilization of thermal camera imaging is a highly acccurate method for detecting water stress and utilization thereof could have a positive impact on reduction of yield losses. Aforesaid is also in accordance with a study which found out that utilization of thermal imaging is the most suitable technology for monitoring and assessment of crop water status *(Ezenne et al., 2019)*.

CONCLUSIONS

The measuring of the rape plant proved clearly that the plant is able to resist to the stress impact without an obvious damage for nearly three hours. After this time period first consequences start to appear. The rape plant ceases to cool down leaves in the bottom level. They cease to transpire as well as the photosynthesis stops and leaves wither away. Upon reaching this breakpoint, the damage on the rape plant is irreversible. From 6:59 p.m. to 21:59 when the stress affected the plant, the transpiration area decreased by almost 90%. The withering of the plant proceeds from the lower levels to the top floors of the plant, which are cooled down and provide photosynthesis as the last leaves from the rape plant. The measuring also proved the existence of connection between the heat and water stress. Since the first water stress started to appear, the average leaf temperature increases up to the point where the whole rape plant withers away.

Performance of experiments of water and heat stress could help to set the stress damage breaking points and help to prevent damages and yield losses in the plant production.

ACKNOWLEDGEMENT

REFERENCES

1. Banerjee, K., Krishnan, P., & Mridha, N. (2018). Application of thermal imaging of wheat crop canopy to estimate leaf area index under different moisture stress conditions. *Biosystems Engineering*, *166*, 13-27.

2. Behmann, J., Steinrücken, J., & Plümer, L. (2014). Detection of early plant stress responses in hyperspectral images. *ISPRS Journal of Photogrammetry and Remote Sensing*, (93), 98-111.

3. Bláha, L. (2003). *The Plant and the Stress) (1 ed.)* (in Czech). Prague: Výzkumný ústav rostlinné výroby (Crop Research Institute).

4. Mangus, D., Sharda, A., & Zhang, N. (2016). Development and evaluation of thermal infrared imaging system for high spatial and temporal resolution crop water stress monitoring of corn within a greenhouse. *Computers and Electronics in Agriculture*, *121*, 149-159.

5. Mohanta, T., Bashir, T., Hashem, A., & Abdalleah, E. (2017). Systems biology approach in plant abiotic stresses. *Plant Physiology and Biochemistry*, *2017*(121), 58-73.

6. Prasad, P., Bheemanahalli, R., & Jagadish, S. (2017). Field crops and the fear of heat stress—Opportunities, challenges and future directions. *Field Crops Research*, *200*, 114-121.

7. Procházka, S. (1998). *Plant Physiology (1. ed.)*. Prague: Academia. (in Czech).

8. Tester, M., & Langridge, P. (2010). Breeding Technologies to Increase Crop Production in a Changing World. *Science*, *327*(5967), 818-822.

9. Pullens, J. W. M., Sharif, B., Trnka, M., Balek, J., Semenov, M. A., & Olesen, J. E. (2019). Risk factors for European winter oilseed rape production under climate change. *Agricultural and Forest Meteorology*, 272-273, 30-39.

10. Ezenne, G. I., Jupp, L., Mantel, S. K., & Tanner, J. L. (2019). Current and potential capabilities of UAS for crop water productivity in precision agriculture. *Agricultural Water Management, 218*, 158-164.

11. Sabagh, A. E. L., Hossain, A., Barutçular, C., Islam, M. S., Ratnasekera, D., Kumar, N., et al. (2019). Drought and salinity stress management for higher and sustainable canola (Brassica napus L.) production: a critical review. *Australian Journal Of Crop Science*, 13(01), 88-97.

Corresponding author:
Ing. Karel Starý, Department of Machinery Utilization, Faculty of Engineering, Czech University of Life Sciences Prague, Kamýcká 129, Praha 6, Prague, 16521, Czech Republic, phone: +420 723641581, e-mail: staryk@tf.czu.cz

RELIABILITY OF SELECTED BIOMETRIC IDENTIFICATION SYSTEMS

Veronika ŠTEKEROVÁ[1]

[1]*Department of Vehicles and Ground Transport, Faculty f Engineering, Czech University of Life Sciences Prague*

Abstract
Biometric identification systems are increasingly being used today. Face recognition biometry is the second most common biometric identification right after the fingerprint recognition. The paper is focused on the reliability of systems in difficult conditions, which were gradually simulated and the time of acceptance or incorrect rejection of the user was measured. Measurements were made in a laboratory environment where two biometric sensors were available.
The results show that the time of acceptance or rejection was to some extent influenced by the users themselves. Users have influenced the system with their reference frame, their position and facial expression in front of the reader. The paper showed these biometric readers are not suitable for areas where difficult conditions can occur.

Key words: *biometrics; face recognition; identification; difficult conditions.*

INTRODUCTION

The face is one of the best known biometric features. It is intuitively used every day without a person realizing that now there is a biometric identification. The ability to respond to facial stimuli is one of the first cognitive functions acquired by newborns (*Rak, Matyáš & Říha, 2008; Eysenck, Michael & Keane, 2010).* It is the most natural and widely used method of identification with a high level of reliability. In fact, the human brain stores the faces of people with whom it comes into contact. However, biometric identification itself is known for over 30 years, although identifying people by recognizing human faces is as old as humanity itself *(Ježek, 1996).*

Due to the development and development of technology, the cost of manufacturing of electronic components is constantly decreasing, making biometric systems affordable. Biometric identification systems are increasingly being used today, in quite common devices such as mobile phones or computers. Due to their high reliability they are not only suitable for smaller or larger companies and corporations, but they are the main domain of the army, securing nuclear weapons, sharply guarded financial sector, stadiums, airport areas, reception of major sites or other significantly guarded places and locations. Governments all over the world demand for biometric security of integrated border protection systems. In the commercial sector, biometric security systems are among the main factors that attract potential clients, as identity protection and cyber-attack prevention are in high demand today (*Drahanský, Orság, 2011).* The aim of this study is reliability of selected biometric identification systems under difficult conditions.

MATERIALS AND METHODS

The whole measurement took place in the laboratory of the department where constant conditions were ensured. Two biometric readers were available in the laboratory to recognize the face-based user. It was a biometric reader Multibio 700 and Aktion AFT-500.

Biometric Reader Aktion AFT-500

Biometric Reader Aktion AFT-500 (Fig. 1) is a terminal with built-in face recognition system, integrated card reader and keyboard. It is a biometric face reader that supports identification (1:N) as well as verification (1:1). The verification method is possible with a combination of RFID card / chip or PIN code. The reader processor has a frequency of 600 MHz. The device is designed with IP54 protection, which allows it to be used outdoors, where higher water contact is expected.

Biometric Reader Multibio 700
This reader, which can be seen in Fig. 2, is elegant, robust, and ergonomic in design, combining face recognition, fingerprinting, and PIN added to the integrated RFID module. It captures the relative position, size and shape of the user's eyes, nose, cheekbones and jaw. The reader enables identification (1:N) and verification (1:1).

Luxmetr - CEM-DT-8809A
Another equipment used is the Luxmeter - CEM-DT-8809A (Fig. 3), which was used to simulate one of the difficult conditions. It is a measuring instrument that measures light intensity. This photometric quantity is defined as the luminous flux that falls on the unit of surface. It can therefore be said that it is the ratio of luminous flux, which is given in lumens and area, which is given in square meters.

Fig. 1 Biometric reader Aktion AFT-500, SOURCE: http://shop.efg.cz/z19476-aft-500
Fig. 2 Biometric Reader MultiBio 700, SOURCE: http://www.zkteco.com/product/Multi-Bio700_241.html
Fig. 3 Luxmetr - CEM-DT-8809A

The same difficult conditions were simulated for both biometric readers. Both of these readers are located on a panel whose graphical representation can be seen in Fig 4.
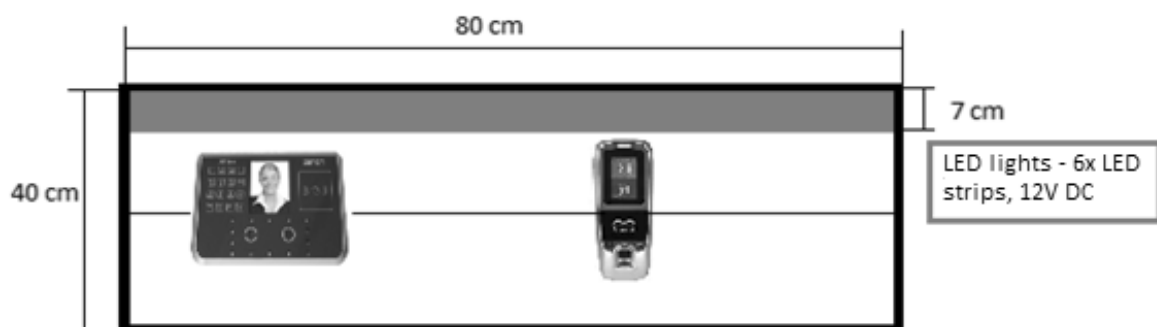

Fig. 4 Graphic representation of the panel

Fig. 5 shows the real photo of the reader panel, which is located in the laboratory. Among other things, the photo and LED strips, which consists of six-meter strips and each of them has 30 high-luminous RGB LEDs - in total, this LED strips 180 has RGB LEDs.

Fig. 5 Panel of biometric readers

Difficult conditions

These are various factors that can occur and affect the reliability of face recognition systems. A total of 11 difficult conditions were tested. Each difficult condition was measured a total of ten times. The following difficult conditions were chosen: brown curly wig, black straight wig, sunglasses, eyeglasses, winter hat, baseball cap, distinctive make-up, soiling with coal, foil scan and artificial light conditions. In one case it will be to ensure the greatest possible darkness and in the second case to ensure as much light as possible, which will be provided by the LED strips. The room will be obscure for the dark.

Measurement procedure

In order to be able to make measurements, it was first necessary to take a user's reference image to create a user profile. A total of 10 people participated in the measurement, namely: 6 men and 4 women. Volunteers were between the ages of 23 and 27.

During the measurement, individual identification times were recorded, for each difficult condition, and any false rejections or false admissions were recorded. All measured times were recorded in pre-prepared tables. Subsequently, the measured data from the tables were analyzed and the FRR was calculated for the individual difficult conditions.

The time of identification was determined for testing, for one identification attempt. This limit was 10 seconds from the start of shooting. If the person was not identified within 10 seconds, the identification was considered unsuccessful. This measurement was then marked with the X symbol in the pre-prepared measurement tables.

First, it was necessary to record each volunteer as a user in the reader and take a reference picture. The reference picture was taken without glasses in normal daylight.

The measurement started with the measurement of the shooting time when the glasses were attached. Next was a measurement with a headgear like a winter hat and a cap. It was used two wigs - black straight with bangs and dark brown curls without bangs. Then followed a scan through the foil. Conversely, for a larger amount of light in the room was used a light in the form of LED strips, which can be controlled by the remote control and adjust its intensity differently. In the end, there was a strong make-up, both for women and men. Rich red lipstick, strong blush and dark blue eyeshadow were used. The last time was measured by the time of scrubbing the face with coal. To obtain reliability data, it was necessary to use a formula that determines the level of false acceptance. This formula is part of one of the two basic types of biometric errors and reads as follows:

$$FRR = \frac{N_{FR}}{N_{EIA}} = \frac{N_{FR}}{N_{EVA}} \qquad (1)$$

where *FRR* is False Rejection Rate, N_{FR} is Number of False Rejection, N_{EIA} is Enrolle Identification Attempt.

RESULTS AND DISCUSSION

A total of 2,200 measurements were taken. In order to evaluate the measurement results, it was necessary to first average all the measurement times we obtained, and this is shown in Tab. 1.

Tab. 1 Average acceptance times for measurements (sec)

	Aktion AFT-500	Multibio 700
Sunglasses	x	x
Eyeglasses	x	x
Cap	1,72	2,2
Winter hat	2,13	1,07
Curly wig	2,18	2,31
Straight wig with bangs	1,93	1,95
Foil	x	x
LED strips	1,29	1,52
Dark	x	x
Soiling with coal	1,51	2,07
Make up	1,49	2,38

As a result of the measurement, the FRR was calculated for each difficult condition. Formula 1 was used to determine this value.

The FRR results for the Aktion AFT - 500 reader are as follows: 100% eyeglasses, 100% sunglasses, 12% cap, winter hat 35%, black bangs 22%, dark brown curly wig 51%, 100% foil, LED strips 0%, dark 100%, soiled face with 3% charcoal and 33% distinct makeup.

The results of the Multibio 700 reader are: prescription glasses 100%, sunglasses 100%, cap 33%, winter hat 44%, black wig with bangs 51%, dark brown curly wig 51%, foil 100%, LED strips 0%, darkness 100%, soiled face with charcoal 28% and distinctive makeup 25%.

Tab. 2 shows the overall error rejection rate for all difficult conditions for each reader.

Tab. 2 Total False Rejection Rate (sec)

	Aktion AFT - 500	Multibio 700
N_{EIA}	1100	1100
N_{FR}	556	632
FRR	51 %	57 %

It has been found that the reliability of readers is relatively low under difficult conditions. Difficult conditions can occur under different circumstances and nowadays biometric readers need to be able to respond. The overall false rejection rate (FRR) was relatively high. This is the frequency of rejection of authorized users. The rate of false rejection does not directly threaten the system's security, but it causes complications to the user and the identification process needs to be repeated or a new identification key generated. The Aktion AFT-500 reader had a FRR of 51% while the Multibio 700 reader had a FRR of 57%. Not only because of the FRR value, but also for its user-friendliness, the Aktion AFT-500 biometric reader was found to be a better choice than the Multibio 700 reader. As a further disadvantage,

the Multibio 700 reader does not even signal when it starts to scan. The Aktion AFT-500 reads that it scans because a square is visible around the face it focuses and detects. The Multibio 700 did not display anything at all, displaying only the quality of the scanned image - if the image quality was not higher than 5, the user was not authenticated at all. Another disadvantage is its very small touch screen, where it was quite difficult to work. From the user's point of view, the Aktion AFT-500 reads better than the MultiBio 700 and can be used as a sound or light signal for MultiBio 700 readers. Fig. 6 shows the rate of mis-acceptance for individual difficult conditions for biometric readers.
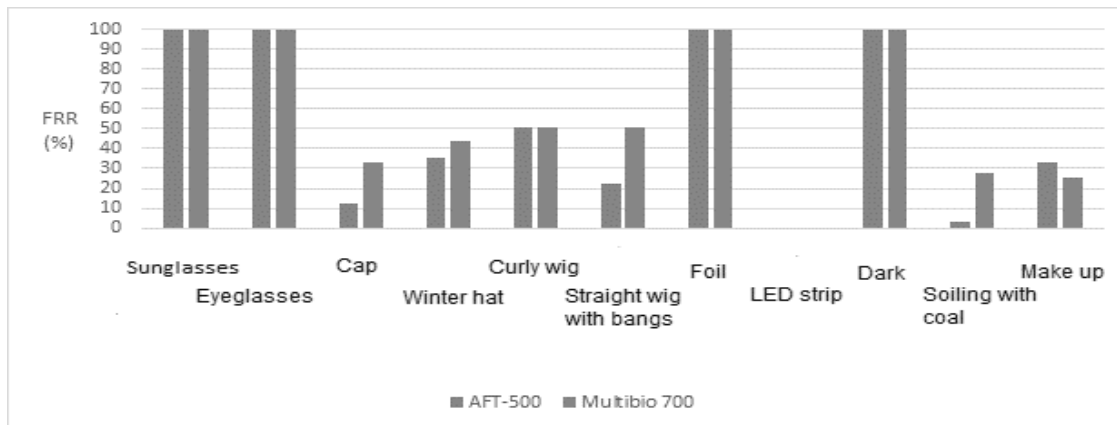
Fig. 6 FRR for individual difficult conditions for biometric readers

Technavio is predicted to grow by more than 79% by 2021 to further enhance security, mainly because the technology based on biometric identification becomes affordable.

Due to the low reliability of biometric readers, it is advisable to provide them with a more appropriate recognition algorithm. This problem could be solved by face recognition based on dictionary learning *(Liao & Gu, 2019)*. Dictionary learning plays an important role in sparse representation based face recognition. In their paper, they propose a face recognition algorithm based on dictionary learning and subspace learning.

Facial recognition is a challenging task, *Abudarham N., Shkiller L., Yovel G.,* comes with a study where they use reverse engineering to discover which facial features are critical to familiar face recognition. As a result, they propose a new framework that assumes a similar perception of all faces and integrates knowledge and perception to take account of the excellent human knowledge of familiar faces.

Toshiba has developed face recognition software, as face recognition technology is used in a wide variety of applications, including identifying individuals in video surveillance systems used in public spaces, identifying airports and financial institutions, and marketing activities to identify personal attributes such as age, gender, or expression. Toshiba has more than 20 years of experience in face recognition technology and achieves excellent face recognition results. Among other things, it has a high processing speed and has also received excellent feedback.

CONCLUSIONS

Biometrics is an area where new technology is constantly developing. Recently, this is a security method that ensures a high level of security, and that is why this type of security is being sought and is becoming more and more used. It is important to keep in mind that it is a matter of protecting property or just taking an attendance system to select a suitable reader. This research means that it should be used in common commercial spaces

This research shows that the selected biometric readers are not suitable for use in more demanding areas and shows that the reliability of biometric systems under difficult conditions is low.

These readers are suitable for environments where they do not experience difficult conditions - for example use in attendance systems in companies. These biometric readers are not suitable for property security.

REFERENCES

1. Aburddarham, N., Shkiller, L., & Yovel, G., 2019, Critical features for face recognition. *Cognition, 182*, 73-83.

2. Biometrics in 2018: For ever more secure security. Retrieved from http://www.businessit.cz/cz/biometricke-prvky-v-roce-2018-pro-stale-dokonalejsi-zabezpeceni.php.

3. Digital luxmetr CEM DT-8809A. gme.cz. Retrieved from https://www.gme.cz/digitalni-luxmetr-cem-dt-8809#product-detail

4. Drahanský, M., Doležel M., & Orság, F. (2011). *Biometrie* . Brno: Computer Press. ISBN 978-80-254-8979-6.

5. Eysenck, M., W., & Keane, M., T. (2010). *Cognitive psychology: a student's handbook.* 6th ed. New York: Psychology Press. ISBN 978-1841695402.

6. Ježek, V. (1996). *Systémy automatické identifikace: aplikace a praktické zkušenosti*. Praha: Grada. ISBN 80-7169-282-4

7. Liao M. & Ge, X., (2019), Face recognition based on dictionary learning and subspace learning. *Digital Signal Processing*, *90*, 110-124.

8. Putting More Than Just a Name to a Face. Retrieved from https://www.nec.com/en/global/solutions/safety/face_recognition/

9. Rak, R., Matyáš, V., Říha, & Z. (2008). *Biometrie a identita člověka ve forenzních a komerčních aplikacích*. Praha: Grada. Profesionál. ISBN 978-80-247-2365-5.

10. The Rise of Biometric Security. Retrieved from http://www.fastlane-turnstiles.com/press-releases/biometric-security/

Corresponding author:

Ing. Veronika Štekerová, Department of Vehicles and Ground Transport, Faculty f Engineering, Czech University of Life Sciences Prague, Kamýcká 129, Prague, Czech Republic, stekerova@tf.czu.cz

YIELD PREDICTION OF POTATO BY UNMANNED AERIAL VEHICLE

Dai TANABE[1], Shigeru ICHIURA[1], Ayumi NAKATSUBO[2], Takashi KOBAYASHI[2], Mitsuhiko KATAHIRA[2]

[1]*The United Graduate School of Agricultural Sciences, Iwate University*
[2]*Yamagata University*

Abstract
We built an analysis system that combined image data from UAV and Deep-Learning AI to investigate the relationship between image data and actual yield. The experiment was designed with 6 fertilizer treatments in the potato field, aerial images were obtained and plant growth and yield was measured. A potato yield prediction model was then built with AI on the basis of the aerial image and potato yield. Results showed a difference in plant cover between each plot, but no difference in NDVI value. Each fertilizer treatment produced a variation in plant growth as time progressed. There was a correlation between potato yield and NDVI value in etiolation stage. Yield prediction model accuracy with RGB image during the growth stage was the highest.

Keywords: UAV; NDVI; IoT; AI; Potato.

INTRODUCTION

At present, the number of agricultural workers is decreasing in Japan *(Ministry of Agriculture, Forestry and Fisheries, 2015)* and there is a concern that the agronomic technology that comes from experience will be lost. Therefore, new approaches such as robotization and introduction of AI (artificial intelligence) technology are being promoted. As part of that, UAV (Unmanned Aerial Vehicle) has been used as a new platform for efficiently acquiring information in the field. In addition, NDVI (None Differential Vegetation Index) is most commonly used as a vegetation index for evaluating the growth of plants from aerial images such as UAV. On the other hand, AI technology has been rapidly developed against the background of GPU (Graphics Processing Unit) and Big Data, and in the field of agriculture, attempts are being made to classify crop species at the field level and to detect disease of crops using deep learning *(Yaping, et al., 2018; Jun, et al., 2017)*. However, since large amount of learning data is essential for accurate learning, only few cases have been reported in literature were AI was applied to yield prediction of land use type crops which have many fluctuation factors outdoors.

This research aims to establish a new method to predict potato yield by analyzing the data obtained from UAV with AI.

MATERIALS AND METHODS
Agricultural summary

The experiment was conducted at Takasaka Agricultural field centre of Yamagata University, located in Tsuruoka City, Yamagata Prefecture. The field dimensions were length 40m, width 7.5m, with an area of 300m². Test crop was potato (Solanum tuberosum L. "Toyoshiro") and was transplanted on May 1st 2018. The row spacing was 0.75 m, plant spacing 0.3 m and the planting density was 4.44 strains / m². 3kg /m² of barnyard manure, 100 g/m² of bitter lime, 40 g/m² of fused magnesium phosphate, 10 g/m² of heavy roasted phosphorus were spread as soil improvement material before transplanting. Base fertilization was 2 ~ 10 g-N/m² of chemical fertilizer (N: P_2O_5: K_2O= 14:14:14) and additional fertilization was 2 g-N/m² of ammonium sulphate. Additional fertilizer was applied on June 4.

UAV flights and aerial images

Aerial image was obtained by the multi-copter (S900, DJI) equipped with a multispectral camera (Micro MCA RGB+3, Tetracam). The shooting altitude was 30 m, and approx. 100 images were acquired. The aerial image was acquired with overlap rate was 75 % or more and the side wrap rate was 60 % or more. The ground resolution of the aerial image was approx. 0.015 m / pixel. The aerial photograph was obtained during 10:00 to 14:00 hrs after emergence of potato in each week. Individual plants were selected to measure growth in advance and set up some marks before the flight. Aerial images were processed with Pixel Wrench2 (Tetracam) and ortho-mosaic images built with Photoscan (Agisoft). Ortho-

mosaic images were evaluated and mapped by calculating NDVI. Moreover, the band values for each pixel was extracted from the ortho-mosaic image, it correlated with ground truth data and used for analysis of plant growth.

Construction of test area

Six test areas were created by combining the amount of base fertilizer and the additional fertilization in the test field described above: A) 10 g-N/m^2 of base fertilizer and 2 g-N/m^2 of additional fertilizer. B) Only 10 g-N/m^2 of base fertilizer. C) 6 g-N/m^2 of base fertilizer and 2 g-N/m^2 of additional fertilizer. D) Only 6 g-N/m^2 of base fertilizer. E) 2 g-N/m^2 of base fertilizer and 2 g-N/m^2 additional fertilizer. F) Only 2 g-N/m^2 of base fertilizer. Fig.1 showed the arrangement of each test field.
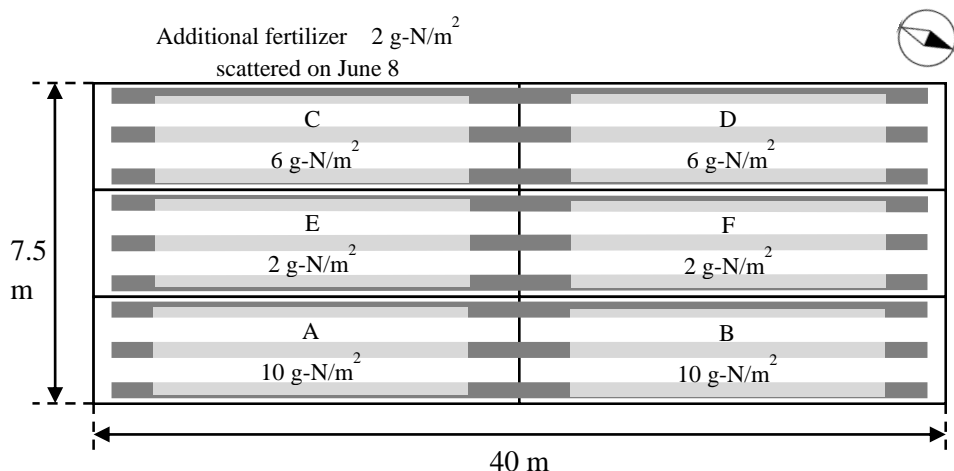
Fig. 1 Construction of test area

Plant growth survey

The plant growth survey was conducted on May 28, June 14, 25, July 9 in 2018. Three individual plants were selected in each survey area and the measurement parameters were plant height, total weight, and plant dry weight. In this report, only the data of plant height is published.

Yield survey

The potato harvest survey was conducted on August 6, 2018. Five survey plots of 1.8 m × 1.8 m were chosen in each test area of the field. 4 individual plants were harvested from each survey plot surveyed. The measurement parameters were total tuber weight (g) and number of tubers (piece).

Yield prediction

Multiple regression analysis based on growth data and deep learning artificial intelligence was used for potato yield prediction.

The statistical software R (ver. 3.5.1) was used for the multiple regression analysis with yield (g/m^2) as the dependent variable while the explanatory variables were the NDVI value and plant height for each growth survey.

The data set for construction potato yield prediction model was created as follows: 1) The plot portion used for the yield survey was cut from the aerial photographs of each growth stage from May to July 2018. 2) Plot portion image's angle was changed by 90, 180, 270, 360 degrees. 3) They were classified by yield (kg/m^2) calculated from the yield survey results. 4) Classified images were organized at each growth stage, and a total of 1080 images were used for training each time. 5) Images in which the left and right of the plot image were inverted were created and used as test data. The Chainer framework (ver. 1.23.0) and Alex Net neural network was used for building the AI with a batch size 32 and epoch number 100 used for learning.

RESULTS AND DISCUSSION

Aerial photographs

Fig.2 (a) shows RGB aerial images for each season. Aerial image of May 28 shows a clear difference in emergence due to difference in base fertilization condition. Area A and B had the strongest growth in the test field. On June 14, the difference in the size of the plant body and the size of the plant canopy

due to variation in base fertilization is evident, also the difference in growth due to the presence or absence of additional fertilizer can be slightly confirmed in comparison with the area E and F. In the image taken on June 25, due to size of the canopy the space between the rows was obscured in area A and B. There was also a mixture of plants with respect to maturity and growth of secondary plants.

Fig.2 (b) shows NDVI aerial images for each stage. The height of the NDVI is expressed in grayscale, where white indicates high NDVI and black low NDVI. The image on May 28 is similar to the RGB image, and the difference in emergence can be confirmed clearly. Although the difference is not seen in NDVI. In the image on June 14, the difference is not seen in NDVI, In the image on June 25, there is a tendency for NDVI to be slightly higher in the high fertility area. In the image of July 9, NDVI appears to be uniform overall. The average NDVI value has changed each area: A) 0.62, 0.80, 0.74, 0.79. B) 0.64, 0.80, 0.77, 0.77. C) 0.64, 0.77, 0.68, 0.73.D) 0.58, 0.77, 0.77, 0.77. E) 0.53, 0.78, 0.75, 0.74. F) 0.57, 0.78, 0.75, 0.74. The same trend is observed in all treatment areas, but NDVI, which dropped by one in the third to fourth surveys, raised again. At the time of the third survey, most plants yellowed and NDVI decreased, but at the time of the fourth survey, new leaves with high photosynthetic activity had grown secondarily, and the NDVI levels increased.
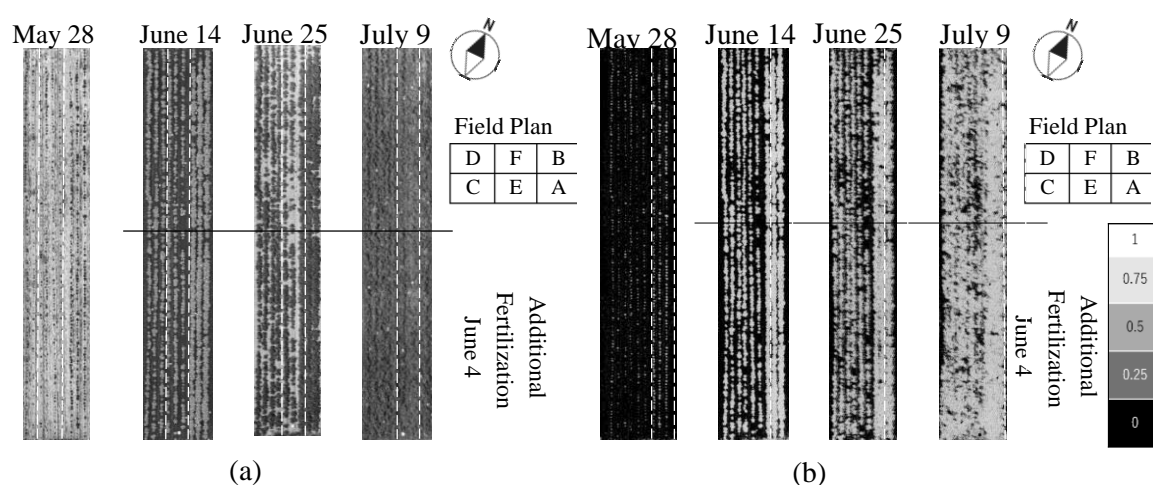

Fig. 2 The aerial image. (a) RGB aerial image; (b) NDVI aerial image.

Plant Growth Survey

The transition of plant height is shown in Fig.3 (a). The plant height has changed in each area: A) 0.21 m, 0.46 m, 0.63 m, 0.75 m. B) 0.19 m, 0.48 m, 0.63 m, 0.67 m. C) 0.15 n, 0.42 m, 0.52 m, 0.60 m. D) 0.17 m, 0.43 m, 0.53 m, 0.63 m. E) 0.16 m, 0.41 m, 0.53 m, 0.63 m. F) 0.21 m, 0.38 m, 0.51 m, 0.55 m. Although there was little difference in the growth survey during the early stages of growth in the test period, plant height increased during test interval in accordance with age and the amount of nitrogen applied. In addition, the growth rate of plant height was low at the fourth growth survey in the B, D, and F areas where no additional fertilization was performed, and the additional fertilization affected the growth of plant height at the later growth stage for areas A, C and E.

Fig.3 (b) shows the correlation between NDVI and plant height. The coefficient of determination R^2 was 0.58. The plant height and NDVI showed the higher correlation than the total weight and the plant dry weight ($R^2 = 0.24, 0.41$). This suggests that it is possible to construct a growth, yield prediction model using NDVI and the plant height as parameters.

According to the report of Hunt, E.R., et al., Potato with different nitrogen conditions tended to show no difference in LAI, NDVI, etc. during tuberization *(Hunt, E.R., et al., 2018)*. This is the same result for NDVI in this test. However, in the tests where nitrogen and phosphoric acid application conditions were changed respectively, it has been reported that frequent use of N and P promotes the increase of plant height and biomass etc. *(Zelalem, et al., 2016)*. Also in this test, there is a tendency that there is a difference in treatment area in plant height. It can be said that the effect of the difference in fertilization amount is larger in plant height than in NDVI.
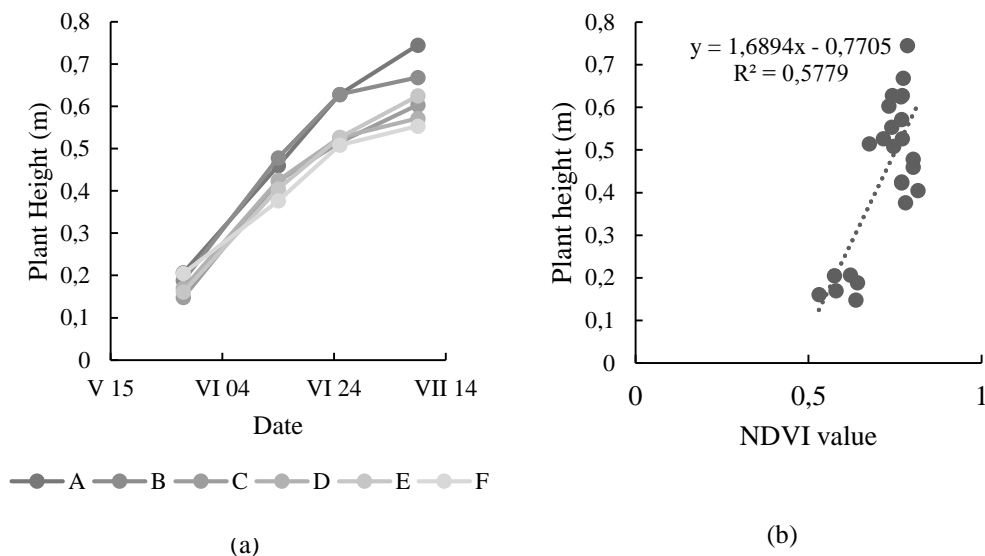
(a)

(b)

Fig. 3 The result of plant survey. (a) The transition of plant height; (b) The correlation of NDVI and plant height.

Table 1 shows the yield of potato and the number of tubers per individual plants in each test section. The total yield varied with the amount of fertilization mostly: A) 4230 g/m². B) 4371 g/m². C) 2543 g/m². D) 2913 g/m². E) 2936 g/m². F) 2061 g/m². Regarding the yield, the standard deviation tends to be high in B, D and F areas where no additional fertilization was performed. This indicates that the nitrogen supply at the late growth stage was insufficient due to the absence of additional fertilization, and the translocation of nutrients to the tuber was uneven.

Tab. 1 Yield and number of tubers

Area	Yield (g/m²)	Number of Tubers
A	4230 (515.0)	10.3 (2.67)
B	4371 (1252.1)	12.5 (4.12)
C	2543 (667.5)	7.0 (3.25)
D	2913 (824.5)	7.8 (1.26)
E	2936 (343.6)	10.2 (1.44)
F	2061 (738.1)	8.3 (2.85)

Note: The numbers in parentheses indicate the standard deviation

The coefficient of determination between the NDVI value of each period and the yield is shown in Table 2. The yield of potato was highly correlated ($R^2 = 0.67$) with the NDVI value on July 9, and the number of tubers per individual plant was highly correlated with the NDVI value on June 14 ($R^2 = 0.67$). The flowering period of the potato corresponds to the tuber period, which was June 14 in this test. Therefore, the correlation between the NDVI value of this day and the number of tubers has increased. In addition, the fourth NDVI value has a strong correlation with the yield and the number of tubers because nitrogen absorption by secondary growth of plants affected tuber growth. For these reasons, the construction of potato yield prediction model with the potential to predict yield or number tubers, based on the aerial image of the plant at flowering or late growth stage is suggested.

Khalid et al. Examine the relationship between NDVI from satellites and potato yield, and report that they can be predicted with an accuracy of $R^2 = 0.39$ to 0.65 *(Khalid, et al, 2016)*. The accuracy in this research is $R^2 = 0.02$ to 0.67, which is the same as or lower than that of previous researches. These facts show that even with high-resolution aerial images, it is difficult to predict potato yield with only NDVI, and another method is needed to accurately predict potato yield.

Tab. 2 Coefficient of determination of NDVI value each of season and potato yield

	R^2	Yield (g/m^2)	Number of tubers
NDVI	May 28	0.24	0.02
	Jun 14	0.31	0.67
	Jun 25	0.18	0.23
	Jul 9	0.67	0.47

Yield Prediction by multiple regression analysis

The results of multiple regression analysis of yield, NDVI value and plant height for each survey period are shown in Table 3.

The yield was predicted with high accuracy from the NDVI value and plant height on June 14 (early flowering season) and June 25 (late flowering season). This indicates that the growth of plant height at the flowering stage and the photosynthetic activity affect the yield.

Tab. 2 The results of multiple regression analysis

$Y=-4466.08+11380.94*X_1+46.96*X_2$ （May 28）
$R^2=-0.1252$
$Y=-18851.5+11698.7*X_1+222.4*X_2$ （June 14）
$R^2=0.9998$
$Y=-3397.2-3108.6*X_1+159.5*X_2$ （June 25）
$R^2=0.8199$
$Y=-10917.02+11393.95*X_1+86.36*X_2$ （July 9）
$R^2=0.5835$

Y: yield (kg/10a), X_1: NDVI value and X_2: Plant height (cm).

Yield prediction by Deep Learning

Fig.4 shows accuracy of yield prediction model based RGB image (a) and NDVI image (b). As shown in Fig.9 (a), the prediciton accuracy of each class is 12.2%, 50.2%, 37.1%, 60.3%, 5.1% in the growing stage, 2.5 %, 64.7 %, 46.8 % 37.3 %, 6.1 % in the flowering stage, 4.2 %, 22.1 %, 40.9 %, 28.3 %, 4.5% in the etiolation stage. On the other hand, as shown Fig. 9 (b), 5.7 %, 14.2 %, 25.4 %, 56.1 %,12.9 % in the growth stage, 0.0 %, 15.8 %, 45.1 %, 0.2 %, 0.1 % in the flowering stage, 4.2 %, 22.1 %, 40.9 %, 28.3 %, 4.5 % in the etiolation stage.

The RGB image-based model had better overall prediction accuracy than the NDVI image based one. Among those modelled on RGB images, the yield prediction accuracy at the growth stage and the flowering stage was higher than that the etiolation stage. The prediction accuracy was 33.0%, 31.5% and 20.0% in each stage. This caused no difference in plant canopy with the progress of time. Additionally, the accuracy rate of 1 - 2 kg/m^2 and 6 - 7 kg/m^2 classes were lower than any other classes. This was due to the number of data set being less than other classes.

The NDVI image-based model had a large difference in prediction accuracy depending on the stage. The prediction accuracy is biased to 4 - 5 kg/m^2 in growth stage, 3 - 4 kg/m^2 in flowering stage and 2 - 3 kg/m^2 in etiolation stage. This indicates that the model unable to differentiatie between plots, and NDVI image is not suitable to build a yield prediction model.

Therefore, RGB aerial image in growth or flowering stage is suitable for constructing a potato yield prediction model by Deep Learning. However, it is necessary to improve accuracy because Deep Learning model accuracy is lower than multiple regression analysis.

The low accuracy and bias of the prediction by AI in this test is due to the Imbalanced Data Set. There are two approaches to learning correctly with the Imbalanced Data Set. One is to assign high cost to minority class misclassification to minimize the overall cost, and the other is to adjust the number of samples by sampling. If the total number of data sets is small as in this test, it is considered that the former is applicable. In addition, accumulation of data sets will be required from now on.
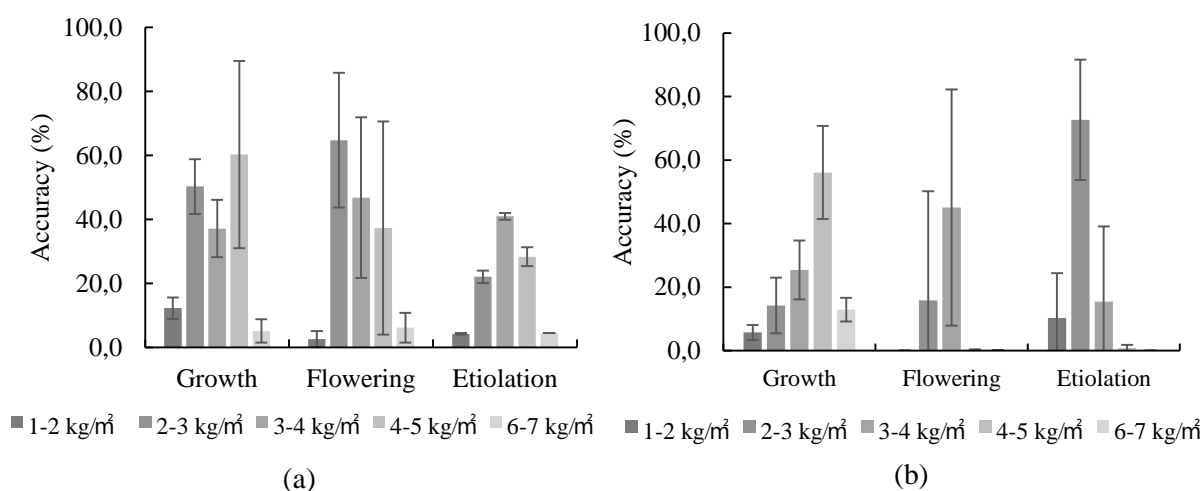
Fig. 4 Accuracy of the yield prediction model. (a) Based RGB image; (b) Based NDVI image.

CONCLUSIONS

This research was aimed at the establishment of the next generation of agriculture by IoT and tried to build a new monitoring system that combined aerial image data with UAV and analysis method by Deep Learning AI. The tests were conducted in the potato field under different fertilization treatments. The aerial image showed the difference of canopy by the difference of the fertilization treatment, but the difference was not seen in the NDVI value. NDVI value was correlated with plant height and the yield was correlated with the NDVI value in the yellowing stage, while the number of tubers were correlated with the NDVI value in the flowering stage. In the multiple regression model with NDVI value and plant height as explanatory variables and yield (g/m^2) as the target variable, the data at flowering stage gave high prediction accuracy. The yield prediction model with AI based RGB image in the growth stage was the highest prediction accuracy, but further improvement of this method is required.

REFERENCES

1. Alex, K., et al. (2012). ImageNet Classification with Deep Convolutional Neural Networks. *COMMUNICATIONS OF THE ACM, 60*, 84-90, 2017

2. Hunt, E.R., et al. (2018). Monitoring nitrogen status of potatoes using small unmanned aerial vehicles. *Precision Agriculture, 19*, 314-333

3. Japkowicz, N., & Stephen, S. (2002). The class imbalance problem: A systematic study. *Intelligent Data Analysis, 6*(5), 429-449

4. Jin, G. H., et al. (2017). Deep convolutional neural network for classifying Fusarium wilt of radish from unmanned aerial vehicles. *Journal of Applied Remote Sensing, 11*(4), 042621

5. Khalid, A. A., et al. (2016). Prediction of Potato Crop Yield Using Precision Agriculture Techniques. *PLOS ONE, 11*(9), e0162219

6. Ministry of Agriculture, Forestry and Fisheries (2015). CENSUS OF AGRICULTURE AND FORESTRY IN JAPAN Report and Data on the results. Retrieved from http://www.est at.go.jp/SG1/estat/ListE.do?bid=0000010858 18&cycode=0.

7. Yaping, C., et al. (2018). A high-performance and in-season classification system of field-level crop types using time-series Landsat data and a machine learning approach. *Remote Sensing of Environment, 210*, 35-47

8. Zelalem, A., et al. (2016). Response of potato (Solanum tuberosum L.) to different rates of nitrogen and phosphorus fertilization on vetisols at Debre Berhan, in the central highlands of Ethiopia. *African Journal of plant Science, 3*(2), 016-024.

Corresponding author:

Dai Tanabe, The United Graduate School of Agricultural Sciences, Iwate University, Nishishinsai-machi, 10-35, Tsuruoka-city, Japan , 997-0045, tanabe.d.zc32s@gmail.com

ZIGBEE PROTOCOL AND MICROCONTROLLER ON A PV SYSTEM FOR A MILKING CATTLE ROBOT

Tomáš TESAŘ[1], Petr VACULÍK[1], Rui MELICIO[2], Victor M.F. MENDES[3]

[1]Department of Technological Equipment of Buildings, Czech University of Life Sciences Prague
[2]ICT, Departamento de Física, Escola de Ciências e Tecnologia, Universidade de Évora, Portugal
[3]CISE, Electromechatronic Systems Research Centre, Universidade da Beira Interior, Portugal

Abstract
This paper is about a system for supporting action of management in an industrial building integrated photovoltaic system by a supervising and monitoring data collector system of environmental data. The integrated photovoltaic system is a grid-connected rooftop-mounted having energy storage with the main purpose of supplying energy for an industrial milking cattle robot. The main equipment of the robot, the photovoltaic system is summarized and the equipment for supporting the assessment of the environmental data is further addressed. This equipment play an important role in nowadays for industrial milking and even more important in a smart grid context. Sensors, actuators and ZigBee technology are used in an association with Arduino allowing to have available information to carry way the management. Finally, conclusions are addressed about the hardware for the supervising and monitoring.

Key words: PV system; milking cattle robot; monitoring; wireless sensors; microcontroller; ZigBee.

INTRODUCTION

The study in this paper is about a Building Integrated PV (BIPV) roofing system with a wireless monitoring and control based on the ZigBee protocol. As main downstream devices, the roofing system accommodates power for a milking cattle robot and an energy storage intended to partially or fully side-step the supplying of energy from the electric utility. The system under study can enable further functionality, for instance, can enable control of sun radiance and temperature in rooms, protection or safety control of the building. The International Energy Agency Implement of Photovoltaic Power Systems Operational Performance of PV Systems and Subsystems (IEA PVPS Task 2) has established a set of parameters describing the operational performance of PV systems in buildings (*Batista et al., 2014; Boonmee et al., 2009*). The main parameters associated with the performance are: module temperatures, solar irradiation, wind speed, the DC power generated by the PV system, the AC grid voltage, and the AC current injected into the grid (*Batista et al., 2014; Boonmee et al., 2009*). The ZigBee technology has been gathering great acceptance (*Fadlullah et al., 2011*), advantaging from having low power consumption, low cost and an outstanding wireless networking protocol to be used in wireless connections in automation and remote-control (*Batista et al., 2014*). The IEEE 802.15.4 is a standard for a Low-Rate Wireless Personal Area Network (LR-WPAN) defining the Physical Layer (PHY) and Media Access Control (MAC) and is maintained by the IEEE 802.15 working group (*Batista et al., 2014*). LR-WPAN supports low cost modules, low power consumption, secure communication, data collision avoidance and power management (*Batista et al., 2012a; Batista et al., 2012b*). The ZigBee technology is a specification based on the IEEE 802.15.4 standard extending that definition by developing extra new higher layers. ZigBee technology can be implemented in mesh networks, with a larger range, than the Bluetooth technology. This technology is expected to transmit from 1 m to 100 m, depending of the in-situ environment sources of interference and of the power output consumption (*Batista et al., 2012a*). The IEEE 802.15.4 standard defines two different types of devices: Full Function Devices (FFD) or Reduced Function Devices (RFD). An FFD can communicate with any other device and perform all the functions defined on the standard, including relaying messages and sensor/actuator tasks. An FFD can play the role of coordinator, router or end device in the Personal Area Network (PAN) powered from an AC supply to be always active and monitoring the PAN (*Batista et al., 2012b*). An RFD requires relatively small resources memory size, compatible with a lower processing capability and allowing a decrease on the final cost. Typically, an RFD must be connected to an FFD and are not used to act as a coordinator or as a router but as an end device such as a sensor or

an actuator performing limited tasks (*Batista et al., 2012b*). There are two types in IEEE 802.15.4 for the topology: Peer to Peer or Star. The Peer to Peer topology as shown allows the creation of Cluster-tree networks. This topology also as shown allows the creation of mesh networks, allowing all messages to be routed to any other FFD. In the Star topology the FFD acting as a coordinator is the central node having other FFD and RFD nodes attached directly to the coordinator (*Batista et al., 2012a; Batista et al., 2012b*). ZigBee technology has a wide acceptance and successful operates in many applications (*Batista et al., 2012b*). A wireless sensor network is valuable technology for monitoring a PV system using radio frequency transceivers, sensors and microcontrollers. Wireless sensor networks have embedded self-organizing, self-configuring, self-diagnosing and self-healing capability. The aim of this study about a BIPV real implementation with a remote monitoring data system for the PV system having a storage battery, supplying power to a milking cattle robot, situated in Žďár nad Sázavou, Czech Republic. The main parameters collected on in situ are: solar irradiance, wind speed and temperature. Prototypes of sensors for temperature, pyranometer and one anemometer are performed using microcontroller Arduino hardware and software and the ZigBee network technology interfaces the system with a Python software. The rest of the paper is organized as follows. Section II presents the main framework the followed procedure a summarizes the robot and the PV systems. Section III presents the Monitoring Data Collector. Finally, concluding remarks are in Section IV.

MATERIALS AND METHODS

The sensor prototypes implemented for the tests are: a ZigBee coordinator module with processing capability offered by an Arduino board as in (*Batista et al., 2014*; *Georgitzikis et al., 2012*); a ZigBee end-nodes connected to the Arduino board; and a ZigBee module that will function only as router. The ZigBee end-node in the receiver side is also attached to an Arduino board that reads the Received Signal Strength Indicator (RSSI) and displays the value in an LCD screen in decibel-milliwatts [*dBm*]. The field tests test the RSSI information and the loss of data. The ZigBee communication devices are configured to operate in an Application Programming Interface (API) mode, delivering the RSSI information of a module. This module receives the message and the checksum byte of the packets data frame validating if the data arrives without errors (*Batista et al., 2014*). The relation between transmitted power and the received power is given by the Friis transmission equation (*Batista et al., 2014*) given by:

$$\frac{P_r}{P_t} = G_t . G_r . \left(\frac{\varphi}{4.\pi.d}\right)^2 \tag{1}$$

In (1) where P_t and P_r are respectively the transmitted power and the received power which has to be higher than the sensitive of the receiver, P_t and P_r are in the same units of power; G_t and G_r are respectively the gains of the transmitter and the receiver antennas; φ is the wavelength given by the channel in the ZigBee devices; d is the distance between the transmitter and the receiver antennas. φ and *d* are in the same units of length. The received signal strength indicator final $\overline{RSSI}$ value is taken in the ZigBee (*Batista et al., 2014*). The signal strength is given by:

$$\overline{RSSI} = \frac{1}{n} \sum_{i=1}^{n} RSSI_i \tag{2}$$

In (2) n is the number of samples. The RSSI value only reflects the received signal strength of the last message hop and not the signal strength of all the routers (multihops), neither the general quality of the transmission. So, if a device is connected to a router, the RSSI value only represents the signal strength between the last router and the device and not between the ZigBee coordinator sending the message and the device (*Batista et al., 2014*). Before the sensor modules installation, an evaluation of the ZigBee devices location is made by evaluating the RSSI value for different positions. At the transmitter side the Arduino board with the ZigBee coordinator operating in API mode is configured to send data packets to a predefined ZigBee device under analysis for the RSSI signal analysis, which has a predetermined 64 bit network address. These packets are sent in intervals of 5 s. At the receiver side the ZigBee end-node has a microcontroller Arduino board that reads the RSSI value by taking n samples in intervals of 5 s and then averaging the samples to be displayed. Concerns with the installation of sensors, for instance, information to be delivered to the destination, insurance of delivering without errors or faults (*Batista et al., 2017*) have been taken into consideration. The data collector is a

support information system for the schedule of needed energy considering the capture by BIPV roof system and the stored energy, having the main purpose of supplying power to a milking cattle robot situated in a farm in Žďár nad Sázavou, Czech Republic. The objective is avoiding as much as possible the usage of electric energy from the electric grid utility. The farm has around 70 cows to be milked and installed the milking cattle robot in 2008. The milking cattle robot is one of the first milking cattle robots installed in the Czech Republic by the company DeLaval. The Robot installed is a single-blade milking robot having two parts. The first part consists of a cage box in the form of a container and is made of stainless-steel resistant to corrosion. The box is very spacious, the teat cups can be deployed in the teats of the cow by human intervention. The entrance and exit doors are electronically controlled to be opened and closed by a hydraulic motor. The doors positioning is on the side of the box and the dairy cows pass through the arc when passing through the milking robot. There is an identification set on the box structure. The floor is a non-slip rubber with built-in nozzles to easily clean the dirt from a hygienic point of view. The second part of the milking robot is the engine room where the hydraulic two-articulated rotary milking arm of the stainless steel is located. The milking arm performs the test preparation before milking, the teat cup deployment and re-deployment. If necessary, then a correction is made for the position of the milk hose and teats disinfection after milking. This arm is inspired in the human hand and easily responds to the tear irregularities with a deflection of up to 45° in a wide range, of high or low seated of mammary gland of the cows. There is on the shoulder an optical camera and a double laser. There are four teat cups hanging beside their shoulders able to drip and remain free of dirt, and the fifth handpiece cleaning the udder is placed under the same principle as the teat cups of the quarter. The robot is equipped with an oil-free air compressor and four optical milk counters for each area to monitor deviations and abnormalities in flow, bed, admixture and blood flow rates. The Robot LCD displays information coming from the software processing decision making and recording event and data. The energy for the Robot is supplied by the: PV system, 15 battery system installed in the farm or the local electric grid. The PV array has a power of 5.25 kWp and is composed by 21 PV panels of Polycrystalline technology Omsun 250 W with an allowed module operating temperature of -40 to 85℃ and the Normal Operating Cell Temperature (NOTC) is 45±2℃. More data at standard test conditions (STC) for the modules Omsun 250 W (*Omsun, 2019*) are shown in Tab. 1.

Tab. 1 STC DATA OF OMSUN 250 W

Technology	V_{MP}	I_{MP}	V_{OC}	I_{SC}	Efficiency
Polycrystalline	31.36 V	7.98 A	38.41 V	8.51 A	15.20 %

In Tab. 1 the values for the voltage and current at maximum power give a power of 250 Wp per PV module and a form factor of 76 % at STC, but due to ageing a value of 0.60 %/year of degradation is to be expected. The balance-of-system has a battery management system as usually included in the DC circuit and the power inverter implemented has anti-islanding protection. The inverter is compatible with the PV systems power and with the three-phase bus bar of the AC circuit connecting to the electric grid utility. The inverter implemented is a three-phase PV power inverter GoodWe GW10K-DT. The sensors and the data transmitter are installed near the PV arrays on the roof of one of the buildings. While the receiver and monitoring data collector are installed in another, see Fig. 1 a). The PV array and the monitoring by the sensors of wind speed, irradiance and temperature in situ are near of the PV arrays as shown for the pyranometer and the anemometer respectively in Fig. 1 a), b), c), d). In Fig. 1 b) the cup anemometer shown has a range between 0.9 m/s and 40 m/s and the electrical output has a frequency of 100 Hz for a wind speed of 40 m/s. This anemometer, 4.3515.51.105 is produced by (*Thies Clima, 2019)*. In Fig. 1 c) the pyranometer shown has the spectral range between 310 nm and 2800 nm, the time response is less than 18 s. Although this time is greater than the response of the PV modules, this difference is not relevant for the purpose of monitoring PV modules (*Boonmee et al., 2009*). This pyranometer, CM6B (*Thies Clima, 2019*), is produced by Kipp and Zonenand is based on a thermocouple device. In Fig. 1 d) the temperature sensor shown is a digital thermometer, DS18B20, produced by Maxim Integrated (*Maxim Integrated, 2019*), providing 9 bit to 12 bit Celsius measure-

ments in a range between -55 °C and +125 °C and has an alarm function with non-volatile user programmable upper and lower trigger points.

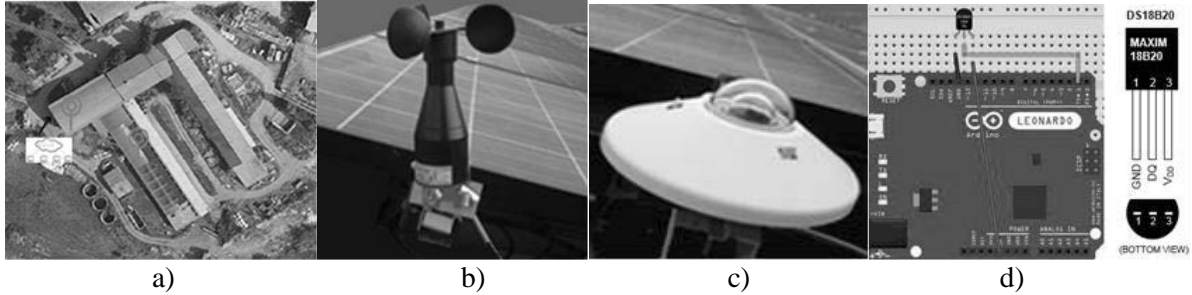a)   b)   c)   d)

Fig. 1 Sensors: a) PV array, b) anemometer, c) pyranometer, d) temperature sensor and Arduino.

RESULTS AND DISCUSSION

The distance between the transmitter antenna near the PV arrays and the receiving antenna at the building where the monitoring data collector is located is about 40 m and the wireless transmission shown in Fig. 1 a) is implemented by ZigBee network technology. Normally, a linear increase on the maximum power is expected with the increase in the irradiance. Also, the power output of a PV cell can be considered as an affine function of the PV cell temperature (*Woyte et al. 2013*): a reduction on power for the OMSUN 250 W of 0.475 % is expected per 1 °C of increase in the PV module. The energy capture by the PV arrays for one day depends on the in situ peak sun-hours, which is the in situ irradiation per unit of area in $[kWh/m^2]$ computed by the integral of the irradiance over the time. So, the parameters influencing the capturing of energy by the PV system in situ are: the horizontal component of the wind speed, the irradiance, the temperature where the PV modules are implemented. The cup anemometer produced by Thies Clima, 4.3515.51.105 (*Thies Clima, 2019*), measures the value of the angular frequency of the anemometer which is considered as an affine function of the wind speed. So, the anemometer transfer function (*Pindado el at., 2012*) is given by:

$$V = A.f + B \qquad (3)$$

In (3) V is the wind speed [*m/s*], f is the output frequency [*Hz*], A and B are coefficients of the transfer function, the slope and the offset of the anemometer, respectively. The coefficients of the transfer function are established by a calibration process that correlates the wind speed and the output frequency. The global irradiance (*Thies Clima, 2019*) measured by a pyranometer is given by:

$$E_{\downarrow Solar} = \frac{U_{emf}}{S_{ensivity}} \qquad (4)$$

In (4) $E_{\downarrow Solar}$ is the global irradiance in $[W/m^2]$, U_{emf} is voltage at the thermocouple in response of the subjected global irradiance in [μV] and $S_{ensivity}$ is the sensitivity of the pyranometer in [$\mu V m^2/W$]. The calibration of the pyranometer is performed in accordance with ISO 9846 ISO 9847 (*Boonmee et al., 2009*; *Kipp and Zonen, 2019*), i.e., under indoor and outdoor conditions. The temperature sensor used is the digital thermometer produced by Maxim Integrated, DS18B20, (*Maxim Integrated, 2019*). The DS18B20 connected to the Arduino shown in Fig. 1 d) provides 9 bit to 12 bit Celsius measurements in a range between -55 °C and +125 °C and has an alarm function with non-volatile user programmable upper and lower trigger points. The supervising and monitoring data collector system of environmental data is equipped with a computer having a program in Python for recording and processing the collected data. The network node with the Arduino, the transmitting ZigBee and the prototype sensors is interfaced with the other equipment as shown in Fig. 2.
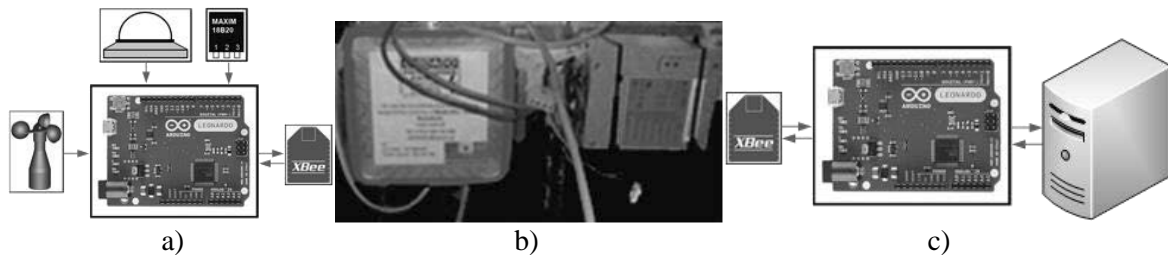
Fig. 2 a) Network node with the sensors, Arduino and ZigBee data transmitter; b) AC/DC onsite installation; c) Node with ZigBee data receiver and computer for recording and processing data.

In Fig. 2 a) the network node shown is for collecting and transmission of data, the input information from the anemometer 4.3515.51.105, the pyranometer CM6B and temperature sensor DS18B20 is sent to the Arduino and there is a bidirectional flow of information between the Arduino and the ZigBee. In Fig. 2 b) the power AC/DC installation is shown under the roof of the building where the PV modulus are installed. In Fig. 2 c) the network node shown is for receiving and processing the information: another bidirectional flow of information is implemented between the ZigBee and the Arduino and from the Arduino to a computer to be analyzed and process the data by a Python script. An instance of historical data for the wind speed, the irradiance and temperature collected during a day are respectively shown in Fig. 3 a), Fig. 3 b) and Fig. 3 c).
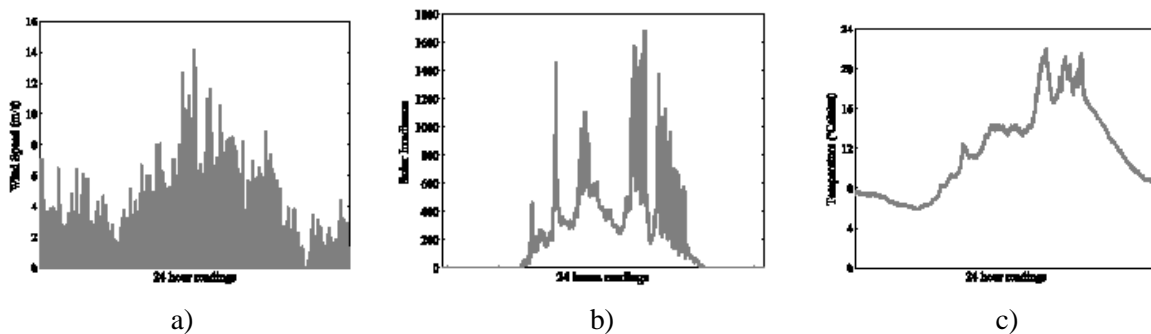
Fig. 3 Data collected in a day: a) wind speed, b) solar irradiance, c) ambient temperature.

In Fig. 3 the wind speed, solar irradiance and ambient temperature data shown can to use as an instance of historical data to predict the power and energy captured by the PV system, considering the NOCT (*Omsun, 2019*), the ambient temperature, the irradiance and the temperature of the PV cell can be computed. Also, $P_{MP} = V_{MP} \times I_{MP}, V_{OC}$ and I_{SC} can be computed using the temperature coefficients (*Omsun, 2019*), the change on the irradiance relatively to the one Sun irradiance, i.e., STC irradiance of $1 \ kW/m^2$, and the wind speed: an increase on the wind speed extracts more thermal energy from the modules, implying that the temperature of the module decreases.

CONCLUSIONS

The BIPV system with the PV system installed on the roof of the Žďár nad Sázavou, Czech Republic, is an instance of a grid-connected rooftop-mounted system aiming at a sustainable EU industrial milking by a milking cattle robot. This BIPV systems reduces or off-sets the usage of electric energy from the grid of the electric utility. Further, as the BIPV has storage and PV energy, the industrial milking has electric power without too much concern about the continuity of energy supply from the utility. So, the stored and PV energy avoids stopping the operation of the milking cattle robot with a jumpy cow stuck inside of the robot due to an eventual discontinuity of energy supply from the utility. But needs a convenient system for supporting the action of management in the BIPV and a part of that systems is a supervising and monitoring data collector of environmental data. The monitoring data collector for the PV system installed is hardware and software to collect, send and process the values of wind speed, irradiance and temperature in the environment where PV modules are located. The monitoring is addressed for the data collector collecting data from the sensors of wind speed, irra-

diance and temperature in order to be processed to deliver information on the operation condition of the PV modules. The development of prototypes of sensors using low power wireless networks is based on the Arduino microcontroller hardware and ZigBee protocol. The ZigBee standard proved to be a reliable approach for the creation of wireless network for monitoring at a reasonable cost.

REFERENCES

1. Batista, N.C, Melício, R., & Mendes, V.M.F. (2014). Layered smart grid architecture approach and field tests by ZigBee technology. *Energy Conversion and Management, 88*, 49-59.

2. Batista, N.C., Melício, R., & Mendes, V.M.F. (2017). Services enabler architecture for smart grid and smart living services providers under industry 4.0. *Energy and Buildings*, *141*, 16-27.

3. Batista, N.C., Melício, R., Matias, J.C.O., & Catalão, J.P.S. (2012a). ZigBee devices for distributed generation management: field tests and installation approaches. In *Proc. of the 6th IET International Conference on Power Electronics, Machines and Drives - PEMD 2012* (pp. 1-5). Bristol, UK.

4. Batista, N.C., Melício, R., Matias, J.C.O., & Catalão, J.P.S. (2012b). ZigBee standard in the creation of wireless networks for advanced metering infrastructures. In *Proc. of 16th IEEE Mediterranean Electrotechnical Conference* (pp. 220-223). Yasmine Hammamet, Tunisia.

5. Boonmee, C., Plangklang, B., & Watjanatepin, N. (2009). System performance of a three-phase PV-grid-connected system installed in Thailand: data monitored analysis. *Renewable Energy, 34*, 384-389.

6. Fadlullah, Z.M., Fouda, M.M., Kato, N., Takeuchi, A., Iwasaki, N., & Nozaki, Y. (2011). Toward intelligent machine-to-machine communications in smart grid. *IEEE Communications Magazine, 49*, 60-65.

7. Georgitzikis, V., Akribopoulos, O., & Chatzigiannakis, I. (2012). Controlling physical objects via the internet using the Arduino platform over 802.15.4 networks. *IEEE Latin America Transactions*, *10*, 1686-1689.

8. Kipp & Zonen. (2019). Retrieved from http://www.kippzonen.com/Product/12/CMP-6-Pyranometer#.VUaeePlVhBc.

9. Maxim Integrated. (2019). Retrieved from http://www.maximintegrated.com/.

10. Omsun. (2019). Retrieved from http://www.kazan-haz.hu/files/napelem/omsun-250w-poly.pdf

11. Pindado, S., Sanz, A., & Wery, A. (2012). Deviation of cup and propeller anemometer calibration results with air density. *Energies*, *5*, 683-701.

12. Thies Clima (2019). Retrieved from http://www.thiesclima.com/.

13. Woyte, A., Richter, M., Moser, D., Mau, S., Reich, N., & Jahn, U. (2013). Monitoring of photovoltaic systems: good practices and systematic analysis. In *Proc. of 28th European Photovoltaic Solar Energy Conference and Exhibition – PVSEC (*pp. 1-9). Paris, France.

Corresponding author:

Ing. Tomáš Tesař, Department of Mechanical Engineering, Faculty of Engineering, Czech University of Life Sciences Prague, Kamýcká 129, Praha 6, Prague, 16521, Czech Republic, phone: +420 22438 3178, e-mail: tesart@tf.czu.cz

STATIC AND DYNAMIC MECHANICAL PROPERTIES OF COMPOSITE FROM TYRE WASTE MICROPARTICLES/EPOXY RESIN

Martin TICHÝ[1], Viktor KOLÁŘ[1], Miroslav MÜLLER[1]

[1]*Department of Material Science and Manufacturing Technology, Czech University of Life Sciences Prague, Kamýcká 129, 165 00 Praha 6 – Suchdol, Czech Republic*

Abstract

The world-wide year production of tyres is over 1.5 billion and 6 % of scrap is used as a recycle product for engineering. The research finding an use of tyre waste in the engineering field. This research deals with the recycle product from tyre waste as rubber powder (RP) in microparticles form. To ensure an application of composite material in production engineering, it is necessary to meet appropriate mechanical properties to be able to compete with conventional materials. The aim of this research was specification of an absorption effect of tyre waste microparticles/epoxy resin composite by the impact strength and determination the fracture process by SEM analyses. The research finds a dependency between the impact strength and static mechanical properties i.e. tensile strength, elongation and hardness. Results of the research proved that the filler in rubber powder form has absorbing effect in matrix. The composite is suitable for application where are stiffness and ductility needed.

Key words: impact strength; tensile strength; elongation at break; hardness; rubber powder; SEM.

INTRODUCTION

A waste from worn out tyres from road transportation are serious environmental problem. The world-wide year production of tyres is over 1.5 billion and scrap of the tyre production is over 300 million only for the United States. An use of this tyre wastes is dived into 40 % as fuel for power station, 26 % ground into granulate rubber, 13 % landfills and 6 % as recycle product for engineering *(Karakurt, 2015; Sienkiewicz et al. 2017).*

For these reasons are necessary to develop new materials to find a use of tyre waste and increase the number of products in engineering field.

However, the recycling methods can reach several products from a tyre waste which is steel wires, textile fibres and rubber *(Fang et al., 2001).* All these products can be used in a composite. In general, a composite is based form matrix and reinforcing phase *(Pihtili & Tosun, 2002).* According to phase is composite marked as fibre *(Singh & Garg, 2000)* or particle composite *(Fu et al. 2008).* The filler reinforce a matrix which is a thermosetting polymer or a thermoplastic.

This research deals with recycle product from tyre waste as the rubber powder (RP) in microparticles form. There are many researches about interaction of rubber particles on total characteristic of composite *(Müller et al. 2018; Krmela & Tomanova, 2010; Sienkiewicz et al. 2017; Valášek, 2015).* The problem of rubber powder from tyre waste is that the vulcanisation process cannot be applicable repeatedly, for this reason it is good filler in composite *(Sienkiewicz et al. 2017).* The most common characteristic of rubber powder is an absorbing "toughening" effect which leads to significant influence on mechanical properties *(Ahmed et al. 2015).* Another useful feature of rubber powder is, that the particles can be added into various matrix *(Sienkiewicz et al. 2017).*

To ensure an application of composite material in production engineering, it is necessary to meet appropriate mechanical properties to be able to compete with conventional materials. Each composite needs different mechanical properties according to application field i.e. high strength and brittleness or otherwise stiffness and ductility *(Yang et al., 2011).* Tests of composite materials must be as close as possible to real condition, for these reasons it´s necessary to measure static and dynamic mechanical properties.

In this research the tensile strength, elongation and hardness were measured as the static mechanical properties. The impact strength was measured for the dynamic mechanical properties, which is very

important factor especially for determination of fracture process. Good impact strength is needed for application where is absorbing effect required e.g. automotive components *(Yang et al., 2011)*.

The aim of research was specification of absorption effect of tyre waste microparticles/epoxy resin composite by the impact strength and determination of the fracture process by SEM analyses. The research finds dependency between the impact strength and mechanical properties i.e. the tensile strength, elongation and hardness.

MATERIALS AND METHODS

In the research static and dynamic mechanical properties of tyre waste microparticles/epoxy resin composite were measured. The composite is divided in two phases i.e. a matrix and a filler. The matrix of the composite presents thermosetting epoxy resin by Havel Composite LH 288 with Hardener H 282. The filler of the composite presents rubber powder (RP) with two sizes of microparticles fracture i.e. sizes 0.0 – 0.4 mm and 0.4 – 0.8 mm. This rubber powder (RP) is product from tyre waste recycle process. The rubber powder AGP4 (0.0 – 0.4) and AGP8 (0.4 – 0.8) was add in concentration 30 wt.%.

The test samples were created by the vacuum infusion method with flow 16 $m^3.h^{-1}$ and vacuum pressure 2 mbar. The composite plate from vacuum infusion was cut into test samples by abrasive water jet (AWJ) on the machine AWAC CT 0806. The test samples meet the standard ČSN EN ISO 3167.

The composite was tested on static mechanical properties i.e. the tensile strength, elongation at break and hardness. The tensile strength and the elongation at break were measured on universal testing machine LABTest 5.50ST with measure hardware AST KAF 50 kN and software Test & Motion with loading speed 2 $mm.min^{-1}$. The hardness was measured according to ČSN EN ISO 2039-1 (Plastic – determination of hardness – Part 1: Ball indentation method) on device DuraJet G5 Rockwell Hardness tester with diameter of ball 5 mm and loading force 358 N.

The dynamic mechanical properties of composite were tested on the impact strength by Dynstat. The impact strength test was measured according to ČSN 64 0611.

Determination of fracture process and interactions between filler and matrix were evaluated by SEM analyses on electron microscope TESCAN MIRA 3. The shape and dimension of rubber powder (RP) were examined by SEM images with Gwyddion program, where the test group was 100 values. The samples for SEM analyses were prepared by gold-plating on Quarum Q150R ES.

The measured values were evaluated by statistical analyses ANOVA (Analysis of Variance) F-test with established p-values. The difference between p-values of F-test was analyse be hypothesis. Hypothesis H_0 establish no statistically significant difference between measured value: *p > 0.05*.

RESULTS AND DISCUSSION

The first part of results presents measured values of static mechanical properties i.e. the tensile strength, elongation at break and hardness. Measured values of tensile strength (Fig. 1) confirmed statistically significant difference between matrix and composite with filler AGP4 and AGP8 i.e. the hypothesis H_0 was rejected: *p = 0.00001*. The average tensile strength was 30.31 ± 1.21 MPa for matrix (concentration 0 wt.%), 32.83 ± 3.78 MPa for composite with filler AGP4 (concentration 30 wt.%) and 25.94 ± 1.40 MPa for composite with filler AGP8 (concentration 30 wt.%). The Fig. 1 presents increase of the tensile strength on composite with filler AGP4 with dimension 0.0 – 0.4 mm.
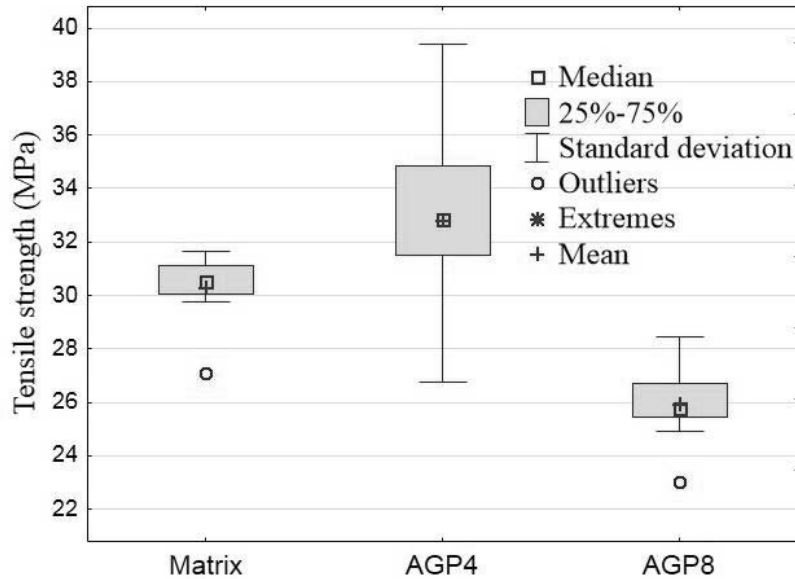
Fig. 1 Influence of the AGP4 and AGP8 filler on tensile strength

Measured values of elongation at break (Fig. 2) confirmed statistically significant difference between matrix and composite with filler AGP4 and AGP8 i.e. the hypothesis H_0 was rejected: *p = 0.00000*. The average elongation at break was 1.51 ± 0.45 % for matrix (concentration 0 wt.%), 2.00 ± 0.12 % for composite with filler AGP4 (concentration 30 wt.%) and 2.46 ± 0.27 % for composite with filler AGP8 (concentration 30 wt.%). The Fig. 2 presents biggest increase of the elongation at break at composite with filler AGP8 with dimension 0.4 – 0.8 mm. This fact is given by larger dimension of filler which also influence elasticity.
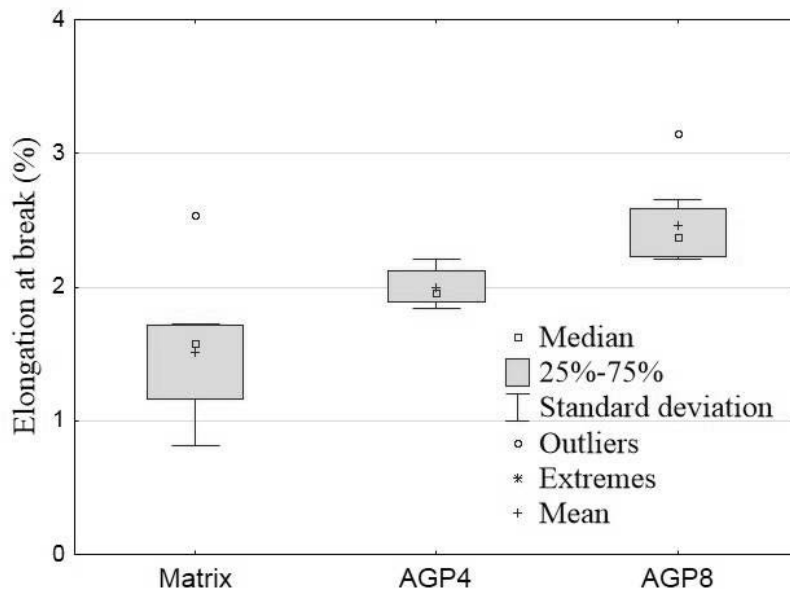
Fig. 2 Influence of the AGP4 and AGP8 filler on elongation at break

Measured values of hardness (Fig. 3) confirmed statistically significant difference between matrix and composite with filler AGP4 and AGP8 i.e. the hypothesis H_0 was rejected: *p = 0.00000*. The average hardness was 205.98 ± 7.15 HB for matrix (concentration 0 wt.%), 22.93 ± 4.64 HB for composite with filler AGP4 (concentration 30 wt.%) and 30.31 ± 3.08 HB for composite with filler AGP8 (concentration 30 wt.%). The Fig. 3 present decrease of the hardness at composite with filler AGP4 and AGP8 which is caused by adding elastic elements in rubber powder form into the matrix.
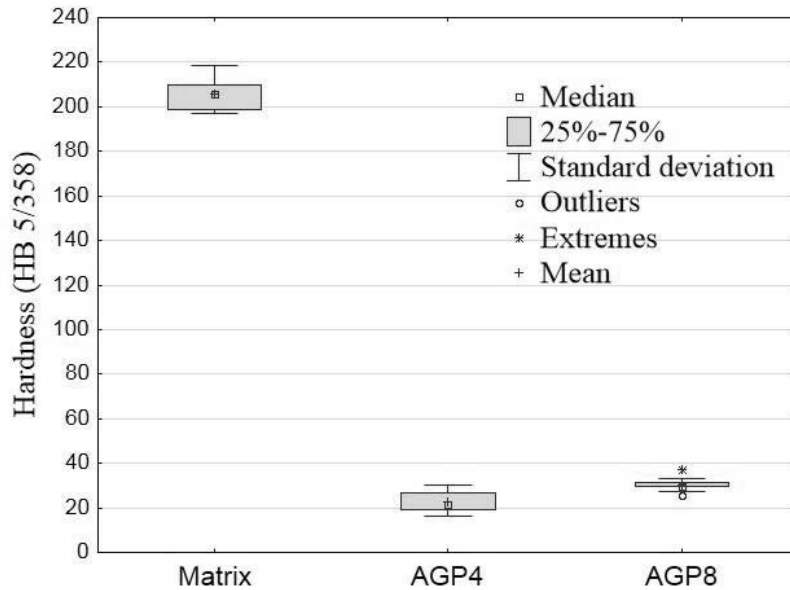
Fig. 3 Influence of the AGP4 and AGP8 filler on hardness

The Fig. 4 presents values of impact strength from test on the dynamic mechanical properties. Measured values confirmed statistically significant difference between matrix and composite with filler AGP4 and AGP8 i.e. the hypothesis H_0 was rejected: $p = 0.0347$. The average impact strength was 2.87 ± 0.29 $kJ.m^{-2}$ for matrix (concentration 0 wt.%), 3.55 ± 0.84 $kJ.m^{-2}$ for composite with filler AGP4 (concentration 30 wt.%) and 4.12 ± 0.49 $kJ.m^{-2}$ for composite with filler AGP8 (concentration 30 wt.%). The Fig. 4 presents increase of the impact strength at composite with the filler AGP4 and AGP8. This fact confirmed the absorbing effect of rubber powder (RP) *(Ahmed et al. 2015)*.
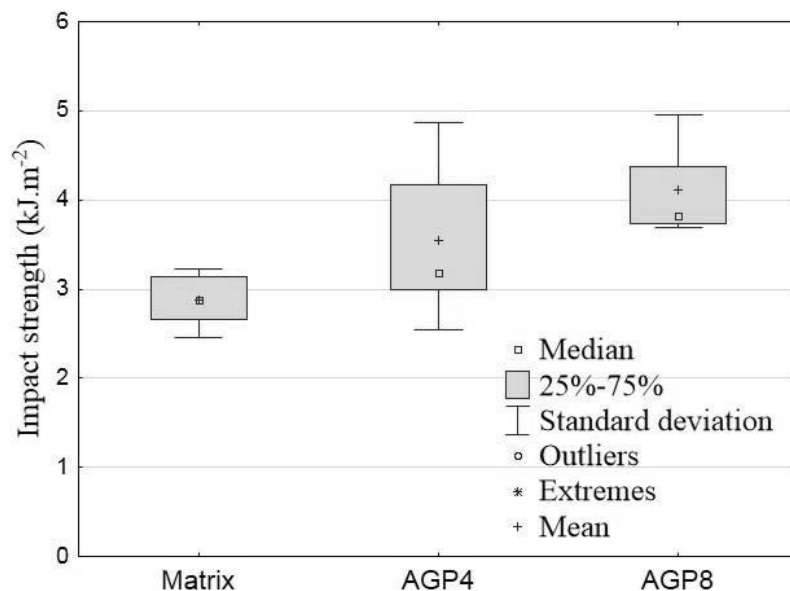

Fig. 4 Influence of the AGP4 and AGP8 filler on impact strength

Comparison of another composite is shown in Tab. 1, where are main factor a different matrix, ratio of RP and RP size. Tensile strength and elongation at break of composite types decrease with increasing amount of RP particles, which is different from this study. Hardness in the table decrease with increasing amount of RP particles, which was also proved in this study.

Tab. 1 Comparation of another composite in view of matrix and RP composition, components ratio, RP size and mechanical properties from other studies *(Sienkiewicz et al. 2017, Müller et al., 2017).*

Composition of matrix and RP	Components ratio [%]	RP size [µm]	Results on mechanical properties	Reference
Linear low-density polyethylene/rubber powder/ethylene-1-octene copolymers	50/0/50 – 50/50/0	425 – 500	Tensile strength increase with amount of RG decrease Elongation at break decrease with amount of RP increase	(Rocha et al., 2014)
Polyvinyl chloride/rubber powder	100/0 – 30/70	200 200 – 500 >500	Reducing in tensile strength, toughness and stiffness with amount of RP increasing	(Orrit et al., 2011)
Epoxy resin/ rubber powder	100/0 – 70/30	0 – 400	The tensile strength was reduced with increasing concentration of RP. The material hardness reduction was increased with increasing concentration of RP.	(Müller et al., 2018)

On Fig. 5 is shown SEM analyse of used filler. There is evident iregular geometric shape (Fig. 5 A, B, C, D, E, F). From Fig. 5 is evidetn that the particle is composed by groupe of aggregates.
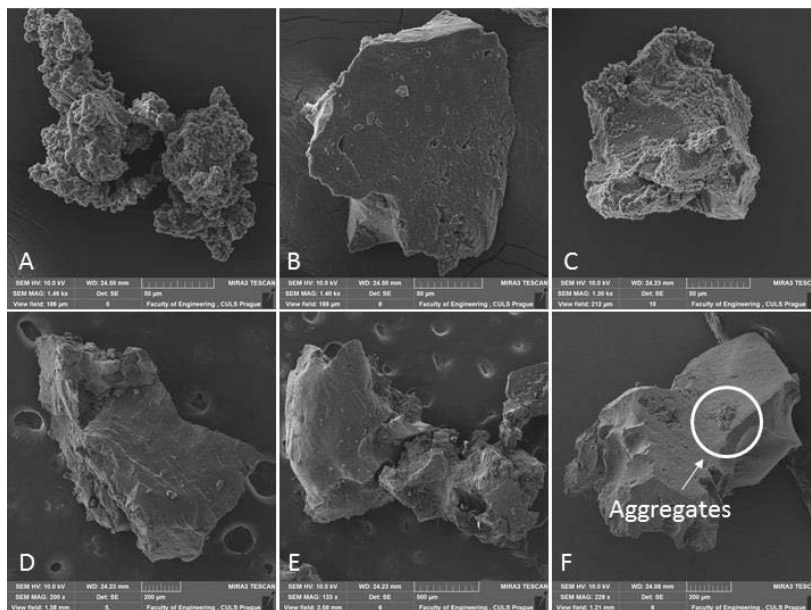

Fig. 5 SEM analyses of filler: A – microparticle of filler AGP4 composed by aggregates (MAG 1.49 kx), B – microparticle of filler AGP4 without aggregates (MAG 1.40 kx), C – microparticle of filler AGP4 with aggregate surface (MAG 1.30 kx), D – microparticle of filler AGP8 (MAG 200 x), E – microparticle of filler AGP8 with fracture (MAG 133 x), F – microparticle of filler AGP8 with small aggragates on surface (MAG 229 x)

SEM analyse proved good interaction between the matrix and the filler i.e. good wettablity (Fig. 6 A, F). From Fig. 6 C is evdent fragile fracture of the matrix. On Fig. 6 D is evident pulled-out particle of filler from the matrix and aggregates in the fracture area. On Fig. 6 E is evident that microparticles are not completely separated. The small agregates and incomplete separation of microparticles decrease adhesion to the matrix and negatively influence mechanical properties, which is evident on tensile

stregth on Fig. 1 at filler AGP8. This fact was also confirmed by other authors *(Aoudia et al., 2017; Müller et al. 2018)*.
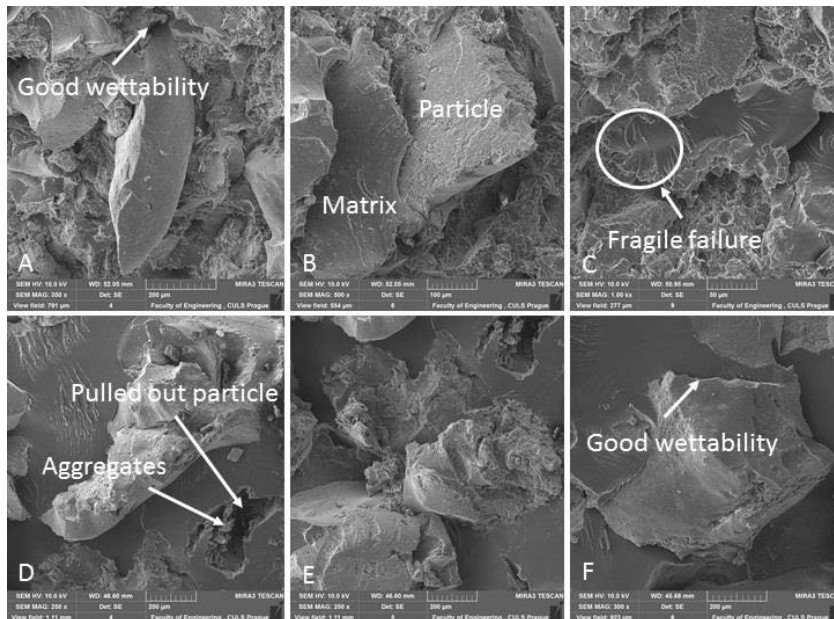

Fig. 6 SEM analyses of fracture surface: A – good wettability of the matrix and the filler (MAG 350 x), B – the matrix and the filler (MAG 500 x), C – fragile fracture of matrix (MAG 1 kx), D – the pulled-out particle and aggregates (MAG 250 x), E – exposition of not completely separated microparticles of filler (MAG 250 x) F – good wettability of the matrix and the filler (MAG 300 x).

The SEM analyse of rubber powder dimensions report average dimension of individual microparticles. Results of analyse present average dimension 174 ± 77.8 µm on the filler AGP4 and 995 ± 178.8 on the filler AGP8. This result show that filler AGP8 has larger dimension than stated by the manufacturer.

CONCLUSION

The results of impact strength proved significant increase with rubber powder AGP4 and AGP8 i.e. the main aim has been met. The result of SEM analyses confirmed good wettability of filler which positively influenced the impact strength and elongation. The tensile strength was positively increased only with filler AGP4 i.e. filler is resistant only with particle dimension to 0.4 mm. On the other hand, filler AGP8 positively increased at the elongation at break, which is given by larger base for elasticity than the filler AGP4. From the results is evident dependence of the impact strength and elongation at break of the composite. The hardness rapidly decreased with the filer AGP4 and AGP8 which is given by the elasticity of rubber particles. The results of the research proved that the filler in rubber powder form has absorbing effect in the matrix. The composite is suitable for application where are stiffness and ductility required.

ACKNOWLEDGEMENT

REFERENCES

1. Ahmed, M. A., Kandil, U. F., Shaker, N. O., & Hashem, A. I. (2015). The overall effect of reactive rubber nanoparticles and nano clay on the mechanical properties of epoxy resin. *Journal of Radiation Research and Applied Sciences, 8(4),* 549-561.

2. Aoudia, K., Azem, S., Hocine, N. A., Gratton, M., Pettarin, V., & Seghar, S. (2017). Recycling of waste tire rubber: Microwave devulcanization and incorporation in a thermoset resin. *Waste management, 60,* 471-481.

3. Fang, Y., Zhan, M., & Wang, Y. (2001). The status of recycling of waste rubber. *Materials & Design, 22*(2), 123-128.

4. Fu, S. Y., Feng, X. Q., Lauke, B., & Mai, Y. W. (2008). Effects of particle size, particle/matrix interface adhesion and particle loading on mechanical properties of particulate–polymer composites. *Composites Part B: Engineering, 39*(6), 933-961.

5. Karakurt, C. (2015). Microstructure properties of waste tire rubber composites: an overview. *Journal of Material Cycles and Waste Management, 17*(3), 422-433.

6. Krmela, J., & Tomanova, V. (2010). Microstructure of tire composite after corrosion. *International Journal of Applied Mechanics and Engineering, 15*(2), 433-439.

7. Müller, M., Valášek, P., Rudawska, A., & Chotěborský, R. (2018). Effect of active rubber powder on structural two-component epoxy resin and its mechanical properties. *Journal of adhesion science and Technology, 32*(14), 1531-1547.

8. Orrit-Prat, J., Mujal-Rosas, R., Rahhali, A., Marin-Genesca, M., Colom-Fajula, X., & Belana-Punseti, J. (2011). Dielectric and mechanical characterization of PVC composites with ground tire rubber. *Journal of Composite Materials, 45*(11), 1233-1243.

9. Pıhtılı, H., & Tosun, N. (2002). Effect of load and speed on the wear behaviour of woven glass fabrics and aramid fibre-reinforced composites. *Wear, 252*(11-12), 979-984.

10. Rocha, M. C. G., Leyva, M. E., & Oliveira, M. G. D. (2014). Thermoplastic elastomers blends based on linear low density polyethylene, ethylene-1-octene copolymers and ground rubber tire. *Polímeros, 24*(1), 23-29.

11. Sienkiewicz, M., Janik, H., Borzędowska-Labuda, K., & Kucińska-Lipka, J. (2017). Environmentally friendly polymer-rubber composites obtained from waste tyres: A review. *Journal of cleaner production, 147*, 560-571.

12. Singh, M., & Garg, M. (2000). Fibre reinforced gypsum binder composite, its microstructure and durability. *Materials and Structures, 33*(8), 525.

13. Valášek, P. (2015). Polymeric microparticles composites with waste EPDM rubber powder. *Agronomy Research, 13*(3), 723-731.

14. Yang, H. S., Gardner, D. J., & Nader, J. W. (2011). Characteristic impact resistance model analysis of cellulose nanofibril-filled polypropylene composites. *Composites Part A: Applied Science and Manufacturing, 42*(12), 2028-2035.

Corresponding author:

Ing. Martin Tichý, Department of Material Science and Manufacturing Technology, Czech University of Life Sciences Prague, Kamýcká 129, 165 00 Praha 6 – Suchdol, Czech Republic, e-mail: martintichy@tf.czu.cz

USING MOTIVATIONAL SYSTEMS TO SORT WASTE EFFECTIVELY IN CZECH MUNICIPALITIES

Eva URBANOVÁ[1], Vlastimil ALTMANN[1]

[1]Department of Machinery Utilization, Faculty of Engineering, Czech University of Life Sciences Prague, Kamýcká 129, Prague 6, 165 21, Czech Republic

Abstract

In order to sort the utilizable elements of communal waste in municipalities of the Czech Republic more effectively, we can use the methods of the PAYT motivational systems ("Pay as you throw"), which respect to the economical, ecological and technological aspects of the given process. The implementation of the motivational system based on the collection of sorted waste from door to door and filing the collection containers and bags by means of bar codes was monitored in a selected town in the Central Bohemian Region. Over the monitored pilot period of the last quarter of 2018, the implementation of the MESOH system in the monitored town demonstrably reduced the amount of mixed communal waste by 5.1 tons compared with the same period in 2017. At the same time, there was an increase in the production of the monitored commodities - paper and cardboard by 7.5 tons, plastics by 2.5 tons. When the motivational system went into live operation in the first quarter of 2019, there was a reduction in the amount of mixed communal waste by 52.8 tons, and the production of paper and cardboard increased by 1 ton, with plastic increasing by 0.7 tons, compared with the last quarter of 2018. Based on detailed monitoring of the potential amount of different waste to be separated, we can state that the potential of raw materials to be sorted amounts to 76 or 83 % of all house waste, depending on the type of the built-up area, which documents the possibility to meet EU requirements. Mixed communal waste only represents 17 or 24 % in the monitored built-up areas.

Key words: *municipal solid waste; motivation; waste sorting.*

INTRODUCTION

In order to reduce the costs of waste management, many municipalities in the Czech Republic have started to implement different motivational measures with the aim of increasing the amount of sorted waste and decreasing the amount of mixed communal waste (SKO) deposited in landfills. Regarding the given motivational system, it is important to make sure that citizens don't start creating illegal landfills in order to reduce the amount of mixed communal waste. This negative feature can be prevented by implementing motivational criteria that do not compensate the citizens only on the basis of the amount of sorted waste, but also on the basis of a reduced amount of mixed communal waste. The main emphasis is on the prevention of the generation of waste *(Xevgenos, Papadaskalopoulou, Panaretou, Moustakas, & Malamis, 2015; Sakai et al., 2017).*

Waste recycling is one of the conditions of waste management sustainability. As the production of waste increases, the environmental capacity decreases, increasing the demand to transport waste to greater distances *(Ferrão et al., 2014; Bonelli, Bosio, Cavallo, Gianolio, & Marengo, 2016).*

Goals have been set regarding the production of communal waste stemming from the goals of the EU. The current goal is to increase the recycling of communal waste to one half of the current amount by 2020. This will bring about a reduction in the amount of mixed communal waste in landfills. According to available data for 2015, the Czech Republic was currently at 36 % *(Expósito & Velasco, 2018; Kling, Seyring, & Tzanova, 2016; Seyring, Dollhofer, Weißenbacher, Bakas, & McKinnon, 2016).*

Key tools for greater effectiveness in sorting waste in Czech municipalities are legislative, economical and institutional tools. Economical tools are namely represented by a fee for mixed communal waste *(Puig-Ventosa & Sastre Sanz, 2017; Chifari, Lo Piano, Matsumoto, & Tasaki, 2017).*

It is possible to achieve greater effectiveness of sorting utilizable elements of communal waste in municipalities by means of implementing the methods of motivational systems ("Pay as you throw"). When implementing this system, the system of waste collection must be changed. The methods are either based on charging mixed communal waste or implementing a system of discounts based on the amount of sorted waste. "Door to door" waste collection is associated with these methods. The principle

of these systems lies in the filing of collected containers and bags by means of bar codes *(Brown & Johnstone, 2014; Morlok, Schoenberger, Styles, Galvez-Martos, & Zeschmar-Lahl, 2017; Šauer, Pařízková, & Hadrabová, 2008).*

The aim of this study is to gradually analyze data regarding the amount of individual commodities based on monitoring the implementation of the MESOH motivational system in a selected town in the Central Bohemian Region, and to determine the possible annual potential of the amount of sorted elements within the municipality based on monitoring 6 households that monitored their household waste for 4 months. The MESOH motivational system is based on the volume of main commodities (plastics, paper, mixed communal waste) collected by the waste collection company. The containers and bags are marked with bar codes, which simplifies the identification of individual households, determining the amount of waste in the household and the level of sorting of individual elements of communal waste. By means of bonus compensations, MESOH not only takes into account waste collection but also the effectiveness of filling up the containers, bags, and the reduction of waste production.

MATERIALS AND METHODS

The actual analysis of the current state of waste management and determining the costs of its individual activities was realized in a monitored town in the Central Bohemian Region with 4,770 citizens (as of 2019). The composition of mixed municipal waste was analyzed and a solution for a better yield of sorted collected waste was suggested. Data were processed using Excel (proportional representation, frequency of occurrence) and basic statistical methods (averages and deviations of values). There are 2 main types of built-up areas in the town (central and suburban).

Based on the analysis, the town has determined the main goals in changing the waste management system:

- Greater utilization of waste container volume
- Implementation of a container registry
- A proposal for a change to choose a more economical and effective system of the town's waste management
- Improvement of the town's waste management services for citizens

The implementation of the registration system for containers and newly also for bags, distributed to the town citizens free of charge, was the main tool for change.

The next part of the analysis within the monitored location dealt with the assessment of the potential amounts of all basic separated commodities with the aim of reducing non-utilizable mixed communal waste. Based on EU directives, it will be necessary to sort 60 % of the overall municipal waste in individual municipalities for recycling in 2025, and this number will grow to 70 % in 2030. There were 6 households that took part in detailed monitoring (3 from the central built-up area and 3 from the suburban built-up area). There were 9 citizens altogether in both types of built-up areas. The households monitored the production of their waste for a period of 4 months (1 month in each quarter), focusing on the possible sorted segments.

RESULTS AND DISCUSSION

Based on the results of the town's waste management analysis, there was a change in the approach to waste sorting as of October 1, 2018, when the MESOH system was launched in pilot mode. The traditional container collection of sorted waste was extended by the collection of plastic and paper in bags directly in the households. Each household received bags and bar codes to attach to the bags. Within the monitored period of the pilot implementation of the MESOH system from October 1, 2018 to December 31, 2018, there were 26.97 % of participating households.

The result of the MESOH system assessment in the reference location over the first monitored period (pilot implementation in the last quarter of 2018) demonstrated an increase in sorting of communal waste segments and a concurrent reduction in mixed municipal waste production, which brings about a reduction of costs for mixed communal waste collection and the lowering of costs for the removal of this waste for the citizens. To ensure comparable conditions, the last two quarters of 2017 and 2018 were compared (Tab. 1).

Tab. 1 Production of waste in the town over the last quarters of 2017 and 2018

Commodities	4Q 2017 t	4Q 2018 t
Mixed communal waste (SKO)	315.2641	310.1554
Paper and cardboard	36.9231	44.4203
Plastic	26.3912	28.9139
Total	378.5784	383.4896

Tab. 1 and Fig. 1 - 2 show that the production of SKO decreased by 5.1 tons (2 %) upon the implementation of the MESOH system, and there was also an increase in the production of the monitored commodities - by 7.5 tons (2 %) of paper and cardboard and by 2.5 tons (1 %) of plastic.
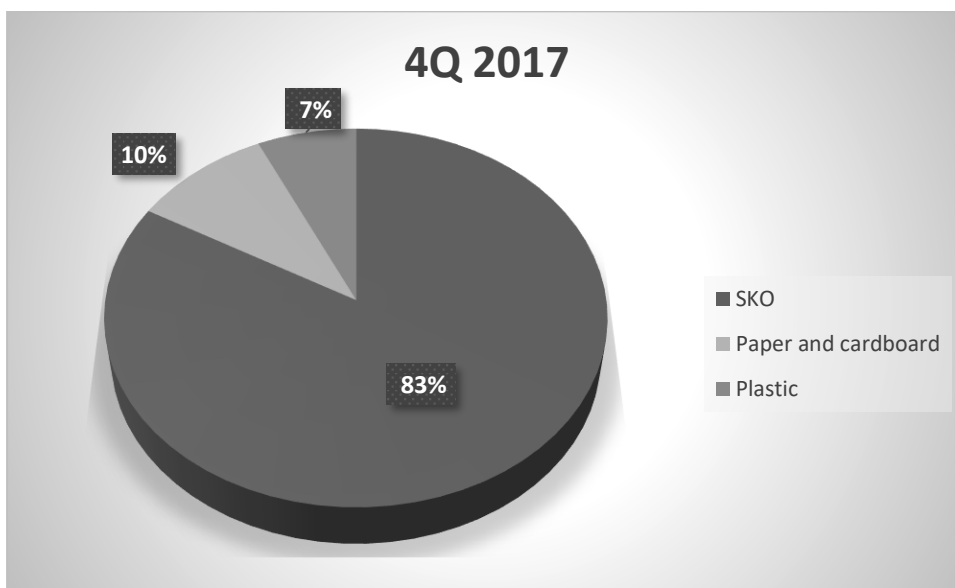
Fig. 1 Graphic representation of the production of monitored commodities in the town over the last quarter of 2017
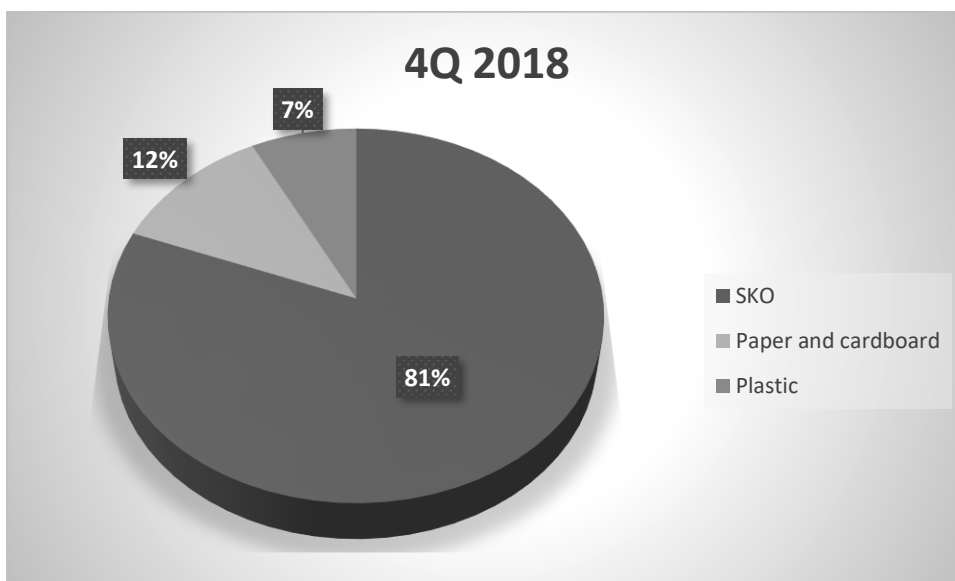

Fig. 2 Graphic representation of the production of monitored commodities in the town over the last quarter of 2018

The MESOH motivational system was implemented full-scale in the monitored reference locality as of January 1, 2019. According to the results shown in Tab. 2, it is obvious that over the first quarter of 2019 there was a reduction of the production of SKO by 52.8 tons (4 %) compared with the fourth quarter of 2018 (Fig. 2), and by 55.3 tons (8 %) compared with the first quarter of 2018 (Fig. 3).

Tab. 2: Production of waste in the town over the first quarter of 2018 and 2019

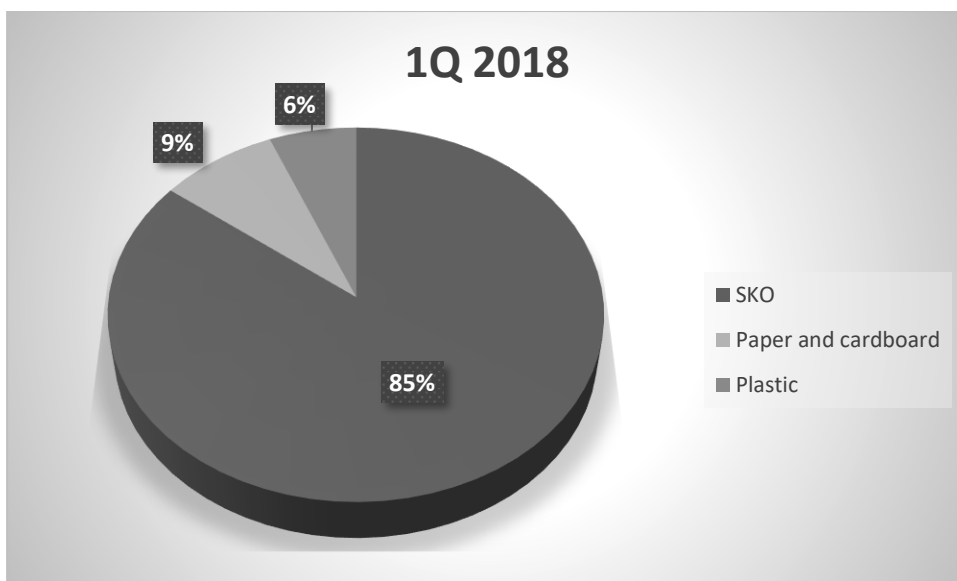| Commodities	1Q 2018 t	1Q 2019 t
Mixed communal waste (SKO)	312.5722	257.3154
Paper and cardboard	30.7320	45.4651
Plastic	22.7261	29.6649
Total	366.0303	332.4454

Fig. 3: Graphic representation of the production of monitored commodities in the town over the first quarter of 2018
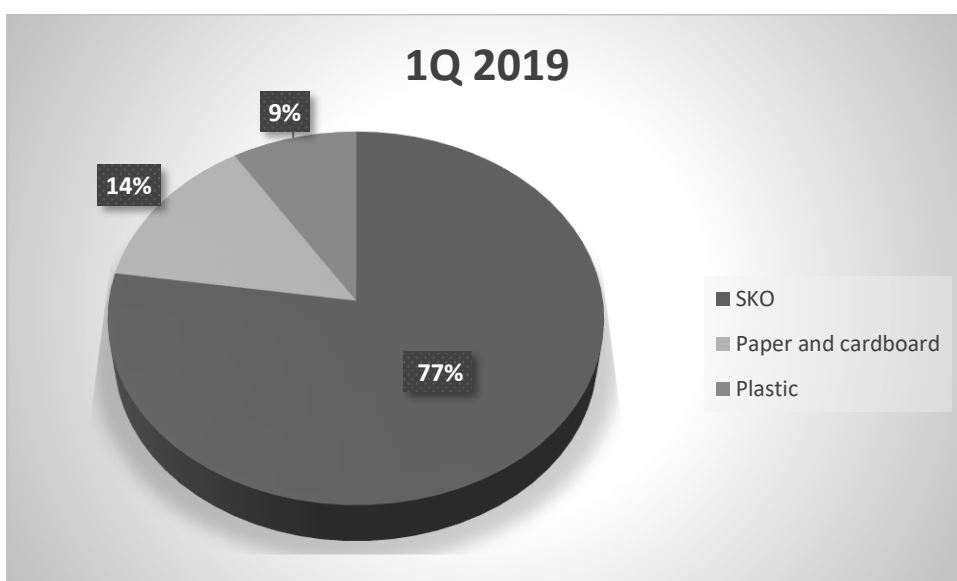

Fig. 4: Graphic representation of the production of monitored commodities in the town over the first quarter of 2019

The results of monitoring the potential production of all basic separated raw materials in the monitored households are shown in Tab. 3. Apart from paper and glass, raw materials like glass, metals, Tetrapak and bio waste were also sorted. For the sake of comparison carried out in Fig. 1- 4, other commodities besides paper and glass were labelled as other sorted commodities, see Tab. 4 and Fig. 5 and 6.

Tab. 3: Production of basic sorted commodities per citizen according to the type of built-up area

Built-up area	SKO	Paper and cardboard	Plastic	Glass	Metal	Bio waste	Tetrapak	Total
	kg	kg	kg	kg	kg	kg	kg	kg
Central	8,683	3,545	13,277	4,582	1,087	17,657	1,931	50,761
Suburban	10,847	4,810	10,914	4,699	1,354	9,630	3,446	45,70

Tab. 4: Production of monitored commodities per citizen according to the type of built-up area

Built-up area	SKO	Paper and cardboard	Plastic	Other sorted commodities
	kg	kg	kg	kg
Central	8,683	3,545	13,277	25,257
Suburban	10,847	4,810	10,914	19,129

Table 4 clearly indicates that there is still a high potential for sorting other commodities in the households within the monitored location and that the amount of SKO in both types of built-up areas decreased significantly, see Fig. 5 and 6.
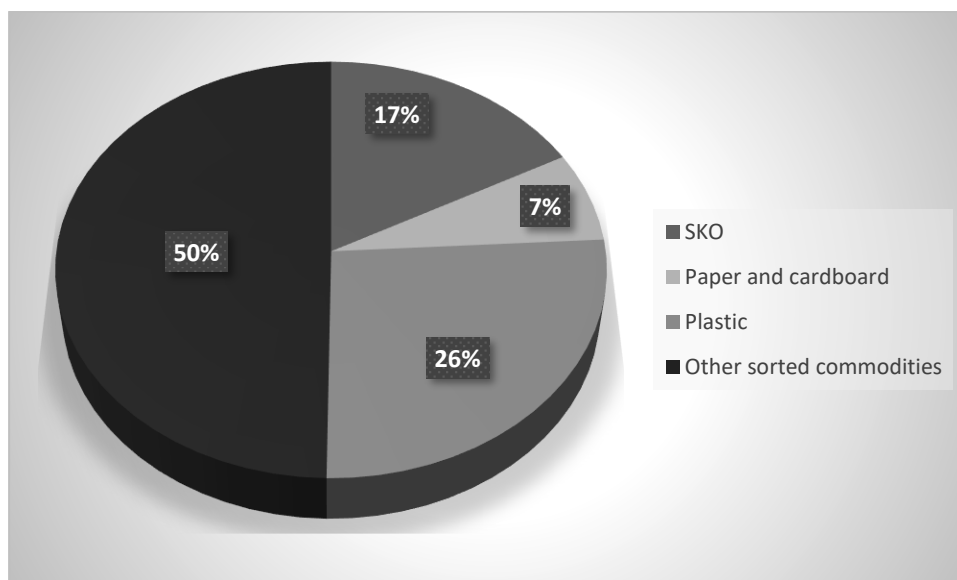

Fig. 5: Graphic representation of the production of individual commodities per citizen in the central built-up area
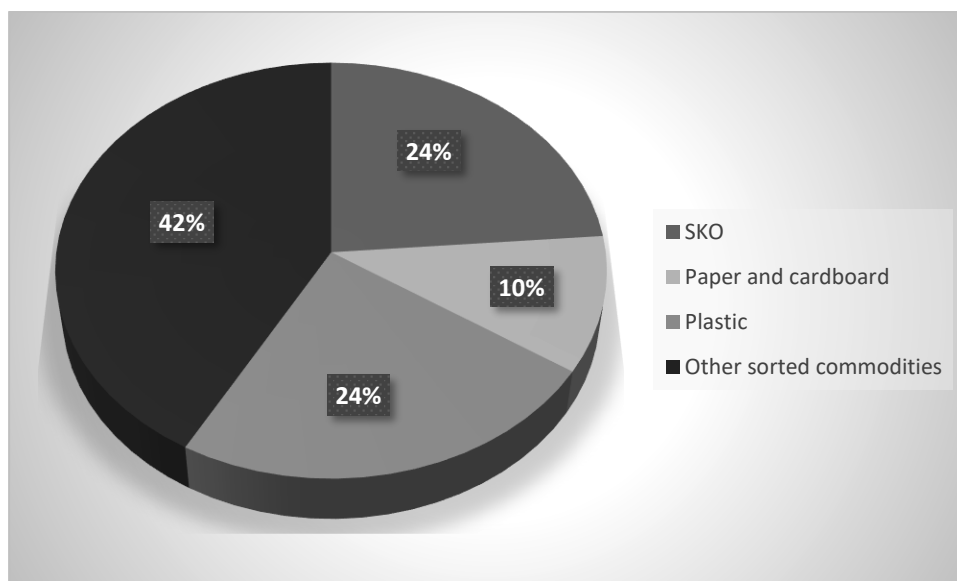
Fig. 6: Graphic representation of the production of individual commodities per citizen in the suburban built-up area

For the sake of comparison and making a prediction of waste development in the monitored town, Table 5 shows the results of waste production in a selected municipality in the South Moravian Region, which has been using the MESOH system since 2018. It is obvious that the amount of SKO decreased by nearly 45 tons, the production of paper and cardboard increased by 6.6 tons, and the production of plastic increased by 13 tons over the course of 5 years.

The measurement results are comparable to those reported by other authors (Benešová, L. a kol. (2011), Kaufman, P. & Báreková, A. (2010); Kotoulová, Z. (2001); Slejška, A. (2004)).

Tab. 5: Results of waste production in the selected municipality following the implementation of the MESOH system in 2013

Year	SKO	Paper and cardboard	Plastic
	t	t	t
2013	282.69	36.56	30.26
2014	276.38	41.42	40.12
2015	229.67	37.44	42.09
2016	243.55	42.28	41.18
2017	237.74	43.17	43.23

CONCLUSIONS

In association with the implementation of the new waste sorting system in the monitored town, changes were observed although the new system has only been implemented recently. The amount of SKO decreased demonstrably by 5.1 tons over the period of pilot implementation and the amount of individual sorted segments increased, especially regarding monitored plastic - by 2.5 tons, and paper and cardboard - by 7.5 tons. There was a further reduction in the amount of SKO by 52.8 tons over the first quarter of full-scale operation of the new motivational system in town, with the amount of plastic increasing by 0.7 tons and paper and cardboard increasing by 1 ton.

When monitoring the potential amount of sorted waste, it is apparent in both types of built-up areas that out of the overall amount of communal waste within households, it is possible to sort up to 76 or 83 % of all waste in the monitored built-up areas. SKO only represented 17 or 24 % in the monitored built-up areas.

Consistent sorting also brought about an increase in paper and plastic collection by 10 - 11 % compared with the monitored period of 1Q 2019.

Based on these detailed analyses of 6 households and based on results from other municipalities that have been participating in the MESOH system for a longer period of time, it is possible to state that a transformation is achievable in meeting the EU requirements for increasing the amount of sorted communal waste for recycling in such a way that 50 % of all communal waste is recycled in 2020, and up to 70 % in 2030. The monitored households have already achieved this. It will therefore be necessary to change the system of collection and removal within the municipality's territory regarding the potentially higher amount of all sorted waste in such a way so as to ensure that all sorted amounts are actually removed from the municipalities. This may be achieved by changing technological parameters such as the amount and size of containers, the interval of collection and the carrying distance.

ACKNOWLEDGMENT

REFERENCES

1. Benešová, L. et al. (2011). Characteristics of Municipal Solid Waste in the Czech Republic. *The 26th International Conference on Solid Waste Technology and Management* (pp. 358 – 350). Philadelphia.

2. Bonelli, M., Bosio, L., Cavallo, R., Gianolio, U., & Marengo, P. (2016). Waste prevention impacts on small municipalities: Three experiences from northern Italy. *Waste Management & Research*, *34*(10), 1014–1025. doi: https://doi.org/10.1177/0734242X16661054

3. Brown, Z. S., & Johnstone, N. (2014). Better the devil you throw: Experience and support for pay-as-you-throw waste charges. *Environmental Science & Policy*, *38*, 132–142. doi: https://doi.org/10.1016/j.envsci.2013.11.007

4. Chifari, R., Lo Piano, S., Matsumoto, S., & Tasaki, T. (2017). Does recyclable separation reduce the cost of municipal waste management in Japan? *Waste Management*, *60*, 32–41. doi: https://doi.org/10.1016/j.wasman.2017.01.05

5. Expósito, A., & Velasco, F. (2018). Municipal solid-waste recycling market and the European 2020 Horizon Strategy: A regional efficiency analysis in Spain. *Journal of Cleaner Production*, *172*, 938–948. doi: https://doi.org/10.1016/j.jclepro.2017.10.221

6. Ferrão, P., Ribeiro, P., Rodrigues, J., Marques, A., Preto, M., Amaral, M., … Costa, e I. (2014). Environmental, economic and social costs and benefits of a packaging waste management system: A Portuguese case study. *Resources, Conservation and Recycling*, *85*, 67–78. doi: https://doi.org/10.1016/j.resconrec.2013.10.2

7. Kaufman, P. & Báreková, A. (2010). Structure of municipal solid waste composition. In *Waste Forum,* 3, 192 – 198. ISSN: 1804-0195.

8. Kling, M., Seyring, N., & Tzanova, P. (2016). Assessment of economic instruments for countries with low municipal waste management performance: An approach based on the analytic hierarchy process. *Waste Management & Research*, *34*(9), 912–922. doi: https://doi.org/10.1177/0734242X16644521

9. Kotoulová, Z. (2001). Recommended methodology for determining the amount and composition of municipal waste. In: *Odpadové fórum,* 10, 10 – 13. ISSN 1212/7779.

10. Morlok, J., Schoenberger, H., Styles, D., Galvez-Martos, J.-L., & Zeschmar-Lahl, B. (2017). The Impact of Pay-As-You-Throw Schemes on Municipal Solid Waste Management: The Exemplar Case of the County of Aschaffenburg, Germany. *Resources*, *6*(1), 8. doi: https://doi.org/10.3390/resources6010008

11. Puig-Ventosa, I., & Sastre Sanz, S. (2017). An exploration into municipal waste charges for environmental management at local level: The case of Spain. *Waste Management & Research*, *35*(11), 1159–1167. doi: https://doi.org/10.1177/0734242X17727067

12. Sakai, S., Yano, J., Hirai, Y., Asari, M., Yanagawa, R., Matsuda, T., … Moore, S. (2017). Waste prevention for sustainable resource and waste management. *Journal of Material Cycles and Waste Management*, *19*(4), 1295–1313. doi: https://doi.org/10.1007/s10163-017-0586-4

13. Šauer, P., Pařízková, L., & Hadrabová, A.

(2008). Charging systems for municipal solid waste: Experience from the Czech Republic. *Waste Management*, 28(12), 2772–2777. doi: https://doi.org/10.1016/j.wasman.2008.03.00

14. Seyring, N., Dollhofer, M., Weißenbacher, J., Bakas, I., & McKinnon, D. (2016). Assessment of collection schemes for packaging and other recyclable waste in European Union-28 Member States and capital cities. *Waste Management & Research*, *34*(9), 947–956. doi: https://doi.org/10.1177/0734242X16650516

15. Slejška, A. (2004). Possibilities of reducing the amount of landfilled biodegradable municipal waste. ISSN: 1801-2655. *Retrieved from* https://biom.cz/cz/odborne-clanky/moznosti-snizovani-mnozstvi-skladkovanych-brko.

16. Xevgenos, D., Papadaskalopoulou, C., Panaretou, V., Moustakas, K., & Malamis, D. (2015). Success Stories for Recycling of MSW at Municipal Level: A Review. *Waste and Biomass Valorization*, *6*(5), 657–684. doi: https://doi.org/10.1007/s12649-015-9389-9

Corresponding author:
RNDr. Ing. Eva Urbanová, Department of Machinery Utilization, Faculty of Engineering, Czech University of Life Sciences Prague, Kamýcká 129, Prague 6, 165 21, Czech Republic, e-mail: urbanovae@tf.czu.cz

ENERGY RECOVERY OF WASTE FROM THE VINEYARD AND WINERY

Lukáš VAŠTÍK[1], Vladimír MAŠÁN[1], Patrik BURG[1], Jakub SIKORA[2]

[1]*Department of Horticultural Machinery, Faculty of Horticulture, Mendel University in Brno, Czech Republic*
[2]*Institute of Agricultural Engineering and Computer Science, Faculty of Production and Power Engineering, University of Agriculture in Krakow, Poland*

Abstract

Viticulture and viniculture processes produce different organic waste, particularly grape marc (pomace), wood mass, to name but a few. Concerning the waste management, research finds out new, waste-free technologies and the use of waste as biofuel. The objective of this work is to determine the net calorific value of selected waste materials by the calorimetric method for its further use in solid biofuels production. Results show that comparable values of net calorific value are for the samples of wood cane, wood trunk, grape marc, grape stalks, cane pellets and ranged from 16.24 to 17.79 MJ·kg^{-1}. The higher net calorific value had grape seeds (21.14 MJ·kg^{-1}) and grape bagasse pellets (19.62 MJ·kg^{-1}) and the lowest net calorific value was determined for filter cellulose sheets (9.38 MJ·kg^{-1}). Based on data of the calorific values of tested samples, it is clear, that the majority of tested materials have very good calorific values.

Key words: *organic waste; solid biofuels; calorific values; pomace; wood mass.*

INTRODUCTION

Grapes are one of the most cultivated fruits worldwide (*FAO, 2017*). For this reason, it is important to think about produced waste and other secondary products. The waste management leads the research to new, waste-free technologies and the technologies where waste is used for biofuels (*Boulton et al., 2010*). A sizeable portion of wastes is from timber after the cut of vineyards (*Burg et al., 2017*), and also from the processing of grape and its processing during the production of wine (*Burg, Masan & Ludin, 2017*).

The production value from vineyards wood mass was evaluated by *Michálek, Burg, & Zemánek (2013)*, according to them this depends on the buckle in the planting and varies from 1,600 to 2,500 kg·ha^{-1}. Many other authors (*Rosúa & Pasadas, 2012; Boschiero et al., 2016*) agreed on the average production with value 1,000 kg·ha^{-1}. During compressing of 1,000 kg of grapes, the waste produced contains the amount of 40-60 kg of stems, 230-300 kg of pomace, with the part of seeds which is approximately from 50 till 100 kg and grape marc which amount is between 150 until 250 kg (*Baydar, Özkan & Çetin, 2007; Hugh, 2002; Muhlack, Potumarthi, & Jeffery, 2018; Rubio, Álvarez-Orti & Pardo, 2009; Schieber, Stintzing & Carle, 2001*). During winemaking, the other waste is produced as well such as used filter cellulose sheets.

This waste material has a large variation in its properties and produced amounts, but they represent an important amount of raw material that can be utilize as well. An interesting alternative is either technology that uses these wastes, as an input material for biogas plants, or the technology that uses grapeseed oil as a fuel substitute (*Chelladorai et al., 2018*), or the one which exploits the energy content of waste in technology of pyrolysis (*Zhang et al., 2017*). The easiest and most straightforward method of use applicable on a wide scale is the energetic combustion. These technologies are also established in practice, from wood shredding, or pelleting to combustion in the boiler and overall, financially accessible affordable too for smaller winery.

The objective of the work is to determine the net calorific value of selected waste materials by the calorimetric method for its further use in solid biofuels production.

MATERIALS AND METHODS

Waste mass

The subject of the research is wood mass produced from grape cane and trunk, grape pomace, grape marc without seeds, grape seeds, grape bagasse pellets (secondary product from grape seed oil pressing), grape stalks, filter cellulose sheets (type S 10) and commercial grape cane pellets used as a standard. The waste mass was produced and collected in South Moravia, Czech Republic in the year 2018. Samples of vines and old trunks were taken from the wine mill in Velké Žernoseky, the year of planting 1971, the wine type Pinot Blanc. The filter plates were used to filter Savilon 2018 in a volume of 2500 liters of wine. Grape marc in its original state, grape marc after seed separation, and in seeds themselves was from wine variety Sauvignon. Grape bagasse pellets were produced during the grape seed oil pressing on screw press and were from the wine variety Sauvignon too.

Laboratory methods

Determination of moisture content and dry mass was carried out accordingly to standard laboratory procedures ISO 18134-3 (total content of carbon, hydrogen and nitrogen), ISO 16948, ISO 16994 (total content of sulfur) and ISO 18122 (total content of ash). All procedures were evaluated in accredited laboratories TÜV NORD Czech, Ltd.

The Determination of the Energy Value

Determination of the gross calorific value was performed accordingly to the standard for solid biofuels ISO 1928. The obtained gross calorific values were converted into net calorific value according by equation (1)

$$Q^r{}_i = Q^r{}_s - \gamma \cdot (W^r_t + 8.94 \cdot H^r_t) \tag{1}$$

where

$Q^r{}_i$ – net calorific value of the evaluated sample, MJ·kg^{-1};

$Q^r{}_s$ – gross calorific value of the original sample, MJ·kg^{-1};

γ – ratio of evaporation of 1% H_2O, MJ·kg^{-1}, at temperature 25°C, γ = 0,02442 MJ·kg^{-1};

8,94 – hydrogen to water conversion ratio of, –;

W^r_t – total water content in the original sample, %;

H^r_t – total hydrogen content in the original sample, %.

Statistic

Every sample and determinations were done in triplicate and the data were reported as means ± standard deviation. Analysis of variance was conducted and the results were tested and compared using Tukey's multiple range test (α=0.05). A statistical analysis was carried out using the software package "Statistica 12.0" (StatSoft Inc., Tulsa, Oklahoma, USA).

RESULTS AND DISCUSSION

The basic precondition for using the solid biofuels is to reduce their humidity to a technologically acceptable value from the perspective of storage, but also to convert it into biofuel. From this point of view, the most problematic materials are filter cellulose sheets with wet basic moisture 67.61%, grape marc 63.47% and grape pomace 59.53%. Overall, the moisture samples fluctuated within a relatively wide range of values from 8.43 to 67.61%. Wood cane and wood trunk have low wet basic moisture, because they were harvested during the winter, when plants do not transplant.

The highest dry moisture content (set at the combustion tests) was then determined for the wood cane at 17.86% and the lowest at filter cellulose sheets at 3.54%. The highest moisture loss would be seen with filter cellulose sheets and grape pomace, which is logical in view of the production method, but may in practice represent increased drying costs. On the other hand, the change in humidity was the lowest in grape bagasse pellets, which, due to their compactness, do not have the prerequisite to attract more air humidity. Samples used in the tests met the basic processing condition, namely the content of dry moisture under 20%. In the content of elements, there was no significant difference between the samples. The hydrogen content required for calculating the calorific value according to equation (1), ranged from 4.14 to 6.49% in the measured samples. Overview of these average values for each samples are shown in Tab. 1.

The ash content samples fluctuated within a relatively narrow range of values from 2.63 to 8.83%, with exception of filter cellulose sheets where the value was 37.06%. This is caused by the material from which the sheets are made (in general, cellulose generates a significant amount of ash during combustion), but also by trapping sediments in the filtering of the wine, which are unburnable (mainly bentonite). For the same reason, their calorific value is also low compared to other samples. Overview of these average values for each samples are shown in Tab. 2.

Manzone et al. (2016) claims that the average ash content from pruning residue was 3.85% during a period of 15 years and average moisture content was 50%. *Burg & Souček (2008)* presents the average basic wet moisture at 40.70%. *Fernández-Puratich, Hernández & Tenreiro (2015)* discuss the average basic wet moisture 53.5% and average ash content 4.4%.

Tab. 1 Average values of moisture and composition of different organic waste

Samples	Wet basic moisture (%)	Dry moisture (%)	Composition (%)				
			H	C	N	H	S
Wood cane	36.29±0.72[d]	17.86±0.10[h]	5.10	50.40	0.85	40.22	0.02
Wood trunk	21.53±1.59[c]	7.62±0.34[a]	5.75	50.89	0.53	39.36	0.06
Grape pomace	59.53±2.86[e]	11.76±0.33[e]	6.07	54.01	2.84	29.73	0.15
Grape marc	63.47±1.15[f]	13.37±0.23[g]	6.16	55.72	2.46	30.07	0.13
Grape seeds	13.89±0.22[b]	7.45±0.04[a]	6.49	56.48	1.95	32.06	0.11
Grape bagasse pellets	8.43±0.06[a]	8.49±0.02[d]	5.78	53.42	2.12	34.89	0.13
Grape stalks	18.09±0.40[c]	12.50±0.15[f]	5.30	50,23	2.04	32.78	0.09
Filter cellulose sheets	67.61±1.91[g]	3.54±0.09[b]	4.14	29.08	0.49	28.96	0.01
Cane pellets	6.24±0.10[a]	6.23±0.09[c]	5.72	45.23	1.31	37.96	0.09

Tab. 2 Average values of ash content and calorific values of different organic waste

Samples	Ash (%)	Gross calorific value (MJ·kg^{-1})	Net calorific value (MJ·kg^{-1})
Wood cane	3.33±0.08[a]	18.7616±0.06[ab]	17.2070±0.06[ab]
Wood trunk	2.63±0.06[b]	18.5402±0.75[ab]	16.9856±0.75[ab]
Grape pomace	7.11±0.04[d]	20.9403±0.33[c]	19.3857±0.33[c]
Grape marc	6.47±0.10[c]	19.3467±1.06[b]	17.7921±1.06[b]
Grape seeds	3.39±0.19[a]	22.6945±0.04[e]	21.1399±0.04[e]
Grape bagasse pellets	3.18±0.05[a]	21.1788±0.01[c]	19.6242±0.01[c]
Grape stalks	8.83±0.15[e]	18.1606±0.15[ab]	16.6060±0.15[ab]
Filter cellulose sheets	37.06±0.24[g]	10.9387±0.45[d]	9.3841±0.45[d]
Cane pellets	9.25±0.05[f]	17.7900±0.10[a]	16.2354±0.010[a]

* Values are means±standard deviations of a triplicate measurements. Alphabetical superscripts indicate significant differences (P<0.05) among values in columns.

The statistical analysis (Tab. 2.) show that comparable values of net calorific value are for the samples wood cane, wood trunk, grape marc, grape stalks, cane pellets. The net calorific values for these samples ranged from 16.24 to 17.79 MJ·kg^{-1}. The higher net calorific value had grape seeds (21.14 MJ·kg^{-1}) and grape bagasse pellets (19.62 MJ·kg^{-1}). This is due to the fact that this material contains considerable amount of oils. On the other hand, the lowest net calorific value was determined for filter cellulose sheets (9.38 MJ·kg^{-1}), which is caused by the high content of ash.

For the evaluation of the energy potential of waste mass, the most important is net calorific value (NCV), even when some authors state their results in gross calorific value (GCV). *Annamalai, Sweeten & Ramalin-gam (1987)* set the GCV of grape pomace at the level of 20.34 MJ·kg^{-1}. *Burg, Masan & Ludin (2017)* report that grape pomace had gross calorific value from 16.07 till 18.97 MJ·kg^{-1}, grape marc of 14.60-17.75 MJ·kg^{-1} and grape seeds have the values of 19.78-21.13 MJ·kg^{-1}. *Manzone et al. (2016)* report the values of average higher heating value of vineyard pruning residue ranged from 17.92 to 18.02

MJ·kg^{-1}, whereas the lower calorific value ranged between 7.34 and 7.96 MJ·kg^{-1}. *Gligorević & Zlatanović (2013)* report the values of gross calorific value at 18,3 MJ·kg^{-1} and NCV at 11,82. *Walg (2007)* set the net calorific value of 12.6 MJ·kg^{-1} and *Burg & Souček (2008)* determined the net calorific value in the range between 14.39 to 16.66 MJ·kg^{-1}.

The main potential problem of grape pomace and filter cellulose sheets used in the production of solid biofuels can be high moisture. On the other hand, *Benetto et al. (2015)* state, that the marc is responsible for the better consistency of the pellets and also prevents the disintegration of the material in the pressing process due to the pulp content of the peel. *Miranda et al. (2012)* reports that as the proportion of marc in the pellets increases, the proportion of ash decreases. On the other hand, pellets with higher marc content show higher values of fixed carbon (*Balaman & Selim, 2015*).

CONCLUSIONS

This thesis brings the results of complexed experiment that was concerned with the possibility of energy utilization of various wastes that arise in the viticulture and viniculture processes. Not just pruning residues but others waste materials have energetic potential too and can be a significant biofuels. This waste material has a large variation in its properties and produced amounts, but they repre-sent an important amount of raw material that can be utilize as well. From the data of the calorific values of tested samples, it is clear, that it is mostly materials with a very good calorific values, which is comparable with the calorific values of e.g. brown coal (18.10 MJ·kg^{-1}). The results show that comparable values of net calorific value are for the samples wood cane, wood trunk, grape marc, grape stalks, cane pellets and ranged from 16.24 to 17.79 MJ·kg^{-1}. The higher net calorific value had grape seeds (21.14 MJ·kg^{-1}) and grape bagasse pellets (19.62 MJ·kg^{-1}) and the lowest net calorific value was determined for filter cellulose sheets (9.38 MJ·kg^{-1}). The results obtained suggest that the waste mass and their use may have an economic and ecological benefit. For greater use, it is necessary to find optimal technological and technical solutions with the aim to obtain energy. From this point of view, filter cellulose sheets with wet basic moisture 67.61%, grape marc 63.47% and grape pomace 59.53% are the most problematic materials, which may in practice represent increased drying costs. Another problem of filter cellulose sheets is the ash content, where the value was 37.06%.

ACKNOWLEDGMENT

REFERENCES

1. Annamalai, K., Sweeten, J.M., & Ramalingam, S.C. (1987). Estimation of grossheating values of biomass fuels. *Transaction of the Asae*, *30*, 1205-1208.
2. Balaman, Ş.Y., & Selim, H. (2015). Biomass to Energy Supply Chain Network Design: An Overview of Models, Solution Approaches and Applications. In *Handbook of Bioenergy* (pp. 1-35). Springer International Publishing.
3. Baydar, N.G., Özkan, G., & Çetin, E.S. (2007). Characterization of grape seed and pomace oil extracts. *Grasas y aceites, 58*, 29-33.
4. Benetto, E., Jury, C., Kneip, G., Vázquez-Rowe, I., Huck, V., & Minette, F. (2015). Life cycle assessment of heat production from grape marc pellets. *Journal of Cleaner Production, 87*, 149-158.
5. Boschiero, M., Cherubini, F., Nati, C., & Zerbe, S. (2016). Life cycle assessment of bioenergy production from orchards woody residues in Northern Italy. *Journal of Cleaner Production, 112,* 2569-2580.
6. Boulton, R.B., Singleton, V.L., Bisson, F.L., & Kunkee, R.E. (2010). *Principles and practices of winemaking.* New York: Springer+Business Media.
7. Burg, P., Ludín, D., Rutkowski, K., Krakowiak-Bal, A., Trávníček, P., Zemánek, P., Turan, J., & Višacki, V. (2016). Calorific evaluation and energy potential of grape pomace. *International Agrophysics*, *30*, 261-265.
8. Burg, P., Mašán, V., Dušek, M., Zemánek, P., & Rutkowski, K. (2017). Review of energy potential of the wood biomass of orchards and vineyards in the Czech Republic. *Research in*

Agricultural Engineering, 63(Special Issue), S1-S7.

9. Burg, P., Masan, V., & Ludin, D. (2017). Possibilities of using grape marc for making fuel pellets. In *16th International Scientific Conference "Engineering for Rural Development"* (pp. 1333-1338). Jelgava, Latvia.

10. Burg, P., & Souček, J. (2008). The classification of wood chips parameters by crushing of waste cane from diff erent varieties of grapevine (in Czech). *Acta univ. agric. et silvic. Mendel. Brun.*, *56*, 51-56.

11. FAO, Food and Agriculture Organization of the United Nations (2017). *FAOSTAT Data: Crops*. Retrieved from http://www.fao.org/faostat/en/#data/QC

12. Fernández-Puratich, H., Hernández, D., & Tenreiro, C. (2015). Analysis of energetic performance of vine biomass residues as an alternative fuel for Chilean wine industry. *Renewable Energy, 83*, 1260-1267.

13. Gligorević, K., & Zlatanović, I. (2013). Aspects of using potential energy products of biomass after pruning fruit and grape plantations in the republic of serbia. *Agriculture & Forestry, 59*, 167-182.

14. Hugh, J. (2002). Der große Johnson: die Enzyklopädie der Weine, Weinbaugebiete und Weinerzeuger der Welt. 15. Aufl. München: Hallwag. (in German).

15. Chelladorai, P., Varuvel, E.G., Martin, L.J., & Bedhannan, N. (2018). Synergistic effect of hydrogen induction with biofuel obtained from winery waste (grapeseed oil) for CI engine application. *International Journal of Hydrogen Energy, 43,* 12473-12490.

16. ISO 1928:2009 Solid mineral fuels. Determination of gross calorific value by the bomb calorimetric method and calculation of net calorific value.

17. ISO 18134-3: 2015 Solid biofuels. Determination of moisture content. Oven dry method. Part 3: Moisture in the analytical sample for general analysis.

18. ISO 18122:2015 Solid biofuels. Determination of ash content.

19. ISO 16948:2015 Solid biofuels. Determination of total content of carbon, hydrogen and nitrogen.

20. Manzone, M., Paravidino, E., Bonifacino, G., & Balsari, P. (2016). Biomass availability and quality produced by vineyard management during a period of 15 years. *Renewable Energy, 99*, 465-471.

21. Michálek, M., Burg, P., & Zemánek, P. (2013). The assessment of the suitability and effectiveness of the technologies for vineyard wood waste utilization for energetic purposes. *Acta Universitatis Agriculturae et Silviculturae Mendelianae Brunensis, 61,* 157-162.

22. Miranda, T., Román, S., Montero, I., Nogales-Delgado, S., Arranz, J.I., Rojas, C.V., & González, J.F. (2012). Study of the emissions and kinetic parameters during combustion of grape pomace: Dilution as an effective way to reduce pollution. *Fuel Processing Technology, 103*, 160-165.

23. Muhlack, R.A., Potumarthi, R., & Jeffery, D.W. (2018). Sustainable wineries through waste valorisation: A review of grape marc utilisation for value-added products. *Waste Management, 72,* 99-118.

24. Rosúa, J.M., & Pasadas, M. (2012). Biomass potential in Andalusia, from grapevines, olives, fruit trees and poplar, for providing heating in homes. *Renewable and Sustainable Energy Reviews, 16*, 4190-4195.

25. Rubio, M., Álvarez-Orti, M., & Pardo, J.E. (2009). A review on the utilization of grape seed oil as an alternative to conventional edible vegetable oils. *La rivista italiana delle sostanze grasse, 84,* 121-129.

26. Schieber, A., Stintzing, F.C., & Carle, R. 2001. By-products of plant food processing as a source of functional compounds- recent developments. *Trends in food science and technology, 12,* 401-415.

27. Walg, O. (2007). *Taschenbuch der Weinbautechnik*. 2. Aufl. Mainz: Fraund. (in German).

28. Zhang, N., Hoadley, A., Patel, J., Lim, S., & Li, Ch. (2017). Sustainable options for the utilization of solid residues from wine production. *Waste Management, 60,* 173-183.

Corresponding author:
Ing. Vladimír Mašán, Ph.D., Department of Horticultural Machinery, Faculty of Horticulture, Mendel University in Brno, Valtická 337, 691 44 Lednice, Czech Republic, phone: +420 519 367 370, e-mail: vladimir.masan@mendelu.cz

ISOTHERMAL KINETIC ANALYSIS OF THE THERMAL DECOMPOSITION OF SPRUCE WOOD

Ivan VITÁZEK[1], Radoslav MAJDAN[1], Rudolf ABRAHÁM[1]

[1]*Department of Transport and Handling, Faculty of Engineering, Slovak University of Agriculture in Nitra, Slovak Republic*

Abstract

The thermal decomposition of pellets made from spruce wood (Picea abies) was studied under isothermal conditions by the thermogravimetric analysis. The Arrhenius parameters, i.e. apparent activation energy (E_a) and pre-exponential factor A, were determined from thermogravimetric experiments in the temperature range of (275–290) °C. Calculated values of E_a and A by a method based on the half-time of reaction are 151 kJ mol^{-1} and 8.09×10^{10} s^{-1}, respectively.

Key words: apparent activation energy; thermal decomposition; woody biomass; spruce wood.

INTRODUCTION

Wood consisting mainly of hemicellulose, celluloses, and lignin, with a small content of inorganic impurities (*Shen, et al., 2009; Harun & Afzal, 2010; Mohan, Pittman & Steele, 2006*). During heating, in the temperature range of 200 °C – 260 °C and 240 °C – 350 °C, the thermal decomposition of the first and second component occurs, respectively. Lignin decomposition in wood was proposed to begin at 280 °C and continues to 450-500 °C (*Mohan, Pittman & Steele, 2006; Brebu & Vasile, 2010*). Generally, the thermal decomposition of woody biomass can be expressed as (*Harun & Afzal, 2010; Slopiecka, Bartocci & Fantozzi, 2011*)

$$Wood \xrightarrow{\ k(T)\ } Char + Volatiles \tag{1}$$

where $k(T)$ is the rate constant and volatiles means the sum of the gas and tar. Besides that, it is believed, that the various factors, such as heating rate, temperature, moisture content, particle size, pressure, and chemical composition, have an influence on thermal decomposition kinetics under an inert and oxidative atmosphere (*Hosoya, Kawamoto & Saka, 2007; Holubčík, Nosek & Jandačka, 2012; Ondro & Trník, 2017*). In general, the reaction order reaction model ($f(\alpha)=(1-\alpha)^n$), where n is the reaction order, is often used to describe this process (*Harun & Afzal, 2010; Slopiecka, Bartocci & Fantozzi, 2011*). However, in (*Liu, et al., 2002*) the authors stated, that the best linear regression of the Arrhenius function is achieved when the first order ($f(\alpha)=(1-\alpha)$) reaction model is used. The aim of this study is the kinetic analysis of the thermal decomposition of pellets made from residual processing spruce wood (Picea abies). Thermogravimetric (TG) analysis was used to obtain data for kinetic analysis, from which the values of apparent activation energy, pre-exponential factor, and the most probable reaction model were determined.

MATERIAL AND METHODS

The experiments were performed on pellets made from residual processing spruce wood (Picea abies) originated in the locality Nitra-Horné Krškany, Slovakia. As was mentioned in Section 1, the particle size is one of the factors which have an influence on thermal decomposition kinetics. For this reason, an analytical sieve shaker Retsch AS200 was used for sieve analysis of sawdust, which was an input material for pelletizing. The 5-minute sieve shaking time with amplitude 2.0 mm g^{-1} was applied. For this analysis, the sieves with opening size 5, 2.5, 1.25, 1, 0.5, 0.2, 0.1 mm and a bottom pan (<0.1 mm) were used. Then, the material was screed to the sieve with the largest opening size. The measurements were carried out on thermogravimetric analyzer Mettler Toledo TGA/SDTA 851^e in a dynamic atmosphere of dry air with a flow rate of 50 ml min^{-1}. The heating rate of 50 °C min^{-1} was used to reach the isothermal temperatures from 275 °C to 290 °C, which corresponds to the major decomposition region.

Kinetic analysis

The rate of reaction can be described by the following equation (*White, Catallo & Legendre, 2011; Vyazovkin, et al., 2011*)

$$\frac{da}{dt} = k(T) f(\alpha) \tag{2}$$

where α is the degree of conversion, t is time, T is absolute temperature, and $f(\alpha)$ characterized the reaction model. The degree of conversion can be calculated from the TG measurements as (*Vyazovkin, et al., 2011; Ondro, Húlan & Vitázek, 2017*)

$$\alpha = \frac{m_i - m}{m_i - m_f} \tag{3}$$

where m is current, m_i is initial, and m_f is the final value of sample mass. Then, the state of the heterogeneous process is expressed by the single degree of conversion. Equation (1) is often used in its integral form, which for isothermal conditions becomes (*Ptáček, et al., 2010*)

$$g(\alpha) = k(T)t \tag{4}$$

where $g(\alpha)$ is the integral form of the reaction model. Then, the dependence of $g(\alpha)$ on time must give a straight line for proper reaction model. The temperature dependence of the reaction rate is typically parameterized through the Arrhenius equation (5) (*Vyazovkin, et al., 2011; Obert & Trník, 2018*)

$$k(T) = A \exp\left(-\frac{E}{RT}\right) \tag{5}$$

where A is the pre-exponential factor, E is the activation energy and R is the universal gas constant. In the case of thermal decomposition of woody biomass, the apparent activation energy E_a is the combination of the partial activation energies of different processes. The determination of A and E_a is based on the half-time of the reaction method ($t_{0.5}$) when the degree of conversion $\alpha = 0.5$. This method is based on the equation (6)

$$\ln t_{0.5} = \ln\left(\frac{g(\alpha)}{A}\right) + \frac{E_a}{RT} \tag{6}$$

The slope of the plot of the $\ln(t_{0.5})$ on T^{-1} must give a straight line, which corresponds to the E_a/R (*Ptáček, et al., 2010*).

RESULTS AND DISCUSSION

The results of sieve analysis (Fig. 1) show, that the more than 30 % of the material was retained on sieves with opening sizes 0.5 and 0.2 mm. Minimum of material (less than 10 %) were captured by the sieves with opening sizes 2.5 mm, 1.25 mm, 1 mm, and 0.1 mm. Further, the material contains ~7.6 % of particles with sizes less than 0.1 mm. On the other hand, the material did not contain particles >5 mm.
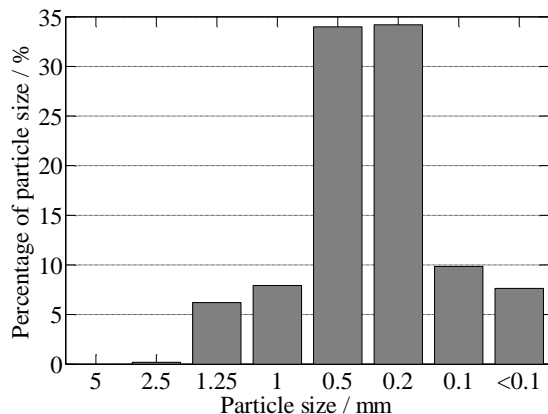

Fig. 1 Particle size distribution.

The isothermal measurements were carried out in temperatures from 275 °C to 290 °C, which correspond to the beginning of the main decomposition region. However, these results also show, that the decomposition process is not complete even if the sample is heated at 290 °C for 10 hours. Based on these measurements, the most probable mechanism of the process was determined from the dependence of $g(\alpha)$ on time for a degree of conversion in the range of $0.1 - 0.7$. The results of linear regression show,

that the best model for this process is the first order reaction (F1), which is consistent with Liu et al. (2002).
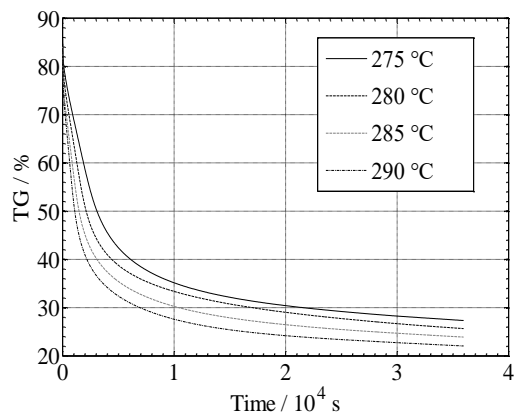

Fig. 2 Results of TG analysis for different isothermal regimes.

Tab. 1 Determined values of $t_{0.5}$.

Temperature	$t_{0.5}$
°C	s
275	2220
280	1628
285	1184
290	925

From the experimental data, the values of $t_{0.5}$ were determined (see Tab. 1). Pertinent kinetic parameters (E_a and A) were determined graphically using the half-time of the reaction method (see Fig. 2). The determined value of E_a by a method based on the half-time of reaction is 151 kJ mol^{-1}. Using the determined reaction model (F1), the calculated value of A is 8.09×10^{10} s^{-1}. The value of E_a is similar to the results obtained by non-isothermal TG analysis *(Ondro et al., 2018)*, where the Friedman, Flynn-Wall-Ozawa and Kissinger-Akahira-Sunose methods were used for kinetic analysis. However, in the aforementioned work, the reaction model was not determined.
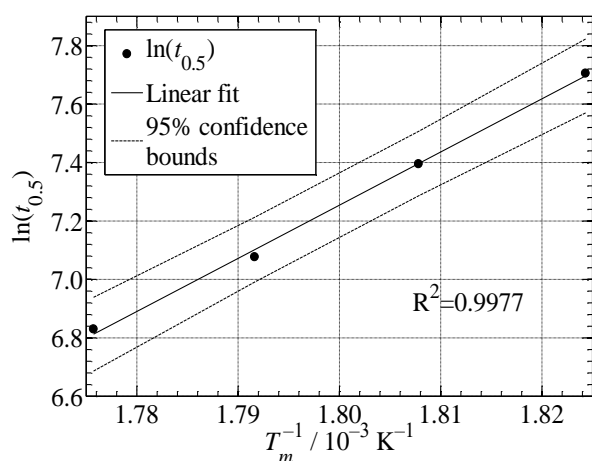
Fig. 3 The $\ln(t_{0.5})$ vs T^{-1} dependence.

CONCLUSIONS

The thermal decomposition of pellets made from spruce wood was studied by the thermogravimetric analysis in an oxidative atmosphere. The reaction model, apparent activation energy (E_a) and pre-exponential factor (A), were determined from thermogravimetric experiments in the temperature range of

(275–290) °C. The results show, that the most probable mechanism of the reaction is the first order reaction (F1). Besides that, the determined value of E_a by a method based on the half-time of reaction is 151 kJ mol^{-1}. Using the determined reaction model (F1), the calculated value of A is 8.09×10^{10} s^{-1}.

ACKNOWLEDGMENT

REFERENCES

1. Brebu, M., & Vasile, C. (2010). Thermal degradation of lignin—a review. *Cellul. Chem. Technol.*, *44*, 353-363.

2. Harun, N.Y., & Afzal, M.T. (2010). Thermal decomposition kinetics of forest residue. *J. Appl. Sci., 10*, 1122-1127.

3. Holubčík, M., Nosek, R., & Jandačka,J. (2012). Optimization of the Production Process of Wood Pellets by Adding Additives. *Inter. Jour. of Energy Optimal. and Engineering, 1(2)*, 20-40.

4. Hosoya, T., Kawamoto, H., & Saka, S. (2007). Cellulose-hemicellulose and cellulose-lignin interactions in wood pyrolysis at gasification temperature. *J. Anal. Appl. Pyrolysis., 80*, 118-125. doi:10.1016/j.jaap.2007.01.006.

5. Liu, N.A., Fan, W., Dobashi, R., & Huang, L. (2002). Kinetic modelling of thermal decomposition of natural cellulosic materials in air atmosphere. *J. Anal. Appl. Pyrolysis, 63*, 303-325. doi:10.1016/S0165-2370(01)00161-9.

6. Obert, F., & Trník, A. (2018). Kinetic analysis of thermal expansion of natural zeolite in temperature interval from 700 °C to 1100 °C during isothermal heating. In *AIP Conf. Proc., p.Article no.020032*. doi:10.1063/1.5047626.

7. Ondro, T., & Trník, A. (2017). Non-isothermal kinetic analysis of processes occurring during thermal treatment of kaolinite. *AIP Conf. Proc., 1866*. doi: 10.1063/1.4994508.

8. Ondro, T., Húlan, T., & Vitázek, I. (2017). Non-isothermal kinetic analysis of the dehydroxylation of kaolinite in dynamic air atmosphere. *Acta Technol. Agric., 20*(2), 52-56. doi:10.1063/1.4994508.

9. Ondro, T., Vitázek, I., Húlan, T., Lawson, M. K., Csáki, Š. (2018). Non-isothermal kinetic analysis of the thermal decomposition of spruce wood in air atmosphere. *Res. Agr. Eng.*, *64*, 41-46. doi: 10.17221/115/2016-RAE.

10. Ptáček, P., Kubátová, D., Havlica, J., Brandštetr, J., Šoukal, F., & Opravil, T. (2010). Isothermal kinetic analysis of the thermal decomposition of kaolinite: The thermogravimetric study. *Thermochim. Acta., 501*, 24-29. doi:10.1016/j.tca.2009.12.018.

11. Shen, D.K., Gu, S., Luo, K.H., Bringwater, A.V., & Fang, M.X. (2009). Kinetic study on thermal decomposition of woods in oxidative environment. *Fuel, 88*, 1024-1030. doi:10. 1016/j.fuel.2008.10.034.

12. Slopiecka, K., Bartocci, P., & Fantozzi, F. (2012). Thermogravimetric analysis and kinetic study of poplar wood pyrolysis. *Appl. Energy, 97*, 491-497. doi:10.1016/ j.apenergy.2011.12.056.

13. Vyazovkin, S., Burnham, A.K., Criado, J.M., Pérez-Maqueda, L.A., Popescu, C., & Sbirrazzuoli, N. (2011). ICTAC Kinetics Committee recommendations for performing kinetic computations on thermal analysis data. *Thermochim. Acta, 520*, 1-19. doi:10. 1016/ j.tca.2011.03.034.

14. White, J.E., Catallo, W.J., & Legendre, B.L. (2011). Journal of Analytical and Applied Pyrolysis Biomass pyrolysis kinetics : A comparative critical review with relevant agricultural residue case studies. *J. Anal. Appl. Pyrolysis. 91* (2011), 1-33. doi:10.1016/ j.jaap.2011.01.004.

Corresponding author:
Ivan Vitázek, Department of Transport and Handling, Faculty of Engineering, Slovak University of Agriculture Nitra, Tr. A. Hlinku 2, Nitra, 94976, Slovak Republic, phone: +421 37 6414 756, e-mail: ivan.vitazek@uniag.sk

METHOD OF PATTERN RECOGNITION OF BIOCHIPS IN GENETIC ENGINEERING

Jaromír VOLF[1], Viktor NOVÁK[1], Vladimír RYŽENKO[1]

[1]Department of Electrical Engineering and Automation, Czech University of Life Sciences Prague, Faculty of Engineering, Kamýcká 129, 165 21 Prague, Czech Republic

Abstract
The article describes the genome analysis based on method of automatic pattern recognition of biochips. The described method enables processing of multitude genetically modified DNA samples. This method can be used for analysing DNA samples in all areas of genetic engineering, particularly for analysing of samples of cattle or corn for agricultural purposes. The image of the samples is obtained by confocal microscopy; it is subsequently digitized and then processed by specific originally developed program Genocol, based on program code Borland Delphi. The program detects the degree of DNA modification of the samples and it represents it graphically by means of representative colour scale.

Key words: *genome; DNA; pattern recognition biochip; genetic engineering.*

INTRODUCTION

By genetic engineering we understand the artificial creation of genetically modified cells or complete organisms by direct manipulation of the organism´s genome on the level of genes. The genome is a set of the complete genetic material of a cell or more generally of an individual. The aim of the study of a genome is the analysis of the genetic structure and function of DNA sequences, detection of the organization of the genome, i.e. regularities of the arrangement of genes in a biological species or detection of similarities and dissimilarities between species and detection of differences between species and detection of the function of protein products which control the genome that creates biochip. Genetic engineering is a constituent of molecular biotechnology *(Bittner, 1999)*. The creating of biochips is described in *(Lyu, 2019)*, using of biochips in biochemistry procedure is described in *(Wan, 2019)* and other methods of analysis of biochips in *(Singla, 2019)*.

The amount of processed data is rapidly expanding and consequently the operation with data must be automated as much as possible, i.e. to apply computational technology in the pattern recognition and analysis and processing of data. The present paper deals with the concept of an appropriate method of the pattern recognition of biochips with individual DNA probes deposited on them. Confocal microscopy is used for the scanning of DNA on biochips. The biochips are placed in the microscope and the colour of the individual biochip DNA probes is scanned. Then the colour of the individual samples is stored in a file and processed by a computer.

The aim of study was automatic creation of biochips and their automatic pattern recognition because their number is about several thousand. This number of biochips is impossible to pattern recognition manually.

MATERIALS AND METHODS

The probe is a section of the DNA or RNA fibre (e.g. 1 gene) with a known sequence. Since it has an ability to be paired with a complementary sequence it can be used for the detection of a certain sequence in the DNA or RNA sample *(e.g. Pardatscher et al., 2016)*. For example if we know the normal sequence of a certain gene and the deviation from this sequence (mutation) which lead to the development of an illness, then by means of the probe we can find out if the gene is in order or mutated. For a known sequence we can even calculate the temperature of denaturation (ion concentration) of the probe. If we set the hybridization temperature of the probe with the investigated DNA exactly on the denaturation temperature of the probe we can even identify the difference between a normal gene (the probe binds) and a mutation (pairing is imperfect, the probe under the given condition does not bind). This is followed by washing when the incorrectly paired probes or absolutely unbound probes are removed. In order to be able to do this the investigated DNA must be fixed to a solid base.

Membranes which are by UV radiation charged positively and DNA charged negatively are used for this purpose.

Hybridization and repeated washing is followed by the detection of the labelled probe by various systems. Radioactive phosphorous is traditionally used for labelling so that each molecule emits β-radiation detected e.g. photographically. New systems are based on fluorescence, luminescence etc. Labelling of the probe is performed by e.g. biotin, fluorescein (fluorescent dye). In practice one of the nucleotides labelled in production with one of the mentioned labels is used in the preparation of the probe. In the case of fluorescein the detection of the labelled probe is performed by UV radiation. Biotin is detected by means of the protein streptavidin which binds to biotin. The producer of streptavidin already adds an enzyme. For the detection of the activity of the enzyme a substrate is added which can be chromogenic (the formed product is coloured, a coloured spot appears on the membrane in the place where the probe binds) or can excite light emission in the form of luminescence. The sensitivity of luminescent systems is equal to that of radioactive systems. In connection with the computational processing of images this makes possible a very fast and precise evaluation.

Biochips are then created by means of probes. From the viewpoint of their function biochips are actually membranes with deposited probes on which complementary sections of DNA (or RNA) are selected by means of hybridization. We can speak about a real biochip when the membrane (probe carrier) to which the DNA is firmly bound is replaced with a glass platelet about the size of a postage stamp and carries hundreds of thousands of functional points *(Ivkovic, N., 2016)*. At present biochips with up to 400 000 different oligonucleotide probes (400 000 functional points – size 1.28x1.28 cm) can be manufactured. The technology of their production is similar to procedures applied in electrical engineering industry.

By gradual and intermittent shading (and irradiating) further nucleotides can be added to the chain of the oligonucleotide probe to make the biochip contain all possible sequences for the given length. For example for an 8nucleitide sequence we need a biochip with 65 536 working spots (4 potential combinations of 4 various nucleotides in an 8nucleitide chain).

All hitherto mentioned biochips are based on the principle of hybridization (joining of complementary sections of nucleotide acids). The hybridization reaction is used for finding complementary sequences in the analysed samples, both for the identification of a particular similarity and for the specification of the sequence of nucleotides in the investigated nucleic acids.

A separate group are biochips the activity of which is not based on the hybridization reaction. Some of them are designed to sort cells according to their size and serve for obtaining DNA from captured leucocytes. In others a polymerase chain reaction (PCR) is executed. Some firms attempt to construct a so-called "mini-machine", which could sort the cells, isolate DNA from them, multiply their corresponding sections (e.g. genes) compare them with the probes, detect the products and finally evaluate all.

For recognition in medicine in many applications it appears that the best method of scanning is confocal microscopy. Due to its great resolution this method is used in genetic engineering to recognize microscopic biochip patterns.

During observation in a confocal microscope the studied sample is illuminated by a point source of light, most frequently a laser beam focused on a diaphragm (so-called first confocal point diaphragm), which is then projected by the microscope objective lens into a point inside the sample. The same objective lens then collects the reflected and scattered light and perhaps even fluorescence. The image of the sample, owing to the space filtration of incident radiation on the detector, does not show any defocused background on extra focal areas of the sample.

Among the main advantages of confocal microscopy compared with optical microscopy is higher axial resolution and suppression of interfering radiation from the defocused areas of the studied sample. Confocal microscopes can image mounts with three-dimensional resolution. Biology and medical research benefit from the fact that confocal microscopy is actually a non-destructive method of study of the special arrangement of cells and tissues.

The benefit of confocal microscopy is that it can distinguish fluorescence from molecules inside and outside cells. By means of immunofluorescence methods which are based on the precise chemical uniqueness of antibodies labelled by fluorescence, not only the distribution of receptors in the membranes can be studied but for instance also the organization of the cycloskeleton. In many cases the

improvement of contrast is so dramatic, that cell structures which could absolutely not be observed with a classical microscope are revealed.

In our case the method of confocal microscopy was based on the simultaneous scanning of fluorescence images by three photomultipliers with spectral filters for the blue, green and red colour. By a recombination of three partial images in basic colours we obtain an optical section in real colours of the emitted fluorescence.

The image from a confocal microscope is then processed by pattern recognition methods, *(Masoud, 2000)*. Image converters with an accuracy of at least 10 bits are used for special photometric purposes. Methods of noise filtration (important for amplified fluorescence microscopy) or on the other hand detection and accentuation of intensity gradients and image segmentation belong to basic methods of computational image processing. Segmentation requires that individual objects must differ from each other by their brightness or colour. Objects labelled during image segmentation can then be counted or their dimensions and brightness statistically evaluated.

Ratio imaging is of basic significance in the biological application of fluorescence microscopy. This method makes it possible to measure the relative variations of fluorescence intensity in the cell compared with an appropriate initial state and to measure the ratios of intensities on two different excitation wavelengths. The measured ratios can then be imaged in imitated colours according to an appropriate colour code. Ratio imaging is used to convert the fluorescence images of cells coloured by indicators into quantitative images of the distribution of these physiologically significant factors in live cells.

RESULTS AND DISCUSSION

For the automatic evaluation of genetic operations a program called Genocol was created for the recognition of the colours of DNA probes located on the biochip and obtained by confocal microscopy.

First of all biochips are created according to the following procedure:

1. The investigated DNA is cloned.
2. Probes are produced from the DNA (DNA is split into smaller sections).
3. DNA is labelled (coloured) by fluorescence colours (green, red – e.g. Biotin).
4. By means of a micro manipulator (see Fig. 1) DNA is deposited on the biochip on which a physiological solution with a certain DNA sequence is located and also a membrane which fixes the DNA in the given position.
5. Now on each point of the biochip follow certain processes which serve for the joining of two fibres of a certain DNA sequence.
6. Complementary DNA sequences are joined and their bond is relatively strong. Partially joined fibres and those that are not joined are washed by the solution.
7. The biochip is completely scanned by a confocal microscope. In our case the colour of individual points on the biochip ranges from deep green to deep red according to which DNA probes joined.
8. The biochip with individual samples can be directly observed by the objective lens of the confocal microscope. A biochip usually has many thousands up to tens of thousands points and this is why most frequently the image is processed by a computer program. And this is the task of the Genocol program.
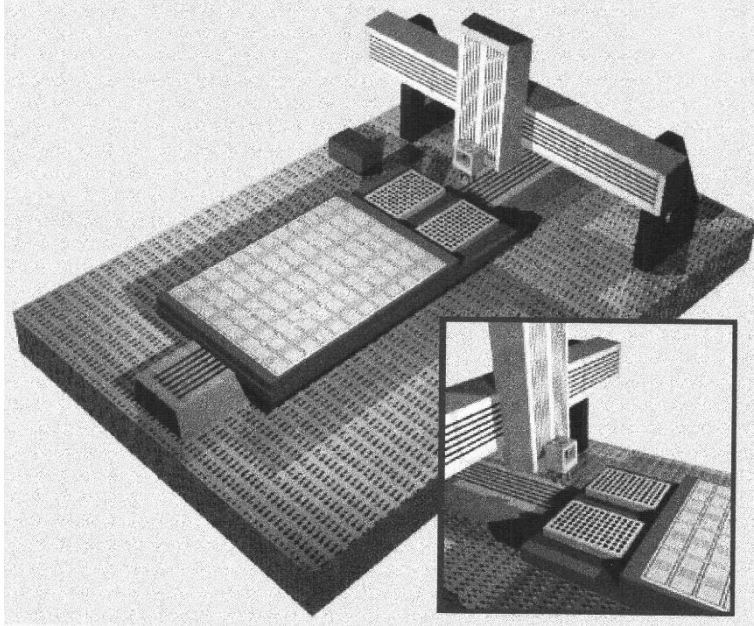
Fig. 1 Micro manipulator depositing the DNA samples.

The Genocol program *(Kolpek, 2003)*, with which the images with the samples of DNA probes are processed is written in the Borland-Delphi programming language. The image data are downloaded directly from the monitor and this is why it is necessary to set the colour deepness to 24 bits (True colour). This method is simpler than downloading data directly from the file because we need not know the exact structure and arrangement of data which are different in each format. The processed file is stored in the BMP file format (Microsoft Windows bitmap image file). This graphical file uses 24 bit imaging. 24 bit images use 3 bytes of colour information per pixel stored in the sequence red, green and blue channel (each 8 bite, i.e. a palette of 256 colours). The BMP format is not a packed format which is essential for dealing with this task since information on the real image in the packed format can be lost due to reduction of data. A section of the recognized bitmap file is in Fig. 2.
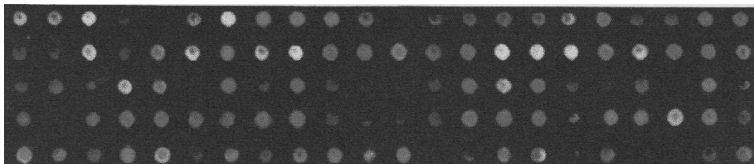
Fig. 2 Section of the recognized bitmap file.

The processed graphical file is a matrix of objects. The pixel which belongs to our searched sample (object) must have a zero or minimum magnitude of the blue colour component. This is due to the fact that DNA probes are labelled only with a red and green colour. However scanning may not be absolutely precise and this is why the tolerance of this colour must be set. Each object on our investigated image is composed of many pixels. This is why the quantity of the red and green colour is obtained by averaging. This means that first all values of the green and red colour are downloaded from one object and then divided by the number of downloaded pixels. This is how the average representation of the red and green colour in the object is obtained. This procedure is performed cyclically in all objects in the image. The result must be stored in two matrices. The coordinates are the same as in the objects on the image. The two matrices containing the values of the representation of the red and green colour are divided one by the other. Thus the resultant matrix is obtained giving the share of the red colour compared with that of the green one in each object (sample). The last operation consists in the ordering of the numbers of the resultant matrix of shares according to their magnitude. In order that the program could recognize which pixels belong to individual objects, grids are formed between

individual objects. The number of grids must be adjustable ("Number of samples, to the right, down") because the number of objects can vary. The program also makes it possible to set various tolerances of the blue colour since this colour is used for specifying if the pixel belongs to the object (sample) investigated by us. The setting of tolerance is also necessary due to the different quality of individual files. The main window with the individual settings is in Fig. 3.
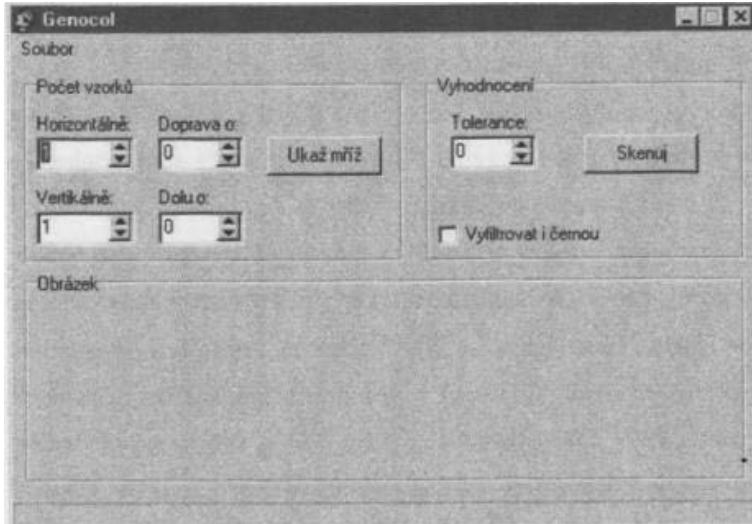

Fig. 3 The main interface window of the application.

The result shows the values of the representation of colours, their share and arrangement according to their magnitude. The program window with results is in Fig. 4.
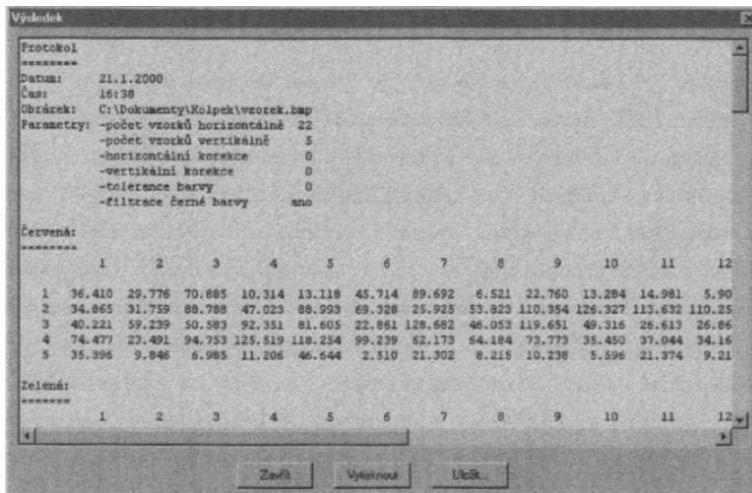
Fig. 4 Program window with results.

In this paper was shown originally methods of creating and automatically patern recognition of bio-chips used in genetics.
Other method of analysis of DMF biochips is described in (*Singla, 2019*).

CONCLUSIONS
The present paper deals with the issue of the recognition of biochip patterns obtained by fluorescence microscopy. The aim was to recognize DNA probes labelled by red and green colour implanted directly into the DNA. These probes were deposited on the biochip where certain processes proceeded, e.g. denaturation, by which the DNA probes were joined with the investigated DNA sections.

By means of this process we can determine the exact sequence of nucleotides in an unknown DNA because the sequence of nucleotides in the DNA probe is precisely known and must be absolutely identical to allow joining of two DNA fibres. The biochip was scanned by a confocal microscope which makes it possible to convert the scanned image into a digital form.

The Genocol program makes it possible to evaluate image information. The recognized file contained a matrix of samples deposited on a biochip. Each sample has a certain colour in dependence on how many DNA probes were complementary and hence were joined. The program screens the quantity of red and green colour in each pixel and sums up these values over the entire surface of the sample. Then it calculates the average representation of the red and green colour. The program distinguishes 256 shades of red and 256 bits of green (8 bite, 3 Byte). The Genocol program makes possible an output to the file and printing. The concept of the program is universal in order to allow recognition of files with a different magnitude and number of samples. The program can also set various tolerances of the blue colour because this colour is used for determining if the pixel belongs to the object (sample) investigated by us. The setting of tolerance is also necessary due to the different quality of individual files.

REFERENCES

1. Bittner, M. (1999). Nature genetics. *Nature Américaine, 21*, 10–14.
2. Ivkovic, N., Golub, M., & Jakobovic, D. (2016). Designing DNA Microarrays with Ant Colony Optimization. *Journal of Computers*, *11*(6), 528–536.
3. Kolpek, V. (2000). *Using of Pattern Recognition Methods in Genome Engineering* (in Czech). Prague: Czech University of Life Sciences.
4. Lyu, Z.M., Zhou, X.L., Wang, X.N., Li, P., Xu, L., & Liu, E.H. (2019). Miniaturized electroluminescent biochip prepared on gold nanoparticles-loaded mesoporous silica film for visual detection of hydrogen peroxide released from living cells. *Sensors and Actuators, B: Chemical, 1. April 2019,* 437-443.
5. Masoud, M. (2000). *New Frontiers in Computational Intelligence and its Application*. Amsterdam: Press IOS.
6. Pardatscher, G., Bracha, D., Daube, S.S., Vonshak, O., Simmel, F.C., & Bar-Ziv, R.H. (2016). DNA Condensation in One Dimension. *Nature Nanotechnology, 11*, 1076–1081.
7. Singla, A., Agarwal, V., Roy, S., & Mondal, A. (2019). Reliability analysis of Mixture Preparation Using Digital Microfluidic Biochips. *IEEE Transaction on Computer-Aided Design of Integrated Circuits and Systems, 38*(4), 654-667.
8. Wan, C., Chen, X., & Liu, D. (2019). A multi-objective-driven placement technique for digital microfluidic biochips. *Journal of Circuits, Systems and Computers*, *28*(5).

Corresponding author:
Prof. Ing. Jaromír Volf, DrSc., Department of Electrical Engineering and Automation, Faculty of Engineering, Czech University of Life Sciences Prague, Kamýcká 129, Praha 6, Prague, 16521, Czech Republic, phone: +420 22438 3203, e-mail: volf@tf.czu.cz

QUALITY ASSESSMENT OF SELECTED TILLAGE MACHINES FOR SECONDARY SOIL TILLAGE

Jiří VOMÁČKA[1], Petr NOVÁK[1], Josef HŮLA[1], Zdeněk KVÍZ[1]

[1]*Department of Agricultural Machines, Faculty of Engineering, Czech University of Life Sciences Prague, Kamýcká 129, Praha 6, Prague, 16521, Czech Republic*

Abstract
The aim of this paper is evaluate the quality of soil tillage with combinator for secondary soil tillage. Measurements of tillage quality parameters were performed on August 2017 in Nesperská Lhota near Benešov (Central Bohemia Region) on sandy-loam soil at an altitude of 390 m. This evaluation was carry out on three-row (working tools) pre-seed combinator for soil bed preparing. Quality of soil tillage was assessed after crossing machine. The evaluated parameters of the quality of work are surface covering by crop residues, size of soil aggregates, surface profile and surface roughness. After secondary tillage was observed small number of clods, low surface roughness and an appropriate spreading crop residues. The results demonstrate the effectiveness of the combinator to create a quality pre-seed bed.

Key words: soil tillage; the quality of the machine work; depth of loosening.

INTRODUCTION

Soil is a non-renewable natural resource that is the main means of producing food in agriculture *(Morgan & Nearing, 2011)*. Over the past hundred years, land has been increasingly used by machinery and technology. However, this is a risk to the sustainability of land use, as damage to the soil environment affects yields for several decades *(Kladivko, 2001)*.

The task of soil cultivation is to prepare the soil for the establishment of stands, for growth, development and yield of cultivated crops and for the proper course of soil processes. When choosing soil tillage, proper soil water management, biological and chemical soil conditions must be taken into account *(Titi, 2002)*.

The soil is threatened by a number of natural phenomena, but also by human activity. According to estimates, 50% of the total original area of productive land has already been destroyed by human activity on Earth, and 10 million square kilometers of cultivated land have been lost over a hundred years *(Morgan, 2005)*. This land is declining mainly in Africa and the Far East. The soil is threatened mainly by water and wind erosion *(Pimentel, 2006)*. The problem is the acidification of soils by acid rain. Another major problem for Africa, Asia and Latin America is desertification because of deforestation *(Lal, 1995)*.

The risk to soil fertility in the Czech Republic is also management at the expense of soil fertility in the future. The detriment to this is, for example, soil compaction in previous operations, inadequate soil organic matter care, extremely simplified crop sequences (lack of improving crops), soil overload with maize for energy purposes, and current water erosion in maize growing *(Kovaříček et al., 2008)*.

About 50% of the total agricultural land is threatened by water erosion in the Czech Republic. This is largely due to the linking of agricultural areas to large units after the Second World War and the current trend of growing wide-row crops as maize without covering the soil surface with organic matter *(Javůrek et al., 2008)*.

Choosing the right soil tillage system and the right machine is crucial to affecting these negative impacts on the soil. Therefore, this issue needs to be addressed. Thus the aim of this paper is evaluate the quality of soil tillage with combinator for secondary soil tillage.

MATERIALS AND METHODS

The measurement was carried out on October 21, 2017 in the area of Nesperská Lhota near Vlašim. The coordinates of the plot are 49 ° 41'30.2 "N 14 ° 48'37.8" E. The soil is loamy-sandy cambisoil, shallow and slightly rocky. The whole plot is located on a gentle slope, the average slope is 4.2°. The altitude is between 450 and 475 meters above sea level. Winter wheat was grown on the plot in

the year of measurement. Straw was baled and taken away. This was followed by medium plowing to a depth of 0.22 m with a ROSS plow. After plowing the land surface was processed by levelling bars and harrows. The soil cultivator Ostroj Saturn with a working width of 6 meters was used for measuring. Combined cultivator was pulled by Zetor Forterra 130 HSX 16V. Tillage was carried out on a contour line. Soil tillage speed was 10 km/h.

Soil roughness was measured by the chain method *(Klik et al. 2002)*. The measurement of clods weight was performed by measuring the weight of the individual clod fractions. Determination of the weight of clods of different size fractions was always performed on an area of 0.25 m² (0.5 x 0.5 m). The soil was uncovered to the depth of soil cultivation. Subsequently, it was screened through a set of 100, 50, 30 and 10 mm sieves. Five measurements were made for both variants (before tillage, after tillage). The results were determined by calculating the arithmetic mean of the fractions weights from which the relative mass fractions were determined.

Measurement of surface coverage by plant residues was performed by image analysis. IrfanView 64.4.44 photo editing software was used for processing. Here, the create photos were edited with color correction and color replacement tools, adjusted to photos with black and white images, where black and white are marked in the bare surface of the soil.

RESULTS AND DISCUSSION

The calculated surface roughness values clearly demonstrate a significant reduction in soil roughness after soil cultivation by combinator. The roughness of the soil surface after tillage has decreased in the longitudinal direction by almost 70% compared to the original state. Soil surface roughness after processing in the cross direction has also decreased, but the difference is not so pronounced due to the surface profile created by the Crosskill rolls. The graphs in Figure 1 show ranges of calculated surface roughness values. According to the Tukey test with homogeneous groups, it is shown that there is a significant statistical difference between the surface roughness before processing and the longitudinal processing of the soil.
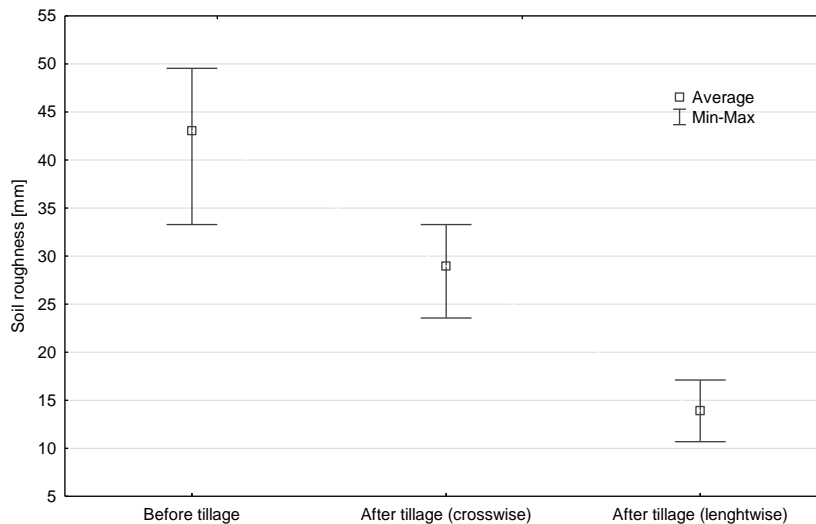

Fig. 1 The calculated surface roughness

The clods weight measurements provided values to generate the graph shown in Figure 2. The values were measured before soil cultivation and immediately after the soil cultivation with a combined cultivator. The results show that the soil is free-flowing and does not produce lumps larger than 100 mm. Even lumps larger than 30 mm are only 4.4% on the site. However, there is a noticeable difference in lumpiness before and after soil tillage. After soil tillage, the proportion of clods over 30 mm and lumps of 10-30 mm were reduced. As a result, the proportion of particles smaller than 10 mm has increased considerably.
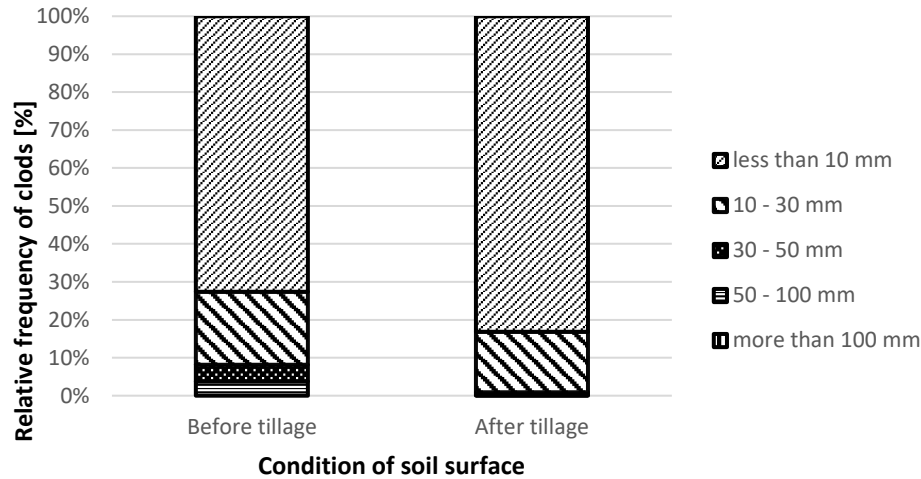
Fig. 2 Relative frequency of clods

The results of the recorded soil cover with plant residues clearly indicate that the vast majority of plant residues on the soil surface have been incorporated. This proves that a small amount of plant residues can reliably incorporate by combined cultivator. Figure 3 shows the ranges of measured values. From Tukey's analysis, there is a significant statistical difference between the pre-cultivation and post-culture values.
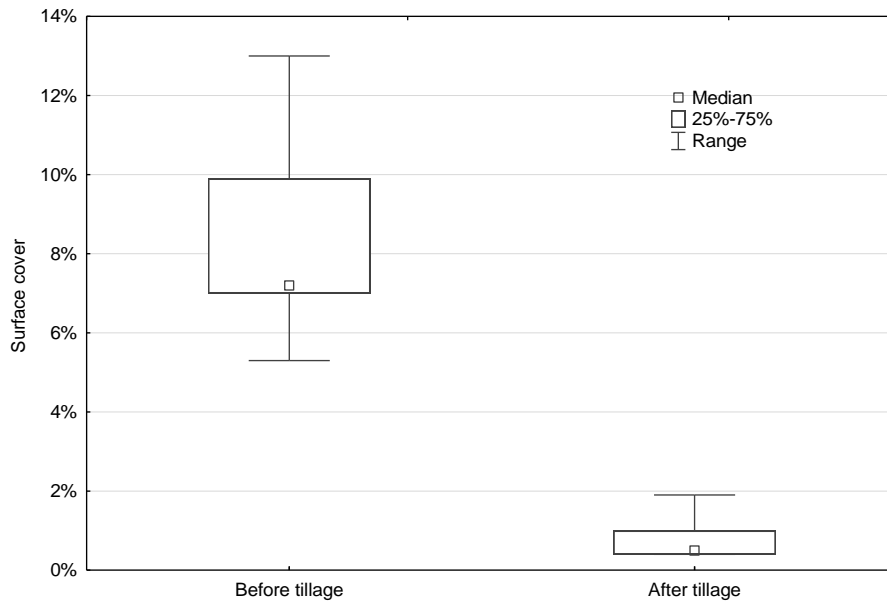

Fig. 3 Soil surface coverage by plant residues

Surface roughness measurements always have pitfalls associated with soil at the measurement site. Very much depends on soil condition, soil type, soil composition, soil moisture, stoniness, etc. When measuring the surface roughness of the chain method, we measured the surface roughness value of 28.96 mm with the transverse direction and 13.90 mm in the longitudinal direction. This significant difference is due to the texture of the soil surface after the Crosskill roll. For comparison, *Duma et al. (2017)* measured the surface roughness by the 2.54 mm chain method, for the Preciser 6000 disc harrow with rod rollers under similar conditions, for the Horsch Tiger 4AS cultivator with tire packer up to 10.36 mm and for Case III Ecolo- tiger 530B surface roughness 10.3 mm finished with gates. These values indicate that the ground surface measured by the Crosskill roller after the soil has been tilled produces a rougher surface when using the gates of the Case Ecolo-tiger or tire packer.

From the soil surface coverage measurements, it was measured that the combined cultivator incorporated 89.5% of the plant residues in the soil, with an average surface coverage of plant residues of 8.5%. This is a good result compared to the values measured by *Novák et al. (2013)* on the Horsch Terrano 3 and Lemken Karat 9/300 cultivators. Horsch Terrano incorporated 71.2% of plant residues and 70.1% of plant residues from Lemken Karat. However, we have to take into account that these measurements initially covered almost 100%, which makes the comparison very difficult.

CONCLUSIONS

The measurement was focused on evaluating the quality of the secondary tillage by the combined Ostroj Saturn cultivator. From the measurement of soil surface roughness by the chain method, we found that the stand creates a good and balanced soil surface suitable for soil preparation before sowing. However, problems occurred in the processing of the soil on a slope when traveling on a contour line, where the machine created some stairs on the land surface. The clods measurement shows that the machine has a good crumbling ability. The proportion of larger clod fractions decreased significantly after soil treatment. In terms of incorporation of plant residues, it was calculated that 89.5% of the plant residues were incorporated. This clearly demonstrates that the machine is able to reliably incorporate a small amount of plant residues.

REFERENCES

1. Duma, C. A., Mihut, C., & Arsene, O. (2017). Optimising mechanized technology in what in the conditions of Bazos Timis County. *Research Journal of Agricultural Science*, *49*(2).
2. Javůrek, M., Hůla, J., Vach, M., & Kroulík, M. (2008). Impact of different soil tillage technologies on soil erosion effect mitigation. *Scientia Agriculturae Bohemica, 39*(2), 218-223.
3. Kladivko, E. J. (2001). Tillage systems and soil ecology. *Soil and Tillage Research*, *61*(1-2), 61-76.
4. Klik, A., Kaitna, R., & Badraoui, M. (2002, May). Desertification hazard in a mountainous ecosystem in the high Atlas region, Morocco. *In 12th International Soil Conservation Organization Conference Proceedings* (pp. 636-644), vol. 4.
5. Kovaříček, P., Šindelář, R., Hůla, J., & Honzík, I. (2008). Measurement of water infiltration in soil using the rain simulation method. *Research in Agricultural Engineering*, *54*(3), 123-129.
6. Lal, R. (1995). Erosion-crop productivity relationships for soils of Africa. *Soil Science Society of America Journal*, *59*(3), 661-667.
7. Morgan, R. P. C. (2005). *Soil erosion and conservation*. Third Edition. Malden, USA: Blackwell Publishing company, p. 304.
8. Morgan, R. P. C., & Nearing, M. A. (Eds.). (2011). *Handbook of erosion modelling*. West Sussex: Wiley-Blackwell, 77 p.
9. Novák, P., Mašek, J., Knap, P., & Petrásek, S. (2013) Quality assessment of selected tillage machines for deeper loosening soil without turning. In *5th International Conference onTrends in Agricultural Engineering 2013* (pp. 456-460).
10. Pimentel, D. (2006). Soil erosion: a food and environmental threat. *Environment, development and sustainability, 8*(1), 119-137.
11. Titi, A. (2002). *Soil tillage in agroecosystems*. USA: CRC press, 384 p.

Corresponding author:
Ing. Jiří Vomáčka, Department of Agricultural Machines, Faculty of Engineering, Czech University of Life Sciences Prague, Kamýcká 129, Praha 6, Prague, 16521, Czech Republic, e-mail: vomacka@tf.czu.cz

MEASUREMENT OF PERFORMANCE PARAMETERS IN SYSTEMS WITH FREQUENCY INVERTERS

Zbyněk VONDRÁŠEK[1], Martin POLÁK[2]

[1]*Department of Electrical Engineering and Automation, Faculty of Engineering, Czech University of Life Sciences in Prague, Kamýcká 129, 165 21 Prague, Czech Republic, e-mail: vondrasek@tf.czu.cz*
[2]*Department of Mechanical Engineering, Faculty of Engineering, Czech University of Life Sciences in Prague, Kamýcká 129, 165 21 Prague, Czech Republic, e-mail: karel@tf.czu.cz*

Abstract
Speed control of AC (alternating current) motors and generators with frequency inverters is becoming increasingly popular, especially due to the decreasing cost of the inverters. This is a positive trend in terms of user comfort, as well as in terms of energy savings. However, besides the undeniable advantages of this technology, it also brings some difficulties arising from the non-harmonic waveforms of the inverters output voltages. This is reflected, for example, in the requirement for greater accuracy in the measurement of electrical input/output power. Conventional wattmeters remain available, but they are mainly designed to measure harmonic waveforms of circumferential parameters. The article experimentally verifies six principles of power system performance measurement and compares them with the YOKOGAWA WT300E digital reference wattmeter, which is specially designed for non-harmonic waveform measurements. The comparison shows that conventional power meters differ from the reference wattmeter up to 12.5%. A set of three conventional wattmeters presents the least deviation from the reference meter, with the range of 0.17 to 7.2%.

Key words: *frequency inverter; wattmeter; power output; asynchronous motor/generator.*

INTRODUCTION

The issue of the three-phase system output measurement was described in (*Dufek & Fajt, 1974*). Measurement applied to a low-output power source with a bladeless turbine and a low voltage synchronous generator was presented in (*Vondrášek & Dlabal, 2016*). (*Gyarfas & Rapant, 1991*) described measurement of output and transmitted energy according to IEEE standards. (*Ďaďo & Sedláček, 1987* ; *Novák & Novák, 2009*) extended the measurements to non-harmonic waveforms of circumferential parameters. (*Chyský, Kořínek, Novák & Novák, 2013*; *Novák, Chyský & Kořínek, 2015*) utilized it for networks with non-harmonic parameters. (*Han, Luo, Hou, Su, Yuan, Liu & Guerrero, 2018*) paid attention to effective inverter control for photovoltaic power system. For the operation of wind power plants, the use of inverters is necessary due to the inconstant speed of the generators; the quality of the supplied energy is evaluated according to IEEE Directives as described in (*Emanuel, Schellschmid, Wachtel, & Adloff, 2009*). A similar situation occurs with small hydropower plants or with the use of pumps as turbines for energy recovery in water distribution networks (WDN). The main interest of the paper is the comparison of measurement results between meters of different constructions.

MATERIALS AND METHODS

Electronic inverters are used to run electric motors with AC (alternating current) and DC (direct current) power systems in regulated drives and in the operation of alternative energy sources. Electric machines with alternating current multiphase systems are used as conventional energy sources with constant speed. The development of power electronics enabled their use in wind power plants and in drives with speed control. The multiphase current system allows creation of a so-called rotating magnetic field.

Alternating machines with a rotating magnetic field are easier to design and cheaper to manufacture compared to DC machines. For speed control, the frequency of the power supply system needs to be changed using inverters. Besides the undeniable advantages, this technology also brings some pitfalls. One of them is the occurrence of non-harmonic waveforms of the output voltages and currents of the inverters.

This is manifested, for example, in the requirement for greater accuracy in the measurement of electrical input/output power. Modern digital devices are already available, but their prices are high. Conventional wattmeters remain available, however they are largely designed to measure harmonic waveforms of circumferential parameters. The article compares the results of six different principles of measuring electrical input, or output power of asynchronous machine in motor, or generator operation. An asynchronous machine AP112M-2s, manufactured by MEZ Mohelnice, was used for the experimental verification. It was mechanically connected to the radial centrifugal pump META Plus 5, manufactured by ISH Pumps Olomouc, which is a part of a hydraulic test circuit described in *(Polák, 2019)* A heavy duty frequency inverter Frecon LSLV0055S100-4EOFNS, manufactured by LS Industrial Systems, with power output of 5.5 kW was used to control the operation. The whole set allowed to measure the performance characteristics in both motor and generator mode, when the pump was operated in pump and also in reverse turbine operation.

Measuring sets
The first of the six measuring sets consisted of three individual electrodynamic wattmeters for harmonic power system. A diagram of connection of the set between the asynchronous machine and the inverter is presented in Fig. 1a (the set is labelled 3W in graphs of performance parameters). Next measuring set was based on the principle of measurement with one three-phase wattmeter described in (*Vondrášek & Dlabal, 2016*). Its connection is shown in Fig. 1b (it is labelled Ganz in graphs).
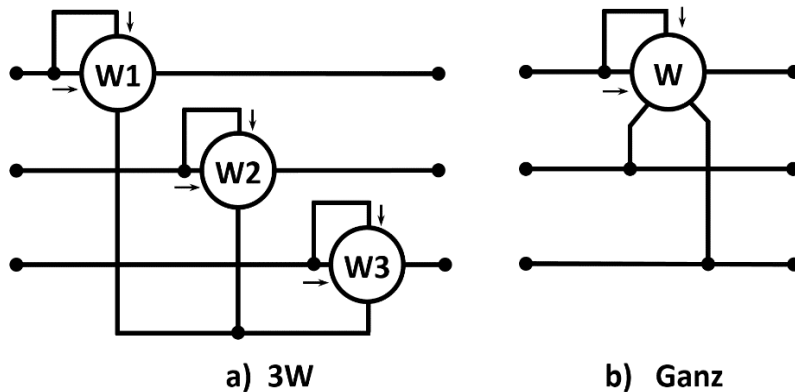

a) 3W   **b) Ganz**

Fig. 1 a) Connection of 3 wattmeters Ganz HEWa-2 with artificial zero point,
b) three-phase wattmeter Ganz HEWa-b with one current circuit.

The third device was a combined measuring set Metra QN10 with a voltmeter, ammeters in each phase and a three-system wattmeter (see Figure 2a). Its connection was similar to the set of the three wattmeters with artificial zero point jointed to the measuring device. Next device was a combined measuring set Metra QW2j with a voltmeter, ammeters in each phase and a two-system ferodynamic wattmeter connected similarly as the pair of wattmeters in Aron's scheme according to (*Brandolini & Gandelli, 2009*), as shown in Figure 2b.

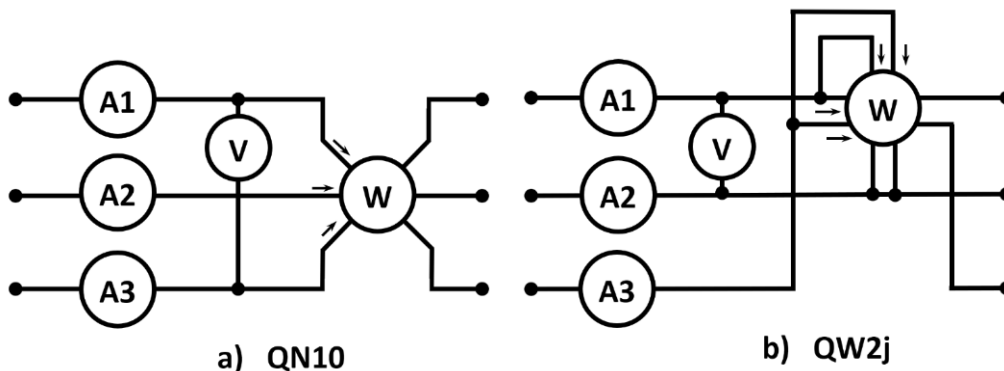**a) QN10**   **b) QW2j**

Fig. 2 a) combined measuring set QN10 with three-system wattmeter,
b) combined measuring set QW2j with two-system wattmeter

The fifth meter is a digital wattmeter YOKOGAWA WT300E (*Zhou, Su, Li, Fang, & Cheng, 2018*). This wattmeter is specially designed to measure the performance of non-harmonic waveforms. In view of this, it was designated as a reference meter. The variant 3V-3A was chosen out of the possible configurations proposed by the manufacturer, and it is presented in Fig. 3.
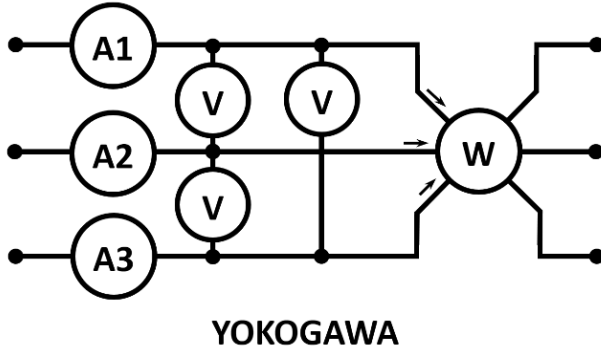

YOKOGAWA

Fig. 3 Digital wattmeter YOKOGAWA WT300E, configuration 3V-3A

The five above described devices were complemented by frequency inverter Frecon, which displayed the active electrical power output. The monitored data were included for comparison with other meters. The built-in algorithm for calculating invertor output power has not been published by the manufacturer. However, it is possible to assume the use of theoretical principle for determining the instantaneous power output p according to:

$$p = u \cdot i \tag{1}$$

where u is instantaneous value of voltage, i is instantaneous value of current.

Evaluation of periodic signal of period T and determination of mean power output P lead to differential equation (2) according to *(Chyský, Kořínek, Novák & Novák, 2013)*

$$P = \frac{1}{T} \int_0^T u(t) \cdot i(t) \cdot dt \tag{2}$$

For numerical evaluation, the integral was replaced by finite number of time periods k forming period T

$$P = \frac{1}{T} \sum_{i=1}^{i=k} u_i \cdot i_i \cdot \Delta t \tag{3}$$

where Δt is period of sampling of instantaneous values of circumferential parameters u and i. At the same time, equation (4) applies:

$$T = k \cdot \Delta t \tag{4}$$

For correct evaluation, it is necessary for the sampling frequency to correspond to at least twice the frequency of the measured signal.

For complete information, mechanical output power data on the motor shaft measured by torque sensor Magtrol TMB 307/411 were added to the output power characteristics.

RESULTS AND DISCUSSION

The test circuit was designed to operate the asynchronous machine in pump mode as a motor, thus it acts as an appliance. In turbine mode, the asynchronous machine operates as a generator.

The measurement of the performance characteristics in the pump mode was carried out at a constant speed of n = 2,950 rpm. During the measurement, the water flow was throttled by a control valve at the discharge from the pump. At the same time, the phase currents between the inverter and the asynchronous motor and the electrical input of the set were measured in steady states. The courses of the monitored parameters depending on the pump flow are presented in Fig. 4.
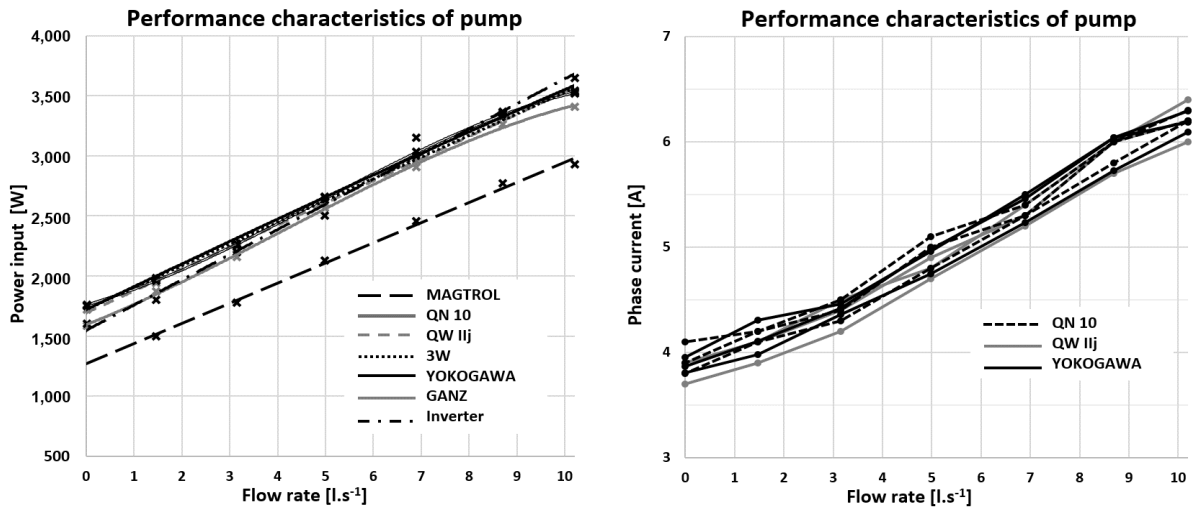
Fig. 4 Input and output powers and phase currents of asynchronous machine depending on pump flow.

The mechanical input of the pump increased with the flow rate – see the MAGTROL curve in Fig. 4 on the left. A similar energy flow situation occurs when the heat pump is powered from the inverter used in the dehumidification experiment according to (*Zhou, Su, Li, Fang, & Cheng, 2018*).

The course of the power input of waterpump was linear, which corresponds to the theoretical assumption. The electric input power of the motor had similar trend, only it was shifted upwards by the energy losses of the pump and the engine. The input power data measured by the various meters had deviations in the range of 3.2 to 10.7%. The biggest deviation of 10.7% was recorded by the Ganz HEWa-b three-phase wattmeter with one current-device at zero pump flow rate. On the other hand, the 3W set presented the best match with the reference meter, with measured values differing from the reference values by 0.40 - 1.17%. The increase of the asynchronous motor current from the initial value in the monitored load range was approximately parabolic. The course corresponded to the theoretical assumption for loading an asynchronous motor with an initial current value different from idle. The difference occurred due to the motor load by pump losses at zero flow rate. The values of phase currents measured by different meters differed from each other minimally – in the range of 4.9 to 10.2%. The greatest percentage differences were recorded at zero pump flow rate and smallest used currents.

Turbine mode measurements were performed at constant feed pump settings, while power outputs and currents at the asynchronous machine in generator mode were monitored. The loading was carried out by gradual reduction of the shaft speed by means of an inverter placed between the asynchronous machine and the load. The measured power outputs and electric currents depending on the shaft speed are shown in Fig. 5. A similar energy flow situation occurs in wind powerplants and the standardized IEEEE energy quality measurement is used in paper by (*Emanuel et al., 2009*).
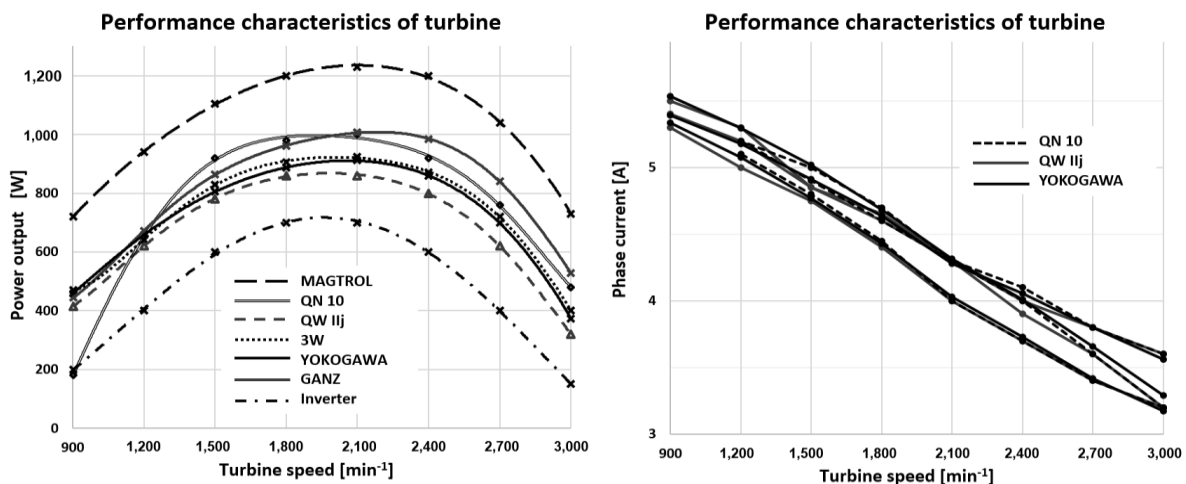

Fig. 5 Power outputs and phase currents of asynchronous machine depending on shaft speed.

When measuring the output power of the asynchronous generator, the 3W set presented the lowest deviation from the reference meter, namely in the range of 1.4 to 7.2%. On the other hand, the QN10 set showed the largest deviation of 60.8% at the lowest speed and 28.7% at the highest speed. In the remaining measured range, the deviation was in the range of 1.1 to 14.1%, similar to other meters. The phase currents of the asynchronous generator decreased with machine speed. The biggest differences between the data from the ammeters were in the area just above the highest output of the asynchronous generator and at the highest speed of the machine when the deviation reached 20.9%. In the remaining monitored speed range, the current deviations oscillated between 10 to 12.5%. The current drop with increasing speed was conditioned by setting the inverter to the so-called full field of the asynchronous machine. The monitored speed range of the set corresponded to the frequency of the current system f_1 which was lower than the nominal one. To prevent over-saturation of the magnetic circuit of the asynchronous machine, a reduced voltage was applied and a constant U_1/f_1 ratio was roughly maintained, so the voltage raised as the speed increased. A lower current was sufficient for a defined output power at a higher voltage.

CONCLUSIONS

Experimental measurements in circuits with non-harmonic waveforms showed that only currents can be measured reliably with conventional ammeters designed for harmonic waveforms. This is partly due to the imperfect symmetry of the set and the load. Combined meters equipped with ammeters presented data comparable to the reference digital meter.

In the case of power output measurement, it appeared that analogue meters compared to the reference digital one were lagging behind. The results of the set of three individual phase electrodynamic wattmeters with an artificial zero point (3W) were the closest to the results of the reference meter, with deviation between 0.17 to 1.17% for motor mode and 1.4 to 7.2% for generator mode. Combined meters QN10 and QW2j were equipped with multi-system wattmeters but with ferromagnetic components of magnetic circuits. This fact distorted the measurements at higher frequencies that occurred in circuits with non-harmonic waveforms of circumferential parameters. This was most evident in the generation operation of the asynchronous machine, where the deviations in the performance measurements from the reference meter were the greatest, depending on the measuring apparatus – up to 60.8% for QN10 meter.

REFERENCES

1. Brandolini, A. &, Gandelli, A. (2009). Power and energy measurements. *Electrical Engineering-Volume II*. Milano: Politecnico di Milano.
2. Chyský, J., Kořínek, P., Novák, J. & Novák, M. (2013). Power output measurement in non-harmonic distribution networks (in Czech). In *New Method and Procedures in Automatic Control, Instrumentation and Informatics*. Turnov.
3. Dufek, M. & Fajt, V. (1974). *Electric measurement 1* (in Czech). SNTL Praha.
4. Ďaďo, S. & Sedláček, M. (1987). *Measurement of active electrical quantities with nonharmonic waveforms* (in Czech). SNTL Praha.
5. Emanuel, H., Schellschmidt, M., Wachtel, S., & Adloff, S. (2009). Power quality measurements of wind energy converters with full-scale converter according to IEC 61400-21, Lodź. In *10th International Conference on Electrical Power Quality and Utilisation* (pp. 1-7).
6. Gyarfas, J., & Rapant, S. (1991). Theory and practice of energy measurement of non-sinusoidal and asymmetrical currents and voltages. *European Transactions on Electrical Power, 1*(3), 159-164.
7. Han, H., Luo, Ch., Hou, X., Su, M., Yuan, W., Liu, Z., & Guerrero, J., M. (2018). A Cost-Effective Decentralized Control for AC-Stacked Photovoltaic Inverters. *Energies, 11*(9), *2262*.
8. Novák, J., Chyský, J., & Kořínek, P. (2015). Interference effects of frequency inverters on motor lines (in Czech). *ELEKTRO, 25*(12), 6-7.
9. Novák, J. & Novák, M. (2009). Power measurement in circuits with pulsed voltage sources. *ELEKTRO, 19*(1), 8-12.

10. Polák, M. (2019). The Influence of Changing Hydropower Potential on Performance Parameters of Pumps in Turbine Mode. *Energies, 12*(11), 2103.

11. Vondrášek, Z., & Dlabal, L. (2016). Determination of loading chacacteristics of a generator for a bladeless turbine, Prague. In: *6th International Conference On Trends in Agricultural Engineering 2016* (pp. 690-694).

12. Zhou, G., Su, L., Li, K., Fang, Y., & Cheng, Q. (2018). An experimental investigation of dehumidifying and reheating performances of a dual-evaporator heat pump system in electrified vehicles. *International Journal of Energy Research, 42*(2), 754-763.

Corresponding author:

Ing. Zbyněk Vondrášek, Ph.D., Department of Electrical Engineering and Automation, Faculty of Engineering, Czech University of Life Sciences in Prague, Kamýcká 129, 165 21 Prague, Czech Republic, e-mail: vondrasek@tf.czu.cz

ANALYSIS OF THE EFFICIENCY OF ELECTRONIC MULTIMEDIA EDUCATION AT THE TECHNICAL FACULTY

Zdeněk VOTRUBA[1], Marek PAČES[2]

[1]*Department of Technological Equipment of Buildings, Faculty of Engineering, Czech University of Life Science Prague,*
[2] *Department of Physics, Faculty of Engineering, Czech University of Life Science Prague*

Abstract
The article is focused on the determination of the effectiveness of multimedia e-learning of selected subjects of the Czech University of Life Science in Prague, Faculty of Engineering. The author focuses mainly on the quantification of the relationship between student achievement in a given subject and the quality and scope of electronic support. Data from several years of monitoring are statistically pro-cessed and relations are sought to quantify the dependence between the student's final evaluation and the electronic support offered. In the conclusion, another possibility of research and the effectiveness of the mentioned e-learning are discussed.

Key words: *education; e-learning; multimedia; efficiency.*

INTRODUCTION

Supporting education and the entire didactic process at any university is a fundamental prerequisite for a high-quality and recognized university. High-quality and well-prepared graduates are the best criterion for evaluating a university with any type of focus. Of course, it is very difficult to evaluate the quality of the teaching process across faculties, disciplines or subjects; however, it is possible, to some extent, to assess the efforts made in the didactic process and to determine a certain degree of effectiveness in the resources spent in this manner. This, of course, primarily impacts supporting the university's didactic process, better acquisition of funds invested in education support, and, of course, as a tool for successfully combating increased failure rates (*Wagner, 2005*). A secondary, but definitely significant argument is the increase in the university's prestige in global rankings (*Vaindorf-Sysoeva, 2018*), (*Gros Salvat, 2018*).

The use of e-learning for all of the above objectives is already relatively broadly developed in academia. At Czech universities, we have been seeing the basic forms of e-learning since the beginning of this millennium (*Čapek, 2015*), although the form and method of implementation varies significantly at individual universities not only in time, but above all with the willingness of guarantors of individual subjects and programs to include these schemes in normal teaching (and in what scope) (*Eger, 2014*), (*Vaněček, 2011*). In addition, stagnation in this area has been evident since about 2014, despite the fact that the technical and technological resources that can be used in e-learning are still being expanded. The prospective means of multimedia e-learning are very difficult to achieve, despite the great interest among students in promoting the aforementioned didactic process. The problem is both the majority approach of teachers and the relatively high reluctance of university management to devote relatively large amounts of funds into the investment of technical equipment, the necessary organizational development and targeted support for this form of teaching. Moreover, there is a fundamental terminological misunderstanding, similarly as when in the past the concept of e-learning itself was misunderstood. Even today, most educators still believe that multimedia e-learning is basically a common form of e-learning supplemented by instructional videos or recordings. It is up to the responsible staff not only at universities, but above all superior components (ministries) to approach multimedia e-learning with full knowledge of this concept and its deployment. Of course, the discussion and definition of the term is not the content of this paper, but it is crucial for any actual implementation. By analysing data from the real implementation of multimedia e-learning, the aim of the paper is primarily to express the conclusiveness of the assumed hypothesis: "**The implementation of multimedia e-learning increases the success of study in selected subjects**".

Given that this concerns proving the existence of statistically significant correlations between the success of the study of the selected subject (the final grade in the subject) and the intensity of e-learning,

more specifically multimedia e-learning (the number and work time of e-learning or multimedia), it is necessary to establish a multi-level comparison, and above all to choose a sufficiently large data set (*Mironova, 2018*). The used inputs and their processing are shown in the next section. When analysing possible processing tools, both classical statistical methods and neural network analysis were considered. Because this is one of the first attempts to determine this dependence, it was finally decided, above all, to use clearer and easier-to-control statistical processing. However, it is evident that analysis using a neural network would ultimately be simpler, but also much more difficult to discuss. However, it is planned as one of the next stages of the ongoing research.

MATERIALS AND METHODS

The first attempts to quantify the effectiveness of multimedia teaching were published in 2015 (*Votruba, 2015*). The results were quite promising, but the fact that the unambiguity of the conclusions had to deal with the high variability of the analyses was evident. It was necessary to significantly increase the number of students and try to refine the own evaluation via a better processing methodology. Therefore, annual data collection has been carried out since 2015. At the moment, a matrix of data from 3 years of teaching (3 semesters of a subject using multi-media e-learning and 3 semesters of a subject where it is not used) is completely available. The data for the analysis is obtained from several independent sources:

   a) study information system - ID of the student, final result in the subject (grade), number of attempted exams;
   b) LMS system – ID of the student, number of accesses to the system, total time of connection in the system, survey of the student expressing his or her opinion of the subject and e-learning support of the subject;
   c) multimedia system – ID of the student, number of accesses to individual records, time of tracking of individual records, total number of accesses, total time of access to the system.

The student's university e-mail was chosen as the ID of the student, under which the student logs into all the above systems. During the course of data processing, it was necessary to significantly simplify the input data, and therefore the following input data were used for the processing:

SIS	LMS	MediaSite
• ID of the student • Final grade • Number of exam attempts	• ID of the student • Number of accesses • Student survey	• ID of the student • Number of accesses to the subject • Time of tracking of the subject

Exports from individual systems were combined into a set, which was subsequently corrected from the perspective of unambiguous identification of the student from all three data sources and subsequently verified in relation to the number of LMS accesses to the number of accesses on MediaSite. Similarly, it was necessary to filter students who completed their studies during the semester. The total number of student records before and after correction is defined in Tab. 1.

Tab. 1 Data counts[*] before and after correction

year	before correction	after correction
2018	336	267
2017	335	269
2016	340	251

•number of students

The resulting data file structure after correction and connection to several initial data *(with regard to GDPR, the email addresses are hidden)* is specified in Tab. 2.

Tab. 2 Data export structure for evaluation

ID user	ID study	Name	Email	Credit	T1	T2	T3	T4	S-mark	Mediasite - total present.	Mediasite - count of view	Mediasite - time of view	Moodle - count of view	Moodle - time of view
185114	209076			Z	1				1	15	31	9:16:24	223	19:23:00
188157	212425			Z	3				3	7	9	3:02:41	182	12:01:00
180498	199266			Z	4				4	1	1	0:00:00	243	23:57:00
161646	209180			Z	4	4	4		12	3	3	0:02:46	172	13:23:00
180499	199267			Z	4	1			5	2	2	0:01:40	217	15:37:00
180654	199823								0	1	1	0:01:37	112	9:02:00
173495	189220			Z	4	3			7	15	23	7:03:57	166	13:23:00
181420	203201			Z	4	4	2		10	11	26	9:55:33	166	14:38:00
175209	202449			Z	3				3	1	1	0:01:29	124	7:59:00
181416	203194			Z	1				1	2	2	0:43:26	115	8:22:00
180428	199224				4	4			8	3	4	1:49:19	84	7:40:00
180502	199270			Z	4	4	3		11	8	12	0:15:00	202	17:38:00
180657	199826			Z	2				2	4	5	1:13:31	126	10:15:00
185120	209087			Z	1				1	20	46	14:49:48	446	12:37:00

The next step was to verify that the three data files could be merged into one and work could continue with only one (merged) file. The results are specified in Tab. 3.

Tab. 3 Statistical processing of input values

	number of accesses			access time		
	2016	2017	2018	2016	2017	2018
number (n)	251	269	267	251	269	267
average (p)	6,66951567	7,565056	7,270758	3:35:03[*]	3:03:32[*]	3:38:44[*]
standard deviation (σ)	5,83428901	6,196327	6,212452	0,225586	0,176729	0,230928
confidence.t	0,612472865	0,743827	0,734818	0,026683	0,021215	0,027314
finv	1,209985796			1,209447		

[*][hh:mm:ss]

Based on the parametric Student's t-test (two selection t-test), the assumption of statistical data consistency with 95% probability was confirmed and data from all three years were still processed collectively. It was thereby possible to work with data from **787 students in two subjects** (full-time and part-time study).

Furthermore, it was necessary to obtain the students' exam results in the monitored subject. This data was exported from the study information system (see Table 2). Since the number of retests, not only the final grade, needs to be taken into account for the evaluation, the resulting grade has been adjusted according to the following formula (1)

$$S = T_1 + T_2 + T_3 + T_4 \qquad\qquad (1)$$

where S is the final grade of the student for evaluation, T_1 to T_4 are grades $(1 - 4)$ from individual exam attempts.
This completed the data acquisition and verification part, and this could then be followed by the dependency analysis and verification of the defined hypothesis.

RESULTS AND DISCUSSION
On the basis of the aforementioned processing of input data, basic statistical processing of the ascertained values was carried out. Above all, there was no significant change in the number of students in the relevant subject in the ascertained time range, see Fig. 1 (TGT25E is a full-time study, TGT75E is part-time study) (*Votruba, 2015*).
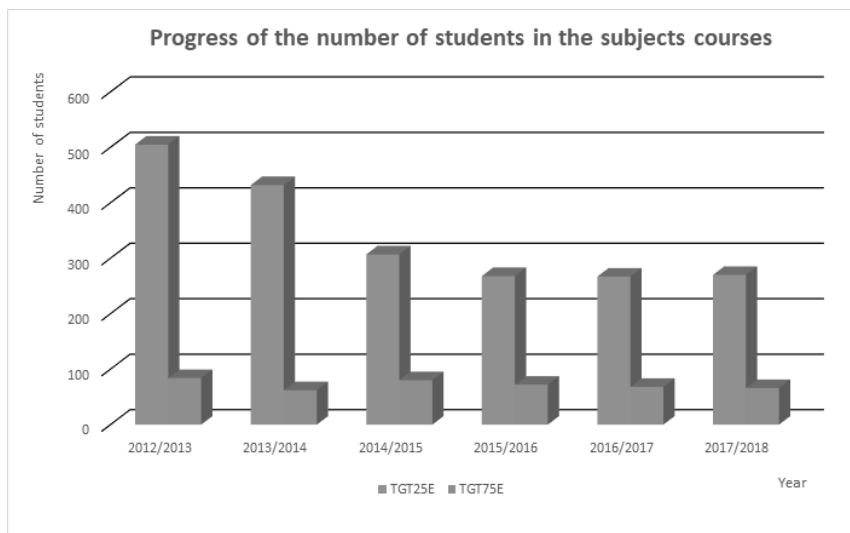
Fig. 1 Development of the number of students in the subject

It is also very interesting to analyse the course of time frequency of access to multimedia support of the relevant subject. It is clear from the graph (Fig. 2) that the maximum monthly number of accesses is achieved both at the end of the semester and in the first half of the exam period. From these values it is possible to conclude that multimedia support becomes the basis for preparation for credit and for preparation for exams, especially for the second and subsequent exam attempts in the subject.
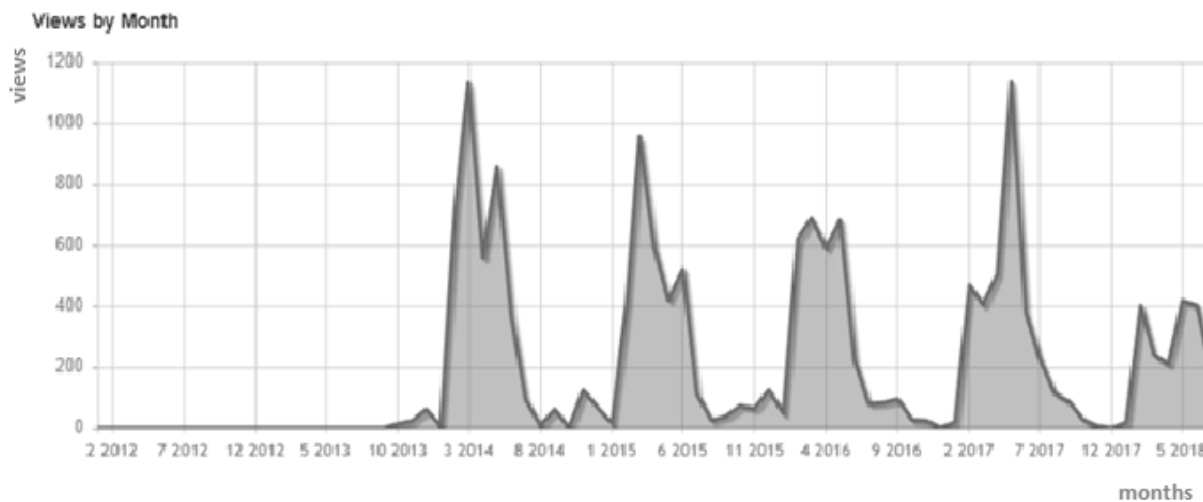
Fig. 2 Peak Connection by Month

Peak Connections by Month
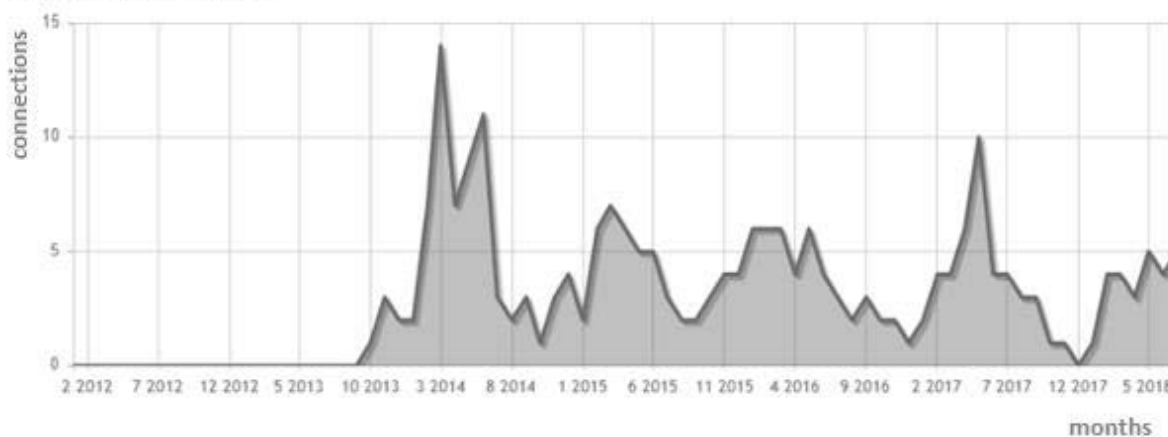
Fig. 3 Views by Month

The subsequent summary table (Tab. 4), together with a summary of the results from the exam via an S-grade, is available after processing input values into a single file and their basic statistical processing.

Tab. 4 Statistical summary of combined input data

	number of accesses	access time	S-grade
number (n)	787	768	768
average (p)	7,0927	3:28:28*	4,8577
standard deviation (σ)	6,0163	0,216245	3,4198

*[hh:mm:ss]

The success of the student (final S-grade) can then be interpreted according to the information system in the subsequent 3 years:
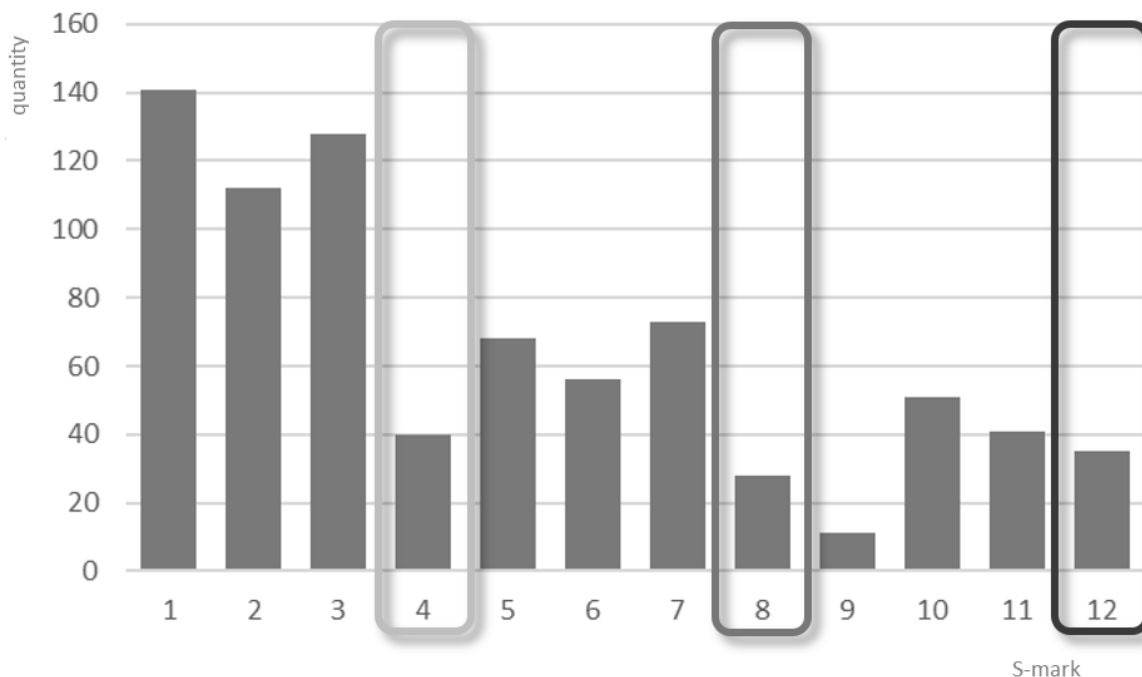
Fig. 4 Success of subject completion

The results shown in Fig. 4 are very interesting, but using a closer analysis, it can be shown that they are somewhat devalued by a systemic error (*Gros Salvat, 2018*). It is obvious that the number of students passing on the second or third attempt is different (lower) than the number of students taking the first exam in the subject in each individual year of study. If this effect and the real number of students recalculated for the given exam are taken into account, the results are significantly more conclusive.
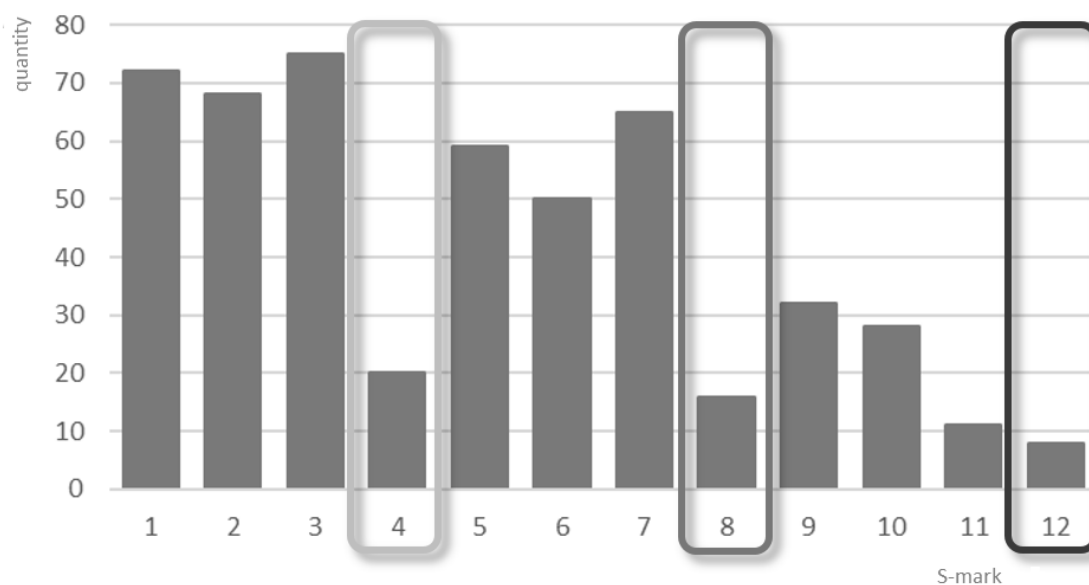
Fig. 5 Success of passing a subject related to the number of students with the relevant grade

It is quite clear from Fig. 5 that multimedia e-learning support is used most by students with a final grade between 1 – 3, the next significant extreme is during a final grade of 3 during the first repetition.

If, for comparison, a subject using only basic e-learning support is processed in a similar manner, the result is demonstrated in Fig. 6.
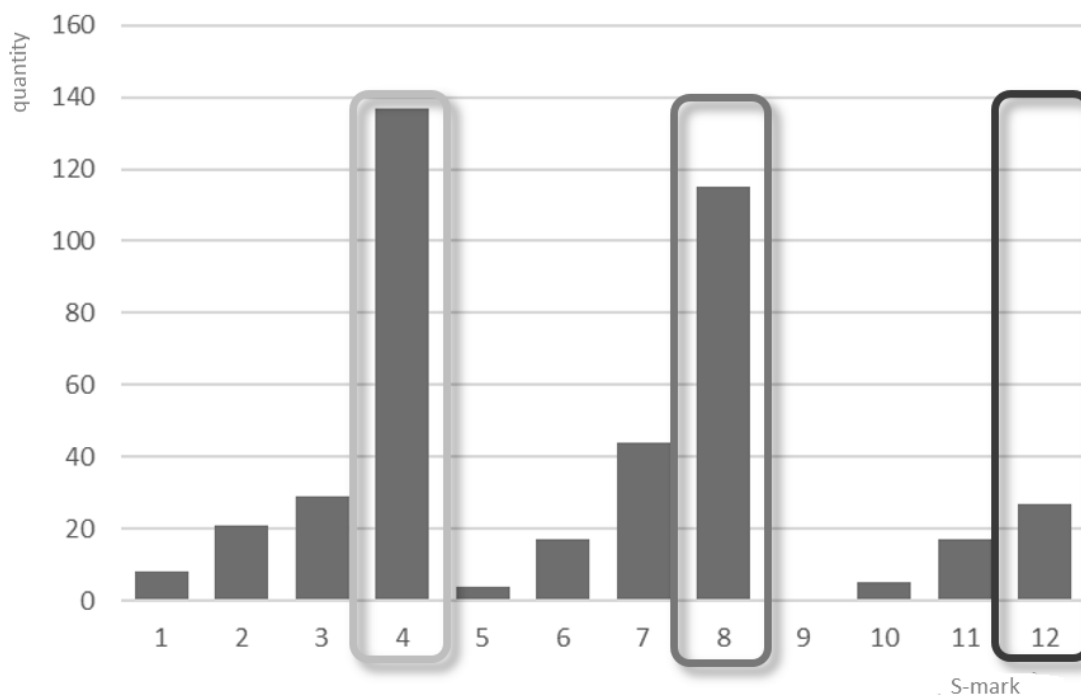
Fig. 6 The success of passing a subject related to the number of students with the relevant grade – control sample

Given the obvious difference between the control sample of the study results and the results discussed in this report, an analysis of statistically significant differences between the compared samples was omitted (*Trilaksono, K.; Santoso, H. 2017*).

CONCLUSIONS

It is possible to formulate the conclusions of this testing on several levels. Above all, it has been statistically confirmed that the results of two different subjects taught in three consecutive semesters are statistically identical. The impact of multimedia e-learning thus manifested itself similarly in various subjects on different groups of students. This is one of the key test conclusions, proving the universal validity of the findings.

Another confirmed conclusion was the verification of the conclusiveness of the impact of multimedia e-learning on a student's final grade (see Fig. 5 and Fig. 6). In this case, the striking difference in the frequency shift of the result "failed" towards the frequency of the result "good", and a certain shift in the frequency of the result "good" towards the frequency of the result "very good" can be seen. In order to unambiguously quantify this result, it will be necessary to expand the monitoring, in particular in the area of "*teaching without e-learning*" and "*teaching with e-learning without multimedia support*", in order to independently assess the impact of e-learning and the impact of multimedia support. Above all, in this monitoring, it is necessary to exclude the influence of the teacher and the subject (topic) area. Therefore, it would be ideal to **have the same teacher teach the subject for various groups of students** with multimedia e-learning, and for a different group without multimedia e-learning, and then in the third group only with classic e-learning support.

From the existing testing, by comparing the results of the specified two groups of students, it can be unequivocally deduced that the use of e-learning shifts the final grade by about **0.4 to 0.7 grade levels** from the subject to a better result, in particular for students around the overall expected result of the S-grade of 3 – 4 and 7 – 8. On the contrary, it is apparent that the impact is **not particularly significant for students repeating an exam for the second time**. Of course, it is not possible to confirm this impact for students with grades from 1 to 2. In any case, the validity of the defined hypothesis that multimedia e-learning has a positive impact on the study results in the given subject has been confirmed.

The survey conducted annually among students shows that the popularity of multimedia e-learning is very high, mainly as a basis for preparation for an exam, and amongst of part-time study students (Fig. 7). The usual claim that multimedia support reduces real participation of students in a lecture is therefore not true.

Fig. 7 Graph of the results of the survey among students on the usefulness of multimedia e-learning (536 respondents)

Without preparing a more detailed analysis, it is interesting to note that the students attach relatively much greater importance to the lecture record than to multimedia support of seminars.

ACKNOWLEDGMENT

REFERENCES

1. Čapek, R. (2015). *Moderní didaktika*. Grada, ISBN: 978-80-247-3450-7.
2. Eger, L. (2014). *Vzdělávání dospělých a ICT*. NAVA, ISBN 978-80-7211-428-3.
3. Gros Salvat, B. (2018). The evaluation of e-learning: from virtual classroom to the network. *Ried-Revista Iberoamericana de Rducation a Distancia, 21*(2), 69-82.
4. Mironova, Y. & Sozontova, E. (2017). Use of modern information technologies in lectures on higher mathematics. *Modern Jurnal of Language Teaching Methods, 7*(12), 196 – 206.
5. Trilaksono, K. & Santoso, H. (2017). Moodle Based Learning Management System Development for Kinesthetic Learning Style. In *Conference: 7th World Engineering Education Forum (WEEF)*. Kuala Lumpur, Malaysia: Univ. Teknologi Petronas, Date: NOV 13-16, 2017.
6. Vaněček, D. (2011). *Elektronické vzdělávání*. ČVUT. ISBN: 978-80-01-04952.
7. Vaindorf-Sysoeva, M. et al. (2018). Improvement of University Ranking by the Level of E-learning Development, *Tomsk State University Journal, 437*, 165-170.
8. Votruba, Z. (2015). Elektronické vzdělávání na ČZU. In *MUG2015 Conference on electronic education via MediaSite, Prague 2015.*
9. Wagner, J. (2005). Nebojme se e-learningu, Česká škola. Retrieved from http://www.ceskaskola.cz/2004/06/jan-wagner-nebojme-se-e-learningu.html.

Coresponding author:
Ing. Zdeněk Votruba, Ph.D., Department of Technological Equipment of Buildings, Faculty of Engineering, Czech University of Life Science Prague, Prague, Kamýcká 129, 16500, Czech Republic, email: votruba@tf.czu.cz.

MATHEMATICAL DESCRIPTION OF NORMAL CONVECTIVE AND VACUUM DRYING PROCESS OF RAPESEEDS

Ling Sze YEE[1], Intan Fazreenna bt Mohd REDZUAN[2]

[1,2] *University of Technology Petronas, Seri Iskandar, Perak, Malaysia*

ABSTRACT
Normal convective drying and vacuum drying of rapeseeds were carried out to conduct the comparison between two different drying process at five different drying temperatures and vacuum pressure of 20 kPa. Mathematical model for description of dependency between weight of rapeseeds and drying time for normal convective and vacuum drying process was determined and statistically verified. From the gained drying characteristics imply that vacuum drying has higher efficiency than convective drying.

Key words: *drying; agricultural; normal drying; vacuum drying*

INTRODUCTION
Rapeseed (*Brassica napus* L), which also known as oilseed rape, is a bright-yellow flowering member of the family Brassicaceae. Like any other seeds, rapeseed are easily affected by the moisture content, temperature and the access to oxygen *(Gawrysiak-Witulska et al., 2012)*. Hence, drying process is one of the methods to produce good quality seed.

The drying process is considered as heat transfer into the product and the moisture of the product evaporated out researched by *Akpinar, Midilli & Bicer (2002)*. Drying process has been enhanced from the past to create an effective and efficient way to produce the products. Study *(Akpinar & Bicer, 2005)*, the need of a drying process is to meet the quality specifications and conserving energy.

Compared to forced convection, natural convection is a slower heat transfer process as forced convection is help with external force (*Hrabě & Herák, 2015*). Moreover, temperature, moisture content and time are some of the factors that might affect the chemical and physical changes that will happen during the process. Therefore, finding the perfect temperature and moisture distribution of the products with a good estimation of the time for the process can improve the quality of the products (*Mizera, Herák & Hrabě, 2017*).

Moreover, *Orikasa et al. (2014)* mentioned that vacuum drying products will have distinctive characteristics compared to convective drying. When using vacuum drying, it tends to retain the integrity of the original product without damaging it with the usage of the heat *(Parikh, 2015)*. Due to that, researchers had found that vacuum drying is generally used for drying products that are heat sensitive. Meanwhile, convection drying focus on high temperatures to properly accelerate the dehydration and absorption process (*Mizera et al., 2018*).

Drying agricultural products has been and still an ongoing research for a lot of researchers out there for examples with kiwi *(Orikasa et al., 2014)*, eggplants *(Akpinar & Bicer, 2005)*, pistachio *(Midilli et al., 2002)*, tomato *(Sacilik et al., 2005)*, apple pomace *(Wang et al., 2006)*, and sultana grapes *(Yaldiz et al., 2000)*.

Thus the aim of this research is to mathematically describe normal convective and vacuum drying process of rapeseeds and to their mutual comparison.

MATERIALS AND METHODS
Rapeseeds used for the experiments were from Czech Republic. The experiments were carried out in Czech University of Life Sciences Prague (CULS).

For each experiment, the seeds were measure to be 100g initially with precision balance shown in Figure 1 (Kern KB 2000-2N, KERN & Sohn GmbH, Balingen, Germany) and the three samples were run together to get the mean results. The weight of the seeds is recorded with the interval of an hour. The oven used for convective drying is from Memmert UF110, Memmert GmbH + Co.KG, Schwabach, Germany shown in Figure 2 whereas the oven used for vacuum drying is from Goldbrunn l450, Expondo GmbH, Berlin, Germany shown in Figure 3. The settings for the convective drying was set to no fan and no flap for the oven. On the other hand, the setting for the vacuum oven, the vacuum pressure was

set to 20kPa throughout the experiment. The data were not collected at night but the drying process was still carried out overnight and the results is taken on the next day. For both convective drying and vacuum drying, the experiments were run under five different temperatures which are 110˚C, 90 ˚C, 70 ˚C, 50 ˚C, and 30 ˚C. The experiment was terminated once the mean of the weight of the seeds had stabilized.

Fig 1: Seeds and precision balance

Fig 2: Memmert UF110 convective dryer for normal drying.

Fig 3: Goldbrunn l450 vacuum dryer for vacuum drying.

RESULTS AND DISCUSSION

In this experiment, rapeseeds were dried under the temperature of 30˚C, 50˚C, 70˚C, 90˚C and 110˚C for both convective drying and vacuum drying. The graphs (Figs. 4, 5, 6, 7, 8, 9, 10, 11, 12, 13) shown is mean weight of the seeds against the heating time. The initial weight of the seeds was measured to be 100g and the data were not collected at night.
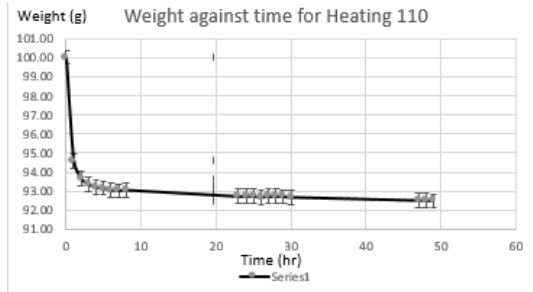
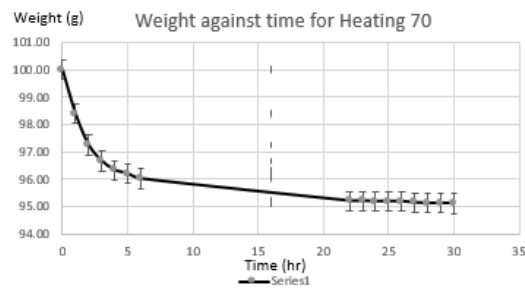**Fig 4**: Normal drying 110 ˚C.
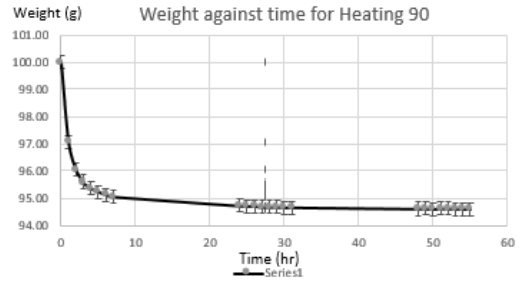
Fig 5: Normal drying 90 ˚C.

Fig 6: Normal drying 70 ˚C.
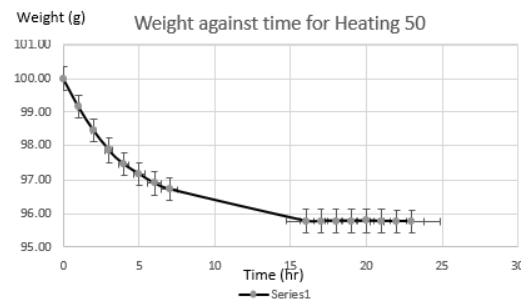
Fig 7: Normal drying 50 ˚C.
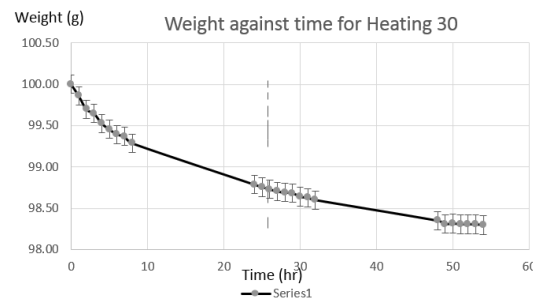
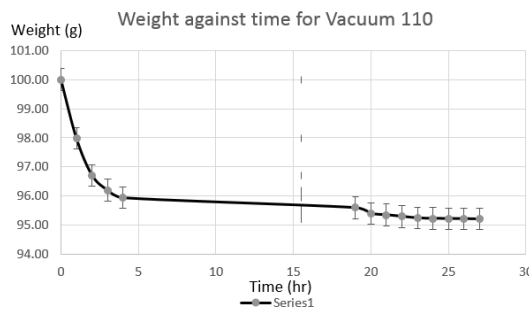**Fig 8**: Normal drying 30 ˚C.

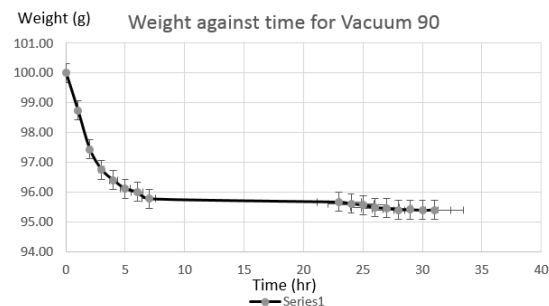**Fig 9**: Vacuum drying 110 ˚C.

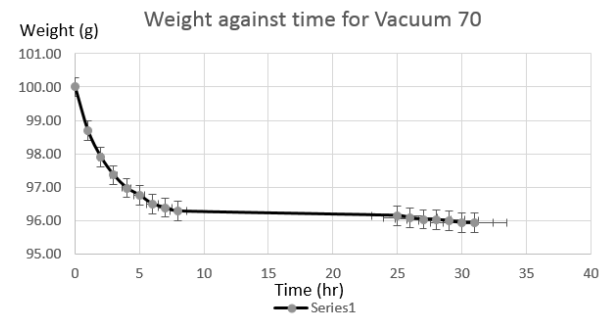
Fig 10: Vacuum drying 90 ˚C.
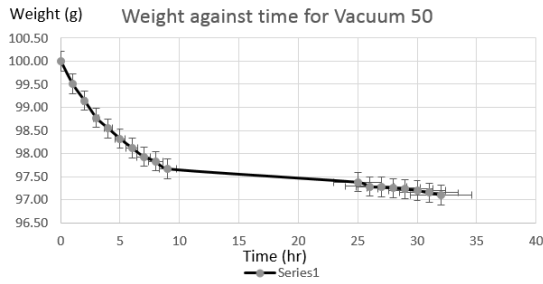
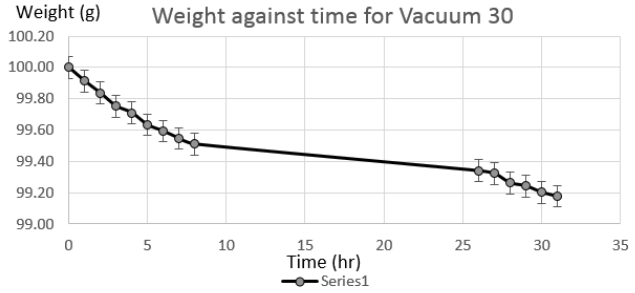**Fig 11**: Vacuum drying 70 ˚C.

Fig 12: Vacuum drying 50 ˚C.

Fig 13: Vacuum drying 30 ˚C.

The mathematical model to describe this heating process is shown in equation 1.

$$\xi\,(d,t) := d_0 + d_1 \cdot e^{d2\,\cdot\,t} + d_3 \cdot e^{d4\,\cdot\,t} \qquad (1)$$

Where d_0 – first coefficient of normalized weight
$\quad$ d_1 – second coefficient of normalized weight
$\quad$ d_2 – third coefficient of normalized weight
$\quad$ d_3 – fourth coefficient of normalized weight
$\quad$ d_4 – fifth coefficient of normalized weight
$\quad$ t – Time

Table 1 lists the coefficient values and statistical values for the model obtained with the data for five different temperatures experiment. An ANOVA (Analysis of variance) statistical analysis of the measured and fitted data shows that the measured data could be mathematically described by Eq. 1. The significance of the ANOVA analysis results was based on the values of F_{crit} being higher than Frat values as well as P_{value} greater than 0.05 with high coefficients of determination R^2 (Table 1).

Tab. 1: Coefficient values and statistical values

	d0	d1	d2	d3	d4	F	Fc	Pv	R^2
H 110	92.419	0.934	-0.046	6.671	-1.607	4.173*10^-11	4.098	1	0.999
H 90	94.62	0.995	-0.097	4.378	-1.024	4.173*10^-11	4.052	1	0.999
H 70	94.923	1.469	-0.072	3.634	-0.597	2.894*10^-11	4.171	1	0.999
H 50	95.688	4.017	-0.202	0.306	-0.694	3.045*10^-11	4.171	1	0.999
H 30	97.89	0.392	-0.335	1.722	-0.027	4.625*10^-11	4.043	1	0.999
V 110	95.311	0.171	-1390	4.518	-0.544	1.524*10^-11	4.225	1	0.994
V 90	95.489	0	0	4.573	-0.401	3.381*10^-11	4.149	1	0.994
V 70	96.018	0.261	-1000	3.722	-0.336	3.126*10^-11	4.171	1	0.998
V 50	97.218	0	0	2.785	-0.191	7.367*10^-11	4.131	1	0.996
V30	99.234	8.012 *10^-4	-1000	0.766	-0.125	1.608*10^-9	4.196	1	0.982

Where $\;$ F - value of the F test
$\quad$ F_c - critical value that compares a pair of models
$\quad$ P_v - hypothesis of the study outcomes significant level
$\quad$ R^2 – coefficient of determination

As expected, the time taken for the drying process of the seeds is longer for normal drying compared to vacuum drying (*Orikasa et al., 2014; Chua et al., 2019; Yaldiz et al., 2001; Akpinar et al., 2003; Wang et al., 2007; Sacilik et al., 2006; Midilli et al., 2003; Akpinar & Bicer, 2005*). From comparison conducted in this study (Figs. 4, 5, 6, 7, 8, 9, 10, 11, 12, 13) of normal drying and vacuum drying,

generally shorter time is required for vacuum drying until the weight of the seeds is stable compared to normal drying. There are some errors during the experiment which caused the time for the vacuum drying at 50 ˚C is longer than the normal drying. Besides, no constant drying rate period is observed in any of the experiments but the drying process happened in decreasing rate based on the observation of the weight of the seeds. This is due to the diffusion of moisture from the centre area of the seeds to the surface is slow and rate limiting mentioned by *Chua et al. (2019).* In already published studies *(Hrabě & Herák, 2015; Mizera et al., 2017; Mizera et al., 2018)* were found that moisture diffusion represents the dominant physical mechanism affecting drying rate decrease during the drying which is a very energy-intensive process and has a significant effect on the quality of the final product.

CONCLUSIONS

- Drying characteristics of rapeseeds under temperature of 30˚C, 50˚C, 70˚C, 90˚C and 110˚C for both convective drying and vacuum drying were determined and described.
- Mathematical model for description of dependency between weight of rapeseeds and drying time for normal convective and vacuum drying process was determined and statistically verified.
- From the determined drying characteristics, it is evident that the time taken for the drying process of the seeds was longer for normal drying compared to vacuum drying
- Vacuum drying has higher efficiency than convective drying.

ACKNOWLEDGEMENTS

REFERENCES

1. Akpinar, E., Midilli, A., & Bicer, Y. (2003). Single layer drying behaviour of potato slices in a convective cyclone dryer and mathematical modelling. *Energy Conversion and Management, 44*, 1689-1705.
2. Akpinar, E.K., & Bicer, Y. (2005). Modeling of the drying of eggplants in thin-layers. *International Journal of Food Sciences and Technology, 40*, 273-281.
3. Fu, D.H., Jiang, L.Y., Mason, A.S., Xiao, M.L., Zhu, L.R., Li, L.Z., Zhou, Q.H., Shen, C.J., & Huang, C.H. (2016). Research progress and strategies for multifunctional rapeseed: A case study of China. *Journal of Integrative Agriculture, 15*(8), 1673-1684.
4. Gawrysiak-Witylska, M., Rudzińska, M., Wawrzyniak, J., & Siger, A. (2012). The effect of temperature and moisture content of stored rapeseed on the phytosterol degradation rate. *Journal of*

The American Oil Chemists' Society, 89(9), 1673-1679.
5. Hrabě, P. & Herák, D. (2015). Mathematical model of sun drying of sliced tomato in Hawassa Region – Ethiopia. Engineering for Rural Development, 14, 174-178.
6. Orikasa, T., Koide, S., Okamoto, S., Imaizumi, T., Muramatsu, Y., Takeda, J., Shiina, T., Tagawa, A. (2014). Impacts of hot air and vacuum drying on the quality attributes of kiwifruit slices. *Journal of Food Engineering, 125*, 51-58.
7. Parikh, D.M. (2015). Vacuum Drying: Basics and Application. *Chemical Engineering-New York-Mcgraw Hill Incorporated then Chemical Week Publishing Llc, 122*(4), 48-54.
8. Chua, L.Y.W., Chua, B.L., Figiel, A., Chong, C.H., Wojdylo, A., Szumny, A., & Lech, K. (2019). Characterisation of the Convective Hot-Air Drying and Vacuum Microwave Drying of Cassia

alata: Antioxidant Activity, Essential Oil Volatile Composition and Quality Studies. Molecules. Retrieved from www.mdpi.com/journal/molecules.

9. Midilli, A., & Kucuk, H. (2003). Mathematical modelling of thin layer drying of pistachio by using solar energy. *Energy Conversion and Management 44*, 1111-1122.

10. Mizera, Č., Herák, D. & Hrabě, P. (2017). Mathematical model describing the drying curves of false banana´s fibre (Ensete ventricosum). Agronomy Research, 15(1), 1094-1100.

11. Mizera, Č., Herák, D., Hrabě, P., Kabutey, A., Wasserbauer, M. & Pouzarová, H. (2018). Describing of drying curves of green coffee beans using mathematical model. IOP Conference Series: Materials Science and Engineering, 420 (1), 1-5.

12. Sacilik, K., Keskin, R., & Elicin, (2006). A.K. Mathematical modelling of solar tunnel drying of thin layer organic tomato. *Journal of Food Engineering, 73*, 231-238.

13. Wang, Z., Sun, J., Liao, X., Chen, F., Zhao, G., Wu, J., & Hu, X. (2007). Mathematical modelling on hot air drying of thin layer apple pomace. *Food Research International, 40*, 39-46.

14. Yaldiz, O., Ertekin, C., & Uzun, H.I. (2001). Mathematical modelling of thin layer solar drying of sultana grapes. *Energy, 26*, 457-465.

Corresponding author:

Ling Sze YEE, University of Technology Petronas, Persiaran UTP, 32610, Seri Iskandar, Perak, Malaysia, email: lingszeyee@gmail.com

THE COMBUSTION PROCESS AND HEAT RELEASE IN THE GAS ENGINE

Mikhail N. YEROKHIN[1], Otari N. DIDMANIDZE[1], Nikolay ALDOSHIN[1], Ramil T. KHAKIMOV[2]

[1] *Russian State Agrarian University - Moscow Timiryazev Agricultural Academy, Russia*
[2] *St. Petersburg State Agrarian University, Russia*

Abstract
The analysis of the material presented in the article showed that the exact mathematical description of the whole gas-dynamic process, the result of which is the effective combustion of the gas-air mixture inside the cylinder, is a difficult task. For this purpose is not appropriate often used option - the creation of a purely empirical regression model, becaus for it would require a very large number of experiments (even in the case of using the method of part factorial experiment); the experience results will be adequate only in the range of changes of parameters in the framework of the conducted experience. Based on the knowledge of modern techniques, it seems appropriate to use the data obtained experimentally as a basis for further recalculation of the parameters taking into account new conditions and physical representations about the working process of gas engines.

Key words: *the process of burning, heat generation, gas engine, flame front, the turbulent velocity.*

INTRODUCTION

The burnout characteristics includes: the duration of the φ1, indicators of the nature of burnout and the proportion of the fuel, burnable in the individual phases of burnout. In the case of diesel engines, there are usually two phases of burnout; in gas and gasoline engines with forced ignition - single-phase heat release (*Vibe i. 1962*),.The purpose of this article is determining the speed of propagation of the frontsevere gas mixture in the combustion chamber, severethrough the angle of rotation of the crankshaft.f

Studies by various authors have confirmed that the angle of the crankshaft rotation (CR) from the beginning of the combustion process to achieve the first maximum rate of heat release in the gas engine under study is practically independent of the operating mode and load characteristics. Accordingly the maximum rate of heat release rate, as indicated above, in the proportion to the heat share released in the first phase of combustion; let us denote it as X_1. According the experimental experience of existing research results and our own tests, the angle φ_1 can be taken equal to $3 - 4°$ CR, since in this case there is an initial process of laminar motion of the flame front, (*Gainullin F. 1986, Birger I. 1978)*. The second phase of heat release is determined according to the presented technique.

MATERIALS AND METHODS

The ratio of burning gas amount to the supplied gas-air mixture gives the additive to the X_1.

$$\tilde{O}_1 = \frac{G_{\tilde{A}\pi}}{\alpha \cdot G_{\tilde{A}}}, \tag{1}$$

where $G_{\Gamma\pi i}$ – the amount of gas mixture consisting of ethane (propane, butane, inert gases, etc.);
α – air excess factor;
G_{Γ} – amount of natural gas.

Thus, for a large class of chain reactions it is possible to write a differential equation. It will relate the total rate of change in the relative density of the effective centers to its density at a given time:

$$\frac{d\rho}{dt} = a\rho - b\rho^2, \tag{2}$$

where a – proportionality coefficient in 1/sec., or constant of circuit development;
b – the proportionality coefficient, which is an abstract number, or the constant of the circuit break.

For non-chain reactions $a = 0$, $b = 0$, so from the equation (3) will obtain that $\frac{d\rho}{dt} = 0$. Therefore $\rho =$ const and the equation for the proportion of the reacted substance turns into the equation of the monomolecular reaction:

$$x = 1 - e^{-n\rho_0^t} = 1 - e^{-kt}, \tag{3}$$

Ratio $a/b = \rho_s$ is equal to the quasi-stationary density of effective centers.

According to equation (3) of the rate constant of monomolecular reactions

$$k = n\rho_0, \tag{4}$$

For very many chemical reactions this constant depends on the temperature according to Arrhenius law, so can write:

$$n\rho_0 = Ae^{-\frac{E}{RT_0}}, \quad \text{or} \quad \rho_0 = \rho_{np}e^{-\frac{E}{RT_0}} \tag{5}$$

where E – activation energy of the initiating reaction;

T$_0$ – absolute temperature at which the heat initiation of the reaction takes place;

R – gas constant;

A constant of co-hit in accordance with the provisions of the gases kinetic theory;

ρ_{np} – the marginal density of the effective centers under a condition T = ∞.

According to equation (5), the initial density of the effective centers of hydrocarbon gas fuels in the combustion process can be calculated for a given temperature.

The process of burning the working mixture consisting of natural gas and air in the main phase is expressed by an angle φ_2, it indicates the flow of the process from the beginning of combustion to the maximum value of the heat release rate in the combustion chamber of the engine. In the formulation of the problem in the process of modeling the heat release process, we believe that this angle shows, ceteris paribus, the determination of the flame front velocityand the distance traveled by the frontal boundary of the flame from the ignition point to the point of the released heat near the walls of the combustion chamber. It follows that the change in the velocity of the turbulent flame propagation in the combustion chamber is directly related to the component composition of the gas-air mixture (*Khakimov R. et al., 2018*).

As a result, the angle φ_2 when the maximum heat release rate in the second combustion phase is reached linearly depends on the turbulent velocity of the flame front propagation in the combustion chamber, according to the data (*Petrichenko R., Rusinova R., 1983*). Based on the above studies on the increasing to the maximum speed of the flame front propagation, we try to determine and construct a type of dependence for the angle of maximum heat release in the main phase of the burn-up process. (*Alumbauch R.L., Keeton I.R, 1984*). Therefore, the expression will have the form that was described (*Khakimov R.T., Didmanidze O.T., 2017*):

$$\bar{u}_T \approx (P)^{a_1}(T)^{a_2}(U_H)^{a_3}(\alpha)^{a_4}(n)^{a_5}(V/n)^{a_6}(q_z)^{a_{11}}, \tag{6}$$

where T - the average temperature of the flame front during its propagation in the combustion chamber; α - air excess factor; U_H - normal speed during the combustion process; P - average combustion pressure during its rise in the combustion chamber; n - the rotational speed of a gas engine a crankshaft; V - volume of gas-air mixture entering the cylinder; q_z – total specific heat of combustion used according Vibe i. (1962), $q_z = \frac{Q_z}{G_{mc}G}$; G_{mc} – the amount of fuel supplied to the engine cylinder in one cycle; G – weight of working fluid per 1 kg of fuel.

Given the fact that $u_H(P,T,\alpha,n)$, add new value q_z so the dependence will take the following form:

$$\bar{u}_T \approx (P)^{a_1}(T)^{a_2}\left((P)^{a_7}(T)^{a_8}(\alpha)^{a_9}(n)^{a_{10}}\right)^{a_4}(n)^{a_5}(V/n)^{a_6}(q_z)^{a_{11}}, \tag{7}$$

Having studied the above, it is necessary to determine the remaining power values in the form of the following coefficients a_1 a_2, a_7, a_8. In this case, we use the ideas about the effect of P, T on the turbulent velocity of the flame in the combustion chamber. Materials on the effect of T on the velocity u_T of a

turbulent flame, degree values of the coefficients sum a_2+(*Kagan L., et al., 2010*). The theory about the relationship between the turbulent flame velocity and *P* can be represented by the values of the following coefficients equal to $a_1 = 0,302$ и $a_7 = -0,305$. (*Austin J.M., Pintgen F., Shepherd J.E – 2005*). To simplify the determination of coefficients a_{11}, a_9, a_6 и a_5, set the value of the coefficient equal to $a_3 = 1$. Further, in order to simplify the expression, let's combine some power values with the same terms, then the calculated dependence will look like this:

$$\bar{u}_T \approx (P)^0 (T)^{1,6} (\alpha)^{a_9} (n)^{a_5} (V/n)^{a_6} (q_z)^{a_7} = (T)^{1,6} (\alpha)^{a_9} (n)^{a_5} (V/n)^{a_6} (q_z)^{a_{11}} \ , \tag{8}$$

The calculated dependence of the angle φ2 characterizing the second phase of the turbulent burning
velocity of flame propagation inside the engine cylinder can be represented by the following formula:

$$\varphi_2 = \frac{l \cdot in}{\bar{u}_T} \ , \tag{9}$$

where *l* - distance from the ignition point to the point of reaching the cylinder walls; *n* - the frequency of the crankshaft rotation; *i* – the number of the engine cylinders.

It follows that the dependence on determining the angle φ_2 of rotation of the crankshaft at the maximum speed of the turbulent flame, taking into account the dependence for u_m will be as follows:

$$\varphi_2 \approx l \cdot n \cdot (T)^{-1,65} (\alpha)^{-a_8} (n)^{a_5-1} (V/n)^{-a_6} (q_z)^{a_{11}} \ , \tag{10}$$

Coefficient a_8 and a_5 values aren't defined we will look for the values of the degree at the excess air ratio and speed, denote them $t>1$ и b_2.

$$\varphi_2 \approx (T)^{-1,65} (\alpha)^{b_1} (n)^{b_2} (V/n)^{b_3} (q_z)^{a_{11}} \ , \tag{11}$$

RESULTS AND DISCUSSION
To determine the degree coefficients, we use the experimental data (*Belyaev A.I., Afanasyev 2016*). As a result, the set values of the coefficients confirm the findings *(Kagan L., et al., 2010)*, about the absence of the relationship between the crankshaft speed and the achievement angle of the maximum value of the turbulent flame velocity in the combustion chamber, expressed by the second combustion phase φ_2; (*Ciccarelli G, 2011*). On the basis of the dependence. (*Oran E.S., Gamezo V.N 2005*) degree value for the coefficient b_3 set equal to $b_3=1$. Next, to determine the degree value of the coefficient b_1, we turn to the experimental data presented in figures 1 and 2. They clearly shows the parabolic nature of the dependence of the normal (u_T) combustion of the gas-air mixture on the coefficient (α) with an extremum corresponding to the composition of the mixture in the stoichiometric ratio.

For gas-air mixtures of methane and oxygen, the stoichiometric composition is equal to the ratio of 17.2%, therefore, the flame propagation velocity of these mixtures will correspond to the maximum limit of 45-55%. This ratio is explained by the weighting of molecules, while the concentration boundaries of ignition are significantly narrowed, hence the curves of the flame propagation velocity in the percentage ratio are also reduced.
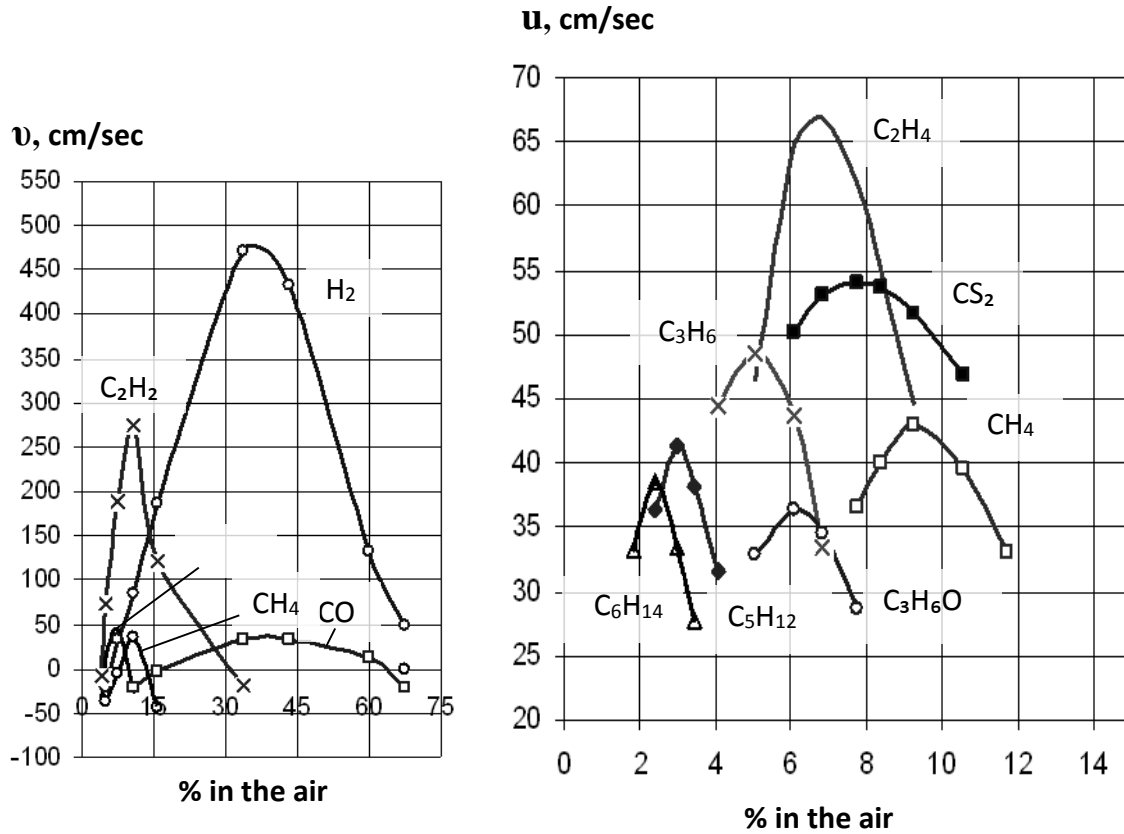
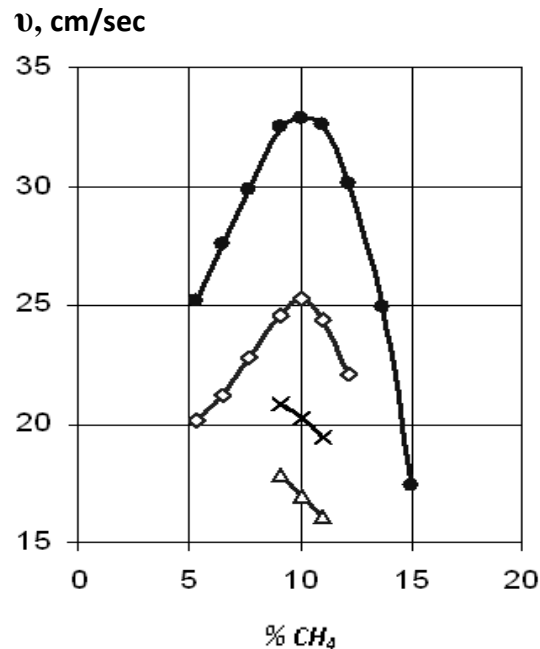**Fig.1** The dependence of the flame spreading speed and the normal speed of the mixture

Fig. 2 The normal velocity of the methane-air mixture flame from the pressure according *(Petrichenko R., Rusinov R., 1983), Novichlov M. (2004).*

1 – velocity of propagation of methane-air mixture at pressure Pz = 5,0…5,4 MPa;
2 – velocity of propagation of methane-air mixture at pressure Pz = 4,5…4,8 MPa;
3 – velocity of propagation of methane-air mixture at pressure Pz = 4,0…4,3 MPa;
4 – velocity of propagation of methane-air mixture at pressure Pz = 3,4…3,8 MPa.

CONCLUSIONS

1. On the basis of theoretical studies of the main parameters of in-cylinder processes influence on the rate of heat release and propagation of the flame front in the second phase of combustion and taking into account the applicability of hydrocarbon fuels of methane series, a physically justified model of the processes was formulated.

2. A mathematical model and an algorithm for calculating the operating cycle of the gas engine, allowing to take into account the peculiarities of the physical processes in the cylinder due to the combustion of the gas-air mixture was developed.

REFERENCES

1. Vibe I. I. New about the working cycle of the engine (combustion rate and engine duty cycle). – M. : Mashgiz, 1962. – 271 p.

2. Gainullin F.G. Natural gas as a motor fuel for transport. - M .: Nedra, 1986. - 327 p.

3. Birger I.A. Technical diagnostics. - M.: Mashinostroenie, 1978. - 240 p.

4. Khakimov R. T., Didmanidze O. N., Afanasiev A. S. Studies of heat dissipation of gas engines // Notes of the Mining Institute. – 2018. – Vol. 229. – P. 50-55.

5. Petrichenko P. M., Rusinov R. V. heat Exchange in the fuel torch // engine building. – 1983. No. I. – P. 9-12.

6. Alumbauch R.L., Keeton I.R., Нитт E.F. Experimental polyurethane roof systems // J. Cellular Plastics. – 1984. – № 4. – P. 257-273.

7. Khakimov R.T., Didmanidze O.T Improving the supply system gas engine to improve energy efficiency // Transportation Research Procedia. – 2017. – P. 183-191.

8. Kagan L., Valiev D., Liberman M., Gamezo V., Oran E., Sivashinsky G. Effects of hydraulic resistance and heat losses on deflagration-to-detonation transition // In Deflagrative and detonative combustion (eds G.D. Roy & S.M. Frolov). – 2010. – pp. 157 – 168.

9. Austin J.M., Pintgen F., Shepherd J.E. Reaction zones in highly unstable detonations // Proc.Combust.Inst. – 2005. – vol. 30. – pp. 1849-1857.

10. Belyaev A.I., Afanasyev, A.S., Efficiency of vehicle operation / International journal of economics and financial issues, № 2, т 6, 2016. P. 24 - 30.

11. Ciccarelli G. Transition in the propagation mechanism during flame acceleration in porous media / G. Ciccarelli, C. Johansen, M. Parravani // Proc. Combust. Inst. 33. – 2011. – pp. 2273 –2278.

12. Oran E.S., Gamezo V.N. Flame acceleration and detonation transition in narrow tubes // Paper presented at 20 th Int. Colloq / On the Dynamics of Explosions and Reactive Systems (ICDERS), McGill University, Montreal, 31 July–5 August – 2005.

13. Yerokhin M. N., Didmanidze O. N., Mityagin G. E. Problems and prospects of import substitution in road transport // In the collection: Information technologies and innovations in transport materials of the 2nd International scientific and practical conference. – Orel state University. I. S. Turgeneva, 2016. – P. 88-96.

Corresponding author:

Prof. Otari Didmanidze, Head of Department of Automobile transport, Russian State Agrarian University-Moscow agricultural academy named K.A. Timiryazev, Russia,Timiryazevskaya str.49,Moscow, Russia, 127550, cxm.msau@yandex.ru

COMMENTS ON THE DEVELOPMENT OF PROSUMER ENERGY IN POLAND

Iwona ŻABIŃSKA[1], Zbigniew MATUSZAK[2]

[1]*Faculty of Organization and Management, Silesian University of Technology, Zabrze, Poland*
[2]*Faculty of Mechanical Engineering, Maritime University of Szczecin, Szczecin, Poland*

Abstract
The aim of study was to analyse and assess the conditions for the development of prosumer energy in Poland. The assessment was based on the analysis of legal and financial aspects, as well as statistical data included in the reports on connected energy installations. The concept of prosumer, micro-installation and energy cluster was defined. The selected legal regulations concerning micro-installation and possibilities of financing prosumer activities were indicated.

Key words: prosumer energy; micro-installation; energy cluster.

INTRODUCTION

The energy and climate policy adopted by various European countries is different and it uses various support mechanisms for renewable energy sources. In connection with the above, each Member State has its national action plan regarding renewable energy in relation to the production of electricity and heating until 2020. For the effective realization of the adopted assumptions, the European Commission has issued a communication concerning the climate and energy framework for the years 2020-2030. The targets specified in this communication are to ensure the implementation of a long-term strategy for building a competitive low-emission economy, assuming the reduction of internal emissions by 80% until 2050 – compared to their level in 1990 (*Communication from the Commission to the European Parliament, 2011a; Communication from The Commission to The European Parliament, 2011b*). In Poland, one of the methods to reduce greenhouse gas emission is the development of prosumer energy. In the prosumer model, the end user installs electricity or heat generating devices in this facility and produces energy for his needs. Moreover, the user has the option of reselling any surplus to the network. It should be emphasized that the energy prosumer is usually characterized by high sensitivity to environmental problems and he consciously takes actions to protect the surrounding nature. Hence, he often has a broaden knowledge of products and services and willingly shares it with others (*Suchacka, 2015; Żabińska, 2017*).

MATERIALS AND METHODS

Data from secondary sources were used for the analysis in this article. The secondary data came from internal sources such as the following:
- data from statistical offices listed in the bibliography;
- data from government administration authorities (including information from the Internet);
- national and international regulations and legal acts;
- studies and publications listed in the bibliography.

The concept of prosumer in legal terms

According to Article 2 point 27a of the Renewable Energy Sources Act (Journal of Laws of 2018, item 1269), the prosumer is a final consumer purchasing electricity on the basis of a comprehensive contract, who generates electricity only from renewable energy sources in micro-installation for his own needs, which are not related to the conducted business activity…".
Currently, prosumers connected to the network operate in the system of discounts. The discount rate is 1:0.8 for installed electrical power not more than 10 kW or 1:0.7 for installed electrical power greater than 10 kW. Therefore, the system of discounts can be compared to an energy accumulator, from which you can recover from 70% to 80% of energy. Pursuant to the Renewable Energy Sources Act, a prosumer provides to the seller (for free) the rest of energy. From the amount of settled electricity, in the manner referred to in section 1, the prosumer does not pay to the seller fees for its settlements and fees for the distribution service, the amount of which depends on the amount of electricity received by

the prosumer. These fees are paid by the seller to the operator of the electricity distribution system, which is connected to the micro-installation.

The concept of microgeneration

Microgeneration is the production of electricity or thermal energy on a small scale with the use of low-emission technologies or technologies based on renewable energy sources. A common feature of microgenerators is their connection to a low voltage network with a rated current, which is not higher than 16A (*PN EN 50549-1:2019*). The Polish legal system includes the concept of micro-installation, which is not synonymous with the term microgeneration, because it concerns a renewable energy sources installation with a total installed electrical power not more than 50 kW, connected to the network with a rated voltage lower than 110 kV or with a heat-generating power in the combination not exceeding 150 kW, in which the total installed electrical power is not higher than 50 kW (*The Renewable Energy Sources Act*). As it was pointed out by one of the researchers, the term "micro-installation" is misleading, because it could also be associated with a low-power installation, in which a non-renewable production source was applied, or with a receiving micro-installation – and the legislator thought about the generating micro-installation.

Energy clusters

Researches conducted by Jabłońska on energy clusters as tools for supporting the development of modern power systems have shown that the majority of cluster initiatives in the field of renewable energy and environmental protection run a little innovative business. However, the author drew attention to their important role in three areas (*Jabłońska, 2015*):
- Education and information through training, expert advices, information campaigns, conferences, etc.;
- Acquisition of EU funds for the purchase of installations in the field of renewable sources;
- Creation of cooperation platforms between cluster participants and creation of cooperation between them.

Therefore, it can be concluded that cluster initiatives have a significant impact on the development of prosumer energy. Their role was also recognized by entities responsible for creating energy policy what ultimately led to the regulating the concept of energy clusters under the current Renewable Energy Sources Act. According to the definition contained in Art. 2 point 15a of the above-mentioned Act, an energy cluster is a civil law agreement that may gather natural persons, legal persons, units, as well as research institutes or local government units. The subject of activity of the energy cluster must be the generation and balancing of the demand, distribution or trade in energy from renewable energy sources or from other sources or fuels, within a framework of distribution network with a rate voltage lower than 110 kV. The area of the cluster's activity may not exceed borders of one district or 5 municipalities. The cluster's activity may not concern cooperation with neighboring countries. Coordinator of the cluster is a cooperative, association, foundation or any member of the energy cluster indicated in a civil law agreement (hereinafter referred to as "energy cluster coordinator") established for this purpose.

In order to cooperate with a given cluster, the operator of the electronic distribution system is obliged to conclude a contract for the provision of distribution services with the cluster coordinator on the basis of Article 38.

In conclusion, it can be stated that the energy cluster is a new approach in running economic projects in the area of energy in Poland. The main goal of energy clusters is to create optimal conditions for the development of distributed energy. Opening of the cluster for different stakeholders should activate the local community to take environmentally friendly actions based on the use of renewable energy sources. The result of the cluster's activity should also be the improvement of local energy security, development of technologies and innovativeness in the area of energy, as well as increase of competitiveness of local enterprises.

Financial support for prosumers

An important element of the growing interest in micro-installations for renewable energy sources is the state policy regarding financial support for this type of installations. Currently, it is possible to

support prosumers under the Renewable Energy Sources Act and within the framework of the ENERGY PLUS program. Until 2016, it was possible to take advantage of the co-financing programs, such as: PROW, Prosumer, LEMUR. Support under the Renewable Energy Sources Act applies only to prosumers producing electricity, while the Rural Development Program (PROW) and the programs of the National Fund for Environmental Protection and Water Management (NFEPWM) also include manufacturers of thermal energy. The Institute for Renewable Energy (IRE) has assessed the impact of the Priority Program of the NFEPWM "Prosumer" on the development of the RES micro-installation sector. In the opinion of the IRE, the "Prosumer" program did not support prosumer activity in a systemic manner, and the funds available in the program could not be "*treated as a basic or even complementary instrument ensuring the profitability of investments in RES micro-installations*" [12]. However, according to the author of this article, the program aroused public interest and disseminated the idea of prosumer energy. The proof of this may be an increase in the number of micro-installations in the last two years (2014-2016). From 1 March 2019, applications within the framework of a new priority program – "Energy Plus" can be submitted. The aim of this program is to reduce the negative impact of enterprises on the environment, including to improve air quality, by supporting investment projects. The program should encourage the installation of own energy source through simplified investments and a lower (8%) VAT tax for installations assembled on land or in farm buildings.

RESULTS AND DISCUSSION
The development of RES and microgeneration
According to the data from the European Statistical Office, the share of energy from renewable sources in final energy consumption among all EU Member States was 17% in 2016 and increased by 0.9 percentage points compared to 2014 and by 3.8 compared to 2011 (*Eurostat Statistic Explained*). Pursuant to the Directive 2009/28/WE, the further increase of this ratio up to 21% in 2020 and up to 24% in 2030 is expected (*Communication from the Commission to The European Parliament, 2014*). Due to the fact that each country set its own target for 2020, as early as in 2014, eleven countries reached the assumed value, and thirteen countries exceeded the value determined in the above-mentioned Directive. In Poland, this goal was set at the level of 15% and in 2016 it reached the value of 11.3% (decreasing by 0.4 percentage points compared to 2015) (*Eurostat Statistic Explained*). Analysis of GUS data shows that both in Poland and in Europe, solid biofuels are the most frequently obtained primary energy from renewable sources. Against the background of the European Union, Poland has worse results in acquiring primary energy from such sources as: municipal waste, geothermal energy, solar energy (Fig. 1 and Fig. 2).
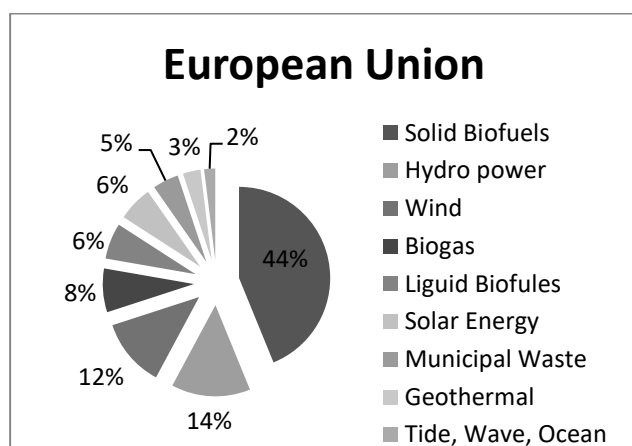

Fig. 1 Structure of primary energy production from renewable sources in EU in 2016 (*Energy 2018*)

The analysis of reports prepared by electricity distribution network operators (DNOs) published in the Public Information Bulletin on the website of the Energy Regulatory Office indicates that the prosumer market in Poland began to develop very dynamically in the last two years (*Energy Regulatory Office, 2019b*). In 2018, the number of customers, who installed their own power sources for the purpose of selling part of the energy to the network, amounted to 51 163, while the total amount of

electricity introduced by the prosumer to the network was 130 370.162 MWh (*Energy Regulatory Office, 2019c*). In 2015, the number of assembled micro-installations amounted to 4 691, while in 2016 – 12 860 – this constituted 75% of all micro-installations. In 2018, the total number of micro-installations amounted to 55 502. According to statistics provided by the Energy Regulatory Office, at the end of December 2018, the total installed power of renewable energy sources in Poland exceeded 8.59 MW. Detailed information on the installed power of micro-installations and its structure is presented in Table 1. The data in the table applies to particular types of installations for renewable energy sources, including installations that obtained:

- concession for the production of electricity;

- entry into the register of regulated activities carried out by the President of the Energy Regulatory Office (register of energy producers in a small installation);

- entry into the register of regulated activities of the President of the Agricultural Market Agency (register of agricultural biogas producers);

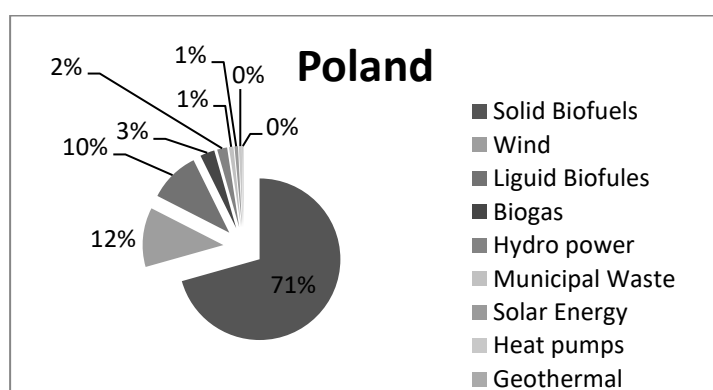- micro-installations applying for the issue of certificates of origin.

Fig. 2 Structure of primary energy production from renewable sources in Poland in 2016 *(Energy, 2018)*

Tab. 1. Installed power [MW], as at 31.12.2018 (*Energy Regulatory Office, 2019*)

Type of RES installation	Installed power [MW]					
	2005	2013	2015	2016	2017	2018
Installations using biogas	31.972	162.241	212,497	233.967	235.377	237.618
Installations using biomass	189.790	986.873	1 122,670	1 281.065	1 362.030	1 362. 870
Installations using solar radiation energy	-	1.901	71.031	99.098	103.896	146,995
Installations using wind energy	83.280	3 389.541	4 582.036	5 807.416	5 848.671	5 864.443
Installations using hydropower	852.495	970.128	981.799	993.995	988.377	981.504
Total	1 157.537	5 510.684	6 970.033	8 415.541	8 538.341	8 593.430

According to the data presented by the DSO in the reports of 2018, the majority of micro-installations were connected to such operators as: TAURON Dystrybucja S.A. (1406 pcs.), PGE Dystrybucja S.A. (1139 pcs.) and Energa Operator (1019 pcs.). The analysis of the data included in these reports also shows that solar installations constitute approx. 99.3%, hydroelectric plants – 0.5% and wind farms – about 0.1%. Biomass and biogas installations have a negligible market share. The significant advantage of photovoltaic power plants is primarily connected with the availability of equipment and specialist assembly companies on the market, as well as with the smallest environmental requirements. The opposite situation occurs in relation to hydroelectric and wind power plants, where the important criterion for the selection of this type of installation is the location conditions. Another factor affecting their lower popularity is the high price of the installation.

Comments on the development of renewable energy sources and microgeneration

The discrepancy in the structure of receiving primary energy from renewable energy results from the geographic conditions of individual countries, but energy policy and the support system for renewable

sources also play an important role (*Piria et al., 2014*). The Polish government is not conducive to the policy of obtaining energy for renewable energy sources, which was reflected in the lack of agreement in terms of climate neutrality of the European Union until 2050. Poland belongs to the group of countries with economy largely based on coal. This is the main problem in the implementation of the European Union's energy and climate strategy. According to the Polish government, coal, as an energy resource located on the territory of the Union, may provide energy security and competitiveness of the EU economy. Furthermore, the development of renewable energy sources (RES) under the current regulations, supply and prices may lead to the increasing exploitation and degradation of the natural environment in third countries.

The Institute for Renewable Energy (IRE) has assessed the impact of the Priority Program of the NFEPWM "Prosumer" on the development of the RES micro-installation sector. In the opinion of the IRE, the "Prosumer" program did not support prosumer activity in a systemic manner, and the funds available in the program could not be "*treated as a basic or even complementary instrument ensuring the profitability of investments in RES micro-installations*" (*Rosołek, Boelsta & Wiśniewski, 2014*). However, according to the author of this article, the program aroused public interest and disseminated the idea of prosumer energy. The proof of this may be the increase in the number of micro-installations in the last two years (2014-2016). In 2018, the government program "Clean Air" was launched. The aim of this program was to support (among others) installation of modern heating devices, including renewable energy sources. Currently, the European Commission's experts warn that in its current form, the program is doomed to failure and it cannot count on the support of EU funds. According to the experts, it is necessary to simplify the application procedures and build an effective system of services for beneficiaries.

CONCLUSIONS

As a result of the analysis of the conditions for the development of prosumer energy, the following conclusions can be drawn:

- Microgeneration is becoming more and more popular in both rich and developing countries. The most important factors for the development of distributed energy include:
- dependence on electricity – the use of an increasing number of electrical devices;
- poor transmission infrastructure;
- insufficient powers in the energy system;
- possibilities resulting from the development of new technologies;
- uncertainty of energy prices.
- Due to the Poland's economic policy, which is largely based on coal, actions for the development of prosumer energy undertaken by the Polish government are moderate in character. This is evidenced by a small number of implemented micro-installations compared to other European countries, critical opinions of institutions and experts dealing with renewable energy in Poland and the lack of systemic support for prosumers. Therefore, there is a need to develop mechanisms / principles of cooperation and exchange of experiences in the promotion and development of innovative pro-ecological society and distributed energy. Clusters are a change to develop effective mechanisms of cooperation between prosumers and entities of the so-called centralized energy.
- Poland, due to the disproportions connected with the distribution of large generating capacities, has favorable conditions for the development of distributed micro-energy. Unfortunately, state actions concerning the removal of barriers (energy and billing, financial and technical) for microgeneration are insufficient. The centralized model of the energy market still dominates in Poland.
- The European Commission has determined targets for renewable energy and greenhouse gas emissions for the successful implementation of EU climate and energy policies. Unfortunately, the Renewable Energy Sources Act provides support only for prosumers, who produce electricity.
- Co-financing for installations that generate thermal energy is provided only by two programs: "Clean Air", for which the EU funding can be suspended, and "Energy Plus".
- Despite insufficient incentives and support from the state in eliminating energy, billing, financial, technical and information barriers, the implementation of micro-installations in Poland is constantly growing, which probably results from the growing environmental awareness of the society, as well as technical and economic opportunities.

REFERENCES

1. Communication from the Commission to The European Parliament. (2014). The Council. The European Economic and Social Committee and The Committee of The Regions. *A policy framework for climate and energy in the period from 2020 to 2030, COM(2014) 015 final*. Bruksela.

2. Communication from the Commission to the European Parliament. (2011a). The Council. The European Economic and Social Committee and The Committee of The Regions. *A Roadmap for moving to a competitive low carbon economy in 2050, COM(2011) 112 final*. Brussels.

3. Communication from The Commission to The European Parliament. (2011b). The Council. The European Economic And Social Committee and The Committee Of The Regions *Energy Roadmap 2050, COM (2011) 885 final*. Brussels.

4. Energy 2018. Warsaw: GUS.

5. Energy Regulatory Office. (2019a). Data on specific types of renewable energy installations. Retrieved from https://www.ure.gov.pl/poze/potencjalkrajowy-oze/5753, Moc-zainstalowana-MW. html

6. Energy Regulatory Office. (2019b). Reports by the Distribution System Operator for the years 2013–2016. Retrieved from http://bip.ure.gov.pl/bip/ mikroinstalacje

7. Energy Regulatory Office. (2019c). REPORT - containing aggregate information on electricity generated from a renewable energy source in micro-installations (including prosumers) and introduced to the distribution network in 2018 (Article 6a of the RES Act) (in Polish). Poland.

8. Eurostat Statistic Explained. Retrieved from https://ec. europa.eu/eurostat/statistics-explained/index. php? title=File:Table_2-Share_of_energy_ from_renewable_sources_in_gross_final_con sumption_of_energy_2004-2016.png

9. Jabłońska, K. A. (2015). Energy Clusters as a Tool of Support of Development of Modern Electroenergy Systems. In *Prace Naukowe Uni-wersytetu Ekonomicznego we Wrocławiu, 402*, 123–132.

10. Piria, R. et al. (2014). Greening the Heartlands of Coal in Europe Insights from a Czech-German-Polish Dialogue on Energy Issues. Czech Republic: Heinrich-Böll-Stiftung.

11. PN EN 50549-1:2019. Requirements for generation installations intended for parallel connection to public distribution networks - Part 1: Connection to the distribution network nN - Generation installations up to and including type B. Polish Committee for Standardization.

12. Rosołek, K., Boelsta, J., & Wiśniewski, G. (2014). Expertise of the Institute of Renewable Energy for the Greenpeace Polska Foundation and WWF Poland. Analysis of the real benefits of the prosumer support mechanisms proposed by the government according to the government draft law on renewable energy sources (in Polish). Instytut Energii Odnawialnej.

13. Suchacka, M. (2015). Consumer or prosumer? Sociological determinants of lifestyle in the perspective of sustainable development (in Polish). Uniwersytet Śląski w Katowicach. In *Prosumenckie społeczeństwo a energetyka prosumencka – problemy wdrażania innowa-cyjnych ścieżek rozwoju OZE* (pp. 13-32).

14. The Renewable Energy Sources Act. (2018). In *Journal of Laws of 2018*, item 1269.

15. Żabińska I. (2017). Development of prosumer energy based on renewable energy sources in Poland (in Polish). Systemy Wspomagania w Inżynierii Produkcji. In *Problemy w zarządzaniu środowiskiem, 6*(1), 83 – 95.

Corresponding author:
Ing. Iwona Żabińska, Ph.D., Silesian University of Technology, Faculty of Organization and Management, Roosevelta 26, 41-800 Zabrze, Poland, e-mail: Iwona.Zabinska@polsl.pl

THE BEATER SHREDDING ASSEMBLY – CLASSIC AND NEW CONSTRUCTION

Marcin ZASTEMPOWSKI[1], Andrzej BOCHAT[1]

[1]Faculty of Mechanical Engineering, UTP University of Science and Technology, Poland.

Abstract

New design solutions of the working assembly of the beater shredder, the traditional construction of which is commonly used in the agri-food industry, are presented in the article. There has been described the test stand, methodology of the studies and the selected results obtained from the experiment. New construction of the beater shredder's rotor is characterised by a lower power consumption, higher effectiveness and better partitioning of the shredded material into fractions as compared to its traditional construction.

Key words: *beater shredder; shredding of grain material; new construction of a beater shredding.*

INTRODUCTION

Shredding of the cereals' grains is one of the main technological operations in the agri-food industry and on farms. From among many types of shredders, that is: radial plate grinding mills, roller mills, crushing mills and beater shredders, these are the beater shredders that are the most widely used ones because of the shredding efficiency *(Bochat, Wesolowski, & Zastempowski, 2015; Bochat & Zastempowski, 2018; Zastempowski & Bochat, 2016)*.

The design solutions of beater shredders existing at present, are characterised by high energy consumption of shredding, as a result of what, for their drive it is necessary to use engine of high powers. The fundamental elements of a typical beater shredder are a rotor with pivotably or rigidly mounted beaters, screens, shredding plates and a supporting structure with a driving system.

The disadvantage and inconvenience of known, traditional design solutions of beater shredders is their low efficiency as compared to energy consumption *(J. Flizikowski, Sadkiewicz, & Tomporowski, 2015; J. B. Flizikowski, Mrozinski, & Tomporowski, 2017; Macko et al., 2017; Tomporowski, Flizikowski, & Al-Zubiedy, 2018; Tomporowski, Flizikowski, & Kruszelnicka, 2017)*. It is most of all determined by a rotor's design, where the beaters are of rectangular plates' shape. As an effect of that, under the influence of the beaters' strokes, the material's particles start to move along the paths similar to a circle. They form a thin layer circulating along the internal perimeter of a shredding chamber, what causes that in spite of sometimes insufficient degree of shredding, the material is not enough shredding degree, material still for a long time circles before it goes through the holes in the screens.

Therefore, the purpose of the article is to determine the efficiency and power consumption in the shredding process for both construction of beater shredder - traditional and new construction as described in the article. For this purpose, the authors conducted tests using their own test stand.

MATERIALS AND METHODS

In fig. 1a there is presented a traditional rotor of a beater shredder from the isometric view with beaters in the form of rectangular plates. The essence of a new construction (fig. 1b) consists in the fact, that the working assembly of a shredder consists of a disk rotor assembled on a shaft to the which there are fixed the self-aligning beaters. These beaters are in the form of plates in the form of circular sectors of the angle of flare of at least 35^0, while the beater's fixing hole lies on the symmetry axis of the circular sector close to its arch base. Such a construction of the beater shredder's rotor causes, that the particles of the shredded material hit by the beaters do not move along the wheel track and do not form a rotating ring, but they move approximately radially as compared to the screens and immediately hit against them. It results in quicker going of the material's through the holes in the screens.
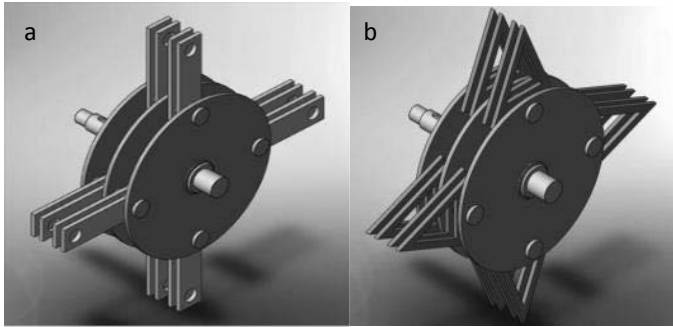
Fig. 1 Isometric view of a beater shredder (own study): a – traditional design solution of the rotor ($\propto = 0^0$) b – new design solution of a rotor with beaters in the shape of a circular sector ($\propto = 45^0$)

The authors have conducted experimental studies of the material's shredding process, aiming at determination the demand for power by the shredders' working assemblies.

For the purposes of the studies' performance, the test stand was designed and constructed, which is presented in fig. 2.
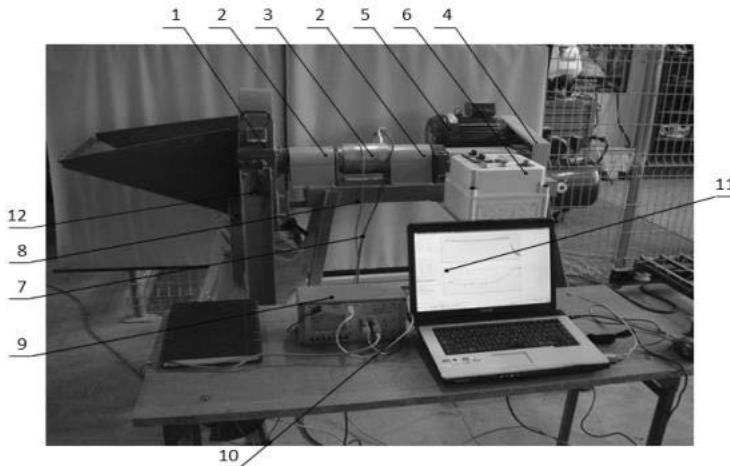
Fig. 2 View of the test stand (own study): 1 – modified beater shredder type WIR RB-1.3, 2 – flexible claw coupling Poly-Norm, 3 – torque measuring device with revolution counter type MIR 20, 4 – belt transmission, 5 – electric engine 7 kW, 380 V, 6 – control box with frequency converter Lenze SMD, 7 – transmission cable of a turning moment, 8 – transmission cable of rotational speed, 9 – two-channel measuring device MW2006-4, 10 – transmission cable type USB, 11 – computer system with a programme for data registering PP203 and an author's computing programme RB01, 12 – supporting structure.

The test bed consists of a modified beater shredder type WIR RB-1.3, equipped for studies with a traditional and a new working assembly – a rotor, control and measuring apparatuses in the form of an electric engine's control system ensuring smooth adjustment of a rotor's rotations and a torque measuring device for determining the power consumption on the rotor's shaft.

Within the frames of the experiment, there were shredded the grains of triticale (winter triticale Krakowiak, of humidity 11,69%, of bulk density 795,15 kg·m^{-3}). That material has been chosen for the studies due to commonness of cultivation and its designation for fodder purposes. The studies were conducted for the diameter of holes in the screens of d =5 mm, size of gap between the endings of the beaters and the surface of screens of s = 10 mm and the peripheral speed of the beater's endings respectively: 38; 45; 52; 59; 66 m·s^{-1}.

RESULTS AND DISCUSSION

The selected results of the tests are presented in fig. 3 and 4.

In fig. 3 there is presented the diagram of power consumption at the time of shredding for both the constructions of the beater's working assemblies.
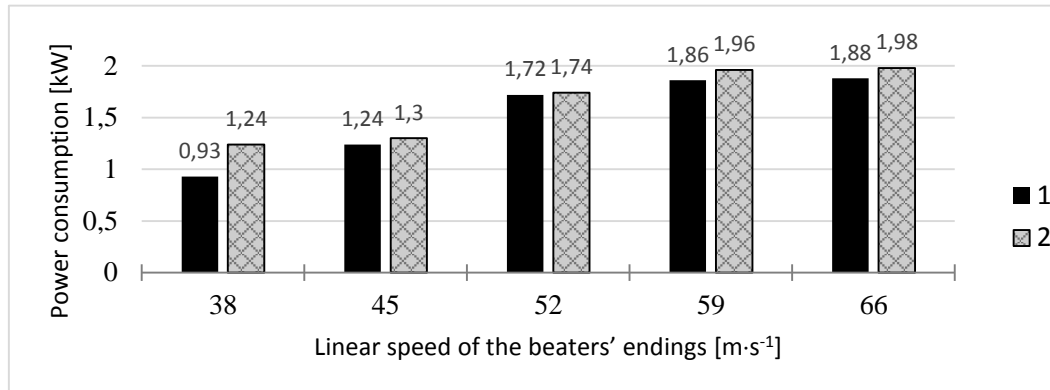

Fig. 3. Comparative diagram of the beater shredder's power consumption (own study): 1 – new design of a rotor, 2 – traditional rotor's design

It results from the conducted experimental studies, that an essential impact on power's consumption on the shredder's shaft and its efficiency at the time of the triticale grain's shredding there have: the design form of a rotor – the angle of the beaters and the peripheral speed of the beaters' endings while maintaining the constant diameter of the holes in the screens and the gaps between the endings of the beaters and the screens' surface.

In fig. 4 there is presented the diagram of efficiencies obtained in the shredding process for a shredder equipped with a traditional and new rotor.
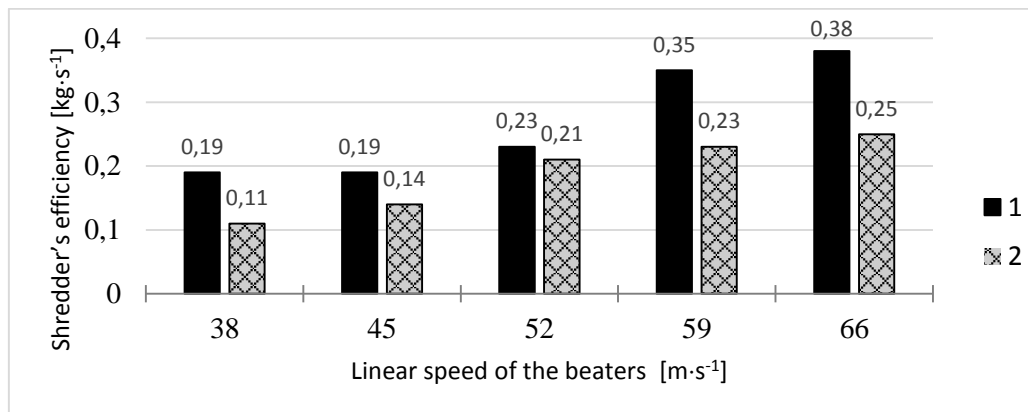

Fig. 4. Comparative diagram of the beater shredder's efficiency (own study): 1 – new construction of the rotor, 2 – traditional rotor's construction

Application in a beater shredder of a new construction of a working assembly (fig. 1b) equipped with beaters of the shape of a circular sector, resulted in a considerable increase of the shredder's efficiency from 11 up to 32%, and minimum decrease of power consumption for about 5% as compared to the traditional rotor's constructional solution. As a final effect, the shredder with a new design of the shredder, has a lower power consumption for shredding of the triticale's grain as compared to the traditional design. Additionally, application of a new construction of the beater shredder's design, equipped with beaters of the shape of a circular sector, results in the decrease of dust fraction in shredded cereal as compared to the traditional design solution.

Application of the beaters of the angle $\propto = 45^0$ has an impact on:
- decrease of the content of dust fraction from 7,26 to 7,75% ,
- decrease of the content of fine fraction from 8,58 to 9,23%,
- increase of the content of heavy fraction from 16,33 to 16,49%.

The conducted assessment of shredding efficiency has proved, that in case of shredding triticale, the most effective design solution of the beater assembly is application of beaters in the shape of circular sector $\propto = 45^0$, a beater's gap of the value of $s = 10\ mm$ and screens of the holes' diameter $d = 5\ mm$. The use of a gap of the value of $s = 15\ mm$ and screens of the diameter $d = 3\ mm$ proved to be less efficient.

The authors of the study did not have an opportunity of direct comparison of the results of their studies with the ones presented in the literature by other researchers. It is caused by the fact, that the results of the studies presented in this article, concern mainly a new construction of the shredder's rotor, which is covered by legal protection. However, for a traditional construction of a shredder's rotor, there is no direct comparison encountered in the world's literature to the data for direct comparison because of: the differences in the shredders designs' solutions *(J. Flizikowski, Sadkiewicz, & Tomporowski, 2015; Tomporowski, Flizikowski, & Kruszelnicka, 2017)*, different materials exposed to the shredding process, *(Macko et al., 2017; Tomporowski, Flizikowski, & Al-Zubiedy, 2018)* and different geometric and dynamic features of the shredders.

CONCLUSIONS

New constructional solutions of the beater shredder with new design of the rotor and its tests presented in the study show unequivocally, that by way of evolutionary changes of the existing constructions, one may contribute to lowering the costs of production of food, fodder or power materials of biomass's type. The new construction of the working assembly developed at the Institute of Mechatronics and Machinery is the subject matter of the patent and is more and more commonly used in new machine's constructions.

REFERENCES

1. Bochat, A., Wesolowski, L., & Zastempowski, M. (2015). A Comparative Study of New and Traditional Designs of a Hammer Mill. *Transactions of the Asabe, 58*(3), 585-596.
2. Bochat, A., & Zastempowski, M. (2018). *Modelling of the grain materials 'shredding process for the purposes of the beater shredders' designing.* Paper presented at the MATEC Web of Conferences.
3. Flizikowski, J., Sadkiewicz, J., & Tomporowski, A. (2015). Functional characteristics of a six-roller mill for grainy or particle materials used in chemical and food industries. *Przemysl Chemiczny, 94*(1), 69-75.
4. Flizikowski, J. B., Mrozinski, A., & Tomporowski, A. (2017). Active Monitoring as Cognitive Control of Grinders Design. *Scientific Session of Applied Mechanics Ix, 1822.*
5. Macko, M., Flizikowski, J., Szczepanski, Z., Tyszczuk, K., Smigielski, G., Mrozinski, A., & Tomporowski, A. (2017). CAD/CAE Applications in Mill's Design and Investigation. In *Proceedings of the 13th International Scientific Conference: Computer Aided Engineering* (pp. 343-351). doi:10.1007/978-3-319-50938-9_35
6. Tomporowski, A., Flizikowski, J., & Al-Zubiedy, A. (2018). An active monitoring of biomaterials grinding. *Przemysl Chemiczny, 97*(2), 250-257.
7. Tomporowski, A., Flizikowski, J., & Kruszelnicka, W. (2017). A new concept of roller-plate mills. *Przemysl Chemiczny, 96*(8), 1750-1755.
8. Zastempowski, M. & Bochat, A. (2016). Innovative Constructions of Cutting and Grinding Assemblies of Agricultural Machinery. In *Proceeding of 6th International Conference on Trends in Agricultural Engineering 2016* (pp. 726-735).

Corresponding author:
Marcin Zastempowski, assocc. prof: Faculty of Mechanical Engineering, UTP University of Science and Technology, Poland., Al. Prof. Kaliskiego 7, 85-796 Bydgoszcz, e-mail: zastemp@utp.edu.pl

PROPERTIES OF FRESH AND FROZEN FISH SKIN AT CYCLIC LOAD

Josef ZEMAN[1], Jan SEDLÁČEK[1]

[1]*Department of Physics, Faculty of Engineering, Czech University of Life Sciences Prague, Kamýcká 129, Praha 6, 165 21 Prague*

Abstract
Our paper deals with the methodology for determining of changes in rheological properties during various technological adjustments of biological structures. An example of the methodology is performed on the deformation curves during the cyclic tensile load in the elastic region. With the number of cycles, the absorption capacity of mechanical energy decreases exponentially during increasing and decreasing of the load. We observed the final value of the percentage of mechanical energy that the skin is able to absorb and the number of cycles that lead to this value. The measurements were made on a sample of freshly decapitated fish and the fish after quick freezing and thawing. We found the effect of this technological process on both the absorption capacity of mechanical energy and the number of stabilization cycles. We also found a strong positive correlation between the number of relaxation stabilization cycles and the thickness of fish skin.

Key words: absorption energy; relaxation time; rheological properties.

INTRODUCTION

The deformation of biological samples often results in the absorption of deformation mechanical energy. The value of this energy is determined as the area of the hysteresis loop, after measuring the curve of loading and unloading. It turns out that when repeating a load cycle, this area (and thus the absorbed energy) decreases, up to the finite non-zero value. This relaxation process can be described as a decreasing exponential function. When we fit the exponentials to the gradually decreasing surfaces of the hysteresis loops, we determine the number of relaxation cycles *ñ*. (Then we relax only 1/e changing parts of the hysteresis loop.) In practice, this relaxation process is often underestimated. This transition state is omitted in many works (see e.g. *Hadraba, Janacek, Filova, Lopot, Paesen, Fanta, Jarman, Necas, Ameloot & Jelen, 2017*) and the properties of the already relaxed material are evaluated. Experimenters tends to determine the number of load cycles, which are used for evaluation, completely arbitrarily. There are two primary reasons for absorbing mechanical energy when deforming biological materials. The first of these mechanisms is wringing (see e.g. *Fransson & Stading, 2003*). This mechanism consists in the fact that the formation of mechanical stress releases the water molecules that are present in the structure. These free molecules pass through the tissue that forms the structure of the biological material. In this process, hydrogen bonding arise and disappear continually. After each release of the bond, a part of the mechanical energy changes to a disordered movement of water molecules. Thus, as the entropy increases, the temperature of the material is increased. The second mechanism of mechanical energy absorption is the release of tertiary bonds of proteins and polymers that are present in the structure. Superfast freezing (*Dinu, Ozmen, Dragan & Okay, 2007*) is a process that is gentlest of all biomaterial storage processes, but it disrupts both types of bonds. It can therefore be expected, that its consequences will be identifiable by this method. The aim of this study is to demonstrate the usefulness of the proposed methodology on the example of determining rheological changes occurring in fish skin under rapid technological freezing.

MATERIALS AND METHODS

A sample of skin 3 cm length (beginning at 2 cm behind the gill arch), 1 cm width and *d* thickness, was attached in the jaws of the DEFORM02 deformation device from the firm of Pemar. The measuring cycles were defined as follows for the material used: The maximum force of 2 N (generated by the sample) was achieved at a constant rate of 0.1 mm / min. Immediately thereafter, the force in the sample was reduced to 0.1 N at the same speed. Again we increased the force to 2 N and decreased the force to 0.1 N at the same speed. We used adult individuals to measure. There were four species: Erpetoichtys calabricus (3 tested fish) - further species A, Gnathonemus petersii (3 tested fish) -

further species B, Oncorhynchus mykiss (8 tested fish) - further species C and Squalius cephalus (3 tested fish) - further species D. The fish sample of skin was always taken from its right flank immediately after being killed. The preparation of the frozen samples was as follows. The fish was shock-frozen and left for 14 days at -40 °C. The fish was taken from the freezer and left at 25 °C for 8 hours. Equally large sample of skin was taken from left side of fish as in the case of fresh samples. Both types of samples were mechanically strained in an isotonic bath of Ringer's solution. The stress was carried out with the above-described 8 cycles at 35-38 °C. The resulting hysteresis loops of the individual cycles were analyzed as follows. For the measured absorbed energy E_i in the i-th cycle:

$$E_i = E_i^{UP} - E_i^{DOWN} = \int_{l\,(F=0.1\,N)}^{l\,(F=2\,N)} F(l)\mathrm{d}l - \int_{l\,(F=2\,N)}^{l\,(F=0.1\,N)} F(l)\mathrm{d}l, \quad i \in \{1,\ldots,8\}, \tag{1}$$

E_i^{UP} – the energy supplied to the sample as it is stretched,
E_i^{DOWN} – the energy taken from the sample as it is shortened,
$l(F)$ – the length of the sample corresponding to the force F,
$F(l)$ – the force induced by the sample with length l in the given direction of deformation.

In this way, we obtain a series of eight absorption energies. The sequence of this series, as mentioned above, can be approximated by the following function:

$$E(i) = E_0 - (E_0 - E_\infty)e^{-i/\tilde{n}}, \tag{2}$$

$E(i)$ – the approximated absorption energy in i-cycle,
E_0 – absorption energy of the initial deformation,
E_∞ – the residual absorption energy required to deform the sample, in the order of the endless cycle of deformation,
$\tilde{n}$ – the number of relaxation stabilization cycles (see Introduction).

The fitting function $E(i)$ to values of E_i was realized by Solver of Excel 2010. Subsequent statistical processing was performed in the R application (ver. 4.3.0).

RESULTS AND DISCUSSION
First, we present a typical example of a measured hysteresis loop - see Fig. 1, from which the value of energy absorbed in one particular cycle was calculated according to (1).
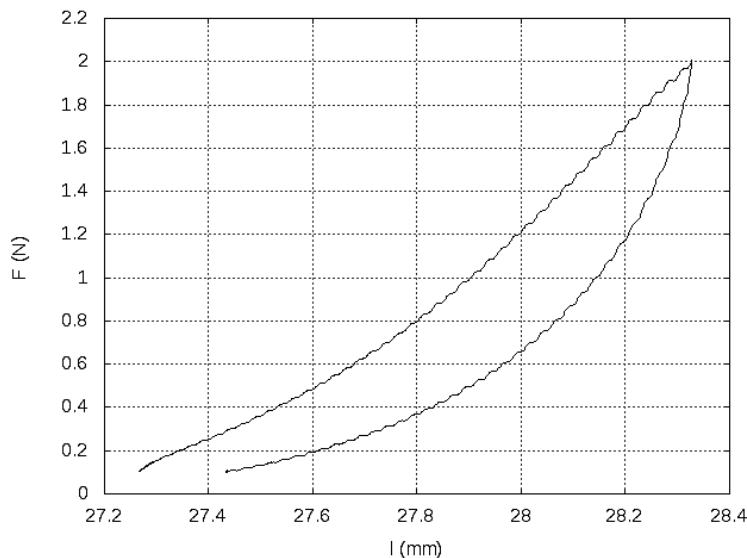

Fig. 1 Third loading and unloading cycle of the fifth sample of species C

If we plot the energies absorbed in eight consecutive cycles, we get the result shown in Fig. 2. The found exponential dependence, that approximates the measured data with equation (2), is shown in this figure too.
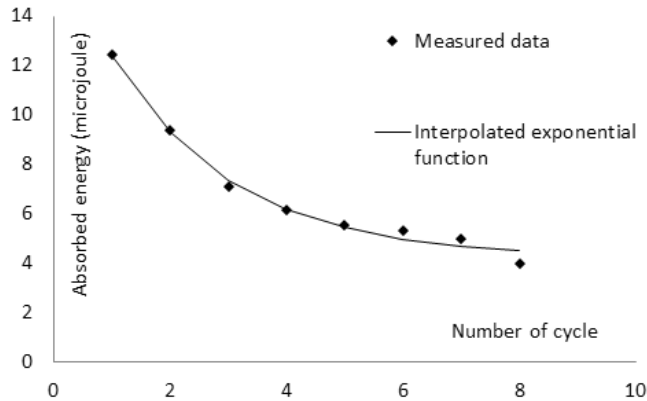

Fig. 2 The energies absorbed in each cycle of the fifth sample of species C

Based on the Kolmogorov-Smirnov test (= 0.65) we were forced to reject the hypothesis of the normality of all the examined quantities. Therefore, no average values are in Tab. 1, but medians of measured values.

Tab. 1 Medians of parameters of individual measured fish species (fresh samples)

Species of fish	$\hat{d}$	$\widehat{E_\infty}$	$\widehat{E_0}$	$\hat{ñ}$
	mm	%	%	
A	0.56	37.7	87.3	2.6
B	0.05	18.9	32.0	3.3
C	0.33	7.8	29.2	16.6
D	0.07	14.5	18.9	19.0
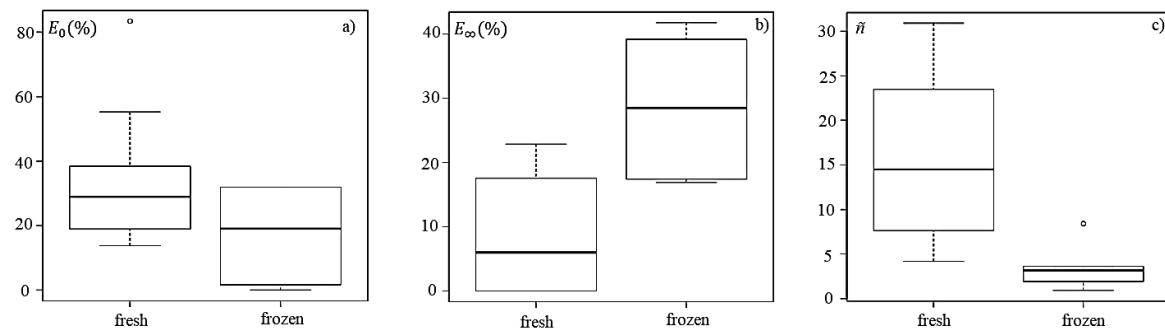
Fig. 3 Comparison of fresh and frozen samples values

A comparison of the fresh and frozen samples is shown in Fig. 3. This statistical comparison was conducted by Wilcoxon unpaired test. We found that the values of the examined parameters $ñ$, E_∞ a E_0 differ at the 10% level of significance for all species, even for our small number of samples (E_0 p-value = 0.1078, E_∞ p-value = 0.004891, $ñ$ p-value = 0.01198). The Kruskal-Wallis test found significant differences also among all four fish species. Subsequently, a moderately strong correlation was found between sample thickness d and the number of relaxation stabilization cycles $ñ$. Pearson correlation coefficient $r = -0.3433$ only and Spearman's rank correlation coefficient $\rho = -0.3904$. This indicates a moderately strong, slightly non-linear negative correlation. Further results (dependence of the number of relaxation stabilization cycles $ñ$ on the thickness d of the fish skin sample) can be seen in Fig. 4.
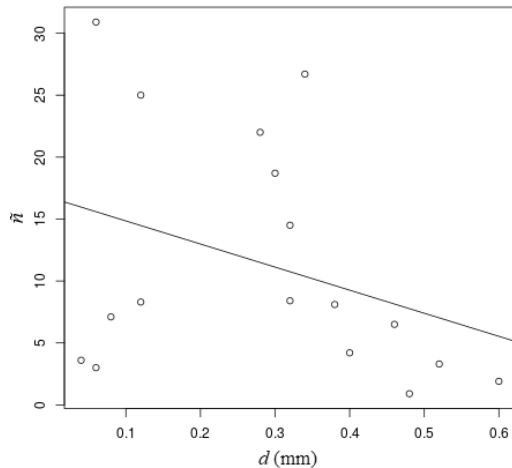
Fig. 4 Dependence of the number of relaxation stabilization cycles $\tilde{n}$ on the thickness d of the fish skin sample

DISCUSSION

On the example of the use of our methodology, we have shown the effect of freezing on the examined mechanical parameters for all examined species A, B, C, D Thus, there appears to be structural changes during the freezing of the fish skin, and the flow of tissue fluid through the microporous medium is increasing. Furthermore, it appears that significant differences among the values of the quantity $\tilde{n}$ exist for individual examined species. Mutual ratio between the energies E_∞ and E_0 is also significantly different for each species. This illustrates the structural differences of skin among individual fish species. The proven negative correlation between $\tilde{n}$ and d indicates that thick skin (probably due to higher collagen content) relaxes at a lower number of load cycles.

CONCLUSIONS

We managed to describe a method of how to effectively use the first load cycles to describe the rheological properties of a material. With this method, not only the ratio between elastic and plastic deformation can be obtained, but also the number of relaxation cycles can be determined. We applied the method to the case of fish skins distribution. It turned out that our method is applicable both to differentiation of individual fish species and to indicating of technological treatments (freezing fish meat).

REFERENCES

1. Dinu, M., V., Ozmen, M., M., Dragan, E., S. & Okay, O. (2007). Freezing as a path to build macroporous structures: Superfast responsive polyacrylamide hydrogels. *Polymer, 48*, 195-204.
2. Fransson, K. & Stading, M. (2003). Methodology and Measurements of Extensional Rheology by Contraction and Squeeze Flow. *Annual transactions of the Nordic rheology society, 11*, 149-152.
3. Hadraba, D., Janacek, J., Filova, E. Lopot, F., Paesen, R., Fanta, O., Jarman, A., Necas, A., Ameloot, M. & Jelen, K. (2017). Calcaneal Tendon Collagen Fiber Morphometry and Aging. *Microscopy and microanalysis, 23*(5), 1040-1047.
4. Hubená, P. & Tůmová, V. (2017). Comparing the physical properties of fresh and frozen fish skin at cyclic load (in Czech). Czech University of Life Sciences Prague.
5. Nachtikal, F. (1912). About the influence of relaxation on the oscillations of the elastic bodies(in Czech). *Magazine for the cultivation of mathematics and physics, 41*(3-4), 423-431.

Corresponding author: Mgr. Josef Zeman, Ph.D., Department of Physics, Faculty of Engineering, Czech University of Life Sciences Prague, Kamýcká 129, Praha 6, Prague, 16521, Czech Republic, phone: +420 22438 3317, e-mail: zeman@dzeta.cz

AN ANALYSIS OF NOISE POLLUTANTS IN CITY SUBWAY TRANSPORTATION

Retta ZEWDIE[1], David MARČEV[1], Martin HALBERŠTÁT[2]

[1]*Department of Vehicles and Ground Transport, Faculty of Engineering, Czech University of Life Sciences in Prague, Czech Republic*
[2]*ŠKODA AUTO, Mladá Boleslav, Czech Republic*

Abstract
Noise in general, is any unwanted sound in any mode of transportation, and exposure to it can be a serious threat to health. Subways are among those considered as sources of urban noise, which adversely affect health. This paper, presents the results of survey conducted on noise levels of Prague City subways transport system. Over 240 noise measurements were made. Noise levels were measured using a sound level meter on both subway lines, Line A (green) and line B (yellow) lines for comparison. On both lines the return measurements were conducted namely in the first, third and fifth compartments. The maximum average noise level measured on the line A (green) subway in all three compartments was 94.1 dBA (decibel-A weighting) and 96 dBA in Line B (yellow) respectively. These results indicate that the maximum noise levels in subway cars have exceeded recommended exposure guidelines from the World Health Organization.

Key words: excessive sound, hearing damage, sound level, rail noise.

INTRODUCTION

Noise irritates or worsens the mood of individuals in passenger compartments and even disturbs or damages hearing capacities if it continues for long periods. In rail transport, the dominant source is the rolling noise caused by speed increase, depending on the acoustic pressure. Traction, chassis, and aerodynamic noises are among the prominent excess noise producing components which should be addressed carefully. Rolling noise is mainly caused by wheel surface contact with the rail. It is also produced at the chassis where friction occurs. Rolling noise is determined by the quality of the track, and the quality of the vehicle, especially the chassis system. A high incidence of noise and long exposure to it often causes permanent effects on to human health. Measurements should be taken both in the daytime and at night.

Noise level measurements serves to find ways to reduce noise and consequently provide guidance to effectively fight for environmental protection. Higher noise levels increase the risk of damage to the body, especially to an individual's hearing. If a person is present long-term in an environment where the noise is 65 dB, the human vegetative reactions change. These are mainly changes in behaviour, irritation and other negative symptoms that are difficult to identify initially. Another signs may be more frequent headaches. In the case of permanent residence in the 85 dB environment, permanent hearing disturbances occur, which can lead to permanent hearing loss. At the same time, the effects on the vegetative system and the whole nervous system become more apparent. Hygiene limits of noise at work stations is provided by Czech Government Decree No. 272/2011 Coll. (*Liberko, 2004*; *Nový, 2001*; *Zewdie & Kic 2016).* These noise limits apply only to the engine-driver cabin and excludes the noise caused in passengers compartments. Neither standard nor law regulate noise limits in public areas of stations and platforms in enclosed spaces such as metro tunnels. From the point of view of passengers in individual cars, the Czech standard CSN 281310 is used *(Nový & Kučera 2009).* However, this standard no longer distinguishes between surface and subsurface transport. The result limits are approved by the manufacturer upon confirmation of the Rail Authority.

The concept of the noise level impacts primarily on passengers and the highly exposed engine-drivers. Researchers *Persinger, 2014; Jandak, 2007* have come to the conclusion that noise is the quality of sound interaction with human biology. The extensive research work led by *Nelson, J. T. et. al., 1997*, states that noise is also included in the provisions of Section 30 of the Public Health Protection Act. The technical sources of noise are the subject of state health surveillance carried out by public health authorities. The research conclusion states that noises and vibration from rapid transit systems are caused by wheel/rail interaction and is influenced by factors such as wheel and rail roughness track supports and variations of surface contact stiffness.

These sources of noise are generated by the interaction of wheel and rail, and radiated by the wheel and rail to the vehicle interior and wayside *(Thopson, 2009)*. The human ear is capable of responding to a very wide range of sound pressures; at the threshold of pain the sound pressure is roughly 1 million times as large as the sound pressure at the threshold of hearing. Physical definitions cannot be determined because noise is a subjective impression and depends on the individual's relationship to the given sound. Recommendations for station platform noise levels should be especially considered because, trains entering and leaving subway stations should not produce noise levels in excess of 85 dB. The noise level limits for above grade stations are 80 and 85 dB for concrete sleeper track beds, respectively. Noise levels 5 dB below these limits are desirable. Compartment noise levels are normally measured at 1.5m above the platform, roughly midway between the platform edge and rear wall, or 1.5m from the platform edge, whichever is closer to the track *(Persinger, 2014)*.

The noise levels apply to the total noise level, including noise due to rail sources as well as traction engine equipment, vehicle ventilation and air conditioning equipment, and brake systems. (The APTA guidelines also provide limits for continuous noise levels caused by station and subway ventilation fans, and recommend station reverberation times to control speech intelligibility of public address systems.) Tangent track rolling and curving noises are due to wheel and rail roughness, which may include rail corrugation and random surface defects. Smooth rolling surfaces produce less vibration The average noise level measured on the line A (green) subway in all three compartments was ~ 76 dB (decibel-A weighting) and ~ 78 dB in Line B (yellow) respectively. These results indicate that the average noise levels in subway cars have exceeded recommended exposure guidelines from the Czech health standard recommendation. The maximum average noise level measured on the line A (green) subway in all three compartments was 94.1 dB (decibel-A weighting) and 96 dB in Line B (yellow) respectively. The results show a breaking of the safe exposure limit of 74 dB.

The aim of this study is to explore specific areas where excessive noise levels appear to be the highest and passengers likely to be adversely affected by the Prague metro's rail transport. The investigation on the cause of noise level presence was carried out on both sides of metro drive.These findings reveal the confirmation that noise potentially poses a health threat to passengers.

MATERIAL AND METHOD

To carry out this research the authors used a very precise measuring instruments which is shown in Fig. 1, and two Prague metro lines, line A (green) and line B (yellow). The measurement was held on both lines in first, third and fifth compartments (wagons) from each line including the reverse ride. The location of the measuring device with the stand is shown in Fig. 2 in the wagon. For the noise level measurement a frequency analyser of the brand made by CESVA instrument, a brand manufactured in Barcelona was applied. The SC 310 has a measurement range that allows it to measure noise without adjusting the range. Device settings have been selected with respect to the required data. The sound pressure level setting with slow time weighing was selected during the measurement.
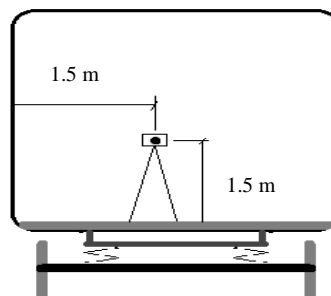

Fig. 1 Measuring device

Fig. 2 Placement of measuring device

Fig. 1 shows noise level measurement device. It is a frequency analyser of the brand made by CESVA instruments, producing acoustic devices and Fig. 2 indicates the placement of the measuring device

CESVA in the wagon for noise levels data collection, which is normally measured at 1.5m above the compartment floor, roughly midway between the side edge and rear /front side, 1.5m from the surface edge.

Line A (green) has a length of 17.129 km. The entire route takes 30 minutes to ride with the shortest train arrival/departure interval of two minutes at peak hours. Up to 200,000 passengers use the line daily. *Motol Hospital* and *Depo Hostivař* stations are surface stations. The deepest place is located in the *Náměstí Míru* station at a depth of 52 meters below the surface. The maximum set speed is 80 km/h one train can accommodate up to 1580 passengers

Line B (yellow) is 25.7 km long and connects the, densely populated western Prague district *Stodůlky,* with the equally populated eastern area of *Černý most*. The route has 24 stations. The peak time train arrival/departure interval is 2.5 minutes. Line B serves (yellow) serves up to 350,000 passengers a day. The total ride time is 41 minutes. The deepest station is *Můstek*, which lies at a depth of 40.3 meters below the surface. The route also has two unusual features and these are transparent overland bridges. These are between the stations *Hůrka - Lužiny* and *Rajská zahrada - Černý most*. The metro line has three surface stations.

Tab. 1 Table of standard CSN 281310 (interior)

Noise interior cabin	
Carriage speed 60 km/h	78 dBA
Noise in the drivers cabin at 60 km/h	74 dBA

(Source: CSN 28 1310 - Subway cars for passenger transport - Basic technical requirements and tests)

Tab. 1 shows the recommended noise level Czech Republic hygiene standard for subway cars passenger transport. Measurements were adapted to individual needs in kits, so as to be able to absorb the noise as well as register most passengers. Measurements were taken over the weekend due to the lower frequency of passengers out of peak hours.

RESULTS AND DISCUSSION

An important factor is the intensity of the noise barriers surrounding distance from the noise source. On most routes subway lines are routed down their own separate tunnel and metro trains visually and acoustically meet only at stations. On some sections however there are metro tunnels for both metro trains. These sections have a larger space where acoustic waves can travel through the environment. Noise from the perspective of long-term load in individual sections of lines, but also selected local and short-term noise impulses. The reasons are different factors, notably the speed and the technical condition of vehicles *(Thopson, 2009)*. However, noise can be accurately determined and analyzed over longer periods of time. When comparing the noise level of individual metro lines, the largest noise load on line B (yellow) was measured with an average value of 78.17 dB (*Zličín - Černý Most*) respectively 78.63 dB in the opposite direction ride. The noisiest sections of the line B have repeatedly exceeded 90 dB and this is more than the Czech standard ČSN 28 1310 prescribes. The measured data confirms at stations between *Jinonice – Radlicka* and *Hloubetín – Rajská Zahrada*. The line A was measured and the average noise was 75.65 dB and 75.94 dB respectively. The highest values then appeared in the *Dejvická - Bořislavka* and *Náměstí Míru - Jiřího z Poděbrad* sections, where they repeatedly reached over 90 dB.

Tab. 2 Measured data of Line A (Green)

Line "A"	Motol to Hostivař			Hostivař to Motol		
	1. wagon	3. wagon	5. wagon	1. wagon	3. wagon	5. wagon
Max [dBA]	97.3	92.8	93.2	91.9	97.3	91.8
Min [dBA]	56.9	54.0	58.4	53.7	56.9	59.8
Average [dBA]	75.83	75.43	75.63	75.33	75.89	76.64
SD [dBA]	8.1	9.1	7.5	9.1	8.1	6.9

Tab. 2 shows the results of the first measurement that took place on March 26, 2016. On this day, data on line A (green) were recorded in both directions. All six records were measured continuously.

Tab. 3 Measured data of Line B (Yellow)

Line "B"	Zličín to Černý Most			Černý Most to Zličín		
	1. wagon	3. wagon	5. wagon	1. wagon	3. wagon	5. wagon
Max [dBA]	95.3	93.9	97.9	96.9	96.3	95.9
Min [dBA]	58.4	61.6	59.4	58.5	60.9	62.5
Average [dBA]	76.97	78.46	79.02	78.04	78.41	79.52
SD [dBA]	8.6	8.0	8.7	8.6	8.6	8.0

Tab. 3 indicates the Line B (yellow) line measurement that took place the following day, ie on March 27, 2016. The last line B was measured 2.3.2016. All six measurements were continuous. On the last day of the measurement, the values from the selected stations were recorded for comparison. The record was recorded at noise level meter CESVA SC310. An illustration of the location of the sound level meter is shown in Fig. 2 for measurements in the wagon interior. The front seat of car was chosen because of the axle and chassis location.
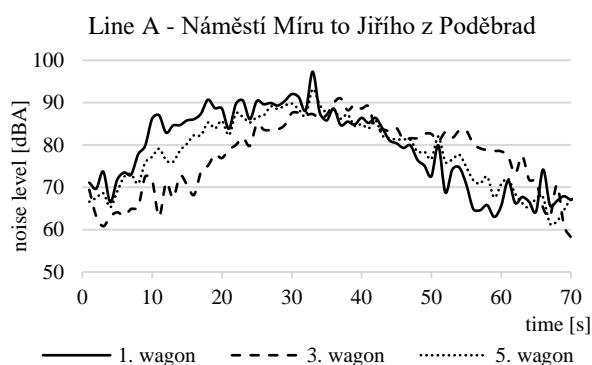
Fig. 3 Graph of the noise level between two stations
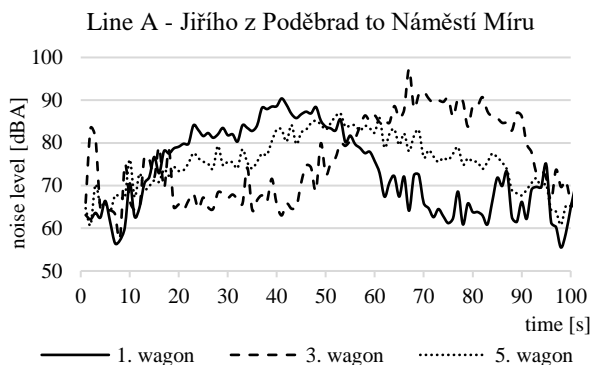
Fig. 4 Graph showing the reverse ride

Fig. 3. Shows the noise level characteristics of line A (Green) from *Náměstí Míru* stop to *Jiřího z Poděbrad*. The maximum values are observed on the 32-33 seconds ride, in the 1st and 5th wagons respectively, 97.3 dB and 93.2 dB. These values could be the result of crossing a rail switch *(Thopson, 2009)*. It is clear from the graph that a similar course of noise level during the ride was recorded during individual rides. This similar pattern is the result of adherence to the timetable, where in this case the metro trains were perfectly on time.

Fig. 4 Shows the reverse ride of line A (green) from *Jiřího z Poděbrad* to *Náměstí Míru,* where very different noise levels were observed. Interestingly, a different style of driving was observed given to compliance with the timetable. From the data the noise level in the third wagon was recorded and there was a maximum 97.3 dB. The noise level between stations on this ride was higher than the noise noise level on the other runs.
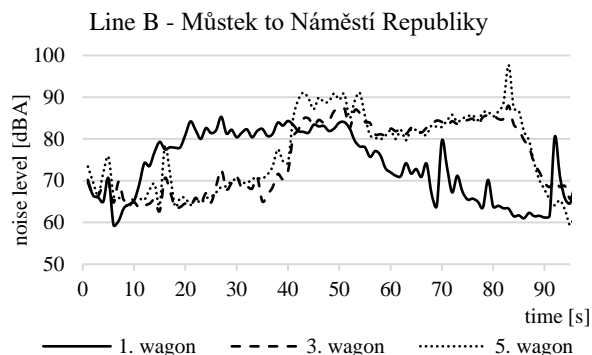

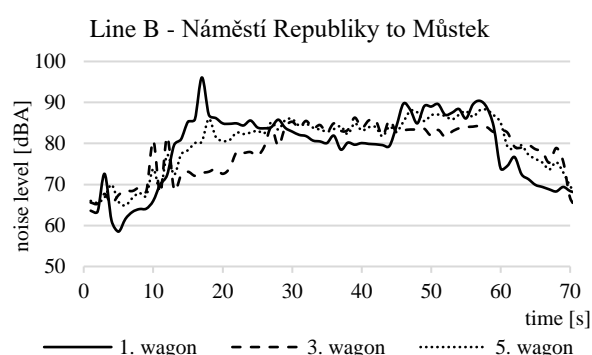**Fig. 5** Graph of the noise level between two stations

Fig. 6 Graph showing the reverse ride

Fig. 5. During measurements on the subway line B (yellow) pronounced maximums were recorded between *Můstek* and *Náměstí Republiky*, and also between stops *Luka* and *Lužiny* stations. The graph shows the record of the measurements between stops *Můstek* and *Náměstí Republiky*, where a different

driving style of metro trains is again evident. The drive recording shows measurements in the first wagon were different from the third and fifth wagon measured.

Fig. 6. In the opposite direction, the trip logs were almost identical, showing the same driving style during all measurements. Only when measuring the noise level in the first wagon a significant peak maximum of 96.1 dB was recorded, which is not reflected in the other runs.
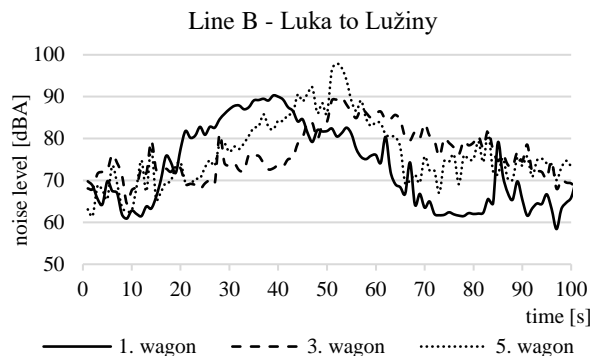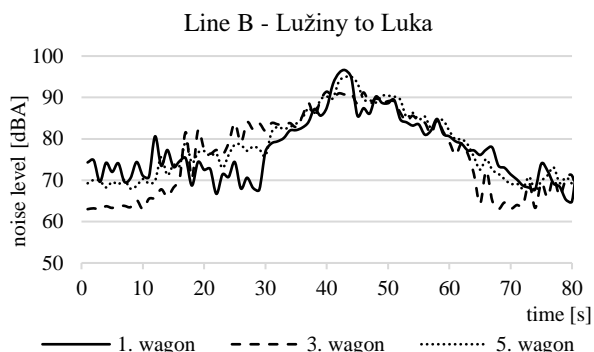

Fig. 7 Graph of the noise level between two stations   **Fig. 8** Graph showing the reverse ride

Fig. 7. On the same route, subway lines maximum noise levels were recorded even during the ride between *Luka* and *Lužiny*. The maximum value was recorded when measuring the noise level in the fifth wagon (97.9 dB).

Fig. 8. When measuring in the opposite direction between *Lužiny* and *Luka*, very similar noise levels were recorded for all rides. The maximum values were recorded in the 1st and 5th wagons measurements (96.6 dB and 95.0 dB). From the measured values it can be seen that the noise level measurement is dependent on the style of driving assembly, which is influenced by the need for punctuality.
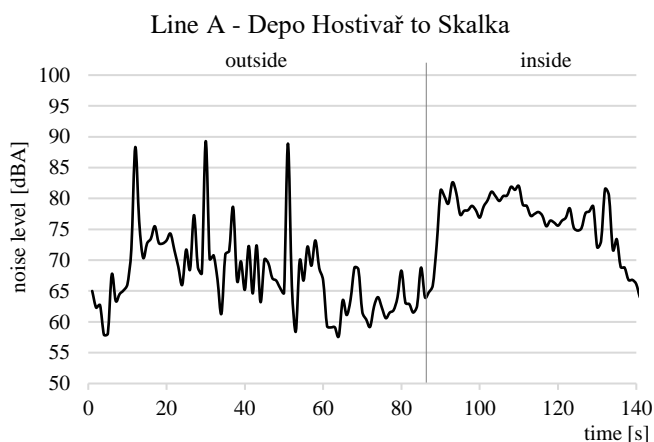

Fig. 9 The metro train noise level of outside and inside ride

The graph on Fig. 9 shows the noise level differences at the surface ride of the subway (0 - 88 s). From the graph, it is clearly observed that as soon as train enters the tunnel the noise level increases. The interior tunnel average surface noise level was 71.5 dB, whereas riding in a tunnel shows 10 dB less noise level. The registered noise level peaks on the surface are caused by crossing the sliding rail.

CONCLUSION

Sound absorption barrier walls made of concrete or brick reflect practically all of the energy contained in the acoustic waves which strike them directly. However, these reflected waves may still find their way over the wall by being subsequently reflected off the train car and then diffracted. That was what has been observed in tunnels of Prague subway tunnels. To prevent this, absorptive material may be fixed to the surface of the wall. The absorbing mechanism is caused by friction between moving air and the loose fibres or pore walls in the sound absorbing treatment. The friction between the air and porous

or fibrous absorptive material converts the acoustic energy to heat, thereby attenuating the sound. The excavated stations include *Dejvice*, *Strašnická* and *Skalka*. Other tunnels are built by punching.

The data obtained from subway line A (green), it is evident that the section between stops *Dejvická – Nemocnice Motol* was higher noise level observed in the recent built tunnel than prior built sections. Tunnels built by *Tunnel Boring Machine* and *Earth Pressure Balance* (TBM – EPB) technologies, with six segments of reinforced concrete thickness of 250 mm and width of 1.5m with insulation clenched in the joints, confirms the theory by *Nový, 2001 & Nelson, 1997,* principles of noise expansion based on ambient conditions. The measured data in general indicate that subway cars riding on the surface satisfy the Czech health standard recommendation, whereas in tunnels exceed. It has also been confirmed that noise levels depend mainly on vehicle speed and associated chassis noise and aerodynamic noise.

REFERENCES

1. Jandak, Z. (2007). *Noise within working environment* (in Czech). State Health Institute. Retrieved from http://www.szu.cz/tema/pracovni-prostredi/hluk-v-pracovnim-prostredi

2. Liberko, M. (2004). *Noise within environment* (in Czech). Ministry of the Environment of the Czech Republic. Retrieved from http://www.ceskyfocalpoint.cz/wp_content/uploads/2015/12/pupr_hluk_text.pdf

3. Nelson, J. T. (1997). Wheel/Rail noise control manual. *Transit Cooperative Research Programme,* Report 23, Washington, D.C.

4. Nový, R., Kučera, M. (2009). *Reducing noise and vibration (in Czech)*. Retrieved from https://www.ib.cvut.cz/sites/default/files/Studijni_materialy/SHV/Novy_Kucera_Snizovani_hluku_a_vibraci.pdf

5. Nový, R. (2001). *Noise and Vibration* (in Czech). Praha: ČVUT. ISBN: 80-01-02246-3

6. Persinger, M. (2014). Infrasound, human health, and adaptation: an integrative overview of recondite hazards in a complex environment. *Natural Hazards*, *70* (1), 501–525.

7. Thopson, D. (2009). *Railway Noise and Vibration: Mechanisms, Modelling and Means of Control*. Southampton: Elsevier, ISBN-13:978-0-08-045147-3

8. Zewdie, R. & Kic, P. (2016). Transport route segments and stress effect on drivers. *Agronomy Research*, *14*(1), 269-279.

Corresponding author:

Dr. Ing. Retta Zewdie, Department of Vehicles and Ground Transport, Faculty of Engineering, Czech University of Life Sciences Prague, Kamýcká 129, Praha 6, Prague, 165 21, Czech Republic, phone: +420 22438 3101, e-mail: zewdie@tf.czu.cz